Functional glycomimetics to explore bacterial adhesion and membrane behaviour: Synthesis and applications

Dissertation

zur Erlangung des Doktorgrades

der Mathematisch-Naturwissenschaftlichen Fakultät

der Christian-Albrechts-Universität

zu Kiel

vorgelegt von

Franziska Reise

Otto Diels-Institut für Organische Chemie

Kiel 2018

Referentin: Prof. Dr. Thisbe K. Lindhorst

Koreferent: Prof. Dr. Frank D. Sönnichsen

Tag der mündlichen Prüfung: 18.01.2019

zum Druck genehmigt:

gez. Prof. Dr. Frank Kempken, Dekan

Die vorliegende Arbeit wurde unter Anleitung von

Prof. Dr. Thisbe K. Lindhorst

am Otto Diels-Institut für Organische Chemie

der Christian-Albrechts-Universität zu Kiel

im Zeitraum von

September 2014 bis November 2018 angefertigt.

Hiermit erkläre ich, Franziska Reise, dass ich die vorliegende Arbeit selbstständig und nur unter Verwendung der angegebenen Quellen und Hilfsmittel angefertigt habe. Inhalt und Form dieser Arbeit sind eigenständig erarbeitet und verfasst worden. Die Arbeit ist unter Einhaltung der Regeln guter wissenschaftlicher Praxis der Deutschen Forschungsgemeinschaft entstanden. Weder die gesamte Arbeit noch Teile davon sind an anderer Stelle im Rahmen eines Prüfungsverfahrens eingereicht worden. Dies ist mein erster Promotionsversuch.

Kiel, 14.11.2018

_____

Franziska Reise

Danksagung

Mein besonderer Dank gilt Frau Prof. Dr. Thisbe K. Lindhorst für die interessante Aufgabenstellung, die Betreuung der Arbeit sowie die vielen anregenden Ideen, Gespräche und Ratschläge in den vergangenen Jahren. Gespräche und Diskussionen waren stets sehr konstruktiv und haben maßgeblich zur Entstehung dieser Arbeit beigetragen. Danke auch für das entgegengebrachte Vertrauen und die gewährten Freiräume bei der Ausgestaltung der Projekte. Beides hat eine angenehme Arbeitsatmosphäre geschaffen.

Weiterhin danke ich Herrn Prof. Dr. Frank D. Sönnichsen zunächst für die Betreuung dieser Arbeit als Zweitgutachter aber vor allem auch für die hilfreichen Diskussionen und Ratschläge, für die er jederzeit zur Verfügung stand.

Meinen Kooperationspartnern Dr. Bridget Murphy und Jonas Warias, Prof. Dr. Laura Hartmann und Sophia Boden sowie Prof. Dr. Arnaud Tatibouët und Giuliano Cutolo danke ich für die erfolgreiche Zusammenarbeit. Dank gilt natürlich auch meinen fleißigen Kollegen im Arbeitskreis für die produktive Zusammenarbeit.

Dank gebührt ebenfalls den Mitarbeitern der analytischen Abteilungen, Holger Franzen, Marion Höftmann, Gitta Kohlmeyer-Yilmaz, Dirk Meyer, Silke Rühl und Rolf Schmied für die Vielzahl an aufgenommenen NMR- und Massenspektren. Auch Rüdiger Kargoll und Andreas Wilms sei für die Erledigung vieler mal kleinerer und mal größerer Aufgaben gedankt.

Ein großes Dankeschön geht an Christine Haug und Elwira Klima-Bartczak, die stets mit großer Hilfsbereitschaft und Engagement für den Arbeitskreis da waren.

Dem aktuellen Arbeitskreis Lindhorst sowie den ehemaligen Mitgliedern danke ich für die angenehme Arbeitsatmosphäre und so manche amüsante Unternehmung.

Weiterhin möchte ich auch meinen Bachelorstudenten Tim Haas, Tobias Romann und Søren Tyldal, meinem F3 Praktikanten Constantin Ruppel sowie meinem fleißigen „Hiwi“ Clemens Lütjohann danken.

Da das beste stets zum Schluss kommt, sei an dieser Stelle meiner Familie gedankt, die mich stets unterstützt, Danke!

Die Bearbeitung der in Kapitel 4 genannten Zielstellung wurde bereits im Rahmen der Masterarbeit begonnen. Es wurden übernommen:

- Die literaturbekannte Syntheseroute von Verbindung **13** in Scheme 10.
- Die teilweise literaturbekannte Syntheseroute von Verbindung **29** und **30** in Scheme 11.
- Die literaturbekannte Synthese von Verbindung **10** in Scheme 19.
- Das ^{1}H-NMR-Spektrum der Verbindung **9** in Figure 43.

Die photochemischen Daten, die in Figure 28 bis Figure 33 und Figure 37 sowie in Table 1 wiedergegeben sind, wurden von Jonas Warias unter der Anleitung von Dr. Bridget Murphy am Institut für Experimentelle und Angewandte Physik der Christian-Albrechts-Universität zu Kiel ermittelt. Die Brewsterwinkel-Mikroskopie (Figure 34) wurde ebenfalls unter der Anleitung von Dr. B. Murphy durchgeführt.

Während der Promotionszeit wurden folgende Arbeiten veröffentlicht:

- F. Reise, J. E. Warias, K. Chatterjee, N. R. Krekiehn, O. Magnussen, B. M. Murphy, Th. K. Lindhorst, Photoswitchable glycolipid mimetics: Synthesis and photochromic properties of glycoazobenzene amphiphiles, *Chem. Eur. J.* **2018**, doi:10.1002/chem.201803112.
- V. Poonthiyil, F. Reise, G. Despras, T. K. Lindhorst, Microwave-assisted facile synthesis of red-shifted azobenzene glycoconjugates, *Eur. J. Org. Chem*. **2018**, doi:10.1002/ejoc.201801078.
- G. Cutolo, F. Reise, M. Schuler, R. Nehmé, G. Despras, J. Brekalo, P. Morin, P.-Y. Renard, Th. K. Lindhorst, A. Tatibouët, Myrosinase substrate and FimH ligand in one: Bifunctional glucosinolate glycoconjugates as enzymatically triggered masked isothiocyanates, *Org. Biomol. Chem.* **2018**, *16*, 4900-4913.

Abstract

Cell surface glycans play an important role in glycobiology since they are essential in cell recognition and cell adhesion. Furthermore, they decide about the health status of mammalians. For instance, bacterial adhesion is mediated by carbohydrate-specific binding of bacteria to glycosylated cell surfaces (‘glycocalyx’) of mammals. Consequently, essential questions in glycobiology are dedicated to the constitution and conformational properties of the glycocalyx in the context of their biological function in general and in particular, in bacterial adhesion processes. Scientists are driven by the need of new inventive tools and methods to gain a deeper and comprehensive insight into the biological role of glycans. This is also the motivation for the projects presented in this thesis.

One of the most common species of bacteria is the pathogenic *Escherichia coli* (*E. coli*) bacterium. They account for several serious diseases such as urinary tract infections, neonatal meningitis and gastroenteritis. Such infections usually start with an initial contact between bacterial fimbriae (adhesive organelles) and the glycosylated cell surface of the target cell. This interaction is mediated by carbohydrate-specific proteins (lectins) which are located at the fimbrial tips. In case of uropathogenic *E. coli* (UPEC) the lectins FimH and PapG are of utmost importance for the adhesion process. Whereas the lectin PapG is highly galabioside (Galα(1→4)Gal)-specific, the lectin FimH binds highly specific α-D-mannosides and is the focus of this work. For a deeper understanding of the binding mechanisms one has to focus on the adhesive surfaces on the one hand and the adhesive organelles on the other hand. Accordingly, the first part of this thesis deals with glycosylated surfaces and the second part deals with the lectin FimH.

In the first project photoswitchable glycolipid mimetics were synthesised and investigated regarding their photochemical properties and their structural changes resulting from light-induced *E*/*Z* isomerisation. These experiments were complemented by X-ray scattering methods and Langmuir isotherm measurements.

In the second project of this thesis the concept of glycoarrays and glyco-SAMs was deepened by establishing new assay set-ups. The first assay has the advantage that any glycan type can be easily immobilised via a light-induced insertion reaction, whereas the second investigated bacterial adhesion assay utilises a polysaccharide surface,

resembling, to some extent, a disordered sweet surface, which might be closer to the natural glycocalyx than a well-ordered and rather artificial glyco-SAM.

The third project aims at enabling photoswitching of mannose-specific adhesion by chemical modification of the adhesive protein FimH. Therefore, azobenzene precursors were synthesised which shall work as photosensitive ‘gate keeper’ molecules which can block the binding site of the lectin in one photochemical state and leave it open in its isomeric form. To realize such a site-directed approach the azobenzene precursors were synthesised with a thioester moiety and can thus be transferred onto an appropriate nucleophile in the proximity of the binding site in a DMAP-catalysed acyl transfer reaction. All azobenzene precursors were tested with respect to their suitability as ‘gate keeper’ moieties by investigation of the photochemical properties and molecular modelling.

The fourth project presents a versatile method for the preparation of red-shifted azobenzene derivatives by tetra-*ortho*-chlorination which feature *E*/*Z* isomerisation with visible light. Thus, damage due to UV light can be prevented in photoswitching experiments in biological systems. This approach widens the application potential of simple azobenzene glycoconjugates. A great advantage of the chosen approach is, that the chlorination can be performed at a ‘late stage’ of the synthesis and thus can be easily adapted to other applications.

Kurzzusammenfassung

Extrazelluläre Glykanstrukturen spielen eine wichtige Rolle in der Glykobiologie, da sie für die Zellerkennung und Zelladhäsion unerlässlich sind. Somit wird auch der Gesundheitszustand von Säugetieren von Glykanstrukturen bestimmt. Beispielsweise wird bakterielle Adhäsion kohlenhydratspezifisch vermittelt: Bakterien adhärieren mit hoher Spezifität an glykosidische Strukturen auf Zelloberflächen. Diese äußere Kohlenhydrathülle von eukaryontischen Zellen wird auch als Glykokalyx bezeichnet. Aus diesem Grund befassen sich die viel untersuchten Fagestellungen der Glykobiologie mit der Konstitution und der Konformation der Glykokalyx und vor allem auch mit dem Aspekt, welcher Zusammenhang daraus für die biologische Funktion im Allgemeinen und im Kontext der bakteriellen Adhäsionsprozesse im Speziellen resultiert. Dabei werden Naturwissenschaftler vor allem von der Notwendigkeit neuer Methoden und Instrumente zur Untersuchung kohlenhydratbasierter Prozesse angetrieben, um langfristig ein genaues und allumfassendes Verständnis der biologischen Rolle von Glykanstrukturen zu erlangen. Dies ist auch die Motivation derer Projekte, die im Folgenden in dieser Dissertation präsentiert werden.

Eine der am häufigsten vorkommenden Bakterienarten ist die des pathogenen *Escherichia coli* (*E. coli*) Bakteriums. Diese ist für eine Vielzahl von ernsthaften Krankheiten verantwortlich zu denen Harnwegsinfekte, Hirnhautentzündung bei Neugeborenen und Gastroenteritis zählen. Solche Infektionen beginnen gewöhnlich mit einem initialen Kontakt der bakteriellen Fimbrien (Adhäsionsorganelle) mit der glykosylierten Zelloberfläche der anvisierten Zelle. Diese Wechselwirkung wird von kohlenhydrat-spezifischen Proteinen (Lektinen), die sich an der Spitze eines Fimbriums befinden, vermittelt. Im Falle von uropathogenen *E. coli* Bakterien sind hauptsächlich die Lektine FimH und PapG von besonderer Bedeutung für den Adhäsionsprozess. Während das Lektin PapG spezifisch Galabioside (Galα(1→4)Gal) bindet, zeichnet sich das Lektin FimH durch eine hohe α-D-Mannosespezifität aus. Diese Arbeit konzentriert sich auf das Lektin FimH. Um den bakteriellen Bindungsmechanismus genauer aufzuklären, ist es nötig, sowohl die adhäsiven Oberflächen als auch die adhäsiven Organellen zu untersuchen. Daher befasst sich der erste Teil dieser Dissertation mit glykosylierten Oberflächen und der zweite Teil mit dem Lektin FimH.

Im ersten Projekt wurden photoschaltbare Glycolipidmimetika synthetisiert. Diese wurden im Hinblick auf ihre photochemischen Eigenschaften und die daraus

resultierenden strukturellen Änderungen während der *E*/*Z*-Isomerisierung untersucht. Diese Experimente wurden durch Röntgenstreuungsexperimente und Messungen der Langmuirisothermen ergänzt.

Das zweite Projekt dieser Arbeit erweiterte das Konzept der Glycoarrays um zwei neue Assaykonzepte. Der erste Assay hat den Vorteil, dass beliebige Glykanstrukturen ohne spezielle Funktionalisierung einfach durch eine lichtinduzierte Insertionsreaktion immobilisiert werden können. Der zweite untersuchte bakterielle Adhäsionsassay nutzt eine Polysaccharidoberfläche, die in gewisser Hinsicht einer ungeordneten, glykosylierten Oberfläche ähnelt, die folglich die natürliche Glycokalyx besser mimikrieren könnte, als es den streng geordneten glykosidischen SAMs möglich ist.

Das Ziel des dritten Projekts war es, ein lichtinduziertes Schalten der mannosespezifischen Adhäsion des Proteins FimH durch eine chemische Modifikation zu etablieren. Für diese Modifikation wurden Azobenzolderivate synthetisiert, die als photosensitive ‚Torhüter'-Moleküle fungieren sollen: In einem der beiden photochemischen Zustände wird die Bindetasche des Lektins durch den Azobenzolliganden verschlossen und in der isomeren Form wird die Bindetasche wieder geöffnet. Für die Durchführung dieser ortsspezifischen Ligationsstrategie wurden die Azobenzolderivate als Thioester synthetisiert, die in einer DMAP-katalysierten Reaktion mit einer geeigneten Aminosäure in der Nähe der Bindetasche des Proteins ligiert werden können. Alle synthetisierten Azobenzolderivate wurden im Hinblick auf ihre Eignung als ‚Torhüter'-Moleküle untersucht, indem ihre photochemischen Eigenschaften ermittelt wurden und computergestützte molekulare Modellierungen durchgeführt wurden.

Das vierte Projekt bietet eine vielseitig anwendbare Methode, die es ermöglicht, Azobenzolderivate zu synthetisieren, die in allen vier *ortho* Positionen chloriert sind. Diese Chlorierung hat zur Folge, dass die *E*/*Z* Isomerisierung durch langwelliges Licht induziert werden kann, sodass Schäden durch die Verwendung von UV Licht, wie es bei herkömmlichen Azobenzolderivaten üblich ist, vermieden werden können. Dies ist vor allem bei der Anwendung bei Photoschaltungsexperimenten in biologischen Systemen ausgesprochen vorteilhaft. Dieser Ansatz stellt eine beträchtliche Erweiterung der zuvor synthetisierten Azobenzolderivate dar. Ein großer Vorteil ist zudem, dass die Chlorierung kompletter Azobenzol- und Azobenzolglykosidderivate am Ende der Synthesesequenz durchgeführt werden kann, sodass die Methode ohne großen Aufwand für andere Anwendungen übernommen werden kann.

Table of contents

A guide to this thesis

This thesis comprises nine chapters as follows:

The first chapter provides a general introduction with basic information about the field of glycobiology and bacterial adhesion. This chapter is especially recommended to all readers who are not familiar with this subject to be able to fully appreciate the described research.

Chapter 2 explains the objectives of this thesis.

Chapters 3-6 present the individual projects. Each chapter starts with a specific introduction followed by a section ‘Results and Discussion’ and a conclusion.

Chapter 7 provides a comprehensive conclusion.

The experimental procedures and the UV/Vis as well as the NMR spectra related to all sub-projects are complied in chapter 8.

Abbreviations are given on page XXI and references in chapter 9.

For the sake of clarity, molecule numbering for each individual project starts with **1**.

Abbreviations

Ac	acetyl
AFM	atomic force microscopy
AGU	anhydroglucose unit
Aha	azidohomoalanine
Amp	ampicillin
aq.	aqueous
Arg	arginine
arom.	aromatic
Asn	asparagine
Boc	*tert*-butyloxycarbonyl
calc.	calculated
CAM	chloramphenicol
cf.	confer
CFG	Consortium for Functional Glycomics
conc.	concentrated
CRD	carbohydrate recognition domain
CuAAC	copper catalysed alkyne azide cycloaddition
d	day
d (NMR)	dublett
DBU	1,8-Diazabicyclo[5.4.0]undec-7-en
DCC	dicyclohexylcarbodiimide
DMAA	*N*,*N*-dimethylacetamide
DCM	dichloromethane

DEPC	diethyl cyanophosphonate
DIPEA	*N*,*N*-diisopropylethylamine
DMAP	dimethylaminopyridine
DMF	N,N-dimethylformamide
DMSO	dimethylsulfoxide
DNA	deoxyribonucleic acid
DPPA	diphenylphosphoryl azide
DPPC	1,2-dipalmitoyl-*sn*-glycero-3-phosphocholine
D_s	degree of substitution
DSC	differential scanning calorimetry
E. coli	*Escherichia coli*
EHEC	enterohemorrhagic *Escherichia coli*
ESI	electrospray ionisation
Fmoc	fluorenylmethyloxycarbonyl
FWHM	full width at half maximum
g	gram
Gal	galactose
GalNAc	*N*-acetylgalactosamine
GlcNAc	*N*-acetylglucosamine
GFP	green fluorescent protein
Gln	glutamine
h	hour
HATU	(1-[Bis(dimethylamino)methylene]-1*H*-1,2,3-triazolo [4,5-b]pyridinium 3-oxid hexafluorophosphate
Hpg	homopropargylglycine

Hz	Hertz
IC_{50}	half maximal inhibitory concentration
IR	infrared
ITC	isothermal titration calorimetry
J	coupling constant
L	litre
L_α	liquid crystalline phase
L_β	lammelar gel phase
L_o	liquid ordered phase
LB	lysogeny broth
LDT chemistry	ligand-directed “tosyl” (LDT) chemistry
LED	light emitting diode
lit.	literature
m	*meta*
m (NMR)	multiplett
M	molarity
MALDI-MS	matrix-assisted laser desorption ionisation mass spectrometry
MALDI-Tof	MALDI time of flight
Me	methyl
MeMan	methyl α-D-mannopyranoside
MeOH	methanol
min	minute
m.p.	melting point
MS	mass spectrometry

m/z	mass-to-charge ratio
NCS	isothiocyanate
NHS	*N*-hydroxysuccinimide
NMEG	neonatal meningitis causing *Escherichia coli*
NMR	nuclear magnetic resonance spectroscopy
o	*ortho*
OD	optical density
p	*para*
$P_{\beta'}$	rippled phase
PBS	phosphate-buffered saline
PBST	phosphate-buffered saline tween
PCR	polymerase chain reaction
PDB	protein data base
PFPA	pentafluorophenylazide
p-IF	*p*-iodophenylalanine
PMDTA	pentamethyldiethylenetriamine
P-ALM	post-affinity labelling modification
P-PALM	post-photoaffinity labelling modification
*p*PKL1162	plasmid Per Klemm 1162
PS	polystyrene
PSS	photostationary state
PVA	polyvinyl alcohol
quant.	quantitative
R	residue

R_f	retention factor
RIP	relative inhibitory potency
RNA	ribonucleic acid
rpm	revolutions per minute
rt	room temperature
s	second
s (NMR)	singulett
SAM	self-assembled monolayer
sat.	saturated
SD	standard deviation
Ser	serine
SPR	surface plasmon resonance spectroscopy
t (NMR)	triplett
TBAI	tetrabutylammonium iodide
TFA	trifluoroacetic acid
THF	tetrahydrofuran
Thr	threonine
TLC	thin layer chromatography
TRIS	*tris*(hydroxymethyl)aminomethane
Ts/tos	tosyl
Tyr	tyrosine
UAA	unnatural amino acids
UPEC	uropathogenic *Escherichia coli*
UV	ultraviolet

1 General introduction

In the attempt to reach a fundamental understanding of life and its regulatory processes, a great number of key achievements became famous, such as the findings of WATSON and CRICK in 1953 who revealed the helical structure of the DNA (deoxyribonucleic acid).[1] Their work paved the way for many more new discoveries within the field of protein biochemistry in the second half of the 20th century. Several Nobel Prizes were awarded for research on decoding of the genetic code[2] and protein biosynthesis.[3] One reason for the great success in this field of research may well lie in the clear structural basis of the investigated molecules. A limited number of nucleotides can be linked in a defined manner. A sequence of three nucleotids forms a so-called codon. Each codon then again represents one amino acid. The number of naturally occurring amino acids is limited and the subsequent connection of amino acids for the formation of peptides can just occur via an amide bond. Eventually, the protein biosynthesis is a well-organised system with an assembly plan which doesn't leave space for much structural diversity – at least not as much structural diversity as we can find for oligosaccharide structures, called glycans. The structural variability of glycans is determined by the connection of monosaccharides to oligo- and polysaccharides and the possible modifications with varying functional groups on the monosaccharide building blocks. Thus regio- and stereochemistry contribute to the huge variety of glycans.[4] Although carbohydrates represent a majority of the organic mass on earth the structural diversity and the resulting functions are not yet fully explained.[5-6] The potential of carbohydrates as energy storage and energy source had already been discovered by the pharmacist CONSTANTIN KIRCHHOFF in 1811.[7] At the same time EMIL FISCHER also investigated carbohydrates such as glucose and published the corresponding structure elucidation.[8-12] Also the photosynthesis research made progress at this time.[13] The knowledge about carbohydrates was limited to the field of energy and nutrition for a long time. Step by step also the connection between health and glycans was perceived. CLAUDE BERNARD mentioned diabetes in 1845 for the first time and opened the field of research about metabolism.[14] Many findings about the intermediary metabolism were published in the beginning of the 20th century.[15-17] Also the realisation that the specific blood groups of the human AB0 system are defined according to their individual saccharide decoration illustrated once more that carbohydrates play an essential role in every area and stage of life.[18-19] Saccharides even play a decisive role in the first second of life since glycans are said to be involved in many stages of the reproductive process – for instance they influence the sperm migration to

the site of fertilisation.[20] Nowadays it is known that carbohydrates also play fundamental roles in biological recognition processes as it is the case in cell recognition,[21,22] communication[23] and invasion[24] – either by commensal or pathogenic species.[5, 25] Although the field of carbohydrate research - also referred to as glycobiology[26] - is growing since the late 1980s there are still a lot of question marks concerning the impact of glycans for life.[5] Thus, there is a great interest to achieve a deeper insight into the function and biology of natural occurring glycans. However, as HANS-JOACHIM GABIUS stated in his book entitled 'The Sugar Code', the diversity of glycan structures is both a blessing and a curse. More ingenious tools for the analysis and synthesis of glycans are still required for the investigation of the diversity of glycoconjugates and their role in nature.[27-28]

1.1.1 Bacterial adhesion as one form of carbohydrate-protein interaction

Cell surface glycans play an important role in glycobiology since they are essential in cell recognition and cell adhesion.[5] More precisely, cell recognition can occur if one counterpart e.g. bacteria can recognize the glycan decoration of a targeted cell via special carbohydrate-binding proteins, so-called lectins.[29] The glycan layer on eukaryotic cells is referred to as 'glycocalyx'.[5, 30] The glycocalyx is an approximately 100 nm thick layer of inhomogenously arranged glycoconjugates.[31] Those oligosaccharides can be embedded into the cell membrane either through proteins (glycoproteins and proteoglycans) or in the form of glycolipids (cf. chapter3.1.1).[32] Glycoproteins can occur either as *N*-linked or *O*-linked oligosaccharides. *N*-linked means that the respective saccharide is β-glycosidically linked to the side chain of asparagine.[33] Whereas *O*-linked means that the particular glycan – which has a *N*-acetylgalactosamine (GalNAc) moiety within its structure - is α-glycosidically linked to the side chain hydroxyl group of serine or threonine, respectively (Figure 1). O-Glycans are often referred to as mucins.[34] Interestingly, the composition of the glycocalyx is highly individual and differs for every cell type. It also changes due to aging processes and in disease.[35] The function of the glycocalyx and the connected biological processes are not yet fully understood and thus are the subject of current research.

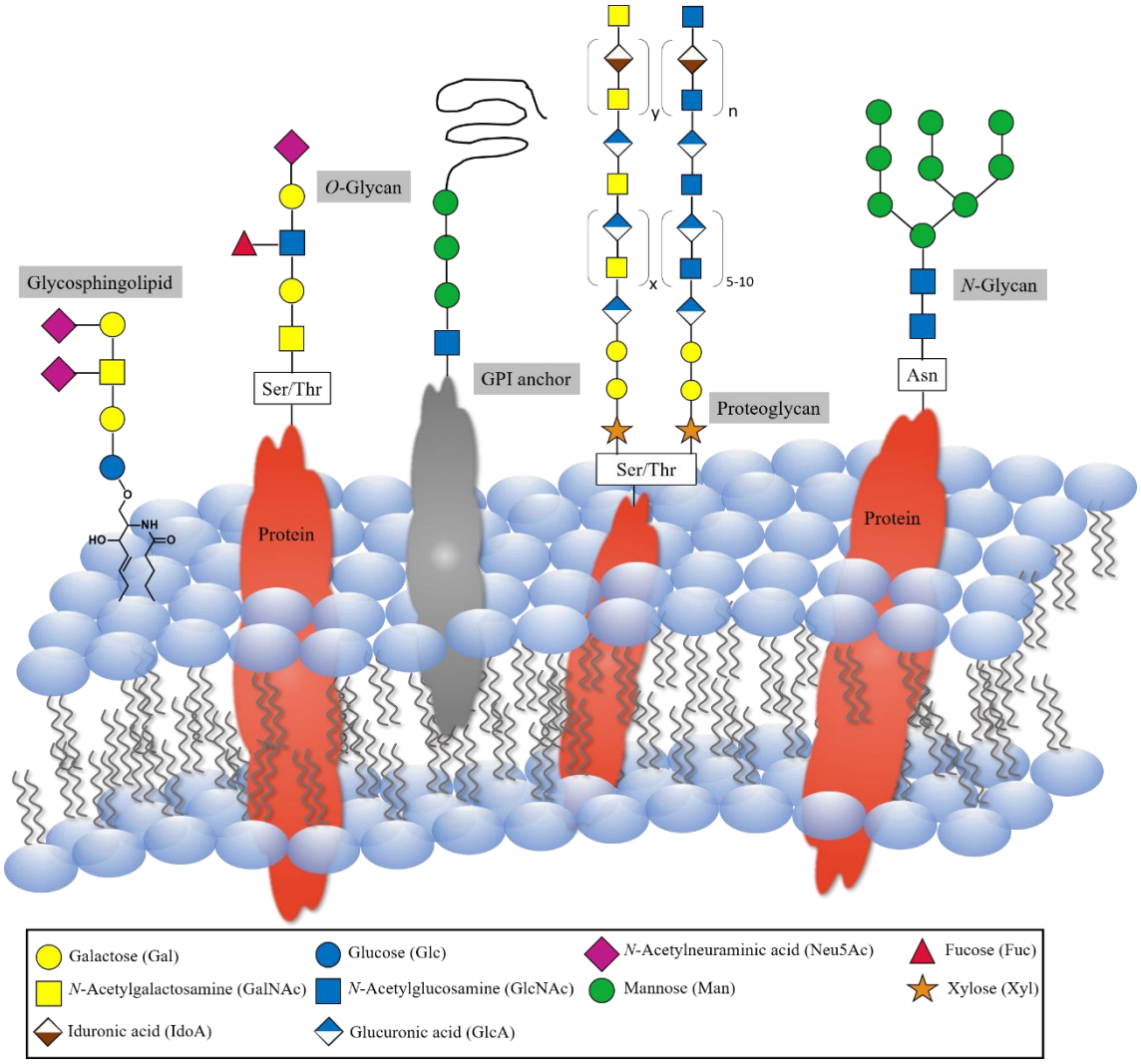

Figure 1: Schematic presentation of a eukaryotic cell membrane with embedded glycans ('glycocalyx'). Glycan structures are commonly linked to the membrane either as proteins (glycoproteins and proteoglycans), GPI anchors or glycolipids. The carbohydrate moieties are depicted according to the conventions introduced by the Consortium for Functional Glycomics (CFG).[36]

The glycocalyx enables the adhesion of bacteria to eukaryotic cells. This process is essential for mammals. The human mucous membranes are colonised by a multitude of commensal bacteria. Those are part of the immune system since they inhibit the colonisation of pathogens. But as soon as those commensal bacteria colonize body regions in which they don't occur under healthy conditions those bacteria become pathogens as well.[37] A well researched example are *E. coli* (*Escherichia coli*) bacteria. Those gram-negative bacteria belong to the family of Enterobacteriaceae and colonize the gastrointestinal tract as commensal bacteria.[38] Nevertheless, some *E. coli* strains are pathogens and cause diseases like urinary tract infections (uropathogenic *E. coli*, UPEC)[39], meningitis (neonatal meningitis causing *E. coli*, NMEC)[40] or diarrhoe

(enterohemorrhagic *E. coli*, EHEC).[41] The adhesion of bacteria on cell surfaces- both commensal and pathogenic- is mediated by adhesive organelles the so-called fimbriae. The surface of bacteria is decorated with different kinds of fimbriae. For example UPEC show a large quantity of type 1 fimbriae which are encoded by the fim gene cluster and P fimbriae which are encoded by the pap gene cluster. The process of bacterial adhesion is mediated by special proteins, the so-called lectins. They are either located directly at the surface of the bacterium or at the tip of fimbriae. Lectins are classified with regard to their structure and function in groups of C-, I- and P-type lectins and galectins for animal lectins for instance.[42] Bacterial type 1 fimbriae considerably contribute to adhesion and virulence. Those fimbriae are 1-2 μm long and around 7 nm in diameter. Type 1 fimbriae can be divided into two units: the fimbrial shaft and the tip. The shaft is built by up to 3000 FimA subunits which are arranged helically. The pilus rod carries one FimF and one FimG unit on top and the last unit of this chain is the lectin FimH (Figure 2). FimH consisting of two domains – the lectin domain and the pilin domain – acts as the carbohydrate recognition domain (CRD) which binds α-D-mannose-specific.[43-45] The entrance of the CRD is flanked by two tyrosine residues (Tyr48 and Tyr137) which form the so-called tyrosine gate.[46] Therefore ligands with an aromatic aglycone show an increased affinity for the lectin FimH due to ππ interactions with the tyrosine gate. This correlation can be considered for the synthesis of α-D-mannose-based FimH antagonists as anti-adhesives in anti-adhesive therapies to prevent bacterial infections.[47-49]

The synthesis of type 1 fimbriae is controlled by the chaperone/usher pathway. The protein FimC as so-called chaperone ensures the correct protein folding of the pilin subunits within the periplasm. As soon as a suitable conformation is obtained the subunits can pass the outer membrane via the protein FimD which therefore is called the usher. Subsequently the passed subunits are integrated in the growing fimbrial rod.[50]

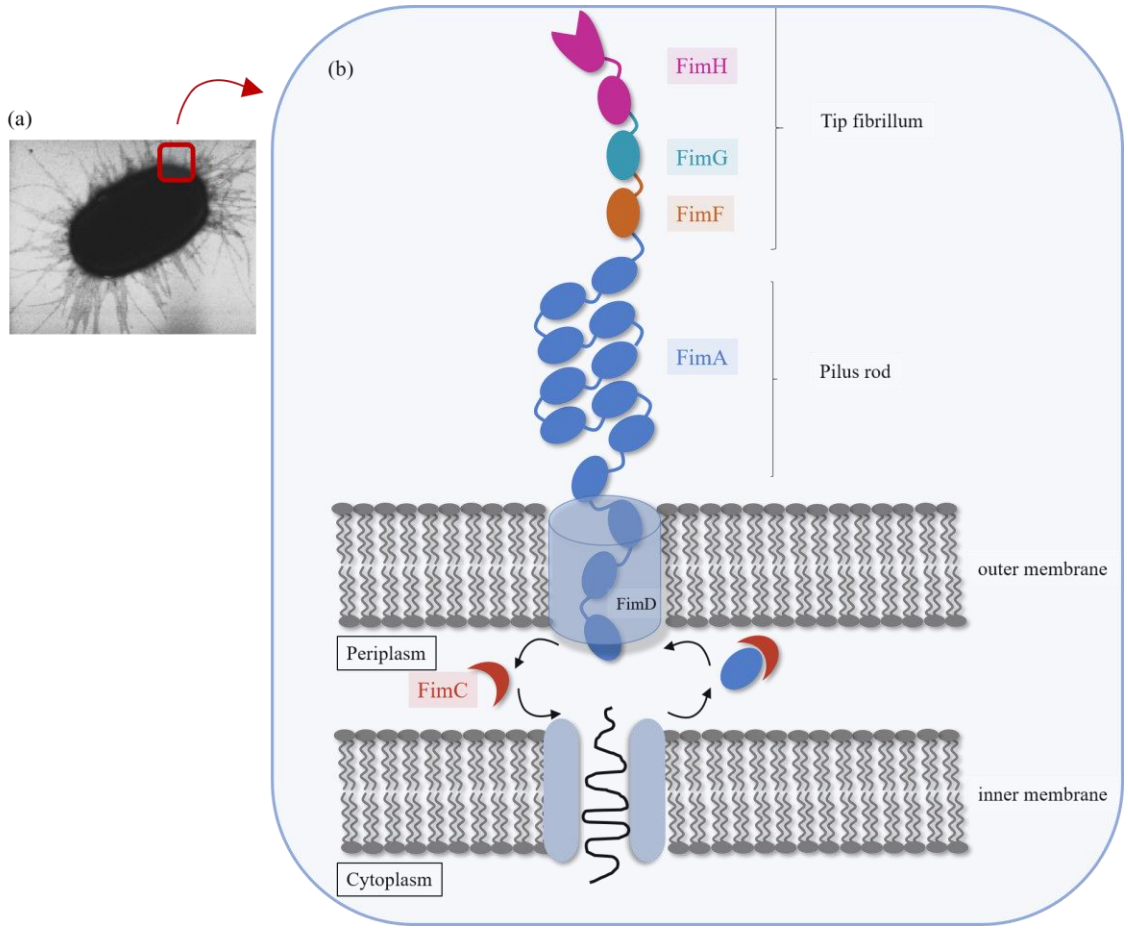

Figure 2: (a) AFM (atomic force microscopy) picture of *E. coli*[51]; (b) Schematic representation of a type 1 fimbria of *E. coli*. The fimbria consists of different subunits and carries the lectin FimH with the α-D-mannose-specific CRD at the tip. Fimbriae are formed via the chaperone/usher pathway in the periplasm.[52]

Although the process of cell adhesion was elucidated as outlined above, many of its details are not yet fully investigated. Glycoarrays have been proven to serve as valuable tools for the investigation of carbohydrate-protein interactions, but there is room for further improvement. Indeed, the glycoscience is still in need of new methods and techniques to provoke significant progress in the field of glycomics as the field of proteomics already experienced.[5, 53]

2 Objectives

The focus of this thesis lies on carbohydrates as mediators of bacterial adhesion. The process of bacterial adhesion was addressed from two perspectives regarding the bacteria and their adhesive organelles on the one hand and considering the adhesive glycosylated surfaces on the other hand (Figure 3). Hence, the first part of this thesis deals with various glycosylated surfaces in the context of FimH-mediated bacterial adhesion. The glycosylated surfaces were investigated both on the molecular level and in a broader context as glycosylated lipid layers. For the investigation of glycosylated surfaces as adhesive films, polystyrene surfaces were modified with different glycoside derivatives (cf. chapter 4). This project was focussed on the different parameters which influence the binding process. The density of the glycosidic layer, the arrangement as well as the orientation were considered as well as how close the respective glycoarray resemble their natural counterparts. The focus of the project dealing with lipid layers (cf. chapter 3) was motivated by the dynamic processes occurring in lipid bilayers. In this context, the influence of carbohydrate moieties of special tailor-made glycolipid mimetics was investigated regarding structure and dynamics. As functional handle the glycolipid mimetics were equipped with an azobenzene moiety to make the structure of those amphiphiles sensitive to irradiation with UV light. The incorporation of the glycolipid mimetics created a dynamic membrane system which is an interesting model system for the mimicry and investigation of processes occurring within cell membranes. This work was performed in collaboration with Dr. BRIDGET MURPHY at the Institute of Experimental and Applied Physics at Kiel University.

The project dealing with FimH as adhesive organelle (cf. chapter 5) took an approach which comprises organic synthesis and biochemistry. The goal of this project was to enable photoswitching of mannose-specific adhesion by chemical modification of the adhesive protein FimH. The project aimed at attaching an azobenzene at the entrance of the FimH carbohydrate binding site by a site-specific bioorthogonal reaction. The azobenzene moiety is meant to function as a photosensitive ‘gate keeper’ molecule that can block the binding site in one photochemical state and leaves it open in its isomeric form. Thus, labelling and the control of adhesivity can be achieved in one step and will enable new methods for the investigation of the binding mechanism of the lectin FimH. In the course of this project, a library of potential ‘gate keeper’ moieties as thioester precursors were synthesised. The synthesis was accompanied by molecular modelling

studies and molecular dynamics studies for the investigation of the opening and closing process of the binding site by photoswitching. In addition, photochemical properties of all synthetic molecules were investigated to validate their intended use. Eventually, the biochemical ligation will be performed by CARINA SPORMANN under the supervision of Prof. Dr. THISBE K. LINDHORST at the Otto Diels Institute of Organic chemistry at Kiel University.

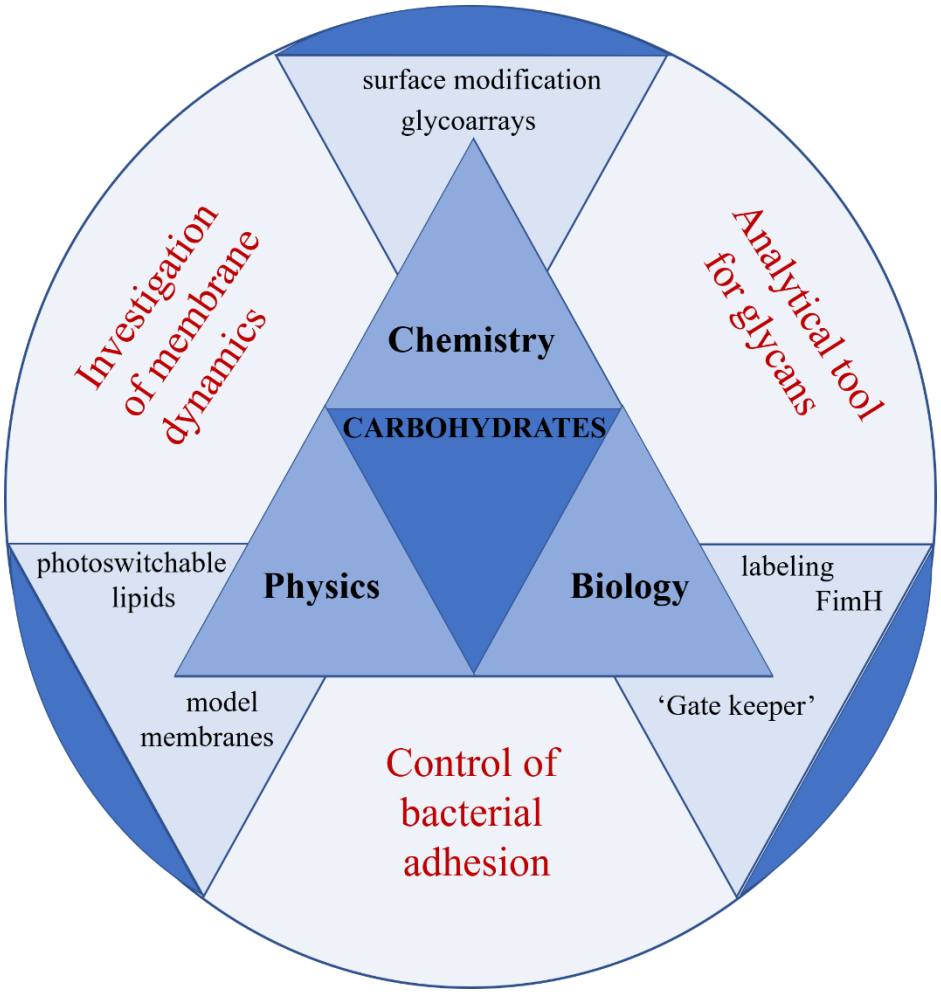

Figure 3: Overview of the interdisciplinary projects of this thesis.

Finally, work aiming at the synthesis of red-shifted azobenzene glycoconjugates was also performed (cf. chapter 6). [54-55]

3 Photoswitchable glycolipids for the investigation in lipid layers

3.1 Introduction

Glycolipids are amphiphilic molecules and important constituents of cell membranes. Membranes as special representatives of liquid-liquid interfaces are of great importance for biological systems. They do not only operate as barrier between cells but also play a key role in regulatory processes.[32] Whereas solid interfaces were thoroughly investigated, liquid interfaces offer a wide sphere of aspects for research. Hence, it is known, for example, that there is a direct link between the lipid environment of ion channels in membranes and their structure and function.[56] Photoisomerizable molecules are valuable tools in investigating the details for such important biological processes. There are studies about rather artificial amphiphilic molecules which can indeed mimic dynamic changes within membranes by isomerisation of a photoswitchable unit but lack the comparability to naturally occuring lipids though.[57-65] On these grounds we designed photoswitchable glycolipid mimetics for spectroscopic studies and for the investigation of Langmuir Blodgett films composed thereof (Figure 4). The integration of tailor-made photoswitchable glycolipids into phospholipid membranes will enable the analysis of biologically relevant characteristics of the membrane-host system regarding structure and kinetics.

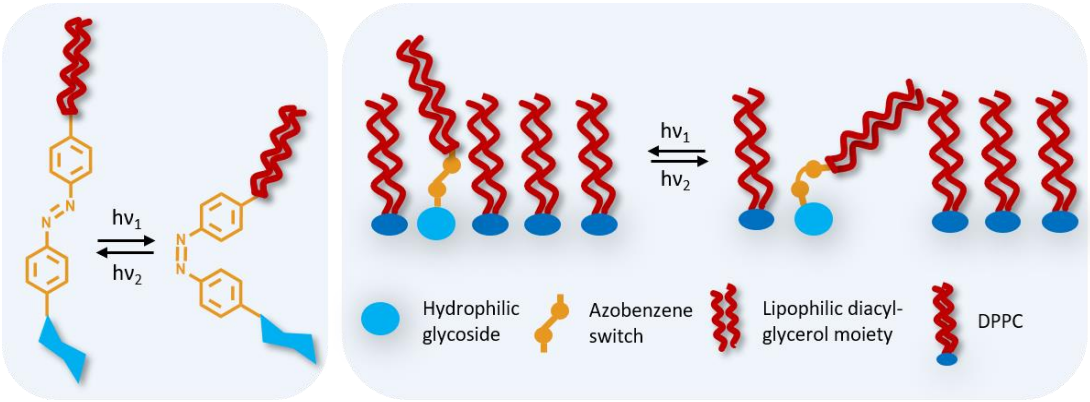

Figure 4: Light-induced switching of azobenzene glycolipids embedded into a DPPC (1,2-dipalmitoyl-*sn*-glycero-3-phosphocholine) monolayer can mimic dynamic changes within lipid monolayers. Conformational changes can be triggered due to the *E*/*Z* isomerisation of the azobenzene moiety and can be investigated regarding structure and kinetics.

3.1.1 Amphiphiles and lipid layers in biological systems

Lipids are one of the main groups of functional biomolecules in addition to carbohydrates, nucleotides and amino acids. Whereas the three last-mentioned classes build up polymers by covalent bonds, lipids form macromolecular entities by supramolecular interactions. Lipids can be categorised into fatty acids, triglycerides, wax, isoprenoids, phospholipids and glycolipids. Many lipids resemble amphiphiles, namely phospholipids and glycolipids.[66-67] Amphiphiles are characterised by a hydrophilic headgroup on the one hand, and on the other hand by a lipophilic tailgroup. Hence, amphiphilic lipids aggregate in water to form micelles or lipid bilayers, respectively. Lipid bilayers form compartments both between cells theirselves and between the cell's organelles: this spatial separation is essential for many processes of live e.g. signalling, regulation, transport and cell communication.[32] Since every system seeks for a state of equilibrium which is characterised by a minimum of lowest GIBBS free energy, membranes are essential for living systems as they function as fundamental barriers. Membranes provide distinct cellular regions which come along with a differential of various concentrations for instance ATP, the currency of energy in cells. Those concentration-dependent potentials are the impetus for life. In absence of barriers both cellular ingredients like proteins, nucleic acids, nucleotides and carbohydrates and ATP would diffuse away from the cell totally uncontrolled. The scattered diffusion would happen so fast that live would not be possible.[68]

As already mentioned above cell membranes are constituted by phospholipids, glycolipids and cholesterol, which is an important structure factor. Due to its rigid structure, cholesterol makes the membrane less fluid, indeed, but at the same time it prevents a too large density of the hydrocarbon residues which belong to the other membrane constituents and therefore precludes crystallisation of the bilayer.[69] The class of phospholipids includes glycerophospholipids and sphingophospholipids. Glycerophospholipids feature a glycerol core structure. In contrast to triglycerides just two of the three hydroxyl groups are esterified with fatty acids, whereas the third hydroxyl group of the glycerol unit is connected via a phosphordiester bond with either aminoalcohols, more precisely choline, serine or ethanolamine or polyols, for instance inositol. Sphingophospholipids in contrast to glycerol lipids are composed of a sphingosin (1-amino-4-*trans*-octadecene-1,3-diol) backbone which is just monoacylated at the amino functionality (ceramide structure). One of the hydroxyl groups remains unmodified, whereas the second OH group is either esterified as a phosphordiester resulting in

sphingomyelins or it is glycoslated, resulting in glycosphingolipids. The simplest representatives of glycosphingolipids are cerebrosides, which are functionalised with just one carbohydrate moiety which is in most cases glucose or galactose. More complex derivatives are called gangliosides which are equipped with complex oligosaccharides containing sialic acid derivatives. In particular, those negatively charged sialic acid residues give distinction to the cell surface (Figure 5).[32]

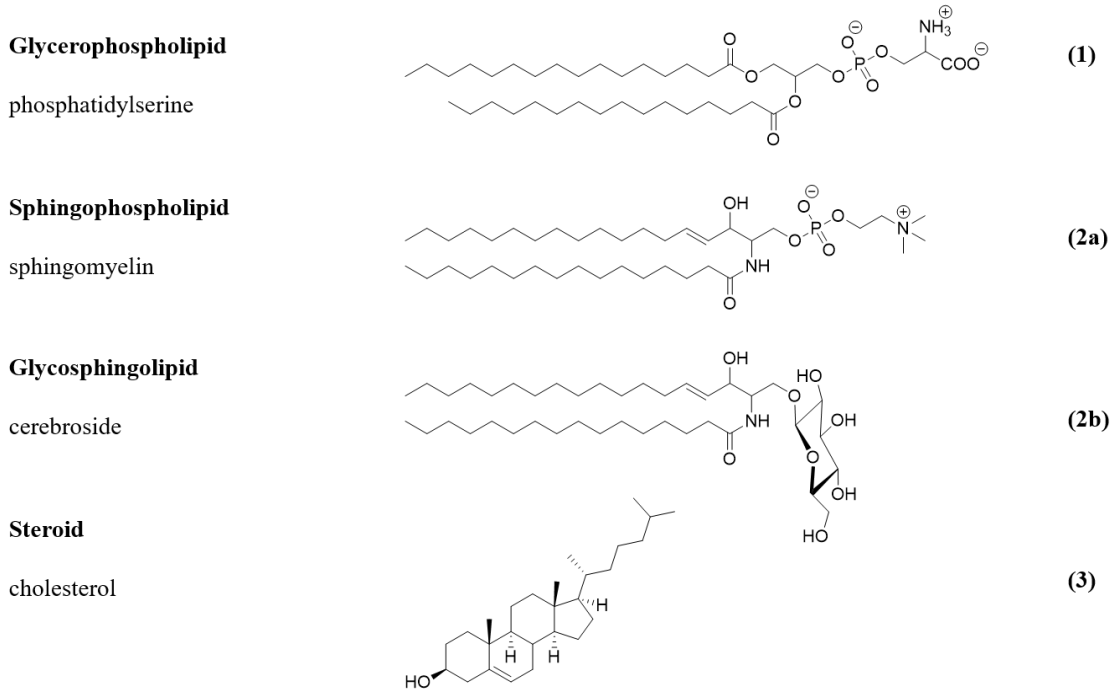

Figure 5: Representatives for the three classes of membrane lipids: Glycerophospholipids, e.g phosphatidylserine (**1**), the class of sphingolipids, which can be divided into sphingophospholipids, e.g. sphingomyelin (**2a**) and glycosphingolipids, e.g. cerebroside (**2b**) and steroids, e.g. cholesterol (**3**).[32]

Membrane features are influenced by different parameters such as pressure, temperature and the composition of the hydrophilic as well as the lipophilic parts. Depending on these parameters, membranes adopt various phases and phase transitions. Phase transitions are connected to function and in order to elucidate such structure-function relationships, suitable model systems are required. Monolayers are outstanding model systems for membranes since lipid bilayers consist of two interacting monolayers.[70-71] If amphiphilic lipids are deposited on a water surface, they arrange due to their bipolarity. The hydrophilic headgroup orients towards the water surface and the lipophilic tailgroup angles off towards the air. The resulting monomolecular insoluble films are called Langmuir monolayers. Langmuir monolayers can be studied with respect to various (thermodynamical) variables. Langmuir-Blodgett troughs for example are used to

investigate the surface pressure of an amphiphilic monolayer on a specific subphase (commonly water) by varying the surface dimension by a movable barrier. The results can be depicted in the form of a Langmuir isotherm.[72] A schematic Langmuir isotherm is shown in Figure 6. Monolayers with a spacious allocation of molecules on the subphase, where the area per molecule is large, can be described as two-dimensional gases. By increasing the surface pressure and hence decreasing the area per molecule on the subphase the monolayer can be converted into a so-called liquid expanded phase. Continuing compression leads in the first instance to a plateau of surface pressure despite compression. This fact indicates a first-order transition. After transcending this plateau, the monolayer converts into a condensed phase. Further compression leads to a kink of the isotherm and ends in an untilted condensed phase. The kink originates from a decreased compressibility. The untilted condensed phase is often referred to as solid phase. But in both cases of condensed phases the hydrocarbon chains of the lipophilic part are straightened in parallel merely differing in their orientation in relation to the subphase.[71]

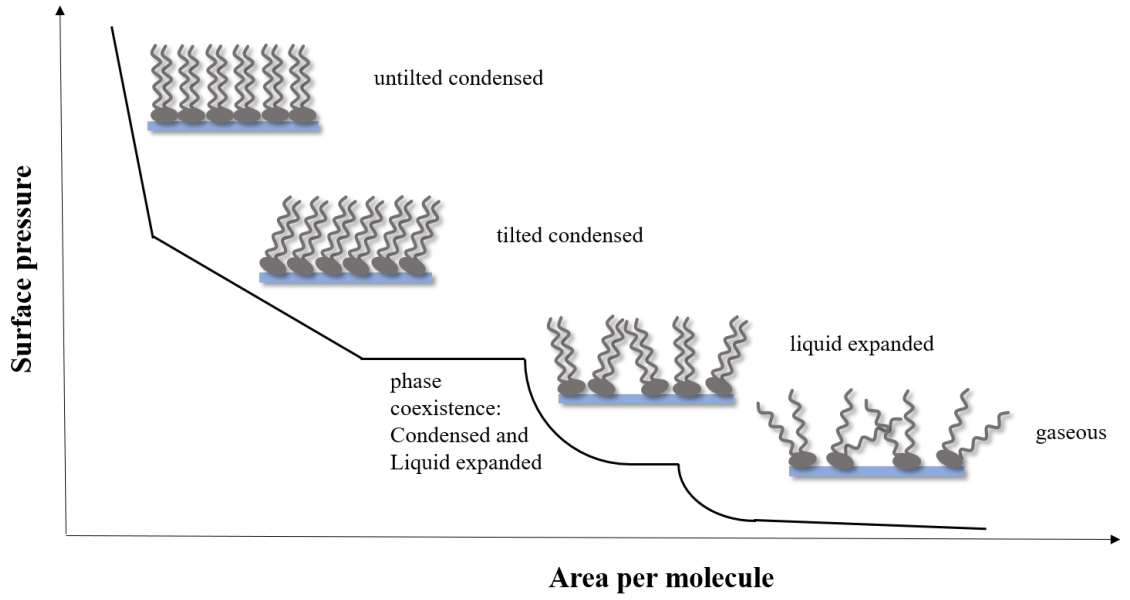

Figure 6: A schematic Langmuir isotherm for some monolayer of amphiphiles on a water subphase. A horizontal trend of the isotherm shows an area in which two phases can coexist due to a first-order transition. The kink in contrast suggests a continuous transition[71]

Lipid bilayers can also be classified with respect to their occurence. A distinction is drawn between lamellar and non-lamellar phases. Whereas there are different lamellar phases there is just one non-lamellar phase, the liquid crystalline L_α phase. Many biologically

relevant processes happen in the liquid crystalline L_α phase and therefore many investigations focus on this state of bilayers. Nevertheless, it is worth mentioning that those processes occur in dependence of temperature or surface pressure as already discussed before for monolayers. In the context of non-lamellar bilayers the terms subgel L_c gel phase L_β and $L_{\beta'}$ as well as rippled phase $P_{\beta'}$ are commonly used. The subgels L_c are characterised by a high organisation of the hydrocarbon chains, therefore also referred to as liquid ordered phase (L_o), and a tilt angle with respect to the bilayer. By increasing the temperature, for instance, the system can be converted to a lamellar gel phase (L_β or $L_{\beta'}$). In analogy to the tilted condensed phase in case of monolayers, the lipids lipophilic parts are arranged with a tilted angle relating to the bilayer normal in case of $L_{\beta'}$ phases. In the L_β phase the lipophilic parts are disposed parallel to the bilayer normal. When the temperature is further increased, a transition to a liquid crystalline phase occurs which is characterised by a disordered arrangement of the lipid tails. The transition from the gel phase to the liquid crystalline phase can arise either directly or via a rippled phase $P_{\beta'}$. For that purpose, the gel phase first converts to the rippled phase which is not just rippled but also tremendously swollen; nevertheless, the lipophilic tails are still ordered. During further increase of the temperature the rippled phase can melt to a L_α phase (Figure 7).[73]

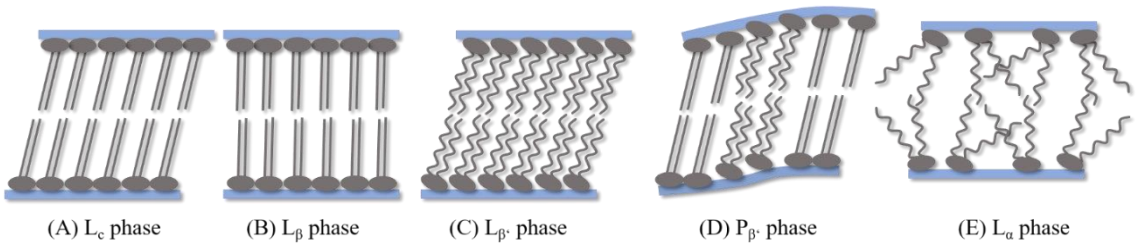

Figure 7: Schematic representation of known membrane patterns. The state of highest organisation is the L_c phase (A) followed by the lamellar gel phases L_β (B) and $L_{\beta'}$ (C). The lamellar gel phases can convert into a liquid crystalline L_α phase (E) either directly or via a rippled phase $P_{\beta'}$ (D).[74]

All descriptions outlined above are models which apply best for homogenous lipid layers. However, biological relevant membranes always consist of different constituents such as glycolipids and cholesterol. This mixed composition leads to variable interactions of the various components and therefore, the naturally occurring membranes are not always homogenous as described above in a simplified way. Often, membrane lipids build domains due to their heterogeneity. Lipid domains differ from the surrounding parts of the bilayer. Domains of high glycosphingolipid and cholesterol concentration are called lipid rafts. Whereas sphingolipids interact via weak attractive forces between the

glycoside headgroups, occurring voids are filled by cholesterol molecules. Lipid rafts are more ordered and more tightly packed than the surrounding and moreover, they float freely within the bilayer.[32, 75-76] Until to date, lipid rafts are not conclusively understood and especially photoswitchable lipid derivatives might be valuable tools for their further investigations and thus the key for remaining questions.[77-78]

3.1.2 Azobenzenes as molecular switching lever of biological function

Molecules which can function as switchable hinges or molecular joint, respectively, triggered by distinct stimuli are of great importance and interest in research fields ranging from material science to biological chemistry. Molecular switches can be toggled between at least two distinct thermodynamically stable states by exposure to an external stimulus. As stimuli light, heat, mechanical stress[79] and pH can be considered.[80] Molecular switches open a wide field of fascinating applications. They can be used for optical devices and for imaging,[81] as molecular machines[82-85] and for tailor-made functional materials like polymers.[86-89] Furthermore, a lot of promising applications can be considered in the field of life sciences where especially photoswitches find applications owing to non or little invasive stimulation. In addition, they are beneficial due to their high temporal and spatial resolution. Photoswitches can be used in photopharmacology e.g. for drug delivery[90-91] or as modulators of protein activity.[92-95] Current photoswitches are spiropyranes, diarylethenes, fulgides and probably the most famous and longest investigated representative of molecular photoswitches are azobenzenes.[96] They show favourable photochromic properties, as azobenzenes are characterised by an effective *E*/*Z* isomerisation: The planar *E*-isomer is the thermodynamically more stable form which can be converted to its bent *Z*-isomer by irradiation with UV light.[97-98] The back isomerisation Z → *E* can be triggered either by heat leading to thermal relaxation, by irradiation with visible light[99] or electrochemically.[100] Not only the angle of the molecules does change upon irradiation but also the dipole moment, thus, the polarity and the volume expansion change upon isomerisation. Whereas the end-to-end distance of the *E*-isomer adds up to 9 Å, for the *Z*-isomer this value is reduced to 5.5 Å.[101-104] Ideally, the properties of azobenzene derivatives can be tuned with regard to the requirements of the targeted application.[105-108] For instance, azobenzenes can be grouped into slow and fast switches depending on their half-life. The velocity of the switching process in turn is dependant on the mechanism of isomerisation. A distinction is drawn between four

proposed mechanisms, namely rotation, inversion, concerted inversion and inversion assisted rotation (Scheme 1).[109-113] 'Fast switches' can be addressed by short pulses of light and are characterised by a short half-life due to immediate thermal relaxation. Consequently after withdrawal of the stimulus the *E*-state can be retrieved in the range of microseconds time scale.[114] Those properties are ideal for the use as optical oscillators[115] and for applications like data exchange and real time information transmitting.[116] Nevertheless, the focus on science is on the development of even shorter time scales of nano-, respectively, picoseconds which were realised for spiropyrane[117-119] and diarylethene[120] derivatives up to now but not for azobenzenes.[116] 'Fast switches' are in many ways of great importance since they might be used for future applications in cell communication processes,[121-122] for the imitation of cilia movement[123-124] and as molecular muscles.[125-127] In contrast, 'slow switches' like photoswitchable derivatives for data storage need a long durability and prevention of photobleaching to enable countless switching cycles.[116, 128-132] To adapt the language of data storage the 'written state' should be stable but erasable. The same holds true for many biological, medical and pharmaceutical applications such as the manipulation of ion channels for the regulation of nociception.[133-135] 'Fast switches' can be realised by push-pull azobenzene derivatives which are equipped with a strong electron donor on the *para*-position of one phenyl ring and a strong electron acceptor on the far side *para*'-position of the second phenyl ring. This substitution pattern lowers the energy of the ππ* state and thus promotes thermal *Z*→*E* relaxation.[113] In addition to the substitution pattern which can increase the dipole character[136] of those molecules, the thermal relaxation is also favoured by polar solvents[137] and increased pressure.[138-140] Due to the asymmetric electron distribution and the resulting high dipole moment, push-pull azobenzene derivatives undergo isomerisation, albeit much discussed,[141-142] in many cases pursuant to a rotational isomerisation mechanism (Scheme 1).[143-146] Push-pull azobenzene derivatives with an especially fast thermal *Z*→*E* relaxation were introduced by VELASCO and coworkers. Those molecules are in shape of bithionylpyrrole-based azo dyes,[147] azopyridines and azopyrimidines,[114] cationic azo dyes[146] and cationic bis-azo derivatives.[148]

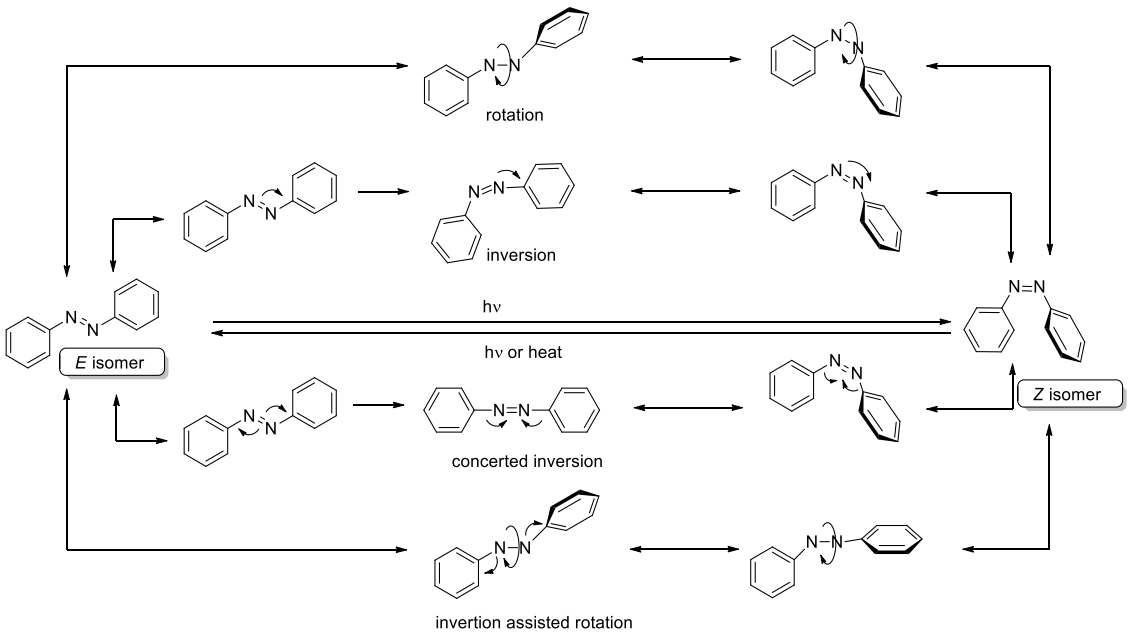

Scheme 1: Proposed mechanisms for the *E* → *Z* isomerisation of azobenzenes. All steps are supposed to be reversible in case of thermal or light-induced back isomerisation *Z* → *E*.[113]

Biological applications for instance require photoswitches which can be excited by longer wavelength ('red-shift') to prevent damage on the targeted system or the surrounding tissue in case of *in vivo* applications.[149-151] Furthermore, azobenzene derivatives for use in biological systems also have to fulfil further requirements besides the wavelength for isomerisation, namely water solubility, biocompatibility and stability towards hydrolysis and reduction.[152] Besides this, not just the life-time of an azobenzene compound in general is of scientific interest but also the half-life is in focus of potential applications. As every material, molecular switches must also pass a quality check and have to be characterised and evaluated in view of the requirements mentioned above. For that purpose a variety of analytical methods can be executed. Some methods which are relevant for this project are presented in the next chapter.

3.1.3 Tools for the investigation of lipid layers

Many publications are known reporting about the effects and processes which azobenzene derivatives can evoke when embedded to a lipid layer like membranes or liposomes.[90, 153-163] MORGAN et al. for instance investigated the release of a fluorescent marker from a liposome due to photoinduced isomerisation of azobenzene derivatives which are embedded in the respective liposome.[159] Although the effect of the photoswitches in

those experiments are known, it still has to be encoded which events run down during isomerisation on the nanoscale of the lipid systems.[164] For those investigation methods like X-ray reflectivity in combination with Langmuir Blodgett troughs, atomic force microscopy (AFM)[165-166] and differential scanning calorimetry (DSC)[167] lend themselves. X-ray reflectivity is an interferometric method to analyse surfaces, thin films and multilayers.[168-169] The basic concept of this method is that an incoming X-ray beam with a wave vector k_{in} and entrance angle α_{in} is reflected on the interface between two layers n and n_0. For flat angles of incidence total reflectance occurs (entrance angle α_{in} = exit angle α_{out}) and the intensity of the emergent beam can be detected (Figure 8). This setting which assumes a perfectly flat surface and excludes absorption was theoretical described by FRESNEL.[170] Since many surfaces are rough by nature, and besides, it is not trivial to prepare perfectly flat surfaces, the FRESNEL equitation has to be considered as a model which needs modifications to describe real systems. One reliable roughness model has been proposed by NÉVOT and CROCE.[171] Two aspects have to be considered in case of larger angles. First of all, one has to consider that not the complete incoming beam is reflected but a minor lot can pass the interface and transmission of the other phase can occur. Secondly, in case of surfaces which are not perfectly flat e.g. rough surfaces or lipid layers the beam is not perfectly reflexed with $\alpha_{in} = \alpha_{out}$ but scattered. Besides some percentage of the beam is also subjected to transmission. This part is characterised by a wave vector k_t and enters the second phase n_0 with an entrance angle α_t. Refraction in dependence of the material befalls the transmitting beam. For X-rays the refractive index n is defined as:

$$n = 1 - \delta - i\beta$$

The real number δ terms the dispersion which is dependant on the electron density, the classical electron radius and the wavelength. The imaginary number β terms the absorption which is dependant on the wavelength and the linear absorption coefficient μ. The electron density is the crucial parameter for the reflectivity of an interface.[172] First and foremost X-ray reflectivity is a good method to investigate the thickness of films and also to provide a profile of layer thickness. From the measured data it is also possible to determine the electron density with the aid of computer-based models and the surface roughness. The surface roughness is defined as a statistical deviation of the local surface from the mean surface. Thus the roughness can be mathematically considered as the root mean square deviation from the mean surface.[173]

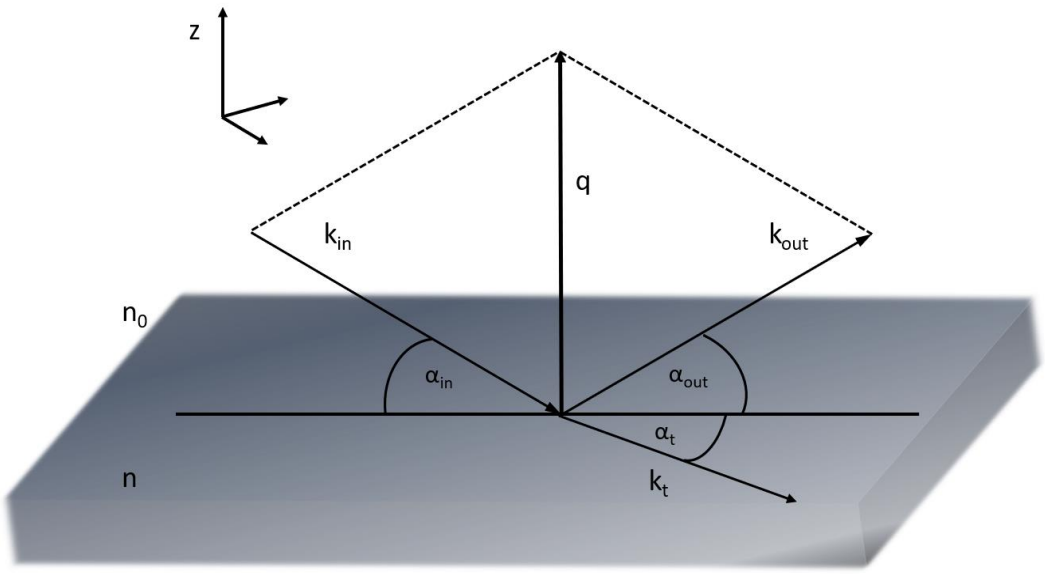

Figure 8: Schematic representation of the interaction of an incoming beam k_{in} with an interface between one phase with a refractive index n and a second phase with a refractive index n_o. The entrance beam k_{in} is partly reflected (k_{out}) and partly scattered (k_t).

To gain dependable results from X-ray reflectivity measurements of liquid interfaces a high-grade surface must be prepared. Such research can be performed within Langmuir Blodgett troughs. These are temperature-controlled troughs which are filled with a carrier material, usually water, to create a liquid-air interface. After addition of molecules to be investigated, e.g. lipids, those ingredients can align themselves with the interface, in case of lipids the polar headgroups dip into the water surface and the lipophilic tail portions straighten up towards the air forming monolayers. Furthermore, Langmuir Blodgett troughs are equipped with a barrier which can be piloted within the trough for compression of the layer. The resulting surface pressure can be detected with a Wilhelmy plate. The resulting Langmuir isotherms were already discussed in chapter 3.1.1.

3.2 Results and discussion

3.2.1 Synthesis of azobenzene glycolipid mimetics

The targeted photoswitchable glycolipids are composed of two parts, a hydrophilic oligoethylene glycol glycoside headgroup and a lipophilic 1-*O*-azobenzene diacylglycerol ether tailgroup. Both components were functionalised to allow ligation by copper(I)-catalysed 1,3-dipolar cycloaddition ('click chemistry'). Whereas the aglycon of the glycoside was equipped with an azido substituent, the azobenzene moiety of the tailgroup was alkyne-functionalised. In addition, control compounds were designed lacking the azobenzene or the carbohydrate moiety, respectively. This molecular design is the basis for a library of three different hydrophilic building blocks on the one hand and four different lipophilic components on the other hand (Figure 9). Their combination by click chemistry resulted in a library of twelve different (glyco)lipid mimetics which were compared regarding their physico-chemical properties. As hydrophilic headgroup, D-glucose- and D-lactose-functionalised oligoethylene portions were chosen. The hydrophilic component was based on a glycerol ether, esterified either with lauric acid (C12) or palmitic acid (C16).[174]

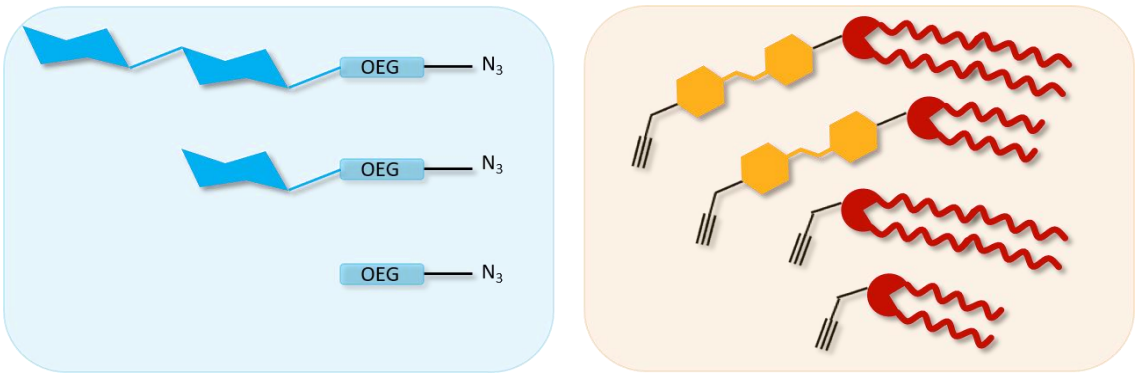

Figure 9: Schematic representation of the building blocks for amphiphile synthesis via click chemistry: Hydrophilic parts are shown on the left and lipophilic parts are shown on the right.

For the synthesis of the hydrophilic part mono-tosylated triethylene glycol **2** was synthesised according to the literature (Scheme 2).[175] Tosylate **2** was then easily converted into the respective azide **3**[175-178] by nucleophilic substitution with sodium azide. However, glycosylation to form glycosides **6** and **7**, respectively, was best performed with the tosylate **2** rather than with **3**. The glycosylation step is the limiting factor of the entire synthetic sequence. As glycosyl donors, glucose pentaacetate **4** and lactose octaacetate **5** were used as anomeric mixtures. The boron trifluoride diethyl

etherate-catalysed reaction yielded the glycosides **6** and **7**, respectively, as pure β-anomers in yields of 58 % and 50 %, respectively. The following nucleophilic substitution with sodium azide gave the azido-functionalised glycosides **8** and **9**, respectively, in high yields.[176] Subsequent deacetylation under ZEMPLÉN conditions[179] quantitatively led to the desired compounds **10** and **11**. (Scheme 2).[176]

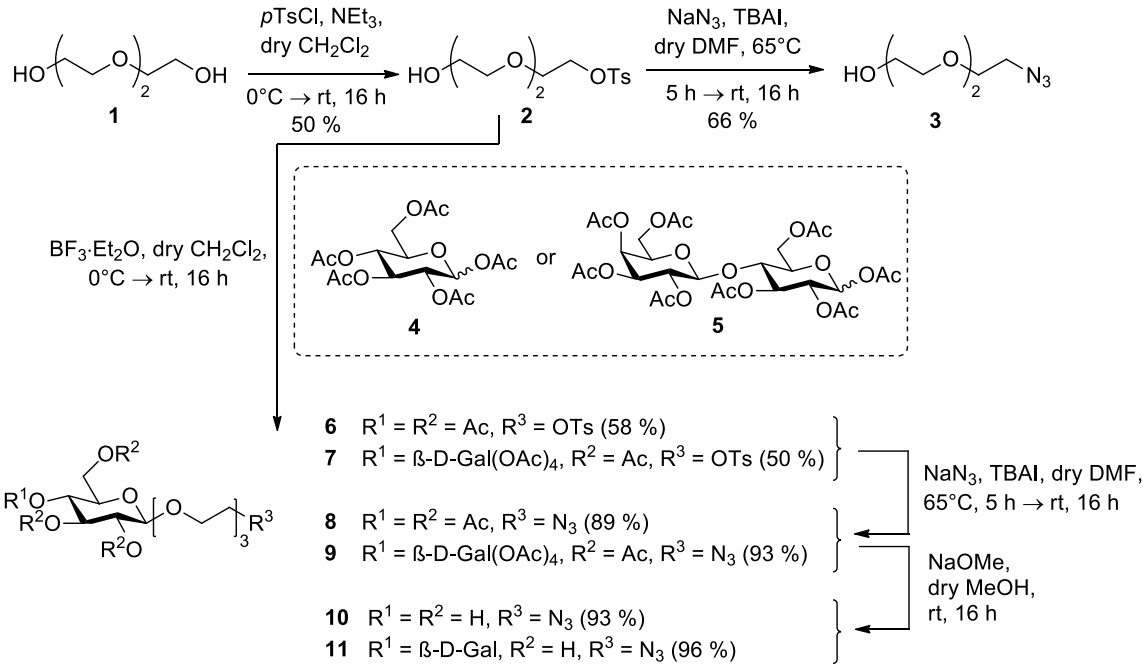

Scheme 2: Synthesis of azido-functionalised hydrophilic building blocks **3**, **10** and **11** for amphiphile synthesis.

Next, the lipophilic tailgroups which were based on a 1-*O*-[(propargyloxy)azobenzene] diacylglycerol ether core were synthesised (Scheme 3). For that purpose, first the propargylated azobenzene **12** was prepared according to the literature[180] and employed in a WILLIAMSON ether synthesis with the tosylated isopropylidene-protected glycerol derivative **13** in the next step to obtain **14** in a high yield of 86 %. The glycerol derivative **13** was synthesised as enantiomeric mixture of (*R*)- and (*S*)-configured stereoisomers according to PFAENDLER.[181] For the removal of the isopropylidene protecting group, **14** was treated with hydrochloric acid in THF to furnish the the desired diol **15** in a yield of 56 % together with the starting material **12**, which was recovered in a yield of 30 %. For the synthesis of the required lipophilic building block, diol **15** was subjected to a STEGLICH esterification using dicyclohexylcarbodiimide (DCC) and dimethylaminopyridine (DMAP).[182] Lauric acid (C12 derivative) and palmitic acid (C16

derivative) were employed for esterification to obtain the diacylglycerol derivatives **16** and **17** in a yield of 48 % and 80 %, respectively (Scheme 3).

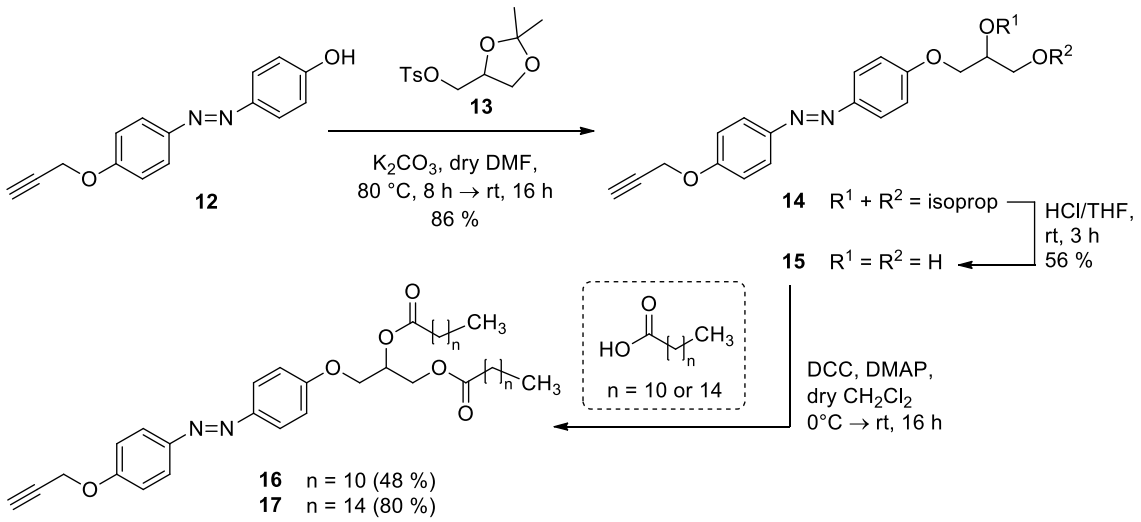

Scheme 3: Preparation of the lipophilic building block: Synthesis of the 1-*O*-[(propargyloxy)azobenzene] diacylglycerol ethers **16** and **17** was performed according to STEGLICH's procedure.[182]

Finally, the targeted photoswitchable amphiphiles were obtained by ligation of the hydrophilic azido-functionalised derivatives **3**, **10** and **11**, respectively, with the lipophilic 1-*O*-[(propargyloxy)azobenzene] diacylglycerol ethers **16** and **17** by copper(I)-catalysed 1,3-dipolar cycloaddition (Scheme 4). Addition of pentamethyldiethylene-triamine (PMDTA) as an copper (I)-ion stabilising reagent[183] was essential to improve poor yields (~10 %) to 83 % and 73 %, respectively, for the photoswitchable C12-diacyl β-D-glucoside **20** and the respective C16-diacyl β-D-glucoside **21**. Hence, PMDTA was used for all click reactions in connection with this project. The photoswitchable C12-diacyl β-D-lactoside amphiphile **22** was obtained in a yield of 71 % and the respective C16-diacyl β-D-lactoside amphiphile **23** in a yield of 70 %. To facilitate the investigation of the influence of the carbohydrate headgroups in lipid layers in context of dynamics and structural changes, two derivatives **18** and **19** with just an oligoethylene glycol headgroup, lacking the carbohydrate portion, were synthesised as well and obtained in yields of 87 % for the C12 derivative **18** and 85 % for the respective C16 derivative **19**.

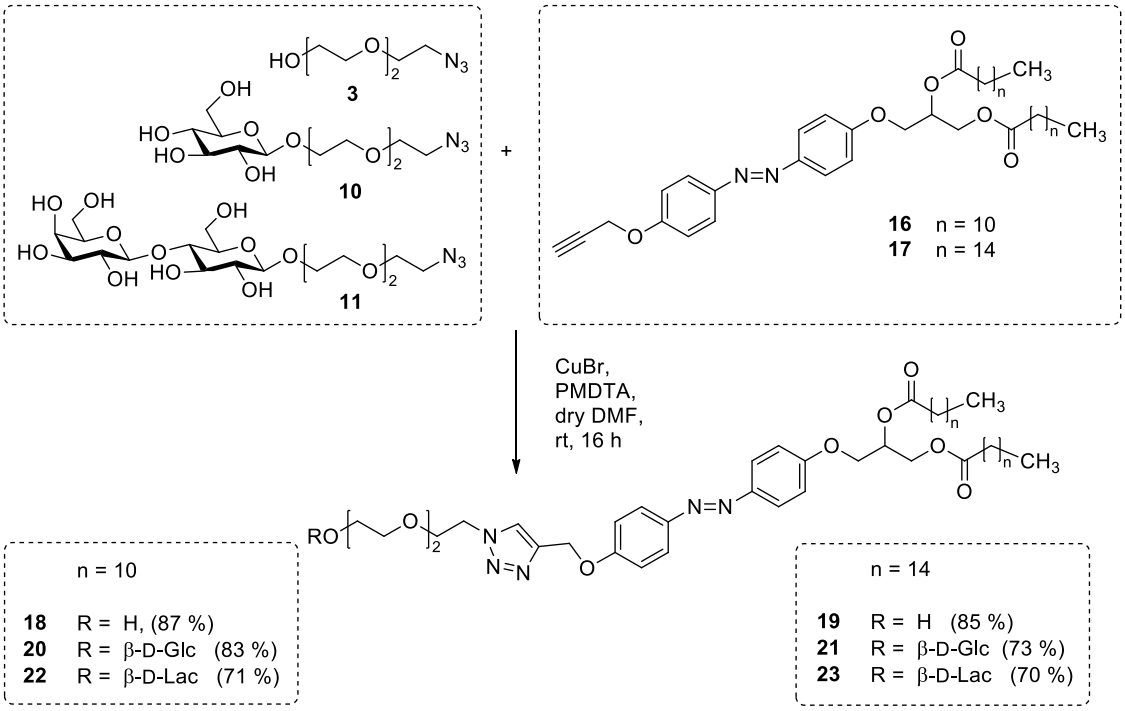

Scheme 4: Synthesis of photoswitchable target amphiphiles by click chemistry: Hydrophilic building blocks **3**, **10** and **11** were ligated via copper(I)-catalysed 1,3-dipolar cycloaddition with lipophilic building blocks **16** and **17** to achieve amphiphiles **18**-**23**.

For a reliable evaluation of the photoswitchable properties of amphiphiles **18**-**23**, control compounds, lacking the azobenzene moiety, **29**-**34** were required. Therefore, the synthetic pathway outlined above was modified according to Scheme 5. Starting from the isopropylidene-protected glycerol derivative **24**, the known propargyl glycerol ether **25** was synthesised as (*R*,*S*) mixture according to a procedure of LATXAGUE et al.[184] Removal of the isopropylidene protecting group with hydrochloric acid in THF amounts to diol **26** in a yield of 75 %. Then, the diol **26** was subjected to esterification with lauric and palmitic acid in analogy to the preparation of the respective photoswitchable diacyl glycerol derivatives **16** and **17**. The resulting propargyl diacyl derivatives **27** and **28** were utilised in a 1,3-dipolar cycloaddition using the hydrophilic counterparts **3**, **10**, **11** to obtain the C12 diacyl glycerol mimetics **29**, **31**, **33** and the respective C16 diacyl glycerol mimetics **30**, **32** and **34**.

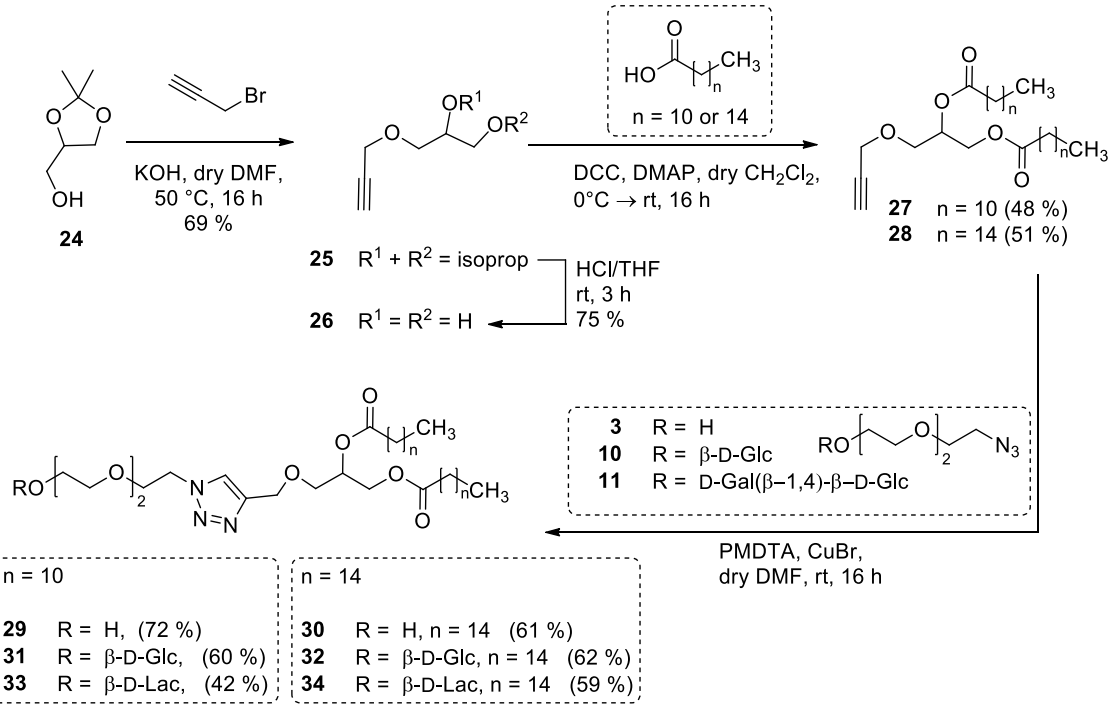

Scheme 5: Synthesis of non-photoswitchable control compounds **29**-**34**.

3.2.2 Results of molecular modelling

For the validation of measured data in X-ray and Langmuir Blodgett film experiments it is important to have an idea about the three-dimensional structure of the amphiphilic molecules. Therefore, molecular dynamics simulations for amphiphiles **18** to **23** as well as the non-photoswitchable control compounds **29** to **34** were performed. For this, the program *MacroModel*[185] as implemented in the Schrödinger *Maestro* software package was used.[186] The calculations provided the atomic distances of different conformers and their occurence. For all twelve synthesised molecules, **18** to **23** and **29** to **34**, 3D structures were first set-up with *Maestro*[186] and then their energy was minimised within an OPLS 2005 force field with *MacroModel*.[185] In addition, the *MacroModel* software has the feature to perform molecular dynamics simulations which are based on classical mechanics (Newton`s equitation of motion). The results of the molecular dynamics simulations delivered the occurence of single conformers as characterised by their intramolecular distances and are depicted below in Figure 10 to Figure 27. The photoswitchable C12-diacyl β-D-glucoside **20** is depicted in Figure 10. The molecular dynamics simulations are focused on four parts of the molecule which are shown in Figure 10. The intramolecular distances were screened for the hydrophilic part (highlighted in blue), the azobenzene moiety (highlighted in grey) and two lipophilic

parts, starting from the central part (N=N double bond) of the azobenzene moiety towards one or the other alkyl chain (highlighted in yellow and red, respectively) (Figure 10). The numbering of the atoms indicated in Figure 10 to Figure 27was adapted from the Maestro software.[186]

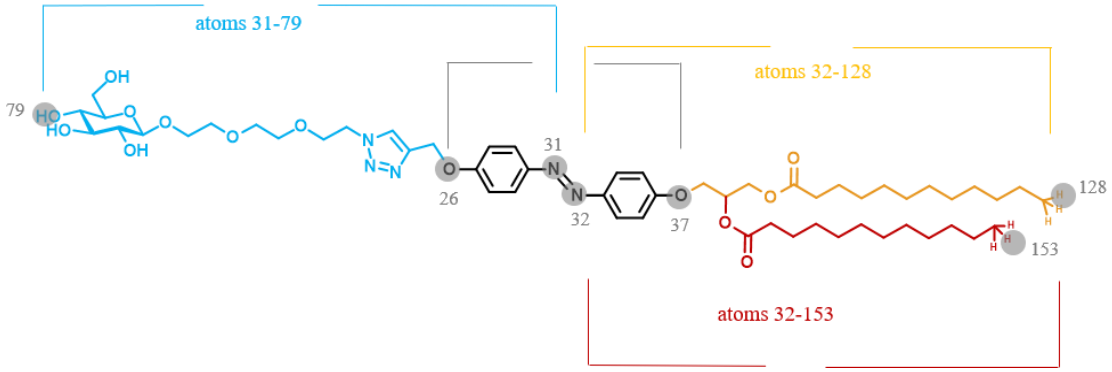

Figure 10: Molecular dynamics simulation with the photoswitchable C12-diacyl β-D-glucoside **20**. The molecul was divided into four parts: the hydrophilic headgroup (blue), the azobenzene moiety (grey), and two lipophilic parts, one for each alkyl chain (yellow and red, respectively).

The distribution of occurring intramolecular distances for the azobenzene portion (measured from atom 26 to 37) is depicted in Figure 11. The *E*-state showed possible distances from 11.2 Å up to 12.1 Å with a highest probability around 11.8 Å. As expected, a contraction of the intramolecular distance was observed for the *Z*-isomer of the molecule with distances from 8.6 Å up to 9.2 Å and approximately 9.0 Å as the most probable one.

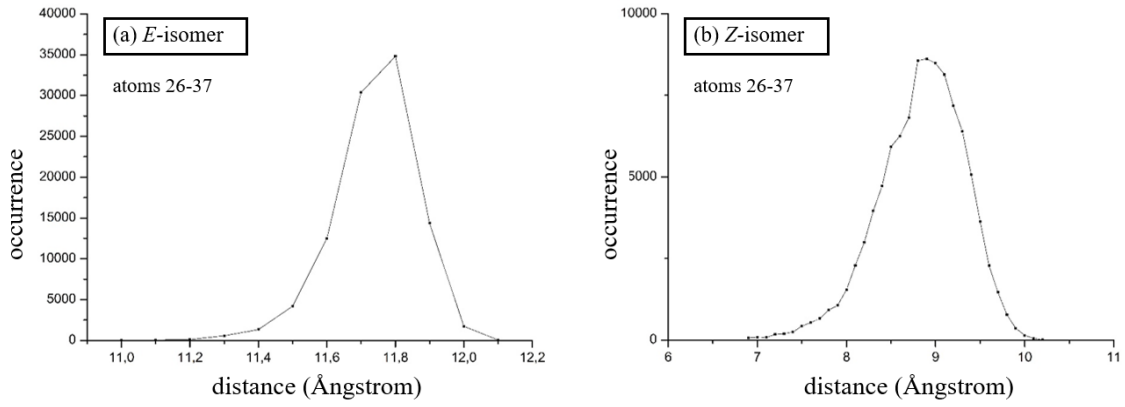

Figure 11: Intramolecular distances and their occurence as determined for the possible conformers of amphiphile **20**. The distances were screened for the azobenzene moiety from atom 26 to 37 as *E*-isomer (left, (a)) and the related *Z*-isomer (right, (b)).

The distribution of occurring intramolecular distances for the hydrophilic part (measured from atom 31 to 79) of the inspected molecule **20** as *E*-isomer and the lipophilic tails (measured from atom 32 to 153 and 32 to 128, respectively) are depicted in Figure 12.

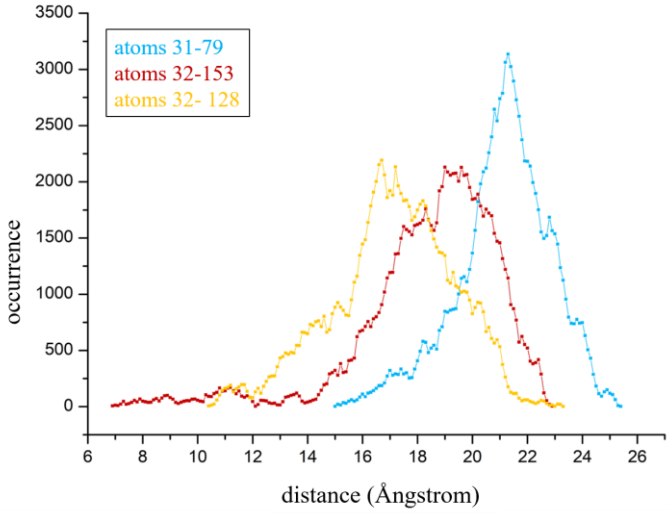

Figure 12: Intramolecular distances and their occurence as determined for the possible conformers of amphiphile **20** (*E*-isomer). The distances were screened for three parts of the molecule: the hydrophilic headgroup (blue) and two lipophilic parts, one for each alkyl chain (yellow and red, respectively).

In Figure 13, the distribution of occurring intramolecular distances for the three molecular parts (as detailed above) of *Z*-**20** is depicted. The distribution of possible distances for the alkyl chains is suggested to be rather broad for both the *E*-isomer and the *Z*-isomer resembling a multitude of sterically unhindered conformers. A slight contraction for the C12 chain length can be observed for the *Z*-isomer in comparison to the *E*-isomer. The curve of the hydrophilic part (blue) shows a clear maximum at approximately 22 Å in the *E*-state whereas the distance range is broadened to 19 Å to 24 Å for the *Z*-isomer.

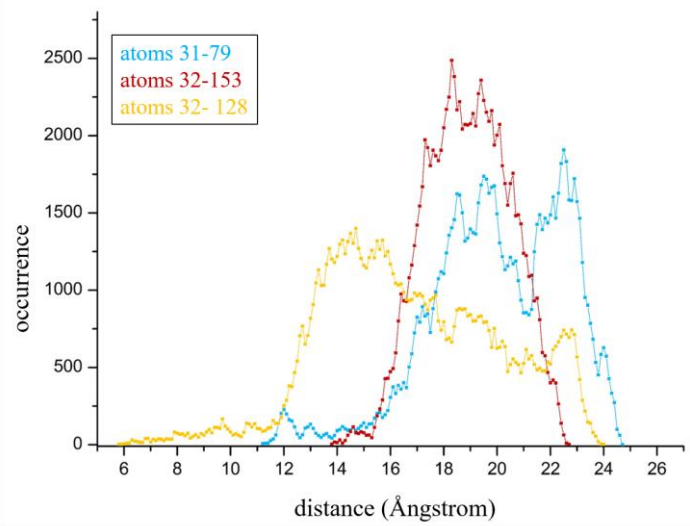

Figure 13: Intramolecular distances and their occurence as determined for the possible conformers of amphiphile **20** (*Z*-isomer). The distances were screened for three parts of the molecule: the hydrophilic headgroup (blue) and two lipophilic parts, one for each alkyl chain (yellow and red, respectively).

As before, also molecule **21** was divided into four parts for distance analysis.

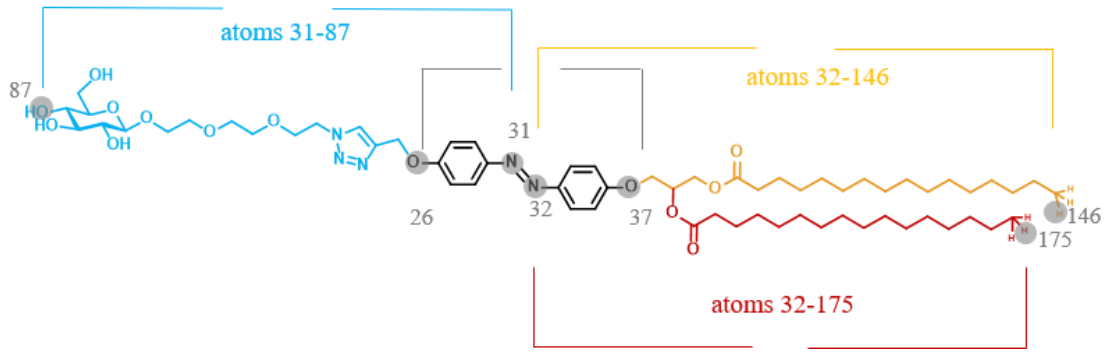

Figure 14: Molecular dynamics simulations with the photoswitchable C16-diacyl β-D-glucoside **21**. The molecule was divided into four parts: the hydrophilic headgroup (blue), the azobenzene moiety (grey), and two lipophilic parts, one for each alkyl chain (yellow and red, respectively).

The distribution of occurring intramolecular distances for the azobenzene part of compound **21** (determined from atom 26 to 37) is depicted in Figure 15. In this case, the simulation led to nearly the same data as with compound **20**.

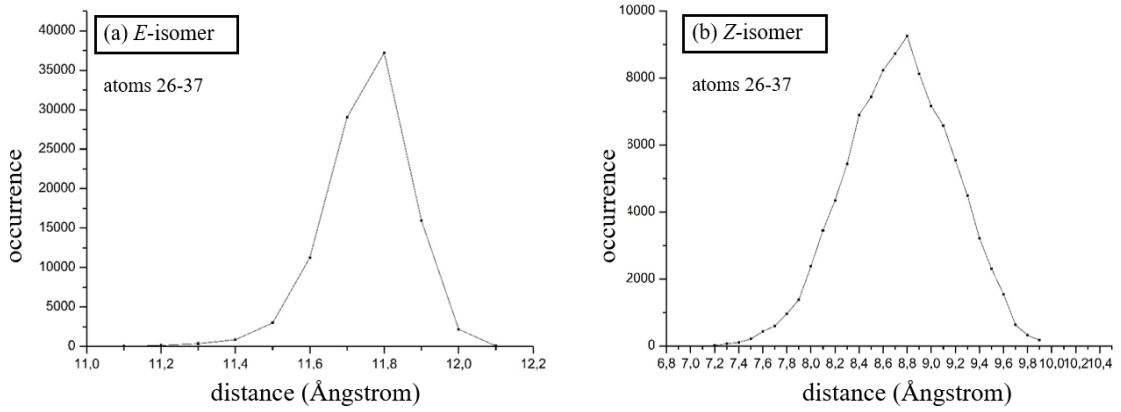

Figure 15: Intramolecular distances and their occurence as determined for the possible conformers of amphiphile **21**. The distances were screened for the azobenzene moiety from atom 26 to 37 as *E*-isomer (left, (a)) and the related *Z*-isomer (right, (b)).

The distribution of occurring intramolecular distances for the hydrophilic part (measured from atom 31 to 87) and the lipophilic tails (measured from atom 32 to 146 and 32 to 175, respectively) for the *E*-isomer of **21** are depicted in Figure 16.

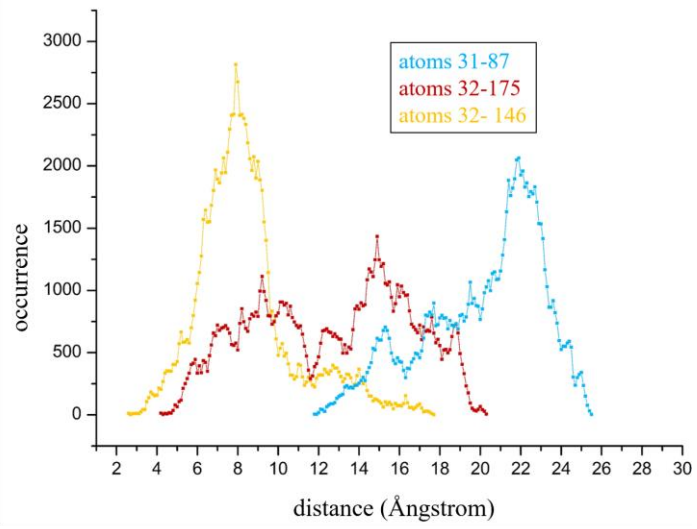

Figure 16: Intramolecular distances and their occurence as determined for the possible conformers of amphiphile **21** (*E*-isomer). The distances were screened for three parts of the molecule: the hydrophilic headgroup (blue) and two lipophilic parts, one for each alkyl chain (yellow and red, respectively).

The distribution of occurring intramolecular distances for the three parts of *Z*-**21** as exemplified above are depicted in Figure 17. For the one lipophilic part (highlighted in yellow) the distribution of occurring distances shows both for *E*-**21** and *Z*-**21** a rather clear maximum. The second lipophilic tail (highlighted in red) shows a rather broad distribution of conformers for the *E*-isomer and an even broader distribution for the

Z-isomer, with a maximum emerging at 9 Å. In comparison with the shorter C12 derivative **20**, the alkyl chains of compound **21** in the three-dimensional representation are obviously shortened due to clumping. The hydrophilic part shows a distance maximum at approximately 22 Å for the *E*-isomer and a slightly reduced distance for the *Z*-isomer (20 Å).

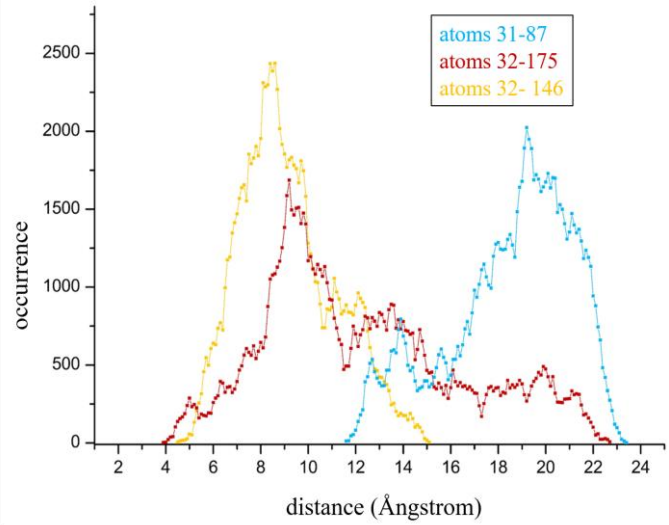

Figure 17: Intramolecular distances and their occurence as determined for the possible conformers of amphiphile **21** (*Z*-isomer). The distances were screened for three parts of the molecule: the hydrophilic headgroup (blue) and two lipophilic parts, one for each alkyl chain (yellow and red, respectively).

The results of the molecular dynamics simulations with the non-photoswitchable C12-diacyl β-D-glucoside **31** are depicted in Figure 19. The molecular dynamics simulation was focused on three parts of the molecule which are shown in Figure 18. The intramolecular distances were screened for the hydrophilic part (highlighted in blue), and two lipophilic parts, starting from the central glycerol ether moiety towards one or the other alkyl chain (highlighted in yellow and red, respectively).

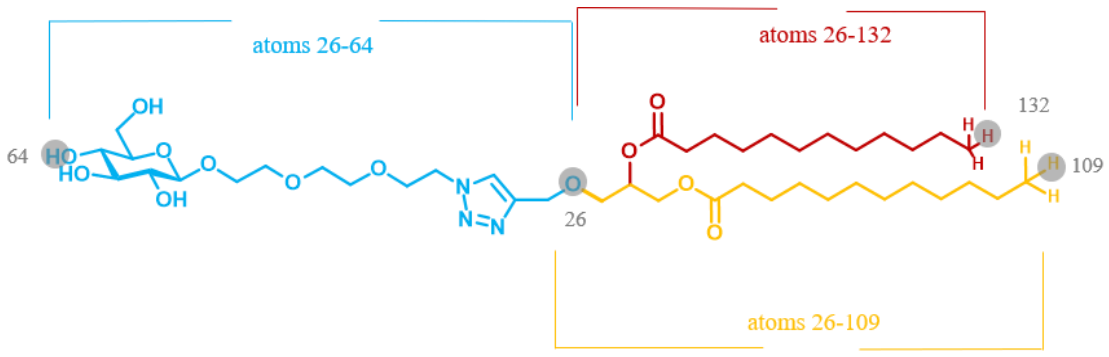

Figure 18: Molecular dynamics simulation with the non-photoswitchable C12-diacyl β-D-glucoside **31** regarding three parts of the molecule: the hydrophilic headgroup (blue) and the two lipophilic parts (yellow and red), starting from the glycerol ether moiety.

The distribution of occurring intramolecular distances for the three parts of C12 control compound **31** is depicted in Figure 19.

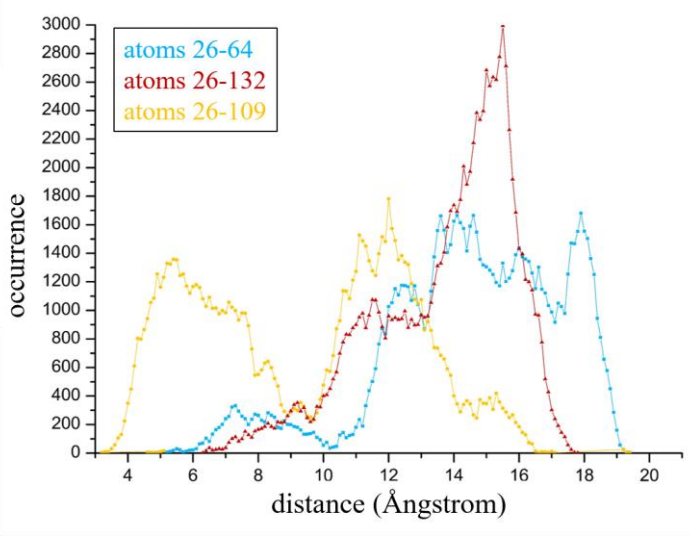

Figure 19: Intramolecular distances and their occurence as determined for the possible conformers of amphiphile **31**. The distances were screened for three parts of the molecule: the hydrophilic headgroup (blue) and two lipophilic parts, one for each alkyl chain (yellow and red, respectively).

Non-photoswitchable C16-diacyl β-D-glucoside **32** is depicted in Figure 20.

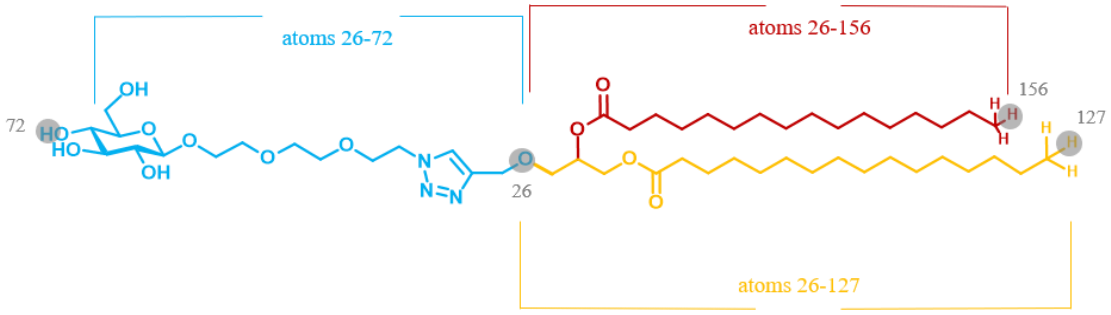

Figure 20: Molecular dynamics simulation with the non-photoswitchable C16-diacyl β-D-glucoside **32** regarding three parts of the molecule: the hydrophilic headgroup (blue) and the two lipophilic parts (yellow and red), starting from the glycerol ether moiety.

The distribution of occurring intramolecular distances for the three parts of C16 control compound **32** are depicted in Figure 21.

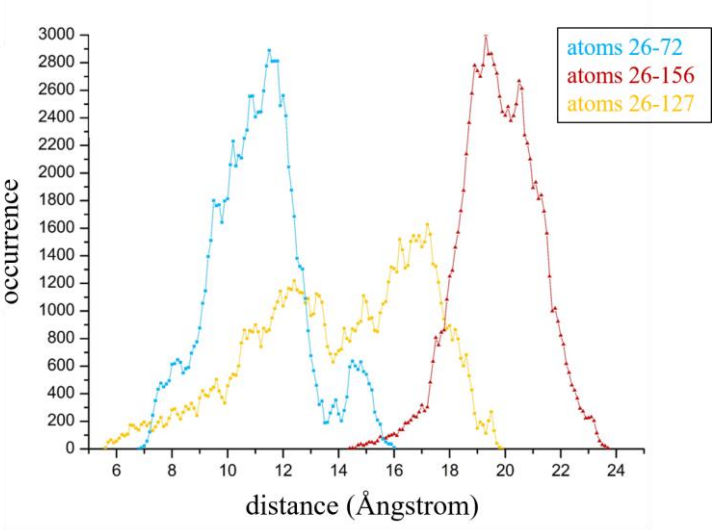

Figure 21: Intramolecular distances and their occurence as determined for the possible conformers of amphiphile **32**. The distances were screened for three parts of the molecule: the hydrophilic headgroup (blue) and two lipophilic parts, one for each alkyl chain (yellow and red, respectively).

In coincidence with the increasing chain length, both the distribution for the one chain (yellow) and the other chain (red) are shifted to longer distances in case of the C16 derivative **32**. It is conspicuous that the one alkyl chain (yellow) shows a broad distribution of conceivable distances whereas the other one shows a narrow range of possible distances, highlighted by a maximum at about 16 Å for the C12 compound **31** and 20 Å for the C16 compound **32**. The hydrophilic part of the molecule **31** shows a rather broad distribution of occurring distances from 12 Å to 18.5 Å whereas the long-chained analogue shows a compacted range from 19 Å to 22 Å with a maximum at about 20 Å.

Furthermore, the distances of the lactose derivatives **22**, **23**, **33** and **34** as well as for the solely ethylene glycol-equipped derivatives **18**, **19**, **29** and **30** were calculated similarly. The results for the lactose derivatives are given in Figure 22 to Figure 24. The distances for the azobenzene moiety for all three kinds of amphiphiles are the same as shown exemplarily for compound **20** (Figure 11) and **21** (Figure 15), respectively.

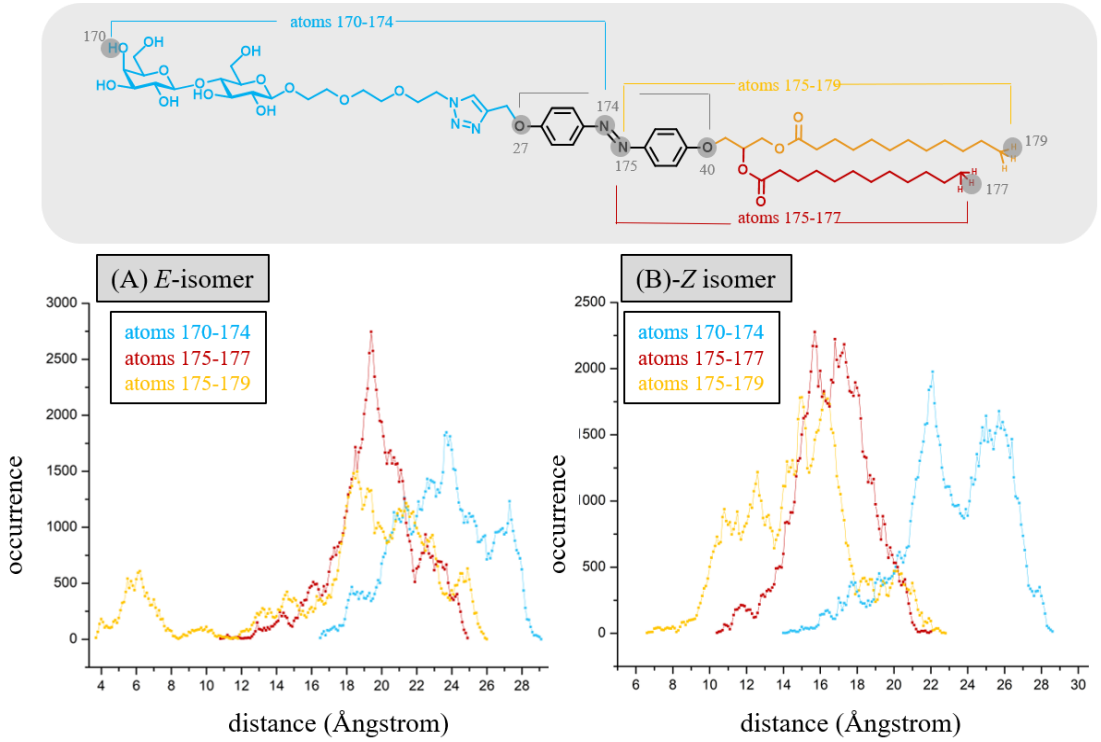

Figure 22: Molecular dynamics simulations with the photoswitchable lactoside **22**. Top: The molecule was divided into four parts: the hydrophilic headgroup (blue), the azobenzene moiety (grey), and two lipophilic parts, one for each alkyl chain (yellow and red, respectively). Bottom: Intramolecular distances and their occurence as determined for the possible conformers of amphiphile **22**. The distances were screened for three parts (as detailed above) of the molecule *E*-**22** ((A), left) and *Z*-**22** ((B), right)**,** respectively.

The distribution of the occurring distances for the *E*-isomer of compound **22** resembles that one of the respective glucose derivative **20**. The curve of the distances of the hydrophilic part (blue) is shifted to longer distances between 17 and 29 Å due to the increased size of the carbohydrate moiety. The same shift could be observed for the C16 derivatives with a lactose moiety (Figure 23). It is noteworthy that also the curves for the lipophilic alkyl chains are shifted to increased distances. This might result from the increased hydrophilicity of the lactose moiety which might result in a more unbent structure of the chains.

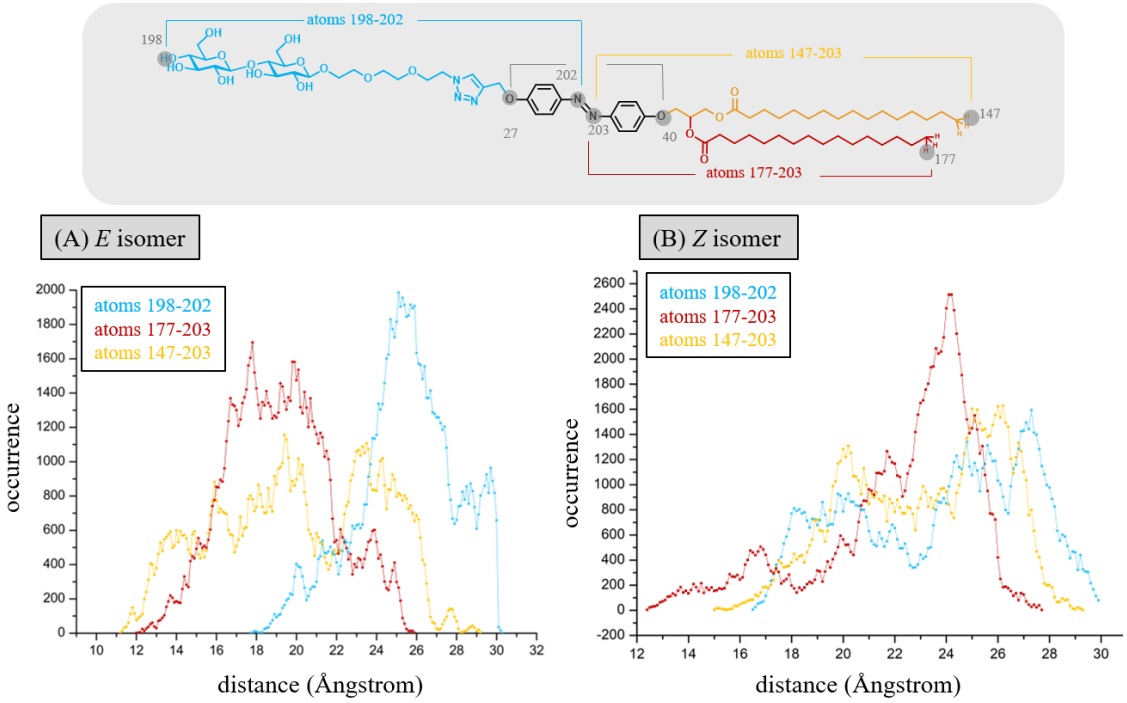

Figure 23: Molecular dynamics simulations with the photoswitchable lactoside **23**. Top: The molecule was divided into four parts: the hydrophilic headgroup (blue), the azobenzene moiety (grey), and two lipophilic parts, one for each alkyl chain (yellow and red, respectively). Bottom: Intramolecular distances and their occurence as determined for the possible conformers of amphiphile **23**. The distances were screened for three parts (as detailed above) of the molecule *E*-**23** ((A), left) and *Z*-**23** ((B), right)**,** respectively.

The results for the non-photoswitchable derivatives **33** and **34** are given in Figure 24.

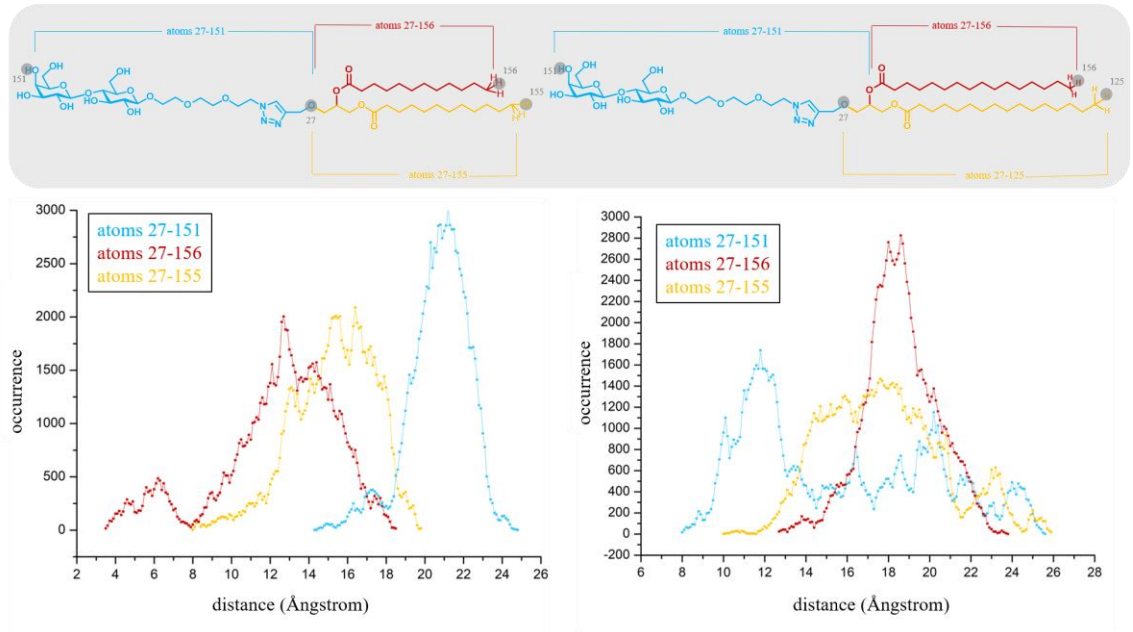

Figure 24: Intramolecular distances were determined by molecular dynamics simulations for compounds **33** (left) and **34** (right). The different possible conformers and the respective distances were observed by occurence. The distances were screened for three parts of the molecule (atoms are marked in blue, red and yellow).

The results for the solely ethylene glycol-equipped derivatives are depicted in Figure 25 to Figure 27. Both for the C12 and the C16 derivatives **18** and **19**, respectively, the occurring distances for the hydrophilic moiety are lower due to the reduced size.

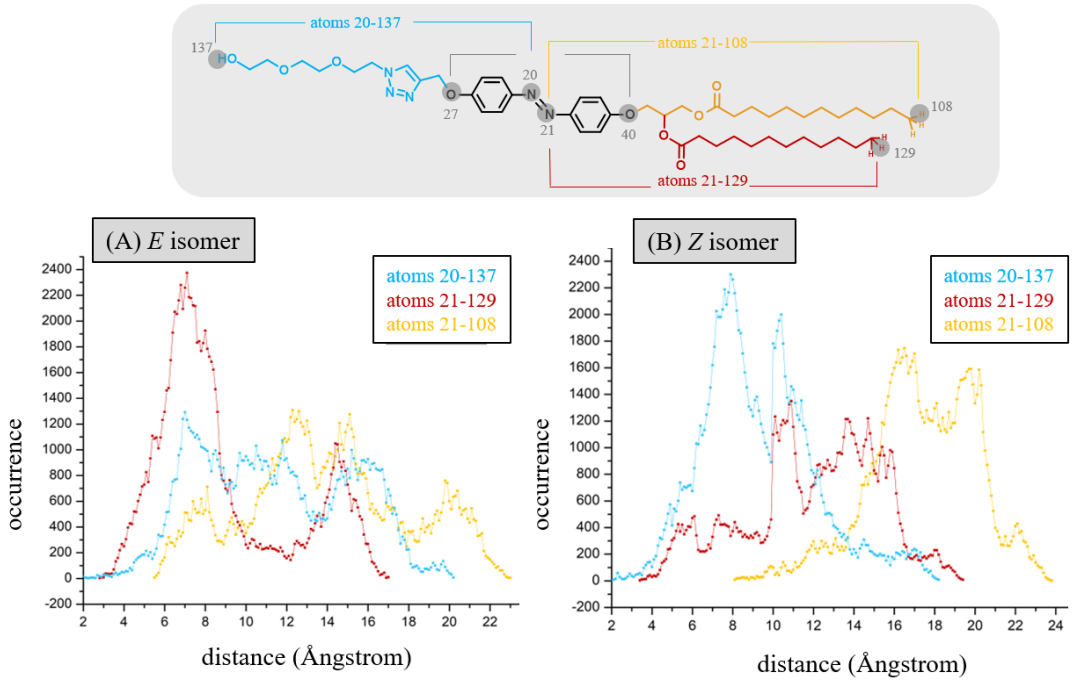

Figure 25: Bottom: Intramolecular distances were determined by molecular dynamics simulations for compound **18** in its *E*-state (A) as well as for the *Z*-isomer (B). The different possible conformers and the respective distances were observed by occurrence. Top: The distances were screened for three parts of the molecule (atoms are marked in blue, red and yellow).

Also, the lipophilic alkyl chains of compound **18** and **19** show lower distances. It seems that the alkyl chains can form more bundled structures due to the reduced size of the hydrophilic counterpart within the amphiphilic structures.

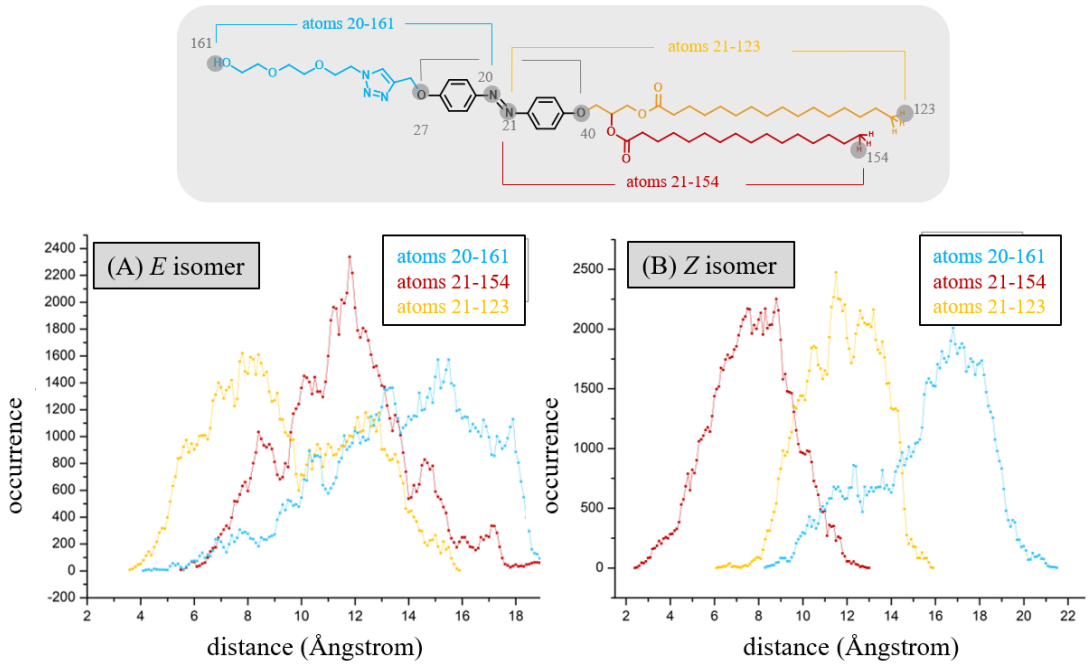

Figure 26: Bottom: Intramolecular distances were determined by molecular dynamics simulations for compound **19** in its *E*-state (A) as well as for the *Z*-isomer (B). The different possible conformers and the respective distances were observed by occurrence. Top: The distances were screened for three parts of the molecule (atoms are marked in blue, red and yellow).

The results for the non-photoswitchable derivatives **29** and **30** are given in Figure 27.

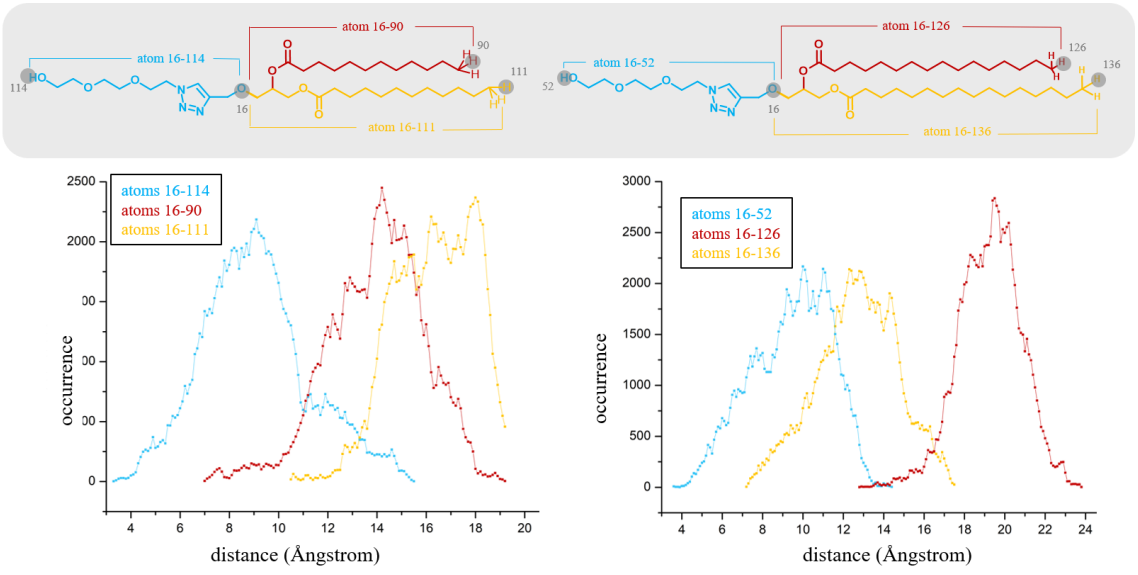

Figure 27: Bottom: Intramolecular distances were determined by molecular dynamics simulations for compounds **29** (left) and **30** (right). The different possible conformers and the respective distances were observed by occurence. Top: The distances were screened for three parts of the molecule (atoms are marked in blue, red and yellow).

3.2.3 Photochemical properties

For the evaluation of every potential photochemical application the photochromic properties of the azobenzene derivatives **18**-**23** are essential. Therefore, photochromic data were obtained by UV/Vis spectroscopy. The photoirradiation was performed using a UV LED (2.7 mW, λ = 365 nm for *E*→*Z* isomerisation) and a blue LED (2.6 mW, λ = 455 nm for *Z*→*E*), respectively. For UV measurements the *E*-configured azobenzene derivatives **18**-**23** were dissolved in $CHCl_3$ at 1 mM and irradiated at 365 nm (*E*→*Z* isomerisation), respectively 455 nm (Z→*E* isomerisation) for 1 min. Detailed setup information according the procedure of the UV/Vis measurements can be found in the literature.[187] UV/Vis spectra were recorded immediately afterwards. The photochromic properties of the synthetic azobenzene derivatives **18**-**23** were investigated with a Cary 4000 double-beam spectrometer (Varian Inc.).

The UV/Vis spectra (Figure 28 to Figure 33) were collected with 1 nm resolution from 260 nm to 600 nm. After irradiation with 365 nm the absorption spectra showed an increase of the absorbance in the n-π* transition and simultaneous decrease in the π-π* transition, indicating the formation of the respective *Z*-isomer. The *E*-isomer absorbance maxima of all compounds (**18**-**21**) were measured around 355 nm and the *Z*-isomer absorbance maximum was determined at 312 nm for each compound. A slight shift towards higher wavelength was detected for lactoside derivatives **22** and **23**. (Figure 32 and Figure 33)

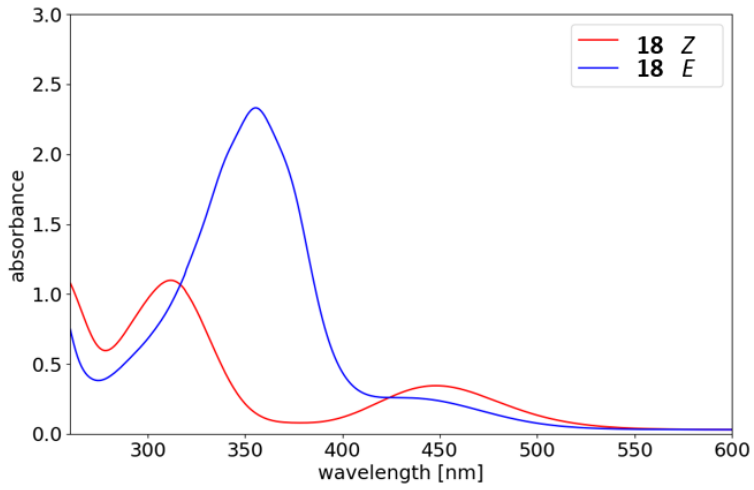

Figure 28: UV/Vis spectra for the steady state of compound **18**: The *E*-isomer is shown in blue and the *Z*-isomer in red. Irradiation was performed with 365 nm (*E*→*Z*) and 465 nm (*Z*→*E*) in chloroform.

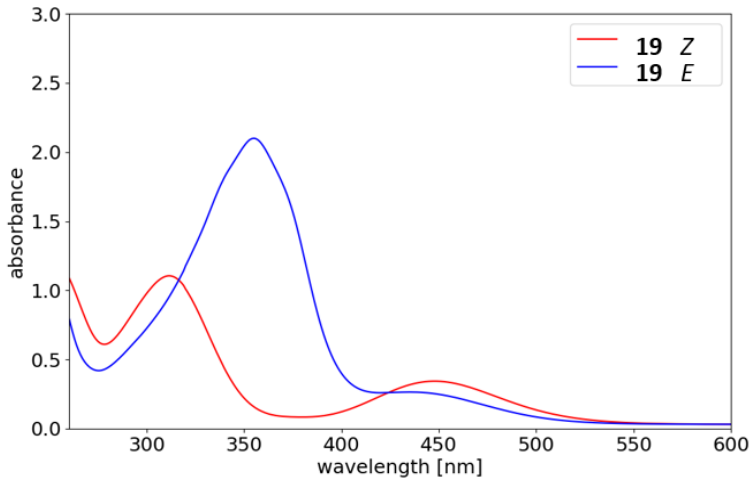

Figure 29: UV/Vis spectra for the steady state of compound **19**: The *E*-isomer is shown in blue and the *Z*-isomer in red. Irradiation was performed with 365 nm (*E*→*Z*) and 465 nm (*Z*→*E*) in chloroform.

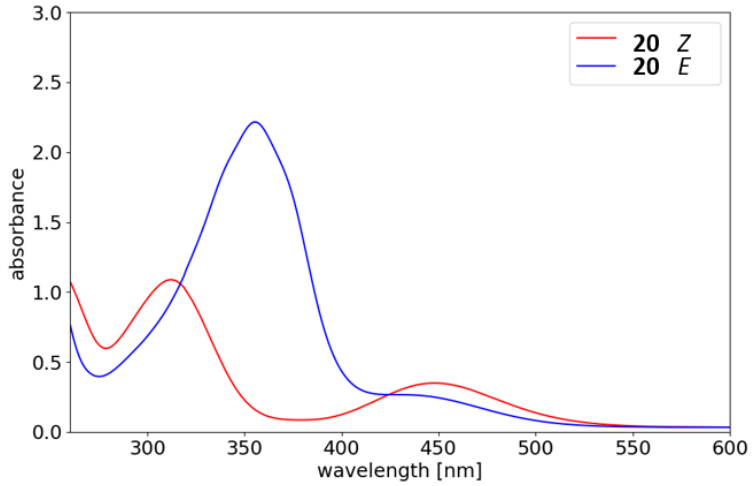

Figure 30: UV/Vis spectra for the steady state of compound **20**: The *E*-isomer is shown in blue and the *Z*-isomer in red. Irradiation was performed with 365 nm (*E*→*Z*) and 465 nm (*Z*→*E*) in chloroform.

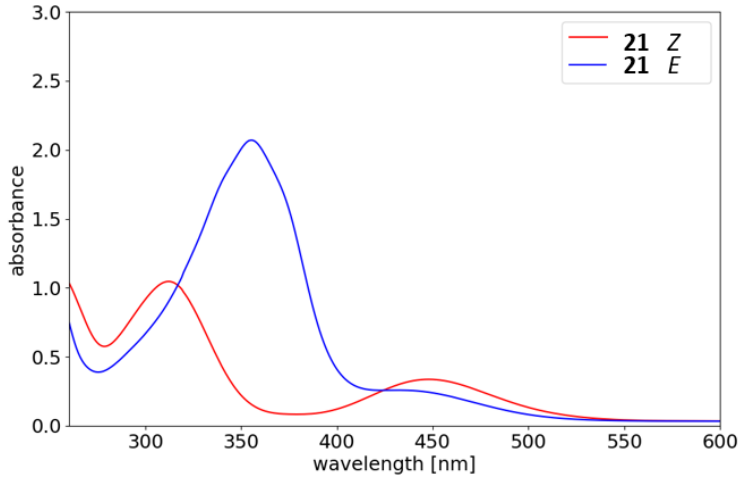

Figure 31: UV/Vis spectra for the steady state of compound **21**: The *E*-isomer is shown in blue and the *Z*-isomer in red. Irradiation was performed with 365 nm (*E*→*Z*) and 465 nm (*Z*→*E*) in chloroform.

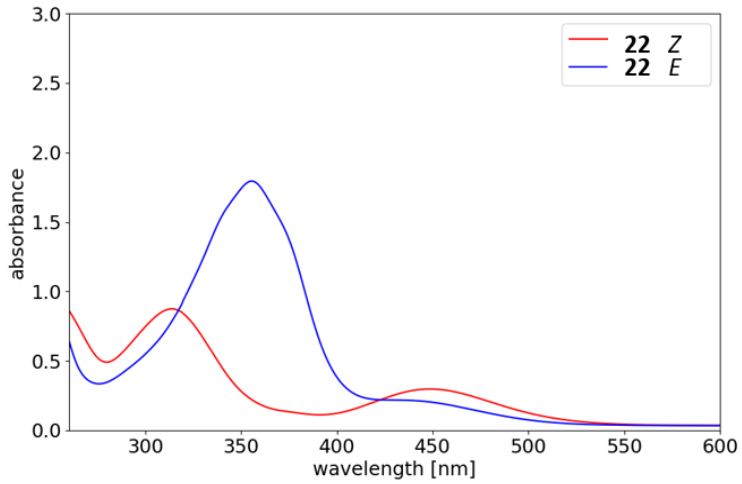

Figure 32: UV/Vis spectra for the steady state of compound **22**: The *E*-isomer is shown in blue and the *Z*-isomer in red. Irradiation was performed with 365 nm (*E*→*Z*) and 465 nm (*Z*→*E*) in chloroform.

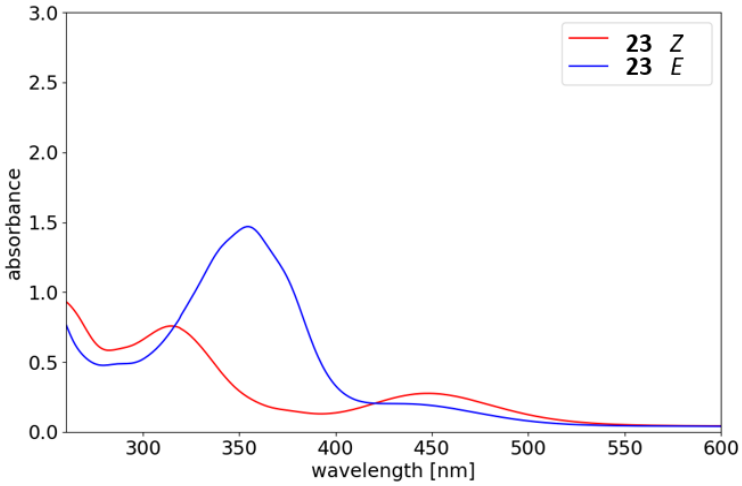

Figure 33: UV/Vis spectra for the steady state of compound **23**: The *E*-isomer is shown in blue and the *Z*-isomer in red. Irradiation was performed with 365 nm (*E*→*Z*) and 465 nm (*Z*→*E*) in chloroform.

The kinetic behaviour of the thermal *Z*⟶*E* relaxation process was also investigated by UV/Vis spectroscopy by monitoring the intensity of the *E*-isomer at maximum wavelength. The mean lifetime τ was determined as $abs = A * (1 - e^{-t/\tau})$ with time t, absorbence abs, and amplitude A. The half-life $T_{1/2}$ was calculated using $T_{1/2} = \ln 2 * \tau$. Regarding the half-life, an influence of the chain length of the azobenzene derivatives could be observed. A longer chain length triggers a longer half-life. Likewise, an influence of the carbohydrate moiety was observed. The glucoside residues of **20** and **21** increased the half-life whereas the lactose moieties in **22** and **23** decreased the half-life compared to the non-glycosylated reference lipids **18** and **19**. Besides, all six azobenzene-equipped glycolipid mimetics **18** to **23** showed a half-life greater than 5 h and hence both

isomeric states can be investigated independently from one another (Table 1). Thus, photochromic properties of the azobenzene derivatives enable the performance of planned X-ray experiments as well as Langmuir film isotherm experiments.

Table 1: Photochemical characterisation of the *E*- and *Z*-isomers of the azobenzene lipids **18** and **19** and the corresponding azobenzene glycolipids **20** to **23**.

Compound	**λ_{max} (nm) (*E*-isomer)**	**λ_{max} (nm) (*Z*-isomer)**	***E*/*Z* (PSS)**	**Half-life $T_{1/2}$ (min)**
18	356	312	0/ 100	411
19	355	312	0/ 100	516
20	356	312	0/ 100	686
21	355	312	0/ 100	1119
22	355	314	0/ 100	343
23	355	315	5 / 95	443

To examine the feasibility of the glycolipid mimetics for Langmuir film isotherm experiments preliminary tests were performed. For this, a Langmuir film was produced from 95 % 1,2-dipalmitoyl-*sn*-glycero-3-phosphocholine (DPPC) and 5 % of the synthetic glycolipid mimetic **20** and compared with pure DPPC Langmuir films on the one hand and a pure water surface on the other hand. Those produced Langmuir films were subjected to Brewster angle microscopy as shown in Figure 34. The pure water surface is depicted on the left (Figure 34A) showing a clear difference to the other two micrographs. The azobenzene derivative **20** employed in a 5:95 mixture with DPPC (Figure 34C) shows no difference from the pure DPPC (Figure 34B) matrix and therefore it can be concluded that a stable Langmuir film is formed which is suitable for eventual X-ray experiments.

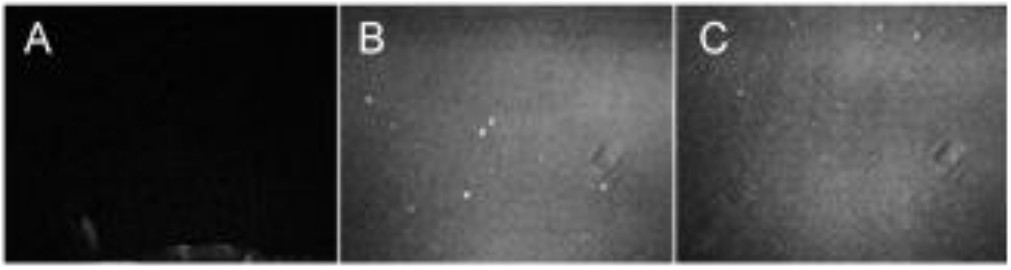

Figure 34: Pictures recorded on a Brewster angle microscope of pure water (A), a DPPC monolayer (B) and a monlayer containing 95 % DPPC and 5 % of compound **20**.

The results of the Brewster angle microscopy as well as the photochemical data obtained from the UV/Vis spectroscopy are very promising. On the one hand, the half-lifes of all *Z*-isomers of the synthetic glycolipid mimetics were long enough to be investigated independently from the *E*-isomer. On the other hand, also the formation of monolayers with embedded mimetics worked nicely as shown in Figure 34. This in turn will allow future experiments which both follow structural changes in a membrane on the nanoscale during photoswitching and study the dynamics via X-ray investigations. Those experiments partly were, and party will be performed by JONAS WARIAS under the supervision of Dr. BRIDGET MURPHY at the Institute of Experimental and Applied Physics at Kiel University.

3.2.4 Next generation of photoswitchable glycolipid mimetics

To further extend the work with photoswitchable glycomimetics, an azobenzene derivative was targeted in which a push-pull azobenzene is ligated to form one bis-azo derivative (Figure 35). This work is based on research published by VELASCO et al. (cf. chapter 3.1.2).[148]

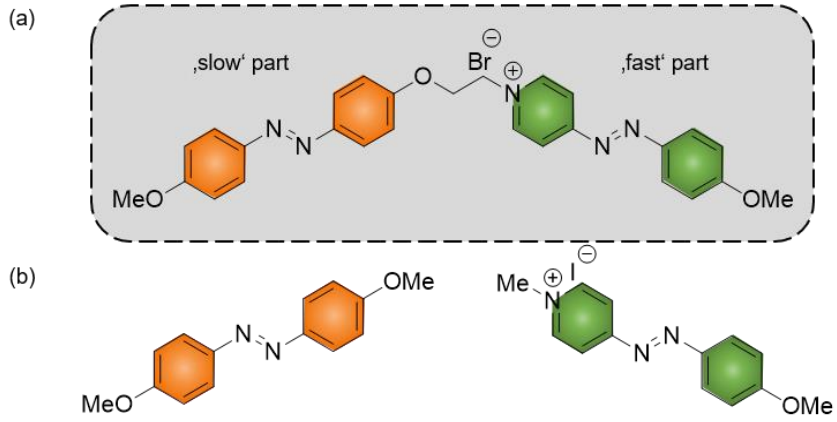

Figure 35: (a) Structure of the bis-azo derivative synthesised by VELASCO et al.; (b) Two reference molecules were synthesised which are comparable to the constituent parts.[148]

Photoswitchable materials which are based on azobenzene photoswitches are typically fabricated by incorporation of one kind of azobenzene derivatives. Depending on the employed stimulus the entire molecular entity is triggered to result in a specific effect to which all incorporated azobenzene moieties add synergistically. Such materials can just perform one function at a time. In order to establish multifunctionality in the field of photoswitchable materials, VELASCO et al. synthesised a bis-azo derivative as shown in Figure 35. They combined an azobenzene unit with a slow thermal relaxation rate with a push-pull derivative, which shows a fast thermal relaxation. This combination furnished a new photoswitch featuring a high temporal resolution of 2 x 10^8 times between the rates for thermal $Z \rightarrow E$ isomerisation of both building blocks. Such bis-azo photoswitches can be orthogonally addressed by two different wavelengths since $E \rightarrow Z$ isomerisation of the 'slow' part is triggered by UV light whereas the 'fast' part can also be addressed by green light.[148] To tie in with the idea of VELASCO et al. to perform isochronous switching on two different timescales, we designed bis-azo glycolipids to enhance the multifunctionality of photoswitching in the field of lipid bilayers (Figure 36).

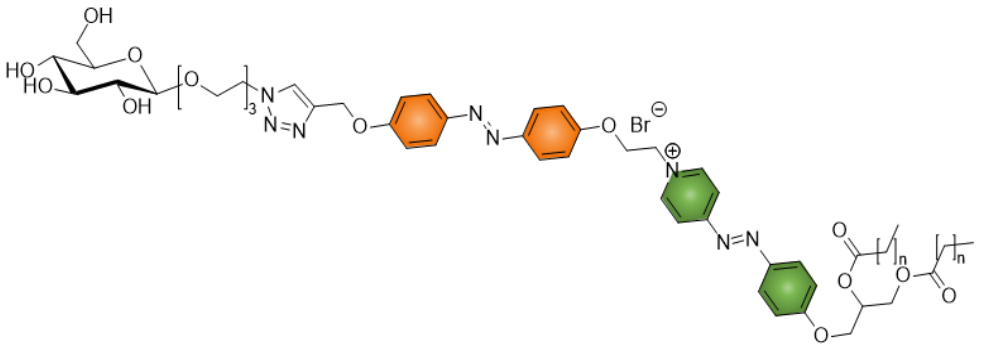

Figure 36: Chemical structure of the targeted bis-azo glycolipid.

The lipophilic building block for the second generation of photoswitchable glycolipids was synthesised in analogy to the pathway for the synthesis of compounds **16** and **17** (Scheme 3). Starting from literature-known compound **35**,[146, 188] the glycerol-equipped azobenzene **36** was obtained as a (*R*,*S*) mixture in a yield of 80 % via etherification with the tosylate **13**. Successive acidic deprotection of the isopropylidene protection group led to diol **37** which was subsequently submitted to esterification with lauric, respectively palmitic acid. The esterification product **38** was obtained with a yield of 61 % and the corresponding long-chain fatty acid ester **39** in 79 % (Scheme 6).

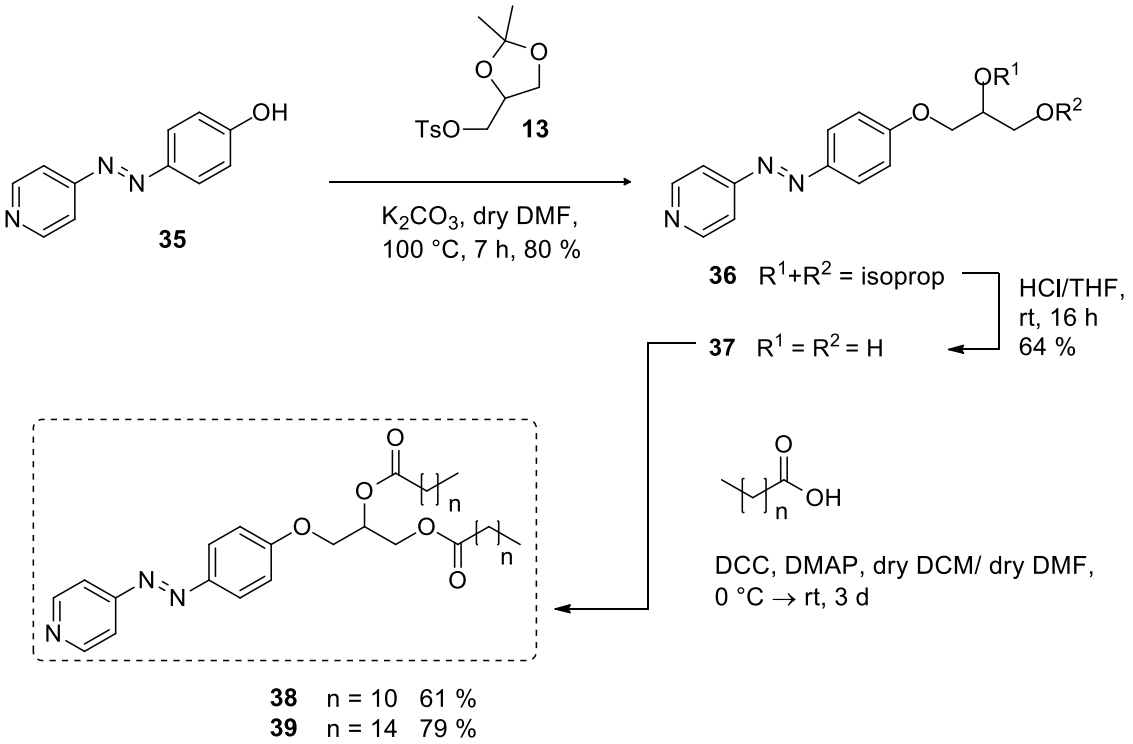

Scheme 6: Preparation of the lipophilic building blocks for glycolipids of the second generation: Lipophilic components **38** and **39** were deduced from *p*-phenylazopyridine **35** via ether synthesis with the glycerol core structure **13** and subsequent esterification.

Since amphiphiles **20** and **21** showed good results during initial investigations, the hydrophilic β-D-glucoside **10** was employed for the preparation of the second generation of glycolipids. Therefore, the glucoside **10** was conjugated to the azobenzene **40** in a PMDTA (pentamethyldiethylenetriamine) supported 1,3-dipolar cycloaddition. The resulting glycoconjugate **41** is equipped with a bromine substituent and can thus undergo substitution with the pyridine moiety of the lipophilic building block **38** and **39**, respectively. The nucleophilic substitution was performed in dry acetonitrile at 80 °C. After cooling the reaction mixture to room temperature, glycolipid **42** precipitated in a yield of 75 %. Surprisingly, the long-chained analogue **43** did not precipitate from the reaction mixture and could thus not be obtained (Scheme 7).

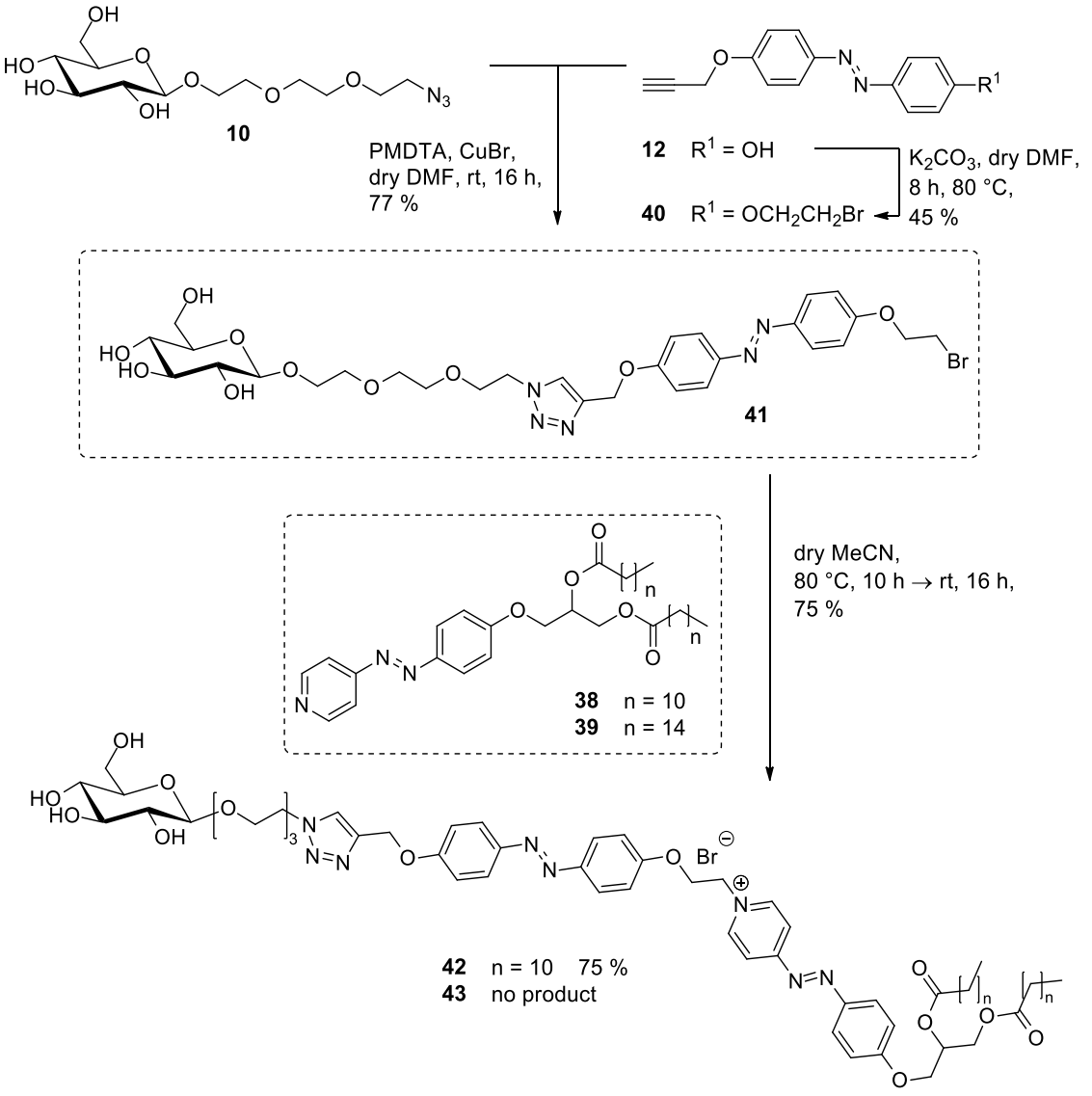

Scheme 7: The hydrophilic building block **41** for glycolipid formation was synthesised via click chemistry. Both building blocks are individually photoswitchable and can be combined via nucleophilic substitution to one photoswitchable glycolipid.

To confirm that the synthesised bis-azobenzene glycolipid mimetic **42** has similar photochemical properties as the model system of VELASCO et al.,[148] photochemical investigations were performed both for the target molecule **42** and the building blocks **38** and **41**. The UV/Vis spectrum of the bis-azo derivative **42** is shown in Figure 37. After irradiation with 365 nm the absorption spectra showed an increase of the absorbance in the n-π* transition and simultaneous decrease in the π-π* transition, indicating the formation of the respective *Z*-isomer.

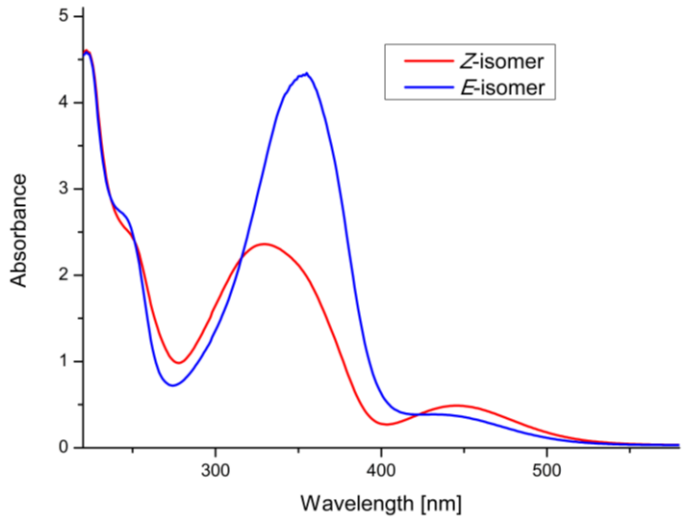

Figure 37: UV/Vis spectra for the steady state of compound **42**: The *E*-isomer is shown in blue and the *Z*-isomer in red. Irradiation was performed with 365 nm (*E*→*Z*) and 465 nm (*Z*→*E*) in chloroform.

Half-lifes were determined by NMR spectroscopy according to the procedure described in chapter 5.3.4. The half-life for the target molecule **42** was determined as 16.2 h. For the glycoside **41** the half-life was 25.4 h. For the second building block, the phenylazopyridine derivative **38**, no half-life could be determined, neither via NMR spectroscopy nor via UV/Vis spectroscopy. UV/Vis spectroscopy features the advantage that the measurement can be performed with solutions of low concentrations. Thus, the suppression of photoswitching due to high concentrations can be excluded. Presumably the thermal relaxation of compound **38** proceeds in a very short time which is too fast to be detectable by NMR or UV/Vis measurements. Indeed, for phenylazopyridinum derivatives half-lifes of less than one second were reported.[116] Nevertheless, the obtained results already indicate that the bis-azobenzene derivative **42** has two constituent parts with different half-lifes. The NMR spectra of compound **42** for the *E*- and the *Z*-isomer are shown in Figure 38. Although the preliminary NMR spectrum of the building block **38** suggested a thermal relaxation which cannot be detected, the spectrum of compound **42**

shows that all aromatic signals are shifted. The chemical shift in the aromatic region of the *Z*-isomer can be traced to the switching of the azobenzene derivative located on the triazole moiety, the slowly switching moiety.

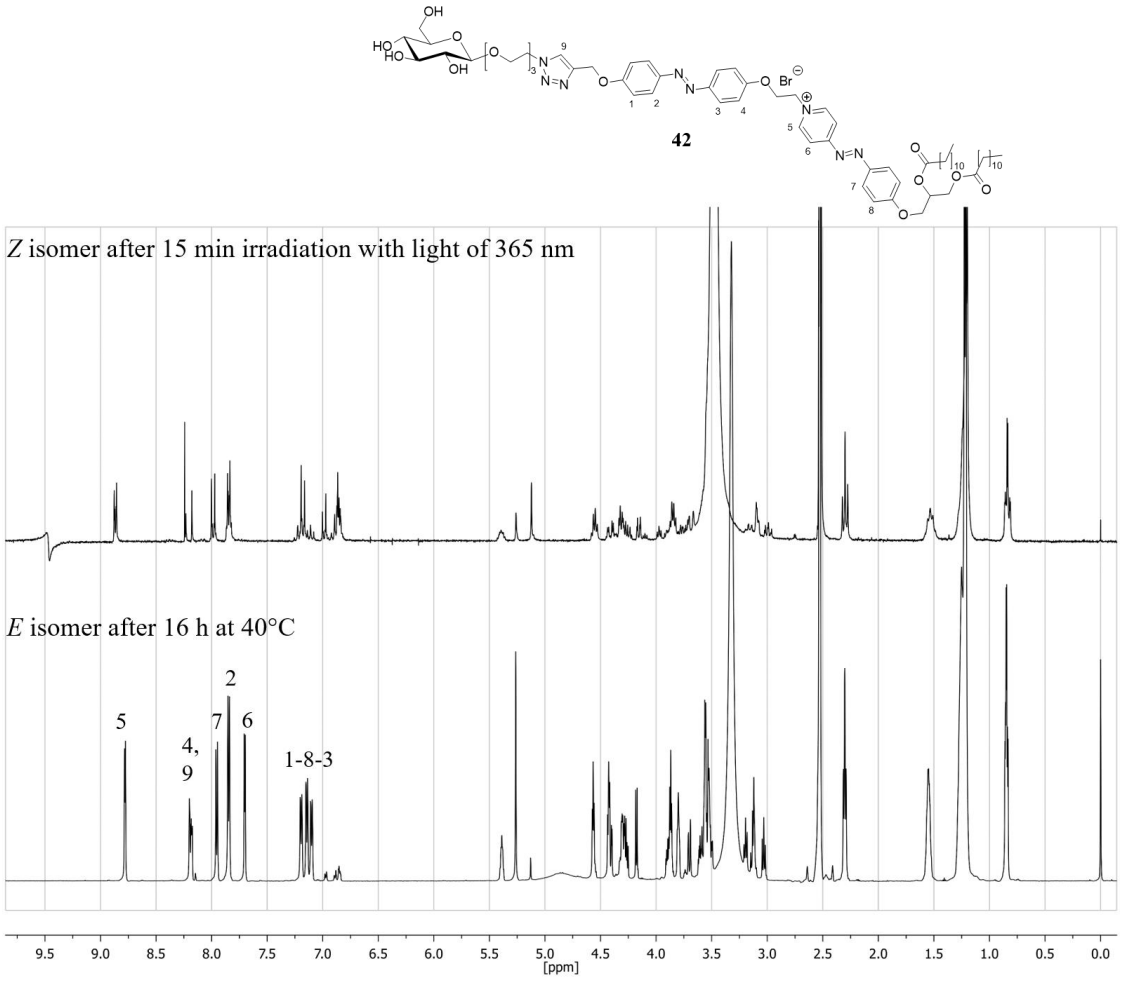

Figure 38: NMR spectra of the *Z*- and the *E*-isomer of compound **42** in DMSO-*d6*: The spectrum of the *E*-isomer was recorded after keeping the probe at 40 °C for 16 h (bottom) and the spectrum of the *Z*-isomer was recorded after irradiating the probe with a 365 nm LED for 15 min (top).

3.3 Conclusion

In the course of this sub-project, a series of novel photoswitchable glycolipids and corresponding non-photoswitchable derivatives was prepared. Photochemical investigations showed that both the nature of the hydrophilic headgroup and the chain length of the lipophilic tail influence the half-life of the thermal relaxation. Especially the influence of the carbohydrate moiety shows a clear impact on photoswitching: The glucoside residues of compounds **20** and **21** almost double the relaxation time for both chain lengths whereas the β-D-lactoside moiety of compounds **22** and **23** diminished the half-lifes. For derivatives with longer chain length, thermal $Z \rightarrow E$ relaxation is slowed down. The glycolipid mimetics **18**-**23** and **42** can now be embedded into lipid monolayers for the investigation of the effects of photoswitching. Since all derivatives form stable *Z*-isomers, Langmuir isotherm and X-ray investigations can be performed for each isomer independently from one another. The examination of the conformational changes triggered by photoswitching will create a useful model system on the nanoscale for the investigation of dynamic transformations of and within membranes. The bifunctional glycolipid **42** will be a special tool for triggering dynamic changes within a membrane. Since the molecule has two azobenzene moieties with different photochromic properties, both photoswitches can be addressed orthogonally and this may result in the induction of special dynamic processes within the lipid layer. A special focus will eventually lie on the influence carbohydrates play within membranes regarding stabilisation of the lipid layer for instance. In addition, the application of glycolipid derivatives will not only allow new insights into the field of membrane dynamics but can also open the field of potential applications, for example in drug delivery.

4 Assay systems for bacterial adhesion studies

Carbohydrates play an essential role in cell-cell recognition, microbial adhesion and microbe invasion as well as for pathogenity. All three processes are based on the specific interactions of lectins and cell surface carbohydrates.[5] To elucidate such processes and to get a deeper insight into biological function of glycoconjugates and lectins much effort has been spent to date. Nevertheless, the mechanisms of carbohydrate-mediated interactions are not yet conclusively understood. Also, it has to be stated that in comparison to the field of nucleic acids and proteins the field of the glycosciences is still lacking versatile methods for structural and functional investigations.[28] Whereas the fields of proteomics and genomics hold valuable tools like polymerase chain reaction (PCR), automated sequencing or automated synthesis ready, much more effort has to be spent for investigations in the field of glycomics.[27] First of all, glycoconjugates have to be either isolated from naturally occurring sources or synthesised. Secondly, gained carbohydrate derivatives must be analysed and characterised and finally the interactions with proteins, e.g. lectins, bacteria, cells or viruses must be investigated. For the exploration of carbohydrate-cell interactions different methods are provided for selection depending on the individual objective. Particularly with regard to structure determination either of the glycoconjugate or the carbohydrate-lectin complex, mass spectrometry[189-191] and nuclear magnetic resonance spectroscopy (NMR)[46, 192-193] are appropriate. Besides, isothermal titration calorimetry (ITC),[194-195] surface plasmon resonance spectroscopy (SPR)[196-197] and atomic force microscopy (AFM)[198] are expedient tools. Last but not least, glycoarrays have to be mentioned necessarily in this context. Glycoarrays are an advancement of microarrays which have been applied for the investigation of DNA, proteins, tissues and antibodies since the early 1980s.[199] The benefit of glycoarrays lies in their feasible handling which can be combined with different analytical procedures ranging from surface investigations e.g. via SPR spectroscopy, reflection absorption infrared spectroscopy or by mass spectrometry via MALDI ToF[200-201] to biochemical procedures like adhesion studies.[202-203] In addition, they are not very much time-consuming and can be performed with just little quantities of precious glycans.[204] Albeit it is extremely challenging to imitate the complex structures of naturally occuring glycan structures, glycoarrays represent versatile model systems for the mimicry of such glycosylated surfaces, their molecular interactions and supramolecular relations on cell surfaces.[205] It permits the reverse conclusion that glycoarrays at least constitute well-defined systems which can be investigated with a view

to particular glycosides as well as defined parameters as density, orientation, pH, temperature and ionic concentration. Glycoarrays are composed of immobilised glycans. Immmobilisation can be realised either non-covalently by adsorption or covalently by chemical ligation.[206] In most cases, gold, glass or polystyrene surfaces are employed. The non-covalent fixation is based on ionic and hydrophobic interactions.[207] In case of non-amphiphilic compounds this method is limited by the molecular weight which has to amount to 3.3-2000 kDa, consequently small mono- or oligosaccharides can only be immobilised in the form of glycoconjugates like glycoproteins or glycolipids.[208] A range of well-established methods for the covalent immoblisation of glycosides is shown in Scheme 8. Most common glycans are immobilised on prefunctionalised surfaces either by amide formation on amino-functionalised surfaces[209] or by depositing amines to active esters e.g. immobilised pyrrolidine derivatives.[210-214] Further methods are based on thiol-maleimide ligation[215-217] or on cycloaddition ranging from click chemistry[213, 218-221] to Diels-Alder reactions.[222] An interesting method is shown under entry (f) (Scheme 8) which shows the covalent immoblisation on a non-prefunctionalised surface by light-induced insertion to the surface material.[223]

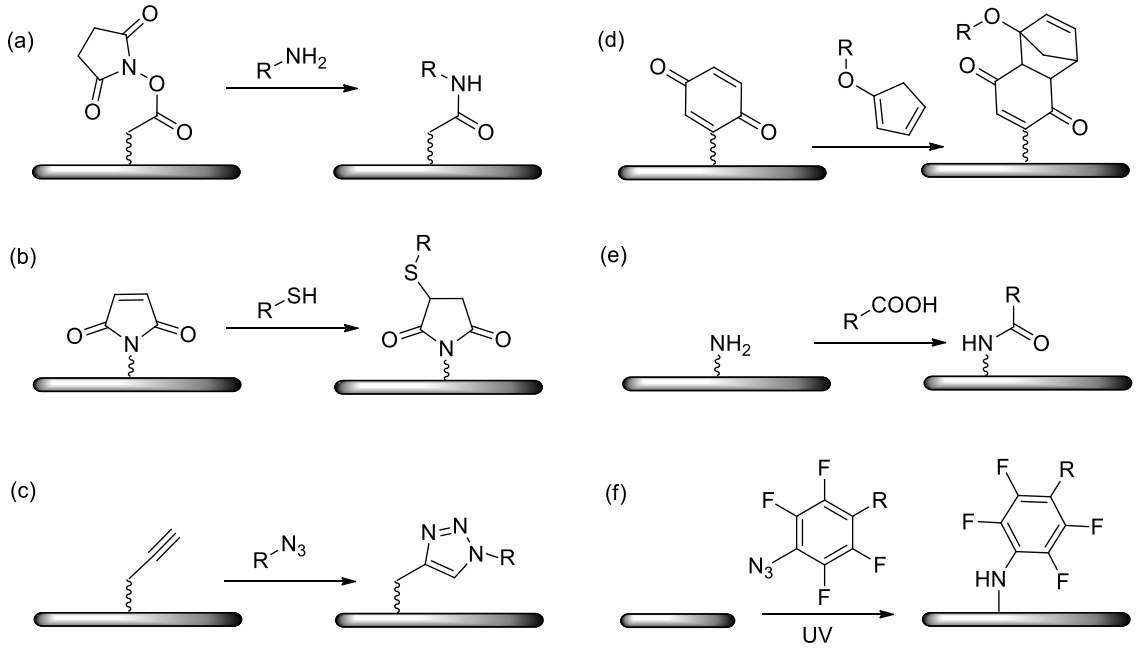

Scheme 8: Methods for the immobilisation of glycans (R) on surfaces: (a) amide formation via active ester; (b) thiol maeimide ligation; (c) (3+2) cycloaddition; (d) Diels-Alder reaction; (e) amide formation; (f) photochemical fixation.[206]

To gain reliable results from glycoarrays such as in adhesion studies, some requirements must be fulfilled. As a start, unspecific interactions of the adhering species, e.g. bacteria,

with the pristine surface must be supressed by using blocking agents or intrinsically little adhesive materials. Secondly, during glycoarray fabrication the occurrence of clustering effects which would lead to an irregular density of glycans on the surface should be avoided. For comparability of results it is important that glycosides are arranged regularly and homogenously so that every immobilised glycoside ligand has the same accessibility for adhering species. Finally, one has to keep in mind to choose a surface which is applicable for common investigation methods.[205] To fulfill all these aspects, the concept of self-assembled monolayers (SAMs) was introduced to the field of glycoarray fabrication some time ago.[222] SAMs can be constructed on metal or metal oxide surfaces either by covalent bond formation with the respective molecules or by their adsorption or by hydrophobic interactions. Established systems for SAM fabrication are silanes on silicium, carboxylic acids on metal oxides and especially organosulfur compounds on gold.[200] For glycoarray fabrication, glycans thus have to be equipped with a hydrophobic residue for adsorption. Alternatively, the glycoarray can be prepared starting with SAM formation of linker molecules, which are equipped with a functional group for subsequent ligation with glycoside derivatives.[224] Unspecific binding can be prevented by using oligoethylene glycol linkers.[204, 218, 222, 225-231] The experience from glycoarray studies was also transferred to investigations of molecular interactions of organisms with glycan-decorated particles of different shape and material to enlarge the variety of methods and applications. The scope varies from nanodiamonds,[232-233] quantum dots[234-235] and gold beads[236] to polymer beads which can feature fluorescence[237] or magnetism.[234, 238] Although the beads concept gives more experimental flexibility, all methods described prior to this lack the ability to mimic convincingly the adhesive recognition processes which take place in every eukaryotic cell in every second of life. Therefore, one general aim in science is to establish glycoarrays with higher flexibility and a surface decoration which can describe and imitate nature more satisfactorily. For this purpose, two approaches were taken. In the first approach, glycoarray fabrication is facilitated to produce glycoarrays with formidable glycan decoration. In the second approach, glycosylated surfaces were prepared which are on a par with naturally occurring glycosylated surfaces. In connection with earlier works performed in the LINDHORST group,[239-241] we performed adhesion assays with type 1 fimbriated *E. coli*, mediated by the lectin FimH. Lectin FimH mediates the adhesion of UPEC (uropathogenic *E. coli*) to α-D-mannosides which are displayed on urothelial epithelial cells.[242]

4.1 Simple fabrication of glycosylated surfaces for bacterial adhesion studies by using pentafluorophenylazides as linkers

4.1.1 Introduction

Pentafluorophenylazides (PFPA) are known for their reliable atom-economic photochemistry. Hence, PFPA linkers can be used for glycan immobilisation without the need of prior functionalisation of the glycan. Therefore, it was the objective of this sub-project to utilise PFPA-functionalised surfaces for glycoarray fabrication. The azido functional group of PFPAs is photoactivatable and in addition, PFPAs can be further functionalised in *para*-position with great ease.[223] Hence, PFPA building blocks were used for many applications in material sciences including surface functionalisation and their implementation in polymer synthesis.[243-253] With regard to glycobiology, PFPA chemistry found applications for the fabrication of glycosylated surfaces[250, 254-263] and glyconanoparticles[264-265] in order to investigate biomolecular recognition processes and also antiviral antibodies were produced by PFPA ligation.[266] PFPA chemistry provides the opportunity for simple glycoarray fabrication with unmodified glycoconjugates since light triggers the chemoselective ligation. This also embraces the possibility for spatial resolution. Advantageously, PFPA chemistry works under mild reaction conditions in aqueous media and does not require any additional reagents and in addition does not release any side products.[223] Besides, the probability of effective insertion of PFPA-functionalised molecules to substrates increases with the number of CH bonds within a molecule (Figure 39). Therefore, PFPA chemistry for glycoarray formation was also employed to glycoclusters (Figure 40) since multivalent ligands have increased numbers of CH bonds for photochemical insertion reactions.[267-270]

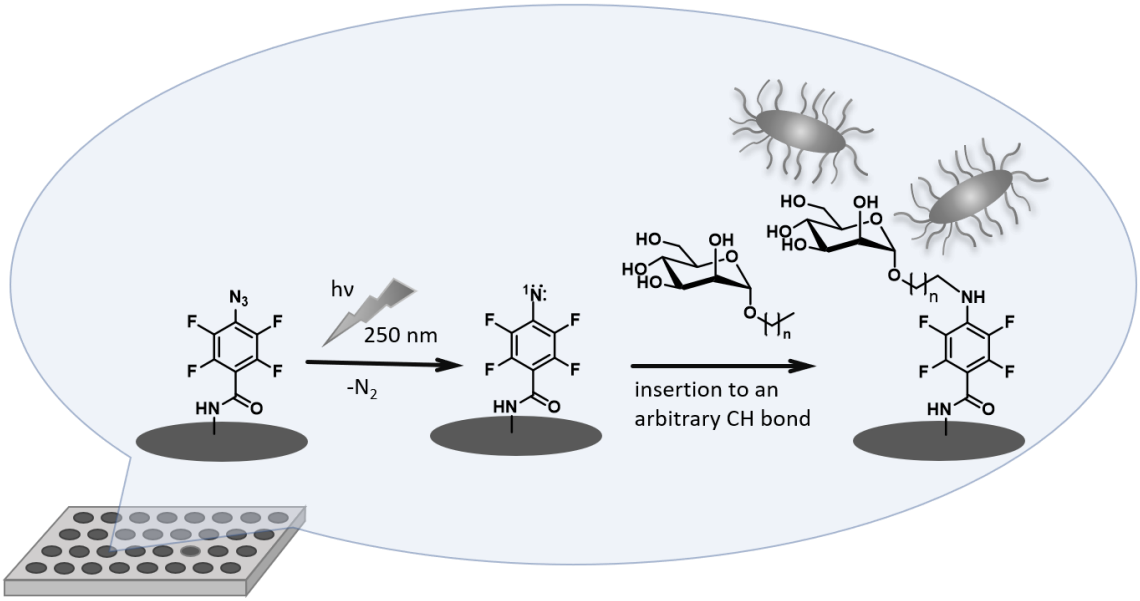

Figure 39: Schematic representation of the glycoarray fabrication by PFPA chemistry. Carbohydrates can be immobilised to a pentafluorophenylazide-prefunctionalised surface by UV light. Under irradiation with UV light of 250 nm, PFPAs release elementary nitrogen resulting in a highly reactive nitrene intermediate which can undergo an insertion reaction to CH bonds.

4.1.2 Results and discussion

Glycoarray synthesis was focussed on mono-, di and trivalent mannosides to look at possible multivalency and density effects. Finally, those arrays were subjected to bacterial adhesion studies with type 1 fimbriated *E. coli* (PKL1162 strain) (Figure 39). First, the synthetic part of the project is described below. A photoreactive linker molecule **7** composed of a biorepulsive ethylene glycol unit and a terminal azido functionality for light-driven insertion was synthesised according to literature procedures.[271-273] Methyl pentafluorobenzoate **1** was equipped with an azido group in *para*-position by substitution. After deprotection of the methyl ester **2** under basic conditions, the resulting acid **3** was converted to a NHS (*N*-hydroxysuccinimide) active ester **4**. Since the PFPA compound **4** shall be used as a functional coating of surfaces, a functional group for the immobilisation of the respective surface is required. Therefore triethylene glycol derivative **5** was synthesised[274] which is biorepulsive and accessorily suppresses unspecific binding of bacteria to the polystyrene surface.[275] Active ester **4** and amine **5** were reacted to yield compound **6** which was subsequently deprotected to produce amine **7** with an overall yield of 85 % after five steps (Scheme 9).

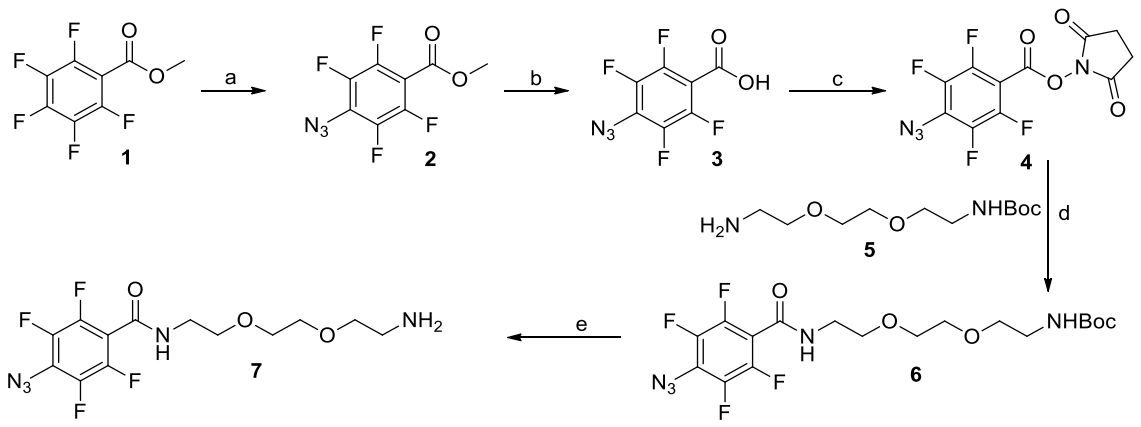

Scheme 9: Synthesis of PFPA linker **7**: (a) NaN_3, acetone/H_2O, Δ, 8 h, 95 %; (b) NaOH, MeOH/ H_2O, rt, 20 h, 95 %; (c) NHS, DCC, DCM, rt, 19 h, 99 %; (d) DCM, rt, 16 h, 95 %; (e) TFA, DCM, rt, 4 h, quant.

To test pentafluorophenylazide-mediated glycoarray fabrication, four different glycosides were prepared, the two monovalent glycosides **12** and **13** and and two mannoside clusters, the divalent derivative **30** and the trivalent cluster **31**. All glycosides are equipped with an alkyl chain for the photochemical ligation. Both monomeric compounds were synthesised according to the literature.[276-278] Starting from the glycosyl donors **8** and **9**, respectively, 1-octanol (**10**) was glycosylated under Lewis acid catalysis to obtain the mannoside **11** and the glucoside **12** in 81 % and 77 % respective yields. Following deprotection under ZEMPLÉN conditions[179] gave the unprotected glycosides **13** and **14** in quantitative yields (Scheme 10).

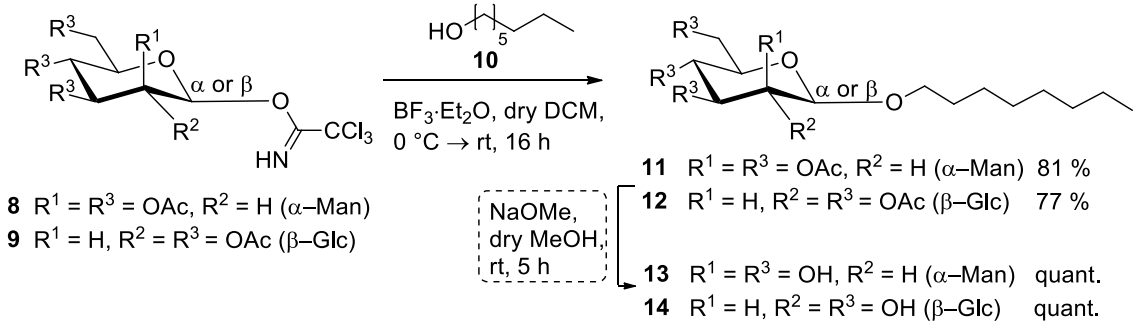

Scheme 10: Synthesis of monovalent glycosides **13** and **14** via $BF_3{\cdot}Et_2O$ promoted glycosylation.[276]

Di- and trivalent cluster mannosides were designed according to work published by ROY et al.[279-280] as shown in Figure 40. Two different synthetic pathways were considered, one starting with the construction of the cluster and subsequent functionalisation of the

molecular core (Figure 40, (A)), in the other approach, the core was functionalised first and then the cluster was built up (Figure 40, (B)).

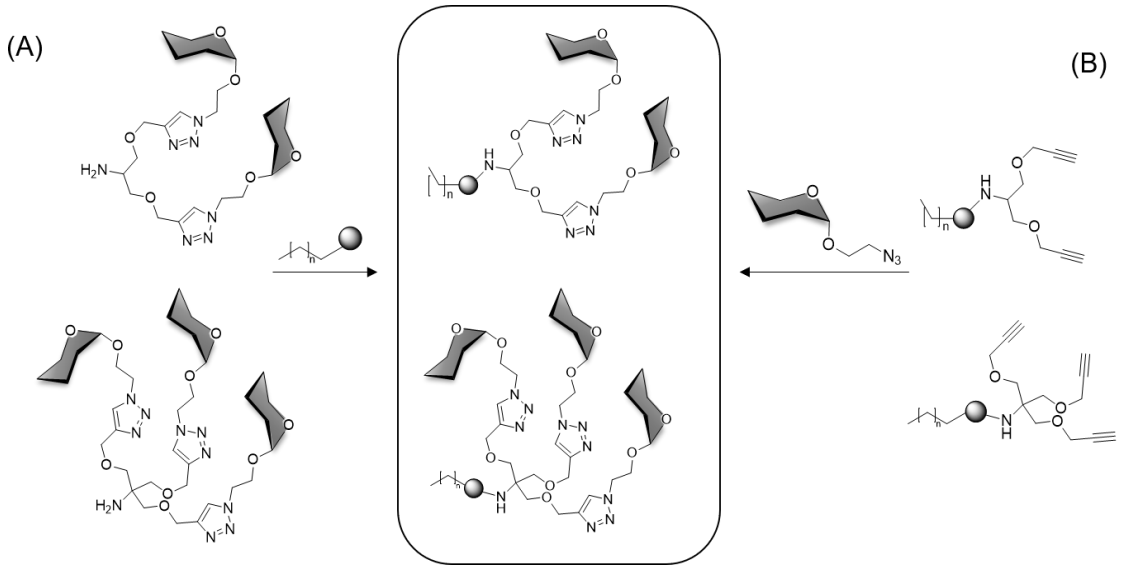

Figure 40: Schematic representation of the approaches for glycocluster formation. The first synthetic pathway started with the construction of the cluster and subsequent core functionalisation (A). The second approach provided the functionalisation of the core first and then the build-up of the cluster (B).

The first considered reaction pathway (A) is advantageous as it allows to equip the synthesised glycoclusters with any required focal moiety afterwards. Here, alkyl chains were desired, to facilitate glycoarray functionalisation by photochemical nitrene insertion. Starting from serinol **15** and tris(hydroxymethyl)aminomethane (TRIS) **16**, Boc protection was performed initially with high yields.[281] The resulting alcohols **17** and **18**, respectively, were equipped with alkyne functionalities by WILLIAMSON etherification with propargyl bromide to obtain versatile core molecules **20** and **21** in 83 % and 41 % respective yields.[279, 282] Next, **20** and **21** were employed in a click reaction with the azidoethylmannoside **22**[283] under copper (I) catalysis by using sodium ascorbate and copper sulphate ($CuSO_4 \cdot 5H_2O$) which led to the desired clusters **23** and **24** in yields of 72 % and 86 %, respectively.[280] Then, the focal amino functionality was liberated with trifluoroacetic acid to yield free amines **25** and **26** in quantitative yields (Scheme 11).[284] The introduction of the desired alkyl chains was then attempted with hexanoic acid **27** and DCC but **25** gave only minor amounts of the expected derivative **28** and the trivalent analogue was achieved in unsatisfactory 10 %. Nevertheless, **28** and **29** were deprotected to furnish **30** and **31**, respectively.

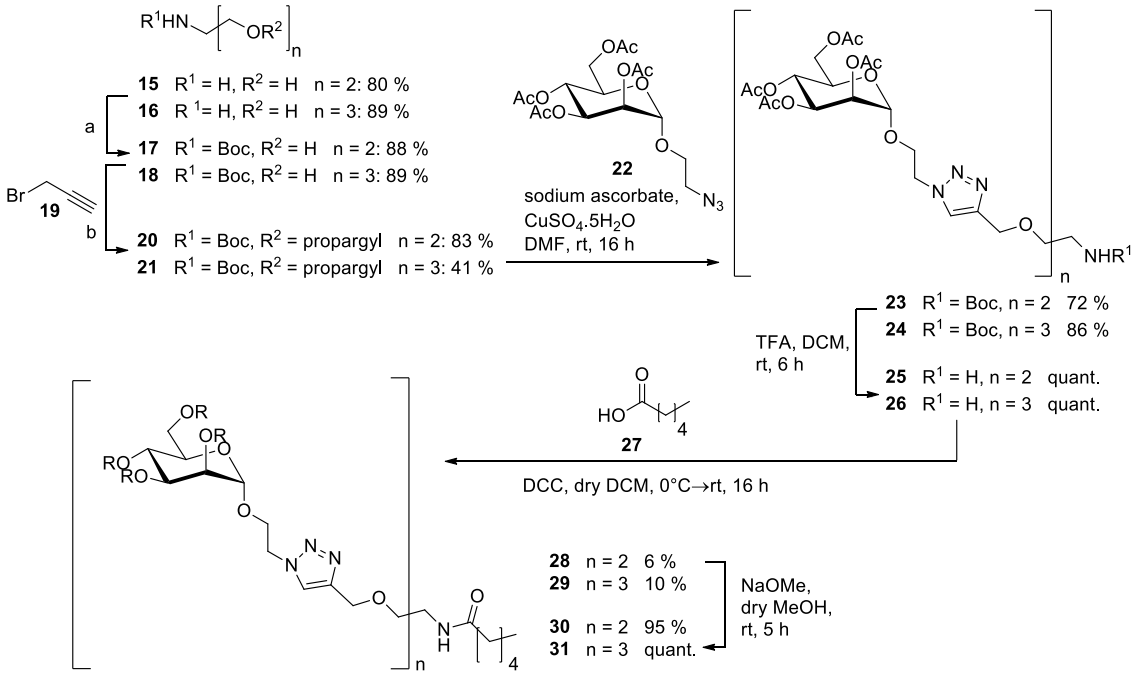

Scheme 11: First synthetic strategy: Di- and trivalent cluster molecules **25** and **26** were synthesised starting from serinol **15** and TRIS **16**, respectively. The amino functionality allowed adjacent functionalisation of the molecules with a favoured core. Reacction conditions: (a) Boc_2O, MeOH, rt, 42 %; (b) KOH, dry DMF, 0 °C → 35 °C, 4h.

The subsequent attempts to improve the alkyl functionalisation at the focal point of glycocluster **26** are summarised in Scheme 12. First, amide bond formation was further investigated. Hence, the amine **26** was reacted with the known NHS active ester of hexanoic acid **32** (Scheme 12(A)[285-286] under three different conditions. The first reaction was performed with K_2CO_3 in dry acetonitrile. The reaction stirred under reflux for 15 h.[287] The second reaction required 1,8-diazabicyclo[5.4.0]undec-7-en (DBU). The reaction mixture in dry acetonitrile was stirred for 16 h at room temperature.[288] Both reactions showed no conversion according to thin layer chromatography (TLC). The third entry used triethylamine (NEt_3) at 0 °C. After warming up to room temperature, the mixture was stirred for another 40 h at room temperature.[289] This approach also only gave a small amount of the crude product which does not justify the longer synthetic pathway via the NHS active ester. Then, another coupling reagent, namely HATU ((1-[Bis(dimethyl-amino)methylene]-1*H*-1,2,3-triazolo[4,5-b]pyridinium 3-oxid hexafluorophosphate) and DIPEA (*N,N*-Diisopropylethylamine) were employed for amide formation. The reaction was performed in dry DMF and stirred at room temperature for 16 h to yield 17 % of the crude product (Scheme 12(B)). When **26** was dissolved with hexanoyl chloride **33** and NEt_3 in dry DCM and reacted at room

temperature,[290] no product was obtained (Scheme 12(C)). Since functionalisation at the focal point of **26** via amide bond formation was not successful, thiourea bridging as alternative ligation chemistry was tried out next (Scheme 12(D)).[291] However, also this reaction did not yield the expected product neither with **26** nor with **25** as starting material. Finally, the focal amino function was converted into an azido functionality by the azide transfer reagent imidazol-1-sulfonylazide hydrochloride **35** (Scheme 12(E)), however, TLC control indicated no conversion even after 16 h.

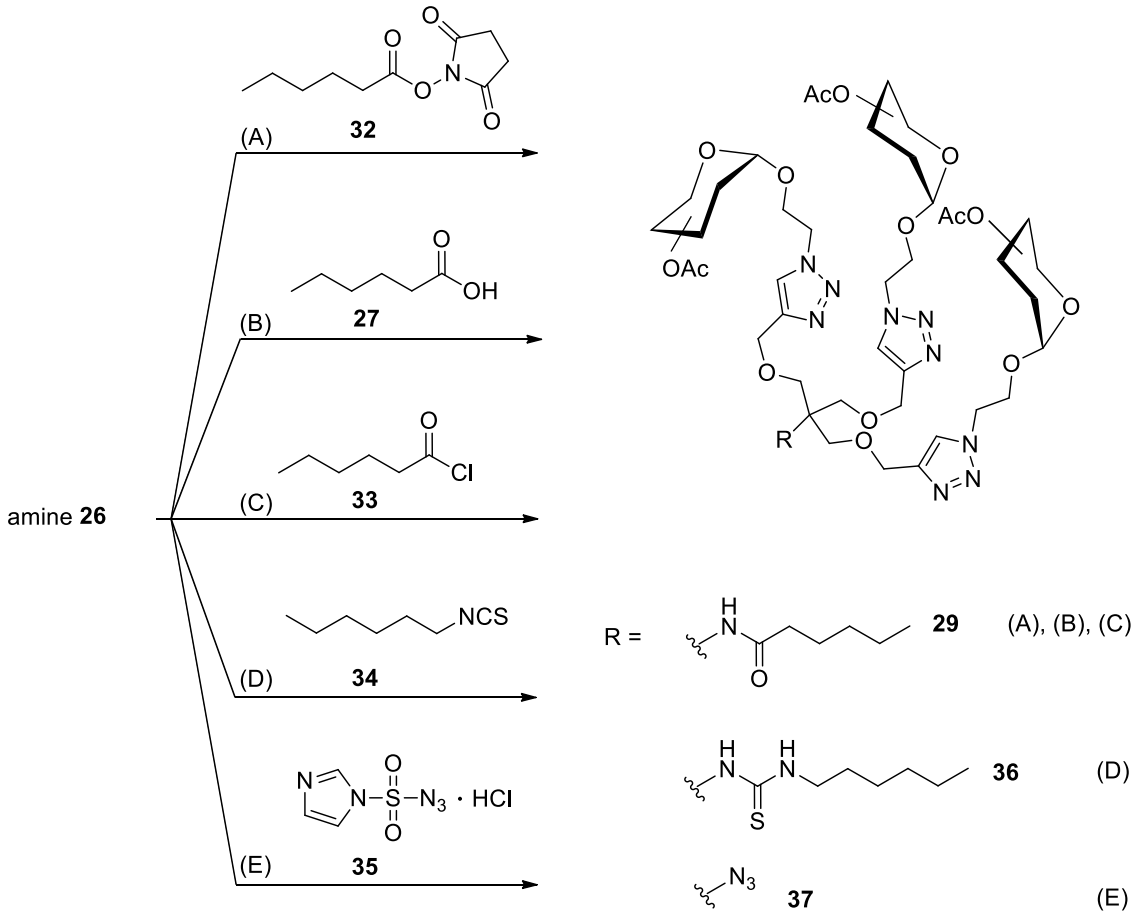

Scheme 12: Overview of the approaches which were investigated to find an effective route towards the fabrication of core-functionalised glycoclusters. Several reagents and conditions were tested commencing from amine **26**.

As all attempts made here to functionalise the focal point of glycoclusters **25** and **26** were unsuccessful, the synthetic strategy was changed, and the core molecule functionalised prior to sugar conjugation (Figure 40 (B)). It can be anticipated that also during this strategy all performed syntheses worked successfully in case of divalent molecules, but some effort was made to finally obtain a trivalent cluster (Scheme 16).

Hence, the core molecules **20** and **21** were deprotected with trifluoroacetic acid[292] to obtain amines **38** and **39** which were utilised for amide bond formation with hexanoic acid **27** with DCC as coupling agent. Core molecules **40** and **41** were obtained in 51 % yield (**40**) and 68 % (**41**). The successive synthesis of the cluster with mannoside **22**[283] was performed under copper (I) catalysis by using sodium ascorbate and $CuSO_4 \cdot 5H_2O$. The divalent cluster **28** was obtained with an auspicious yield of 74 % with slight impurities after column chromatography (Scheme 13). However, the same click reaction with the trivalent core molecule **41** gave no product at all, neither when the catalytic system for the cycloaddition was changed to CuBr and PMDTA (cf. chapter 3.2.1). Although the results for the divalent cluster **28** were promising, further efforts were needed for the synthesis of the trivalent analogue.

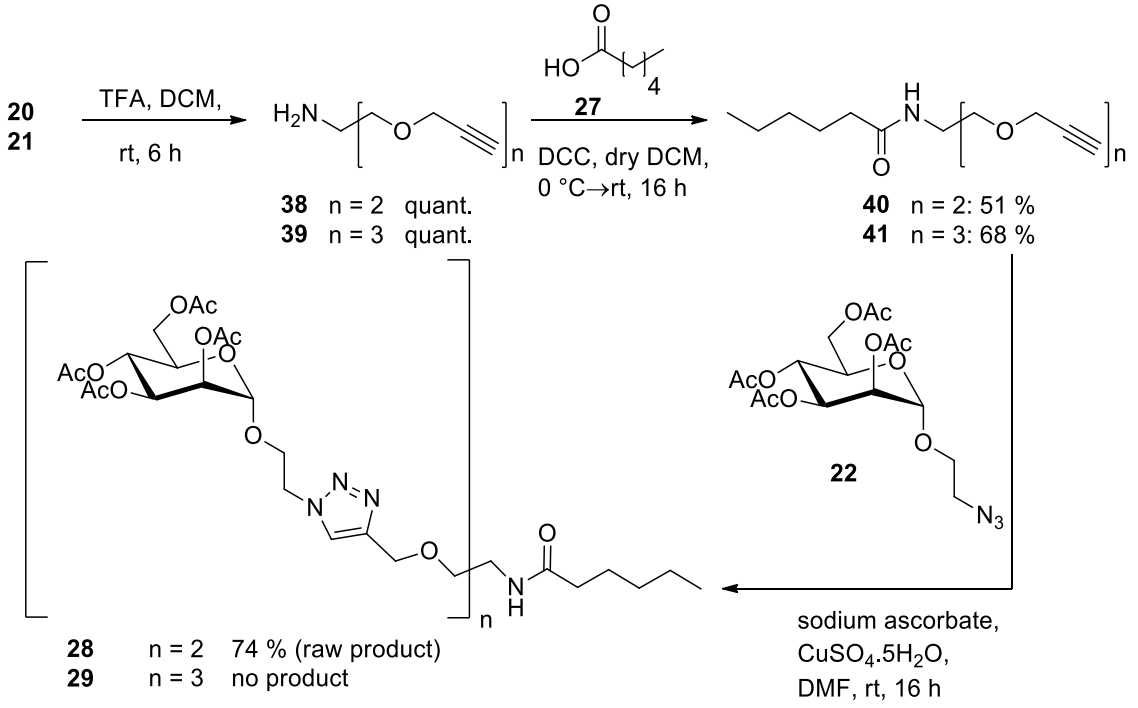

Scheme 13: Second strategy for cluster synthesis: Starting from compounds **20** and **21**, respectively, the alkyl chain was first introduced and the cluster constructed secondly.

To try thiourea bridging next, the alkyl chain-equipped core molecules **48** and **49**, respectively, were prepared according to two synthetic pathways. The first synthesis started with serinol **15**, respectively **16** and hexyl isothiocyanate **41** to obtain molecules **43** and **44**. Then, the di- and trivalent alcohols **43** and **44** were employed in a WILLIAMSON ether synthesis with propargyl bromide **19**. Etherification yielded the divalent core molecule **48** in 74 % yield, but no product was obtained in case of the

trivalent alcohol **44**. The same outcome resulted from the second reaction pathway which started from amino-functionalised compound **38** and **39**, respectively. First, both amines were converted to the corresponding isothiocyanates using thiophosgene. The reactions provided the desired products in 26 % yield for compound **45** and 73 % for compound **46**. To avoid thiophosgene as reagent, amine **37** was first converted into the azide **50** with imidazol-1-sulfonylazide hydrochloride **35** and afterwards reacted with carbon disulfide and triphenylphosphine to yield isothiocyanate **46** in an excellent yield of 89 %. With both isothiocyanates **45** and **46** in hand, thiourea bridging was performed with hexylamine **47**. The divalent core molecule **48** was obtained in 74 % yield whereas the synthesis of the trivalent analogue remained unsuccessful. Continuing from the divalent core molecule **48**, glycocluster **51** was obtained by click reaction with azido-functionalised mannoside **22**[283] in 62 % yield (Scheme 14).

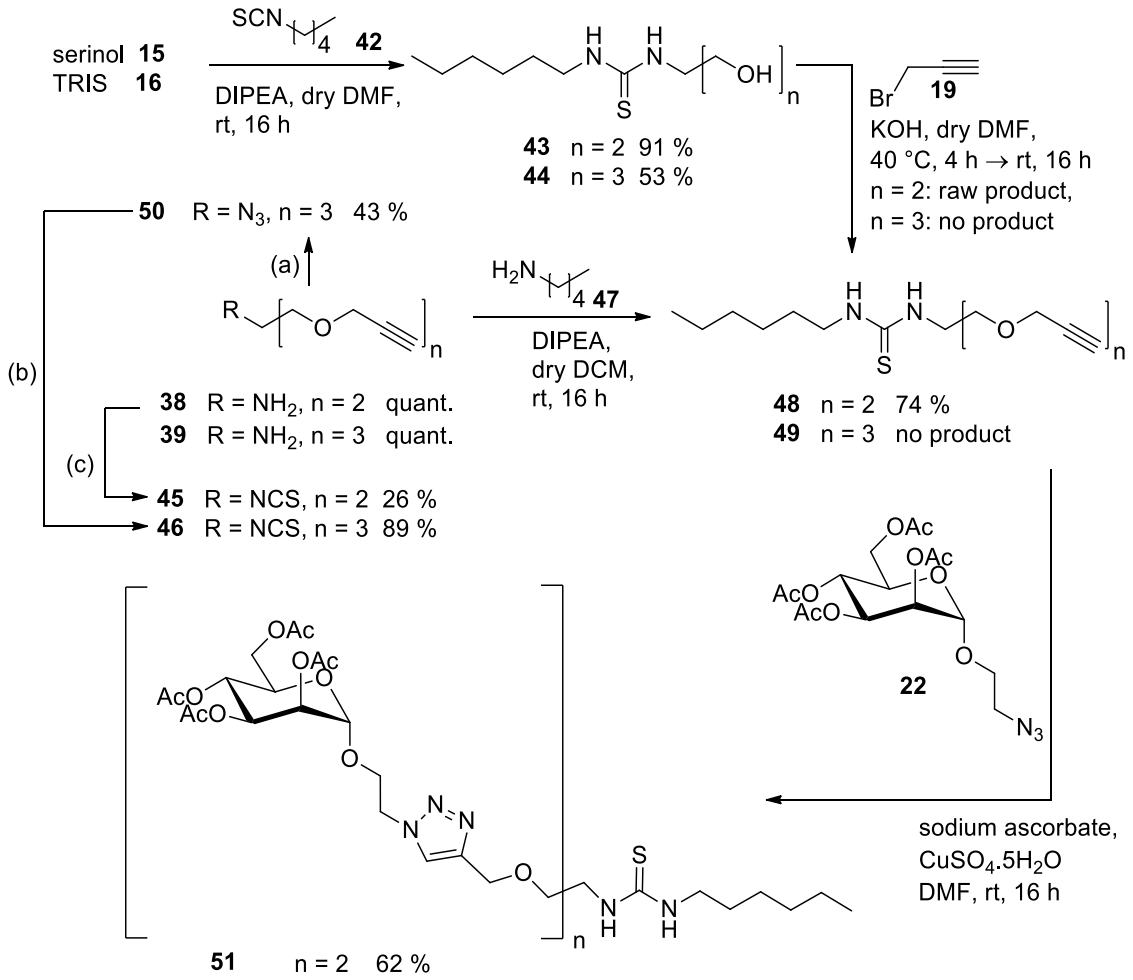

Scheme 14: Synthesis of glycocluster **51** starting with the functionalisation of the core via thiourea bridging and subsequent build-up of the cluster through click chemistry with azide **22**. Conditions: (a) imidazol-1-sulfonylazide hydrochloride **35**, $CuSO_4 \cdot 5H_2O$, MeOH, rt, 16 h; (b) CS_2, PPh_3, $CHCl_3$, rt, 16 h; (c) thiophosgene, NEt_3, dry DCM, rt, 16 h.

In conclusion, the synthesis of divalent glycoclusters could be easily achieved whereas synthesis of the trivalent analogue remained problematic. The next attempts which were made are depicted in Scheme 15. Therefore amines **15** and **16** were employed in a reaction with butyl chloroformate **52** to form carbamates **53** and **54**, respectively.[293] Both molecules were submitted to WILLIAMSON ether synthesis with propargyl bromide **19**. Again, just the divalent molecule delivered **55** in a yield of 36 %. The following click reaction proceeded without difficulty to yield cluster **57** in 76 %.

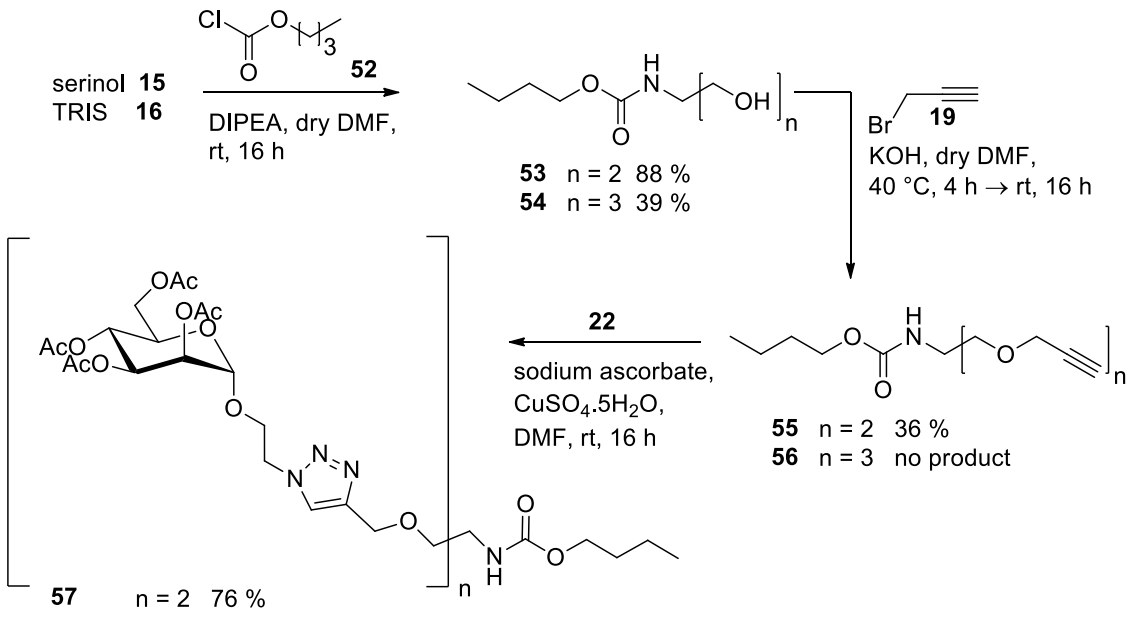

Scheme 15: Synthesis towards glycocluster **57** employing butyl chloroformate **52** for ligation with amines **15** and **16**, respectively.

In a next attempt, carbamate formation was tried with glycoclusters **25** and **26**, which were deacetylated beforehand due to solubility issues. In this approach, ultimately the trivalent core molecule could also be functionalised at the focal point allowing to finally proceed with the project in bacterial adhesion studies as outlined above. The focal points of **25** and **26**, respectively, were functionalised with an alkyne chain by carbamate formation with butyl chloroformate **52** making carbamates **57** and **60** available with a yield of 72 % and 59 %, respectively. Acetylation was performed for facile purification. The last step of the synthesis route was the removal of the *O*-acetylated protecting groups under ZEMPLÉN conditions[179] resulting in compound **61** and **62** in quantitative yields which were then applicable for bacterial adhesion studies (Scheme 16).

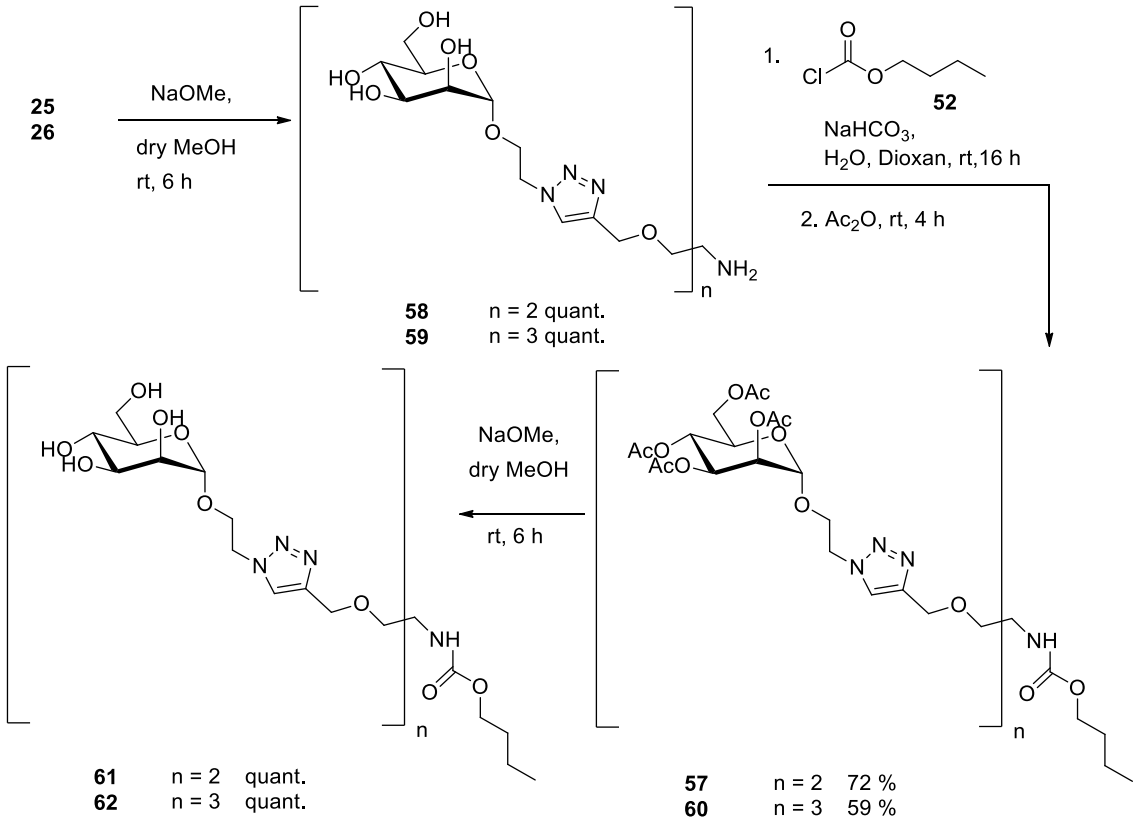

Scheme 16: Successful synthesis of glycoclusters **61** and **62** via carbamate formation between amines **58** and **59**, respectively, with butyl chloroformate **52**.

In summary, for the fabrication of glycosylated surfaces for bacterial adhesion studies by light-induced pentafluorophenylazide-mediated insertion reaction four different glycosides were prepared, the two monosaccharides **13** and **14** and the di- and trivalent glycoclusters **61** and **62**, respectively.

For glycoarray formation, commercially available preactivated Nunc polystyrene 96 well microtiter plates were used. After incubation with the amine **7**, the PFPA-modified surface **63** was formed which was then applicable for subsequent immobilisation of the prepared carbohydrates, **13**, **14**, **61** and **62** which were employed in serial dilutions in PBS buffer. (Scheme 17).

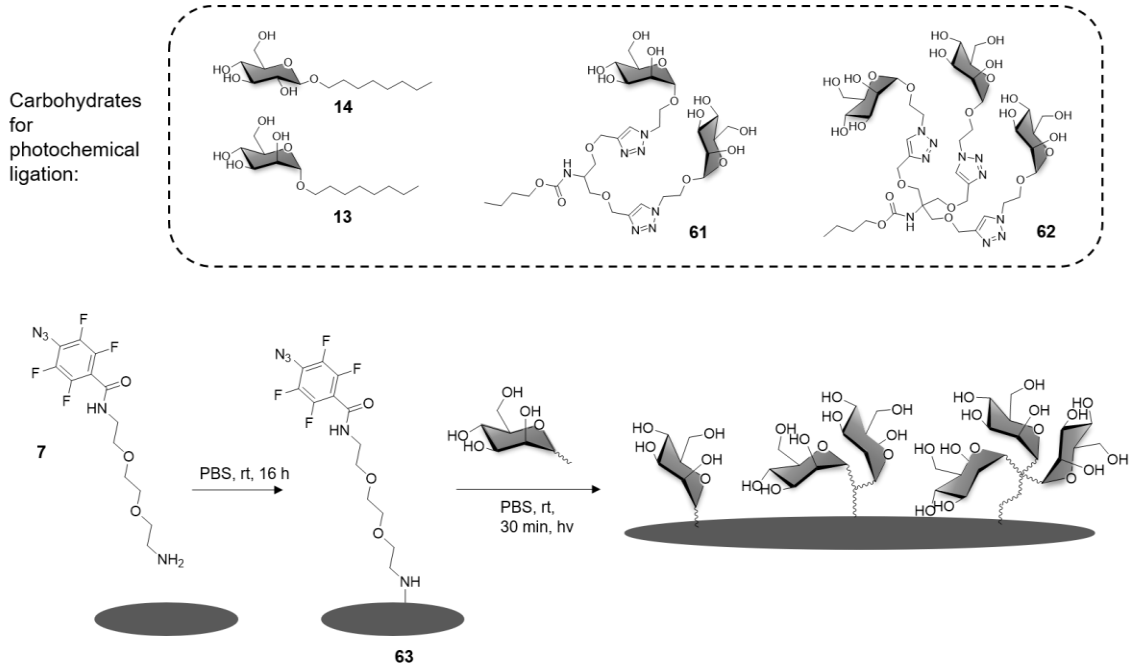

Scheme 17: Synthesis of the PFPA-functionalised surface **63** and schematic picture of the glycoarray surface after irradiation. All four immobilised carbohydrate derivatives **13**, **14**, **61** and **62** are shown in the box above.

The microtiter plate was irradiated with a mercury vapour discharge lamp with a wavelength of 254 nm for 30 minutes. Photofixation was followed by washing steps with PBST (phosphate buffered saline with tween) to remove unreacted glycoconjugates and incubation with ethanolamine to block unreacted surface groups. Finally, the glycoarrays were used in bacterial adhesion studies. Microtiterplates were incubated with type 1 fimbriated *E. coli* (PKL1162 strain). Since the PKL 1162 strain contains the GFP (green fluorescent protein) gene, bacterial adhesion was quantified by fluorescence read out in the end.[239, 270] The results of adhesion studies are depicted in Figure 41.

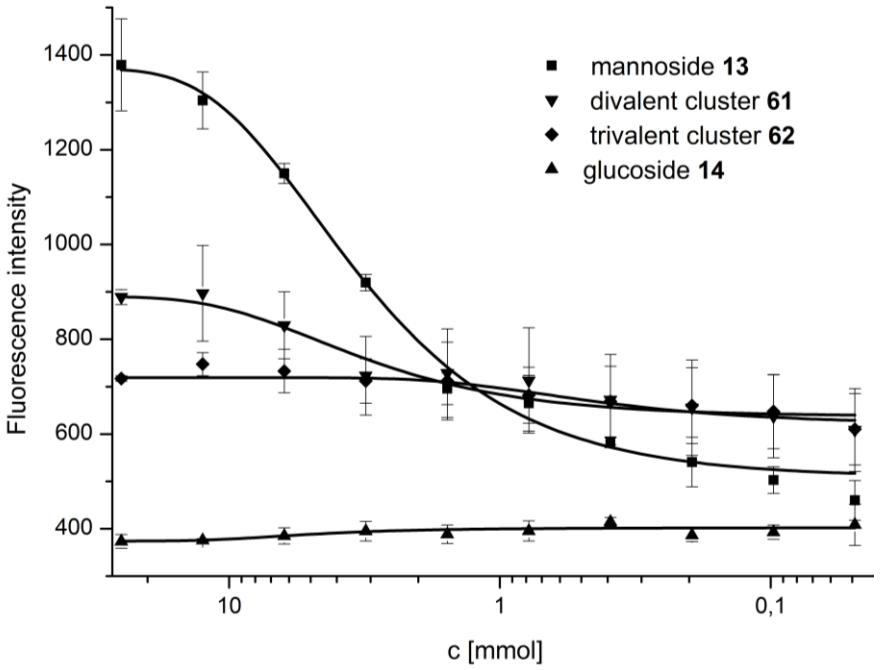

Figure 41: Bacterial adhesion (quantified by fluorescence intensity) to glycosylated surfaces fabricated by PFPA linkers as measured with the described assay. Three mannoside derivatives **13**, **61** and **62** were tested in comparison to a glucoside derivative **14**. Given concentrations are based on solutions which were used for the irradiation reaction. Error bars are standard deviations generated from triplicate values on one plate.

An almost four times higher adhesion for mannoside **13** in comparison to glucoside **14** for the starting concentration of 25 mM was detected and can be taken as a proof of successful array formation. As expected, glucoside **14** showed just little fluorescence independent of the applied the concentration. This confirmed that there was no adhesion for glucoside **14**. Surprisingly, divalent mannoside cluster **61** showed way less adhesion for the same concentrations than the monovalent mannoside **13** at least in the range of 25 mM to 1.5 mM concentrations. Above all, the trivalent mannoside cluster **62** shows the same behaviour and consequently the least adhesion of all three mannoside ligands. For lower concentrations (1 mM and lower) the observation is reversed: di- and trivalent clusters **61** and **62**, respectively, show rather similar adhesion which is then higher than the adhesion of monovalent mannoside **13**. Similar multivalency effects were investigated on glycoarrays conventionally fabricated from amino-equipped mannose derivatives on prefunctionalised polystyrene surfaces.[270]

4.1.3 Conclusion

Different glycoarray surfaces with mono- to trivalent mannoside derivatives were successfully synthesised by PFPA-mediated photo-immobilisation The immobilisation was proven by bacterial adhesion studies which showed concentration-dependent high adhesion for the mannose derivatives immobilised on the PFPA-functionalised surface. The glucose-configured control showed no adhesion as expected. Even though effects of multivalency could not be investigated completely since the orientation of immobilised molecules is unknown, we observed that the affinity for di- and trivalent clusters is proportionally higher at lower surface concentrations. This effect could be rationalised by better exposure and therefore better accessibility of the single cluster molecules on the surface at lower concentrations. Those results regarding the multivalency effect of di-and trivalent glycoside clusters are in accordance with studies which were performed earlier on by WEHNER et al. on glycoarrays formed of amino-equipped cluster molecules on prefunctionalized polystyrene surfaces.[270]

4.2 Bioorthogonal click chemistry on glycosylated surfaces for the investigation of bacterial adhesion

4.2.1 Introduction

Using bioorthogonal click chemistry, a second approach towards tailor-made glycoarrays was taken aiming at mimicking more of nature's complexity. Bioorthogonal reactions are reactions that according to BERTOZZI "neither interact with nor interfere with a biological system".[294-295] For a successful bioorthogonal reaction a high rate and inertness against other functionalities which can occur in biological systems such as hydroxyl groups, thiols or amines is required.[296-297] Two prominent bioorthogonal ligation methods are widely-used in biological chemistry. First, the reaction of an azide with a triarylphosphane which was investigated by STAUDINGER in 1919[298] and refined by BERTOZZI such as a stable amide bond can be formed after reduction of the azide to an amine.[295] The second well-known reaction is the click reaction which occurs between an azide and an alkyne in presence of a copper (I) catalyst to yield triazoles. This copper-catalysed strategy was developed by SHARPLESS[299] and MELDAL[300] after HUISGEN[301-302] had already explored the formation of triazoles from azides and alkynes by thermal activation. As described above (chapter 4), glyco-SAMs do not mimick the chaotic structure of the glycocalyx and therefore the tools for the investigation of carbohydrate-lectin interactions were further extended towards glyconanoparticles[234, 236-238, 303-307], glycosylated polymers[308-310] and glycosylated polysaccharides.[311-317] The characteristics of polysaccharides are dependent on their monomers, the connection pattern of monomers, functional groups which might be attached on the polysaccharide and the occurrence of branching.[318] This can be exemplified by cellulose, amylose and dextran. Whereas all three constitute D-glucose, the specific features of cellulose arise from β(1,4) glycosidic linkages, from α(1,4) glycosidic linkages for amylose and dextran is characterised by α(1,4), α(1,2) and α(1,3) glycosidic linkages.[319-320] Water solubility increases from cellulose over amylose to dextran.[321-322] Especially dextran derivatives can resemble a large glyco-flexibility and a variety of structures. Thus, MELNYK and coworkers equipped a dextran derivative with azido functionalities, performed click chemistry with alkyne-equipped glycosides and finally immobilised the whole dextran-glycoside conjugate on microtiter plates.[323] BÖCHER and coworkers pursued a likewise approach. They used dextran as a carrier molecule for the fabrication of monofunctional peptide-dextran conjugates by amide bond formation. The immobilised peptides were

then immunodetected and compared to the results for peptides which were directly immobilised on ELISA plates. This method led to an improvement of the required amount of peptides by 2 to 3 order of magnitudes.[324]

In this sub-project, click chemistry was applied for conjugation of alkyne-equipped ligands on the azido-equipped dextran surface. Thus, a less ordered but in return more natural orientation of the surface glycosides was provided. A microtiter plate was first decorated with an azido dextran derivative to form a glycoarray which was decorated with irregularily presented azido functionalities on its surface. This set-up should mimic the naturally occurring situation of adhesion to the glycocalyx appropriately (Figure 42, (C)). To evaluate the outcome of the polysaccharide-based glycoarray, two reference arrays were designed. One, fabricated from an azido oligoethylene glycol derivative, representing highly ordered SAM surfaces (Figure 42, (A)) and another surface was created by immobilising β-D-glucosides which carry an azido functionality at the 6-position. Immobilisation was performed via a terminal amine on the aglycone (Figure 42, (B)). Eventually, click chemistry was performed on the three microtiter plates to introduce the mannoside residues before bacterial adhesion studies were performed.

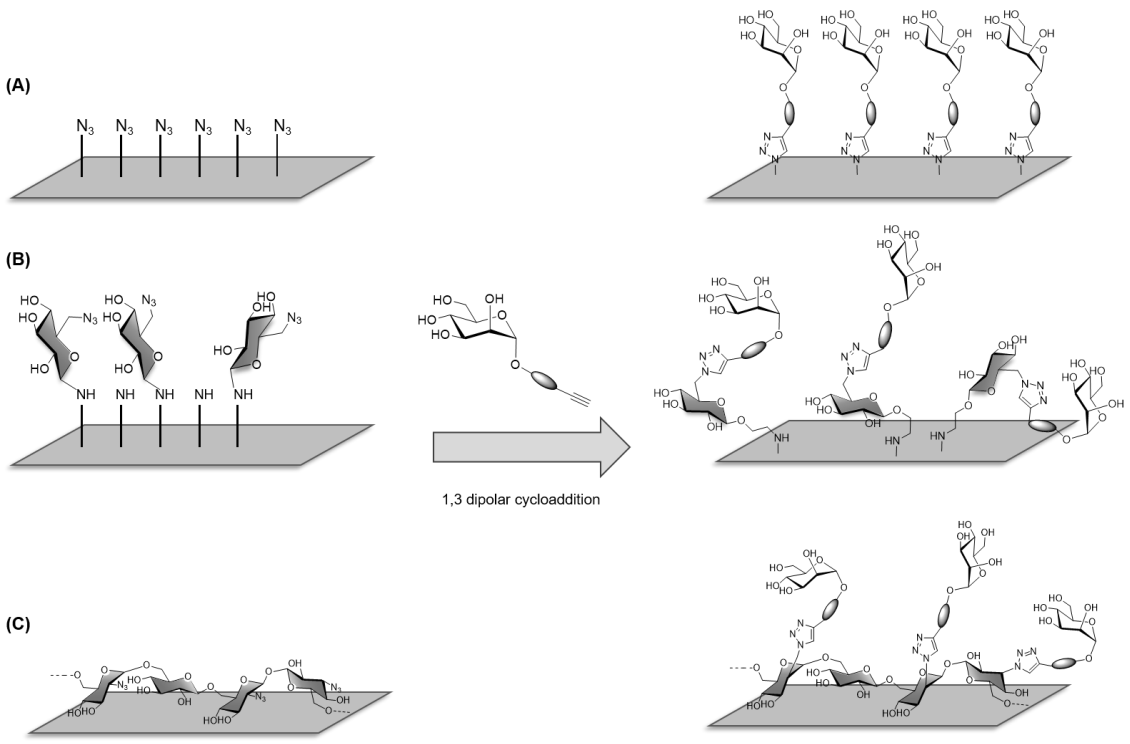

Figure 42: Schematic representation of the three microtiter plate surfaces which were prepared for this project: (A) an azido functionalisation was realised by immobilising azido-equipped triethylene glycol derivatives representing a well-ordered system; (B) immobilisation of an amino ethyl glucoside which carries an azido functionality at the 6-position to enable further ligation of mannosides; (C) immobilisation of an azido dextran derivative as a natural source coating for glycoarray formation via click chemistry.

4.2.2 Results and discussion

Azido-functionalised glucoside **69** was synthesised according to the literature[325] starting from peracetylated azidoethyl glucoside **64** leading to compound **68** in four steps. By deprotection of compound **68** with trifluoroacetic acid, the free amine **69** was obtained quantitatively (Scheme 18).

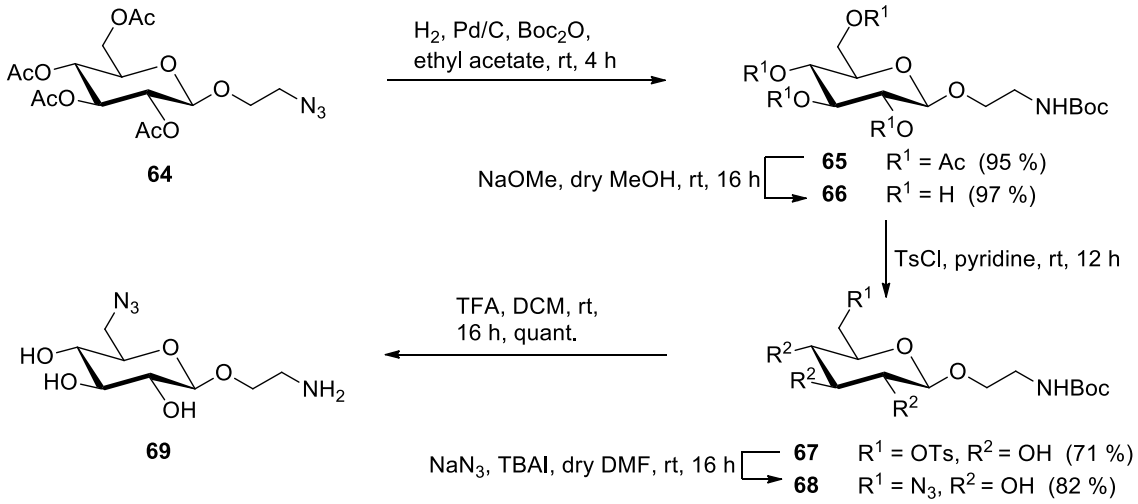

Scheme 18: Synthesis of amino-equipped glucoside **69** for the immobilisation on prefunctionalised microtiter plates.

The synthesis of azido derivatives of cellulose and starch malfunctioned since the starting material did not solve properly in appropriate solvents.[326] Thus, dextran, which features a higher solubility, was chosen since solubility is essential for the synthesis and adjacent glycoarray fabrication. Azido dextran **72** was prepared in two steps according to a procedure described by HEINZE et al.[327] using *N,N'*-dimethylacetamide (DMAA) and lithium chloride as a solvation system. Starting from dextran **70**, first, tosylation with tosyl chloride and triethylamine was performed and then a nucleophilic substitution with sodium azide gave azido dextran **72** with a yield of 80 %. (Scheme 19).

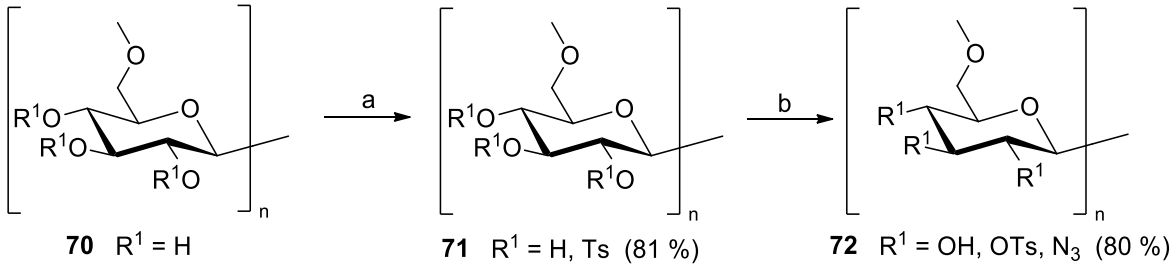

Scheme 19: Synthesis of azido dextran derivative **72**: (a) TsCl, NEt_3, dry DMAA, 0 °C, 3 h → rt, 16 h, 81 %; (b) NaN_3, dry DMSO, 100 °C, 20 h, 80 %.

Both, the tosylated dextran **71** and the azido dextran **72** could be characterised by IR spectroscopy and also NMR spectra were recorded. One NMR spectrum of compound **71** is shown in Figure 43.

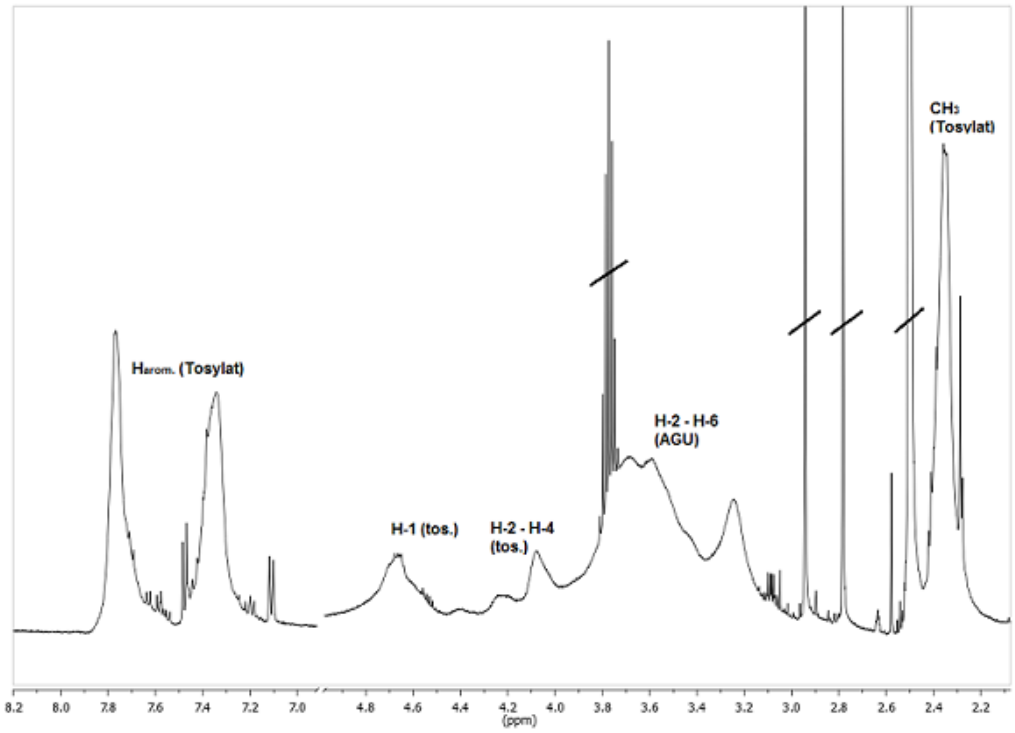

Figure 43: ^{1}H NMR spectrum of tosylated dextran **71**. Protons which are located at a C atom which also carries a tosyl group are marked '(tos.)'.

With the help of NMR spectroscopy the degree of substitution (D_s) was determined according to the formula of LEMECHKO (Formula 1)[328]. The D_s value describes the number of substituents located on one monomeric unit of a polysaccharide. For a linear polysaccharide such as cellulose the D_s can be at the most $D_s = 3$.

$$D_s \text{ (tosyl)} = \frac{I_{8.0 - 7.0 \text{ ppm}}}{I_{5.9 - 3.9 \text{ ppm}}}$$

Formula 1: Quotient for the calculation of the degree of substitution by tosyl groups based on ^{1}H NMR integrals.

According to Formula 1 the degree of substitution with tosyl groups relates to the quotient of the integrals of the four aromatic protons of the tosyl substituents ($I_{8.0\text{-}7.0 \text{ ppm}}$) and the sum of integrals of the remaining hydroxyl groups, the anomeric proton and the protons on the tosyl-substituted positions ($I_{5.9\text{-}3.9 \text{ ppm}}$). Thus, the prepared tosyl dextran **71** has a

degree of substitution of D_s(tos.) = 1.25 which is reduced to D_s(tos.) = 0.72 in **72** after substitution with sodium azide. Consequently, the D_s for azidation amounts to $D_s(N_3)$ = 0.53, that means that every second glucoside monomer of dextran carries one azido functionality. The degrees of substitution as determined with Formula 1 were confirmed by elemental analysis.

For the following modification of the dextran surface by click chemistry, the five alkyne-functionalised mannosides **75**, **79**, **83** and **86** as well as the glucoside control compound **84** were synthesised (Scheme 20 to Scheme 22). The mannoside **75** was synthesised according to a procedure published by POLÁKOVÁ et al.[329] in an overall yield of 77 %. To take advantage of the possible ππ interactions which can occur between the tyrosine gate of the FimH binding site and an aromatic aglycon of a potential ligand, a glycoside with aromatic aglycon moiety, **79**, was also prepared.[47, 330] For this, aminophenyl α-D-mannopyranoside **77** was coupled with propiolic acid using *N*,*N*'-dicyclohexylcarbodiimide (DCC) to yield compound **78** in 73 % which was then subsequently deprotected under ZEMPLÉN conditions[179] to obtain compound **79** (Scheme 20).

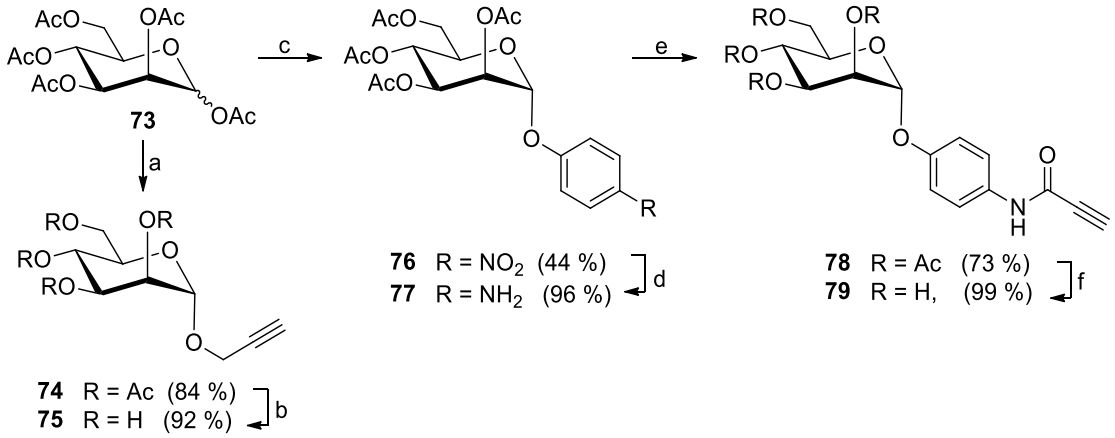

Scheme 20: Synthesis of mannose derivatives **75** and **79**: (a) propargyl alcohol, $BF_3{\cdot}Et_2O$, dry DCM, 0 °C → rt, 20 h, 84 %; (b) NaOMe, dry MeOH, rt, 16 h, 92 %; (c) *p*-nitrophenol, $BF_3{\cdot}Et_2O$, dry DCM, 0 °C → rt, 42 h, 44 %; (d) H_2, Pd/C, methanol, rt, 70 h, 96 %; (e) propiolic acid, DCC, dry DCM, rt, 16 h, 73 %; (f) NaOMe, dry MeOH, rt, 16 h, 99 %.

Since preliminary binding tests showed unspecific results, glycosides **83** and **84** were also synthesised which should suppress unspecific binding due to their biorepulsive ethylene glycol units and the glucoside **84** should also work as negative control in FimH-mediated binding. Both compounds were synthesised starting from trichloroacetimidate glycosyl donors **8** and **9**, respectively, to glycosylate 2-[2-[2-(2-propynyloxy)ethoxy]ethoxy] ethanol **20**[257] under the catalysis of boron trifluoride. This gave glycosides **81** and **82**[331]

in moderate yields (32 % and 46 %, respectively) and after ZEMPLÉN deprotection[179] the OH-free products **83** and **84** (Scheme 21).

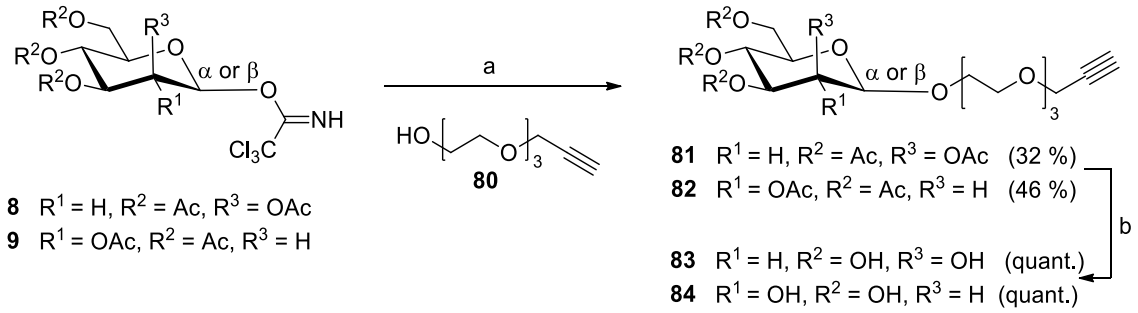

Scheme 21: Synthesis of glycosides **83** and **84**: (a) 2-[2-[2-(2-propynyloxy)ethoxy]ethoxy]ethanol **80**, $BF_3 \cdot Et_2O$, dry DCM, 0 °C → rt, 20 h, 32 % (**81**), 46 % (**82**); (b) NaOMe, dry MeOH, rt, 16 h, quant.

The trivalent glycocluster **86** was also synthesised to investigate possible multivalency effects within this assay system. The previously reported trivalent glycocluster **26** (cf. chapter 4.1.2) which carries an amino functionality at its focal point for further functionalisation, was subjected to amidation with propargyl chloroformate making carbamate **85** available in a yield of 42 %. After ZEMPLÉN deprotection,[179] the trivalent cluster mannoside **86** was obtained in quantitative yield.

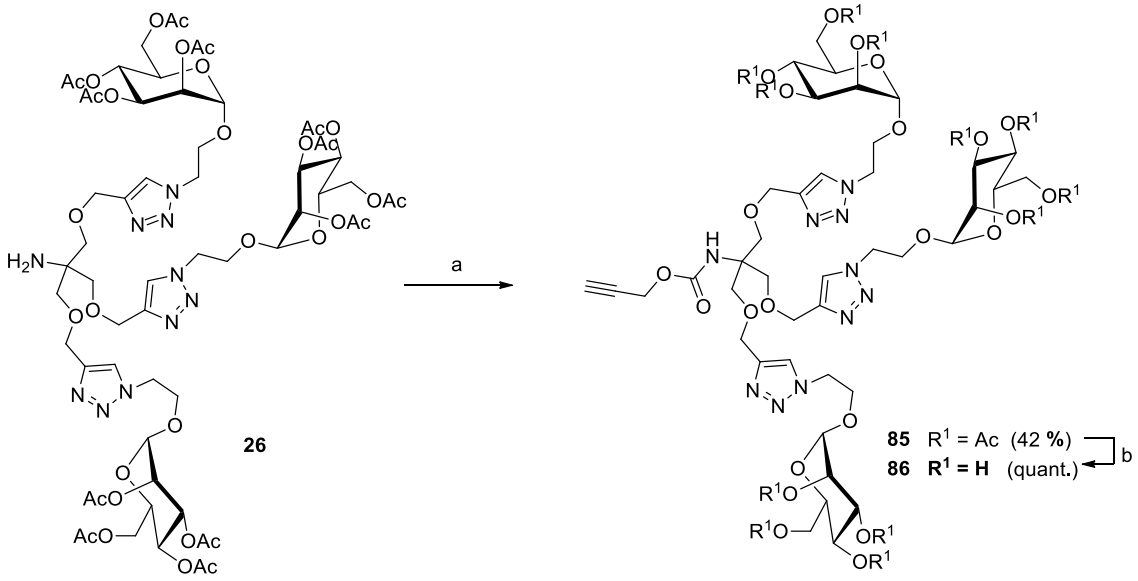

Scheme 22: Synthesis of trivalent derivative **86**: (a) 1. NaOMe, dry MeOH, rt, 16 h, quant.; 2. Na_2CO_3, propargyl chloroformate, H_2O/1,4 dioxane, rt, 60 h, 3. Ac_2O, pyridine, rt, 4 h, 42 %; (b) NaOMe, dry MeOH, rt, 16 h, quant.

For glycoarray formation commercially available preactivated Nunc polystyrene 96 well microtiter plates were used. After incubation with amines **69** and **87** and polysaccharide **72**, respectively, and incubation with ethanolamine to block the unreacted surface (polyvinylalcohol in case of surface **C**) surfaces were prepared with azido groups for further functionalisation by copper (I)-catalysed click chemistry. Therefore, solutions of the glycosides **75**, **79**, **83**, **84** and **86** in PBS buffer with serial dilution were added to the microtiter plates followed by solutions of copper(I)sulphate and sodium ascorbate in PBS buffer which were also added in serial dilution. Click reaction on surface was performed at 37 °C at 100 rpm for 3 hours. Afterwards washing steps with PBST and PBS removed unreacted glycoconjugates followed (Scheme 23).

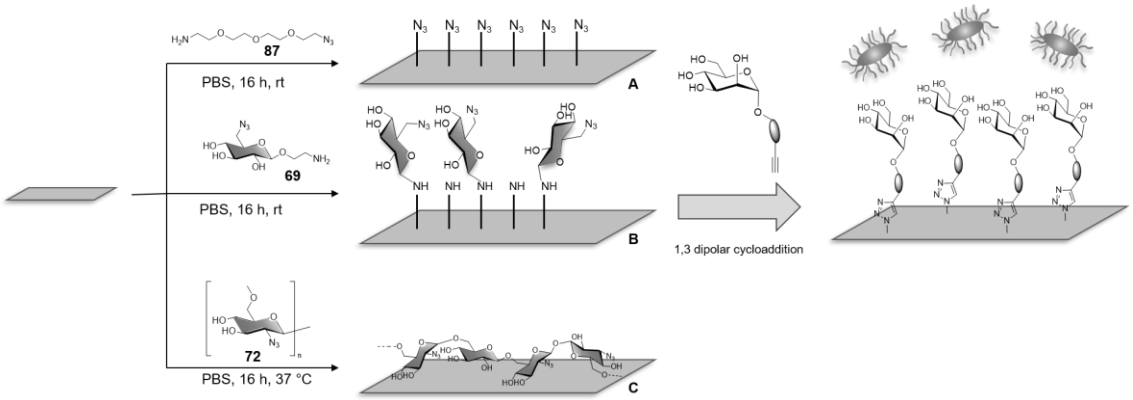

Scheme 23: Overview of the three different prepared azido-functionalised surfaces A, B and C. After decoration of all three surfaces with α-D-mannosides, bacterial adhesion studies were performed.

Finally, the fabricated glycoarrays were subjected to bacterial adhesion studies. Microtiter plates were incubated with type 1 fimbriated *E. coli* (PKL1162 strain) and non-adhered bacteria were washed away afterwards. Since the PKL 1162 strain contains the GFP (green fluorescent protein) gene, bacterial adhesion was quantified by fluorescence read out in the end.[239, 270] The results of adhesion studies are depicted in Figure 44, Figure 45 and Figure 46.

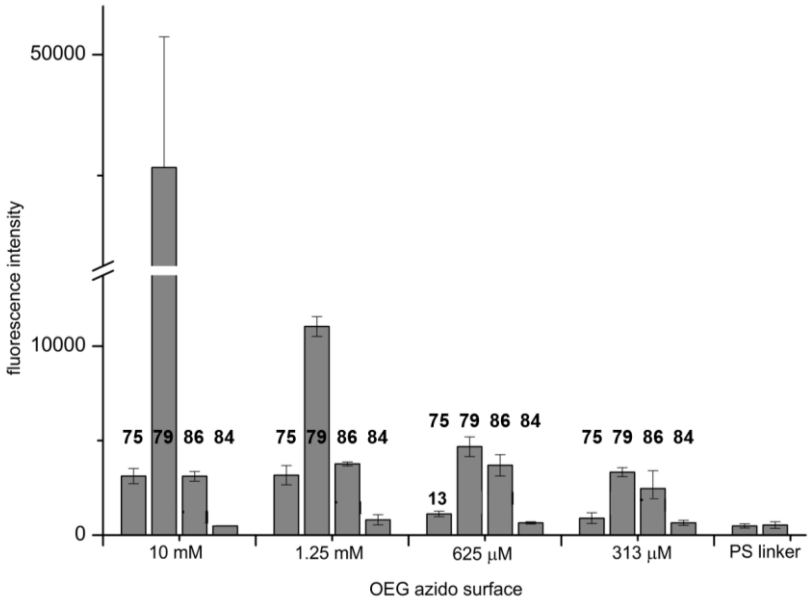

Figure 44: Bacterial adhesion (quantified by fluorescence intensity) to glycosylated surface **A** fabricated by click chemistry as measured with the described assay. Three mannoside derivatives **75**, **79** and **86** were tested in comparison to a glucose derivative **84**. Given concentrations are based on solutions of the alkyne-functionalised glycosides which were used for the 1,3-dipolar cycloaddition. Error bars are standard deviations generated from triplicate values on one plate.

As a proof of successful array formation, an almost six times higher adhesion was measured for mannoside **75** in comparison to glucoside **84** employed at a concentration of 10 mM in case of surface **A**. The adhesivity of mannoside **75** decreases with concentration. As expected glucoside **84** shows just little fluorescence which is independent of the concentration and in the range of the unmodified plate surface ('PS') and the only with linker **87** functionalised surface ('linker'). Also compound **79** shows the expected decrease of adhesivity with lower concentrations used for sugar decoration of the surface. Nevertheless, due to its aromatic aglycon the adhesive potential of compound **79** is 15 times higher than in case of compound **75**. With the trivalent cluster **86**, the adhesion is just slightly higher than for the monovalent analogue **75** and hence **86** does not show the expected multivalency effect in this system.

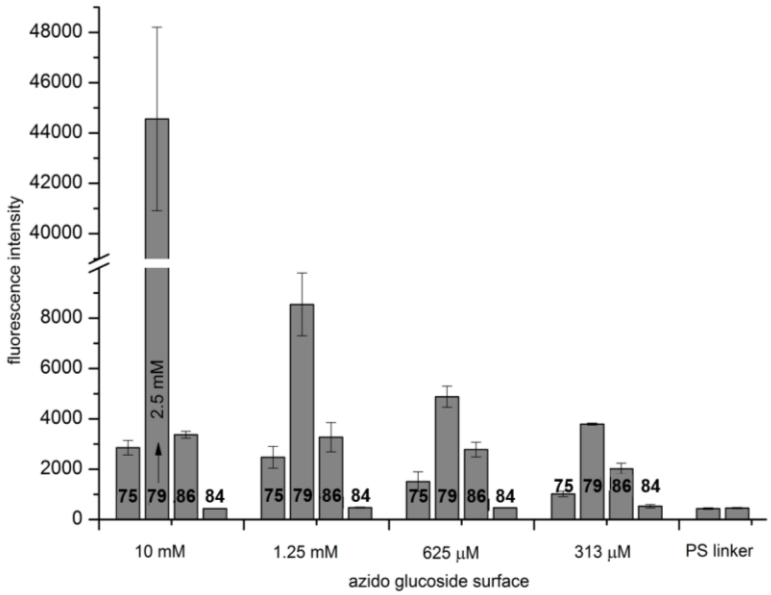

Figure 45: Bacterial adhesion (quantified by fluorescence intensity) to glycosylated surface **B** fabricated by click chemistry as measured with the described assay. Three mannoside derivatives **75**, **79** and **86** were tested in comparison to a glucose derivative **84**. Given concentrations are based on solutions of the alkyne-functionalised glycosides which were used for the 1,3-dipolar cycloaddition. Error bars are standard deviations generated from triplicate values on one plate.

Also in the case of surface **B** which is functionalised with azido glucoside **69** to allow subsequent click chemistry with alkyne-functionalised glycosides for glycoarray formation, a 15 times higher adhesivity for aromatic mannoside **79** than for mannoside **83** was observed - even though compound **79** was compared with a reduced concentration of 2.5 mM to compounds **83**, **84** and **86** in concentrations of 10 mM. Again, a concentration dependency as for the adhesion experiment on surface **A** was observed and also the trivalent cluster **86** shows a similar behaviour in this assay set-up.

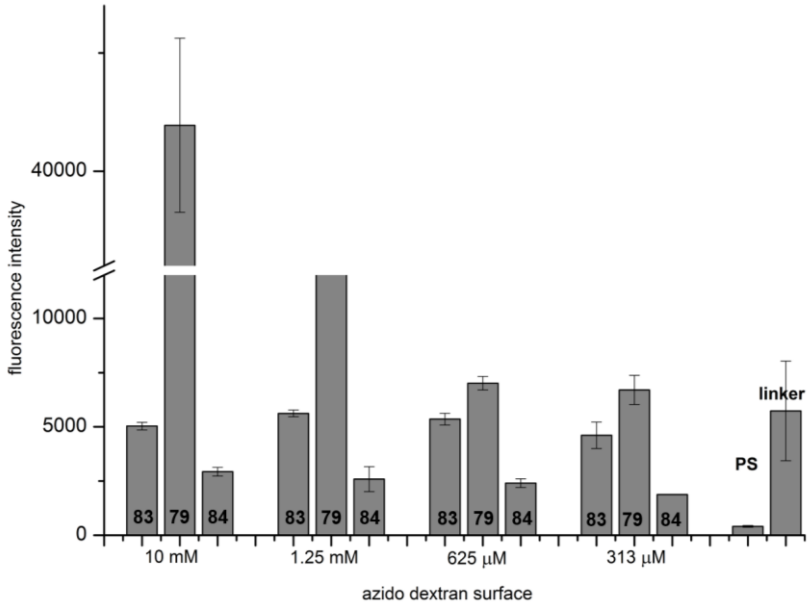

Figure 46: Bacterial adhesion (quantified by fluorescence intensity) to glycosylated surface **C** fabricated by click chemistry as measured with the described assay. Two mannoside derivatives **83** and **79** were tested in comparison to a glucose derivative **84**. Given concentrations are based on solutions of the alkyne-functionalised glycosides which were used for the 1,3-dipolar cycloaddition. Error bars are standard deviations generated from triplicate values on one plate.

In case of surface **C**, an unexpected and likewise undesired high adhesivity of the surface which is just covered with azido-functionalised dextran **72** was observed. To suppress such unspecific binding, ethylene glycol derivatives **83** and **84** were used. It was verified that the cycloaddition occurred on surface because glucoside **84** led to reduced adhesion so that consequently unspecific binding can be neglected. Ethylene glycol-equipped mannoside **83** shows on the contrary higher adhesion than compound **84**. Aromatic mannoside **79** shows adhesivity in similar range to surfaces **A** and **B**, merely reduced by 10 % which is remarkable since surface **C** has a considerably reduced density of azido groups on its surface. Whereas surfaces **A** and **B** resulted from modification with 20 mM solutions, just 1.2 mg/mL of compound **72** was used for this array surface**.** That conforms to a concentration of 5 mM. Additionally, one has to keep in mind the degree of substitution of $D_s(N_3) = 0.53$ which means that just every second monomer unit of dextran carries an azido group.

4.2.3 Conclusion

Different glycoarray surfaces were successfully fabricated by 1,3-dipolar cycloaddition of alkyne-functionalised sugar ligands on various azido-functionalised microtiter plate surfaces leading to glycoside-decorated surfaces for bacterial adhesion studies. Whereas surfaces fabricated with azido-equipped triethylene glycol derivatives **87** (Scheme 23, (**A)**) and amino ethyl glucoside **69** (Scheme 23, (**B)**), respectively -which were chosen as model systems for the more complex dextran surface- showed rather similar behaviour, the more complex dextran surface (Scheme 23, (**C**)) showed a stronger adhesivity. This observation confirms that a potent surface for adhesivity studies was developed. Thus, this finding suggests that the objective of this sub-project, that is using a complex unordered carbohydrate environment for cell adhesion studies, indeed results in potent adhesive surfaces which might reflect the properties for the unordered natural glycocalyx better than glyco-SAMs, for example.

5 Labelling FimH: Towards the photochemical control of carbohydrate recognition

5.1 Introduction

5.1.1 Switching biological function

Already back in 1979, the Nobel laureate FRANCIS CRICK dreamt of a tool to manipulate the brain by writing about "a method by which all neurons of just one type could be inactivated, leaving the others more or less unaltered"[332-333] and in 1999 he suggested light for the control of cellular activation accurately as to space and time.[334-335] Those ideas are nowadays realised in the field of optogenetics.[333, 336] In the meantime a whole research field deals with the use of light to control cells (optogenetics) and molecular function (molecular machines).[337-338] Photosensitive molecules which allow to reversibly manipulate a particular system are called photoswitches (cf. chapter 3.1.2) and found applications in whole organisms and cells but also in biological chemistry for the manipulation of, for example, DNA and RNA [339-340], enzymes[341-343], receptors, channel proteins and also smaller peptides.[344-346] To obtain photoresponsive proteins, they are modified with a photoswitchable unit by chemical ligation. In many cases azobenzene derivatives are used as photoswitches due to their excellent (photo)chemical properties.[101] In the protein field, especially protein folding and protein-ligand interactions were photoswitched.[344, 347-349] For example, TRAUNER and coworkers introduced azobenzene derivatives for light-triggered opening and closing of ion channels[95, 350-353] *in vitro* as well as *in vivo* (Figure 47).[347]

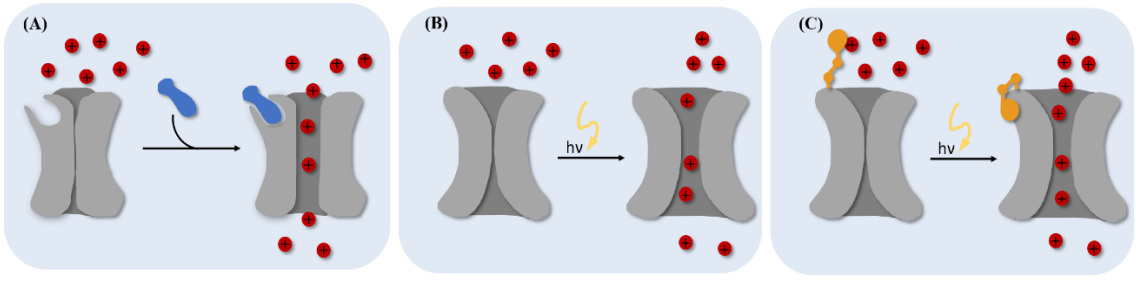

Figure 47: Different approaches to control protein function: (A) Naturally occurring ion channels which can be opened by neurotransmitter (blue ligand) activation; (B) mimicry of neurotransmitter-activated ion channels which can be triggered by inserted light-activatable channelrhodopsins; (C) mimicry of neurotransmitter-activated ion channels which can be triggered by attached light-responsive azobenzene moieties.[335, 354]

5.1.2 Chemical protein modification

Proteins can be modified in their native form and in addition, unnatural amino acids (UAA) can be introduced into proteins to facilitate their modification. In any case, the modification should be protein-specific and site-selective. Additionally, control over the number of occurring modifications is desirable. For site-selective modifications, the introduction of UAA can be advantageous. Commonly employed UAA have their side chain modified with a bioorthogonal functionality such as azides (azidohomoalanine, Aha), alkynes (homopropargylglycine, Hpg) or halogens (*p*-iodophenylalanine, *p*-IF).[355-357] Such modifications, for example, allow for STAUDINGER ligation[295, 298], click chemistry (CuAAC)[299] or SUZUKI-MIYAURA cross coupling reactions (Figure 48).[358]

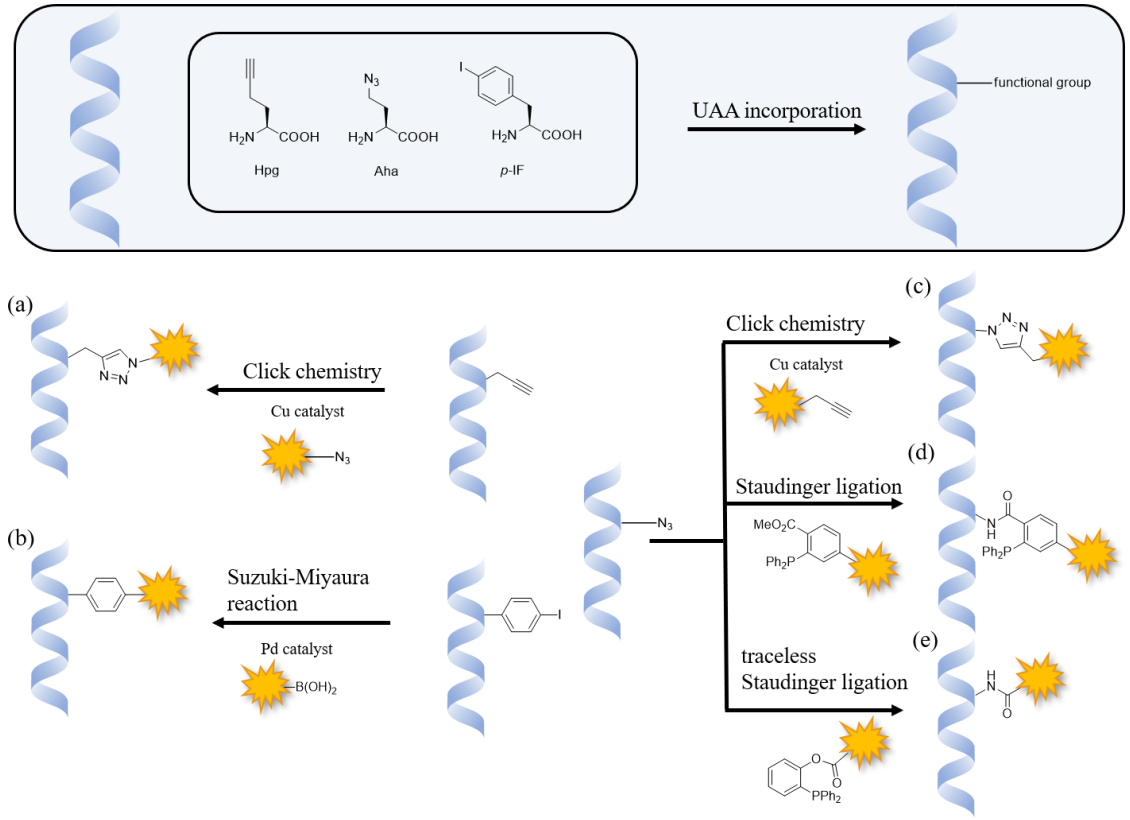

Figure 48: Bioorthogonal ligation methods enabled by the incorporation of unnatural amino acids. (a) click chemistry on an alkyne-equipped protein, (b) SUZUKI-MIYAURA coupling, (c) click chemistry on an azido-equipped protein, (d) STAUDINGER ligation, (e) traceless STAUDINGER ligation.[359]

As the synthesis of UAA-modified proteins requires some know-how and effort,[359-360] the modification of natural proteins is also desirable. In addition, in unmodifed proteins, their natural form and function remains unimpaired. Hence, their posttranslational modification is attractive for many applications from biochemistry to medicine.[361] Ligation chemistry which is suited for the modification of natural proteins targets amino

acids such as lysine, cysteine and tyrosine. Lysine is widely spread in proteins and therefore can be easily addressed for applications which do not require a single or a site-specific modification.[296-297] Cysteine on the contrary is suited for single modifications due to its minor abundance in proteins.[362] Numerous successful ligation methods targeting at cysteine can be found in the literature.[363-366] Moreover, cysteine can be introduced at a favoured position of a protein by site-directed mutagenesis. However, ligation via cysteine is limited to *in vitro* experiments due to disulfide formation which could occur with free thiols within cell systems.

An additional methodology for the posttranslational modifications of endogenous proteins uses affinity-driven methods. First attempts were reported in the 1960s when matching ligands were equipped with a reactive group, e.g. a diazonium or an iodoacetamide group. The target protein was incubated with the applicable ligand for covalent bond formation after complex formation at the close proximity of the ligand binding site or the active site of an enzyme, for example.[367-369] In 2012, HAMACHI and coworkers started to develop new methods for the traceless modification of proteins, which preserve their function after labelling.[370] HAMACHI's work and other methods for site-specific modification of proteins can be classified into two types, which are here referred to as type I reactions and type II reactions. Type I reactions (exchange/cleavage reaction type) are based on ligands which are equipped with a predetermined breaking point. Type II reactions (catalyst tethering type) embrace strategies for traceless protein modification using a ligand-tethered catalyst (Figure 49).[370]

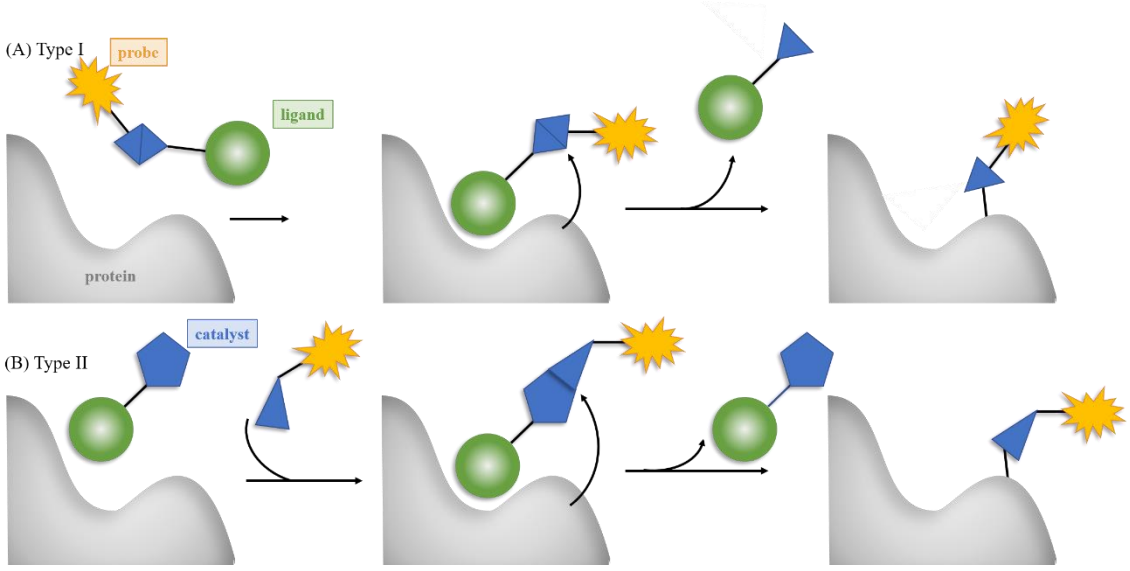

Figure 49: Schematic representation of traceless affinity-based protein labelling. (A) Type I (exchange/cleavage type): The probe is attached to a high affinity ligand via a predetermined breaking point. (B) Type II (catalyst tethering type): A ligand-tethered catalyst fosters the reaction with the probe.[370]

The first generation of the exchange/cleavage type reactions (type I) is called post-photoaffinity labelling modification (P-PALM). Firstly, a prepared high-affinity ligand binds to the active site, secondly the reaction of, for example, a photoreactive diazirine moiety which is attached on the ligand via, for example, a disulfide bond can occur in the proximity of the ligand binding site. Finally, the disulfide bond is cleaved and the ligand is released from the active site. The resulting thiol moiety can react with an electrophile which is equipped with the desired moiety (hereinafter referred to as 'probe'). It should be noted however, that the use of disulfides is limited to applications *in vitro* and additionally laborious purification is required to yield the targeted protein (Figure 50).[371]

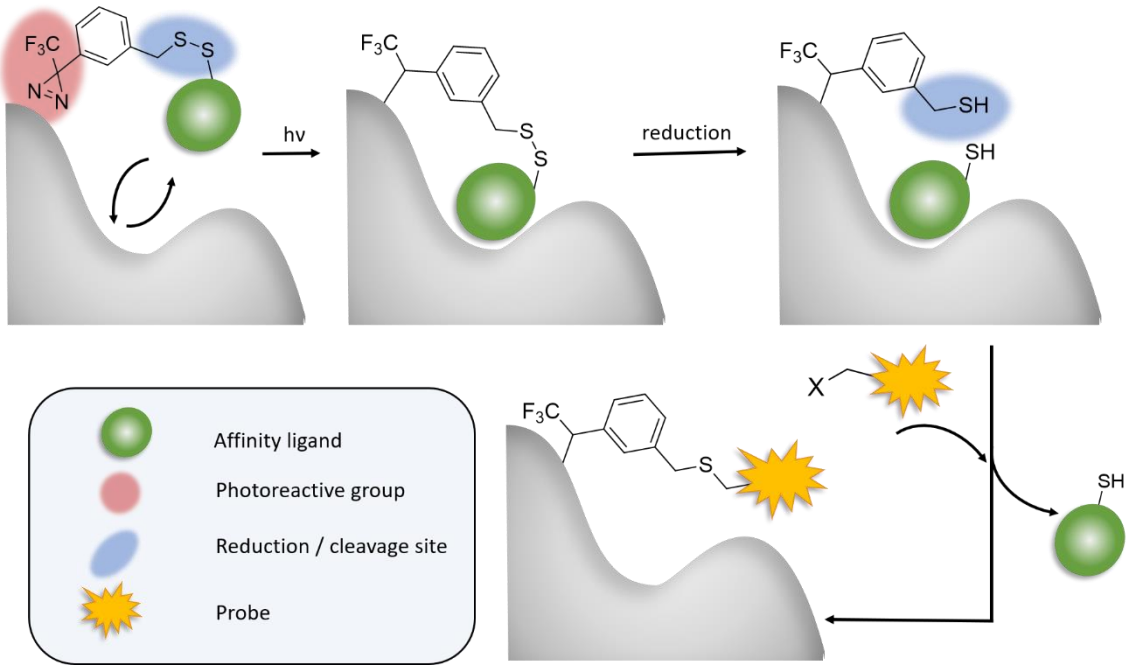

Figure 50: Schematic representation of the P-PALM (post-photoaffinity labelling modification) method for protein labelling.[370]

The second-generation protein modification is called post-affinity labelling modification (P-ALM). Here, the same principle is applied as in P-PALM, but the photoreactive site is replaced by a chemically reactive moiety such as an epoxide. After formation of the protein-ligand complex, the epoxide can react with a nucleophile in the proximity of the ligand binding site. For P-ALM, the disulfide linkage of the ligand is exchanged by a hydrazone unit which can be substituted by aminooxy or hydrazine derivatives to release the ligand after successful labelling of the protein.[372-374] However, also this modified protein modification is not fully bioorthogonal and hence not suited for *in vivo* applications (Figure 51).

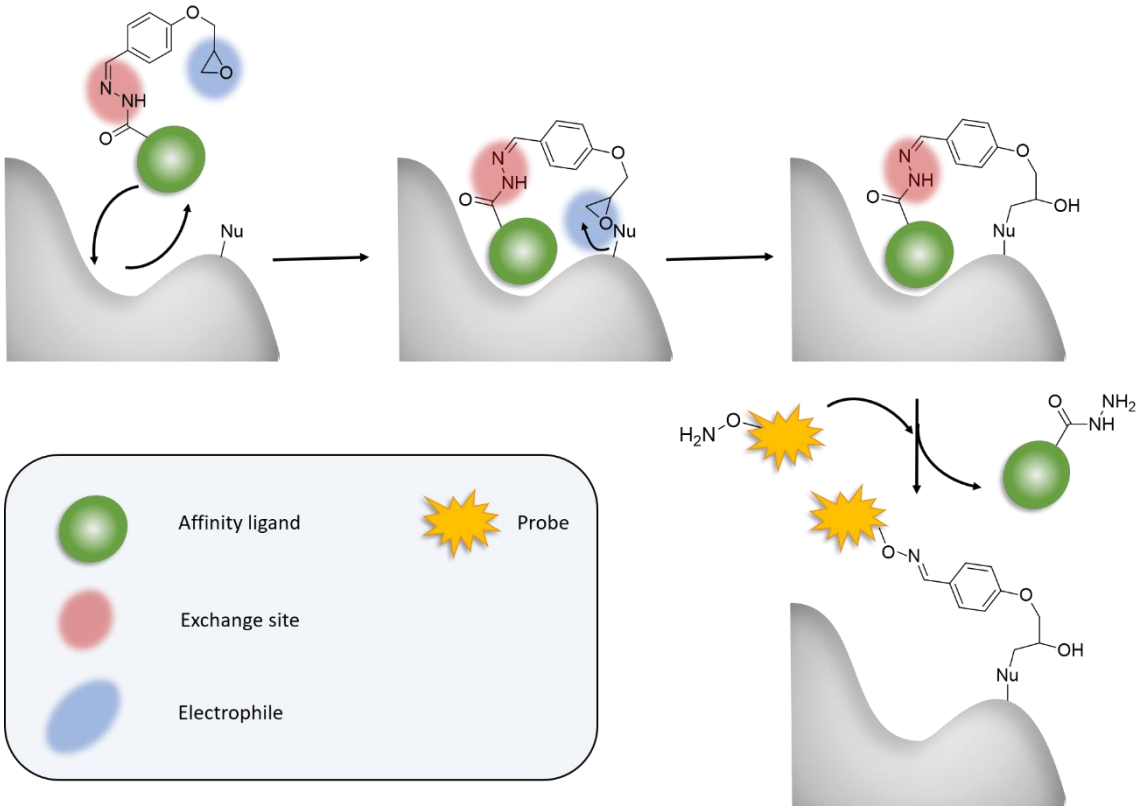

Figure 51: Schematic representation of the P-ALM (post-affinity labelling modification) method for protein labelling.[370]

The question of bioorthogonality was also addressed by HAMACHI and coworkers. They established a new way of traceless chemical labelling which they called ligand-directed "tosyl" (LDT) chemistry. In this case, the ligand has two functions, it operates as linker between the probe and the ligand and as the reactive group. The phenylsulfonate ('tosyl') can react with a nucleophilic amino acid in a S_N2-type reaction and hence, after successful modification of the target protein the ligand can be removed (Figure 52).[375-377]

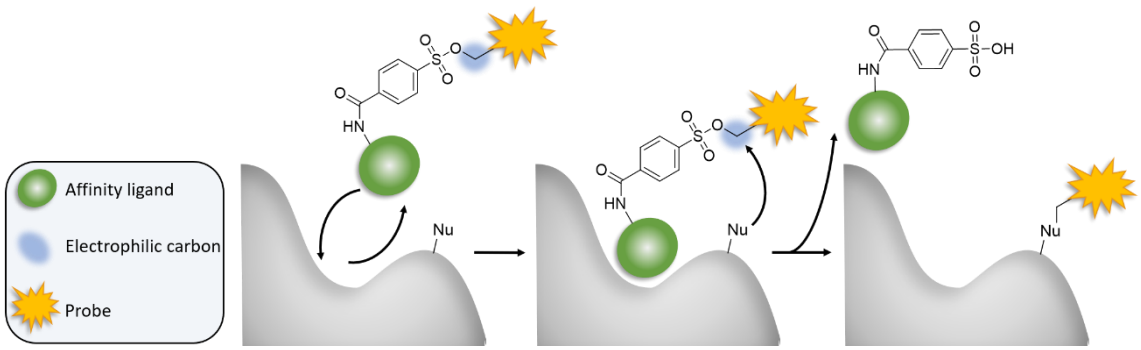

Figure 52: Schematic representation of the LDT (ligand-directed tosyl) chemistry for protein labelling.[370]

Type II reactions are strategies for traceless protein modification in which a ligand-tethered catalyst is used. HAMACHI and coworkers used 4-dimethylaminopyridine (DMAP) as acyl transfer catalyst, ligated to the protein ligand.[375] The probe can then be introduced as a thioester, which reacts with the DMAP moiety of the ligand and the resulting conjugate can be attacked in the next step by an endogenous nucleophilic protein residue to result in the labelled protein; whereas the ligand is released from the binding site (Figure 53).[378]

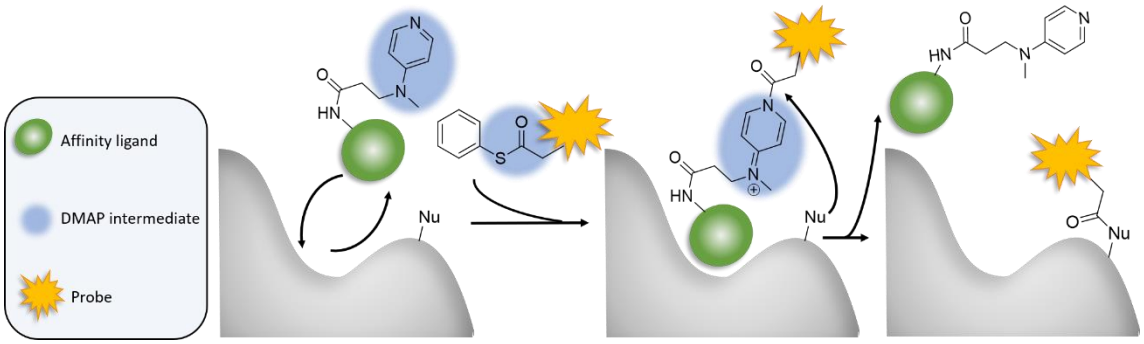

Figure 53: Schematic representation of HAMACHI's affinity-guided DMAP-catalysed protein labelling.[370]

This strategy for affinity-driven protein labelling was already earlier used by F. Beiroth[379]and was also employed here for labelling of FimH. Based on work by HAMACHI and coworkers on the graded reactivity of different thioesters (cf. Figure 54),[380] phenylthioesters were employed in the current project.

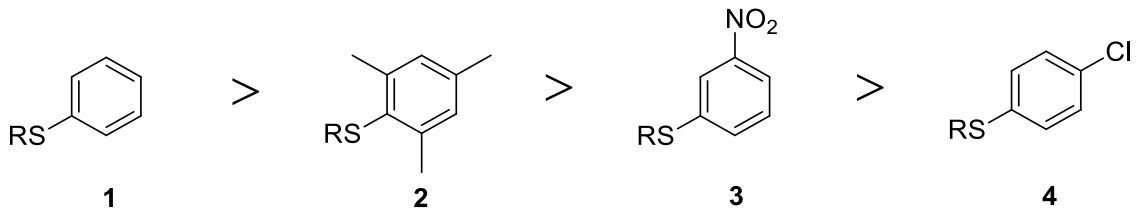

Figure 54: Graded reactiviy of thioesters **1**-**4** as studied by HAMACHI and coworkers (for specific residues R see literature).[380]

5.2 Project idea

It was the objective of this sub-project to utilise HAMACHI's DMAP-mediated affinity-guided method for protein labelling for the photochemical control of the function of FimH. An azobenzene moiety attached at the proximity of the carbohydrate binding site of FimH would act as a photosensitive 'gate keeper' molecule, allowing to block and open

the sugar binding site of the bacterial lectin on demand. This would involve the perspective to control bacterial cell adhesion (Figure 55).

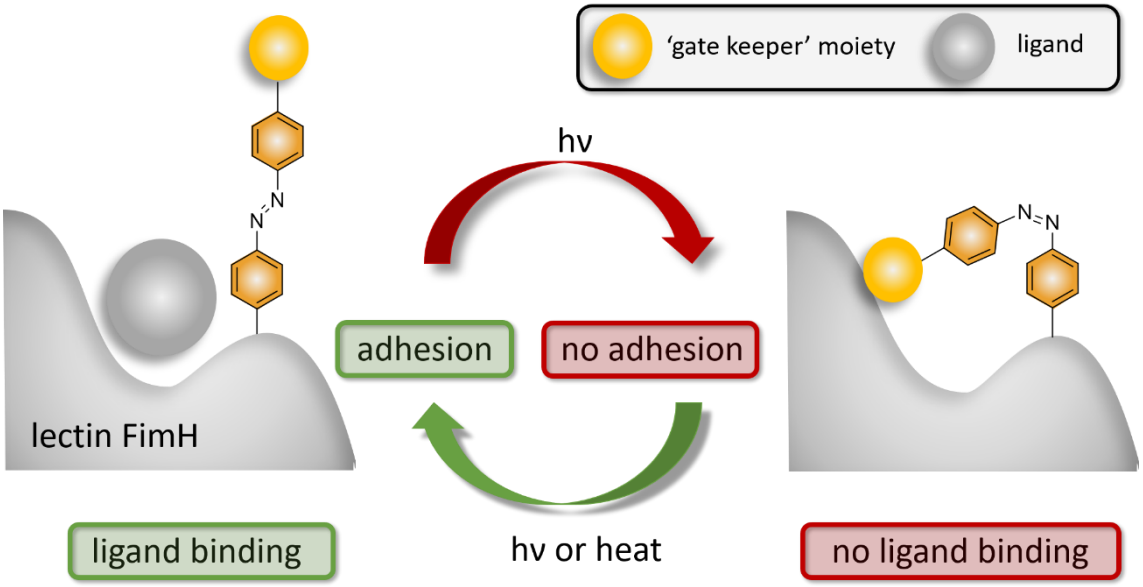

Figure 55: Site-directed labelling of the lectin FimH to enable photocontrol of cell adhesion: The azobenzene 'gate keeper' moiety is meant to leave the binding site open in its *E*-state and close it in its *Z*-state.

HAMACHI's method is based on 4-dimethylaminopyridine (DMAP) as an acyl transfer catalyst.[378] Since the DMAP-catalyst is linked to a high-affinity ligand for FimH, the addition of an azobenzene thioester will lead to an activated pyridinium intermediate which is oriented close to the carbohydrate binding site. Thus, the activated azobenzene derivative can be transferred onto an appropriate nucleophilic amino acid in the proximity of the FimH carbohydrate binding site. After successful transfer of the azobenzene moiety to the lectin, the DMAP ligand can be removed from the binding site to release the binding site. Thereafter, the opening and closing of the binding site can be realised by a photoinduced isomerisation between the *E*- and the *Z*-state (Scheme 24).

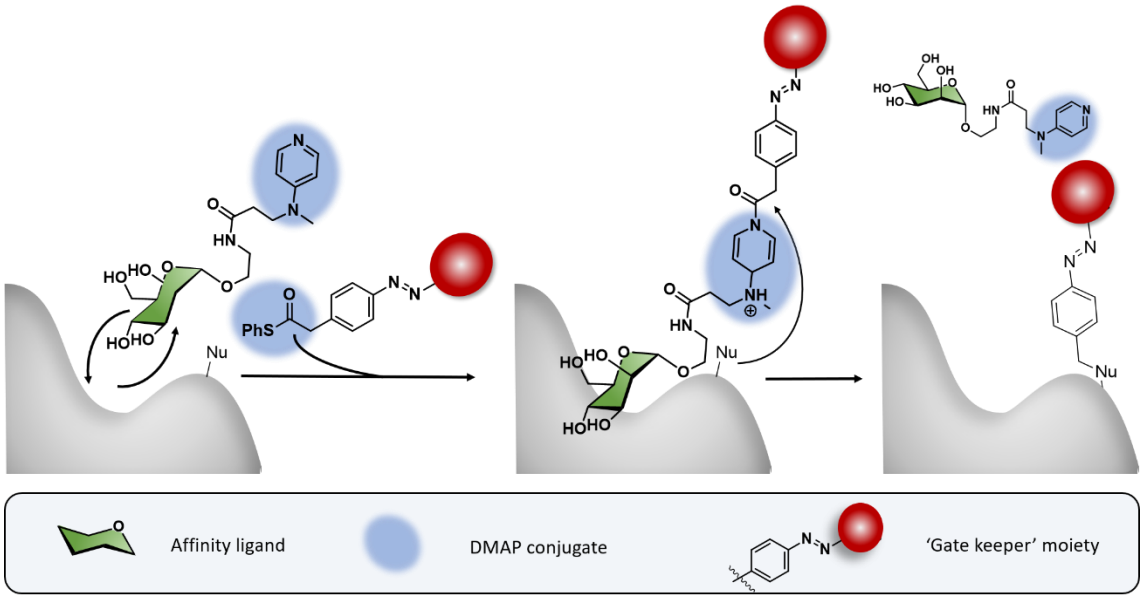

Scheme 24: FimH carbohydrate binding function could become photoswitchable by the site-specific attachment of a photosensitive 'gate keeper' molecule at the entrance of the binding site.[379]

F. BEIROTH[379] and I. STAMER[381] started this project in the LINDHORST group by the synthesis and partial evaluation of a couple of DMAP affinity ligands and thioesters.

First, high affinity α-D-mannoside ligands equipped with a DMAP moiety as acyl transfer catalytic part were required. The higher the affinity of the directing DMAP ligand the greater the possibility to suppress undesired side reactions which could for example occur on serine residues which are present on the protein surface of FimH away from the binding site. Two such derivatives, **5** and **6** (Figure 56) were introduced by F. BEIROTH in her PhD thesis.[379] Docking studies with Glide as implemented in the Schrödinger software[382] confirmed the suitability of the ligands for the purpose of the site-directed labelling.[379] Both ligands are soluble in water, so that the reaction can be performed under physiological conditions.

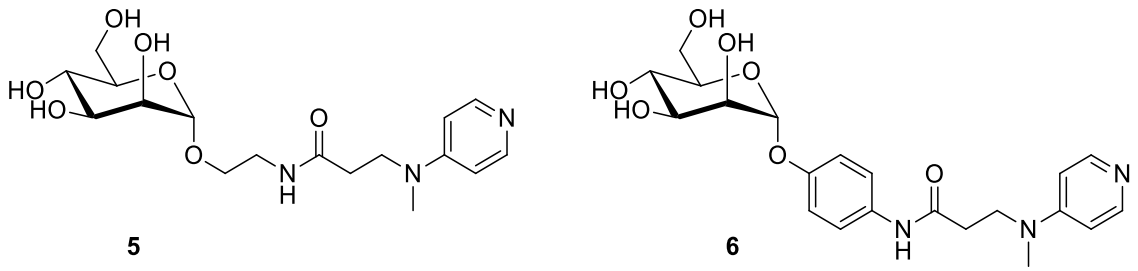

Figure 56: DMAP-functionalised mannosides **1** and **2** which were synthesised by F. BEIROTH.[379]

Mannoside **5** carries an aromatic moiety within the aglycon which could induce accessory hydrophobic ππ interactions with the tyrosine gate of the FimH binding site and thus also may support an optimal orientation of the reactive site at the FimH binding site.

In this thesis, the objective was to expand the collection of thioesters for site-specific FimH labeling and to investigate their properties. Different thioester derivatives were discussed as leaving groups for the DMAP-catalysed acylation by HAMACHI and coworkers.[380]

To allow protein modification under physiological conditions, some requirements must be met, such as water solubility. In addition, it would be desirable to modify FimH in a way to allow switching of function by visible light (cf. chapter 6). Furthermore, there are some requirements for structure and size of the 'gate keeper' moiety to allow an optimal closing of the binding site. First and foremost, the 'gate keeper' precursor should boast a perfect shape which enables the reversible opening and closing of the binding site due to its sterical hindrance in the *Z*-state. Also, it could be advantageous if the 'gate keeper' moiety shows some affinity for the protein. Thus, affinity must be ideally fine-tuned to trigger site-specific binding on the one hand, and to allow for release of this moiety from the binding site upon Z→*E* isomerisation on the other hand. With respect to these considerations, three glycoside 'gate keeper' molecules were designed. All designed thioester derivatives were evaluated by molecular docking studies and the switching process was simulated. The calculations were performed in parallel with the synthesis since they are rather time-consuming.[185, 383] Additionally the photochemical properties of the azobenzene derivatives were determined in order to estimate the switching performance. The ultimate goal is the testing of the switchable adhesion which could be detected by an assay system and observed by NMR studies. When all parts of this demanding project can be accomplished (synthesis, efficient switching, protein labelling) FimH-mediated bacterial adhesion could be controllable. In the future, this approach could be employed for other lectins, which could then be used as photoswitchable diagnostic tools or targeted drug release could be realised.

5.3 Results and discussion

5.3.1 Determination of ligation site

Three amino acids in FimH are eligible for this site-directed approach, namely tyrosine 48, tyrosine 137 and threonine 51 (Figure 57). Arginine 98 can also react as a nucleophile in dependence of the pH. Since the DMAP-tethered labelling strategy requires a pH in the range of 8.0, arginine will not be targeted as at pH 8 it exists in its protonated (guanidinium) form due to a pK_a value of 12.48.

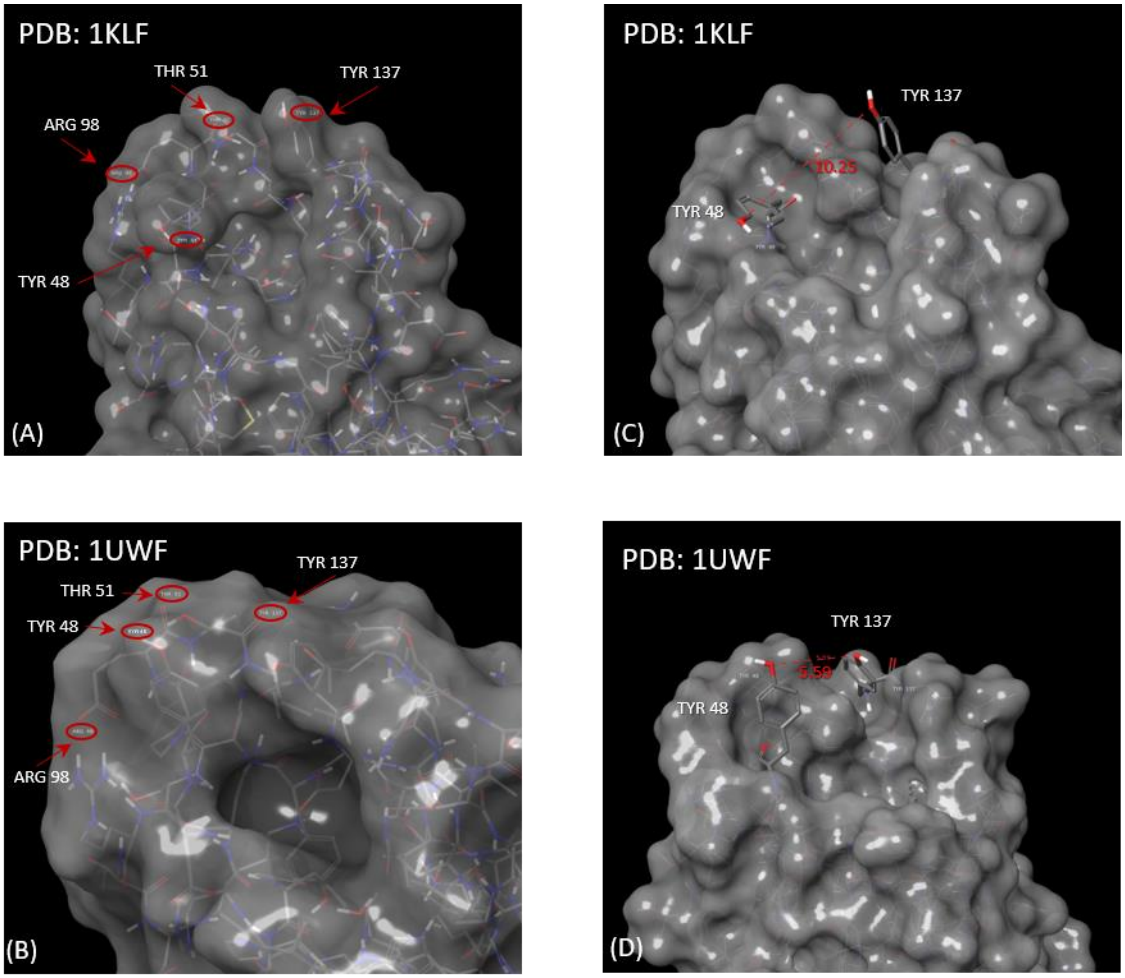

Figure 57: Surface representation of the lectin FimH in the open gate conformation (A, PDB code: 1KLF) and closed gate conformation (B, PDB code: 1UWF). Nucleophilic residues in proximity of the binding site are marked in red. The denotation open gate and closed gate conformation, respectively, is based on the two known crystal structures, 1KLF and 1UWF. In the 1KLF conformation the two tyrosine moieties at the binding site have a major distance (10.3 Å), leaving the binding site open and in the 1UWF conformation the two tyrosine residues have a minor distance (5.6 Å) resulting in a shielding of the binding site.

In addition to DMAP-activated mannosides, appropriate azobenzene-based ‘gate keeper’ molecules are required. Whereas the *para*-position of the azobenzene derivatives is

allocated to the thioester moiety for ligation, the *para'*-position can be modified for optimal closing and opening of the FimH binding site. The suitability of 'gate keeper' molecules can be evaluated by molecular modelling. The results of the molecular modelling are discussed in chapter 5.3.5**.**

5.3.2 Synthesis of thioester-equipped 'gate keeper' precursors: non-glycoside derivatives

Thioester derivatives were synthesised using thiophenol, following HAMACHI's work.[378] In the first place a library of thioesters was designed which showed different sterical dimensions (Figure 58).[379]

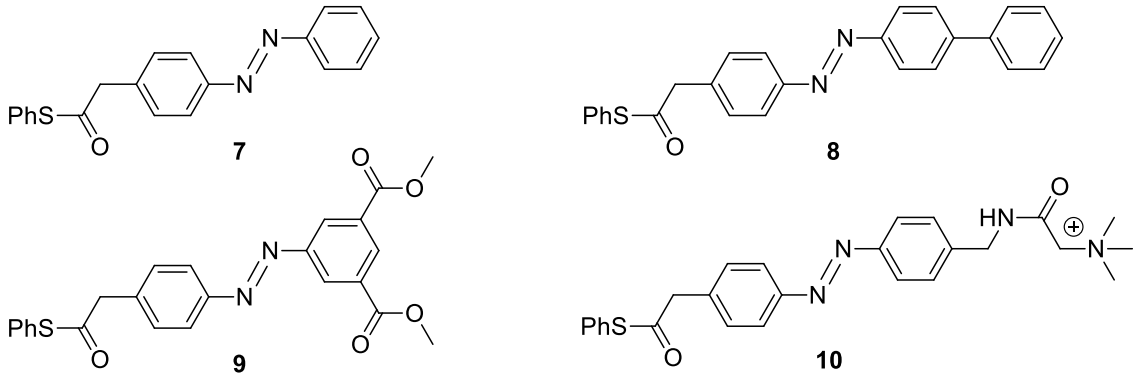

Figure 58: Four thioester derivatives **7**-**10** had been designed by F. BEIROTH which varied in the bulkiness of the substitution of the terminal phenyl ring as well as in polarity since compound **10** is positively charged.[379]

Compounds **7** to **9** were synthesised and isolated as pure material whereas the cationic derivative **10** had just been detected by MALDI MS spectroscopy.[379] To expand the library of sterically different thioesters, SUZUKI-MIYAURA coupling was employed to devise new 'gate keeper' precursors with a backbone similar to compound **8**. The advantage of 'gate keeper' molecules with a biphenyl residue is that the aromatic ring of the biphenyl unit can interact with the tyrosine residues Tyr48 and Tyr137 at the entrance of the binding site via ππ interactions. ππ Interactions might favourably direct a 'gate keeper' molecule in its *Z*-state to block the binding site. Thus, four thiophenol derivatives **11 12**, **13** and **14** shown in Figure 59 were designed with a biphenyl moiety. In addition, all four thioesters shown in Figure 59 comprise hydrogen bond acceptors and compounds **11** and **13** also contain hydrogen bond donors. Phenylpyridine derivatives **12**

and **14** vary in the orientation of the potential hydrogen bond acceptors. The different affinities of the 'gate keeper' moieties **11-14** towards the lectin binding site resulting from the different patterns of hydrogen bond acceptors and donors was evaluated by molecular modelling.

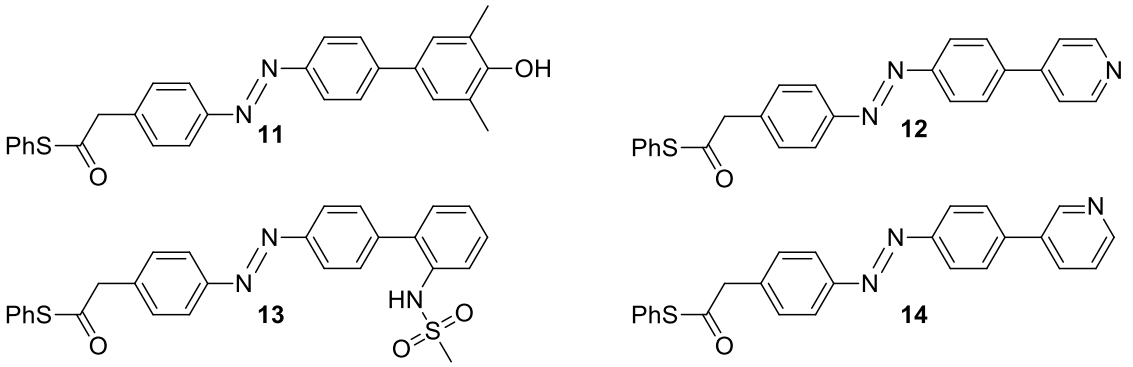

Figure 59: Four new thioester derivatives **12** to **14** which have a biphenyl unit in common but vary in their steric demand as well as in the orientation of potential hydrogen bond acceptors (**12** and **14**).

All four compounds **11** to **14** were synthesised employing azobenzene precursor **25** which is equipped with an iodine substituent which allows SUZUKI-MIYAURA coupling with organoboronic derivatives.[384] SUZUKI-MIYAURA coupling leads to carbon-carbon bond formation between aryl or alkylhalogenides, respectively, with organoboron compounds.[385-386] The iodine-substituted compound **25** was chosen since iodo-equipped compounds are the most reactive electrophilic reagents for SUZUKI cross coupling reactions.[386] Azobenzene **25** was synthesised starting from amines **17** and **20**, respectively, which were synthesised according to literature-known procedures (Scheme 25).[387] The synthesis started from nitrophenyl acetic acid **15** which was protected with two different protecting groups. On the one hand *tert*-butanol and on the other hand methanol was employed for esterification of acid **15**.[387-388] Subsequently the nitro group of **16** and **19**, respectively, was converted into amines **17** and **20**, respectively, by hydrogenolysis with gaseous hydrogen and palladium catalyst on activated charcoal in quantitative yields. Both synthetic pathways were performed to compare yields and to optimize the reaction conditions. With amines **17** and **20** in hand, azobenzene derivatives **23** and **24** were synthesised via MILLS coupling. For this, amines **17** and **20** were subjected to oxidation with oxone® to obtain nitroso compounds **18** and **21**. Nitroso derivatives **18** and **21** were reacted with *p*-iodoaniline **22** to form azobenzene derivative **23** and **24**. Following deprotection under acidic conditions in case of *tert* butyl ester **23** and under basic conditions in case of methyl ester **24** originated acid **25**. Compound **25** provides a

versatile precursor which can be employed for cross coupling reactions with numerous reaction partners (Scheme 25).

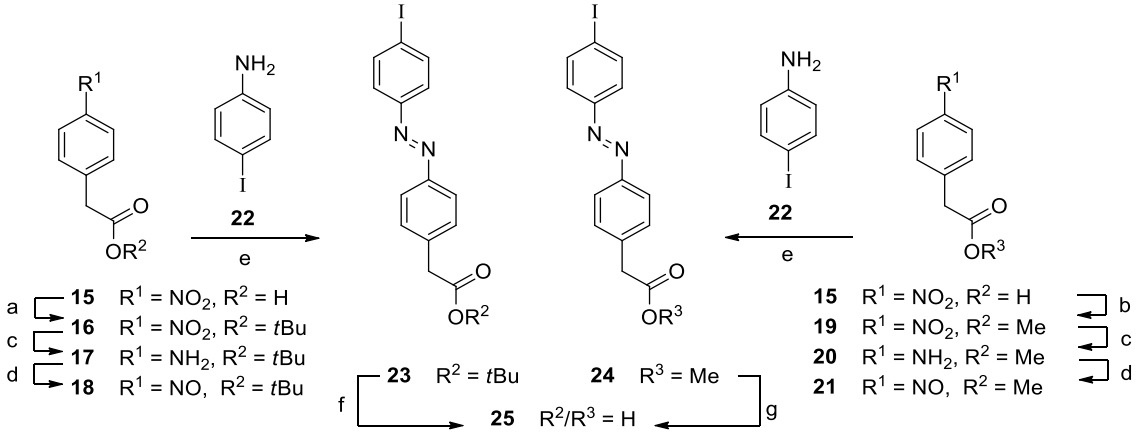

Scheme 25: Synthesis of the iodo-equipped azobenzene precursor **25** which can be employed for SUZUKI coupling reactions for further functionalisation: (a) *t*BuOH, $POCl_3$, pyridine, 0 °C → rt, 16 h, 85 %; (b) $SOCl_2$, methanol, 0 °C → rt, 4 h, 98 %; (c) H_2, Pd/C, methanol, rt, 4 h, 99 %; (d) oxone®, DCM/H_2O, rt, 4 h, 72 % (**18**), 55 % (**21**); (e) CH_3COOH, rt, 16 h, 59 % (**23**), 65 % (**24**); (f) TFA, DCM, rt, 4 h, 90 %; (g) LiOH, THF/H_2O (2:1), rt, 16 h, 98 %.

Precursor **25** was then submitted to SUZUKI-MIYAURA coupling reactions with four different phenylboronic acid pinacol esters **26** to **29**. Reactions were carried out under basic conditions employing potassium carbonate to yield acids **30**-**33**. Compounds **30** and **32** were obtained in rather poor yields of 35 % and 41 %, respectively, whereas compounds **31** and **33** were obtained in good yields of 94 % and 72 %, respectively. Finally, the acids **30**-**33** were converted to the corresponding thioesters employing thiophenol and diethylcyano phosphonate (DECP) as activating agent for the carboxylic acid. The formation of thioesters turned out to be the yield limiting step for synthetic pathways towards a thioester precursor for the labelling of FimH.[379] It can be anticipated at this point, that diethylcyano phosphonate (DECP) proved to not just being be the most practicable reagent but also led to the highest yields. Thioester derivatives **11**-**14** were obtained in yields ranging from 45 % in case of compound **12** to 65 % for compound **13** (Scheme 26).

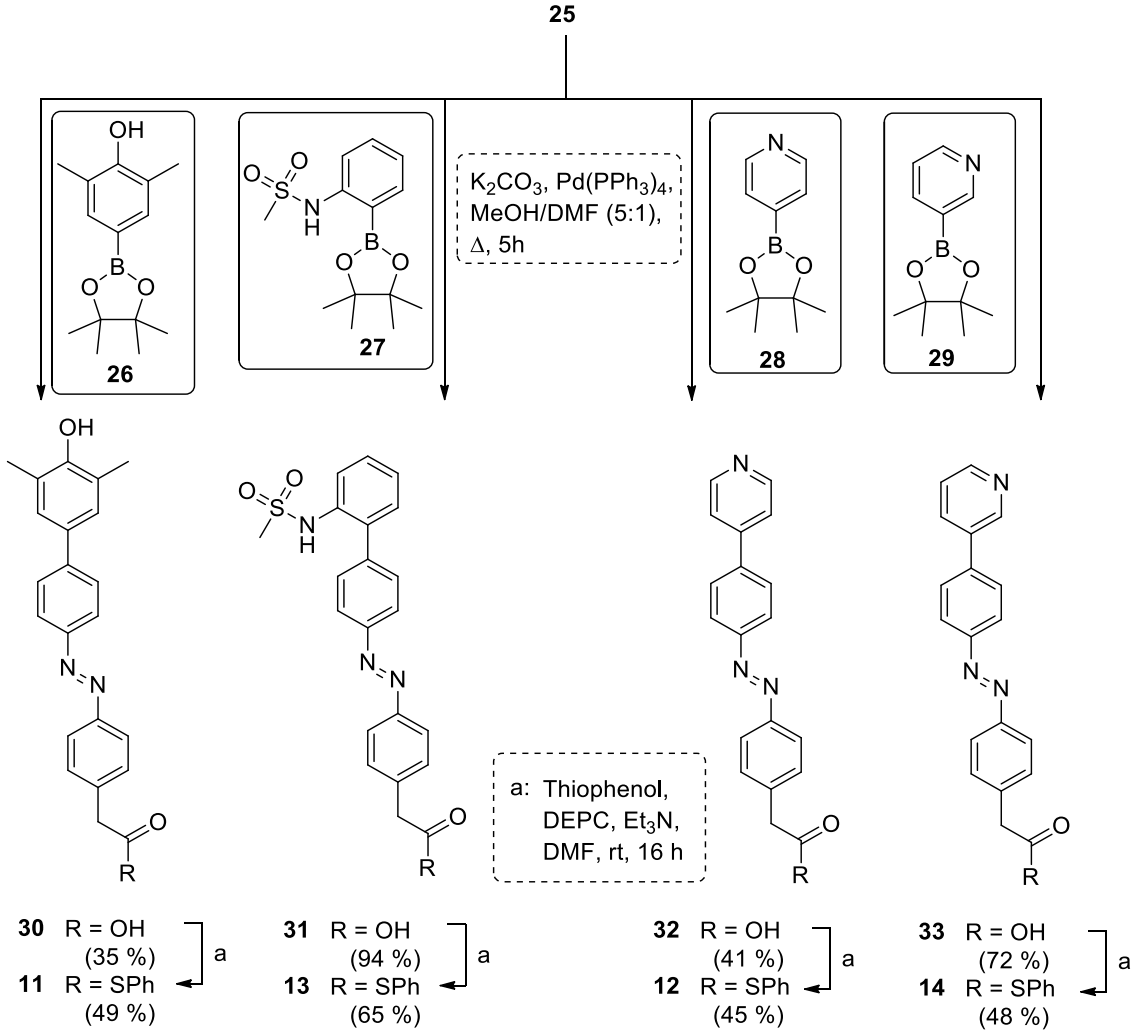

Scheme 26: Synthetic route for SUZUKI-MIYAURA coupling reactions between compound **25** and phenylboronic acid pinacolesters **26** to **29**. Adjacent thioester formation led to 'gate keeper' precursors **11** to **14.**

The polarity of 'gate keeper' molecules is a significant requirement which must be considered for the synthesis of 'gate keeper' moieties. Molecules with increased polarity have two main advantages. On the one hand, polar compounds can interact individually with the binding site and on the other hand, they show a higher water solubility. For this purpose F. BEIROTH designed the cationic trimethylamine derivative **10**,[379] which could not be isolated as pure material, and I. STAMER synthesised α-D-mannoside-decorated thioester **34** (Figure 60).[381]

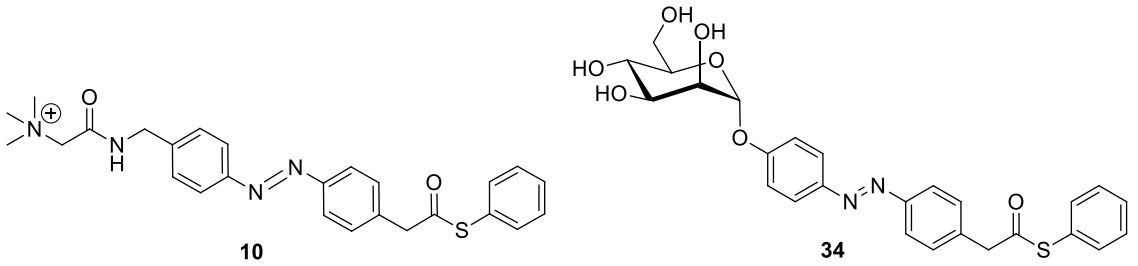

Figure 60: Thioester derivatives with increased polarity synthesised by F. BEIROTH[379] and I. STAMER[381].

The substitution pattern of the azobenzene might also have a great influence on the 'gate keeper' moiety. Depending on the introduction of the thioester residue in the *ortho*-, *meta*- or *para*-position of the azobenzene 'gate keeper' moiety, the angle of the photoswitchable 'gate keeper' varies significantly. Therefore, structures **10** and **35**-**39** were designed with either a trimethylamine residue or a triethylamine residue as ionic 'gate keepers' on the one hand and with varying substitution patterns on the other hand (Figure 61).

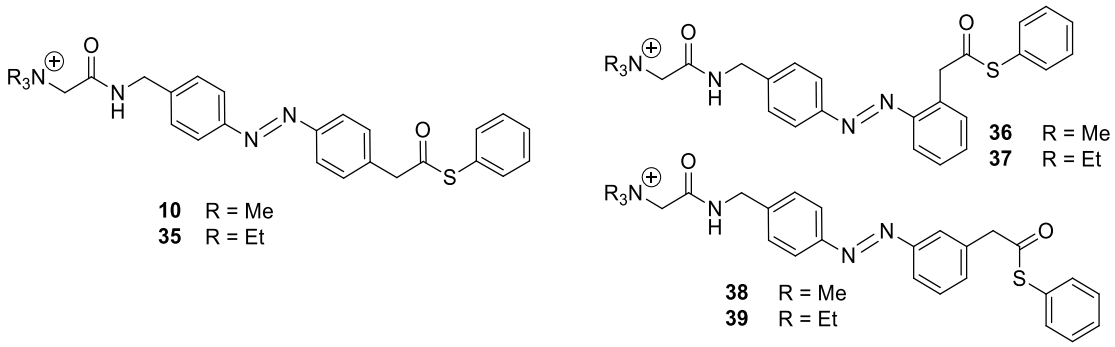

Figure 61: Six potential 'gate keeper' precursor which vary in their substitution pattern.

To establish an efficient synthesis strategy for cationic derivatives as shown in Figure 61 the work in this thesis is focussed on the *para* and *para'* substituted derivatives. In addition, precursors for compounds **36** to **39** were prepared. Amines **17**, **20**, **44** and **45** were synthesised according to literature starting from the respective nitro phenylacids **15**, **40** and **41**.[389-392] First, the reaction pathway of F. BEIROTH was repeated to obtain acyl precursor **66** which can be employed for the investigation of thioester formation which was the crux of matter in the thesis of F. BEIROTH. Therefore amine **17** was converted to the respective nitroso compound **18** by oxidation with oxone®. Nitroso compound **18** was then subjected to MILLS coupling with the 4-amino benzylamine derivative **51** which is selectively Fmoc-protected at the benzylic position.[393-394] The resulting azobenzene derivative **56** was obtained in a yield of 44 %. For removal of the Fmoc protecting group

compound **56** was treated with piperidine leading to free amine **57** in a yield of 61 %.[395] Since the deprotection does not work quantitatively as expected, remaining amines **20** and **44** were employed for MILLS coupling with literature-known nitroso compound **48**[396-397] to obtain Boc-protected azobenzenes **52** and **53**.[398] Amines **20** and **44** were converted according to this synthetic strategy. The yields for the MILLS coupling amount to 50 % for the *para*-substituted derivative **53** and 23 % for the *ortho*-substituted derivative **52**. Boc-protected derivatives **52** and **53** were easily converted to the respective amines **54** and **55** using trifluoroacetic acid (Scheme 27).

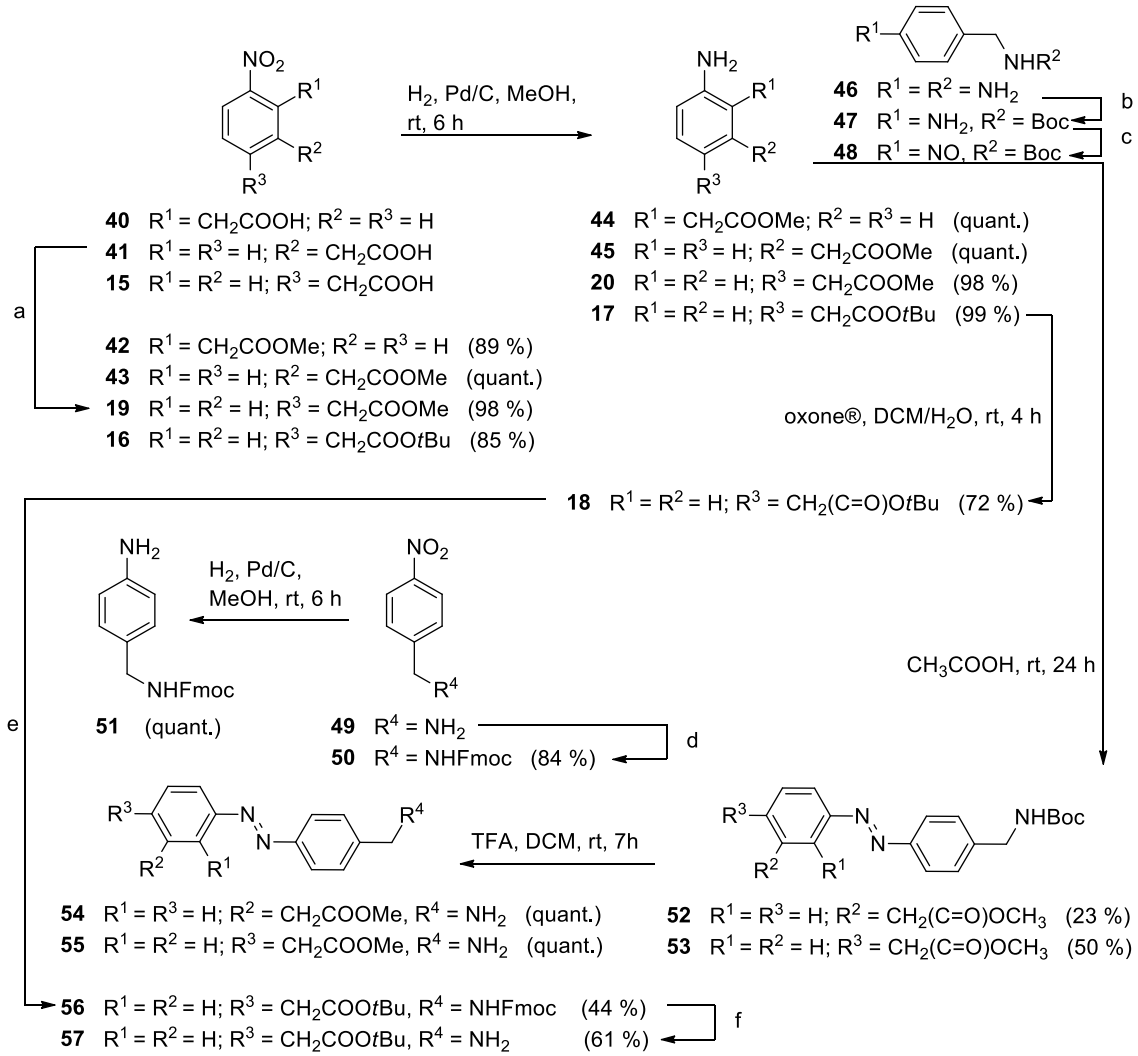

Scheme 27: Synthesis of amino-equipped azobenzene precursors **54**, **55**, **57**: (a) $SOCl_2$, methanol, 0 °C → rt, 4 h, 89 % (**42**), quant. (**43**); (b) Boc_2O, THF, rt, 16 h, 88 %; (c) oxone®, DCM/H_2O, rt, 4 h, 62 % (d) Fmoc chloride, DIPEA, DCM, rt, 16 h, 84 %; (e) CH_3COOH, rt, 24 h, 44 %; (f) piperidine, dry DMF, rt, 16 h, 61 %.

For the synthesis of cationic derivative **65** the acyl chloride of betaine **64** was prepared and reacted with amine **55** to yield compound **65-I** in 68 % yield. Compound **65** was

quantitatively deprotected with lithium hydroxide and acid **66** was then activated with diethyl cyanophosphonate (DEPC, **77**) for thioester formation which occurred with a yield of 44 %. Nevertheless, traces of betaine **64** could not be removed neither by repeated column chromatography on silica gel nor on Sephadex. Thus, an alternative synthesis was established. Starting from amines **54**, **55** and **57** amidation was performed with bromo acetylchloride **58** to obtain azobenzene derivatives **59**-**61** in moderate yields. The best result was obtained for the *tert* butyloxycarbonyl-protected compound **61** which was synthesised in a yield of 76 %. The bromine substituent offers the opportunity of a nucleophilic substitution to introduce the trimethyl- respectively the triethylamine moiety. Methyl ester **60** was subjected to a solution of trimethylamine in methanol (30 wt. %) to obtain compound **65-II** in a yield of 50 %. Due to an excess of trimethylamine, the methyl ester of compound **65-II** was partly deprotected after the substitution reaction. Compound **65-II** was fully deprotected with lithium hydroxide and esterification with thiophenol was subsequently performed as already stated above for compound **65-I**. Bromine-equipped derivative **61** was subjected to a solution of triethylamine (25 wt. % in methanol) and substitution originated triethylamine-equipped azobenzenes **62** with a yield of 43 %. Deprotection with trifluoroacetic acid led to acid **63** which was then subjected to esterification with thiophenol under DEPC (**77**) catalysis to obtain azobenzene derivative **35** with 54 % yield. For the synthesis of cationic compounds **10** and **35** the problem emerged, that traces of DEPC (**77**) remained after purification (Scheme 28).

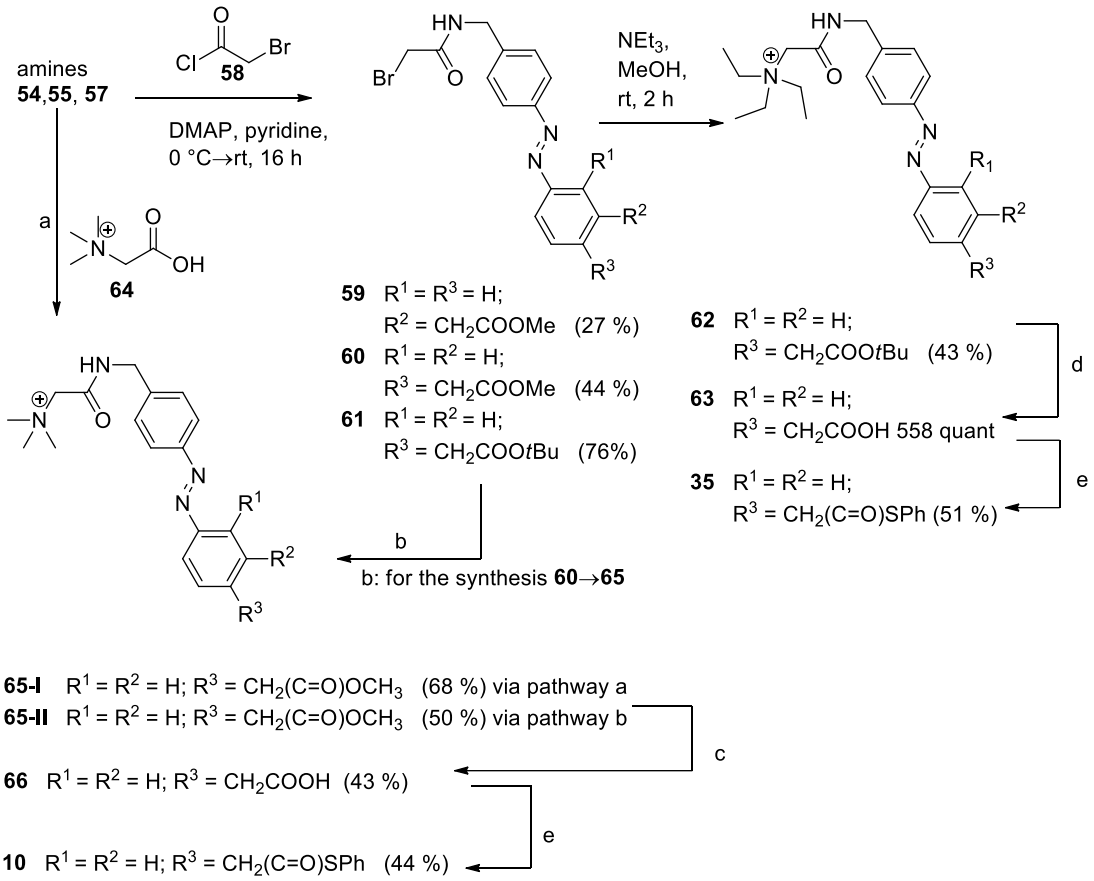

Scheme 28: Synthesis of cationic compounds as 'gate keeper' precursors: (a) 1. betaine **64**, oxalylchloride, DMF, dry acetonitrile, rt, 20 min, 2. amine **55**, DIPEA, dry DMF, rt, 16 h; (b) trimethylamine, methanol, rt, 2 h, quant.; (c) LiOH, THF/H_2O, rt, 5 h, quant.; (d) trifluoroacetic acid, DCM, rt, 6 h, quant.; (e) thiophenol, DEPC (**77**), Et_3N, 0 °C→rt, 16 h.

5.3.3 Synthesis of thioester-equipped 'gate keeper' precursors: glycoside derivatives

Regarding the water solubility of the 'gate keeper' precursors thioester-equipped glycoside derivatives were designed. In addition, glycoside headgroups for the 'gate keeper' molecules also offer the opportunity to synergistically support the closing of the binding site by the 'gate keeper' group due to attractive interactions. Nonetheless the opposite situation might disrupt the opening and closing process because in case of too high affinity a strong binding ligand might suppress the reversible opening of the binding site. Thus, three derivatives **78-80** -one mannoside (α-D-mannoside as 1,2-*trans*-glycoside) and two glucosides (β-D-glucoside as 1,2-*trans*-glycoside and α-D-glucoside as 1,2-*cis*-glycoside)- were outlined which vary in their anomeric configuration and the configuration of the 2-position of the carbohydrate ring. Amino phenyl glycosides were synthesised according to the literature[239, 399] and adjacently

subjected to MILLS coupling with nitroso compound **21** to obtain glycoside azobenzene derivatives **70**-**72** with yields ranging from 40 % to 50 %. Methyl esters **70**-**72** were treated with lithium hydroxide to obtain the acids **73**-**75** in practically quantitative yields. Acids **73**-**75** were then applicable for thioester formation. The α-mannoside **78** and β-glucoside **80** were used for investigating different methods for thioester synthesis. The most successful method was to use diphenylphosphoryl azide (DPPA, **76**) and DEPC (**77**) which form a highly reactive acyl azide or acyl cyanide intermediate, respectively, which can then undergo a nucleophilic attack of thiophenol for instance. In case of glucoside **80** DEPC (**77**) proved to be the more powerful activating reagent (51 % yield with DEPC (**77**), 45 % yield with DPPA (**76**) (Scheme 29). Therefore, DEPC (**77**) was utilised as reagent for most of the thioester syntheses within the course of this thesis as it could already be recognised in the previously described synthesis in Scheme 26 and Scheme 28. The α-mannoside **78** was obtained in 58 % and the α-glucoside in 63 % respective yield. Secondary, the usage of DEPC (**77**) respectively DPPA (**76**) enabled the purification of glycosides **78**-**80**. In case of HATU-mediated thioester formation the yield was lower and additionally the purification was rather demanding since traces of tetramethylurea and the pyridine derivative released during the synthesis were remaining after several steps of purification.

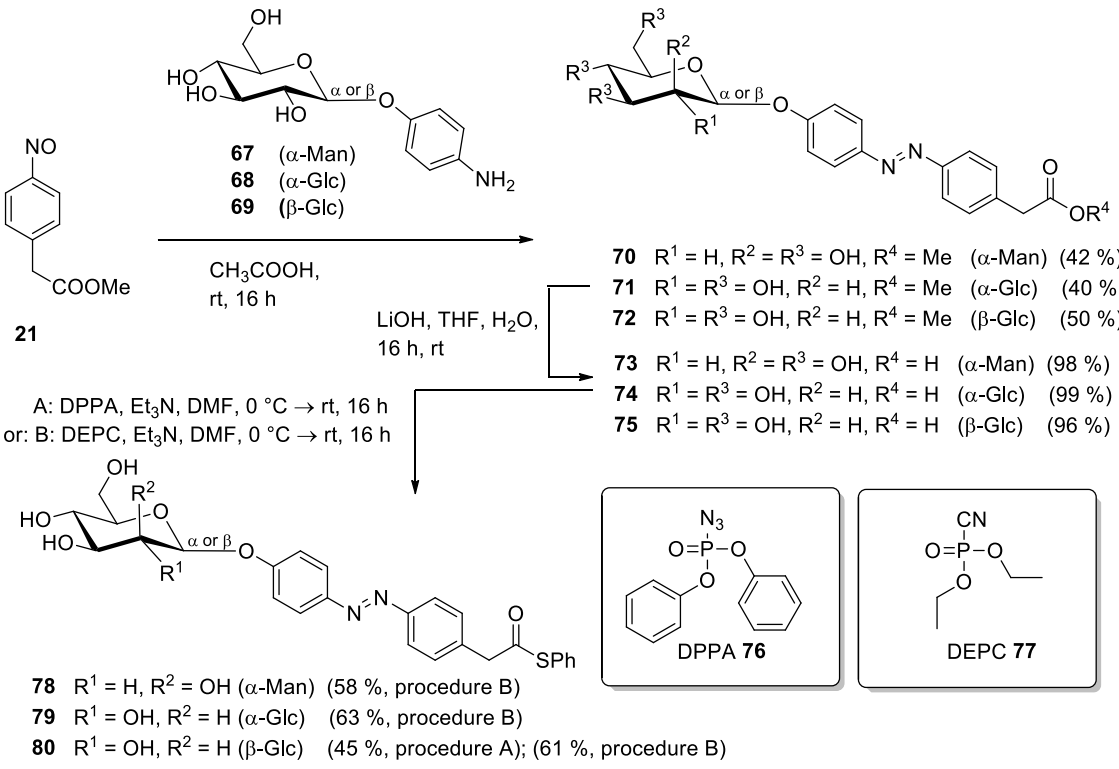

Scheme 29: Synthesis of thioester glycosides **78**-**80**: Carboxylic acids **73**-**75** were activated by DEPC (**77**) or DPPA (**76**) for thioester formation.

To evaluate the general potency of DPPA (**76**) and DEPC (**77**) as reagents for thioester synthesis, the compounds **81**-**83** which are already known from F. BEIROTH were synthesised according to the literature.[379] Those three carboxylic acids were then subjected to thioester synthesis with DPPA (**76**) for the comparison of yields. Previously those thioesters **7**-**9** had been synthesised by common methods like the use of HATU as coupling reagent or by activation of the acid by acyl chloride. Nevertheless, the yields were rather poor, especially for compound **9** the yield just amounted to 11 %.[379] With DPPA (**76**) all three synthesis results were improved at least about 12 percentage point and in case of compound **9** the yield could even be enlarged from 11 % to 42 %. In this way the general applicability of DPPA (**76**) as capable esterification reagent was proved (Scheme 30).

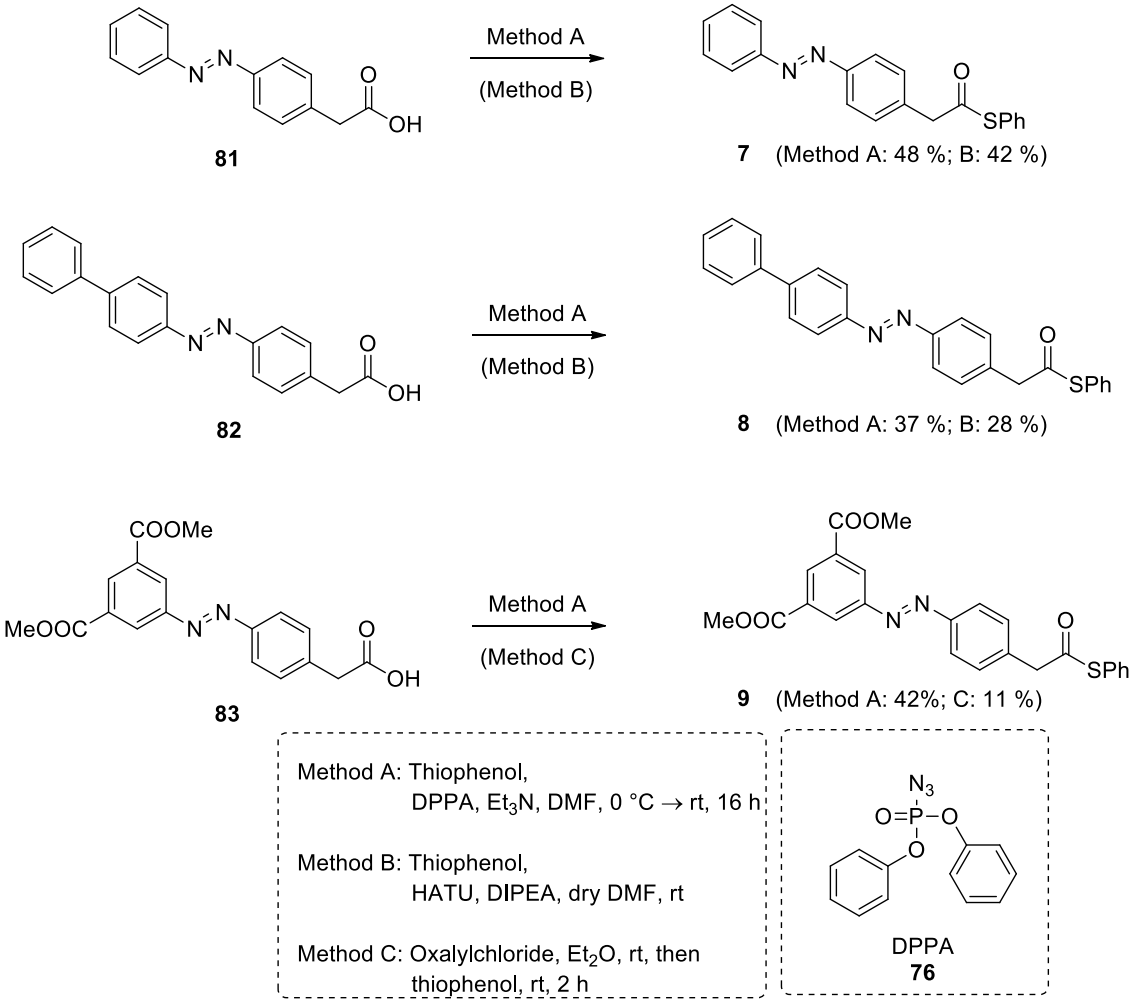

Scheme 30: Improving the synthesis of the known thioesters **7**-**9**[379]: Method A, employing DPPA (**76**), led to increased yields in comparison to the published procedures.

Further hydrophilic thioesters were targeted based on findings published by CHANDRASEKARAN et al. that certain *ortho*-substitution improves water solubility of glycoazobenzene derivatives. In particular, it was shown that the *ortho*'-substituted glycoazobenzene methyl esters **84** and **86** (Scheme 31) possess an increased water solubility compared to the respective carboxylic acids **85** and **87**.[400]

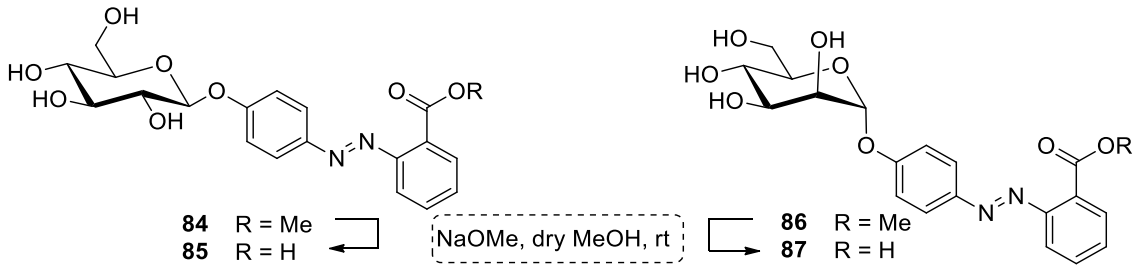

Scheme 31: Glycoazobenzene derivatives **84**-**87** which were synthesised by CHANDRASEKARAN et al. for the investigation of the photochromic properties which are influenced by the *ortho*'-substitution pattern.[400]

Consequently, the literature-known methyl ester **91** was synthesised[401] and glycosylated under $BF_3 \cdot Et_2O$ catalysis with a glycosyl donor, **88** or **89** (Scheme 32). The nitrophenyl glucoside **92** was obtained in 61 % and the respective mannoside **93** in 84 % yield. Subsequent reduction of the nitro group led to the amines **94** and **95**, respectively, which were employed in a MILLS coupling reacting with the nitroso compound **18**. Azobenzene glycoside **96** and azobenzene mannoside **97** were obtained in rather mediocre yields of 31 % and 25 %, respectively. Both azobenzene derivatives **96** and **97**, respectively, were successively treated with sodium methoxide and trifluoroacetic acid to obtain the fully deprotected acids **98** and **99**, which were finally employed for thioester synthesis by DEPC (**77**) activation resulting in thioesters **102** and **103** in yields of 50 % and 47 %, respectively. Although both compounds were purified by column chromatography and crystallisation several times, the NMR spectra of **102** and **103** showed slight impurities. The reason might be that either the ester bond at the aromatic ring or the thioester are labile and decompose during isolation.

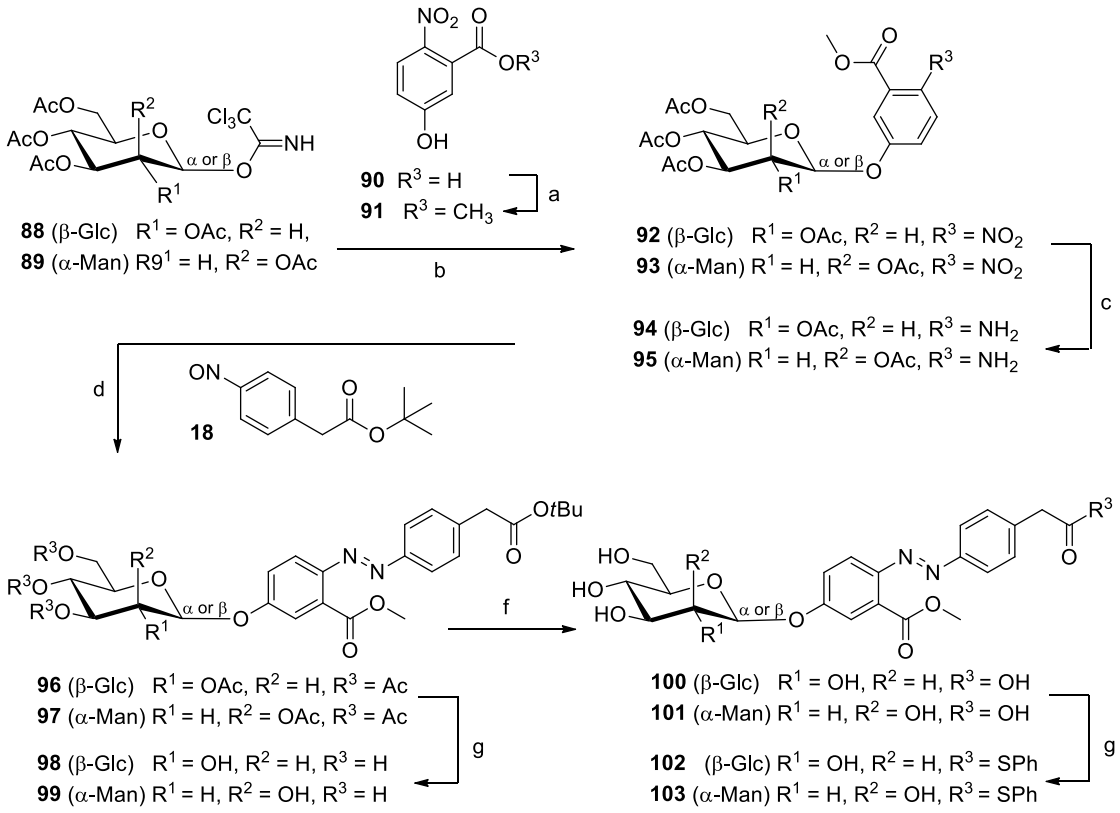

Scheme 32: Synthesis of thioesters **102** and **103**: (a) $SOCl_2$, MeOH, 0 °C→Δ, 8 h, 67 % (b) $BF_3 \cdot Et_2O$, dry DCM, 0 °C → rt, 2 d, 61 % (**92**), 84 % (**93**), (c) H_2, Pd/C, ethyl acetate, rt, 16 h, quant., (d) CH_3COOH, rt, 24 h, 31 % (**96**) 25 % (**97**), (e) 1M NaOMe, dry MeOH, rt, 16 h, 89 % (**98**), 95 % (**99**), (f) TFA, DCM, rt, 5 h, quant., (g) DEPC **77**, Et_3N, dry DMF, 0 °C→rt, 16 h, 50 % (**102**), 47 % **(103** %).

Furthermore, three especially hydrophilic thioesters **104**, **105** and **106** (Figure 62) were designed and the respective methyl ester precursors were synthesised, but the thioester products could not be obtained in pure form. Hence, these three target molecules were not further investigated in spite of the fact that according to molecular modelling they are suited as 'gate keeper' moieties to reversibly block and open the binding site of the lectin FimH.

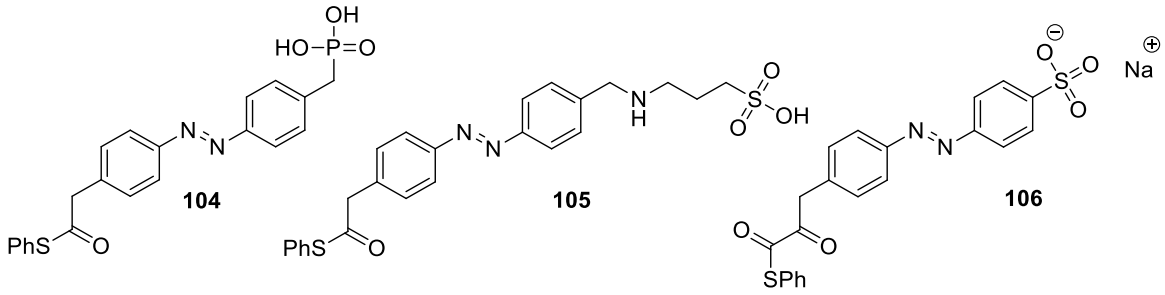

Figure 62: Hydrophilic thioesters **104** to **106**. Under physiological conditions, the acids **104** and **105** can also occur as the respective conjugated bases.

5.3.4 Investigation of photochemical properties

The photochemical properties of the thioesters **7**-**14**, **35**, **78**, **79**, **102** and **103** were determined to evaluate the suitability of these molecules as photoswitchable 'gate keepers' for the lectin FimH. Since it is known that the switching behaviour of azobenzene derivatives is affected by their substituents, one has to consider that the results obtained for the thioester precursors might not perfectly represent the situation after FimH ligation Hence, *N*-(Acetyl)-L-tyrosine ethyl ester **107** was used as model system, resembling a FimH side chain, and ligated with acid **81** to form **108** which can be compared to the thioester **7** itself (Scheme 33).

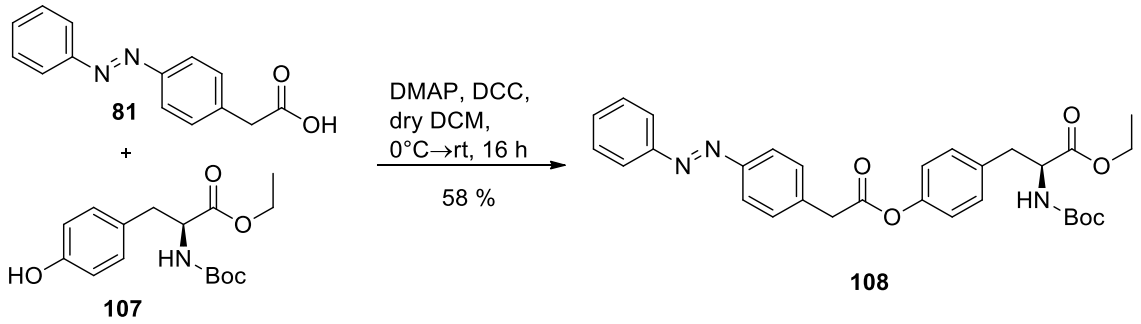

Scheme 33: Ligation of acid **81** with *N*-(Acetyl)-L-tyrosine ethyl ester **107** for the investigation of photochemical properties.

The photochromic properties were investigated by UV and NMR spectroscopy. All obtained data are collected in Table 2, recorded NMR spectra are shown in chapter 8.5.3 and UV spectra in chapter 8.5.4. The wavelength of the maximal absorption was determined for the *Z*- and the *E*-isomer via UV/Vis spectroscopy and the photostationary state (PSS) and most half-lifes were determined by NMR spectroscopy. Some half-lifes were determined by UV/Vis spectroscopy. Either, because they did not show an isolated signal in the ^{1}H NMR which could be used for integration or since photoswitching could just be realised at low concentrations. *E*-isomers were obtained by storing the respective probe at 40 °C overnight and *Z*-isomers were obtained by irradiation with a light emitting diode with an irradiation wavelength of 365 nm. The photostationary state (PSS) describes the ratio of the *E*- and the *Z*-isomer after irradiation with 365 nm for at least 15 min respectively a maximum time of 30 min.

Table 2: Characterisation of the *E*- and *Z*-isomers of compound **121** and thioesters **7** to **14**, **35**, **78**, **79**, **80**, **102** and **103**.

Compound	λ_{max} (nm) (*E*-isomer)	λ_{max} (nm) (*Z*-isomer)	*E*/*Z* (PSS)	Half-life $T_{1/2}$ (h)
7	324	296	25 / 75	27.3
108[a]	322	306	21 / 79	129.9
8	356	443	13 / 87	1.27
9	327	433	16 / 84	15.8
10	344	438	17 / 83	16.9
11	367	441	55 / 45[b]	0.11[d]
12	340	438	79/20[e]	0.72[d]
13	339	438	8 / 92	19.7
14	336	439	7 / 93	55.8
35	328	434	12 / 88	48.1
78	345	302	11 / 89	2.5
79	345	304	9 / 91	0.9
80	344	302	2 / 98	4
102	343	423	[c]	59.7[d]
103	345	424	30 / 70	88.3[d]

[a] **108** was used as a model system, resembling a FimH side chain equipped with the azobenzene moiety of compound **7**
[b] No photoswitching observed until a dilution of 0.5 mg substance / 500 µL was reached;
[c] Photoswitching was observed, but no separate proton signal was existing for integration;
[d] Half-life was determined via UV/Vis spectroscopy with 80 µM solutions (5 µM in case of compound **11**);
[e] Low *E*/*Z* ratio due to the poor half-life.

For photoswitching of FimH function, high *E*/*Z* ratios in the photostationary state and rather long half-lifes are required. In comparison to the thioester **7**, the ligation product **108** showed more advantageous photochromical properties. This confirms that the photochemical properties can be investigated for the precursor molecules to decide if the molecules are suitable in general since the switching behaviour does not get worse after ligation – at least in the case of compound **7**. Both compounds **7** and **108** show similar switching behaviour which was also confirmed by UV/Vis spectroscopy. The UV/Vis spectra of compound **7** and **121** are shown in Figure 63 and Figure 64. The *E*-isomer is shown in blue. It is characterised by a strong absorbance in the π -π^* transition (around 330 nm). After irradiation with 365 nm the absorption spectra of the *Z*-isomer

(red) showed an increase of the absorbance in the n-π* transition and simultaneously a decrease in the π-π* transition.

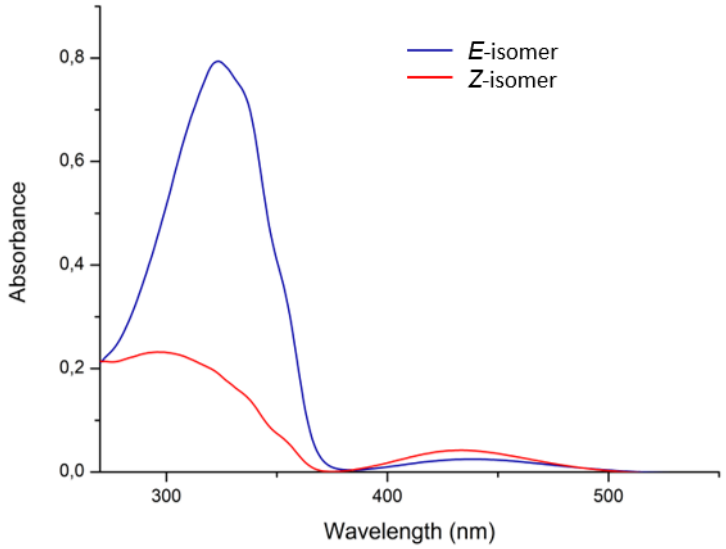

Figure 63: UV spectra of compound **7**. The spectrum of the *E*-isomer (in blue) was recorded after 16 h storage at 40 °C and the spectrum of the *Z*-isomer (in red) was recorded after irradiation with 365 nm for 15 min. Irradiation with 440 nm restored the *E*-isomer. Spectra were recorded in DCM at 293 K.

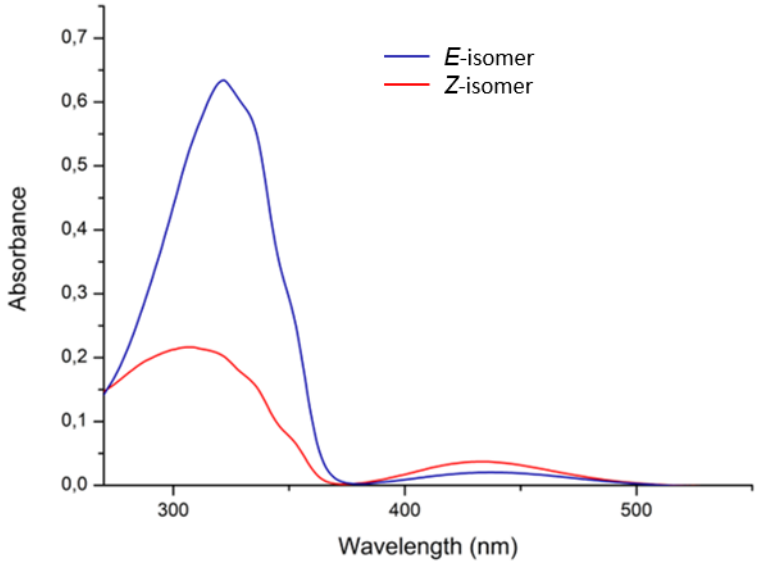

Figure 64: UV spectra of compound **108**. The spectrum of the *E*-isomer (in blue) was recorded after 16 h storage at 40 °C and the spectrum of the *Z*-isomer (in red) was recorded after irradiation with 365 nm for 15 min. Irradiation with 440 nm restored the *E*-isomer. Spectra were recorded in DCM at 293 K.

UV/Vis spectra for compounds **8**-**14**, **35**, **78**, **79**, **102** and **103** are shown in chapter 8.5.4.

5.3.5 Molecular modelling and docking

For the determination of the suitability of 'gate keeper' molecules for effective switching between the carbohydrate binding (adhesion) and the non-carbohydrate binding (no adhesion) function of the azobenzene-labelled lectin the system was investigated *in silico*. First, the binding event between the reactive conjugate and the lectin FimH was observed. For the labelling experiment lectin FimH will be incubated with the DMAP ligand **6** before thioesters (exemplified by compound **11** in Scheme 34) will be added. A nucleophilic attack of compound **6** on thioester **11** leads to a reactive conjugate (**6**+**11**) (highlighted in red, Scheme 34). This conjugate was employed for docking studies to predict the affinity of the ligand towards FimH on the one hand and to get a deeper knowledge about the orientation of the reactive conjugate in and at the binding site, respectively. Finally, one nucleophilic amino acid side chain will attack the conjugate (**6**+**11**) to form the labelled protein. Since FimH can occur in two conformations, namely the open gate conformation (PDB code 1KLF[402]) and the closed gate conformation (PDB code 1UWF[403]) docking studies were performed for both states of the azobenzene, the *E*- and the *Z* form. (Figure 57)

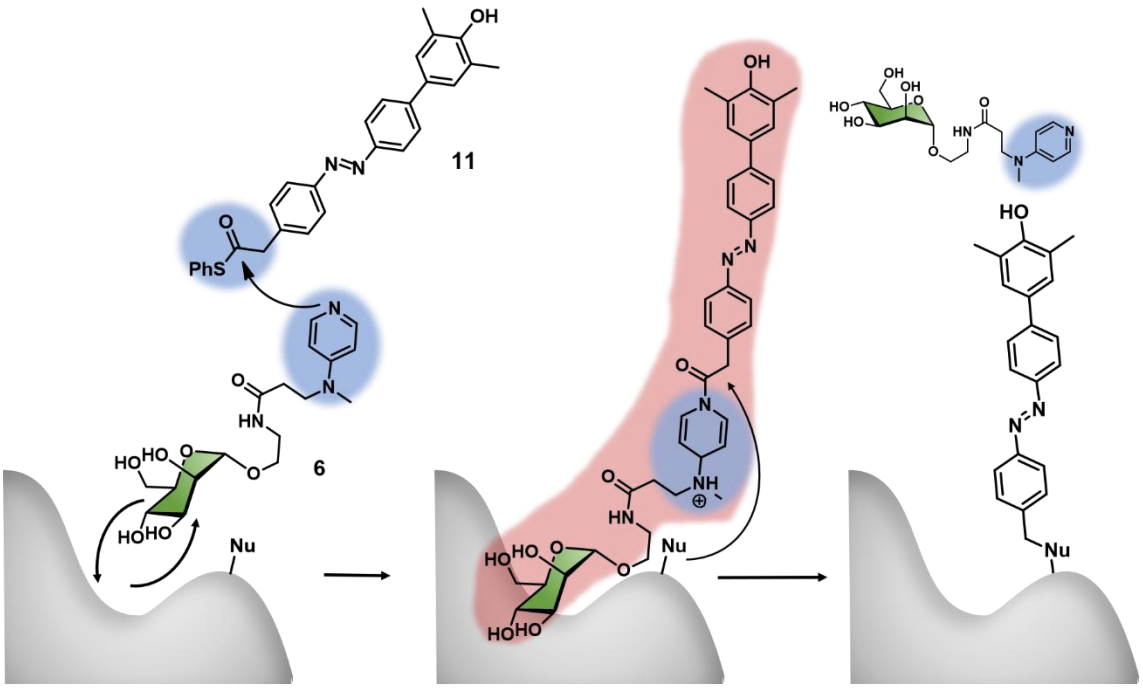

Scheme 34: Mechanism of the DMAP-catalysed ligation reaction shown exemplified by DMAP ligand **6** and thioester **11**. The resulting conjugate (**6**+**11**) (highlighted in red) was applied for docking studies with Glide.[382]

Docking studies were performed with the software Glide[382] which is implemented in the Schrödinger software package.[404] Ligands were prepared by transforming a 2D structure into a 3D structure by energy minimisation and conformer generation. The 2D and the resulting 3D structure of compound **11** (after ligand preparation with LigPrep from the Schrödinger software package[405]) is shown as an example in Figure 65.

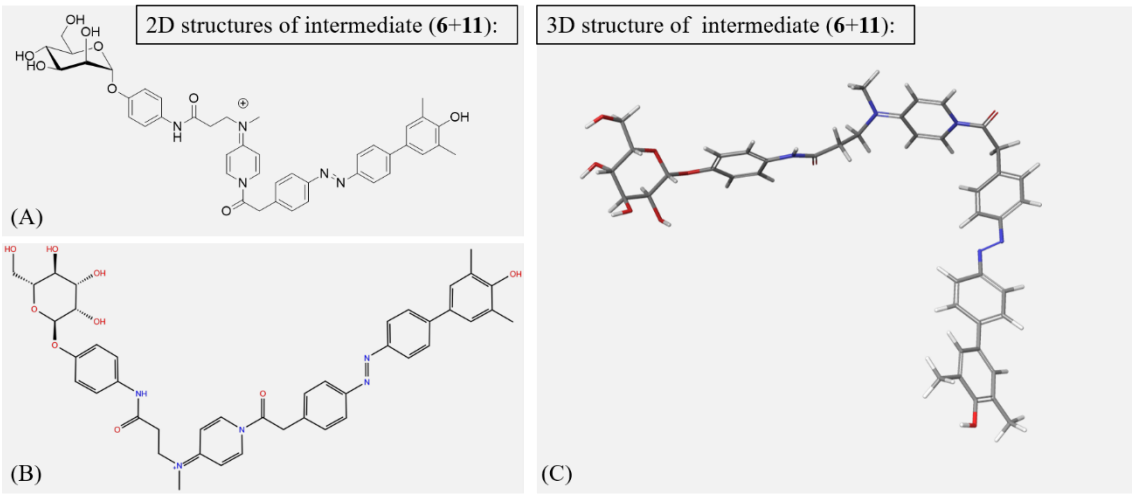

Figure 65: 2D (left, (A) and (B)) and 3D (right, (C)) structures for the conjugate (**6**+**11**) which was applied for the docking study.

The conjugate (**6**+**11**) was disposed to docking studies with Glide. For this, both protein conformers (1KLF and 1UWF) were prepared for docking with the implemented 'Protein Preparation Wizard' tool.[406-407] Docking was performed in a high precision mode which fixed the lectin in a rigid conformation whereas the ligand is flexible during the docking process. The results with the best docking scores for conjugate (**6**+**11**) are shown in Figure 66. The more negative the docking score, the higher is the predicted ligand affinity for the lectin. Unexpectedly, in case of conjugate (**6**+**11**) the mannoside residue did not enter the binding site of the lectin during the docking process. Instead, it was orientated next to the binding site at a hypothetic second carbohydrate binding site (hereafter referred to as 'putative binding site') where the mannoside residue formed stabilising hydrogen bonds. Nevertheless, the resulting complex showed the 'gate keeper' moiety orientated ideally in front of the binding site and additionally the reactive centre of the conjugate is in proximity to the potential nucleophilic residue of Tyr137. Thus, the result of this docking emboldened to use compound **11** as a precursor for the attachment of the 'gate keeper' moiety.

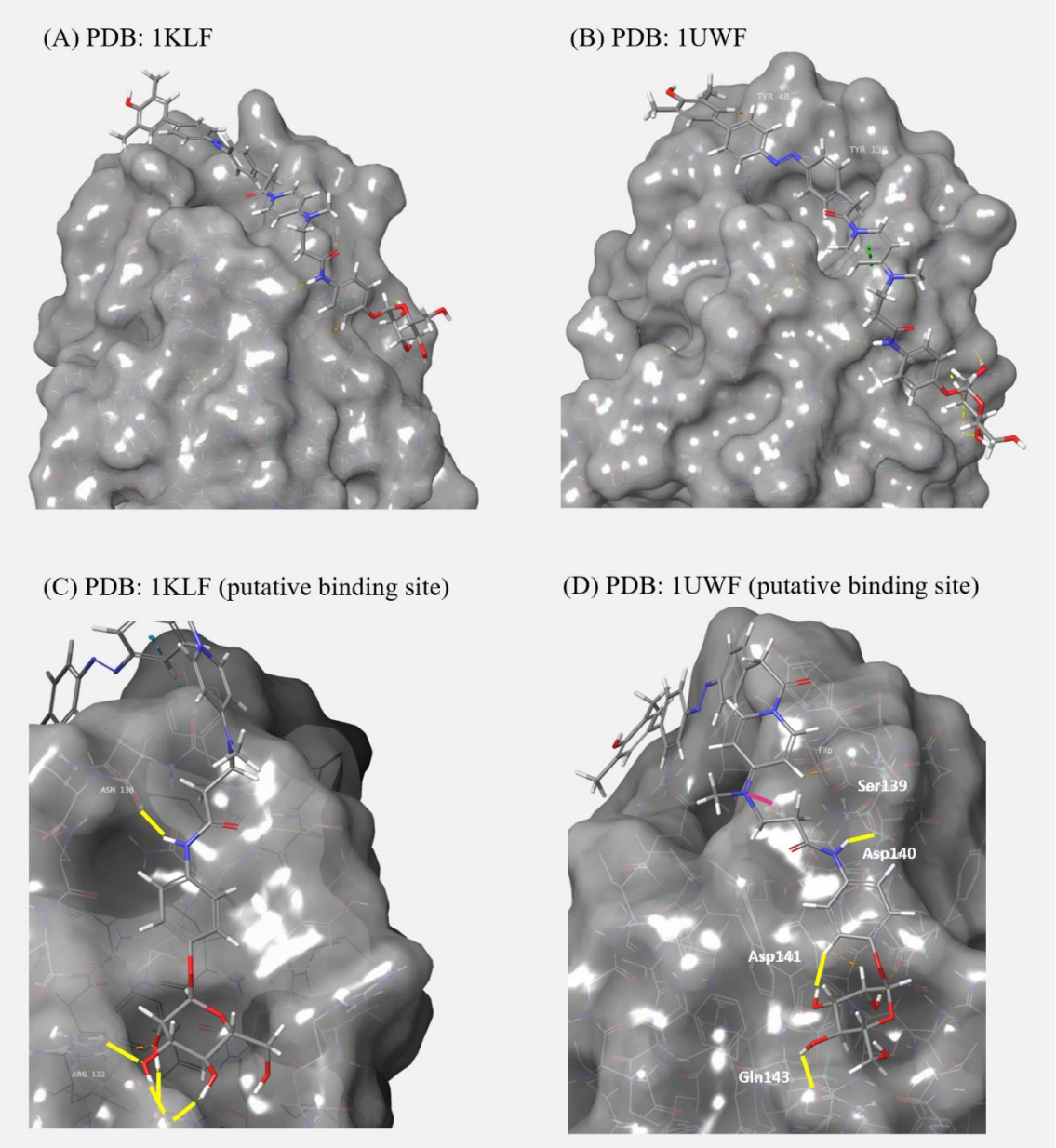

Figure 66: Results of the docking of conjugate (**6**+**11**) with Glide: (A) Docking was performed with the open gate conformation of lectin FimH (PDB code: 1KLF) and (B) with the closed gate conformation of lectin FimH (PDB code: 1UWF). Location of the mannoside moiety at the putative binding site of the 1KLF structure (C) and of the 1UWF structure (D). Stabilising hydrogen bonds are marked in yellow, stabilising ππ interactions are marked in green and salt bridges are shown in pink.

Hydrogen bonds at the putative binding site were formed with aspartic acid Asp140, Asp140 and glutamine Gln143 (Figure 66, (C)). Significant interactions between the ligand and the lectin are shown in 2D in Figure 67. The same situation, the mannoside residue being orientated at the putative binding site, was observed also for other conjugates after docking.

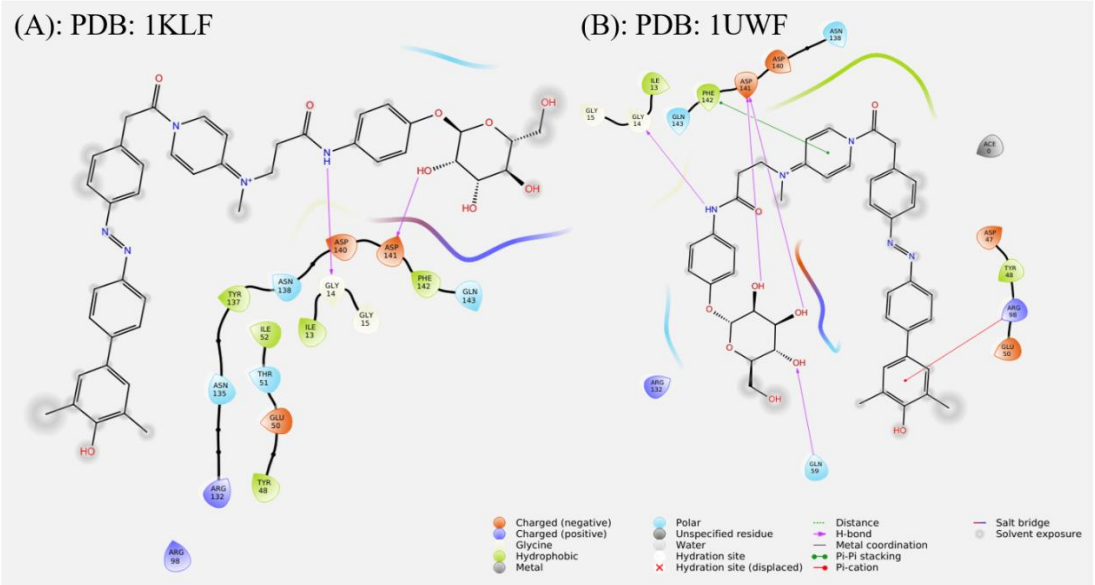

Figure 67: Interaction diagrams for the conjugate (**6**+**11**) with lectin FimH in the open gate conformation (left, (A), 1KLF) and the closed gate conformation (right, (B), 1UWF). Stabilising hydrogen bonds are highlighted in violet and stabilising ππ interactions are highlighted in red. Additionally the proximity of nucleophilic amino acid residues to the reactive centre of the conjugate can be estimated.

The results of the docking of the conjugate (**6**+**14**) are depicted in Figure 68. In case of the closed gate conformation the conjugate (**6**+**14**) was positioned within the binding site with a resulting docking score of -7.94. However, for the 1KLF conformation the binding site remains unoccupied and the ligand is positioned beneath the binding site.

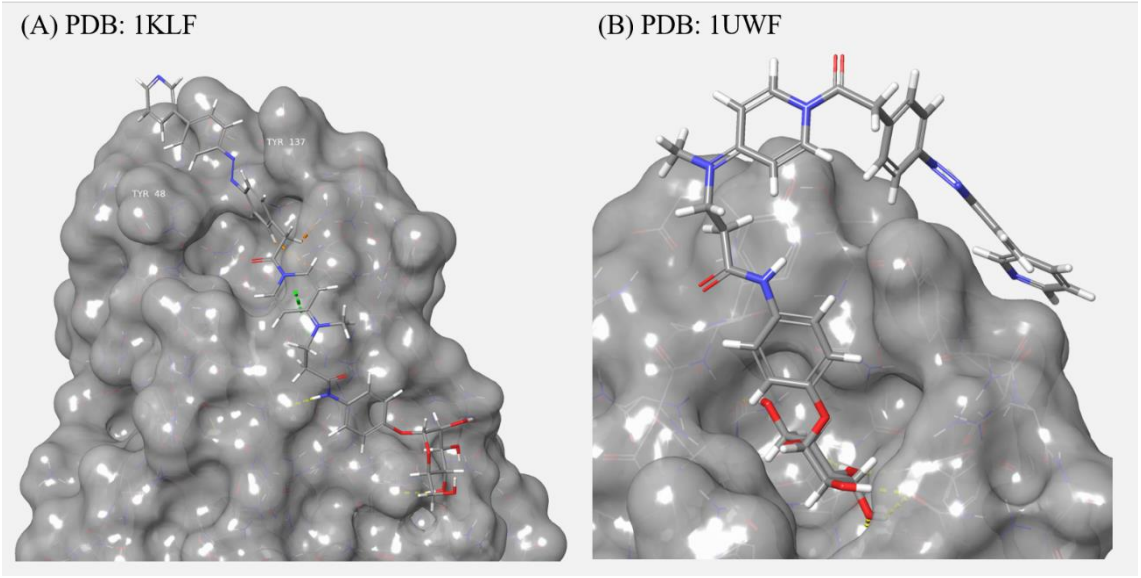

Figure 68: Results of the docking of conjugate (**6**+**14**) with Glide: (A) Docking was performed with the open gate conformation of lectin FimH (PDB code: 1KLF) and (B) with the closed gate conformation of lectin FimH (PDB code: 1UWF). Stabilising ππ interactions are marked in green.

Nevertheless, compound (**6**+**14**) extended to the entrance of the binding site and is also pre-oriented for ligation with the lectin FimH (Figure 69).

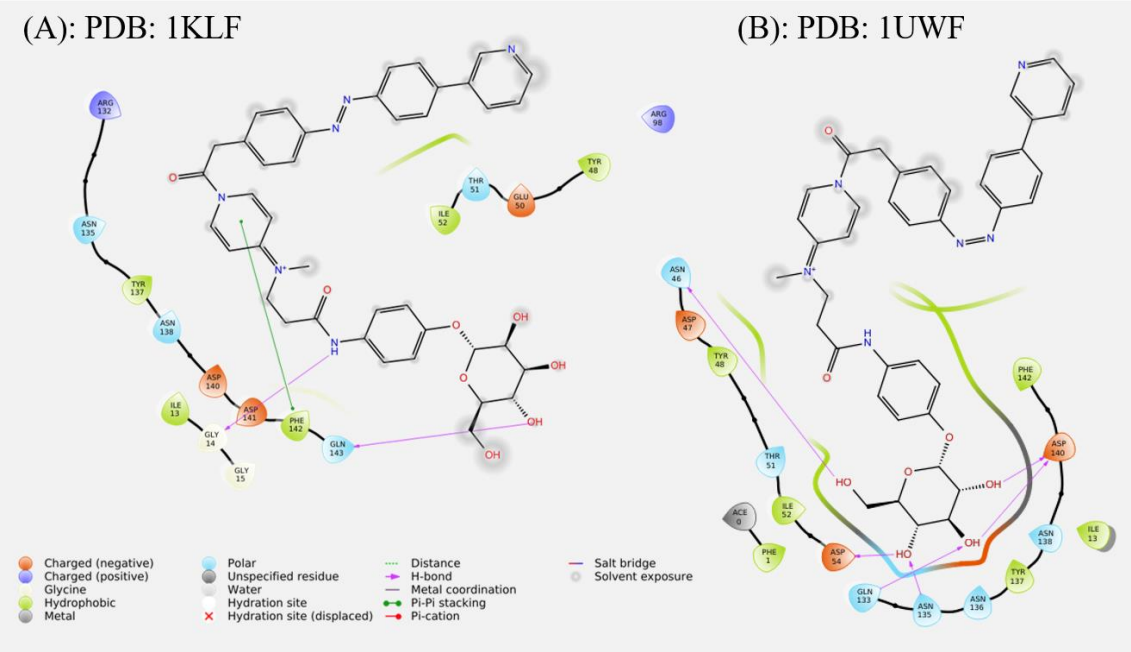

Figure 69: Interaction diagrams for the conjugate (**6**+**14**) with lectin FimH in the open gate conformation (left, (A), 1KLF) and the closed gate conformation (right, (B), 1UWF). Stabilising hydrogen bonds are highlighted in violet and stabilising ππ interactions are highlighted in green. Additionally, the proximity of nucleophilic amino acid residues to the reactive centre of the conjugate can be estimated.

For the pyridinium derivative **12** and the conjugate (**6**+**12**), respectively, both the 1KLF conformation and the 1UWF conformation stayed unoccupied by the ligand. In both cases the mannoside residue was located alongside the binding site at the putative binding site which was already sighted before (cf. Figure 66). Hydrogen bonding with Asp141 is stabilising the constellation. Figure 70 shows the location of the conjugate at the putative binding site of the open gate conformation (A and B) and the closed gate conformation (C). In both cases the conjugate was located above the binding site and the active ester of the compound (**6**+**12**) is in proximity of potential nucleophiles at the entrance of the binding site.

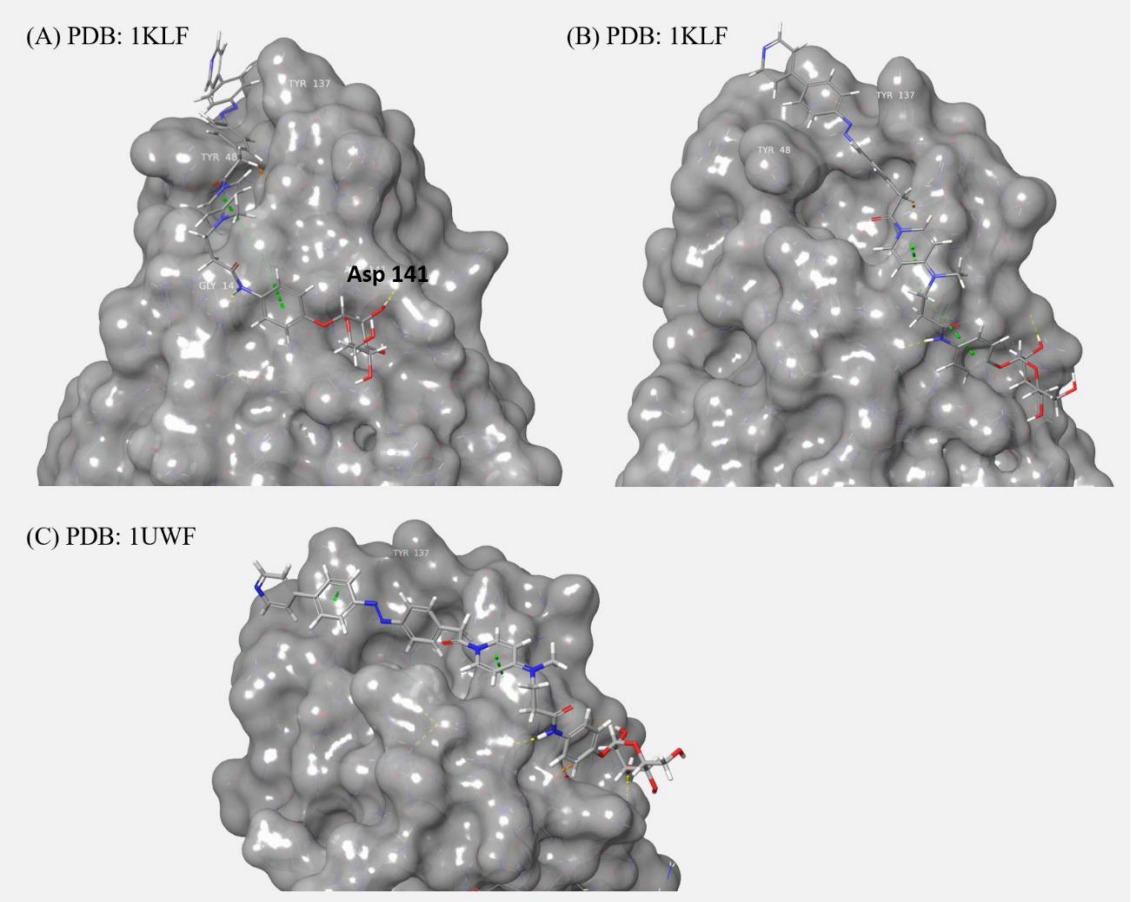

Figure 70: Results of the docking of conjugate (**6**+**12**) with Glide: (A) Docking was performed with the open gate conformation of lectin FimH (PDB code: 1KLF). (B) shows the location of the mannoside residue at the putative binding site. (C) shows the result of the docking with the closed gate conformation of lectin FimH (PDB code: 1UWF). Stabilising hydrogen bonds are marked in yellow, and stabilising ππ interactions are marked in green.

Interaction diagrams for conjugate (**6**+**12**) with the lectin conformations 1KLF and 1UWF are shown in Figure 71. Hydrogen bonds which stabilise the compound at the putative binding site are highlighted in violet.

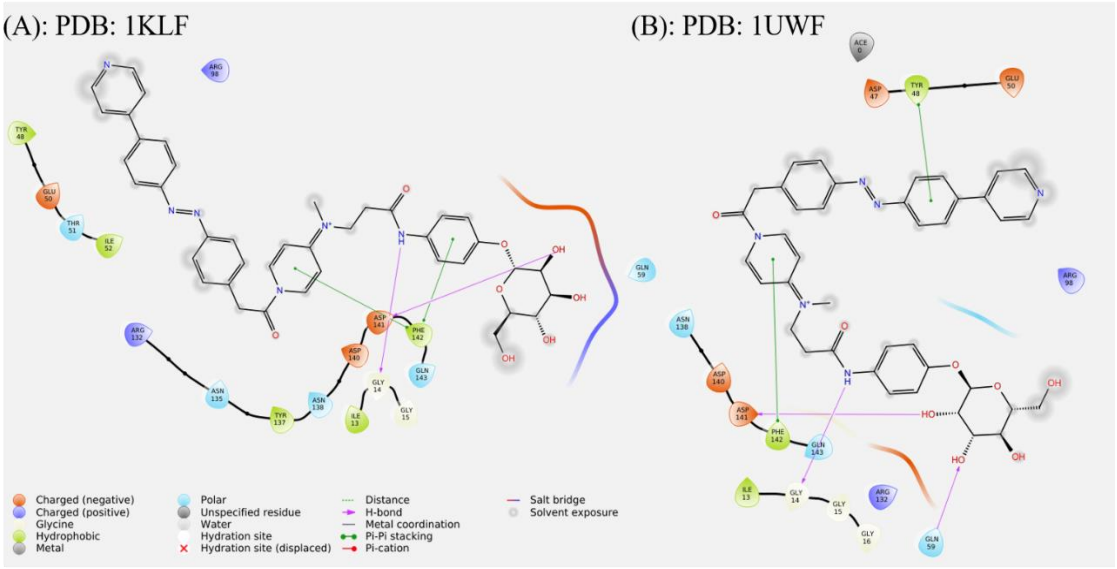

Figure 71: Interaction diagrams for the conjugate (**6**+**12**) with lectin FimH in the open gate conformation (left, (A), 1KLF) and the closed gate conformation (right, (B), 1UWF). It is evident that Tyr137 is in ideal proximity of the reactive active ester in case of the 1KLF conformation. Stabilising hydrogen bonds are highlighted in violet and stabilising ππ interactions are highlighted in green.

In case of conjugate (**6**+**13**) the ligand was also located beside the binding site. In both cases (1KLF and 1UWF) the mannoside residue was located at the putative binding site. The docking result for the 1UWF conformation showed that the azobenzene moiety was lying above the entrance of the binding site. Thus, an optimal pre-orientation of the conjugate for ligation with nucleophile Tyr137 was provided. (Figure 72)

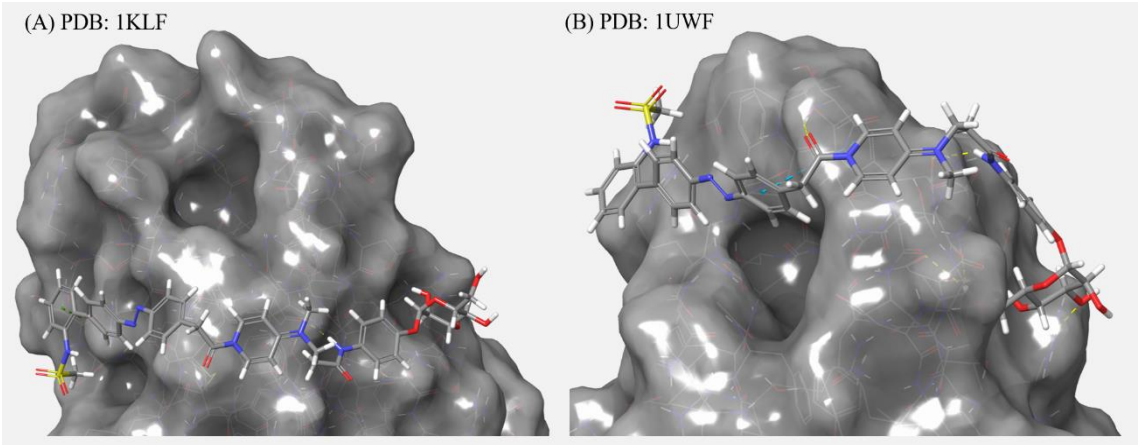

Figure 72: Results of the docking of conjugate (**6**+**13**) with Glide: (A) Docking was performed with the open gate conformation of lectin FimH (PDB code: 1KLF) and (B) with the closed gate conformation of lectin FimH (PDB code: 1UWF). Stabilising hydrogen bonds are marked in yellow, and stabilising ππ interactions are marked in green.

Interaction diagrams for the conjugate (**6**+**13**) are shown in Figure 73. The orientation of the conjugate at the surface of the 1UWF lectin was stabilised by ππ stacking of the azobenzene phenyl ring and Tyr137 and hydrogen bonding of Tyr137 with the amide functional groups of the conjugate (**6**+**13**).

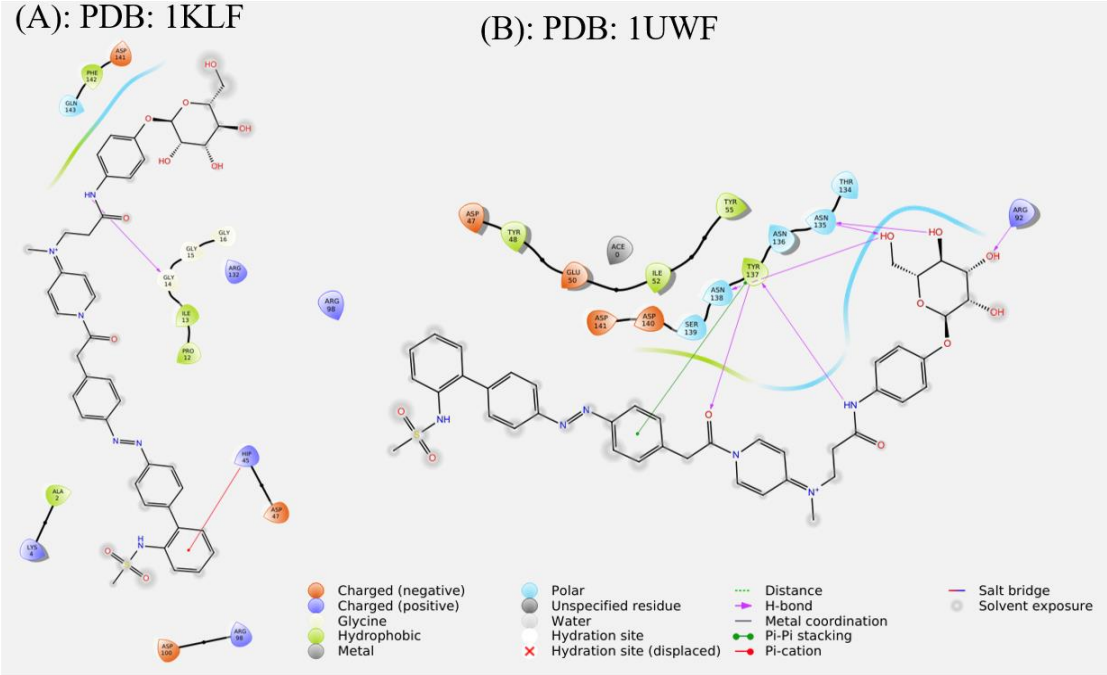

Figure 73: Interaction diagrams for the conjugate (**6**+**13**) with lectin FimH in the open gate conformation (left, (A), 1KLF) and the closed gate conformation (right, (B), 1UWF). Stabilising hydrogen bonds are highlighted in violet and stabilising ππ interactions are highlighted in green.

The cationic ‘gate keeper’ precursors **35** and **38** were also investigated via docking studies. The respective compound **10** had already been investigated by F. BEIROTH who observed unspecific binding for conjugate (**6**+**10**).[379] The respective triethylamine derivative **35** was investigated in the course of this thesis and the docking results are shown in Figure 74. With respect to the mannoside residue also compound (**6**+**35**) showed unspecific binding. Nevertheless, in case of the 1KLF conformation a good pre-orientation was observed since the ‘gate keeper’ moiety of the conjugate is located within the binding site and the active ester is in proximity of the nucleophilic residues. In case of the 1UWF conformation the ‘gate keeper’ moiety was at least cutting across the entrance of the binding site. Again, in both constellations the mannoside residue was located at the putative binding site.

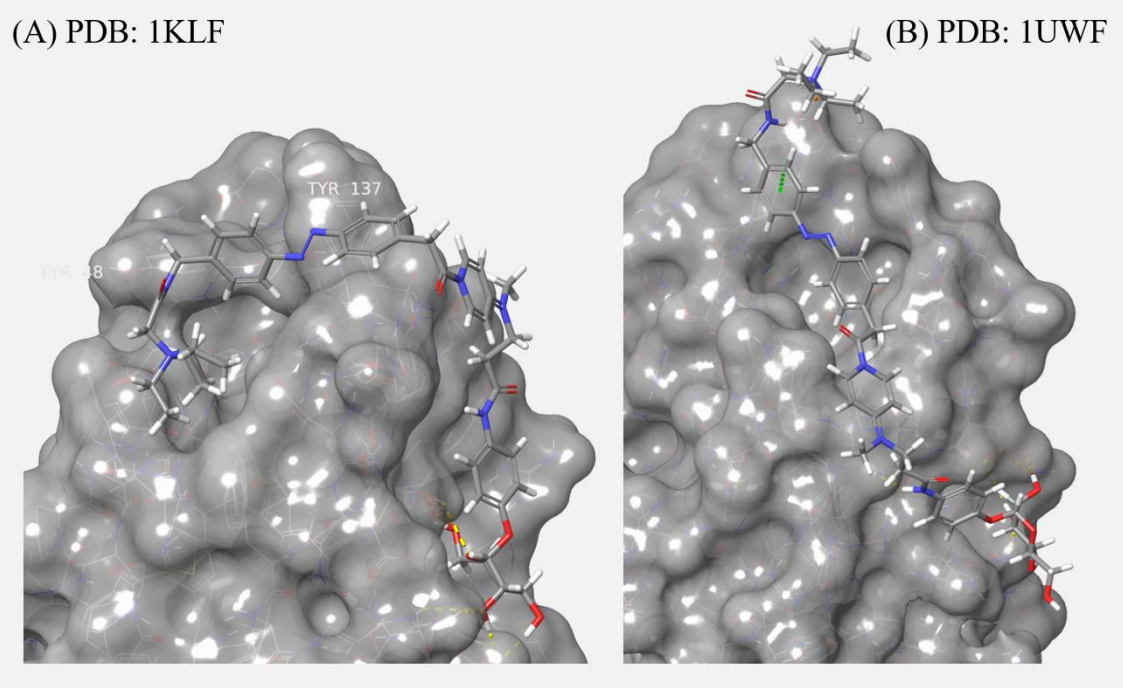

Figure 74: Results of the docking of conjugate (**6**+**35**) with Glide: (A) Docking was performed with the open gate conformation of lectin FimH (PDB code: 1KLF) and (B) with the closed gate conformation of lectin FimH (PDB code: 1UWF). Stabilising hydrogen bonds are marked in yellow, and stabilising ππ interactions are marked in green.

Interaction diagrams for the conjugate (**6**+**35**) are shown in Figure 75.

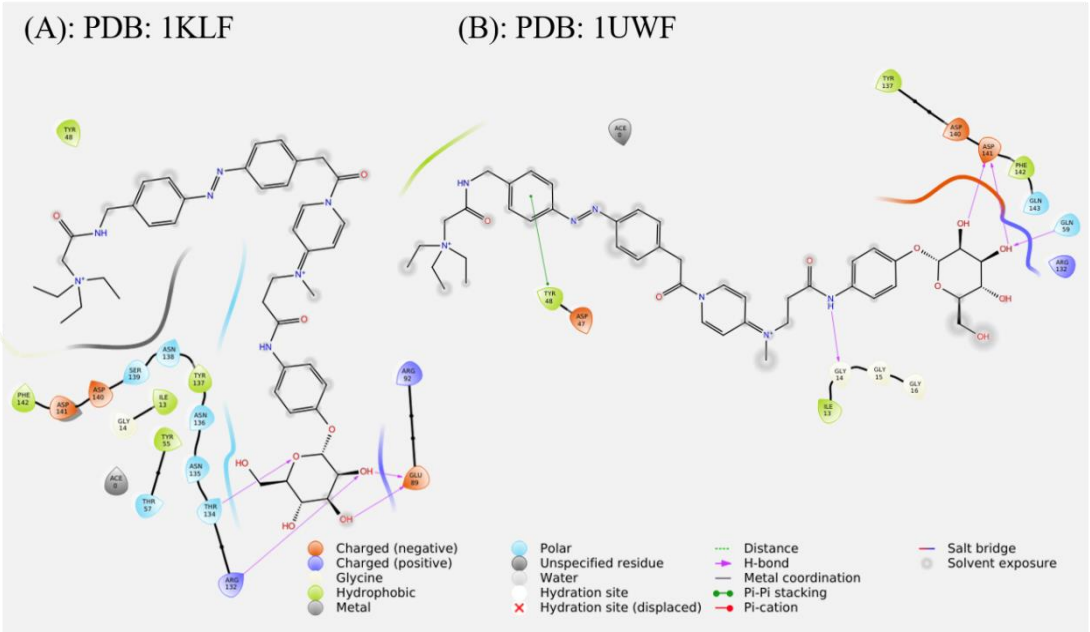

Figure 75: Interaction diagrams for the conjugate (**6**+**35**) with lectin FimH in the open gate conformation (left, (A), 1KLF) and the closed gate conformation (right, (B), 1UWF). Stabilising hydrogen bonds are highlighted in violet and stabilising ππ interactions are highlighted in green.

The substitution pattern of the azobenzene might also have a great influence on the applicability as ‘gate keeper’ molecules. Depending on attachment of the thioester residue in the *ortho*-, *meta*- or *para*-position of the azobenzene ‘gate keeper’ moiety, the angle of the photoswitchable ‘gate keeper’ vary significantly. Thus, compound **38** was designed and subjected to docking studies. The results of the docking are depicted in Figure 76. Conjugate (**6**+**38**) showed unspecific binding related to the 1KLF conformation but the orientation above the binding site was still promising for ligation experiments. In case of the 1UWF conformation a weak binding characterised by a very mean docking score of -3.93 was observed.

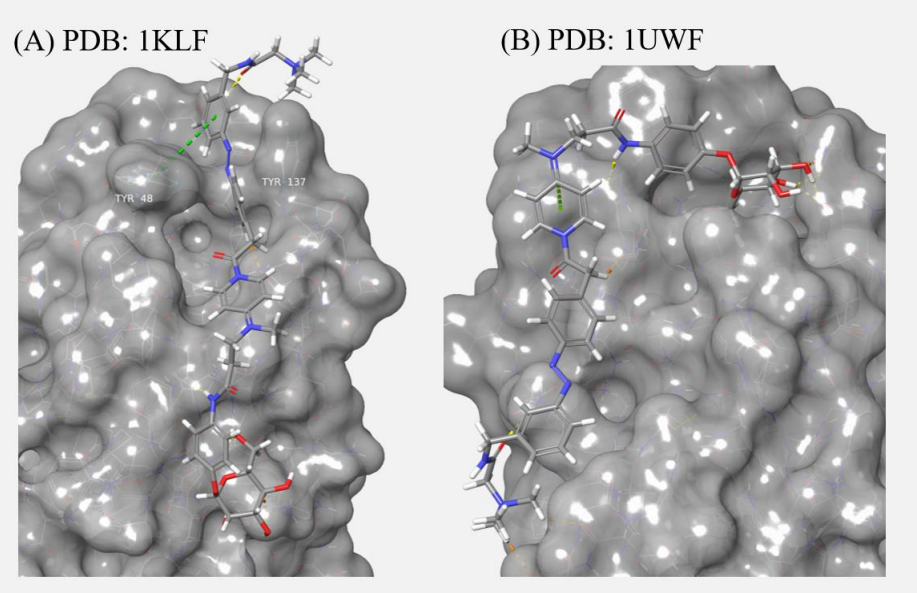

Figure 76: Results of the docking of conjugate (**6**+**38**) with Glide: (A) Docking was performed with the open gate conformation of lectin FimH (PDB code: 1KLF) and (B) with the closed gate conformation of lectin FimH (PDB code: 1UWF). Stabilising hydrogen bonds are marked in yellow, and stabilising ππ interactions are marked in green.

Interaction diagrams for the conjugate (**6**+**38**) are shown in Figure 77.

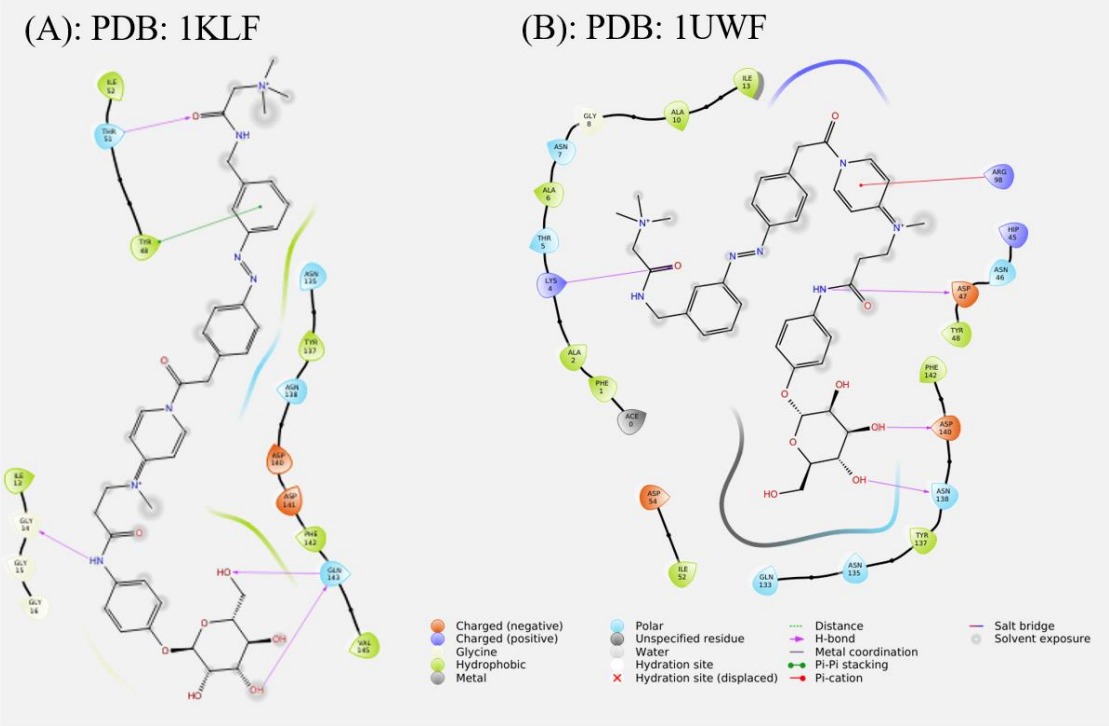

Figure 77: Interaction diagrams for the conjugate (**6**+**38**) with lectin FimH in the open gate conformation (left, (A), 1KLF) and the closed gate conformation (right, (B), 1UWF). Stabilising hydrogen bonds are highlighted in violet and stabilising ππ interactions are highlighted in green.

The next group of potential 'gate keeper' precursors which were estimated by docking studies are the carbohydrate-based derivatives **79**, **80**, **102** and **103**. The mannoside **78** had already been investigated by I. STAMER, who observed docking scores which were at least in the range of methyl α-D mannoside.[381] Derivatives **79** and **80** were investigated here. First, α-D-glucoside **79** was subjected to docking studies as conjugate (**6**+**79**) (Figure 78). The conjugate (**6**+**79**) showed affinity both for the 1KLF conformation of FimH (docking score -5.73) and the 1UWF conformation (docking score -10.76). It must be taken in account that the α-D-glucoside moiety was located within the binding site and not as expected the α-D-mannoside residue. Thus, the conjugate was perfectly oriented for ligation with the lectin and subsequent use as 'gate keeper' molecule.

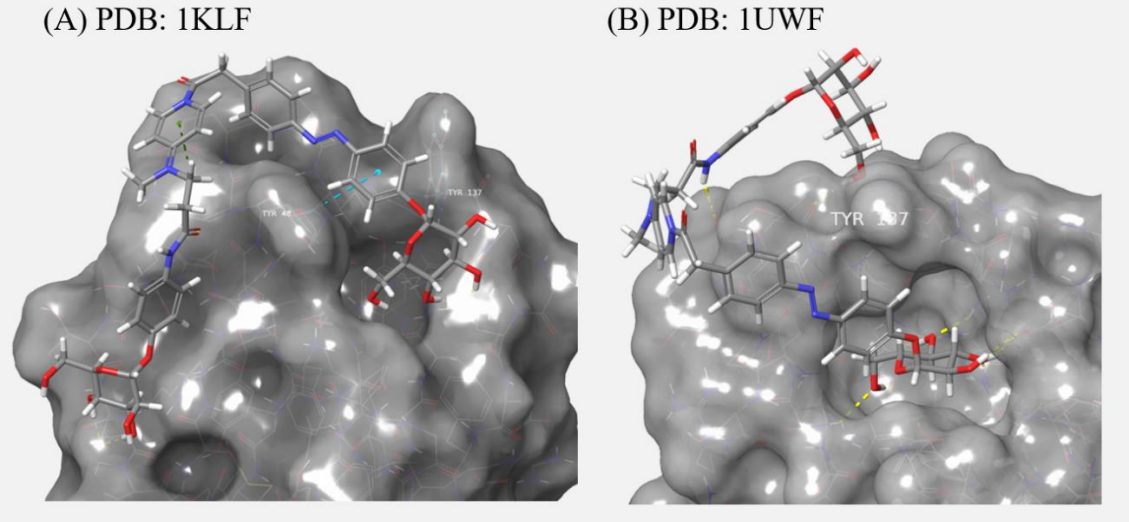

Figure 78: Results of the docking of conjugate (**6**+**79**) with Glide: (A) Docking was performed with the open gate conformation of lectin FimH (PDB code: 1KLF) and (B) with the closed gate conformation of lectin FimH (PDB code: 1UWF). Stabilising hydrogen bonds are marked in yellow.

Interaction diagrams for the conjugate (**6**+**79**) are shown in Figure 79.

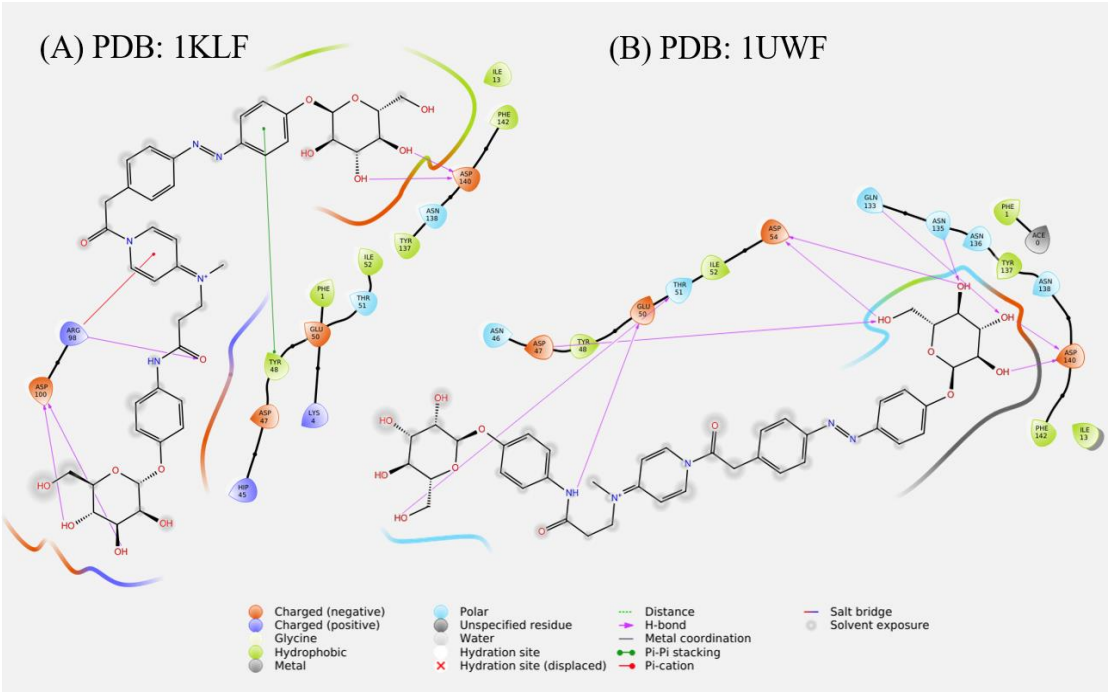

Figure 79: Interaction diagrams for the conjugate (**6**+**79**) with lectin FimH in the open gate conformation (left, (A), 1KLF) and the closed gate conformation (right, (B), 1UWF). Stabilising hydrogen bonds are highlighted in violet and stabilising $\pi\pi$ interactions are highlighted in green.

However, the formation of conjugate (**6**+**79**) was intended to be a site-directing aid. Since the result of the docking showed that this does not work as expected via the mannoside

moiety, a conjugate of compound **79** and DMAP (Figure 81) was submitted to docking studies to evaluate the influence of the affinity driven DMAP ligand **6**. The docking results for the conjugate (DMAP+**79**) are shown in Figure 80. The glucoside moiety was located beneath the entrance of the binding site. This result supported the idea that the labelling of the binding site might work affinity-driven, albeit the mannoside DMAP catalyst **6** is located at the putatitive binding site which led in case of conjugate (**6**+**79**) to a suitable preorientation of the 'gate keeper' moiety within the binding site. The (DMAP+**79**) conjugate was not able to provide this preorientation.

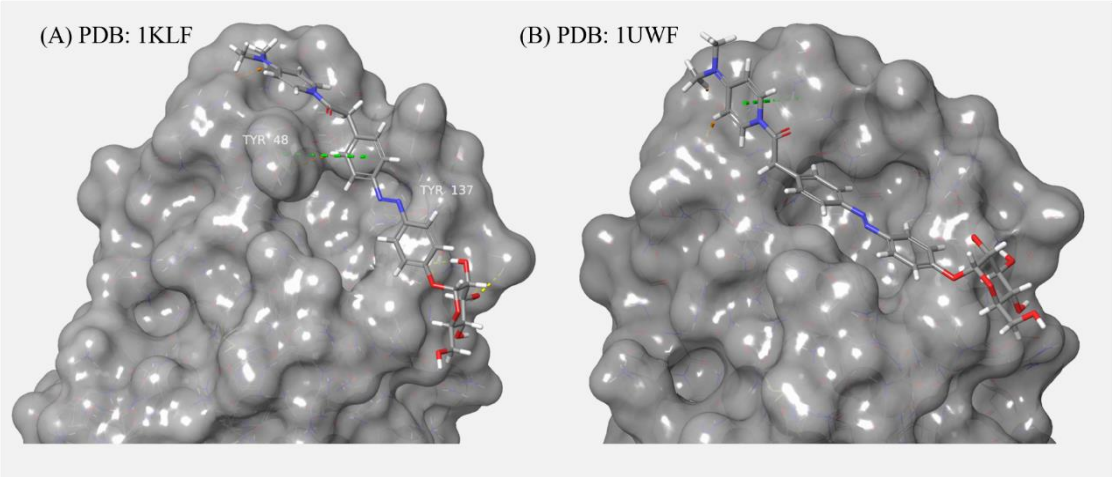

Figure 80: Results of the docking of conjugate (DMAP+**79**) with Glide: (A) Docking was performed with the open gate conformation of lectin FimH (PDB code: 1KLF) and (B) with the closed gate conformation of lectin FimH (PDB code: 1UWF). Stabilising hydrogen bonds are marked in yellow, and stabilising ππ interactions are marked in green.

Interaction diagrams for the conjugate (DMAP+**79**) are shown in Figure 81.

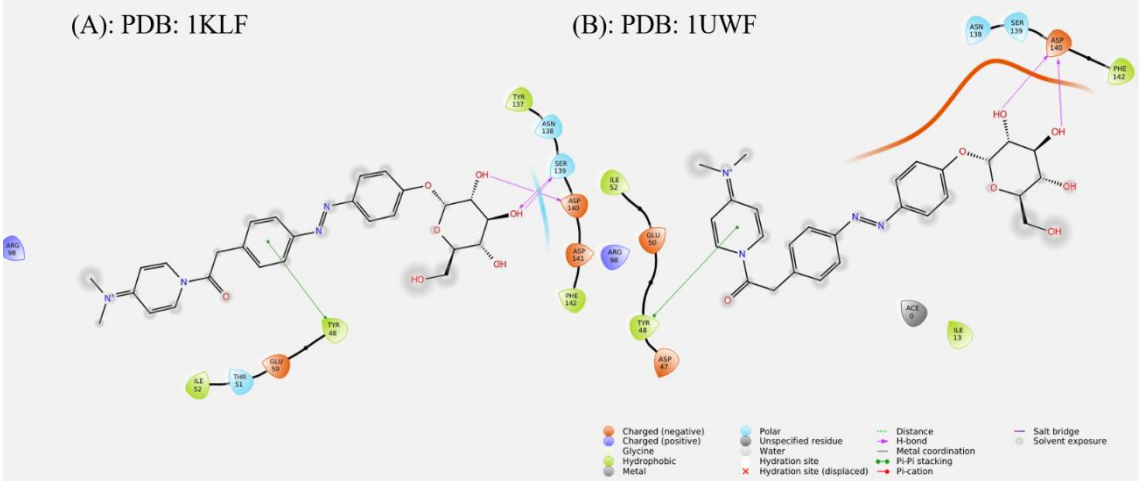

Figure 81: Interaction diagrams for the conjugate (DMAP+**79**) with lectin FimH in the open gate conformation (left, (A), 1KLF) and the closed gate conformation (right, (B), 1UWF). Stabilising hydrogen bonds are highlighted in violet and stabilising ππ interactions are highlighted in green.

The β-D-glucoside **80** was subjected to docking studies as conjugate (**6**+**80**). The results are shown in Figure 82. The docked structure of conjugate (**6**+**80**) with the 1KLF conformation of the CRD ensued a docking score of -6.64.

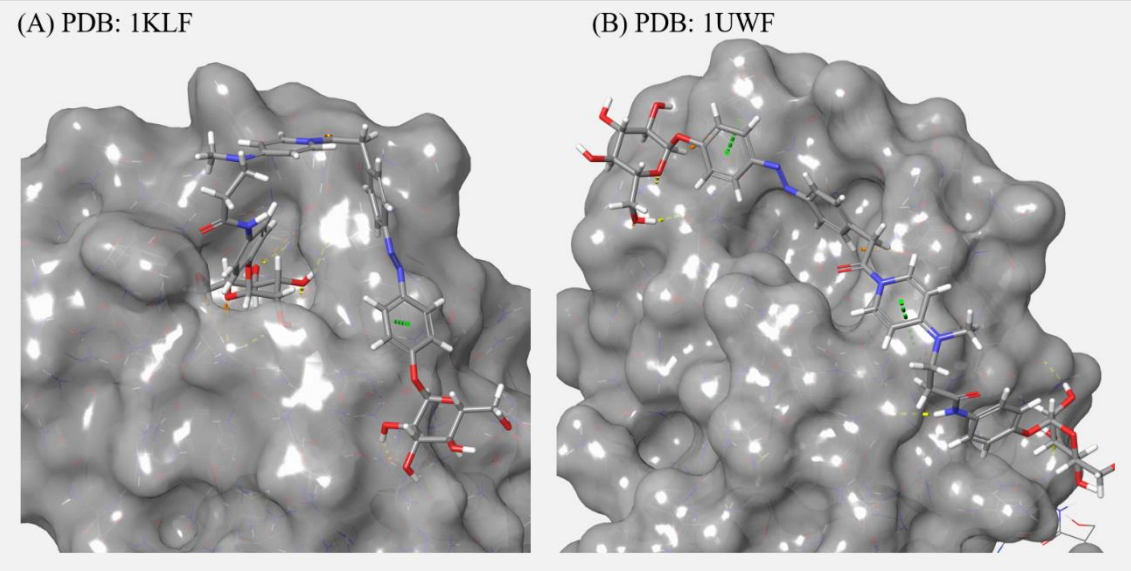

Figure 82: Results of the docking of conjugate (**6**+**80**) with Glide: (A) Docking was performed with the open gate conformation of lectin FimH (PDB code: 1KLF) and (B) with the closed gate conformation of lectin FimH (PDB code: 1UWF). Stabilising hydrogen bonds are marked in yellow, and stabilising ππ interactions are marked in green.

Interaction diagrams for the conjugate (**6**+**80**) are shown in Figure 83. Especially Tyr137 was in proximity of the reactive active ester of the conjugate.

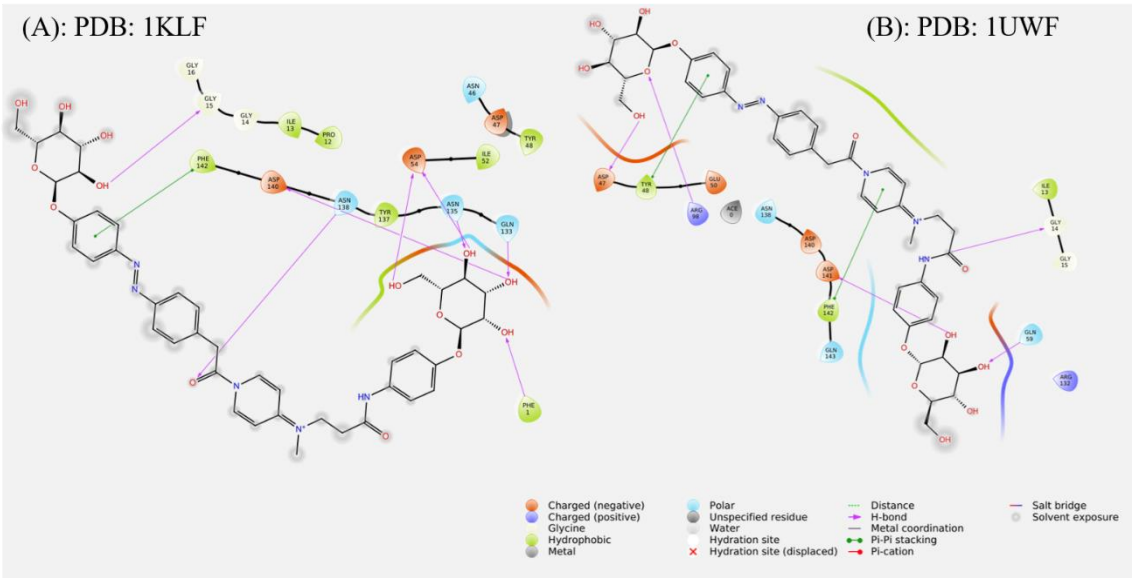

Figure 83: Interaction diagrams for the conjugate (**6**+**80**) with lectin FimH in the open gate conformation (left, (A), 1KLF) and the closed gate conformation (right, (B), 1UWF). Stabilising hydrogen bonds are highlighted in violet and stabilising ππ interactions are highlighted in green.

The results for the methoxy-substituted azobenzene derivative **102** are shown in Figure 84. Both, for the 1KLF and the 1UWF conformation of the CRD the mannoside residue was located at the putative binding site instead of the CRD. However, the methoxy substituent was located in the binding site like a 'gate keeper' and the active ester was located at the rim of the binding site.

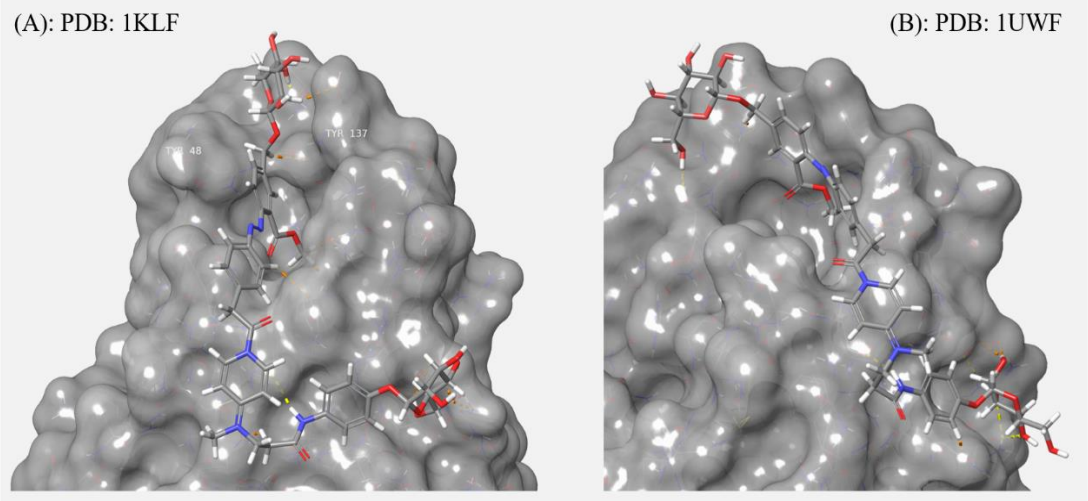

Figure 84: Results of the docking of conjugate (**6**+**102**) with Glide: (A) Docking was performed with the open gate conformation of lectin FimH (PDB code: 1KLF) and (B) with the closed gate conformation of lectin FimH (PDB code: 1UWF). Stabilising hydrogen bonds are marked in yellow.

Interaction diagrams for the conjugate (**6**+**102**) are shown in Figure 85.

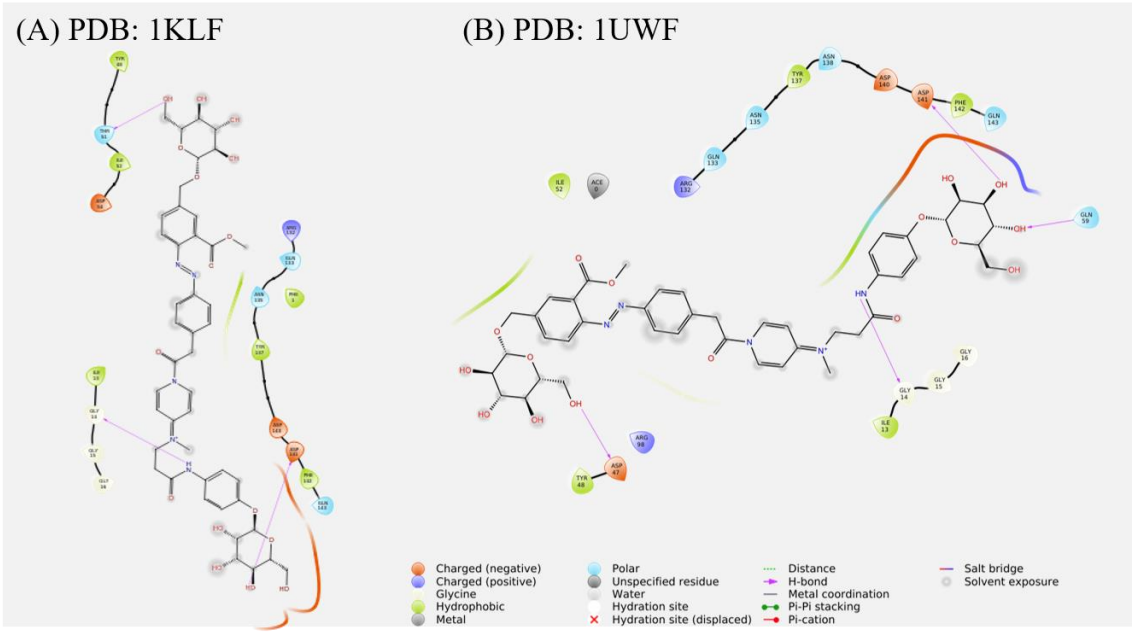

Figure 85: Interaction diagrams for the conjugate (**6**+**102**) with lectin FimH in the open gate conformation (left, (A), 1KLF) and the closed gate conformation (right, (B), 1UWF). Stabilising hydrogen bonds are highlighted in violet.

In case of the analogous mannoside **103** the same situation with the azobenzene moiety across the binding site was observed for the closed gate conformation. In case of the 1KLF conformation of the CRD the mannoside residue of the 'gate keeper' unit was docked within the binding site. The docking score accounts for -7.17 (Figure 86).

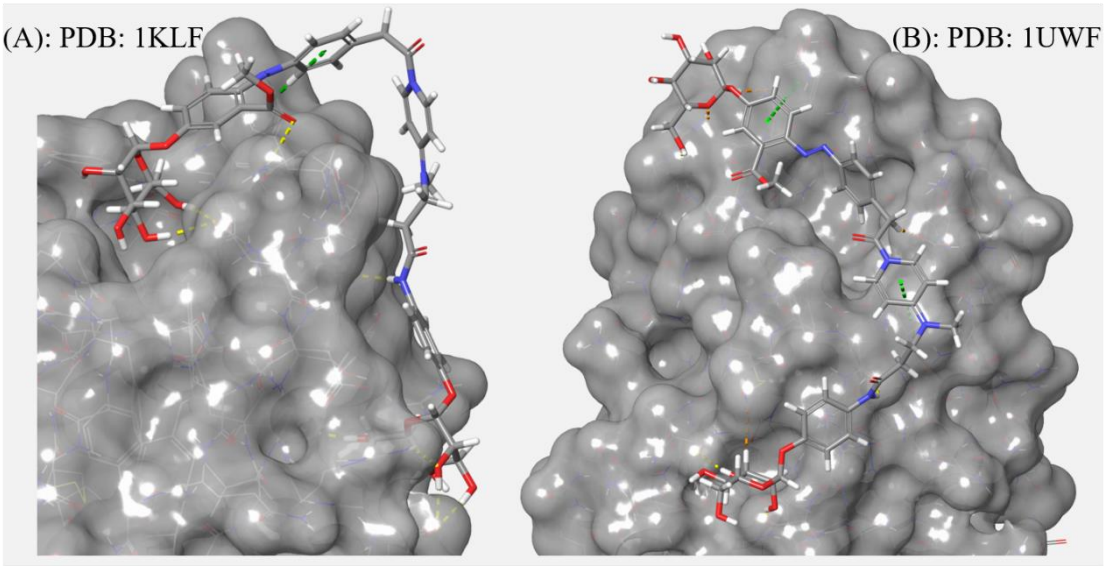

Figure 86: Results of the docking of conjugate (**6**+**103**) with Glide: (A) Docking was performed with the open gate conformation of lectin FimH (PDB code: 1KLF) and (B) with the closed gate conformation of lectin FimH (PDB code: 1UWF). Stabilising hydrogen bonds are marked in yellow, and stabilising ππ interactions are marked in green.

Interaction diagrams for the conjugate (**6**+**103**) are shown in Figure 87. Especially Tyr137 was in proximity of the conjugate's reactive centre.

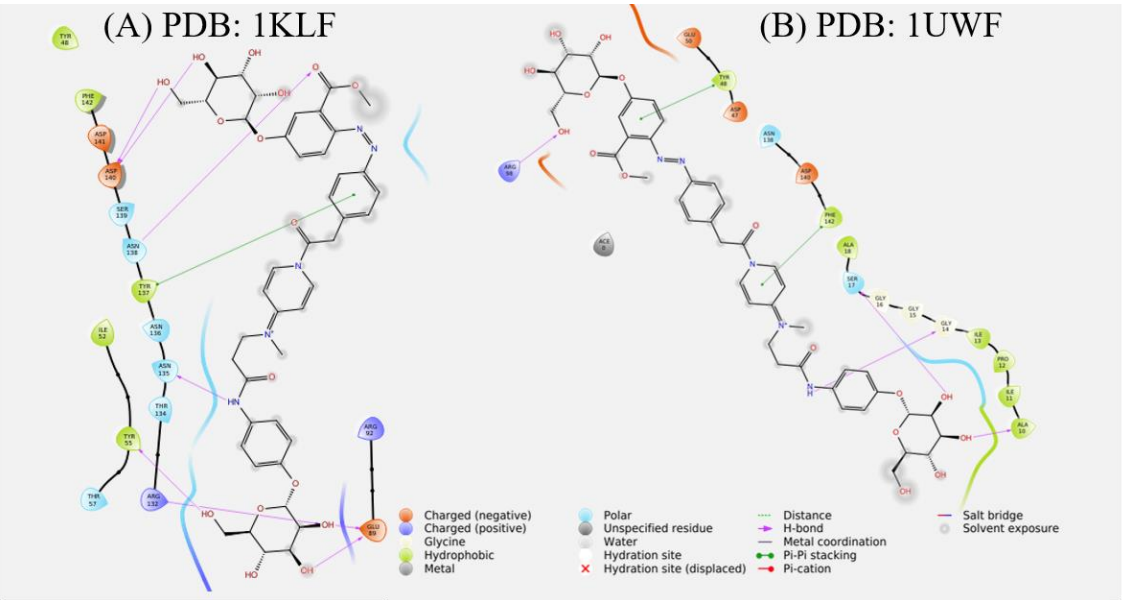

Figure 87: Interaction diagrams for the conjugate (**6**+**103**) with lectin FimH in the open gate conformation (left, (A), 1KLF) and the closed gate conformation (right, (B), 1UWF). Stabilising hydrogen bonds are highlighted in violet and stabilising ππ interactions are highlighted in green.

Since the docking scores which result from the docking experiments depend on many parameters which can be individually set-up, they are slightly difficult to compare and assess specially if the experiments are performed by different users or with varying releases of the Schrödinger software package. Thus, it is always favourable to have a well-known and reliable reference. Therefore, docking studies were performed with methyl α-D-mannoside (MeMan) and *para*-nitrophenyl α-D-mannoside (*p*NP). The results for MeMan are given in Figure 88. The docking score of methyl mannoside with the 1KLF conformation is –8.18 and with the 1UWF conformation is -7.28.

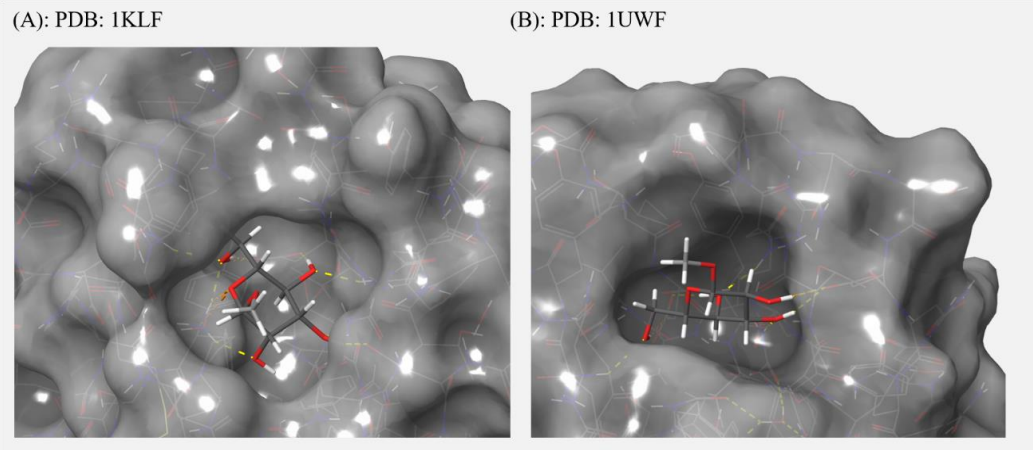

Figure 88: Results of the docking of MeMan with Glide: (A) Docking was performed with the open gate conformation of lectin FimH (PDB code: 1KLF) and (B) with the closed gate conformation of lectin FimH (PDB code: 1UWF). Stabilising hydrogen bonds are marked in yellow.

Interaction diagrams for the methyl mannoside are shown in Figure 89.

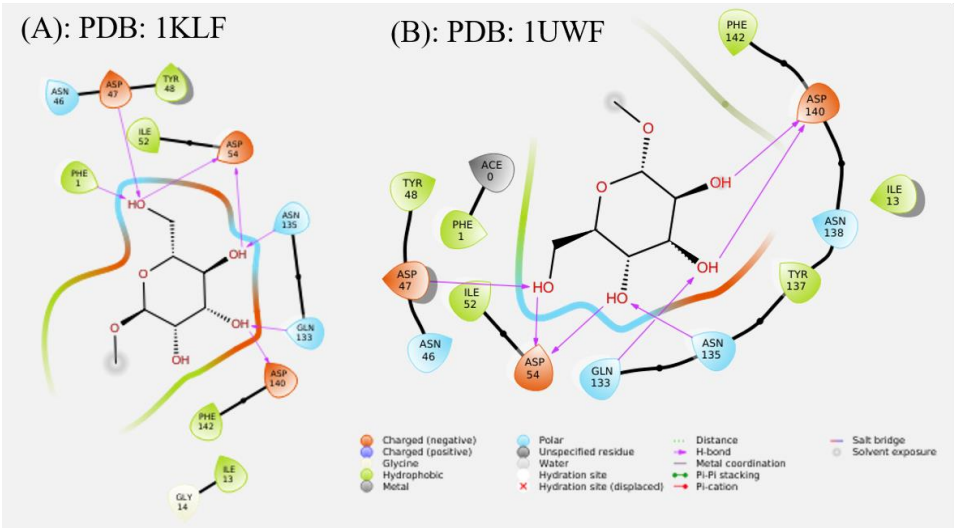

Figure 89: Interaction diagrams for MeMan with lectin FimH in the open gate conformation (left, (A), 1KLF) and the closed gate conformation (right, (B), 1UWF). Stabilising hydrogen bonds are highlighted in violet.

The results for *p*NP mannoside are given in Figure 90. The docking score of *p*NP mannoside with the 1KLF conformation is -8.53 and with the 1UWF conformation is -8.23.

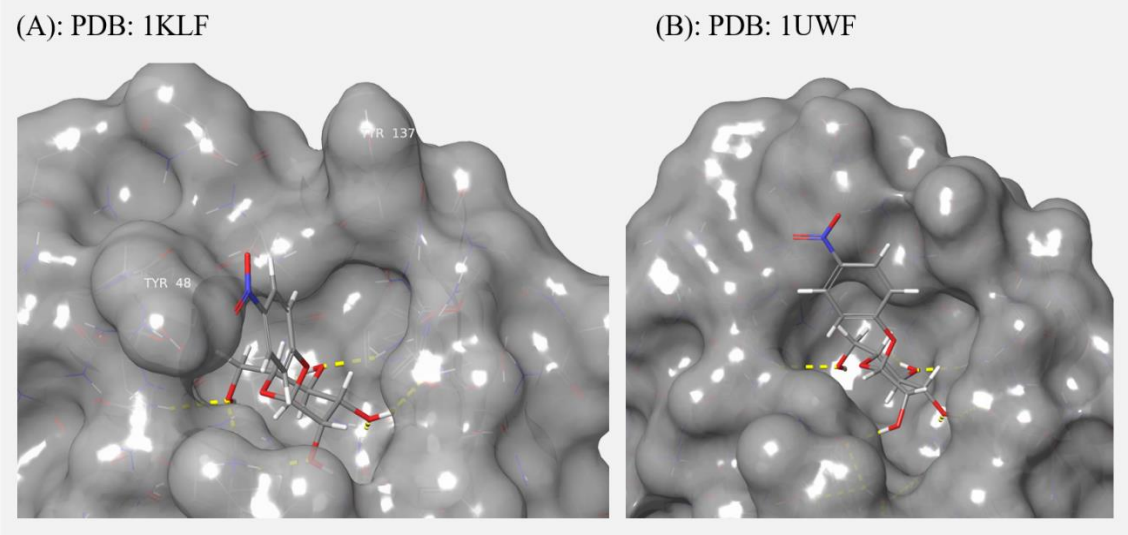

Figure 90: Results of the docking of *p*NP mannoside with Glide: (A) Docking was performed with the open gate conformation of lectin FimH (PDB code: 1KLF) and (B) with the closed gate conformation of lectin FimH (PDB code: 1UWF). Stabilising hydrogen bonds are marked in yellow.

Interaction diagrams for the *p*NP mannoside are shown in Figure 91.

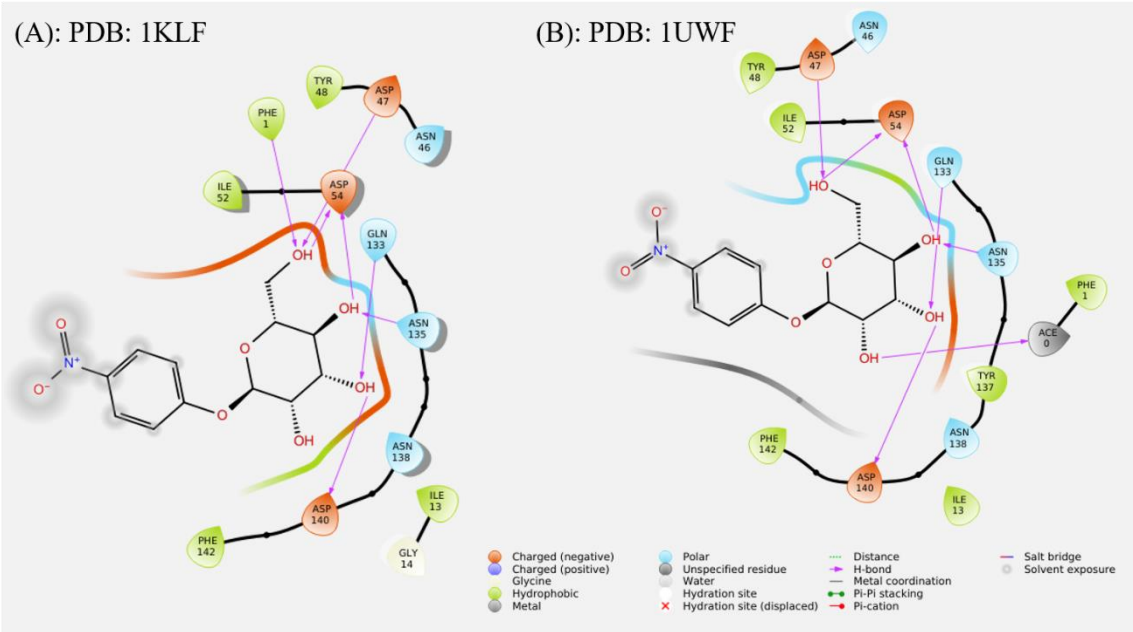

Figure 91: Interaction diagrams for the *p*NP mannoside with lectin FimH in the open gate conformation (left, (A), 1KLF) and the closed gate conformation (right, (B), 1UWF). Stabilising hydrogen bonds are highlighted in violet.

The results of all performed docking studies are summarised in Table 3.

Table 3: Summary of all performed docking studies (1KLF: open gate conformation; 1UWF closed gate conformation of FimH).

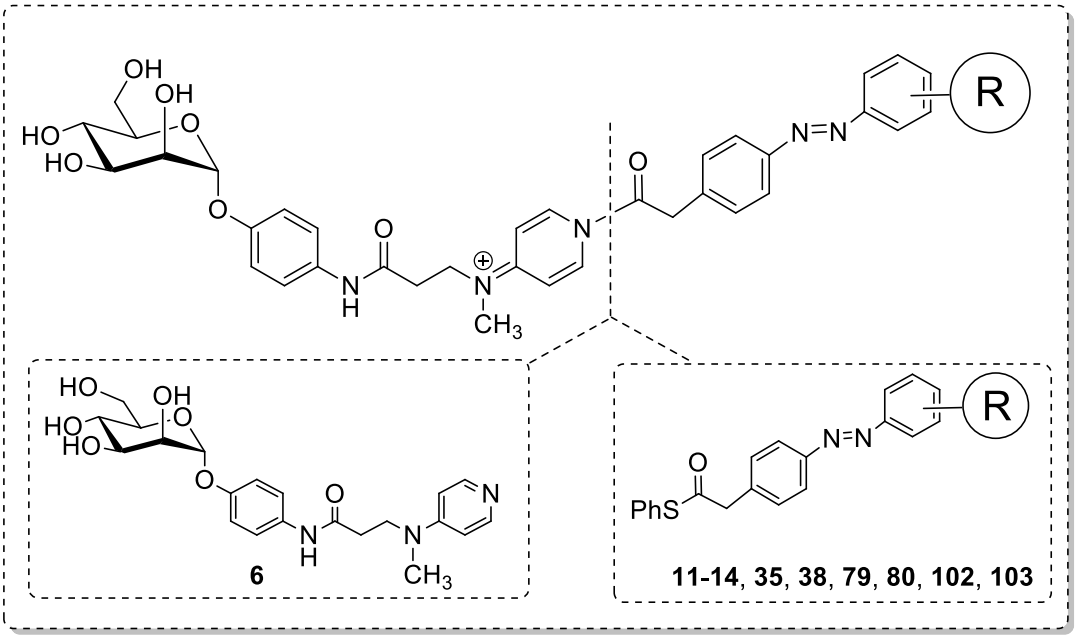

Docked conjugate	Ligand binding in CRD: Glide docking scores	Ligand bound to putative binding site*
6+11	--	1KLF and 1UWF
6+12	--	1KLF and 1UWF
6+13	--	1KLF and 1UWF
6+14	-7.94 (1UWF)	1KLF
6+35	--	1KLF and 1UWF
6+38	-3.93 (1UWF)	1KLF: unspecific
6+79	-10.76 (1UWF) -5.73 (1KLF)	--
DMAP + **79**	--	1KLF and 1UWF
6+80	-6.64 (1KLF)	1UWF
6+102	--	1KLF and 1UWF
6+103	-7.17[b] (1KLF)	1UWF: unspecific

Docked conjugate	Ligand binding in CRD: Glide docking scores	Ligand bound to putative binding site*
MeMan[c]	-7.28 (1UWF) -8.18 (1KLF)	
*p*NPMan[c]	-8.23 (1UWF) -8.53 (1KLF)	

* No docking scores are obtained when the conjugate is not located in the CRD
[a] the glucoside residue of the 'gate keeper' moiety instead of the site directing DMAP mannoside moiety is located within the binding site.
[b] the mannoside residue of the 'gate keeper' moiety instead of the site directing DMAP mannoside moiety is located within the binding site.
[c] MeMan and *p*NPMan were docked as references and thus used without previous conjugation.

In summary, all structures designed to function as 'gate keeper' molecules after ligation form a strong complex with FimH, although the affinity moiety of the reactive conjugates is not in all cases located within the carbohydrate binding site. Nevertheless, the conjugates are at least located at the putative binding site in such a way that a pre-orientation for the ligation with one of the amino acids Tyr48, Tyr137 or Thr51 is provided. At the putative binding site hydrogen bonds with the glycoside moiety of the conjugates are formed and the reactive active ester part of the conjugates is adjusted towards the edge of the binding site.

Furthermore, also the eligibility of the molecules as 'gate keeper' molecules after ligation with Tyr48, Tyr137 and Thr51 was investigated by molecular modelling. Ligation was performed manually based on the docking results which were obtained for each conjugate of the DMAP mannoside **6** with the respective thioester. Thus, six structures resulted for each 'gate keeper' precursor since ligation was performed with all three relevant amino acids and both for the 1KLF and the 1UWF conformation. The resulting structures were energetically minimised by MacroModel.[408] An efficient 'gate keeper' should leave the binding site open in its one isomeric state and close the binding site in its second isomeric state. Consequently, both states should be attainable in the form of an energetically advantageous state. Thus, a multitude of alignments of the azobenzene moiety were studied. The alignments were obtained by a rotational scan with MacroModel.[408] The azobenzene moiety was rotated about two dihedral angles which are shown in Figure 92. Each dihedral angle, respectively dihedral angle 1 and dihedral angle 2, were changed in steps of 10° and the potential energy of each resulting conformation was recorded. Thus,

1369 structures and the corresponding potential energies were obtained for each ligated amino acid and for each CRD conformation. Additionally, all rotational scans were performed for the *Z*- and the *E*-configuration of the 'gate keeper' molecules. For the *Z*-configuration the angle and the dihedral angle of the azo moiety were defined.[103]

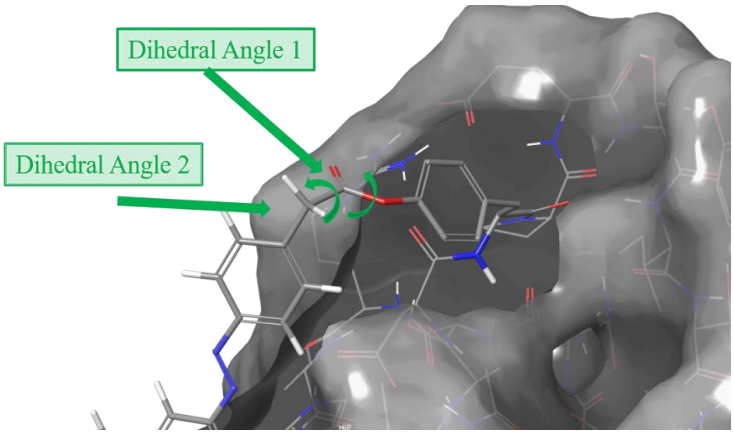

Figure 92: For the evaluation of the 'gate keeper' molecules the ligated azobenzene moieties were rotated about the dihedral angle 1 and dihedral angle 2 while the resulting potential energies were recorded. The potential energies are plotted as a contour plot depending on the two dihedral angles afterwards.

The evaluation of all structures must be performed manually and consequently is very time consuming. A contour plot proved helpful to visualise the potential energies resulting for each conformation. The dihedral angle 2 was plotted on the x-axis and the dihedral angle 1 was plotted on the y-axis. The plot was coloured as a contour diagram by the potential energies which occurred for each single combination of dihedral angle 1 and 2. In the contour diagram red indicates a high potential energy and blue indicates a low potential energy. These diagrams allow to identify regions of energetically advantageous conformers. Nevertheless, all structures were also sighted manually to find good conformations which show the binding site either opened or closed. Finally, the energetically advantageous structures were matched to find those promising 'gate keeper' moieties which have a suitable state of low energy for the *E*- and for the *Z*-state. The results of the rotational scans for all compounds in Table 3 are discussed in the following paragraphs. The results for the biphenyl derivative **11** are shown in Figure 93 to Figure 98. For the 1KLF open gate conformation positive matches were observed for the ligation of compound **11** to Tyr48 and Tyr137. In both cases the *E*-configuration left the binding site open in many of the calculated conformations during the rotational scan. In case of the *Z*-configured 'gate keeper' molecule, conformations of

low potential energy were observed which close the binding site and are thus able to avoid binding of ligands at the binding site.

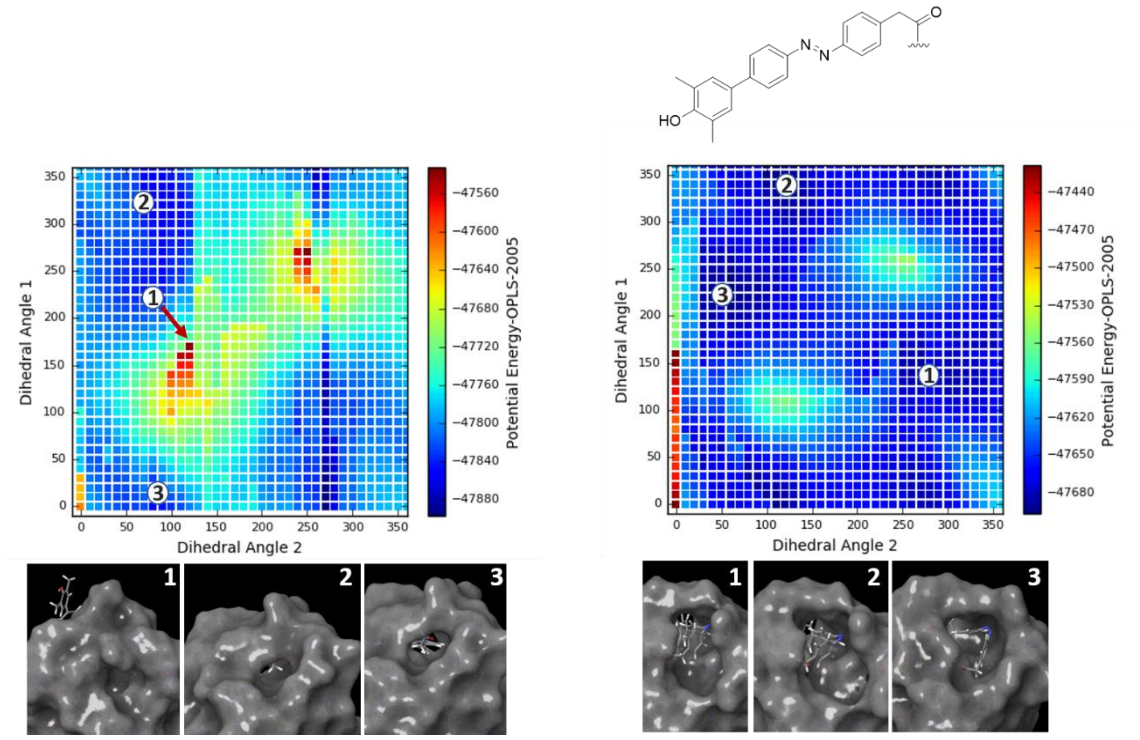

Figure 93: Results of the rotational scan with MacroModel for the azobenzene derivative **11** ligated to the amino acid Tyr48 (open gate conformation 1KLF) in *E*- (left) and *Z*-conformation (right). The potential energy is plotted as a contour diagram in relation to the dihedral angles 2 (x-axis) and 1 (y-axis).

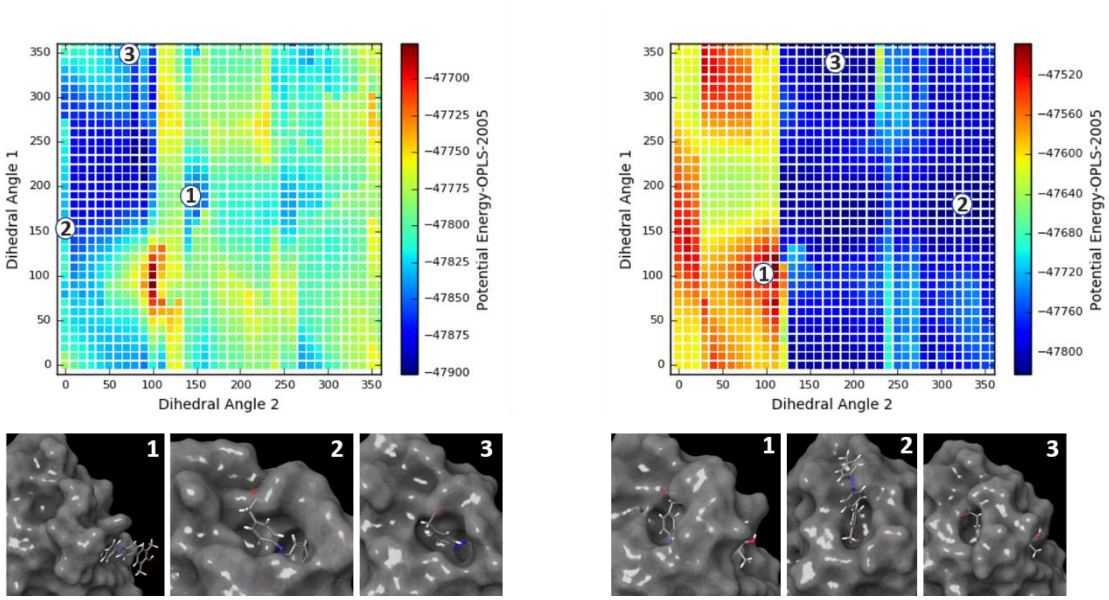

Figure 94: Results of the rotational scan with MacroModel for the azobenzene derivative **11** ligated to the amino acid Tyr137 (open gate conformation 1KLF) in *E*- (left) and *Z*-conformation (right). The potential energy is plotted as a contour diagram in relation to the dihedral angles 2 (x-axis) and 1 (y-axis).

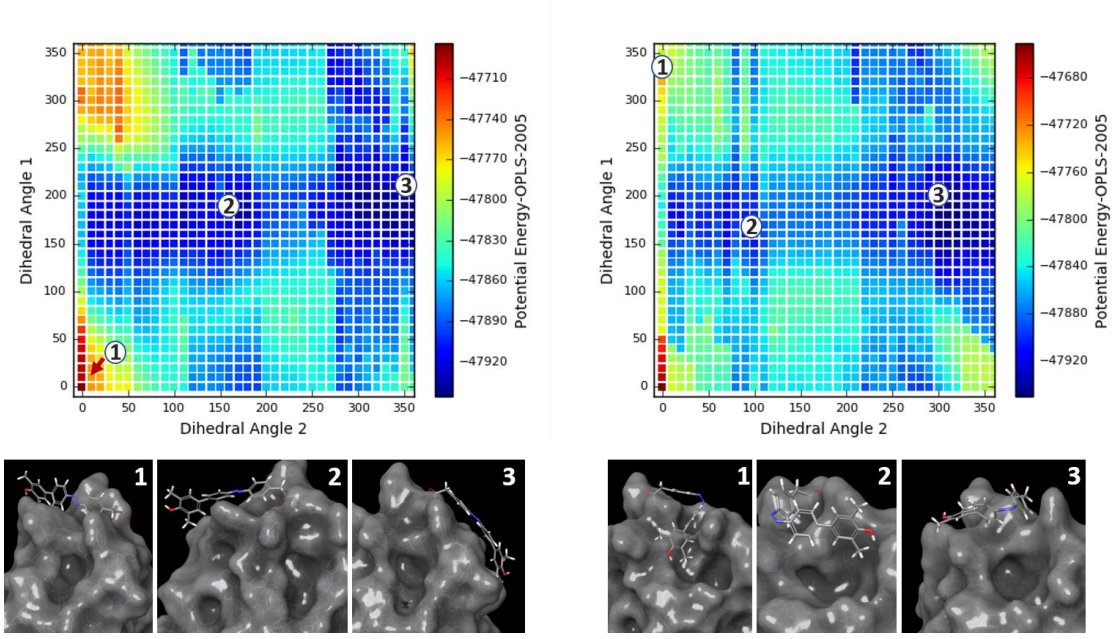

Figure 95: Results of the rotational scan with MacroModel for the azobenzene derivative **11** ligated to the amino acid Thr51 (open gate conformation 1KLF) in *E*- (left) and *Z*-conformation (right). The potential energy is plotted as a contour diagram in relation to the dihedral angles 2 (x-axis) and 1 (y-axis).

For the closed gate conformations only one positive match was observed. In case of the protein which was ligated at the Tyr48 the binding site stayed open when the azobenzene moiety was in its *E*-state and was at least covered by the biphenyl residue in its *Z*-state in some energetically favoured conformations.

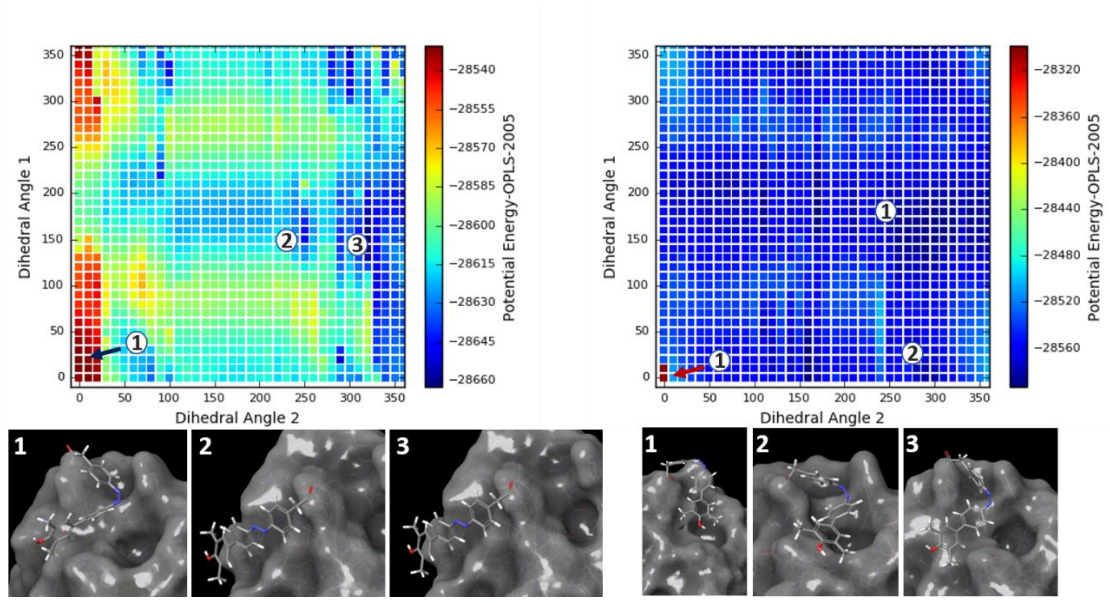

Figure 96: Results of the rotational scan with MacroModel for the azobenzene derivative **11** ligated to the amino acid Tyr48 (closed gate conformation 1UWF) in *E*- (left) and *Z*-conformation (right). The potential energy is plotted as a contour diagram in relation to the dihedral angles 2 (x-axis) and 1 (y-axis).

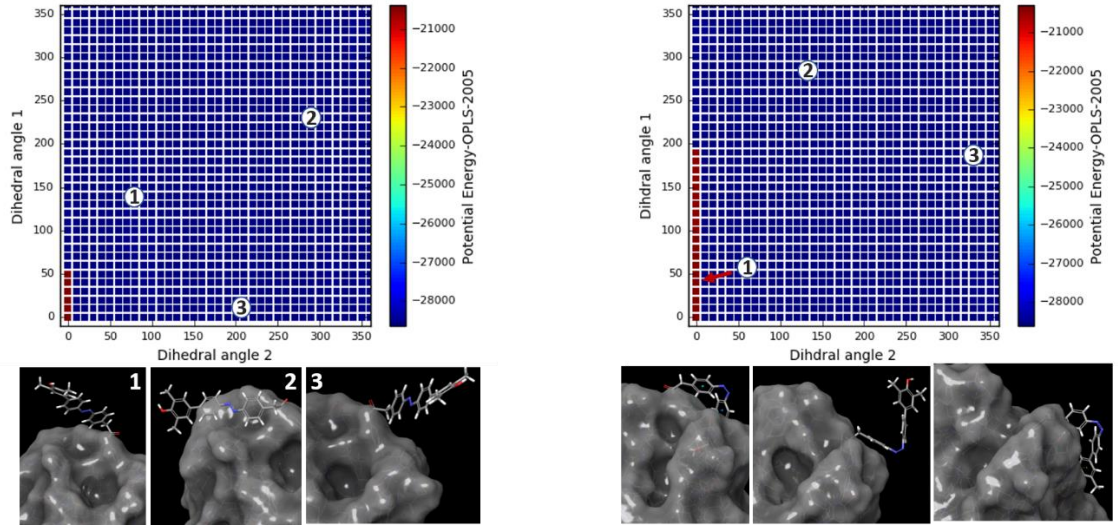

Figure 97: Results of the rotational scan with MacroModel for the azobenzene derivative **11** ligated to the amino acid Tyr137 (closed gate conformation 1UWF) in *E*- (left) and *Z*-conformation (right). The potential energy is plotted as a contour diagram in relation to the dihedral angles 2 (x-axis) and 1 (y-axis).

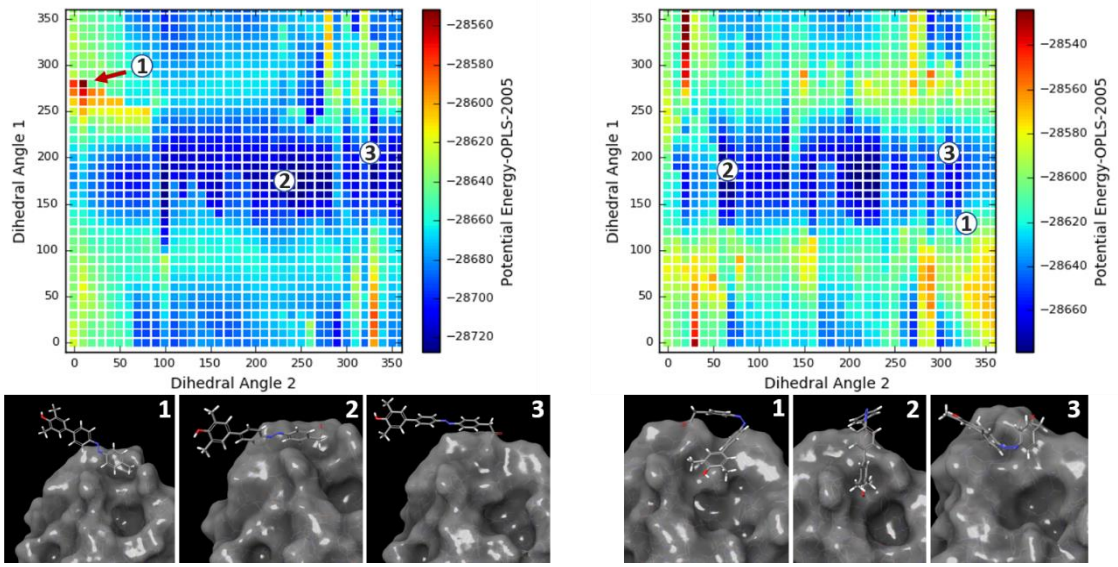

Figure 98: Results of the rotational scan with MacroModel for the azobenzene derivative **11** ligated to the amino acid Thr51 (closed gate conformation 1UWF) in *E*- (left) and *Z*-conformation (right). The potential energy is plotted as a contour diagram in relation to the dihedral angles 2 (x-axis) and 1 (y-axis).

The results for the pyridine derivative **14** are shown in Figure 99: to Figure 104:. A positive match was observed for the protein-ligated with the 'gate keeper' moiety at the amino acid Tyr48 both for the open and the closed gate structure. Additionally, also the Tyr137-ligated protein structure in the open gate conformation was a positive match. For

the closed gate conformation of the Tyr137-ligated protein structure only one closed structure (picture 1 on the right side of Figure 103) was observed.

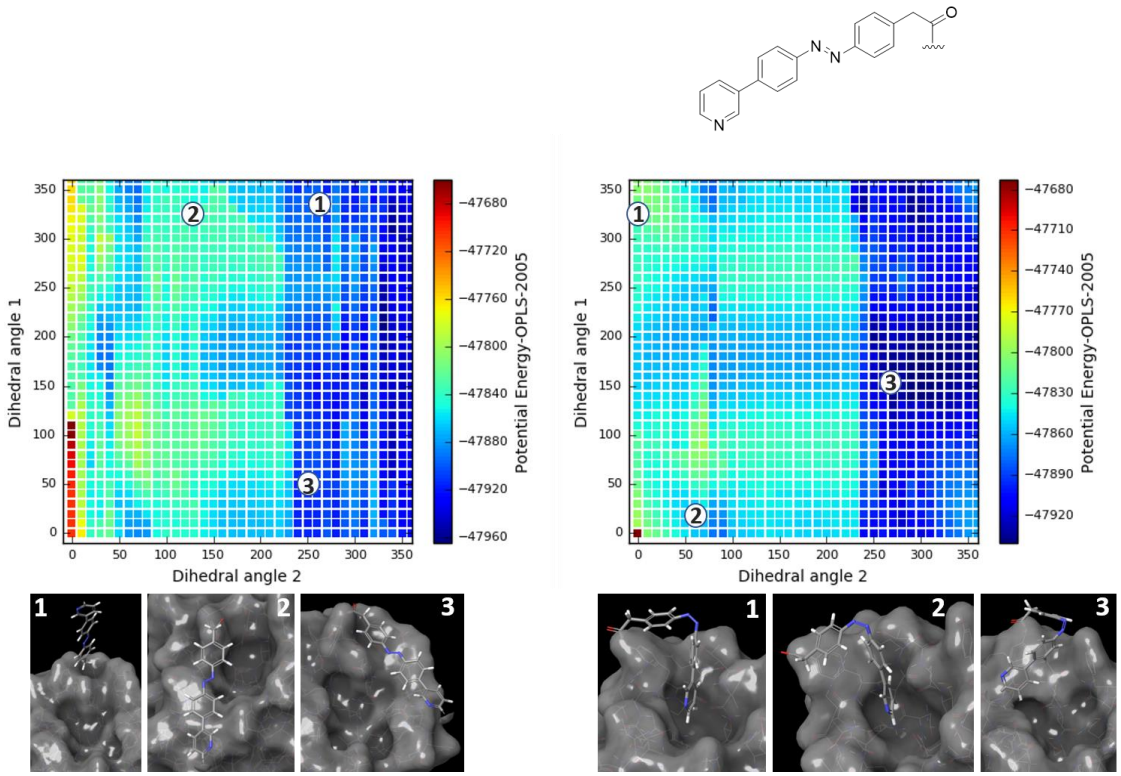

Figure 99: Results of the rotational scan with MacroModel for the azobenzene derivative **14** ligated to the amino acid Tyr48 (open gate conformation 1KLF) in *E*- (left) and *Z*-conformation (right). The potential energy is plotted as a contour diagram in relation to the dihedral angles 2 (x-axis) and 1 (y-axis).

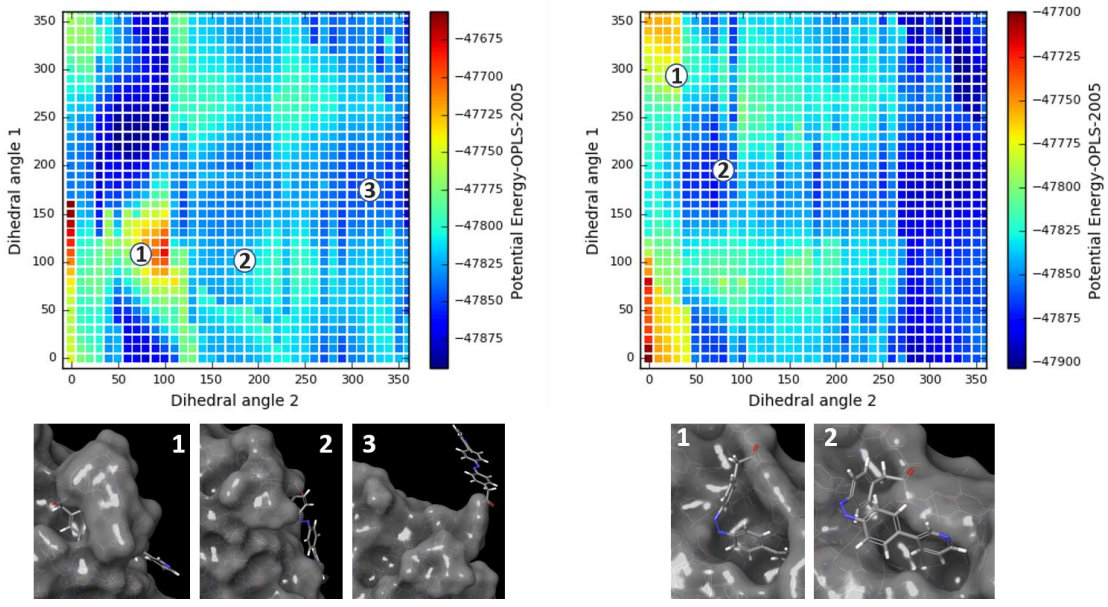

Figure 100: Results of the rotational scan with MacroModel for the azobenzene derivative **14** ligated to the amino acid Tyr137 (open gate conformation 1KLF) in *E*- (left) and *Z*-conformation (right). The potential energy is plotted as a contour diagram in relation to the dihedral angles 2 (x-axis) and 1 (y-axis).

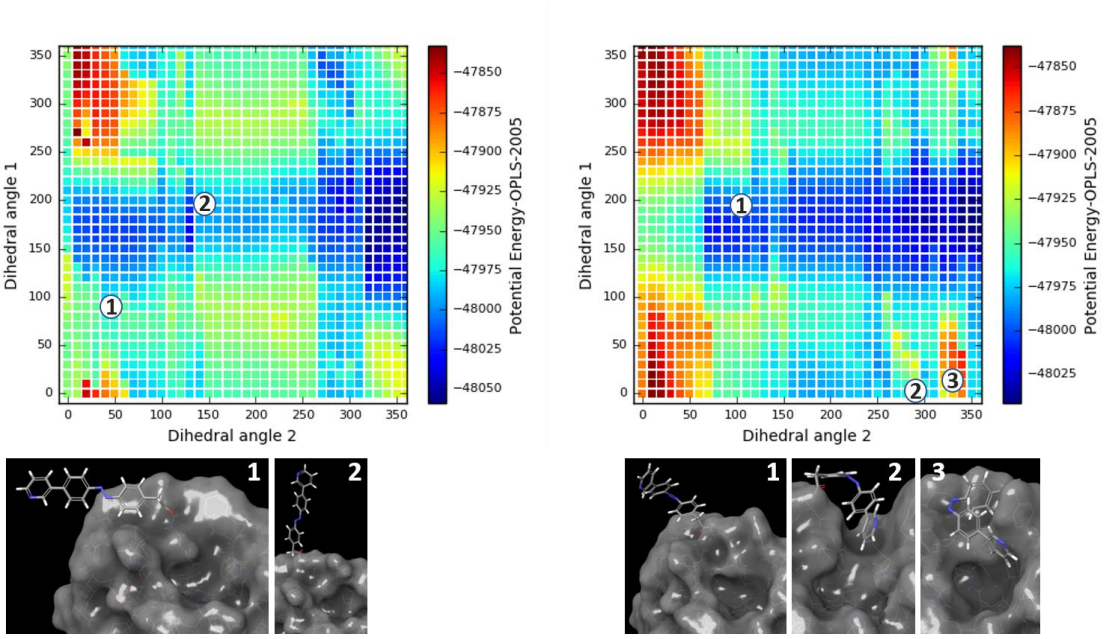

Figure 101: Results of the rotational scan with MacroModel for the azobenzene derivative **14** ligated to the amino acid Thr51 (open gate conformation 1KLF) in *E*- (left) and *Z*-conformation (right). The potential energy is plotted as a contour diagram in relation to the dihedral angles 2 (x-axis) and 1 (y-axis).

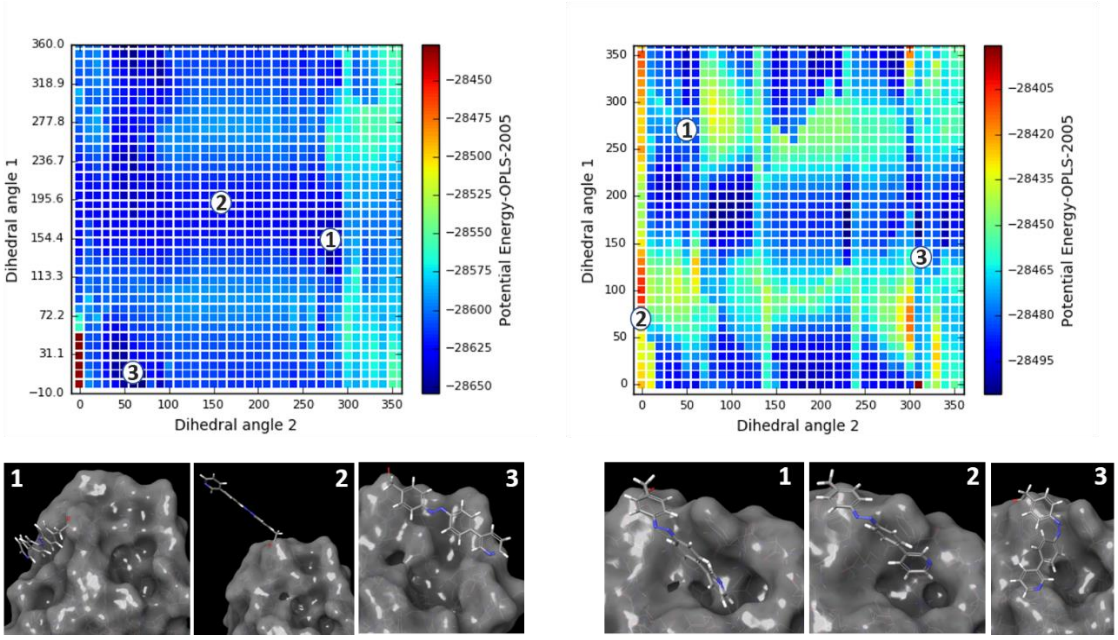

Figure 102: Results of the rotational scan with MacroModel for the azobenzene derivative **14** ligated to the amino acid Tyr48 (closed gate conformation 1UWF) in *E*- (left) and *Z*-conformation (right). The potential energy is plotted as a contour diagram in relation to the dihedral angles 2 (x-axis) and 1 (y-axis).

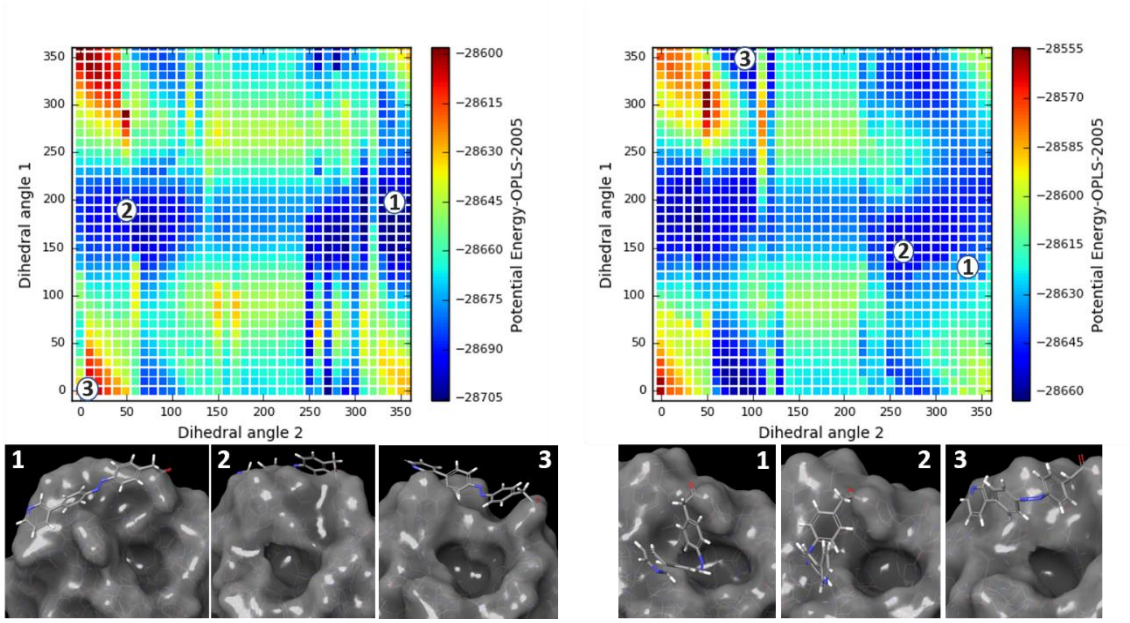

Figure 103: Results of the rotational scan with MacroModel for the azobenzene derivative **14** ligated to the amino acid Tyr137 (closed gate conformation 1UWF) in *E* (left) and *Z* conformation (right). The potential energy is plotted as a contour diagram in relation to the dihedral angles 2 (x-axis) and 1 (y-axis).

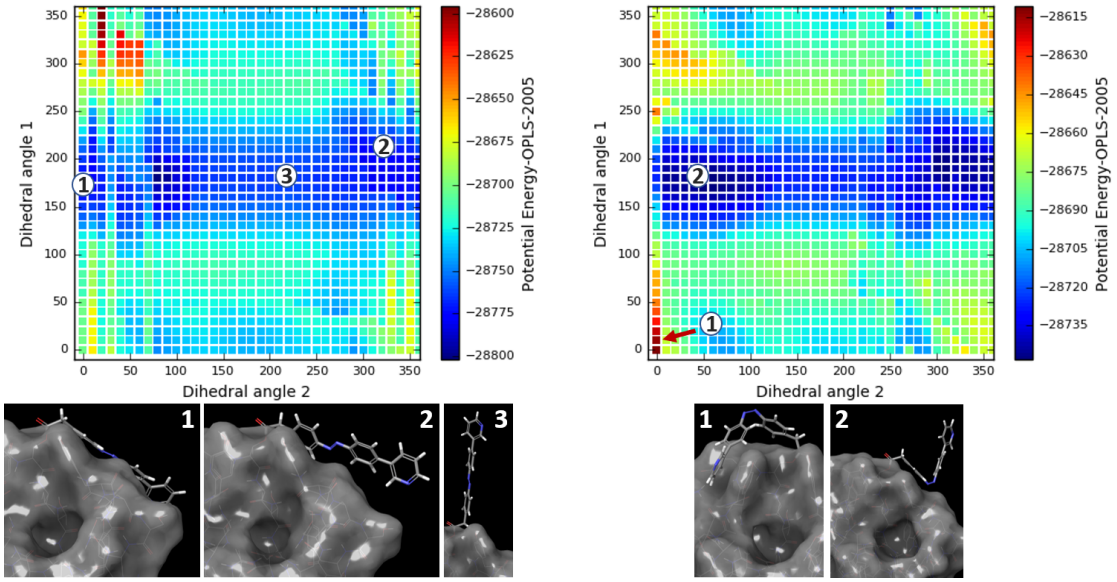

Figure 104: Results of the rotational scan with MacroModel for the azobenzene derivative **14** ligated to the amino acid Thr51 (closed gate conformation 1UWF) in *E*- (left) and *Z*-conformation (right). The potential energy is plotted as a contour diagram in relation to the dihedral angles 2 (x-axis) and 1 (y-axis).

The results for the pyridine derivative **12** are shown in Figure 105 to Figure 110. A positive match was observed for the protein ligated with the 'gate keeper' moiety at the amino acid Tyr48 both for the open and the closed gate structure. Additionally, also the

Tyr137-ligated protein structure in the closed gate conformation was a positive match. For the open gate conformation of the Tyr137-ligated protein structure only one closed structure (picture 1 on the right side of Figure 106) was observed.

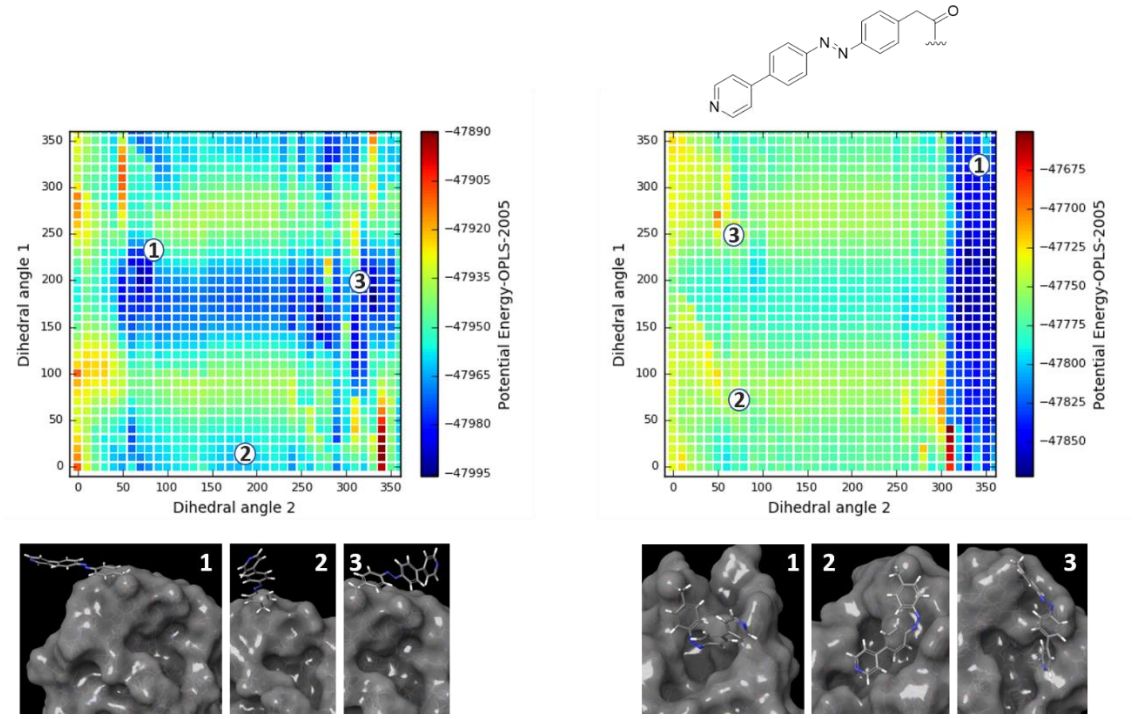

Figure 105: Results of the rotational scan with MacroModel for the azobenzene derivative **12** ligated to the amino acid Tyr48 (open gate conformation 1KLF) in *E*- (left) and *Z*-conformation (right). The potential energy is plotted as a contour diagram in relation to the dihedral angles 2 (x-axis) and 1 (y-axis).

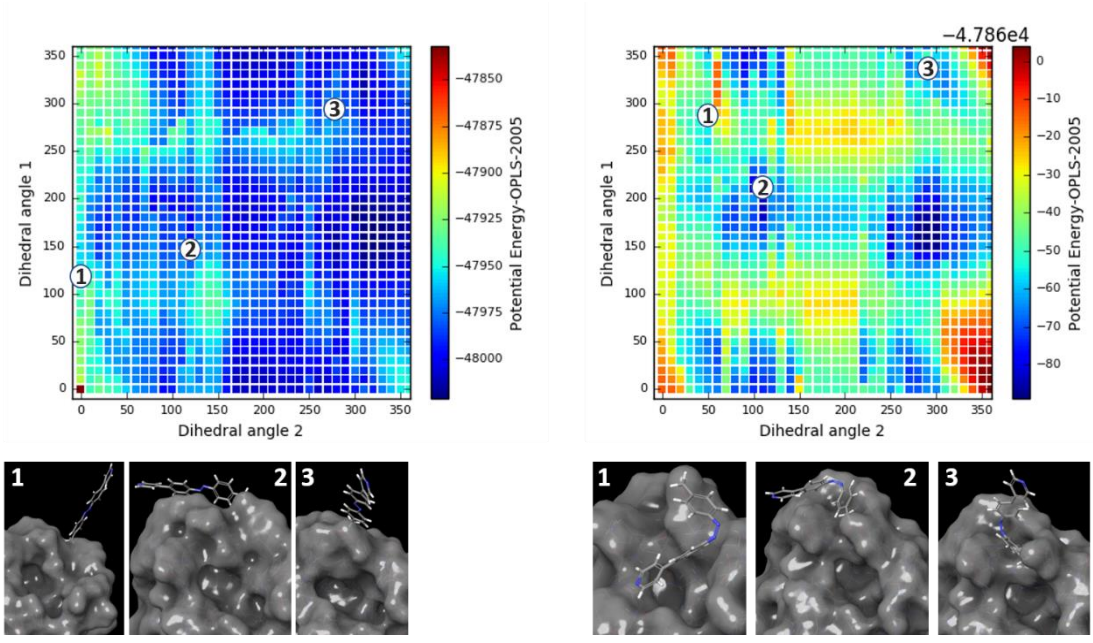

Figure 106: Results of the rotational scan with MacroModel for the azobenzene derivative **12** ligated to the amino acid Tyr137 (open gate conformation 1KLF) in *E*- (left) and *Z*-conformation (right). The potential energy is plotted as a contour diagram in relation to the dihedral angles 2 (x-axis) and 1 (y-axis).

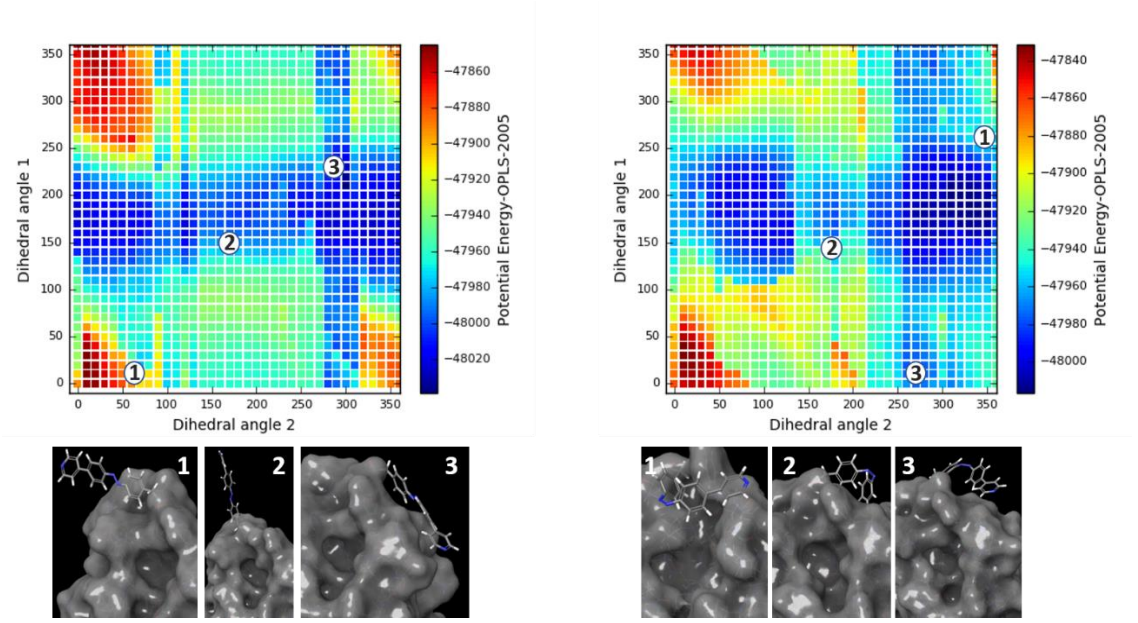

Figure 107: Results of the rotational scan with MacroModel for the azobenzene derivative **12** ligated to the amino acid Thr51 (open gate conformation 1KLF) in *E*- (left) and *Z*-conformation (right). The potential energy is plotted as a contour diagram in relation to the dihedral angles 2 (x-axis) and 1 (y-axis).

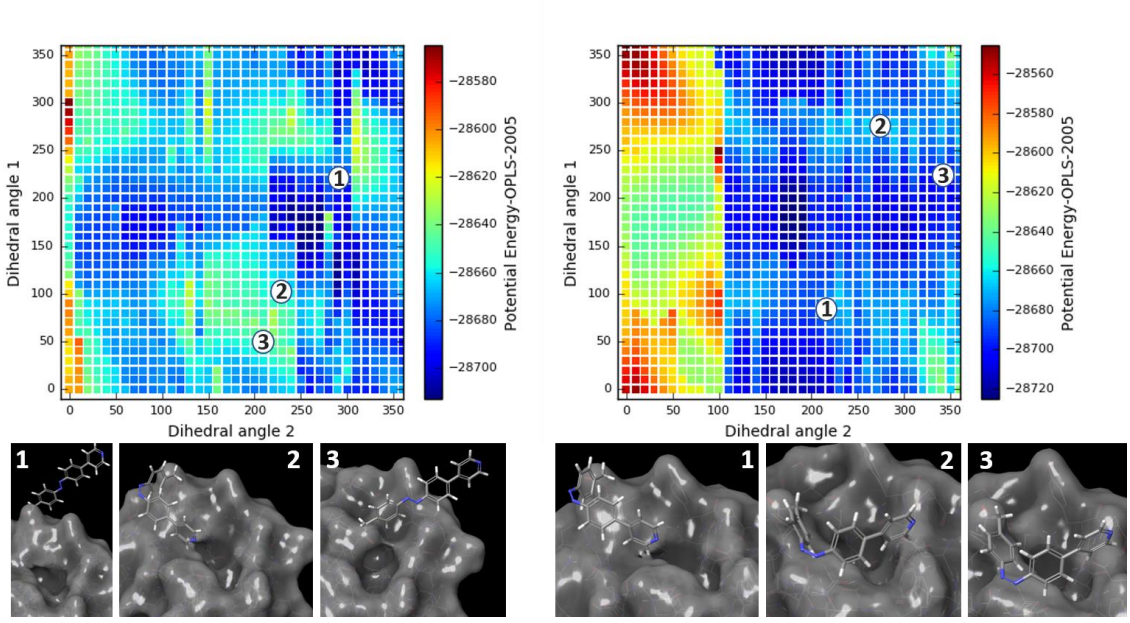

Figure 108: Results of the rotational scan with MacroModel for the azobenzene derivative **12** ligated to the amino acid Tyr48 (closed gate conformation 1UWF) in *E* (left) and *Z* conformation (right). The potential energy is plotted as a contour diagram in relation to the dihedral angles 2 (x-axis) and 1 (y-axis).

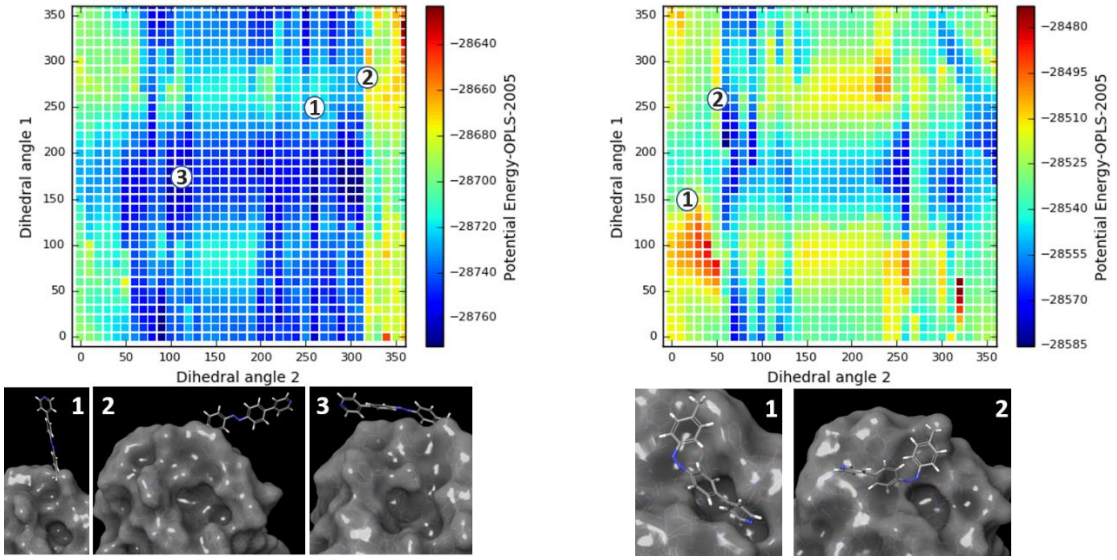

Figure 109: Results of the rotational scan with MacroModel for the azobenzene derivative **12** ligated to the amino acid Tyr137 (closed gate conformation 1UWF) in *E*- (left) and *Z*-conformation (right). The potential energy is plotted as a contour diagram in relation to the dihedral angles 2 (x-axis) and 1 (y-axis).

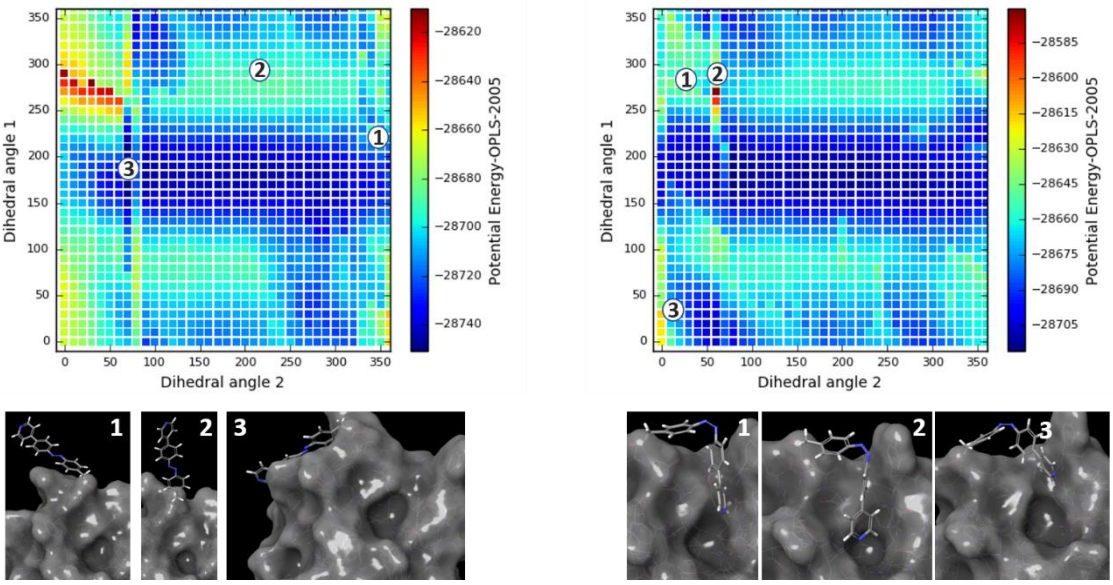

Figure 110: Results of the rotational scan with MacroModel for the azobenzene derivative **12** ligated to the amino acid Thr51 (closed gate conformation 1UWF) in *E*- (left) and *Z*-conformation (right). The potential energy is plotted as a contour diagram in relation to the dihedral angles 2 (x-axis) and 1 (y-axis).

The results for the sulfonamide derivative **13** are shown in Figure 111 to Figure 116. Derivative **13** showed positive matches for the Tyr48-ligated KLF derivative and the Thr51-ligated UWF derivative. In case of the Tyr137-ligated UWF derivative an inversed photoswitching might be possible since the binding site was closed in the *E*-configuration of the azobenzene moiety and thus was opened in the *Z*-configuration. Nevertheless, for most of the twelve ligated protein structures the ‘gate keeper’ shows a high affinity to the

binding site and its proximity might impede the opening of the binding site significantly. The responsible interactions are shown as an example for the Tyr137-ligated UWF structure in Figure 115 (left, third picture).

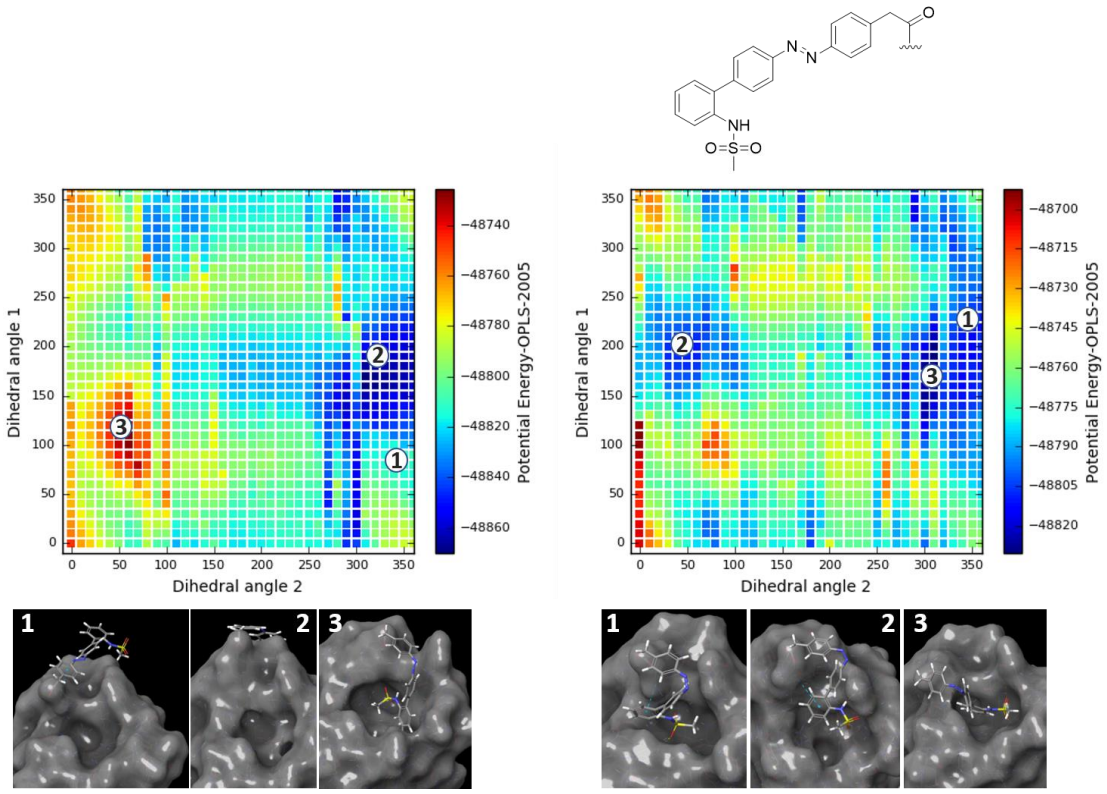

Figure 111: Results of the rotational scan with MacroModel for the azobenzene derivative **13** ligated to the amino acid Tyr48 (open gate conformation 1KLF) in *E*- (left) and *Z*-conformation (right). The potential energy is plotted as a contour diagram in relation to the dihedral angles 2 (x-axis) and 1 (y-axis).

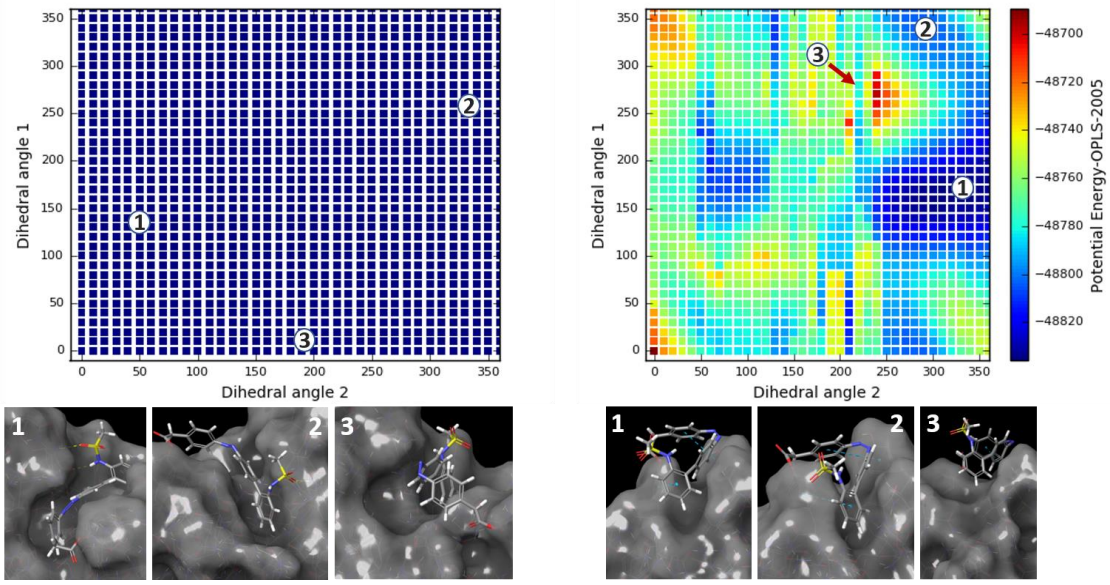

Figure 112: Results of the rotational scan with MacroModel for the azobenzene derivative **13** ligated to the amino acid Tyr137 (open gate conformation 1KLF) in *E*- (left) and *Z*-conformation (right). The potential energy is plotted as a contour diagram in relation to the dihedral angles 2 (x-axis) and 1 (y-axis).

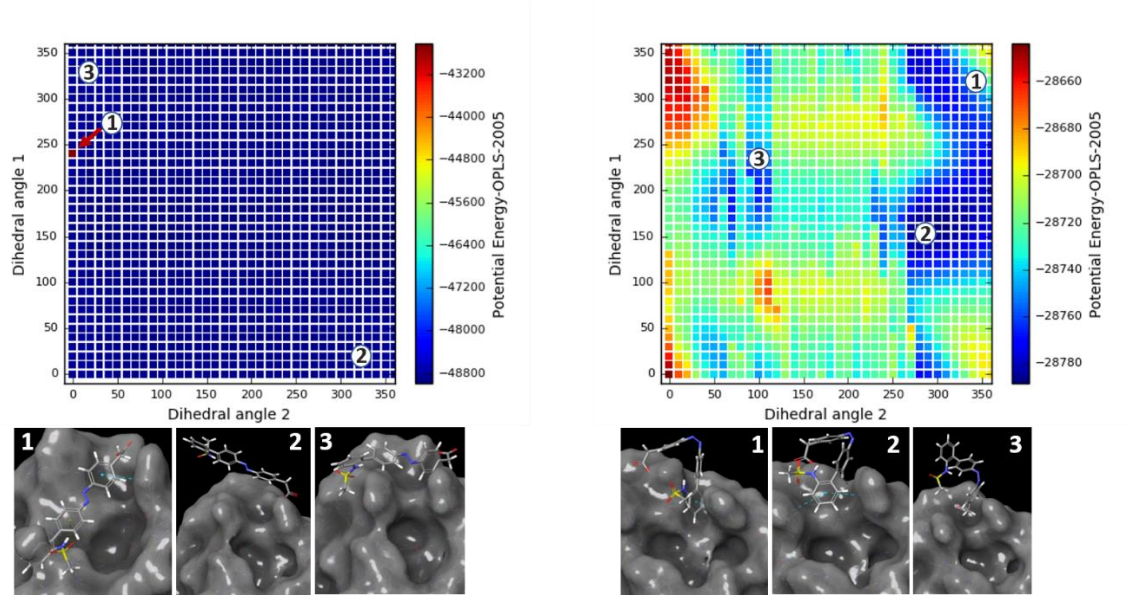

Figure 113: Results of the rotational scan with MacroModel for the azobenzene derivative **13** ligated to the amino acid Thr51 (open gate conformation 1KLF) in *E*- (left) and *Z*-conformation (right). The potential energy is plotted as a contour diagram in relation to the dihedral angles 2 (x-axis) and 1 (y-axis).

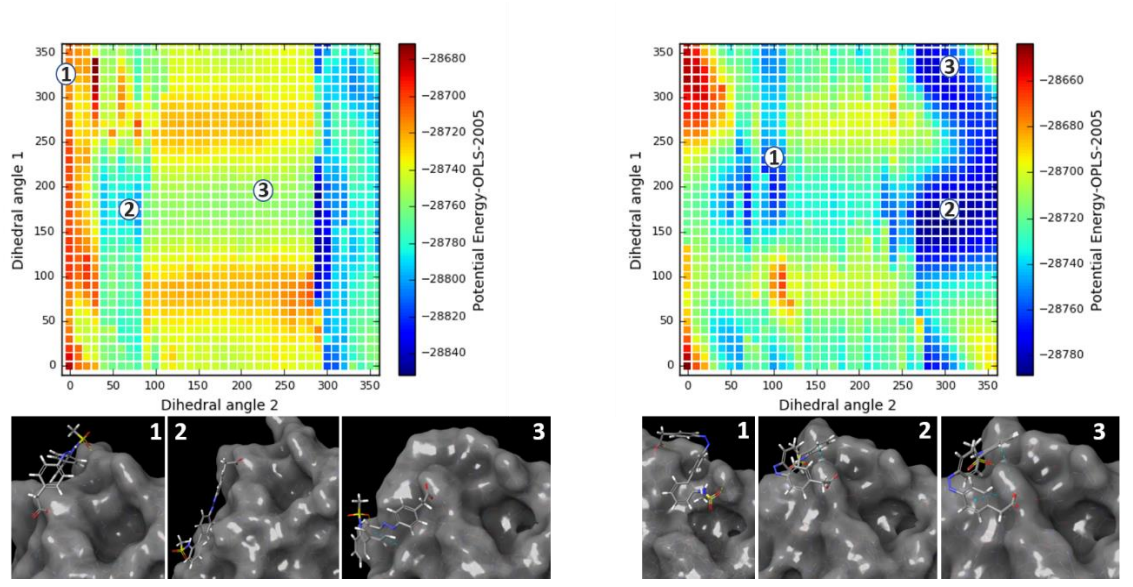

Figure 114: Results of the rotational scan with MacroModel for the azobenzene derivative **13** ligated to the amino acid Tyr48 (closed gate conformation 1UWF) in *E*- (left) and *Z*-conformation (right). The potential energy is plotted as a contour diagram in relation to the dihedral angles 2 (x-axis) and 1 (y-axis).

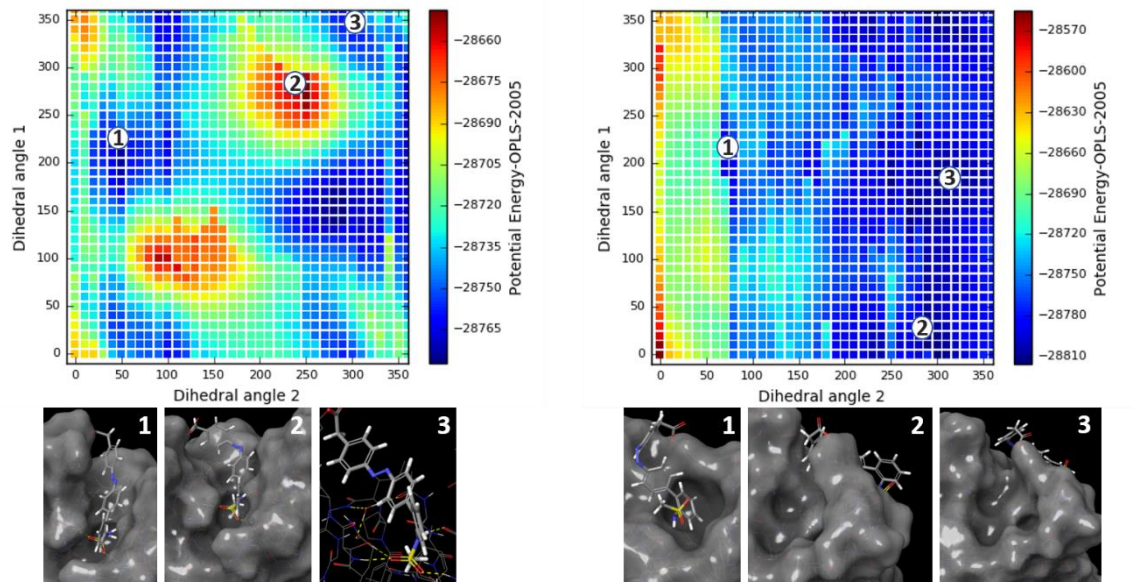

Figure 115: Results of the rotational scan with MacroModel for the azobenzene derivative **13** ligated to the amino acid Tyr137 (closed gate conformation 1UWF) in *E*- (left) and *Z*-conformation (right). The potential energy is plotted as a contour diagram in relation to the dihedral angles 2 (x-axis) and 1 (y-axis).

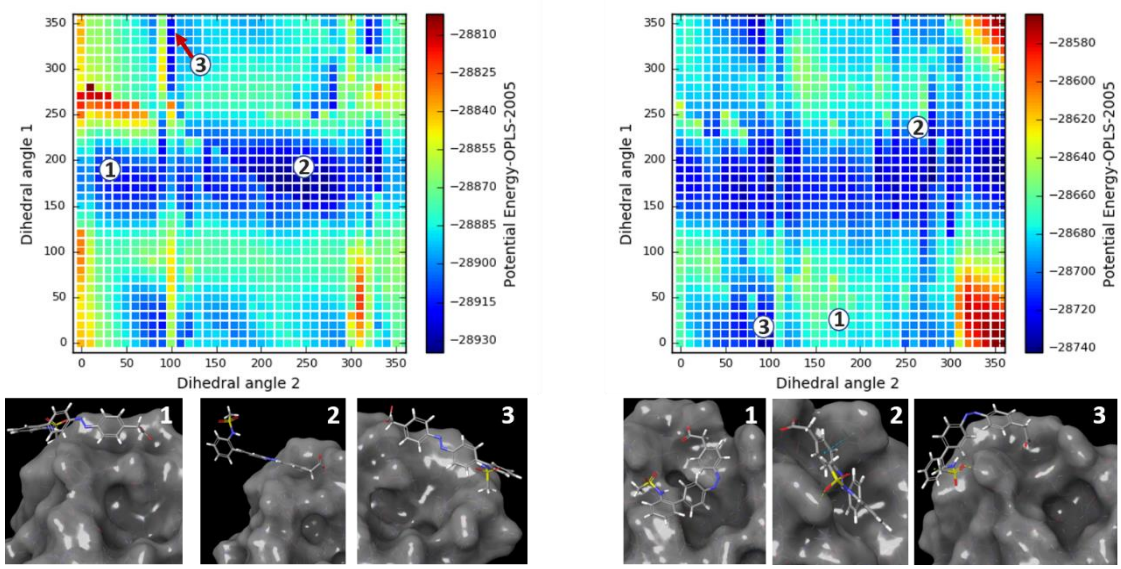

Figure 116: Results of the rotational scan with MacroModel for the azobenzene derivative **13** ligated to the amino acid Thr51 (closed gate conformation 1UWF) in *E*- (left) and *Z*-conformation (right). The potential energy is plotted as a contour diagram in relation to the dihedral angles 2 (x-axis) and 1 (y-axis).

The results for the triethylammonium derivative **35** are shown in Figure 117 to Figure 122. Positive matches were observed for the proteins ligated with the ‘gate keeper’ at Tyr48 and Tyr137 in the open gate conformation and for the proteins ligated at Tyr137 for the closed gate conformation. In case of the Thr51-ligated protein the ‘gate keeper’ moiety closes the binding site both in the *E*- and its *Z*-configuration. In case of the Thr51-

ligated protein (closed gate conformation) reversed switching might be successful since only in the *E*-configuration of the 'gate keeper' conformations of the protein with a closed binding site were observed (Figure 122).

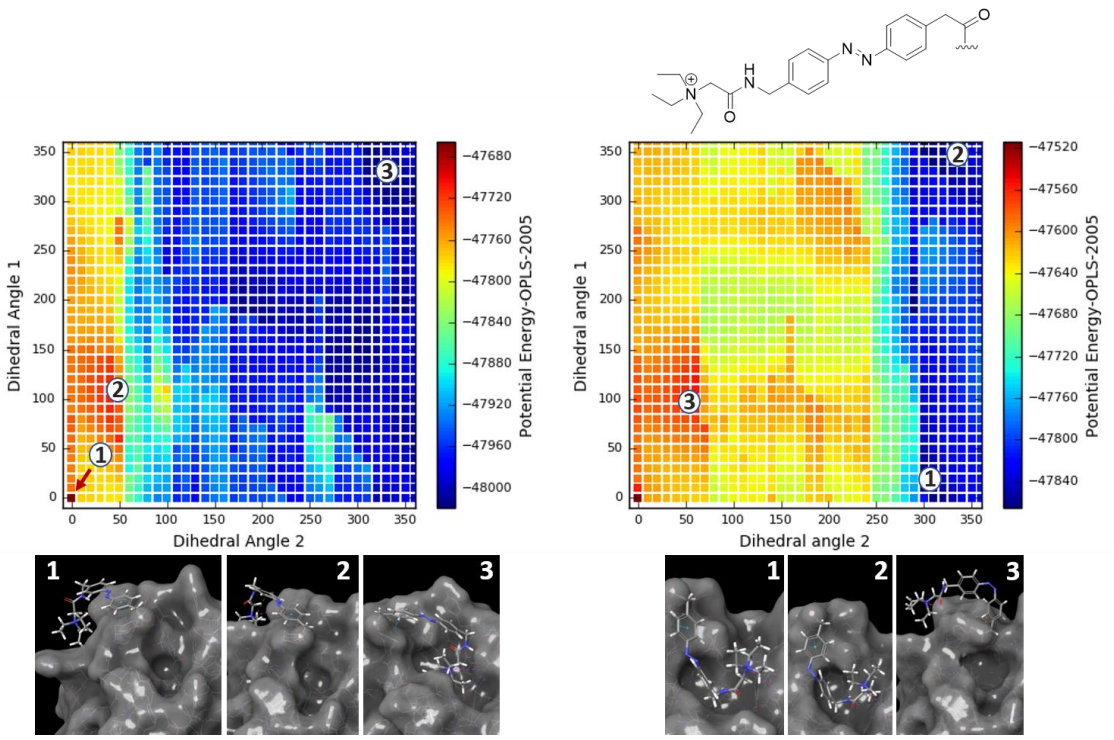

Figure 117: Results of the rotational scan with MacroModel for the azobenzene derivative **35** ligated to the amino acid Tyr48 (open gate conformation 1KLF) in *E*- (left) and *Z*-conformation (right). The potential energy is plotted as a contour diagram in relation to the dihedral angles 2 (x-axis) and 1 (y-axis).

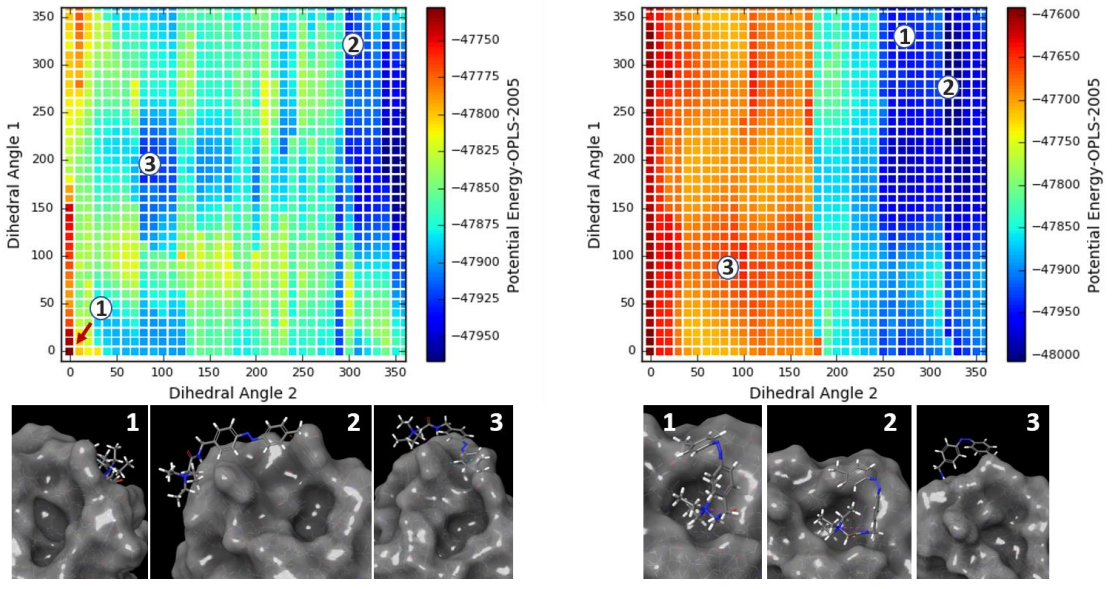

Figure 118: Results of the rotational scan with MacroModel for the azobenzene derivative **35** ligated to the amino acid Tyr137 (open gate conformation 1KLF) in *E*- (left) and *Z*-conformation (right). The potential energy is plotted as a contour diagram in relation to the dihedral angles 2 (x-axis) and 1 (y-axis).

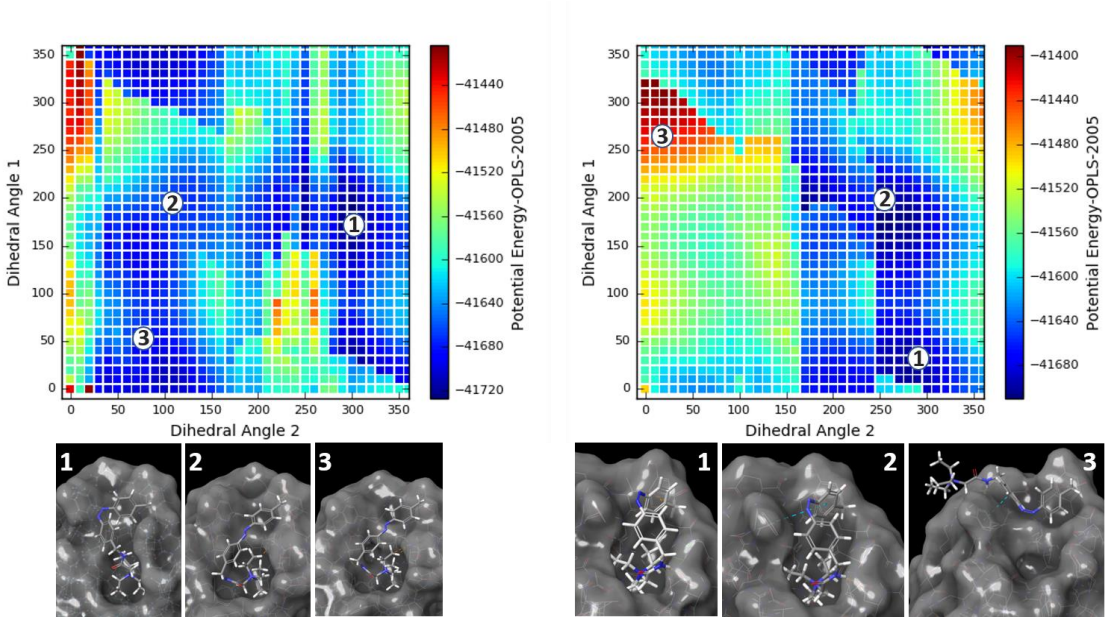

Figure 119: Results of the rotational scan with MacroModel for the azobenzene derivative **35** ligated to the amino acid Thr51 (open gate conformation 1KLF) in *E*- (left) and *Z*-conformation (right). The potential energy is plotted as a contour diagram in relation to the dihedral angles 2 (x-axis) and 1 (y-axis).

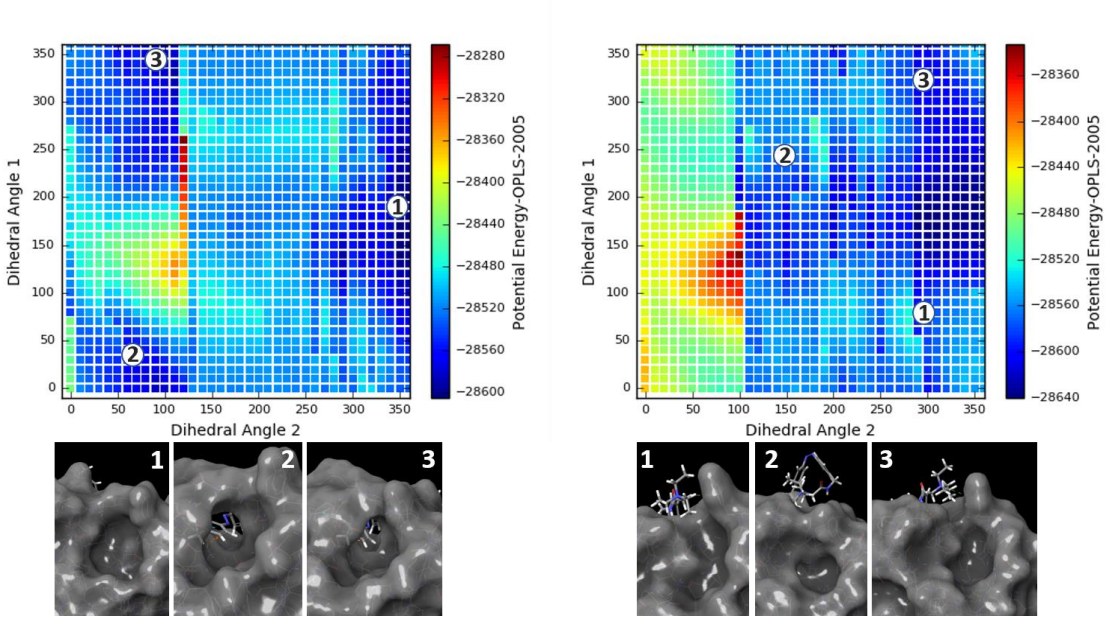

Figure 120: Results of the rotational scan with MacroModel for the azobenzene derivative **35** ligated to the amino acid Tyr48 (closed gate conformation 1UWF) in *E*- (left) and *Z*-conformation (right). The potential energy is plotted as a contour diagram in relation to the dihedral angles 2 (x-axis) and 1 (y-axis).

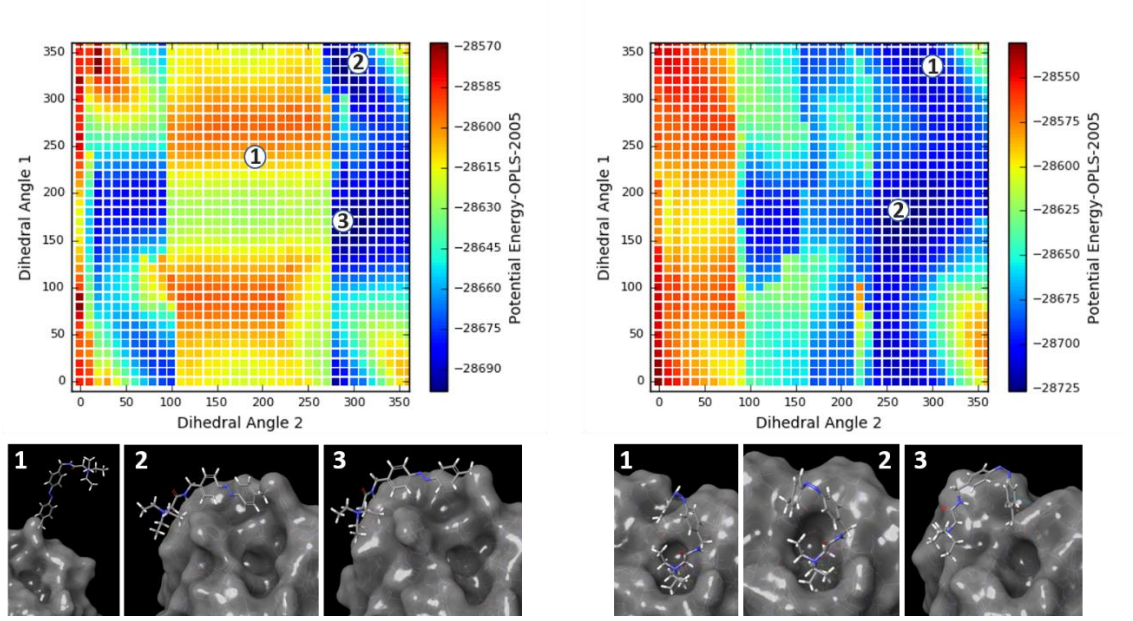

Figure 121: Results of the rotational scan with MacroModel for the azobenzene derivative **35** ligated to the amino acid Tyr137 (closed gate conformation 1UWF) in *E*- (left) and *Z*-conformation (right). The potential energy is plotted as a contour diagram in relation to the dihedral angles 2 (x-axis) and 1 (y-axis).

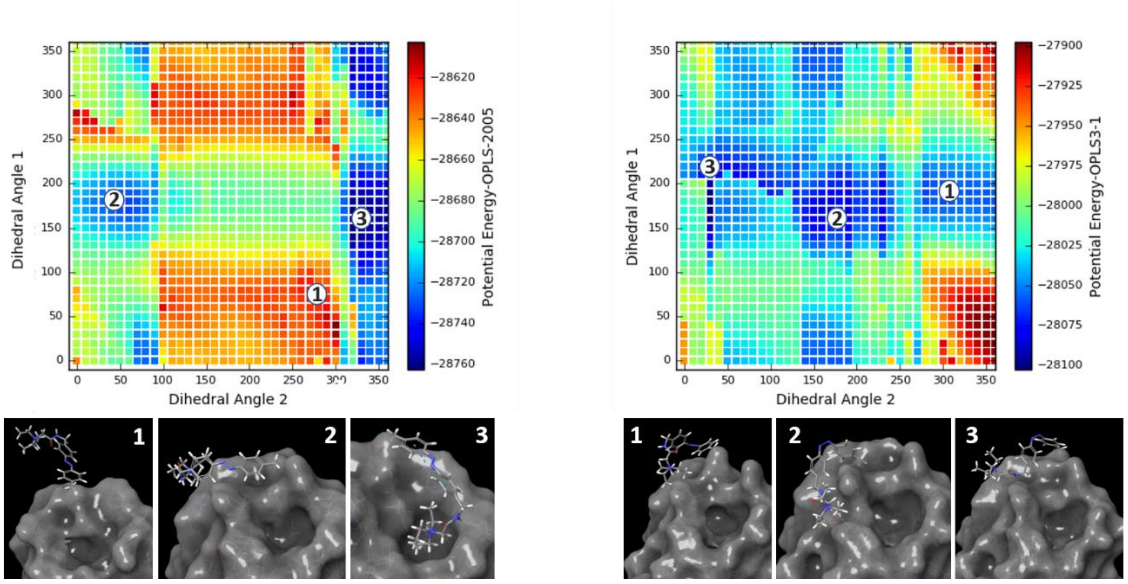

Figure 122: Results of the rotational scan with MacroModel for the azobenzene derivative **35** ligated to the amino acid Thr51 (closed gate conformation 1UWF) in *E*- (left) and *Z*-conformation (right). The potential energy is plotted as a contour diagram in relation to the dihedral angles 2 (x-axis) and 1 (y-axis).

The results for the trimethylammonium derivative **38** are shown in Figure 123 to Figure 128. Positive matches were observed for the ligation of the 'gate keeper' molecule with Tyr48 both in the open and in the closed gate conformation. Additionally, the

Tyr137-ligated KLF structure and the Thr51-ligated UWF structure can be evaluated as suitable ‘gate keeper’ molecules.

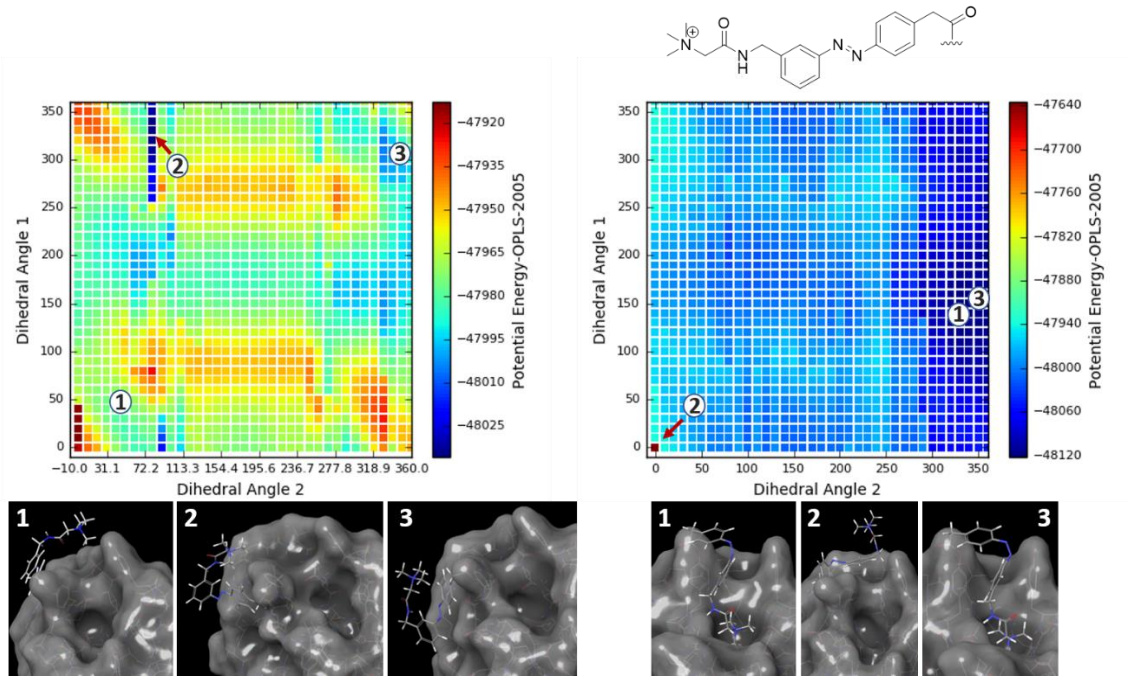

Figure 123: Results of the rotational scan with MacroModel for the azobenzene derivative **38** ligated to the amino acid Tyr48 (open gate conformation 1KLF) in *E*- (left) and *Z*-conformation (right). The potential energy is plotted as a contour diagram in relation to the dihedral angles 2 (x-axis) and 1 (y-axis).

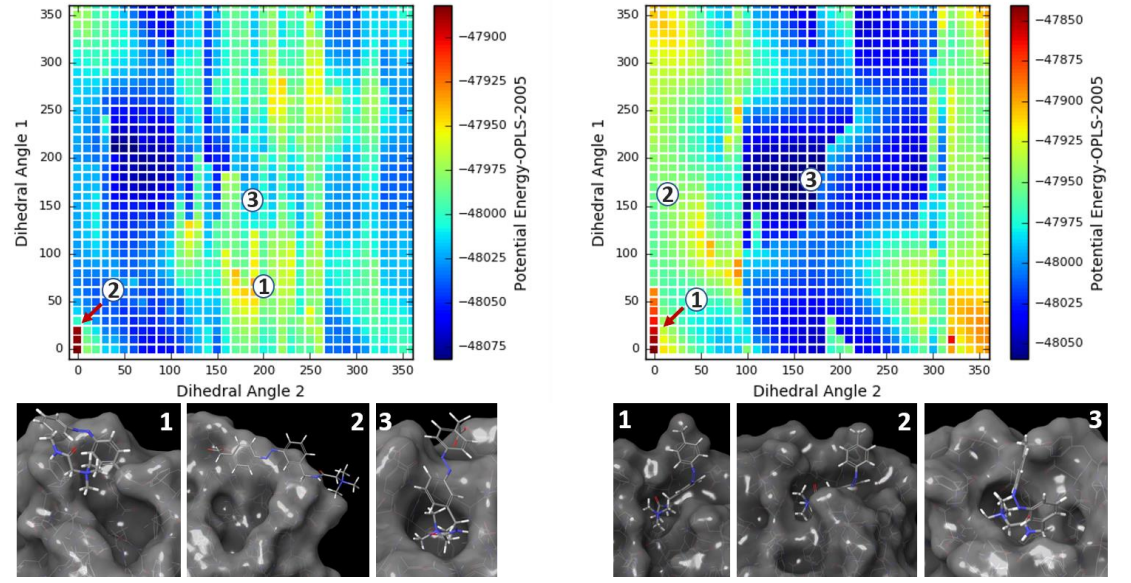

Figure 124: Results of the rotational scan with MacroModel for the azobenzene derivative **38** ligated to the amino acid Tyr137 (open gate conformation 1KLF) in *E*- (left) and *Z*-conformation (right). The potential energy is plotted as a contour diagram in relation to the dihedral angles 2 (x-axis) and 1 (y-axis).

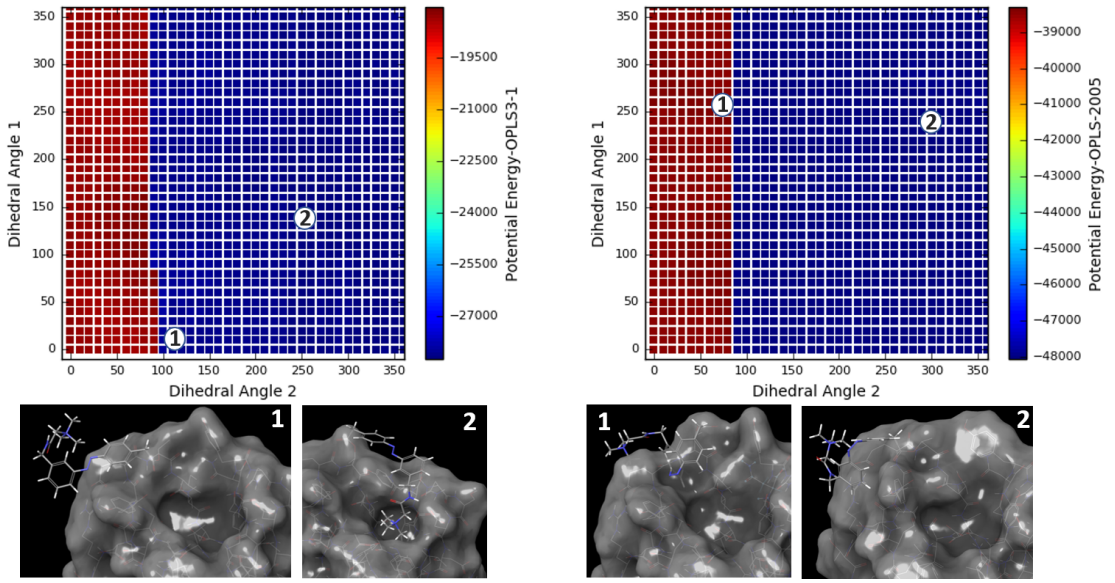

Figure 125: Results of the rotational scan with MacroModel for the azobenzene derivative **38** ligated to the amino acid Thr51 (open gate conformation 1KLF) in *E*- (left) and *Z*-conformation (right). The potential energy is plotted as a contour diagram in relation to the dihedral angles 2 (x-axis) and 1 (y-axis).

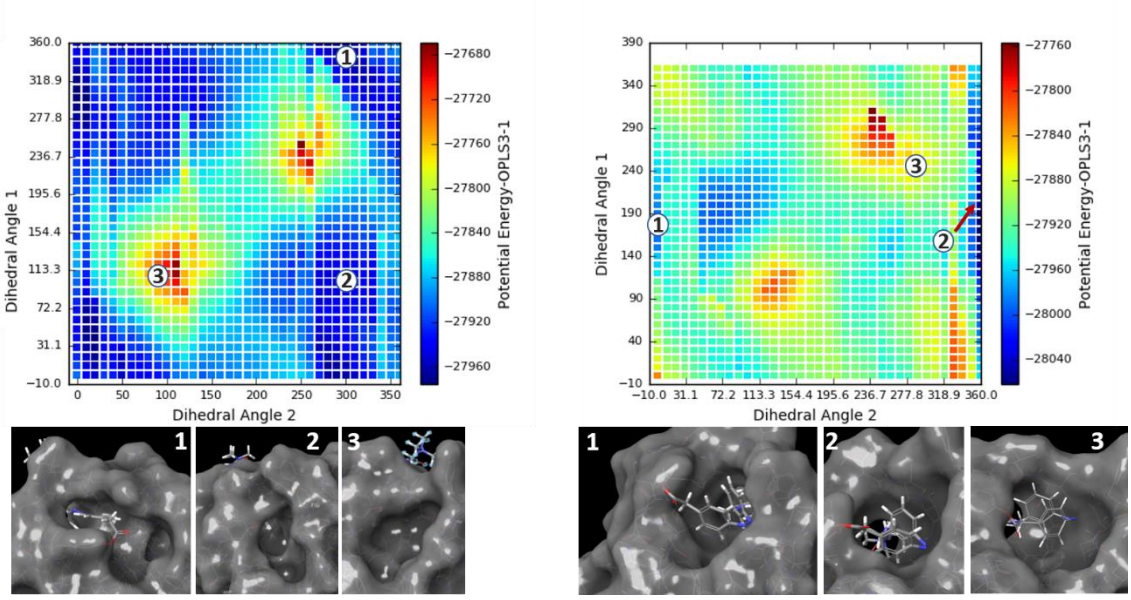

Figure 126: Results of the rotational scan with MacroModel for the azobenzene derivative **38** ligated to the amino acid Tyr48 (closed gate conformation 1UWF) in *E*- (left) and *Z*-conformation (right). The potential energy is plotted as a contour diagram in relation to the dihedral angles 2 (x-axis) and 1 (y-axis).

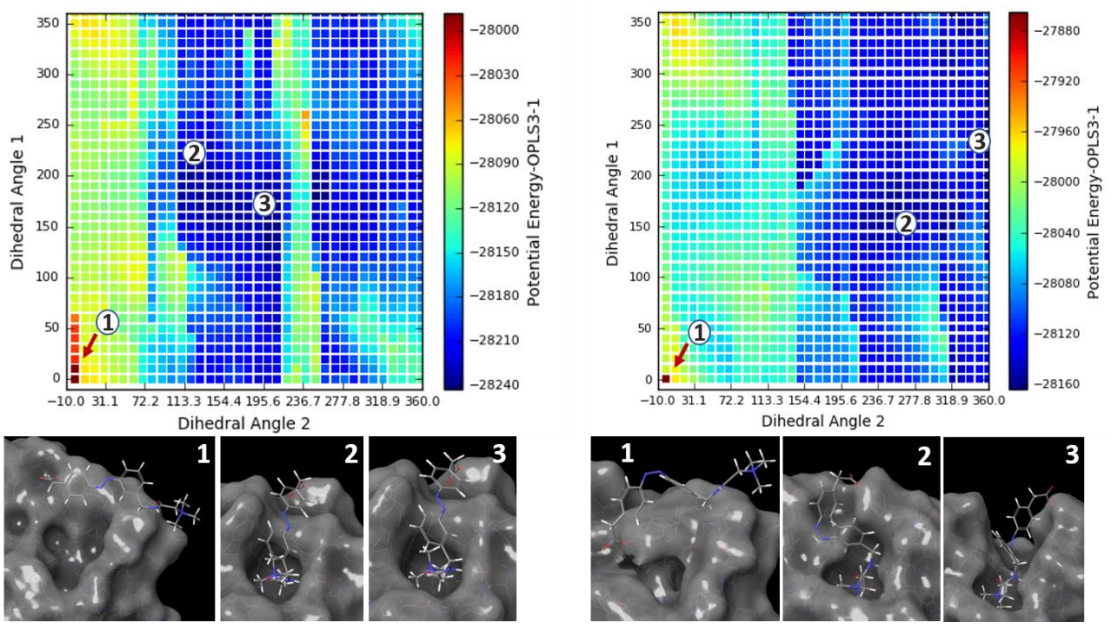

Figure 127: Results of the rotational scan with MacroModel for the azobenzene derivative **38** ligated to the amino acid Tyr137 (closed gate conformation 1UWF) in *E*- (left) and *Z*-conformation (right). The potential energy is plotted as a contour diagram in relation to the dihedral angles 2 (x-axis) and 1 (y-axis).

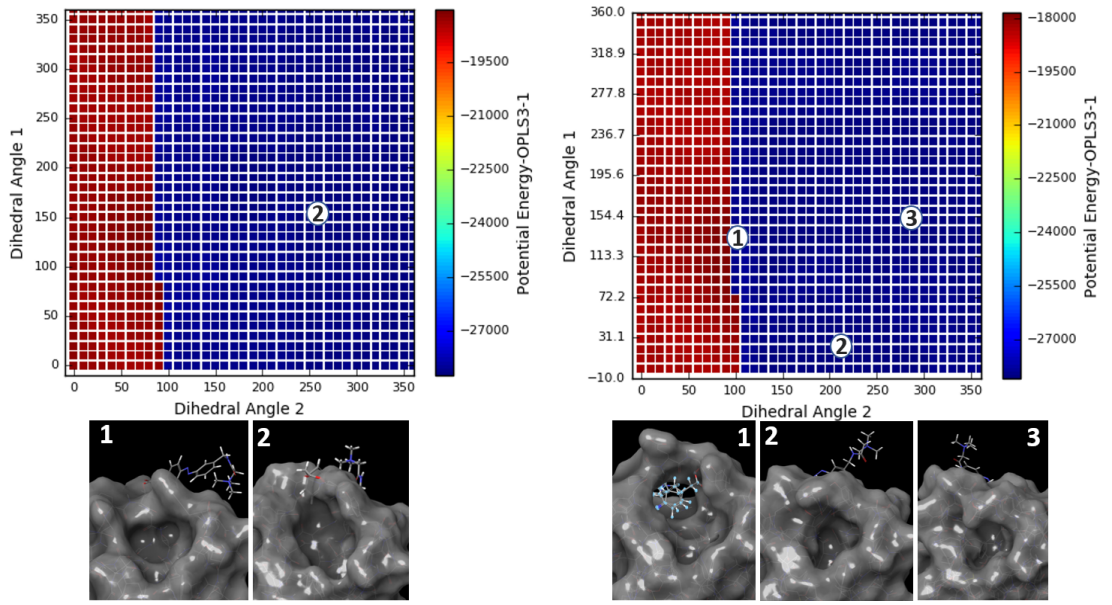

Figure 128: Results of the rotational scan with MacroModel for the azobenzene derivative **38** ligated to the amino acid Thr51 (closed gate conformation 1UWF) in *E*- (left) and *Z*-conformation (right). The potential energy is plotted as a contour diagram in relation to the dihedral angles 2 (x-axis) and 1 (y-axis).

The results for the alpha glucoside **79** are shown in Figure 129 to Figure 134. For compound **79** as 'gate keeper' molecule only one positive match was observed namely the Tyr48-ligated UWF protein structure. The remaining UWF structures with Tyr137 and Thr51, respectively, attached just showed unspecific results with a partly closed

binding site for the *E*- as well as the *Z*-configuration of the 'gate keeper' moiety. The binding sites of the modified KLF protein structures all stay opened both in the *E*- and in the *Z*-configuration.

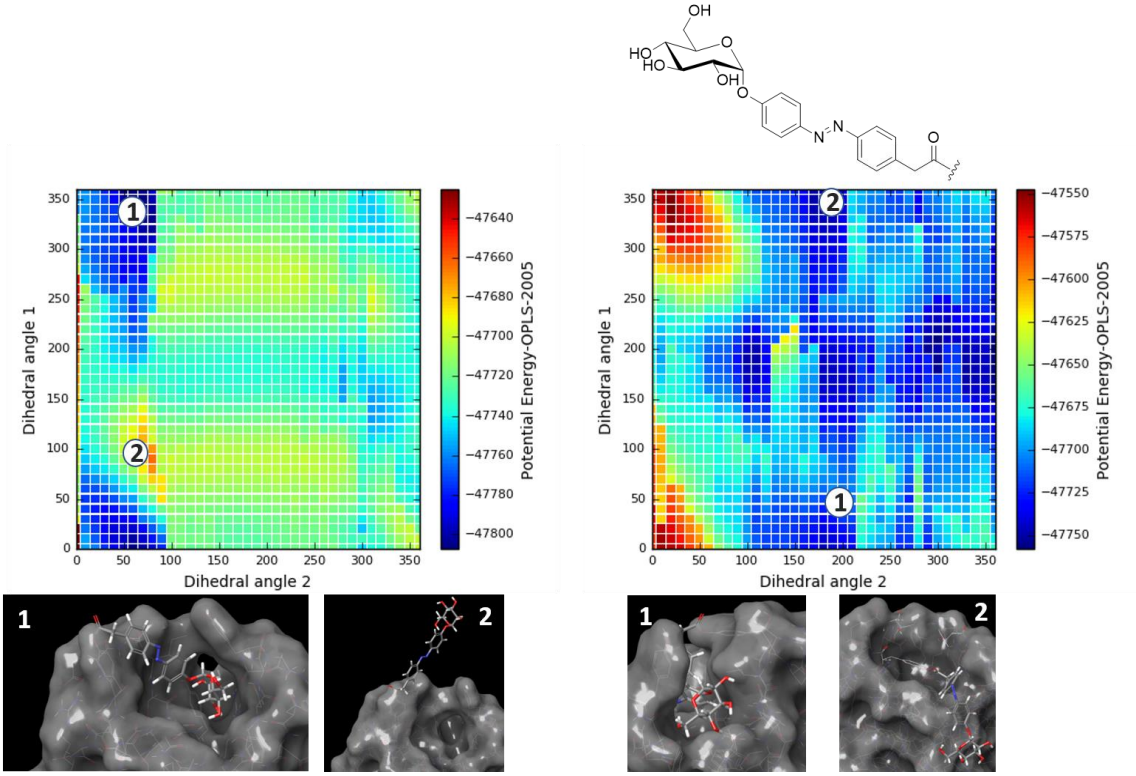

Figure 129: Results of the rotational scan with MacroModel for the azobenzene derivative **79** ligated to the amino acid Tyr48 (open gate conformation 1KLF) in *E*- (left) and *Z*-conformation (right). The potential energy is plotted as a contour diagram in relation to the dihedral angles 2 (x-axis) and 1 (y-axis).

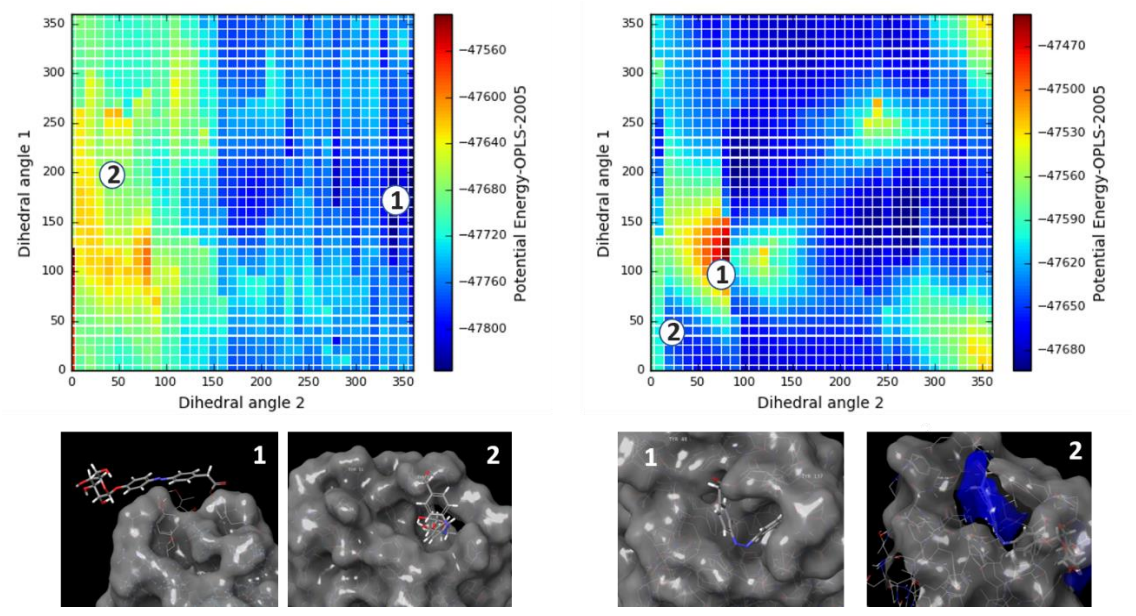

Figure 130: Results of the rotational scan with MacroModel for the azobenzene derivative **79** ligated to the amino acid Tyr137 (open gate conformation 1KLF) in *E*- (left) and *Z*-conformation (right). The potential energy is plotted as a contour diagram in relation to the dihedral angles 2 (x-axis) and 1 (y-axis).

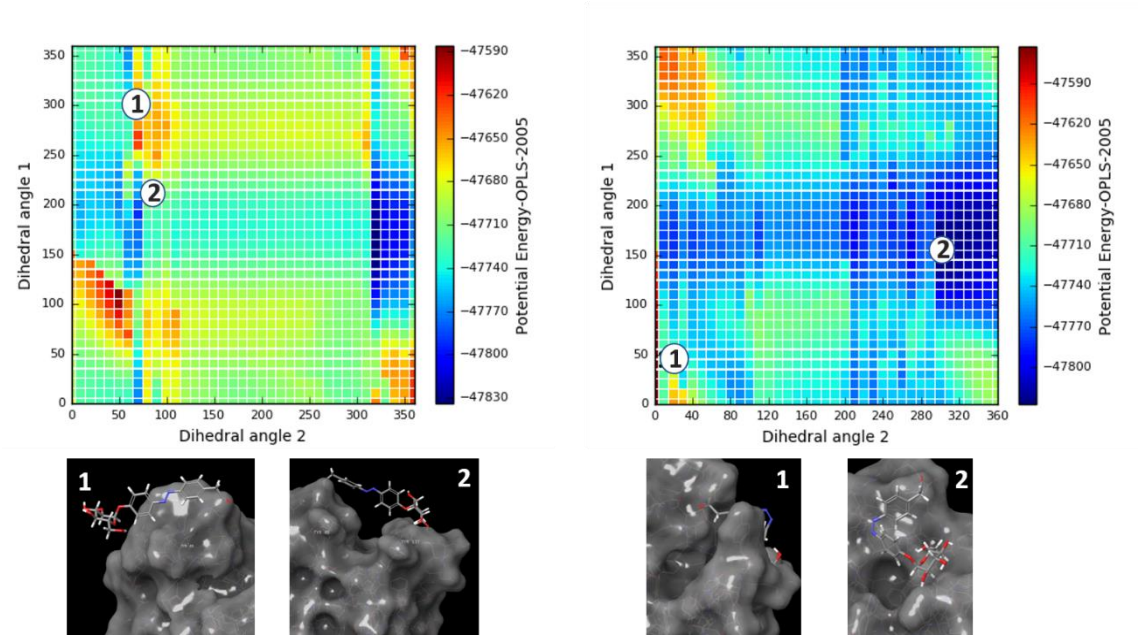

Figure 131: Results of the rotational scan with MacroModel for the azobenzene derivative **79** ligated to the amino acid Thr51 (open gate conformation 1KLF) in *E*- (left) and *Z*-conformation (right). The potential energy is plotted as a contour diagram in relation to the dihedral angles 2 (x-axis) and 1 (y-axis).

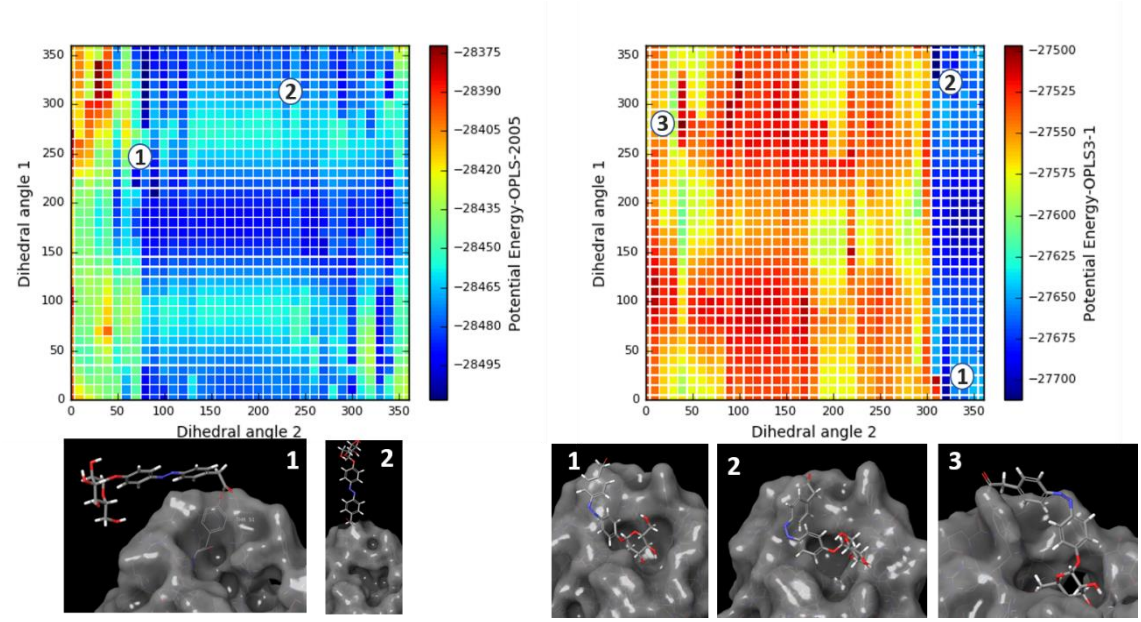

Figure 132: Results of the rotational scan with MacroModel for the azobenzene derivative **79** ligated to the amino acid Tyr48 (closed gate conformation 1UWF) in *E*- (left) and *Z*-conformation (right). The potential energy is plotted as a contour diagram in relation to the dihedral angles 2 (x-axis) and 1 (y-axis).

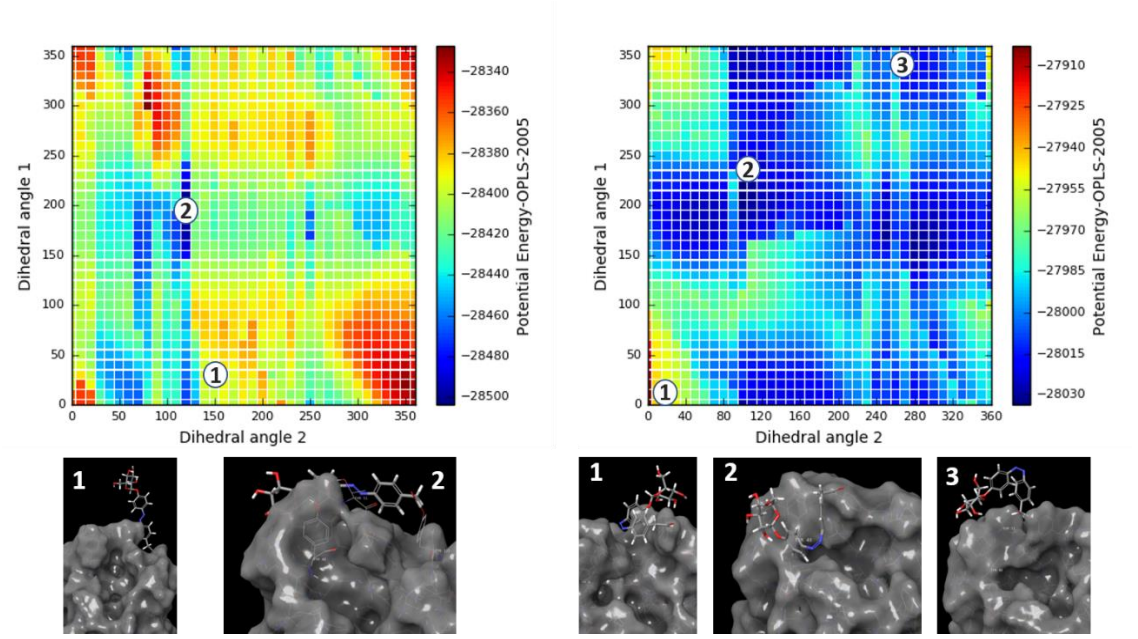

Figure 133: Results of the rotational scan with MacroModel for the azobenzene derivative **79** ligated to the amino acid Tyr137 (closed gate conformation 1UWF) in *E*- (left) and *Z*-conformation (right). The potential energy is plotted as a contour diagram in relation to the dihedral angles 2 (x-axis) and 1 (y-axis).

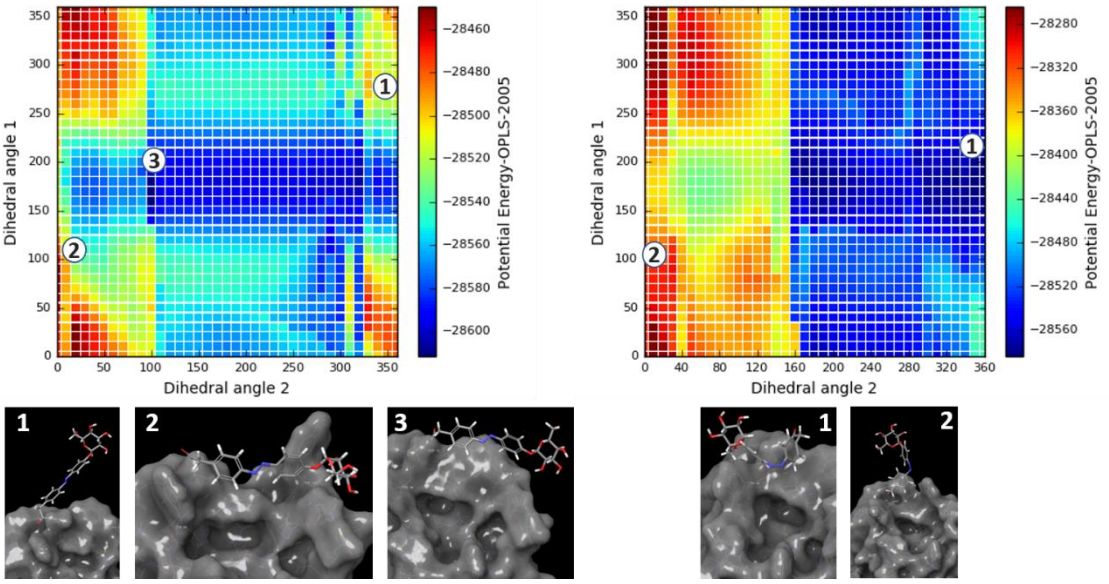

Figure 134: Results of the rotational scan with MacroModel for the azobenzene derivative **79** ligated to the amino acid Thr51 (closed gate conformation 1UWF) in *E*- (left) and *Z*-conformation (right). The potential energy is plotted as a contour diagram in relation to the dihedral angles 2 (x-axis) and 1 (y-axis).

The results for the beta glucoside **80** are shown in Figure 135 to Figure 140. The most promising matches were found for the Tyr48-ligated protein derivatives both for the open and the closed gate conformation. In both cases the binding site stayed opened in several

energetically favourable conformations in its *E*-configuration and closed in several conformations of low energy in its *Z*-state.

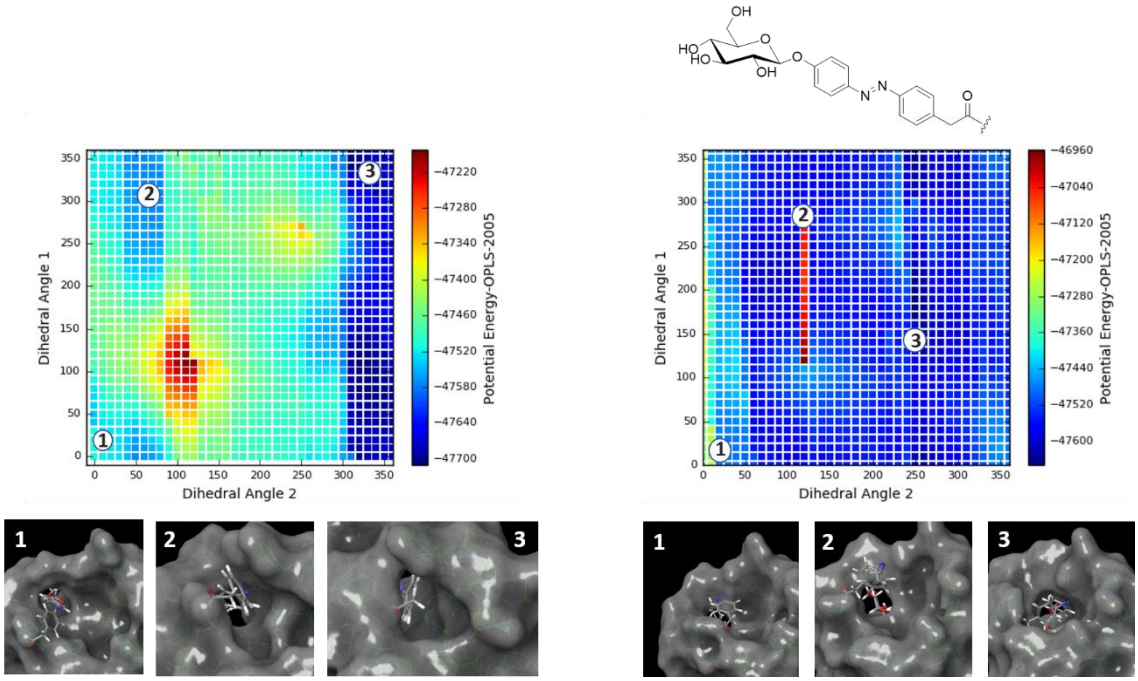

Figure 135: Results of the rotational scan with MacroModel for the azobenzene derivative **80** ligated to the amino acid Tyr48 (open gate conformation 1KLF) in *E*- (left) and *Z*-conformation (right). The potential energy is plotted as a contour diagram in relation to the dihedral angles 2 (x-axis) and 1 (y-axis).

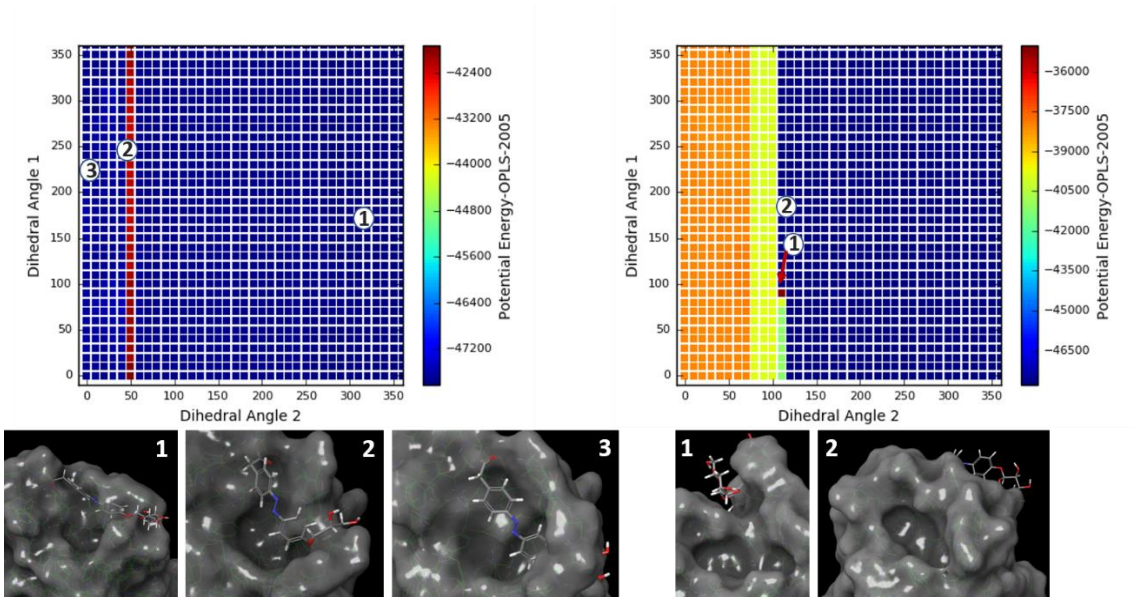

Figure 136: Results of the rotational scan with MacroModel for the azobenzene derivative **80** ligated to the amino acid Tyr137 (open gate conformation 1KLF) in *E* (left) and *Z* conformation (right). The potential energy is plotted as a contour diagram in relation to the dihedral angles 2 (x-axis) and 1 (y-axis).

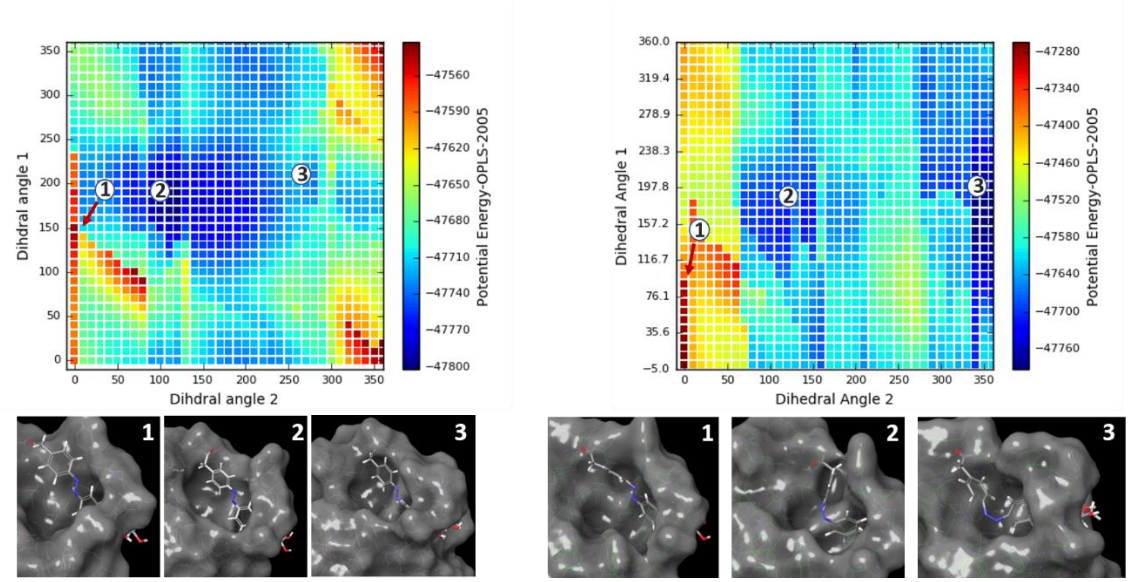

Figure 137: Results of the rotational scan with MacroModel for the azobenzene derivative **80** ligated to the amino acid Thr51 (open gate conformation 1KLF) in *E*- (left) and *Z*-conformation (right). The potential energy is plotted as a contour diagram in relation to the dihedral angles 2 (x-axis) and 1 (y-axis).

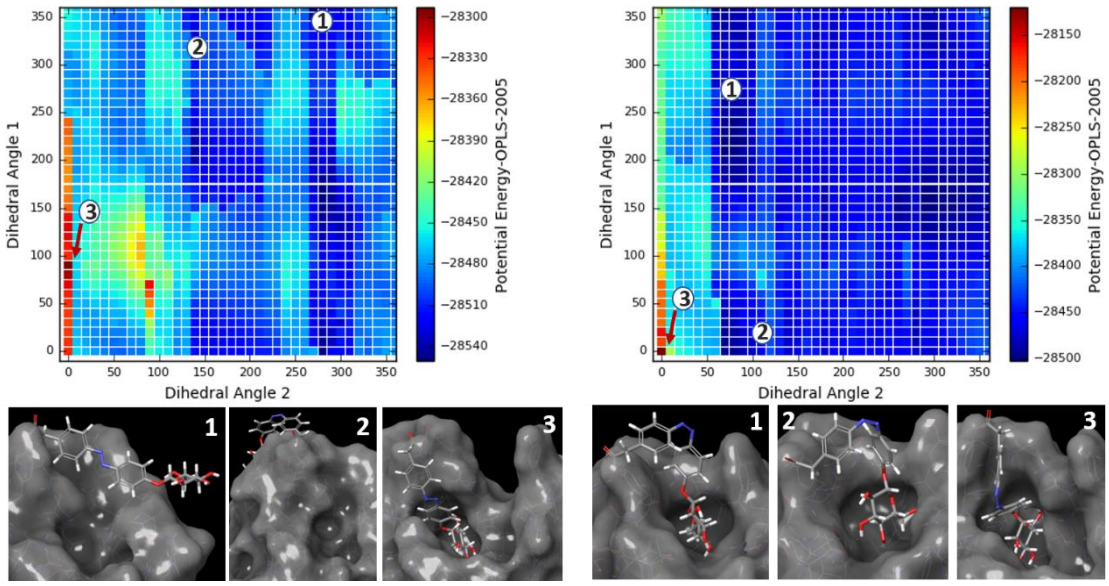

Figure 138: Results of the rotational scan with MacroModel for the azobenzene derivative **80** ligated to the amino acid Tyr48 (closed gate conformation 1UWF) in *E*- (left) and *Z*-conformation (right). The potential energy is plotted as a contour diagram in relation to the dihedral angles 2 (x-axis) and 1 (y-axis).

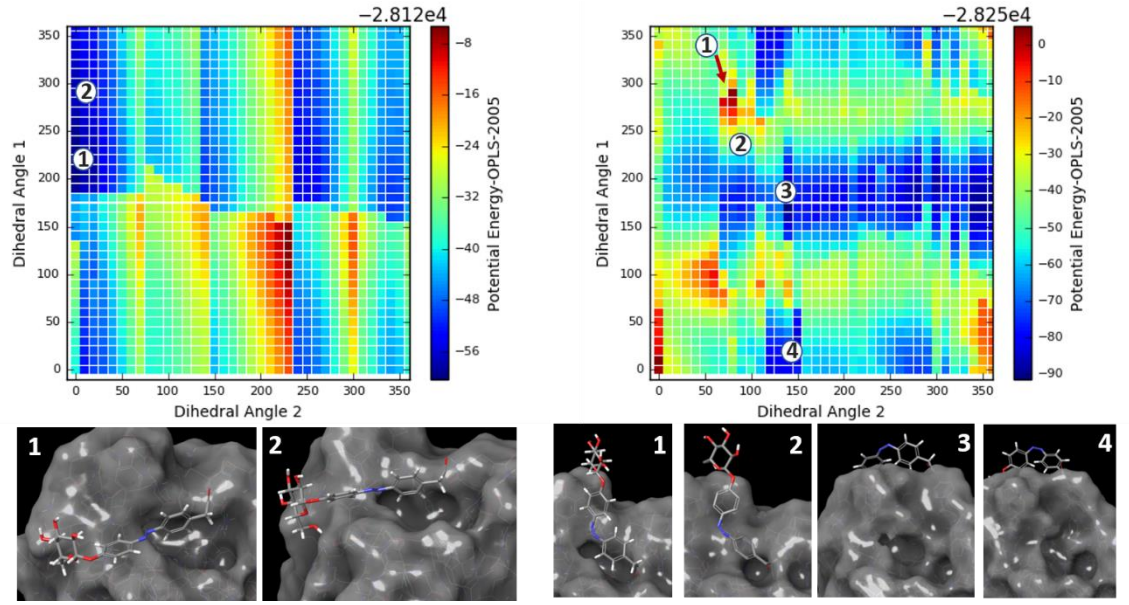

Figure 139: Results of the rotational scan with MacroModel for the azobenzene derivative **80** ligated to the amino acid Tyr137 (closed gate conformation 1UWF) in *E*- (left) and *Z*-conformation (right). The potential energy is plotted as a contour diagram in relation to the dihedral angles 2 (x-axis) and 1 (y-axis).

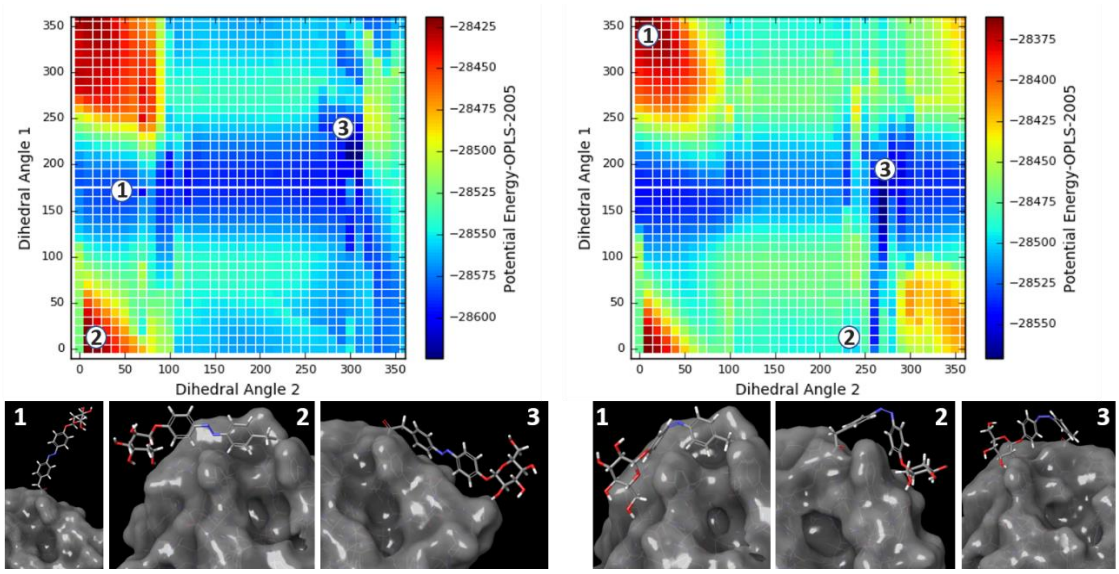

Figure 140: Results of the rotational scan with MacroModel for the azobenzene derivative **80** ligated to the amino acid Thr51 (closed gate conformation 1UWF) in *E*- (left) and *Z*-conformation (right). The potential energy is plotted as a contour diagram in relation to the dihedral angles 2 (x-axis) and 1 (y-axis).

The results for the β-glucoside **102** are shown in Figure 141 to Figure 146. The Tyr48- and the Tyr37-modified closed gate conformations of the protein show a positive match. In case of the open gate conformation of the Thr51-labelled protein an inversed switching of the binding affinity would be possible since the binding site is closed in the *E*-configuration of the azobenzene 'gate keeper' moiety. At first glance also the Tyr137-ligated open gate conformation and the Thr51-ligated closed gate conformation of the

protein seem to show a positive match. But the conformations of the proteins which exhibit the binding site closed by a *Z* configured 'gate keeper' moiety are characterised by significantly high potential energies and thus their occurrence is rather unlikely.

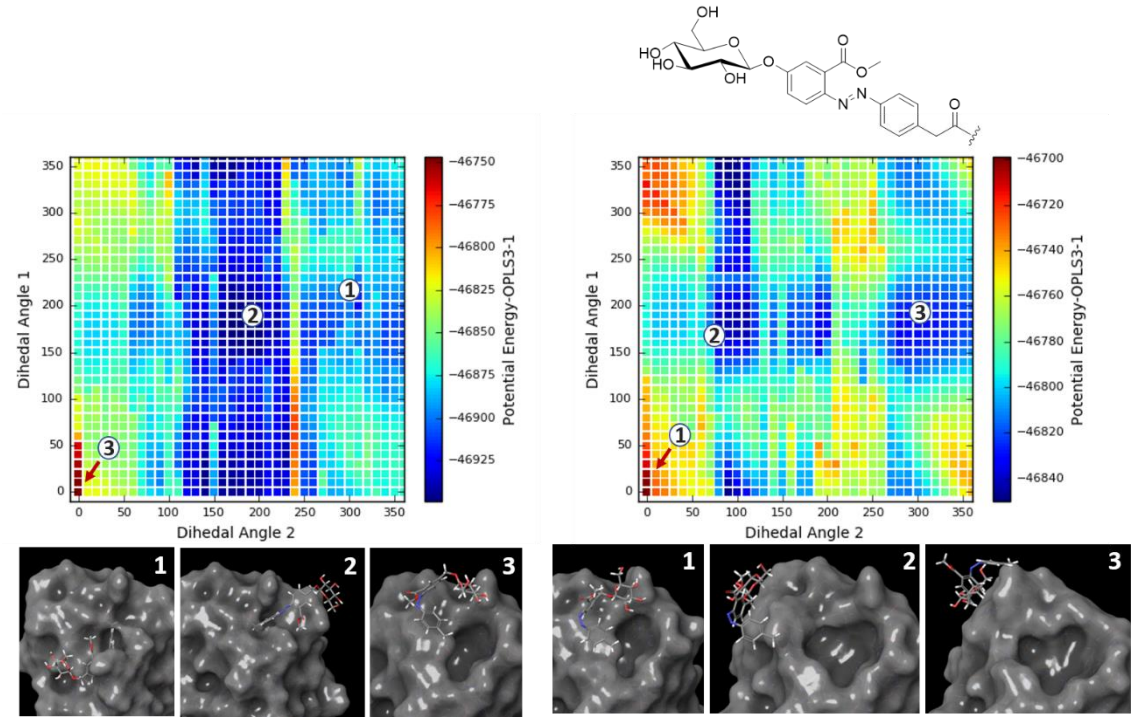

Figure 141: Results of the rotational scan with MacroModel for the azobenzene derivative **102** ligated to the amino acid Tyr48 (open gate conformation 1KLF) in *E*- (left) and *Z*-conformation (right). The potential energy is plotted as a contour diagram in relation to the dihedral angles 2 (x-axis) and 1 (y-axis).

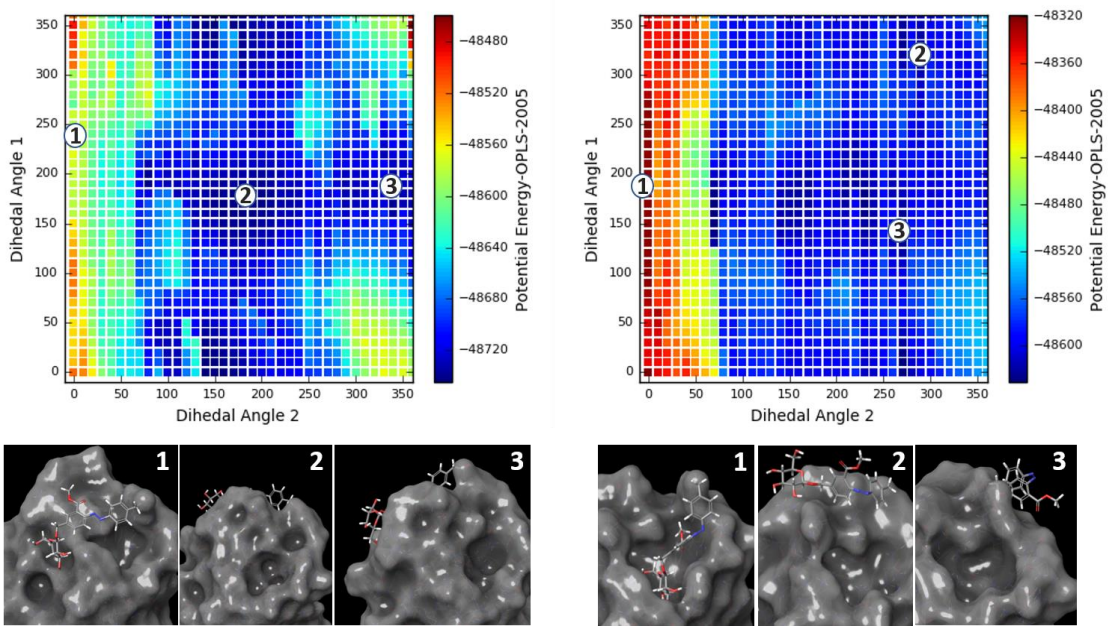

Figure 142: Results of the rotational scan with MacroModel for the azobenzene derivative **102** ligated to the amino acid Tyr137 (open gate conformation 1KLF) in *E*- (left) and *Z*-conformation (right). The potential energy is plotted as a contour diagram in relation to the dihedral angles 2 (x-axis) and 1 (y-axis).

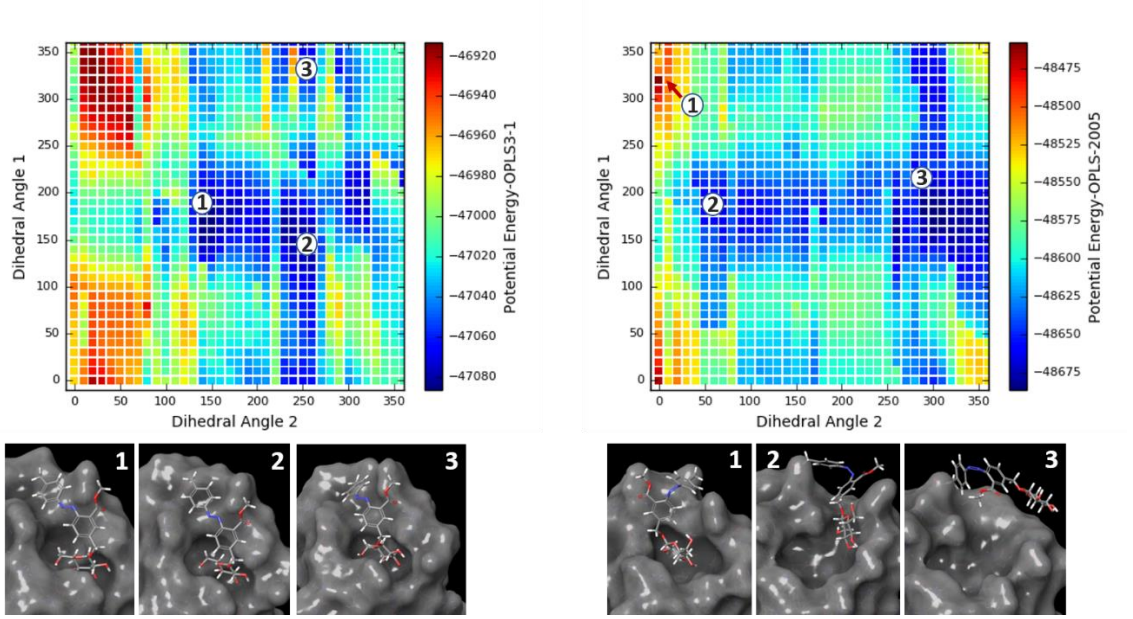

Figure 143: Results of the rotational scan with MacroModel for the azobenzene derivative **102** ligated to the amino acid Thr51 (open gate conformation 1KLF) in *E*- (left) and *Z*-conformation (right). The potential energy is plotted as a contour diagram in relation to the dihedral angles 2 (x-axis) and 1 (y-axis).

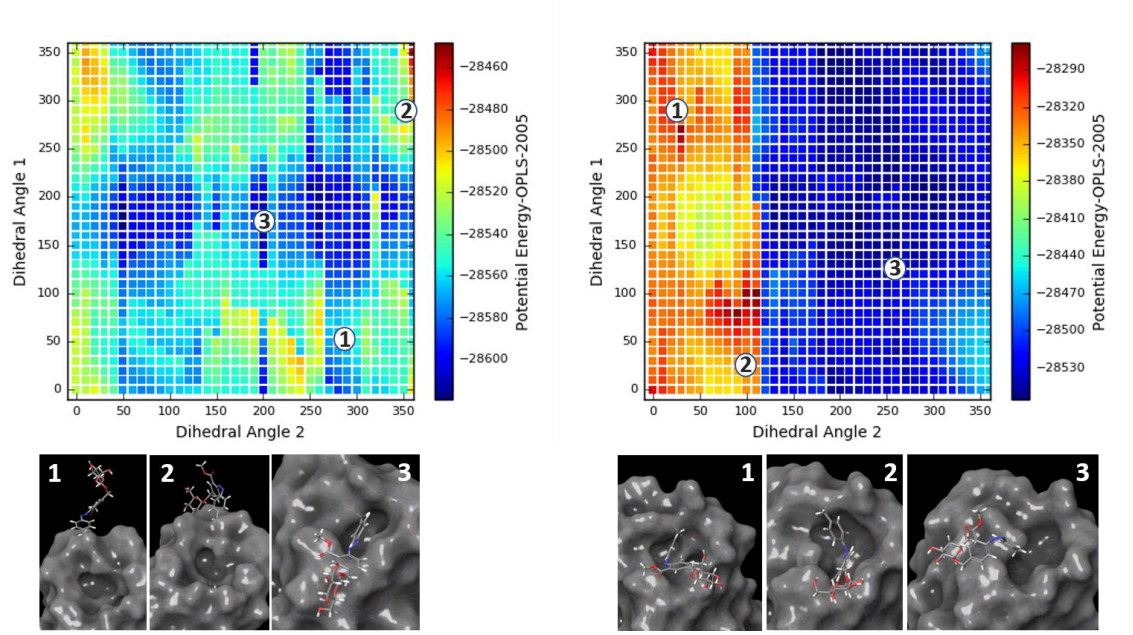

Figure 144: Results of the rotational scan with MacroModel for the azobenzene derivative **102** ligated to the amino acid Tyr48 (closed gate conformation 1UWF) in *E*- (left) and *Z*-conformation (right). The potential energy is plotted as a contour diagram in relation to the dihedral angles 2 (x-axis) and 1 (y-axis).

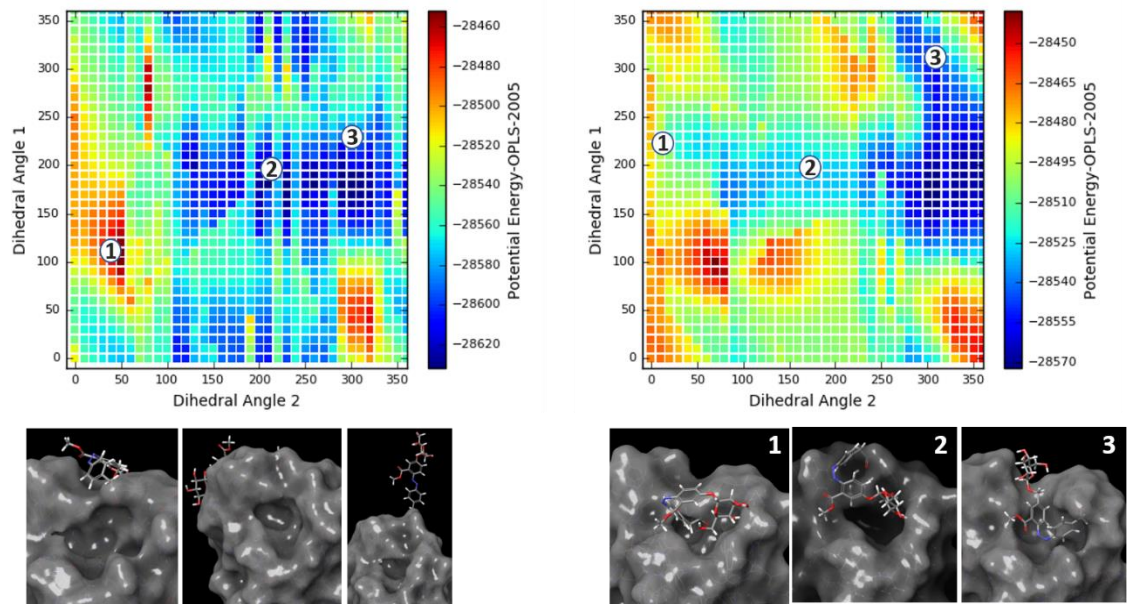

Figure 145: Results of the rotational scan with MacroModel for the azobenzene derivative **102** ligated to the amino acid Tyr137 (closed gate conformation 1UWF) in *E*- (left) and *Z*-conformation (right). The potential energy is plotted as a contour diagram in relation to the dihedral angles 2 (x-axis) and 1 (y-axis).

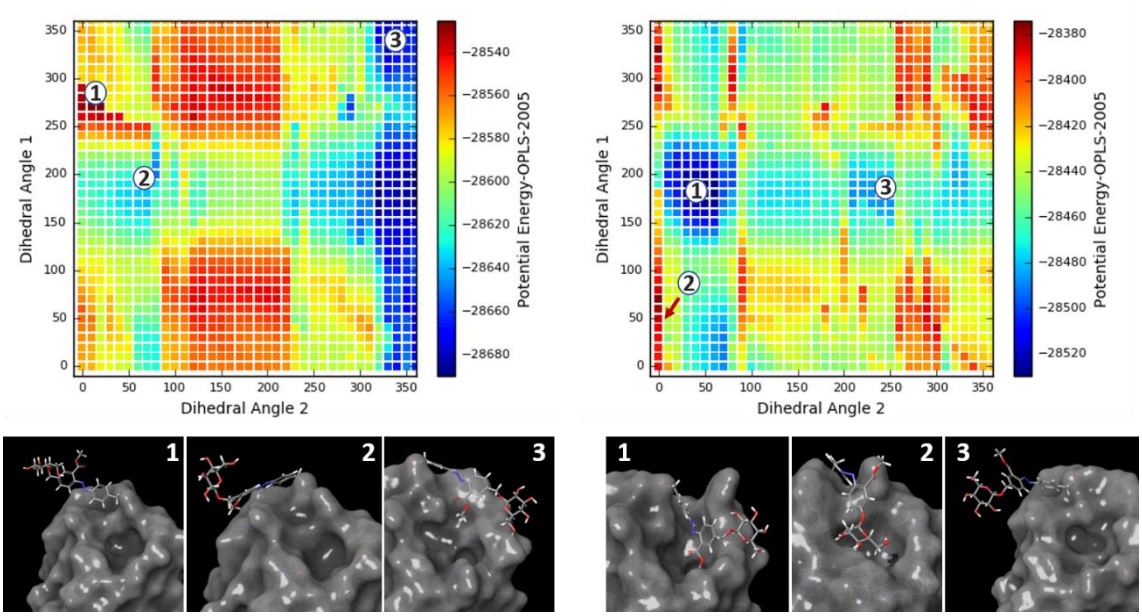

Figure 146: Results of the rotational scan with MacroModel for the azobenzene derivative **102** ligated to the amino acid Thr51 (closed gate conformation 1UWF) in *E*- (left) and *Z*-conformation (right). The potential energy is plotted as a contour diagram in relation to the dihedral angles 2 (x-axis) and 1 (y-axis).

The results for the α-mannoside **103** are shown in Figure 147 to Figure 152. For the ligated structures of the KLF FimH positive matches were observed for the 'gate keeper' moieties ligated on the amino acids Tyr48 and Thr51. In case of the Tyr137-ligated UWF structure only one closed binding site with the 'gate keeper' in *Z*-configuration was

observed and moreover, this structure showed a rather high potential energy. The same can be stated for the Thr51-ligated UWF protein. Furthermore, a positive match was observed for the Tyr137-ligated UWF protein derivative.

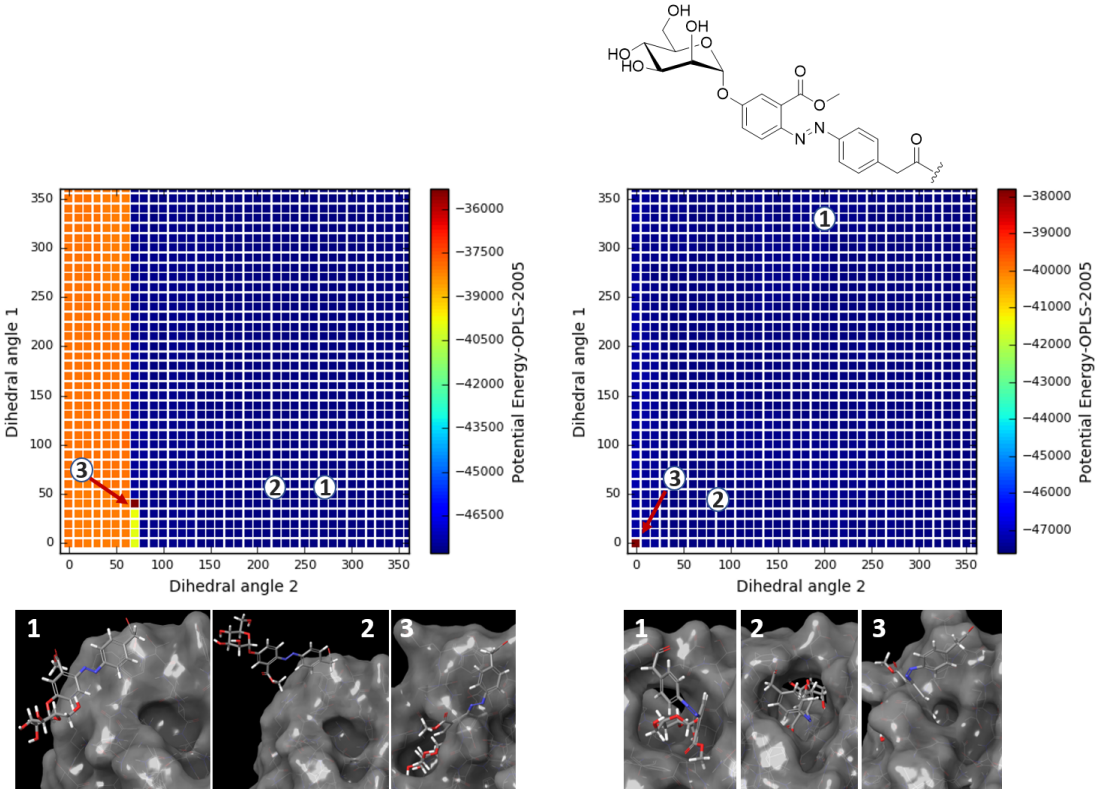

Figure 147: Results of the rotational scan with MacroModel for the azobenzene derivative **103** ligated to the amino acid Tyr48 (open gate conformation 1KLF) in *E*- (left) and *Z*-conformation (right). The potential energy is plotted as a contour diagram in relation to the dihedral angles 2 (x-axis) and 1 (y-axis).

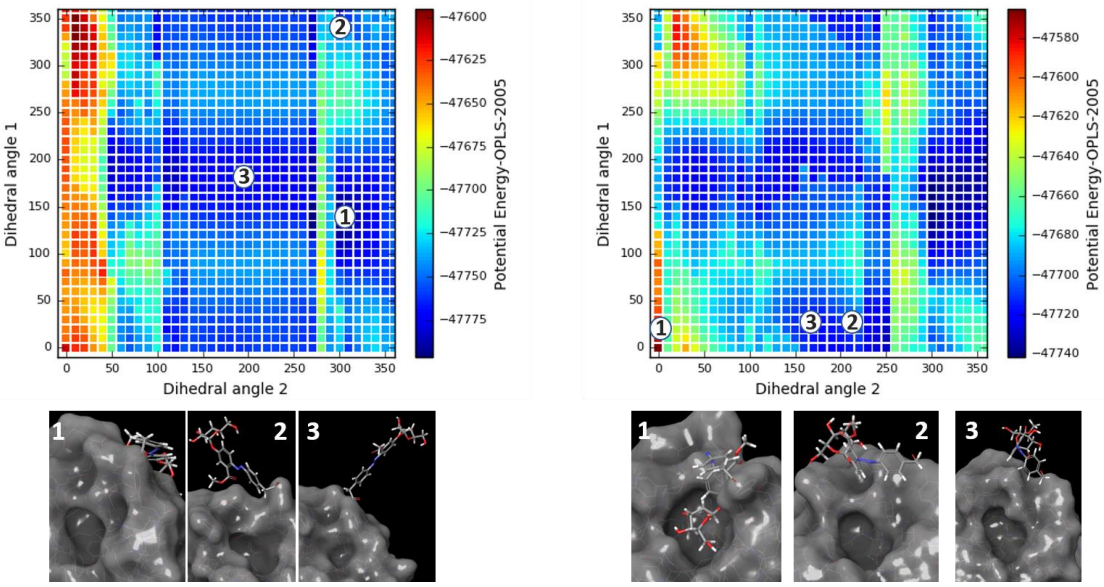

Figure 148: Results of the rotational scan with MacroModel for the azobenzene derivative **103** ligated to the amino acid Tyr137 (open gate conformation 1KLF) in *E*- (left) and *Z*-conformation (right). The potential energy is plotted as a contour diagram in relation to the dihedral angles 2 (x-axis) and 1 (y-axis).

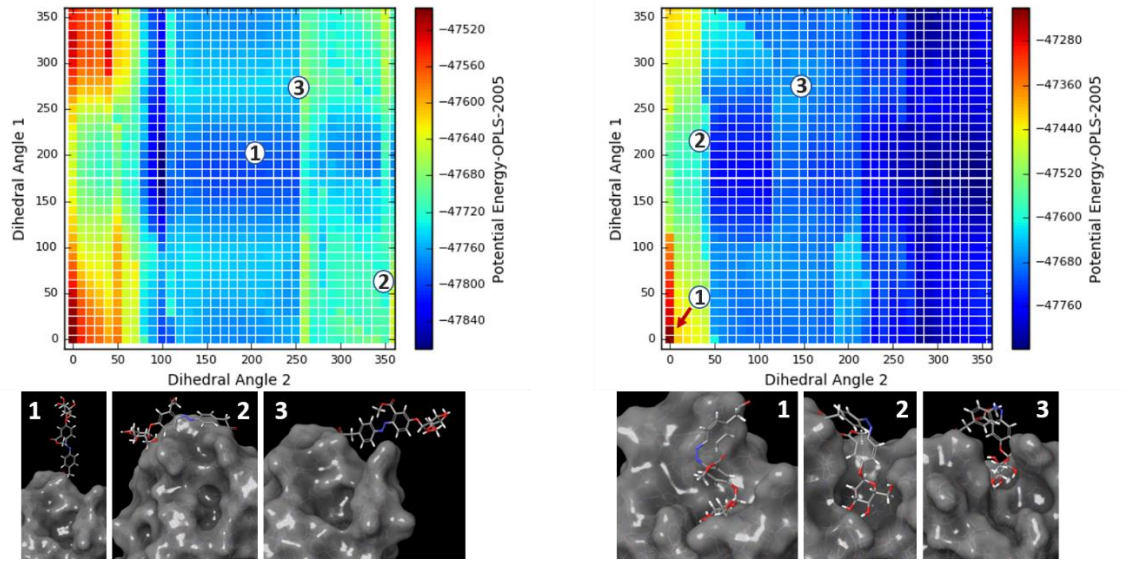

Figure 149: Results of the rotational scan with MacroModel for the azobenzene derivative **103** ligated to the amino acid Thr51 (open gate conformation 1KLF) in *E*- (left) and *Z*-conformation (right). The potential energy is plotted as a contour diagram in relation to the dihedral angles 2 (x-axis) and 1 (y-axis).

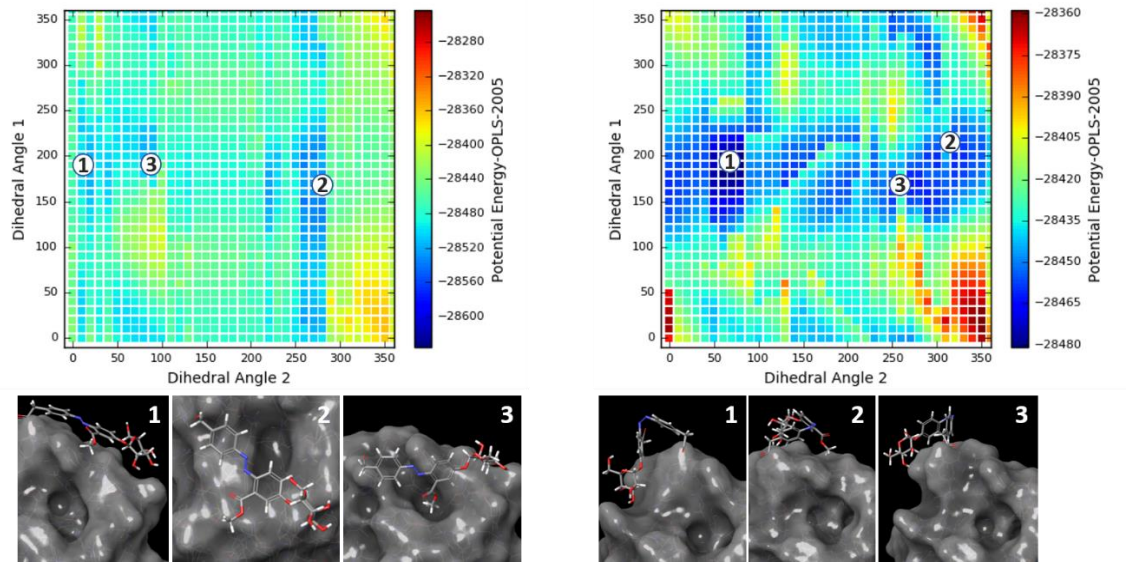

Figure 150: Results of the rotational scan with MacroModel for the azobenzene derivative **103** ligated to the amino acid Tyr48 (closed gate conformation 1UWF) in *E*- (left) and *Z*-conformation (right). The potential energy is plotted as a contour diagram in relation to the dihedral angles 2 (x-axis) and 1 (y-axis).

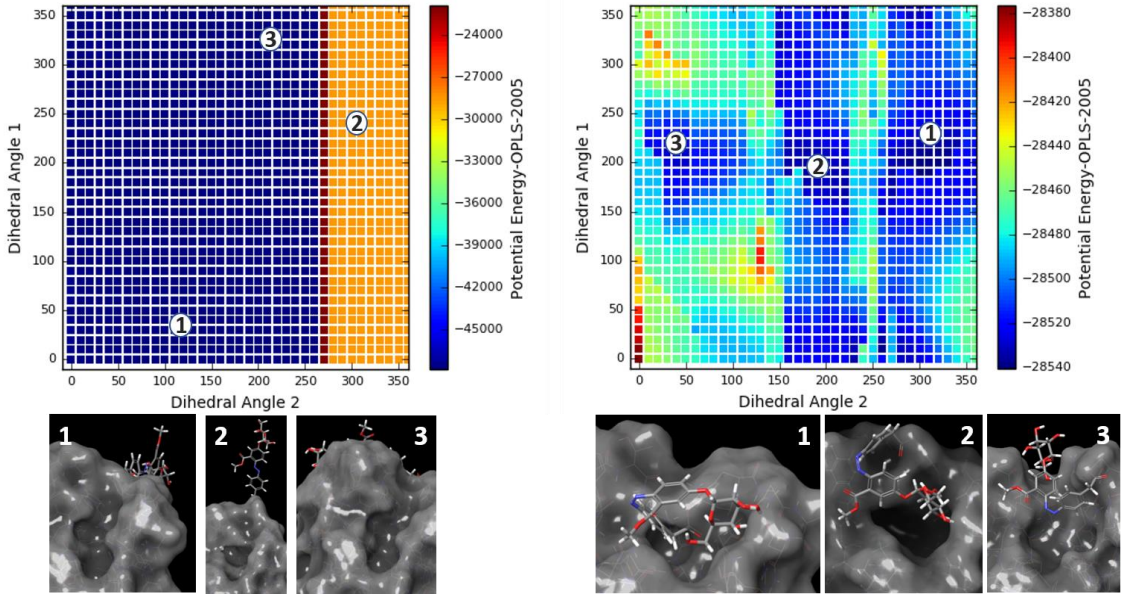

Figure 151: Results of the rotational scan with MacroModel for the azobenzene derivative **103** ligated to the amino acid Tyr137 (closed gate conformation 1UWF) in *E*- (left) and *Z*-conformation (right). The potential energy is plotted as a contour diagram in relation to the dihedral angles 2 (x-axis) and 1 (y-axis).

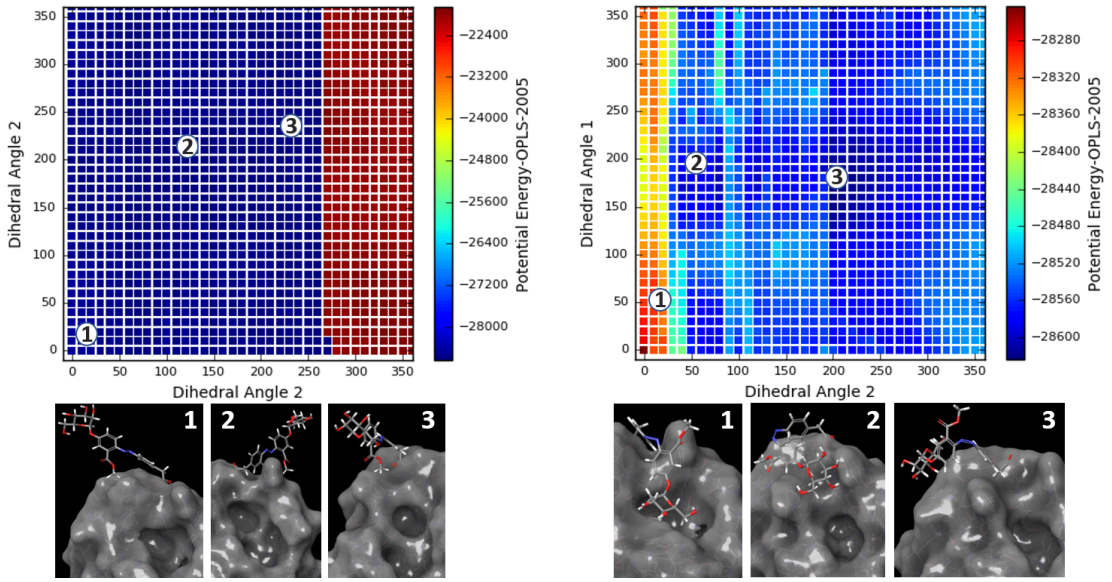

Figure 152: Results of the rotational scan with MacroModel for the azobenzene derivative **103** ligated to the amino acid Thr51 (closed gate conformation 1UWF) in *E*- (left) and *Z*-conformation (right). The potential energy is plotted as a contour diagram in relation to the dihedral angles 2 (x-axis) and 1 (y-axis).

5.4 Conclusion

In conclusion, all structures (**11**-**14**, **35**, **79**, **80**, **102**, **103**) were successfully synthesized by a versatile strategy using DPPA (**76**), respectively DEPC (**77**) and submitted to a scan of the dihedral angles with MacroModel.[185] The rotational scans showed at least two positive matches for each compound with exception of compound **79** which showed just one positive match. That means that one protein structure (KLF or UWF) is existing with a ligated 'gate keeper' moiety on one of the considered amino acids (Tyr48, Tyr137, Thr51) which leaves the binding site open in several energetically favoured structures during the dihedral angle scan for the *E*-configuration of the azobenzene moiety and accordingly shows also several energetically favoured structures during the scan for the *Z*-configuration of the azobenzene moiety which close the binding site or at least cover or distort it in such a way that binding of a ligand would be impeded. Thus, all those *in silico* results in chapter 5.3.5 recommend to perform the respective ligation and photoswitching experiments with lectin FimH *in vitro* as next step of the project.

It is advisable to establish both the labeling of FimH *in vitro* and the adjacent NMR studies with the bipyridinyl derivative **14**, which showed the required 'gate keeper' properties *in silico* both for the docking and the rotational scan. Afterwards, it would be particularly interesting to investigate the carbohydrate series **78**-**80**. Those derivatives feature a biocompatible glycoside 'gate keeper' moiety and in addition the influence of the graded affinity to the CRD on the reversible opening and closing of the binding site is of great interest.

6 Red-shifted azobenzene glycoconjugates for *in vivo* photoswitching expriments

6.1 Introduction

The wavelengths which are required for the *E*/*Z* isomerisation of basic azobenzene derivatives are too low not to harm living systems. Therefore, they are not suited for *in vivo* experiments. Consequently, so-called red-shifted azobenzene derivatives were introduced in which the wavelength required for photoswitching is shifted from UV light to visible ligtht (bathochromic shift). A number of reports appeared in the literature. For example, WOOLLEY et al. discovered that azobenzene derivatives which are substituted at all four *ortho*-positions of the azobenzene can be isomerised at increased wavelength while the thermal stability of the molecules is still ensured.[149-151, 350] Particularly advantageous are chloro-substituents and thus both WARREN and WOOLLEY pursued this research. WARREN et al. synthesised tetra-*ortho*-chloro-substituted azobenzenes by oxidative aniline dimerisation[409-410] and WOOLLEY et al. used azocoupling.[411] In the following, further work on the synthesis of tetra-*ortho*-chloro-substituted azobenzenes was published by TRAUNER and coworkers[54] who used a 'late stage chlorination approach'. FERINGA and coworkers established the synthesis of tetra-*ortho*-substituted azobenzenes by a lithiation of an aromatic substrate first and subsequent coupling with a diazonium salt.[412-413] Our objective was to build on this work for the synthesis of red-shifted azobenzene glycoconjugates to eventually facilitate *in vivo* investigations. This work was performed in collaboration with Dr. VIVEK POONTHIYIL in the LINDHORST group.[55]

6.2 Results and discussion

WOOLLEY's procedure[411] was followed in order to achieve tetra-*ortho*-chloro-substituted azobenzene derivatives for the synthesis of photoswitchable glycoconjugates. Thus amine **1** was employed in a diazotation reaction according to a procedure of RULLO et al.[350] using sodium nitrite for the formation of the diazonum salt which should then be reacted with the phenol derivative **2** to form the azobenzene derivative **3**. Unfortunately, this reaction did not generate any product (Scheme 35).

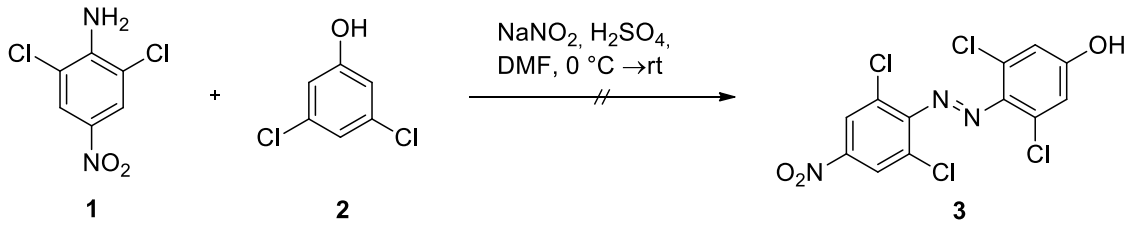

Scheme 35: Synthetic pathway for the formation of azobenzene derivative **3** via diazotation.

Since varying the reaction conditions did not lead to success, MILLS coupling was used as alternative. Therefore the nitro compound **5** was synthesised starting from the phenol derivative **4** via nitration with sodium nitrite under acidic conditions.[414] The nitro compound **5** was subsequently reduced via hydrogenation to obtain amine **6**, which was employed for MILLS coupling with the nitroso compound **8** prepared from amine **7** with oxone®. However, also this approach remained unsuccessful and the desired azobenzene derivative **3** was not obtained (Scheme 36).

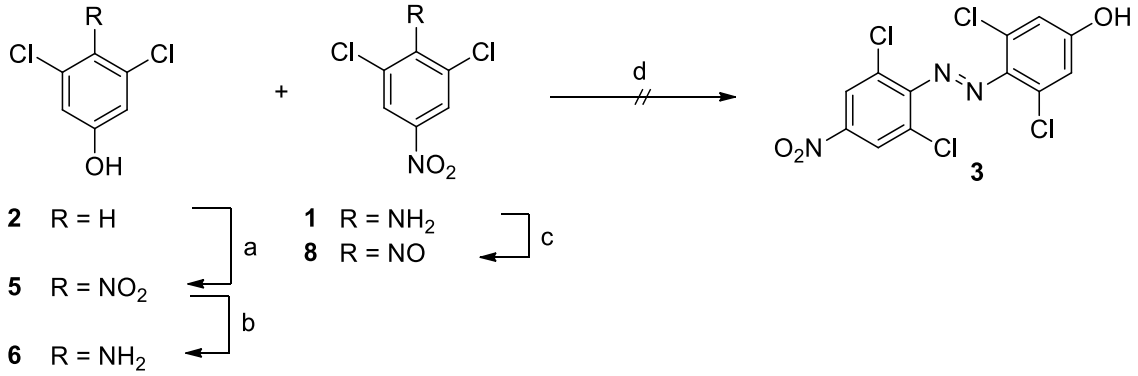

Scheme 36: Synthetic pathway for the synthesis of desired azobenzene derivative **3**: (a) $NaNO_2$, H_2SO_4, H_2O, 0 °C → reflux, 6 h → rt, 16 h, 37 %; (b) H_2, Pd/C, MeOH, rt, 16 h, quant.; (c) oxone®, H_2O, DCM, acetone, rt, 16 h, raw product; (d) CH_3COOH, rt, 16 h.

Since MILLS coupling had worked out quite nicely for many reactions with aminophenyl glycosides as described in chapter 5.3.2, the starting materials were varied. Hence, the aminophenyl mannoside **11** was applied in a MILLS coupling. Compound **11** was prepared by glycosylation of **5** with the trichloroacetimidate **9** followed by hydrogenation (Scheme 37). Then, MILLS coupling with the nitroso compound **8** delivered the azobenzene mannoside **12** as a raw product which however could not be fully purified (Scheme 37).

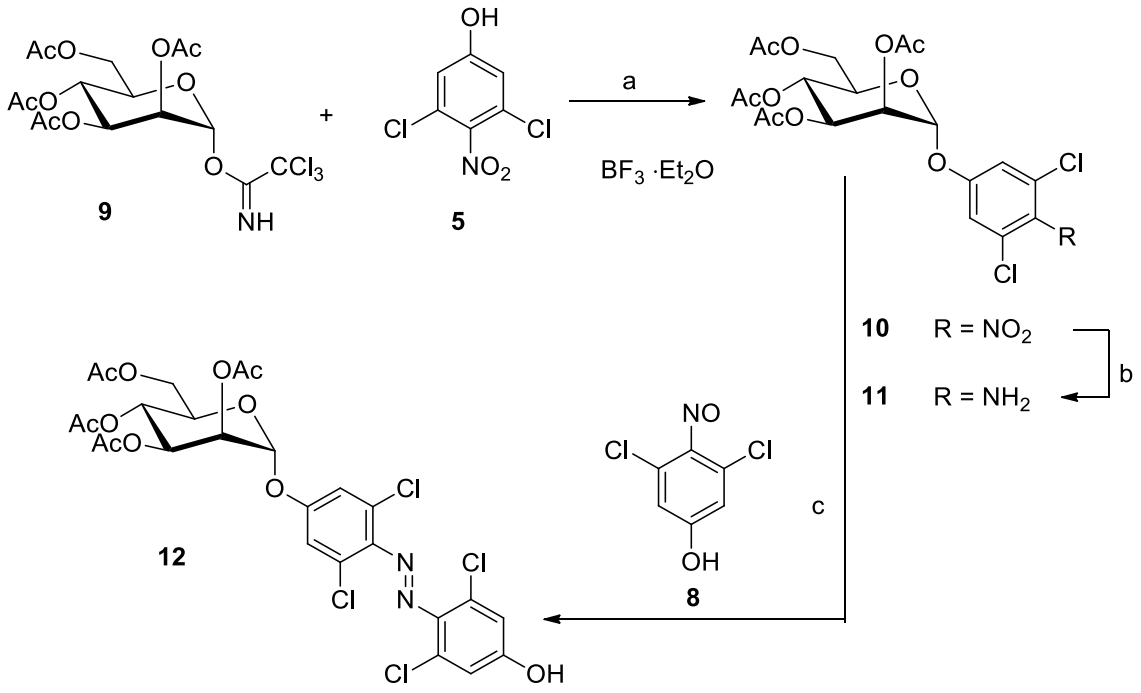

Scheme 37: Synthetic pathway for the synthesis of azobenzene-equipped mannoside **12**: (a) $BF_3 \cdot Et_2O$, dry DCM, 0 °C → rt, 16 h, 71 %; (b) H_2, Pd/C, MeOH, 4 h, quant.; (c) CH_3COOH/DMSO (1:1), rt, 16 h, raw product.

In conclusion the common methods for the synthesis of glycoazobenzene derivatives failed for the synthesis of tetra-*ortho*-chlorinated azobenzene derivatives. When TRAUNER and coworkers[54] published the late stage chlorination approach in 2016, this chemistry was adapted to the synthesis of azobenzene glycoconjugates. By using a palladium (II) catalyst, the azobenzene *ortho*-positions can be activated and subsequently chlorinated with *N*-chlorosuccinimide. This method was applied to standard azobenzene derivative **13** and the propargylated derivative **14** which proved to be versatile building blocks for the synthesis of glycoazobenzenes before. In case of the dihydroxy derivative **13** the late stage chlorination produced a raw product, which was not obtained in pure form even after repeated column chromatography. In case of the propargylated derivative **14** no product was obtained which suggests that the late stage chlorination method is not compatible with alkyne groups within the substrate. (Scheme 38)

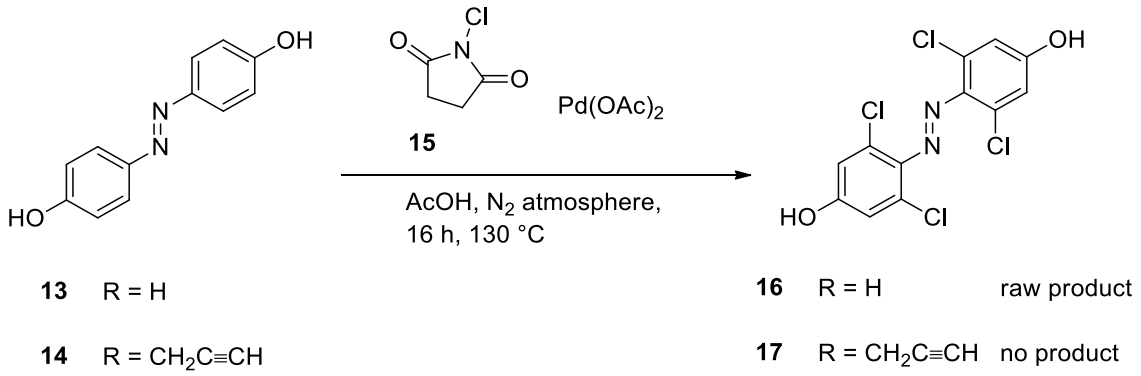

Scheme 38: Late stage chlorination of the azobenzene derivatives **13** and **14** with *N*-chlorosuccinimide and $Pd(OAc)_2$ catalyst.

Nevertheless, since the target molecule was a red-shifted glycoazobenzene derivative, raw product **16** was submitted to a glycosylation reaction with the trichloroacetimidate **9** under Lewis acid catalysis with boron trifluoride diethyl etherate (Scheme 39). The result of this reaction was a colourless solid so that the formation of the targeted compound **12** was excluded. Instead of the targeted compound the formation of the hydrazine derivative **18** was indicated by NMR spectroscopy and confirmed by mass spectrometry. This outcome confirmed the formation of a chloro-substituted azobenzene derivative in the reaction step shown in Scheme 38 was successful but the targeted glycoazobenzene derivative **12** was not originated.

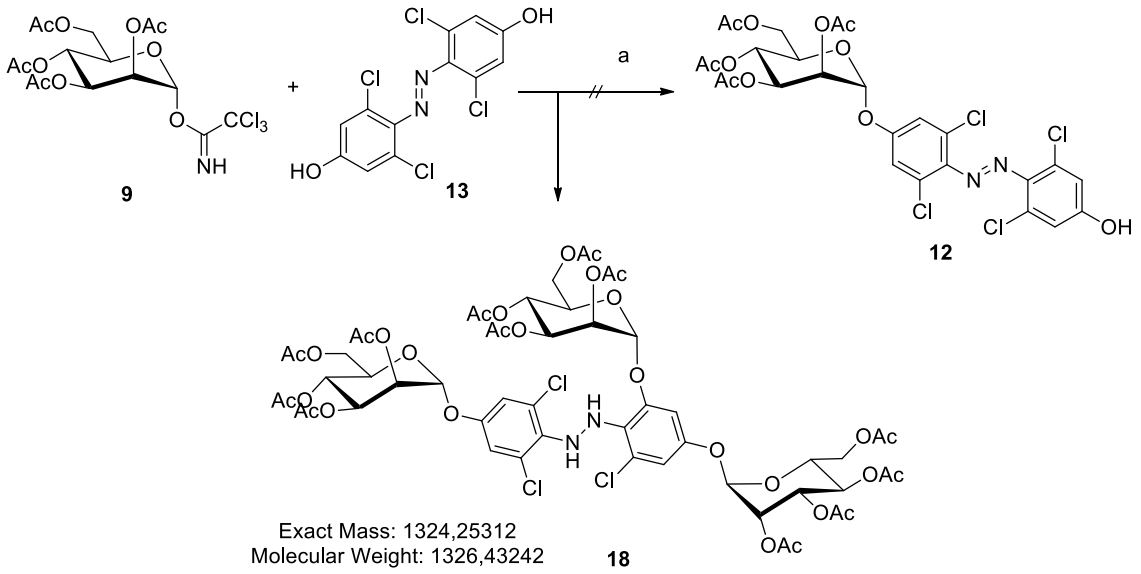

Scheme 39: Synthesis plan for the glycosylation of azobenzene **13** with trichloroacetimidate **9** to obtain the targeted compound **12**. (a) $BF_3 \cdot Et_2O$, dry DCM, 0 °C → rt, 16 h.

Finally, although the reaction conditions of the late stage chlorination seem rather harsh with respect to the stability of carbohydrates, the method was yet applied to a glycoazobenzene derivative. Thus, the reaction was performed with the azobenzene derivative **19** (cf. 5.3.2). It was necessary to first fully acetylate **19** to result in **20** which was then subjected to the chlorination reaction with NCS and $Pd(OAc)_2$ (Scheme 40). Heating was performed in a microwave reactor. The desired product **21** was obtained with a yield of 33 %. Taken together, late stage chlorination after a proceeding glycosylation step is the clearly more advantageous route to synthesize red-shifted azobenzene glycoconjugates.

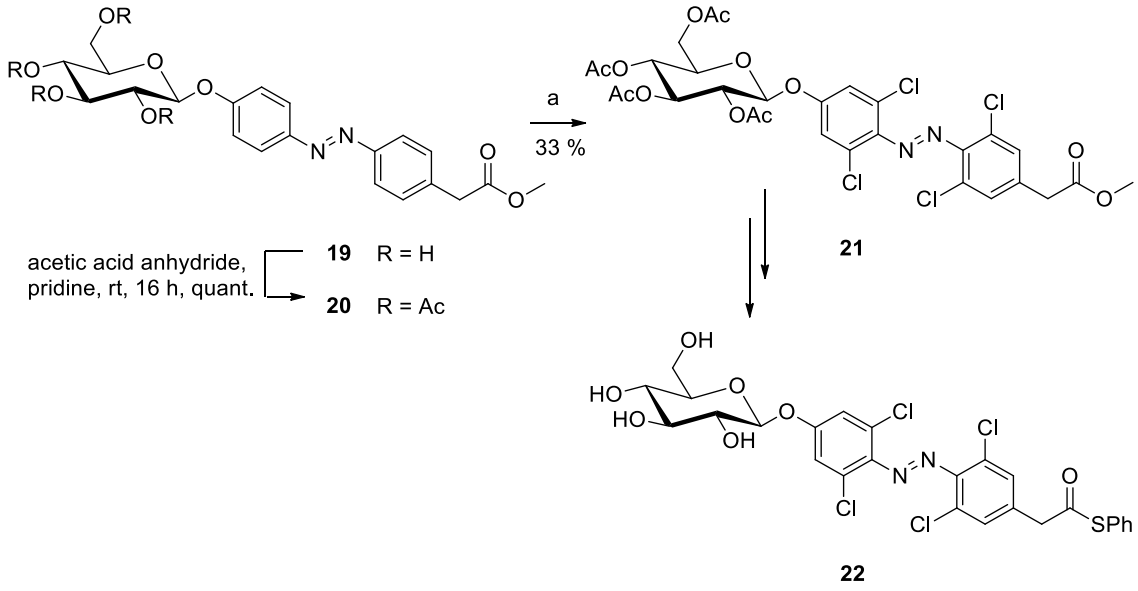

Scheme 40: Synthesis of the tetra-*ortho*-chloro-substituted glycoazobenzene derivative **21** via late stage chlorination which can be converted into a thioester **22** for subsequent ligation with lectin FimH: (a) NCS, $Pd(OAc)_2$, CH_3COOH, 140 °C (microwave), 2 h, 33 %.

The azobenzene derivative **21** can be employed in the preparation of the thioester **22** in order to achieve red-shifted 'gate keeper' molecules for the switching of FimH function (cf. chapter 5). Docking studies and also a rotational scan with the Schrödinger software was used to evaluate the suitability of **22** as FimH gate keeper. The results of the coordinate scan are shown in Figure 153 to Figure 158. Positive matches were observed for the protein derivative which is ligated with the 'gate keeper' moiety at the Tyr137 residue both in the open and the closed gate conformation. Additionally, also the Tyr48-ligated protein in the open gate conformation showed a closed binding site when the azobenzene 'gate keeper' was in its *Z*-state.

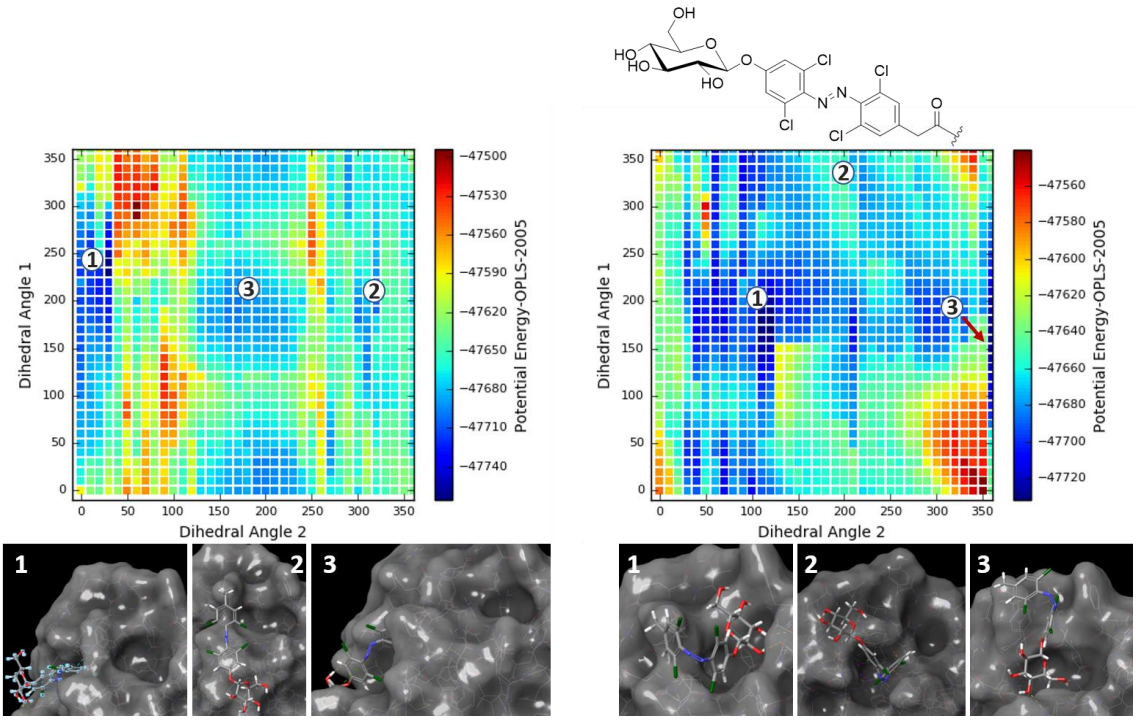

Figure 153: Results of the rotational scan with MacroModel for the azobenzene derivative **22** ligated to the amino acid Tyr48 (open gate conformation 1KLF) in *E*- (left) and *Z*-conformation (right). The potential energy is plotted as a contour diagram in relation to the dihedral angles 2 (x-axis) and 1 (y-axis).

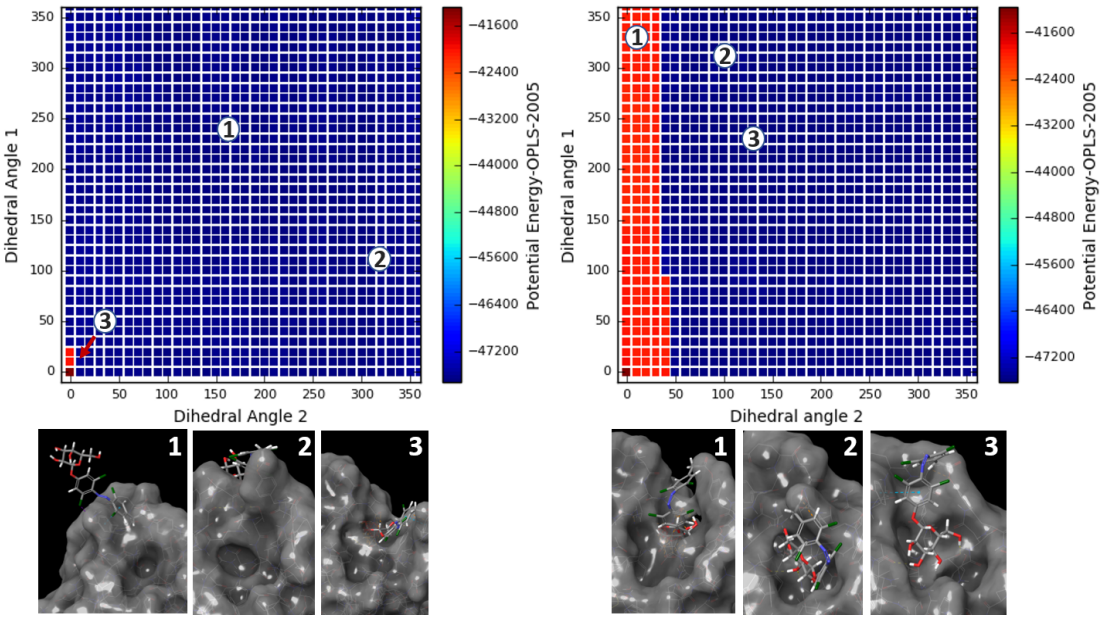

Figure 154: Results of the rotational scan with MacroModel for the azobenzene derivative **22** ligated to the amino acid Tyr137 (open gate conformation 1KLF) in *E*- (left) and *Z*-conformation (right). The potential energy is plotted as a contour diagram in relation to the dihedral angles 2 (x-axis) and 1 (y-axis).

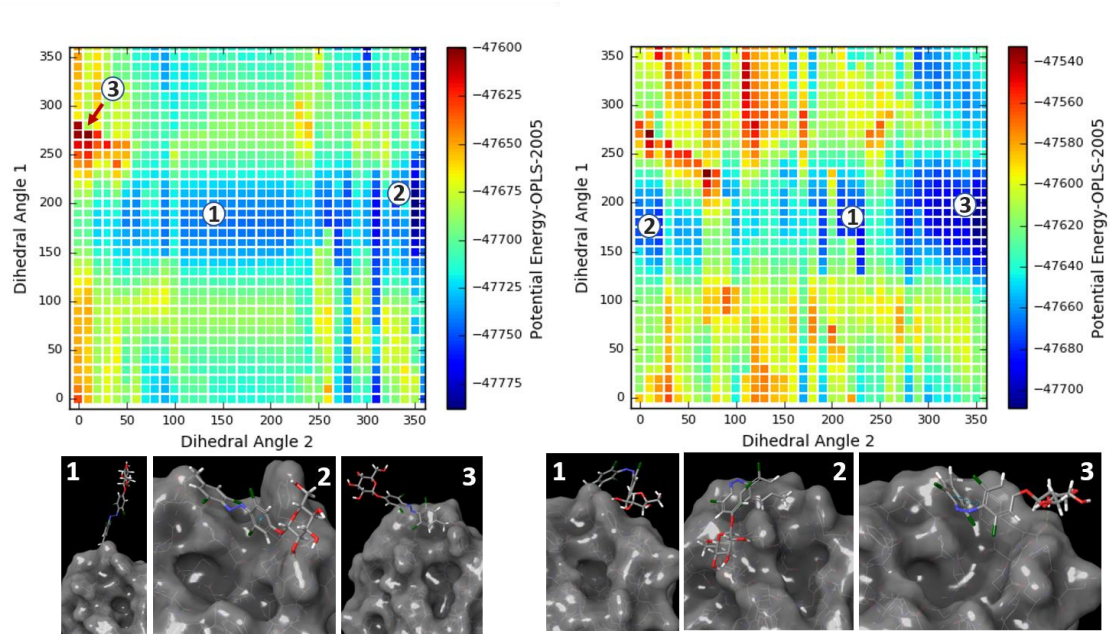

Figure 155: Results of the rotational scan with MacroModel for the azobenzene derivative **22** ligated to the amino acid Thr51 (open gate conformation 1KLF) in *E*- (left) and *Z*-conformation (right). The potential energy is plotted as a contour diagram in relation to the dihedral angles 2 (x-axis) and 1 (y-axis).

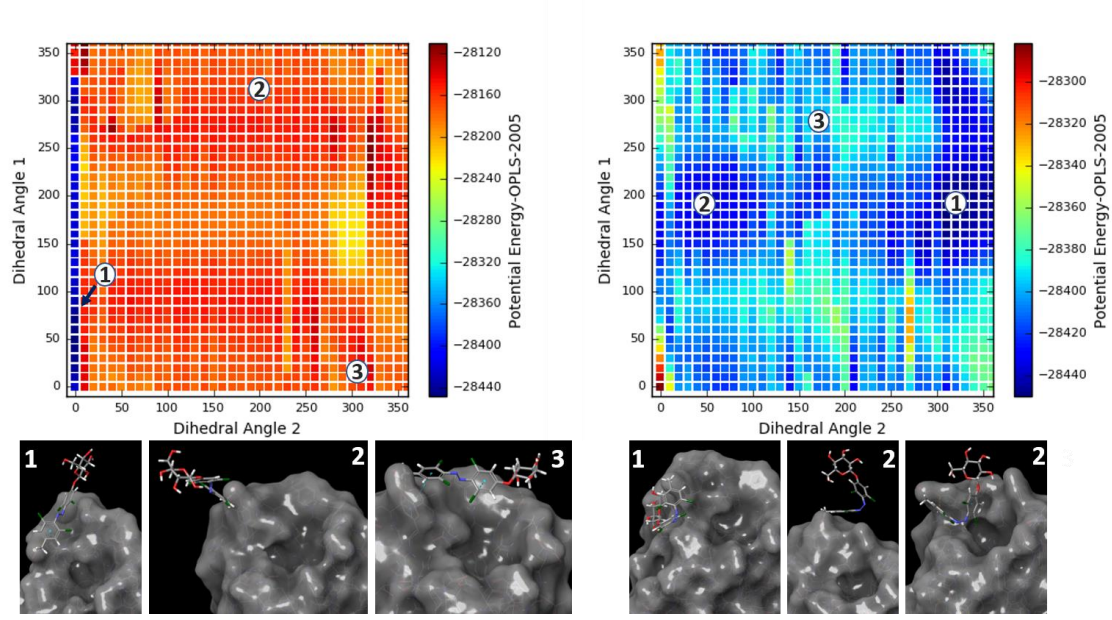

Figure 156: Results of the rotational scan with MacroModel for the azobenzene derivative **22** ligated to the amino acid Tyr48 (closed gate conformation 1UWF) in *E*- (left) and *Z*-conformation (right). The potential energy is plotted as a contour diagram in relation to the dihedral angles 2 (x-axis) and 1 (y-axis).

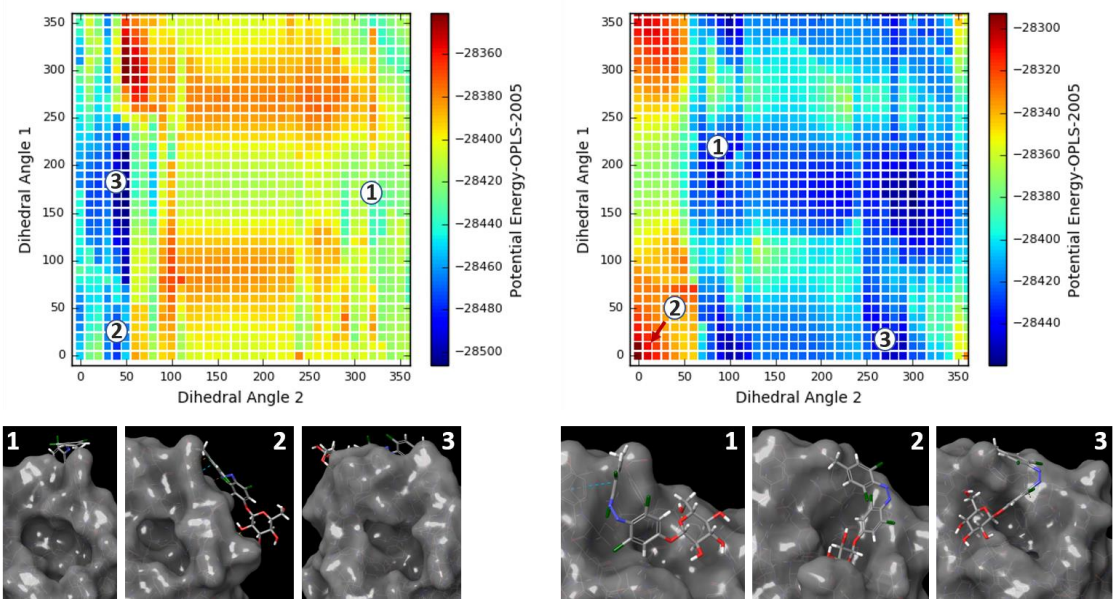

Figure 157: Results of the rotational scan with MacroModel for the azobenzene derivative **22** ligated to the amino acid Tyr137 (closed gate conformation 1UWF) in *E*- (left) and *Z*-conformation (right). The potential energy is plotted as a contour diagram in relation to the dihedral angles 2 (x-axis) and 1 (y-axis).

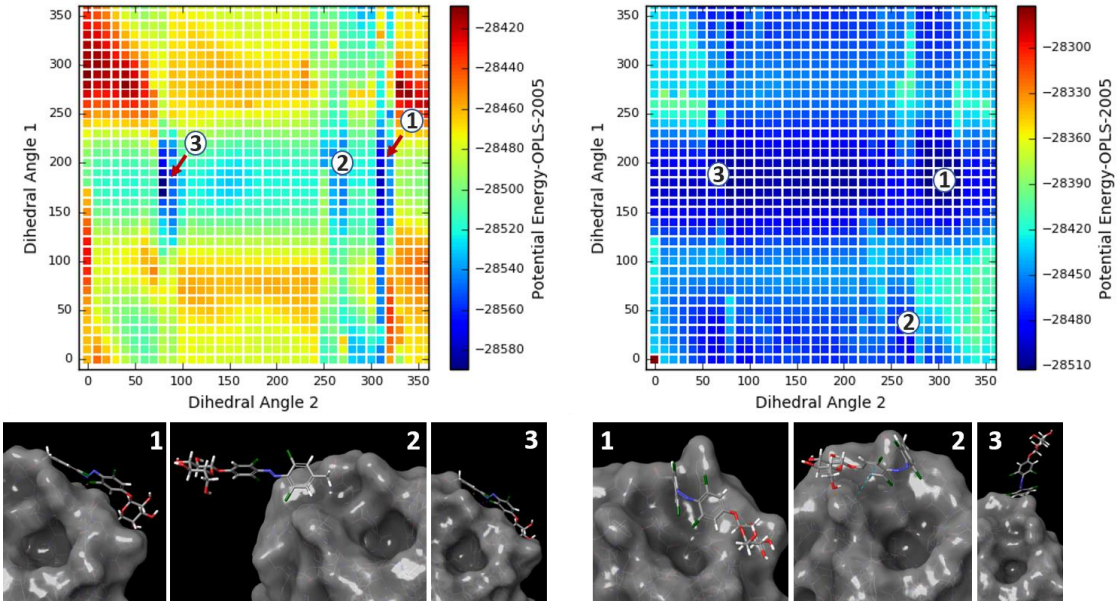

Figure 158: Results of the rotational scan with MacroModel for the azobenzene derivative **22** ligated to the amino acid Thr51 (closed gate conformation 1UWF) in *E*- (left) and *Z*-conformation (right). The potential energy is plotted as a contour diagram in relation to the dihedral angles 2 (x-axis) and 1 (y-axis).

6.3 Conclusion

Late stage chlorination was established as a versatile method to synthesize red-shifted glycoconjugates. In addition, molecular modelling regarding the ‘gate keeper’ project (chapter 5) was performed. The results confirm that also the tetra-*ortho*-chloro-substituted derivative **22** showed positive matches for the *E*/*Z* isomerisation along with the opening respectively closing of the binding site. Thus, this derivative might be a good ‘gate keeper’ moiety. Besides that, the red shift of azobenzene isomerisation would allow to switch the function of FimH under physiological conditions (and eventually *in vivo*).

7 Conclusion: Insights gained and following challenges

Four projects were investigated in this thesis aiming at providing tools for the investigation of carbohydrate binding and carbohydrate function within a supramolecular biological context.

The first project dealt with photoswitchable glycolipid mimetics, which could be embedded into DPPC monolayers for the eventual investigation of membrane dynamics in collaboration with Dr. B. MURPHY. A library of 13 glycolipid mimetics was successfully synthesised. The synthetic azobenzene glycoconjugates were photochemically characterised and an influence of the carbohydrate moiety on the switching behaviour could be registered. In addition, the ability of those glycolipids to form a monolayer with DPPC was confirmed and Langmuir isotherm and X-ray investigations were performed by the physics departement of Kiel University.

During the second project two new glycoarrays which enrich the previous experience in the field of glyco-SAMs and glycosylated surfaces in the LINDHORST group. were developed. One, which is photoactivatable and another, which is based on a polysaccharide platform. The photoactivatable glycoarray is based on a light-induced PFPA ligation strategy which was performed for mono-, di- and trivalent mannoside derivatives. The second assay aimed for the design of a ‘chaotic’ glycosylated surface which can mimic naturally occurring surfaces better than the established glyco-SAMs. Therefore, a polysaccharide (dextran) was equipped with azido functionalities and immobilised by adsorption on a polystyrene surface. Then, the azido moieties were used for the attachment of glycosides via copper-catalysed azide alkyne click chemistry resulting in a surface which has no defined orientation of its glycoside constituents.

The aim of the third project was the bioorthogonal and site-specific modification of the lectin FimH with suitable azobenzene precursors to create a labelled protein which can be photochemically switched between an adhesive and a non-adhesive state. Therefore, a library of thioester-equipped azobenzene derivatives was synthesised. The thioester moiety enables a DMAP-catalysed ligation with nucleophilic residues like those from tyrosine or threonine in the proximity of the binding site. For the design of the ‘gate keeper’ precursors different requirements like size, polarity and affinity were considered. Moreover, a versatile method using DPPA (**76**) respectively DEPC (**77**) for the synthesis of thioesters could be established and increased the yields of formerly synthesised

thioesters. All synthesised ‘gate keeper’ precursors were also investigated photochemically and by molecular modelling to evaluate their eligibility as ‘gate keeper’ moieties. All synthesised ‘gate keeper’ molecules are depicted in (Figure 159).

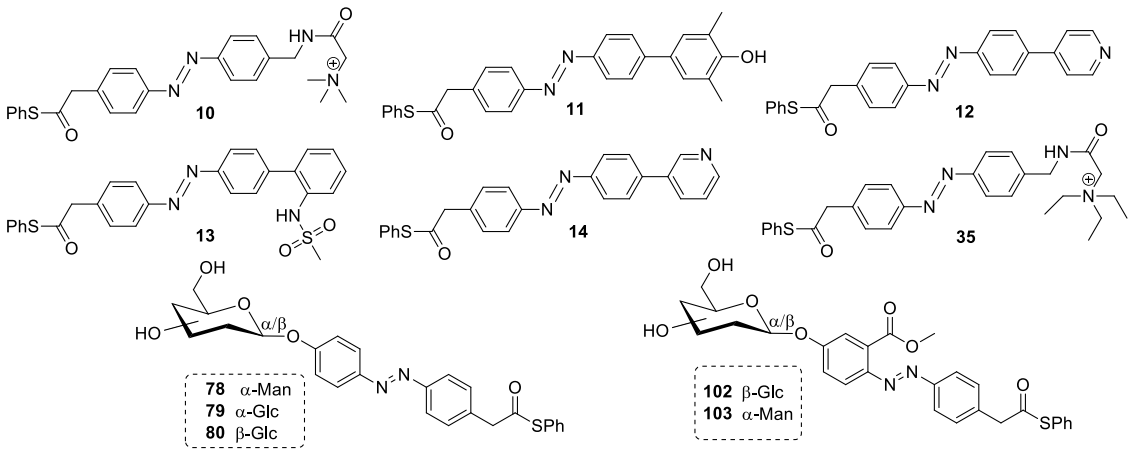

Figure 159: Summary of all thioesters, prepared as photosensitive “gate keeper” molecules for FimH labelling.

The next challenge in the context of this project will be the proof of principle for the labelling and subsequent switching of the bacterial lectin FimH. Hopefully this method will become a versatile and potent tool in glycobiology which combines labelling and controlling in one modification which can be attached on the native protein without preceding protein engineering.

The last part of this thesis dealed with the synthesis of tetra-*ortho*-chloro-substituted azobenzene derivatives which can be addressed for *E* to *Z* isomerisation with long waved light. Thus, those red-shifted azobenzene derivatives are especially useful in biological applications since they provoke less damage on tissues than their unsubstituted counterparts. A general procedure based on a method by TRAUNER was modified and established for glycoazobenzene derivatives. From now on, the microwave-assisted method allows the simple preparation of tetra-*ortho*-chloro-substituted azobenzene glycosides. This strategy is a very promising approach which can be introduced to all projects which deal with the photochemical control of biological function. Especially for the project which aims for the labelling and control of FimH (cf. chapter 5) this represents a useful expansion. By using red-shifted azobenzene moieties as ‘gate keeper’ molecules, damages on the protein can be prevented. Concerning this matter, for the long term there are no impediments for the expansion of the ‘gate keeper’ project towards labelled and controlled bacteria.

8 Experimental section

8.1 General methods

Reactions, chemicals and solvents

All reactions were carried out under atmospheric conditions (unless stated otherwise). Moisture sensitive reactions were carried out in dry glass ware under nitrogen atmosphere. All chemicals were purchased from abcr, Acros, Alfa Aesar, Gruessing, Merck, Sigma-Aldrich and TCI and used without further purification. Only ion exchange resins were washed with methanol before use. Solvents were purchased as technical grade solvents and purified by distillation before use. Methanol was dried over magnesium and acetonitrile over calciumhydride under a nitrogen atmosphere. Dry *N*,*N*'-dimethyl-formamide over molecular sieves was purchased from Acros Organics and used without further purification. Dry dichloromethane, diethylether and tetrahydrofurane were obtained by the PureSolv MD5 Solvent Purification System from Inert Technology.

Thin layer chromatography (TLC)

Analytical thin layer chromatography (TLC) was performed on silica-gel plates (GF 254, Merck). Visualisation was achieved by UV light and/or with a solution of vanillin in 10% sulfuric acid in ethanol followed by heat treatment at ~180 °C.

Flash chromatography

Flash chromatography was performed on silica gel 60 (Merck, 230-400 mesh, particle size 0.040-0.063 mm) by using distilled solvents.

NMR spectroscopy

Proton (^{1}H) nuclear magnetic resonance spectra and carbon (^{13}C) nuclear magnetic resonance spectra were recorded on a Bruker Avance 200, Bruker ARX300, Bruker AvanceNeo 500 and Bruker Avance 600 spectrometer. Chemical shifts are referenced to internal tetramethylsilane or to the residual proton of the NMR solvent. Data are presented as follows: chemical shift, multiplicity (s=singlet, d=doublet, t=triplet, q=quartet,

m=multiplet, and br=broad signal), coupling constant in Hertz (Hz) and, integration. Full assignment of the peaks was achieved with the aid of 2D NMR techniques ($^{1}H/^{1}H$ COSY and $^{1}H/^{13}C$ HSQC). All NMR spectra of the *E*-isomers of the azobenzene derivatives were recorded after they were kept for 16 h in the dark at 40 °C. *Z*-isomers of the azobenzene derivatives were recorded after irradiation with a UV LED (365 nm) for 15 min.

Infrared (IR) spectroscopy

Infrared (IR) spectra were measured with a Perkin Elmer FT-IR Paragon 1000 (ATR) spectrometer and were reported in cm^{-1}.

UV/Vis spectroscopy

UV-Vis absorption spectra were recorded on a Agilent Cary 4000 spectrometer (for chapter 3) or on a Lambda-41 spectrometer from PerkinElmer equipped with a Büchi thermostat. Samples were measured in quartz cuvettes with a diameter of 1 cm at a temperature of 20 °+/- 1 °C.

Mass spectrometry

EI mass spectra were recorded on a Jeol AccuTOF 4GCV and Finnigan MAT 8230 or MAT 8200 devices. ESI mass spectra were recorded on an Applied Biosystems (Applera) Mariner ESI-TOF and HR (high resolution) MS ESI spectra on a ThermoFisher Orbitrap (Q Exactive Plus from Thermo Scientific). MALDI MS were measured on a Bruker Bioflex III instrument and a Bruker MALDI-TOF Autoflex.

Melting points

Melting points were determined on a Büchi M-560 apparatus.

Photoirradiation

Photoirradiation was performed using either a UV LED (emitting 365 nm light, 2.7 mW) or a blue LED (emitting 455 nm light, 2.6 mW). *E* → *Z* isomerisation was induced by

irradiation using a LED (emitting 365 nm light) from the Nichia Corporation (NC4U133A) with a FWHM (full width at half maximum) of 10 nm and an intensity of 25 mW/cm^2. *Z* → *E* isomerisation was performed by irradiation of the probe with a LED (emitting 365 nm light) from the Nichia Corporation with a FWHM of 45 nm and an intensity of 1 mW/cm^2.

ELISA reader

Fluorescence and absorbance were measured on a Tecan infinite F200 and a Tecan infinite M200 Pro multifunction microplate reader. A bandpass filter was used with 485 nm for excitation and 535 nm for emission in case of Tecan reader F200.

Optical rotations

Optical rotations were measured on a PerkinElmer 241 polarimeter (sodium D-line: 589 nm, cell length: 1 dm) in the solvents indicated.

Microwave

Microwave reactions were performed with a Discover SP Microwave Synthesizer from CEM Corporation (model: Explorer 12 Hybrid) The temperature, pressure, and power settings used for all reactions were 140 °C, 10 bar and 200 W.

Purity of compounds

The purity of synthesised compounds was ensured by validation of the corresponding ^{1}H and ^{13}C NMR spectra in combination with the HR-MS spectra.

8.2 Supporting information for chapter 3: Photoswitchable glycolipids for the investigation in lipid layers

8.2.1 Synthesis of amphiphiles

(*E*)-[*p*-((2,2-Dimethyl-1,3-dioxan-4-yl)methoxy)-*p*'-(propargyloxy)] azobenzene (14)

To a suspension of azobenzene **12** (8.00 g, 31.7 mmol) and potassium carbonate (10.1 g, 73.1 mmol) in dry DMF (100 mL) compound **13** (9.08 g, 31.7 mmol) was added and stirred for 10 h at 100 °C. Then the solvent was removed, the residue resolved in ethyl acetate (250 mL) and washed with water (2 x 200 mL). It was dried over $MgSO_4$, filtered and the filtrate was concentrated under reduced pressure. Purification of the crude product by column chromatography (cyclohexane/ethyl acetate 6:1 → 4:1) gave **14** as an orange solid.

Yield: 10.0 g (27.3 mmol, 86 %);

TLC: R_f = 0.30 (cyclohexane/ethyl acetate 4:1);

^{1}H NMR (600 MHz, $CDCl_3$, 300 K): δ = 7.90-7.86 (m, 4H, Ar-H*$_{ortho}$*, Ar-H*$_{ortho'}$*), 7.08 (m, 2H, Ar-H*$_{meta}$*), 7.02 (m, 2H, Ar-H*$_{meta'}$*), 4.77 (d, $^4J_{OCH2,C\equiv CH}$ = 2.3 Hz, 2H, OCH_2), 4.51 (m, 1H, Ar-$COCH_2C\underline{H}$), 4.19 (dd, $^2J_{CHH'}$ = 8.6 Hz, $^3J_{CHCHH'}$ = 6.5 Hz, 1H, Ar-$COCH_2CHC\underline{H}H'$), 4.13 (dd, $^3J_{CHH'CH}$ = 5.4 Hz, $^2J_{CHH'}$ = 9.5 Hz, 1H, Ar-$COC\underline{H}H'CH$), 4.03 (dd, $^3J_{C\underline{H}H'C\underline{H}}$ = 5.9 Hz, $^2J_{C\underline{H}H'}$ = 9.5 Hz, 1H, Ar-$COCH\underline{H}'CH$), 3.93 (dd, $^2J_{CHH'}$ = 8.6 Hz, $^3J_{C\underline{H}CH\underline{H}'}$ = 5.9 Hz, 1H, Ar-$COCH_2CHCH\underline{H}'$), 2.56 (t, $^4J_{CH2C\equiv CH}$ = 2.4 Hz, 1H, C≡CH), 1.48 (s, 3H, CH_3), 1.42 (s, 3H, CH_3) ppm;
^{13}C NMR (126 MHz, $CDCl_3$, 300 K): δ = 160.8 (Ar-C*$_{para'}$*), 159.6 (Ar-C*$_{para}$*), 147.7 (Ar-C*$_{ipso}$*), 147.4 (Ar-C*$_{ipso'}$*), 124.6, 124.5 (Ar-C*$_{ortho}$*, Ar-C*$_{ortho'}$*), 115.3 (Ar-C*$_{meta}$*), 114.9 (Ar-C*$_{meta'}$*), 110.0 ($O\underline{C}CH_3$), 78.3 ($\underline{C}\equiv CH$), 76.1 ($C\equiv\underline{C}H$), 74.1 ($OCH_2\underline{C}H$), 69.2 (Ar-$CO\underline{C}H_2CH$), 66.9 (Ar-$COCH_2CH\underline{C}H_2$), 56.2 ($\underline{C}H_2C\equiv CH$), 29.9, 27.0 ($CH_3$) ppm;

Ir (ATR): $\tilde{\nu}$ = 3400, 3276, 1594, 1497, 1234, 1014, 844 cm^{-1};

EI-MS: *m/z* = 366.15796, $[M]^+$; (calc. 366.15796 for $C_{21}H_{22}N_2O_4$).

(*E*)-[*p*-((1,2-Dihydroxypropyloxy)-*p*'-(propargyloxy)] azobenzene (15)

1 M HCl (200 mL) was added to a solution of azobenzene **14** (10.5 g, 28.7 mmol) in THF (300 mL). The reaction mixture was stirred for 2 h at room temperature. Afterwards the

reaction was neutralised by adding 1 M NaOH solution and the mixture was extracted with ethyl acetate (3 x 150 mL). It was dried over $MgSO_4$, filtered and the filtrate was concentrated under reduced pressure. Purification of the crude product by column chromatography (cyclohexane/ethyl acetate 6:1 → ethyl acetate → ethyl acetate/methanol 3:1) gave **15** as an orange solid.

Yield: 5.26 g (16.1 mmol, 56 %);

TLC: R_f = 0.37 (ethyl acetate);

^{1}H NMR (500 MHz, DMSO-*d6*, 300 K): δ = 7.86-7.82 (m, 4H, Ar-H$_{ortho}$, Ar-H$_{ortho'}$), 7.18-7.15 (m, 2H, Ar-H$_{meta'}$), 7.13-7.10 (m, 2H, Ar-H$_{meta}$), 5.00 (d, $^3J_{CHOH}$ = 5.1 Hz, 1H, CHO<u>H</u>), 4.91 (d, $^4J_{CH2C\equiv CH}$ = 2.3 Hz, 2H, C<u>H</u>$_2$C≡CH), 4.70 (t, $^3J_{CH2OH}$ = 5.7 Hz, 1H, CH$_2$O<u>H</u>), 4.12-4.10 (dd, $^3J_{OC\underline{H}H'C\underline{H}}$ = 4.0 Hz, $^2J_{OCHH'}$ = 9.9 Hz, 1H, OC<u>H</u>H'CH), 3.99-3.96 (dd, $^3J_{OCH\underline{H}'C\underline{H}}$ = 6.2 Hz, $^2J_{OCHH'}$ = 9.9 Hz, 1H, OCH<u>H</u>'CH), 3.86-3.80 (m, 1H, C<u>H</u>OH), 3.63 (t, $^4J_{CH2C\equiv CH}$ = 2.4 Hz, 1H, C≡CH), 3.47 (t, 2H, $^3J_{CH2OH}$ = 5.7 Hz, C<u>H</u>$_2$OH) ppm;

^{13}C NMR (126 MHz, DMSO-*d6*, 300 K): δ = 161.1 (Ar-C$_{para}$), 159.3 (Ar-C$_{para'}$), 146.6, 146.1 (Ar-C$_{ipso}$, Ar-C$_{ipso'}$), 124.2, 124.0 (Ar-C$_{ortho}$, Ar-C$_{ortho'}$), 115.4(Ar-C$_{meta'}$), 115.0 (Ar-C$_{meta}$), 78.9 (<u>C</u>≡CH), 78.6 (C≡<u>C</u>H), 70.0 (O<u>C</u>H$_2$CH), 69.9 (OCH$_2$<u>C</u>H), 62.6 (CH$_2$OH), 55.8 (<u>C</u>H$_2$C≡CH) ppm;

IR (ATR): $\tilde{\nu}$ = 3400, 3276, 2934, 1594, 1497, 1234, 1014, 844 cm^{-1};

EI-MS: *m/z* = 326.12666, [M]$^+$; (calc. 326.12666 for $C_{18}H_{18}N_2O_4$).

General Procedure A for the Esterification of glycerol derivatives (16, 17, 27, 28, 38, 39): Dicyclohexylcarbodiimide (2 eq) was added to an ice-cold solution of the glycerol derivative (1 eq), fatty acid (4 eq) and dimethylaminopyridine (2 eq) in dry DMF. The reaction mixture was then stirred for 16 h at room temperature. Afterwards the mixture was diluted with DCM (200 mL) and washed with 0.5 N HCl (150 mL) and aq. $NaHCO_3$ solution (150 mL). It was dried over $MgSO_4$, filtered and the filtrate was concentrated under reduced pressure. Unless otherwise noted in the individual procedures, the raw product was purified by column chromatography (cyclohexane → cyclohexane/ethyl acetate 6:1) and subsequent crystallisation from acetone.

(*E*)-[*p*-((1,2-Didodecanoyloxycarbonyl)propyloxy)-*p*'-propargyloxy)] azobenzene (16)

According to the General Procedure A compound **15** (1.43 g, 4.38 mmol) and dodecanoic acid (3.51 g, 17.5 mmol) were reacted to yield **16** as an orange solid.

Yield: 1.45 g (2.10 mmol, 48 %);

TLC: R_f = 0.32 (cyclohexane/ethyl acetate 8:1);

^{1}H NMR (600 MHz, $CDCl_3$, 300 K): δ = 7.91-7.87 (m, 4H, Ar-H*ortho*, Ar-H*ortho'*), 7.10-7.07 (m, 2H, H(Ar-H*meta'*), 7.02-6.99 (m, 2H, (Ar-H*meta*), 5.44-5.40 (m, 1H, $CH_2C\underline{H}$), 4.77 (d, $^4J_{CH2C\equiv CH}$ = 2.4 Hz, 2H, $C\underline{H_2}C\equiv CH$), 4.46 (dd, $^3J_{C\underline{H}C\underline{H}H'}$ = 4.1 Hz, $^2J_{CHC\underline{H}H'}$ = 12.0 Hz, 1H, $CHC\underline{H}H$'), 4.32 (dd, $^3J_{C\underline{H}CH\underline{H}'}$ = 6.0 Hz, $^3J_{CHC\underline{H}H'}$ = 12.0 Hz 1H, $CHCH\underline{H}$'), 4.19 (d, $^3J_{OCH2CH}$ = 5.3 Hz, 2H, Ar-$COC\underline{H_2}CH$), 2.56 (t, $^4J_{CH2C\equiv CH}$ = 2.4 Hz, 1H, C≡CH), 2.36-2.31 (m, 4H, $(C=O)CH_2$), 1.66-1.59 (m, 4H, $(C=O)CH_2C\underline{H_2}$), 1.33-1.23 (m, 32H, $(C=O)CH_2CH_2(C\underline{H_2})_{12}CH_3$), 0.87 (t, $^3J_{CH2CH3}$ = 7.0 Hz, 6H, CH_3) ppm;

^{13}C NMR (126 MHz, $CDCl_3$, 300 K): δ = 173.4, 173.1 (C=O), 160.4 (Ar-C*para*), 159.6 (Ar-C*para'*), 147.5 (Ar-C*ipso'*), 147.3 (Ar-C*ipso*), 124.5, 124.4 (Ar-C*ortho*, Ar-C*ortho'*), 115.2, 114.8 (Ar-C*meta*, Ar-C*meta'*), 78.1 ($\underline{C}\equiv CH$), 75.9 ($C\equiv\underline{C}H$), 69.4 (Ar-$COCH_2\underline{C}H$), 66.4 (Ar-$CO\underline{C}H_2CH$), 62.2 (Ar-$COCH_2CH\underline{C}H_2$), 56.0 ($\underline{C}H_2C\equiv CH$), 34.3, 34.1 ($(C=O)\underline{C}H_2$), 31.9 ($(C=O)CH_2\underline{C}H_2$), 29.6, 29.5, 29.4, 29.3, 29.1, 29.0 25.0, 22.7 ($(C=O)CH_2CH_2(\underline{C}H_2)_{12}CH_3$), 14.1 ($CH_3$) ppm;

IR (ATR): $\tilde{\nu}$ = 3306, 2918, 2849, 2317, 1734, 1597, 1503, 1246, 1171, 1149, 1017, 841, 722 cm^{-1};

EI-MS: *m/z* = 690.46079, $[M]^+$; (calc. 690.46079 for $C_{42}H_{62}N_2O_6$).

(*E*)-[*p*-((1,2-Dihexadecanoyloxycarbonyl)propyloxy)-*p*'-(propargyloxy)] azobenzene (17)

According to the General Procedure A compound **15** (4.86 g, 14.9 mmol) and hexadecanoic acid (15.6 g, 60.8 mmol) were reacted to yield **17** as an orange solid.

Yield: 9.61 g (12.0 mmol, 80 %);

TLC: R_f = 0.50 (cyclohexane/ethyl acetate 6:1);

^{1}H NMR (600 MHz, $CDCl_3$, 300 K): δ = 7.90-7.86 (m, 4H, Ar-H_{ortho}, Ar-$H_{ortho'}$), 7.09-7.07 (m, 2H, H(Ar-$H_{meta'}$), 7.02-6.99 (m, 2H, (Ar-H_{meta}), 5.43-5.40 (m, 1H, CH_2CH), 4.77 (d, $^4J_{CH2C\equiv CH}$ = 2.4 Hz, 2H, $CH_2C\equiv CH$), 4.46 (dd, $^3J_{CHCHH'}$ = 4.2 Hz, $^2J_{CHCHH'}$ = 12.0 Hz, 1H, CHCHH'), 4.32 (dd, $^3J_{CHCHH'}$ = 6.0 Hz, $^3J_{CHCHH'}$ = 12.0 Hz 1H, CHCHH'), 4.19 (d, $^3J_{OCH2CH}$ = 5.1 Hz, 2H, Ar-$COCH_2CH$), 2.56 (t, $^4J_{CH2C\equiv CH}$ = 2.4 Hz, 1H, C≡CH), 2.36-2.31 (m, 4H, $(C=O)CH_2$), 1.66-1.59 (m, 4H, $(C=O)CH_2CH_2$), 1.34-1.21 (m, 48H, $(C=O)CH_2CH_2(CH_2)_{12}CH_3$), 0.88 (t, $^3J_{CH2CH3}$ = 7.0 Hz, 6H, CH_3) ppm;

^{13}C NMR (126 MHz, $CDCl_3$, 300 K): δ = 173.5, 173.24 (C=O), 160.5 (Ar-C_{para}), 159.6 (Ar-$C_{para'}$), 147.7 (Ar-$C_{ipso'}$), 147.6 (Ar-C_{ipso}), 124.6, 124.5 (Ar-C_{ortho}, Ar-$C_{ortho'}$), 115.3 (Ar-$C_{meta'}$), 114.9 (Ar-C_{meta}), 77.4 ($C\equiv CH$), 77.0 ($C\equiv CH$), 69.5 (Ar-$COCH_2CH$), 66.5 (Ar-$COCH_2CH$), 62.4 (Ar-$COCH_2CHCH_2$), 56.2 ($CH_2C\equiv CH$), 34.4 ($(C=O)CH_2$), 34.3 ($(C=O)CH_2CH_2$), 32.1, 29.8, 29.6, 29.5, 29.4, 29.2, 25.1, 22.8 ($(C=O)CH_2CH_2(CH_2)_{12}CH_3$), 14.3 ($CH_3$) ppm;

IR (ATR): ṽ = 3311, 2918, 2850, 1736, 1596, 1470, 1201, 1244, 1222, 1172, 1149, 1030, 840 cm^{-1}.

General Procedure B for the Synthesis of Glycolipids (18-23, 29-34): To a solution of the glucoside (1 eq), alkyne derivative (1 eq) and copper(I)bromide (0.21 eq) in a 1:1 mixture of dry DCM and dry DMF (50 mL) pentamethyldiethylenetriamine (PMDTA) (0.20 eq) was added. The reaction mixture was then stirred for 16 h at room temperature. Then the solvent was removed, the residue resolved in a 1:1 mixture of DCM and ethyl acetate (250 mL) and washed with water (200 mL). Afterwards the aqueous phase was extracted with a 1:1 mixture of DCM and ethyl acetate (2 x 200 mL) and again with ethyl acetate (100 mL). It was dried over $MgSO_4$, filtered and the filtrate was concentrated under reduced pressure. The raw product was purified by column chromatography (ethyl acetate → ethyl acetate/ methanol 6:1).

(*E*)-[*p*-[(1,2-Didodecanoyloxycarbonyl)propyloxy]-*p*'-(2-{2-[2-(1-ethoxy-4-methoxy-1,2,3-triazolyl)]ethoxythyl)]azobenzene (18)

According to the General Procedure B compound **16** (60.9 mg, 347 μmol) and compound **3** (240 mg, 347 μmol) were reacted to yield **18** as a colourless solid.

Yield: 209 mg (241 μmol, 87 %);

TLC: R_f = 0.23 (ethyl acetate);

^{1}H NMR (500 MHz, $CDCl_3$, 300 K): δ = 7.90-7.85 (m, 5H, Ar-H*ortho*, Ar-H*ortho'*, $H_{triazole}$), 7.12-7.08 (m, 2H, Ar-H), 7.01-6.98 (m, 2H, Ar-H) 5.44-5.40 (m, 1H, $CH_2C\underline{H}$), 5.33-5.27 (s, 2H, $C_{triazole}CH_2$), 4.59-4.54 (t, 2H, $^3J_{CH2CH2}$ = 5.0 Hz, CH_2N), 4.47-4.43 (dd, 1H, $^2J_{CHCHH'}$ = 12.0 Hz, $^3J_{CHCHH'}$ = 4.1 Hz, CHC$\underline{H}$H'), 4.33-4.29 (dd, 1H, $^2J_{CHCHH'}$ = 12.0 Hz, $^3J_{CHCHH'}$ = 6.0 Hz, CHC$\underline{H}$H'), 4.19 (d, 2H, $^3J_{CH2CH}$ = 5.2 Hz, Ar-COC$\underline{H}_2$CH), 3.90 (t, 2H, $^3J_{CH2CH2}$ = 5.0 Hz, C$\underline{H}_2CH_2N$), 3.71-3.69 (m, 2H, CH_2), 3.60-3.57 (m, 4H, CH_2), 3.56-3.53 (m, 2H, CH_2), 2.37-2.30 (m, 4H, (C=O)CH_2), 1.66-1.58 (m, 4H, (C=O)$CH_2C\underline{H}_2$), 1.33-1.20 (m, 32H, (C=O)$CH_2CH_2(C\underline{H}_2)_{12}CH_3$), 0.87 (t, 6H, $^3J_{CH2CH3}$ = 6.9 Hz, CH_3) ppm;

^{13}C NMR (126 MHz, $CDCl_3$, 300 K): δ = 173.5, 173.2 (C=O), 160.4 (Ar-C*para*, Ar-C*para'*), 147.6, 147.5 (Ar-C*ipso'*, Ar-C*ipso*, $C_{triazole}$), 124.6 (Ar-C*ortho*, Ar-C*ortho'*, $C_{triazole}H$), 115.2, 114.9 (Ar-C*meta'*, Ar-C*meta*), 72.6 (CH_2), 70.7, 70.4 (CH_2), 69.5 (CH_2, propargyloxy-COC$H_2\underline{C}$H), 66.5 (propargyloxy-CO$\underline{C}H_2$CH), 62.4 (propargyloxy-COCH_2CH$\underline{C}H_2$, $C_{triazole}\underline{C}H_2$), 61.9, 50.6 ($CH_2$), 34.4, ((C=O)$\underline{C}H_2$), 34.3, 32.1, 29.8, 29.6, 29.5, 29.4, 29.3, 29.2 (((C=O)$CH_2CH_2(\underline{C}H_2)_{12}CH_3$), 25.1 (((C=O)$CH_2\underline{C}H_2$)), 22.8 ($\underline{C}H_2CH_3$), 14.3 ($CH_3$) ppm;

IR (ATR): ṽ = 2919, 2850, 2357, 1736, 1598, 1499, 1238, 1149, 842, 750 cm^{-1};

EI-MS: *m/z* = 865.56, $[M]^+$; (calc. 865.556 for $C_{48}H_{75}N_5O_9$).

(*E*)-[*p*-[(1,2-Dihexadecanoyloxycarbonyl)propyloxy]-*p*'-[(2-{2-[2-(1-ethoxy-4-methoxy-1,2,3-triazolyl)]ethoxy}ethyl)]azobenzene (19)

According to the General Procedure B compound **17** (917 mg, 1.14 mmol) and compound **3** (200 mg, 1.14 mmol) were reacted to yield **19** as a colourless solid.

Yield: 945 mg (966 µmol, 85 %);

TLC: R_f = 0.36 (ethyl acetate);

^{1}H NMR (600 MHz, $CDCl_3$, 300 K): δ = 7.88-7.85 (m, 4H, Ar-H*ortho*, Ar-H*ortho'*), 7.85 (s, 1H, $H_{triazole}$), 7.11-7.08 (m, 2H, Ar-H), 7.01-6.98 (m, 2H, Ar-H) 5.43-5.40 (m, 1H, $CH_2C\underline{H}$), 5.30 (s, 2H, $C_{triazole}CH_2$), 4.57-4.55 (m, 2H, $^3J_{CH2CH2}$ = 5.1 Hz, CH_2N), 4.45 (dd, 1H, $^2J_{CHCHH'}$ = 11.9 Hz, $^3J_{CHCHH'}$ = 4.1 Hz, CHC$\underline{H}$H'), 4.31 (dd, 1H, $^2J_{CHCHH'}$ = 12.0 Hz,

$^{3}J_{CHCHH'}$ = 6.0 Hz, CHC<u>H</u>H'), 4.19 (d, 2H, $^{3}J_{CH2CH}$ = 5.2 Hz, Ar-COC<u>H</u>$_2$CH), 3.90 (t, 2H, $^{3}J_{CH2CH2}$ = 5.0 Hz, C<u>H</u>$_2$CH$_2$N), 3.71-3.69 (m, 2H, CH$_2$), 3.59 (s, 4H, CH$_2$), 3.55-3.52 (m, 2H, CH$_2$), 2.36-2.31 (m, 4H, (C=O)CH$_2$), 1.66-1.58 (m, 4H, (C=O)CH$_2$C<u>H</u>$_2$), 1.33-1.22 (m, 48H, (C=O)CH$_2$CH$_2$(C<u>H</u>$_2$)$_{12}$CH$_3$), 0.87 (t, 6H, $^{3}J_{CH2CH3}$ = 7.0 Hz, CH$_3$) ppm;

^{13}C NMR (151 MHz, CDCl$_3$, 300 K): δ = 173.5, 173.2 (C=O), 160.4 (Ar-C$_{para}$, Ar-C$_{para'}$), 147.6, 147.5 (Ar-C$_{ipso'}$, Ar-C$_{ipso}$), 143.8 (C$_{triazole}$), 124.5 (Ar-C$_{ortho}$, Ar-C$_{ortho'}$), 124.3 (C$_{triazole}$H), 115.2, 114.9 (Ar-C$_{meta'}$, Ar-C$_{meta}$), 72.5 (CH$_2$), 70.7, 70.4 (CH$_2$), 69.5 (CH$_2$, propargyloxy-COCH$_2$<u>C</u>H), 66.5 (propargyloxy-CO<u>C</u>H$_2$CH), 62.4 (propargyl-COCH$_2$CH<u>C</u>H$_2$, C$_{triazole}$<u>C</u>H$_2$), 61.8, 50.5 (CH$_2$), 34.4, ((C=O)<u>C</u>H$_2$), 34.3, 32.1, 29.8, 29.6, 29.5, 29.4, 29.3, 29.2 ((C=O)CH$_2$CH$_2$(<u>C</u>H$_2$)$_{12}$CH$_3$), 25.1 ((C=O)CH$_2$<u>C</u>H$_2$), 22.8 (<u>C</u>H$_2$CH$_3$), 14.3 (CH$_3$) ppm;

IR (ATR): ṽ = 2917, 2849, 2365, 1735, 1598, 1498, 1469, 1243, 1148, 1041, 841, 721 cm^{-1};

EI-MS: *m/z* = 977.68, [M]$^{+}$; (calc. 977.682 for C$_{59}$H$_{91}$N$_5$O$_9$).

(*E*)-[*p*-[(1,2-Didodecanoyloxycarbonyl)propyloxy]-*p*'-[(2-{2-[2-(1-ethoxy-4-methoxy-1,2,3-triazolyl)]ethoxy}ethyl) β-D-glucopyranosyloxy]]azobenzene (20)

According to the General Procedure B compound **16** (819 mg, 1.19 mmol) and glucoside **10** (400 mg, 1.19 mmol) were reacted to yield **20** as an orange solid.

Yield: 1.02 g (989 μmol, 83 %);

TLC: R_f = 0.18 (ethyl acetate/methanol 6:1);

^{1}H NMR (500 MHz, CDCl$_3$, 300 K): δ = 8.10-7.78 (m, 5H, Ar-H$_{ortho}$, Ar-H$_{ortho'}$, H$_{triazole}$), 7.15-6.90 (m, 4H, (Ar-H$_{meta'}$,Ar-H$_{meta}$), 5.44-5.37 (m, 1H, CH$_2$C<u>H</u>), 5.35-5.17 (s, 2H, C$_{triazole}$CH$_2$), 4.65-4.54 (t, $^{3}J_{CH2CH2}$ = 4.6 Hz, 2H, CH$_2$N), 4.47-4.43 (dd, $^{2}J_{CHCHH'}$ = 12.0 Hz, $^{3}J_{CHCHH'}$ = 4.0 Hz, 1H, CHC<u>H</u>H'), 4.35-4.32 (d, $^{3}J_{1,2}$ = 8.4 Hz, 1H, H-1), 4.32-4.27 (dd, $^{2}J_{CHCHH'}$ = 12.0 Hz, $^{3}J_{CHCHH'}$ = 6.1 Hz, 1H, CHCH<u>H</u>'), 4.20-4.18 (d, $^{3}J_{OCH2CH}$ = 5.1 Hz, 2H, Ar-COC<u>H</u>$_2$CH), 4.00-3.96 (dt, $^{2}J_{CHH'}$ = 11.3 Hz, $^{3}J_{CHH',CH2}$ = 4.1 Hz, 1H, C$_{glc}$OC<u>H</u>H'), 3.93-3.88 (m, 3H, C<u>H</u>$_2$CH$_2$N, H-6), 3.82-3.78 (dd, $^{3}J_{5,6'}$ = 5.1 Hz, $^{3}J_{6,6'}$ = 11.6 Hz, 1H, H-6'), 3.71-3.67 (m, 1H, C$_{glc}$OCH<u>H</u>'), 3.61-3.52 (m, 8H, H-3, H-4, 3 x CH$_2$), 3.39-3.35 (m, 2H, H-2, H-5), 2.36-2.29 (m, 4H, (C=O)CH$_2$),

1.65-1.58 (m, 4H, (C=O)$CH_2C\underline{H}_2$), 1.34-1.19 (m, 32H, (C=O)$CH_2CH_2(C\underline{H}_2)_{12}CH_3$), 0.89-0.84 (m, 6H, CH_3) ppm;

^{13}C NMR (126 MHz, $CDCl_3$, 300 K): δ = 173.5, 173.2 (C=O), 160.5, 160.4 (Ar-C_{para}, Ar-$C_{para'}$), 147.6, 147.5 (Ar-$C_{ipso'}$, Ar-C_{ipso}), 124.6 (Ar-C_{ortho}, Ar-$C_{ortho'}$), 115.3, 115.2 (Ar-$C_{meta'}$, Ar-C_{meta}), 103.2 (C-1), 75.9 (C-4), 73.7 (C-5), 72.5 (C-2), 70.7 (CH_2), 70.5 (C-3), 70.4 (Ar-$COCH_2\underline{C}H$), 69.5, 68.9 (CH_2), 66.5 (Ar-$CO\underline{C}H_2CH$), 62.4 (Ar-$COCH_2CH\underline{C}H_2$), 62.4 ($C_{triazole}\underline{C}H_2$), 61.9, 50.6 ($CH_2$), 34.4, ((C=O)$\underline{C}H_2$), 34.3, 32.0, 29.8, 29.6, 29.5, 29.3, 29.2 (((C=O)$CH_2CH_2(\underline{C}H_2)_{12}CH_3$), 25.1 (((C=O)$CH_2\underline{C}H_2$)), 22.8 ($\underline{C}H_2CH_3$), 14.3 ($CH_3$) ppm;

IR (ATR): $\tilde{\nu}$ = 3365, 2919, 2851, 1737, 1598, 1581, 1466, 1238, 1149, 1100, 1075, 1036, 841 cm^{-1};

ESI-MS: *m/z* = 1028.61658, $[M+H]^+$; (calc. 1028.61713 for $C_{54}H_{85}N_5O_{14}$+H).

(*E*)-[*p*-[(1,2-Dihexadecanoyloxycarbonyl)propyloxy]-*p*'-[(2-{2-[2-(1-ethoxy-4-methoxy-1,2,3-triazolyl)]ethoxy}ethyl) β-D-glucopyranosyloxy]]azobenzene (21)

According to the General Procedure B compound **17** (2.50 g, 3.11 mmol) and glucoside **10** (1.05 g, 3.11 mmol) were reacted to yield **21** as an orange solid.

Yield: 2.60 g (2.28 mmol, 73 %);

TLC: R_f = 0.18 (ethyl acetate/methanol 6:1);

^{1}H NMR (500 MHz, $CDCl_3$, 300 K): δ = 7.91-7.82 (m, 5H, Ar-H_{ortho}, Ar-$H_{ortho'}$, $H_{triazole}$), 7.11-7.05 (m, 2H, Ar-$H_{meta'}$), 6.99-6.96 (m, 2H, Ar-H_{meta}), 5.43-5.39 (m, 1H, $CH_2C\underline{H}$), 5.28-5.20 (s, 2H, $C_{triazole}CH_2$), 4.59-4.56 (t, $^3J_{CH2CH2}$ = 5.0 Hz, 2H, CH_2N), 4.47-4.44 (dd, $^3J_{C\underline{H}C\underline{H}H'}$ = 3.9 Hz, $^2J_{CHC\underline{H}H'}$ = 12.0 Hz, 1H, CHC$\underline{H}$H'), 4.36-4.33 (d, $^3J_{1,2}$ = 7.8 Hz, 1H, H-1), 4.33-4.29 (dd, $^3J_{C\underline{H}CHH'}$ = 6.1 Hz, $^3J_{CHC\underline{H}H'}$ = 12.0 Hz 1H, CHCH$\underline{H}$'), 4.17 (d, $^3J_{OCH2CH}$ = 5.1 Hz, 2H, Ar-COC$\underline{H}_2$CH), 4.06-3.95 (dt, $^2J_{C\underline{H}H'}$ = 11.5 Hz, $^3J_{CHH',CH2}$ = 4.1 Hz, 1H, $C_{glc}OC\underline{H}H'$), 3.92-3.90 (t, $^3J_{CH2CH2}$ = 4.9 Hz, 2H, C$\underline{H}_2CH_2N$), 3.90-3.88 (dd, $^3J_{5,6}$ = 3.2 Hz, $^3J_{6,6'}$ = 11.6 Hz, 1H, H-6), 3.81-3.77 (dd, $^3J_{5,6'}$ = 5.1 Hz, $^3J_{6,6'}$ = 11.6 Hz, 1H, H-6'), 3.72-3.67 (m, 1H, $C_{glc}OCH\underline{H}'$), 3.62-3.52 (m, 8H, H-3, H-4, 3 x CH_2), 3.39-3.34 (m, 2H, H-2, H-5), 2.36-2.30 (m, 4H, (C=O)CH_2), 1.65-1.57 (m, 4H, (C=O)$CH_2C\underline{H}_2$), 1.32-1.21 (m, 48H, (C=O)$CH_2CH_2(C\underline{H}_2)_{12}CH_3$), 0.87 (t, $^3J_{CH2CH3}$ = 6.9 Hz, 6H, CH_3) ppm;

^{13}C NMR (126 MHz, $CDCl_3$, 300 K): δ = 173.5, 173.2 (C=O), 160.5 (Ar-C_{para}, Ar-$C_{para'}$), 147.5, 147.4 (Ar-$C_{ipso'}$, Ar-C_{ipso}), 124.6 (Ar-C_{ortho}, Ar-$C_{ortho'}$), 115.2 (Ar-$C_{meta'}$), 114.9 (Ar-C_{meta}), 103.2 (C-1), 76.1 (C-4), 75.2 (C-5), 73.3 (C-2), 70.4 (C-3), 70.3 (CH_2), 69.2 ($\underline{C}H_2CH_2N$), 69.1 (Ar-$COCH_2\underline{C}H$), 68.9 ($C_{glc}O\underline{C}HH'CH_2$), 66.5 (Ar-$CO\underline{C}H_2CH$), 62.4 (Ar-$COCH_2CH\underline{C}H_2$), 62.2 ($C_{triazole}\underline{C}H_2$), 62.1 (C-6), 50.6 ($CH_2N$), 34.4 ((C=O)$\underline{C}H_2$), 34.2, 32.1, 29.8, 29.6, 29.5, 29.4, 29.3 29.2, 25.1, 25.0 ((C=O)$CH_2\underline{C}H_2$), 22.8 ($\underline{C}H_2CH_3$), 14.3 (CH_3) ppm;

IR (ATR): $\tilde{\nu}$ = 3383, 2917, 2849, 1736, 1243, 1104, 1077, 1036, 841, 721 cm^{-1};

ESI-MS: *m/z* = 1140.73931, $[M+H]^+$; (calc. 1140.74233 for $C_{62}H_{101}N_5O_{14}$+H).

(*E*)-[*p*-[(1,2-Didodecanoyloxycarbonyl)propyloxy]-*p*'-[(2-{2-[2-(1-ethoxy-4-methoxy-1,2,3-triazolyl)]ethoxy}ethyl) β-D-galactopyranosyl-(1→4)β-D-glucopyranosyloxy]]azobenzene (22)

According to the General Procedure B compound **16** (300 mg, 601 µmol) and lactoside **11** (300 mg, 601 µmol) were reacted to yield **22** as an orange solid.

Yield: 630 mg (529 µmol, 71 %);

TLC: R_f = 0.18 (ethyl acetate/methanol 6:1);

^{1}H NMR (500 MHz, DMSO-*d6*, 600 K): δ = 8.25 (s, 1H, $H_{triazole}$), 7.85-7.82 (m, 4H, Ar-H_{ortho}, Ar-$H_{ortho'}$), 7.24-7.21 (m, 2H, Ar-H), 7.13-7.10 (m, 2H, Ar-H), 5.39-5.35 (m, 1H, $CH_2C\underline{H}$), 5.25 (s, 2H, $C_{triazole}CH_2$), 5.12 (d, $^3J_{HCOH}$ = 5.1 Hz, 1H, C2-OH), 5.07 (d, $^3J_{HCOH}$ = 4.4 Hz, 1H, C2'-OH), 4.79 (d, $^3J_{HCOH}$ = 5.2 Hz, 1H, $OH_{Lactoside}$), 4.68-4.65 (m, 2H, $OH_{Lactoside}$) 4.58-4.50 (m, 4H, C6-OH, CH_2N), 4.39 (dd, $^2J_{CHCHH'}$ = 12.0 Hz, $^3J_{CHCHH'}$ = 3.5 Hz, 1H, CHC$\underline{H}$H'), 4.31-4.24 (m, 3H, Ar-CO$C\underline{H}_2$CH, CHC$\underline{H}$H'), 4.22-4.20 (d, $^3J_{1,2}$ = 7.8 Hz, 1H, H-1), 4.20-4.18 (d, $^3J_{1,2}$ = 7.4 Hz, 1H, H-1'), 3.86-3.82 (m, 3H, H-$6_{Lactoside}$, CH_2CH_2N), 3.74 (dd, $^3J_{CHCH}$ = 5.8 Hz, $^2J_{CHCH}$ = 11.2 Hz, 1H, $C_{Glc}OC\underline{H}H'$), 3.63-3.43 (m, 14H, 3 x CH_2, 3 x H-$6_{Lactoside}$, $C_{Glc}OCH\underline{H}'$, 4 x $H_{Lactoside}$), 3.37-3.26 (m, 5H, H-2', H-3, 3 x $H_{Lactoside}$), 3.04-3.00 (m, 1H, H-2), 2.32-2.27 (m, 4H, (C=O)CH_2), 1.53-1.47 (m, 4H, (C=O)$CH_2C\underline{H}_2$), 1.26-1.17 (m, 32H, (C=O)$CH_2CH_2(C\underline{H}_2)_{12}CH_3$), 0.85-0.81 (m, 6H, CH_3) ppm;

^{13}C NMR (151 MHz, DMSO-*d6*, 300 K): δ = 172.6, 172.3 (C=O), 160.3, 160.2 (Ar-C), 146.5, 146.3 (Ar-C), 142.1 ($C_{triazole}$), 125.2 (Ar-C), 124.1 ($C_{triazole}H$), 115.3, 115.1 (Ar-C),

103.9 (C-1'), 102.7 (C-1), 80.8, 75.5, 75.0, 74.9, 73.3, 73.1 ($C_{Lactoside}$), 70.6 (Ar-$COCH_2\underline{C}H$), 69.5 (CH_2), 69.3 (CH_2CH_2N), 68.7 (Ar-$CO\underline{C}H_2CH$), 68.1 ($C_{Glc}O\underline{C}HH'$), 68.0 (CH_2), 61.9 (Ar-$COCH_2CH\underline{C}H_2$), 61.5 ($C_{triazole}\underline{C}H_2$), 60.5, 60.4 (C-6, C-6'), 49.5 (CH_2N), 33.6, 33.4, 31.3, 29.0, 28.9, 28.7, 28.4, 28.3, 24.5, 22.1 (CH_2), 13.9 (CH_3) ppm;

IR (ATR): $\tilde{\nu}$ = 3347, 2920, 2850, 2364, 1735, 1599, 1583, 1469, 1244, 1168, 1150, 1107, 1071, 1037, 842, 722 cm^{-1};

ESI-MS: *m/z* = 1190.66940, $[M+H]^+$; (calc. 1190.66995 for $C_{60}H_{95}N_5O_{19}$+H).

(*E*)-[*p*-[(1,2-Dihexadecanoyloxycarbonyl)propyloxy]-*p*'-[(2-{2-[2-(1-ethoxy-4-methoxy-1,2,3-triazolyl)]ethoxy}ethyl) β-D-galactopyranosyl-(1→4)β-D-glucopyranosyloxy]]azobenzene (23)

According to the General Procedure B compound **17** (402 mg, 501 µmol) and lactoside **11** (250 mg, 501 µmol) were reacted to yield **23** as an orange solid.

Yield: 458 mg (352 µmol, 70 %);

TLC: R_f = 0.18 (ethyl acetate/methanol 6:1);

^{1}H NMR (600 MHz, DMSO-*d6*, 600 K): δ = 8.25 (s, 1H, $H_{triazole}$), 7.86-7.80 (m, 4H, Ar-H_{ortho}, Ar-$H_{ortho'}$), 7.25-7.20 (m, 2H, Ar-H), 7.14-7.09 (m, 2H, Ar-H), 5.39-5.35 (m, 1H, $CH_2C\underline{H}$), 5.25 (s, 2H, $C_{triazole}CH_2$),), 5.13-5.09 (d, $^3J_{HCOH}$ = 4.9 Hz, 1H, C2-OH), 5.09-5.06 (d, $^3J_{HCOH}$ = 4.1 Hz, 1H, C2'-OH) 4.79 (d, $^3J_{CHCH}$ = 4.6 Hz, 1H, $OH_{Lactoside}$), 4.68-4.65 (m, 2H, $OH_{Lactoside}$), 4.59-4.50 ((m, 4H, C6-OH, CH_2N), 4.42-4.38 (m, 1H, CHC$\underline{H}$H'), 4.31-4.23 (m, 3H, Ar-CO$C\underline{H}_2$CH, CHC$\underline{H}$H'), 4.22-4.20 (m, 1H H-1), 4.20-4.17 (m, 1H, H-1'), 3.86-3.82 (m, 3H, H-$6_{Lactoside}$, CH_2CH_2N), 3.77-3.70 (dd, $^3J_{CHCH}$ = 5.4 Hz, $^3J_{CHCH}$ = 10.9 Hz, 1H, $C_{Glc}OC\underline{H}$H'), 3.69-3.41 (m, 14H, 3 x CH_2, 3 x H-$6_{Lactoside}$, $C_{Glc}OCH\underline{H}$', 4 x $H_{Lactoside}$), 3.41-3.25 (m, 5H, H-2', H-3, 3 x $H_{Lactoside}$), 3.04-2.99 (m, 1H, H-2), 2.32-2.25 (m, 4H, (C=O)CH_2), 1.53-1.47 (m, 4H, (C=O)$CH_2C\underline{H}_2$), 1.27-1.16 (m, 48H, (C=O)$CH_2CH_2(C\underline{H}_2)_{12}CH_3$), 0.84 (t, $^3J_{CH2CH3}$ = 6.6 Hz, 6H, CH_3) ppm;

^{13}C NMR (151 MHz, DMSO-*d6*, 300 K): δ = 172.6, 172.3 (C=O), 160.3, 160.2 (Ar-C), 146.5, 146.3 (Ar-C), 142.1 ($C_{triazole}$), 125.1 (Ar-C), 124.1 ($C_{triazole}H$), 115.3, 115.1 (Ar-C), 103.9 (C-1'), 102.7 (C-1), 80.8, 75.5, 75.0, 74.9, 73.3, 73.1 ($C_{Lactoside}$), 70.6

(Ar-COCH$_2$<u>C</u>H) 69.7 (CH$_2$), 69.3 (CH$_2$CH$_2$N), 68.7 (Ar-CO<u>C</u>H$_2$CH), 68.1 (C$_{Glc}$O<u>C</u>HH'), 68.0 (CH$_2$), 61.9 (Ar-COCH$_2$CH<u>C</u>H$_2$), 61.5 (C$_{triazole}$<u>C</u>H$_2$), 60.4, 60.3 (C-6, C-6'), 49.4 (CH$_2$N), 33.6, 33.4, 31.3, 29.0, 28.9, 28.7, 28.4, 28.3, 24.5, 24.4, 22.1 (CH$_2$), 13.9 (CH$_3$) ppm;

IR (ATR): $\tilde{\nu}$ = 3341, 2918, 2849, 2364, 1736, 1599, 1585, 1470, 1245, 1224, 1040, 841, 720 cm^{-1};

ESI-MS: *m/z* = 1302.79548, [M+H]$^+$; (calc. 1302.79515 for $C_{68}H_{111}N_5O_{19}$+H).

2,2-Dimethyl-4-[(2-propargyloxy)methyl]-1,3-dioxolane (25)[184]

Propargyl bromide (80 % wt. % solution in toluene, 13.9 mL, 129 mmol) was added to an ice-cold solution of D, L-isopropylideneglycerol (**24**) (6.00 mL, 43.0 mmol) in dry DMF (45 mL). Potassium hydroxide (9.65 g, 172 mmol) was added in portions. The reaction mixture was stirred for 16 h at 50 °C. Afterwards the solvent was removed under reduced pressure and the residue was resolved in ethyl acetate (300 mL). The organic phase was washed with water (2 × 200 mL). It was dried over $MgSO_4$, filtered and the filtrate was concentrated under reduced pressure. Purification of the crude product by column chromatography (cyclohexane / ethyl acetate) gave **25** as a brown oil.

Yield: 8.46 g (49.7 mmol, 69%);

TLC: R_f = 0.35 (cyclohexane / ethyl acetate, 6:1);

^{1}H-NMR (200 MHz, $CDCl_3$, 300 K): δ = 4.31-4.26 (m, 1H, CH), 4.20 (m, 2H, C<u>H$_2$</u>C≡CH), 4.08-4.04 (m, 1H, CH$_2$CHC<u>H</u>H'), 3.76-3.72 (m, 1H, CH$_2$CHCH<u>H</u>'), 3.61-3.55 (m, 2H, C<u>H$_2$</u>CHCHH'), 2.44 (t, $^2J_{CH2C≡CH}$ = 2.4 Hz, 1H, C≡CH), 1.42 (s, 3H, CH$_3$), 1.35 (s, 3H, CH$_3$) ppm;

^{13}C NMR (126 MHz, $CDCl_3$, 300 K): δ = 109.5 (<u>C</u>(CH$_3$)$_2$), 79.3 (CH$_2$<u>C</u>≡CH), 74.7 (CH$_2$C≡<u>C</u>H), 74.5 (CH), 70.7 (<u>C</u>H$_2$CHCH$_2$), 66.7 (CH$_2$CH<u>C</u>H$_2$), 58.7 (<u>C</u>H$_2$C≡CH), 26.7 (CH$_3$), 25.3 (CH$_3$) ppm.

3-Propargyloxy-1,2-propanediol (26)

Compound **25** (5.00 g, 29.4 mmol) was dissolved in THF (50 mL) and 1 M HCl (50 mL) was added and the reaction mixture was stirred for 2 h. After neutralisation with 1 M

sodium hydroxide solution, the mixture was extracted with ethyl acetate (3 x 100 mL). The organic phase was dried over $MgSO_4$, filtered and the filtrate was concentrated under reduced pressure. Purification of the crude product by column chromatography (cyclohexane / ethyl acetate 1:1 → 4:1) gave **26** as a colourless oil.

Yield: 2.88 g (22.1 mmol, 75 %);

TLC: R_f = 0.11 (cyclohexane / ethyl acetate, 1:1);

^{1}H-NMR (200 MHz, $CDCl_3$, 300 K): δ = 4.19 (d, $^2J_{C\underline{H}2C\equiv C\underline{H}}$ = 2.4 Hz, 2H, $C\underline{H}_2C\equiv CH$), 3.96-3.86 (m, 1H, CH), 3.76-3.54 (m, 4H, $C\underline{H}_2CHC\underline{H}_2$), 2.46 (t, $^2J_{C\underline{H}2C\equiv C\underline{H}}$ = 2.4 Hz, 1H, C≡CH) ppm;

^{13}C NMR (126 MHz, MeOD, 300 K): δ = 80.6 ($CH_2\underline{C}\equiv CH$), 75.97 ($CH_2C\equiv\underline{C}H$), 72.3 ($\underline{C}H_2CHCH_2$), 72.1 (CH), 66.4 ($CH_2CH\underline{C}H_2$), 59.3 ($\underline{C}H_2C\equiv CH$) ppm.

(2,3-Didodecanoyl)-(1-Propargyloxy)propionate (27)

According to the General Procedure A compound **26** (835 mg, 6.42 mmol) and dodecanoic acid (5.14 g, 25.7 mmol) were reacted to yield **27** as a colourless solid.

Yield: (1.52 g, 3.08 mmol, 48 %);

TLC: R_f = 0.67 (cyclohexane/ethyl acetate 6:1);

^{1}H NMR (500 MHz, $CDCl_3$, 300 K): δ = 5.24-5.20 (m, 1H, $CH_2C\underline{H}$), 4.33 (dd, $^3J_{C\underline{H}C\underline{H}H'}$ = 3.9 Hz, $^2J_{CHC\underline{H}\underline{H}'}$ = 12.0 Hz, 1H, CHC$\underline{H}$H'), 4.19-4.15 (m, 3H, $C\underline{H}_2C\equiv CH$, CHCH$\underline{H}$'), 3.68-3.66 (m, 2H, $OC\underline{H}_2CH$), 2.43 (t, $^4J_{CH2C\equiv CH}$ = 2.4 Hz, 1H, C≡CH), 2.43-2.40 (m, 4H, $(C=O)CH_2$), 1.65-1.57 (m, 4H, $(C=O)CH_2C\underline{H}_2$), 1.32-1.23 (m, 32H, $(C=O)CH_2CH_2(C\underline{H}_2)_{12}CH_3$), 0.88 (t, $^3J_{CH2CH3}$ = 7.0 Hz, 6H, CH_3) ppm;

^{13}C NMR (126 MHz, $CDCl_3$, 300 K): δ = 173.5, 173.2 (C=O), 79.2 ($\underline{C}\equiv CH$), 75.1 ($C\equiv\underline{C}H$), 70.0 ($Ar\text{-}COCH_2\underline{C}H$), 68.1 ($Ar\text{-}CO\underline{C}H_2CH$), 62.7 ($Ar\text{-}COCH_2CH\underline{C}H_2$), 58.7 ($\underline{C}H_2C\equiv CH$), 34.5, 34.3 ($(C=O)\underline{C}H_2$), 32.1, 29.8, 29.6, 29.5, 29.4, 29.3, 29.2 ($(C=O)CH_2CH_2(\underline{C}H_2)12CH3$), 25.0 ($(C=O)CH_2\underline{C}H_2$), 22.8 ($CH_2$) 14.1 ($CH_3$) ppm;

IR (ATR): $\tilde{\nu}$ = 3269, 2919, 2851, 2326, 1737, 1470, 1353, 1171, 1111, 1091, 1043, 718 cm^{-1};

EI-MS: *m/z* = 494.39712, $[M]^+$; (calc. 494.3971 for $C_{30}H_{54}O_5$).

(2,3-Dihexadecanoyl)-(1-Propargyloxy)propionate (28)

According to the General Procedure A compound **26** (835 mg, 6.42 mmol) and hexadecanoic acid (6.49 g, 25.3 mmol) were reacted to yield **27** as a colourless solid.

Yield: 2.00 g (3.30 mmol, 51 %);

TLC: R_f = 0.73 (cyclohexane/ethyl acetate 6:1);

Melting point: 63 °C;

^{1}H NMR (500 MHz, $CDCl_3$, 300 K): δ = 5.24-5.20 (m, 1H, $CH_2C\underline{H}$), 4.33 (dd, $^3J_{C\underline{H}C\underline{H}H'}$ = 3.9 Hz, $^2J_{CHC\underline{H}\underline{H}'}$ = 11.9 Hz, 1H, CHC$\underline{H}$H'), 4.19-4.15 (m, 3H, C$\underline{H}_2$C≡CH, CHCH$\underline{H}$'), 3.68-3.66 (m, 2H, OC$\underline{H}_2$CH), 2.43 (t, $^4J_{CH2C\equiv CH}$ = 2.4 Hz, 1H, C≡CH), 2.34-2.29 (m, 4H, (C=O)CH_2), 1.65-1.58 (m, 4H, (C=O)$CH_2C\underline{H}_2$), 1.32-1.23 (m, 48H, (C=O)$CH_2CH_2(C\underline{H}_2)_{12}CH_3$), 0.88 (t, $^3J_{CH2CH3}$ = 7.0 Hz, 6H, CH_3) ppm;

^{13}C NMR (126 MHz, $CDCl_3$, 300 K): δ = 179.5, 179.2 (C=O), 79.2 (C≡CH), 75.1 (C≡CH), 70.0 (Ar-$COCH_2\underline{C}H$), 68.1 (Ar-$CO\underline{C}H_2CH$), 62.7 (Ar-$COCH_2CH\underline{C}H_2$), 56.9 ($\underline{C}H_2C\equiv CH$), 34.5, 34.3 ((C=O)$\underline{C}H_2$), 32.1, 29.9, 29.8, 29.6, 29.5, 29.4, 29.3, 29.2 ((C=O)$CH_2CH_2(\underline{C}H_2)$12CH3), 25.1 ((C=O)$CH_2\underline{C}H_2$), 22.8 ($CH_2$) 14.3 ($CH_3$) ppm;

IR (ATR): $\tilde{\nu}$ = 3269, 2916, 2850, 2365, 1731, 1472, 1354, 1172, 1112, 1045, 719 cm^{-1};

EI-MS: *m/z* = 606.52232, $[M]^+$; (calc. 606.5223 for $C_{38}H_{70}O_6$).

1-{2-[2-(2-Hydroxyethoxy)ethoxy]ethyl]}-4-{[(1,2-Didodecanoyloxy-carbonyl) propyloxy]methoxy}-1,2,3-triazole (29)

According to the General Procedure B compound **27** (1.13 g, 2.28 mmol) and compound **3** (400 mg, 2.28 mmol) were reacted to yield **29** as a colourless solid.

Yield: 1.09 g (1.63 μmol, 72 %);

TLC: R_f = 0.26 (ethyl acetate/methanol 6:1);

^{1}H NMR (500 MHz, $CDCl_3$, 300 K): δ = 7.95 (s, 1H, $H_{triazole}$), 5.22 (s, 1H, $CH_2C\underline{H}$), 4.72-4.60 (s, 2H, $C_{triazole}CH_2$), 4.60-4.52 (s, 2H, CH_2N), 4.34-4.29 (m, 1H, CHC$\underline{H}$H'), 4.17-4.11 (dd, $^3J_{C\underline{H}C\underline{H}H'}$ = 5.7 Hz, $^2J_{CHC\underline{H}\underline{H}'}$ = 11.7 Hz, 1H, CHC$\underline{H}$H'), 3.92-3.88 (t, $^3J_{CH2CH2}$ = 4.5 Hz, 2H, $C\underline{H}_2CH_2N$), 3.75-3.71 (m, 2H, CH_2), 3.70-3.65 ($CH_2OC\underline{H}_2CH$), 3.64-3.60 (m, 2H, CH_2), 3.58-3.55 (m, 10H, CH_2), 2.33-2.26 (m, 4H, (C=O)CH_2),

1.63-1.55 (m, 4H, (C=O)$CH_2C\underline{H}_2$), 1.32-1.20 (m, 32H, (C=O)$CH_2CH_2(C\underline{H}_2)_{12}CH_3$), 0.87 (t, $^3J_{CH2CH3}$ = 7.0 Hz, 6H, CH_3);

^{13}C NMR (126 MHz, $CDCl_3$, 300 K): δ = 173.6, 173.3 (C=O), 72.6, 70.7, 70.4 (CH_2), 70.1 ($OCH_2\underline{C}H$), 69.5, ($\underline{C}H_2CH_2N$), 68.8 (CH_2), 65.0 ($C_{triazole}\underline{C}H_2O$), 62.8 ($OCH_2CH\underline{C}H_2$), 61.7 ($O\underline{C}H_2CH$), 50.5 ($CH_2N$), 34.4, 34.3 ((C=O)$\underline{C}H_2$), 32.0, 29.7, 29.6, 29.5, 29.4, 29.3 29.2 ((C=O)$CH_2CH_2(\underline{C}H_2)_{12}CH_3$), 25.1, 25.0 ((C=O)$CH_2\underline{C}H_2$), 22.8 ($\underline{C}H_2CH_3$), 14.2 ($CH_3$) ppm;

IR (ATR): $\tilde{\nu}$ = 3446, 2918, 2850, 2367, 1729, 1464, 1225, 1178, 1114, 1097, 860, 720 cm^{-1};

EI-MS: *m/z* = 668.43, $[M-H]^+$; (calc. 669.493 for $C_{36}H_{67}N_3O_8$).

1-{2-[2-(2-Hydroxyethoxy)ethoxy]ethyl]}-4-{[(1,2-Dihexadecanoyloxy-carbonyl) propyloxy]methoxy}-1,2,3-triazole (30)

According to the General Procedure B compound **28** (693 mg, 1.14 mmol) and compound **3** (200 mg, 1.14 mmol) were reacted to yield **30** as a colourless solid.

Yield: 548 mg (701 μmol, 61 %);

TLC: R_f = 0.24 (ethyl acetate/methanol 6:1);

^{1}H NMR (600 MHz, $CDCl_3$, 300 K): δ = 7.78 (s, 1H, $H_{triazole}$), 5.23-5.19 (m, 1H, $CH_2C\underline{H}$), 4.69-4.63 (s, 2H, $C_{triazole}CH_2$), 4.55 (t, $^3J_{CH2CH2}$ = 5.0 Hz, 2H, CH_2N), 4.31 (dd, $^3J_{C\underline{H}C\underline{H}H'}$ = 3.6 Hz, $^2J_{CHC\underline{H}H'}$ = 11.9 Hz 1H, CHC$\underline{H}$H'), 4.13 (dd, $^3J_{C\underline{H}C\underline{H}H'}$ = 6.5 Hz, $^2J_{CHC\underline{H}H'}$ = 11.9 Hz, 1H, CHC$\underline{H}$H'), 3.88 (t, $^3J_{CH2CH2}$ = 5.0 Hz, 2H, $C\underline{H}_2CH_2N$), 3.73 (t, $^3J_{CH2CH2}$ = 9.2 Hz, 2H, CH_2), 3.68-3.60 ($CH_2OC\underline{H}_2CH$, CH_2), 3.58-3.56 (m, 10H, CH_2), 2.32-2.26 (m, 4H, (C=O)CH_2), 1.62-1.56 (m, 4H, (C=O)$CH_2C\underline{H}_2$), 1.31-1.23 (m, 48H, (C=O)$CH_2CH_2(C\underline{H}_2)_{12}CH_3$), 0.87 (t, $^3J_{CH2CH3}$ = 7.0 Hz, 6H, CH_3);

^{13}C NMR (126 MHz, $CDCl_3$, 300 K): δ = 173.6, 173.3 (C=O), 144.7 ($C_{triazole}$), 124.1 ($C_{triazole}H$), 72.6, 70.7 (CH_2), 70.4 ($\underline{C}H_2CH_2N$), 70.1 ($OCH_2\underline{C}H$), 69.5, ($CH_2\underline{C}H_2N$), 68.8 (CH_2), 65.0 ($C_{triazole}\underline{C}H_2O$), 62.8 ($OCH_2CH\underline{C}H_2$), 61.9 ($O\underline{C}H_2CH$), 50.4 ($CH_2N$), 34.4, 34.3 ((C=O)$\underline{C}H_2$), 32.1, 29.8, 29.6, 29.5, 29.4, 29.3 29.2 ((C=O)$CH_2CH_2(\underline{C}H_2)_{12}CH_3$), 25.1, 25.0 ((C=O)$CH_2\underline{C}H_2$), 22.8 ($\underline{C}H_2CH_3$), 14.3 ($CH_3$) ppm;

IR (ATR): $\tilde{\nu}$ = 3446, 2917, 2849, 2367, 1730, 1463, 1388, 1247, 1196, 1178, 1115, 1099, 867, 719 cm^{-1};

EI-MS: *m/z* = 780.52, $[M-H]^+$; (calc. 781.618 for $C_{44}H_{83}N_3O_8$).

1-{2-[2-(2-(β-D-Glucopyranosyloxy)ethoxy)ethoxy]ethyl]}-4-{[(1,2-di-dodecanoyl-oxycarbonyl)propyloxy] methoxy}-1,2,3-triazole (31):

According to the General Procedure B compound **27** (589 mg, 1.19 mmol) and glucoside **10** (400 mg, 1.19 mmol) were reacted to yield **31** as a colourless solid.

Yield: 594 mg (713 µmol, 60 %);

TLC: R_f = 0.24 (ethyl acetate/methanol 6:1);

^{1}H NMR (500 MHz, $CDCl_3$, 300 K): δ = 7.86 (s, 1H, $H_{triazole}$), 5.22 (s, 1H, $CH_2C\underline{H}$), 4.66 (s, 2H, $C_{triazole}CH_2$), 4.57 (s, 2H, CH_2N), 4.35 (d, $^3J_{1,2}$ = 7.4 Hz, 1H, H-1), 4.31 (dd, $^3J_{C\underline{H}C\underline{H}H'}$ = 2.9 Hz, $^2J_{CHC\underline{H}\underline{H}'}$ = 11.9 Hz, 1H, CHC$\underline{H}$H'), 4.15-4.10 (m, 1H, CHCH$\underline{H}$'), 4.00-3.95 (m, 1H, H-6), 3.92-3.87 (m, 2H, CH_2), 3.88-3.80 (m, 2H, CH_2), 3.76-3.50 (m, 15H, H-4, H-5, H-6', 3 x CH_2, $C_{triazole}CH_2O$, 4 x OH), 3.39-3.32 (m, 2H, H-2, H-3), 2.33-2.25 (m, 4H, (C=O)CH_2), 1.63-1.55 (m, 4H, (C=O)$CH_2C\underline{H}_2$), 1.32-1.20 (m, 32H, (C=O)$CH_2CH_2(C\underline{H}_2)_{12}CH_3$), 0.87 (t, $^3J_{CH2CH3}$ = 7.0 Hz, 6H, CH_3);

^{13}C NMR (126 MHz, $CDCl_3$, 300 K): δ = 173.7, 173.4 (C=O), 103.3 (C-1), 76.6, 70.2 (C-4, C-5), 75.9, 73.6 (C-2, C-3), 70.5, 70.4 (CH_2), 70.1 ($OCH_2\underline{C}H$), 69.5, (CH_2), 68.9 (C-6), 68.8 ($O\underline{C}H_2CH$), 64.8 ($C_{triazole}\underline{C}H_2O$), 62.9 (($OCH_2CH\underline{C}H_2$), 62.1, 50.6 ($CH_2$), 34.5, 34.3 ((C=O)$\underline{C}H_2$), 32.0, 29.8, 29.6, 29.5, 29.4, 29.3 29.2 ((C=O)$CH_2CH_2(\underline{C}H_2)_{12}CH_3$), 25.1, 25.0 ((C=O)$CH_2\underline{C}H_2$), 22.8 ($\underline{C}H_2CH_3$), 14.2 ($CH_3$) ppm;

IR (ATR): $\tilde{\nu}$ = 3387, 2957, 2918, 2851, 2365, 1736, 1467, 1166, 1100, 1076, 1035, 721 cm^{-1};

ESI-MS: *m/z* = 832.55292, $[M+H]^+$; (calc. 832.55346 for $C_{42}H_{77}N_3O_{13}$+H).

1-{2-[2-(2-(β-D-Glucopyranosyloxy)ethoxy)ethoxy]ethyl]}-4-{[(1,2-Di-hexadeca-noyl-oxycarbonyl)propyloxy] methoxy}-1,2,3-triazole (32)

According to the General Procedure B compound **28** (722 mg, 1.19 mmol) and glucoside **10** (400 mg, 1.19 mmol) were reacted to yield **32** as a colourless solid.

Yield: 693 mg (734 µmol, 62 %);

TLC: R_f = 0.21 (ethyl acetate/methanol 6:1);

Melting point: 171 °C;

^{1}H NMR (500 MHz, $CDCl_3$, 300 K): δ = 7.86 (m, 1H, $H_{triazole}$), 5.24-5.20 (m, 1H, $CH_2C\underline{H}$), 4.71-4.66 (m, 2H, $C_{triazole}CH_2$), 4.59 (t, 2H, $^3J_{CH2CH2}$ = 4.86 Hz, CH_2N), 4.36 (d, $^3J_{1,2}$ = 7.7 Hz, 1H, H-1), 4.32 (dd, $^3J_{C\underline{H}C\underline{H}H'}$ = 3.2 Hz, $^2J_{CHC\underline{H}\underline{H}'}$ = 11.9 Hz, 1H, CHC$\underline{H}$H'), 4.13 (m, 1H, CHCH$\underline{H}$'), 4.00-3.97 (m, 1H, H-6), 3.92-3.89 (m, 2H, CH_2), 3.89-3.81 (m, 2H, CH_2), 3.75-3.59 (m, 13H, H-6', 3 x CH_2, $C_{triazole}CH_2O$, 4 x OH), 3.58-3.51 (m, 2H, H-4, H-5), 3.37-3.33 (m, 2H, H-2, H-3), 2.33-2.26 (m, 4H, $(C=O)CH_2$), 1.62-1.55 (m, 4H, $(C=O)CH_2C\underline{H}_2$), 1.32-1.22 (m, 48H, $(C=O)CH_2CH_2(C\underline{H}_2)_{12}CH_3$), 0.87 (t, $^3J_{CH2CH3}$ = 7.0 Hz, 6H, CH_3);

^{13}C NMR (126 MHz, $CDCl_3$, 300 K): δ = 173.8, 173.5 (C=O), 141.1 ($NCH\underline{C}_{triazole}$), 124.8 ($NC_{triazole}H$), 103.4 (C-1), 76.6, 70.1 (C-4, C-5), 75.9, 73.7 (C-2, C-3), 70.51, 70.4 (CH_2), 70.2 ($OCH_2\underline{C}H$), 69.5, (CH_2), 69.0 (C-6), 68.9 ($O\underline{C}H_2CH$), 64.6 ($C_{triazole}\underline{C}H_2O$), 62.9 (($OCH_2CH\underline{C}H_2$), 62.2, 50.7 ($CH_2$), 34.5, 34.3 (($C=O)\underline{C}H_2$), 32.1, 29.9, 29.7, 29.5, 29.3, (($C=O)CH_2CH_2(\underline{C}H_2)_{12}CH_3$), 25.1, 25.0 (($C=O)CH_2\underline{C}H_2$), 22.8 ($\underline{C}H_2CH_3$), 14.3 ($CH_3$) ppm;

IR (ATR): ṽ = 3370, 2956, 2917, 2850, 1736, 1467, 1079, 1039, 721 cm^{-1};

ESI-MS: *m/z* = 944.67812, $[M+H]^+$; (calc. 944.67867 for $C_{50}H_{93}N_3O_{13}$+H).

1-{2-[2-(2-(β-D-Galactopyranosyl-(1→4)β-D-glucopyranosyloxy)ethoxy)ethoxy] ethyl]}-4-{[(1,2-didodecanoyloxycarbonyl)propyloxy] methoxy}-1,2,3-triazole (33)

According to the General Procedure B compound **27** (297 mg, 601 µmol) and lactoside **11** (300 mg, 601 µmol) were reacted to yield **33** as a colourless solid.

Yield: 250 mg (252 µmol, 42 %);

TLC: R_f = 0.24 (ethyl acetate/methanol 6:1);

^{1}H NMR (600 MHz, DMSO-*d6*, 300 K): δ = 8.06 (s, 1H, $H_{triazole}$), 5.14-5.12 (m, 1H, $CH_2C\underline{H}$), 5.11-5.10 (d, $^3J_{HCOH}$ = 5.1 Hz, 1H, C2-OH), 5.10-5.08 (d, $^3J_{HCOH}$ = 4.2 Hz, 1H, C2'-OH), 4.80-4.77 (d, $^3J_{HCOH}$ = 4.4 Hz, 1H, $OH_{Lactoside}$), 4.67 (s, 1H, C3-OH), 4.66-4.64 (t, $^3J_{HCOH}$ = 5.1 Hz, 1H, C5-$OH_{Lactoside}$), 4.56-4.49 (m, 6H, $C_{triazole}CH_2$, CH_2N, 2 x $OH_{Lactoside}$), 4.26-4.23 (dd, $^3J_{C\underline{H}C\underline{H}H'}$ = 3.1 Hz, $^2J_{CHC\underline{H}\underline{H}'}$ = 12.0 Hz, 1H, CHC$\underline{H}$H'), 4.21 (d, $^3J_{1,2}$ = 8.0 Hz, 1H, H-1), 4.20 (d, $^3J_{1,2}$ = 7.5 Hz, 1H, H-1'), 4.08-4.05 (dd, $^3J_{C\underline{H}C\underline{H}H'}$ = 7.1 Hz, $^2J_{CHC\underline{H}\underline{H}'}$ = 12.0 Hz, 1H, CHC$\underline{H}$H'), 3.87-3.83 (m, 1H, $C_{Glc}OC\underline{H}$H'), 3.82 (t, $^3J_{CH2CH2}$ = 5.3 Hz, 2H, $\underline{C}H_2CH_2N$), 3.77-3.74 (dd, $^3J_{CHCH}$ = 5.6 Hz, $^3J_{CHCH}$ = 11.0 Hz, 1H, H-6$_{Lactoside}$), 3.63-3.43 (m, 14H, 3 x CH_2, 3 x H-6$_{Lactoside}$, $OC\underline{H}_2CH$, $C_{Glc}OCH\underline{H}$', 2 x $H_{Lactoside}$), 3.34-3.27 (m, 5H, H-2', H-3, H-4, H-5, 1 x $H_{Lactoside}$), 3.04-2.99 (m, 1H, H-2), 2.28-2.23 (m, 4H, $(C=O)CH_2$), 1.53-1.46 (m, 4H, $(C=O)CH_2C\underline{H}_2$), 1.29-1.19 (m, 48H, $(C=O)CH_2CH_2(C\underline{H}_2)_{12}CH_3$), 0.85 (t, $^3J_{CH2CH3}$ = 7.0 Hz, 6H, CH_3);

^{13}C NMR (150 MHz, DMSO-*d6*, 300 K): δ = 173.5, 172.3 (C=O), 143.4 ($C_{triazole}$), 124.4 ($C_{triazole}H$), 103.9 (C-1'), 102.7 (C-1), 80.7 ($C_{Lactoside}$), 75.5, 75.0, 74.8 ($C_{Lactoside}$), 73.3 ($C_{Lactoside}$), 73.1 (C-2), 70.6 ($OCH_2\underline{C}H$), 69.8 (C-4), 69.5 (CH_2), 68.9 ($\underline{C}H_2CH_2N$), 68.7 ($O\underline{C}H_2CH$), 68.1 ($C_{glc}O\underline{C}HH'$), 68.0, 67.9 (CH_2), 63.8 ($C_{triazole}\underline{C}H_2O$), 62.3 ($OCH_2CH\underline{C}H_2$), 60.6, 60.4 (C-6, C-6'), 49.3 (CH_2N), 33.5, 33.4 ($(C=O)\underline{C}H_2$), 31.3, 29.0, 28.9, 28.7, 28.4, 28.3 ($(C=O)CH_2CH_2(\underline{C}H_2)_{12}CH_3$), 24.5, 24.4 ($(C=O)CH_2\underline{C}H_2$), 22.1 ($\underline{C}H_2CH_3$), 13.9 ($CH_3$) ppm;

IR (ATR): ṽ = 3353, 2921, 2852, 2365, 1736, 1467, 1260, 1032, 798, 704 cm^{-1};

ESI-MS: *m/z* = 994.60574, $[M+H]^+$; (calc. 994.60629 for $C_{48}H_{87}N_3O_{18}$+H).

1-{2-[2-(2-(β-D-Galactopyranosyl-(1→4)β-D-glucopyranosyloxy)ethoxy)ethoxy] ethyl]}4-{[(1,2-dihexadecanoyloxycarbonyl)propyl-oxy]methoxy}-1,2,3-triazole (34)

According to the General Procedure B compound **28** (243 mg, 400 µmol) and lactoside **11** (200 mg, 400 µmol) were reacted to yield **34** as a colourless solid.

Yield: 262 mg (237 µmol, 59 %);

TLC: R_f = 0.25 (ethyl acetate/methanol 6:1);

^{1}H NMR (600 MHz, DMSO-*d6*, 300 K): δ = 8.06 (s, 1H, $H_{triazole}$), 5.14-5.11 (m, 1H, $CH_2C\underline{H}$), 5.11-5.10 (d, $^{3}J_{HCOH}$ = 5.1 Hz, 1H, C2-OH), 5.10-5.08 (d, $^{3}J_{HCOH}$ = 4.2 Hz, 1H, C2'-OH), 4.77 (d, $^{3}J_{HCOH}$ = 4.8 Hz, 1H, $OH_{Lactoside}$), 4.67 (d, $^{3}J_{HCOH}$ = 1.0 Hz, 1H, C3-OH), 4.64 (t, $^{3}J_{HCOH}$ = 5.1 Hz, 1H, C5-$OH_{Lactoside}$), 4.56-4.49 (m, 6H, $C_{triazole}CH_2$, CH_2N, 2 x $OH_{Lactoside}$), 4.26-4.24 (dd, $^{3}J_{C\underline{H}C\underline{H}H'}$ = 3.0 Hz, $^{2}J_{CHC\underline{H}H'}$ = 12.0 Hz, 1H, CHC$\underline{H}$H'), 4.22 (d, $^{3}J_{1,2}$ = 7.9 Hz, 1H, H-1), 4.20 (d, $^{3}J_{1,2}$ = 7.4 Hz, 1H, H-1') 4.07 (dd, $^{3}J_{C\underline{H}C\underline{H}H'}$ = 7.2 Hz, $^{2}J_{CHC\underline{H}H'}$ = 12.0 Hz, 1H, CHC$\underline{H}$H'), 3.87-3.83 (m, 1H, $C_{Glc}OC\underline{H}$H'), 3.82 (t, $^{3}J_{CH2CH2}$ = 5.3 Hz, 2H, $\underline{C}H_2CH_2N$), 3.75 (dd, $^{3}J_{CHCH}$ = 5.6 Hz, $^{3}J_{CHCH}$ = 11.0 Hz, 1H, H-$6_{Lactoside}$), 3.63-3.43 (m, 14H, 3 x CH_2, 3 x H-$6_{Lactoside}$, $OC\underline{H}_2CH$, $C_{Glc}OCH\underline{H}$', 2 x $H_{Lactoside}$), 3.35-3.26 (m, 5H, H-2', H-3, H-4, H-5, 1 x $H_{Lactoside}$), 3.04-2.99 (m, 1H, H-2), 2.29-2.22 (m, 4H, $(C=O)CH_2$), 1.53-1.46 (m, 4H, $(C=O)CH_2C\underline{H}_2$), 1.29-1.19 (m, 48H, $(C=O)CH_2CH_2(C\underline{H}_2)_{12}CH_3$), 0.85 (t, $^{3}J_{CH2CH3}$ = 7.0 Hz, 6H, CH_3);

^{13}C NMR (150 MHz, DMSO-*d6*, 300 K): δ = 173.5, 172.3 (C=O), 143.4 ($C_{triazole}$), 124.4 ($C_{triazole}H$), 103.9 (C-1'), 102.7 (C-1), 80.7 ($C_{Lactoside}$), 75.5, 75.0, 74.8 ($C_{Lactoside}$), 73.3 ($C_{Lactoside}$), 73.1 (C-2), 70.6 ($OCH_2\underline{C}H$), 69.8 (C-4), 69.5 (CH_2), 68.9 ($\underline{C}H_2CH_2N$), 68.7 ($O\underline{C}H_2CH$), 68.1 ($C_{glc}O\underline{C}HH'$), 68.0, 67.9 (CH_2), 63.8 ($C_{triazole}\underline{C}H_2O$), 62.3 ($OCH_2CH\underline{C}H_2$), 60.6, 60.4 (C-6, C-6'), 49.3 (CH_2N), 33.5, 33.4 ($(C=O)\underline{C}H_2$), 31.3, 29.0, 28.9, 28.7, 28.4, 28.3 ($(C=O)CH_2CH_2(\underline{C}H_2)_{12}CH_3$), 24.5, 24.4 ($(C=O)CH_2\underline{C}H_2$), 22.1 ($\underline{C}H_2CH_3$), 13.9 ($CH_3$) ppm;

IR (ATR): $\tilde{\nu}$ = 3416, 2917, 2850, 2367, 1735, 1467, 1062, 784, 720 cm^{-1};

ESI-MS: *m/z* = 1106.73094, $[M+H]^+$; (calc. 1106.73149 for $C_{56}H_{103}N_3O_{18}$+H).

(*E*)-*p*-{*p'*-[(2,2-Dimethyl-1,3-dioxan-4-yl)methoxy]phenylazo}pyridine (36)

Azobenzene **35** (2.54 g, 12.8 mmol), compound **13** (3.66 g, 12.8 mmol) and freshly pestled potassium carbonate (5.31 g, 38.4 mmol) were dried in vacuo for 45 min before solvation in dry DMF (60 mL). The mixture was stirred at 100 °C for 7 h. The solvent was removed under reduced pressure and the residue was suspended in water (150 mL) and sat. NaCl solution (150 mL) and subsequently extracted with ethyl acetate (4 x 250 mL) and DCM (2 x 200 mL). The combined organic layers were dried over $MgSO_4$, filtered and the solvent removed under reduced pressure. The crude product was purified by column chromatography (cyclohexane / ethyl acetate 4:1 → 1:1) to yield compound **36** as an orange solid.

Yield: 3.23 g (10.3 mmol, 80 %);

TLC: R_f = 0.24 (cyclohexane / ethyl acetate 2:1);

^{1}H-NMR ($CDCl_3$, 500 MHz, 300 K): δ = 8.79-8.77 (dd, $^3J_{Ar-H}$ = 4.5 Hz, $^4J_{Ar-H}$ = 1.6 Hz, 2H, Ar-H*,meta‘*), 7.98-7.95 (m, 2H, Ar-H*,ortho*), 7.68-7.66 (dd, $^3J_{Ar-H}$ = 4.5 Hz, $^4J_{Ar-H}$ = 1.6 Hz, 2H, Ar-H*,ortho‘*), 7.07-7.04 (m, 2H, Ar-H*,meta*), 4.55-4.50 (m, 1H, $OCH_2C\underline{H}$), 4.22-4.18 (dd, $^2J_{CHH'}$ = 8.6 Hz, $^3J_{CHCHH'}$ = 6.4 Hz, 1H, $OCH_2CHC\underline{H}H$‘), 4.17-4.13 (dd, $^2J_{CHH}$ = 9.5 Hz, $^3J_{CHCHH'}$ = 5.4 Hz, 1H, $OC\underline{H}H$‘CH), 4.09-4.03 (dd, $^2J_{Ar-H}$ = 9.5 Hz, $^3J_{Ar-H}$ = 5.7 Hz, 1H, $OCH\underline{H}$‘CH), 3.96-3.92 (dd, ^2J = 8.6 Hz, ^3J = 5.7 Hz, 1H, $OCH_2CHCH\underline{H}$‘), 1.49 (s, 3H, CH_3), 1.42 (s, 3H, CH_3) ppm;

^{13}C-NMR (DMSO-d_6, 126 MHz, 300 K): δ = 162.7 (Ar-C*para*), 157.1 (Ar-C*ipso‘*), 151.9 (Ar-C*meta‘*), 146.7 (Ar-C*ipso*), 125.9 (Ar-C*ortho*), 116.3 (Ar-C*ortho‘*), 115.8 (Ar-C*meta*), 109.5 ($\underline{C}(CH_3)_2$), 74.0 ($OCH_2\underline{C}H$), 69.7 ($O\underline{C}H_2CH$), 66.0 ($OCH_2CH\underline{C}H_2$), 27.0 (CH_3), 25.8 (CH_3) ppm;

IR (ATR): $\tilde{\nu}$ = 2458, 1579, 1402, 1291, 1135, 1009, 826, 732, 553, 495 cm^{-1};

EI-MS: *m/z* = 313.14, $[M]^+$; (calc. 313,14 for $C_{17}H_{19}N_3O_3$).

(*E*)-*p*-[*p‘*-(1,2-Dihydroxypropyloxy)phenylazo]pyridine (37)

Azobenzene **36** (4.12 g, 13.1 mmol) was dissolved in a 1:1 mixture of THF and 1 N HCl (600 mL) and stirred at room temperature for 16 h. After neutralisation with 1 N NaOH, the mixture was extracted with ethyl acetate (5 x 300 mL). The combined organic layers were dried over $MgSO_4$, filtered and the solvent removed under reduced pressure. Column chromatography (cyclohexane/ethyl acetate 1:1→ ethyl acetate → ethyl acetate/methanol 4:1) gave compound **37** as an orange solid.

Yield: 2.29 g (8.37 mmol, 64 %);

TLC: R_f = 0.25 (ethyl acetate);

^{1}H-NMR (MeOD/DMSO-*d_6*, 500 MHz, 300 K): δ = 8.74-8.72 (dd, $^3J_{Ar-H}$ = 4.6 Hz, $^4J_{Ar-H}$ = 1.6 Hz, 2H, Ar-H*,meta‘*), 8.01-7.98 (m, 2H, Ar-H*,ortho*), 7.79-7.77 (dd, $^3J_{Ar-H}$ = 4.6 Hz, $^4J_{Ar-H}$ = 1.6 Hz, 2H, Ar-H*,ortho‘*), 7.18-7.15 (m, 2H, Ar-H*,meta*), 4.22-4.18 (dd, $^2J_{CHH'}$ = 9.9 Hz, $^3J_{CHCHH'}$ = 4.2 Hz, 1H, $OC\underline{H}H$‘CH), 4.12-4.07 (dd, $^2J_{CHH'}$ = 9.9 Hz,

$^{3}J_{CHCHH'}$ = 6.1 Hz, 1H, OCHH‘CH), 4.02-3.97 (m, 1H, OCH_2CH), 3.70-3.63 (m, 2H, $CHCH_2OH$) ppm;

^{13}C-NMR (MeOD/DMSO-*d_6*, 126 MHz, 300 K): δ = 164.4 (Ar-C_{para}), 159.1 (Ar-$C_{ipso'}$), 151.9 (Ar-$C_{meta'}$), 148.1 (Ar-C_{ipso}), 126.7 (Ar-C_{ortho}), 117.6 (Ar-$C_{ortho'}$), 116.2 (Ar-C_{meta}), 71.5 (OCH_2CH), 70.9 (OCH_2CH), 63.9 (OCH_2CHCH_2) ppm;

IR (ATR): ṽ = 3045, 2960, 2562, 1580, 1403, 1259, 116, 1009, 797, 554, 495 cm^{-1};

EI-MS: *m/z* = 273.11086, $[M]^+$; (calc. 273.1113 for $C_{14}H_{15}N_3O_3$).

(*E*)-*p*-{[*p'*-(1,2-Didodecanoyloxycarbonyl)propyloxy]phenylazo}pyridine (38)

According to the General Procedure A azobenzene **37** (1.14 g, 4.17 mmol) and dodecanoic acid (3.34 g, 16.7 mmol) were reacted to yield **38** after column chromatography (cyclohexane/ethyl acetate 9:1 → 2:1) as an orange solid.

Yield: 1.62 g (2.54 mmol, 61 %);

TLC: R_f = 0.35 (cyclohexane/ ethyl acetate 4:1);

^{1}H-NMR ($CDCl_3$, 200 MHz, 300 K): δ = 8.82-8.76 (dd, $^{3}J_{Ar-H}$ = 4.7 Hz, $^{4}J_{Ar-H}$ = 1.4 Hz, 2H, Ar-$H_{meta'}$), 8.00-7.93 (m, 2H, Ar-H_{ortho}), 7.72-7.66 (dd, $^{2}J_{Ar-H}$ = 4.6 Hz, $^{3}J_{Ar-H}$ = 1.6 Hz, 2H, Ar-$H_{ortho'}$), 7.07-7.01 (m, 2H, Ar-H_{meta}), 5.49-5.38 (m, 1H, OCH_2CH), 4.51-4.41 (dd, $^{2}J_{CHH'}$ = 12.0 Hz, $^{3}J_{CHCHH'}$ = 4.2 Hz, 1H, CHCHH’O(C=O)), 4.37-4.26 (dd, $^{2}J_{CHH'}$ = 12.0 Hz, $^{3}J_{CHCHH'}$ = 5.9 Hz, 1H, CHCHH’O(C=O)), 4.25-4.19 (d, $^{3}J_{CH2CH}$ = 5.1 Hz, 2H, Ar-CCH_2CH), 2.40-2.26 (m, 4H, $((C=O)CH_2CH_2$), 1.68-1.57 (m, 4H, $(C=O)CH_2$), 1.35-1.19 (m, 32H, $(CH_2)_xCH_3$), 0.92-0.82 (t, $^{3}J_{CH2CH3}$ = 7.0 Hz, 6H, CH_3) ppm;

IR (ATR): ṽ = 2956, 2918, 2851, 1741, 1731, 1586, 1455, 1265, 1163, 1144, 836, 721, 558 cm^{-1};

EI-MS: *m/z* = 637.44409, $[M]^+$; (calc. 637.44547 for $C_{38}H_{59}N_3O_5$).

(*E*)-*p*-{[*p'*-(1,2-Dihexadecanoyloxycarbonyl)propyloxy]phenylazo}pyridine (39)

According to the General Procedure A azobenzene **37** (1.14 g, 4.17 mmol) and palmitic acid (4.28 g, 16.7 mmol) were reacted to yield **39** after column chromatography (cyclohexane/ethyl acetate 9:1 → 2:1) as an orange solid.

Yield: 2.46 g (3.28 mmol, 79 %);

TLC: R_f = 0.38 (cyclohexane/ ethyl acetate 4:1);

^{1}H-NMR ($CDCl_3$, 500 MHz, 300 K): δ = 8.79-8.76 (dd, $^3J_{Ar\text{-}H}$ = 4.6 Hz, $^4J_{Ar\text{-}H}$ = 1.6 Hz, 2H, Ar-H*$_{meta'}$*), 7.98-7.95 (m, 2H, Ar-H*$_{ortho}$*), 7.69-7.67 (dd, $^3J_{Ar\text{-}H}$ = 4.6 Hz, $^4J_{Ar\text{-}H}$ = 1.6 Hz, 2H, Ar-H*$_{ortho'}$*), 7.06-7.02 (m, 2H, Ar-H*$_{meta}$*), 5.46-5.41 (m, 1H, $OCH_2C\underline{H}$), 4.48-4.44 (dd, $^2J_{CHH'}$ = 12.0 Hz, $^3J_{CHCHH'}$ = 4.1 Hz, 1H, $CHC\underline{H}H'O(C{=}O)$), 4.35-4.30 (dd, $^2J_{CHH'}$ = 12.0 Hz, $^3J_{CHCHH'}$ = 5.9 Hz, 1H, $CHCH\underline{H}'O(C{=}O)$), 4.24-4.21 (d, $^3J_{CH2CH}$ = 5.2 Hz, 2H, Ar-$CC\underline{H}_2CH$), 2.38-2.31 (m, 4H, $((C{=}O)CH_2C\underline{H}_2$), 1.67-1.59 (m, 4H, $(C{=}O)CH_2$), 1.29-1.22 (m, 48H, $(C\underline{H}_2)_xCH_3$), 0.88 (t, $^3J_{CH2CH3}$ = 7.0 Hz, 6H, CH_3) ppm;

^{13}C-NMR ($CDCl_3$, 126 MHz, 300 K): δ = 173.4 (C=O), 173.1 ($CH_2O(C{=}O)$), 161.8 (Ar-C*$_{para}$*), 157.4 (Ar-C*$_{ipso'}$*), 151.1 (Ar-C*$_{meta'}$*), 147.2 (Ar-C*$_{ipso}$*), 125.6 (Ar-C*$_{ortho}$*), 116.2 (Ar-C*$_{ortho'}$*), 115.0 (Ar-C*$_{meta}$*), 69.2 ($OCH_2\underline{C}H$), 66.4 ($O\underline{C}H_2CH$), 62.2 ($OCH_2CH\underline{C}H_2$), 34.3 ($(C{=}O)CH_2\underline{C}H_2$), 34.1, 31.9, 29.7, 29.6, 29.4 (CH_2), 24.9 ($(C{=}O)CH_2$), 22.7 (CH_2), 14.1 (CH_3) ppm;

IR (ATR): $\tilde{\nu}$ = 2957, 2917, 2850, 1741, 1731, 1586, 1455, 1264, 1145, 836, 727, 558 cm^{-1};

EI-MS: *m/z* = 749.56984, $[M]^+$; (calc. 749.57076 for $C_{46}H_{75}N_3O_5$).

(*E*)-[*p*-(2-Bromoethoxy)-*p'*-(propargyloxy)]azobenzene (40)

Azobenzene **12** (200 mg, 793 µmol), 1,2 dibromoethane (273 µL, 3.17 mmol) and potassium carbonate (438 mg, 3.17 mmol) were dissolved in dry DMF (10 mL) and stirred for 8 h at 80 °C. The solvent was removed under reduced pressure and the residue dissolved in DCM (150 mL) and subsequently washed with water (50 mL) and sat. NaCl solution (50 mL). The organic layer was dried over Mg_2SO_4, filtered and the solvent

removed under reduced pressure. The crude product was purified by column chromatography (toluene) to yield compound **40** as an orange solid.

Yield: 128 mg (356 µmol, 45 %);

TLC: R_f = 0.57 (toluene);

^{1}H-NMR ($CDCl_3$, 500 MHz, 300 K): δ = 7.83-7.79 (m, 4H, Ar-H_{ortho}, Ar-$H_{ortho'}$), 7.03-6.99 (m, 2H, Ar-$H_{meta'}$), 6.96-6.93 (m, 2H, Ar-H_{meta}), 4.70 (d, ^{4}J = 2.4 Hz, 2H, $C\underline{H}_2C{\equiv}CH$), 4.30 (t, ^{3}J = 6.3 Hz, 2H, OCH_2), 3.60 (t, ^{3}J = 6.3 Hz, 2H, CH_2Br), 2.49 (t, ^{4}J = 2.4 Hz, 1H, $CH_2C{\equiv}C\underline{H}$) ppm;

^{13}C-NMR ($CDCl_3$, 126 MHz, 300 K): δ = 160.1 (Ar-C_{para}), 159.5 (Ar-$C_{para'}$), 147.6 (Ar-$C_{ipso'}$), 147.5 (Ar-C_{ipso}), 124.5 (Ar-C_{ortho}), 124.3 (Ar-$C_{ortho'}$), 115.1 (Ar-$C_{meta'}$), 114.9 (Ar-C_{meta}), 78.1 ($\underline{C}H_2C{\equiv}CH$), 75.9 ($\underline{C}H_2C{\equiv}CH$), 68.0 ($CH_2Br$), 56.0 ($CH_2C{\equiv}\underline{C}H$), 28.8 ($CH_2$) ppm;

IR (ATR): $\tilde{\nu}$ = 3274, 1593, 1496, 1455, 1376, 1240, 1144, 1013, 844, 670, 557 cm^{-1};

EI-MS: *m/z* = 359.94, $[M]^+$; (calc. 359.22 for $C_{17}H_{15}N_2BrO_2$).

(*E*) [*p*-(2-Bromoethoxy)-*p'*-[(2-{2-[2-(1-ethoxy-4-methoxy-1,2,3-triazolyl)]ethoxy} ethyl)β-D-glucopyranosyloxy]]azobenzene (41)

Glucoside **10** (69.5 mg, 206 µmol), alkyne **40** (74.0 mg, 206 µmol) and copper (I) bromide (6.21 mg, 43.3 µmol) were dissolved in dry DMF (6 mL) and after addition of PMDTA (8.60 µL, 41.2 µmol) the mixture was stirred at room temperature for 16 h. The solvent was then removed under reduced pressure, the residue was dissolved in ethyl acetate (200 mL) and washed with water (70 mL). The aqueous phase was extracted with DCM (3 x 50 mL) and the combined organic layers were dried over $MgSO_4$, filtered and the solvent removed under reduced pressure. The crude product was purified by column chromatography (ethyl acetate → ethyl acetate/ methanol 8:1) to yield compound **41** as an orange solid.

Yield: 106 mg (158 µmol, 77 %);

TLC: R_f = 0.20 (ethyl acetate / methanol 8:1);

^{1}H-NMR (MeOD, 600 MHz, 300 K): δ = 8.16 (s, 1H, $CH_{triazole}$), 7.88-7.84 (m, 4H, Ar-H_{ortho}, Ar-$H_{ortho'}$), 7.18-7.14 (m, 2H, Ar-H_{meta}), 7.09-7.06 (m, 2H, Ar-$H_{meta'}$), 5.28 (s,

2H, $C_{triazole}CH_2$), 4.62-4.59 (t, ^3J = 5.0 Hz, 2H, $\underline{C}H_2CH_2N_{triazole}$), 4.41-4.38 (t, ^3J = 5.6 Hz, 2H, $OC\underline{H}_2CH_2Br$), 4.27-4.25 (d, ^3J = 7.8 Hz, 1H, H-1), 3.98-3.94 (ddd, ^2J = 10.9 Hz, ^3J = 5.1 Hz, ^3J = 3.6 Hz, 1H, $C_{glc}OC\underline{H}H$‘), 3.91-3.88 (t, ^3J = 5.0 Hz, 2H, $C\underline{H}_2N_{triazol}$), 3.85-3.82 (dd, $^2J_{6,6‘}$ = 11.9 Hz, $^3J_{5,6}$ = 2.1 Hz, 1H, H-6), 3.75-3.72 (t, ^3J = 5.7 Hz, 2H, CH_2Br), 3.70-3.57 (m, 8H, H-6‘, $C_{glc}OCH\underline{H}$‘, OCH_2), 3.36-3.32 (m, 1H, H-3), 3.29-3.22 (m, 2H, H-4, H-5), 3.20-3.17 (dd, $^3J_{1,2}$ = 7.9 Hz, $^3J_{2,3}$ = 9.1 Hz, 1H, H-2) ppm;

^{13}C-NMR (MeOD, 151 MHz, 300 K): δ = 162.0 (Ar-$C_{para‘}$), 161.9 (Ar-C_{para}), 148.6 (Ar-$C_{ipso,}$ Ar-$C_{ipso‘}$), 144.5 ($\underline{C}_{triazole}CH_2$), 126.4 ($\underline{C}H_{triazole}C_{triazole}$), 125.4 (Ar-$C_{ortho,}$ Ar-$C_{ortho‘}$), 116.3 (Ar-C_{meta}), 116.1 (Ar-$C_{meta‘}$), 104.5 (C-1), 78.1 (C-4), 78.0 (C-3), 75.1 (C-2), 71.6, 71.4, 71.2 (OCH_2), 70.4 ($CH_2N_{triazole}$), 69.7 ($C_{glc}O\underline{C}HH$‘), 69.6 ($O\underline{C}H_2CH_2Br$), 62.8 (C-6), 62.7 ($C_{triazole}\underline{C}H_2$), 51.5 ($\underline{C}H_2CH_2N_{triazole}$), 30.3 ($CH_2Br$) ppm;

IR (ATR): ṽ = 3397, 2932, 1654, 1217, 1107, 1038, 814, 676, 552 cm^{-1};

ESI-MS: *m/z* = 718.2, $[M+Na]^+$; (calc. 718.17 for $C_{28}H_{38}N_5BrO_{10}$+Na).

p-(2-{*p‘*-[(2-{2-[2-(1-Ethoxy-4-methoxy-1,2,3-triazolyl)]ethoxy}ethyl) β-D-glucopyranosyloxy]phenyl}diazenyl)-*N*-{2-[*p*-(2-{*p‘*[(1,2-Didodecanoyloxycarbonyl) propyl-oxy]phenyl}diazenyl)phenoxy]ethyl}pyridinum bromide (42)

Glucoside **41** (313 mg, 470 µmol) and compound **38** (300 mg, 470 µmol) were dissolved in dry acetonitrile (40 mL) and stirred at 80 °C for 10 h and further 16 h at room temperature. The precipitate was subsequently filtered off and washed with cold acetonitrile to yield compound **42** as an orange solid.

Yield: 436 mg (351 µmol, 75 %);

^{1}H-NMR ($CDCl_3$/DMSO-*d6*, 600 MHz, 300 K): δ = 8.80-8.77 (m, 2H, Ar-$H_{py,\ meta}$), 8.21-8.16 (m, 2H, $CH_{triazole}$, Ar-$H_{meta(1)}$), 7.97-7.93 (m, 2H, Ar-$H_{py,\ ortho‘}$), 7.89-7.81 (m, 3H, Ar-$H_{meta(2)}$, Ar-$H_{ortho‘}$), 7.72-7.68 (m, 2H, Ar-$H_{py,\ ortho}$), 7.21-7.08 (m, 2H, Ar-$H_{meta‘}$), 7.16-7.13 (m, 2H, Ar-$H_{py,\ meta’}$), 7.12-7.08 (Ar-H_{ortho}), 5.41-5.37 (m, 1H, Ar-$COCH_2C\underline{H}$), 5.26 (s, 2H, $C_{triazole}CH_2$), 4.58-4.55 (t, ^3J = 5.0 Hz, 2H, $CH_2\underline{C}H_2N_{triazole}$), 4.45-4.38 (m, 3H, $OC\underline{H}_2CH_2N^+$, $CHC\underline{H}H’(C=O)$), 4.32-4.24 (m, 3H, Ar-$COC\underline{H}_2CH$, $CHCH\underline{H}’(C=O)$), 4.19-4.16 (s, ^3J = 7.8 Hz, 1H, H-1), 3.92-3.84 (m, 3H, $C_{glc}OC\underline{H}H$‘, $C\underline{H}_2CH_2N_{triazole}$), 3.82-3.78 (m, 2H, $C_{glc}OCH_2C\underline{H}_2$), 3.72-3.68 (m, 1H, H-6), 3.62-3.49 (m, 8H, H-6‘, $C_{glc}OCH\underline{H}$‘, $OCH_2C\underline{H}_2N^+$, OCH_2), 3.22-3.17 (m, 1H, H-3), 3.15-3.09 (m, 2H, H-4, H-5),

3.05-3.00 (dd~t, ^{3}J = 8.3 Hz, 1H, H-2), 2.32-2.28 ((C=O)CH_2), 1.58-1.52 ((C=O)$CH_2C\underline{H}_2$), 1.29-1.19 ((C$\underline{H}_2$)$_n$$CH_3$), 0.87-0.82 ($CH_3$) ppm;

^{13}C-NMR ($CDCl_3$/DMSO-*d6*, 151 MHz, 300 K): δ = 172.2, 171.9 (C=O), 161.7 (Ar-$C_{py,\ para'}$), 160.1 (Ar-$C_{para'}$), 159.8 (Ar-$C_{ipso)}$, 151.0 (Ar-$C_{py,\ ipso}$), 150.8 (Ar-$C_{py,\ meta}$), 146.4 (Ar-$C_{ipso'}$), 146.5 (Ar-$C_{py,\ ipso'}$), 146.4 ($\underline{C}_{triazole}CH_2$), 125.3 (Ar-$C_{ortho'}$), 124.8 (Ar-$C_{ipso'}$) 124.1 (Ar-$C_{meta}$, $\underline{C}H_{triazole}$), 115.7 (Ar-$C_{py,\ ortho}$), 115.1 (Ar-$C_{py,\ meta'}$, Ar-$C_{meta'}$, Ar-$C_{ortho}$), 115.0 (Ar-$C_{ortho'}$), 102.9 (C-1), 76.6 (C-3, C-4), 73.2 (C-2), 70.1 (C-5), 69.9, 69.8, 69.7 (OCH_2), 68.9 (Ar-$COCH_2C\underline{H}$), 68.6 ($C_{glc}OCHH'\underline{C}H_2$, $CH_2N_{triazole}$), 68.0 ($OCH_2\underline{C}H_2N^+$), 68.0 ($C_{glc}O\underline{C}HH'$), 66.6 (Ar-$CO\underline{C}H_2CH$), 61.8 (Ar-$COCH_2CH\underline{C}H_2$), 61.5 ($C_{triazole}\underline{C}H_2$), 61.2 (H-6), 49.4 ($\underline{C}H_2N_{triazole}$), 33.5 ((C=O)$CH_2\underline{C}H_2$), 31.3 ($CH_2$), 28.9 ($CH_2N^+$), 28.8, 28.6, 28.4, 28.3 (CH_2), 24.3 ((C=O)CH_2), 22.0 (CH_2), 13.7 (CH_3) ppm;

IR (ATR): $\tilde{\nu}$ = 2957, 2919, 2850, 1732, 1599, 1585, 1501, 1456, 1248, 1144, 841, 722, 559 cm^{-1};

ESI-MS: *m/z* = 1253.7, $[M]^+$; (calc. 1253.7 for $C_{66}H_{95}N_8O_{15}$).

8.2.2 ^{1}H and ^{13}C NMR spectra of synthesised amphiphiles

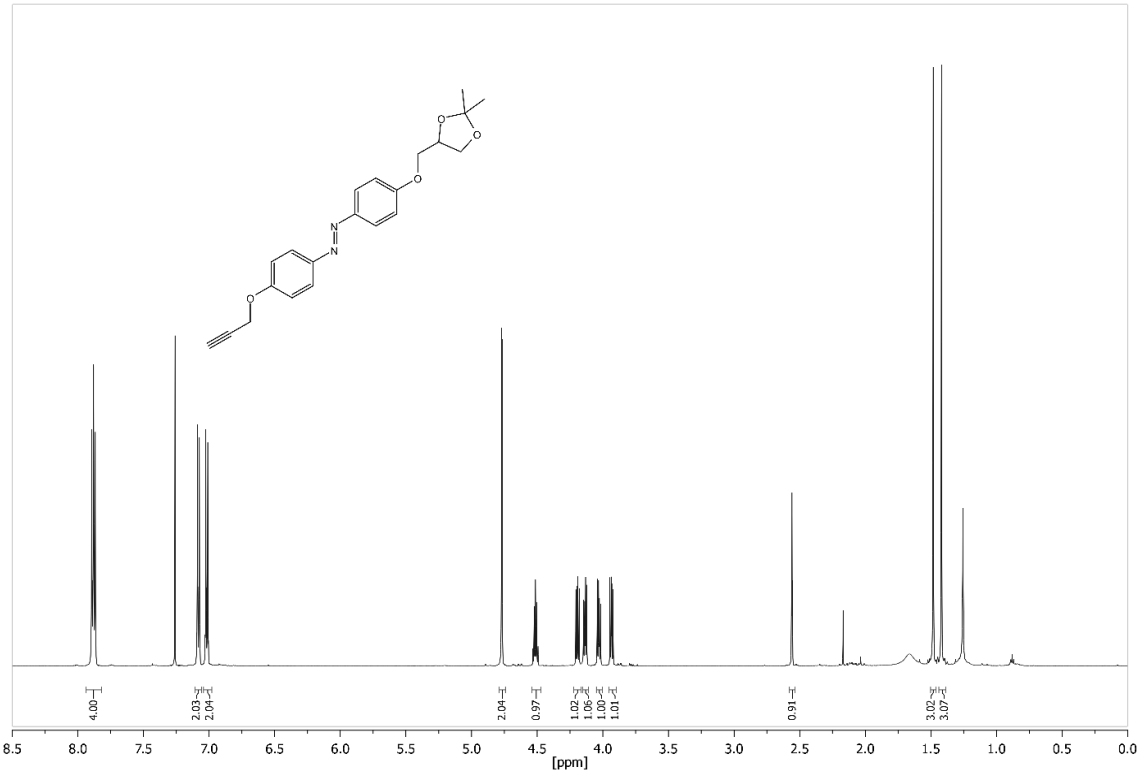

Figure 160: ^{1}H NMR spectrum of **14** (600 MHz, $CDCl_3$, 300 K).

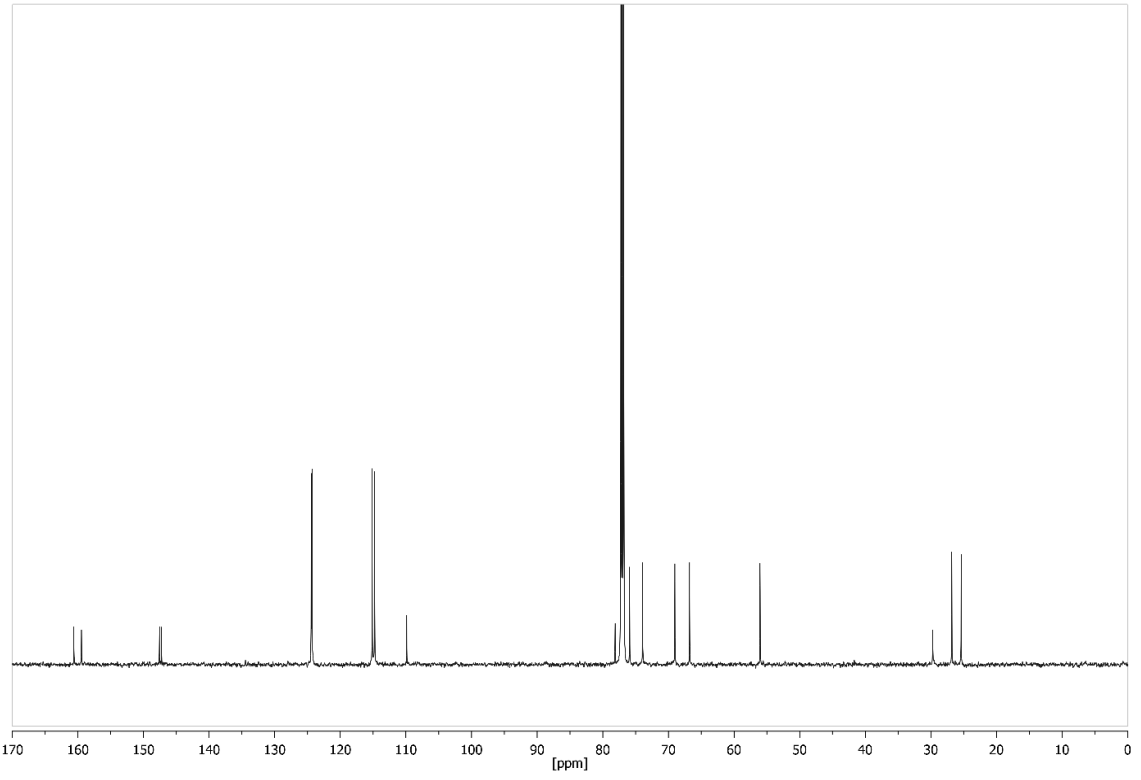

Figure 161: ^{13}C NMR spectrum of **14** (126 MHz, $CDCl_3$, 300 K).

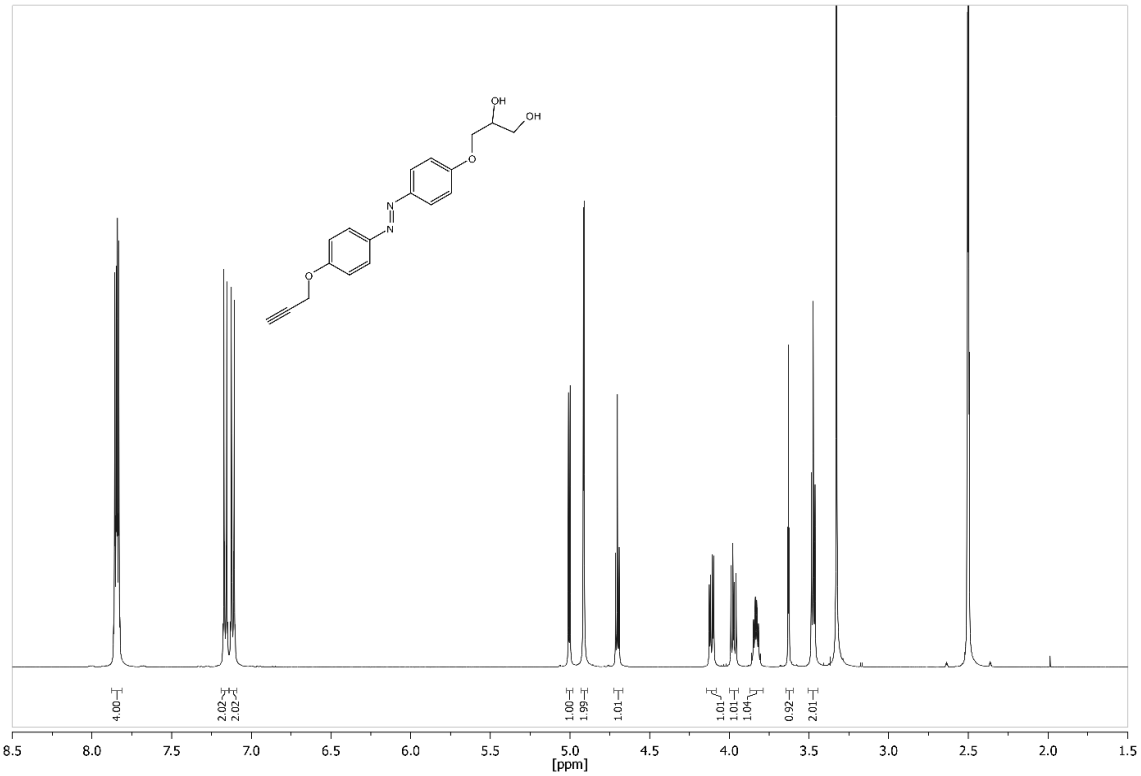

Figure 162: ^{1}H NMR spectrum of **15** (500 MHz, DMSO-*d6*, 300 K).

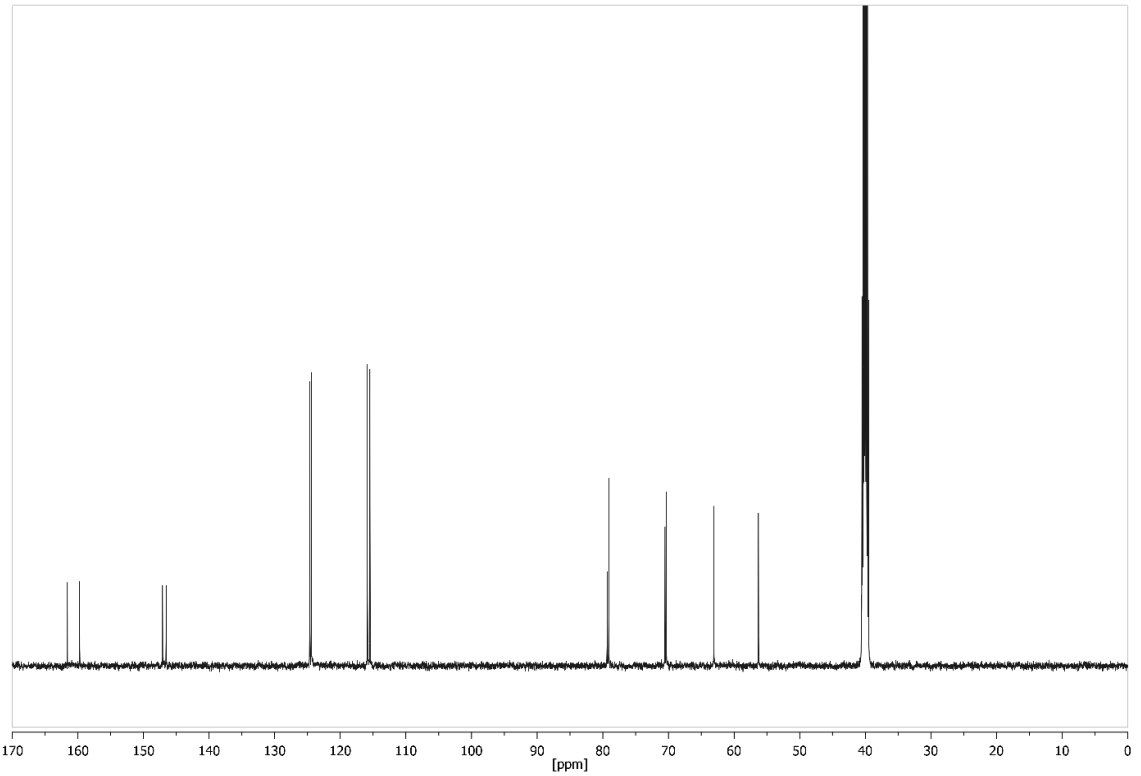

Figure 163: ^{13}C NMR spectrum of **15** (126 MHz, DMSO-*d6*, 300 K).

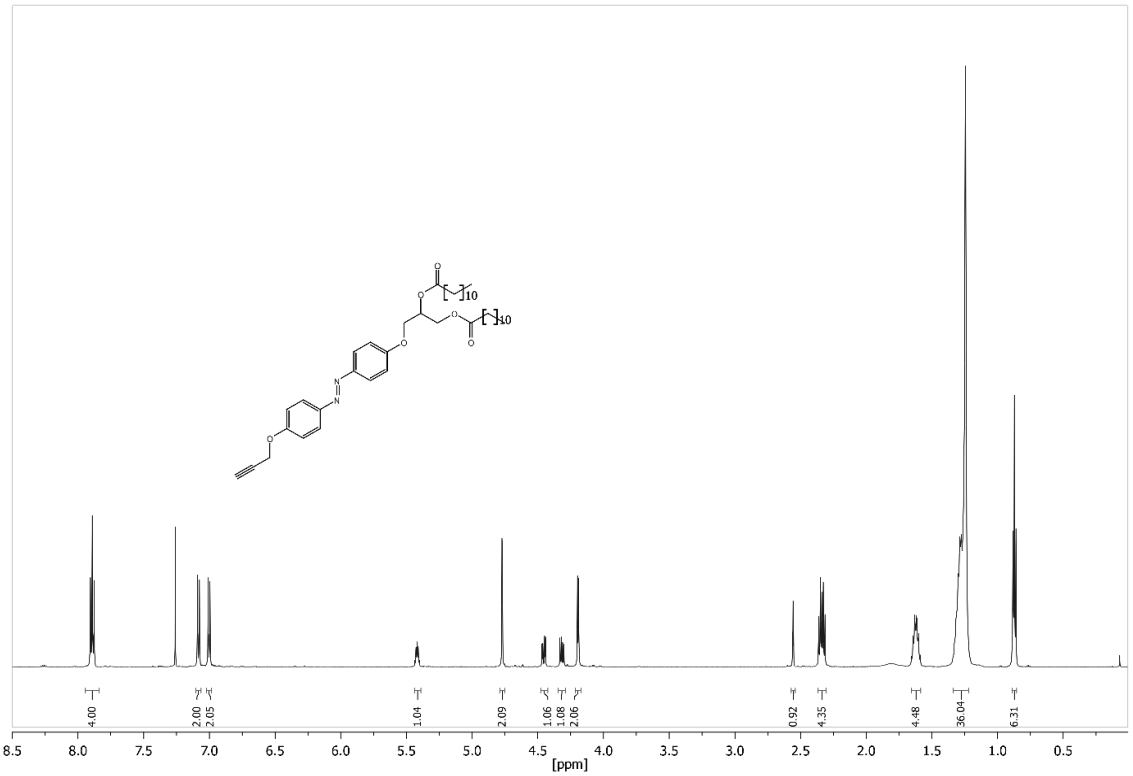

Figure 164: ^{1}H NMR spectrum of **16** (600 MHz, $CDCl_3$, 300 K).

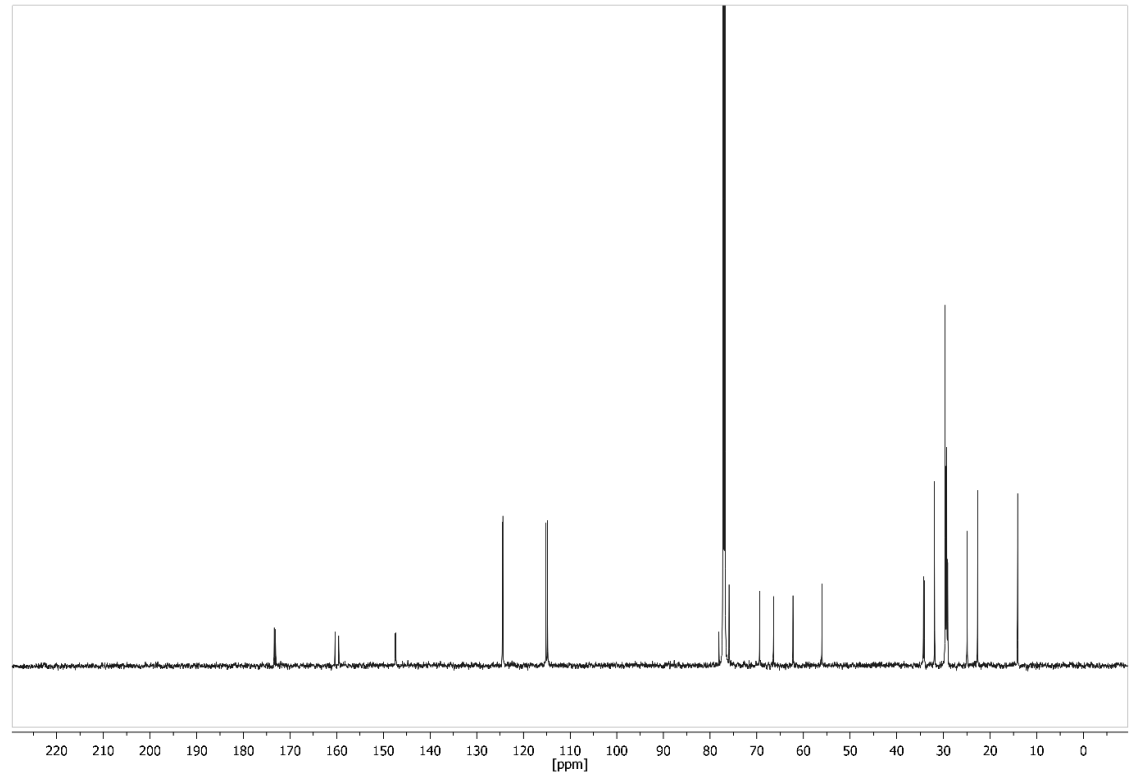

Figure 165: ^{13}C NMR spectrum of **16** (126 MHz, $CDCl_3$, 300 K).

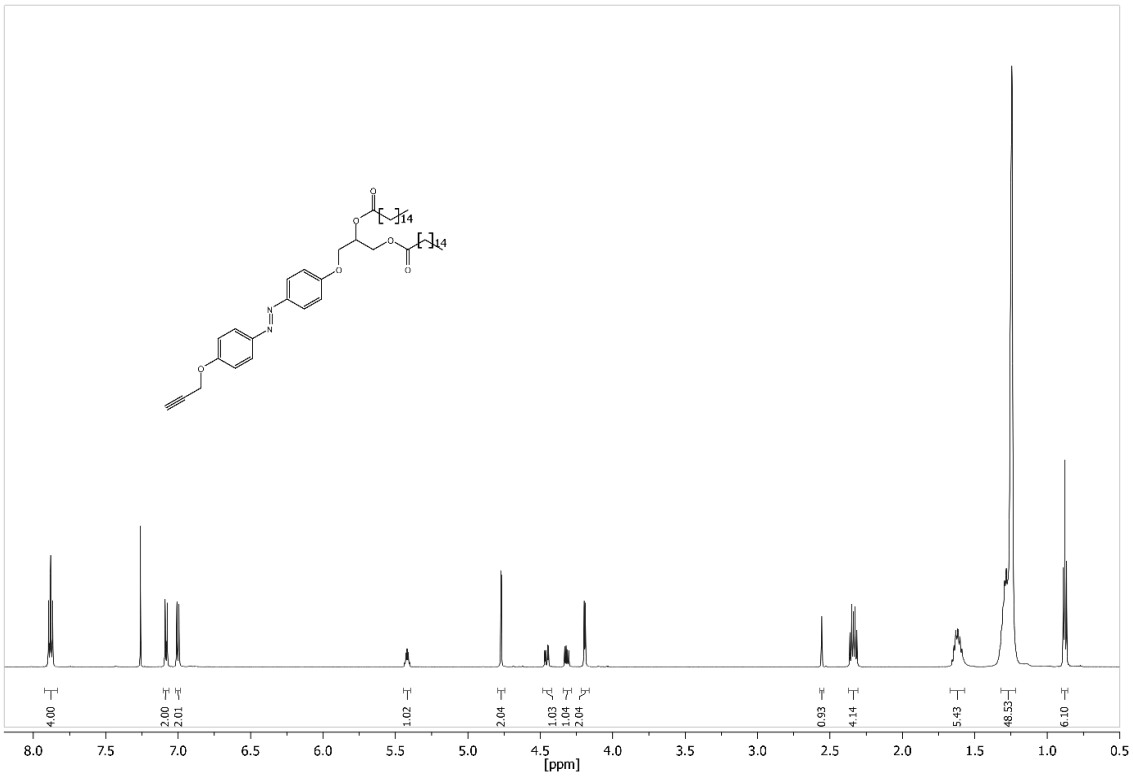

Figure 166: ^{1}H NMR spectrum of **17** (600 MHz, $CDCl_3$, 300 K).

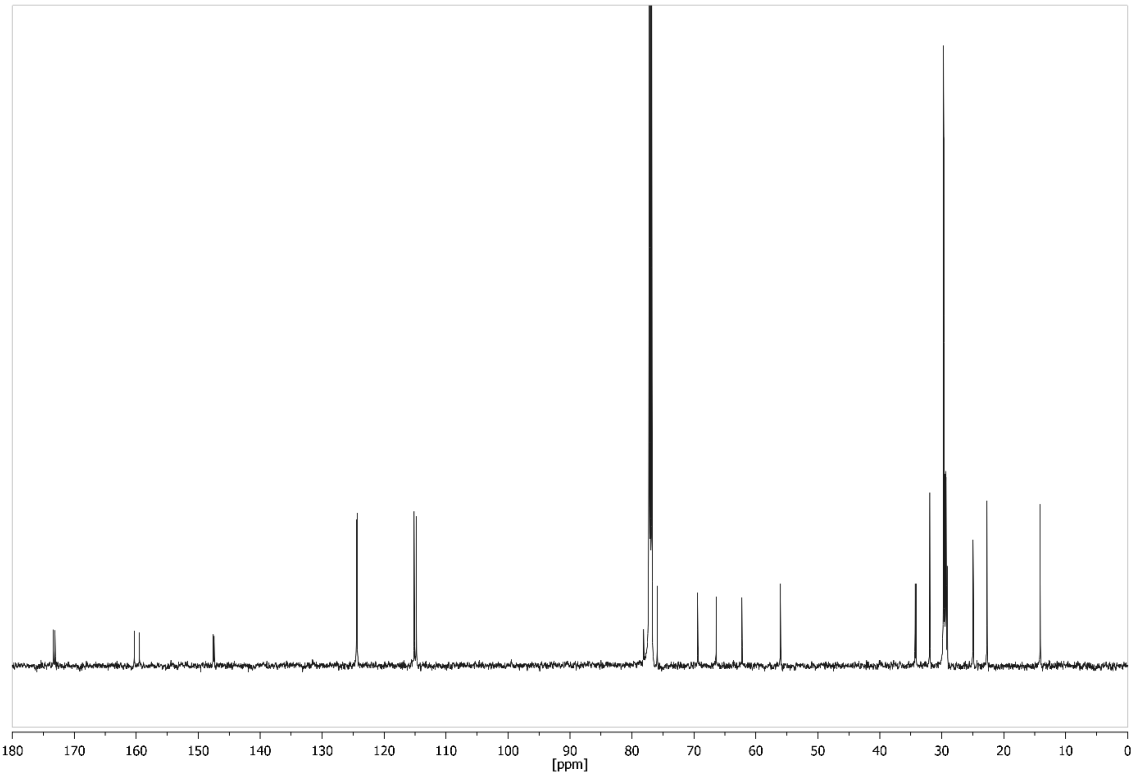

Figure 167: ^{13}C NMR spectrum of **17** (126 MHz, $CDCl_3$, 300 K).

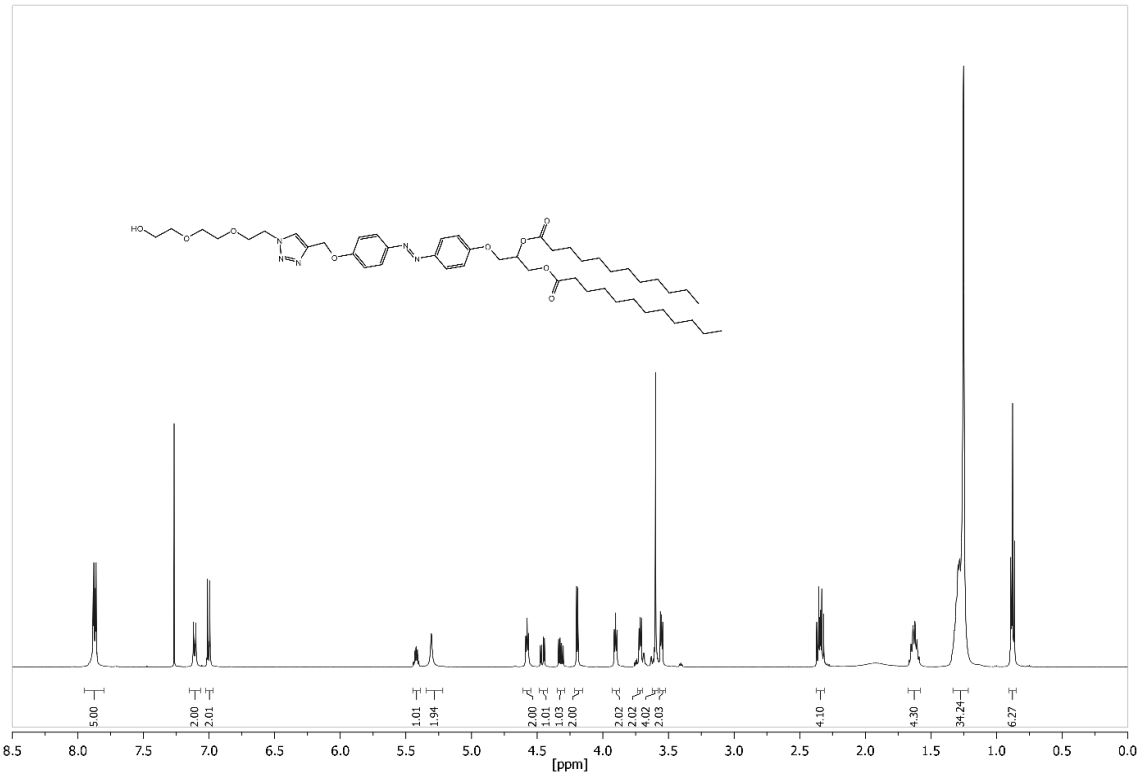

Figure 168: ^{1}H NMR spectrum of **18** (500 MHz, $CDCl_3$, 300 K).

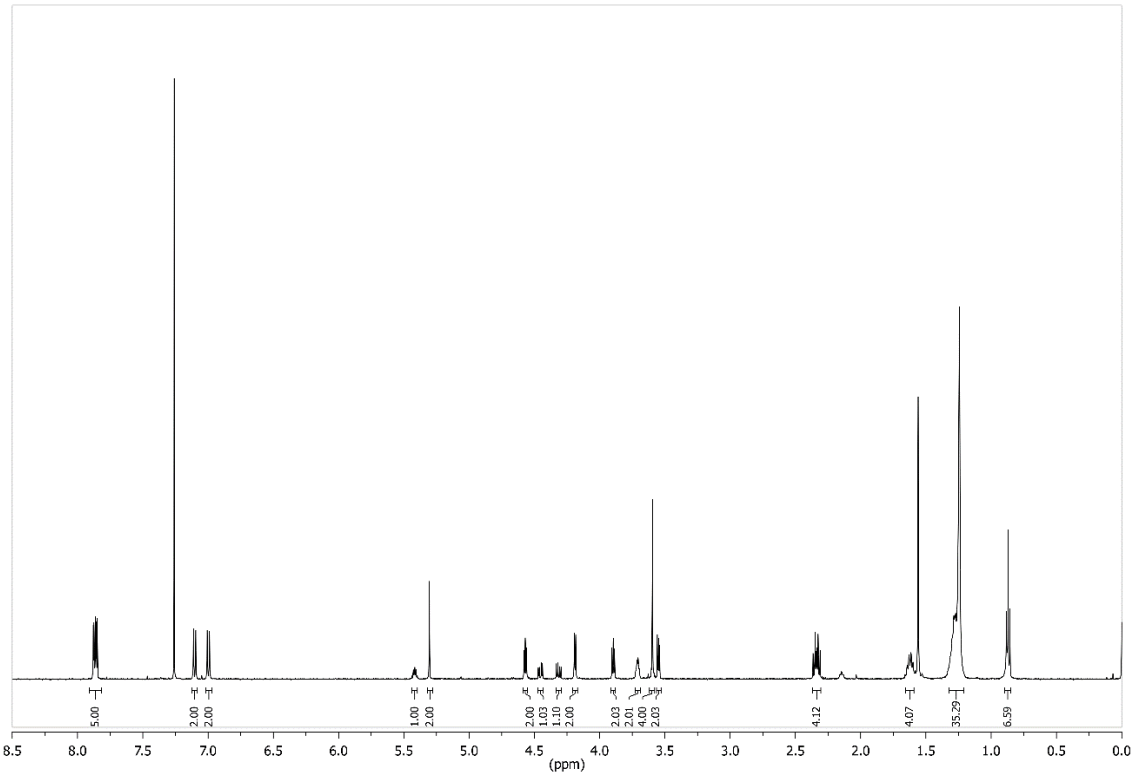

Figure 169: ^{1}H NMR spectrum of **18** (*Z*-isomer after irradiation with 365 nm) (500 MHz, $CDCl_3$, 300 K).

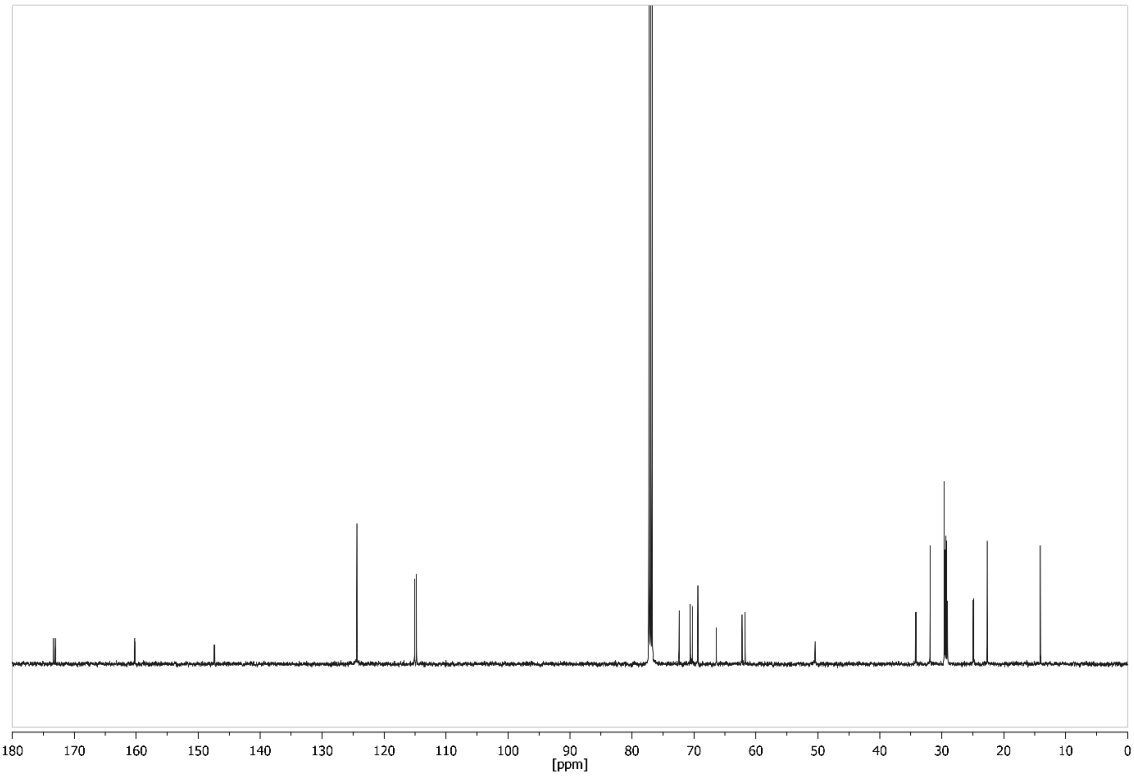

Figure 170: ^{13}C NMR spectrum of **18** (126 MHz, $CDCl_3$, 300 K).

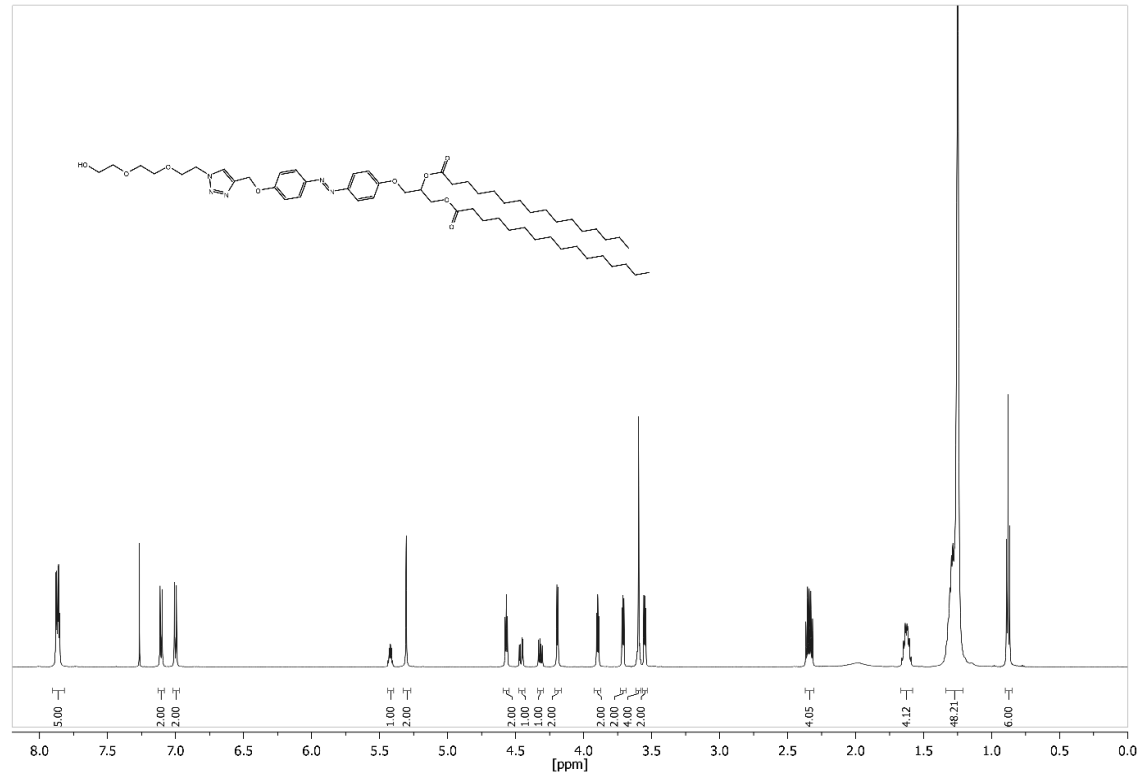

Figure 171: ^{1}H NMR spectrum of **19** (600 MHz, $CDCl_3$, 300 K).

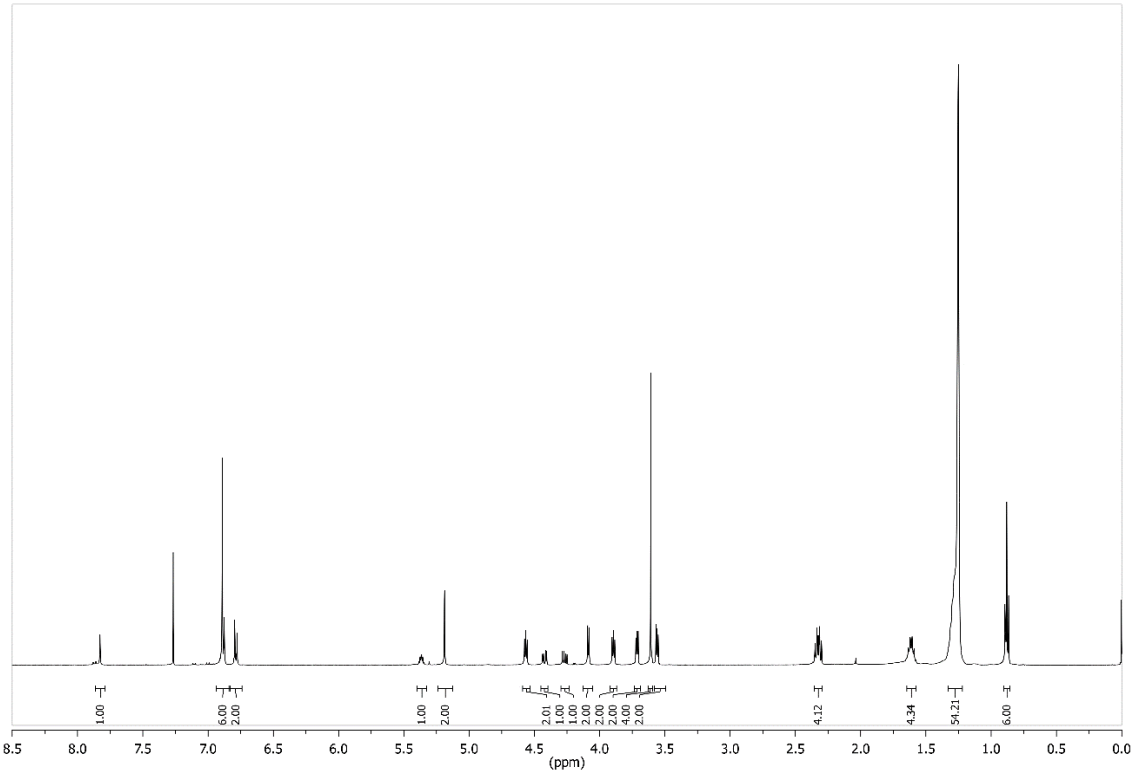

Figure 172: ^{1}H NMR spectrum of **19** (*Z*-isomer after irradiation with 365 nm) (500 MHz, $CDCl_3$, 300 K).

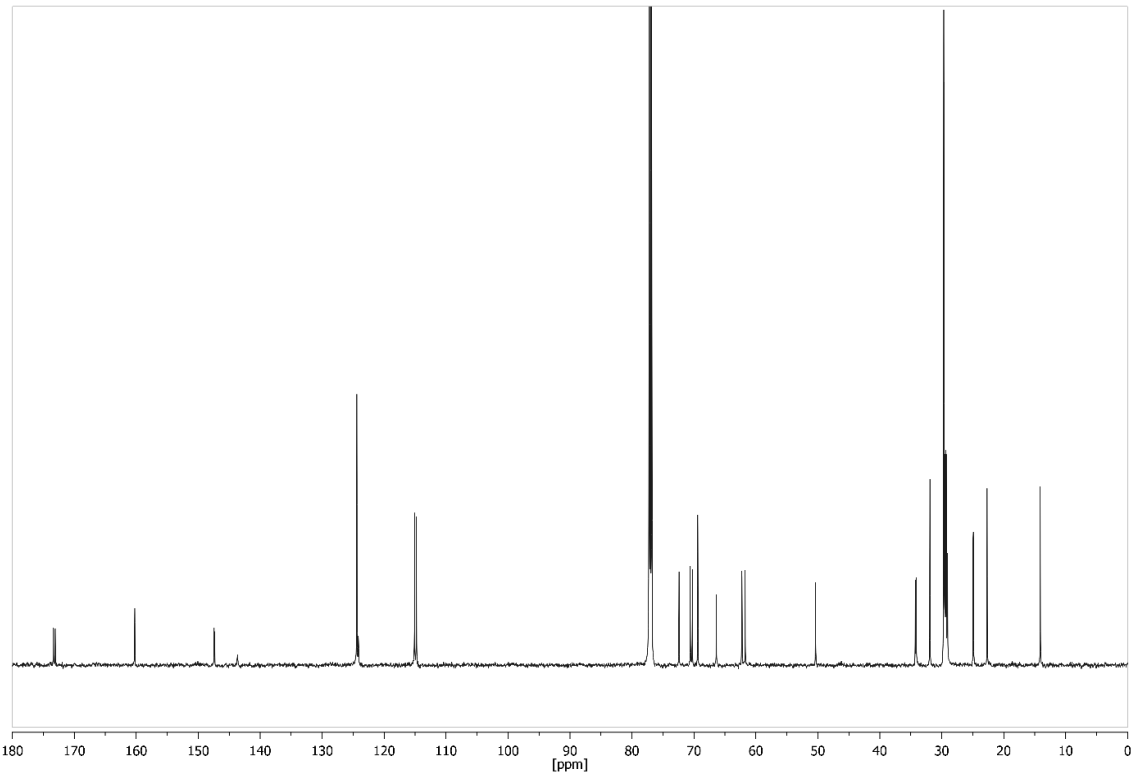

Figure 173: ^{13}C NMR spectrum of **19** (151 MHz, $CDCl_3$, 300 K).

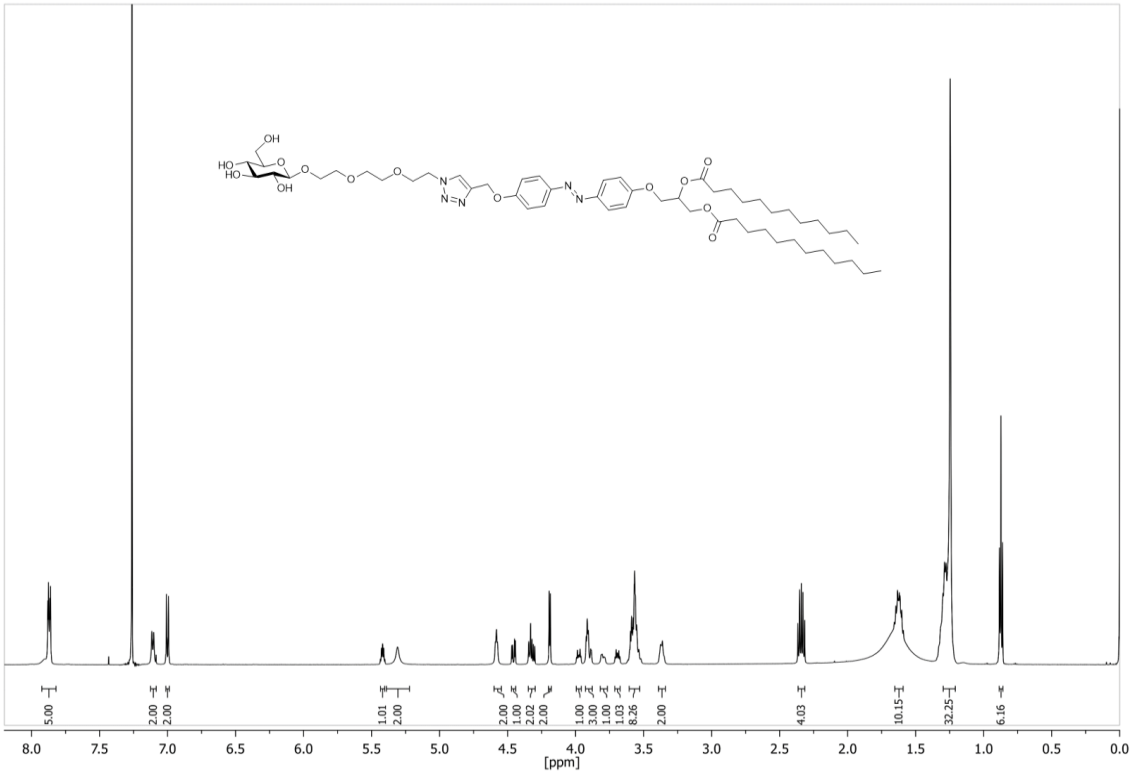

Figure 174: ^{1}H NMR spectrum of **20** (500 MHz, $CDCl_3$, 300 K).

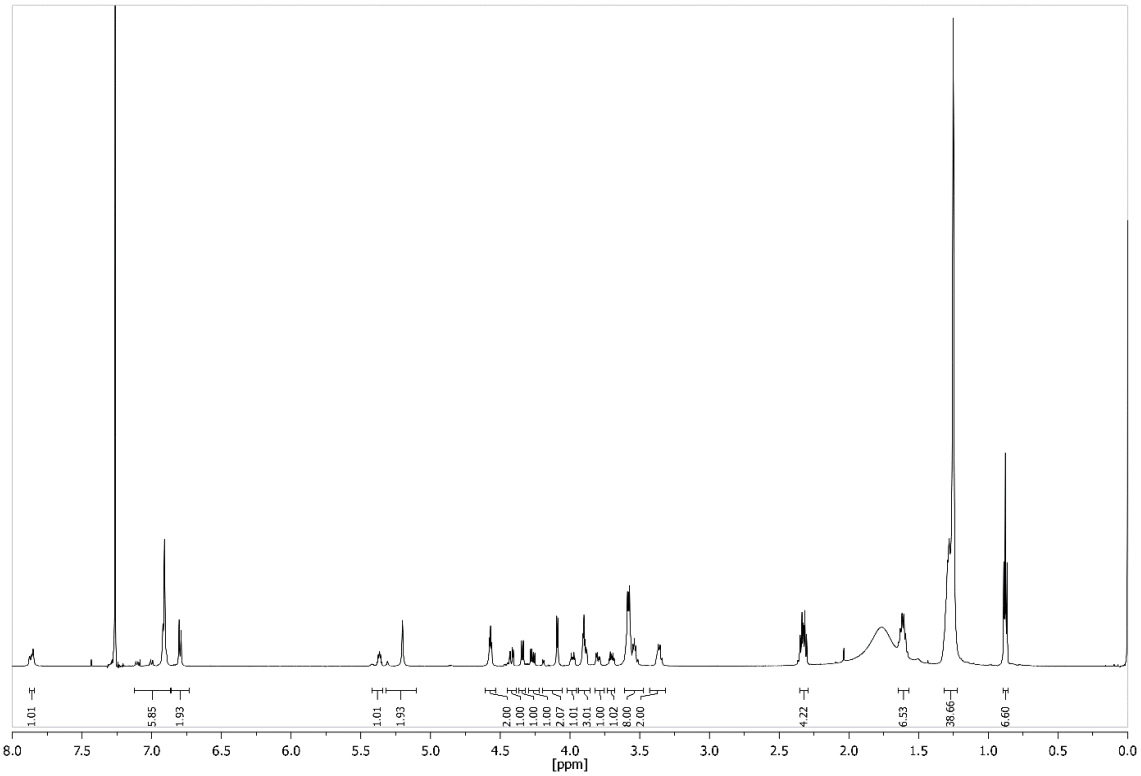

Figure 175: ^{1}H NMR spectrum of **20** (*Z*-isomer after irradiation with 365 nm) (500 MHz, $CDCl_3$, 300 K).

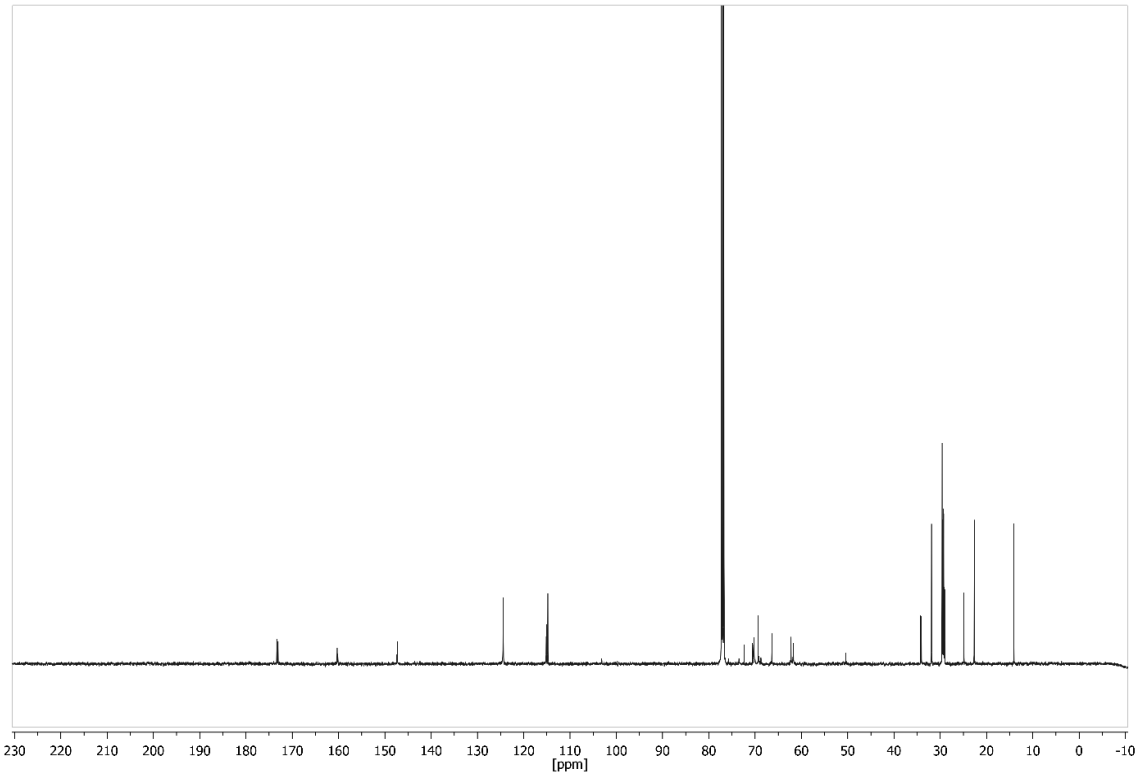

Figure 176: ^{13}C NMR spectrum of **20** (126 MHz, $CDCl_3$, 300 K).

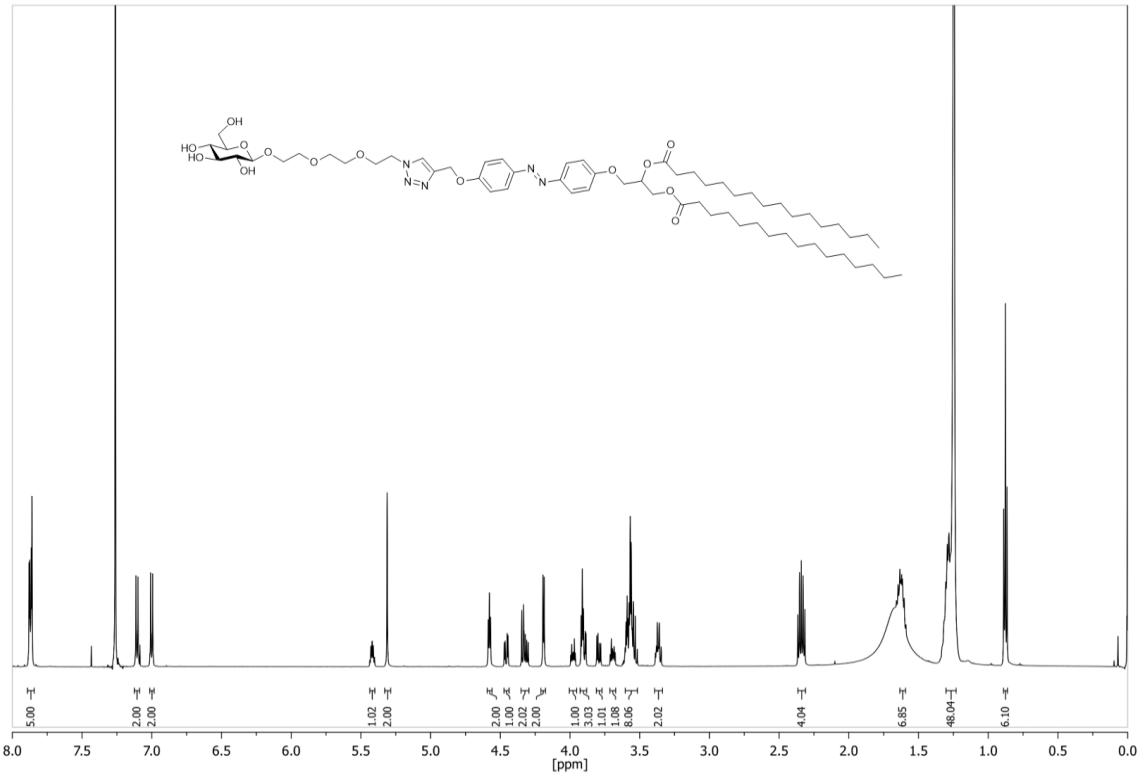

Figure 177: ^{1}H NMR spectrum of **21** (500 MHz, $CDCl_3$, 300 K).

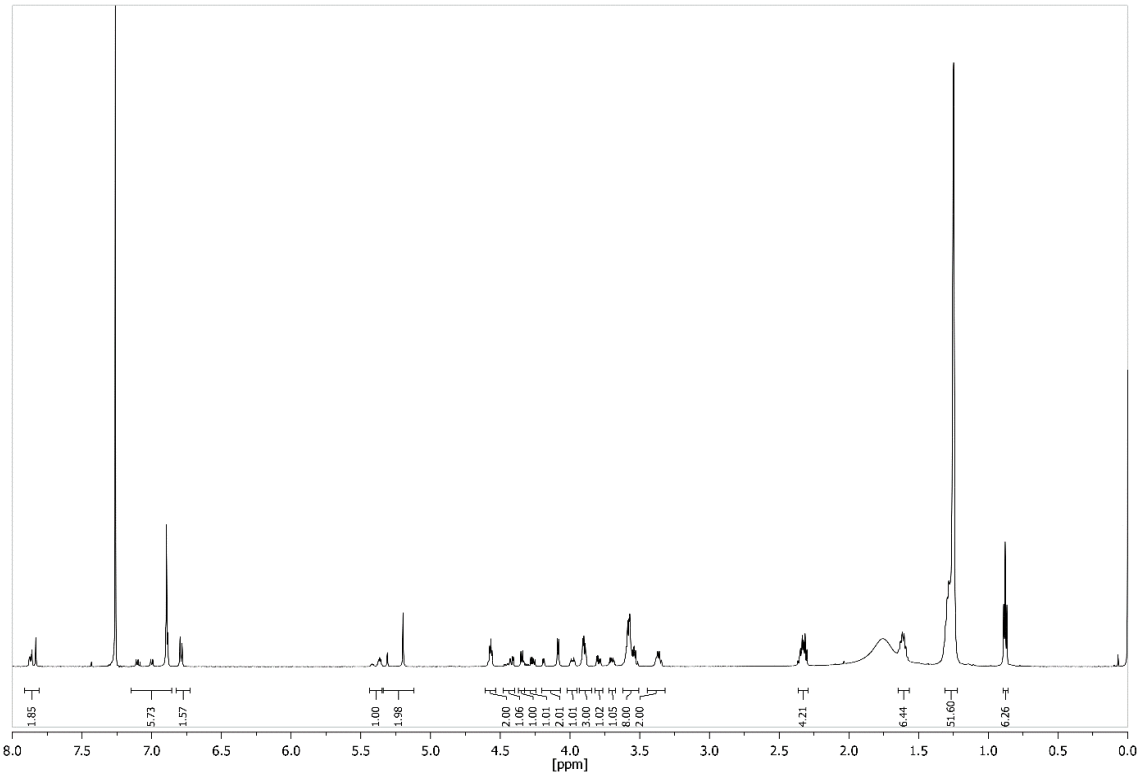

Figure 178: ^{1}H NMR spectrum of **21** (*Z*-isomer after irradiation with 365 nm) (500 MHz, $CDCl_3$, 300 K).

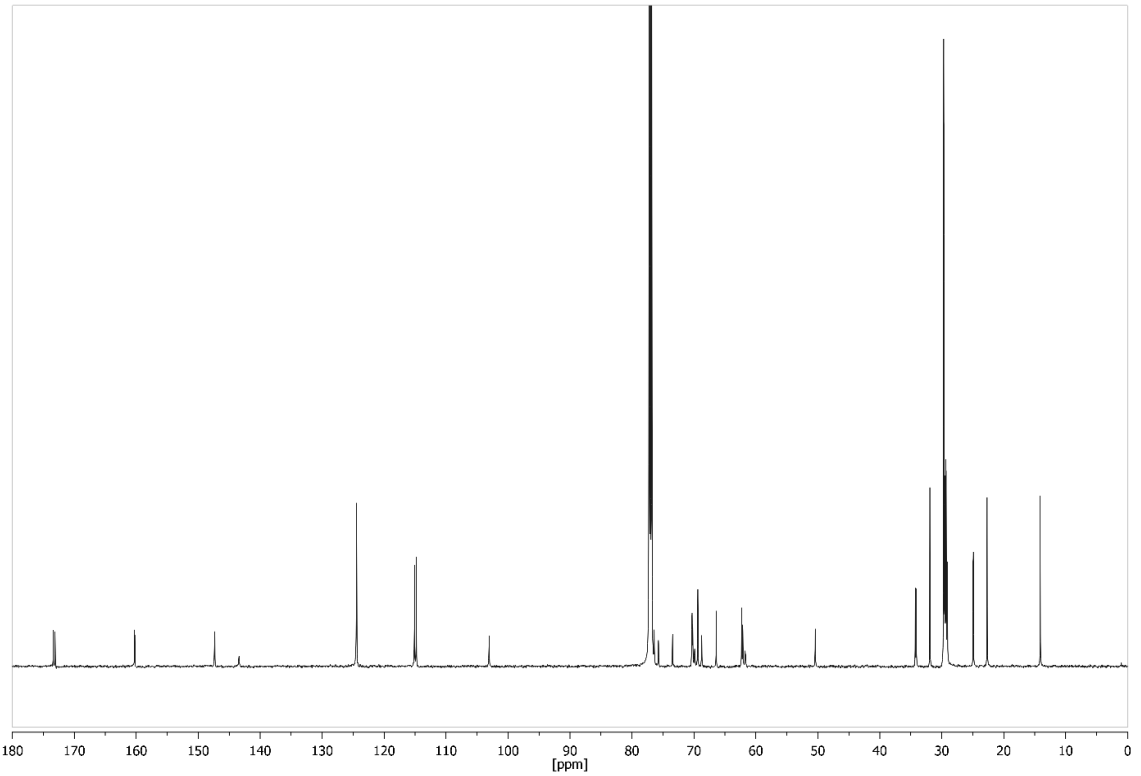

Figure 179: ^{13}C NMR spectrum of **21** (126 MHz, $CDCl_3$, 300 K).

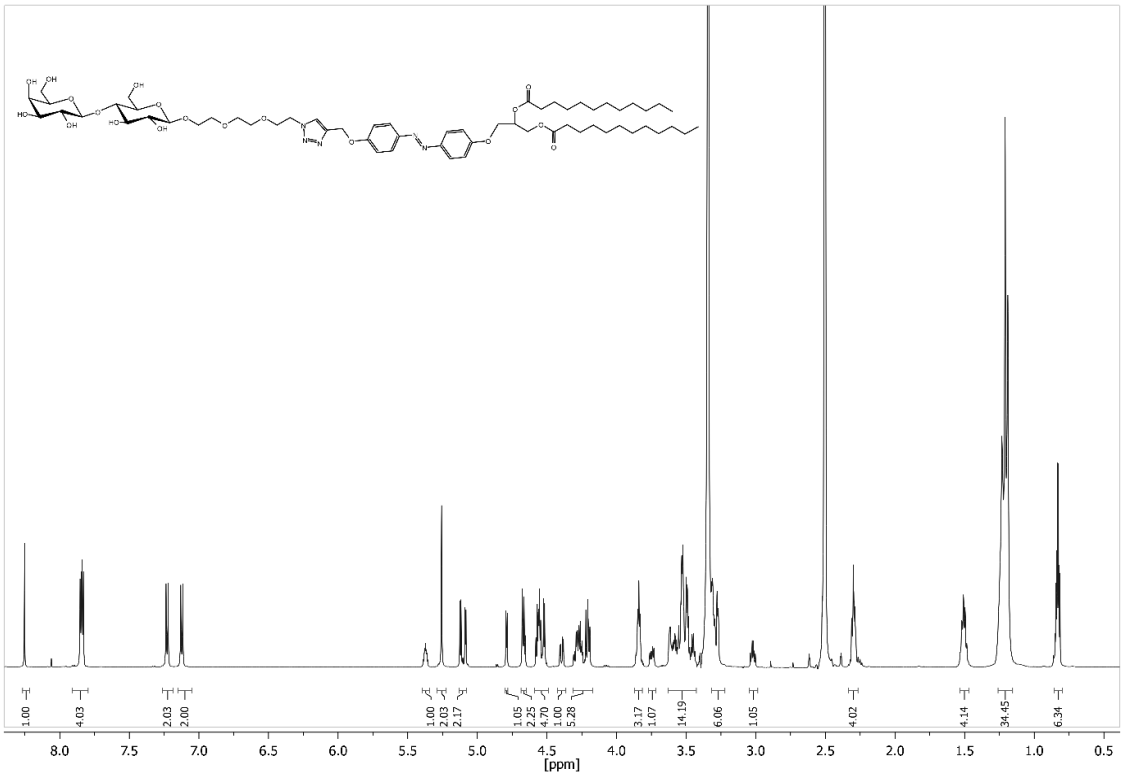

Figure 180: ^{1}H-NMR spectrum of **22** (600 MHz, DMSO-*d6*, 300 K)

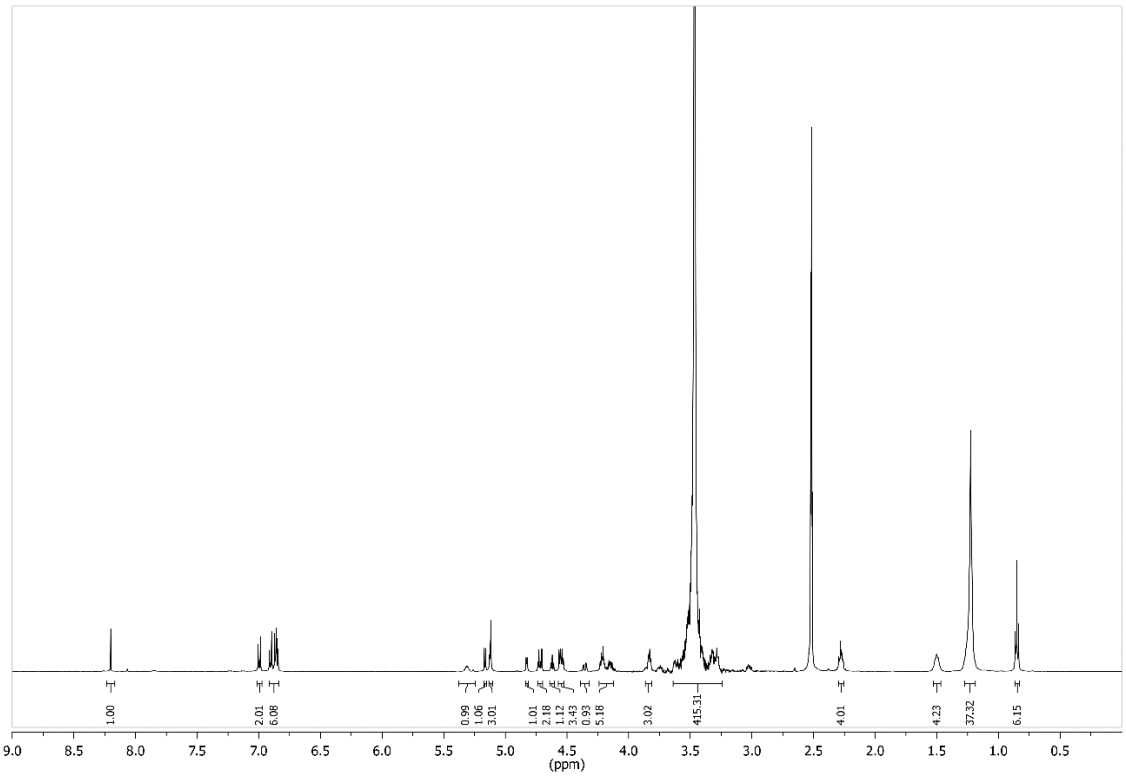

Figure 181: ^{1}H NMR spectrum of **22** (*Z*-isomer after irradiation with 365 nm) (500 MHz, DMSO-*d6*, 300 K).

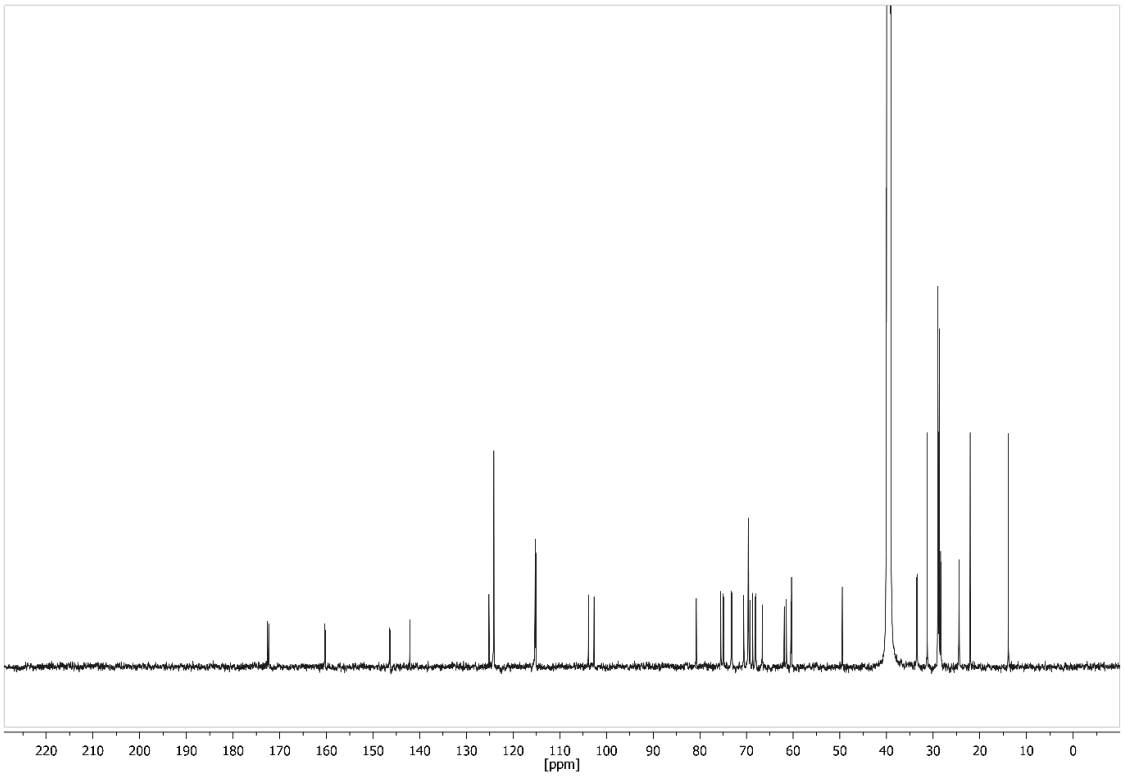

Figure 182: ^{13}C-NMR spectrum of **22** (150 MHz, DMSO-*d6*, 300 K)

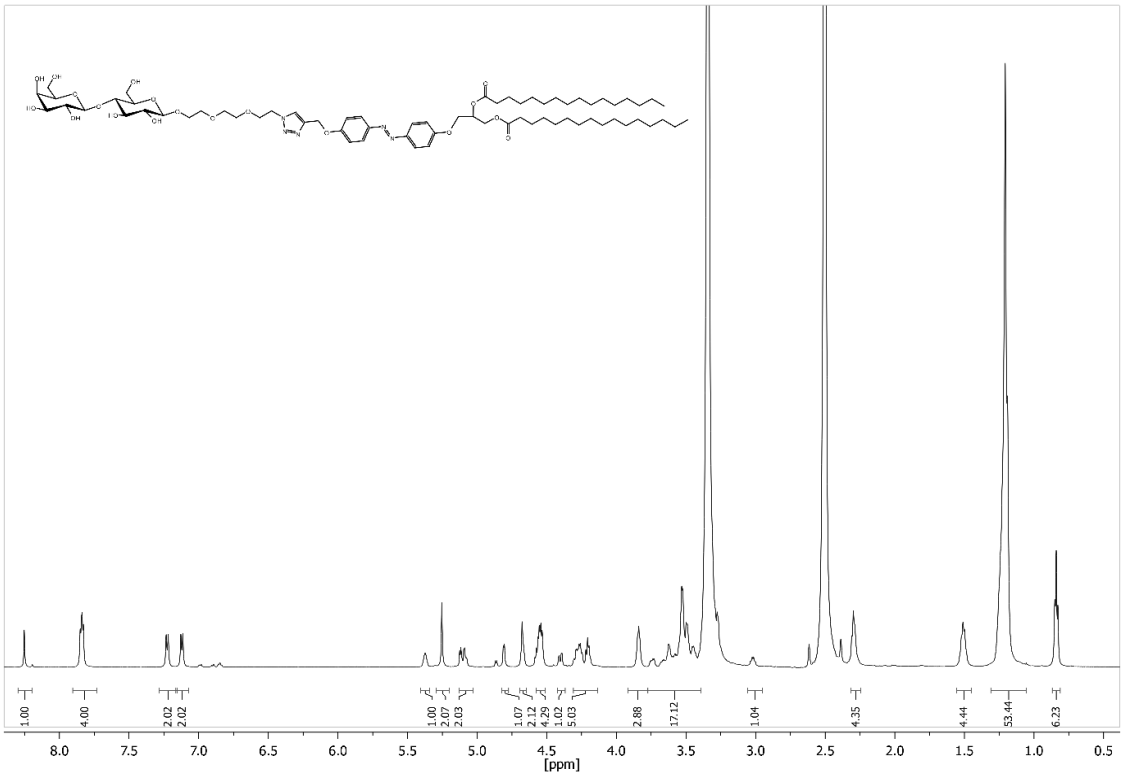

Figure 183: ^{1}H-NMR spectrum of **23** (600 MHz, DMSO-*d6*, 300 K).

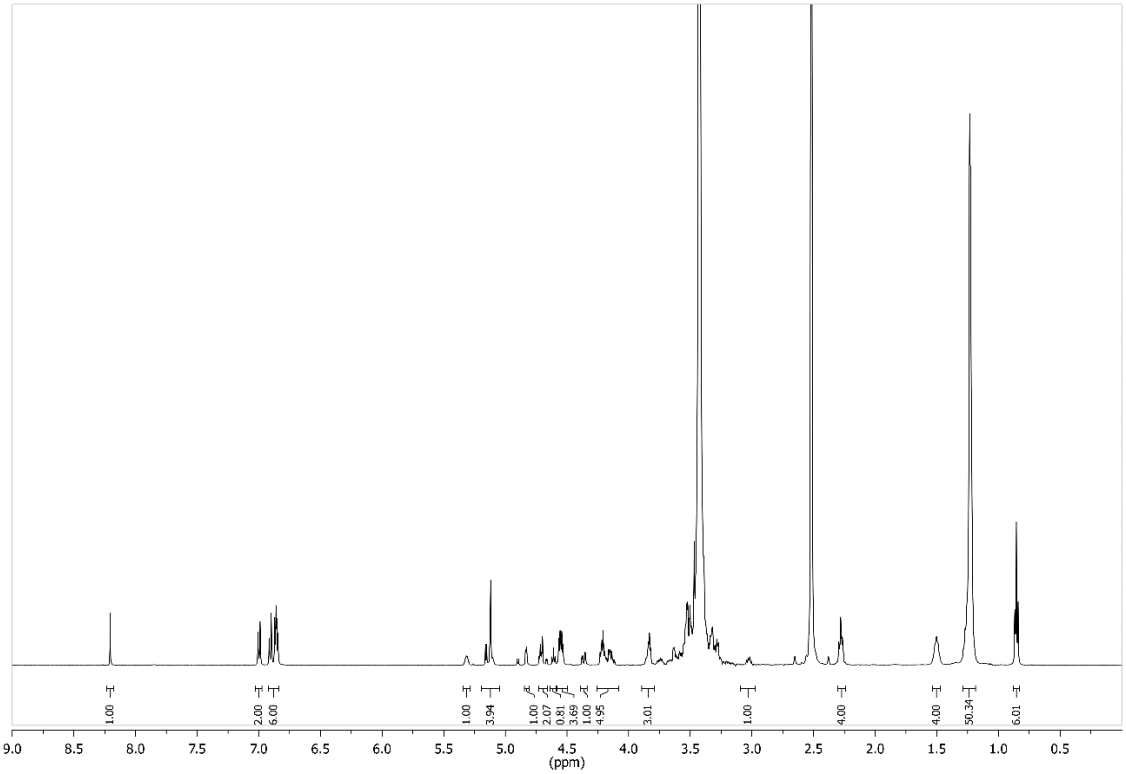

Figure 184: ^{1}H NMR spectrum of **23** (*Z*-isomer after irradiation with 365 nm) (500 MHz DMSO-*d6*, 300 K).

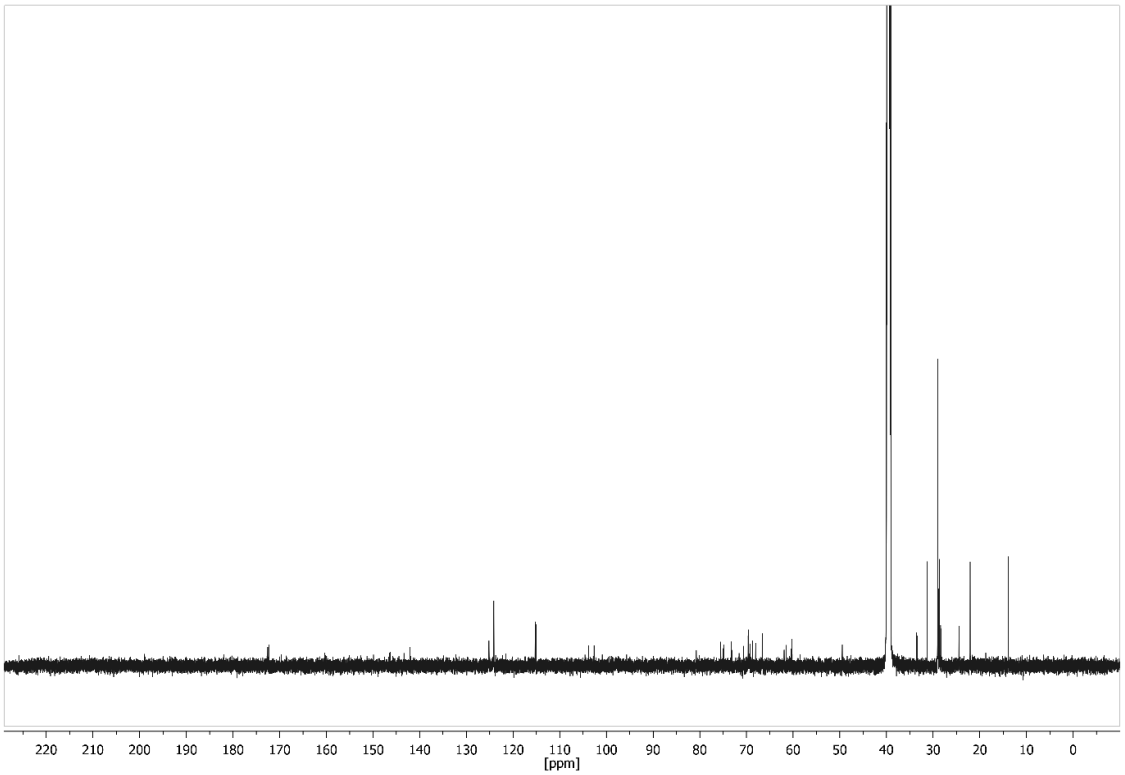

Figure 185: ^{13}C-NMR spectrum of **23** (150 MHz, DMSO-*d6*, 300 K)

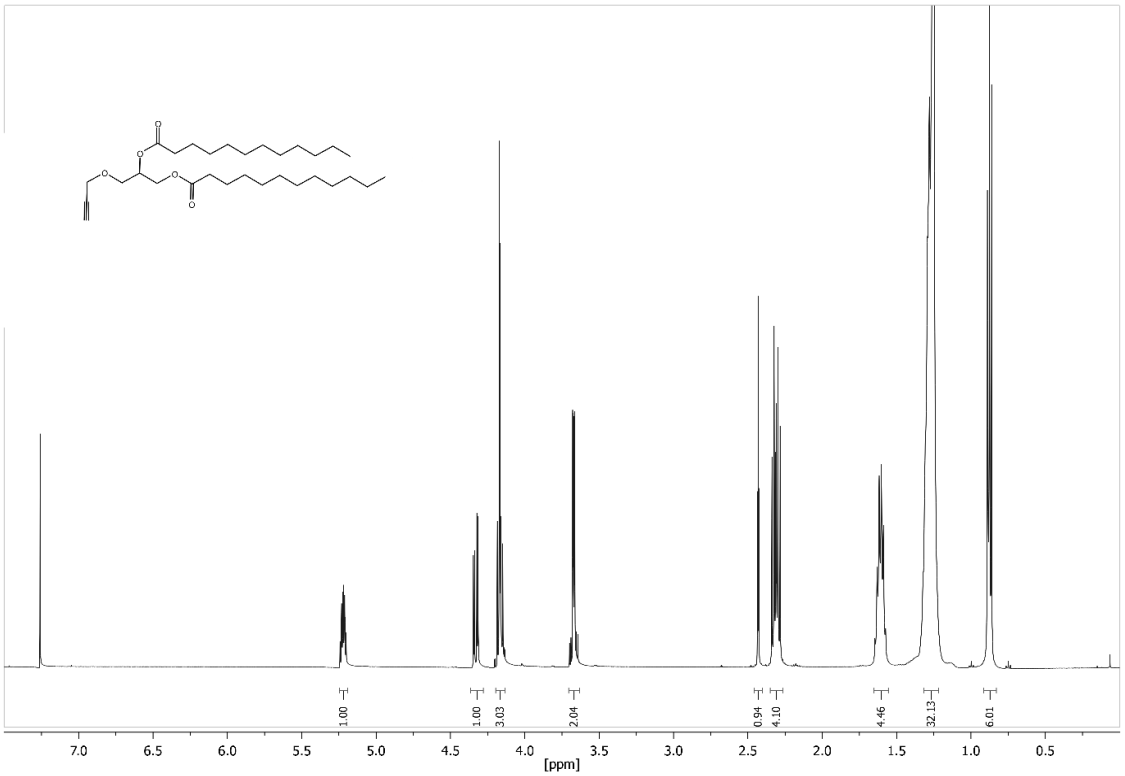

Figure 186: ^{1}H NMR spectrum of **27** (500 MHz, $CDCl_3$, 300 K).

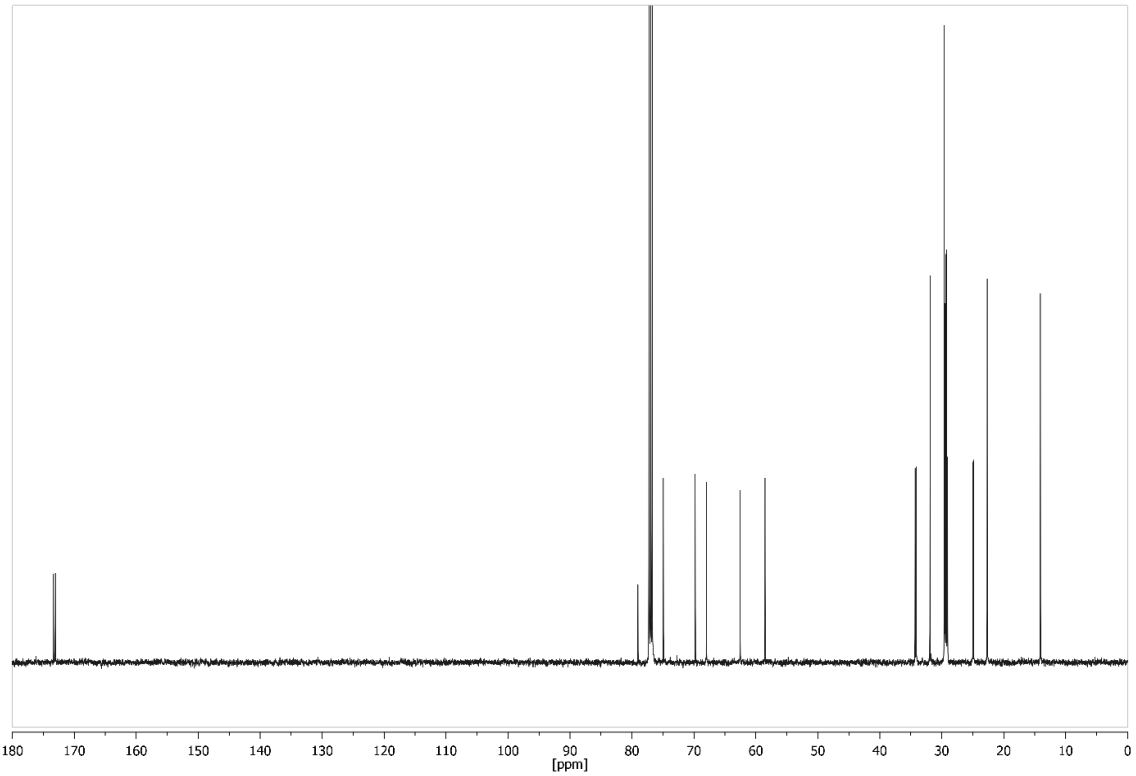

Figure 187: ^{13}C NMR spectrum of **27** (126 MHz, $CDCl_3$, 300 K).

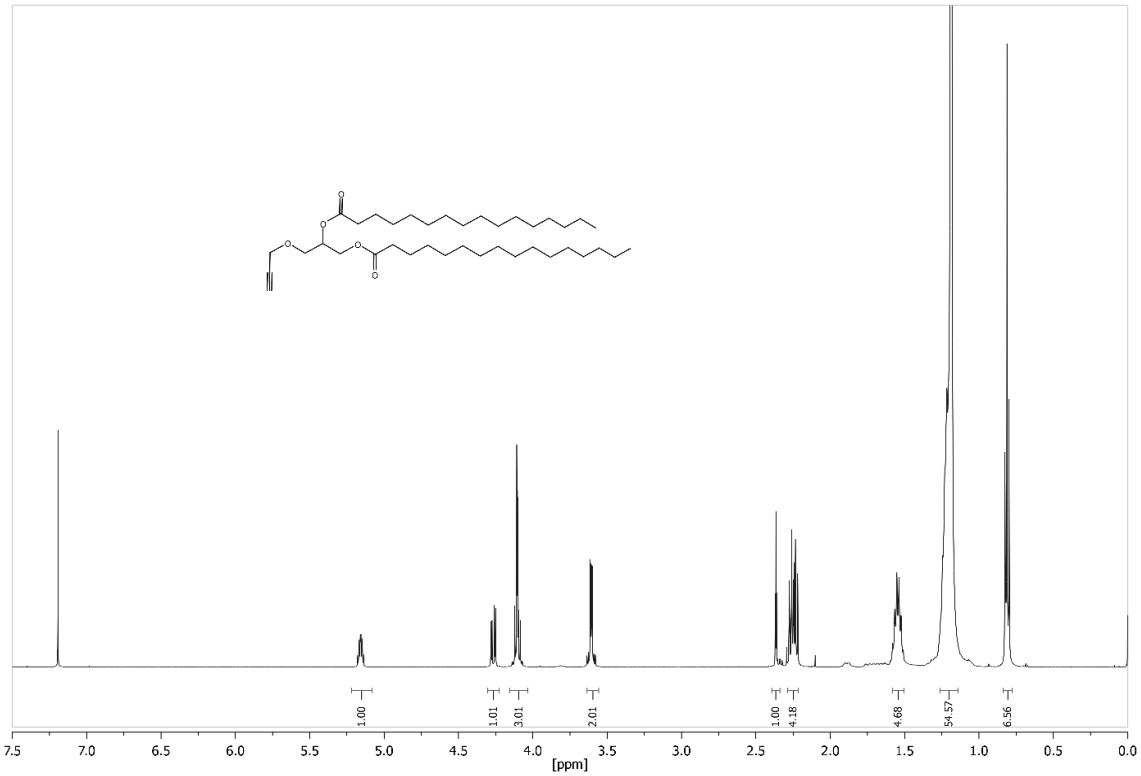

Figure 188: ^{1}H NMR spectrum of **28** (500 MHz, $CDCl_3$, 300 K).

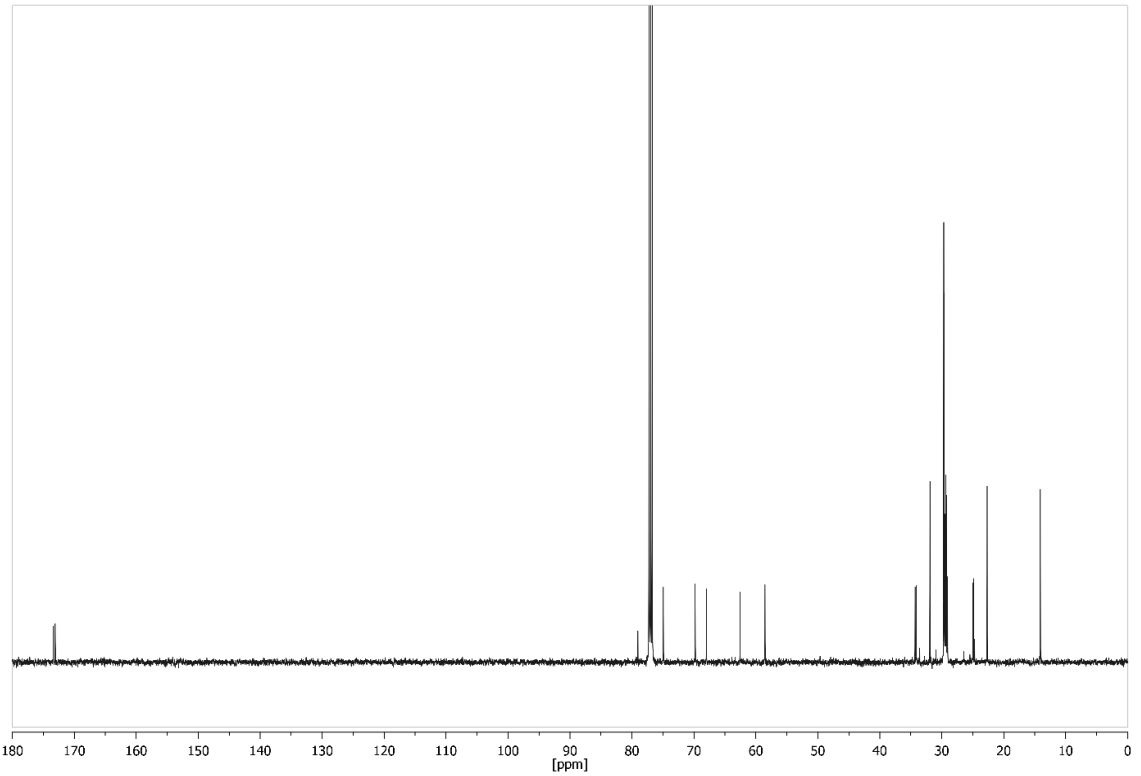

Figure 189: ^{13}C NMR spectrum of **28** (126 MHz, $CDCl_3$, 300 K).

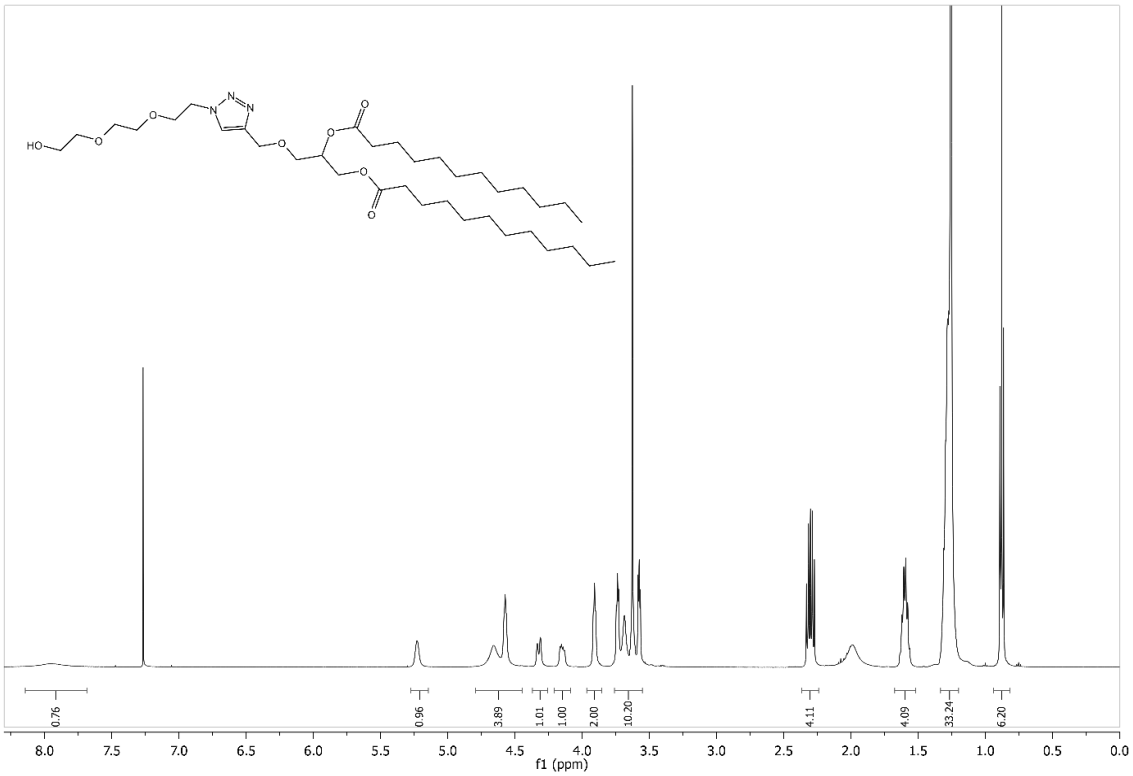

Figure 190: ^{1}H NMR spectrum of **29** (500 MHz, $CDCl_3$, 300 K).

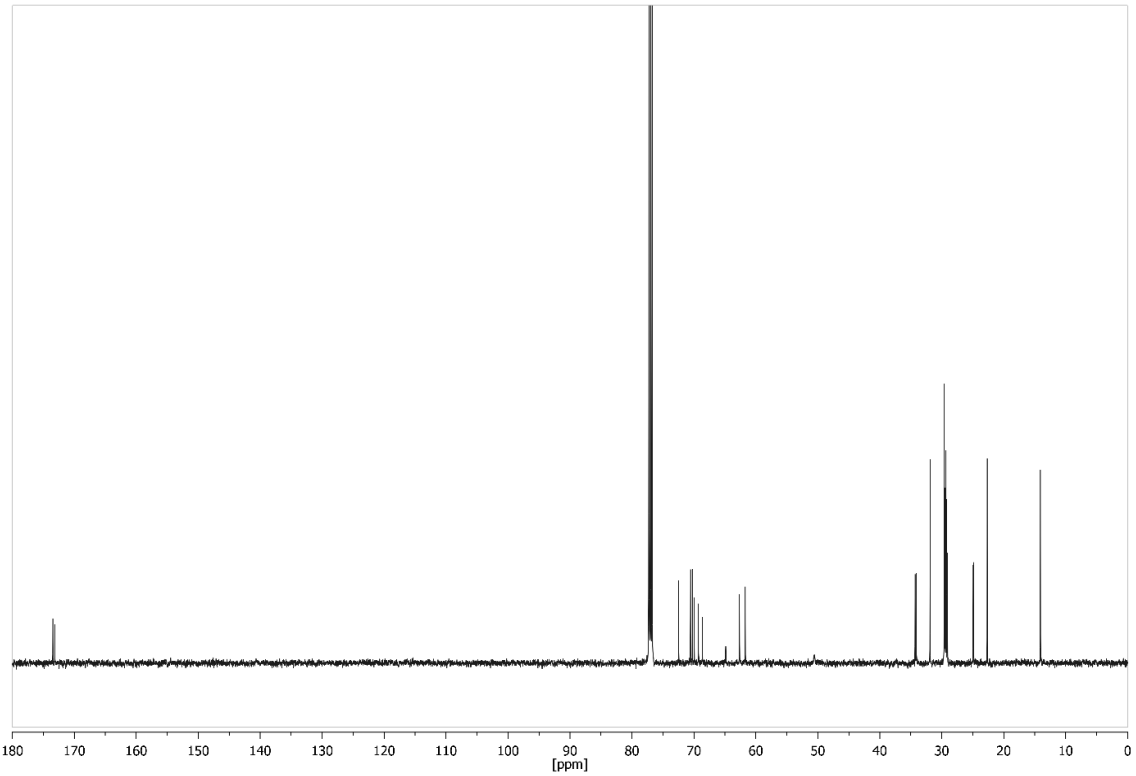

Figure 191: ^{13}C NMR spectrum of **29** (126 MHz, $CDCl_3$, 300 K).

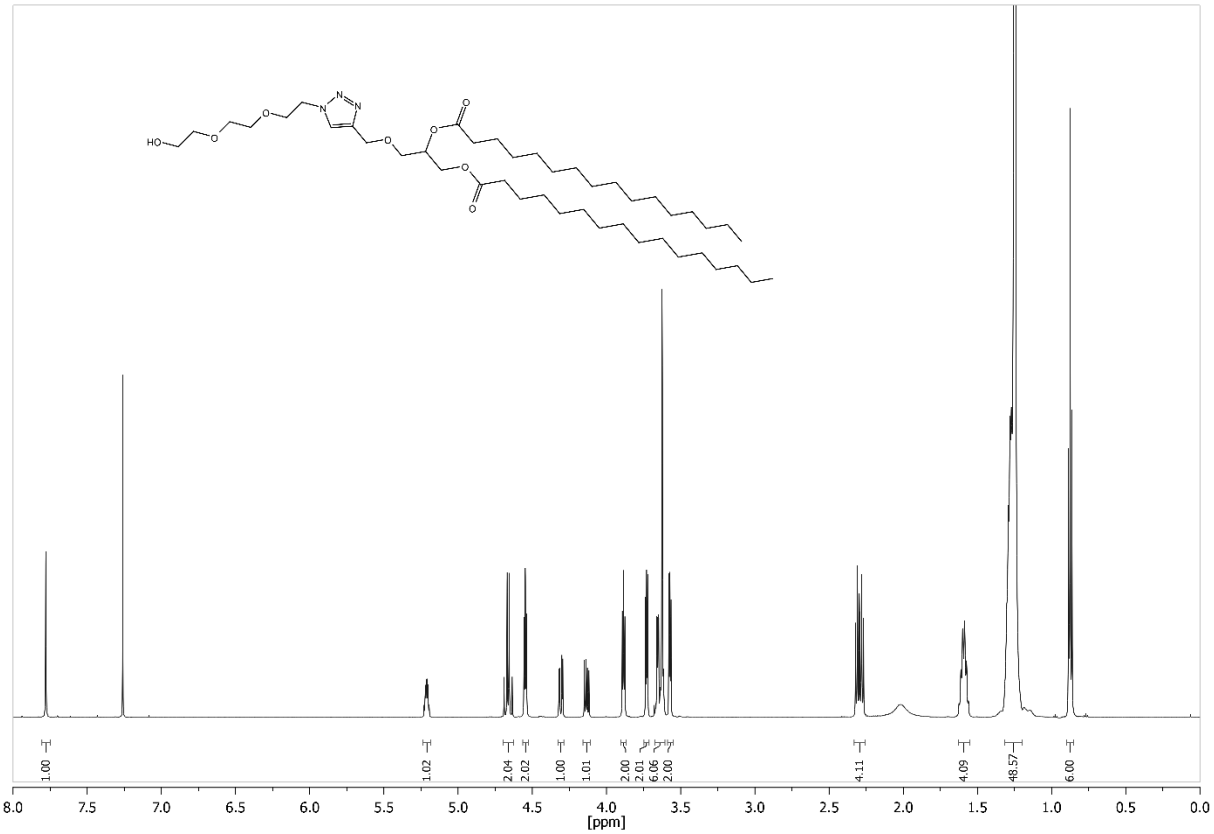

Figure 192: ^{1}H NMR spectrum of **30** (600 MHz, $CDCl_3$, 300 K).

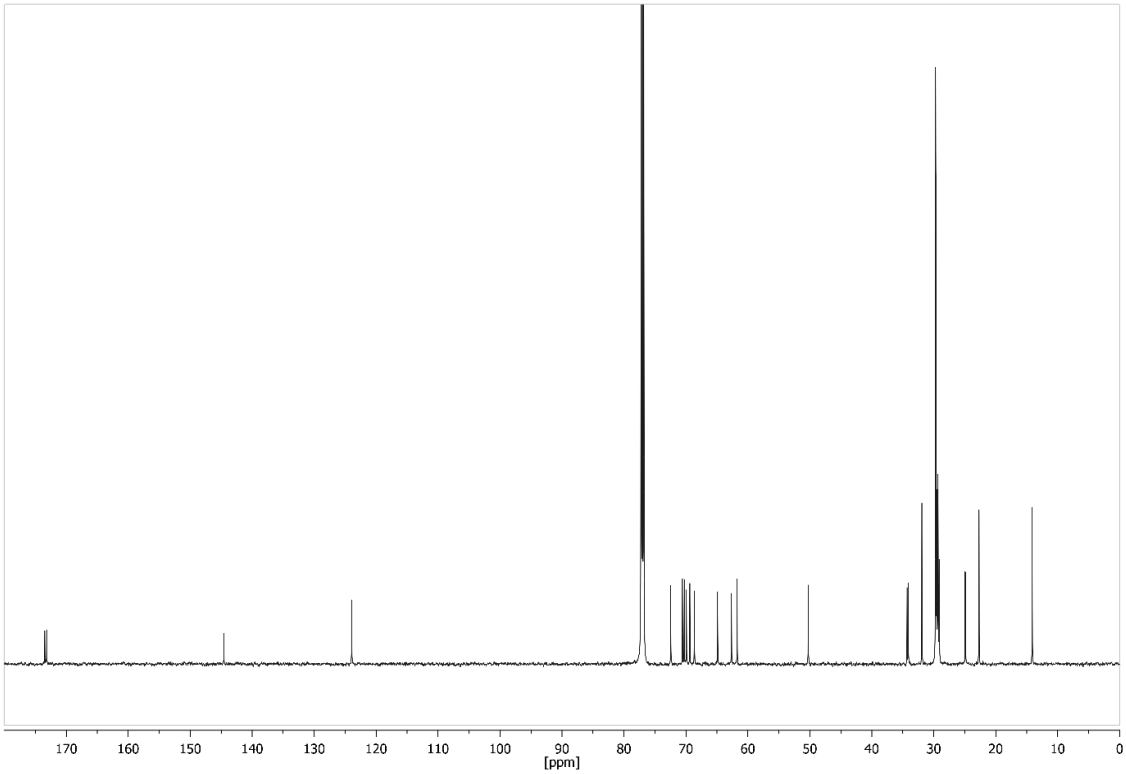

Figure 193: ^{13}C NMR spectrum of **30** (126 MHz, $CDCl_3$, 300 K).

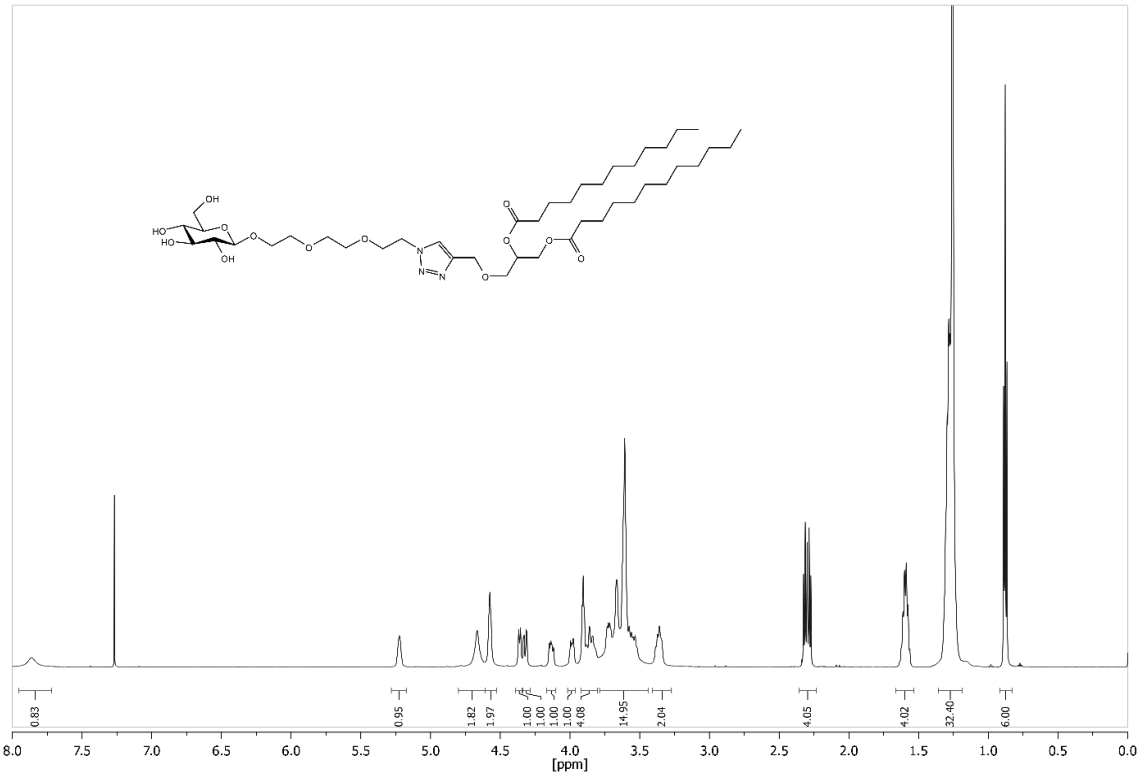

Figure 194: ^{1}H NMR spectrum of **31** (500 MHz, $CDCl_3$, 300 K).

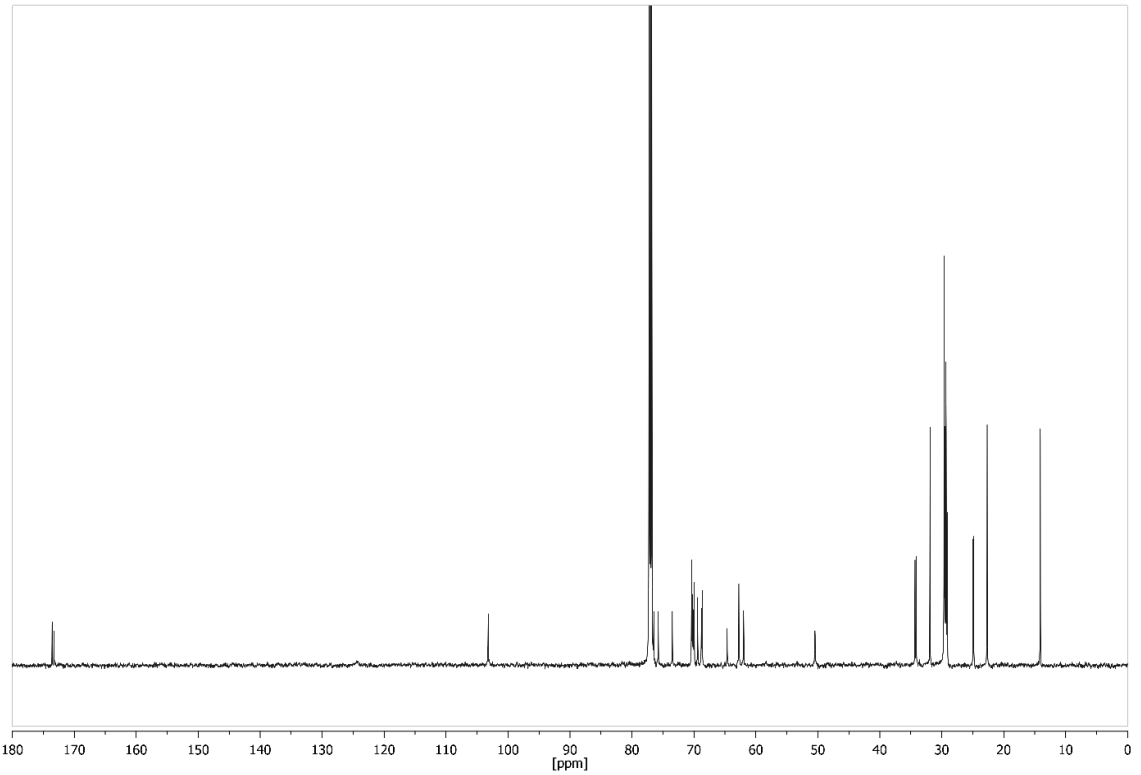

Figure 195: ^{13}C NMR spectrum of **31** (126 MHz, $CDCl_3$, 300 K).

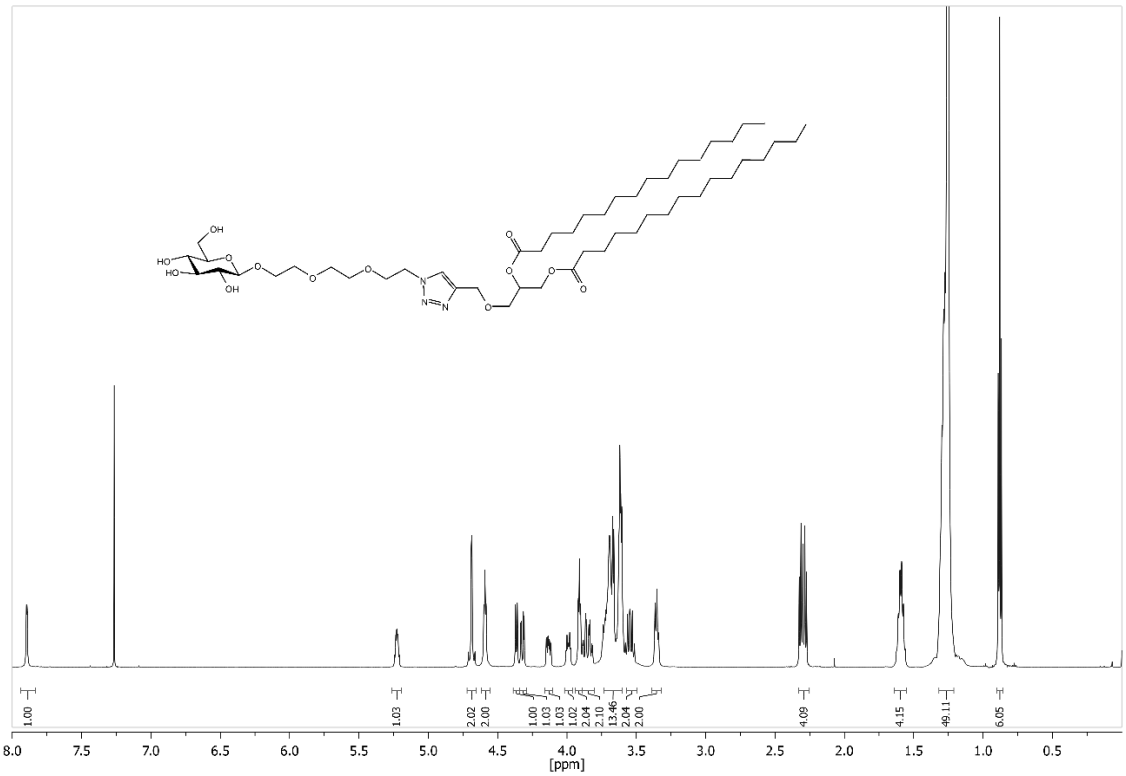

Figure 196: ^{1}H NMR spectrum of **32** (500 MHz, $CDCl_3$, 300 K).

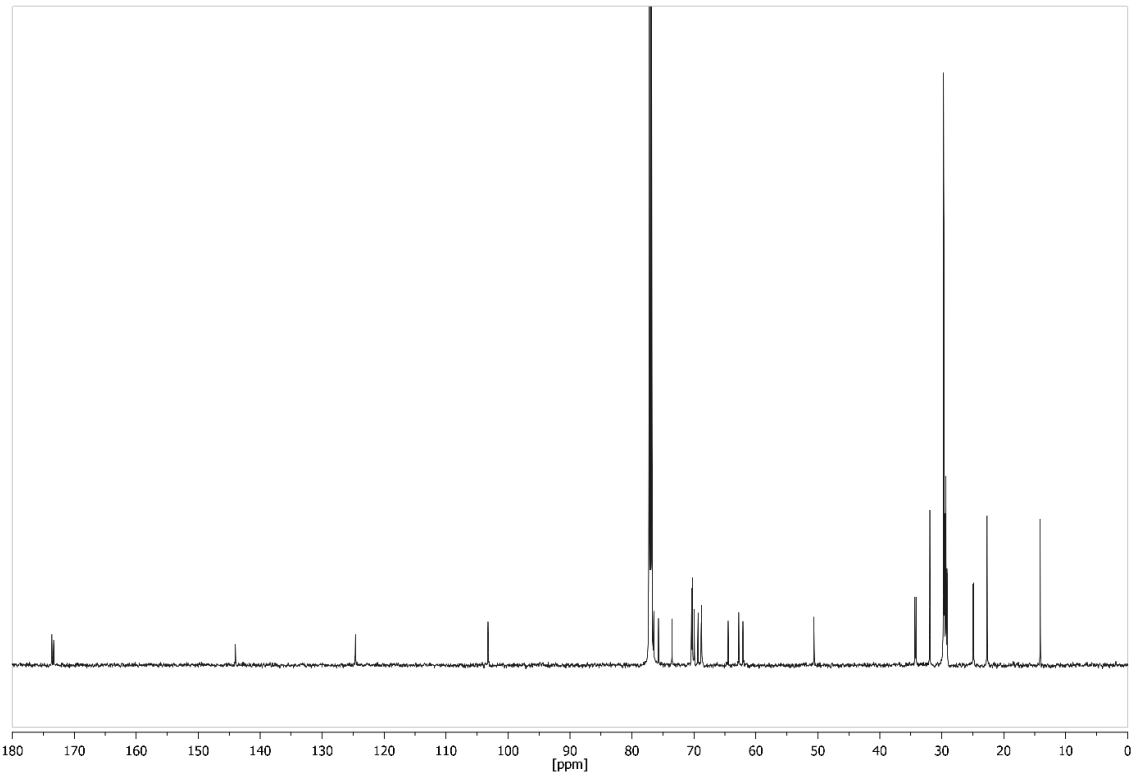

Figure 197: ^{13}C NMR spectrum of **32** (126 MHz, $CDCl_3$, 300 K).

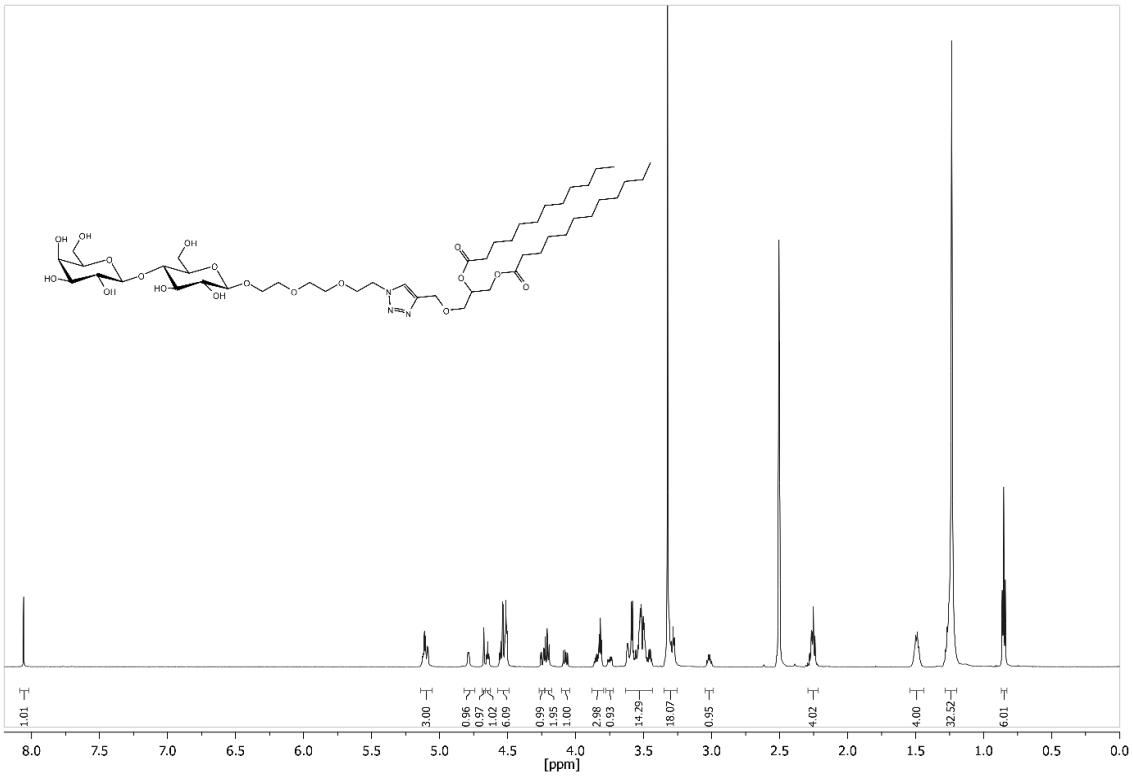

Figure 198: ^{1}H NMR spectrum of **33** (600 MHz, DMSO-*d6*, 300 K).

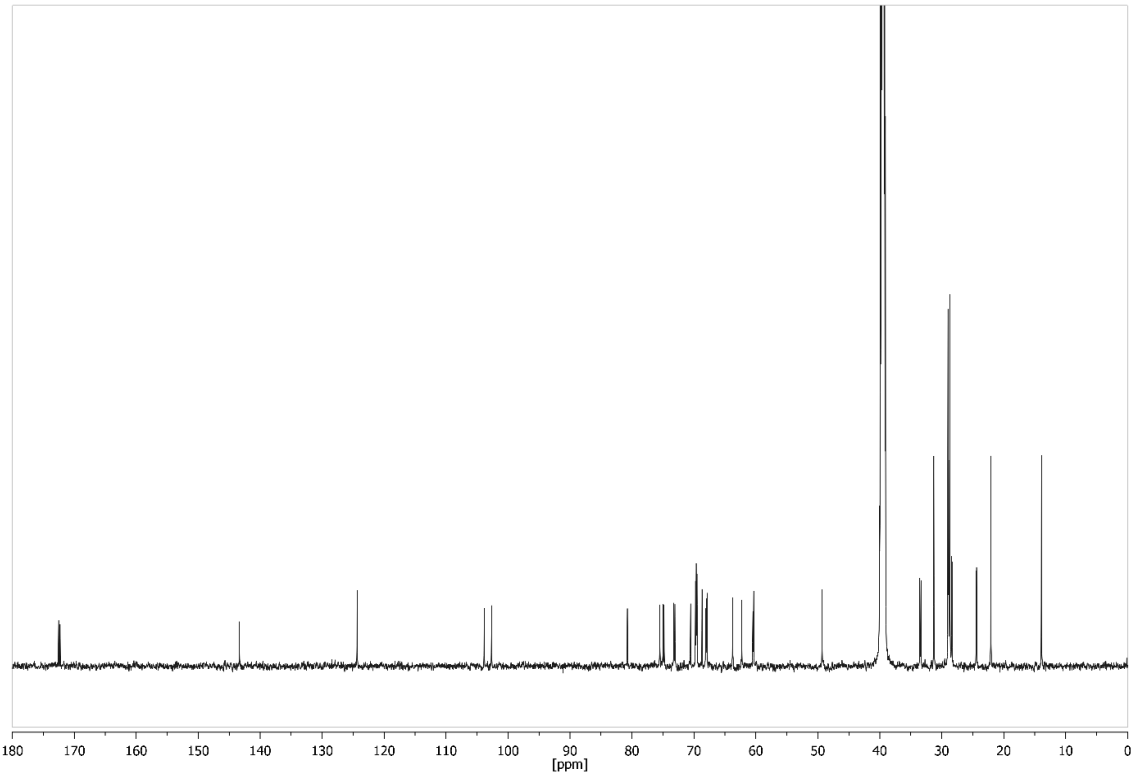

Figure 199: ^{13}C NMR spectrum of **33** (150 MHz, DMSO-*d6*, 300 K).

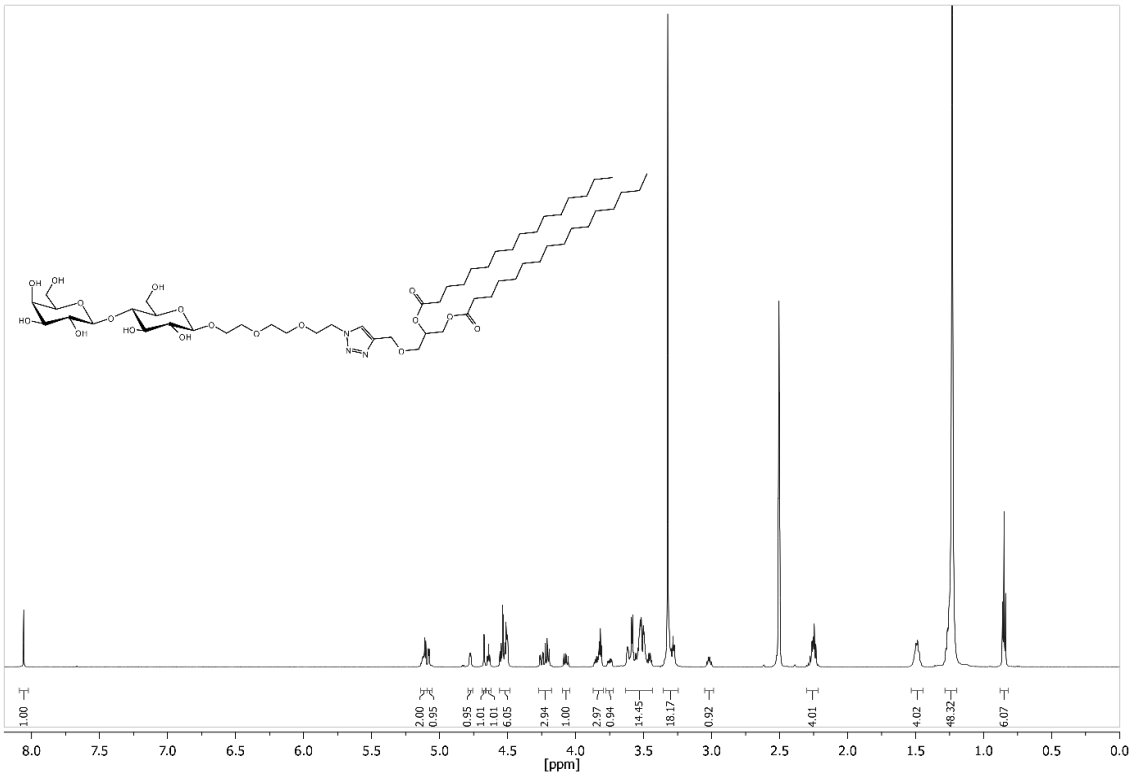

Figure 200: ^{1}H NMR spectrum of **34** (600 MHz, DMSO-*d6*, 300 K).

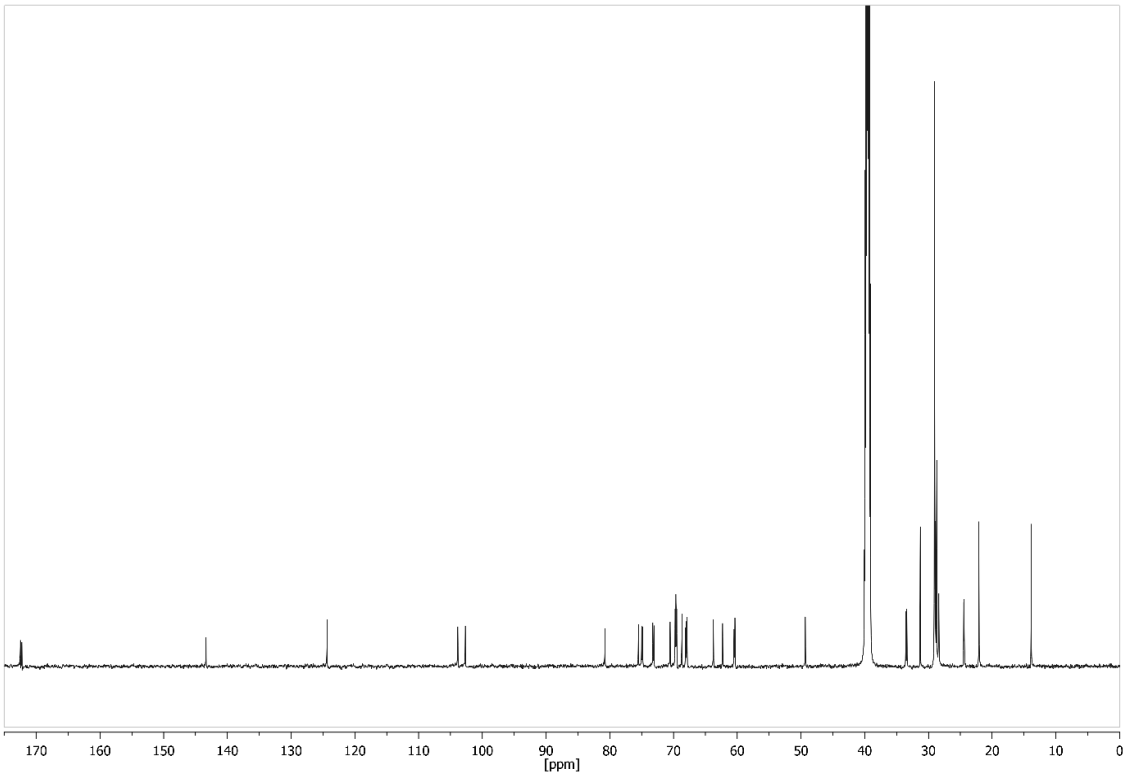

Figure 201: ^{13}C NMR spectrum of **34** (150 MHz, DMSO-*d6*, 300 K).

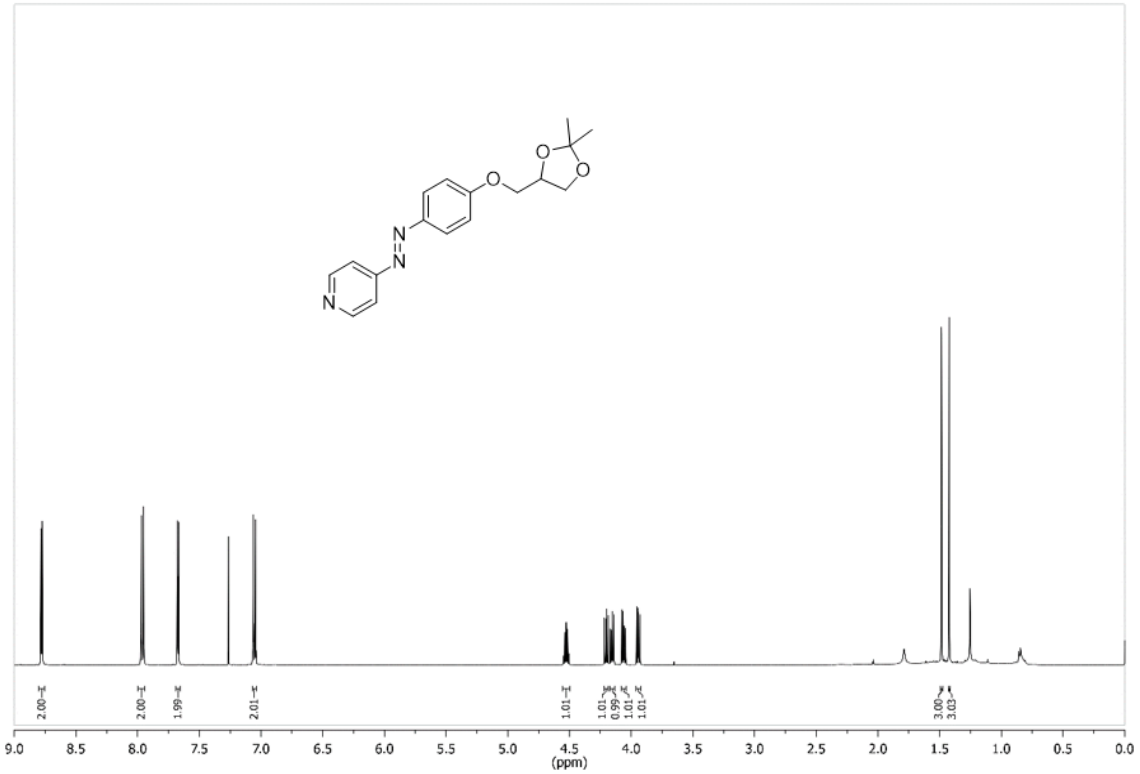

Figure 202: ^{1}H NMR spectrum of **36** (500 MHz, $CDCl_3$, 300 K, TMS).

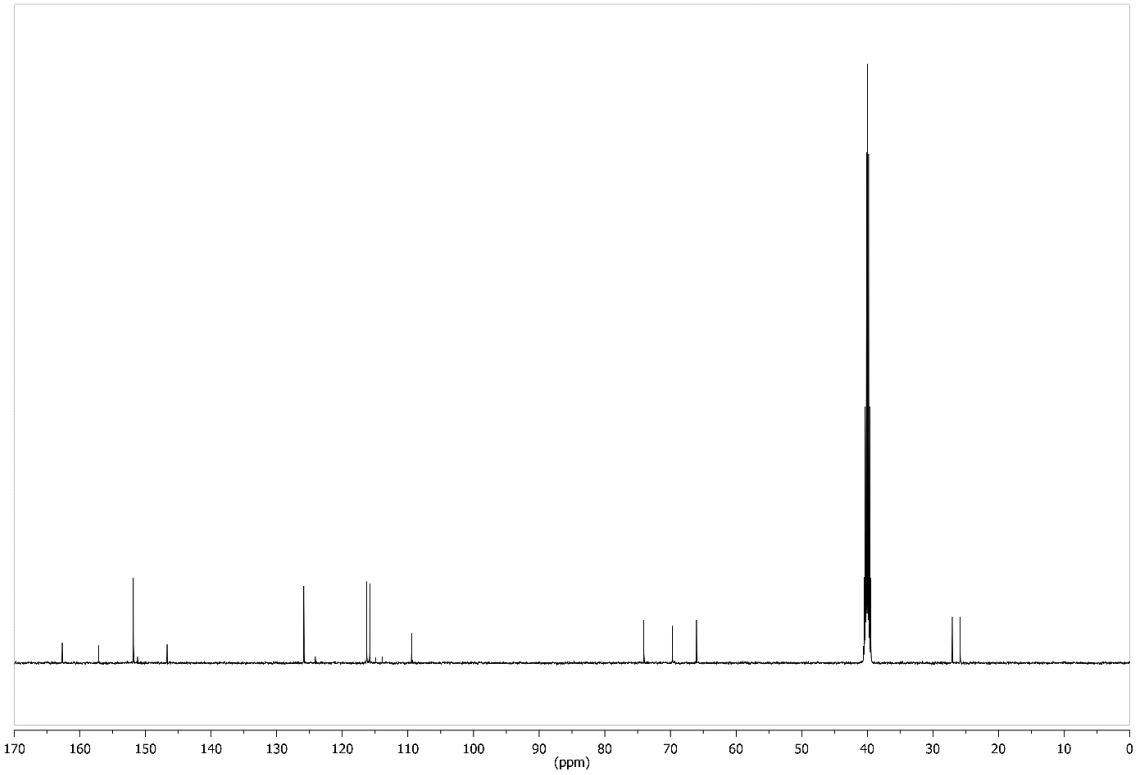

Figure 203: ^{13}C NMR spectrum of **36** (126 MHz, DMSO-*d6*, 300 K).

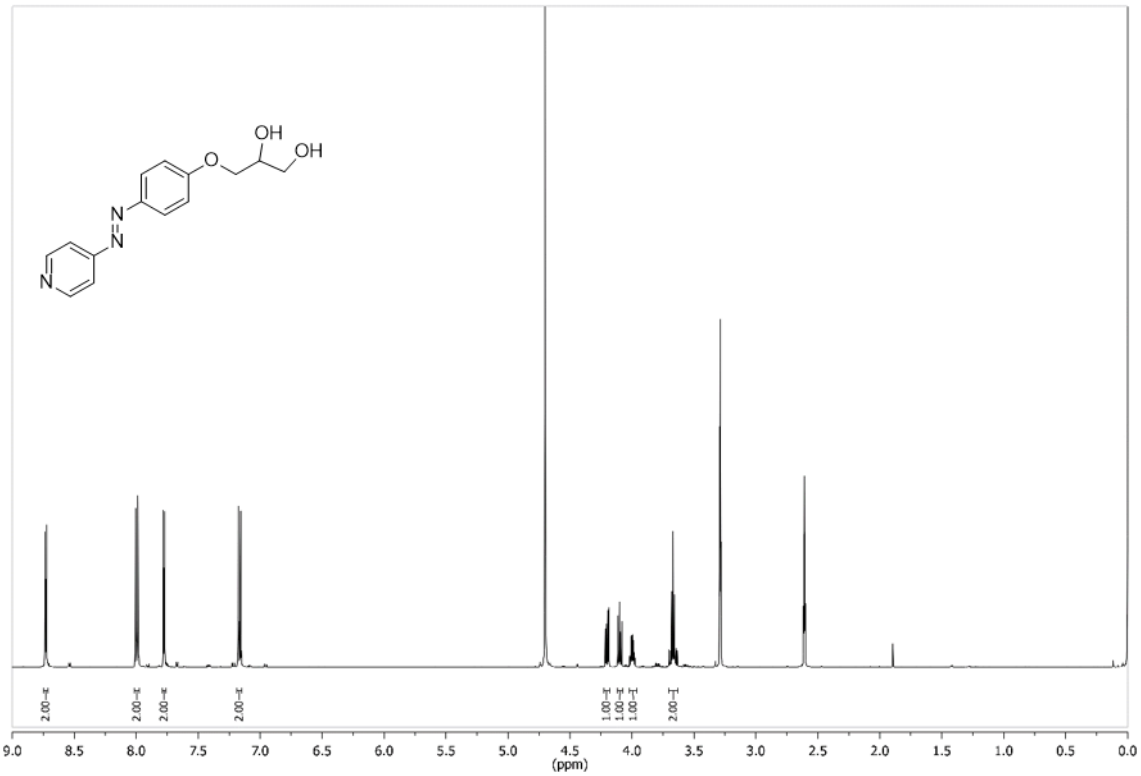

Figure 204: ^{1}H NMR spectrum of **37** (500 MHz, MeOD/ DMSO-*d6*, 300 K, TMS).

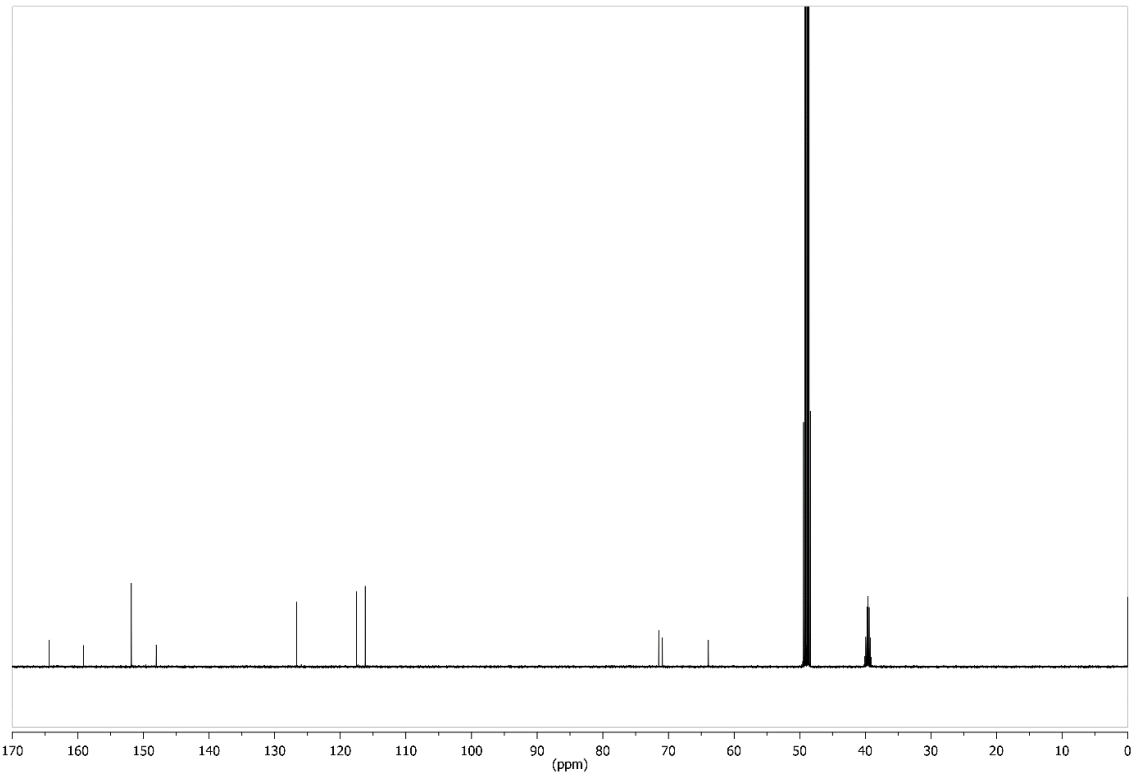

Figure 205: ^{13}C NMR spectrum of **37** (126 MHz, MeOD/ DMSO-*d6*, 300 K, TMS).

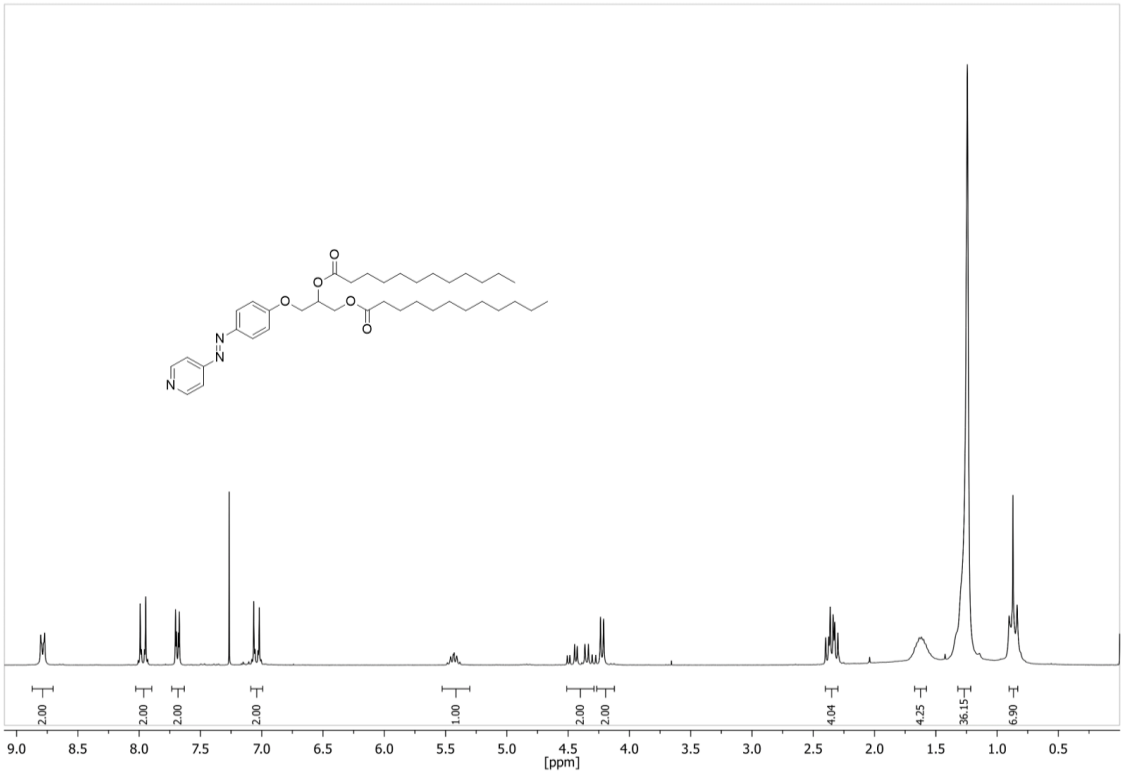

Figure 206: ^{1}H NMR spectrum of **38** (200 MHz, $CDCl_3$, 300 K, TMS).

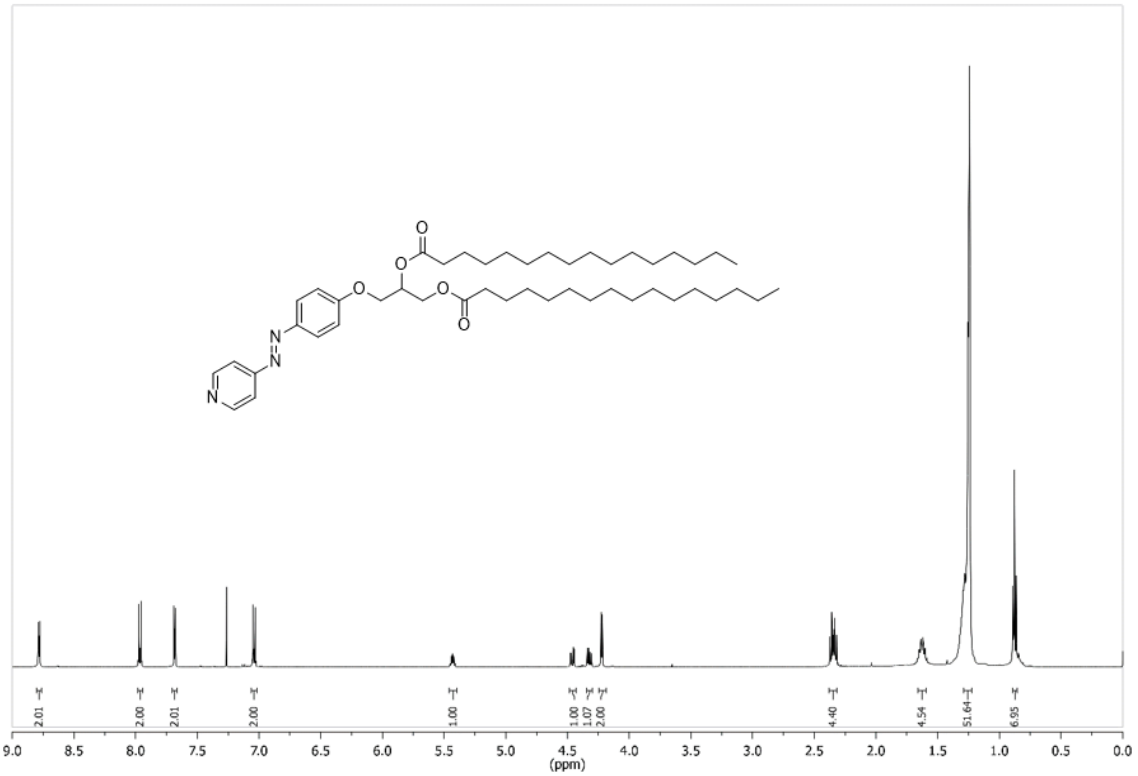

Figure 207: ^{1}H NMR spectrum of **39** (500 MHz, $CDCl_3$, 300 K, TMS).

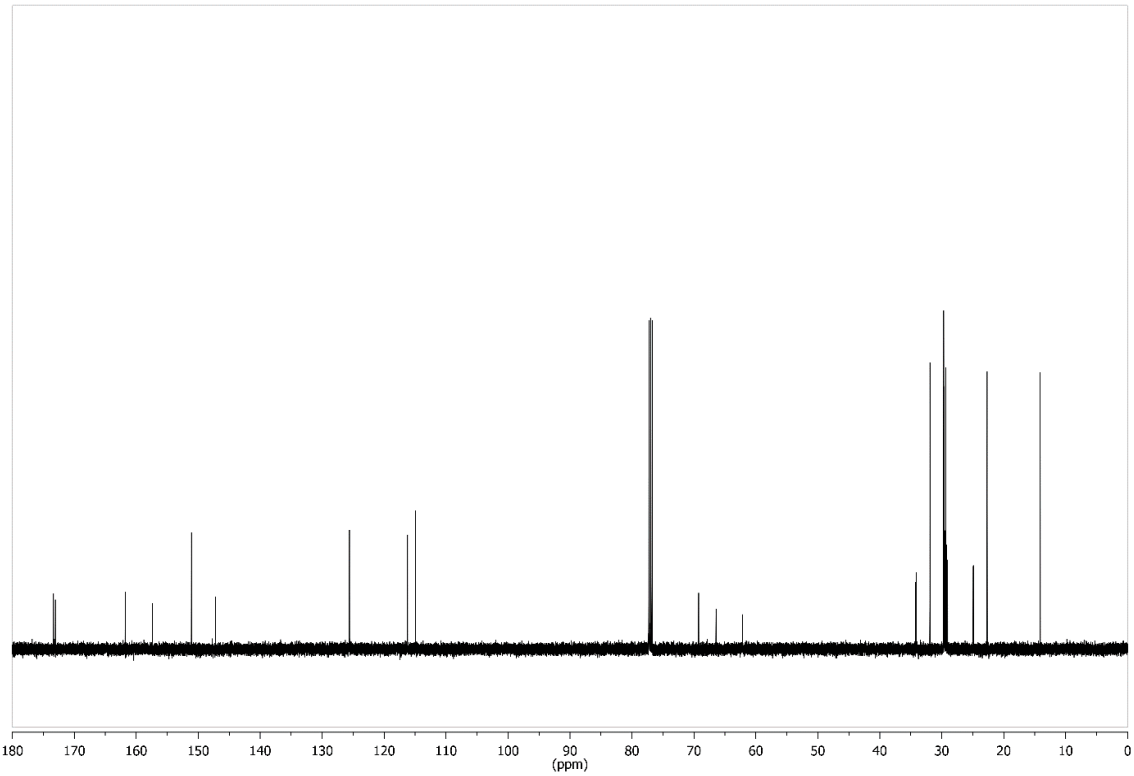

Figure 208: ^{13}C NMR spectrum of **39** (126 MHz, $CDCl_3$, 300 K, TMS).

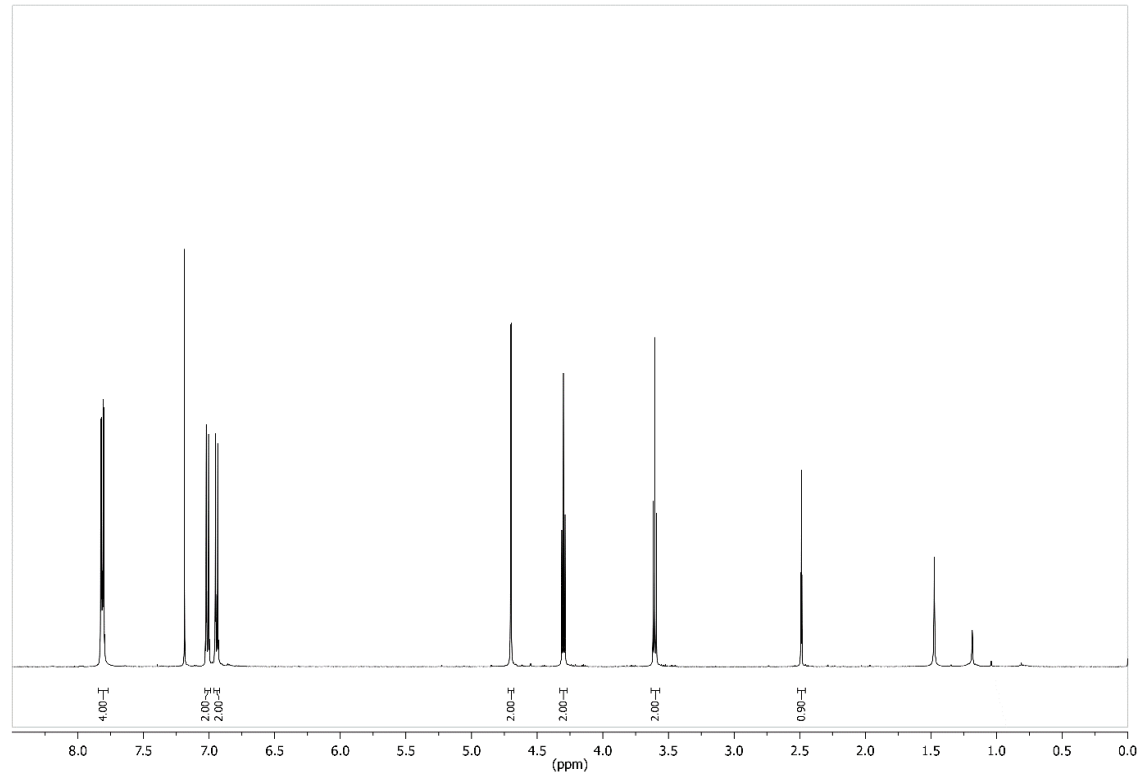

Figure 209: ^{1}H NMR spectrum of **40** (500 MHz, $CDCl_3$, 300 K, TMS).

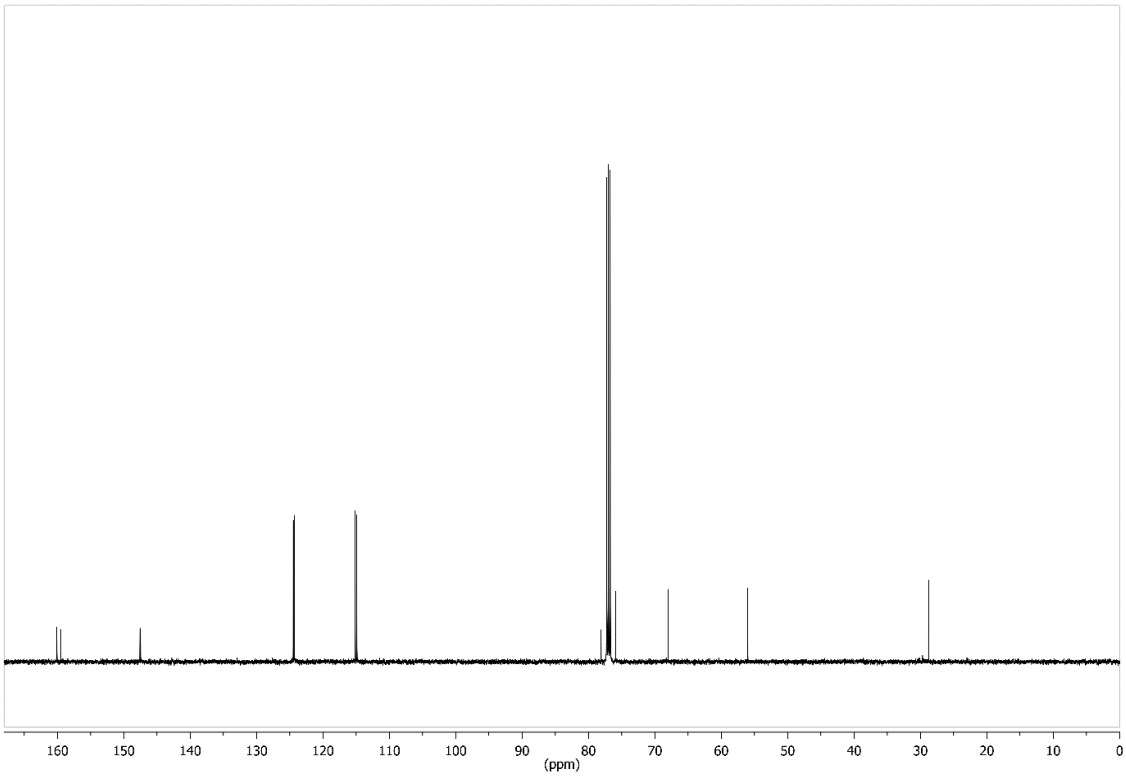

Figure 210: ^{13}C NMR spectrum of **40** (126 MHz, $CDCl_3$, 300 K, TMS).

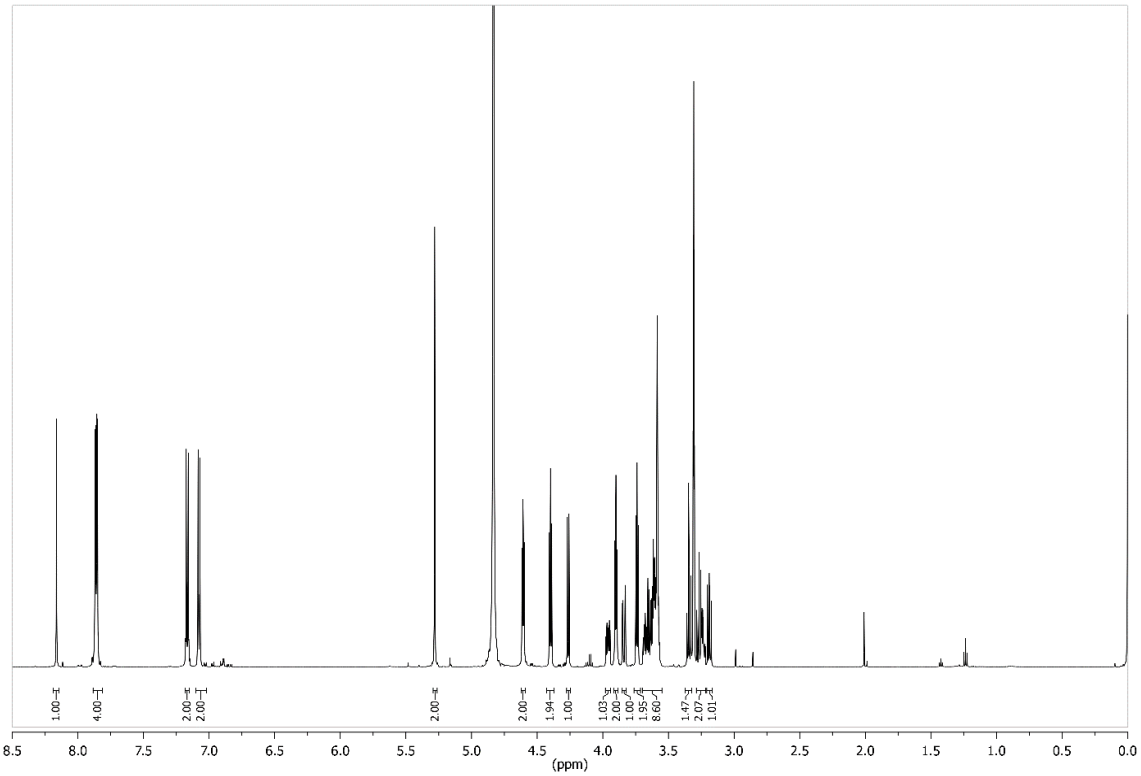

Figure 211: ^{1}H NMR spectrum of **41** (600 MHz, MeOD, 300 K, TMS).

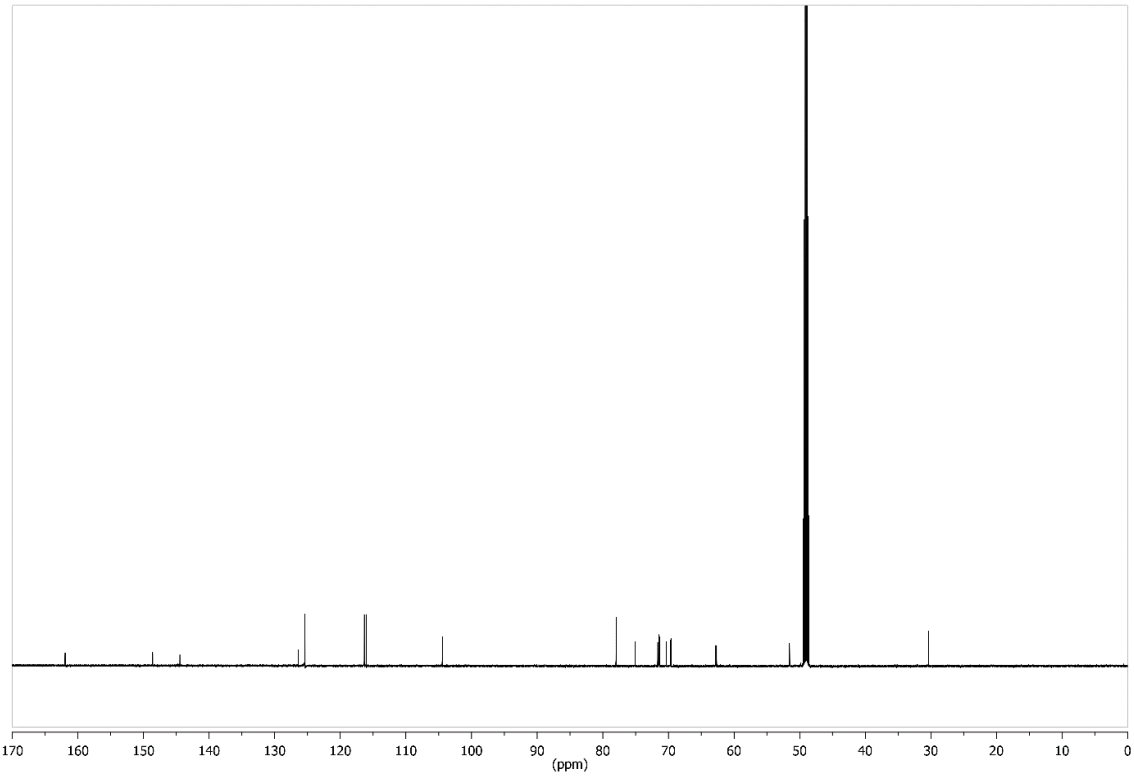

Figure 212: ^{13}C NMR spectrum of **41** (151 MHz, MeOD, 300 K, TMS).

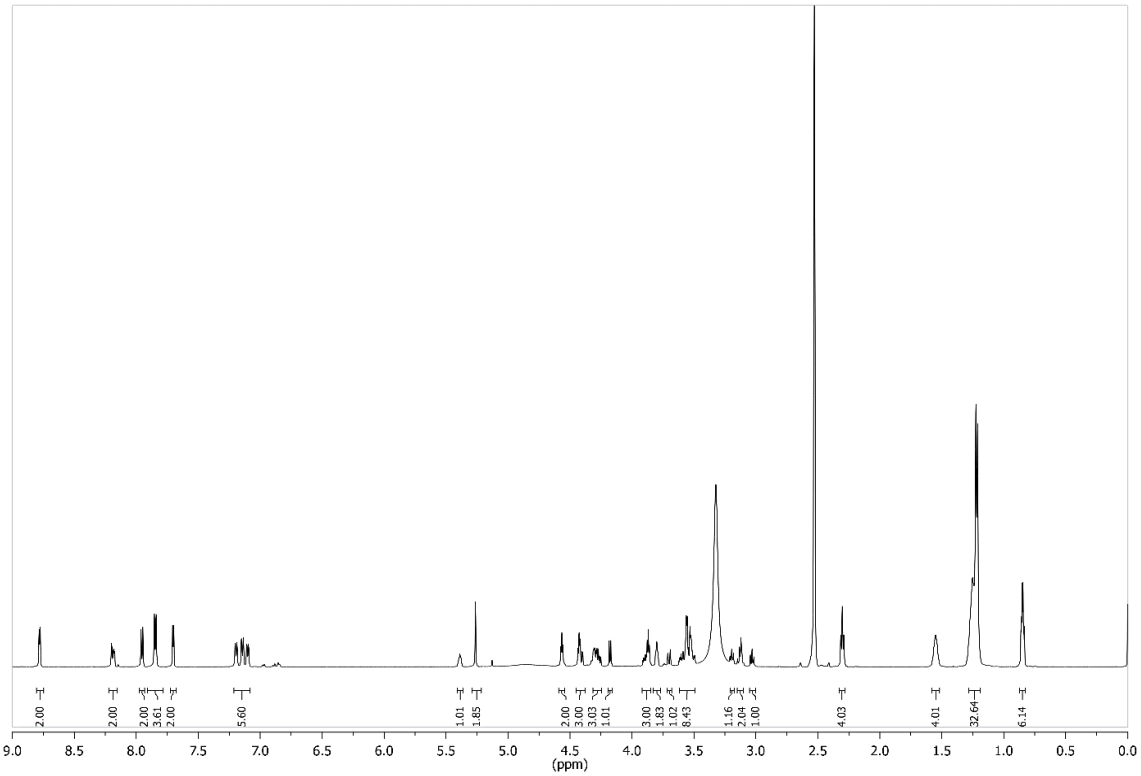

Figure 213: ^{1}H NMR spectrum of **42** (600 MHz, $CDCl_3$/ DMSO-*d6*, 300 K, TMS).

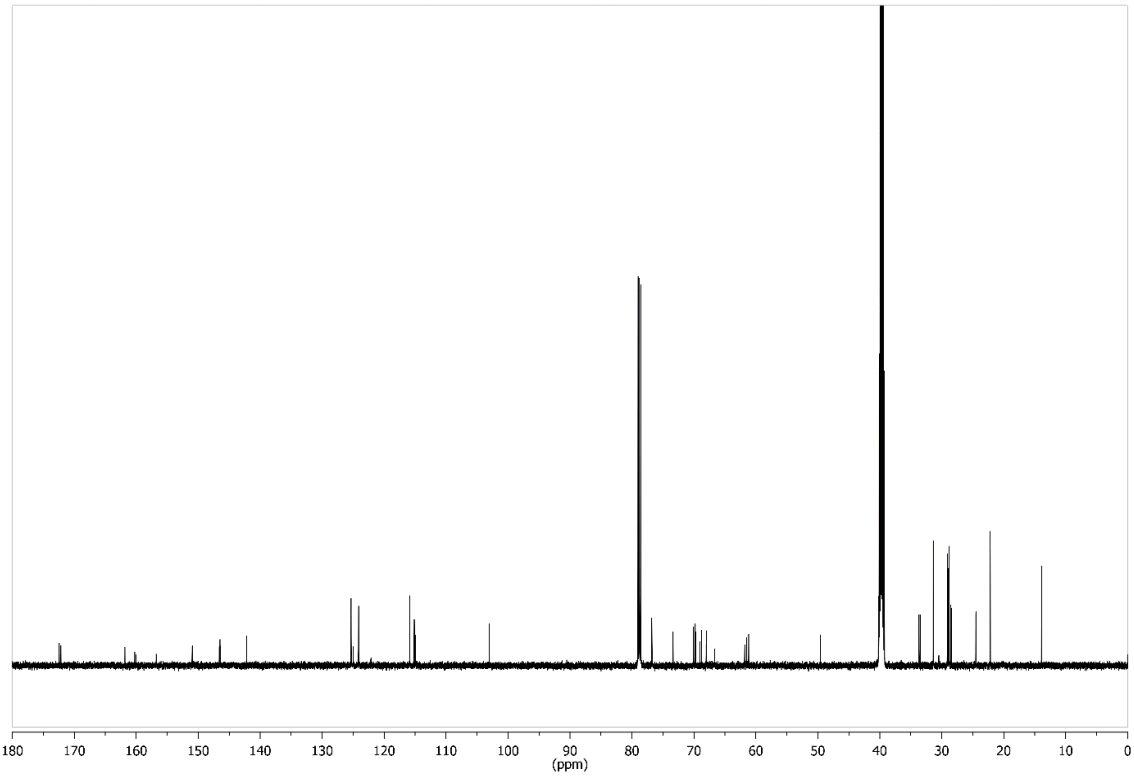

Figure 214: ^{13}C NMR spectrum of **42** (151 MHz, $CDCl_3$/ DMSO-*d6*, 300 K, TMS).

8.3 Supporting information for chapter 4.1: Simple fabrication of glycosylated surfaces for bacterial adhesion studies by using pentafluorophenylazides as linkers

8.3.1 Synthesis of PFPA linker and glycosides

4-Azido-2,3,5,6-Tetrafluorobenzoic acid methyl ester 2[415]

Sodium azide (1.38 g, 21.2 mmol) was added to a solution of methyl pentafluorobenzoate **1** (5.16 g, 22.8 mmol) in H_2O (50 mL) and acetone (120 mL). The mixture was stirred 8 h under reflux and additional 16 h at room temperature. After the addition of water (100 mL) the mixture was extracted with ethyl acetate (3 x 100 mL). The combined organic layers were dried over $MgSO_4$, filtered and the solvent removed under reduced pressure. Compound **2** was obtained as a coloress solid.

Yield: 5.42 g (21.8 mmol, 95 %); lit.[415]: 87 %;

Melting point 56 °C; lit.[415]: 54-55 °C;

^{1}H NMR (500 MHz, $CDCl_3$, 300 K, TMS): δ = 3.97 (s, 3H, $COCH_3$) ppm;

^{19}F-NMR: (470.6 MHz, $CDCl_3$, 300 K): δ = -138.66 (m, 2F), -150.93 (m, 2F) ppm;

^{13}C-NMR: (126 MHz, $CDCl_3$, 300 K): δ = 160.0 (C=O), 145.4 (Ar-CF), 140.7 (Ar-CF), 123.4 (C(C=O)), 107.8 (CN_3), 53.3 (CH_3);

IR (ATR): ṽ = 2972, 2130, 1732, 1645, 1479, 1434, 1259, 991, 758 cm^{-1};

EI-MS: *m/z* = 249.016, $[M]^+$; 221.009, $[M\text{-}N_2]^+$; 161.996 $[M\text{-}N_2\text{-}COOCH_3]^+$, (calc. 249.016 for $C_8H_3F_4N_3O_2$).

4-Azido-2,3,5,6-Tetrafluorobenzoic acid 3[415]

Methyl ester **2** (4.60 g, 18.5 mmol) was dissolved in methanol (60 mL) and water (6 mL). After addition of a sodium hydroxide solution (20 %, 5.4 mL) the mixture was stirred at room temperature for 16 h. The mixture was then acidified with 2N hydrochloric acid until pH 1 was reached. The mixture was extracted with chloroform (3 x 90 mL) and the combined organic layers were dried over $MgSO_4$. The solvent was removed under reduced pressure to obtain compound **3** as a colourless solid.

Yield: 4.13 g (17.6 mmol, 95 %); lit.:[415] 95 %;

Melting point 142 °C; lit.[415]: 140-141 °C;

^{1}H-NMR: (200 MHz, $CDCl_3$, 300 K, TMS): δ = 8.57 (s (br), 1H, COOH) ppm;

^{19}F-NMR: (470.6 MHz, $CDCl_3$, 300 K): δ = -137.10 (m, 2F), -150.74 (m, 2F) ppm;

^{13}C-NMR: (126 MHz, $CDCl_3$, 300 K): δ = 164.1 (C=O), 146.0 (Ar-CF), 140.6 (Ar-CF), 124.8 (C(C=O)), 106.1 (CN_3);

IR (ATR): ṽ = 2835, 2128, 1699, 1642, 1481, 1420, 1259, 991, 720, 461 cm^{-1};

EI-MS: *m/z* = 235.917, $[M+H]^+$; (calc. 235.000 for $C_7HF_4N_3O_2$).

4-Azido-2,3,5,6-Tetrafluorobenzoic acid *N*-hydroxysuccinimidyl ester 4[271]

Benzoic acid **3** (4.00 g, 17.0 mmol) and *N*-hydroxysuccinimide (1.96 g, 17.0 mmol) were dissolved in DCM (60 mL). DCC (3.58 g, 17.3 mmol) was added dropwise before the mixture was stirred at room temperature for 19 h. Finally the mixture was filtered before the solvent was removed under reduced pressure to obtain compound **4** as a colourless solid.

Yield: 5.61 g (16.9 mmol, 99 %); lit.:[416] 99 %;

Melting point 101 °C; lit. [415]: 103-104 °C;

^{1}H-NMR: (500 MHz, $CDCl_3$, 300 K, TMS): δ = 2.91 (s, 4H, $COCH_2CH_2$) ppm;

^{19}F-NMR: (470.6 MHz, $CDCl_3$, 300 K): δ = -133.53 (m, 2F), -149.84 (m, 2F) ppm;

^{13}C-NMR: (126 MHz, $CDCl_3$, 300 K): δ = 168.3 (C=O), 146.3 (Ar-CF), 140.5 (Ar-CF), 126.3 (C(C=O)), 102.0 (CN_3), 25.7 (CH_2);

IR (ATR): ṽ = 2127, 1738, 1646, 1485, 1417, 1252, 1134, 1069, 993, 894, 640 cm^{-1};

EI-MS: *m/z* = 332.016, $[M]^+$; 218.002, $[M-C_4H_4NO_3]^+$, (calc. 332.017 for $C_{11}H_4F_4N_4O_4$).

(2,2-Dimethylpropionamide)-2-[2-[2-[4-Azido-2,3,4,5-tetrafluorobenzoyl)amino] ethoxy]ethoxy]ethyl ester 6

Active ester **4** (770 mg, 2.32 mmol) and amine **5** (576 mg, 2.32 mmol) were dissolved in DCM (30 mL) and stirred at room temperature in the dark for 16 h. The solvent was removed under reduced pressure and the crude product was purified by column chromatography (ethyl acetate/ cyclohexane 2:1 → ethyl acetate) to yield compound **6** as a colourless liquid.

Yield: 1.02 g (2.20 mmol, 95 %);

DC: R_f = 0.36 (ethyl acetate);

^{1}H-NMR: (500 MHz, $CDCl_3$, 300 K): δ = 3.70-3.60 (m, 8H, OCH_2), 3.59-3.52 (m, 2H, OCH_2), 3.33-3.29 (OCH_2) ppm;

^{19}F-NMR: (470.6 MHz, $CDCl_3$, 300 K): δ = -141.0 (m, 2F), -150.8 (m, 2F) ppm;

EI-MS: *m/z* = 465.12, $[M]^+$; 218.002, $[M\text{-}C_4H_4NO_3]^+$, (calc. 465.164 for $C_{18}H_{23}F_4N_5O_5$).

2-[2-(2-Aminoethoxy)ethoxy]ethyl-(4-Azido-2,3,5,6-tetrafluorobenzoic) amide7

Trifluoroacetic acid (2.50 mL) was added to a solution of compound **6** (1.02 g, 2.20 mmol) in DCM (50 mL) and the mixture was stirred at room temperature in the dark for 4 h. The solvent was removed under reduced pressure and the crude product was codestilled with DCM (3 x 50 mL) to obtain compound **7** as a colourless liquid.

Yield: 799 mg (2.19 mmol, 99 %);

DC: R_f = 0.45 (ethyl acetate/methanol 4:1);

^{1}H-NMR: (200 MHz, $CDCl_3$, 300 K, TMS): δ = 3.72-3.65 (m, 8H, OCH_2), 3.60-3.56 (t, $^3J_{CH2CH2}$ = 5.5 Hz, 2H, OCH_2), 3.14-3.09 (t, $^3J_{CH2CH2}$ = 5.5 Hz, 2H, OCH_2) ppm;

^{19}F-NMR: (470.6 MHz, $CDCl_3$, 300 K): δ = -143.6 (m, 2F), -152.1 (m, 2F) ppm;

^{13}C-NMR: (126 MHz, $CDCl_3$, 300 K): δ = 71.4, 70.3, 67.8, 41.1, 40.7 (OCH_2);

IR (ATR): $\tilde{\nu}$ = 2885, 2126, 1651, 1485, 1132, 992, 798, 722, 706 cm^{-1};

EI-MS: *m/z* = 465.12, $[M]^+$; 218.002, $[M\text{-}C_4H_4NO_3]^+$, (calc. 465.164 for $C_{18}H_{23}F_4N_5O_5$).

Octyl 2,3,4,6 tetra-*O*-acetyl-α-D-mannopyranoside 11[276]

Mannose trichloroacetimidate **8** (2.00 g, 4.06 mmol) and 1-octanol **10** (956 µL, 6.09 mmol) were dissolved in dry DCM (12 mL). The mixture was cooled to 0 °C before $BF_3 \cdot Et_2O$ (1.02 mL, 8.12 mmol) was added dropwise. The mixture was stirred at room temperature for 16 h. The reaction mixture was diluted with DCM (200 mL) and washed with sat. $NaHCO_3$ solution (100 mL) and sat. NaCl solution (100 mL). The combined organic layers were dried over $MgSO_4$, filtered and the solvent removed under reduced pressure. The crude product was purified by column chromatography (cyclohexane/ ethyl acetate 4:1 → 3:1) to yield mannoside **11** as a colourless syrup.

Yield: 1.48 g (3.21 mmol, 79 %); lit.:[276] 46 %;

DC: R_f = 0.41 (cyclohexane/ ethyl acetate 2:1);

Rotational value: $[\alpha]_{20}^{D}$ = -18.9 (c = 0.62 in ethyl acetate);

^{1}H-NMR: (500 MHz, $CDCl_3$, 300 K, TMS): δ = 5.39-5.31 (dd, $^3J_{2,3}$ = 3.5 Hz, $^3J_{3,4}$ = 10.0 Hz, 1H, H-3), 5.27 (dd~t, $^3J_{3,4}$ = 10.0 Hz, 1H, H-4), 5.23 (dd, $^3J_{1,2}$ = 1.7 Hz, $^3J_{2,3}$ = 3.5 Hz, 1H, H-2), 4.80 (d, $^3J_{1,2}$ = 1.7 Hz, 1H, H-1), 4.32-4.24 (dd, $^3J_{5,6}$ = 5.3 Hz, $^2J_{6,6'}$ = 12.2 Hz, 1H, H-6), 4.15-4.07 (dd, $^3J_{5,6'}$ = 2.4 Hz, $^2J_{6,6'}$ = 12.2 Hz, 1H, H-6'), 4.01-3.97 (ddd, $^3J_{5,6'}$ = 2.4 Hz, $^3J_{5,6}$ = 5.3 Hz, $^3J_{4,5}$ = 10.0 Hz, 1H, H-5), 3-71-3.65 (dt, $^2J_{OCHH'}$ = 9.6 Hz, $^3J_{OCH2CH2}$ = 6.6 Hz, 1H, OC<u>H</u>H'), 3.49-3.43 (dt, $^2J_{OCHH'}$ = 9.6 Hz, $^3J_{OCH2CH2}$ = 6.6 Hz, 1H, OCH<u>H</u>'), 2.15, 2.10, 2.04, 1.99 (each s, each 3H, O(C=O)CH_3), 1.65-1.54 (m, 2H, OCH_2CH_2), 1.31-1.27 (m, 10H, CH_2), 0.89 (t, $^3J_{CH2CH3}$ = 7.0 Hz, 3H, CH_3) ppm;

^{13}C-NMR: (126 MHz, $CDCl_3$, 300 K, TMS): δ = 170.7, 169.7 (<u>C</u>OCH_3), 97.7 (C-1), 69.9 (C-2), 69.3 (C-3), 68.7 (O<u>C</u>H_2CH_2), 68.5 (C-5), 66.5 (C-4), 62.7 (C-6), 32.0, 29.5, 29.4, 29.3, 26.2, 22.8 (CH_2), 21.1, 20.9, 20.8 (OCO<u>C</u>H_3), 14.2 (CH_3) ppm;

IR (ATR): ṽ = 2922, 2855, 1742, 1367, 1224, 1033 cm^{-1};

ESI-MS: *m/z* = 483.223, $[M+Na]^+$ (calc. 483.221 for $C_{22}H_{36}O_{10}$ + Na).

Octyl 2,3,4,6-tetra-*O*-acetyl-β-D-glucopyranoside 12[276]

Glucose trichloroacetimidate **9** (1.20 g, 2.44 mmol) and 1-octanol **10** (573 µL, 3.65 mmol) were dissolved in dry DCM (12 mL). The mixture was cooled to 0 °C before

$BF_3 \cdot Et_2O$ (615 µL, 4.88 mmol) was added dropwise. The mixture was stirred at room temperature for 16 h. The reaction mixture was diluted with DCM (150 mL) and washed with sat. $NaHCO_3$ solution (70 mL) and sat. NaCl solution (70 mL). The combined organic layers were dried over $MgSO_4$, filtered and the solvent removed under reduced pressure. The crude product was purified by column chromatography (cyclohexane/ ethyl acetate 4:1 → 3:1) to yield glucoside **12** as a colourless solid.

Yield: 869 mg (1.89 mmol, 77 %); lit.:[276] 47 %;

DC: R_f = 0.43 (cyclohexane/ ethyl acetate 2:1);

Melting point: 67 °C; lit.[417]: 68-68.5 °C;

Rotational value: $[\alpha]_{20}^{D}$ = -20.8 (c = 0.29 in ethyl acetate); lit.[418]: $[\alpha]_{27}^{D}$ = -20.2 (c = 0.59 in chloroform);

^{1}H-NMR: (500 MHz, $CDCl_3$, 300 K, TMS): δ = 5.24-5.14 (dd~t, $^3J_{2,3}$ = 9.5 Hz, 1H, H-3), 5.13-5.05 (dd~t, $^3J_{3,4}$ = 9.9 Hz, 1H, H-4), 5.03-4.92 (dd, $^3J_{1,2}$ = 8.0 Hz, $^3J_{2,3}$ = 9.5 Hz, 1H, H-2), 4.50-4.46 (d, $^3J_{1,2}$ = 8.0 Hz, 1H, H-1), 4.29-4.22 (dd, $^3J_{5,6}$ = 4.7 Hz, $^2J_{6,6'}$ = 12.3 Hz, 1H, H-6), 4.15-4.11 (dd, $^3J_{5,6'}$ = 2.5 Hz, $^2J_{6,6'}$ = 12.3 Hz, 1H, H-6'), 3.89-3.83 (dt, $^2J_{OCHH'}$ = 9.6 Hz, $^3J_{OCH2CH2}$ = 6.4 Hz, 1H, OC<u>H</u>H'), 3.72-3.66 (ddd, $^3J_{5,6'}$ = 2.5 Hz, $^3J_{5,6}$ = 4.7 Hz, $^3J_{4,5}$ = 10.0 Hz, 1H, H-5), 3.50-3.43 (dt, $^2J_{OCHH'}$ = 9.6 Hz, $^3J_{OCH2CH2}$ = 6.8 Hz, 1H, OCH<u>H</u>'), 2.08, 2.03, 2.02, 2.00 (each s, each 3H, O(C=O)CH_3), 1.62-1.51 (m, 2H, OCH_2CH_2), 1.32-1.23 (m, 10H, CH_2), 0.87 (t, $^3J_{CH2CH3}$ = 7.0 Hz, 3H, CH_3) ppm;

^{13}C-NMR: (126 MHz, $CDCl_3$, 300 K, TMS): δ = 170.9, 170.5, 169.6, 169.4 (<u>C</u>OCH_3), 101.0 (C-1), 73.0 (C-3), 71.9 (C-5), 71.5 (C-2), 70.4 (O<u>C</u>H_2CH_2), 68.7 (C-4), 62.2 (C-6), 31.9, 29.5, 29.4, 25.9, 22.8 (CH_2), 20.9, 20.8, 20.7 (OCO<u>C</u>H_3), 14.2 (CH_3) ppm;

IR (ATR): ṽ = 2922, 2855, 1742, 1367, 1225, 1034, 623 cm^{-1};

ESI-MS: *m/z* = 483.21963, $[M+Na]^+$ (calc. 483.22007 for $C_{22}H_{36}O_{10}$ + Na).

Octyl α-D-mannopyranoside 13[276]

Freshly prepared sodium methoxide solution (1 M, 2.50 mL) was added to a solution of compound **11** (1.38 g, 3.00 mmol) in dry methanol (25 mL). After stirring at room temperature for 16 h the mixture was neutralised with Amberlite® IR 120 and filtered.

The solvent was removed under reduced pressure to yield compound **13** quantitatively as a colourless syrup.

Yield: quant.; lit.[276]: 95 %;

TLC: R_f = 0 (cyclohexane/ ethyl acetate 4:1);

Optical rotation: $[\alpha]^{22}_D$ = +55.0 (c = 1.04 in methanol); lit.[276]: $[\alpha]^{24}_D$ = +56.0 (c = 0.85 in water);

^{1}H-NMR: (500 MHz, MeOD, 300 K): δ = 4.73 (d, $^3J_{1,2}$ = 1.5 Hz, 1H, H-1), 3.84-3.80 (dd, $^3J_{5,6'}$ = 2.3 Hz, $^2J_{6,6'}$ = 11.7 Hz, 1H, H-6'), 3.80-3.76 (dd, $^3J_{1,2}$ = 1.5 Hz, $^3J_{2,3}$ = 3.4 Hz, 1H, H-2), 3.75-3.67 (m, 3H, -OCHH', H-6, H-3), 3.60 (t, $^3J_{3,4}$ = 9.7 Hz, 1H, H-4), 3.56-3.50 (ddd, $^3J_{5,6'}$ = 2.3 Hz, $^3J_{5,6}$ = 5.8 Hz, $^3J_{4,5}$ = 9.7 Hz, 1H, H-5), 3.46-3.38 (dt, $^2J_{OCHH'}$ = 9.6 Hz, $^3J_{OCH2CH2}$ = 6.4 Hz, 1H, OCHH'), 1.63-1.57 (m, 2H, OCH_2CH_2), 1.38-1.28 (m, 10H, CH_2), 0.90 (t, $^3J_{CH2CH3}$ = 7.0 Hz, 3H, CH_3) ppm;

^{13}C-NMR: (126 MHz, MeOD, 300 K): δ = 101.6 (C-1), 74.6 (C-5), 72.7 (C-3), 72.3 (C-2), 68.6 (OCH_2), 68.6 (C-4), 62.9 (C-6), 33.0, 30.6, 30.5, 30.4, 27.4, 23.7 (CH_2), 14.4 (CH_3) ppm;

IR (ATR): ṽ = 3364, 2924, 2856, 1131, 1056, 1026, 677 cm^{-1};

ESI-MS: *m/z* = 315.180, $[M+Na]^+$ (calc. 315.178 for $C_{14}H_{28}O_6$ + Na).

Octyl β-D-glucopyranoside 14[419]

Freshly prepared sodium methoxide solution (1 M, 1.00 mL) was added to a solution of compound **12** (547 mg, 1.19 mmol) in dry methanol (25 mL). After stirring at room temperature for 16 h the mixture was neutralised with Amberlite® IR 120 and filtered. The solvent was removed under reduced pressure to yield compound **14** quantitatively as a colourless syrup.

Yield: quant.;

TLC: R_f = 0 (cyclohexane/ ethyl acetate 4:1);

Rotational value: $[\alpha]_{20}^D$ = -21.5(c = 0.30 in methanol);

^{1}H-NMR: (500 MHz, MeOD, 300 K): δ = 4.27-4.22 (d, $^3J_{1,2}$ = 7.8 Hz, 1H, H-1), 3.92-3.84 (m, 2H, H-6, OCHH'), 3.68-3.64 (dd, $^3J_{5,6'}$ = 5.5 Hz, $^2J_{6,6'}$ = 11.9 Hz, 1H, H-6'),

3.56-3.50 (dt, $^{2}J_{OCHH'}$ = 9.5 Hz, $^{3}J_{OCH2CH2}$ = 6.8 Hz, 1H, OCH<u>H</u>'), 3.36-3.31 (m, 1H, H-3), 3.28-3.23 (m, 2H, H-4, H-5), 3.18-3.14 (dd, $^{3}J_{1,2}$ = 7.8 Hz, $^{3}J_{2,3}$ = 9.1 Hz, 1H, H-2), 1.65-1.58 (m, 2H, $OCH_2C\underline{H}_2$), 1.39-1.25 (m, 10H, CH_2), 0.90 (t, $^{3}J_{CH2CH3}$ = 7.0 Hz, 3H, CH_3) ppm;

^{13}C-NMR: (126 MHz, MeOD, 300 K): δ = 104.4 (C-1), 78.2 (C-3), 77.9 (C-5), 75.1 (C-2), 71.7 (C-4), 70.9 (OCH_2), 62.8 (C-6), 33.0, 30.8, 30.6, 30.4, 27.1, 23.7 (CH_2), 14.4 (CH_3) ppm;

IR (ATR): ṽ = 3355, 2924, 2855, 1377, 1075, 1018, 614 cm^{-1};

ESI-MS: *m/z* = 293.19526, $[M+H]^+$ (calc. 293.19587 for $C_{14}H_{28}O_6$ + H).

tert-Butyl-1,3-dihydroxypropane-2-yl-carbamate 17

Di-*tert*-butyldicarbonate (13.2 g, 60.4 mmol) was added to a solution of serinol **15** (5.00 g, 54.9 mmol) in methanol (250 mL). The mixture was reacted at room temperature for 18 h. The crude was then concentrated and product **17** was precipitated with cold ethyl acetate (100 mL). Compound **17** was obtained after filtration as a colourless solid.

Yield: 9.22 g (48.2 mmol, 88 %); lit.: 92 %;

Melting point: 86 °C, lit.: 84-85 °C;

^{1}H-NMR: (500 MHz, $CDCl_3$, 300 K, TMS): δ = 5.28 (br s, 1H, NH), 3.83-3.79 (dd, 2H, $^{2}J_{CHCH2}$ = 11.1 Hz, $^{3}J_{CHCH2}$ = 4.4 Hz, 2H, C<u>H</u>H'OH), 3.76-3.73 (dd, 2H, $^{2}J_{CHCH2}$ = 11.1 Hz, $^{3}J_{CHCH2}$ = 4.4 Hz, 2H, CH<u>H</u>'OH), 3.68-3.65 (m, 1H, CH), 2.65 (br s, 2H, OH), 1.44 (s, 9H, CH_3) ppm;

^{13}C-NMR: (126 MHz, $CDCl_3$, 300 K): δ = 156.5 (C=O), 80.1 ($\underline{C}(CH_3)_3$), 63.6 (CH_2), 53.3 (CH), 28.5 (CH_3) ppm;

IR (ATR-IR): ṽ = 3301 (νOH), 2983, 2960, 2885 (νCH_2), 1684 (νC=O), 1531 (νCONH) 1392, 1364 (ν$C(CH_3)_3$), 1309, 1246 (νCH_2), 1162, 1040, 1021 (νCOC) cm^{-1};

ESI-MS: *m/z* = 214.107, $[M+Na]^+$ (calc. 214.106 for $C_8H_{17}NO_4$ + Na).

***N*-(*tert*-Butyloxycarbonyl)tris(hydroxymethyl)aminomethane 18**

Di-*tert*-butyldicarbonate (11.8 g, 53.9 mmol) was added to a solution of serinol **16** (5.00 g, 41.3 mmol) in methanol/ *tert* butyl alcohol (1:1, 90 mL). The mixture was reacted at room temperature for 40 h. The crude was then concentrated and product **18** was precipitated with cold ethyl acetate (100 mL). Compound **18** was obtained after filtration as a colourless solid.

Yield: 8.13 g (36.7 mmol, 89 %); lit.: 90 %;

Melting point: 86 °C, lit.: 84-85 °C;

^{1}H-NMR: (500 MHz, DMSO-*d6*, 300 K): δ = 5.75 (br s, 1H, NH), 4.49 (t, $^{3}J_{CH2OH}$ = 5.6 Hz, 3H, OH), 3.52 (d, $^{3}J_{CH2OH}$ = 5.6 Hz, 6H, CH_2), 1.37 (s, 9H, CH_3) ppm;

^{13}C-NMR: (126 MHz, DMSO-*d6*, 300 K): δ = 155.0 (C=O), 77.8 ($\underline{C}(CH_3)_3$), 60.5 (CH_2), 60.2 ($\underline{C}(CH_2)_3$), 28.2 (CH_3) ppm;

IR (ATR-IR): ṽ = 3293 (νOH), 2986, 2964 (νCH_2), 1677 (νC=O), 1544 (νCONH) 1393, 1368 (ν$C(CH_3)_3$), 1291, 1257 (νCH_2), 1163, 1029, 1016 (νCOC) cm^{-1};

ESI-MS: *m/z* = 222.16, $[M+H]^+$ (calc. 221.126 for $C_9H_{19}NO_5$).

***tert*-Butyl(1,3-bis(prop-2-in-1-yloxy)propan-2-yl)-carbamate 20[420]**

Propargyl bromide **19** (80 % in toluene, 28.1 mL, 261 mmol) was added to an ice-cold solution of diol **17** in dry DMF (60 mL). Freshly pestled potassium hydroxide (18.4 g, 328 mmol) was added in portions before the reaction was stirred at 40 °C for 4 h and subsequently at room temperature for additional 16 h. The crude mixture was then diluted with ethyl acetate (350 mL). After washing with water (3 x 200 mL) the organic layer was dried over $MgSO_4$, filtered and the solvent removed under reduced pressure. Compound **20** was obtained after column chromatography (cyclohexane → cyclohexane/ ethyl acetate 8:1) as a yellow oil.

Yield: 9.67 g (36.2 mmol, 83 %); lit.: 39 %;[420]

TLC: R_f = 0.33 (cyclohexane/ ethyl acetate 5:1);

^{1}H-NMR: (500 MHz, $CDCl_3$, 300 K, TMS): δ = 4.90 (br s, 1H, NH), 4.16 (d, $^{4}J_{CH2≡CH}$ = 2.4 Hz, 4H, $C\underline{H}_2C{\equiv}CH$), 3.92 (s, 1H, NHC$\underline{H}$), 3.63 (dd, $^{2}J_{CHCH2}$ = 9.2 Hz,

$^{3}J_{CHCH2}$ = 4.5 Hz, 2H, CHC<u>H</u>H‘), 3.60-3.55 (m, 2H, CHCH<u>H</u>‘), 2.43 ($^{4}J_{CH2\equiv CH}$ = 2.4 Hz, 2H, $CH_2C\equiv C\underline{H}$), 1.44 (s, 9H, CH_3) ppm;

^{13}C-NMR: (126 MHz, $CDCl_3$, 300 K, TMS): δ = 155.6 (C=O), 79.7 (<u>C</u>≡CH), 77.8 ($\underline{C}(CH_3)_3$), 74.7 (C≡<u>C</u>H), 68.7 (CH<u>C</u>H_2), 58.6 ($C\underline{H}_2C\equiv CH$), 49.6 (<u>C</u>$HCH_2$), 28.5 ($CH_3$) ppm;

ESI-MS: *m/z* = 265.16779, [M]; (calc. 265.16779 for $C_{15}H_{23}NO_3$);

IR (ATR-IR): ṽ = 3292 (νC≡CH), 2977 (νCH_2), 1697 (νC=O), 1504 (νCONH) 1392, 1366 (ν$C(CH_3)_3$), 1166, 1097, 1058 (νCOC) cm^{-1}.

N-(*tert*-Butyloxycarbonyl)tris[(propargyloxy)methyl]aminomethane 21[284]

Propargyl bromide **19** (80 % in toluene, 25.9 mL, 240 mmol) was added to an ice-cold solution of triol **18** in dry DMF (60 mL). Freshly pestled potassium hydroxide (17.0 g, 303 mmol) was added in portions before the reaction was stirred at 40 °C for 4 h and subsequently at room temperature for additional 16 h. The crude mixture was then diluted with ethyl acetate (350 mL). After washing with water (3 x 200 mL) the organic layer was dried over $MgSO_4$, filtered and the solvent removed under reduced pressure. Compound **21** was obtained after column chromatography (cyclohexane → cyclohexane/ ethyl acetate 8:1) as a yellow oil.

Yield: 5.61 g (16.7 mmol, 41 %); lit.: 67 %;[284]

TLC: R_f = 0.28 (cyclohexane/ ethyl acetate 9:1);

^{1}H-NMR: (500 MHz, $CDCl_3$, 300 K, TMS): δ = 4.92 (br s, 1H, NH), 4.15 (d, $^{4}J_{CH2\equiv CH}$ = 2.4 Hz, 6H, $C\underline{H}_2C\equiv CH$), 3.79 (s, 6H, CCH_2), 2.42 ($^{4}J_{CH2\equiv CH}$ = 2.4 Hz, 3H, $CH_2C\equiv C\underline{H}$), 1.42 (s, 9H, CH_3) ppm;

^{13}C-NMR: (126 MHz, $CDCl_3$, 300 K, TMS): δ = 154.9 (C=O), 79.8 (<u>C</u>≡CH), 79.4 ($\underline{C}(CH_3)_3$), 74.7 (C≡<u>C</u>H), 69.1 (C<u>C</u>H_2), 58.8 ($C\underline{H}_2C\equiv CH$), 58.2 (<u>C</u>$CH_2$), 28.5 ($CH_3$) ppm;

MALDI-MS: *m/z* = 373.974, $[M+K]^+$; (calc. 374.137 for $C_{18}H_{25}NO_5$+K);

IR (ATR-IR): ṽ = 3292 (νC≡CH), 2977, 2850, 2790 (νCH_2), 1702 (νC=O), 1517 (νCONH) 1393, 1361 (ν$C(CH_3)_3$), 1166, 1088, 1075 (νCOC) cm^{-1}.

2-Cascade: *N*-(*tert*-butylcarbamate)aminomethane[2-1,1]:methoxymethyl: 1*H* [1,2,3]triazole-1-ethyl: 2,3,4,6-tetra-O-acetyl-α-D-mannopyranoside 23

To a solution of (2-Azidoethyl) 2,3,4,6-tetra-*O*-acetyl-α-D-manno-pyranoside **22** (2.50 g, 5.99 mmol) and *tert*-Butyl(1,3-bis(prop-2-in-1-yloxy)propan-2-yl) carbamate **20** (801 mg, 3.00 mmol) in DMF (100 mL) was added a solution of copper(II) sulphate pentahydrate (632 mg, 2.53 mmol) in water (20 mL) and sodium ascorbate (1.00 g, 5.05 mmol) in water (20 mL). After stirring at room temperature for five hours, a 1:1 mixture of saturated ammonium chloride and water (200 mL) was added and the mixture was extracted with ethyl acetate (3 x 200 mL). The combined organic layers were dried over $MgSO_4$ and filtered. The solvent was removed under reduced pressure and the crude product was purified by column chromatography (ethyl acetate/cyclohexane/methanol 6:4:1) to yield compound **23** as a colourless solid.

Yield: 2.94 g (2.67 mmol, 89 %);

TLC: R_f = 0.38 (ethyl acetate/cyclohexane/methanol, 6:4:1);

Melting point: 86 °C;

Rotational value: $[\alpha]_{25}^{D}$ = +29.7 (8.7 mM CH_2Cl_2);

^{1}H-NMR (500 MHz, MeOD, 300 K): δ = 8.03 (s, 2H, $H_{triazole}$), 5.21-5.12 (m, 6H, H-2, H-3, H-4), 4.84 (d, $^3J_{1,2}$ = 1.6 Hz, 2H, H-1), 4.69 (m, 4H, $NC\underline{H}_2CH_2$), 4.62 (s, 4H, $OCH_2C_{triazole}$), 4.17-4.10 (m, 4H, H-6, $NCH_2C\underline{H}_2$), 4.02 (dd, $^2J_{6,6'}$ = 12.4 Hz, $^3J_{5,6'}$ = 2.2 Hz, 2H, H-6'), 3.95 (m, 2H, $NCH_2C\underline{H}'_2$), 3.86 (m, 1H, H_{core}), 3.59-3.46 (m, 6H, H-5, $C_{core}CH_2O$), 2.12, 2.05, 2.03, 1.95 (each s, 24H, 8 $COCH_3$), 1.43 (s, 9H, CH_3) ppm;

^{13}C-NMR (126 MHz, MeOD, 300 K): δ = 172.3, 171.6, 171.5, 171.4 (8 $_COCH_3$), 146.1 ($OCH_2\underline{C}_{triazole}$), 126.0 ($C_{triazole}$), 98.3 (C-1), 70.3, 70.2 (C-2, C-3), 70.1 ($C_{core}\underline{C}H_2O$), 69.8 (C-5), 67.0 ($NCH_2\underline{C}H_2$), 66.6 (C-4), 64.8 ($O\underline{C}H_2C_{triazole}$), 63.0 (C-6), 51.1 ($C_{core}$), 50.7 ($N\underline{C}H_2CH_2$), 28.5 ($CH_3$), 20.4, 20.3 (8 $COCH_3$) ppm;

ESI-MS: *m/z* = 1102.43062, [M+H]; (calc. 1102.43157 for $C_{46}H_{67}N_7O_{24}$+H);

IR (ATR-IR): $\tilde{\nu}$ = 2946, 1742, 1367, 1218, 1138, 1087, 1042 cm^{-1}.

3-Cascade: *N*-(*tert*-butylcarbamate)aminomethane[3-1,1,1]:methoxymethyl:1*H*-[1,2,3]triazole-1-ethyl: 2,3,4,6-tetra-O-acetyl-α-D-mannopyranoside 24[284]

To a solution of (2-Azidoethyl) 2,3,4,6-tetra-*O*-acetyl-α-D-mannopyranoside **22** (3.45 g, 8.27 mmol) and *N*-(*tert*-Butyloxycarbonyl)tris[propargyloxy) methyl]amino-methane **21** (926 mg, 2.76 mmol) in DMF (50 mL) was added a solution of copper(II) sulphate pentahydrate (861 mg, 3.45 mmol) in water (20 mL) and sodium ascorbate (1.39 g, 6.56 mmol) in water (20 mL). After stirring at room temperature for 14 hours, a 1:1 mixture of saturated ammonium chloride and water (200 mL) was added and the mixture was extracted with ethyl acetate (3 x 200 mL). The combined organic layers were dried over $MgSO_4$ and filtered. The solvent was removed under reduced pressure and the crude product was purified by column chromatography (ethyl acetate/cyclohexane/methanol 6:4:1→7:3:1) to yield compound **24** as a colourless solid.

Yield: 3.27 g (2.06 mmol, 75 %), lit.: 87 %;[284]

TLC: R_f = 0.22 (ethyl acetate/cyclohexane/methanol, 7:3:1);

Melting point: 90 °C;

Optical rotation: $[\alpha]^{22}_D$ = +31.5 (c = 1.0 in dichloromethane);

^{1}H-NMR (500 MHz, MeOD, 300 K): δ = 8.03 (s, 3H, $H_{triazole}$), 5.21-5.13 (m, 9H, H-2, H-3, H-4), 4.85 (d, $^3J_{1,2}$ = 1.3 Hz, 3H, H-1), 4.71-4.69 (m, 6H, $NC\underline{H}_2CH_2$), 4.60 (s, 6H, $OCH_2C_{triazole}$), 4.17-4.11 (m, 6H, *H*-6, $NCH_2C\underline{H}_2$), 4.03 (dd, $^2J_{6,6'}$ = 12.3 Hz, $^3J_{5,6'}$ = 2.3 Hz, 3H, H-6'), 3.98-3.94 (m, 3H, H-7'), 3.74 (s, 6H, $C_{core}CH_2O$), 3.52 (ddd, $^3J_{4,5}$ = 9.4 Hz, $^3J_{5,6}$ = 4.7 Hz, $^3J_{5,6'}$ = 2.3 Hz, 3H, H-5), 2.11, 2.05, 2.02, 1.95 (each s, 36H, 12 $COCH_3$), 1.39 (s, 9H, CH_3) ppm; **^{13}C-NMR** (126 MHz, MeOD, 300 K): δ = 172.3, 171.5, 171.4 (12 $\underline{C}OCH_3$), 145.0 ($OCH_2\underline{C}_{triazole}$), 126.0 ($C_{triazole}N$), 98.4 (C-1), 70.3, 70.2 (C-2, C-3), 69.8 (C-5), 69.6 ($C_{core}\underline{C}H_2O$), 67.0 ($NCH_2\underline{C}H_2$), 66.7 ($\underline{C}$-4), 65.2 ($O\underline{C}H_2C_{triazole}$), 63.0 (C-6), 50.7 ($CN\underline{C}H_2CH_2$), 28.5 ($CH_3$), 20.4, 20.3 (12 $CO\underline{C}H_3$) ppm;

ESI-MS: *m/z* = 1587.59606, [M+H]; (calc. 1587.59613 for $C_{66}H_{94}N_{10}O_{35}$+H);

IR (ATR-IR): $\tilde{\nu}$ = 2977 (νCH_2), 1742 (νC=O), 1368 (ν$C(CH_3)_3$), 1218 (δCH_2), 1138, 1086, 1043 (νCOC) cm^{-1}.

2-Cascade: Aminomethane[2-1,1]:methoxymethyl:1*H*[1,2,3]triazole-1-ethyl: 2,3,4,6-tetra-O-acetyl-α-D-mannopyranoside 25

Trifluoroacetic acid (3.17 mL, 41.4 mmol) was added to a solution of compound **23** (2.28 g, 2.07 mmol) in DCM (40 mL). After stirring for 16 h at room temperature the solvent was removed under reduced pressure and the crude product was codestilled with toluene (3 x 50 mL) and DCM (2 x 40 mL) to yield the free amine of compound **25** quantitatively as colourless syrup.

Yield: quant.;

Optical rotation: $[\alpha]^{20}_D$ = +22.7 (c = 0.42 in ethyl acetate);

^{1}H-NMR (500 MHz, $CDCl_3$, 300 K): δ = 7.94-7.91 (m, 2H, $H_{triazole}$), 6.03-5.86 (s (br), NH_2), 5.27-5.22 (dd~t, $^3J_{3,4}$= 10.2 Hz, 2H, H-3), 5.18-5.12 (m, 4H, H-2, H-4), 4.79-4.74 (m, 6H, H-1, $OCH_2C_{triazole}$), 4.71-4.66 (m, 2H, $NC\underline{H}_2CH_2$), 4.63-4.57 (m, 2H, $NC\underline{H}'_2CH_2$), 4.22 (2 x ddd, $^3J_{5,6'}$ = 5.2 Hz, $^2J_{6,6'}$ = 12.3 Hz, 1H, H-6), 4.17-4.12 (ddd, $^3J_{CH2H}$ = 4.2 Hz, $^3J_{CH2H}$ = 6.6 Hz, $^2J_{CHH'}$ = 10.6 Hz, 2H, $NCH_2C\underline{H}H'$), 4.09 (dd $^3J_{5,6}$ = 2.4 Hz, $^2J_{6,6'}$ = 12.3 Hz, 1H, H-6'), 3.91-3.75 (m, 7H, $NCH_2CH\underline{H}'$, $C\underline{H}C\underline{H}_2O$), 3.72-3.67 (m, 2H, H-5), 2.13, 2.10 (each s, 12H, CH_3), 2.05, 1.98 (each m, 12H, CH_3);

^{13}C-NMR: (126 MHz, $CDCl_3$, 300 K): δ = 171.3, 171.0, 170.5, 169.9 (C=O), 143.5 ($\underline{C}_{triazole}CH$), 124.9 ($C_{triazole}\underline{C}H$), 97.6 (C-1), 69.1, 67.3, 67.2 (C-2, C-4, C-5), 66.0 ($N_{triazole}CH_2\underline{C}H_2$), 65.7 (C-3), 65.6 ($O\underline{C}H_2C_{triazole}$), 62.5 (C-6), 51.1 ($C_{core}$), 50.5 ($N_{triazole}CH_2$), 20.9, 20.8 ($CH_3$) ppm;

IR (ATR): $\tilde{\nu}$ = 3453, 2932, 1738, 1678, 1372, 1225, 1225, 1133, 1088, 1043 cm^{-1};

MALDI-MS: *m/z* = 1002.387, $[M+H]^+$; (calc. 1002.379 for $C_{41}H_{59}N_7O_{22}$+H).

3-Cascade: Aminomethane[3-1,1,1]:methoxymethyl:1*H*[1,2,3]triazole-1-ethyl: α-D-mannopyranoside 26[284]

Trifluoroacetic acid (2.60 mL, 34.0 mmol) was added to a solution of compound **24** (1.26 g, 794 µmol) in DCM (50 mL). After stirring for 16 h at room temperature the solvent was removed under reduced pressure and the crude product was codestilled with toluene (3 x 50 mL) and DCM (2 x 40 mL) to yield the free amine of compound **26** quantitatively as colourless solid.

Yield: quant.; lit.[284]: quant.;

Melting point: 69 °C;

Optical rotation: $[\alpha]^{20}_{D}$ = +28.5 (c = 0.80 in ethyl acetate);

^{1}H-NMR (600 MHz, $CDCl_3$, 300 K): δ = 7.76 (s, 3H, $H_{triazole}$), 5.27-5.22 (dd~t, $^{3}J_{3,4}$= 9.7 Hz, 3H, H-3), 5.21-5.17 (m, 6H, H-2, H-4), 4.81 (d, $^{3}J_{1,2}$ = 1.1 Hz, 3H, H-1), 4.66-4.56 (m, 12H, $OCH_2C_{triazole}$, $NC\underline{H}_2CH_2$), 4.23-4.18 (dd, $^{3}J_{5,6}$ = 5.1 Hz, $^{2}J_{6,6'}$ = 12.3 Hz, 3H, H-6), 4.15-4.11 (ddd, 3H, $^{3}J_{CH2H}$ = 4.2 Hz, $^{3}J_{CH2H}$ = 6.6 Hz, $^{2}J_{CHH'}$ = 10.6 Hz, $NCH_2C\underline{H}H$‘), 4.07-4.03 (dd, $^{3}J_{5,6'}$ = 2.4 Hz, $^{2}J_{6,6'}$ = 12.3 Hz, 3H, H-6‘), 3.93-3.88 (ddd, $^{3}J_{CH2H'}$ = 4.2 Hz, $^{3}J_{CH2H'}$ = 6.3 Hz, $^{2}J_{CHH'}$ = 10.6 Hz, $NCH_2CH\underline{H}$‘), 3.64-3.60 (ddd, 2.4 Hz, 5.1 Hz, 9.6 Hz, 3H, H-5), 3.58-3.52 (m, 6H, $C_{core}CH_2O$), 2.13, 2.09, 2.04, 1.99 (each s, 9H, CH_3);

^{13}C-NMR: (151 MHz, $CDCl_3$, 300 K): δ = 170.7, 170.3, 170.2, 169.8 (C=O), 145.2 ($\underline{C}_{triazole}CH$), 124.0 ($C_{triazole}\underline{C}H$), 97.6 (C-1), 69.3, 69.1 (C-2, C-4, C-5), 66.4 ($N_{triazole}CH_2\underline{C}H_2$), 65.82 (C-3), 65.0 ($O\underline{C}H_2C_{triazole}$), 62.4 (C-6), 49.8 ($N_{triazole}CH_2$), 20.9, 20.7 ($CH_3$) ppm;

IR (ATR): ṽ = 3300, 2928, 1737, 1370, 1222, 1135, 1087, 1041 cm^{-1};

MALDI-MS: *m/z* = 1487.517, $[M+H]^+$; (calc. 1487.544 for $C_{61}H_{86}N_{10}O_{33}$+H).

2-Cascade: *N*-(1-oxo-hexyl)aminomethane[2-1,1]: methoxymethyl: 1*H*[1,2,3] triazole-1-ethyl: 2,3,4,6-tetra-*O*-acetyl-α-D-mannopyranosid 28

2-Cascade: aminomethane[2-1,1]:methoxymethyl:1*H*[1,2,3]triazole-1-ethyl: 2,3,4,6-tetra-*O*-acetyl-α-D-mannopyranoside **25** (1.00 g, 896 µmol) and HATU (511 mg, 1.34 mmol) were predried for 30 min in vacuo. After addition of dry DMF (24 mL) and hexanoic acid **27** (112 µL, 986 mmol) the mixture was cooled to 0 °C before DIPEA (187 µL, 1.08 mmol) was added. The mixture was stirred at room temperature for 16 h. Finally, the solvent was removed under reduced pressure and the crude product purified twice by column chromatography (ethyl acetate/ methanol 9:1 and ethyl acetate/ cyclohexane/ methanol 6:4:1) to obtain compound **28** as a colourless solid.

Yield: 63.8 mg (58.0 µmol; 6 %);

DC: (ethyl acetate/ methanol, 9:1): R_f = 0.51;

Melting point: 65 °C;

Optical rotation: $[\alpha]^{22}_D$ = +31.1 (c = 0.97 in dichloromethane);

^{1}H-NMR (500 MHz, MeOD, 300 K): δ = 8.03, 8.02 (2 s, each 1H, $H_{triazole}$), 5.21-5.12 (m, 6H, H-2, H-3, H-4), 4.84 (s, 2H, H-1), 4.72-4.68 (m, 4H, $NC\underline{H}_2CH_2$), 4.62 (s, 4H, $OC\underline{H}_2C_{triazole}$), 4.20 (quint, 1H, $^3J_{CH,CH_2}$ = 5.4 Hz, H_{core}), 4.17-4.11 (m, 4H, H-6, $NCH_2C\underline{H}_2$), 4.02 (2 dd, $^2J_{6,6'}$ = 12.3 Hz, $^3J_{5,6'}$ = 2.4 Hz, 2H, H-6'), 3.95 (m_c, 2H, $NCH_2C\underline{H}'_2$), 3.63-3.52 (m, 5H, H-5 (1), $C_{core}C\underline{H}_2O$), 3.49 (ddd, $^3J_{4,5}$ = 9.6 Hz, $^3J_{5,6}$ = 4.7 Hz, $^3J_{5,6'}$ = 2.4 Hz, 1H, H-5 (2)), 2.19 (t, $^3J_{NHCOCH_2CH_2}$ = 7.5 Hz, 2H, $NHCOC\underline{H}_2$), 2.12, 2.06, 2.03, 1.95 (each s, 24H, 8 $COCH_3$), 1.59 (quin, $^3J_{NHCOCH_2CH_2}$ = 7.5 Hz, 2H, $NHCOCH_2C\underline{H}_2$), 1.36-1.27 (m, 4H, $NHCO(CH_2)_2C\underline{H}_2$, $C\underline{H}_2CH_3$), 0.89 (t, $^3J_{CH_2CH_3}$= 7.1 Hz, 3H, $C\underline{H}_3$) ppm;

^{13}C-NMR (126 MHz, MeOD, 300 K): δ = 176.3 (CONH), 172.3, 171.6, 171.5, 171.4 (8 $\underline{C}OCH_3$), 146.0 ($OCH_2\underline{C}_{triazole}$), 125.9 ($C_{triazole}N$), 98.6 (C-1), 70.6, 70.4 (C-2, C-3), 70.0 (C-5), 70.0 ($C_{core}\underline{C}H_2O$), 67.3, 67.2 (2 s, $NCH_2\underline{C}H_2$), 66.9 (C-4), 65.1, 65.0 ($O\underline{C}H_2C_{triazole}$), 63.3 (C-6), 51.0 ($N\underline{C}H_2CH_2$), 51.0 ($NH\underline{C}HCH_2$), 37.0 ($CNHCOC\underline{H}_2$), 32.5 ($NHCO(CH_2)_2C\underline{H}_2$), 26.7 ($NHCOCH_2C\underline{H}_2$), 23.4 ($\underline{C}H_2CH_3$), 20.7, 20.4 (8 $CO\underline{C}H_3$), 14.3 ($\underline{C}H_3$) ppm;

IR (ATR-IR): $\tilde{\nu}$ = 3433 (νCONH), 2944 (νCH_2), 1736 (νC=O), 1648 (νCONH), 1372 (νCH_2, νCH_3), 1227 (δCH_2), 1139, 1087, 1046 (νCOC), 836 (νC=CH) cm^{-1};

MALDI-MS: *m/z* = 1122.441, [M+Na]; (calc. 1122.434 for $C_{47}H_{69}N_7O_{23}$+Na).

3-Cascade: *N*-(1-oxo-hexyl)-aminomethane[3-1,1,1]: methoxymethyl: 1*H*[1,2,3] triazole-1-ethyl: 2,3,4,6-tetra-*O*-acetyl-α-D-mannopyranosid 29

Amino-tris{[1-(2,3,4,6-tetra-*O*-acetyl-α-D-mannopyranosyloxy)ethyl]-(4-methoxy)-1*H*-[1,2,3]-triazolyl}isobutan **26** (600 mg, 375 µmol) and HATU (214 mg, 563 µmol) were predried for 30 min in vacuo. After addition of dry DMF (20 mL) and hexanoic acid **27** (47.0 µL, 376 mmol) the mixture was cooled to 0 °C before DIPEA (77.0 µL, 442 µmol) was added. The mixture was stirred at room temperature for 16 h. Finally, the solvent was removed under reduced pressure and the crude product purified by column

chromatography (ethyl acetate/ cyclohexane/ methanol 6:4:1) to obtain compound **29** as a colourless foam.

Yield: 59.5 mg (44.9 μmol; 10 %);

DC: (ethyl acetate/ cyclohexane/ methanol, 8:2:1): R_f = 0.24;

Optical rotation: $[\alpha]^{20}_D$ = +31.6 (c = 0.23 in ethyl acetate);

^{1}H-NMR (600 MHz, MeOD, 300 K): δ = 8.00 (s, 3H, $H_{triazole}$), 5.20-5.14 (m, 6H, H-4, H-2), 5.15 (dd, $^3J_{2,3}$ = 3.2 Hz, $^3J_{3,4}$ = 10.2 Hz, 3H, H-3), 4.85 (s, 3H, H-1), 4.71-4.65 (m, 6H, $NC\underline{H}_2CH_2$), 4.59 (s, 6H, $OC\underline{H}_2C_{triazole}$), 4.16-4.11 (m, 6H, H-6, $NCH_2C\underline{H}_2$), 4.02 (dd, $^2J_{6,6'}$ = 12.3 Hz, $^3J_{5,6'}$ = 2.3 Hz, 3H, H-6'), 3.96-3.94 (m, 3H, H-7'), 3.80 (s, 6H, $C_{core}C\underline{H}_2O$), 3.52 (ddd, $^3J_{4,5}$ = 9.6 Hz, $^3J_{5,6}$ = 4.6 Hz, $^3J_{5,6'}$ = 2.3 Hz, 3H, H-5), 2.15 (t, $^3J_{NHCOCH_2CH_2}$ = 7.5 Hz, 2H, $NHCOC\underline{H}_2$), 2.12, 2.05, 2.02, 1.95 (each s, 36H, 12 $COCH_3$), 1.54 (quin, $^3J_{NHCOCH_2CH_2}$ = 7.5 Hz, 2H, $NHCOCH_2C\underline{H}_2$), 1.32-1.26 (m, 4H, $NHCO(CH_2)_2C\underline{H}_2$, $C\underline{H}_2CH_3$), 0.87 (t, $^3J_{CH_2CH_3}$= 7.0 Hz, 3H, $C\underline{H}_3$) ppm;

^{13}C-NMR (126 MHz, MeOD, 300 K): δ = 172.3 (CONH), 171.7, 171.3, 171.2 (12 $\underline{C}OCH_3$), 145.9 ($OCH_2\underline{C}_{triazole}$), 125.6 ($C_{triazole}\underline{C}N$), 98.3 (C-1), 70.3, 70.1 (C-2, C-3), 69.8 (C-5), 69.1 ($C_{core}\underline{C}H_2O$), 67.0 ($NCH_2\underline{C}H_2$), 66.6 (C-4), 65.1 ($O\underline{C}H_2C_{triazole}$), 63.0 (C-6), 61.1 ($NH\underline{C}CH_2$), 50.7 ($N\underline{C}H_2CH_2$), 37.4 ($NHCOC\underline{H}_2$), 32.2 ($NHCO(CH_2)_2C\underline{H}_2$), 26.5 ($NHCOCH_2C\underline{H}_2$), 23.2 ($\underline{C}H_2CH_3$), 20.4, 20.3 (12 $CO\underline{C}H_3$), 14.1 ($\underline{C}H_3$) ppm;

IR (ATR-IR): $\tilde{\nu}$ = 3436 (νCONH), 2930 (νCH_2), 1734 (νC=O), 1660 (νCONH), 1381 (νCH_2, νCH_3), 1241 (δCH_2), 1241, 1140, 1052 (νCOC), 839 (νC=CH) cm^{-1};

MALDI-MS: *m/z* = 1608.333, [M+Na]; (calc. 1607.599 for $C_{67}H_{96}N_{10}O_{34}$+Na).

2-Cascade: *N*-(1-oxo-hexyl)-aminomethane[2-1,1]: methoxymethyl: 1*H*[1,2,3] triazole-1-ethyl :*α*-D-mannopyranoside 30

Freshly prepared sodium methoxide solution (1 M, 50.0 μL) was added to a solution of compound **28** (63.8 mg, 58.0 μmol) in dry methanol (10 mL). After stirring at room temperature for 20 h the mixture was neutralised with Amberlite® IR 120 and filtered. The solvent was removed under reduced pressure to yield compound **30** as a colourless foam.

Yield: 41.9 mg (54.9 µmol; 95 %);

DC: (ethyl acetate/ methanol, 9:1): $R_f = 0$;

^{1}H-NMR (500 MHz, MeOD, 300 K): δ = 8.00 (2H, $H_{triazole}$), 4.73 (s, 2H, H-1) 4.86-4.62 (m, 4H, $NC\underline{H}_2CH_2$), 4.60 (s, 4H, $OC\underline{H}_2C_{triazole}$), 4.19 (quint, 1H, $^3J_{CH,CH_2}$ = 5.4 Hz, H_{core}), 4.14-4.10 (m, 2H, $NCH_2C\underline{H}_2$), 3.89-3.85 (m, 2H, $NCH_2C\underline{H}'_2$), 3.77 (dd, $^2J_{6,6'}$ = 11.8 Hz, $^3J_{5,6}$ = 2.2 Hz, 2H, H-6), 3.74 (dd, $^3J_{1,2}$ = 1.5 Hz, $^3J_{2,3}$ = 2.9 Hz, 2H, H-2), 3.65 (dd, $^2J_{6,6'}$ = 11.8 Hz, $^3J_{5,6'}$ = 5.9 Hz, 2H, H-6'), 3.60-3.52 (m, 4H, H-3, H-4, $C_{core}C\underline{H}_2O$), 3.24-3.19 (m, 2H, H-5), 2.20 (t, $^3J_{NHCOCH_2CH_2}$ = 7.5 Hz, 2H, $NHCOC\underline{H}_2$), 1.59 (quin, $^3J_{NHCOCH_2CH_2}$ = 7.5 Hz, 2H, $NHCOCH_2C\underline{H}_2$), 1.35-1.26 (m, 4H, $NHCO(CH_2)_2C\underline{H}_2$, $C\underline{H}_2CH_3$), 0.90 (t, $^3J_{CH_2CH_3}$ = 6.9 Hz, 3H, $C\underline{H}_3$) ppm;

^{13}C-NMR (126 MHz, MeOD, 300 K): δ = 176.3 (CONH), 145.8 ($OCH_2\underline{C}_{triazole}$), 125.5 ($C_{triazole}N$), 101.4 (C-1), 74.7 (C-5), 72.2, 68.1 (C-4, C-3), 71.6 (C-2), 69.8 ($C_{core}\underline{C}H_2O$), 66.4 ($NCH_2\underline{C}H_2$), 64.7 ($O\underline{C}H_2C_{triazole}$), 62.5 (C-6), 51.0 ($N\underline{C}H_2CH_2$), 50.1 ($NH\underline{C}HCH_2$), 36.7 ($CNHCOC\underline{H}_2$), 32.2 ($NHCO(CH_2)_2C\underline{H}_2$), 26.4 ($NHCOCH_2C\underline{H}_2$), 23.2 ($\underline{C}H_2CH_3$), 14.3 ($\underline{C}H_3$) ppm;

MALDI-MS: *m/z* = 802.598, [M+K]; 764.607, [M+H]; (calc. 802.324 for $C_{31}H_{53}N_7O_{15}$+K);

IR (ATR-IR): $\tilde{\nu}$ = 3324, 2924, 1640, 1546, 1367, 1226, 1134, 1091, 1052 cm^{-1}.

3-Cascade: *N*-(1-oxo-hexyl)-aminomethane[3-1,1,1]: methoxymethyl: 1*H*[1,2,3] triazole-1-ethyl: α-D-mannopyranosid 31

Freshly prepared sodium methoxide solution (1 M, 45.0 µL) was added to a solution of compound **29** (59.5 mg, 44.9 µmol) in dry methanol (10 mL). After stirring at room temperature for 20 h the mixture was neutralised with Amberlite® IR 120 and filtered. The solvent was removed under reduced pressure to yield compound **31** as a colourless syrup.

Yield: quant.;

DC: (ethyl acetate/ methanol, 9:1): $R_f = 0$;

^{1}H-NMR (500 MHz, MeOD, 300 K): δ = 7.98 (3H, $H_{triazole}$), 4.74 (d, $^{3}J_{1,2}$ = 1.54 Hz, 3H, H-1) 4.68-4.60 (m, 6H, $NC\underline{H}_2CH_2$), 4.57 (s, 6H, $OC\underline{H}_2C_{triazole}$), 4.14-4.10 (m, 3H, $NCH_2C\underline{H}_2$), 3.90-3.85 (m, 3H, $H_{NCH_2CH\underline{H}'}$), 3.79-3.75 (m, 12H, H-2, H-6, $C_{core}C\underline{H}_2O$), 3.66 (dd, $^{2}J_{6,6'}$ = 11.8 Hz, $^{3}J_{5,6'}$ = 5.9 Hz, 3H, H-6'), 3.61-3.57 (m, 6H, H-3, H-4), 3.27-3.23 (m, 3H, H-5), 2.17 (t, $^{3}J_{NHCOCH_2CH_2}$ = 7.5 Hz, 3H, $NHCOC\underline{H}_2$), 1.54 (quin, $^{3}J_{NHCOCH_2CH_2}$ = 7.6 Hz, 3H, $NHCOCH_2C\underline{H}_2$), 1.33-1.27 (m, 4H, $NHCO(CH_2)_2C\underline{H}_2$, $C\underline{H}_2CH_3$), 0.88 (t, $^{3}J_{CH_2CH_3}$= 7.0 Hz, 3H, $C\underline{H}_3$) ppm;

^{13}C-NMR (126 MHz, MeOD, 300 K): δ = 176.6 (CONH), 145.9 ($OCH_2\underline{C}_{triazole}$), 125.8 ($C_{triazole}\underline{C}N$), 101.7 (C-1), 74.9 (C-5), 72.5, 68.4 (C-4, C-3), 71.9 (C-2), 69.3 ($C_{core}\underline{C}H_2O$), 66.8 ($NCH_2\underline{C}H_2$), 65.2 ($O\underline{C}H_2C_{triazole}$), 62.8 (C-6), 51.3 ($N\underline{C}H_2CH_2$), 37.6 ($CNHCOC\underline{H}_2$), 32.4 ($NHCO(CH_2)_2C\underline{H}_2$), 26.7 ($NHCOCH_2C\underline{H}_2$), 23.5 ($\underline{C}H_2CH_3$), 14.3 ($\underline{C}H_3$) ppm;

MALDI-MS: *m/z* = 1082.060, [M+H]; (calc. 1081.490 for $C_{43}H_{72}N_{10}O_{22}$);

IR (ATR-IR): $\tilde{\nu}$ = 3323 (br, OH), 2925 (νCH_2), 1647 (νC=O), 1547 (CONH), 1365 (δOH), 1227 (δCH_2), 1134, 1090, 1052 (νCOC) cm^{-1}.

N-(Hexanoyloxy)succinimide 32[285, 289]

Hexanoic acid **27** (1.88 mL, 20.0 mmol) and DCC (3.73 g, 24.0 mmol) were dissolved in dry THF (40 mL), stirred for 10 min and then a solution of *N*-hydroxysuccinimide (2.08 g, 24.0 mmol) was added. The reaction mixture was stirred at room temperature for 60 h. The solvent was removed under reduced pressure and the crude product was purified by column chromatography (cyclohexane → cyclohexane/ ethyl acetate 5:1) to obtain compound **32** as a colourless oil which contained unreacted hexanoic acid. Compound **32** was used without further purification.

Yield: 3.48 g (16.3 mmol; 82 %), lit.[289]: 74 %;

TLC: R_f = 0.38 (cyclohexane/ ethyl acetate 7:1).

1,3-Bis(propargyloxy)-2-propanamine 38[420]

Trifluoroacetic acid (5.00 mL, 65.3 mmol) was added to a solution of Boc-protected compound **20** (3.23 g, 12.1 mmol) in DCM (40 mL). The mixture was stirred at room

temperature for 5 h before the solvent was removed under reduced pressure. The crude product was codestilled with DCM (3 x 60 mL) to obtain amine **38** quantitatively.

Yield: quant., lit.[420]: quant.;

TLC: R_f = 0.28 (cyclohexane/ ethyl acetate 9:1);

^{1}H-NMR: (500 MHz, $CDCl_3$, 300 K, TMS): δ = 6.65 (s, 1H, NH_2), 4.32-4.26 (m, 1H, $NH_2C\underline{H}$), 4.19-4.18 (d, ^4J = 2.4 Hz, 2H, $C\underline{H}H'C{\equiv}CH$), 4.18-4.17 (d, ^4J = 2.4 Hz, 2H, $CH\underline{H}'C{\equiv}CH$), 3.74-3.70 (dd, ^2J = 9.6 Hz, ^3J = 4.5 Hz, 2H, $NH_2C(C\underline{H}H')$), 3.67-3.64 (dd, ^2J = 9.6 Hz, ^3J = 5.5 Hz, 2H, $NH_2C(CH\underline{H}')$),2.47-2.46 (t, 2H, $CH_2C{\equiv}C\underline{H}$) ppm;

^{13}C-NMR (126 MHz, $CDCl_3$, 300 K, TMS): δ = 79.1 ($\underline{C}{\equiv}CH$), 75.3 ($C{\equiv}\underline{C}H$), 67.4 ($CH(\underline{C}H_2)_2$), 58.7 ($\underline{C}H_2C{\equiv}CH$), 49.2 ($\underline{C}H(CH_2)_2$) ppm;

EI-MS: *m/z* = 154.10, [M-CH]; (calc. 167.0946 for $C_9H_{13}NO_2$).

Tris[(propargyloxy)methyl]aminomethane 39[292]

Trifluoroacetic acid (5.00 mL, 65.3 mmol) was added to a solution of Boc-protected compound **21** (3.00 g, 8.94 mmol) in DCM (30 mL). The mixture was stirred at room temperature for 16 h before the solvent was removed under reduced pressure. The crude product was codestilled with DCM (3 x 60 mL) to obtain amine **39** quantitatively.

Yield: quant., lit.[292]: quant.;

TLC: R_f = 0.28 (cyclohexane/ ethyl acetate 9:1);

^{1}H-NMR: (500 MHz, MeOD, 300 K, TMS): δ = 4.22 (m, 6H, $C\underline{H}_2C{\equiv}CH$), 3.72 (s, 6H, $NH_2C(C\underline{H}_2)$), 2.93 (m, 3H, $CH_2C{\equiv}C\underline{H}$) ppm;

^{13}C-NMR (126 MHz, $CDCl_3$, 300 K, TMS): δ = 78.8 ($\underline{C}{\equiv}CH$), 75.7 ($C{\equiv}\underline{C}H$), 67.2 ($C(\underline{C}H_2)_3$), 59.5 ($\underline{C}(CH_2)_3$), 58.9 ($\underline{C}H_2C{\equiv}CH$) ppm;

IR (ATR): $\tilde{\nu}$ = 3299, 2899, 2859, 1656, 1179, 1142, 1098, 1019, 802, 722, 684, 629 cm^{-1};

EI-MS: *m/z* = 236.12887, [M+H]; (calc. 236.12867 for $C_{13}H_{17}NO_3$).

***N*-[1,3-Bis(propargyloxy)-2-propyl]hexylamide 40**

Amine **38** (327 mg, 1.96 mmol) and HATU (1.12 g, 2.95 mmol) were predried for 30 min in vacuo. After addition of hexanoic acid **27** (250 µL, 2.00 mmol) and dry DMF (12 mL) the mixture was cooled to 0 °C before DIPEA (410 µL, 2.35 mmol) was added. The mixture was stirred at 0 °C for 1 h and additional 16 h at room temperature. The solvent was removed under reduced pressure before the crude product was purified by column chromatography (cyclohexane/ ethyl acetate 4:1 → 1:1) to obtain compound **40** as a colourless oil.

Yield: 263 mg (991 µmol, 51 %);

TLC: R_f = 0.12 (cyclohexane/ ethyl acetate 4:1);

^{1}H-NMR: (500 MHz, $CDCl_3$, 300 K, TMS): δ = 5.84 (d, $^3J_{NHCH}$ = 8.01 Hz, 1H, NH), 4.31-4.25 (m, 1H, NHC<u>H</u>), 3.71-3.62 (dd, $^2J_{CHCH2}$ = 9.4 Hz, $^3J_{CHCH2}$ = 4.4 Hz, 2H, CHC<u>H</u>H‘), 3.61-3.55 (dd, $^2J_{CHCH2}$ = 9.4 Hz, $^3J_{CHCH2}$ = 5.7 Hz, 2H, CHCH<u>H</u>‘), 4.18-4.17 (d, $^4J_{CH2≡CH}$ = 2.4 Hz, 2H, C<u>H</u>H‘C≡CH), 4.17-4.16 (d, $^4J_{CH2≡CH}$ = 2.4 Hz, 2H, CH<u>H</u>‘C≡CH), 2.48-2.41 (t, $^4J_{CH2≡CH}$ = 2.3 Hz, 2H, CH_2C≡C<u>H</u>), 2.20-2.16 (dd, $^2J_{CH2}$ = 9.7 Hz, $^3J_{CH2CH2}$ = 5.6 Hz, 2H, (C=O)CH_2), 1.67-1.60 (m, 2H, CH_2), 1.35-1.27 (m, 4H, CH_2), 0.92-0.87 (t, $^3J_{CH2CH3}$ = 7.0 Hz 3H, CH_3) ppm;

^{13}C-NMR (126 MHz, $CDCl_3$, 300 K, TMS): δ = 173.0(C=O), 79.6 (<u>C</u>≡CH), 74.8 (C≡<u>C</u>H), 68.4 (CH(<u>C</u>H_2)$_2$), 58.6 (<u>C</u>H_2C≡CH), 48.1 (<u>C</u>H(CH_2)$_2$), 36.9 ((C=O)CH_2), 31.5, 25.5, 22.5 (CH_2), 14.1 (CH_3) ppm;

IR (ATR): ṽ = 3291, 2956, 2929, 1643, 1536, 1240, 1096, 663, 630 cm^{-1};

EI-MS: *m/z* = 265.16779, [M]; (calc. 265.16779 for $C_{15}H_{23}NO_3$).

***N*-{Tris[(propargyloxy)methyl]methyl]}hexylamide 41**

DCC (1.13 g, 8.93 mmol) and hexanoic acid **27** (1.06 mL, 8.50 mmol) were dissolved in ice-cold dry DCM (12 mL). After addition of a solution of amine **39** (1.00 g, 4.25 mmol) in dry DCM, the reaction mixture was stirred at 0 °C for 1 h and at room temperature for additional 16 h. The crude product was then filtered to remove precipitated dicyclohexylurea. The solvent was removed under reduced pressure and the crude product

was purified by column chromatography (cyclohexane/ ethyl acetate 4:1) yielding compound **41** as a colourless oil.

Yield: 964 mg (2.89 mmol, 68 %);

TLC: R_f = 0.38 (cyclohexane/ ethyl acetate 4:1);

^{1}H-NMR: (500 MHz, $CDCl_3$, 300 K, TMS): δ = 6.59 (s, 1H, NH), 4.19-4.15 (d, $^4J_{CH2≡CH}$ = 2.4 Hz, 6H, $C\underline{H}_2C≡CH$), 3.87 (s, 6H, $NHC(C\underline{H}_2)$), 2.48-2.43 (t, $^4J_{CH2≡CH}$ = 2.3 Hz, 3H, $CH_2C≡C\underline{H}$), 2.39-2.31 (m, 2H, $(C=O)CH_2$), 1.70-1.58 (m, 2H, CH_2), 1.39-1.27 (m, 4H, CH_2), 0.95-0.85 (t, $^3J_{CH2CH3}$ = 7.1 Hz 3H, CH_3) ppm;

^{13}C-NMR (126 MHz, $CDCl_3$, 300 K, TMS): δ = 179.8 (C=O), 79.2 ($\underline{C}≡CH$), 75.4 ($C≡\underline{C}H$), 67.7 ($C(\underline{C}H_2)_3$), 60.3 ($\underline{C}(CH_2)_3$), 58.7 ($\underline{C}H_2C≡CH$), 33.8 ($(C=O)CH_2$), 31.4, 24.3, 22.4 (CH_2), 13.9 (CH_3) ppm;

IR (ATR): $\tilde{\nu}$ = 3294, 2935, 1708, 1214, 1159, 1093, 632 cm^{-1};

EI-MS: *m/z* = 332.05, [M-H], 262.02 $[M-(CH_2)_4CH_3]$; (calc. 333.19401 for $C_{19}H_{27}NO_4$).

N-[1-(hydroxymethyl)-3-hydroxypropyl]-*N*-(hexyl)thiourea 43

A solution of serinol **15** (1.00 g, 11.0 mmol) and DIPEA (3.43 mL, 19.7 mmol) in dry DMF (12 mL) was prepared and subsequently added to a solution of hexyl isothiocyanate **42** (2.02 mL, 13.2 mmol) in dry DMF (12 mL). The mixture was stirred at room temperature for 16 h. The solvent was removed under reduced pressure and the crude product was purified by column chromatography (ethyl acetate) to obtain compound **43** as a colourless solid.

Yield: 2.34 g (9.98 mmol, 91 %);

TLC: R_f = 0.28 (ethyl acetate);

Melting point 52 °C;

^{1}H-NMR: (200 MHz, MeOD, 300 K): δ = 4.81 (s, 2H, OH), 4.41-4.28 (m, 1H, $NHC\underline{H}$), 3.76-3.59 (m, 4H, $CHC\underline{H}_2$), 3.51-3.39 (t, $^3J_{CH2CH2}$ = 6.9 Hz, 2H, $(NHCH_2)$, 1.66-1.48 (m, 2H, CH_2), 1.43-1.23 (m, 6H, CH_2), 0.96-0.87 (t, $^3J_{CH2CH3}$ = 6.8 Hz 3H, CH_3) ppm;

^{13}C-NMR (126 MHz, $CDCl_3$, 300 K, TMS): δ = 158.7 (C=S), 62.8 ($\underline{C}H(CH_2)_2$), 62.5 ($CH(\underline{C}H_2)_2$,), 31.7 ($(C=O)CH_2$), 26.8 (CH_2), 22.7 (CH_2), 14.2 (CH_3) ppm;

IR (ATR): $\tilde{\nu}$ = 3269, 2926, 2856, 1554, 1356, 1049, 1031, 673, 559 cm^{-1};

EI-MS: *m/z* = 234.14020, [M]; (calc. 234.14020 for $C_{10}H_{22}N_2O_2S$).

N-[*tert*-Butyl(1,3-bis(prop-2-in-1-yloxy)propan-2-yl)]-*N*-(hexyl)thiourea 44

A suspension of TRIS **16** (1.00 g, 8.25 mmol) and DIPEA (2.59 mL, 14.9 mmol) in dry DMF (40 mL) was prepared and subsequently added to a solution of hexyl isothiocyanate **42** (1.52 mL, 9.91 mmol) in dry DMF (12 mL). The mixture was stirred at room temperature for 16 h. The solvent was removed under reduced pressure and the crude product was purified by column chromatography (ethyl acetate) to obtain compound **43** as a colourless solid.

Yield: 1.16 g (4.39 mmol, 53 %);

TLC: R_f = 0.19 (ethyl acetate);

Melting point 84 °C;

^{1}H-NMR: (200 MHz, MeOD, 300 K): δ = 4.76 (s, 3H, OH), 3.65 (s, 6H, $C(CH_2)_3$), 3.50-3.40 (t, $^3J_{CH2CH2}$ = 6.9 Hz, 2H, ($NHCH_2$), 1.61-1.47 (m, 2H, CH_2), 1.40-1.21 (m, 6H, CH_2), 0.94-0.81 (t, $^3J_{CH2CH3}$ = 6.8 Hz 3H, CH_3) ppm;

^{13}C-NMR (126 MHz, $CDCl_3$, 300 K, TMS): δ = 157.6 (C=S), 64.7 ($\underline{C}(CH_2)_3$), 62.5 ($C(\underline{C}H_2)_3$), 32.7 ($(C=O)CH_2$), 30.0, 27.8, 23.7 (CH_2), 14.4 (CH_3) ppm;

IR (ATR): $\tilde{\nu}$ = 3282, 3251, 1246, 1091, 986, 646, 633 cm^{-1};

EI-MS: *m/z* = 264.15076, [M]; (calc. 264.15076 for $C_{11}H_{24}N_2O_3S$).

2-Isothiocyanato-1,3-dipropargyloxypropane 45

A solution of thiophosgene (1.85 mL, 24.1 mmol) in dry DCM (14 mL) was added dropwise to an ice-cold solution of amine **38** (2.00 g, 12.0 mmol) and triethylamine (4.94 mL, 35.6 mmol). The mixture was stirred at room temperature for 16 h. The solvent was removed under reduced pressure and the residue was dissolved in ethyl acetate (400 mL) and washed with H_2O (300 mL). The organic layer was dried over $MgSO_4$, filtered and the solvent removed under reduced pressure. The crude product was purified

by column chromatography (cyclohexane/ ethyl acetate 7:1) to yield compound **45** as a brownish oil.

Yield: 661 mg (3.16 mmol, 26 %);

TLC: R_f = 0.27 cyclohexane/ ethyl acetate 6:1);

^{1}H-NMR: (200 MHz, $CDCl_3$, 300 K): δ = 4.25-4.18 (d, $^4J_{CH2≡CH}$ = 2.4 Hz, 4H, C<u>H</u>$_2$C≡CH), 4.08-3.96 (m, 1H, (NCS)C<u>H</u>), 3.77-3.66 (m, 4H, CHC<u>H</u>$_2$), 2.50-2.44 (t, $^4J_{CH2≡CH}$ = 2.4 Hz, 2H, $CH_2C≡C$<u>H</u>) ppm;

EI-MS: *m/z* = 208.05, [M-H]; (calc. 209.05105 for $C_{10}H_{11}NO_2S$);

Tris(propargyloxymethyl)isothiocyanatomethane 46

Procedure A

A solution of thiophosgene (1.31 mL, 17.1 mmol) in dry DCM (10 mL) was added dropwise to an icecold solution of amine **39** (2.00 g, 8.50 mmol) and triethylamine (3.50 mL, 25.2 mmol). The mixture was stirred at room temperature for 16 h. The solvent was removed under reduced pressure and the residue was dissolved in ethyl acetate (400 mL) and washed with H_2O (300 mL). The organic layer was dried over $MgSO_4$, filtered and the solvent removed under reduced pressure. The crude product was purified by column chromatography (cyclohexane/ ethyl acetate 7:1) to yield compound **46** as a brownish oil.

Yield: 1.73 g (6.24 mmol, 73 %);

TLC: R_f = 0.34 cyclohexane/ ethyl acetate 6:1);

Procedure B

Azide **50** (600 mg, 2.30 mmol) was dissolved in $CHCl_3$ (20 mL) and carbon disulfide (5.63 mL, 93.2 mmol) and triphenyl phosphine (2.41 g, 9.20 mmol) were added. The mixture was stirred for 16 h at room temperature before the solvent was removed under reduced pressure. The crude product was purified by column chromatography (cyclohexane / ethyl acetate 6:1 → 2:1) to obtain compound **46** as a brownish oil.

Yield: 570 mg (2.06 mmol, 89 %);

TLC: R_f = 0.34 (cyclohexane/ ethyl acetate 6:1);

^{1}H-NMR: (500 MHz, $CDCl_3$, 300 K, TMS): δ = 4.18-4.16 (d, $^4J_{CH2≡CH}$ = 2.4 Hz, 6H, C<u>H</u>$_2$C≡CH), 3.87 (s, 6H, C(C<u>H</u>$_2$)$_3$), 2.47-2.45 (t, $^4J_{CH2≡CH}$ = 2.4 Hz, 3H, CH$_2$C≡C<u>H</u>) ppm;

^{13}C-NMR (126 MHz, $CDCl_3$, 300 K, TMS): δ = 157.0 (NCS), 79.2 (<u>C</u>≡CH), 75.2 (C≡<u>C</u>H), 67.8 (CH<u>C</u>H$_2$), 60.3 ((NCS)C$_q$), 58.9 (<u>C</u>H$_2$C≡CH) ppm;

EI-MS: *m/z* = 276.04, $[M-H]^+$; (calc. 277.07726 for $C_{14}H_{15}NO_3S$).

***N*-[1-(propargyloxymethyl)-3-propargyloxypropyl]-*N*-(hexyl)thiourea 48**

A solution of hexylamine **47** (283 µL, 2.15 mmol) and DIPEA (678 µL, 3.89 mmol) in dry DCM (5 mL) was prepared and then added to a solution of isothiocyanate **45** (542 mg, 2.59 mmol) in dry DCM (7 mL). The mixture was stirred at room temperature for 16 h. The solvent was removed under reduced pressure. Column chromatography (cyclohexane/ ethyl acetate 4:1) yielded compound **48** as a colourless oil.

Yield: 596 mg (1.92 mmol, 74 %);

TLC: R_f = 0.23 (cyclohexane/ ethyl acetate 4:1);

^{1}H-NMR: (500 MHz, $CDCl_3$, 300 K): δ = 4.19-4.18 (d, $^4J_{CH2≡CH}$ = 2.4 Hz, 2H, CH<u>H</u>‘C≡CH), 4.18-4.17 (d, $^4J_{CH2≡CH}$ = 2.4 Hz, 2H, CH<u>H</u>‘C≡CH), 4.45-4.32 (m, 1H, (NHC<u>H</u>), 3.75-3.65 (m, 4H, CHC<u>H</u>$_2$), 3.46-3.28 (m, 2H, NHC<u>H</u>$_2$), 2.46-2.44 (t, $^4J_{CH2≡CH}$ = 2.4 Hz, 2H, CH$_2$C≡C<u>H</u>), 1.61-1.55 (m, 2H, NHCH$_2$C<u>H</u>$_2$), 1.38-1.25 (m, 6H, CH$_2$), 0.90-0.86 (t, $^3J_{CH2CH3}$ = 6.9 Hz, 3H, CH$_3$) ppm;

^{13}C-NMR (126 MHz, $CDCl_3$, 300 K, TMS): δ = 181.9 (C=S), 79.2 (<u>C</u>≡CH), 75.2 (C≡<u>C</u>H), 69.3 (CH<u>C</u>H$_2$), 68.7 (NHCH$_2$), 58.7 (<u>C</u>H$_2$C≡CH), 53.9 (NHCH), 31.6, 28.9, 26.7, 22.6 (CH$_2$), 14.1 (CH$_3$) ppm;

IR (ATR): ṽ = 3297, 2918, 2850, 1649, 1248, 1097, 630 cm^{-1};

EI-MS: *m/z* = 152.12, $[M-NH(C=S)NH(CH)_2CH_3+H]^+$; (calc. 310.17150 for $C_{16}H_{26}N_2O_2S$).

Tris(propargyloxymethyl)azidomethane 50

Amine **39** (1.27 g, 5.41 mmol), potassium carbonate (1.49 g, 10.8 mmol) and $CuSO_4 \cdot 5H_2O$ (13.5 mg, 54.1 µmol) were dissolved in methanol (30 mL). After addition of imidazol-1-sulfonylazide hydrochloride **35** (1.81 g, 8.66 mmol) the reaction mixture was stirred at room temperature for 16 h. The solvent was removed under reduced pressure and the residue was dissolved in ethyl acetate (100 mL) and washed with H_2O (100 mL). The organic layer was dried over $MgSO_4$, filtered and the solvent removed under reduced pressure. The crude product was purified by column chromatography (cyclohexane/ ethyl acetate 3:1 → 1:1) to obtain compound **50** as raw product which was used without further purification.

Yield: 608 mg (2.33 mmol, 43 %);

TLC: R_f = 0.42 (cyclohexane/ ethyl acetate 1:1);

IR (ATR): $\tilde{\nu}$ = 3260, 2878, 2114, 1092 cm^{-1};

MALDI-MS: *m/z* = 284.3, [M+Na]; (calc. 284.10 for $C_{13}H_{15}N_3O_3$+Na).

2-Cascade: *N*-(1-hexylthioureamethane)[2-1,1]: methoxymethyl: 1*H*[1,2,3] triazole-1-ethyl: 2,3,4,6-tetra-*O*-acetyl-α-D-mannopyranosid 51

Alkyne **48** (435 mg, 1.40 mmol), mannoside **22** (1.17 g, 2.80 mmol) and copper bromide (80.3 mg, 560 µmol) were dissolved in dry DMF (12 mL). After addition of PMDTA (118 µL, 560 µmol) the mixture was stirred at room temperature for 16 h. The solvent was removed under reduced pressure end the residue dissolved in ethyl acetate (200 mL) and washed with H_2O (3 x 150 mL). The organic layer was dried over $MgSO_4$ and the solvent was removed under reduced pressure. Compound **51** was obtained as colourless solid after column chromatography (ethyl acetate/ cyclohexane 7:3 → ethyl acetate/ cyclohexane/methanol 7:3:1).

Yield: 987 mg (862 µmol, 62 %);

TLC: R_f = 0.17 (ethyl acetate/ cyclohexane/ methanol 7:3:1);

Melting point: 64 °C;

Rotational value: $[\alpha]_{20}^{D}$ = +24.8 (c = 0.28 in ethyl acetate);

^{1}H-NMR (500 MHz, $CDCl_3$, 300 K): δ = 7.72 (s, 2H, $H_{triazole}$), 6.38 (br s, 2H, NH), 5.28-5.15 (m, 6H, H-2, H-3, H-4), 4.80 (s, 2H, H-1), 4.70-4.55 (m, 8H, $NC\underline{H}_2CH_2$, $OCH_2C_{triazole}$), 4.23-4.17 (m, 2H, H-6), 4.16-4.10 (m, 2H, $NCH_2C\underline{H}H'$), 4.07-4.02 (m, 2H, H-6'), 3.92-3.87 (m, 2H, $NCH_2CH\underline{H}'$), 3.75-3.69 (m, 4H, $C_{core}CH_2O$), 3.60-3.53 (m, 2H, H-5), 3.48 (m, 1H, H_{core}), 2.14, 2.10, 2.04, 2.00 (each s, each 6H, 8 x $COCH_3$), 1.58-1.51 (dt, ^{2}J = 14.8 Hz, ^{3}J = 7.2 Hz, 2H, $NHC\underline{H}_2$), 1.36-1.25 (m, 6H, $(CH_2)_3$), 0.91-0.86 (t, ^{3}J = 6.9 Hz, 3H, CH_3) ppm;

^{13}C-NMR (126 MHz, $CDCl_3$, 300 K): δ = 170.8, 170.7, 170.2, 169.7 (8 $COCH_3$), 170.2 (C=S) 145.1, 145.0 ($OCH_2\underline{C}_{triazole}$), 124.1, 123.9 ($C_{triazole}$), 97.6 (C-1), 69.3 (C-2, C-3, C-5), 69.1 (C_{core}), 66.4 ($NCH_2\underline{C}H_2$), 66.3 ($C_{core}\underline{C}H_2O$), 65.8, 65.7 (C-4), 64.6, 64.5 ($O\underline{C}H_2C_{triazole}$), 62.3 (C-6), 49.8 ($N\underline{C}H_2CH_2$), 31.6, 29.1, 26.7 ($CH_2$), 22.6, 20.9, 20.8 ($C=O\underline{C}H_3$), 14.1 ($CH_3$) ppm;

IR (ATR): ṽ = 2931, 1742, 1368, 1217, 1087, 1043, 599 cm^{-1};

ESI-MS: *m/z* = 1183.46910, [M+K]; (calc. 1183.41189 for $C_{48}H_{72}N_8O_{22}S$+K).

Butyl-(1,3-dihydroxypropan-2-yl)carbamate 53[293]

Butyl chloroformate **52** (14.2 mL, 110 mmol) was added to an ice-cold solution of serinol **15** (10.0 g, 110 mmol) and sodium carbonate (23.3 g, 220 mmol) in H_2O (150 mL) and THF (80 mL). The mixture was stirred at room temperature for 16 h. H_2O (50 mL) was added to the mixture and it was extracted with ethyl acetate (4 x 200 mL). The combined organic layers were dried over $MgSO_4$, filtered and the solvent removed under reduced pressure. The residue was dissolved in a small amount of ethyl acetate and precipitated by adding cyclohexane (200 mL). Filtration yielded compound **53** as a colourless solid.

Yield: 18.5 g (96.9 mmol, 88 %); lit.[293]: 98 %;

TLC: R_f = 0.13 (cyclohexane/ ethyl acetate 2:1);

Melting point 64 °C;

^{1}H-NMR: (500 MHz, MeOD, 300 K): δ = 4.84 (s, 2H, OH), 4.03 (t, $^{3}J_{CH2CH2}$ = 6.5 Hz, 2H, $CH_2O(C=O)$), 3.66-3.56 (m, 5H, $CH(CH_2)_2$), 1.63-1.57 (m, 2H, $C\underline{H}_2CH_2CH_3$), 1.46-1.37 (m, 2H, $C\underline{H}_2CH_3$), 0.95 (t, $^{3}J_{CH2CH3}$ = 7.4 Hz, 3H, CH_3);

^{13}C-NMR (126 MHz, MeOD, 300 K, TMS): δ = 159.1 (C=O), 65.7 ($\underline{C}H_2O(C=O)$), 62.3 ($CH(C\underline{H}_2)_2$), 55.8 (CH), 32.3 ($\underline{C}H_2CH_2CH_3$), 20.1 ($\underline{C}H_2CH_3$), 14.1 (CH_3);

IR (ATR): ṽ = 3279, 2955, 2873, 1683, 1544, 1307, 1241, 1069, 1041, 741, 621 cm^{-1};

EI-MS: *m/z* = 191.11576, [M]; (calc. 191.11576 for $C_8H_{17}NO_4$).

Butyl-(2-Hydroxy-(1,1-Bishydroxymethyl)ethyl)carbamate 54

Butyl chloroformate **51** (24.0 mL, 186 mmol) was added to an icecold solution of TRIS **16** (15.0 g, 124 mmol) and sodium carbonate (26.3 g, 248 mmol) in H_2O (250 mL) and THF (140 mL). The mixture was stirred at room temperature for 16 h. H_2O (70 mL) was added to the mixture and it was extracted with ethyl acetate (5 x 200 mL). The combined organic layers were dried over $MgSO_4$, filtered and the solvent removed under reduced pressure. The residue was dissolved in a small amount of ethyl acetate and precipitated by adding cyclohexane (200 mL). Filtration yielded compound **54** as a colourless oil.

Yield: 10.8 g (48.8 mmol, 39 %);

TLC: R_f = 0.11 (cyclohexane/ ethyl acetate 2:1);

^{1}H-NMR: (500 MHz, MeOD, 300 K): δ = 4.84 (s, 3H, OH), 4.01 (t, $^{3}J_{CH2CH2}$ = 6.5 Hz, 2H, $CH_2O(C=O)$), 3.72 (s, 6H, CH_2), 1.63-1.58 (m, 2H, $C\underline{H}_2CH_2CH_3$), 1.44-1.37 (m, 2H, $C\underline{H}_2CH_3$), 0.95 (t, $^{3}J_{CH2CH3}$ = 7.4 Hz, 3H, CH_3);

^{13}C-NMR (126 MHz, MeOD, 300 K, TMS): δ = 158.6 (C=O), 65.7 ($\underline{C}H_2O(C=O)$), 62.6 ($CH(C\underline{H}_2)_2$), 61.7 (C_q), 32.2 ($\underline{C}H_2CH_2CH_3$), 20.1 ($\underline{C}H_2CH_3$), 14.1 (CH_3);

IR (ATR): ṽ = 3396, 2960, 2875, 1748, 1696, 1241, 1050, 789 cm^{-1};

EI-MS: *m/z* = 208.05, [M-2 x CH_2OH], 116.02, [M-$C(CH_2OH)_3$]; (calc. 221.12632 for $C_9H_{19}NO_5$).

Butyl-(1,3-dipropargyloxypropan-2-yl)carbamate 55

Diol **53** (700 mg, 3.66 mmol) and freshly pestled potassium hydroxide (1.69 g, 30.1 mmol) were dissolved in dry DMF (20 mL) and cooled to 0 °C. Propargyl bromide **19** (80 % in toluene, 2.60 mL, 23.4 mmol) was added and the mixture stirred at

40 °C for 4 h and additional 16 h at room temperature. The solvent was removed under reduced pressure and the residue dissolved in ethyl acetate (50 mL). After washing with H_2O (3 x 40 mL) the organic layer was dried over $MgSO_4$, filtered and the solvent removed under reduced pressure. Column chromatography (cyclohexane/ ethyl acetate 6:1 → 2:1) yielded compound **55** as a brown oil.

Yield: 255 mg (955 µmol, 36 %);

TLC: R_f = 0.45 (cyclohexane/ ethyl acetate 2:1);

^{1}H-NMR: (200 MHz, $CDCl_3$, 300 K): δ = 4.41-4.27 (s, 2H, NH), 4.17-4.08 (m, 6H, CH_2O(C=O), C$\underline{H}_2$C≡CH), 3.81-3.73 (m, 4H, CH_2), 2.44-2.40 (t, $^4J_{CH2≡CH}$ = 2.0 Hz, 2H, CH_2C≡C$\underline{H}$), 2.20-2.13 (m, 1H, NHC$\underline{H}$), 1.68-1.55 (m, 2H, C$\underline{H}_2CH_2CH_3$), 1.47-1.33 (m, 2H, C$\underline{H}_2CH_3$), 0.97-0.88 (t, $^3J_{CH2CH3}$ = 7.3 Hz, 3H, CH_3);

^{13}C-NMR (126 MHz, $CDCl_3$, 300 K, TMS): δ = 156.5 (C=O), 79.6 (C≡CH), 74.8 (C≡$\underline{C}$H), 68.6 (CH$\underline{C}H_2$), 58.6 ($\underline{C}H_2$C≡CH), 53.9 (NHCH), 49.9 (CH_2(C=O)), 31.1, 19.2 (CH_2), 13.9 (CH_3) ppm;

IR (ATR): ṽ = 3292, 2959, 2873, 1704, 1513, 1239, 1096, 1075, 630 cm^{-1};

EI-MS: *m/z* = 268.15456, [M+H]; (calc. 268.15488 for $C14H_{21}NO_4$+H).

2-Cascade: (Butylchloroformate)-methane[2-1,1,1]:methoxymethyl: 1*H*[1,2,3] triazole-1-ethyl: tetra-O-acetyl-α-D-mannopyranoside 57

Variante A Click

Alkyne **55** (1.12 g, 4.18 mmol), mannoside **22** (3.49 g, 8.36 mmol) and copper bromide (246 mg, 1.67 mmol) were dissolved in dry DMF (24 mL). After addition of PMDTA (351 µL, 1.67 mmol) the mixture was stirred at room temperature for 16 h. The solvent was removed under reduced pressure and the residue dissolved in ethyl acetate (250 mL) and washed with H_2O (3 x 200 mL). The organic layer was dried over $MgSO_4$ and the solvent was removed under reduced pressure. Compound **57** was obtained after column chromatography (ethyl acetate/ cyclohexane/methanol 6:4:1 → ethyl acetate/ cyclohexane/methanol 7:3:1).

Yield: 3.50 g (3.18 mmol, 76 %);

TLC: R_f = 0.24 (ethyl acetate/ cyclohexane/methanol 7:3:1);

Variante B Butyl chloroformate

To an ice-cold solution of compound **58** (1.28 g, 1.93 mmol) and sodium bicarbonate (551 mg, 6.56 mmol) in water (50 mL) and 1,4 dioxane (20 mL) was added butylchloroformate **52** (375 µL, 2.90 mmol). After stirring at room temperature for 60 h the solvent was removed at reduced pressure and the mixture was codestilled with methanol (2 x 60 mL). The residue was dissolved in acetic anhydride (4.00 mL) and stirred for 4 h. The solvent was removed under reduced pressure again and the remaining crude product was purified by column chromatography (ethyl acetate → ethyl acetate/methanol 15:1) to yield compound **57** as a colourless foam.

Yield: 1.53 g (1.39 mmol, 72 %);

TLC: R_f = 0.24 (ethyl acetate/ cyclohexane/methanol 7:3:1);

Melting point: 63 °C;

Rotational value: $[\alpha]_{25}^{D}$ = +28.3 (c = 1.12 in dichloromethane);

^{1}H-NMR: (500 MHz, $CDCl_3$, 300 K): δ = 7.73 (each s, each 1H, $CH_{triazole}$), 5.43-5.37 (m, 1H, $NH_{carbamate}$), 5.29-5.16 (m, 6H, H-2, H-3, H-4), 4.81, 4.80 (each d, $^3J_{1,2}$ = 1.3 Hz, each 1H, H-1), 4.68-4.57 (m, 8H, $N_{triazole}CH_2$, $OCH_2C_{triazole}$), 4.21 (dd, $^3J_{5,6}$ = 5.1 Hz, $^2J_{6,6'}$ = 12.4 Hz, 2H, H-6), 4.16-4.11 (m, 2H, $N_{triazole}CH_2C\underline{H}$), 4.07-4.02 (m, 4H, H-6', $O_{carbamate}CH_2$), 3.99-3.95 (m, 1H, $N_{carbamate}CH$), 3.93-3.87 (m, 2H, $N_{triazole}CH_2C\underline{H}$'), 3.68-3.55 (m, 6H, $N_{carbamate}CHCH_2$, H-5), 2.14, 2.10, 2.09, 2.04, 2.00 (each s, 24H, $OCOCH_3$), 1.61-1.54 (m, 2H, $C\underline{H}_2CH_2CH_3$), 1.40-1.32 (m, 2H, $CH_2C\underline{H}_2CH_3$), 0.92 (t, $^3J_{CH2CH3}$ = 7.4 Hz 3H, CH_3) ppm;

^{13}C-NMR: (126 MHz, $CDCl_3$, 300 K): δ = 170.7, 170.1, 169.7 ($\underline{C}OCH_3$), 156.1 (OC=O), 145.1 ($\underline{C}_{triazole}CH$), 124.2 ($C_{triazole}\underline{C}H$), 97.7 (C-1), 69.3, 69.1 (CCH_2), 69.0, 65.8 (C-2, C-3, C-4, C-5), 66.3 ($N_{triazole}CH_2\underline{C}H_2$), 64.7 ($O\underline{C}H_2C_{triazole}$), 64.4 ($O_{carbamate}CH_2$), 62.3 (C-6), 58.8 ($\underline{C}_qCH2$), 49.8 ($N_{triazole}CH_2$), 31.2 ($\underline{C}H_2CH_2CH_3$), 20.9, 20.8 ($OCO\underline{C}H_3$), 19.2 ($CH_2\underline{C}H_2CH_3$), 13.9 ($CH_2\underline{C}H_3$) ppm;

IR (ATR-IR): $\tilde{\nu}$ = 2359, 2139, 1225, 1043, 753, 746 cm^{-1};

ESI-MS: *m/z* = 1102.4, [M+Na]; (calc. 1102.432 for $C_{46}H_{67}N_7O_{24}$+H).

2-Cascade: Aminomethane[2-1,1]: methoxymethyl: 1*H*[1,2,3]triazole-1-ethyl: 2,3,4,6-tetra-*O*-α-D-mannopyranosid 58

The crude product **25** (921 mg, 619 µmol) was subsequently dissolved in dry methanol (30 mL) and 1M sodium methoxide solution (1.55 mL) was added. After stirring for 16 h at room temperature the mixture was neutralised with ion exchanger Amberlite® IR 120. The resin was filtered off and the solvent was removed under reduced pressure to yield compound **58** quantitatively as a colourless syrup.

Yield: quant.;

TLC: R_f = 0.0 (ethyl acetate/ cyclohexane/methanol 7:3:1);

Rotational value: $[\alpha]_{20}^{D}$ = +30.7 (c = 0.05 in methanol);

^{1}H-NMR (500 MHz, MeOD, 300 K): δ = 8.03 (s, 2H, $H_{triazole}$), 4.72-4.71 (d, $^3J_{1,2}$ = 1.4 Hz, 2H, H-1), 4.68-4.62 (m, 8 H, $OCH_2C_{triazole}$, $NC\underline{H}_2CH_2$), 4.14-4.09 (m, 2H, $NCH_2C\underline{H}H$‘), 3.94-3.84 (m, 3H, $NCH_2CH\underline{H}$‘, $C\underline{H}(CH_2)_2$), 3.75-3.69 (m, 6H, H-2, H-6, H-6‘), 3.69-3.50 (m, 8H, $C_{core}CH_2O$, H-3, H-4), 3.10-3.05 (m, 2H, H-5);

^{13}C-NMR: (126 MHz, MeOD, 300 K): δ = 145.3 ($\underline{C}_{triazole}CH$), 125.9 ($C_{triazole}\underline{C}H$), 101.1 (C-1), 74.7 ($C_q$), 74.6 (C-5), 72.1 (C-3), 71.4 (C-2), 68.0 ($NH_2CH\underline{C}H_2$), 67.9 (C-4), 66.1 ($N_{triazole}CH_2\underline{C}H_2$), 64.6 ($O\underline{C}H_2C_{triazole}$), 62.3 (C-6), 52.1 ($\underline{C}H(CH_2)_2$), 50.9 ($N_{triazole}CH_2$) ppm;

IR (ATR-IR): $\tilde{\nu}$ = 3324, 2948, 2837, 1650, 1449, 1016, 750, 578, 517 cm^{-1};

ESI-MS: *m/z* = 666.29288, [M+H]; (calc. 666.29408 for $C_{25}H_{43}N_7O_{14}$+H).

3-Cascade: Aminomethane[3-1,1]: methoxymethyl: 1*H*[1,2,3]triazole-1-ethyl: 2,3,4,6-tetra-*O*-α-D-mannopyranosid 59

The crude product **26** (921 mg, 619 µmol) was subsequently dissolved in dry methanol (30 mL) and 1M sodium methoxide solution (1.55 mL) was added. After stirring for 16 h at room temperature the mixture was neutralised with ion exchanger Amberlite® IR 120. The resin was filtered off and the solvent was removed under reduced pressure to yield compound **59** quantitatively as colorless syrup.

Yield: quant.;

TLC: R_f = 0.0 (ethyl acetate/ cyclohexane/methanol 7:3:1);

Rotational value: $[\alpha]_{20}^{D}$ = +23.6 (c = 0.01 in methanol);

^{1}H-NMR (600 MHz, MeOD, 300 K): δ = 8.03 (s, 3H, $H_{triazole}$), 4.73-4.71 (m, 3H, H-1), 4.67-4.62 (m, 12 H, $OCH_2C_{triazole}$, $NC\underline{H}_2CH_2$), 4.15-4.10 (m, 3H, $NCH_2C\underline{H}H$'), 3.90-3.85 (m, 3H, $NCH_2CH\underline{H}$'), 3.77-3.73 (m, 6H, H-2, H-6), 3.66-3.61 (m, 9H, H-6', $C_{core}CH_2O$), 3.61-3.53 (m, 6H, H-3, H-4), 3.16-3.12 (m, 3H, H-5);

^{13}C-NMR: (151 MHz, MeOD, 300 K): δ = 145.1 ($\underline{C}_{triazole}CH$), 126.0 ($C_{triazole}\underline{C}H$), 101.6 (C-1), 74.9 (C-5), 72.5 (C-3), 71.9 (C-2), 69.8 (NH_2CCH_2), 68.4 (C-4), 66.7 ($N_{triazole}CH_2\underline{C}H_2$), 65.2 ($O\underline{C}H_2C_{triazole}$), 62.8 (C-6), 51.4 ($N_{triazole}CH_2$) ppm;

IR (ATR-IR): $\tilde{\nu}$ = 3325, 2923, 1596, 1369, 1226, 1133, 1090, 1052, 1031, 977, 578 cm^{-1};

ESI-MS: *m/z* = 983.41443, $[M+H]^+$ (calc. 983.41692 for $C_{37}H_{63}N_{10}O_{21}$ + H).

3-Cascade: (Butylchloroformate)-methane[3-1,1,1]:methoxymethyl:1*H*[1,2,3] triazole-1-ethyl: tetra-O-acetyl-α-D-mannopyranoside 60

To an ice-cold solution of compound **59** (660 mg, 672 µmol) and sodium bicarbonate (192 mg, 2.28 mmol) in water (40 mL) and 1,4 dioxane (20 mL) was added butylchloroformiate **52** (131 µL, 1.01 mmol). After stirring at room temperature for 60 h the solvent was removed at reduced pressure and the mixture was codestilled with methanol (2 x 60 mL). The residue was dissolved in acetic anhydride (4.00 mL) and stirred for 4 h. The solvent was removed under reduced pressure again and the remaining crude product was purified by column chromatography (ethyl acetate → ethyl acetate/methanol 30:1) to yield compound **60** as a colourless foam.

Yield: 633 mg (399 µmol, 59 %);

TLC: R_f = 0.35 (ethyl acetate / cyclohexane / methanol, 8:2:1);

Melting point: 79 °C;

Rotational value: $[\alpha]_{20}^{D}$ = +28.7 (c = 0.28 in ethyl acetate);

^{1}H-NMR: (500 MHz, $CDCl_3$, 300 K): δ = 7.75 (s, 3H, $CH_{triazole}$), 5.31 (s, 1H, $NH_{carbamate}$), 5.27-5.19 (m, 9H, H-2, H-3, H-4), 4.82 (s, 3H, H-1), 4.65-4.62 (m, 12H, $N_{triazole}CH_2$, $OCH_2C_{triazole}$), 4.23-4.19 (dd, $^3J_{5,6}$ = 5.1 Hz, $^2J_{6,6'}$ = 12.3 Hz, 3H, H-6), 4.16 (m, 3H,

$N_{triazole}CH_2C\underline{H}$), 4.02 (dd, $^2J_{6,6'}$ = 12.3 Hz, $^3J_{5,6'}$ = 2.4 Hz, 3H, *H*-6'), 3.97 (t, $^3J_{CH2CH3}$ = 6.7 Hz, 2H, $O_{carbamate}CH_2$), 3.94-3.89 (m, 3H, $N_{triazole}CH_2C\underline{H}$'), 3.77 (m, 6H, $N_{carbamate}CCH_2$), 3.63 (ddd, $^3J_{4,5}$ = 9.4 Hz, $^3J_{5,6}$ = 5.1 Hz, $^3J_{5,6'}$ = 2.4 Hz, 3H, *H*-5), 2.14, 2.09, 2.04, 1.99 (each s, each 9H, $OCOCH_3$), 1.58-1.53 (m, 2H, $C\underline{H}_2CH_2CH_3$), 1.39-1.31 (m, 2H, $CH_2C\underline{H}_2CH_3$), 0.91 (t, $^3J_{CH2CH3}$ = 7.4 Hz 3H, CH_3) ppm;

^{13}C-NMR: (126 MHz, $CDCl_3$, 300 K): δ = 170.7, 170.2, 170.1, 169.7 ($\underline{C}OCH_3$), 156.5 (OC=O), 145.2 ($\underline{C}_{triazole}CH$), 124.0 ($C_{triazole}\underline{C}H$), 97.6 (C-1), 69.3, 69.0 (CCH_2), 69.1, 66.3 (C-2, C-3, C-4, C-5), 66.4 ($N_{triazole}CH_2\underline{C}H_2$), 65.8 ($O\underline{C}H_2C_{triazole}$), 64.8 ($O_{carbamate}CH_2$), 64.6 (C-6), 50.2 ($NH\underline{C}CH_2$), 49.8 ($N_{triazole}CH_2$), 31.2 ($\underline{C}H_2CH_2CH_3$), 20.9, 20.8, 20.7 ($OCO\underline{C}H_3$), 19.2 ($CH_2\underline{C}H_2CH_3$), 13.9 ($CH_2\underline{C}H_3$) ppm**;**

IR (ATR-IR): $\tilde{\nu}$ = 2960, 1741, 1434, 1368, 1216, 1137, 1085, 1042, 980, 600 cm^{-1};

ESI-MS: *m/z* = 1609.5, [M+Na]; (calc. 1609.578 for $C_{66}H_{94}N_{10}O_{35}$+Na).

2-Cascade: (Butylchloroformate)-methane[2-1,1,1]:methoxymethyl:1*H*[1,2,3] triazole-1-ethyl: α-D-mannopyranoside 61

To a solution of compound **57** (1.45 g, 1.32 mmol) in dry methanol (15 mL) was added a 1M sodium methoxide solution (2.30 mL). After stirring for 16 h at room temperature the mixture was neutralised with ion exchanger Amberlite® IR 120. The resin was filtered off and the solvent was removed under reduced pressure to yield compound **61** quantitatively as a colourless solid.

Yield: quant.;

TLC: R_f = 0.05 (ethyl acetate / cyclohexane / methanol, 8:2:1);

Rotational value: $[\alpha]_{25}^{D}$ = +32.7 (c = 0.97 in methanol);

^{1}H-NMR: (600 MHz, MeOD, 300 K, TMS): δ = 7.99 (s, 2H, $CH_{triazole}$), 4.83 (s, 8H, OH), 4.72 (s, 2H, H-1), 4.67-4.60 (m, 4H, $N_{triazole}CH_2$), 4.60 (s, 4H, $OCH_2C_{triazole}$), 4.14-4.09 (m, 2H, $N_{triazole}CH_2C\underline{H}$), 4.02 (t, $^3J_{CH2CH3}$ = 6.4 Hz, 2H, $O_{carbamate}CH_2$), 3.91-3.84 (m, 3H, $N_{triazole}CH_2C\underline{H}$', NHC$\underline{H}$), 3.78-3.73 (m, 4H, H-2, H-6), 3.64 (dd, $^2J_{6,6'}$ = 11.8 Hz, $^3J_{5,6'}$ = 6.0 Hz, 2H, *H*-6'), 3.60-3.52 (m, 8H, $N_{carbamate}CCH_2$, H-3, H-4), 3.23-3.19 (m, 2H, H-5), 1.62-1.56 (m, 2H, $C\underline{H}_2CH_2CH_3$), 1.42-1.35 (m, 2H, $CH_2C\underline{H}_2CH_3$), 0.94 (t, $^3J_{CH2CH3}$ = 7.4 Hz 3H, CH_3) ppm;

^{13}C-NMR: (126 MHz, MeOD, 300 K, TMS): δ = 159.0 (OC=O), 145.9 ($\underline{C}_{triazole}CH$), 125.8 ($C_{triazole}\underline{C}H$), 101.7 (C-1), 75.0 (C-5), 72.5 (C-3), 71.9 (C-2), 70.4 ($N_{carbamate}CCH_2$), 68.4 (C-4), 66.8 ($N_{triazole}CH_2\underline{C}H_2$), 65.8 ($O_{carbamate}CH_2$), 65.1 ($O\underline{C}H_2C_{triazole}$), 62.9 (C-6), 51.4 (NHCH), 51.3 ($N_{triazole}CH_2$), 32.3 ($\underline{C}H_2CH_2CH_3$), 20.2 ($CH_2\underline{C}H_2CH_3$), 14.1 ($CH_2\underline{C}H_3$) ppm;

IR (ATR-IR): $\tilde{\nu}$ = 3309, 1692, 1055, 806, 6721368 cm^{-1};

ESI-MS: *m/z* = 765.19759, [M]; (calc. 765.33923 for $C_{30}H_{51}N_7O_{16}$).

3-Cascade: (Butylchloroformate)-methane[3-1,1,1]:methoxymethyl:1*H*[1,2,3] triazole-1-ethyl: tetra-O-acetyl-α-D-mannopyranoside 62

To a solution of compound **60** (500 mg, 315 µmol) in dry methanol (10 mL) was added a 1M sodium methoxide solution (788 µL). After stirring for 16 h at room temperature the mixture was neutralised with ion exchanger Amberlite® IR 120. The resin was filtered off and the solvent was removed under reduced pressure to yield compound **62** quantitatively as a colourless foam.

Yield: quant.;

TLC: R_f = 0.35 (ethyl acetate / cyclohexane / methanol, 8:2:1);

Rotational value: $[\alpha]_{25}^{D}$ = +34.6 (c = 0.96 in methanol);

^{1}H-NMR: (600 MHz, MeOD, 300 K): δ = 7.98 (s, 3H, $CH_{triazole}$), 4.83 (s, 12H, OH), 4.73 (d, $^{3}J_{1,2}$ = 1.3 Hz, 3H, H-1), 4.68-4.60 (m, 6H, $N_{triazole}CH_2$), 4.58 (s, 6H, $OCH_2C_{triazole}$), 4.14-4.10 (m, 3H, $N_{triazole}CH_2C\underline{H}$), 3.96 (t, $^{3}J_{CH2CH3}$ = 6.7 Hz, 2H, $O_{carbamate}CH_2$), 3.90-3.85 (m, 3H, $N_{triazole}CH_2C\underline{H}$‘), 3.79-3.75 (m, 6H, H-2, H-6), 3.70 (m, 6H, $N_{carbamate}CCH_2$), 3.66 (dd, $^{2}J_{6,6'}$ = 11.8 Hz, $^{3}J_{5,6'}$ = 5.9 Hz, 3H, *H*-6’), 3.63-3.57 (m, 6H, H-3, H-4), 3.28-3.26 (m, 3H, H-5), 1.60-1.55 (m, 2H, $C\underline{H}_2CH_2CH_3$), 1.41-1.34 (m, 2H, $CH_2C\underline{H}_2CH_3$), 0.93 (t, $^{3}J_{CH2CH3}$ = 7.4 Hz 3H, CH_3) ppm;

^{13}C-NMR: (126 MHz, MeOD, 300 K): δ = 158.0 (OC=O), 145.8 ($\underline{C}_{triazole}CH$), 125.7 ($C_{triazole}\underline{C}H$), 101.6 (C-1), 74.8 (C-5), 72.3 (C-3), 71.7 (C-2), 69.5 ($N_{carbamate}CCH_2$), 68.3 (C-4), 66.7 ($N_{triazole}CH_2\underline{C}H_2$), 65.3 ($O_{carbamate}CH_2$), 65.1 ($O\underline{C}H_2C_{triazole}$), 62.7 (C-6), 60.1 ($CCH_2$), 51.1 ($N_{triazole}CH_2$), 32.1 ($\underline{C}H_2CH_2CH_3$), 20.0 ($CH_2\underline{C}H_2CH_3$), 14.0 ($CH_2\underline{C}H_3$) ppm;

ESI-MS: *m/z* = 1105.44910, [M+Na]; (calc. 1105.45130 for $C_{42}H_{70}N_{10}O_{23}$+Na);

IR (ATR-IR): $\tilde{\nu}$ = 3332 (νOH), 1261, 1053, 765 cm^{-1}.

8.3.2 Bacterial adhesion assay

Buffers: PBS buffer: PBS tablets were obtained from GIBCO containing phosphate (as sodium phosphates), 10 mM, potassium chloride (KCl), 2.68 mM, sodium chloride (NaCl), 140 mM, pH = 7.45; PBST buffer: PBS buffer + 0.05% v/v Tween®20; carbonate buffer solution (pH 9.6): sodium carbonate (10.6 g) and sodium hydrogen carbonate (8.40 g) were dissolved in bidest. Water (1.0 L), pH values were adjusted by using 0.1 M HCl or 0.1 M NaOH.

Bacterial culture: The GFP-tagged strain PKL1162 was constructed in the KLEMM group by introduction of the plasmid pPKL174 into strain SAR18. Plasmid pPKL174 contains the fim gene cluster, which is required for type 1 fimbriae assembly and expression. The chromosome of strain SAR18 from the REISNER group contains the GFP gene, controlled by a constitutive promotor.[239, 421] The bacterial strain PKL1162[421] was cultured from a frozen stock in LB media (+ampicillin 100 mg/mL and chloramphenicol 50 mg/mL) overnight at 37 °C. The bacterial pellet resulting after centrifugation and decantation of media was washed twice with PBS (2 mL) and suspended in PBS buffer afterwards. The bacterial suspension was adjusted to OD_{600} = 0.4 with PBS.

Functionalisation of microtiter plates and the adhesion assay was performed according to HARTMANN et al.[239] Black Immobilizer Amino™ F96 MicroWell™ plates (Nunc) were incubated overnight with a 25 mM solution of amine **7** in PBS buffer (100 µL/well, 100 rpm, room temperature). Plates were washed with PBST three times and afterwards glucosides **13**, **14**, **61** and **62** were added to the plate with serial dilution, starting from a 25 mM solution in PBS (50 µL/well). Microtiter plates were subsequently irradiated with a mercury vapour discharge lamp with a wavelength of 254 nm for 30 minutes. After washing three times with PBST, functional groups which remained unreacted on the microtiter plate were blocked with a 20 mM solution of ethanolamine in carbonate buffer (120 µL/well, room temperature, 100 rpm, 2.5 h). Afterwards, wells were washed with PBST twice and finally once with PBS. The prepared bacterial suspension was added then (50 µL/well). After incubation for one hour at 37 °C and 100 rpm, microtiter plates were washed three times with PBS and filled with PBS (100 µL/well) for terminal fluorescence intensity read out (excitation wavelength 485 nm, emission wavelength 535 nm).

8.3.3 ^{1}H and ^{13}C NMR spectra of synthesised compounds

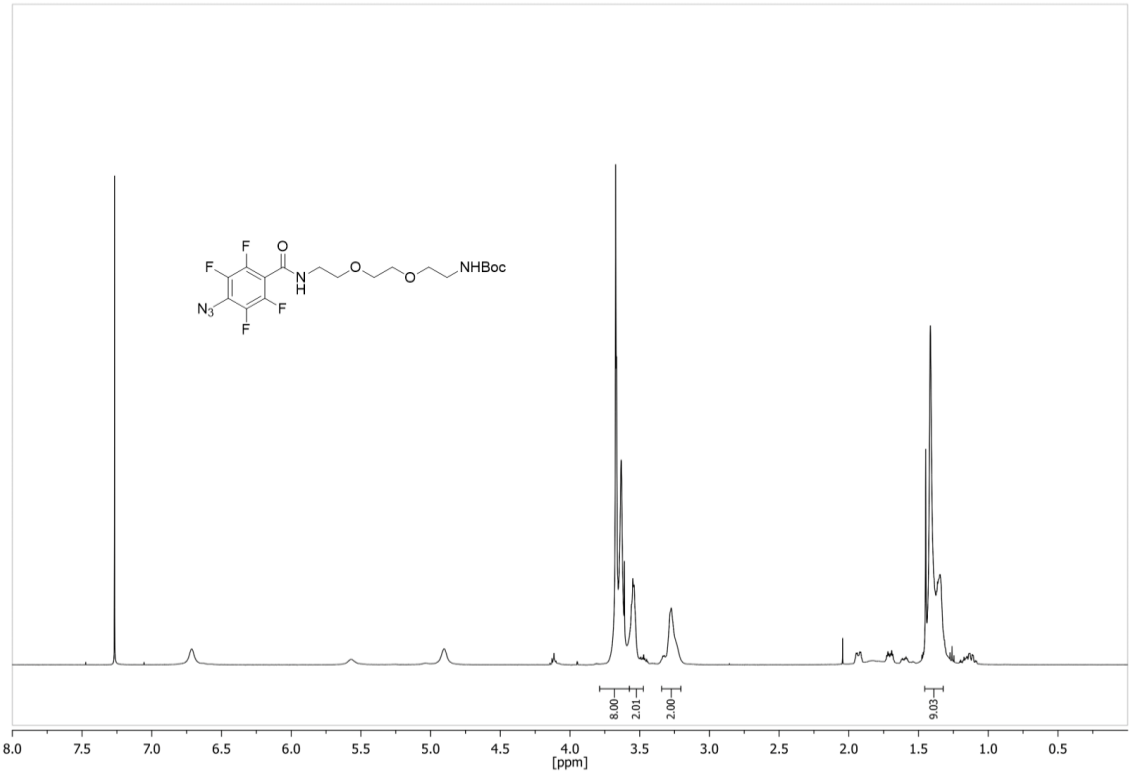

Figure 215: ^{1}H NMR spectrum of **6** (500 MHz, $CDCl_3$, 300 K).

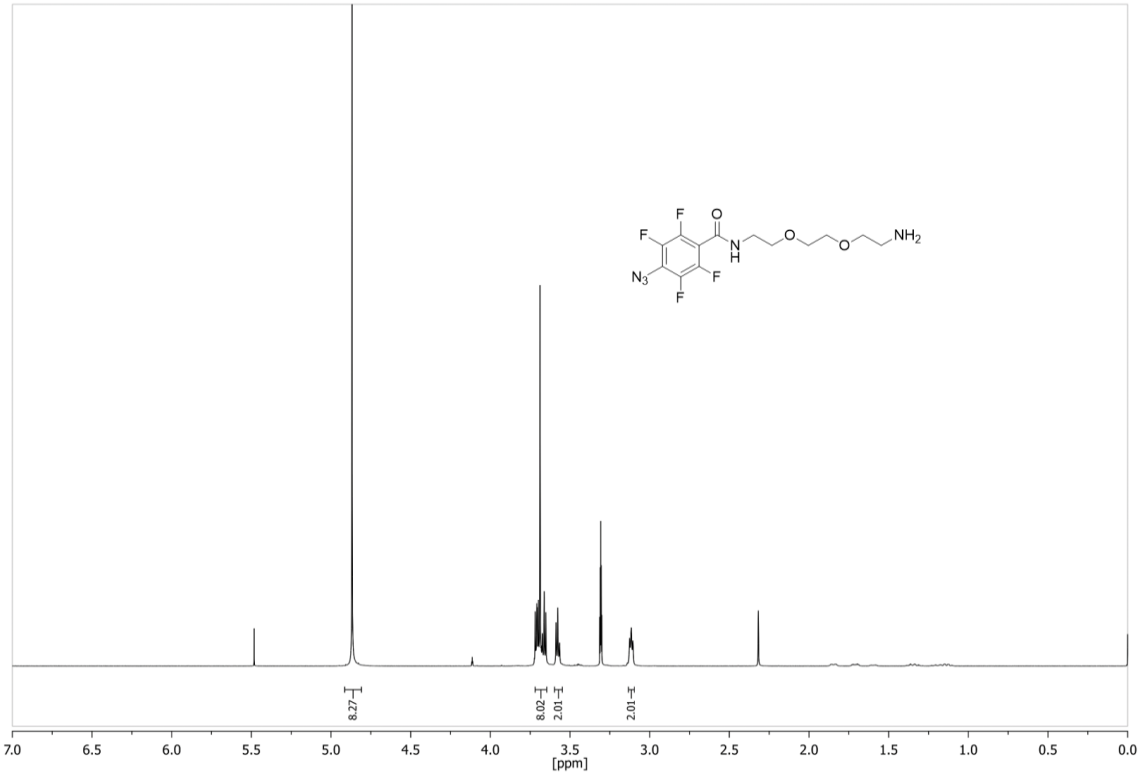

Figure 216: ^{1}H NMR spectrum of **7** (500 MHz, MeOD, 300 K).

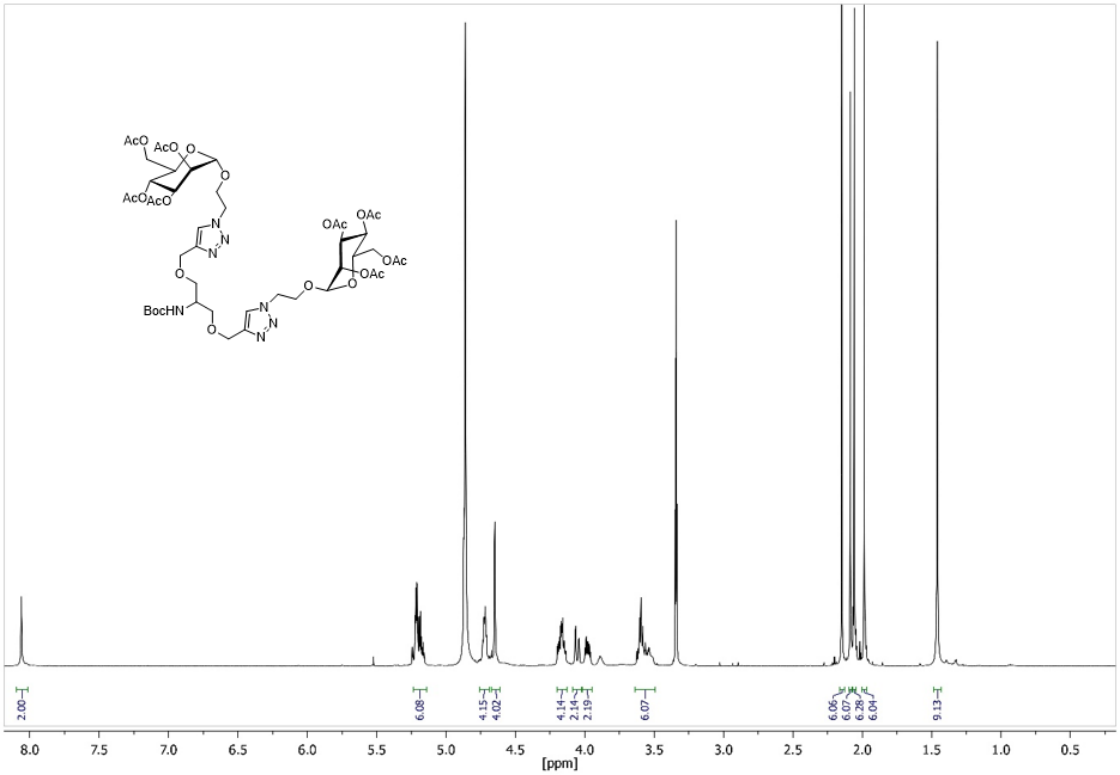

Figure 217: ^{1}H NMR spectrum of **23** (500 MHz, MeOD, 300 K).

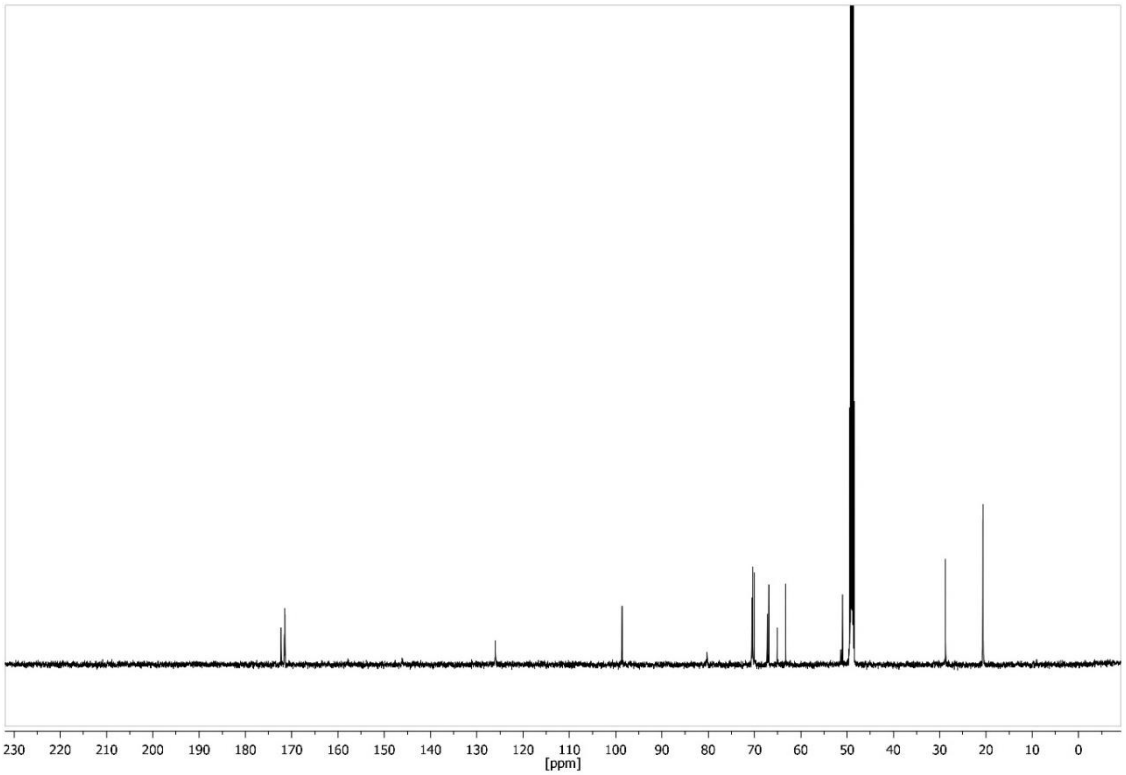

Figure 218: ^{13}C NMR spectrum of compound **23** (126 MHz, MeOD, 300 K).

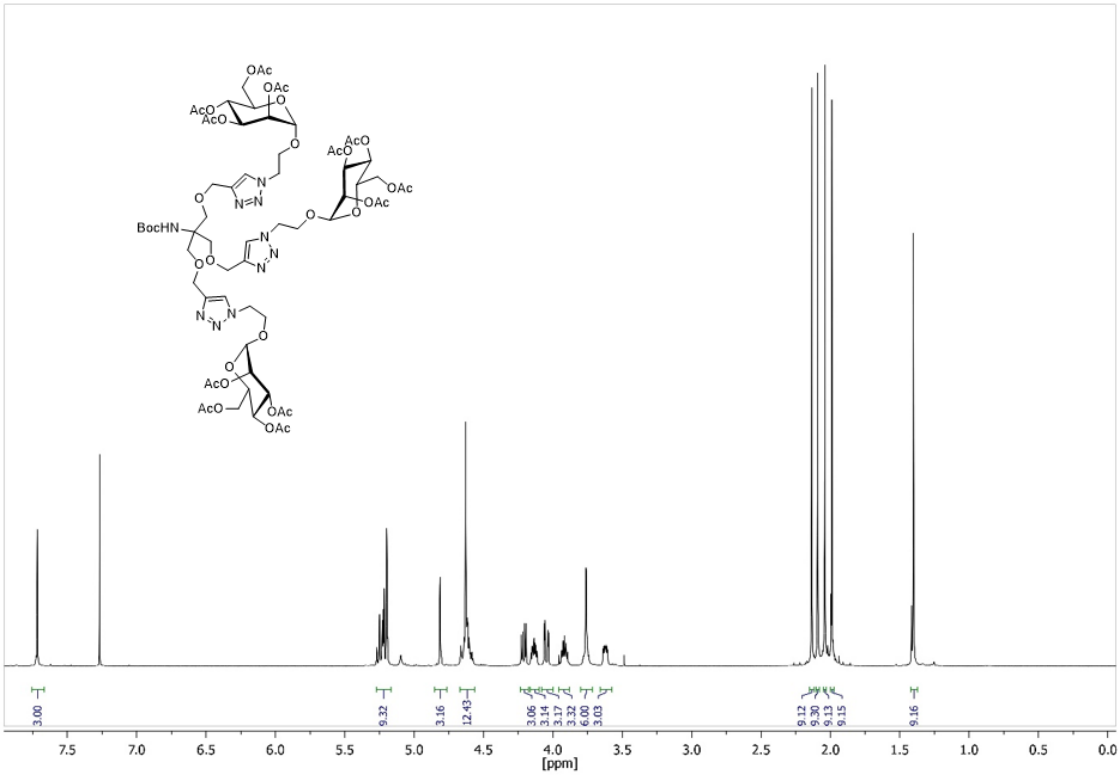

Figure 219: ^{1}H NMR spectrum of **24** (500 MHz, MeOD, 300 K).

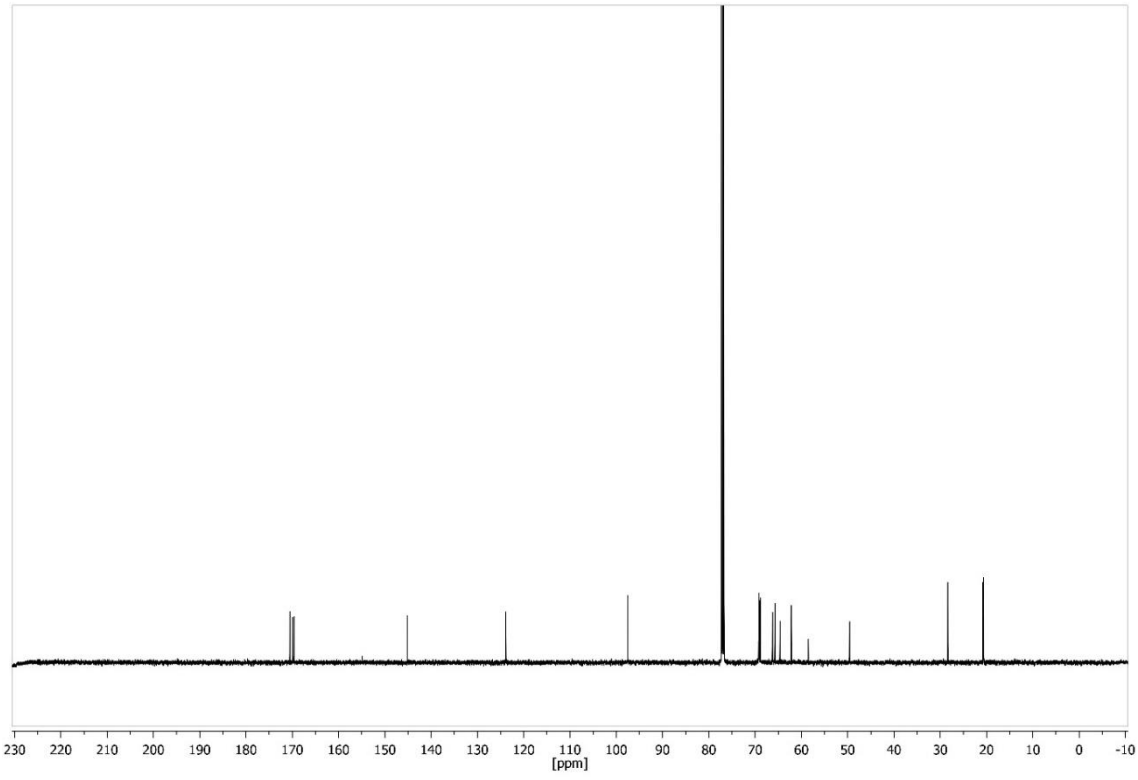

Figure 220: ^{13}C NMR spectrum of **24** (126 MHz, MeOD, 300 K).

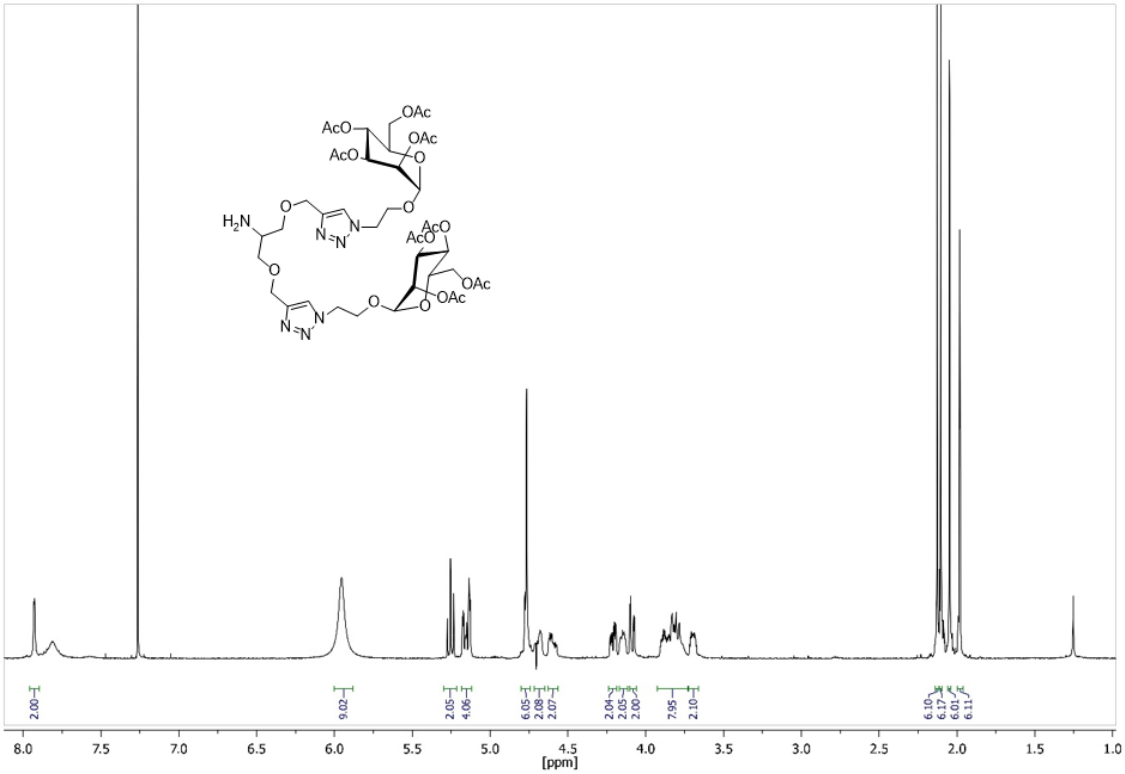

Figure 221: ^{1}H NMR spectrum of deprotected amine **25** (500 MHz, $CDCl_3$, 300 K).

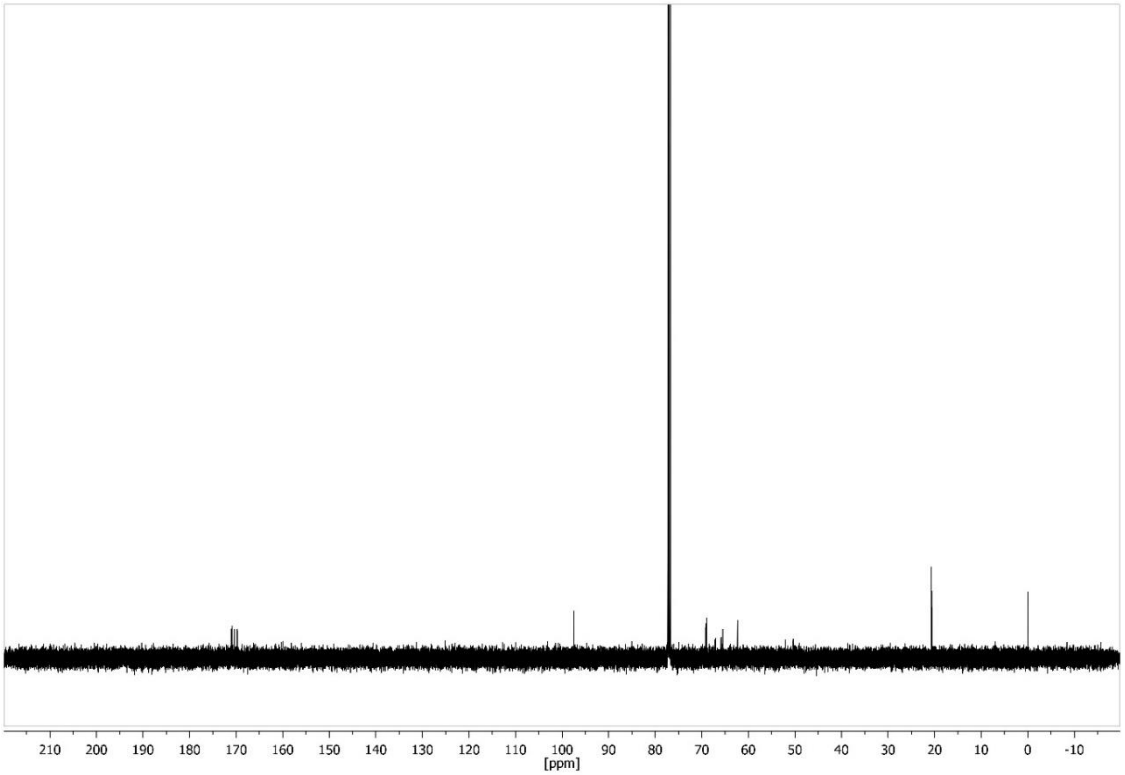

Figure 222: ^{13}C NMR spectrum of deprotected amine **25** (126 MHz, $CDCl_3$, 300 K).

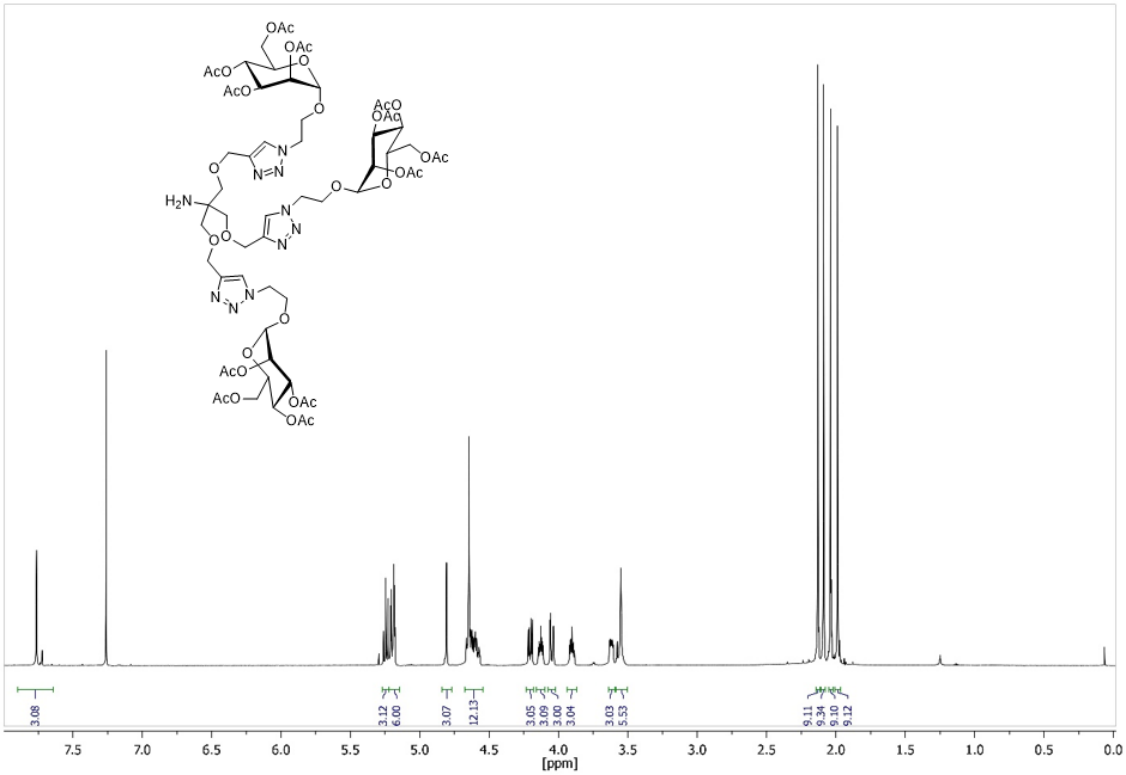

Figure 223: ^{1}H NMR spectrum of deprotected amine **26** (600 MHz, $CDCl_3$, 300 K).

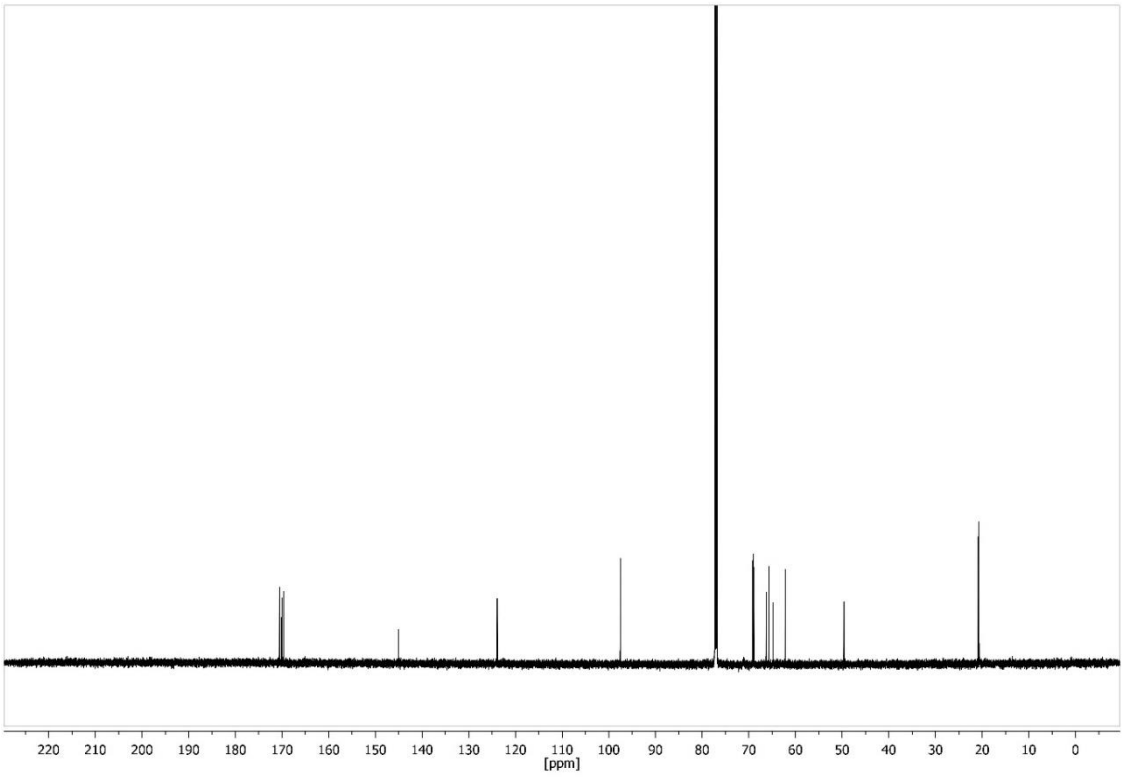

Figure 224: ^{13}C NMR spectrum of deprotected amine **26** (151 MHz, $CDCl_3$, 300 K).

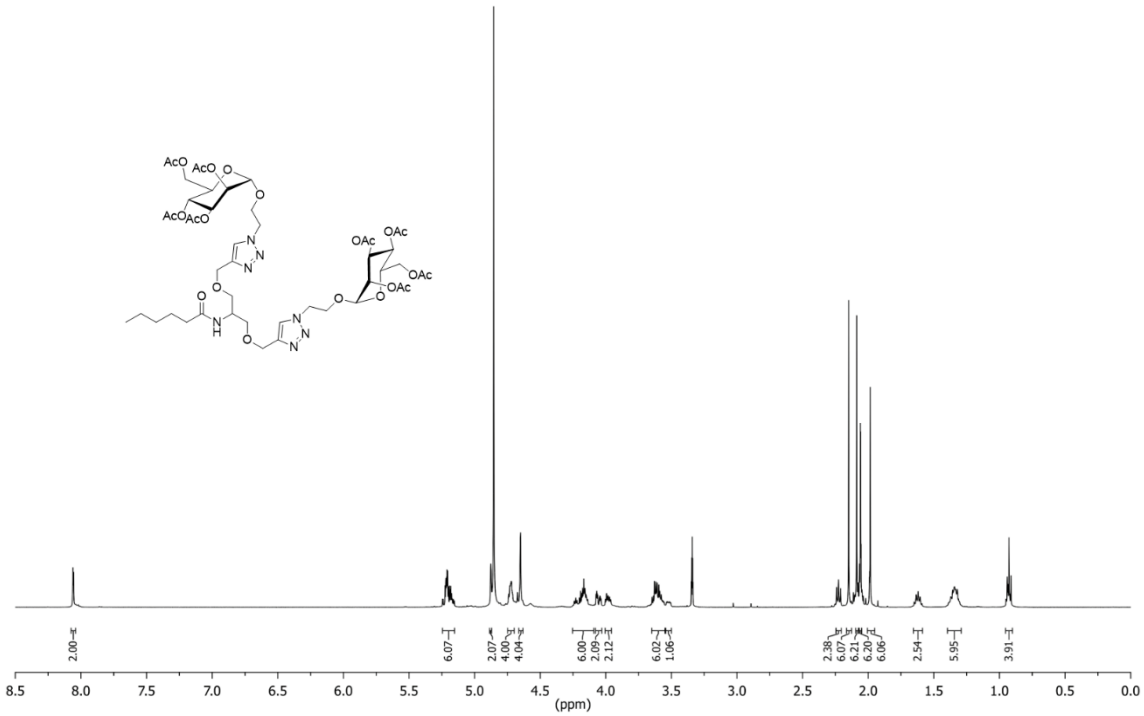

Figure 225: ^{1}H NMR spectrum of compound **28** (500 MHz, $CDCl_3$, 300 K).

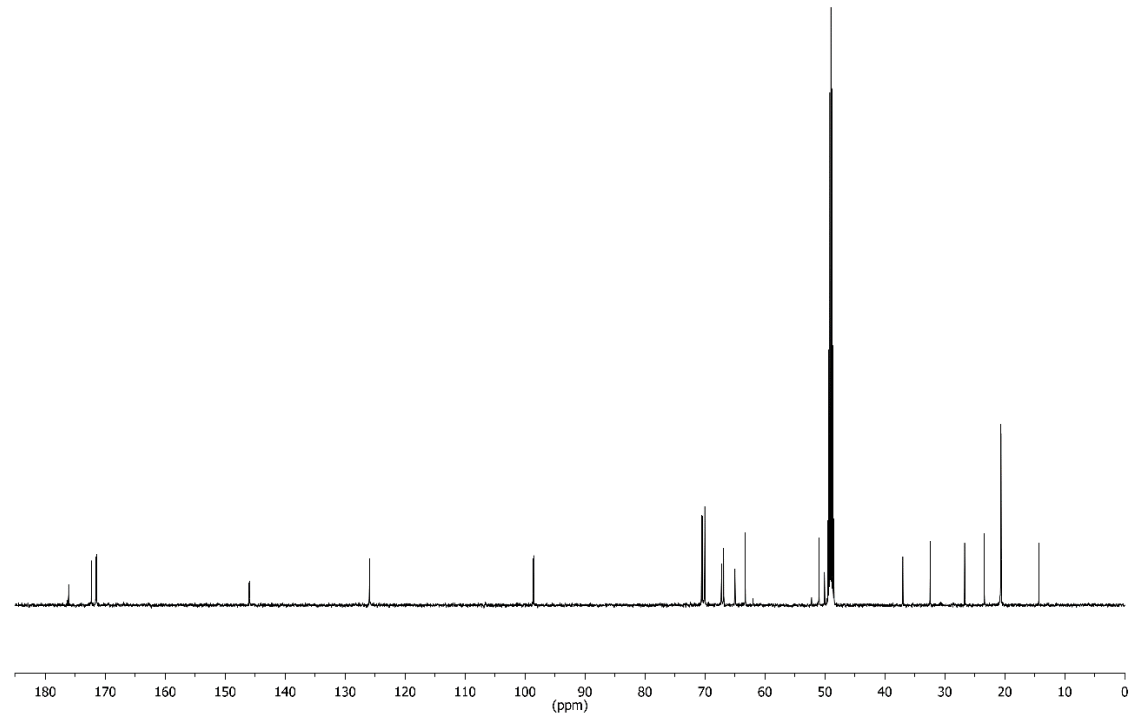

Figure 226: ^{13}C NMR spectrum of compound **28** (126 MHz, $CDCl_3$, 300 K).

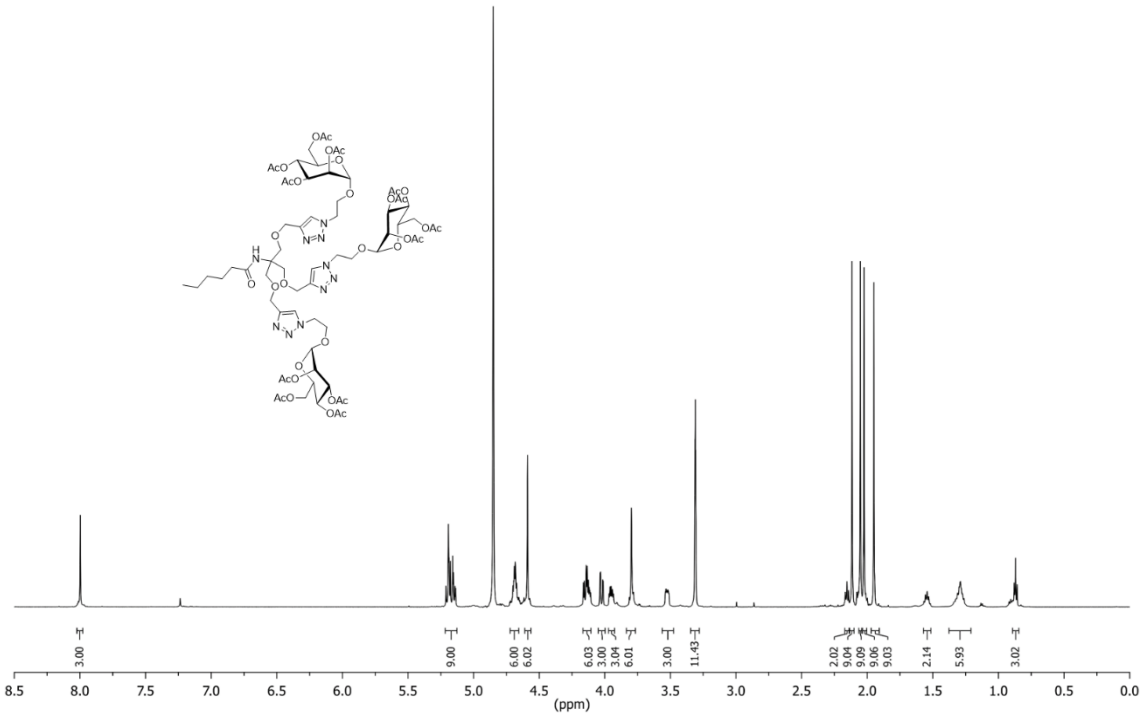

Figure 227: ^{1}H NMR spectrum of compound **29** (600 MHz, $CDCl_3$, 300 K).

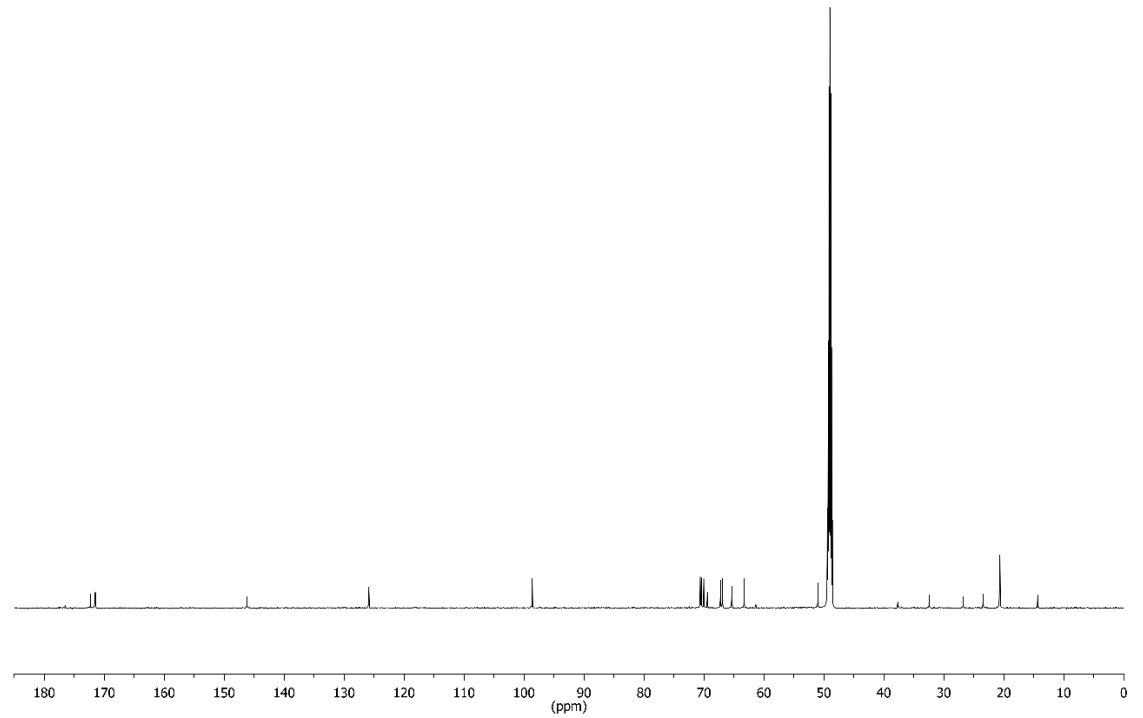

Figure 228: ^{13}C NMR spectrum of compound **29** (151 MHz, $CDCl_3$, 300 K).

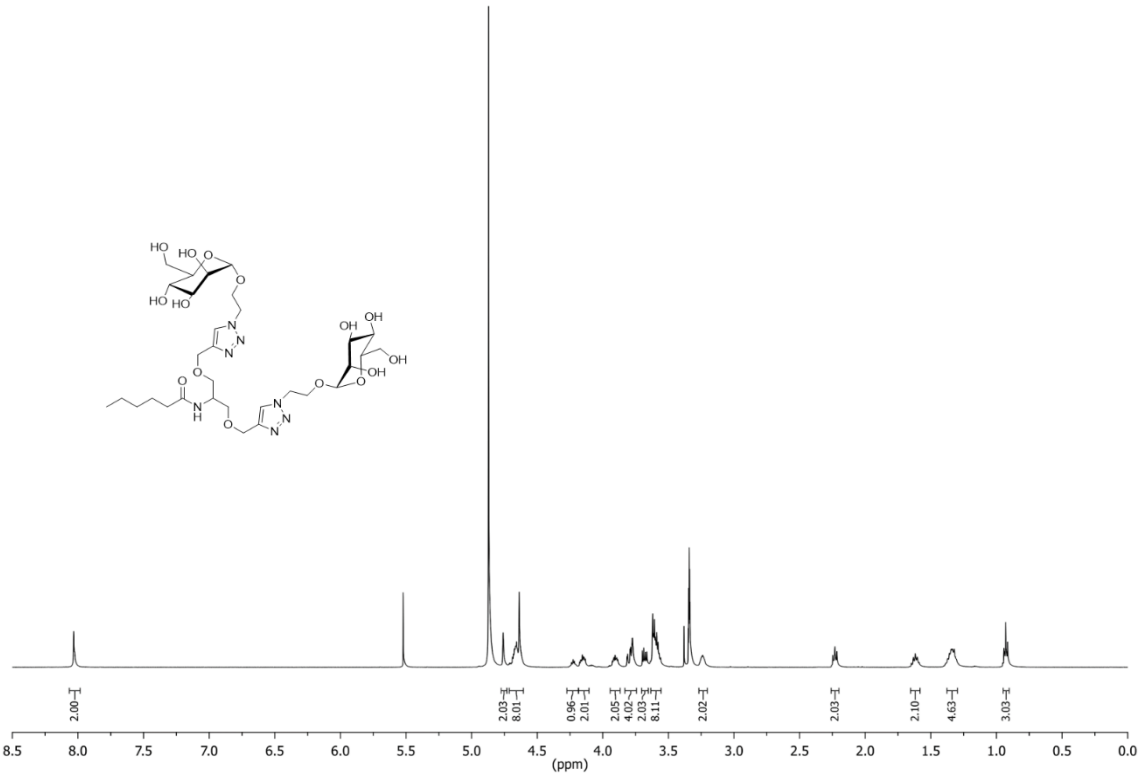

Figure 229: ^{1}H NMR spectrum of compound **30** (500 MHz, $CDCl_3$, 300 K).

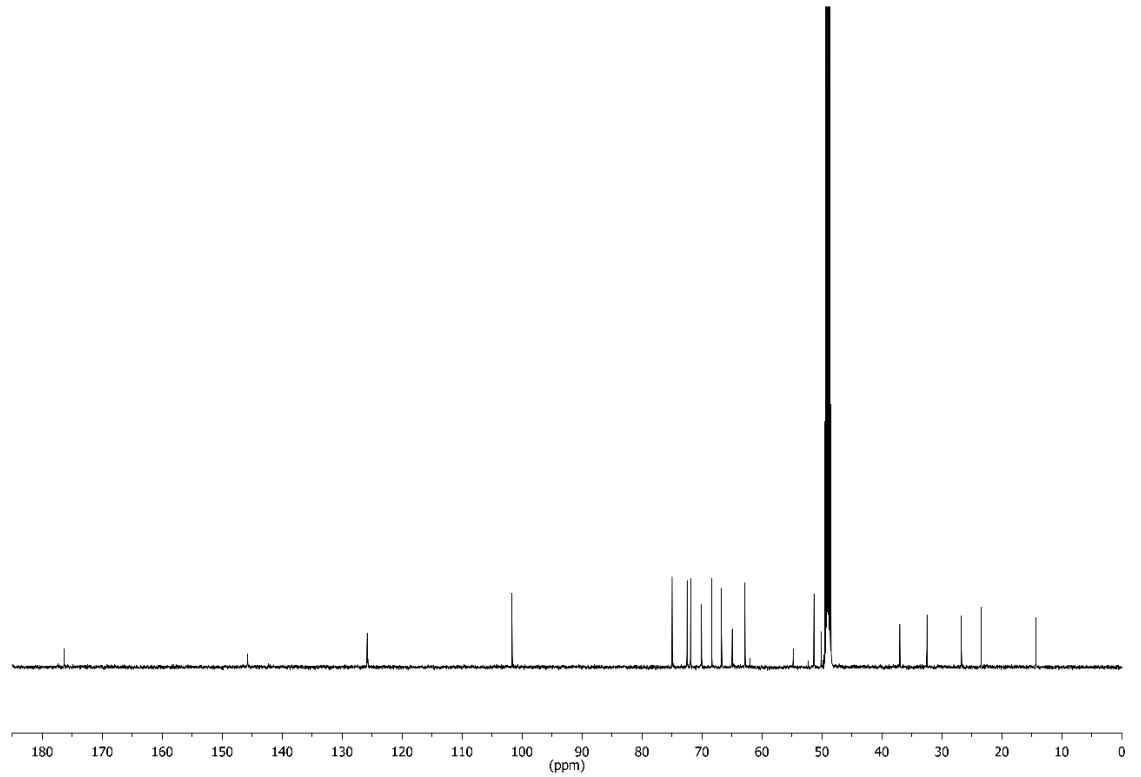

Figure 230: ^{13}C NMR spectrum of compound **30** (126 MHz, $CDCl_3$, 300 K).

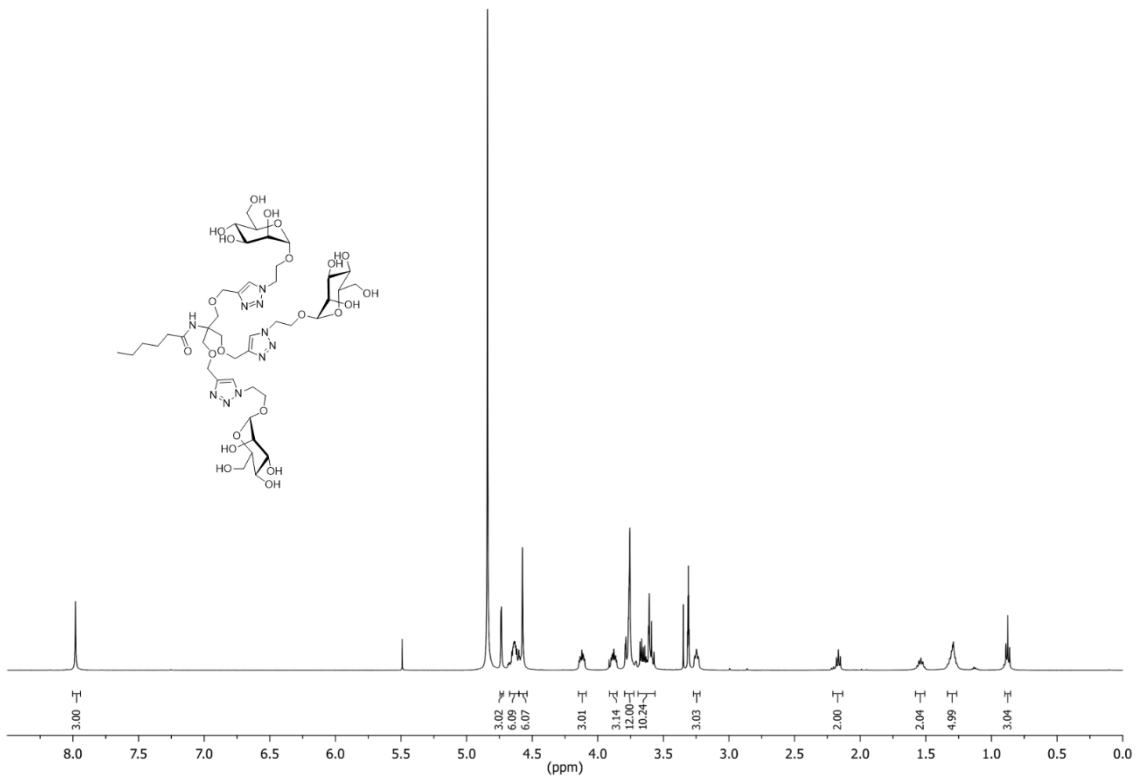

Figure 231: ^{1}H NMR spectrum of compound **31** (500 MHz, $CDCl_3$, 300 K).

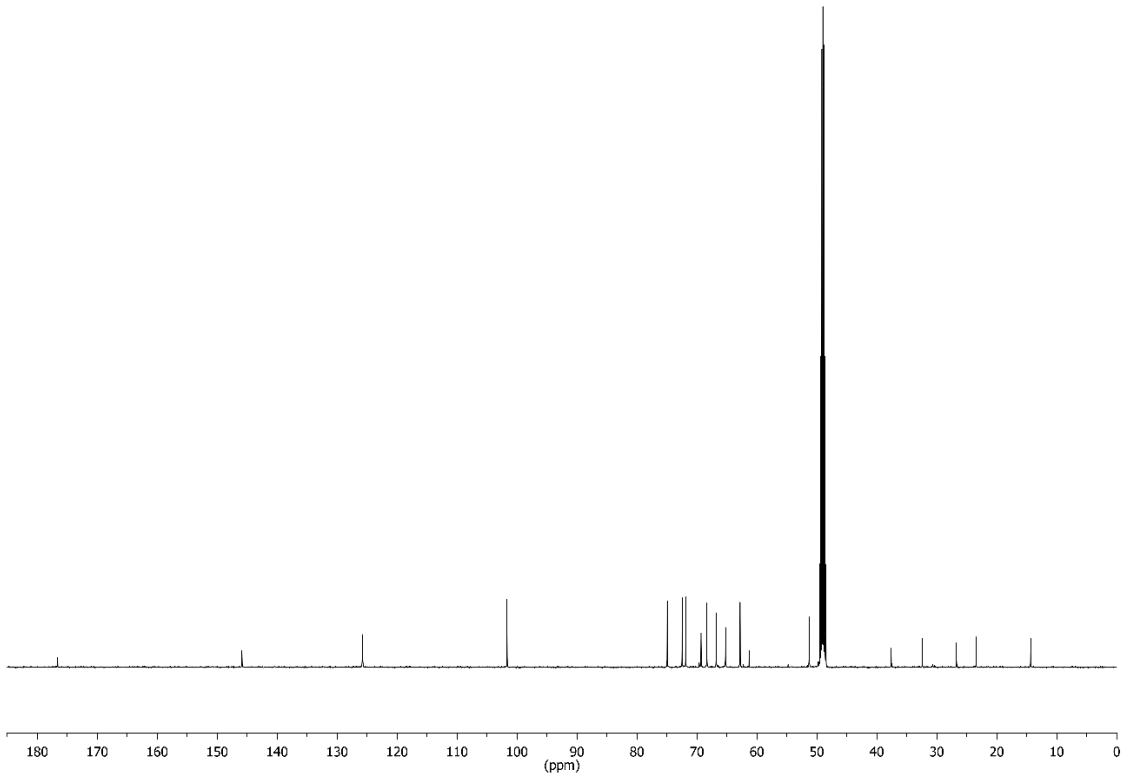

Figure 232: ^{13}C NMR spectrum of compound **31** (126 MHz, $CDCl_3$, 300 K).

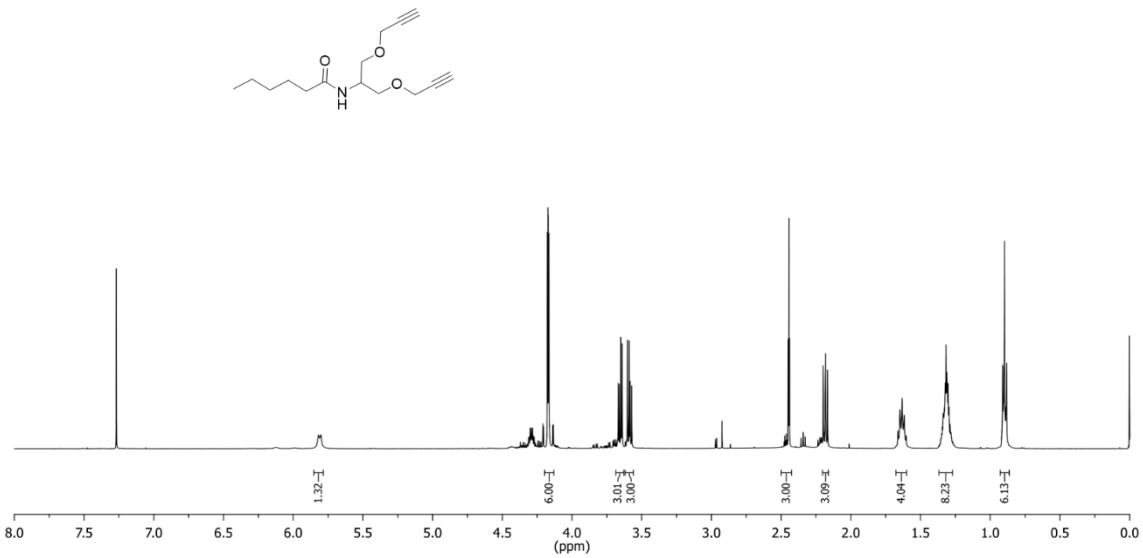

Figure 233: ^{1}H NMR spectrum of compound **40** (500 MHz, $CDCl_3$, 300 K).

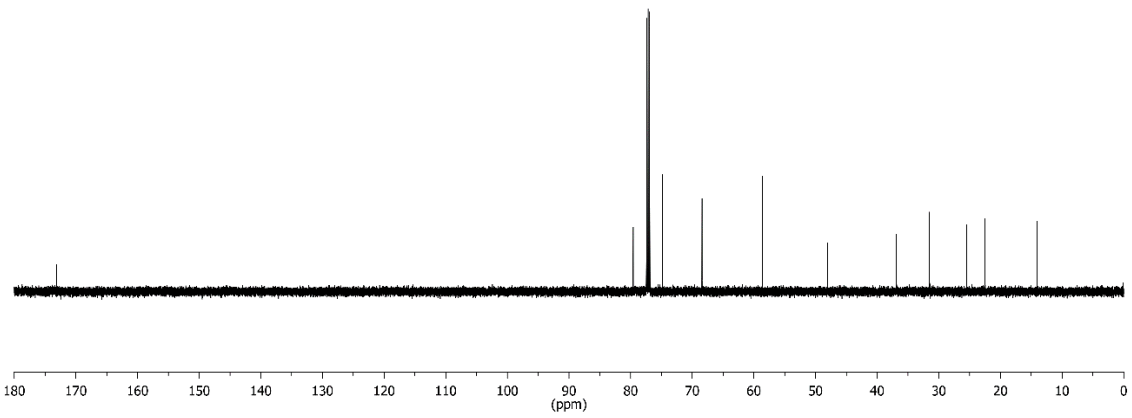

Figure 234: ^{13}C NMR spectrum of compound **40** (126 MHz, $CDCl_3$, 300 K).

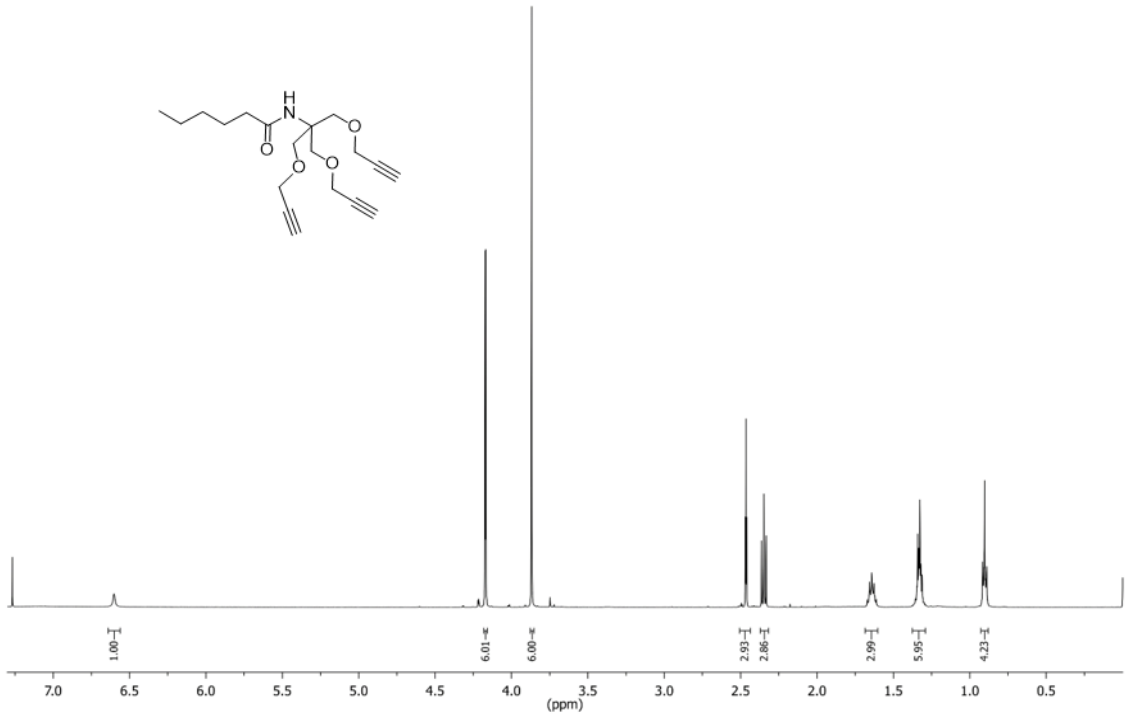

Figure 235: ^{1}H NMR spectrum of compound **41** (500 MHz, $CDCl_3$, 300 K).

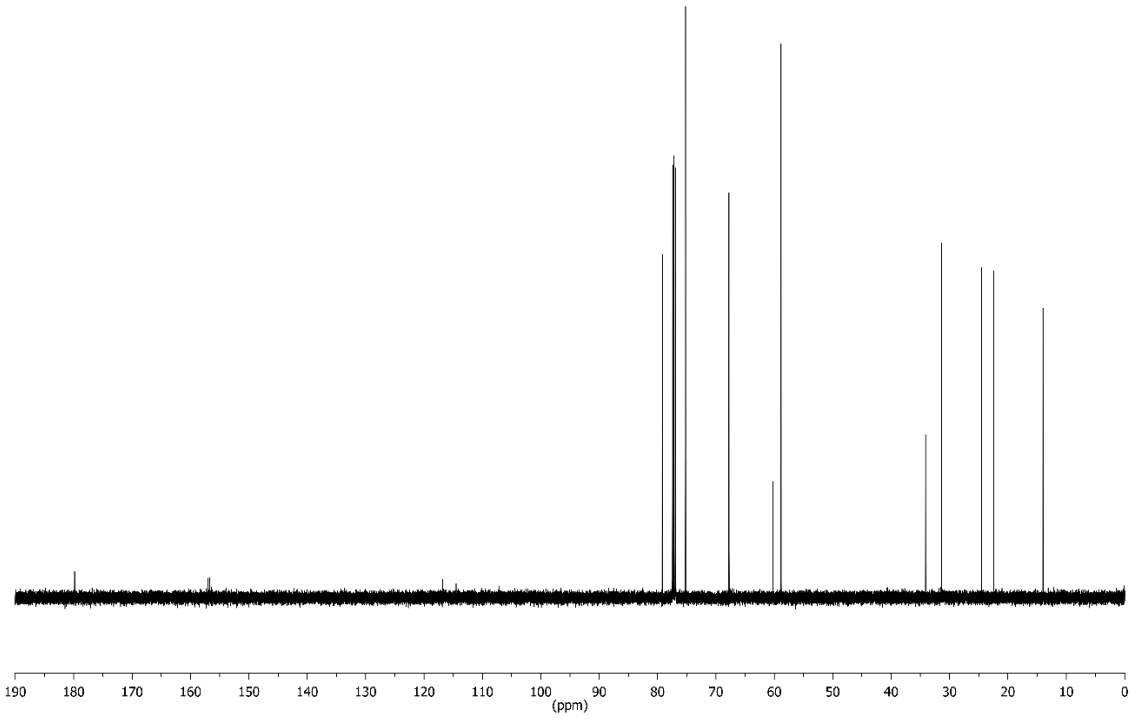

Figure 236: ^{13}C NMR spectrum of compound **41** (126 MHz, $CDCl_3$, 300 K).

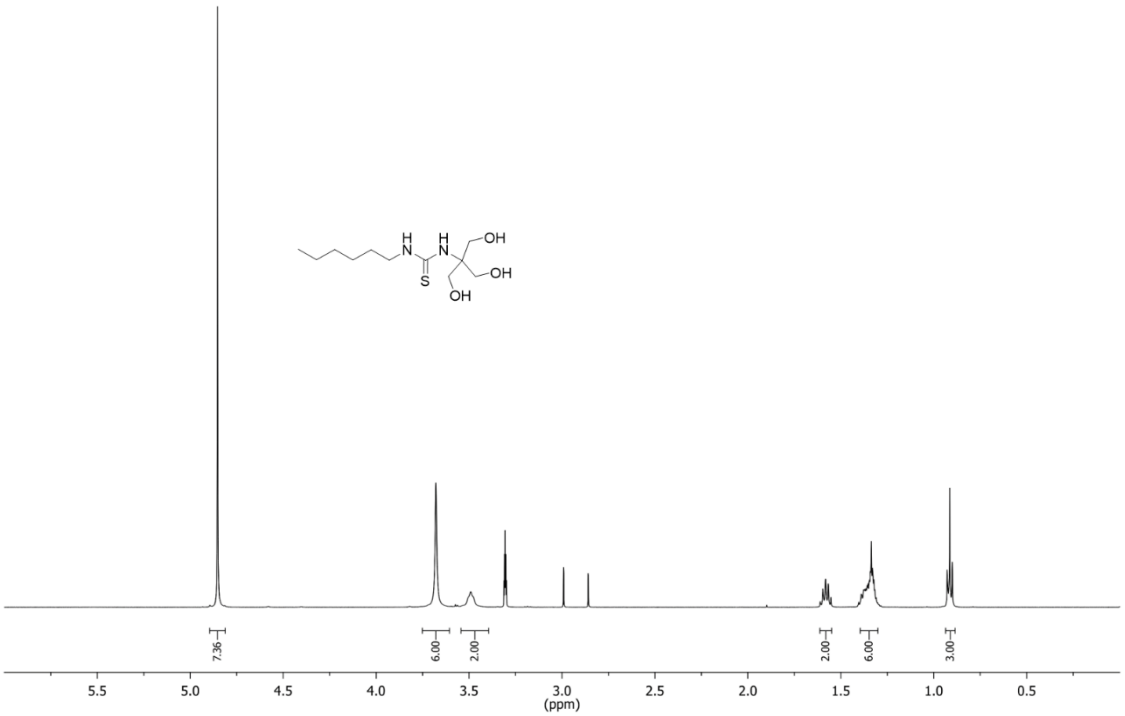

Figure 237: ^{1}H NMR spectrum of compound **44** (500 MHz, MeOD, 300 K).

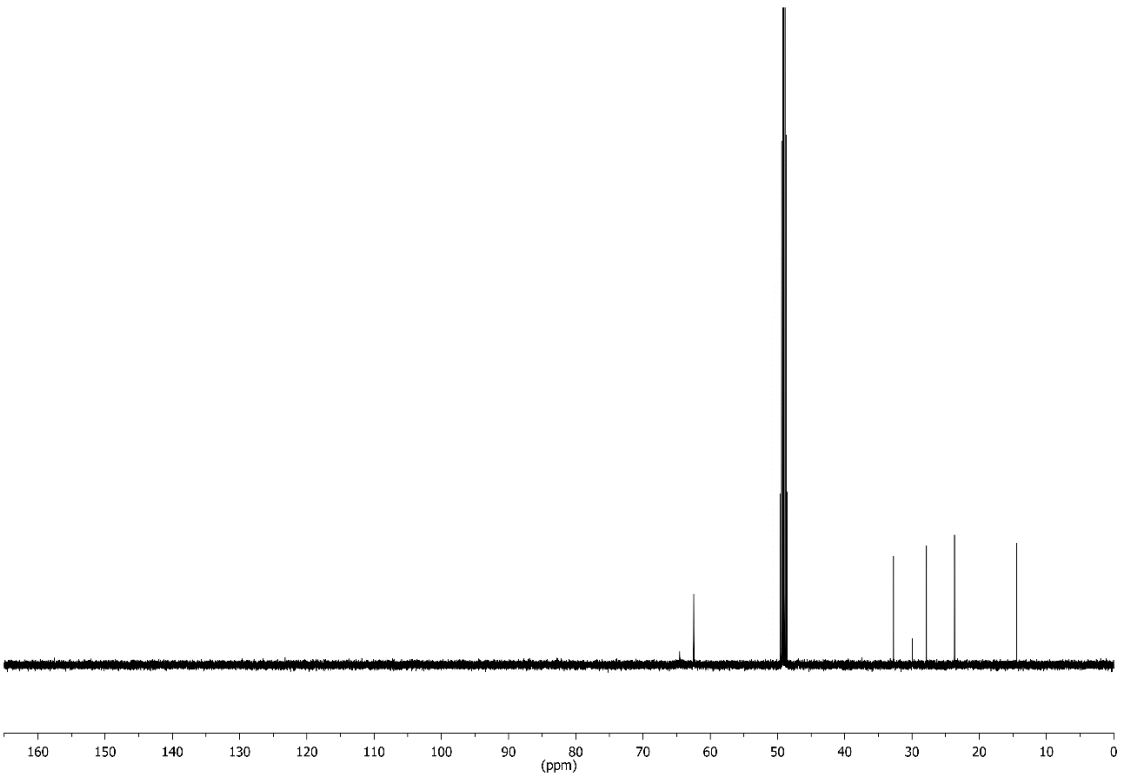

Figure 238: ^{13}C NMR spectrum of compound **44** (126 MHz, MeOD, 300 K).

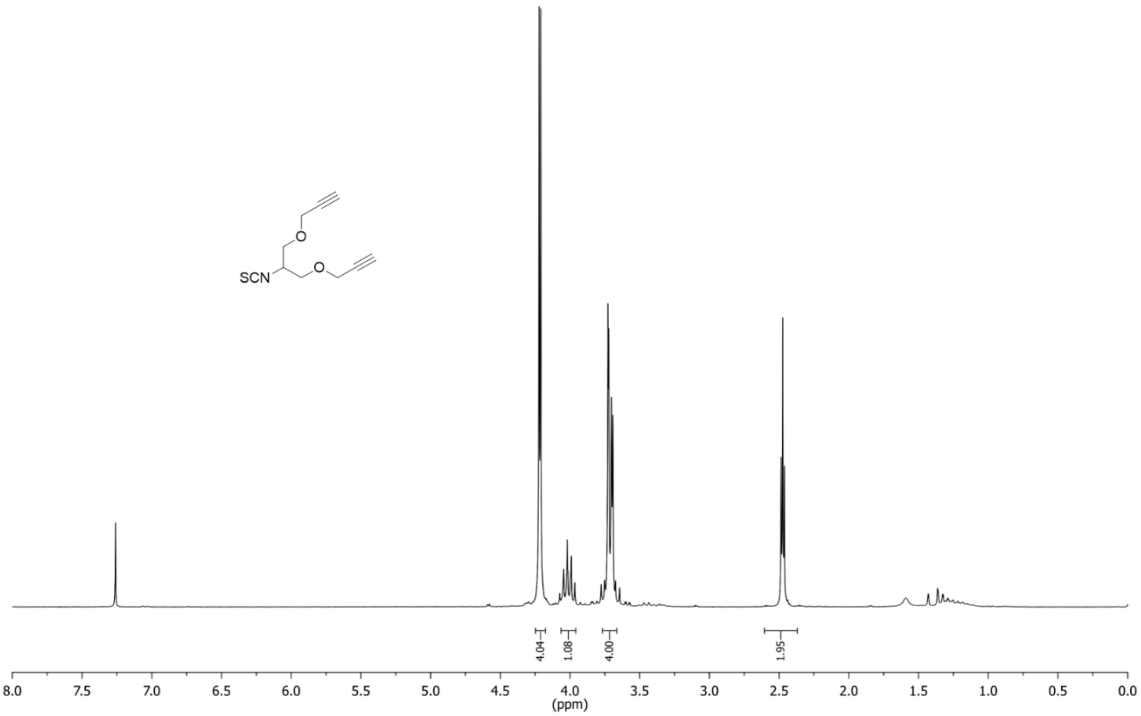

Figure 239: ^{1}H NMR spectrum of compound **45** (200 MHz, $CDCl_3$, 300 K).

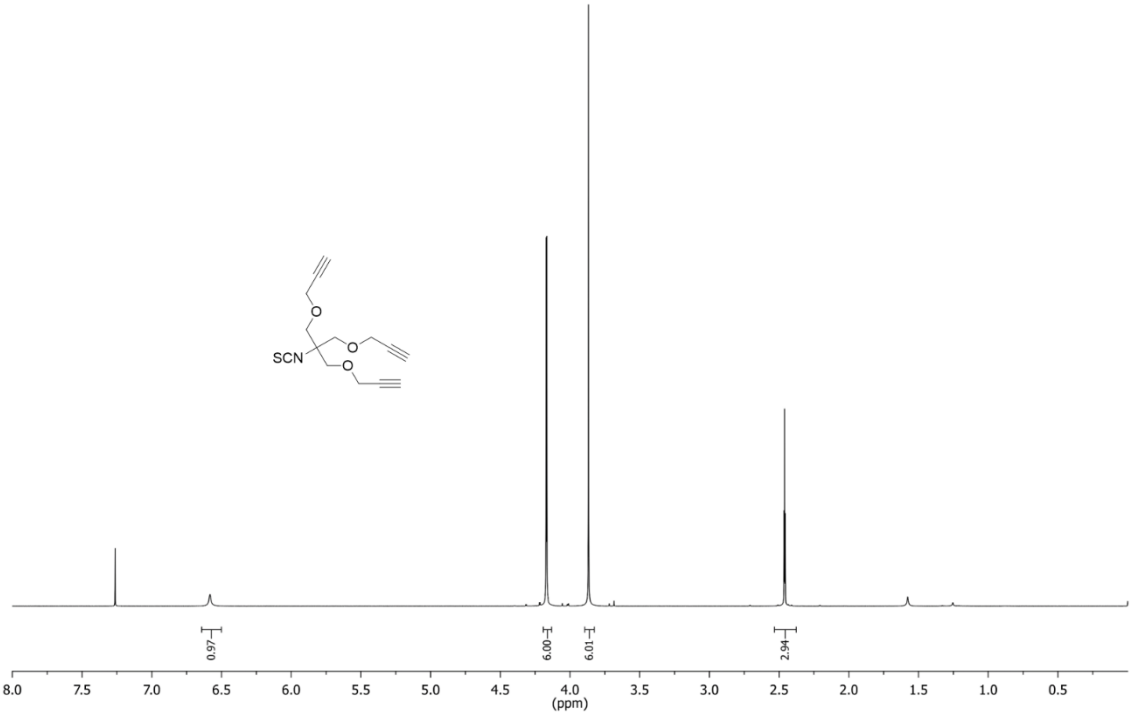

Figure 240: ^{1}H NMR spectrum of compound **46** (500 MHz, $CDCl_3$, 300 K).

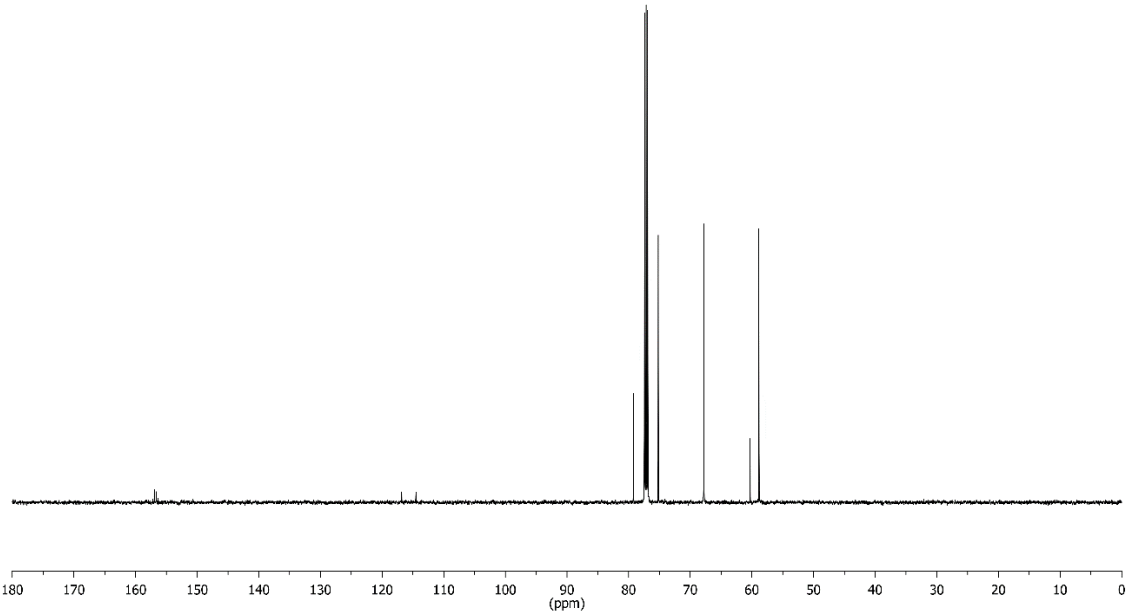

Figure 241: ^{13}C NMR spectrum of compound **46** (126 MHz, $CDCl_3$, 300 K).

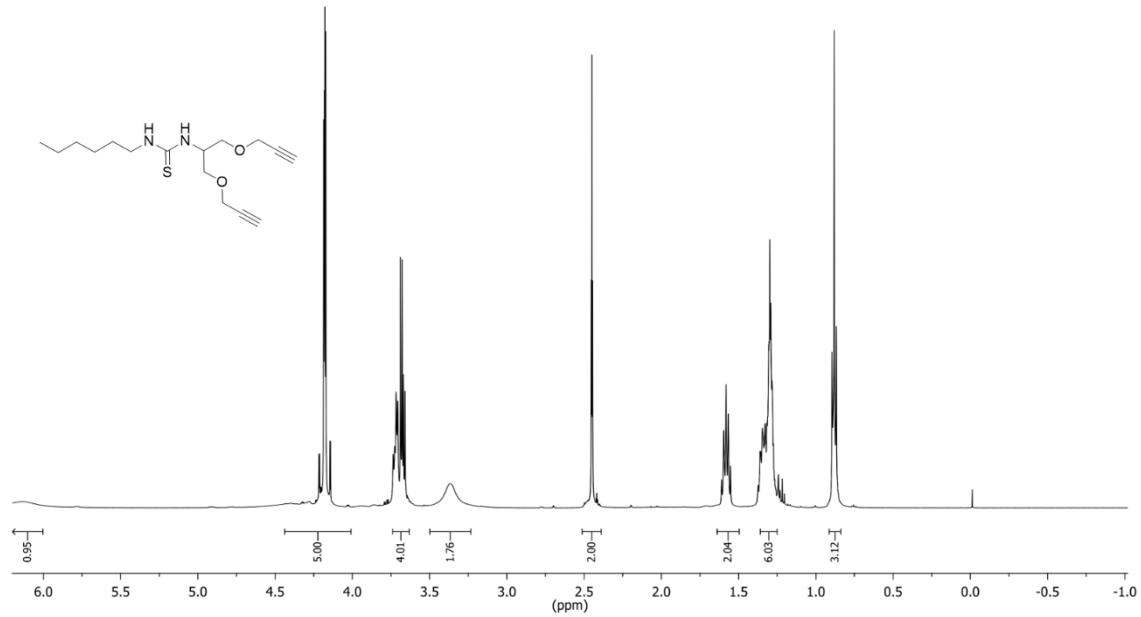

Figure 242: ^{1}H NMR spectrum of compound **48** (500 MHz, $CDCl_3$, 300 K).

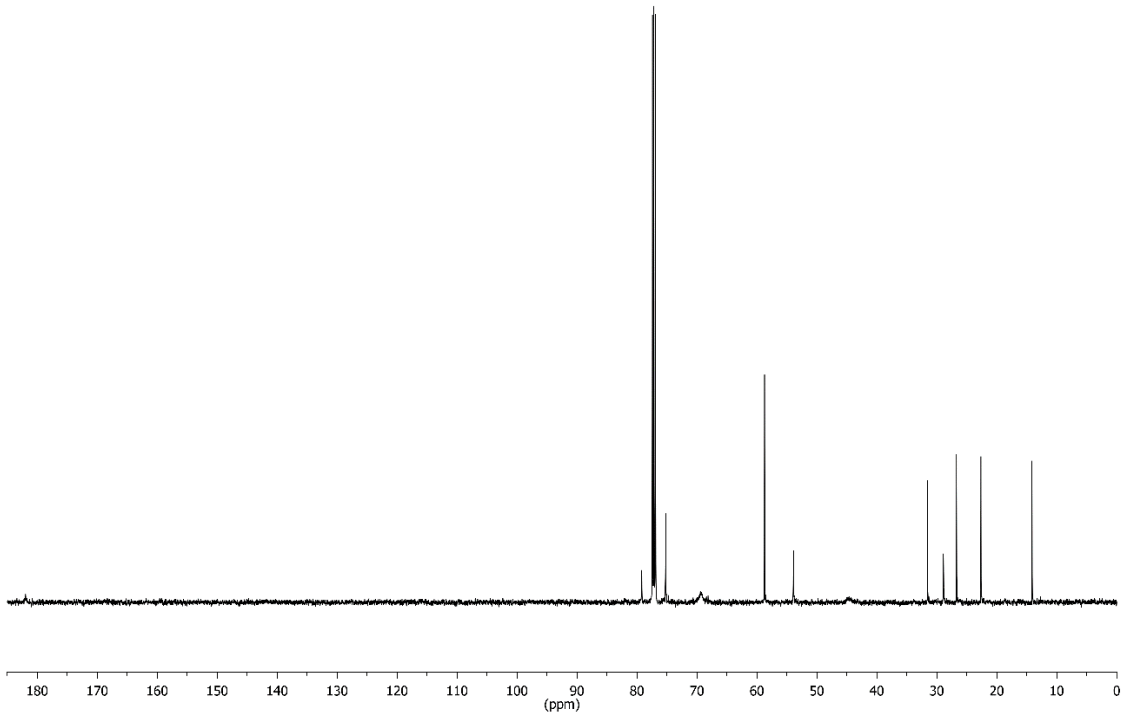

Figure 243: ^{13}C NMR spectrum of compound **48** (126 MHz, $CDCl_3$, 300 K).

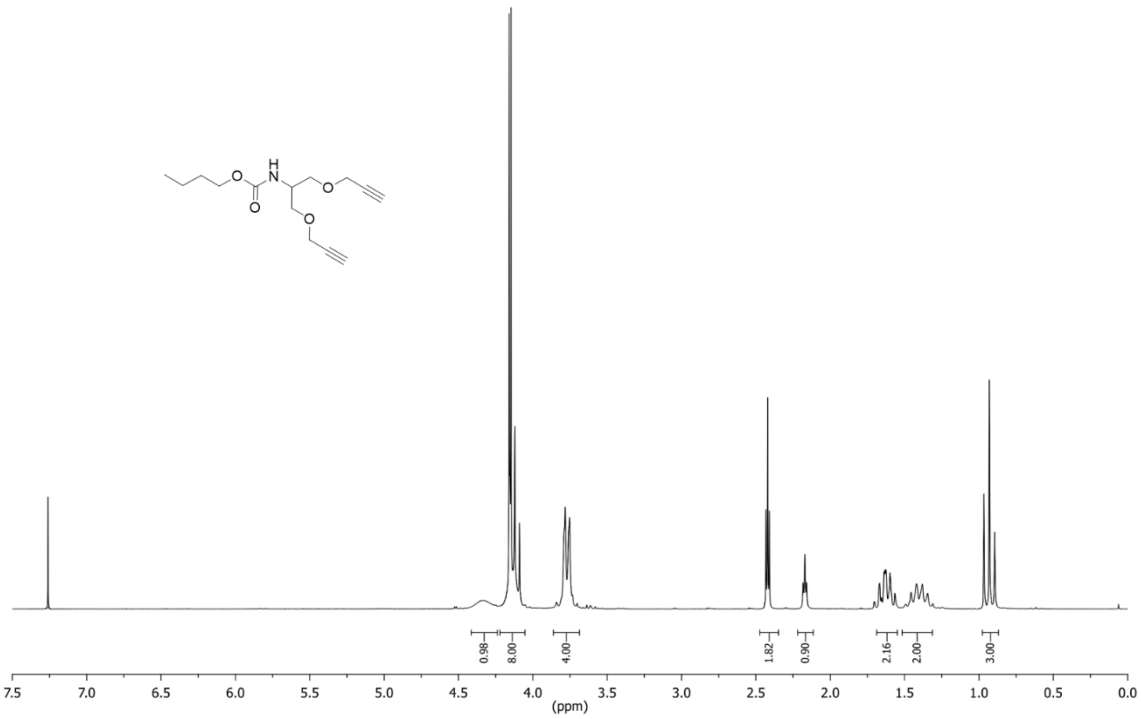

Figure 244: ^{1}H NMR spectrum of compound **55** (500 MHz, $CDCl_3$, 300 K).

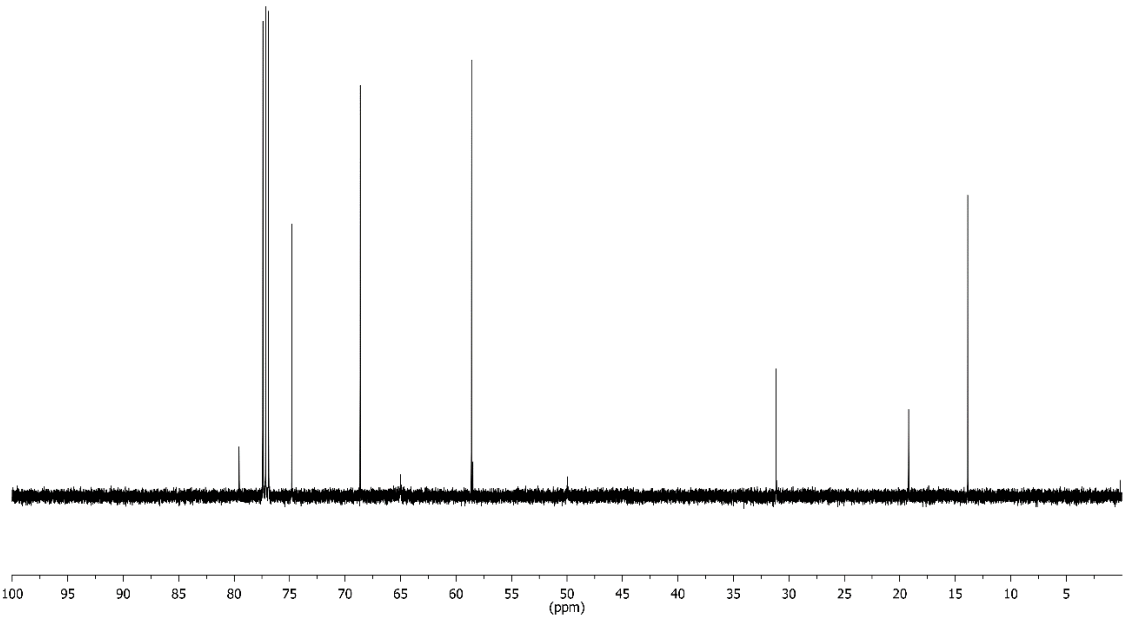

Figure 245: ^{13}C NMR spectrum of compound **55** (126 MHz, $CDCl_3$, 300 K).

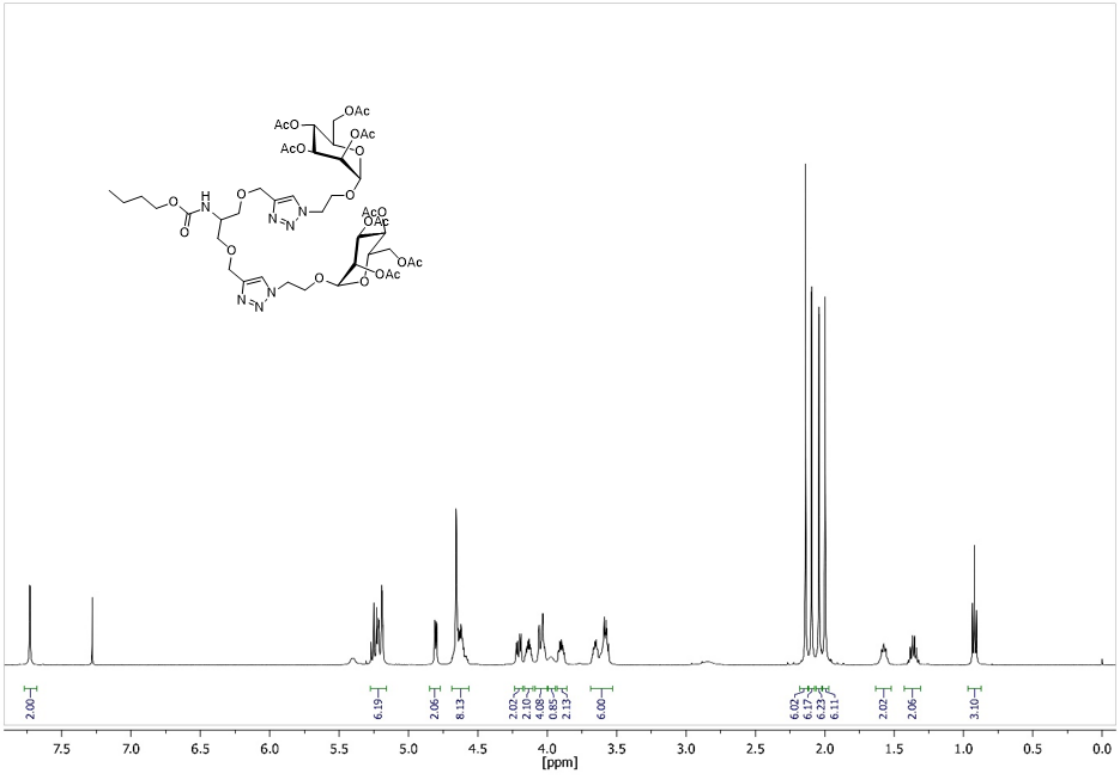

Figure 246: ^{1}H NMR spectrum of **57** (500 MHz, $CDCl_3$, 300 K).

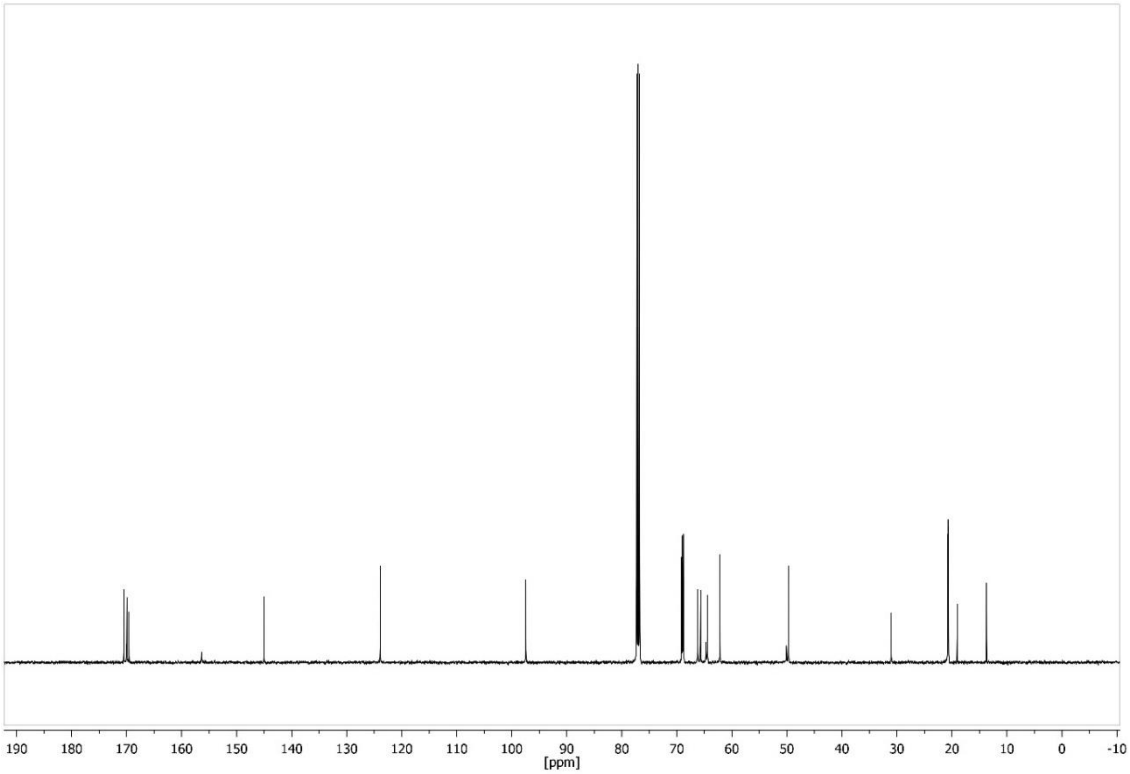

Figure 247: ^{13}C NMR spectrum of **57** (126 MHz, $CDCl_3$, 300 K).

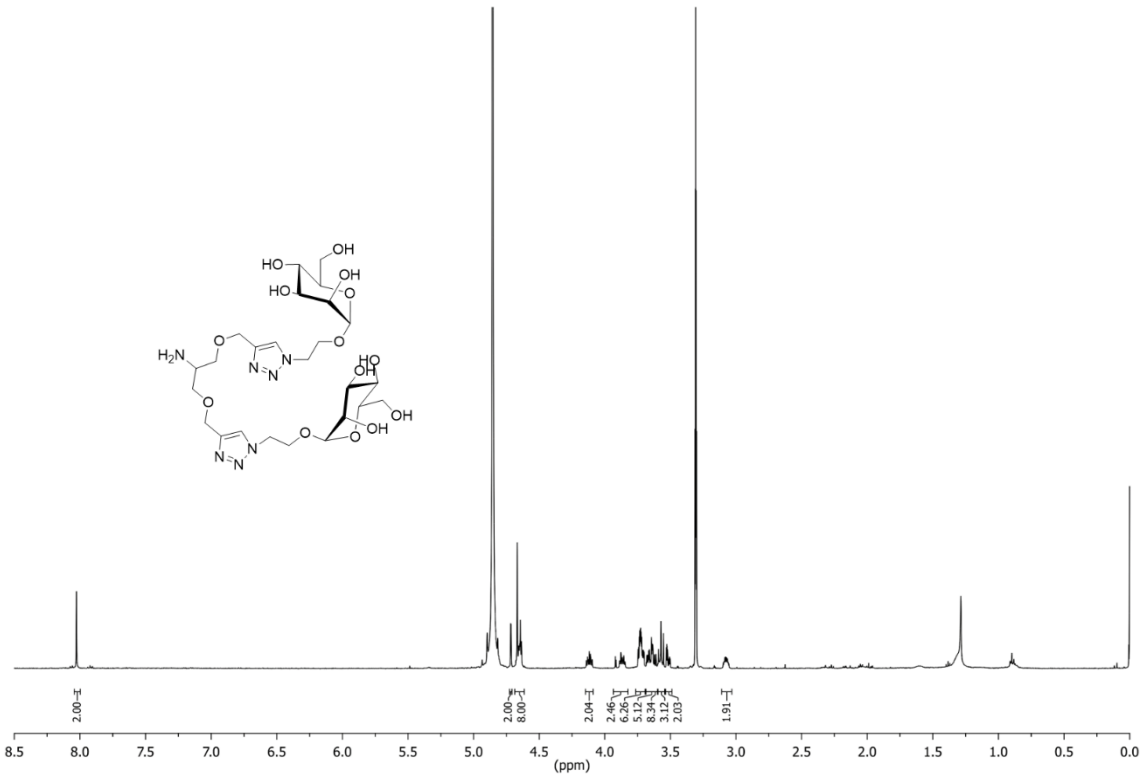

Figure 248: ^{1}H NMR spectrum of **58** (500 MHz, MeOD, 300 K).

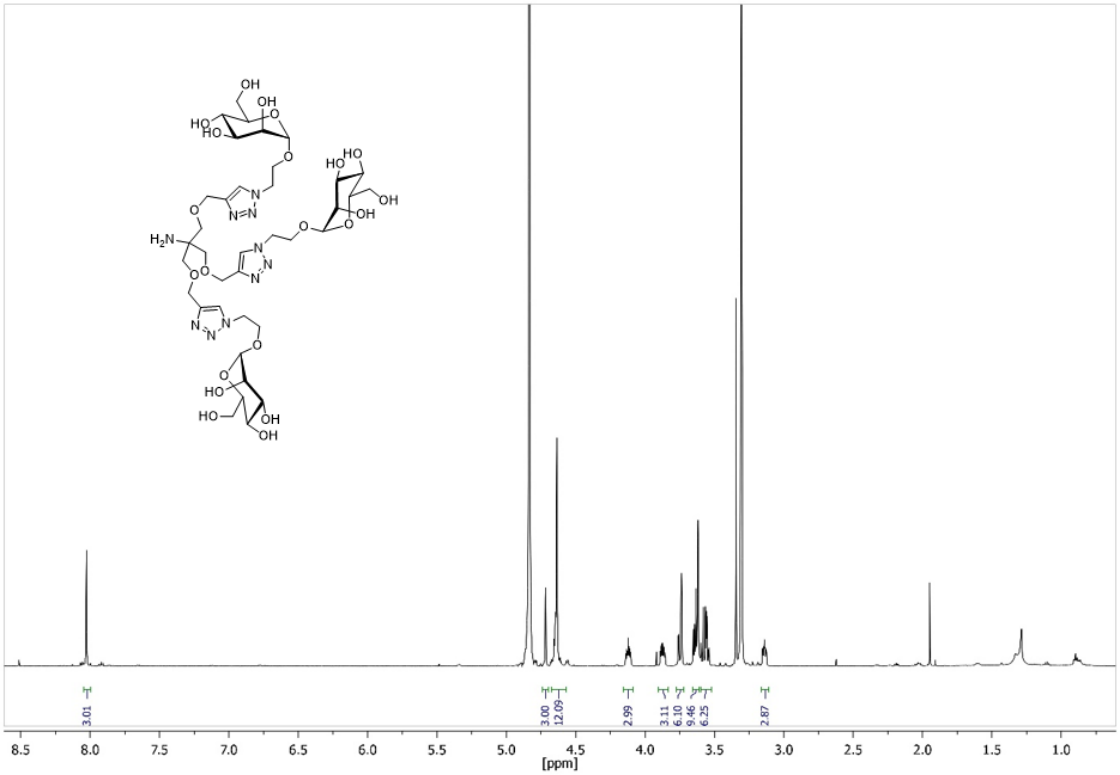

Figure 249: ^{1}H NMR spectrum of **59** (600 MHz, MeOD, 300 K).

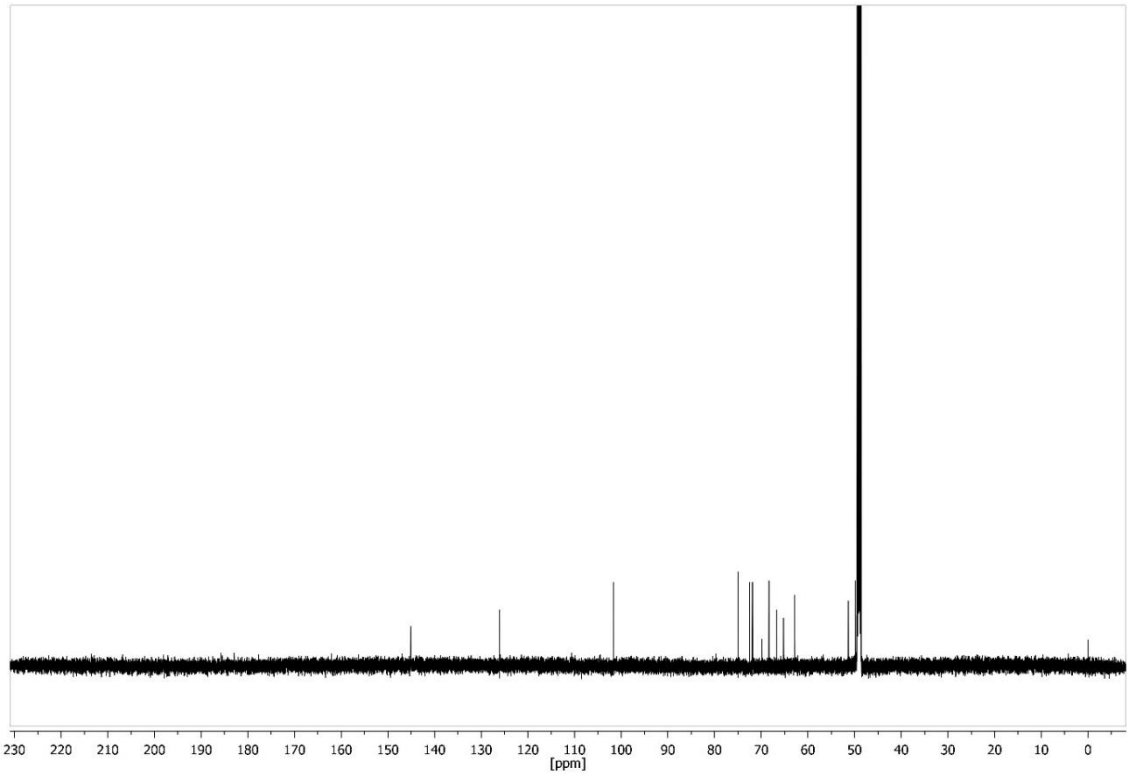

Figure 250: ^{13}C NMR spectrum of **59** (126 MHz, MeOD, 300 K).

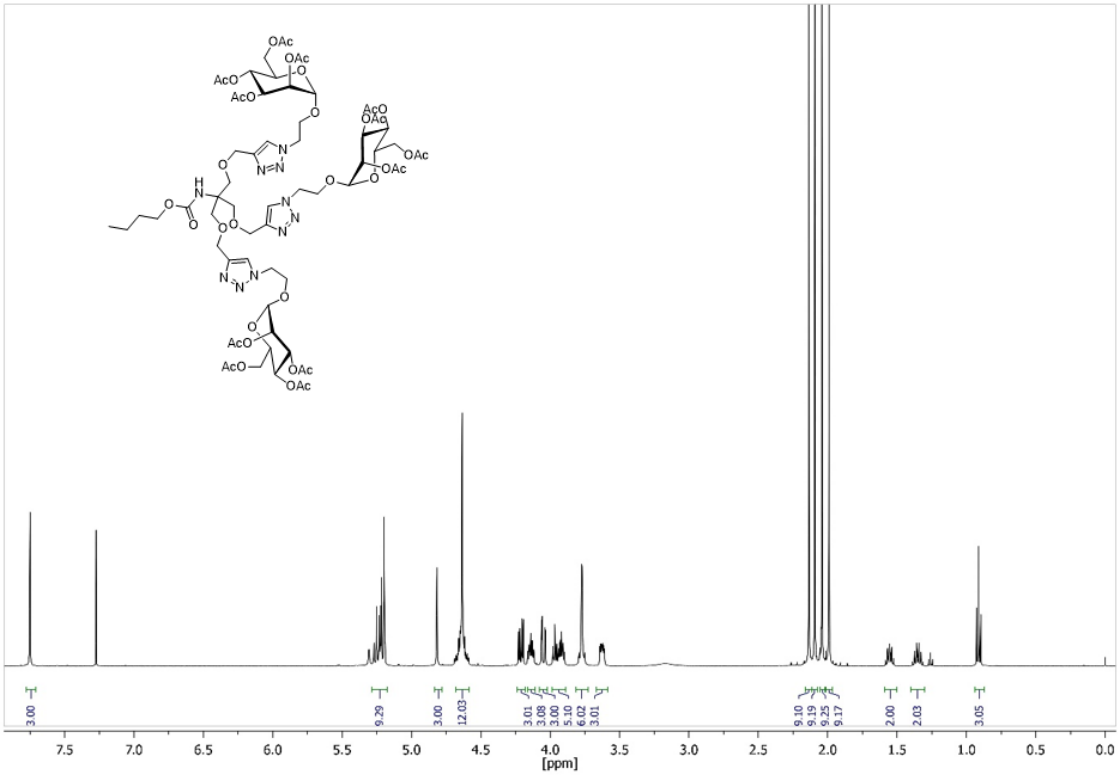

Figure 251: ^{1}H NMR spectrum of **60** (500 MHz, $CDCl_3$, 300 K).

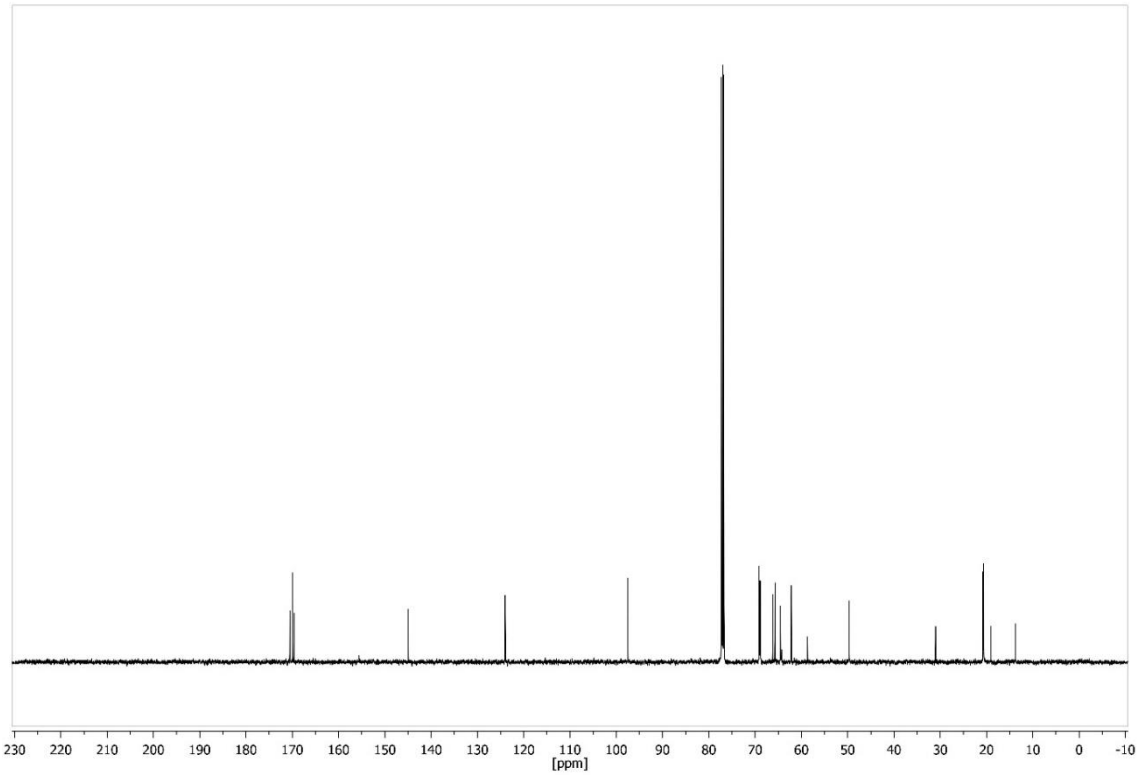

Figure 252: ^{13}C NMR spectrum of **60** (126 MHz, $CDCl_3$, 300 K).

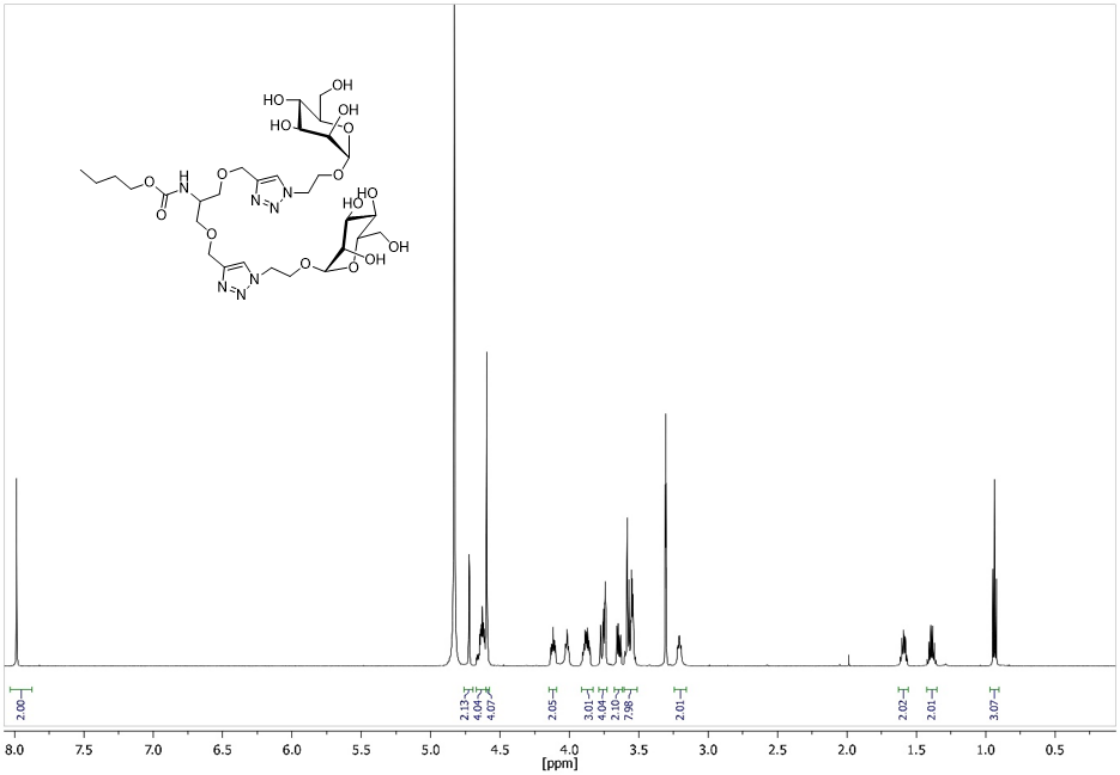

Figure 253: ^{1}H NMR spectrum of **61** (600 MHz, MeOD, 300 K).

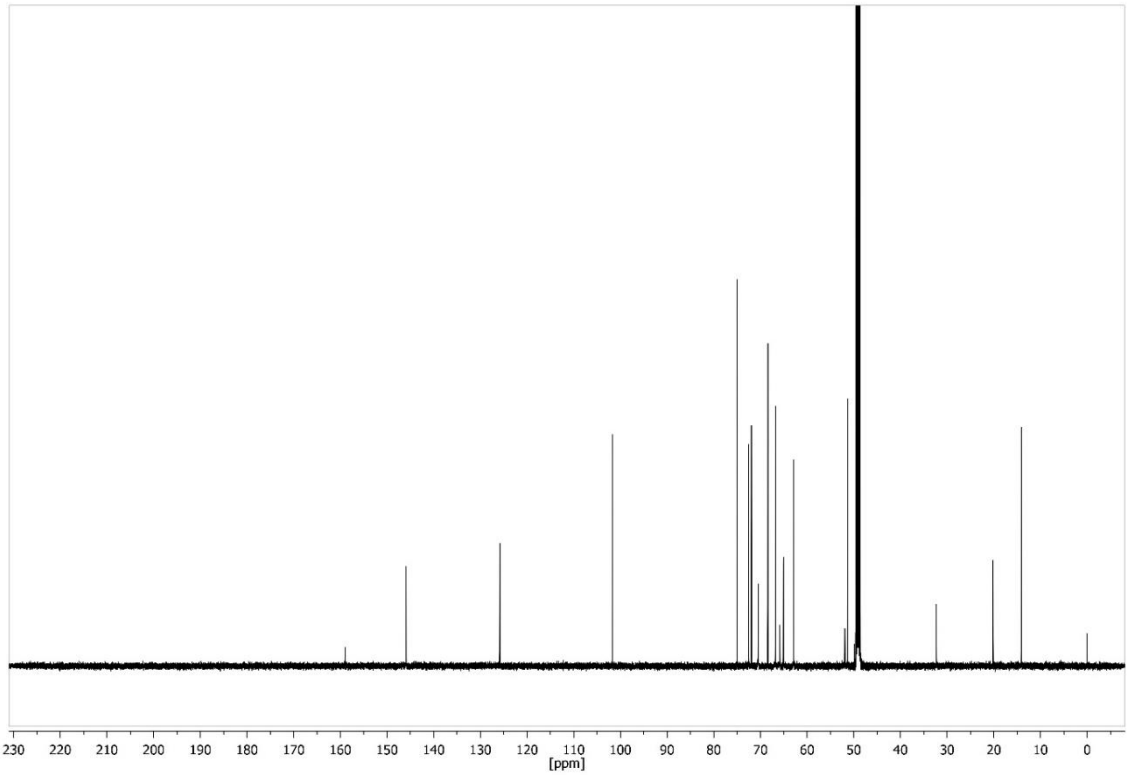

Figure 254: ^{13}C NMR spectrum of **61** (126 MHz, MeOD, 300 K).

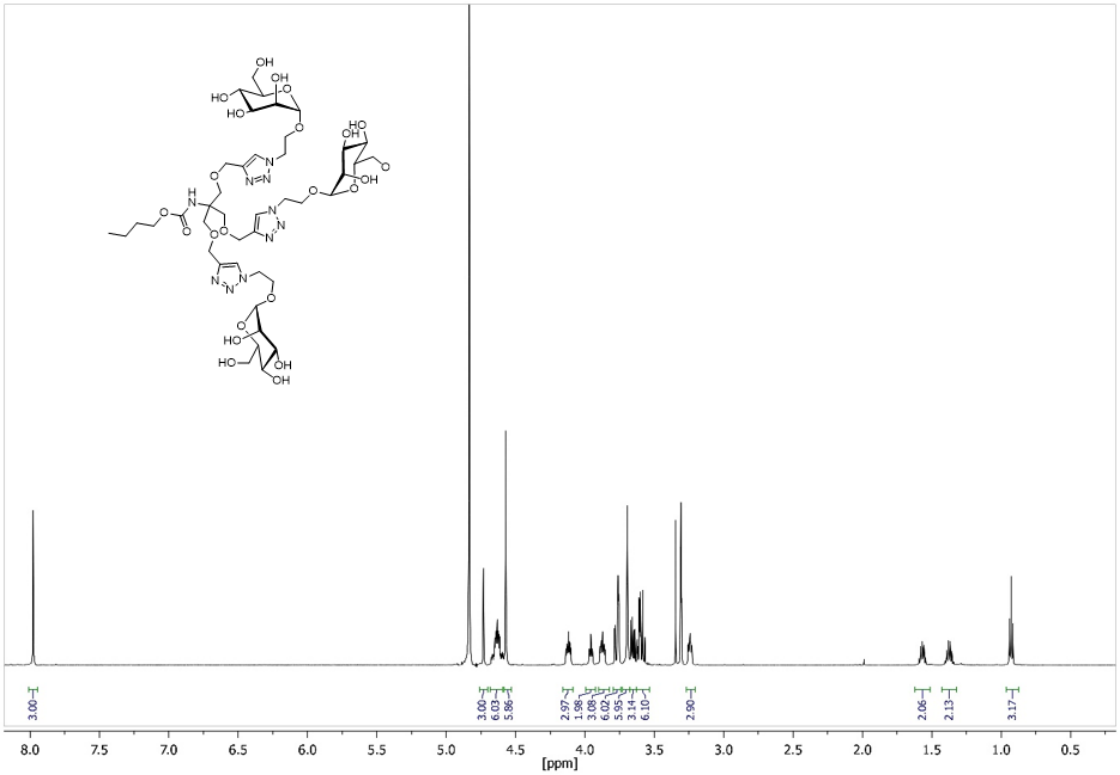

Figure 255: ^{1}H NMR spectrum of **62** (600 MHz, MeOD, 300 K).

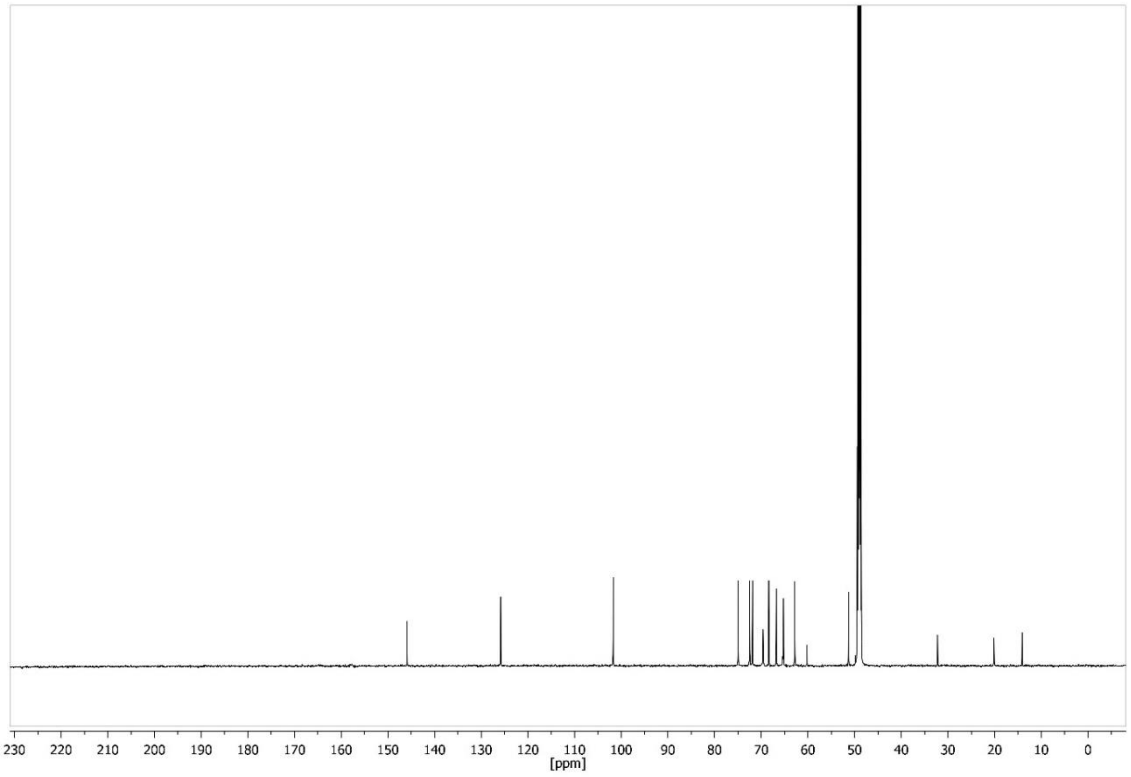

Figure 256: ^{13}C NMR spectrum of **62** (126 MHz, MeOD, 300 K).

8.4 Supporting information for chapter 4.2: Bioorthogonal click chemistry on glycosylated surfaces for the investigation of bacterial adhesion

8.4.1 Synthesis of glucosides and polysaccharides

2-*tert*-Butyloxycarbonylamidoethyl 2,3,4,6-tetra-*O*-acetyl-β-D-glucopyranoside 65[325]

A catalytic amount of activated palladium catalyst (10 % on charcoal) was added to a solution of glucoside **64** (550 mg, 1.32 mmol) and di-*tert*-butyl dicarbonate (431 mg, 1.98 mmol) in ethyl acetate (35 mL). Hydrogenation was completed after stirring under hydrogen atmosphere for 4 h. The catalyst was removed by filtration with a syringe filter device (Ø = 0.45 µm). The filtrate was washed with water (40 mL) and saturated sodium chloride solution (40 mL). The organic layers were dried over $MgSO_4$ and filtered. The solvent was removed under reduced pressure and the crude product was purified by column chromatography (cyclohexane/ ethyl acetate 1:1) to yield compound **65** as a colourless foam.

Yield: 616 mg (1.25 mmol, 95 %); lit.[325]: 90 %;

TLC: R_f = 0.33 (cyclohexane/ ethyl acetate 1:1);

Rotational value: $[\alpha]_D^{20}$ = +5.6 (c = 0.33 in dichloromethane); lit.[325]: $[\alpha]_D^{20}$ = -14 (c = 1.0 in chloroform);

^{1}H-NMR: (600 MHz, $CDCl_3$, 300 K, TMS): δ = 5.19 (t~dd, $^3J_{3,4}$ = 9.6 Hz, 1H, H-3), 5.07 (dd~t, $^3J_{3,4}$ = 9.6 Hz, 1H, H-4), 4.98 (dd, $^3J_{1,2}$ = 8.0 Hz, $^3J_{2,3}$ = 9.6 Hz, 1H, H-2), 4.90 (s, 1H, NH), 4.48 (d, $^3J_{1,2}$ = 8.0 Hz, 1H, H-1), 4.24 (dd, $^3J_{5,6}$ = 4.9 Hz, $^2J_{6,6'}$ = 12.3 Hz, 1H, H-6), 4.13 (dd, $^3J_{5,6'}$ = 2.1 Hz, $^2J_{6,6'}$ = 12.3 Hz, 1H, H-6'), 3.85 (ddd, $^3J_{CHCHH}$ = 3.8 Hz, $^3J_{CHCHH}$ = 5.8 Hz, $^2J_{CHH}$ = 9.9 Hz, 1H, $C_1OC\underline{H}H$'), 3.69 (ddd, $^3J_{5,6'}$ = 2.4 Hz, $^3J_{5,6}$ = 4.9 Hz, $^3J_{4,5}$ = 10.0 Hz, 1H, H-5), 3.66-3.62 (m, 1H, $C_1OCH\underline{H}$'), 3.36-3.24 (m, 2H, CH_2N), 2.08, 2.05, 2.01, 1.99 (each s, each 3H, $OCOCH_3$), 1.41 (s, 9H, CH_3) ppm;

^{13}C-NMR: (151 MHz, $CDCl_3$, 300 K, TMS): δ = 170.7, 170.4, 169.6, 169.5 ($\underline{C}OCH_3$), 155.9 (NC=O), 101.2 (C-1), 79.5 (C-3), 72.8 (C-5), 72.0 (C-2), 71.4 (OCH_2), 68.4 (C-4), 62.0 (C-6), 40.5 (CH_2N), 28.5 ($C(CH_3)$), 20.8, 20.7 ($OCOCH_3$) ppm;

IR (ATR): $\tilde{\nu}$ = 3408, 2984, 1749, 1712, 1340, 1211, 1116, 1060, 1034 cm^{-1};

ESI-MS: *m/z* = 514.1, [M+Na]+; (calc. 514.19 for C21H33NO12+Na).

2-*tert*-Butyloxycarbonylamidoethyl β-D-glucopyranoside 66[325]

To a solution of glucoside **65** (1.80 g, 3.66 mmol) in dry methanol (15 mL) was added a 1M sodium methoxide solution (3.33 mL). After stirring for 16 h at room temperature the mixture was neutralised with ion exchanger Amberlite® IR 120. The resin was filtered off and the solvent was removed under reduced pressure to yield compound **66** as a colourless foam.

Yield: 1.15 g (3.56 mmol, 97 %);

TLC: R_f = 0.54 (DCM/methanol 9:1);

Rotational value: $[\alpha]_D^{20}$ = -11.3 (c = 0.15 in methanol);

^{1}H-NMR: (500 MHz, MeOD, 300 K, TMS): δ = 4.26 (d, $^3J_{1,2}$ = 7.8 Hz, 1H, H-1), 3.90-3.84 (m, 2H, H-6, $C_1OC\underline{H}H$‘), 3.68-3.59 (m, 2H, H-6’, $C_1OCH\underline{H}$’), 3.37-3.19 (m, 6H, H-2, H-3, H-4, H-5, CH_2NH), 1.44 (s, 9H, CH_3) ppm;

^{13}C-NMR: (126 MHz, MeOD, 300 K, TMS): δ = 158.5 (NC=O), 104.5 (C-1), 80.1 ($\underline{C}(CH_3)_3$), 77.9 (C-3, C-5), 75.1 (C-2), 71.6 (C-4), 70.1 (OCH_2), 62.7 (C-6), 41.5 (CH_2N), 28.8 ($C(\underline{C}H_3)$) ppm;

IR (ATR-IR): $\tilde{\nu}$ = 3341, 2976, 2927, 1683, 1365, 1162, 1073, 1029 cm^{-1};

ESI-MS: *m/z* = 346.1, $[M+Na]_+$; (calc. 346.15 for $C_{13}H_{25}NO_8$+Na);

2-*tert*-Butyloxycarbonylamidoethyl6-*O*-(toluene-4-sulfonyl)β-D-glucopyranoside 67[325]

4-Methylbenzenesulfonyl chloride (1.13 g, 5.94 mmol) was added to an ice-cold solution of glucoside **66** (1.28 g, 3.96 mmol) in pyridine (30 mL). After stirring at room temperature for 12 h the reaction was quenched with methanol at 0 °C. The solvent was evaporated under reduced pressure and the crude product subsequently purified by column chromatography (DCM→DCM/methanol 9:1) to yield compound **67** as a colourless foam.

Yield: (1.34 g, 2.81 mmol, 71 %); lit.[325]: 70 %;

TLC: R_f = 0.50 (DCM/methanol 9:1);

Rotational value: $[\alpha]_D^{20}$ = -6.58 (c = 0.15 in ethyl acetate); lit.: $[\alpha]_D^{20}$ = -5.0 (c = 1.0 in methanol);

^{1}H-NMR: (500 MHz, MeOD, 300 K, TMS): δ = 7.80-7.77 (m, 2H, Ar-H$_{meta}$), 7.44-7.41 (m, 2H, Ar-H$_{ortho}$), 4.32 (dd, $^3J_{5,6}$ = 1.96 Hz, $^2J_{6,6'}$ = 10.8 Hz, 1H, H-6), 4.19 (d, $^3J_{1,2}$ = 7.8 Hz, 1H, H-1), 4.14 (dd, $^3J_{5,6'}$ = 5.9 Hz, $^2J_{6,6'}$ = 10.8 Hz, 1H, H-6'), 3.73 (ddd, $^3J_{CHCHH}$ = 4.6 Hz, $^3J_{CHCHH}$ = 6.0 Hz, $^2J_{CHH}$ = 10.4 Hz, 1H, C$_1$OC<u>H</u>H'), 3.53-3.47 (m, 1H, C$_1$OCH<u>H</u>'), 3.40 (ddd, $^3J_{5,6'}$ = 1.9 Hz, $^3J_{5,6}$ = 5.9 Hz, $^3J_{4,5}$ = 9.7 Hz, 1H, H-5), 3.29-3.26 (m, 2H, H-3, C<u>H</u>H'N), 3.22-3.13 (m, 2H, H-4, CH<u>H</u>'N), 3.11 (dd, $^3J_{1,2}$ = 7.8 Hz, $^3J_{2,3}$ = 9.2 Hz, 1H, H-2), 2.45 (s, 3H, Ar-CCH$_3$), 1.43 (s, 9H, C(CH$_3$)$_3$) ppm;

^{13}C-NMR: (126 MHz, MeOD, 300 K, TMS): δ = 158.5 (NC=O), 146.5 (Ar-C$_{para}$), 134.4 (Ar-C$_{ipso}$), 131.0 (Ar-C$_{ortho}$), 129.1 (Ar-C$_{meta}$), 104.4 (C-1), 80.2 (<u>C</u>(CH$_3$)$_3$), 77.7 (C-3), 75.0 (C-5), 74.8 (C-2), 71.1 (C-4), 70.7 (C-6), 70.1 (OCH$_2$), 41.4 (CH$_2$N), 28.8 (C(<u>C</u>H$_3$)), 21.6 (Ar-C<u>C</u>H$_3$) ppm;

IR (ATR-IR): $\tilde{\nu}$ = 3364, 2977, 2930, 1685, 1359, 1173, 1083, 970, 552 cm^{-1};

ESI-MS: *m/z* = 500.15538, $[M+Na]^+$ (calc. 500.15609 for $C_{20}H_{31}NO_{10}S$ + Na).

2-*tert*-Butyloxycarbonylamidoethyl 6-azido-6-deoxy-β-D-glucopyranoside 68[325]

Glucoside **67** (1.10 g, 2.30 mmol), sodium azide (449 mg, 6.90 mmol) and tetrabutylammonium iodide (40.0 mg, 108 µmol) were dissolved in dry DMF (24 mL). The mixture was stirred at 60 °C for 6 h before the solvent was removed under reduced pressure. The crude product was purified by column chromatography (ethyl acetate → ethyl acetate/methanol 30:1) to yield compound **68** as a colourless foam.

Yield: 658 mg (1.89 mmol, 82 %); lit.[325]: 81 %;

TLC: R_f = 0.28 (ethyl acetate/methanol 30:1);

Rotational value: $[\alpha]_D^{20}$ = -37.8 (c = 0.15 in methanol); lit.: $[\alpha]_D^{20}$ = -13.0 (c = 1.0 in methanol);

^{1}H-NMR: (500 MHz, MeOD, 300 K, TMS): δ = 4.58 (s, 1H, NH), 4.30 (d, $^3J_{1,2}$ = 7.2 Hz, 1H, H-1), 3.90-3.85 (m, 1H, C$_1$OC<u>H</u>H'), 3.62-3.57 (m, 1H, C$_1$OCH<u>H</u>'), 3.51-3.38 (m,

3H, H-5, H-6, H-6‘), 3.37-3.32 (m, 2H, H-3, C<u>H</u>H‘N), 3.27-3.18 (m, 3H, H-2, H-4, CH<u>H</u>‘N), 1.44 (s, 9H, $C(CH_3)_3$) ppm;

^{13}C-NMR: (126 MHz, MeOD, 300 K, TMS): δ = 104.4 (C-1), 80.2 ($\underline{C}(CH_3)_3$), 77.7 (C-3), 77.1 (C-5), 75.1 (C-2), 72.4 (C-4), 70.1 (OCH_2), 52.8 (C-6), 41.8 (CH_2N), 28.8 ($C(\underline{C}H_3)$) ppm;

IR (ATR): ṽ = 3355), 2978, 2930), 2097), 1683, 1367, 1162, 1049 cm^{-1};

ESI-MS: *m/z* = 371.1, $[M+Na]^+$; (calc. 371.15 for $C_{13}H_{24}N_4O_7$+Na).

2-Aminoethyl 6-azido-6-deoxy-β-D-glucopyranoside 69

To a solution of glucoside **68** (339 mg, 973 µmol) in DCM (30 mL) was added trifluoroacetic acid (372 µL, 4.87 mmol). The reaction mixture was stirred for 16 h at room temperature and the solvent was evaporated under reduced pressure afterwards. After codestillation with toluene (3 x 30 mL) and DCM (3 x 40 mL) compound **69** was obtained quantitatively as a colourless syrup.

Yield: quant.;

TLC: R_f = 0.05 (ethyl acetate/methanol 6:1);

Rotational value: $[\alpha]_D^{20}$ = -16.8 (c = 0.15 in methanol);

^{1}H-NMR: (500 MHz, MeOD, 300 K, TMS): δ = 4.39 (d, $^3J_{1,2}$ = 7.7 Hz, 1H, H-1), 4.10-4.06 (ddd, $^3J_{CHCHH}$ = 4.0 Hz, $^3J_{CHCHH}$ = 5.2 Hz, $^2J_{CHH}$ = 11.4 Hz 1H, $C_1OC\underline{H}H$‘), 3.83-3.77 (ddd, $^3J_{CHCHH}$ = 4.3 Hz, $^3J_{CHCHH}$ = 6.8 Hz, $^2J_{CHH}$ = 11.4 Hz 1H, $C_1OCH\underline{H}$‘), 3.54 (dd, $^3J_{5,6}$ = 1.7 Hz, $^2J_{6,6'}$ = 12.4 Hz, 1H, H-6), 3.51-3.46 (m, 1H, H-5), 3.44 (dd, $^3J_{5,6'}$ = 6.6 Hz, $^2J_{6,6'}$ = 10.8 Hz, 1H, H-6’), 3.37 (dd~t, $^3J_{2,3}$ = 8.9 Hz, 1H, H-3), 3.28-3.24 (m, 2H, H-2, H-4), 3.20-3.16 (m, 2H, CH_2NH_2) ppm;

^{13}C-NMR: (126 MHz, MeOD, 300 K, TMS): δ = 104.1 (C-1), 77.7 (C-3), 77.2 (C-5), 75.0, 72.3 (C-2, C-4), 66.6 (OCH_2), 52.7 (C-6), 40.9 (CH_2N) ppm;

ESI-MS: *m/z* = 249.2, $[M+H]^+$; (calc. 249.11 for $C_8H_{16}N_4O_5$+H);

IR (ATR): ṽ = 3264, 2932, 2101, 1662, 1201, 1180, 1129, 1060 cm^{-1}.

Tosylated dextran 71

After one hour of pre-drying, dextran **70** (1.00 g, 6.17 mmol) and lithium chloride (600 mg, 14.2 mmol) were suspended in *N*,*N*' dimethylacetamide (30 mL) and stirred for two hours at 80 °C until the suspension became clear and was cooled to 0 °C subsequently. After addition of a solution of triethylamine (5.12 mL, 36.9 mmol) in DMAA (5 mL) a solution of 4-methylbenzenesulfonyl chloride (3.52 g, 18.5 mmol) in DMAA (10 mL) was added dropwise. The reaction mixture was stirred at 0 °C for 3 h and then for additionally 16 h at room temperature. The crude mixture was poured onto ice and the precipitate isolated by centrifugation. The crude product was resuspended several times in isopropanol (5 x 35 mL) and water (5 x 10 mL) and regained by centrifugation after each washing step to yield compound **71** as a brownish solid.

Yield: 1.59 g (5.03 mmol, 81 %);

D_s (Tosyl): 1.25;

^{1}H-NMR: (500 MHz, DMSO-*d6*, 300 K): δ = 7.77 (CAr-H$_{ortho}$), 7.35 (CAr-H$_{meta}$), 5.70-5.00 (OH), 5.00-4.50 (H-1, if C-2 is tosylated), 4.50-3.90 (H-2$_{tos}$, H-3$_{tos}$, H-4$_{tos}$) 3.70-3.10 (H-2, H-3, H-4, H-5, H-6 (AGU)), 2.36 (CH_3) ppm;

^{13}C-NMR: (126 MHz, DMSO-*d6*, 300 K): δ = 145.0 (Ar-C$_{ipso}$), 133.5 (Ar-C$_{para}$), 129.9 (Ar-C$_{meta}$), 128.0 (Ar-C$_{ortho}$), 95.1 (C-1 if C-2 tosylated), 79.7 (C-2$_{tos}$), 70.9-67.9 (C-2, C-3, C-4, C-5 (AGU)), 65.3 (C-6), 20.8 (CH_3) ppm;

IR (ATR-IR): $\tilde{\nu}$ = 3380 (vOH), 2900 (vCH), 1600 (vC=Ar-C), 1350 ($\nu_{asym}SO_2$), 1174 ($\nu_{sym}SO_2$), 1019 (vCOC), 811 (δCAr-H) cm^{-1};

elemental analysis: calcd for D_s = 1.25 (%) $(C_{13}H_{16}O_7S)_n$: C 49.92 %, H 4.97 %, S 11.29 %; found: C 49.00 %, H 5.31 %, S 9.87 %.

Azido dextran 72

Sodium azide (1.44 g, 22.1 mmol) was added to a solution of tosylated dextran **71** (1.00 g, 3.16 mmol) in dimethylsulfoxid (20 mL) and the mixture was stirred for 20 h at 100 °C. The mixture was then cooled to room temperature and poured onto isopropanol (100 mL). The crude product was resuspended several times in isopropanol (5 x 30 mL) and water

(2 x 10 mL) and regained by centrifugation after each washing step to yield compound **72** as a brownish solid.

Yield: 500 mg (2.13 mmol, 80 %);

D_s (Tosyl): 0.72;

D_s (Azid): 0.53;

^{1}H-NMR: (500 MHz, DMSO-*d6*, 300 K): δ = 7.79 (CAr-H_{ortho}), 7.37 (CAr-H_{meta}), 6.15-5.12 (OH), 4.92-4.51 (H-1, if C-2 is tosylated or azido-functionalised, respectively), 4.28-3.90 (H-2_{tos}, H-3_{tos}, H-4_{tos}) 3.80-3.41 (H-2, H-3, H-4, H-5, H-6 (AGU)), 2.37 (CH_3) ppm;

^{13}C-NMR: (126 MHz, DMSO-*d6*, 300 K): δ = 144.7 (Ar-C_{ipso}), 133.3 (Ar-C_{para}), 129.8 (Ar-C_{meta}), 127.8 (Ar-C_{ortho}), 100.1 (C-1 if C-2 azido-functionalised), 95.5 (C-1 if C-2 is tosylated), 79.9 (C-2_{tos}), 71.7-69.0 (C-2, C-3, C-4, C-5 (AGU)), 65.0 (C-6), 21.1 (CH_3) ppm;

IR (ATR-IR): $\tilde{\nu}$ = 3500 (vOH), 2930 (vCH), 2112 (νN_3), 1600 (vC=Ar-C), 1348 ($\nu_{asym}SO_2$), 1173 ($\nu_{sym}SO_2$), 1019 (vCOC), 813 (δCAr-H) cm^{-1};

elemental analysis: calcd for D_s(Tos) = 0.72 and $D_s(N_3)$ = 0.53 (%) $(C_6H_9N_3O_4)_n$: C 47.14 %, H 4.79 %, S 9.21 %, N 6.70 %; found: C 45.21 %, H 4.88 %, S 7.36 %, N 5.49 %.

4-Propiolamidophenyl 2,3,4,6-tetra-*O*-acetyl-α-D-mannopyranoside 78

4-Aminophenyl 2,3,4,6-tetra-*O*-acetyl-α-D-mannopyranoside **77** (810 g, 1.84 mmol) was added to a solution of propiolic acid (133 µL, 2.15 mmol) and *N,N'*-dicyclohexylcarbodiimide (442 mg, 2.14 mmol) in dry DCM (10 mL). The reaction mixture was stirred at room temperature for 16 h before removing the solvent under reduced pressure. The crude product was purified by column chromatography (cyclohexane/acetone 3:1 → 2:1) to yield compound **78** as a colourless foam.

Yield: 663 mg (1.35 mmol, 73 %);

TLC: R_f = 0.15 (cyclohexane/actone 2:1);

Melting point: 83 °C;

Rotational value: $[\alpha]_D^{25}$ = +132.7 (c = 0.23 mM, CH_2Cl_2);

^{1}H-NMR: (500 MHz, $CDCl_3$, 300 K, TMS): δ = 7.61 (s, 1H, NH), 7.47-7.44 (m, 2H, Ar-H_{ortho}), 7.07-7.04 (m, 2H, Ar-H_{meta}), 5.55-5.41 (dd, $^{3}J_{2,3}$ = 3.5 Hz, $^{3}J_{3,4}$ = 10.0 Hz, 1H, H-3), 5.47 (d, $^{3}J_{1,2}$ = 1.8 Hz, 1H, H-1), 5.44-5.42 (dd, $^{3}J_{1,2}$ = 1.8 Hz, $^{3}J_{2,3}$ = 3.5 Hz, 1H, H-2), 5.38-5.33 (dd~t, $^{3}J_{3,4}$ = 10.0 Hz, $^{3}J_{4,5}$ = 10.0 Hz, 1H, H-4), 4.29-4.25 (m, 2H, H-6), 4.10-4.04 (m, 2H, H-5, H-6‘), 2.93 (s, 1H, C≡CH), 2.19, 2.05, 2.03 (each s, each 3H, CH_3) ppm;

^{13}C-NMR: (126 MHz, $CDCl_3$, 300 K, TMS): δ = 170.7, 170.1, 169.9 ($\underline{C}OCH_3$), 152.9 (Ar-C_{ipso}), 149.7 (NC=O), 132.3 (Ar-C_{para}), 121.8 (Ar-C_{meta}), 117.3 (Ar-C_{ortho}), 96.2 (C-1), 77.7 ($\underline{C}$≡CH), 74.3 (C≡$\underline{C}$H), 69.5 (C-2), 69.4 (C-5), 69.0 (C-3), 66.1 (C-4), 62.3 (C-6), 21.0, 20.8 (CO$\underline{C}H_3$) ppm;

ESI-MS: m/z = 514.2, $[M+Na]^+$, (calc. 514.4 for $C_{23}H_{25}NO_{11}$+Na);

IR (ATR): $\tilde{\nu}$ = 3261, 2107, 1744, 1508, 1369, 1213, 1035, 835 cm^{-1}.

4-Propiolamidophenyl α-D-mannopyranoside 79

To a solution of mannoside **78** (214 mg, 436 µmol) in dry methanol (8 mL) was added a 1M sodium methoxide solution (16.0 µL). After stirring for 16 hours at room temperature the mixture was neutralised with ion exchanger Amberlite® IR 120. The resin was filtered off and the solvent was removed under reduced pressure to yield compound **79** as a colourless foam.

Yield: 140 mg (3.56 mmol, 99 %);

TLC: R_f = 0.18 (DCM/methanol 9:1);

Rotational value: $[\alpha]_{20}^{D}$ = +125.1 (c = 0.09 in methanol);

^{1}H-NMR: (500 MHz, MeOD, 300 K, TMS): δ = 7.47-7.44 (m, 2H, Ar-H_{ortho}), 7.07-7.04 (m, 2H, Ar-H_{meta}), 5.40 (d, $^{3}J_{1,2}$ = 1.8 Hz, 1H, H-1), 4.80 (s, 4H, OH), 3.95 (dd, $^{3}J_{1,2}$ = 1.8 Hz, $^{3}J_{2,3}$ = 3.4 Hz, 1H, H-2), 3.84 (dd, $^{3}J_{2,3}$ = 3.4 Hz, $^{3}J_{3,4}$ = 9.4 Hz, 1H, H-3), 3.80-3.70 (m, 3H, H-4, H-6) 3.56 (ddd, $^{3}J_{5,6}$ = 2.5 Hz, $^{3}J_{5,6‘}$ = 5.3 Hz, $^{3}J_{4,5}$ = 9.8 Hz, 1H, H-5), 3.35 (s, 1H, C≡CH) ppm;

^{13}C-NMR: (126 MHz, MeOD, 300 K, TMS): δ = 155.0 (Ar-C_{ipso}), 152.2 (NC=O), 133.7 (Ar-C_{para}), 122.8 (Ar-C_{meta}), 118.1 (Ar-C_{ortho}), 100.5 (C-1), 78.7 ($\underline{C}$≡CH), 76.4 (C≡$\underline{C}$H), 75.4 (C-5), 72.4 (C-3), 72.0 (C-2), 68.4 (C-4), 62.9 (C-6) ppm;

IR (ATR): $\tilde{\nu}$ = 3280, 2931, 2108, 1645, 1508, 1225, 1010, 822, 510 cm^{-1};

ESI-MS: m/z = 346.08944, $[M+Na]^+$, (calc. 346.09027 for $C_{23}H_{25}NO_{11}$+Na).

3-Cascade:(Propargylchloroformate)-methane[3-1,1,1]:methoxymethyl:1*H*[1,2,3] triazole-1-ethyl: tetra-*O*-acetyl-α-D-mannopyranoside (85)

To an ice-cold solution of deprotected compound **26** (634 mg, 619 µmol) and sodium bicarbonate (177 mg, 2.10 mmol) in water (40 mL) and 1,4 dioxane (20 mL) was added propargyl chloroformate (90.2 µL, 929 µmol). After stirring at room temperature for 60 h the solvent was removed at reduced pressure and the mixture was codestilled with methanol (2 x 60 mL). The residue was dissolved in acetic anhydride (20.0 mL) and pyridine (3 mL) and stirred for 3 h. The solvent was removed under reduced pressure again and the remaining crude product was dissolved in DCM (100 mL) and washed with water (50 mL). The organic layer was dried over $MgSO_4$ and filtered. The solvent was removed under reduced pressure and the crude product was purified by column chromatography (DCM/ methanol 19:1) to yield compound **85** as a colourless foam.

Yield: 406 mg (258 µmol, 42 %);

TLC: R_f = 0.37 (DCM/ methanol 19:1);

Rotational value: $[\alpha]_{20}^{D}$ = +19.3 (c = 0.16 in ethyl acetate);

^{1}H-NMR: (500 MHz, $CDCl_3$, 300 K): δ = 7.73 (s, 3H, $CH_{triazole}$), 5.55 (s, 1H, $NH_{Carbamat}$), 5.27-5.18 (m, 9H, H-2, H-3, H-4), 4.81 (d, $^3J_{1,2}$ = 1.0 Hz, 3H, H-1), 4.68-4.60 (m, 12H, $N_{triazole}CH_2$, $OCH_2C_{triazole}$), 4.59-4.57 (d, $^4J_{CH2C\equiv CH}$ = 2.4 Hz, 2H, $CH_2C\equiv C$), 4.23-4.18 (dd, $^3J_{5,6}$ = 5.2 Hz, $^2J_{6,6'}$ = 12.3 Hz, 3H, H-6), 4.16-4.11 (m, 3H, $N_{triazole}CH_2C\underline{H}$), 4.04 (dd, $^2J_{6,6'}$ = 12.3 Hz, $^3J_{5,6'}$ = 2.4 Hz, 3H, H-6'), 3.93-3.88 (m, 3H, $N_{triazole}CH_2C\underline{H}$'), 3.77 (s, 6H, $_{Carbamat}CCH_2$), 3.63-3.59 (ddd, $^3J_{4,5}$ = 9.4 Hz, $^3J_{5,6}$ = 5.1 Hz, $^3J_{5,6'}$ = 2.4 Hz, 3H, H-5), 2.46 (t, 1H, $^4J_{CH2C\equiv CH}$ = 2.4 Hz, C≡CH), 2.13, 2.09, 2.04, 1.99 (each s, each 9H, $OCOCH_3$) ppm;

^{13}C-NMR: (126 MHz, $CDCl_3$, 300 K): δ = 170.7, 170.1, 169.8 ($\underline{C}OCH_3$), 155.8 (OC=O), 145.2 ($\underline{C}_{triazole}CH$), 124.1 ($C_{triazole}\underline{C}H$), 97.7 (C-1), 78.8 ($CH_2\underline{C}\equiv C$), 74.7 ($C\equiv\underline{C}H$), 69.3, 69.1, 69.0 (C-2, C-3, C-5, CCH_2), 66.4 ($N_{triazole}CH_2\underline{C}H_2$), 65.9 (C-4), 64.8 ($O\underline{C}H_2C_{triazole}$), 62.4 (C-6), 59.2 ($NH\underline{C}CH_2$), 52.1 ($\underline{C}H_2C\equiv C$), 49.8 ($N_{triazole}CH_2$), 21.0, 20.9, 20.8, ($OCO\underline{C}H_3$) ppm;

ESI-MS: *m/z* = 1569.54774, $[M+H]^+$ (calc. 1569.54863 for $C_{65}H_{88}N_{10}O_{35}$ + H).

3-Cascade:(Propargylchloroformate)-methane[3-1,1,1]:methoxymethyl:1*H*[1,2,3] triazole-1-ethyl: α-D-mannopyranoside 86

Compound **85** (200 mg, 127 µmol) was dissolved in dry methanol (10 mL) and 1M sodium methoxide solution (40 µL) was added. After stirring for 16 h at room temperature the mixture was neutralised with ion exchanger Amberlite® IR 120. The resin was filtered off and the solvent was removed under reduced pressure to yield compound **86** quantitatively as a colourless syrup.

Yield: quant.;

TLC: R_f = 0 (ethyl acetate/ methanol 4:1);

Rotational value: $[\alpha]_{20}^{D}$ = +74.9 (c = 0.42 in methanol);

^{1}H-NMR: (500 MHz, MeOD, 300 K): δ = 7.98 (s, 3H, $CH_{triazole}$), 5.49 (s, 1H, $NH_{Carbamate}$), 4.86 (s, 12H, OH), 4.73 (d, $^3J_{1,2}$ = 1.2 Hz, 3H, H-1), 4.69-4.59 (m, 8H, $N_{triazole}CH_2$, $C\underline{H}_2C{\equiv}CH$), 4.58 (s, 6H, $OCH_2C_{triazole}$), 4.15-4.09 (m, 3H, $N_{triazole}CH_2C\underline{H}$), 3.90-3.84 (m, 3H, $N_{triazole}CH_2C\underline{H}$‘), 3.80-3.74 (m, 6H, H-2, H-6), 3.70 (s, 6H, $N_{Carbamate}CCH_2$), 3.68-3.55 (m, 9H, H-3, H-4, H-6‘), 3.27-3.22 (m, 3H, H-5), 2.89 (m, 1H, C≡CH) ppm;

^{13}C-NMR: (126 MHz, MeOD, 300 K): δ = 145.8 ($\underline{C}_{triazole}CH$), 125.8 ($C_{triazole}\underline{C}H$), 101.6 (C-1), 79.4 ($CH_2\underline{C}{\equiv}C$), 75.0 (C-5), 74.9 ($C{\equiv}\underline{C}H$), 72.5 (C-3), 71.9 (C-2), 69.4 ($N_{Carbamate}CCH_2$), 68.4 (C-4), 66.7 ($N_{triazole}CH_2\underline{C}H_2$), 65.2 ($O\underline{C}H_2C_{triazole}$), 62.9 (C-6), 60.4 ($CCH_2$), 52.8 ($\underline{C}H_2C{\equiv}C$), 51.3 ($N_{triazole}CH_2$) ppm;

IR (ATR): $\tilde{\nu}$ = 3356, 2926, 1712, 1242, 1055, 1026, 976, 675 cm^{-1};

ESI-MS: m/z = 1087.40215, $[M+Na]^+$, (calc. 1087.40435 for $C_{41}H_{64}N_{10}O_{23}$+Na).

8.4.2 Bacterial adhesion assay

Buffers: PBS buffer: PBS tablets were obtained from GIBCO containing phosphate (as sodium phosphates), 10 mM, potassium chloride (KCl), 2.68 mM, sodium chloride (NaCl), 140 mM, pH = 7.45; PBST buffer: PBS buffer + 0.05% v/v Tween®20; carbonate

buffer solution (pH 9.6): sodium carbonate (10.6 g) and sodium hydrogen carbonate (8.40 g) were dissolved in bidest. Water (1.0 L), pH values were adjusted by using 0.1 M HCl or 0.1 M NaOH.

Bacterial culture: The GFP-tagged strain PKL1162 was constructed in the KLEMM group by introduction of the plasmid pPKL174 into strain SAR18. Plasmid pPKL174 contains the fim gene cluster, which is required for type 1 fimbriae assembly and expression. The chromosome of strain SAR18 from the REISNER group contains the GFP gene, controlled by a constitutive promotor.[239, 421] The bacterial strain PKL1162[421] was cultured from a frozen stock in LB media (+ampicillin 100 mg/mL and chloramphenicol 50 mg/mL) overnight at 37 °C. The bacterial pellet resulting after centrifugation and decantation of media was washed twice with PBS (2 mL) and suspended in PBS buffer afterwards. The bacterial suspension was adjusted to OD_{600} = 0.4 with PBS.

Functionalisation of microtiter plates and the adhesion assay was performed in dependence on HARTMANN et al.[239, 270] Black Immobilizer Amino™ F96 MicroWell™ plates (Nunc) were incubated overnight with a 20 mM solution of amine **69** respectively 2-[2-[2-(2-Azidoethoxy)ethoxy]ethoxy]ethan amine **87** in PBS buffer (100 µL/well, 100 rpm, room temperature). Black microtiter plates (Nunc, MaxiSorp) were incubated overnight with azido-functionalised dextran **72** (1.2 mg/mL carbonate buffer/ DMSO 9:1, 120 µL/well) at 37 °C at 100 rpm. Plates were washed with PBST three times. Dextran-functionalised microtiter plates were blocked with PVA (poly vinyl alcohol) by adding a solution of 1 % PVA in PBS (120 µL/well) and incubation at room temperature, 3 h, 100 rpm. Amine-prefunctionalised plates were blocked with a 20 mM solution of ethanolamine in carbonate buffer (120 µL/well, room temperature, 100 rpm, 2.5 h). Afterwards, wells were washed with PBST three times. Then, click reactions were performed on the microtiter plates. Therefore glycosides **75**, **79**, **83**, **84**, **86** were added to the plates with serial dilution starting from a 20 mM solution in case of compounds **75** and **83**, and 10 mM solutions in case of compounds **79**, **84**, **86**. Solutions of copper sulphate (10 mM) and sodium ascorbate (19.2 mM) in PBS were prepared on separate microtiter plates in serial dilution and subsequently transferred to the azido-functionalised microtiter plates (25 µL/well of sodium ascorbate solution and 25 µL/well of copper sulphate solution). After a reaction time of 3 h at 37 °C and 100 rpm plates were washed with PBST twice and finally once with PBS. The prepared bacterial suspension was added (50 µL/well) then. After incubation for one hour at 37 °C and 100 rpm, microtiter plates were washed three times with PBS and filled with PBS (100 µL/well) for terminal

fluorescence intensity read out (excitation wavelength 485 nm, emission wavelength 535 nm).

8.4.3 ^{1}H and ^{13}C NMR spectra of synthesised compounds

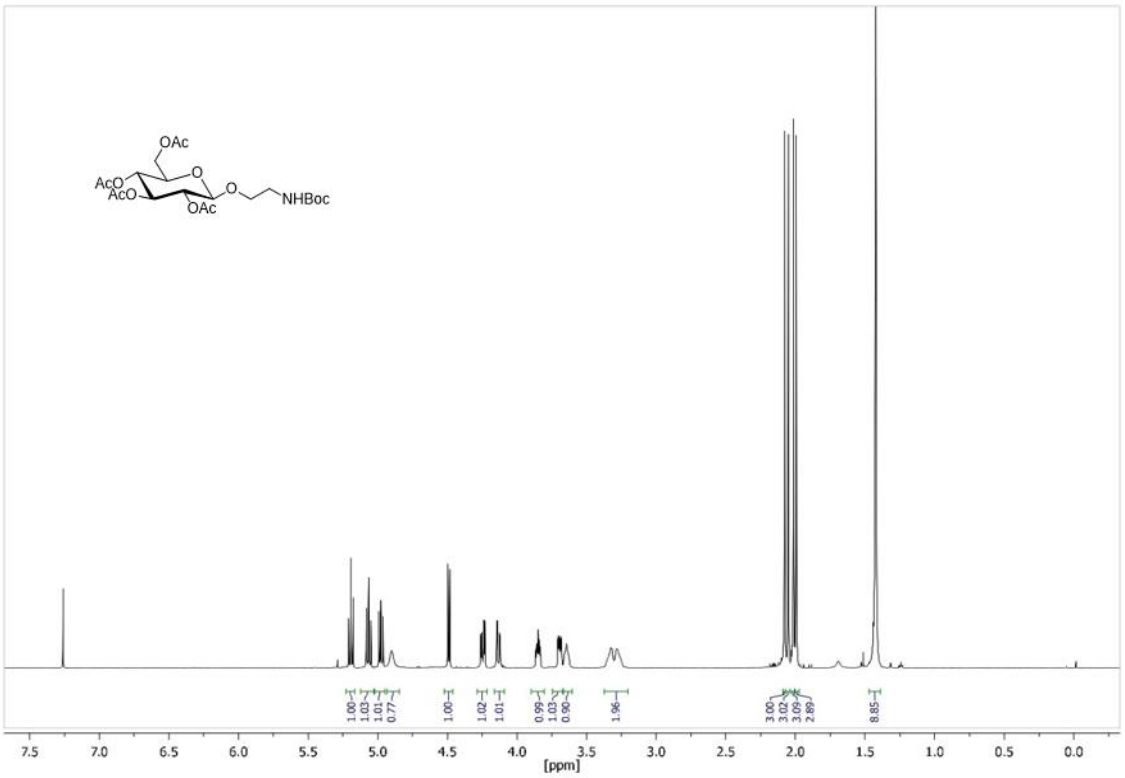

Figure 257: ^{1}H NMR spectrum of compound **65** (600 MHz, $CDCl_3$, 300 K, TMS).

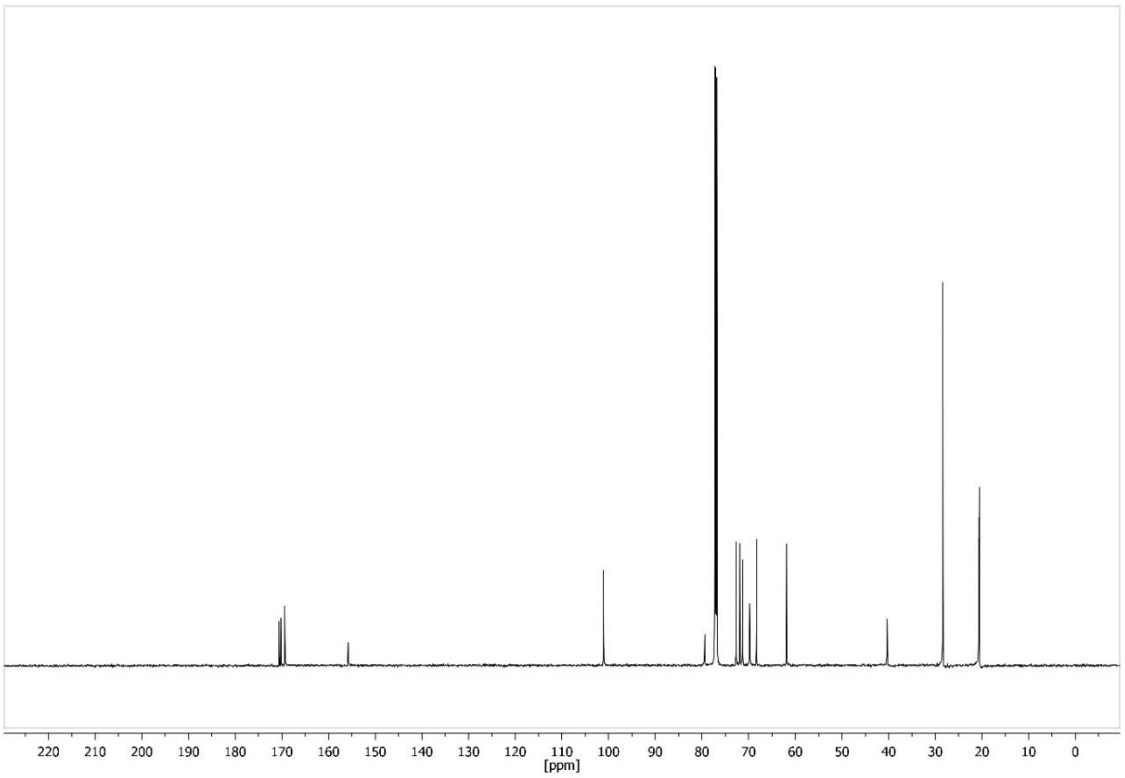

Figure 258: ^{13}C NMR spectrum of compound **65** (151 MHz, $CDCl_3$, 300 K, TMS).

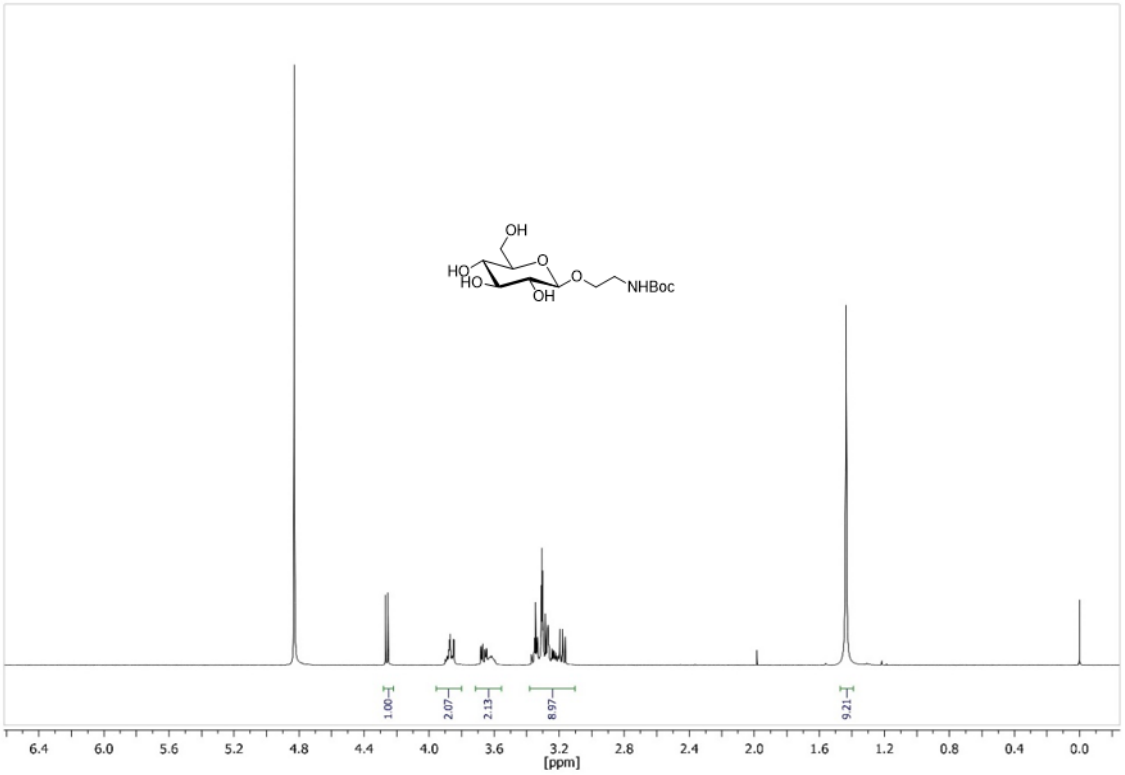

Figure 259: ^{1}H NMR spectrum of compound **66** (500 MHz, MeOD, 300 K, TMS).

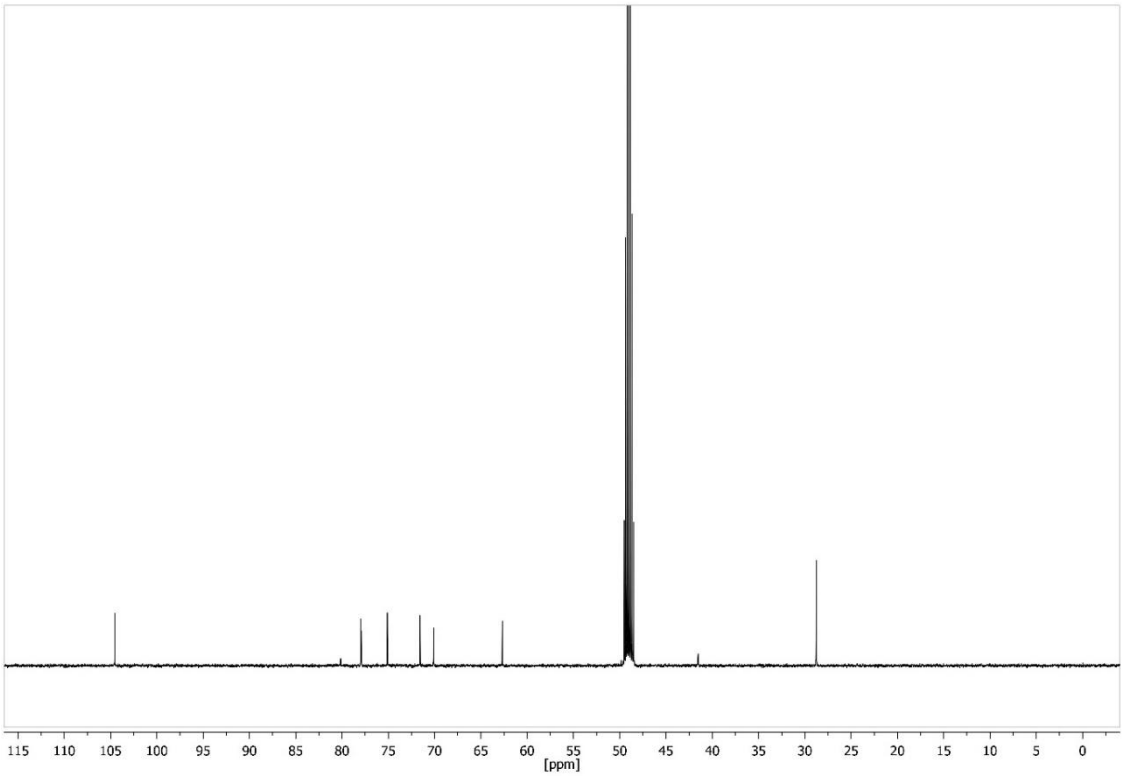

Figure 260: ^{13}C NMR spectrum of compound **66** (126 MHz, MeOD, 300 K, TMS).

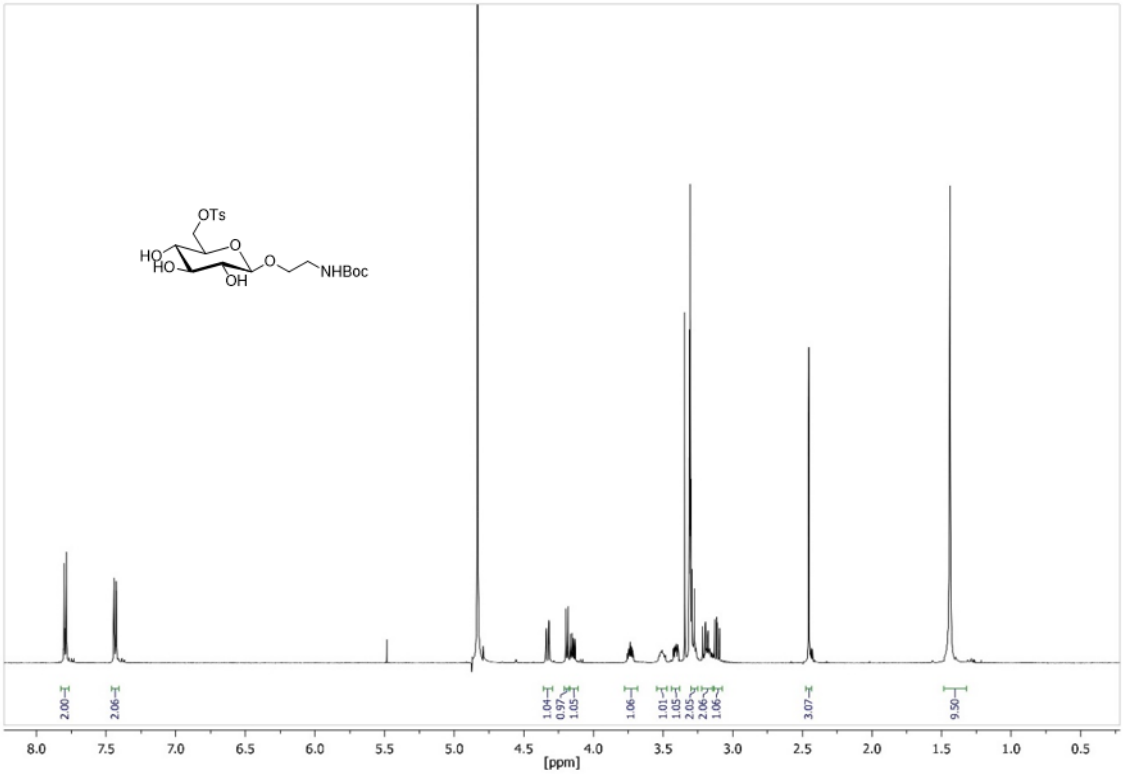

Figure 261: ^{1}H NMR spectrum of compound **67** (500 MHz, MeOD, 300 K, TMS).

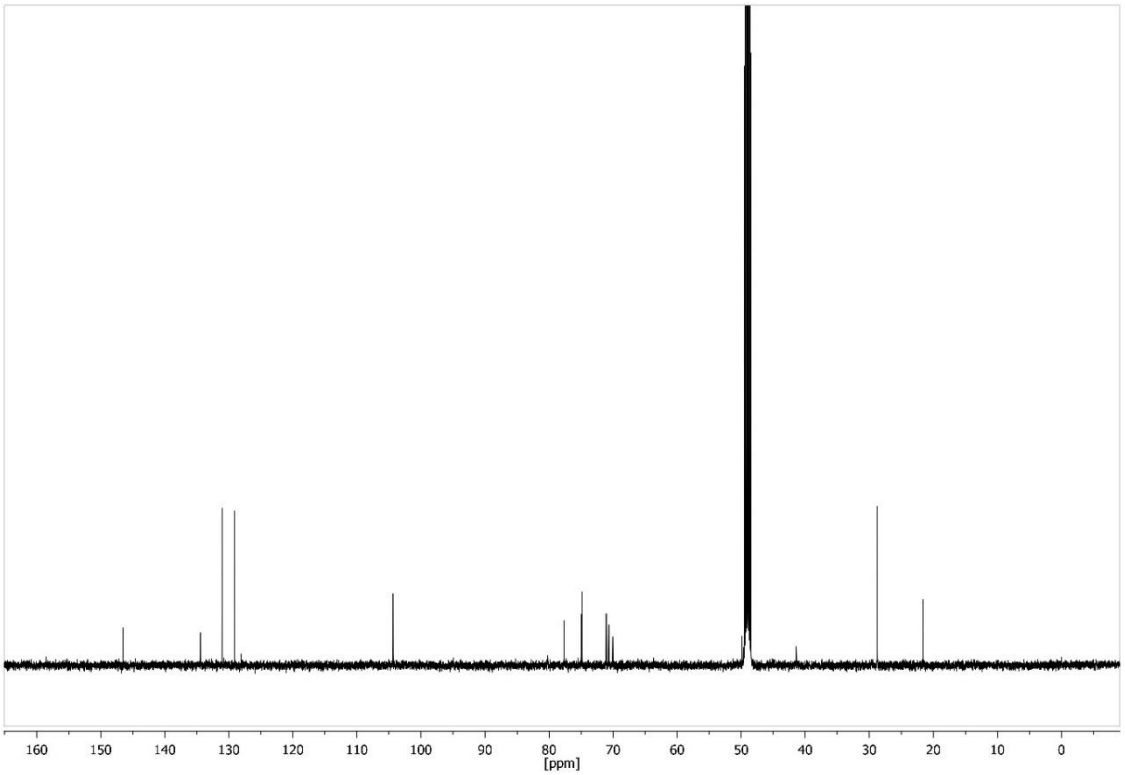

Figure 262: ^{13}C NMR spectrum of compound **67** (126 MHz, MeOD, 300 K, TMS).

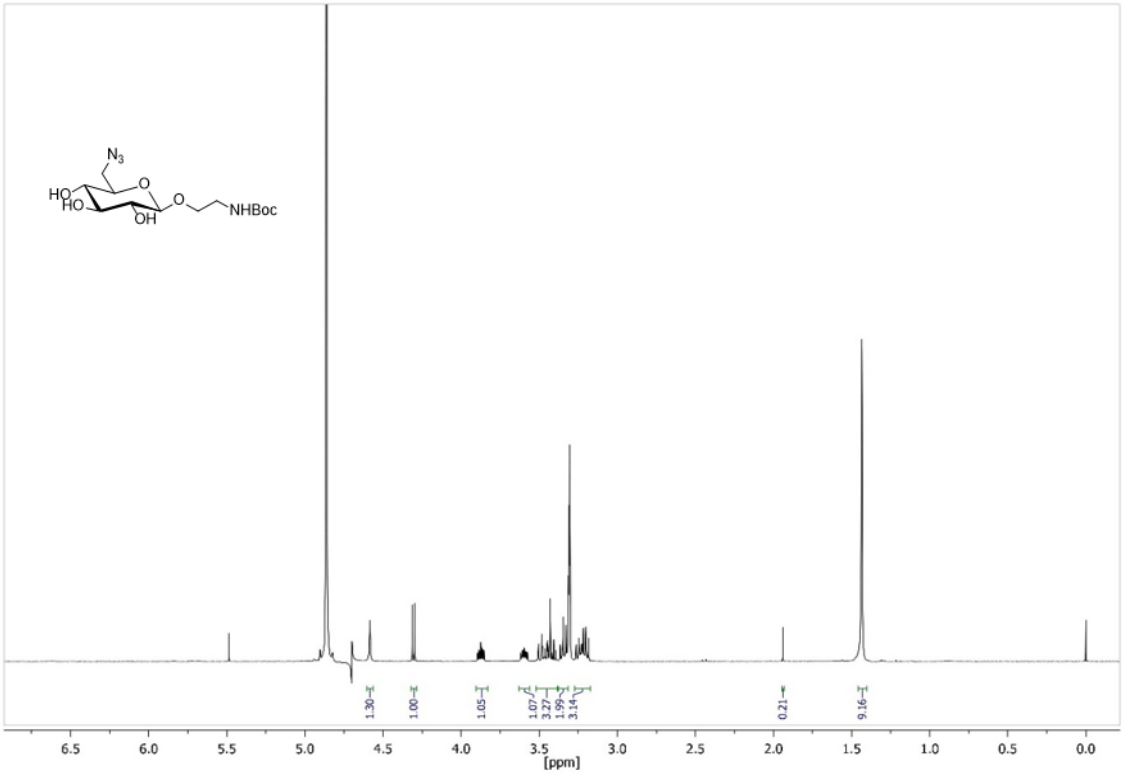

Figure 263: [1]H NMR spectrum of compound **68** (500 MHz, MeOD, 300 K, TMS).

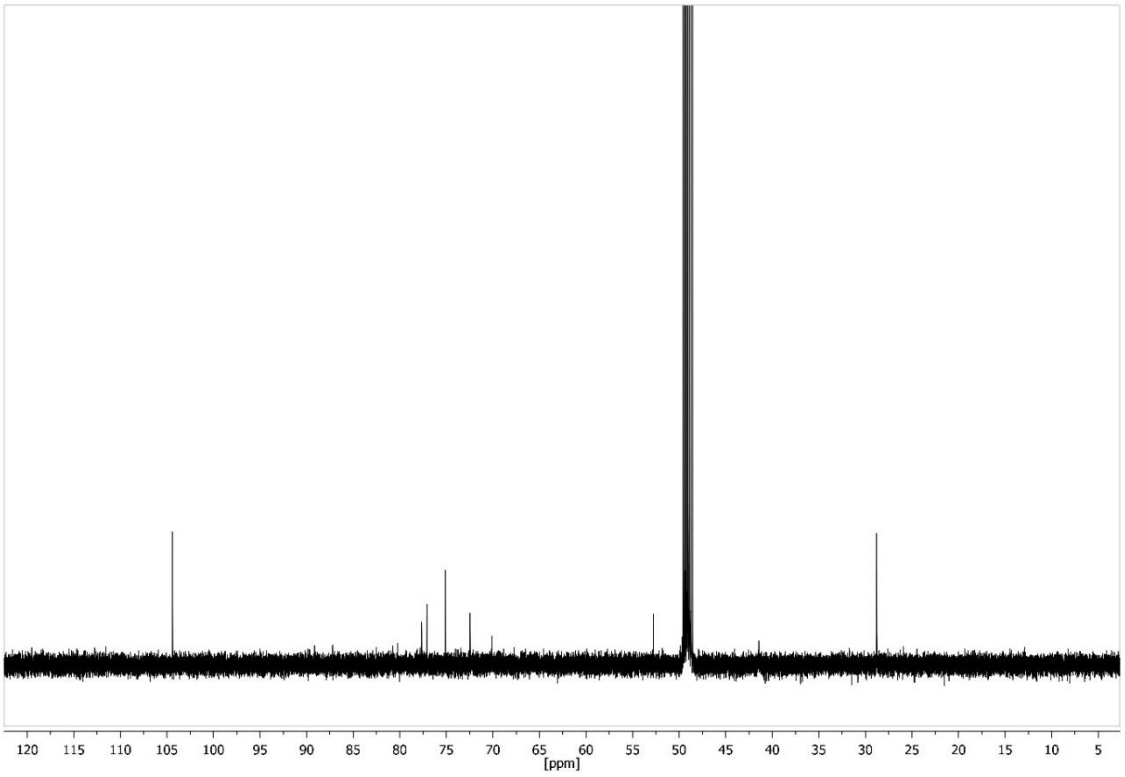

Figure 264: [13]C NMR spectrum of compound **68** (126 MHz, MeOD, 300 K, TMS).

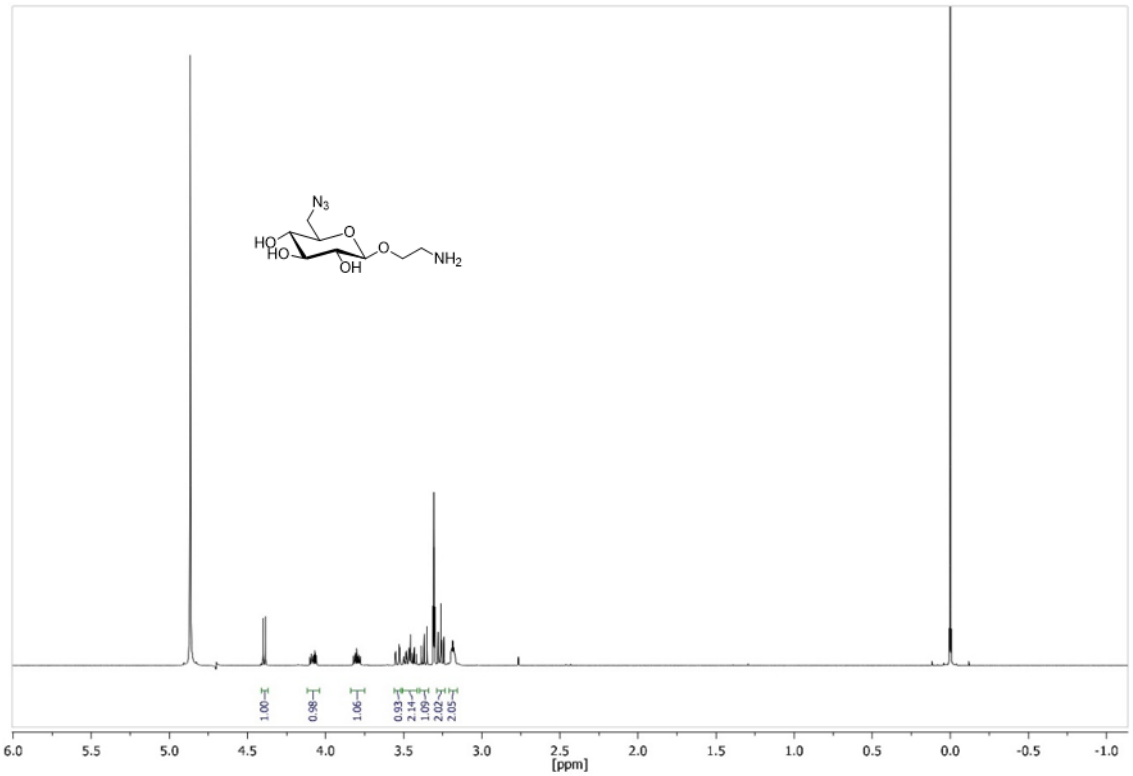

Figure 265: ^{1}H NMR spectrum of compound **69** (500 MHz, MeOD, 300 K, TMS).

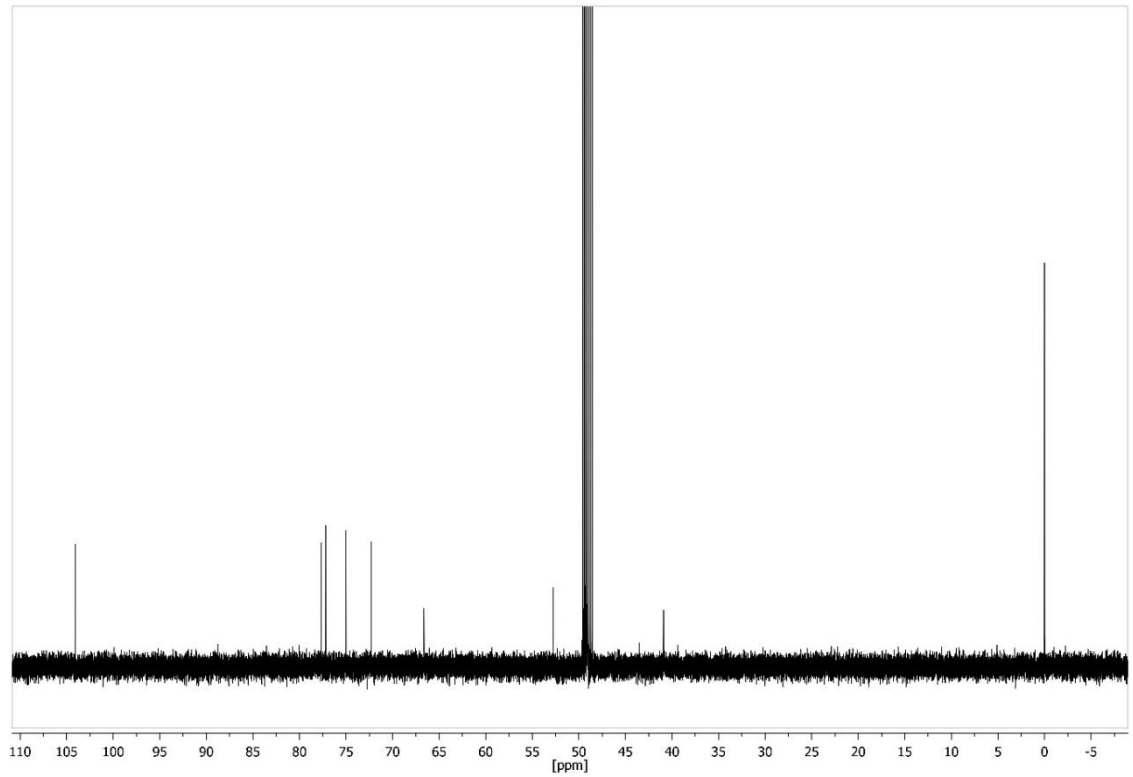

Figure 266: ^{13}C NMR spectrum of compound **69** (126 MHz, MeOD, 300 K, TMS).

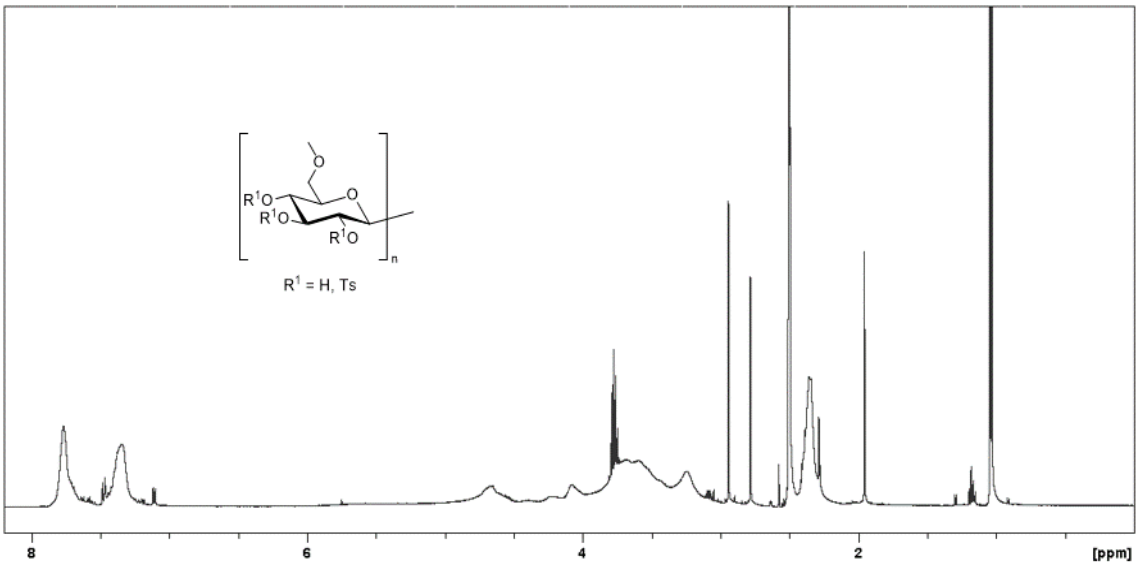

Figure 267: ^{1}H NMR spectrum of compound **71** (500 MHz, DMSO-*d6*, 300 K).

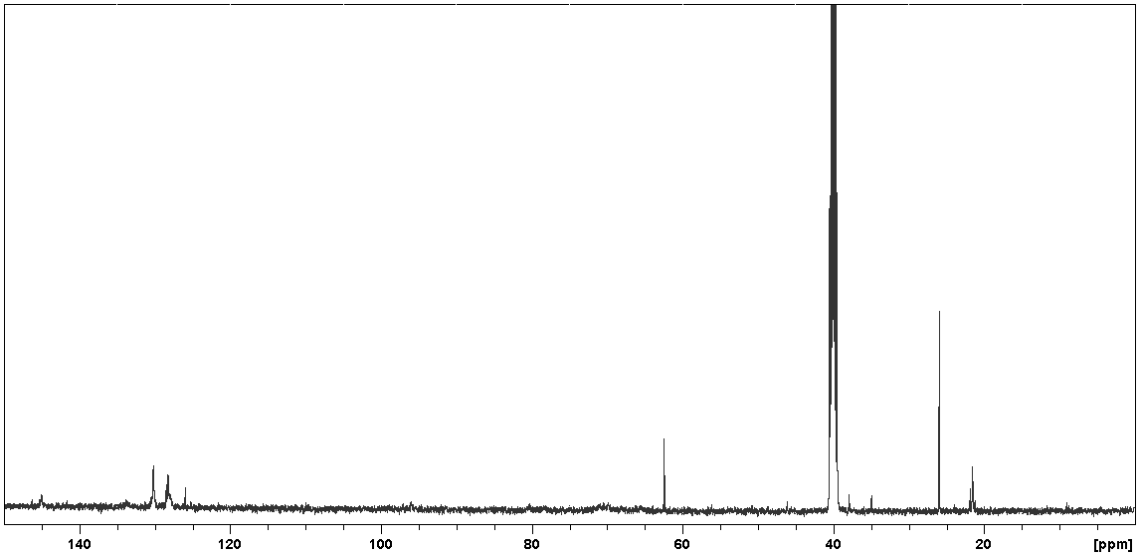

Figure 268: ^{13}C NMR spectrum of compound **71** (126 MHz, DMSO-*d6*, 300 K).

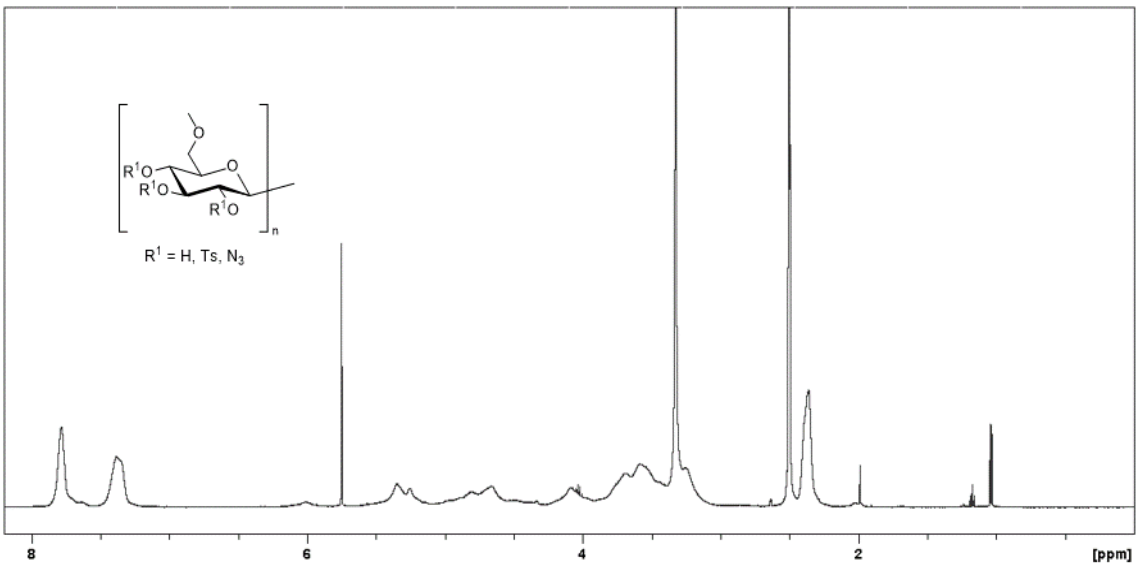

Figure 269: ^{1}H NMR spectrum of compound **72** (500 MHz, DMSO-*d6*, 300 K).

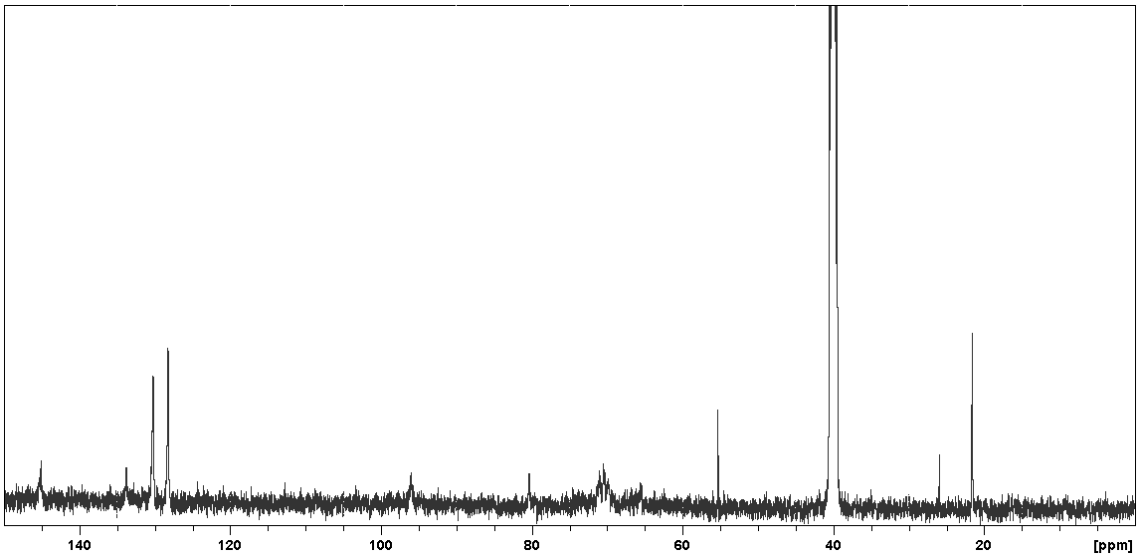

Figure 270: ^{13}C NMR spectrum of compound **72** (126 MHz, DMSO-*d6*, 300 K).

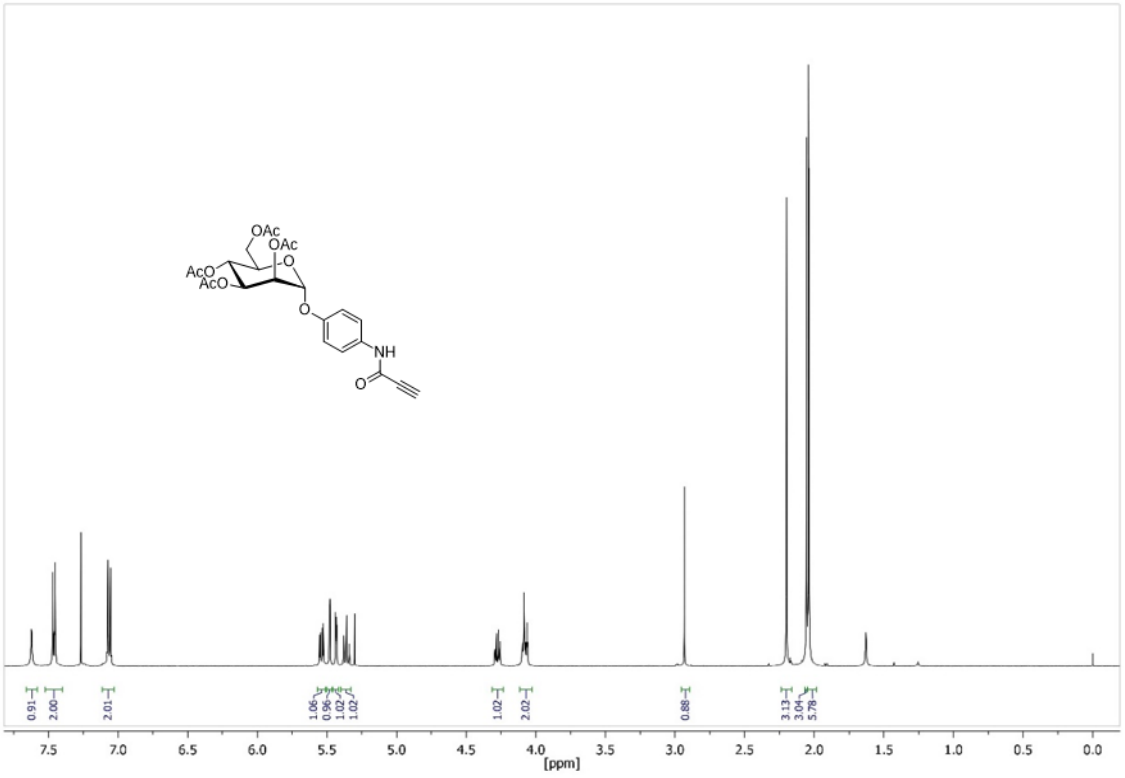

Figure 271: ^{1}H NMR spectrum of compound **78** (500 MHz, $CDCl_3$, 300 K, TMS).

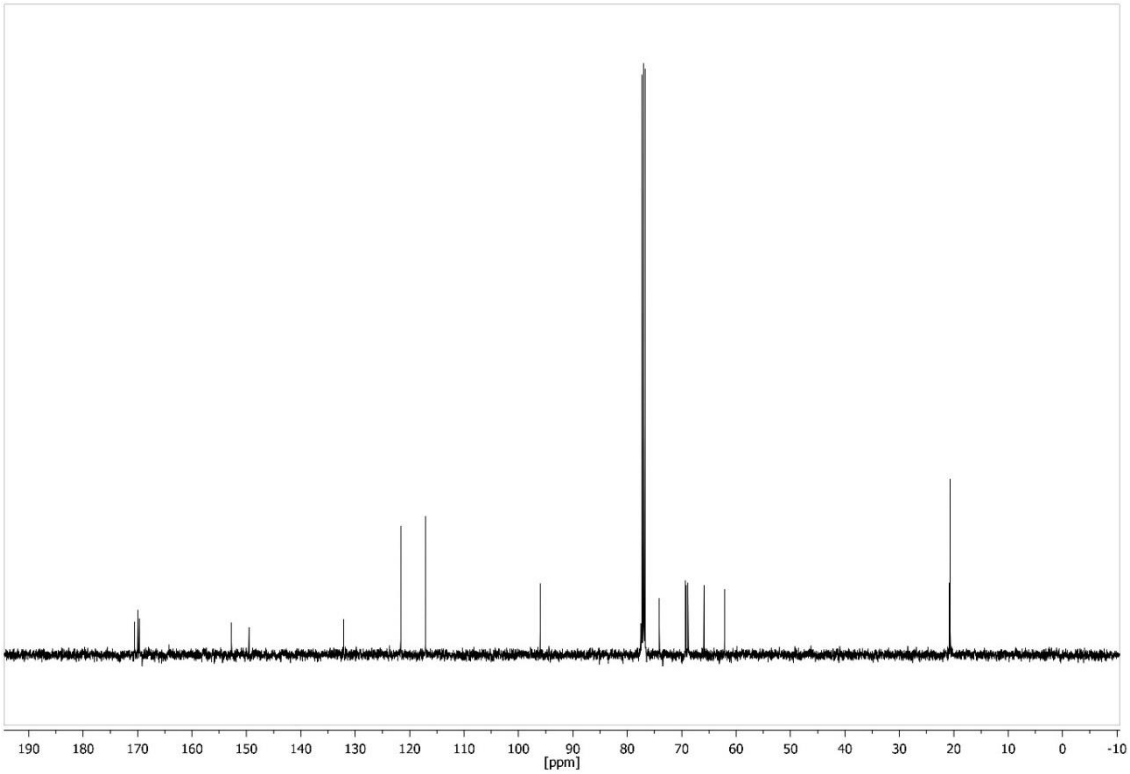

Figure 272: ^{13}C NMR spectrum of compound **78** (126 MHz, $CDCl_3$, 300 K, TMS).

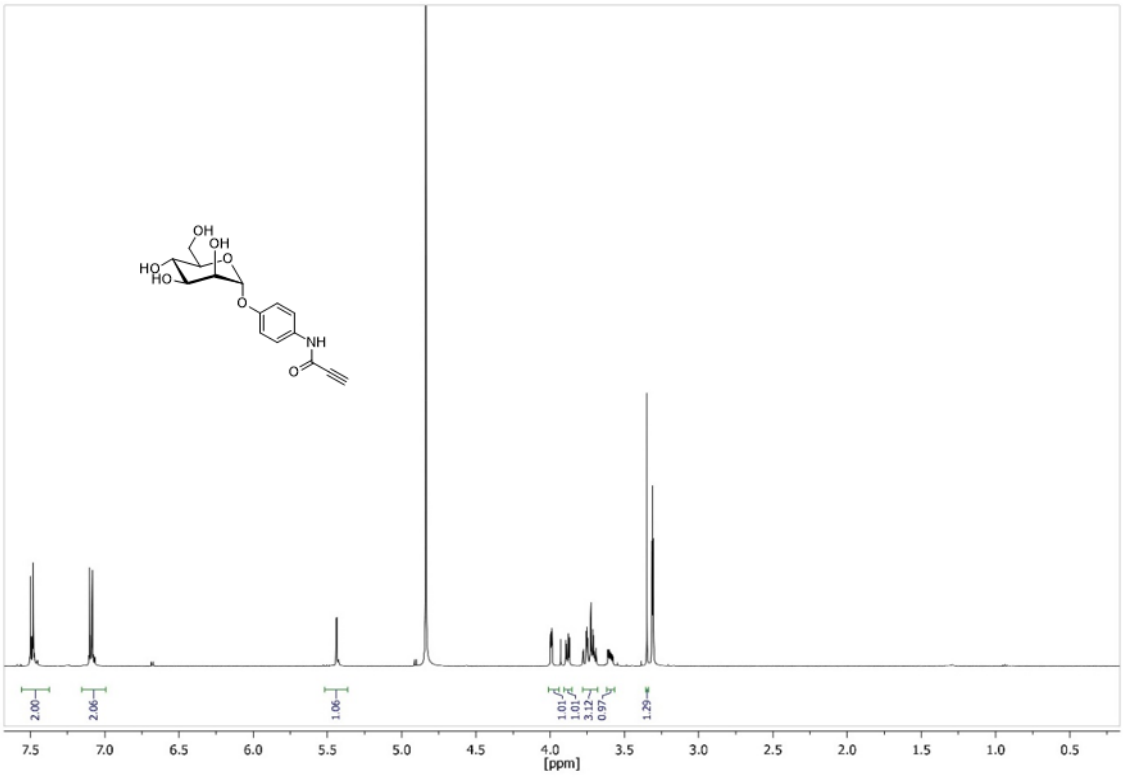

Figure 273: ^{1}H NMR spectrum of compound **79** (500 MHz, MeOD, 300 K, TMS).

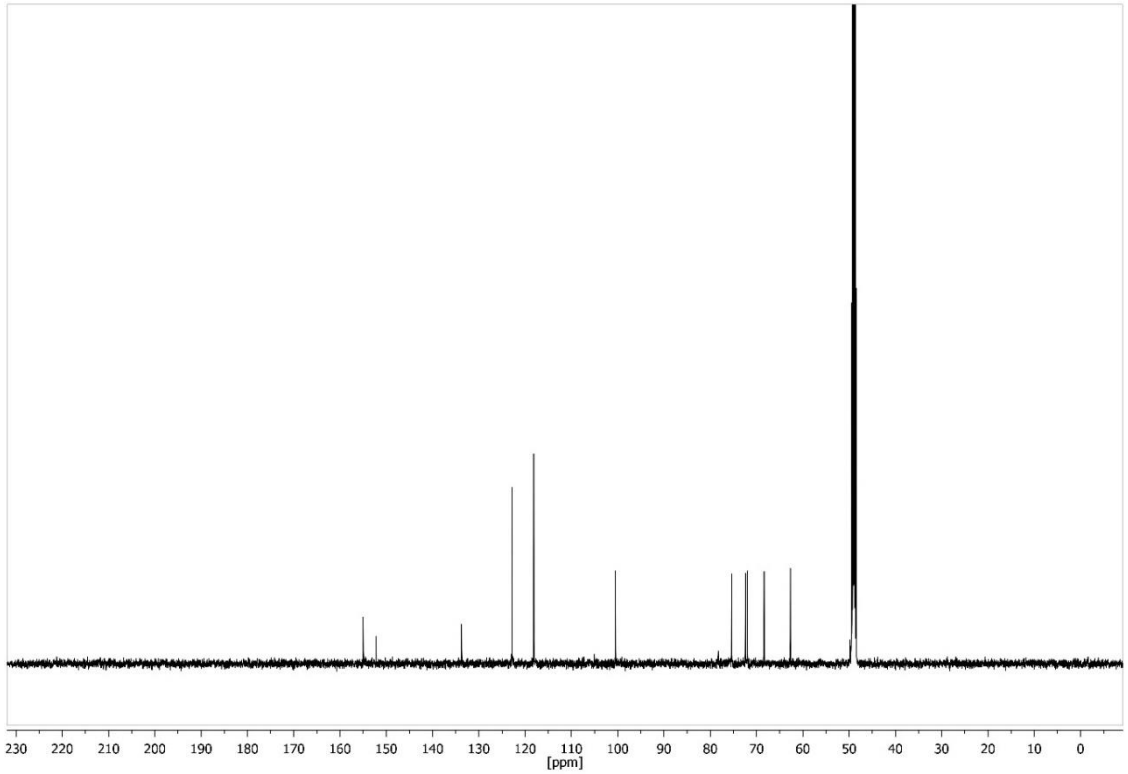

Figure 274: ^{13}C NMR spectrum of compound **79** (126 MHz, MeOD, 300 K, TMS).

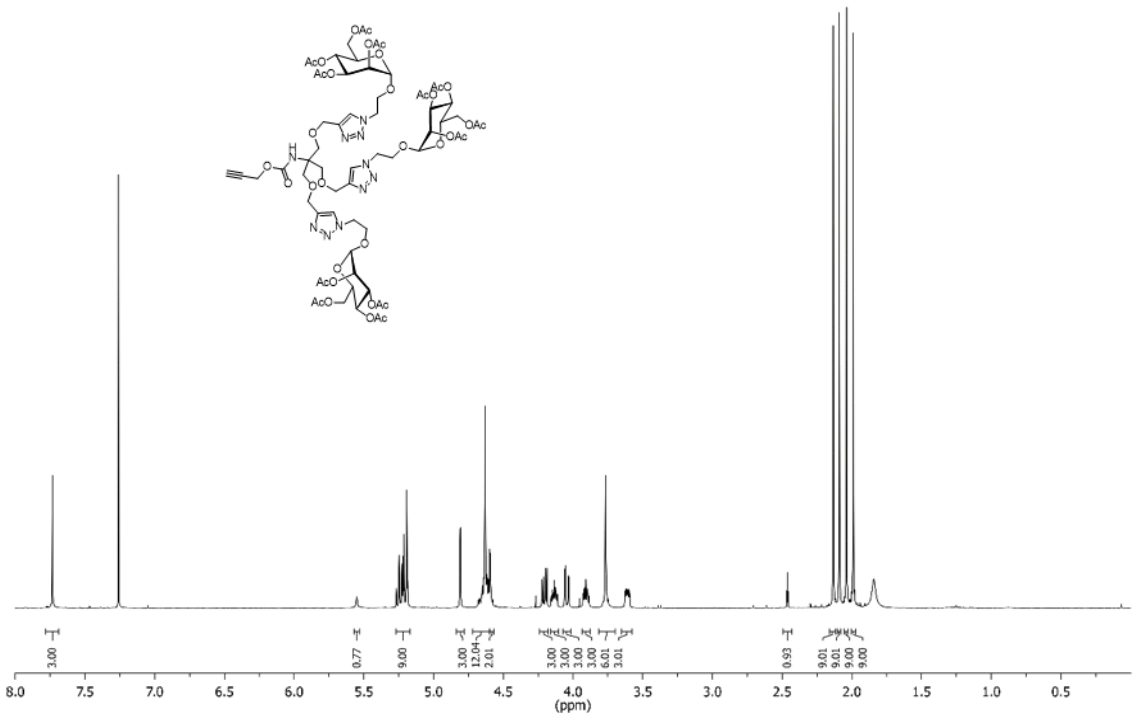

Figure 275: ^{1}H NMR spectrum of compound **85** (500 MHz, $CDCl_3$, 300 K, TMS).

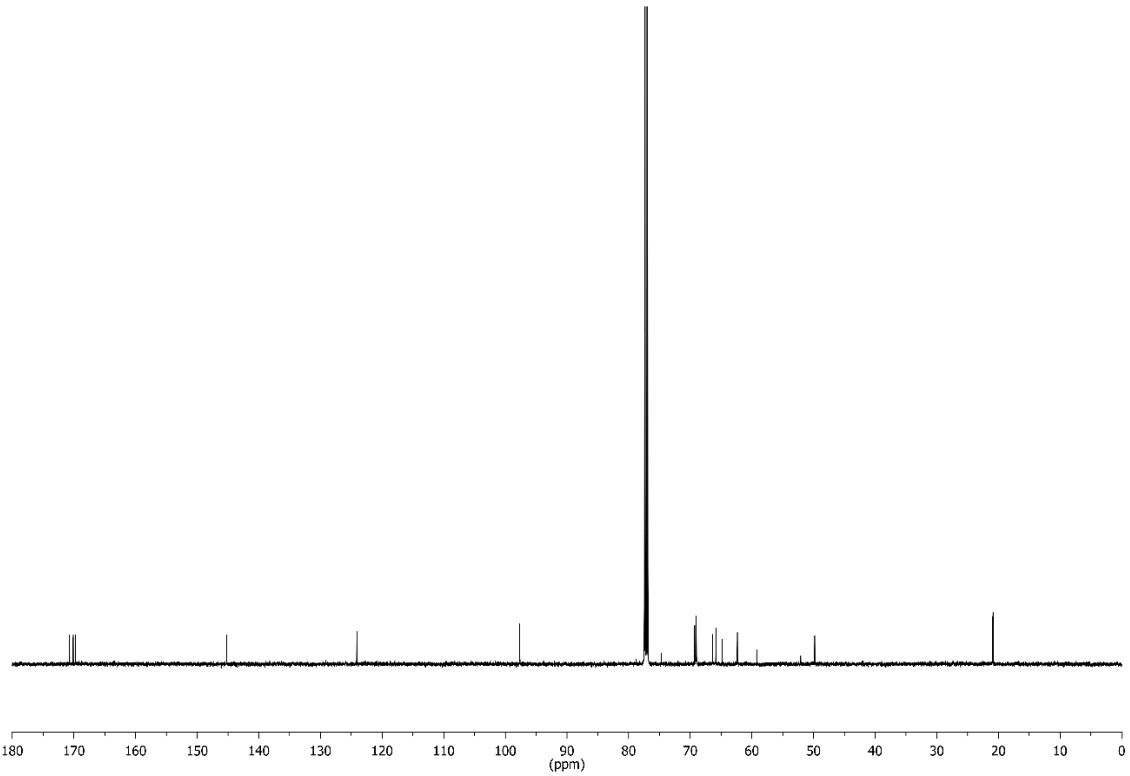

Figure 276: ^{13}C NMR spectrum of compound **85** (126 MHz, $CDCl_3$, 300 K, TMS).

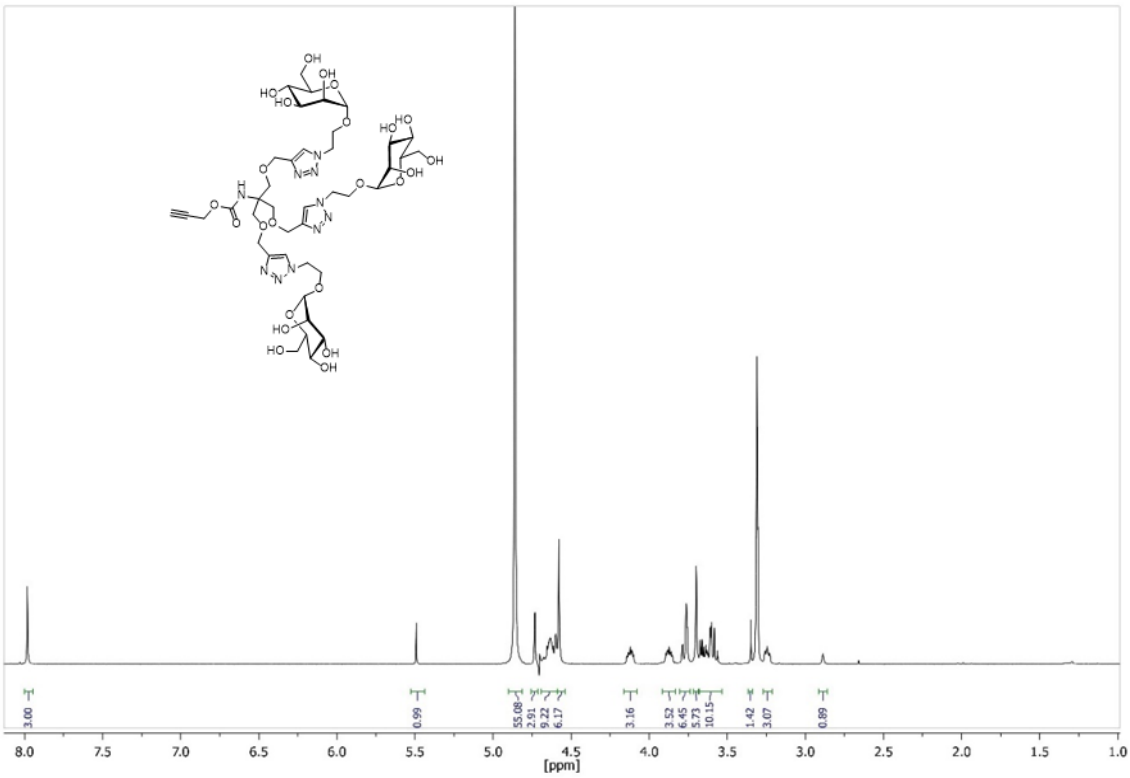

Figure 277: ^{1}H NMR spectrum of compound **86** (500 MHz, MeOD, 300 K, TMS).

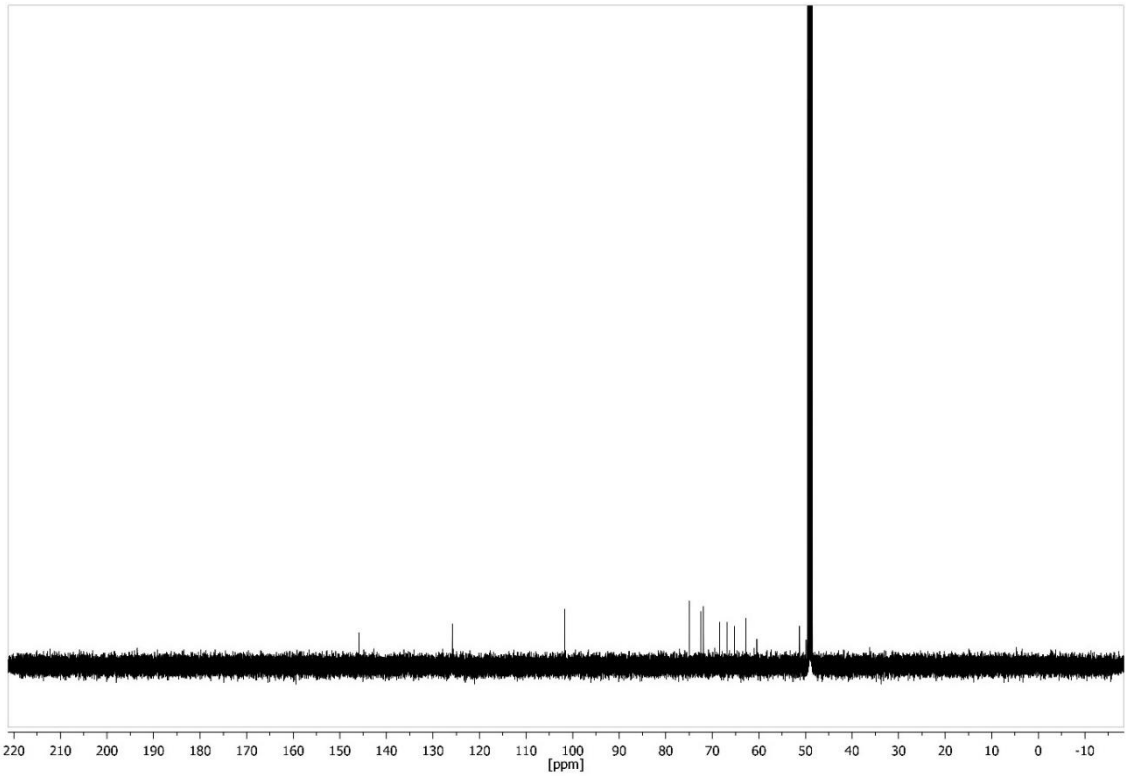

Figure 278: ^{13}C NMR spectrum of compound **86** (126 MHz, MeOD, 300 K, TMS).

8.5 Supporting information for chapter 5: Labelling FimH: Towards the photochemical control of carbohydrate recognition

8.5.1 Synthesis

_S_-Phenyl-2-[4-(2-phenylazo)phenyl]thioacetate 7

Triethylamine (326 µL, 2.35 mmol) was added to an ice-cold solution of acid **81** (470 mg, 1.96 mmol), DPPA (**76**) (506 µL, 2.35 mmol) and thiophenol (998 µL, 9.78 mmol) in DMF (10 mL). The mixture was stirred at room temperature for 16 h. The mixture was then diluted with DCM (200 mL) and washed with 1 N HCl (aq) (70 ml) and sat. NaCl solution (70 mL). The solvent was removed under reduced pressure and the residue dissolved in diethyl ether. After washing with H_2O (70 mL) the organic phase was dried over $MgSO_4$, filtered and the solvent removed under reduced pressure. Compound **7**was obtained as an orange solid after column chromatography (toluene).

Yield: 310 mg (932 µmol; 48 %);

TLC: R_f = 0.58 (cyclohexane/ ethyl acetate 6:1);

Melting point: 100 °C;

^{1}H-NMR: ($CDCl_3$, 500 MHz, 300 K): δ = 7.94-7.90 (m, 4H, Ar-$H_{ortho,}$ Ar-$H_{ortho'}$), 7.55-7.46 (m, 5H, Ar-H_{meta}, Ar-$H_{meta'}$, Ar-$H_{para'}$), 4.00 (s, 2H, CH_2) ppm;

^{13}C-NMR: ($CDCl_3$, 126 MHz, 300 K): δ = 195.0 (C=O), 152.8 (Ar-$C_{ipso'}$), 152.1 (Ar-C_{ipso}), 136.4 (Ar-C_{para}), 134.6 (SPh), 131.2 (Ar-$C_{para'}$), 130.6 (Ar-C_{meta}), 129.7, 129.4 (SPh), 129.3 (Ar-$C_{meta'}$), 127.7 (SPh), 123.3, 123.0 (Ar-C_{ortho}, Ar-C_{ortho}), 50.1 (CH_2) ppm;

IR (ATR): $\tilde{\nu}$ = 2922, 1699, 1439, 1008, 998, 774, 684, 549 cm^{-1};

EI-MS: *m/z* = 254.06, $[M\text{-}C_6H_6]^+$; (calc. 332.0983 for $C_{20}H_{16}N_2OS$).

_S_-Phenyl-2-[4-(2-biphenylazo)phenyl]thioacetate 8

Triethylamine (44.7 µL, 322 µmol) was added to an ice-cold solution of acid **82** (85.0 mg, 269 µmol), DPPA (**76**) (69.3 µL, 322 µmol) and thiophenol (137 µL, 1.34 mmol) in DMF (10 mL). The mixture was stirred at room temperature for 3 h. The solvent was removed under reduced pressure and the residue was dissolved in diethyl ether (80 mL). After washing with 1 N HCl (aq) (40 ml) and sat. NaCl solution (40 mL) the organic phase was

dried over $MgSO_4$, filtered and the solvent removed under reduced pressure. Compound **8** was obtained as an orange solid after column chromatography (toluene).

Yield: 40.7 mg (99.6 µmol; 37 %);

TLC: Rf = 0.43 (toluene);

Melting point: 176 °C (decomposition);

^{1}H-NMR: ($CDCl_3$, 500 MHz, 300 K): δ = 8.02-7.99 (m, 2H, Ar-$H_{ortho'}$), 7.96-7.92 (m, 2H, Ar-H_{ortho}), 7.77-7.74 (m, 2H, Ar-$H_{meta'}$), 7.69-7.66 (m, 2H, Ar-$H_{ortho''}$) 7.52-7.46 (m, 4H, Ar-H_{meta}, Ar-$H_{meta''}$), 7.42-7.38 (m, 6H, SPh, Ar-$H_{para''}$), 4.01 (s, 2H, CH_2) ppm;

^{13}C-NMR: ($CDCl_3$, 126 MHz, 300 K): δ = 194.9 (C=O), 152.3 (Ar-C_{ipso}), 151.9 (Ar-$C_{ipso'}$), 144.0 (Ar-$C_{para'}$), 140.4 (Ar-$C_{ipso''}$), 136.4 (Ar-C_{para}), 134.6 (SPh), 130.6 (Ar-C_{meta}), 129.7, 129.4 (SPh), 129.1 (Ar-$C_{meta''}$), 128.1 (SPh), 128.0 (Ar-$C_{para''}$), 127.4 (Ar-$C_{ortho''}$), 123.6 (Ar-$C_{ortho'}$), 123.4 (Ar-C_{ortho}), 50.1 (CH_2) ppm;

IR (ATR): $\tilde{\nu}$ = 3055, 2919, 1699, 1598, 1484, 984, 846, 766, 687 cm^{-1};

EI-MS: *m/z* = 408.12599, $[M]^+$; (calc. 408.12963 for $C_{26}H_{20}N_2OS$).

_S_-Phenyl-2-[4-(2-(3,5-dimethoxycarbonyl)phenylazo)phenyl]thioacetate 9

Triethylamine (56.0 µL, 404 µmol) was added to an ice-cold solution of acid **83** (120 mg, 337 µmol), DPPA (**76**) (87.0 µL, 404 µmol) and thiophenol (172 µL, 1.68 mmol) in DMF (8 mL). The mixture was stirred at room temperature for 2 d. The solvent was removed under reduced pressure and the residue was dissolved in DCM (70 mL). After washing with 1 N HCl (aq) (40 ml) and sat. NaCl solution (40 mL). The solvent was removed under reduced pressure and the residue was dissolved diethyl ether (80 mL). after washing with H_2O (40 mL) the organic phase was dried over $MgSO_4$, filtered and the solvent removed under reduced pressure. Compound **9** was obtained as an orange solid after column chromatography (cyclohexane/ethyl acetate 2:1).

Yield: 48.2 mg (107 µmol; 32 %);

TLC: R_f = 0.39 (cyclohexane/ethyl acetate 2:1);

Melting point: 109 °C ;

^{1}H-NMR: ($CDCl_3$, 500 MHz, 300 K): δ = 8.72-8.71 (t, ^{4}J = 1.6 Hz, 1H, Ar-$H_{para'}$), 8.67-8.66 (d, ^{4}J = 1.6 Hz, 2H, Ar-$H_{ortho'}$), 7.91-7.88 (m, 2H, Ar-H_{ortho}), 7.45-7.43 (m, 2H, Ar-H_{meta}), 7.33 (s, 5H, SPh), 3.95 (s, 2H, CH_2), 3.93 (s, 6H, CH_3) ppm;

^{13}C-NMR: ($CDCl_3$, 126 MHz, 300 K): δ = 194.8 (S(C=O)), 165.9 (COOMe), 152.9 (Ar-$C_{ipso'}$), 151.8 (Ar-C_{ipso}), 137.4 (Ar-C_{para}), 134.6 (SPh), 132.5 (Ar-$C_{para'}$), 130.7 (Ar-C_{meta}), 129.7, 129.4 (SPh), 127.6 (Ar-$C_{ortho'}$), 123.7 (Ar-C_{ortho}), 52.8 (CH3), 50.0 (CH_2) ppm;

IR (ATR): ṽ = 3082, 2657, 2895, 1731, 1721, 1697, 1241, 1214, 986, 755, 745, 688 cm^{-1};

EI-MS: *m/z* = 448.09819, $[M]^+$; (calc. 448.10923 for $C_{24}H_{20}N_2O_5S$).

4-[(*E*)-[4-(2-Trimethylammoniumacetamido)methyl]phenylazo]phenyl-(phenyl-thioacetate) 10

Triethylamine (593 µL, 4.28 µmol) was added to an icecold solution of acid **66** (791 mg, 2.14 mmol), DEPC (**77**) (650 µL, 4.28 mmol) and thiophenol (328 µL, 3.21 mmol) in DMF (12 mL). The reaction mixture was stirred for 16 h at room temperature. The solvent was then removed under reduced pressure. The crude product was purified by column chromatography (DCM → DCM / methanol 6:1) to yield compound **10** as an orange solid.

Yield: 436 mg (945 µmol, 44 %);

TLC: R_f = 0.28 (DCM / methanol 4:1);

Melting point: 198 °C;

^{1}H-NMR ($CDCl_3$, 200 MHz, 300 K): δ = 7.95-7.87 (m, 4H, Ar-H_{ortho}, Ar-$H_{ortho'}$), 7.56-7.48 (m, 4H, Ar-H_{meta}, Ar-$H_{meta'}$), 4.52 (s, 2H, NHCH_2), 4.20 (s, 2H, NCH_2(C=O)), 4.08 (s, 2H, Ar-CCH_2C=O), 3.35 (s, 9H, N(CH_3)$_3$) ppm;

^{13}C-NMR ($CDCl_3$, 126 MHz, 300 K): δ = 173.7 (O(C=O)), 164.9 (N(C=O)), 153.4 (Ar-C_{ipso}), 152.9 (Ar-$C_{ipso'}$), 142.6 (Ar-C_{para}), 140.9 (Ar-$C_{para'}$), 134.2 (SPh), 131.8 (Ar-$C_{meta'}$), 129.8 (Ar-C_{meta}), 129.4, 129.0 (SPh), 122.7 (Ar-$C_{ortho'}$), 122.4 (Ar-C_{ortho}), 65.6 (CH_2NMe_3), 54.9 (N(CH_3)$_3$), 43.8 (NCH_2), 42.2 (CH_2(C=O)) ppm;

IR (ATR): ṽ = 3344, 1693, 1587, 1494, 1231, 1119, 1002, 976, 840, 667, 546 cm^{-1};

EI-MS: *m/z* = 256.05, $[M\text{-}C_6H_4CH_2NHC{=}OCH_2NMe_3{+}H]^+$; (calc. 461.2006 for $C_{26}H_{29}N_4O_2S$).

4-[(*E*)-(4'-Hydroxy-3,4-dimethyl[1,1'-biphenyl]-4-yl)azo]phenylthioacetate 11

Triethylamine (248 µL, 1.79 mmol) was added to an ice-cold solution of acid **30** (323 mg, 896 µmol), DEPC (**77**) (272 µL, 1.79 mmol) and thiophenol (137 µL, 1.34 mmol) in DMF (5 mL). The reaction mixture was stirred for 16 h at room temperature. The solvent was then removed under reduced pressure. The residue was dissolved in diethyl ether (50 mL) and washed with H_2O (25 mL). The organic phase was dried over $MgSO_4$, filtered and the solvent removed under reduced pressure. The crude product was purified by column chromatography (cyclohexane/ethyl acetate 6:1 → 2:1) to yield compound **11** as an orange solid.

Yield: 198 mg (437 µmol, 49 %);

TLC: R_f = 0.50 (cyclohexane/ethyl acetate 2:1);

Melting point: 156 °C;

^{1}H-NMR ($CDCl_3$, 600 MHz, 300 K): δ = 7.90-7.88 (d, ^3J = 8.49 Hz, 2H, Ar-H$_{,meta'}$), 7.86-7.84 (d, ^3J = 8.32 Hz, 2H, Ar-H$_{,ortho}$), 7.63-7.60 (d, ^3J = 8.49 Hz, 2H, Ar-H$_{,ortho'}$), 7.43-7.40 (d, ^3J = 8.31 Hz, 2H, Ar-H$_{,meta}$), 7.33 (s, 5H, SPh), 7.23 (s, 2H, Ar-H$_{,ortho''}$), 4.64 (s, 1H, OH), 3.93 (s, 2H, CH_2), 2.27 (s, 6H, CH_3) ppm;

^{13}C-NMR ($CDCl_3$, 151 MHz, 300 K): δ = 195.0 (C=O), 152.6 (Ar-C$_{para''}$), 152.3 (Ar-C$_{ipso}$), 151.4 (Ar-C$_{,para'}$), 144.0 (Ar-C$_{ipso''}$), 136.2 (Ar-C$_{para}$), 134.6, 132.4 (SPh), 130.6 (Ar-C$_{meta}$), 129.7, 129.4 (SPh), 127.7 (Ar-C$_{ortho''}$), 127.6 (Ar-C$_{meta''}$), 127.4 (Ar-C$_{ortho'}$), 123.6 (Ar-C$_{meta'}$), 123.5 (Ar-C$_{ortho}$), 123.3 (Ar-C$_{ipso'}$), 50.1 (CH_2), 16.2 (CH_3) ppm;

IR (ATR): $\tilde{\nu}$ = 3508, 2917, 1700, 1598, 1478, 1175, 1165, 1008, 999, 835, 740, 686, 554 cm^{-1};

EI-MS: *m/z* = 452.15585, $[M]^+$; (calc. 452.15585 for $C_{28}H_{24}N_2O_2S$).

4-[(*E*)-(4-(4-Pyridinyl)phenyl)azo]phenylthioacetate 12

Triethylamine (247 µL, 1.78 mmol) was added to an ice-cold solution of acid **32** (283 mg, 892 µmol), DEPC (**77**) (270 µL, 1.78 mmol) and thiophenol (137 µL, 1.34 mmol) in DMF (8 mL). The reaction mixture was stirred for 16 h at room temperature. The solvent was then removed under reduced pressure. The residue was dissolved in diethyl ether (50 mL) and washed with H_2O (25 mL). The organic phase was dried over $MgSO_4$, filtered and the solvent removed under reduced pressure. The crude product was purified by column chromatography (cyclohexane/ ethyl acetate 7:1) to yield compound **12** as an orange solid.

Yield: 164 mg (401 µmol, 45 %);

TLC: R_f = 0.35 (DCM/ethyl acetate 9:1);

Melting point: 168 °C;

^{1}H-NMR: ($CDCl_3$, 500 MHz, 300 K): δ = 7.92-7.89 (m, 2H, ˏAr-H$_{meta'}$), 7.88-7.85 (m, 2H, CAr-H$_{meta'}$), 7.66-7.63 (m, 2H, Ar-H$_{ortho'}$), 7.51-7.47 (m, 4H, Ar-H$_{ortho''}$, Ar-H$_{meta}$), 7.39 (s, 5H, SPh), 7.32-7.28 (m, 2H, Ar-H$_{ortho}$), 4.00 (s, 2H, CH_2) ppm;

^{13}C-NMR: ($CDCl_3$, 125 MHz, 300 K): δ = 195.0 (C=O), 152.2 (Ar-C$_{ipso'}$), 152.0 (Ar-C$_{para'}$), 151.7 (Ar-C$_{ipso}$), 138.6 (Ar-C$_{meta''}$), 136.7, 134.7 (SPh), 130.5 (Ar-C$_{meta}$), 129.8, 129.5 (SPh), 129.3 (Ar-C$_{ortho}$), 127.8 (Ar-C$_{ortho''}$), 127.0 (Ar-C$_{para'}$), 124.8 (Ar-C$_{ortho'}$), 123.6 (Ar-C$_{meta'}$), 50.1 (CH_2) ppm;

IR (ATR): $\tilde{\nu}$ = 1692, 1497, 1439, 1299, 1003, 985, 831, 749, 710, 689, 547 cm^{-1};

4-[(*E*)-(2'-Methylsulfonamido[1,1'-biphenyl]-4-yl)azo] phenylthioacetate 13

Triethylamine (136 µL, 981 µmol) was added to an ice-cold solution of acid **31** (170 mg, 464 µmol), DEPC (**77**) (149 µL, 925 µmol) and thiophenol (76.0 µL, 745 µmol) in DMF (7 mL). The reaction mixture was stirred for 16 h at room temperature. The solvent was then removed under reduced pressure. The residue was dissolved in diethyl ether (50 mL) and washed with H_2O (25 mL). The organic phase was dried over $MgSO_4$, filtered and the solvent removed under reduced pressure. The crude product was purified by column chromatography (toluene/methanol 7:1) to yield compound **13** as an orange solid.

Yield: 152 mg (302 µmol, 65 %);

TLC: R_f = 0.24 (toluene/methanol 7:1);

Melting point: 153 °C;

^{1}H-NMR: ($CDCl_3$, 500 MHz, 300 K): δ = 8.06-8.03 (m, 2H, Ar-H*,ortho'*), 7.97-7.94 (d, 2H, Ar-H*,ortho*), 7.69-7.67 (dd, ^3J = 8.3 Hz, ^2J = 0.94 Hz, 1H, Ar-H*,ortho"*), 7.53-7.49 (m, 4H, Ar-H*,meta,* Ar-H*,meta'*), 7.45-7.41 (m, 1H, Ar-H*,para"*), 7.41 (s, 5H, SPh), 7.35-7.32 (dd, ^3J = 7.6 Hz, ^2J = 1.6 Hz, 1H, C(NH)C<u>Ar-H</u>*,meta"*), 7.29-7.25 (m, 1H, Ar-H*,meta"*), 6.48 (s, 1H, NH), 4.02 (s, 2H, CH_2), 2.92 (s, 3H, CH_3) ppm;

^{13}C-NMR: ($CDCl_3$, 125 MHz, 300 K): δ = 194.8 (C=O), 152.0 (Ar-C*ipso,* Ar-C*ipso'*), 140.0 (Ar-C*ipso"*)136.6 (Ar-C*,para*), 134.4 (SPh), 132.4 (Ar-C*para'*), 130.5 (Ar-C*meta*, C(NH)<u>Ar-C</u>*meta"*), 129.9 (Ar-C*meta'*), 129.5 (Ar-C*para"*), 129.3 (SPh), 125.1 (Ar-C*meta"*), 123.8 (Ar-C*ortho'*), 123.3 (Ar-C*ortho*), 120.3 (Ar-C*ortho"*), 49.7 (CH_2), 39.9 (CH_3) ppm;

IR (ATR): $\tilde{\nu}$ = 3271, 1694, 1484, 1402, 135, 1154, 1051, 962, 854, 767, 747, 595, 527 cm^{-1};

EI-MS: *m/z* = 501.04, $[M]^+$; (calc. 501.11808 for $C_{27}H_{23}N_3O_3S_2$).

4-[(*E*)-(4-(3-Pyridinyl)phenyl)azo]phenylthioacetate 14

Triethylamine (507 µL, 3.66 mmol) was added to an ice-cold solution of acid **36** (580 mg, 1.83 mmol), DEPC (**77**) (555 µL, 3.66 mmol) and thiophenol (280 µL, 2.74 mmol) in DMF (15 mL). The reaction mixture was stirred for 16 h at room temperature. The solvent was then removed under reduced pressure. The residue was dissolved in diethyl ether (50 mL), washed with H_2O (25 mL). The organic phase was dried over $MgSO_4$, filtered and the solvent removed under reduced pressure. The crude product was purified by column chromatography (cyclohexane/ ethyl acetate 7:1) to yield compound **37** as an orange solid.

Yield: 360 mg (879 µmol, 48 %);

TLC: R_f = 0.35 (DCM/ethyl acetate 9:1);

Melting point: 135 °C;

^{1}H-NMR: ($CDCl_3$, 500 MHz, 300 K): δ = 8.94-8.92 (d, 1H, ^{4}J = 1.82 Hz, NCAr-H$_{,ortho''}$), 8.65-8.63 (dd, ^{4}J = 1.7 Hz, ^{3}J = 4.8 Hz, 1H, Ar-H$_{,para''}$), 8.05-8.03 (m, 2H, Ar-H$_{,meta'}$), 7.97-7.93 (m, 3H, Ar-H$_{,ortho}$, Ar-H$_{,ortho''}$), 7.76-7.73 (m, 2H, Ar-H$_{,ortho'}$), 7.52-7.49 (m, 2H, Ar-H$_{,meta}$), 7.43-7.7.71 (dd, ^{4}J = 0.8 Hz, ^{3}J = 4.8 Hz, 1H, Ar-H$_{,meta''}$), 7.40 (s, 5H, SPh), 4.04 (s, 2H, CH_2) ppm;

^{13}C-NMR: ($CDCl_3$, 125 MHz, 300 K): δ = 194.8 (C=O), 152.2 (Ar-C$_{ipso'}$), 152.0 (Ar-C$_{ipso}$, Ar-C$_{para'}$), 149.0 (Ar-C$_{para''}$), 148.3 (NCAr-C$_{,ortho''}$), 140.3 (Ar-C$_{,ipso''}$), 136.5 (Ar-C$_{,para}$), 134.4 (SPh), 134.3 (Ar-C$_{ortho''}$), 130.5 (Ar-C$_{meta}$), 129.6, 129.2 (SPh), 127.9 (Ar-C$_{ortho'}$), 127.5 (C_{SPh}C=O), 123.7 (Ar-C$_{meta'}$), 123.5 (Ar-C$_{meta''}$), 123.3 (Ar-C$_{ortho}$), 49.9 (CH_2) ppm;

IR (ATR): ṽ = 2984, 1697, 1472, 1440, 1253, 1013, 986, 806, 751, 704, 561 cm^{-1};

EI-MS: *m/z* = 407.13172, [M+H]; (calc. 410.13216 for $C_{25}H_{20}N_3OS$).

2-(4-Nitrophenyl)acetic acid *tert* butyl ester 16[388]

Phosphorylchloride (9.93 mL, 106 mmol) was added dropwise to an ice-cold solution of nitrophenylacetic acid **15** (15.0 g, 82.8 mmol), pyridine (33.0 mL, 410 mmol) and *tert* butanol (78.0 mL, 831 mmol) in chloroform (250 mL). After stirring at room temperature for 16 h the mixture was diluted with DCM (50 mL) and 10 % aqueous hydrochloric acid was added. The organic layer was separated, washed with sat. NaCl solution (100 mL) and dried over $MgSO_4$. After filtration the solvent was removed under reduced pressure and the crude product was purified by column chromatography (cyclohexane/ ethyl acetate 7:1) to obtain compound **16** as colourless solid.

Yield: 16.7 g (70.4 mmol; 85 %); lit.: 95 %;[388]

TLC: R_f = 0.52 (cyclohexane/ ethyl acetate 7:1);

Melting point: 54 °C; lit.[422]: 55 °C;

^{1}H-NMR: ($CDCl_3$, 500 MHz, 300 K): δ = 8.13-8.10 (m, 2H, Ar-H$_{meta}$), 7.39-7.36 (m, 2H, Ar-H$_{ortho}$), 3.57 (s, 2H, CH_2), 1.37 (s, 9H, CH_3) ppm;

^{13}C-NMR: ($CDCl_3$, 126 MHz, 300 K): δ = 169.5 (C=O), 147.2 (Ar-C$_{para}$), 142.3 (Ar-C$_{ipso}$), 130.3 (Ar-C$_{ortho}$), 123.7 (Ar-C$_{meta}$), 81.8 ($C_q(CH_3)_3$), 42.5 (CH_2), 28.1 (CH_3) ppm;

IR (ATR): $\tilde{\nu}$ = 2979, 2933, 1725, 1514, 1344, 1327, 1235, 1135, 1108, 883, 855, 724 cm^{-1};

EI-MS: *m/z* = 238.08, $[M+H]^+$; (calc. 237.1001 for $C_{12}H_{15}NO_4$).

2-(4-Aminophenyl)acetic acid *tert* butyl ester 17[387]

To a solution of compound **16** (8.00 g, 33.7 mmol) in ethyl acetate (150 mL) was added a catalytic amount of palladium (10 % on activated charcoal) and the reaction mixture was stirred under hydrogen atmosphere for 16 h. The catalyst was removed by filtration over celite and the solvent was removed under reduced pressure to yield compound **17** quantitatively as a colourless oil.

Yield: 6.98 g (33.7 mmol, quant.);

TLC: R_f = 0.17 (cyclohexane/ ethyl acetate 4:1);

^{1}H-NMR: ($CDCl_3$, 500 MHz, 300 K): δ = 7.09-7.05 (m, 2H, Ar-H_{meta}), 6.69-6.65 (m, 2H, Ar-H_{ortho}), 3.41 (s, 2H, CH_2), 1.44 (s, 9H, CH_3), ppm;

^{13}C-NMR: ($CDCl_3$, 126 MHz, 300 K): δ = 171.5 (C=O), 144.6 (Ar-C_{para}), 130.1 (Ar-C_{ortho}), 125.1 (Ar-C_{ipso}), 115.5 (Ar-C_{meta}), 80.5 ($C_q(CH_3)_3$), 41.8 (CH_2), 28.0 (CH_3) ppm;

IR (ATR): $\tilde{\nu}$ = 3421, 3353, 2976, 1715, 1517, 1336, 1232.44, 1139, 659, 527.4, 504 cm^{-1};

EI-MS: *m/z* = 207.10, $[M]^+$; (calc. 207.1259 for $C_{12}H_{17}NO_2$).

2-(4-Nitrosophenyl)acetic acid *tert* butyl ester 18

To a solution of compound **17** (1.50 g, 7.00 mmol) in DCM (50 mL) was added a solution of oxone® (3.23 g, 10.5 mmol) in water (20 mL). After stirring for 6.5 h at room temperature, the mixture was diluted with DCM (100 mL). After separation of the phases the aqueous one was extracted with DCM (4 x 80 mL). The organic phase was washed with 1 M HCl (60 mL). After drying over $MgSO_4$ and filtration the solvent was removed under reduced pressure. The raw product of target compound **18** was isolated as a mixture with compound **16** in a ratio of 85/15 as a green oil and a yield for compound **18** of 72 %. The compound was used without further purification.

^{1}H-NMR ($CDCl_3$, 500 MHz, 300 K): δ = 7.91-7.84 (m, Ar-H), 7.56-7.50 (m, Ar-H), 3.64 (s, 2H, CH_2), 1.45 (s, 9H, CH_3) ppm.

General procedure A for the synthesis of methyl esters

Thionyl chloride (3 eq.) was added dropwise to an ice-cold solution of the particular acid (1 eq.) in methanol (20 mL/10 mmol). The reaction mixture was stirred at 0 °C for 30 minutes and additionally overnight at room temperature. The solvent was removed under reduced pressure and the residue was dissolved in ethyl acetate (50 mL/10 mmol) and washed with water (30 mL/10 mmol) and sat. $NaHCO_3$ solution (30 mL/10 mmol). The organic phase was dried over $MgSO_4$, filtered and the solvent removed under reduced pressure to obtain the respective methyl ester as a colourless solid.

2-(4-Nitrophenyl)acetic acid methyl ester 19[388]

4-nitrophenylacetic acid **15** (10.0 g, 55.2 mmol) was reacted according to General procedure A to obtain compound **19** as a colourless solid.

Yield: 10.7 g (55.0 mmol; quant.);

TLC: R_f = 0.47 (cyclohexane/ ethyl acetate 7:3);

Melting point: 53 °C; lit.[423]: 52.4-53.3 °C;

^{1}H-NMR: ($CDCl_3$, 500 MHz, 300 K): δ = 8.21-8.18 (m, 2H, Ar-H_{meta}), 7.48-7.45 (m, 2H, Ar-H_{ortho}), 3.75 (s, 3H, CH_3), 3.73 (s, 2H, CH_2) ppm;

^{13}C-NMR: ($CDCl_3$, 126 MHz, 300 K): δ = 170.5 (C=O), 147.1 (Ar-C_{para}), 141.3 (Ar-C_{ipso}), 130.4 (Ar-C_{ortho}), 123.8 (Ar-C_{meta}), 52.3 (CH_3), 40.5 (CH_2) ppm;

IR (ATR): $\tilde{\nu}$ = 3078, 2958, 1732, 1509, 1343, 1170, 996, 852, 815, 713, 577 cm^{-1};

EI-MS: m/z = 195.05287 $[M]^+$; (calc. 195.05316 for $C_9H_9NO_4$).

General procedure B for the reduction of nitro groups

To a solution of the respective nitro-substituted compound in methanol (40 mL/10 mmol) was added a catalytic amount of palladium (10 % on activated charcoal) and the reaction

mixture was stirred under hydrogen atmosphere for 24 h. The catalyst was removed by filtration over celite and the solvent was removed under reduced pressure to yield the respective amine quantitatively as an oil.

2-(4-Aminophenyl)acetic acid methyl ester 20

Compound **19** (10.5 g, 53.8 mmol) was reacted according to General procedure B to yield compound **20** quantitatively as a red oil.

Yield: 8.88 g (53.8 mmol, quant.);

TLC: R_f = 0.47 (cyclohexane/ ethyl acetate 1:1);

^{1}H-NMR: ($CDCl_3$, 500 MHz, 300 K): δ = 7.07-7.04 (m, 2H, Ar-H_{meta}), 6.66-6.63 (m, 2H, Ar-H_{ortho}), 3.67 (s, 3H, CH_3), 3.51 (s, 2H, CH_2) ppm;

^{13}C-NMR: ($CDCl_3$, 126 MHz, 300 K): δ = 170.5 (C=O), 145.2 (Ar-C_{para}), 130.0 (Ar-C_{ortho}), 123.7 (Ar-C_{ipso}), 115.1 (Ar-C_{meta}), 51.4 (CH_3), 39.9 (CH_2) ppm;

IR (ATR): $\tilde{\nu}$ = 3450, 3365, 2952, 1723, 1625, 1516, 1560, 1223, 1142, 1010, 821, 519 cm^{-1};

EI-MS: *m/z* = 165.07929 $[M]^+$; (calc. 165.07898 for $C_9H_{11}NO_2$).

General procedure C for the synthesis of nitroso compounds

To a solution of the respective amine (1 eq.) in DCM (15 mL/ mmol) was added a solution of oxone® (1.5 eq.) in water (20 mL). After stirring for overnight at room temperature, the mixture was diluted with DCM (20 mL/mmol). After separation of the phases the aqueous one was extracted with DCM (4 x 15 mL/mmol). The organic phase was washed with 1 M HCl (15 mL/mmol) and sat. $NaHCO_3$ solution (15 mL/mmol) subsequently. After drying over $MgSO_4$ and filtration the solvent was removed under reduced pressure. The raw product of the targeted nitroso compound was isolated as a mixture with the respective nitro compound. The nitroso compounds were used without further purification.

2-(4-Nitrosophenyl)acetic acid methyl ester 21

Compound **20** (1.00 g, 6.05 mmol) was reacted according to general procedure C. The raw product of target compound **21** was isolated as a mixture with compound **19** in a ratio of 86/14 as a green oil and a yield for compound **21** of 55 %. The compound was used without further purification.

^{1}H-NMR ($CDCl_3$, 500 MHz, 300 K): δ = 8.28-8.14 (m, Ar-H_{meta} (**19**)), 7.91-7.83 (m, Ar-H(**21**)), 7.58-7.48 (m, Ar-H(**21**)), 7.51-7.37 (m, Ar-H_{ortho} (**19**)), 3.74-3.70 (m, CH_3, CH_2) ppm.

4-[(4-Iodophenyl)azo]-(1,1-dimethyl)ethylphenylacetate 23

Nitroso compound **18** (2.75 mmol) was added to a solution of 4-iodoaniline **22** (602 mg, 2.75 mmol) in a mixture of glacial acid and DMSO (19:1; 20 mL). After stirring for 48 h at room temperature H_2O (100 mL) was added. The precipitated raw product was separated and the aqueous phase was additionally extracted with DCM (2 x 75 mL). The precipitate was added to the organic phase which was subsequently dried over $MgSO_4$, filtered and the solvent was removed under reduced pressure. Before column chromatography (cyclohexane → cyclohexane/ ethyl acetate 19:1) the raw product was codestilled with toluene (2 x 50 mL). Compound **23** was obtained as an orange solid.

Yield: 690 mg (1.63 mmol, 59 %);

TLC: R_f = 0.75 (cyclohexane / ethyl acetate 6:1);

Melting point: 113 °C;

^{1}H-NMR: ($CDCl_3$, 500 MHz, 300 K): δ = 7.82-7.77 (m, 4H, Ar-$H_{ortho'}$, Ar-H_{meta}), 7.59-7.55 (m, 2H, Ar-H_{ortho}), 7.37-7.33 (m, 2H, Ar-$H_{meta'}$), 3.53 (s, 2H, CH_2), 1.38 (s, 9H, $C(CH_3)_3$) ppm;

^{13}C-NMR: ($CDCl_3$, 126 MHz, 300 K): δ = 170.4 (C=O), 152.1 (Ar-C_{ipso}), 151.6 (Ar-$C_{ipso'}$, Ar-$C_{para'}$), 138.5 (Ar-$C_{ortho'}$), 130.2 (Ar-$C_{meta'}$), 124.6 (Ar-C_{ortho}), 123.3 (Ar-C_{meta}), 97.7 (Ar-C_{para}), 81.3 ($\underline{C}(CH_3)_3$), 42.8 (CH_2), 28.2 ($C(\underline{C}H_3)_3$) ppm;

IR (ATR): $\tilde{\nu}$ = 2976, .1730, 1339, 1235, 1154, 1003, 832 cm^{-1};

EI-MS: *m/z* = 422.04912, $[M]^+$; (calc. 422.04912 for $C_{18}H_{19}N_2O_2I$).

4-[(*E*)-(4-Iodophenyl)azo]-(1,1-dimethyl)ethylphenylacetate 24

Nitroso compound **21** (1.94 mmol) was added to a solution of 4-iodoaniline **22** (425 mg, 1.94 mmol) in glacial acid (8 mL). After stirring for 16 h at room temperature H_2O (100 mL) was added. The precipitated raw product was separated and purified by column chromatography (cyclohexane / ethyl acetate 19:1 → 7:1) Compound **24** was obtained as an orange solid.

Yield: 479 mg (1.26 mmol, 65 %);

TLC: R_f = 0.50 (cyclohexane / ethyl acetate 7:1);

Melting point: 137 °C;

^{1}H-NMR: ($CDCl_3$, 500 MHz, 300 K): δ = 7.90-7.84 (m, 4H, Ar-H$_{,ortho'}$, Ar-H$_{meta}$), 7.66-7.62 (m, 2H, Ar-H$_{ortho}$), 7.45-7.42 (m, 2H, Ar-H$_{meta'}$), 3.72 (s, 3H, CH_3), 3.71 (s, 2H, CH_2) ppm;

^{13}C-NMR: ($CDCl_3$, 126 MHz, 300 K): δ = 171.6 (C=O), 152.0 (Ar-C$_{para}$), 151.7 (Ar-C$_{ipso'}$), 138.5 (Ar-C$_{meta}$), 137.5 (Ar-C$_{para'}$), 130.3 (Ar-C$_{meta'}$), 124.6 (Ar-C$_{ortho}$), 123.3 (Ar-C$_{ortho'}$), 97.8 (Ar-C$_{ipso}$), 81.3 ($\underline{C}(CH_3)_3$), 52.3 (CH_2), 41.2 (CH_3) ppm;

IR (ATR): $\tilde{\nu}$ = 2956, 1732, 1475, 1435, 1296, 1240, 1129, 1000, 836, 820, 803, 712, 549, 528 cm^{-1};

EI-MS: *m/z* = 380.00383, $[M]^+$; (calc. 380.00217 for $C_{15}H_{13}N_2O_2I$).

4-[(*E*)-(4-Iodophenyl)azo]phenylacetic acid 25

Method A

Trifluoroacetic acid (6 mL) was added to a solution of compound **23** (690 mg, 1.63 mmol) in DCM (50 mL) and the mixture was stirred for 4 h at room temperature. After dilution with DCM (75 mL) and acetone (25 mL) the organic phase was washed with H_2O (50 mL), dried over $MgSO_4$ and filtered. The solvent was removed under reduced pressure and the residue was dissolved in DCM (80 mL). After cooling the product **25** precipitated. After filtration the solvent of the remaining filtrate was evaporated and the remaining crude product was purified by column chromatography (cyclohexane/ethyl acetate 4:1 → ethyl acetate→ ethyl acetate/methanol 6:1) to yield compound **25** as an orange solid.

Yield: 535 mg (1.46 mmol, 90 %).

Method B

Lithium hydroxide (50.4 mg, 1.05 mmol) was added to a solution of compound **24** (200 mg, 526 µmol) in THF/H_2O (2:1; 60 mL) and stirred for 16 h at room temperature. The mixture was neutralised with Amberlite® IR 120 and filtered. The solvent was removed under reduced pressure to yield compound **25** as an amorphous orange solid after lyophilisation.

Yield: 188 mg (51.3 µmol, 98 %);

TLC: R_f = 0.64 (ethyl acetate/ methanol, 4:1);

^{1}H-NMR (MeOD, 600 MHz, 300 K): δ = 7.98-7.94 (m, 2H, Ar-H_{meta}), 7.92-7.88 (m, 2H, Ar-$H_{,ortho'}$), 7.71-7.68 (m, 2H, Ar-H_{ortho}), 7.53-7.49 (m, 2H, Ar-$H_{,meta'}$), 3.73 (s, 2H, CH_2) ppm;

^{13}C-NMR (MeOD, 151 MHz, 300 K): δ = 174.7 (C=O), 153.3 (Ar-C_{ipso}), 152.7 (Ar-$C_{ipso'}$), 139.8 (Ar-$C_{para'}$, Ar-C_{meta}), 131.6 (Ar-$C_{meta'}$), 125.5 (Ar-C_{ortho}), 124.0 (Ar-$C_{ortho'}$), 98.6 (Ar-C_{para}), 41.6 (CH_2) ppm;

IR (ATR): $\tilde{\nu}$ = 3404, 2928, 2251, 1692, 1186, 1050, 1023, 1000, 824, 526 cm^{-1};

EI-MS: *m/z* = 365.98652, $[M]^+$; (calc. 365.98652 for $C_{14}H_{11}N_2O_2I$).

4-[(*E*)-(4'-Hydroxy-3,4-dimethyl[1,1'-biphenyl]-4-yl)azo]phenylacetic acid 30

Compound **25** (930 mg, 2.58 mmol), boronic ester **26** (640 mg, 2.58 mmol), potassium carbonate (1.07 g, 7.74 mmol) and $Pd(PPh_3)_4$ catalyst (29.8 mg, 25.8 µmol) were dissolved in a mixture of methanol and DMF (5:1, 60 mL) and stirred under reflux for 5 h. After removal of the solvent under reduced pressure compound **30** was obtained after column chromatography (ethyl acetate→ethyl acetate/ methanol 7:1) as an orange solid.

Yield: 323 mg (896 µmol, 35 %);

TLC: R_f = 0.64 (ethyl acetate/ methanol, 4:1);

Melting point: 186 °C;

^{1}H-NMR: (MeOD, 500 MHz, 300 K): δ = 7.95-7.92 (m, 2H, Ar-H$_{,ortho'}$), 7.89-7.86 (m, 2H, Ar-H$_{,ortho}$), 7.75-7.72 (m, 2H, Ar-H$_{,meta'}$), 7.49-7.46 (m, 2H, Ar-H$_{,meta}$), 7.31 (s, 2H, Ar-H$_{,ortho''}$), 3.71 (s, 2H, CH_2), 2.29 (s, 6H, CH_3) ppm;

^{13}C-NMR: (MeOD, 126 MHz, 300 K): δ = 175.0 (C=O), 155.1 (Ar-C$_{para''}$), 153.1 (Ar-C$_{ipso}$), 152.4 (Ar-C$_{ipso'}$), 145.6 (Ar-C$_{para'}$), 139.6 (Ar-C$_{para}$), 132.5 (Ar-C$_{ipso''}$), 131.5 (Ar-C$_{meta}$), 128.2 (Ar-C$_{ortho''}$), 128.1 (Ar-C$_{meta'}$), 126.2 (Ar-C$_{meta''}$), 124.4 (Ar-C$_{ortho'}$), 123.9 (Ar-C$_{ortho}$), 41.8 (CH_2), 17.0 (CH_3) ppm;

IR (ATR): ṽ = 3267, 2982, 2915, 1710 1480, 1233, 1188, 1157, 1012, 973, 843, 746, 570 cm^{-1};

EI-MS: *m/z* = 360.14739, $[M]^+$; (calc. 360.14739 for $C_{22}H_{20}N_2O_3$).

4-[(*E*)-(2'-Methylsulfonamido[1,1'-biphenyl]-4-yl)azo]phenylacetic acid 31

Compound **25** (180 mg, 492 µmol), boronic ester **27** (146 mg, 492 µmol), potassium carbonate (204 mg, 1.48 mmol) and $Pd(PPh_3)_4$ catalyst (5.69 mg, 4.92 µmol) were dissolved in a mixture of methanol and DMF (5:1, 60 mL) and stirred under reflux for 5 h. After removal of the solvent under reduced pressure compound **31** was obtained after column chromatography (ethyl acetate → ethyl acetate/ methanol 7:1) as an orange solid.

Yield: 189 mg (462 µmol, 94 %);

TLC: R_f = 0.48 (ethyl acetate/ methanol, 8:1);

Melting point: 178 °C;

^{1}H-NMR: (MeOD, 500 MHz, 300 K): δ = 8.01-7.99 (m, 2H, Ar-H$_{,meta'}$), 7.91-7.89 (m, 2H, Ar-H$_{,ortho}$), 7.66-7.63 (m, 2H, Ar-H$_{,ortho'}$), 7.54-7.47 (m, 3H, Ar-H$_{,meta,}$ Ar-H$_{,ortho''}$), 7.45-7.35 (m, 3H, Ar-H$_{,meta''}$, Ar-H$_{,para''}$), 3.72 (s, 2H, CH_2), 2.78 (s, 3H, CH_3) ppm;

^{13}C-NMR: (MeOD, 125 MHz, 300 K): δ = 175.3 (C=O), 153.2 (Ar-C$_{ipso'}$), 153.0 (Ar-C$_{ipso,}$), 143.5 (Ar-C$_{ipso''}$), 139.9 (Ar-C$_{,para}$), 138.9 (Ar-C$_{para'}$), 135.3 (Ar-C$_{,ortho''}$(NH)), 132.1 (Ar-C$_{meta''}$), 131.7 (Ar-C$_{ortho'}$), 131.5 (Ar-C$_{meta}$), 130.1 (C(NH)Ar-C$_{meta''}$), 128.1 (Ar-C$_{para''}$), 127.8 (Ar-C$_{ortho''}$), 124.0 (Ar-C$_{ortho}$, Ar-C$_{meta'}$), 41.7 (CH_2), 39.9 (CH_3) ppm;

IR (ATR): ṽ = 3361, 3282, 1698, 1322, 1149, 849, 768, 539 cm^{-1};

EI-MS: *m/z* = 409.10963, $[M]^+$; (calc. 409.10963 for $C_{21}H_{19}N_3O_4S$).

4-[(*E*)-(4-(4-Pyridinyl)phenyl)azo]phenylacetic acid 32

Compound **25** (802 mg, 2.19 mmol), boronic ester **28** (450 mg, 2.19 mmol), potassium carbonate (908 mg, 6.57 mmol) and $Pd(PPh_3)_4$ catalyst (25.0 mg, 21.9 µmol) were dissolved in a mixture of methanol and DMF (5:1, 60 mL) and stirred under reflux for 5 h. After removal of the solvent under reduced pressure compound **32** was obtained after column chromatography (DCM→methanol 16:1) as an orange solid.

Yield: 283 mg (892 µmol, 41 %);

TLC: R_f = 0.54 (DCM→methanol, 9:1);

^{1}H-NMR: ($CDCl_3$, 500 MHz, 300 K): δ = 8.54-8.51 (m, 4H, CAr-H$_{,ortho''}$, CAr-H$_{,meta''}$), 7-92-7.90 (m, 2H, Ar-H$_{,meta'}$), 7.85-7.82 (m, 4H, Ar-H$_{,ortho}$), 7.67-7.62 (m, 2H, Ar-H$_{,ortho'}$), 7.50-7.47 (m, 2H, Ar-H$_{,meta}$), 3.59 (s, 2H, CH_2) ppm;

EI-MS: *m/z* = 168.99, $[M\text{-}N(C_6H_4)CH_2COOH+H]^+$; (calc. 317.341 for $C_{19}H_{15}N_3O_2$).

4-[(*E*)-(4-(3-Pyridinyl)phenyl)azo]phenylacetic acid 33

Compound **25** (945 mg, 2.58 mmol), boronic ester **29** (529 mg, 2.58 mmol), potassium carbonate (1.07 g, 7.74 mmol) and $Pd(PPh_3)_4$ catalyst (29.8 mg, 25.8 µmol) were dissolved in a mixture of methanol and DMF (5:1, 60 mL) and stirred under reflux for 5 h. After removal of the solvent under reduced pressure compound **33** was obtained after column chromatography (DCM→methanol 16:1) as an orange solid.

Yield: 588 mg (1.85 mmol, 72 %);

TLC: R_f = 0.54 (DCM→methanol, 9:1);

^{1}H-NMR: (DMSO-*d6*, 500 MHz, 300 K): δ = 9.02-8.99 (m, 1H, NCAr-H$_{,ortho''}$), 8.65-8.60 (dd, ^4J = 1.6 Hz, ^3J = 4.8 Hz, 1H, Ar-H$_{,para''}$), 8.23-8.16 (m, 2H, Ar-H$_{,ortho''}$), 8.00-7.98 (m, 4H, Ar-H$_{,ortho}$, Ar-H$_{,meta'}$), 7.90-7.84 (m, 2H, Ar-H$_{,ortho'}$), 7.57-7.46 (m, 3H, Ar-H$_{,meta}$, Ar-H$_{,meta''}$), 3.66 (s, 2H, CH_2) ppm;

EI-MS: *m/z* = 273.14, $[M\text{-}COOH]^+$; (calc. 317.341 for $C_{19}H_{15}N_3O_2$).

4-[(*E*)-[4-(2-Triethylammoniumacetamido)methyl]phenylazo]phenyl-(phenyl-thioacetate) 35

Triethylamine (59.3 µL, 428 µmol) was added to an ice-cold solution of acid **63** (88.1 mg, 214 µmol), DEPC (**77**) (68.9 µL, 68.9 µmol) and thiophenol (33.1 µL, 321 µmol) in DMF (8 mL). The reaction mixture was stirred for 16 h at room temperature. The solvent was then removed under reduced pressure. The crude product was purified by column chromatography (DCM → DCM/ methanol 6:1) to yield compound **35** as an orange syrup.

Yield: 54.6 mg (108 µmol, 51 %);

TLC: R_f = 0.24 (DCM→methanol, 6:1);

^{1}H-NMR ($CDCl_3$, 500 MHz, 300 K): δ = 9.89 (s, 1H, NH), 7.90-7.83 (m, 4H, Ar-H$_{ortho}$, Ar-H$_{ortho'}$), 7.49-7.44 (m, 4H, Ar-H$_{,meta}$, Ar-H$_{meta'}$), 4.50-4.47 (m, 2H, NHC$\underline{H}_2$), 4.39-4.34 (s, 2H, NC$\underline{H}_2$(C=O)), 3.99 (s, 2H, Ar-CCH_2C=O), 3.56-3.48 (m, 6H, C$\underline{H}_2CH_3$), 1.39-1.30 (t, $^3J_{CH2CH3}$ = 6.6 Hz, 9H, $CH_2C\underline{H}_3$) ppm;

^{13}C-NMR ($CDCl_3$, 126 MHz, 300 K): δ = 194.9 (S(C=O)), 163.5 (N(C=O)), 152.0, 151.8 (Ar-C$_{ipso}$, Ar-C$_{ipso'}$), 141.3 (Ar-C$_{para}$), 136.2 (Ar-C$_{para'}$), 134.5 (SPh), 130.4 (Ar-C$_{meta'}$), 129.5, 129.2 (SPh), 128.5 (Ar-C$_{meta}$), 127.5 (SPh), 123.2, 123.1 (Ar-C$_{ortho}$, Ar-C$_{ortho'}$), 56.4 (NCH_2), 54.4 (CH_2), 49.5 (CH_2(C=O)), 43.2 ($NHCH_2$), 7.8 (CH_3) ppm;

IR (ATR): ṽ = 3243, 3058, 2986, 1677, 1478, 1274, 1202, 1126, 1042, 801, 749, 609, 531 cm^{-1};

EI-MS: m/z = 503.24695 $[M]^+$; (calc. 503.24752 for $C_{29}H_{35}N_4O_2S$).

2-(2-Nitrophenyl)acetic acid methyl ester 42[389]

2-Nitrophenylacetic acid **40** (16.8 g, 92.7 mmol) was reacted according to General procedure A to obtain compound **42** as an amorphous colourless solid.

Yield: 16.0 g (82.2 mmol; 89 %); lit.: 97 %;[389]

TLC: R_f = 0.55 (cyclohexane/ ethyl acetate 7:3);

^{1}H-NMR: ($CDCl_3$, 500 MHz, 300 K): δ = 8.13-8.10 (dd, ^{3}J = 8.2 Hz, ^{4}J = 1.3 Hz, 1H, $(CNO_2)CAr\text{-}H_{meta}$), 7.62-7.53 (m, 1H, $Ar\text{-}H_{meta}$), 7.50-7.46 (m, 1H, $Ar\text{-}H_{para}$), (dd, ^{3}J = 7.6 Hz, ^{4}J = 1.1 Hz, 1H, $Ar\text{-}H_{ortho}$), 4.03 (s, 2H, CH_2), 3.72 (s, 3H, CH_3) ppm;

^{13}C-NMR: ($CDCl_3$, 126 MHz, 300 K): δ = 171.2 (C=O), 148.8 ($Ar\text{-}C_{ortho}NO_2$), 133.7 ($Ar\text{-}C_{meta}$), 133.3 ($Ar\text{-}C_{ortho}$), 129.7 ($Ar\text{-}C_{ipso}$), 128.6 ($Ar\text{-}C_{para}$), 125.3 ($(CNO_2)Ar\text{-}C_{meta}$), 52.2 ($CH_3$), 39.5 ($CH_2$) ppm;

IR (ATR): $\tilde{\nu}$ = 3092, 2961, 1720, 1515, 1343, 1254, 1013, 795, 107, 664, 589, 416 cm^{-1};

EI-MS: m/z = 195.07 $[M+H]^+$; (calc. 195.05316 for $C_9H_9NO_4$).

2-(3-Nitrophenyl)acetic acid methyl ester 43[391]

3-Nitrophenylacetic acid **41** (1.00 g, 5.52 mmol) was reacted according to General procedure A to obtain compound **43** as a colourless solid.

Yield: 1.07 g (5.48 mmol; quant.); lit.: 100 %;[391]

TLC: R_f = 0.48 (cyclohexane/ ethyl acetate 7:3);

^{1}H-NMR: ($CDCl_3$, 500 MHz, 300 K): δ = 8.18-8.13 (m, 2H, $(C(NO_2))CAr\text{-}H_{ortho}$, $Ar\text{-}C_{para}$), 7.65-7.62 (m, 1H, $Ar\text{-}H_{ortho}$), 7.54-7.50 (m, 1H, $Ar\text{-}H_{meta}$), 3.75 (s, 2H, CH_2), 3.73 (s, 3H, CH_3) ppm;

^{13}C-NMR: ($CDCl_3$, 126 MHz, 300 K): δ = 170.8 (C=O), 148.3 ($Ar\text{-}C_{meta}NO_2$), 135.7 ($Ar\text{-}C_{,ipso}$), 135.5 ($Ar\text{-}C_{,ortho}$), 129.4 ($Ar\text{-}C_{meta}$), 124.4, 122.2 ($(C(NO_2))\underline{C}Ar\text{-}H_{ortho}$, $Ar\text{-}C_{para}$), 52.2 (CH_3), 40.5 (CH_2) ppm;

EI-MS: m/z = 195.05310 $[M]^+$; (calc. 195.05316 for $C_9H_9NO_4$).

2-(2-Aminophenyl)acetic acid methyl ester 44[390]

Compound **42** (7.50 g, 38.4 mmol) was reacted according to General procedure B to yield compound **44** quantitatively as a red oil.

Yield: 6.34 g (38.4 mmol, quant.); lit.: 100 %;[390]

TLC: R_f = 0.29 (cyclohexane/ ethyl acetate 7:3);

^{1}H-NMR: ($CDCl_3$, 500 MHz, 300 K): δ = 7.12-7.07 (m, 2H, Ar-H_{ortho}, Ar-H_{para}), 6.78-6.71 (m, 2H, Ar-H_{meta}), 3.69 (s, 3H, CH_3), 3.58 (s, 2H, CH_2) ppm;

^{13}C-NMR: ($CDCl_3$, 126 MHz, 300 K): δ = 172.3 (C=O), 145.2 (Ar-$C_{,ortho}$NH), 131.2 (Ar-$C_{,para}$), 128.6 (Ar-$C_{,ortho}$), 115.1 ((CNH)Ar-C_{meta}), 119.1 (Ar-H_{ipso}), 116.7 (Ar-H_{meta}), 52.1 (CH_3), 38.3 (CH_2) ppm;

EI-MS: *m/z* = 165.09 $[M]^+$; (calc. 165.07898 for $C_9H_{11}NO_2$).

2-(3-Aminophenyl)acetic acid methyl ester 45[392]

Compound **43** (1.05 g, 5.40 mmol) was reacted according to General procedure B to yield compound **45** quantitatively as a red oil.

Yield: 892 mg (5.40 mmol, quant.);

TLC: R_f = 0.26 (cyclohexane/ ethyl acetate 7:3);

^{1}H-NMR: ($CDCl_3$, 500 MHz, 300 K): δ = 7.12-7.08 (m, 1H, Ar-H_{meta}), 6.67-6.65 (m, 1H, Ar-H_{ortho}),6.62-6.57 (m, 2H, (C(NO_2))CAr-H_{ortho}, Ar-C_{para}), 3.68 (s, 3H, CH_3), 3.53 (s, 2H, CH_2) ppm;

^{13}C-NMR: ($CDCl_3$, 126 MHz, 300 K): δ = 172.3 (C=O), 146.8 (Ar-$C_{meta}NO_2$), 135.2 (Ar-$C_{,ipso}$), 129.6 (Ar-$C_{,meta}$), 119.6 (Ar-C_{ortho}), 116.0 ((C(NO_2))Ar-C_{ortho}), 114.1 Ar-C_{para}), 52.2 (CH_3), 41.4 (CH_2) ppm;

EI-MS: *m/z* = 165.07879 $[M]^+$; (calc. 165.07898 for $C_9H_{11}NO_2$).

***tert*-Butyl-*N*-(4-aminobenzyl)carbamate 47[397]**

Di-*tert*-butyldicarbonate (20.3 g, 93.1 mmol) was added to a solution of 4-aminobenzylamine **46** (9.30 mL, 84.3 mmol) in THF (100 mL). The mixture was stirred at room temperature over night before the solvent was removed under reduced pressure. The crude product was purified by column chromatography (cyclohexane/ ethyl acetate 2:1) to obtain compound **47** as slightly brown solid.

Yield: 16.4 g (74.0 mmol, 88 %); lit.: 80 %;[397]

TLC: R_f = 0.20 (cyclohexane/ ethyl acetate 2:1);

Melting point: 78 °C, lit.[424]: 74-75 °C;

^{1}H-NMR: ($CDCl_3$, 500 MHz, 300 K): δ = 7.14-6.99 (m, 2H, Ar-H_{ortho}), 6.72-6.55 (m, 1H, Ar-H_{meta}), 4.71 (s, 1H, NH), 4.15 (d, 2H, ^3J = 5.1 Hz, CH_2NH), 3.32 (s, 2H, NH_2), 1.45 (s, 9H, CH_3) ppm;

^{13}C-NMR: ($CDCl_3$, 126 MHz, 300 K): δ = 155.8 (C=O), 145.7 (Ar-C_{para}), 128.9 (Ar-$C_{,ortho}$), 128.8 (Ar-$C_{,ipso}$), 115.2 (Ar-C_{meta}), 79.3 ($\underline{C}(CH_3)_3$), 44.4 (CH_2), 28.4 (CH_3) ppm;

IR (ATR): ṽ = 3427, 3344, 2977, 2932, 1686, 1513, 1363, 1290, 1265, 1172, 817 cm^{-1};

EI-MS: *m/z* = 222.11, $[M]^+$; (calc. 222.1368 for $C_{12}H_{18}N_2O_2$).

tert-Butyl-*N*-(4-nitrosobenzyl)carbamate 48[396]

Compound **47** (10.0 g, 45.0 mmol) was reacted according to general procedure C. The raw product of target compound **48** was isolated as a mixture with the respective nitro compound in a ratio of 84/16 as a green oil and a yield for compound **48** of 62 %. The compound was used without further purification.

^{1}H-NMR ($CDCl_3$, 200 MHz, 300 K): δ = 8.25-8.17 (m, Ar-H(NO_2)), 7.93-7.83 (m, Ar-H(of compound **48**)), 7.58-7.48 (m, Ar-H(of compound **48**)), 7.51-7.37 (m, Ar-H(NO_2)), 4.47-4.37 (m, 2H, CH_2NH), 1.51-1.43 (s, 9H, CH_3) ppm.

(9*H*-Fluoren-9-yl-methyl)-*N*-[(4-nitrophenyl)methyl]carbamate 50[393-394]

Chloroformic acid 9*H*-fluoren-9-yl-methyl ester (1.37 g, 5.30 mmol) was added to a solution of 4-nitrobenzylamine hydrochloride **49** (1.00 g, 5.30 mmol) and DIPEA (4.07 mL, 24.9 mmol) in DCM (50 mL). The mixture was stirred at room temperature for 16 h and then diluted with DCM. The organic layer was washed with aqueous hydrochloric acid (10 %, 2 75 mL) and sat $NaHCO_3$ solution (75 mL) and subsequently dried over $MgSO_4$. The suspension was filtered and the solvent removed under reduced pressure. The crude product was purified by column chromatography and crystallised in DCM to obtain compound **50** as a colourless solid.

Yield: 1.66 g (4.43 mmol, 87 %); lit.: 92 %;[394];

TLC: R_f = 0.32 (cyclohexane/ ethyl acetate 2:1);

Melting point: 155 °C;

^{1}H-NMR ($CDCl_3$, 200 MHz, 300 K): δ = 8.16-8.05 (m, 2H, Ar-H), 7.74-7.66 (m, 2H, Ar-H_{Fmoc}), 7.56-7.48 (m, 2H, Ar-H_{Fmoc}), 7.41-7.21 (m, 6H, Ar-H_{Fmoc}, Ar-H), 5.17-5.06 (m, 1H, NH), 4.54-4.44 (d, $^3J_{CH,\ CH2}$ = 6.2 Hz, 2H, $CH_{2,\ Fmoc}$), 4.42-4.35 (d, $^3J_{NH,CH2}$ = 6.2 Hz, 2H, CH_2NH), 4.20-4.09 (t, $^3J_{CH,\ CH2}$ = 6.2 Hz, 1H, $CHCH_{2,\ Fmoc}$) ppm;

IR (ATR): $\tilde{\nu}$ = 3365, 3322, 2950, 1698, 1525, 1345, 1259, 984, 757, 740, 731 cm^{-1};

EI-MS: *m/z* = 374.12, $[M]^+$; (calc. 374.389 for $C_{22}H_{18}N_2O_4$).

(9*H*-Fluoren-9-yl-methyl)-*N*-[(4-aminophenyl)methyl]carbamate 51[255]

A solution of compound **50** (1.56 g, 4.17 mmol) in ethanol (120 mL) and dioxane (40 mL) was reacted according to general procedure B with a reduced reaction time of 4 h. Amine **51** was obtained as a colourless solid after column chromatography (cyclohexane/ ethyl acetate 2:1).

Yield: 1.09 mg (3.17 mmol, 76 %); lit.: 80 %;[393]

TLC: R_f = 0.26 (cyclohexane/ ethyl acetate 2:1);

^{1}H-NMR ($CDCl_3$, 200 MHz, 300 K): δ = 7.72-7.65 (m, 2H, Ar-H), 7.58-7.50 (m, 2H, Ar-H_{Fmoc}), 7.38-7.17 (m, 2H, Ar-H_{Fmoc}), 7.06-6.97 (m, 6H, Ar-H_{Fmoc}, Ar-H), 6.68-6.58 (m, 1H, NH), 5.77-5.67 (d, $^3J_{CH,\ CH2}$ = 6.2 Hz, 2H, $CH_{2,\ Fmoc}$), 4.39-4.30 (d, $^3J_{NH,\ CH2}$ = 6.2 Hz, 2H, CH_2NH), 4.22-4.09 (t, $^3J_{CH,\ CH2}$ = 6.2 Hz, 1H, $CHCH_{2,\ Fmoc}$) ppm.

3-[(*E*)-(4-*tert*-Butyl-*N*-benzylcarbamate)azo]methylphenylacetate 52

A solution of compound **48** (5.00 mmol) in acetic acid (20 mL) was added to a solution of amine **45** (826 mg, 5.00 mmol) in acetic acid (15 mL) and stirred at room temperature for 1 d. After addition of H_2O (100 mL) the mixture was extracted with ethyl acetate (3 x 100 mL). The combined organic layers were dried over $MgSO_4$, filtered and the solvent was removed under reduced pressure. Column chromatography (toluene → toluene/ethyl acetate 9:1) gave compound **52** as an orange solid.

Yield: 447 mg (1.17 mmol, 23 %);

TLC: R_f = 0.34 (toluene / ethyl acetate 9:1);

Melting point: 96 °C;

^{1}H-NMR ($CDCl_3$, 500 MHz, 300 K): δ = 7.90-7.86 (m, 2H, Ar-$H_{,ortho}$), 7.84-7.81 (m, 2H, Ar-H_{ortho}‘CH, Ar-H_{para}), 7.50-7.39 (m, 4H, Ar-H_{meta}, Ar-$H_{,meta}$‘, Ar-H_{ortho}‘), 4.92 (s, 1H, NH), 4.40 (d, ^{3}J = 4.1 Hz, 2H, $NHCH_2$), 3.74 (s, 3H, CH_3), 3.72 (s, 2H, CH_2), 1.48 (s, 9H, $C(CH_3)_3$) ppm;

^{13}C-NMR ($CDCl_3$, 126 MHz, 300 K): δ = 171.9 (C=O), 152.9 (Ar-C_{ipso}‘), 152.0 (Ar-C_{ipso}), 135.2 (Ar-C_{meta}‘CH_2), 141.9 (Ar-C_{para}), 132.0 (Ar-C_{ortho}‘Ar-C_{meta}‘CH_2), 129.4 (Ar-C_{meta}‘H), 128.0 (Ar-C_{meta}), 123.6 (Ar-C_{para}‘), 123.3 (Ar-C_{ortho}), 122.2 (Ar-C_{ortho}‘), 79.8 ($\underline{C}(CH_3)_3$), 52.3 (CH_3), 44.2 ($NHCH_2$), 41.2 (CH_2), 28.6 ($C(\underline{C}H_3)_3$) ppm;

IR (ATR): $\tilde{\nu}$ = 3338, 2983, 1728, 1505, 1245, 1161, 1052, 876, 849, 717, 523 cm^{-1};

EI-MS: *m/z* = 383.18451, $[M]^+$; (calc. 383.18451 for $C_{21}H_{25}N_3O_4$).

4-[(*E*)-(4-*tert*-Butyl-*N*-benzylcarbamate)azo]methylphenylacetate 53

A solution of compound **48** (3.82 mmol) in acetic acid (20 mL) was added to a solution of amine **20** (631 mg, 3.82 mmol) in acetic acid (10 mL) and stirred at room temperature for 5 d. After addition of H_2O (100 mL) the mixture was extracted with ethyl acetate (3 x 100 mL). The combined organic layers were dried over $MgSO_4$, filtered and the solvent was removed under reduced pressure. Column chromatography (toluene → toluene/ethyl acetate 9:1) gave compound **53** as an orange solid.

Yield: 935 mg (2.44 mmol, 64 %);

TLC: R_f = 0.33 (toluene / ethyl acetate 9:1);

Melting point: 137 °C;

^{1}H-NMR ($CDCl_3$, 500 MHz, 300 K): δ = 7.89-7.86 (m, 4H, Ar-$H_{,ortho}$, Ar-H_{ortho}‘), 7.44-7.40 (m, 4H, Ar-H_{meta}, Ar-$H_{,meta}$‘), 4.93 (s, 1H, NH), 4.40 (d, ^{3}J = 5.4 Hz, 2H, $NHCH_2$), 3.72 (s, 3H, CH_3), 3.71 (s, 2H, CH_2), 1.48 (s, 9H, $C(CH_3)_3$) ppm;

^{13}C-NMR ($CDCl_3$, 126 MHz, 300 K): δ = 171.7 (C=O), 152.2, 151.8 (Ar-C_{ipso}‘, Ar-C_{ipso}), 142.2 (Ar-C_{para}), 137.1 (Ar-C_{para}‘), 130.2 (Ar-C_{meta}‘), 128.2 (Ar-C_{meta}), 123.2 (Ar-$C_{ortho,}$ Ar-C_{ortho}‘), 79.8 ($\underline{C}(CH_3)_3$), 52.1 (CH_3), 44.4 ($NHCH_2$), 41.1 (CH_2), 28.4 ($C(\underline{C}H_3)_3$) ppm;

IR (ATR): $\tilde{\nu}$ = 3324, 2989, 1737, 1675, 1510, 1250, 1160, 840 cm^{-1};

EI-MS: *m/z* = 383.18425, $[M]^+$; (calc. 383.18451 for $C_{21}H_{25}N_3O_4$).

3-[(*E*)-(4-Aminobenzyl)azo]methylphenylacetate 54

Trifluoroacetic acid (1.80 mL) was added to a solution of compound **52** (380 mg, 991 µmol) in DCM (30 mL) and stirred for 5 h at room temperature. The solvent was removed under reduced pressure and the crude product was codestilled with toluene (3 x 40 mL). Compound **54** was obtained quantitatively as an orange solid.

Yield: quant.;

TLC: R_f = 0.0 (toluene / ethyl acetate 9:1);

Melting point: 188 °C;

^{1}H-NMR (MeOD, 500 MHz, 300 K): δ = 8.01-7.97 (m, 2H, Ar-H_{ortho}), 7.87-7.83 (m, 2H, Ar-$H_{ortho'}$), 7.66-7.62 (m, 2H, Ar-H_{meta}), 7.54-7.50 (t, ^{3}J = 7.6 Hz, 1H, Ar-$H_{meta'}$), 7.48-7.45 (t, ^{3}J = 7.6 Hz, 1H, Ar-$H_{para'}$), 4.22 (s, 2H, $NH_2C\underline{H_2}$), 3.79 (s, 2H, CH_2) ppm;

^{13}C-NMR (MeOD, 126 MHz, 300 K): δ = 173.6 (C=O), 154.2 (Ar-C_{ipso}), 154.1 (Ar-$C_{ipso'}$), 137.4 (Ar-C_{para}), 137.2 (Ar-$C_{meta'}$), 133.7 (Ar-$C_{para'}$), 131.0 (Ar-C_{meta}), 130.5 (Ar-$C_{meta'}$), 124.8 (Ar-$C_{ortho'}$) 124.5 (Ar-C_{ortho}), 122.9 ($\underline{\text{Ar-C}}_{ortho'}$CH), 52.6 ($CH_3$), 44.0 ($NHCH_2$), 41.4 ($CH_2$) ppm;

IR (ATR): $\tilde{\nu}$ = 3053, 1738, 1662, 1506, 1436, 1214, 1174, 1129, 841, 802, 725, 559 cm^{-1};

EI-MS: *m/z* = 283.13165, $[M]^+$; (calc. 283.13208 for $C_{16}H_{17}N_3O_2$).

4-[(*E*)-(4-Aminobenzyl)azo]methylphenylacetate 55

Trifluoroacetic acid (3.50 mL) was added to a solution of compound **53** (850 mg, 2.22 mmol) in DCM (40 mL) and stirred for 5 h at room temperature. The solvent was removed under reduced pressure and the crude product was codestilled with toluene (3 x 50 mL). Compound **55** was obtained quantitatively as an orange solid.

Yield: quant.;

TLC: R_f = 0.0 (toluene / ethyl acetate 9:1);

Melting point: 190 °C;

^{1}H-NMR (MeOD, 500 MHz, 300 K): δ = 7.99-7.96 (m, 2H, Ar-H$_{,ortho'}$), 7.90-7.88 (m, 2H, Ar-H$_{ortho}$), 7.65-7.62 (m, 2H, Ar-H$_{meta'}$), 7.49-7.46 (m, 2H, Ar-H$_{,meta}$), 4.22 (s, 2H, NHCH$_2$), 3.77 (s, 2H, CH$_2$), 3.71 (s, 3H, CH$_3$) ppm;

^{13}C-NMR (MeOD, 126 MHz, 300 K): δ = 173.5 (C=O), 154.3 (Ar-C$_{ipso'}$), 152.9 (Ar-C$_{ipso}$), 139.7 (Ar-C$_{para'}$), 137.3 (Ar-C$_{para}$), 131.5 (Ar-C$_{meta'}$), 131.0 (Ar-C$_{meta}$), 124.4 (Ar-C$_{ortho'}$), 124.1 (Ar-C$_{ortho}$), 52.6 (CH$_3$), 44.0 (NHCH$_2$), 41.5 (CH$_2$) ppm;

IR (ATR): ṽ = 2959, 1738, 1663, 1507, 1214, 1130, 841, 725 cm^{-1};

EI-MS: *m/z* = 283.13208, [M]$^+$; (calc. 283.13208 for $C_{16}H_{17}N_3O_2$).

2-(Phenyl)-[(*E*)-4'-azo-(4''-fluorenylmethoxycarbonylaminomethyl)phenyl] acetic acid *tert* butyl ester 56

Amine **51** (947 mg, 2.75 mmol) was dissolved in a mixture of acetic acid and DMSO (20 mL, 19:1) and nitroso compound **18** (2.75 mmol) was subsequently added. The mixture was stirred at room temperature for 5 d. After addition of water (100 mL) the precipitate was isolated and the remaining aqueous phase was extracted with DCM (2 x 75 mL). The precipitate was dissolved in the organic phase which was then dried over $MgSO_4$, filtered and the solvent removed under reduced pressure. The crude product was purified by column chromatography (cyclohexane/ ethyl acetate 6:1 → 2:1) to obtain compound **56** as an orange solid.

Yield: 656 mg (1.20 mmol, 44 %);

TLC: R_f = 0.54 (cyclohexane/ ethyl acetate 3:1);

Melting point: 118 °C;

^{1}H-NMR ($CDCl_3$, 500 MHz, 300 K): δ = 7.83-7.77 (m, 4H, Ar-H$_{ortho}$, Ar-H$_{ortho'}$), 7.71-7.66 (m, 2H, Ar-H$_{Fmoc}$), 7.56-7.48 (m, 2H, Ar-H$_{Fmoc}$), 7.38-7.29 (m, 6H, Ar-H$_{Fmoc}$, Ar-H$_{para}$, Ar-H$_{para'}$), 7.27-7.22 (m, 2H, Ar-H$_{Fmoc}$), 5.08-5.04 (m, 1H, NH), 4.45-4.41 (d, $^3J_{CH,\ CH2}$ = 6.8 Hz, 2H, CH$_{2,\ Fmoc}$), 4.40-4.36 (d, $^3J_{NH,\ CH2}$ = 6.3 Hz, 2H, CH$_2$NH), 4.19-4.14 (t, $^3J_{CH,\ CH2}$ = 6.8 Hz, 1H, CHCH$_{2,\ Fmoc}$), 3.53 (s, 2H, CH$_2$(C=O)), 1.38 (s, 9H, CH$_3$) ppm;

^{13}C-NMR ($CDCl_3$, 126 MHz, 300 K): δ = 170.5 (CH_2(C=O)), 156.4 NH(C=O)), 152.2 (Ar-C_{Fmoc}), 151.7 (Ar-C_{ipso}, Ar-$C_{ipso'}$), 144.0 (Ar-C_{Fmoc}), 141.5 (Ar-C_{para}), 138.1 (Ar-$C_{para'}$), 130.1 (Ar-$C_{meta'}$), 128.2 (Ar-C_{Fmoc}), 127.9 (Ar-C_{meta}), 127.2 (Ar-C_{Fmoc}), 125.1 (Ar-C_{Fmoc}), 123.3, 123.1 (Ar-$C_{ortho'}$, Ar-C_{ortho}), 120.2 (Ar-C_{Fmoc}), 81.3 ($\underline{C}(CH_3)_3$), 66.9 ($CH_{2,Fmoc}$), 47.5 ($CH_{,Fmoc}$), 44.9 ($NHCH_2$), 42.8 (CH_2(C=O)), 28.3 (CH_3) ppm;

IR (ATR): $\tilde{\nu}$ = 3341, 2974, 1728, 1686, 1535, 1272, 1249, 1140, 731, 554, 419, 412 cm^{-1};

EI-MS: *m/z* = 547.24530, $[M]^+$; (calc. 547.24711 for $C_{34}H_{33}N_3O_4$).

4-[(*E*)-(4-Aminobenzyl)azo]-*tert*-butylphenylacetate 57

Piperidine (5.80 mL) was added to a solution of Fmoc protected amine **56** (606 mg, 1.20 mmol) in dry DMF (30 mL) and the mixture was stirred at room temperature for 16 h. The solvent was then removed under reduced pressure and the crude product was purified by column chromatography (DCM/ methanol 9:1) to obtain amine **57** as an amorphous orange solid.

Yield: 238 mg (731 µmol, 61 %);

TLC: R_f = 0.36 (DCM/ methanol 9:1);

^{1}H-NMR (DMSO-*d6*, 500 MHz, 300 K): δ = 7.87-7.81 (m, 4H, Ar-$H_{,ortho}$, Ar-$H_{ortho'}$), 7.58-7.55 (m, 2H, Ar-H_{meta}), 7.49-7.45 (m, 2H, Ar-$H_{meta'}$), 3.85 (s, 2H, NHC$\underline{H}_2$), 3.69 (s, 2H, (C=O)CH_2), 3.34 (s, 1H, NH), 1.41 (s, 9H, CH_3) ppm;

^{13}C-NMR (DMSO-*d6*, 126 MHz, 300 K): δ = 170.5 (C=O), 151.2 (Ar-C_{ipso}, Ar-$C_{ipso'}$), 147.5 (Ar-C_{para}), 138.8 (Ar-$C_{para'}$), 130.8 (Ar-$C_{meta'}$), 128.6 (Ar-C_{meta}), 122.9 (Ar-C_{ortho}, Ar-$C_{ortho'}$), 80.9 ($\underline{C}(CH_3)_3$), 45.4 ($NHCH_2$), 41.8 ((C=O)CH_2), 28.2 (CH_3) ppm;

IR (ATR): $\tilde{\nu}$ = 3431, 2250, 1660, 1052, 1024, 1004, 822, 759, 614 cm^{-1};

EI-MS: *m/z* = 324.15, $[M-H]^+$; (calc. 325.405 for $C19H_{23}N_3O_2$).

3-{(*E*)-[4-(2-Bromoacetamido)methyl]phenylazo}methylphenylacetate 59

Bromo acetylchloride **58** (147 µL, 1.76 mmol) was added dropwise to an ice-cold suspension of compound **54** (250 mg, 882 µmol), pyridine (78.3 µL, 970 µmol) and DMAP (5.39 mg, 44.1 µmol) in DCM (10 mL). The mixture was stirred for another 16 h

at room temperature. After addition of 1 N hydrochloric acid (30 mL) and DCM (100 mL) the phases were separated and the aqueous one was extracted with DCM (2 x 25 mL). The combined organic layers were dried over $MgSO_4$, filtered and the solvent removed under reduced pressure. Column chromatography (cyclohexane/ ethyl acetate 6:1 → 1:1) gave compound **59** as an amorphous orange solid.

Yield: 105 mg (260 µmol, 27 %);

TLC: R_f = 0.74 (ethyl acetate);

^{1}H-NMR ($CDCl_3$, 500 MHz, 300 K): δ = 7.91-7.86 (m, 4H, Ar-$H_{,ortho}$, C_{meta}'CAr-$H_{,ortho}$', Ar-H_{para}'), 7.45-7.42 (m, 4H, Ar-H_{meta}, Ar-$H_{,ortho}$', Ar-$H_{,meta}$'), 4.59-4.56 (m, 2H, NHC$\underline{H}_2$), 4.14 (s, 2H, CH_2Br), 3.72 (s, 2H, CH_2(C=O)), 3.71 (s, 3H, CH_3) ppm;

^{13}C-NMR ($CDCl_3$, 126 MHz, 300 K): δ = 171.7 ((C=O)O), 166.1 ((C=O)NH), 152.3, 151.8 (Ar-C_{ipso}, Ar-C_{ipso}'), 140.4 (Ar-C_{para}), 137.3 ($\underline{\text{Ar-C}}_{meta}$'$CH_2$), 130.3, 128.6 (Ar-$C_{meta}$, C_{meta}'Ar-C_{ortho}', Ar-C_{para}'), 123.5, 123.3 (Ar-C_{ortho}, Ar-C_{ortho}', Ar-C_{meta}'), 52.4 (CH_3), 43.7 ($NHCH_2$), 42.8 (CH_2Br), 41.2 (CH_2) ppm;

IR (ATR): $\tilde{\nu}$ = 3250, 2925, 1745, 1733, 1646, 1557, 1435, 1296, 1251, 1132, 1011, 844, 690, 562, 529 cm^{-1};

EI-MS: *m/z* = 403.05, $[M]^+$; (calc. 403.05315 for $C_{18}H_{18}BrN_3O_3$).

3-[(*E*)-[4-(2-Bromoacetamido)methyl]phenylazo]methylphenylacetate 60

Bromo acetylchloride **58** (130 µL, 1.56 mmol) was added dropwise to an ice-cold suspension of compound **55** (222 mg, 782 µmol), pyridine (69.4 µL, 860 µmol) and DMAP (4.78 mg, 39.1 µmol) in dry DCM (15 mL). The mixture was stirred for another 16 h at room temperature. After addition of 1 N hydrochloric acid (30 mL) and DCM (100 mL) phases were separated and the aqueous one was extracted with DCM (2 x 30 mL). The combined organic layers were dried over $MgSO_4$, filtered and the solvent removed under reduced pressure. Column chromatography (cyclohexane/ ethyl acetate 6:1 → 1:1) gave compound **60** as an orange solid.

Yield: 138 mg (341 µmol, 44 %);

TLC: R_f = 0.73 (ethyl acetate);

Melting point: 124 °C;

^{1}H-NMR ($CDCl_3$, 500 MHz, 300 K): δ = 7.92-7.88 (m, 2H, Ar-$H_{,ortho'}$), 7.85-7.82 (m, 2H, Ar-H_{ortho}), 7.50-7.40 (m, 4H, Ar-$H_{,meta}$, Ar-$H_{,meta'}$), 4.60-4.56 (m, 2H, NHC$\underline{H}_2$), 4.15 (s, 2H, CH_2Br), 3.74 (s, 2H, CH_2(C=O)), 3.72 (s, 3H, CH_3) ppm;

^{13}C-NMR ($CDCl_3$, 126 MHz, 300 K): δ = 171.7 ((C=O)O), 165.9 ((C=O)NH), 152.7 (Ar-C_{ipso}), 152.2 (Ar-$C_{ipso'}$), 140.2 (Ar-$C_{para'}$), 135.2 (Ar-C_{para}), 131.8 (Ar-$C_{meta'}$), 128.3 (Ar-C_{meta}), 123.4 (Ar-$C_{ortho'}$), 121.9 (Ar-C_{ortho}), 52.0 (CH_3), 43.7 ($NHCH_2$), 42.7 (CH_2Br), 41.0 (CH_2) ppm;

IR (ATR): $\tilde{\nu}$ = 3267, 3073, 2953, 1735, 1644, 1553, 1434, 1304, 1248, 1233, 1219, 1128, 1013, 843, 687, 557 cm^{-1};

EI-MS: *m/z* = 267.07, $[M\text{-}NHC{=}OCH_2Br]^+$; (calc. 403.05315 for $C_{18}H_{18}BrN_3O_3$).

4-{(*E*)-[4-(2-Bromoacetamido)methyl]phenylazo}-*tert*-butylphenylacetate 61

Bromo acetylchloride **58** (128 µL, 1.54 mmol) was added dropwise to an ice-cold suspension of compound **57** (250 mg, 768 µmol), pyridine (68.3 µL, 846 µmol) and DMAP (4.54 mg, 37.2 µmol) in DCM (10 mL). The mixture was stirred for another 16 h at room temperature. After addition of 1 N hydrochloric acid (30 mL) and DCM (100 mL) phases were separated and the aqueous one was extracted with DCM (2 x 25 mL). The combined organic layers were dried over $MgSO_4$, filtered and the solvent removed under reduced pressure. Column chromatography (cyclohexane/ ethyl acetate 6:1 → 1:1) gave compound **61** as an orange solid.

Yield: 259 mg (581 µmol, 76 %);

TLC: R_f = 0.75 (ethyl acetate);

^{1}H-NMR ($CDCl_3$, 500 MHz, 300 K): δ = 7.91-7.86 (m, 4H, Ar-$H_{,ortho'}$, Ar-$H_{,ortho'}$), 7.45-7.41 (m, 4H, Ar-H_{meta}, Ar-$H_{,meta'}$), 4.60-4.55 (m, 2H, NHC$\underline{H}_2$), 4.14 (s, 2H, CH_2Br), 3.60 (s, 2H, CH_2(C=O)), 1.45 (s, 9H, CH_3) ppm;

^{13}C-NMR ($CDCl_3$, 126 MHz, 300 K): δ = 170.4 ((C=O)O), 165.7 ((C=O)NH), 152.2 (Ar-C_{ipso}), 151.5 (Ar-$C_{ipso'}$), 140.1 (Ar-C_{para}), 138.1 (Ar-$C_{para'}$), 130.0 (Ar-$C_{meta'}$), 128.4 (Ar-C_{meta}), 123.3 (Ar-C_{ortho}), 123.0 (Ar-$C_{ortho'}$), 81.2 ($\underline{C}(CH_3)_3$), 43.5 ($NHCH_2$), 42.6 (CH_2Br, CH_2(C=O)), 28.0 (CH_3) ppm;

EI-MS: *m/z* = 445.10010, $[M]^+$; (calc. 445.10010 for $C_{21}H_{24}BrN_3O_2$).

4-{(*E*)-[4-(2-Triethylammoniumacetamido)methyl]phenylazo}-*tert*-butylphenyl-acetate 62

A solution of triethylamine in methanol (5 mL) was added to a solution of compound **61** (259 mg, 581 µmol) in methanol (20 mL). The mixture was stirred for 2 h at room temperature before the solvent was removed under reduced pressure. The residue was dissolved in methanol and subsequently poured into diethyl ether. Crude product **62** was obtained by filtration as an orange solid which was purified by column chromatography (DCM → DCM/methanol 4:1) to yield compound **62** as an orange syrup.

Yield: 118 mg (252 µmol, 43 %);

TLC: R_f = 0.25 (ethyl acetate/ methanol 6:1);

^{1}H-NMR ($CDCl_3$, 500 MHz, 300 K): δ = 9.99 (t, $^3J_{NHCH2}$ = 5.9 Hz, 1H, NH), 7.87-7.84 (m, 4H, Ar-H*ortho*, Ar-H*ortho'*), 7.56-7.52 (m, 2H, Ar-H*meta*), 7.43-7.40 (m, 2H, Ar-H*meta'*), 4.60 (s, 2H, NC$\underline{H_2}$C=O), 4.49 (d, $^3J_{NHCH2}$ = 5.9 Hz, 2H, NHC$\underline{H_2}$), 3.60 (s, 2H, Ar-CCH_2C=O), 3.57-3.51 (q, $^3J_{CH2CH3}$ = 7.3 Hz, 6H, C$\underline{H_2}CH_3$), 1.45 (s, 9H, C(CH_3)$_3$), 1.41 (t, $^3J_{CH2CH3}$ = 7.3 Hz, 9H, $CH_2C\underline{H_3}$) ppm;

^{13}C-NMR ($CDCl_3$, 126 MHz, 300 K): δ = 170.4 (O(C=O)), 162.9 (N(C=O)), 151.8 (Ar-C*ipso*), 151.5 (Ar-C*ipso'*), 140.6 (Ar-C*para*), 137.8 (Ar-C*para'*), 129.9 (Ar-C*meta'*), 128.7 (Ar-C*meta*), 122.9 (Ar-C*ortho*, Ar-C*ortho'*), 81.0 ($\underline{C}(CH_3)_3$), 57.0 (NCH_2), 54.7 (CH_2), 42.5 (Ar-CCH_2C=O), 27.8 (C($\underline{C}H_3$)$_3$), 8.0 ($CH_2\underline{C}H_3$) ppm;

IR (ATR): $\tilde{\nu}$ = 3412, 3203, 3057, 2979, 2930, 1722, 1678, 1232, 1141, 1012, 842, 549 cm^{-1};

EI-MS: *m/z* = 438.26, $[M\text{-}CH_2CH_3]^+$; (calc. 467.30167 for $C_{27}H_{39}N_4O_3$).

4-{(*E*)-[4-(2-Triethylammoniumacetamido)methyl}phenylazo]phenylacetic acid 63

Trifluoroacetic acid acid (4.00 mL) was added to a solution of compound **62** (100 mg, 214 µmol) and the mixture was stirred for 4 h at room temperature. Finally, the solvent was removed under reduced pressure and the crude product was codestilled with toluene (2 x 40 mL) and DCM (40 mL) to yield compound **63** quantitatively as an orange syrup.

Yield: quant.;

TLC: R_f = 0 (ethyl acetate/ methanol 6:1);

^{1}H-NMR (MeOD, 500 MHz, 300 K): δ = 7.92-7.86 (m, 4H, Ar-H$_{ortho}$, Ar-H$_{ortho'}$), 7.51-7.46 (m, 4H, Ar-H$_{meta}$, Ar-H$_{meta'}$), 4.51 (s, 2H, NHC$\underline{H}_2$), 4.03 (s, 2H, NC$\underline{H}_2$C=O), 3.72 (s, 2H, Ar-CCH$_2$C=O), 3.63-3.58 (q, $^{3}J_{CH2CH3}$ = 7.3 Hz, 6H, C$\underline{H}_2$CH$_3$), 1.34 (t, $^{3}J_{CH2CH3}$ = 7.3 Hz, 9H, CH$_2$C$\underline{H}_3$) ppm;

^{13}C-NMR (MeOD, 126 MHz, 300 K): δ = 175.3 (O(C=O)), 164.9 (N(C=O)), 153.7 (Ar-C$_{ipso}$), 153.2 (Ar-C$_{ipso'}$), 142.8 (Ar-C$_{para}$), 140.1 (Ar-C$_{para'}$), 131.8 (Ar-C$_{ortho}$), 130.0 (Ar-C$_{meta}$), 124.4 (Ar-C$_{ortho}$, Ar-C$_{ortho'}$), 57.5 (NCH$_2$), 55.9 (CH$_2$), 44.2 (NHCH$_2$), 8.1 (CH$_3$) ppm;

IR (ATR): ṽ = 3263, 2993, 1671, 1601, 1560, 1420, 1200, 1175, 1127, 1012, 832, 800, 720, 598, 530 cm^{-1};

EI-MS: *m/z* = 438.26, [M-CH$_2$CH$_3$]$^{+}$; (calc. 467.302 for C$_{27}$H$_{39}$N$_4$O$_3$).

4-{(*E*)-[4-(2-Trimethylammoniumacetamido)methyl]phenylazo}methylphenyl-acetate 65-I

A solution of trimethylamine in methanol (30 wt.%) (6 mL) was added to a solution of compound **60** (224 mg, 502 μmol) in methanol (20 mL). The mixture was stirred for 2 h at room temperature before the solvent was removed under reduced pressure. The residue was dissolved in methanol and subsequently poured into diethyl ether. Crude product **65-I** was obtained by filtration as an orange solid which was purified by column chromatography (DCM → DCM/methanol 4:1) to yield compound **65-I**.

4-{(*E*)-[4-(2-Trimethylammoniumacetamido)methyl]phenylazo}methylphenyl-acetate 65-II

Oxalyl chloride (10.8 mL, 97.2 mmol) was added to an ice-cold solution of betaine **63** (11.4 g, 97.2 mmol) in dry acetonitrile (120 mL). After adding 20 drops of dry DMF the mixture was stirred for 20 min at room temperature. The solvent was then removed under reduced pressure and the residue dissolved in dry DMF (60 mL). The solution of the acyl chloride of betaine **63** was added dropwise to an ice-cold solution of amine **53** (2.00 g, 4.86 mmol) and DIPEA (1.65 mL, 9.72 mmol) in dry DMF (60 mL). The mixture was stirred at room temperature for 16 h. After removal of the solvent under reduced pressure the crude product was purified by column chromatography twice (DCM/ methanol 9:1

and ethyl acetate/ethanol 9:1). Finally, compound **64-II** was dissolved in ethanol and isolated by precipitation with ethyl acetate. Compound **64-II** was obtained by filtration as an orange solid.

Yield: 1.38 g (3.30 mmol, 68 %);

TLC: R_f = 0.63 (DCM/ methanol 6:1);

Melting point: 172 °C;

^{1}H-NMR (MeOD, 500 MHz, 300 K): δ = 7.90-7.85 (m, 4H, Ar-H$_{ortho}$, Ar-H$_{ortho'}$), 7.53-7.50 (m, 2H, Ar-H$_{,meta}$), 7.48-7.45 (Ar-H$_{meta'}$), 4.52 (s, 2H, NHC$\underline{H}_2$), 4.22 (s, 2H, NC$\underline{H}_2$(C=O)), 3.76 (s, 3H, OCH_3), 3.71 (s, 2H, Ar-CCH_2C=O), 3.36 (s, 9H, $N(CH_3)_3$) ppm;

^{13}C-NMR (MeOD, 126 MHz, 300 K): δ = 173.4 (O(C=O)), 164.8 (N(C=O)), 153.4 (Ar-C$_{ipso}$), 152.9 (Ar-C$_{ipso'}$), 142.6 (Ar-C$_{para}$), 139.4 (Ar-C$_{para'}$), 131.5 (Ar-C$_{meta'}$), 129.7 (Ar-C$_{meta}$), 124.1 (Ar-C$_{ortho'}$), 124.0 (Ar-C$_{ortho}$), 65.6 ($C\underline{H}_2NMe_3$), 55.0 ($N(CH_3)_3$), 52.5 (OCH_3), 43.8 (NCH_2), 41.4 (CH_2(C=O)) ppm;

IR (ATR): $\tilde{\nu}$ = 3356, 3157, 3011, 2948, 1737, 1679, 1416, 1263, 883, 824, 700, 544 cm^{-1};

EI-MS: *m/z* = 323.14, [M-·(C=O)OCH_3-H]$^+$; (calc. 382.20832 for $C_{21}H_{27}N_4O_3$).

4-{(*E*)-[4-(2-Trimethylammoniumacetamido)methyl]phenylazo}phenylacaetic acid 66

Lithium hydroxide (192 mg, 8.00 mmol) was added to a solution of methyl ester **65** (1.53 g, 4.00 mmol) in a mixture of THF and water (2:1, 60 mL). The mixture was stirred at room temperature for 16 h. The mixture was then neutralised with Amberlite® IR 120, filtered and the solvent removed under reduced pressure. Compound **66** was obtained as an amorphous orange solid.

Yield: 1.40 g (3.80 mmol, 95 %);

TLC: R_f = 0.13 (ethyl acetate/ methanol 6:1);

^{1}H-NMR (MeOD, 500 MHz, 300 K): δ = 7.91-7.83 (m, 4H, Ar-H$_{ortho}$, Ar-H$_{ortho'}$), 7.57-7.43 (m, 4H, Ar-H$_{,meta}$, Ar-H$_{meta'}$), 4.52 (s, 2H, NHC$\underline{H}_2$), 4.28 (s, 2H, NC$\underline{H}_2$(C=O)), 3.72 (s, 2H, Ar-CCH_2C=O), 3.37 (s, 9H, $N(CH_3)_3$) ppm;

^{13}C-NMR (MeOD, 126 MHz, 300 K): δ = 172.9 (O(C=O)), 164.7 (N(C=O)), 153.4 (Ar-C_{ipso}), 152.9 (Ar-$C_{ipso'}$), 142.6 (Ar-C_{para}), 139.1 (Ar-$C_{para'}$), 131.4 (Ar-$C_{meta'}$), 129.7 (Ar-C_{meta}), 124.1 (Ar-$C_{ortho'}$), 123.9 (Ar-C_{ortho}), 67.9 ($C\underline{H}_2NMe_3$), 54.8 ($N(CH_3)_3$), 43.8 (NCH_2), 41.4 ($CH_2(C=O)$) ppm;

IR (ATR): $\tilde{\nu}$ = 3369, 1728, 1676, 1473, 1297, 1082, 831, 526 cm^{-1};

EI-MS: *m/z* = 334.92, $[M\text{-}NHC{=}OCH_2N(CH_3)_3{+}Br{+}H]^+$; (calc. 369.192 for $C_{20}H_{25}N_4O_3$).

p-[(*E*)-(*p*'-Acetic acid methyl ester)phenylazo]phenyl α-D-mannopyranoside 70

4-Aminophenyl α-D-mannopyranoside **67** (400 mg, 1.48 mmol) and nitroso compound **21** (1.48 mmol) were dissolved in acetic acid (50 mL) and stirred at room temperature for 2 d. After addition of sat. NaCl solution (200 mL) the mixture was extracted with ethyl acetate (4 x 150 mL). The combined organic layers were dried over $MgSO_4$, filtered and the solvent was removed under reduced pressure. Column chromatography (ethyl acetate → ethyl acetate/ methanol 6:1) gave compound **70** as an orange syrup.

Yield: 267 mg (616 µmol, 42 %);

TLC: R_f = 0.30 (ethyl acetate/ methanol 6:1);

Melting point: 177 °C;

Rotational value: $[\alpha]_{20}^{D}$ = +177.4 (c = 0.06 in methanol);

^{1}H-NMR (MeOD, 600 MHz, 300 K): δ = 7.91-7.88 (m, 2H, Ar-$H_{,ortho}$), 7.84-7.82 (m, 2H, Ar-$H_{ortho'}$), 7.45-7.42 (m, 2H, Ar-$H_{meta'}$), 7.29-7.26 (m, 2H, Ar-H_{meta}), 5.60 (d, $^3J_{H1H2}$ = 1.8 Hz, 1H, H-1), 4.05-4.03 (dd, $^3J_{H1H2}$ = 1.8 Hz, $^3J_{H2H3}$ = 3.4 Hz, 1H, H-2), 3.94-3.91 (dd, $^3J_{H2H3}$ = 3.4 Hz, $^3J_{H3H4}$ = 9.5 Hz, 1H, H-3), 3.80-3.72 (m, 5H, CH_2, H-4, H-6, H-6'), 3.70 (s, 3H, CH_3), 3.51-3.46 (ddd, $^3J_{H4H5}$ = 9.6 Hz, $^3J_{H5H6'}$ = 2.3 Hz, $^3J_{H5H6}$ = 5.3 Hz, 1H, H-5) ppm;

^{13}C-NMR (MeOD, 151 MHz, 300 K): δ = 173.6 (C=O), 160.4 (Ar-C_{para}), 153.1 (Ar-$C_{ipso'}$), 149.2 (Ar-C_{ipso}), 138.6 (Ar-$C_{para'}$), 131.3 (Ar-$C_{meta'}$), 125.6 (Ar-C_{ortho}), 123.7 (Ar-$C_{ortho'}$), 118.1 (Ar-C_{meta}), 100.1 (C-1), 75.7 (C-5), 72.4 (C-3), 71.9 (C-2), 68.3 (C-4), 62.7 (C-6), 52.6 (CH_3), 41.5 (CH_2) ppm;

IR (ATR): $\tilde{\nu}$ = 3309, 2252, 1733, 1601, 1583, 1497, 1229, 1127, 1005, 967, 838, 671, 548 cm^{-1};

ESI-MS: *m/z* = 433.16065, $[M+H]^+$; (calc. 433.16109 for $C_{21}H_{24}N_2O_8$+H).

p-[(*E*)-(*p*'-Acetic acid methyl ester)phenylazo]phenyl α-D-glucopyranoside 71

4-Aminophenyl α-D-glucopyranoside **68** (500 mg, 1.85 mmol) and nitroso compound **21** (1.85 mmol) were dissolved in acetic acid (70 mL) and stirred at room temperature for 2 d. After addition of sat. NaCl solution (200 mL) the mixture was extracted with ethyl acetate (4 x 150 mL). The combined organic layers were dried over $MgSO_4$, filtered and the solvent was removed under reduced pressure. Column chromatography (ethyl acetate → ethyl acetate/ methanol 6:1) gave compound **71** as an orange syrup.

Yield: 317 mg (732 µmol, 40 %);

TLC: R_f = 0.30 (ethyl acetate/ methanol 6:1);

^{1}H-NMR (MeOD, 500 MHz, 300 K): δ = 7.95-7.91 (m, 2H, Ar-$H_{,ortho}$), 7.88-7.85 (m, 2H, Ar-$H_{,ortho'}$), 7.49-7.46 (m, 2H, Ar-$H_{meta'}$), 7.38-7.35 (m, 2H, Ar-H_{meta}), 5.65 (d, $^3J_{H1H2}$ = 3.7 Hz, 1H, H-1), 3.94-3.90 (dd~t, $^3J_{H3H4}$ = 9.2 Hz, 1H, H-3), 3.82-3.75 (m, 3H, CH_2, H-6), 3.76-3.63 (m, 6H, CH_3, H-2, H-5, H-6'), 3.51-3.46 (dd, $^3J_{H3H4}$ = 9.0 Hz, $^3J_{H4H5}$ = 9.9 Hz, 1H, H-4) ppm;

^{13}C-NMR (MeOD, 126 MHz, 300 K): δ = 173.5 (C=O), 161.1 (Ar-C_{para}), 153.1 (Ar-$C_{ipso'}$), 149.2 (Ar-C_{ipso}), 138.6 (Ar-$C_{para'}$), 131.3 (Ar-$C_{meta'}$), 125.5 (Ar-C_{ortho}), 123.7 (Ar-$C_{ortho'}$), 118.3 (Ar-C_{meta}), 99.2 (C-1), 74.9 (C-3), 74.8 (C-2), 73.2 (C-5), 71.4 (C-4), 62.4 (C-6), 52.6 (CH_3), 41.4 (CH_2) ppm;

ESI-MS: *m/z* = 433.16078, $[M+H]^+$; (calc. 433.16109 for $C_{21}H_{24}N_2O_8$+H).

p-[(*E*)-(*p*'-Acetic acid methyl ester)phenylazo]phenyl β-D-glucopyranoside 72

4-Aminophenyl β-D-glucopyranoside **69** (526 mg, 1.94 mmol) and nitroso compound **21** (1.94 mmol) were dissolved in acetic acid (8 mL) and stirred at room temperature for 16 h. After addition of H_2O (150 mL) the mixture was extracted with ethyl acetate (4 x 50 mL). The combined organic layers were dried over $MgSO_4$, filtered and the solvent

was removed under reduced pressure. Column chromatography (ethyl acetate → ethyl acetate/ methanol 6:1) gave compound **72** as an orange syrup.

Yield: 421 mg (973 µmol, 50 %);

TLC: R_f = 0.30 (ethyl acetate/ methanol 6:1);

Melting point: 180 °C;

Rotational value: $[\alpha]_{20}^{D}$ = -50.8 (c = 0.08 in methanol);

^{1}H-NMR (MeOD, 500 MHz, 300 K): δ = 7.91-7.88 (m, 2H, Ar-H*$_{,ortho}$*), 7.85-7.82 (m, 2H, Ar-H*$_{,ortho‘}$*), 7.45-7.42 (m, 2H, Ar-H*$_{meta‘}$*), 7.26-7.23 (m, 2H, Ar-H*$_{meta}$*), 5.04-5.02 (m, 1H, H-1), 3.94-3.90 (dd, $^3J_{H5H6}$ = 2.3 Hz, $^3J_{H6H6‘}$ = 12.1 Hz 1H, H-6), 3.75-3.71 (m, 3H, CH_2, H-6‘), 3.70 (s, 3H, CH_3), 3.53-3.47 (m, 3H, H-2, H-3, H-4), 3.43-3.39 (m, 1H, H-5) ppm;

^{13}C-NMR (MeOD, 126 MHz, 300 K): δ = 171.9 (C=O), 160.2 (Ar-C*$_{para}$*), 151.1 (Ar-C*$_{ipso‘}$*), 149.2 (Ar-C*$_{ipso}$*), 138.7 (Ar-C*$_{para‘}$*), 131.3 (Ar-C*$_{meta‘}$*), 125.5 (Ar-C*$_{ortho}$*), 123.7 (Ar-C*$_{ortho‘}$*), 118.0 (Ar-C*$_{meta}$*), 102.0 (C-1), 78.3, 78.0, 75.0 (C-2, C-3, C-4), 71.3 (C-5), 62.4 (C-6), 52.3 (CH_3), 41.3 (CH_2) ppm;

IR (ATR): $\tilde{\nu}$ = 3413, 3211, 2923, 1720, 1234, 1077, 1048, 1002, 647, 659 cm^{-1};

ESI-MS: *m/z* = 433.16023, $[M+H]^+$; (calc. 433.16109 for $C_{21}H_{24}N_2O_8$+H).

p-[(*E*)-(*p*'-Acetic acid)phenylazo]phenyl 2,3,4,6-tetra-*O*-acetyl-α-D-mannopyranoside 73

Lithium hydroxide (29.5 mg, 1.23 mmol) was added to a solution of compound **70** (267 mg, 616 µmol) in THF/H_2O (2:1; 70 mL) and stirred for 16 h at room temperature. The mixture was neutralised with Amberlite® IR 120 and filtered. The solvent was removed under reduced pressure to yield compound **73** as an orange syrup after lyophilisation.

Yield: 252 mg (603 µmol, 98 %);

TLC: R_f = 0.0 (ethyl acetate/ methanol 6:1);

Melting point: 208 °C (decompodition);

Rotational value: $[\alpha]_{20}^{D}$ = +143.9 (c = 0.06 in methanol);

^{1}H-NMR (MeOD, 500 MHz, 300 K): δ = 7.91-7.88 (m, 2H, Ar-H$_{,ortho}$), 7.85-7.81 (m, 2H, Ar-H$_{,ortho'}$), 7.47-7.44 (m, 2H, Ar-H$_{,meta}$), 7.29-7.26 (m, 2H, Ar-H$_{,meta'}$), 5.60 (d, $^{3}J_{H1H2}$ = 1.8 Hz, 1H, H-1), 4.05-4.01 (dd, $^{3}J_{H1H2}$ = 1.8 Hz, $^{3}J_{H2H3}$ = 3.3 Hz, 1H, H-2), 3.96-3.87 (dd, $^{3}J_{H2H3}$ = 3.3 Hz, $^{3}J_{H3H4}$ = 9.2 Hz, 1H, H-3), 3.77-3.72 (m, 3H, H-4, H-6, H-6'), 3.70 (s, 2H, CH_2), 3.61-3.57 (ddd, $^{3}J_{H5H4'}$ = 9.7 Hz, $^{3}J_{H5H6}$ = 5.3 Hz, $^{3}J_{H5H6'}$ = 2.4 Hz, 1H, H-5) ppm;

^{13}C-NMR (MeOD, 151 MHz, 300 K): δ = 175.1 (C=O), 160.4 (Ar-C$_{para}$), 153.0 (Ar-C$_{ipso'}$), 149.3 (Ar-C$_{ipso}$), 139.2 (Ar-C$_{para'}$), 131.3 (Ar-C$_{meta'}$), 125.6 (Ar-C$_{ortho}$), 123.7 (Ar-C$_{ortho'}$), 118.1 (Ar-C$_{meta}$), 100.1 (C-1), 75.8 (C-5), 72.4 (C-3), 71.9 (C-2), 68.3 (C-4), 62.7 (C-6), 41.8 (CH_2) ppm;

IR (ATR): $\tilde{\nu}$ = 3325, 1694, 1586, 1496, 1327, 1230, 1105, 1002, 840, 665, 579, 551 cm^{-1};

ESI-MS: *m/z* = 419.14516, $[M+H]^+$; (calc. 419.14544 for $C_{20}H_{22}N_2O_8$+H).

p-[(*E*)-(*p*'-Acetic acid)phenylazo]phenyl 2,3,4,6-tetra-*O*-acetyl-α-D-glucopyranoside 74

Lithium hydroxide (35.1 mg, 1.46 mmol) was added to a solution of compound **71** (317 mg, 732 µmol) in THF/H_2O (2:1; 70 mL) and stirred for 16 h at room temperature. The mixture was neutralised with Amberlite® IR 120 and filtered. The solvent was removed under reduced pressure to yield compound **74** as an orange syrup after lyophilisation.

Yield: 303 mg (725 µmol, 99 %);

TLC: R_f = 0.0 (ethyl acetate/ methanol 6:1);

^{1}H-NMR (MeOD, 200 MHz, 300 K): δ = 7.92-7.79 (m, 4H, Ar-H), 7.48-7.40 (m, 2H, Ar-H), 7.35-7.27 (m, 2H, Ar-H), 5.61 (d, $^{3}J_{H1H2}$ = 3.6 Hz, 1H, H-1), 3.93-3.82 (dd, $^{3}J_{H2H3}$ = 8.8 Hz, $^{3}J_{H3H4}$ = 9.9 Hz, 1H, H-3), 3.79-3.67 (m, 4H, CH_2, H_{glc}), 3.65-3.56 (m, 2H, H_{glc}), 3.49-3.37 (m, 1H, H_{glc}) ppm;

ESI-MS: *m/z* = 419.14497, $[M+H]^+$; (calc. 419.14544 for $C_{20}H_{22}N_2O_8$+H).

p-[(*E*)-(*p*'-Acetic acid)phenylazo]phenyl 2,3,4,6-tetra-*O*-acetyl-β-D-glucopyranoside 75

Lithium hydroxide (721 mg, 30.1 mmol) was added to a solution of compound **72** (1.32 g, 2.20 mmol) in THF/H_2O (2:1; 60 mL) and stirred for 16 h at room temperature. The mixture was neutralised with Amberlite® IR 120, diluted with methanol (80 mL) and filtered. The solvent was removed under reduced pressure to yield compound **75** as an orange syrup.

Yield: 884 mg (2.11 mmol, 96 %);

TLC: R_f = 0.0 (ethyl acetate/ methanol 6:1);

Melting point: 193 °C;

Rotational value: $[\alpha]_{20}^{D}$ = -48.0 (c = 0.09 in methanol);

^{1}H-NMR (MeOD, 500 MHz, 300 K): δ = 7.91-7.88 (m, 2H, Ar-H$_{,ortho}$), 7.85-7.82 (m, 2H, Ar-H$_{,ortho'}$), 7.47-7.44 (m, 2H, Ar-H$_{meta'}$), 7.26-7.22 (m, 2H, Ar-H$_{meta}$), 5.04-5.02 (m, 1H, H-1), 3.94-3.90 (dd, $^3J_{H5H6}$ = 2.2 Hz, $^3J_{H6H6'}$ = 12.1 Hz 1H, H-6), 3.74-3.69 (m, 3H, CH_2, H-6'),3.53-3.48 (m, 3H, H-2, H-3, H-4), 3.44-3.39 (m, 1H, H-5) ppm;

^{13}C-NMR (MeOD, 126 MHz, 300 K): δ = 175.0 (C=O), 161.6 (Ar-C$_{para}$), 153.0 (Ar-C$_{ipso'}$), 149.3 (Ar-C$_{ipso}$), 139.3 (Ar-C$_{para'}$), 131.4 (Ar-C$_{meta'}$), 125.5 (Ar-C$_{ortho}$), 123.7 (Ar-C$_{ortho'}$), 118.0 (Ar-C$_{meta}$), 102.0 (C-1), 78.4, 78.0, 74.9 (C-2, C-3, C-4), 71.4 (C-5), 62.6 (C-6), 41.7 (CH_2) ppm;

IR (ATR): $\tilde{\nu}$ = 3269, 2934, 2459, 1704, 1590, 1495, 1239, 1077, 1047, 1077, 838, 553 cm^{-1};

ESI-MS: *m/z* = 419.14438, $[M+H]^+$; (calc. 419.14544 for $C_{20}H_{22}N_2O_8$+H).

p-[(*E*)-*p*'-(Phenylthioacetate)phenylazo]phenyl 2,3,4,6-tetra-*O*-acetyl-α-D-mannopyranoside 78

Triethylamine (170 µL, 1.23 mmol) was added to an ice-cold solution of mannoside **75** (251 mg, 600 µmol), DEPC (**77**) (187 µL, 1.23 mmol) and thiophenol (95.0 µL, 924 µmol) in DMF (10 mL). The reaction mixture was stirred for 16 h at room temperature. The solvent was then removed under reduced pressure and the crude product

was purified by column chromatography (ethyl acetate /methanol 20:1 → 9:1) to yield compound **78** as an orange solid.

Yield: 176 mg (345 µmol, 58 %);

TLC: R_f = 0.38 (ethyl acetate/methanol 9:1);

Melting point: 176 °C;

Rotational value: $[\alpha]_{20}^{D}$ = +96.9 (c = 0.08 in methanol);

^{1}H-NMR (DMSO-*d6*, 500 MHz, 300 K): δ = 7.90-7.82 (m, 4H, Ar-H$_{,ortho}$, Ar-H$_{SPh}$), 7.56-7.52 (m, 2H, Ar-H$_{,meta'}$), 7.48-7.44 (m, 3H, Ar-H$_{SPh}$), 7.43-7.39 (m, 2H, Ar-H$_{ortho'}$), 7.30-7.25 (m, 2H, Ar-H$_{meta}$), 5.53 (d, $^3J_{H1H2}$ = 1.7 Hz, 1H, H-1), 5.08 (d, $^3J_{H2OH}$ = 4.4 Hz, 1H, OH(2)), 4.85 (d, $^3J_{H4OH}$ = 5.8 Hz, 1H, OH(4)), 4.78 (d, $^3J_{H3OH}$ = 6.0 Hz, 1H, OH(3)), 4.45 (d, $^3J_{H6OH}$ = 6.0 Hz, 1H, OH(6)), 4.18 (m, 2H, CH_2), 3.88-3.85 (m, 1H, H-2), 3.73-3.69 (m, 1H, H-3), 3.63-3.58 (m, 1H, H-6), 3.55-3.45 (m, 2H, H-4, H-6'), 3.41-3.36 (ddd, $^3J_{H4H5}$ = 9.2 Hz, $^3J_{H5H6'}$ = 2.6 Hz, $^3J_{H5H6}$ = 5.4 Hz, 1H, H-5) ppm;

^{13}C-NMR (DMSO-*d6*, 126 MHz, 300 K): δ = 194.6 (C=O), 159.0 (Ar-C$_{para'}$), 151.2 (Ar-C$_{ipso'}$), 146.9 (Ar-C$_{ipso}$), 136.6 (Ar-C$_{para}$), 134.4 (Ar-C$_{ortho'}$), 130.8 (Ar-C$_{meta'}$), 129.6, 129.4 (Ar-C$_{SPh}$), 124.4 (Ar-C$_{ortho}$), 122.4 (Ar-C$_{SPh}$), 117.1 (Ar-C$_{meta}$), 98.7 (C-1), 75.2 (C-5), 70.6 (C-3), 69.9 (C-2), 66.6 (C-4), 61.0 (C-6), 48.9 (CH_2) ppm;

ESI-MS: *m/z* = 511.15344, $[M+H]^+$; (calc. 511.15390 for $C_{26}H_{26}N_2O_7$+H);

IR (ATR): ṽ = 3322, 2936, 1697, 1497, 1224, 1024, 832, 745 cm^{-1}.

p-[(*E*)-*p*'-(Phenylthioacetate)phenylazo]phenyl 2,3,4,6-tetra-*O*-acetyl-α-D-gluco-pyranoside 79

Triethylamine (202 µL, 1.46 mmol) was added to an ice-cold solution of glucoside **76** (303 mg, 725 µmol), DEPC (**77**) (222 µL, 1.46 mmol) and thiophenol (112 µL, 1.10 mmol) in DMF (10 mL). The reaction mixture was stirred for 16 h at room temperature. The solvent was then removed under reduced pressure and the crude product was purified by column chromatography (DCM/methanol 30:1 → 9:1) to yield compound **79** as an orange solid.

Yield: 234 mg (458 µmol, 63 %);

TLC: R_f = 0.48 (DCM/methanol 9:1);

Melting point: 148 °C;

Rotational value: $[\alpha]_{20}^{D}$ = +177.4 (c = 0.18 in methanol);

^{1}H-NMR (DMSO-*d6*, 500 MHz, 300 K): δ = 7.91-7.79 (m, 4H, Ar-H$_{ortho}$, Ar-H$_{SPh}$), 7.56-7.51 (m, 2H, Ar-H$_{,meta'}$), 7.48-7.37 (m, 2H, Ar-H$_{ortho'}$, Ar-H$_{SPh}$), 7.30-7.26 (m, 2H, Ar-H$_{meta}$), 5.55 (d, $^3J_{H1H2}$ = 3.5 Hz, 1H, H-1), 5.14 (d, $^3J_{H3OH}$ = 6.3 Hz, 1H, OH(3)), 5.00 (d, $^3J_{H2OH}$ = 5.8 Hz, 1H, OH(2)), 4.97 (d, $^3J_{H2OH}$ = 5.0 Hz, 1H, OH(5)), 4.48 (t, $^3J_{H6OH}$ = 5.8 Hz, 1H, OH(6)), 4.18 (s, 2H, CH_2), 3.68-3.63 (m, 1H, H-3), 3.60-3.55 (m, 1H, H-6), 3.51-3.39 (m, 3H, H-2, H-4, H-6'), 3.24-3.19 (m, 1H, H-5) ppm;

^{13}C-NMR (DMSO-*d6*, 126 MHz, 300 K): δ = 194.6 (C=O), 159.8 (Ar-C$_{para}$), 151.2 (Ar-C$_{para'}$), 146.9 (Ar-C$_{ipso}$), 136.6 (Ar-C$_{ortho'}$), 134.4 (Ar-C$_{SPh}$), 130.8 (Ar-C$_{meta'}$), 130.5 (Ar-C$_{ipso'}$), 129.6, 124.4 (Ar-C$_{SPh}$), 122.4 (Ar-C$_{ortho}$), 117.3 (Ar-C$_{meta}$), 97.7 (C-1), 74.1 (C-2), 73.0 (C-3), 71.5 (C-4), 69.8 (C-5), 60.7 (C-6), 48.9 (CH_2) ppm;

IR (ATR): $\tilde{\nu}$ = 3352, 2161, 1697, 1598, 1497, 1232, 1079, 1025, 841 cm^{-1};

ESI-MS: *m/z* = 511.15360, $[M+H]^+$; (calc. 511.15390 for $C_{26}H_{26}N_2O_7$+H).

p-[(*E*)-*p*'-(Phenylthioacetate)phenylazo]phenyl 2,3,4,6-tetra-*O*-acetyl-β-D-glucopyranoside 80

Variant A

Triethylamine (166 µL, 1.20 mmol) was added to an ice-cold solution of glucoside **77** (500 mg, 1.20 mmol), DPPA (**76**) (258 µL, 1.20 mmol) and thiophenol (616 µL, 6.00 mmol) in DMF (6 mL). The reaction mixture was stirred for 3 h at room temperature. The solvent was then removed under reduced pressure and the crude product was purified by column chromatography (ethyl acetate/ methanol 30:1 → 9:1) to yield compound **80** as an orange solid.

Yield: 276 mg (540 µmol, 45 %);

TLC: R_f = 0.33 (ethyl acetate/ methanol 9:1);

Variant B

Triethylamine (53.0 µL, 382 µmol) was added to an ice-cold solution of glucoside **77** (80.0 mg, 191 µmol), DEPC (**77**) (61.6 µL, 382 µmol) and thiophenol (29.6 µL, 287 µmol) in DMF (10 mL). The reaction mixture was stirred for 16 h at room temperature. The solvent was then removed under reduced pressure and the crude product was purified by column chromatography (ethyl acetate/ methanol 30:1 → 9:1) to yield compound **80** as an orange solid.

Yield: 59.5 mg (117 µmol, 61 %);

Melting point: 149 °C;

Rotational value: $[\alpha]_{20}^{D}$ = -41.6 (c = 0.13 in methanol);

^{1}H-NMR (MeOD, 500 MHz, 300 K): δ = 7.95-7.85 (m, 4H, Ar-H*$_{,ortho}$*, Ar-H*$_{,ortho‘}$*), 7.55-7.50 (m, 2H, Ar-H*$_{meta‘}$*), 7.45-7.41 (m, 5H, SPh), 7.30-7.26 (m, 2H, Ar-H*$_{meta}$*), 5.08-5.05 (m, 1H, H-1), 4.09 (s, 1H, CH_2), 3.98-3.94 (dd, $^{3}J_{H5H6}$ = 2.2 Hz, $^{3}J_{H6H6‘}$ = 12.1 Hz 1H, H-6), 3.78-3.74 (m, 1H, $^{3}J_{H5H6‘}$ = 5.8 Hz, $^{3}J_{H6H6‘}$ = 12.1 Hz, H-6‘), 3.57-3.52 (m, 3H, H-2, H-3, H-4), 3.47-3.43 (m, 1H, H-5) ppm;

^{13}C-NMR (MeOD, 126 MHz, 300 K): δ = 196.6 (C=O), 161.6 (Ar-C*$_{para}$*), 153.2 (Ar-C*$_{ipso‘}$*), 149.2 (Ar-C*$_{ipso}$*), 137.9 (Ar-C*$_{para‘}$*), 136.5, 135.7 (SPh), 131.6 (Ar-C*$_{meta‘}$*), 130.6 (SPh), 125.5 (Ar-C*$_{ortho}$*), 123.8 (Ar-C*$_{ortho‘}$*), 118.0 (Ar-C*$_{meta}$*), 102.0 (C-1), 78.3, 78.0, 74.9 (C-2, C-3, C-4), 71.3 (C-5), 62.4 (C-6), 50.1 (CH_2) ppm;

IR (ATR): ṽ = 3329, 1598, 1234, 1011, 836, 751, 529 cm^{-1};

ESI-MS: *m/z* = 533.13528, $[M+H]^+$; (calc. 533.13584 for $C_{26}H_{26}N_2O_7$+Na).

2-Nitro-5-hydroxy benzoic acid methyl ester 91[401]

2-Nitro-5-hydroxy benzoic acid **90** (5.00 g, 27.3 mmol) was reacted according to General Procedure A to obtain methyl ester **91** as a colourless oil after column chromatography (cyclohexane / ethyl acetate 3:1).

Yield: 4.38 g (22.2 mmol, 81 %); lit.: 76 %;[401]

TLC: R_f = 0.40 (cyclohexane / ethyl acetate 1:1);

^{1}H-NMR ($CDCl_3$, 500 MHz, 300 K): δ = 8.02-7.98 (d, ^{3}J = 8.9 Hz, 1H, Ar-H_{ortho}), 7.02-6.96 (m, 2H, Ar-H_{meta}, Ar-H_{para}), 6.92 (s, 1H, OH), 3.95 (s, 3H, CH_3) ppm;

^{13}C-NMR ($CDCl_3$, 126 MHz, 300 K): δ = 167.7 (C=O), 160.9 (Ar-C_{meta}OH), 140.0 (Ar-$C_{ortho}NO_2$), 131.2 (Ar-C_{ipso}), 127.3 (Ar-C_{ortho}H), 117.7, 115.7 (Ar-C_{meta}H, Ar-C_{para}), 53.9 (CH_3) ppm;

IR (ATR): $\tilde{\nu}$ = 3308, 3080, 2967, 1703, 1581, 1523, 1434, 1348, 1314, 1267, 1223, 979, 839, 640, 580 cm^{-1};

EI-MS: *m/z* = 197.01, $[M]^+$; (calc. 197.032 for $C_8H_7NO_5$).

3-(2,3,4,6-Tetra-*O*-acetyl-β-D-glucopyranosyloxy)-6-(nitro)benzoic acid methyl-ester 92

Glucose trichloroacetimidate **88** (3.75 g, 7.61 mmol) and compound **91** (1.35 g, 6.85 mmol) were predried in vacuo for 15 min and subsequently dissolved in dry DCM (50 mL). After adding BF_3 etherate (2.87 mL, 22.8 mmol) at 0 °C the reaction mixture was stirred at room temperature for 2 d. The mixture was diluted with DCM (200 mL) and washed with saturated $NaHCO_3$ solution (75 mL). The organic layer was dried over $MgSO_4$, filtered and the solvent removed under reduced pressure. The crude product was purified by column chromatography (cyclohexane / ethyl acetate 2:1 → 1:1) to yield compound **92** as a colourless solid.

Yield: 2.19 g (4.15 mmol, 61 %);

TLC: R_f = 0.45 (cyclohexane/ ethyl acetate 1:1);

Melting point: 117 °C;

Rotational value: $[\alpha]_{20}^{D}$ = -22.5 (c = 0.08 in ethyl acetate);

^{1}H-NMR ($CDCl_3$, 500 MHz, 300 K): δ = 8.00 (d, ^{3}J = 9.0 Hz, 1H, Ar-H_{meta}), 7.20 (d, ^{4}J= 2.7 Hz, 1H, C<u>Ar-H</u>$_{ortho}$C(C=O)), 7.14 (dd, ^{3}J = 9.0 Hz, ^{4}J = 2.7 Hz, 1H, Ar-H_{ortho}), 5.34-5.28 (m, 2H, H-2, H-3), 5.24-5.21 (m, $^{3}J_{1,2}$ = 7.5 Hz 1H, H-1), 5.17-5.13 (dd~t, $^{3}J_{3,4}$ = 9.7 Hz, 1H, H-4), 4.26-4.22 (dd, $^{2}J_{H6H6'}$ = 12.4 Hz, $^{3}J_{H5H6}$ = 5.8 Hz, 1H, H-6), 4.20-4.16 (dd, $^{2}J_{H6H6'}$ = 12.4 Hz, $^{3}J_{H5H6'}$ = 2.4 Hz, 1H, H-6‘), 3.96-3.93 (ddd, $^{3}J_{H5H6}$ = 5.8 Hz, $^{3}J_{H5H6'}$ = 2.4 Hz, $^{3}J_{H4H5}$ = 10.0 Hz, 1H, H-5), 3.92 (s, 3H, CH_3), 2.08, 2.07, 2.06, 2.04 (s, each 3H, C=OCH_3) ppm;

^{13}C-NMR ($CDCl_3$, 126 MHz, 300 K): δ = 170.6, 170.2, 169.5, 169.3 ((C=O)CH_3), 166.0 ((C=O)OCH_3), 159.9 (Ar-$C_{,ipso}$), 142.3 (Ar-$C_{,para}$), 131.0 (Ar-$C_{,meta}$C=O), 126.6 (Ar-$C_{,meta}$H), 118.8 (Ar-$C_{,ortho}$Ar-$C_{,meta}$H), 116.9 (Ar-$C_{,ortho}$Ar-$C_{,meta}$C=O), 98.2 (C-1), 72.7 (C-5), 72.5 (C-3), 71.0 (C-2), 68.1 (C-4), 62.0 (C-6), 53.6 (CH_3), 20.8, 20.7 (C=OCH_3) ppm;

IR (ATR): ṽ = 3481, 3373, 2989, 1743, 1697, 1495, 1367, 1207, 1033 cm^{-1};

ESI-MS: *m/z* = 550.11685, $[M+Na]^+$; (calc. 550.11727 for $C_{22}H_{25}NO_{14}$+Na).

3-(2,3,4,6-Tetra-*O*-acetyl-α-D-mannopyranosyloxy)-6-(nitro)benzoic acid methyl-ester 93

Mannose trichloroacetimidate **89** (3.82 g, 7.75 mmol), molecular sieves (3 Å) and compound **91** (1.53 g, 7.76 mmol) were predried in vacuo for 15 min and subsequently dissolved in dry DCM (40 mL). After adding Borontrifluoride diethyletherate (2.92 mL, 23.0 mmol) at 0 °C the reaction mixture was stirred at room temperature for 2 d. The mixture was diluted with DCM (100 mL) and washed with saturated $NaHCO_3$ solution (60 mL). The organic layer was dried over $MgSO_4$, filtered and the solvent removed under reduced pressure. The crude product was purified by column chromatography (cyclohexane / ethyl acetate 2:1 → 1:1) to yield compound **93** as a colourless solid.

Yield: 3.44 g (6.52 mmol, 84 %);

TLC: R_f = 0.23 (cyclohexane/ ethyl acetate 2:1);

Melting point: 63 °C;

Rotational value: $[\alpha]_{20}^{D}$ = +76.4 (c = 0.52 in ethyl acetate);

^{1}H-NMR ($CDCl_3$, 500 MHz, 300 K): δ = 8.03 (d, ^{3}J = 9.1 Hz, 1H, Ar-H_{meta}), 7.36 (d, ^{4}J= 2.7 Hz, 1H, CAr-H_{ortho}C(C=O)), 7.28-7.25 (dd, ^{3}J = 9.1 Hz, ^{4}J = 2.7 Hz, 1H, Ar-H_{ortho}), 5.62 (m, $^3J_{1,2}$ = 1.7 Hz, 1H, H-1), 5.52-5.49 (dd, $^3J_{2,3}$ = 3.5 Hz, $^3J_{3,4}$ = 10.0 Hz, 1H, H-3), 5.45-5.44 (dd, $^3J_{1,2}$ = 1.7 Hz, $^3J_{2,3}$ = 3.5 Hz, 1H, H-2), 5.39-5.34 (dd~t, $^3J_{3,4}$ = 10.0 Hz, 1H, H-4), 4.28-4.23 (dd, $^2J_{H6H6'}$ = 12.4 Hz, $^3J_{H5H6}$ = 5.9 Hz, 1H, H-6), 4.08-4.04 (dd, $^2J_{H6,6'}$ = 12.4 Hz, $^3J_{H5,6'}$ = 2.3 Hz, 1H, H-6'), 4.01-3.96 (ddd, $^3J_{H5,6}$ = 5.8 Hz, $^3J_{H5H6'}$ = 2.3 Hz, $^3J_{H4H5}$ = 10.0 Hz, 1H, H-5), 3.93 (s, 3H, CH_3), 2.21, 2.06, 2.04, 2.03 (s, each 3H, C=OCH_3) ppm;

^{13}C-NMR ($CDCl_3$, 126 MHz, 300 K): δ = 170.6, 170.0, 169.7, 169.3 ((C=O)CH_3), 165.9 ((C=O)OCH_3), 158.9 (Ar-$C_{,ipso}$), 142.2 (Ar-$C_{,para}$), 131.1 (Ar-$C_{,meta}$C=O), 126.7 (Ar-$C_{,meta}$H), 118.5 (Ar-$C_{,ortho}$Ar-$C_{,meta}$H), 116.8 (Ar-$C_{,ortho}$Ar-$C_{,meta}$C=O), 96.0 (C-1), 70.1 (C-5), 68.9 (C-2), 68.5 (C-3), 65.7 (C-4), 62.1 (C-6), 53.6 (CH_3), 20.9, 20.8, 20.7 (C=OCH_3) ppm;

IR (ATR): $\tilde{\nu}$ = 2365, 2162, 1738, 1587, 1525, 1347, 1213, 1026 cm^{-1};

ESI-MS: *m/z* = 550.11673, $[M+Na]^+$; (calc. 550.11727 for $C_{22}H_{25}NO_{14}$+Na).

6-(Amino)-3-(2,3,4,6-tetra-*O*-acetyl-β-D-glucopyranosyloxy)benzoic acid methyl-ester 94

To a solution of glucoside **92** (2.00 g, 3.79 mmol) in ethyl acetate (150 mL) was added a catalytic amount of palladium (10 % on activated charcoal) and the mixture was stirred under hydrogen atmosphere for 16 h. The catalyst was removed by filtration over celite and the solvent was removed under reduced pressure to yield compound **94** quantitatively as a colourless foam.

Yield: quant.;

TLC: R_f = 0.25 (toluene/ ethyl acetate 3:1);

Melting point: 110 °C;

Rotational value: $[\alpha]_{20}^{D}$ = -16.9 (c = 0.57 in ethyl acetate);

^{1}H-NMR ($CDCl_3$, 500 MHz, 300 K): δ = 7.51 (s, 1H, CAr-H$_{ortho}$C(C=O)), 7.05-7.02 (dd, ^3J = 8.9 Hz, ^4J = 2.9 Hz, 1H, Ar-H_{ortho}), 6.75-6.72 (d, ^3J = 8.9 Hz, 1H, Ar-H_{meta}), 5.30-5.25 (dd~t, $^3J_{3,4}$ = 9.5 Hz, 1H, H-3), 5.24-5.19 (dd, $^3J_{1,2}$ = 7.7 Hz, $^3J_{2,3}$ = 9.5 Hz, 1H, H-2), 5.18-5.13 (dd~t, $^3J_{3,4}$ = 9.5 Hz, 1H, H-4), 4.94 (d, $^3J_{1,2}$ = 7.7 Hz, 1H, H-1), 4.31-4.26 (dd, $^2J_{H6H6'}$ = 12.3 Hz, $^3J_{H5H6}$ = 5.2 Hz, 1H, H-6), 4.17-4.13 (dd, $^2J_{H6H6'}$ = 12.3 Hz, $^3J_{H5H6'}$ = 2.4 Hz, 1H, H-6‘), 3.87 (s, 3H, CH_3), 3.83-3.79 (ddd, $^3J_{H5H6}$ = 5.2 Hz, $^3J_{H5H6'}$ = 2.4 Hz, $^3J_{H4H5}$ = 10.0 Hz, 1H, H-5), 2.08, 2.07, 2.03 (s, each 3H, C=OCH_3) ppm;

^{13}C-NMR ($CDCl_3$, 126 MHz, 300 K): δ = 170.8, 170.4, 169.5 ((C=O)CH_3), 167.8 ((C=O)OCH_3), 148.3 (Ar-$C_{,ipso}$), 145.2 (Ar-$C_{,para}$), 125.6 (Ar-$C_{,ortho}$Ar-$C_{,meta}$H), 119.3 (Ar-$C_{,ortho}$Ar-$C_{,meta}$C=O), 118.8 (Ar-$C_{,meta}$H), 111.9 (Ar-$C_{,meta}$C=O), 100.5 (C-1), 72.8

(C-3), 72.1 (C-5), 71.4 (C-2), 68.4 (C-4), 62.0 (C-6), 52.0 (CH_3), 20.8, 20.7 ($C=OCH_3$) ppm;

IR (ATR): $\tilde{\nu}$ = 3464, 3364, 2960, 1741, 1698, 1499, 1374, 1206, 1028, 812 cm^{-1};

ESI-MS: *m/z* = 520.14242, $[M+Na]^+$; (calc. 520.14255 for $C_{22}H_{27}NO_{12}$+Na).

6-(Amino)-3-(2,3,4,6-tetra-*O*-acetyl-α-D-mannopyranosyloxy)benzoic acid methyl-ester 95

To a solution of mannoside **93** (3.44 g, 6.52 mmol) in ethyl acetate (140 mL) was added a catalytic amount of palladium (10 % on activated charcoal) and the mixture was stirred under hydrogen atmosphere for 16 h. The catalyst was removed by filtration over celite and the solvent was removed under reduced pressure to yield compound **95** quantitatively as a colourless foam.

Yield: quant.;

TLC: R_f = 0.25 (toluene/ ethyl acetate 3:1);

Melting point: 133 °C;

Rotational value: $[\alpha]_{20}^{D}$ = +69.7 (c = 0.58 in ethyl acetate);

^{1}H-NMR ($CDCl_3$, 500 MHz, 300 K): δ = 7.61 (d, ^4J = 2.9 Hz, 1H, C<u>Ar-H</u>$_{ortho}$C(C=O)), 7.10-7.07 (dd, ^3J = 8.9 Hz, ^4J = 3.0 Hz, 1H, Ar-H_{ortho}), 6.73 (d, ^3J = 8.9 Hz, 1H, Ar-H_{meta}), 5.54-5.51 (dd, $^3J_{2,3}$ = 3.5 Hz, $^3J_{3,4}$ = 10.0 Hz, 1H, H-3), 5.43-5.42 (dd, $^3J_{1,2}$ = 1.8 Hz, $^3J_{2,3}$ = 3.5 Hz, 1H, H-2), 5.41 (d, $^3J_{1,2}$ = 1.8 Hz, 1H, H-1), 5.38-5.33 (dd~t, $^3J_{3,4}$ = 10.0 Hz, 1H, H-4), 4.32-4.28 (dd, $^2J_{H6H6'}$ = 12.2 Hz, $^3J_{H5H6}$ = 5.4 Hz, 1H, H-6), 4.14-4.10 (ddd, $^3J_{H5H6}$ = 5.4 Hz, $^3J_{H5H6'}$ = 2.3 Hz, $^3J_{H4H5}$ = 10.0 Hz, 1H, H-5), 4.09-4.05 (dd, $^2J_{H6H6'}$ = 12.2 Hz, $^3J_{H5H6'}$ = 2.3 Hz, 1H, H-6‘), 3.87 (s, 3H, CH_3), 2.19, 2.05, 2.04, 2.03 (s, each 3H, $C=OCH_3$) ppm;

^{13}C-NMR ($CDCl_3$, 126 MHz, 300 K): δ = 170.7, 170.1, 169.9 ((<u>C</u>=O)CH_3), 168.0 ((<u>C</u>=O)OCH_3), 147.0 (Ar-$C_{,ipso}$), 145.2 (Ar-$C_{,para}$), 124.6 (<u>Ar-C</u>$_{,ortho}$Ar-$C_{,meta}$H), 118.9 (Ar-$C_{,meta}$H), 118.2 (<u>Ar-C</u>$_{,ortho}$Ar-$C_{,meta}$C=O), 111.8 (<u>Ar-C</u>$_{,meta}$C=O), 96.8 (C-1), 69.6 (C-2), 69.3 (C-5), 69.0 (C-3), 66.1 (C-4), 62.3 (C-6), 52.0 (CH_3), 21.0, 20.9, 20.8 ($C=OCH_3$) ppm;

IR (ATR): $\tilde{\nu}$ = 3483, 3380, 2955, 1742, 1695, 1495, 1368, 1205, 1034, 977 cm^{-1};

ESI-MS: *m/z* = 498.16059, $[M+H]^+$; (calc. 498.16115 for $C_{22}H_{27}NO_{12}$+H).

p-[(*E*)-*p*'-Acetic acid (*tert*-butyl ester)phenylazo]phenyl-*m*-(methyloxycarbonyl) 2,3,4,6-tetra-*O*-acetyl-β-D-glucopyranoside 96

Glucoside **94** (800 mg, 1.61 mmol) and nitroso compound **18** (2.50 mmol) were dissolved in acetic acid (30 mL) and stirred at room temperature for 2.5 d. After addition of H_2O (50 mL) the mixture was extracted with ethyl acetate (3 x 50 mL). The combined organic layers were dried over $MgSO_4$, filtered and the solvent was removed under reduced pressure. Column chromatography (cyclohexane / ethyl acetate 6:1 → 1:1) gave compound **96** as an orange solid.

Yield: 350 mg (499 µmol, 31 %);

TLC: R_f = 0.40 (cyclohexane / ethyl acetate 1:1);

Melting point: 68 °C;

Rotational value: $[\alpha]_{20}^{D}$ = -5.44 (c = 0.07 in ethyl acetate);

^{1}H-NMR ($CDCl_3$, 500 MHz, 300 K): δ = 7.85-7.82 (m, 2H, Ar-$H_{ortho'}$), 7.72-7.69 (d, ^3J = 8.9 Hz, 1H, Ar-H_{ortho}), 7.43-7.40 (m, 2H, Ar-$H_{meta'}$), 7.37-7.36 (d, ^4J = 2.7 Hz, 1H, Ar-H_{meta}C(C=O)), 7.20-7.17 (m, 2H, Ar-H_{meta}), 5.35-5.30 (m, 2H, H-2, H-3), 5.21-5.15 (m, 2H, H-1, H-4), 4.31-4.26 (dd, $^2J_{H6H6'}$ = 12.3 Hz, $^3J_{H5H6}$ = 5.7 Hz, 1H, H-6), 4.21-4.17 (dd, $^2J_{H6H6'}$ = 12.3 Hz, $^3J_{H5H6'}$ = 2.3 Hz, 1H, H-6'), 3.96-3.92 (ddd, $^3J_{H5H6'}$ = 2.3 Hz, $^3J_{H5H6'}$ = 5.7 Hz, $^3J_{H4H5}$ = 10.0 Hz, H-5), 3.91 (s, 3H, CH_3), 3.60 (s, 2H, CH_2) 2.10, 2.08, 2.06, 2.05 (s, each 3H, C=OCH_3), 1.45 (s, 9H, C(CH_3)$_3$) ppm;

^{13}C-NMR ($CDCl_3$, 126 MHz, 300 K): δ = 170.6, 170.2, 169.4, 169.3 (O(C=O)CH_3), 170.3 (CH_2(C=O)), 167.7 (Ar-C(C=O)), 157.7 (Ar-C_{para}), 151.4 (Ar-$C_{ipso'}$), 147.0 (Ar-C_{ipso}), 138.3 (Ar-$C_{para'}$), 131.1 (Ar-C_{ortho}(C=O)), 130.0 (Ar-$C_{meta'}$), 123.2 (Ar-$C_{ortho'}$), 120.6 (Ar-C_{ortho}H), 120.1 (Ar-$C_{meta}$$CH_{ortho}$), 117.0 (Ar-$C_{meta}$C(C=O)), 98.6 (C-1), 81.2 (C(CH_3)$_3$), 72.6 (C-2), 72.3 (C-5), 71.1 (C-3), 68.2 (C-4), 61.9 (C-6), 52.5 (CH_3), 42.3 (CH_2), 28.0 (C(CH_3)$_3$), 20.6 (C=OCH_3) ppm;

IR (ATR): ṽ = 3250, 2922, 2851, 1745, 1733, 1367, 1212, 1133, 1070, 1033, 1013, 838, 562 cm^{-1};

ESI-MS: *m/z* = 533.21278, $[M+H]^+$; (calc. 532.21352 for $C_{26}H_{32}N_2O_{10}$).

_p_-[(_E_)-_p_'-Acetic acid (_tert_-butyl ester)phenylazo]phenyl-_m_-(methyloxycarbonyl) 2,3,4,6-tetra-_O_-acetyl-α-D-mannopyranoside 97

Mannoside **95** (1.04 g, 2.50 mmol) and nitroso compound **18** (2.50 mmol) were dissolved in acetic acid (30 mL) and stirred at room temperature for 2.5 d. After addition of H_2O (50 mL) the mixture was extracted with ethyl acetate (3 x 80 mL). The combined organic layers were dried over $MgSO_4$, filtered and the solvent was removed under reduced pressure. Column chromatography (cyclohexane / ethyl acetate 6:1 → 1:1) gave compound **97** as an orange solid.

Yield: 433 mg (617 µmol, 25 %);

TLC: R_f = 0.53 (cyclohexane / ethyl acetate 1:1);

Melting point: 73 °C;

Rotational value: $[\alpha]_{20}^{D}$ = +62.3 (c = 0.17 in ethyl acetate);

^{1}H-NMR ($CDCl_3$, 500 MHz, 300 K): δ = 7.85-7.82 (m, 2H, Ar-$H_{ortho'}$), 7.73 (d, ^3J = 8.9 Hz, 1H , Ar-H_{ortho}), 7.51 (d, ^4J = 2.7 Hz, 1H , Ar-H_{meta}C(C=O)), 7.43-7.40 (m, 2H, Ar-$H_{meta'}$), 7.29 (dd, ^4J = 2.7 Hz, ^3J = 8.9 Hz, 1H, Ar-H_{meta}), 5.63 (d, $^3J_{1,2}$ = 1.8 Hz, H-1), 5.58-5.54 (dd, $^3J_{2,3}$ = 3.5 Hz, $^3J_{3,4}$ = 10.0 Hz, 1H, H-3), 5.49-5.47 (dd, $^3J_{1,2}$ = 1.8 Hz, $^3J_{2,3}$ = 3.5 Hz, 1H, H-2), 5.40-5.35 (dd~t, $^3J_{3,4}$ = 10.0 Hz, 1H, H-4), 4.32-4.27 (dd, $^2J_{H6H6'}$ = 12.8 Hz, $^3J_{H5H6}$ = 6.3 Hz, 1H, H-6), 4.10-4.05 (m, 2H, H-5, H-6'), 3.92 (s, 3H, CH_3), 3.60 (s, 2H, CH_2) 2.22, 2.07, 2.05, 2.04 (s, each 3H, C=OCH_3), 1.45 (s, 9H, C(CH_3)$_3$) ppm;

^{13}C-NMR ($CDCl_3$, 126 MHz, 300 K): δ = 170.6, 170.3, 169.9, 169.7 (O(C=O)CH_3, CH_2(C=O)), 167.5 (Ar-C(C=O)), 156.5 (Ar-C_{para}), 151.5 (Ar-$C_{ipso'}$), 146.8 (Ar-C_{ipso}), 138.3 (Ar-$C_{para'}$), 131.3 (Ar-C_{ortho}(C=O)), 130.0 (Ar-$C_{meta'}$), 123.3 (Ar-$C_{ortho'}$), 120.5 (Ar-C_{ortho}H), 119.6 (Ar-$C_{meta}$$CH_{ortho}$), 116.7 (Ar-$C_{meta}$C(C=O)), 95.7 (C-1), 81.2 (C(CH_3)$_3$), 69.6 (C-5), 69.1 (C-2), 68.7 (C-3), 65.8 (C-4), 62.1 (C-6), 52.6 (CH_3), 42.6 (CH_2), 28.0 (C(CH_3)$_3$), 20.9, 20.7, 20.6 (C=OCH_3) ppm;

IR (ATR): $\tilde{\nu}$ = 2924, 2853, 1732, 1560, 1436, 1368, 1211, 1132, 1030, 980, 837 cm^{-1};

ESI-MS: *m/z* = 533.21325, $[M+H]^+$; (calc. 532.21352 for $C_{26}H_{32}N_2O_{10}$).

_p_-[(_E_)-_p_'-Acetic acid (_tert_-butyl ester)phenylazo]phenyl-_m_-(methyloxycarbonyl) β-D-glucopyranoside 98

Sodium methoxide (8.40 mg, 156 µmol) was added to a solution of compound **96** (350 mg, 499 µmol) in dry methanol (10 mL). After stirring at room temperature for 16 h the mixture was neutralised with Amberlite® IR 120 and filtered. The solvent was removed under reduced pressure to yield compound **96** after column chromatography (ethyl acetate → ethyl acetate / methanol 9:1) as an orange solid.

Yield: 236 mg (443 µmol, 89 %);

TLC: R_f = 0.49 (ethyl acetate / methanol 7:1);

Melting point: 96 °C;

Rotational value: $[\alpha]_{20}^{D}$ = -32.8 (c = 0.08 in methanol);

^{1}H-NMR (MeOD, 600 MHz, 300 K): δ = 7.83-7.80 (m, 2H, Ar-H$_{ortho'}$), 7.78-7.75 (d, ^{3}J = 8.9 Hz, 1H , Ar-H$_{ortho}$), 7.45-7.42 (m, 3H , Ar-H$_{meta}$C(C=O), Ar-H$_{meta'}$), 7.37-7.35 (dd, ^{4}J = 2.7 Hz, ^{3}J = 8.9 Hz, 1H, Ar-H$_{meta}$), 5.06-5.03 (d, $^3J_{1,2}$ = 7.5 Hz, 1H, H-1), 3.94-3.89 (m, 4H, H-6, CH$_3$), 3.74-3.70 (dd, $^3J_{5,6'}$ = 5.7 Hz, $^2J_{6,6'}$ = 12.1 Hz, 1H, H-6'), 3.64 (s, 2H, CH$_2$), 3.53-3.49 (m, 3H, H-2, H-3, H-4), 3.44-3.40 (m, 1H, H-5), 1.45 (s, 9H, C(CH$_3$)$_3$) ppm;

^{13}C-NMR (MeOD, 151 MHz, 300 K): δ = 172.4 (CH$_2$(C=O)), 169.8 (Ar-C(C=O)), 160.5 (Ar-C$_{para}$), 152.9 (Ar-C$_{ipso'}$), 147.1 (Ar-C$_{ipso}$), 139.8 (Ar-C$_{para'}$), 132.7 (Ar-C$_{ortho}$(C=O)), 131.2 (Ar-C$_{meta'}$), 124.0 (Ar-C$_{ortho'}$), 121.8 (Ar-C$_{ortho}$H), 120.6 (Ar-C$_{meta}$CH$_{ortho}$), 118.0 (Ar-C$_{meta}$C(C=O)), 102.1 (C-1), 82.3 (C(CH$_3$)$_3$), 78.4 (C-4), 77.9 (C-3), 74.8 (C-2), 71.3 (C-5), 62.4 (C-6), 53.0 (CH$_3$), 43.2 (CH$_2$), 28.3 (C(CH$_3$)$_3$) ppm;

IR (ATR): ṽ = 3361, 2927, 1722, 1600, 1438, 1368, 1286, 1150, 1070, 1043, 1013, 834, 528 cm^{-1};

ESI-MS: _m/z_ = 554.5, [M+Na]$^+$; (calc. 532.21352 for $C_{26}H_{32}N_2O_{10}$).

p-[(*E*)-*p*'-Acetic acid (*tert*-butyl ester)phenylazo]phenyl-*m*-(methyloxycarbonyl) α-D-mannopyranoside 99

Sodium methoxide (10.4 mg, 193 µmol) was added to a solution of compound **97** (533 mg, 617 µmol) in dry methanol (30 mL). After stirring at room temperature for 16 h the mixture was neutralised with Amberlite® IR 120 and filtered. The solvent was removed under reduced pressure to yield compound **99** as an orange syrup.

Yield: 312 mg (585 µmol, 95 %);

TLC: R_f = 0.49 (ethyl acetate / methanol 7:1);

Melting point: 55 °C (decomposition);

Rotational value: $[\alpha]_{20}^{D}$ = +120.2 (c = 0.11 in methanol);

^{1}H-NMR (MeOD, 500 MHz, 300 K): δ = 7.82-7.79 (m, 2H, Ar-H*$_{ortho'}$*), 7.76 (d, ^{3}J = 8.9 Hz, 1H , Ar-H*$_{ortho}$*), 7.46-7.45 (d, ^{4}J = 2.7 Hz, 1H , Ar-H*$_{meta}$*C(C=O)), 7.45-7.42 (m, 2H, Ar-H*$_{meta'}$*), 7.40-7.37 (dd, ^{4}J = 2.7 Hz, ^{3}J = 8.9 Hz, 1H, Ar-H*$_{meta}$*), 5.63 (d, $^3J_{1,2}$ = 1.8 Hz, H-1), 4.06-4.04 (dd, $^3J_{1,2}$ = 1.8 Hz, $^3J_{2,3}$ = 3.4 Hz, 1H, H-2), 3.93-3.89 (m, 4H, H-3, CH_3), 3.80-3.70 (m, 3H, H-4, H-6, H-6'), 3.64 (s, 2H, CH_2), 3.59-3.55 (ddd, $^3J_{H5H6}$ = 5.5 Hz, $^3J_{H5H6'}$ = 2.4 Hz, $^3J_{H4H5}$ = 9.7 Hz, 1H, H-5), 1.45 (s, 9H, $C(CH_3)_3$) ppm;

^{13}C-NMR (MeOD, 126 MHz, 300 K): δ = 172.4 (CH_2(C=O)), 169.8 (Ar-C(C=O)), 159.4 (Ar-C*$_{para}$*), 152.9 (Ar-C*$_{ipso'}$*), 147.1 (Ar-C*$_{ipso}$*), 139.9 (Ar-C*$_{para'}$*), 132.9 (Ar-C*$_{ortho}$*(C=O)), 131.3 (Ar-C*$_{meta'}$*), 124.1 (Ar-C*$_{ortho'}$*), 122.0 (Ar-C*$_{ortho}$*H), 120.7 (Ar-C*$_{meta}$*C*H$_{ortho}$*), 117.8 (Ar-C*$_{meta}$*C(C=O)), 100.3 (C-1), 82.4 ($C(CH_3)_3$), 75.9 (C-5), 72.4 (C-3), 71.8 (C-2), 68.3 (C-4), 62.7 (C-6), 53.1 (CH_3), 43.3 (CH_2), 28.3 ($C(CH_3)_3$) ppm;

IR (ATR): ṽ = 3362, 2930, 1697, 1597, 1495, 1438, 1206, 1006, 977, 818, 410 cm^{-1};

ESI-MS: *m/z* = 555.2, $[M+Na]^+$; (calc. 532.21352 for $C_{26}H_{32}N_2O_{10}$).

p-[(*E*)-*p*'-(Acetic acid)phenylazo]phenyl-*m*-(methyloxycarbonyl) 2,3,4,6-tetra-*O*-acetyl-β-D-glucopyranoside 100

Trifluoroacetic acid (1.50 mL, 19.5 mmol) was added to a solution of glucoside **98** (80.0 mg, 164 µmol) in DCM (15 mL). After stirring at room temperature for 16 h the solvent was removed under reduced pressure. Codestillation with toluene (3 x 30 mL) yielded compound **100** as a red syrup in quantitative yield.

Yield: quant.;

TLC: R_f = 0.0 (ethyl acetate / methanol 7:1);

Melting point: 98 °C (decomposition);

Rotational value: $[\alpha]_{20}^{D}$ = -13.1 (c = 0.01 in methanol);

^{1}H-NMR (MeOD, 500 MHz, 300 K): δ = 7.83-7.80 (m, 2H, Ar-H*ortho‘*), 7.77-7.75 (d, ^{3}J = 8.9 Hz, 1H , Ar-H*ortho*), 7.48-7.45 (m, 2H, Ar-H*meta‘*), 7.43-7.42 (d, ^{4}J = 2.7 Hz, 1H, Ar-H*meta*C(C=O)), 7.37-7.34 (dd, ^{4}J = 2.7 Hz, ^{3}J = 8.9 Hz, 1H, Ar-H*meta*), 5.05-5.03 (m, 1H, H-1), 3.93-3.88 (m, 4H, H-6, CH_3), 3.76-3.68 (m, 3H, H-6‘, CH_2), 3.54-3.48 (m, 3H, H-2, H-3, H-4), 3.43-3.38 (m, 1H, H-5) ppm;

^{13}C-NMR (MeOD, 126 MHz, 300 K): δ = 175.0 (CH_2(C=O)), 169.9 (Ar-C(C=O)), 160.8 (Ar-C*para*), 152.7 (Ar-C*ipso‘*), 147.1 (Ar-C*ipso*), 140.0 (Ar-C*para‘*), 132.7 (Ar-C*ortho*(C=O)), 131.5 (Ar-C*meta‘*), 124.0 (Ar-C*ortho‘*), 121.9 (Ar-C*ortho*H), 120.5 (Ar-C*meta*CH_3*ortho*), 118.2 (Ar-C*meta*C(C=O)), 102.1 (C-1), 78.3 (C-4), 77.9 (C-3), 75.0 (C-2), 71.3 (C-5), 62.5 (C-6), 53.2 (CH_3), 41.4 (CH_2) ppm;

IR (ATR): $\tilde{\nu}$ = 3325, 2920, 1716, 1600, 1438, 1288, 1226, 1070, 1013, 831, 801, 559, 518 cm^{-1};

ESI-MS: *m/z* = 516.16645, $[M+K+H]^+$; (calc. 476.14310 for $C_{22}H_{24}N_2O_{10}$).

p-[(*E*)-*p*'-(Acetic acid)phenylazo]phenyl-*m*-(methyloxycarbonyl) 2,3,4,6-tetra-*O*-acetyl-α-D-mannopyranoside 101

Trifluoroacetic acid (2.37 mL, 30.8 mmol) was added to a solution of mannoside **99** (170 mg, 347 µmol) in DCM (20 mL). After stirring at room temperature for 5 h the solvent was removed under reduced pressure. Codestillation with toluene (3 x 30 mL) yielded compound **101** as a red syrup in quantitative yield.

Yield: quant.;

TLC: R_f = 0.0 (ethyl acetate / methanol 7:1);

Melting point: 207 °C (decomposition);

Rotational value: $[\alpha]_{20}^{D}$ = +75.2 (c = 0.11 in methanol);

^{1}H-NMR (MeOD, 500 MHz, 300 K): δ = 7.83-7.79 (m, 2H, Ar-H*ortho‘*), 7.78-7.75 (d, ^{3}J = 8.9 Hz, 1H , Ar-H*ortho*), 7.49-7.43 (m, 3H, Ar-H*meta*C(C=O), Ar-H*meta‘*), 7.40-7.37 (dd, ^{4}J = 2.7 Hz, ^{3}J = 8.9 Hz, 1H, Ar-H*meta*), 5.63 (d, $^{3}J_{1,2}$ = 1.8 Hz, 1H, H-1), 4.06-4.04 (dd, $^{3}J_{1,2}$ = 1.8 Hz, $^{3}J_{2,3}$ = 3.4 Hz, 1H, H-2), 3.93-3.90 (dd, $^{3}J_{2,3}$ = 3.4 Hz, $^{3}J_{3,4}$ = 9.6 Hz, 1H, H-3), 3.90 (s, 3H, CH_3), 3.80-3.70 (m, 5H, H-4, H-6, H-6‘, CH_2), 3.59-3.55 (ddd, $^{3}J_{H5H6}$ = 5.5 Hz, $^{3}J_{H5H6‘}$ = 2.5 Hz, $^{3}J_{H4H5}$ = 9.9 Hz, 1H, H-5) ppm;

^{13}C-NMR (MeOD, 126 MHz, 300 K): δ = 172.0 (CH_2(C=O)), 169.8 (Ar-C(C=O)), 159.4 (Ar-C*para*), 152.7 (Ar-C*ipso‘*), 147.0 (Ar-C*ipso*), 139.4 (Ar-C*para‘*), 132.9 (Ar-C*ortho*(C=O)), 131.5 (Ar-C*meta‘*), 127.9 (Ar-C*ortho‘*), 122.0 (Ar-C*ortho*H), 120.7 (Ar-C*meta*C*ortho*), 117.8 (Ar-C*meta*C(C=O)), 100.3 (C-1), 75.9 (C-5), 72.4 (C-3), 71.8 (C-2), 68.3 (C-4), 62.7 (C-6), 53.1 (CH_3), 40.5 (CH_2) ppm;

IR (ATR): ṽ = 3355, 1678, 1440, 1201, 1135, 1037, 1029, 801, 723, 503 cm^{-1};

ESI-MS: *m/z* = 381.29691, [M-CO_2CH_3-CH_2COOH+Na]$^{+}$; (calc. 476.14310 for $C_{22}H_{24}N_2O_{10}$).

p-[(*E*)-*p*'-(Phenylthioacetate)phenylazo]phenyl-*m*-(methyloxycarbonyl) 2,3,4,6-tetra-*O*-acetyl-β-D-glucopyranoside 102

Triethylamine (45.5 µL, 328 µmol) was added to an icecold solution of glucoside **100** (78.1 mg, 164 µmol), DEPC (**77**) (52.9 µL, 328 µmol) and thiophenol (25.4 µL, 246 µmol) in DMF (10 mL). The reaction mixture was stirred for 16 h at room temperature. The solvent was then removed under reduced pressure and the crude product was purified by column chromatography (ethyl acetate/methanol 30:1 → 9:1) to yield compound **102** as a red solid.

Yield: 46.5 mg (81.8 µmol, 50 %);

TLC: R_f = 0.21 (ethyl acetate/methanol 12:1);

Melting point: 80 °C;

Rotational value: $[\alpha]_{20}^{D}$ = -23.6 (c = 0.12 in methanol);

^{1}H-NMR (MeOD, 500 MHz, 300 K): δ = 7.86-7.82 (m, 2H, Ar-H*ortho‘*), 7.78-7.75 (m, 1H , Ar-H*ortho*), 7.52-7.48 (m, 2H, Ar-H*meta‘*), 7.45-7.31 (m, 7H, Ar-H*meta*C(C=O)), Ar-H*meta*, SPh), 5.06-5.03 (m, 1H, H-1), 4.07 (s, 1H, CH_2), 3.93-3.88 (m, 4H, H-6, CH_3), 3.74-3.70

(dd, $^{3}J_{5,6}$ = 5.7 Hz, $^{2}J_{6,6'}$ = 12.2 Hz, 1H, H-6'), 3.54-3.47 (m, 3H, H-2, H-3, H-4), 3.43-3.39 (m, 1H, H-5) ppm;

^{13}C-NMR (MeOD, 126 MHz, 300 K): δ = 196.5 (CH_2(C=O)), 169.9 (Ar-C(C=O)), 153.1 (Ar-C_{ipso}), 152.9 (Ar-$C_{ipso'}$), 146.7 (Ar-C_{para}), 138.5 (Ar-$C_{para'}$), 135.7 (Ar-C_{meta}C(C=O)), 131.6 (Ar-$C_{meta'}$), 130.7, 130.1 (SPh), 124.1 (Ar-$C_{ortho'}$), 121.9 (Ar-C_{ortho}H), 120.6 (Ar-$C_{meta}CH_{ortho}$), 118.1 (Ar-C_{meta}C(C=O)), 102.2 (C-1), 78.5 (C-4), 74.8 (C-3), 73.0 (C-2), 71.2 (C-5), 62.3 (C-6), 53.1 (CH_3), 50.2 (CH_2) ppm;

IR (ATR): $\tilde{\nu}$ = 3372, 2919, 1703, 1600, 1228, 1071, 1043, 1011, 745 cm^{-1}.

ESI-MS: *m/z* = 569.15937, $[M+H]^+$; (calc. 569.15938 for $C_{28}H_{28}N_2O_9S$+H).

p-[(*E*)-*p*'-(Phenylthioacetate)phenylazo]phenyl-*m*-(methyloxycarbonyl) 2,3,4,6-tetra-*O*-acetyl-α-D-mannopyranoside 103

Triethylamine (83.2 µL, 600 µmol) was added to an icecold solution of glucoside **101** (143 mg, 300 µmol), DEPC (**77**) (96.7 µL, 600 µmol) and thiophenol (46.4 µL, 450 µmol) in DMF (6 mL). The reaction mixture was stirred for 16 h at room temperature. The solvent was then removed under reduced pressure and the crude product was purified by column chromatography (ethyl acetate/methanol 30:1 → 9:1) to yield compound **103** as a red solid.

Yield: 80.2 mg (141 µmol, 47 %);

TLC: R_f = 0.21 (ethyl acetate/methanol 12:1);

Melting point: 53 °C;

Rotational value: $[\alpha]_{20}^{D}$ = +93.0 (c = 0.08 in methanol);

^{1}H-NMR (MeOD, 500 MHz, 300 K): δ = 7.85-7.79 (m, 2H, Ar-$H_{ortho'}$), 7.78-7.75 (m, 1H , Ar-H_{ortho}), 7.52-7.48 (m, 2H, Ar-$H_{meta'}$), 7.47-7.44 (m, 2H, Ar-H_{meta}C(C=O), Ar-H_{meta}), 7.42-7.32 (m, 5H, SPh), 5.63 (s, 1H, H-1), 4.06-4.04 (dd, $^{3}J_{1,2}$ = 1.8 Hz, $^{3}J_{2,3}$ = 3.3 Hz, 1H, H-2), 3.93-3.88 (m, 4H, H-3, CH_3), 3.80-3.67 (m, 5H, H-4, H-6, H-6', CH_2), 3.59-3.55 (ddd, $^{3}J_{H5H6}$ = 5.4 Hz, $^{3}J_{H5H6'}$ = 2.4 Hz, $^{3}J_{H4H5}$ = 9.7 Hz, 1H, H-5) ppm;

^{13}C-NMR (MeOD, 126 MHz, 300 K): δ = 173.6 (CH_2(C=O)), 169.6 (Ar-C(C=O)), 159.5 (Ar-C_{para}), 153.3 (Ar-$C_{ipso'}$), 147.0 (Ar-C_{ipso}), 139.2 (Ar-$C_{para'}$), 135.7 (SPh), 132.7 (Ar-C_{ortho}(C=O)), 131.6 (Ar-$C_{meta'}$), 130.3, 128.6 (SPh), 124.2 (Ar-$C_{ortho'}$), 121.7

(Ar-C_{ortho}H), 120.7 (Ar-$C_{meta}$$CH_{ortho}$), 118.0 (Ar-$C_{meta}$C(C=O)), 100.2 (C-1), 75.8 (C-5), 72.4 (C-3), 71.8 (C-2), 68.3 (C-4), 62.6 (C-6), 53.1 (CH_3), 41.7 (CH_2) ppm;

IR (ATR): $\tilde{\nu}$ = 3358, 1728, 1598, 1436, 1218, 1005, 973, 818, 689, 415 cm^{-1}.

ESI-MS: *m/z* = 569.15878, $[M+H]^+$; (calc. 569.15883 for $C_{28}H_{28}N_2O_9S$+H).

N-(Acetyl)-*O*-[4-[(*E*)-(2-phenyl)azo)phenyl acetate]]-L-tyrosine ethyl ester 108

DCC (227 mg, 1.10 mmol) was added to an ice-cold solution of thioester **81** (240 mg, 1.00 mmol), *N*-(Acetyl)-L-tyrosine ethyl ester **107** (538 mg, 2.00 mmol) and DMAP (61.0 mg, 500 µmol) in dry DCM (40 mL). The mixture was stirred at room temperature for 16 h. The mixture was then diluted with DCM (30 mL) and washed with 1 N HCl (aq.) (40 mL) and subsequently with sat. $NaHCO_3$ solution (40 mL). The organic layer was dried over $MgSO_4$, filtered and the solvent was removed under reduced pressure. Compound **121** was obtained after repeated column chromatography (cyclohexane/ ethyl acetate 4:1 → 1:2; toluene/ ethyl acetate 9:1 → 4:1) as an orange solid.

Yield: 277 mg (585 mmol, 58 %);

TLC: R_f = 0.29 (ethyl acetate/ cyclohexane 2:1);

Melting point: 146 °C;

^{1}H-NMR ($CDCl_3$, 500 MHz, 300 K): δ = 7.95-7.90 (m, 4H, Ar-H_{ortho}, Ar-$H_{ortho'}$), 7.55-7.46 (m, 5H, Ar-H_{meta}, Ar-$H_{meta'}$, Ar-H_{para}), 7.12-7.08 (m, 2H, Ar-$H_{meta, Tyr}$), 7.02-6.98 (m, 2H, Ar-$H_{ortho, Tyr}$), 5.93-5.89 (d, $^3J_{CHNH}$ = 17.6 Hz, NH), 4.86-4.82 (m, 1H, C<u>H</u>NH), 4.19-4.12 (m, 2H, C<u>H</u>$_2$$CH_3$), 3.93 (s, 2H, Ar-$CCH_2$) 3.13-3.10 (dd, $^2J_{CH2}$ = 5.8 Hz, $^3J_{CH2CH}$ = 2.5 Hz, 2H, C<u>H</u>$_2$CH), 1.98 (s, 3H, (C=O)CH_3), 1.26-1.21 (t, $^3J_{CH2CH3}$ = 7.0 Hz, 3H, CH_3) ppm;

^{13}C-NMR ($CDCl_3$, 126 MHz, 300 K): δ = 171.7 ((<u>C</u>=O)OCH_2CH_3), 169.7 (NH(C=O)), 169.6 (CH_2(C=O)), 152.8 (Ar-$C_{ipso'}$), 152.1 (Ar-C_{ipso}), 149.9 (Ar-$C_{ipso, Tyr}$), 136.5 (Ar-C_{para}), 133.9 (Ar-$C_{para, Tyr}$), 131.2 (Ar-$C_{para'}$), 130.5 (Ar-$C_{meta, Tyr}$), 130.3 (Ar-$C_{meta'}$), 129.3 (Ar-C_{meta}), 123.4, 123.0 (Ar-C_{ortho}, Ar-$C_{ortho'}$), 121.6 (Ar-$C_{ortho, Tyr}$), 61.8 (<u>C</u>H_2CH_3), 53.2 (CHNH), 41.5 (Ar-CCH_2), 37.4 (<u>C</u>H_2CH), 23.3 (NH(C=O)CH_3), 14.3 (CH_2<u>C</u>H_3) ppm;

IR (ATR): $\tilde{\nu}$ = 3328, 2984, 1745, 1729, 1648, 1546, 1349, 1218, 1195, 1169, 1148, 1043, 806, 689, 542, 455 cm^{-1};

EI-MS: *m/z* = 473.19459, $[M]^+$; (calc. 473.19507 for $C_{27}H_{27}N_3O_5$).

8.5.2 Procedure for photoirradiation experiments

E → *Z* isomerisation was induced by irradiation using a LED (emitting 365 nm light) from the Nichia Corporation (NC4U133A) with a FWHW of 10 nm and an intensity of 25 mW/cm^2. *Z* → *E* isomerisation was performed by irradiation of the probe with a LED (emitting 440 nm light) from the Nichia Corporation with a FWHW of 45 nm and an intensity of 1 mW/cm^2. Photostationary states were determined by ^{1}H NMR spectroscopy. Therefore, the samples of azobenzene derivatives were dissolved in the respective solvent and were stored at 40 °C overnight to gain the *E*-isomer. Then, the probe was stored in the dark before ^{1}H NMR spectroscopy was performed. Afterwards, the probe was irradiated with a 365 nm emitting LED for 20-30 min (with approximately 5 cm between the LED and the probe) to reach the photostationary state (PSS). The sample again was stored in the dark and ^{1}H NMR spectroscopy was performed immediately afterwards. The PSS was determined by integration of the the *Z* and *E* signals of a well separated signal which is influenced by *E*/*Z* isomerisation. In case of glycosides the H-1 proton lends itself otherwise the CH_2 moiety shows a suitable singulett for integration.

By analogy, samples for UV/Vis spectroscopy were prepared. The *E*-isomers of the azobenzene derivatives were dissolved in the respective solvent in a UV cuvette and then irradiated for 15 min at 365 nm with a distance between the LED and the cuvette of approximately 5 cm. UV/Vis spectra of the *Z*-isomers were recorded immediately afterwards on PerkinElmer Lambda 241. Subsequent irradiation with 440 nm restored the *E*-isomers. Spectra were also recorded.

The kinetics of the thermal Z→E relaxation process were determined by ^{1}H NMR spectroscopy in the dark. The half-life $\tau_{1/2}$ was determined as $\tau_{1/2} = \ln 2/k$. After irradiation, the ^{1}H NMR spectra of the samples were recorded in regular intervals (1 h) over a period of 3 to 5 days. For the determination of the half-life, signals which are influenced by *E*/*Z* isomerisation, were integrated, both for the *Z*- and the *E*-isomer. In case of glycosides the H-1 proton lends itself otherwise the CH_2 shows a suitable singulett for integration. The decay of the integral of the *Z*- and the increase of the integral of the *E*-isomer were charted. The decay of the integral of the *Z*-isomer was plotted and an exponential decay of first order was fitted for the obtained data. Half-lifes for compounds which just show *E*/*Z* isomerisation at low concentrations were determined via UV/Vis spectroscopy (cf. chapter 3.2.3).

8.5.3 ^{1}H and ^{13}C NMR spectra of synthesised compounds

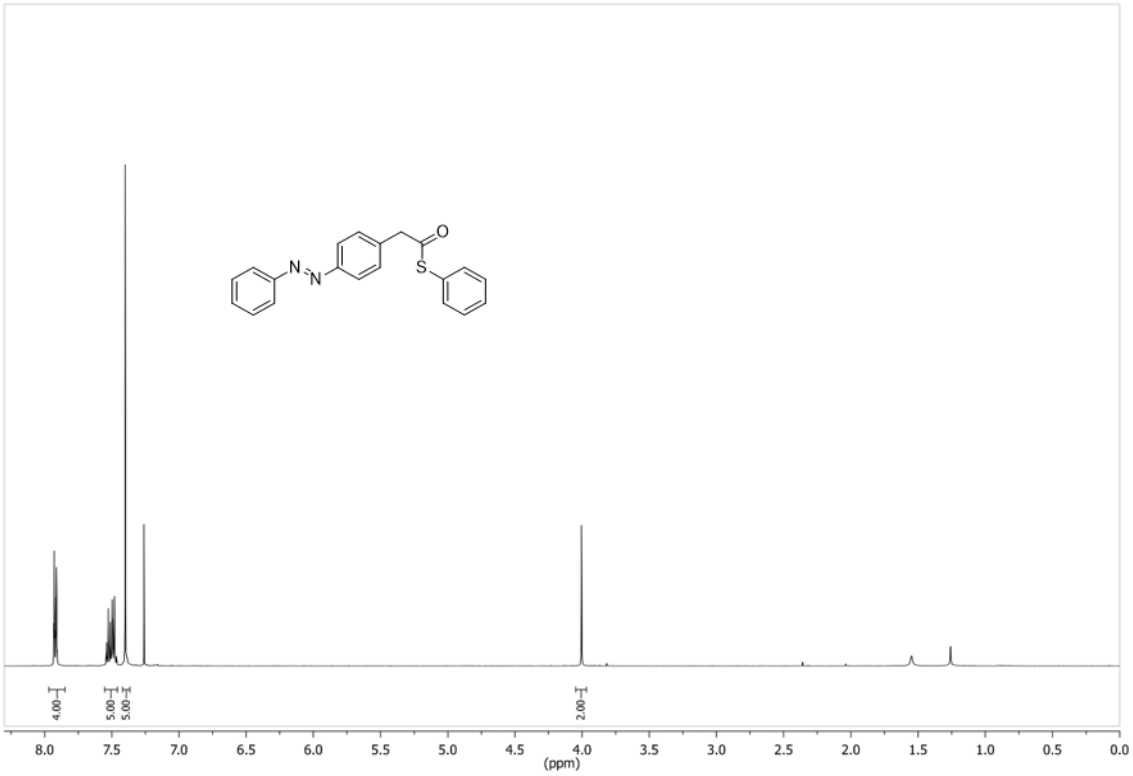

Figure 279: ^{1}H NMR spectrum of compound **7** (500 MHz, $CDCl_3$, 300 K).

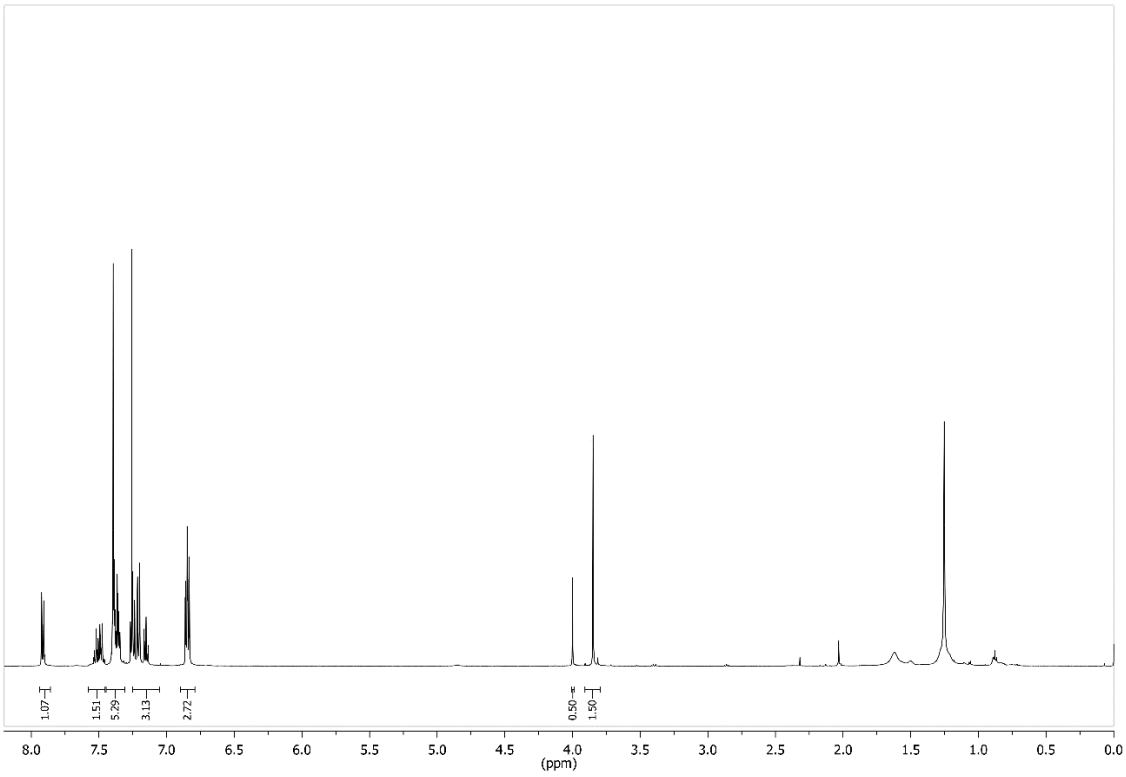

Figure 280: ^{1}H NMR spectrum of compound **7** (*Z*-isomer) (500 MHz, $CDCl_3$, 300 K).

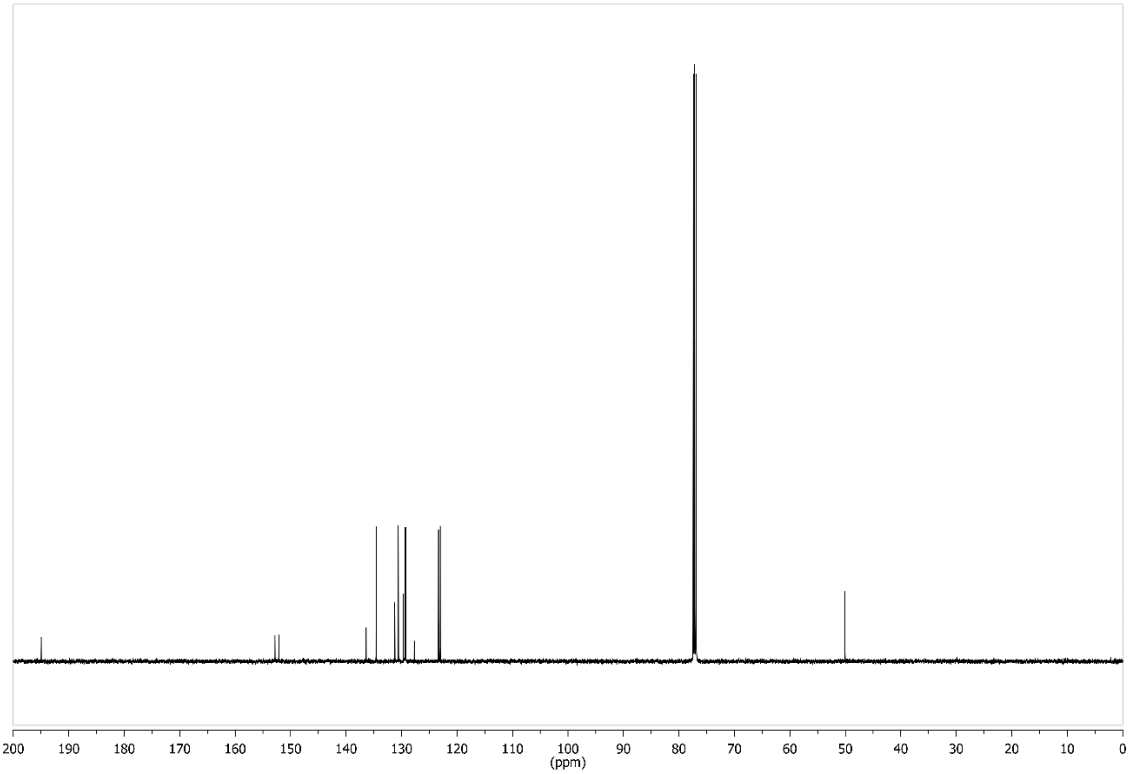

Figure 281: ^{13}C NMR spectrum of compound **7** (126 MHz, $CDCl_3$, 300 K).

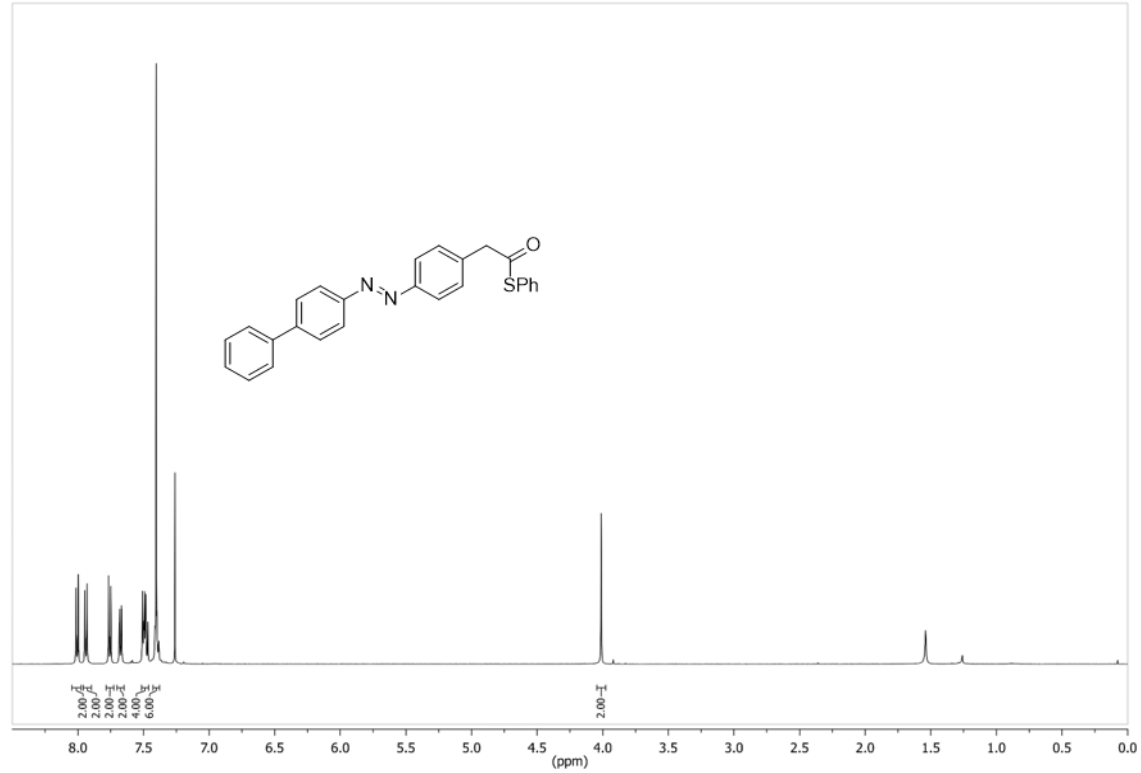

Figure 282: ^{1}H NMR spectrum of compound **8** (500 MHz, $CDCl_3$, 300 K).

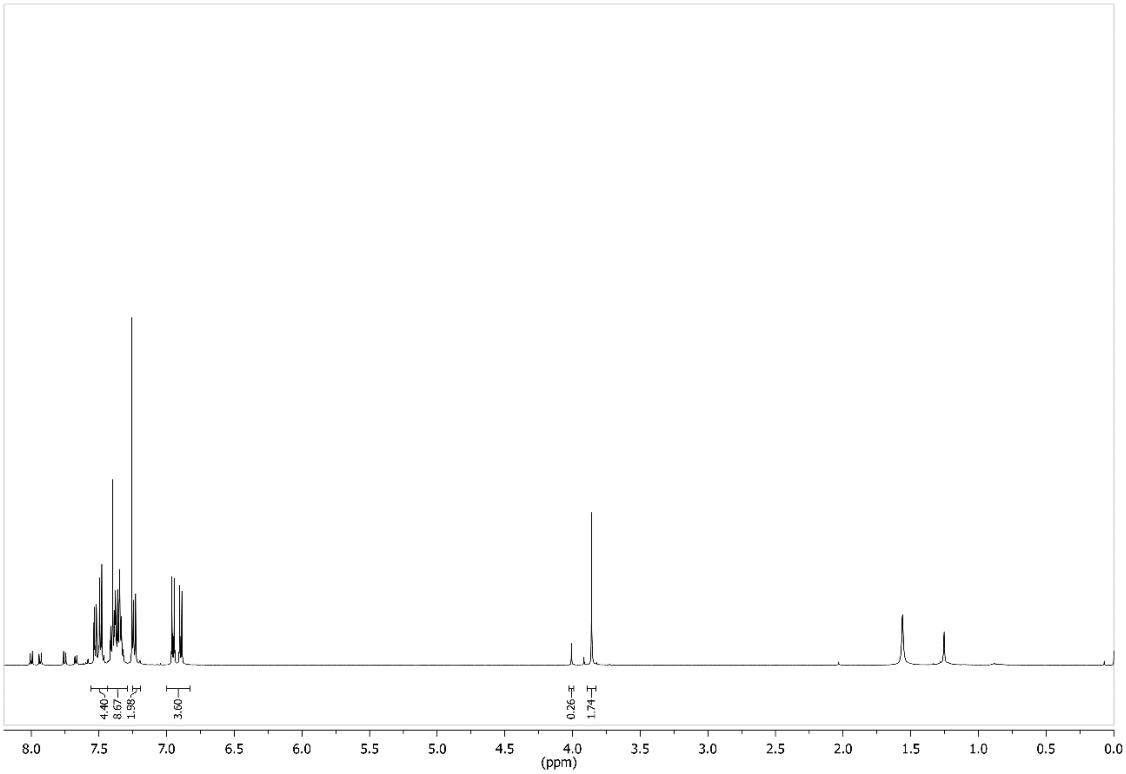

Figure 283: ^{1}H NMR spectrum of compound **8** (*Z*-isomer) (500 MHz, $CDCl_3$, 300 K).

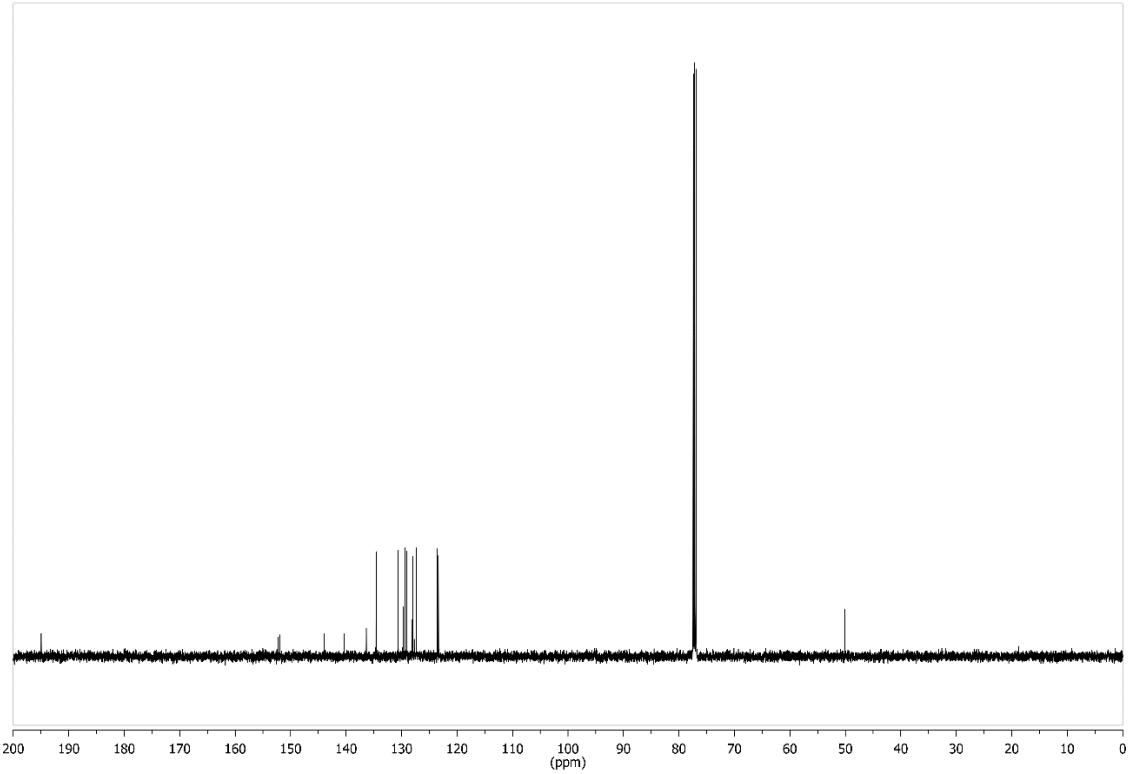

Figure 284: ^{13}C NMR spectrum of compound **8** (126 MHz, $CDCl_3$, 300 K).

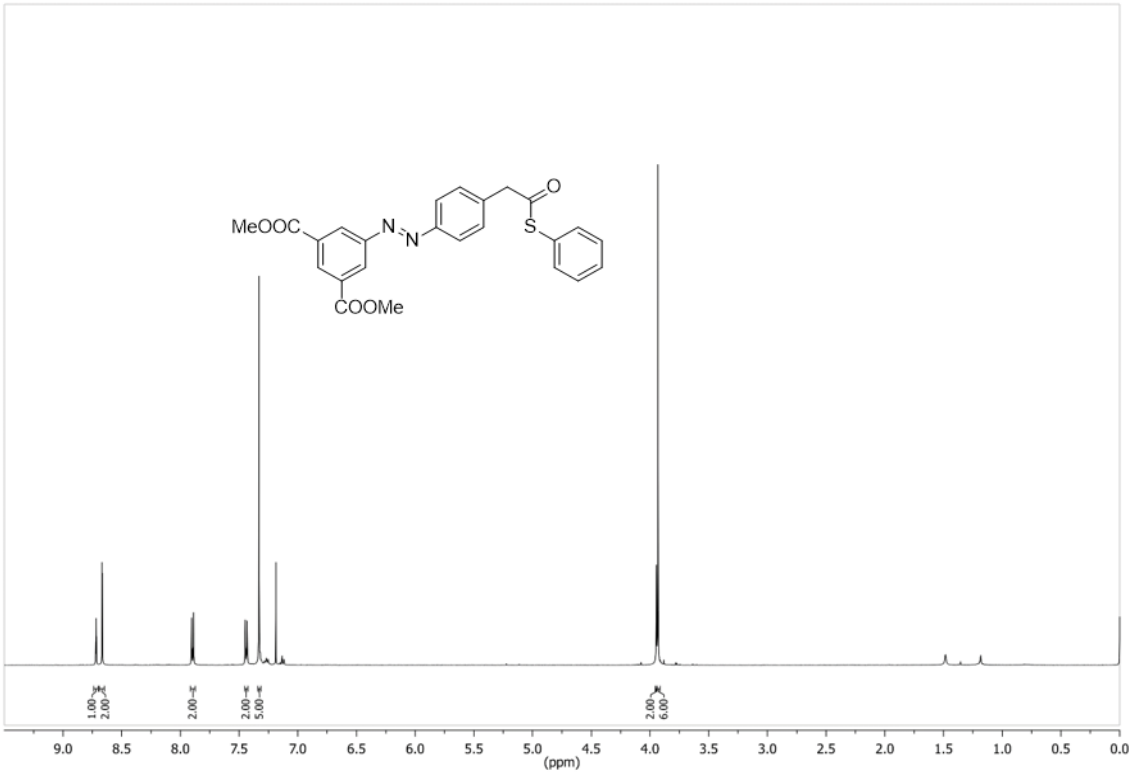

Figure 285: ^{1}H NMR spectrum of compound **9** (500 MHz, $CDCl_3$, 300 K).

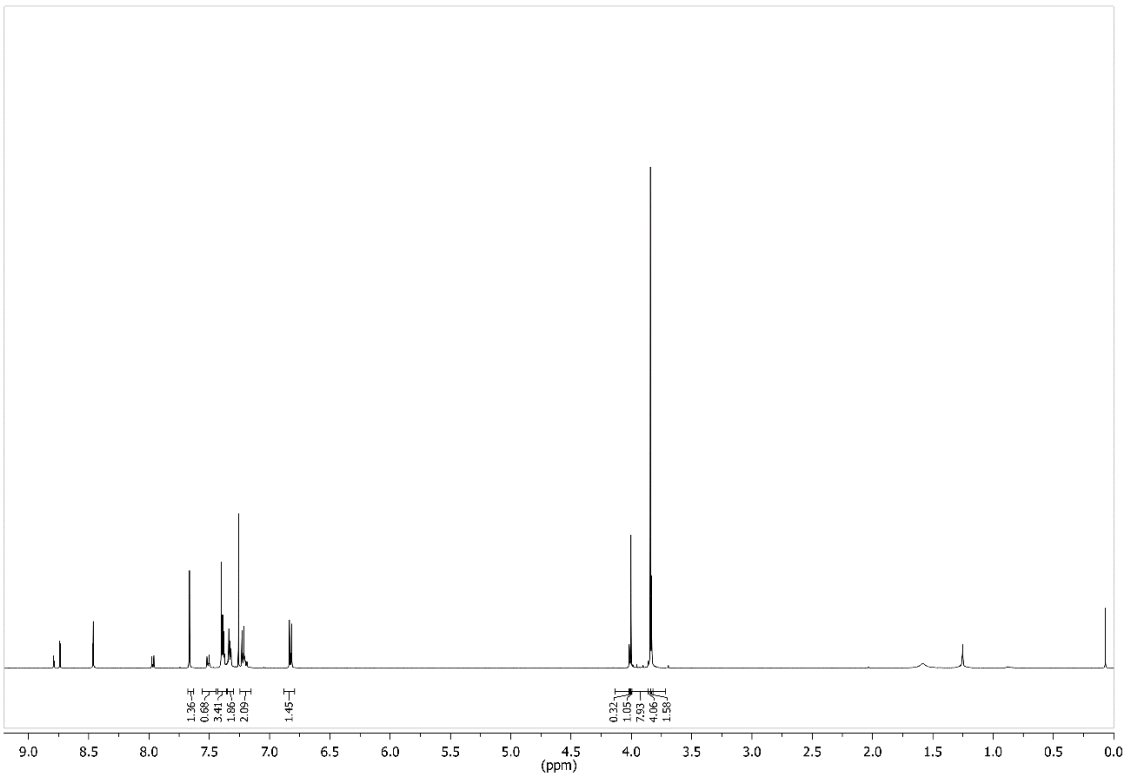

Figure 286: ^{1}H NMR spectrum of compound **9** (*Z*-isomer) (500 MHz, $CDCl_3$, 300 K).

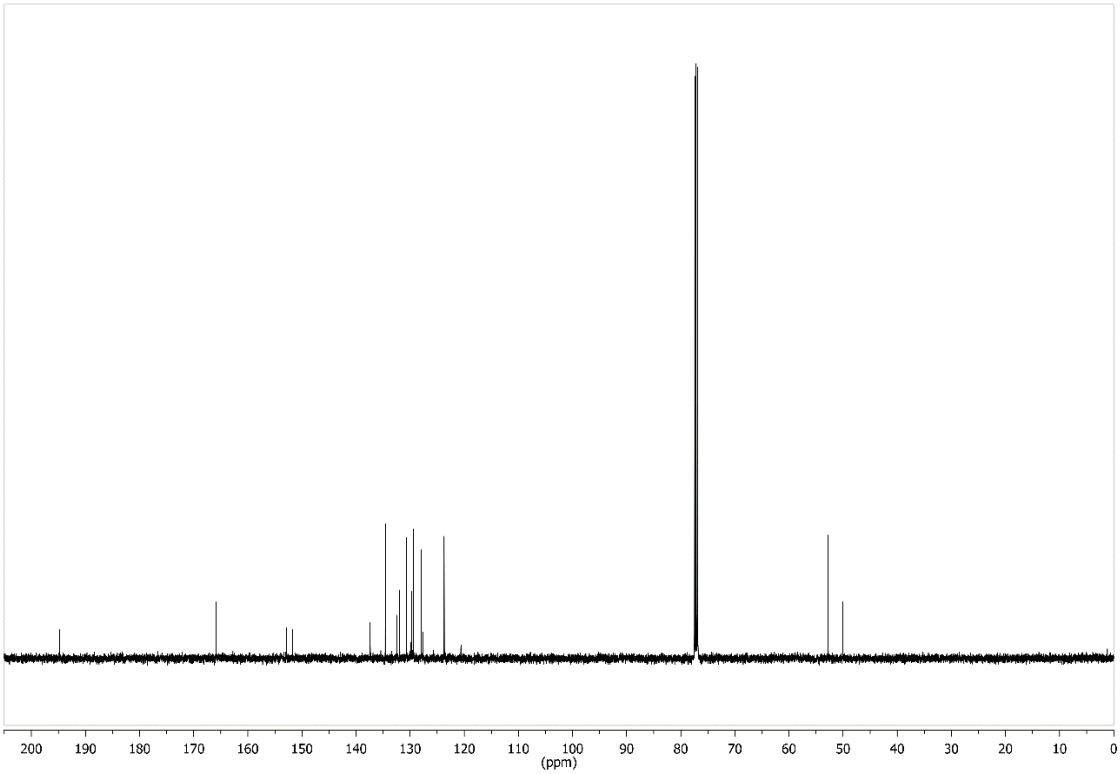

Figure 287: ^{13}C NMR spectrum of compound **9** (126 MHz, $CDCl_3$, 300 K).

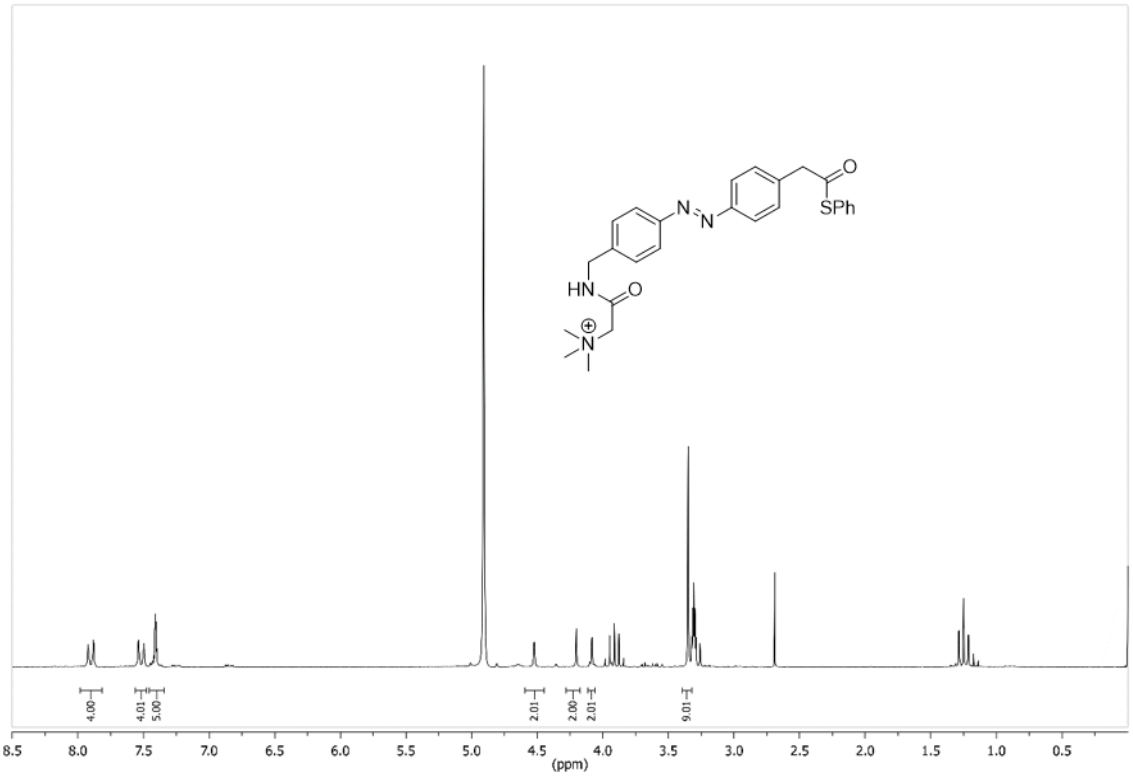

Figure 288: ^{1}H NMR spectrum of compound **10** (500 MHz, $CDCl_3$, 300 K).

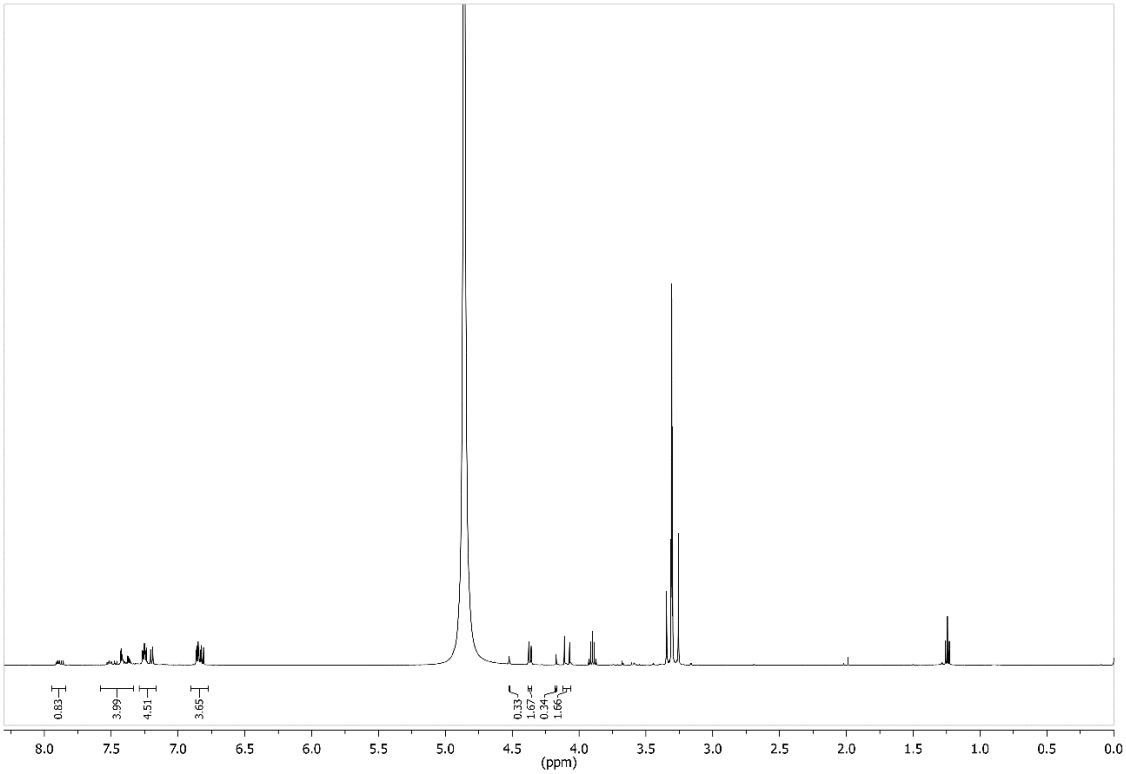

Figure 289: ^{1}H NMR spectrum of compound **10** (*Z*-isomer) (500 MHz, $CDCl_3$, 300 K).

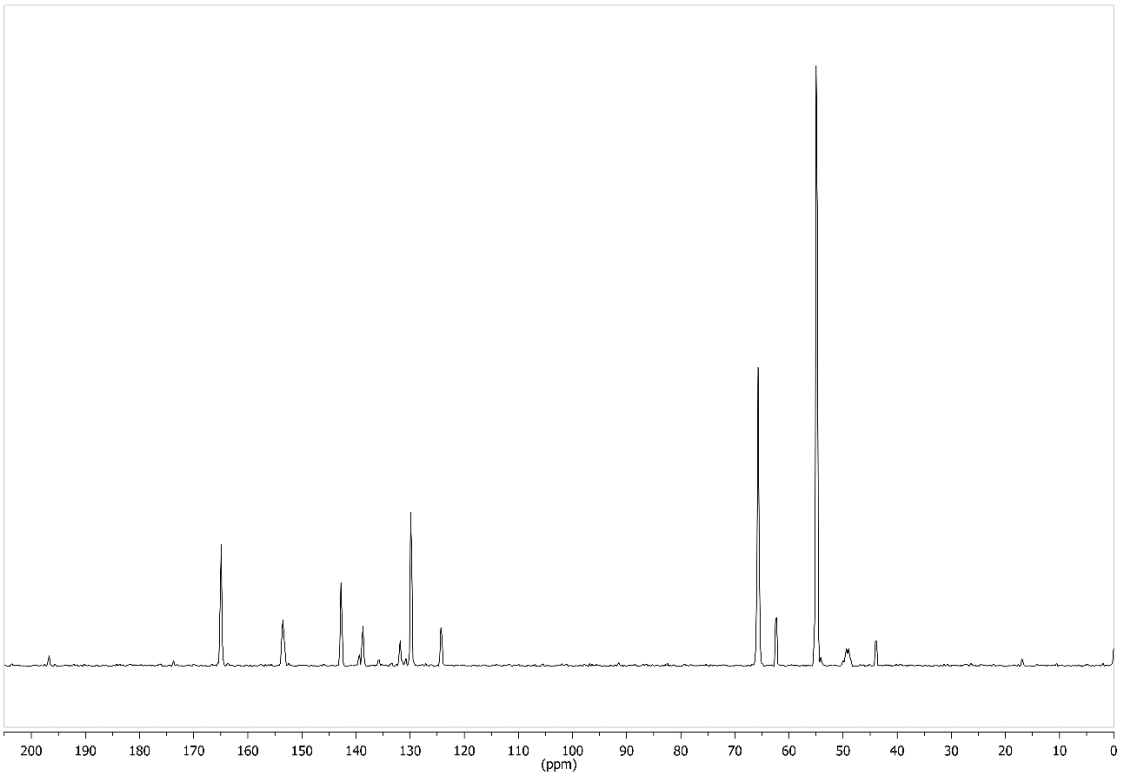

Figure 290: ^{13}C NMR spectrum of compound **10** (126 MHz, $CDCl_3$, 300 K).

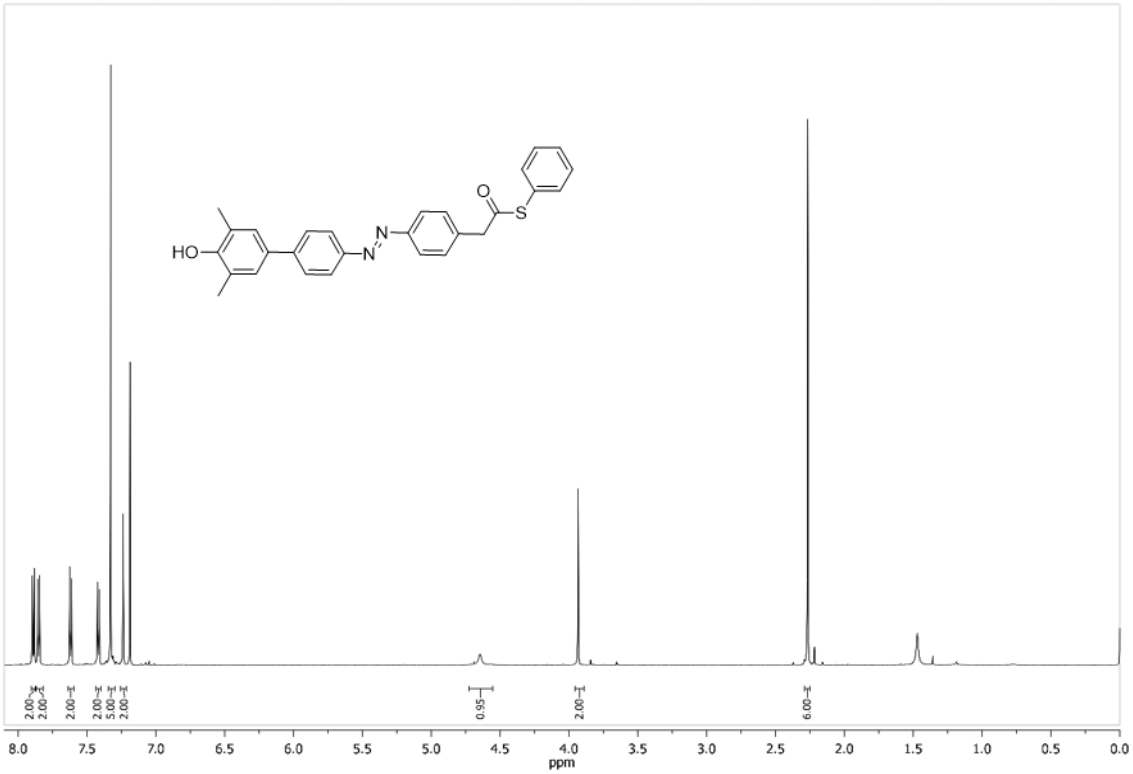

Figure 291: ^{1}H NMR spectrum of compound **11** (600 MHz, $CDCl_3$, 300 K).

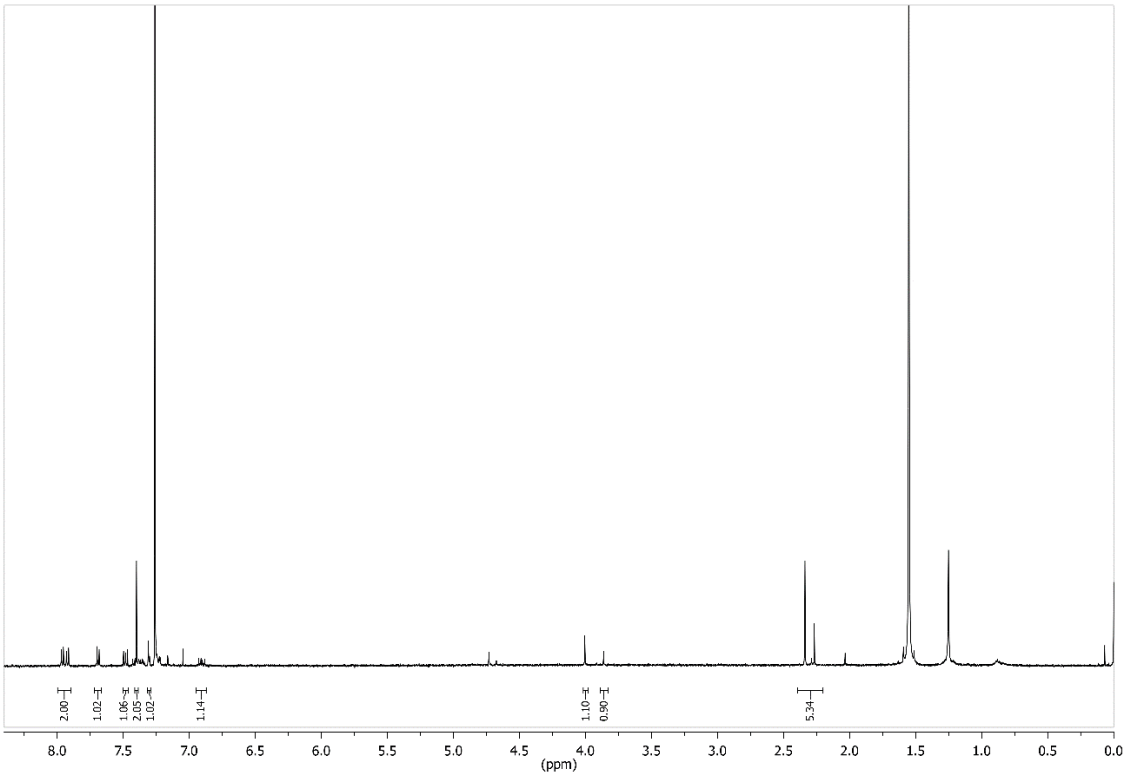

Figure 292: ^{1}H NMR spectrum of compound **11** (*Z*-isomer) (500 MHz, $CDCl_3$, 300 K).

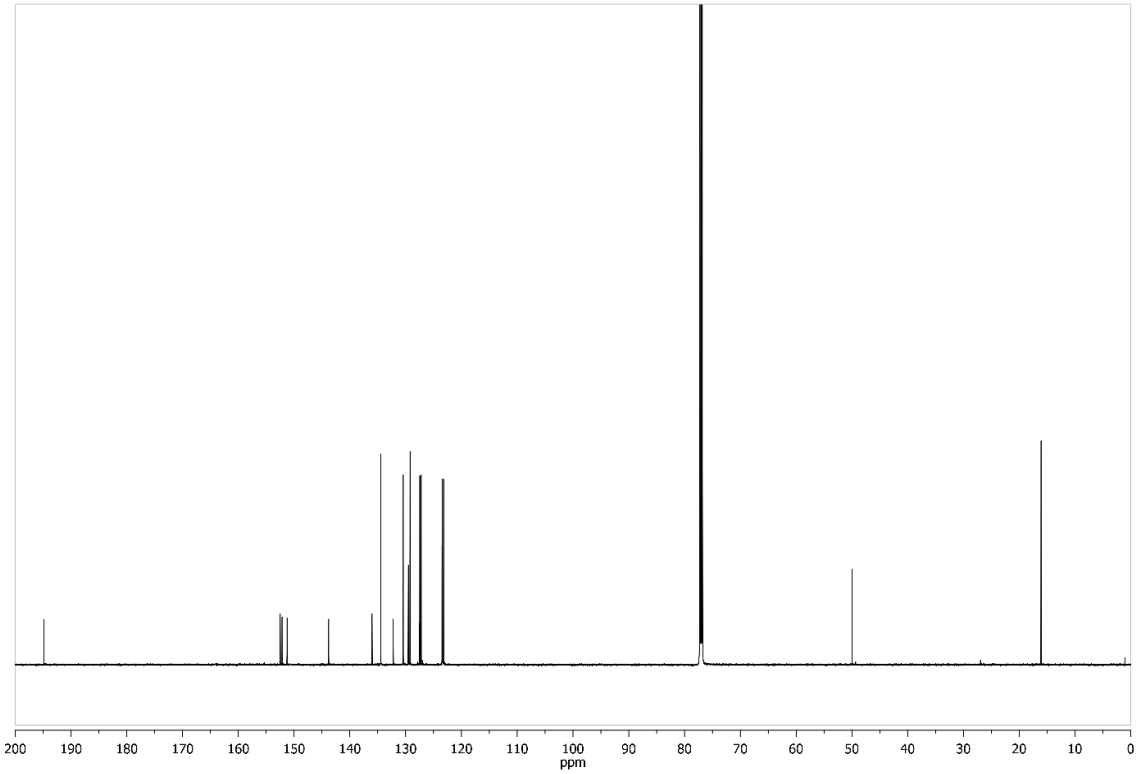

Figure 293: ^{13}C NMR spectrum of compound **11** (151 MHz, $CDCl_3$, 300 K).

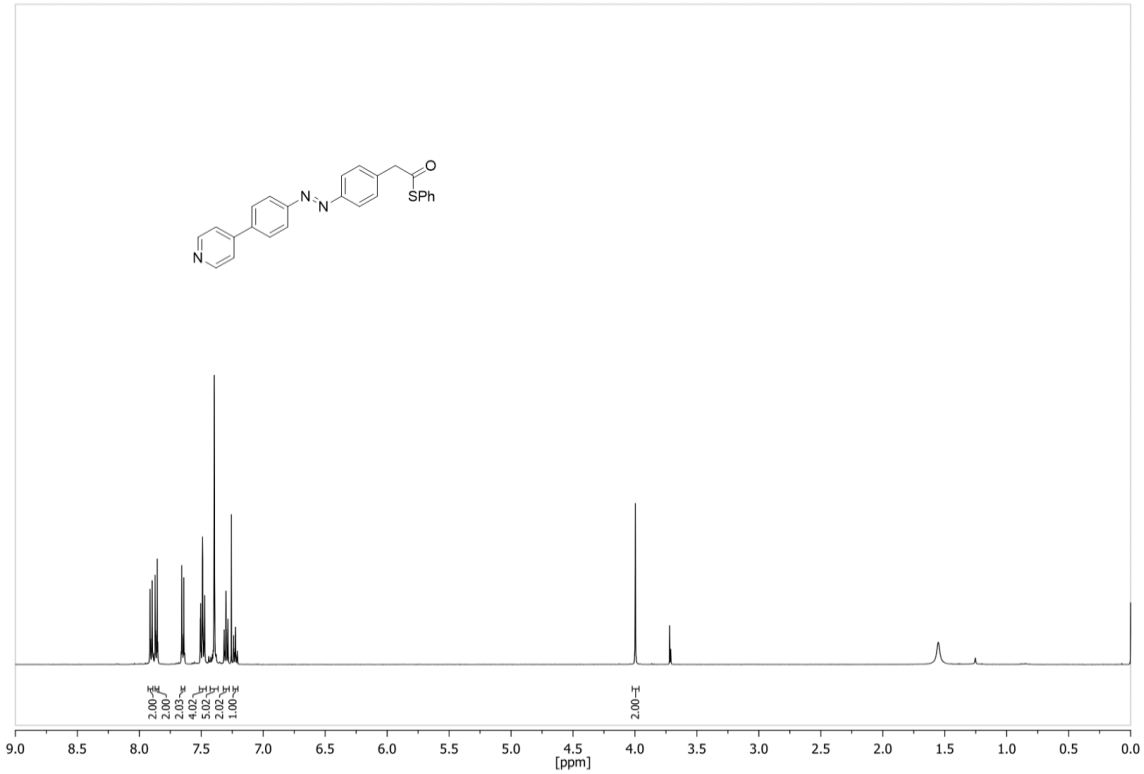

Figure 294: ^{1}H NMR spectrum of compound **12** (500 MHz, $CDCl_3$, 300 K).

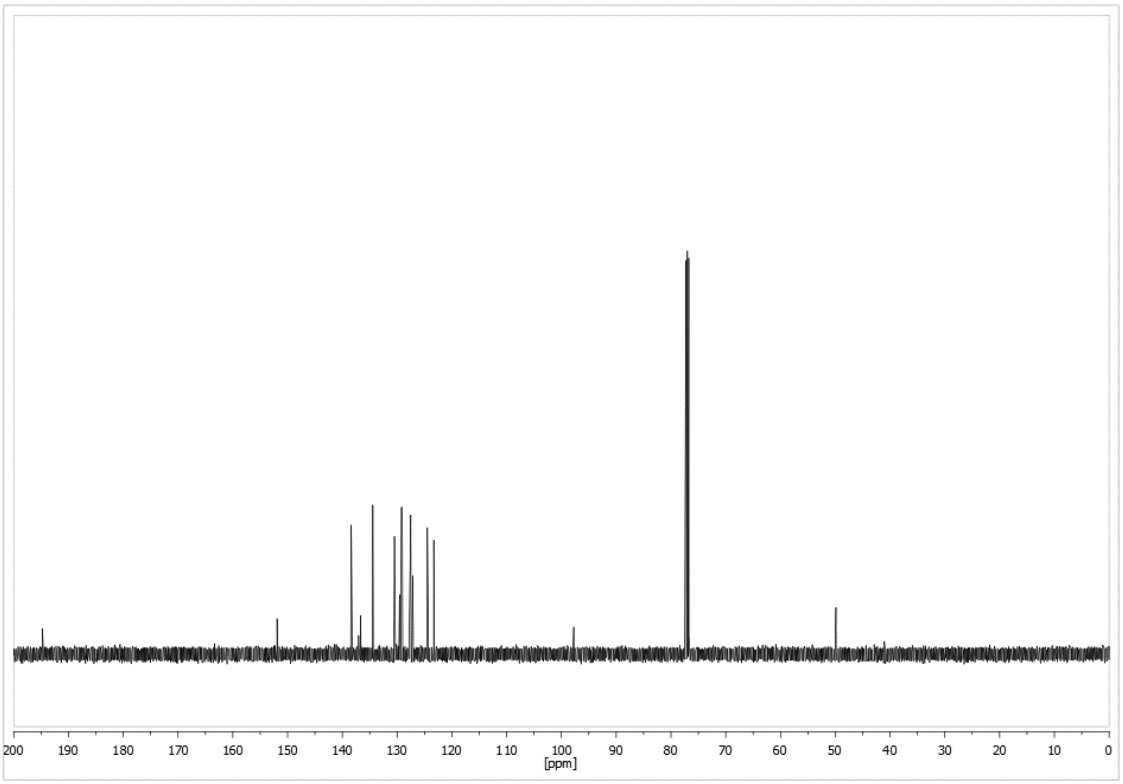

Figure 295: ^{13}C NMR spectrum of compound **12** (126 MHz, $CDCl_3$, 300 K).

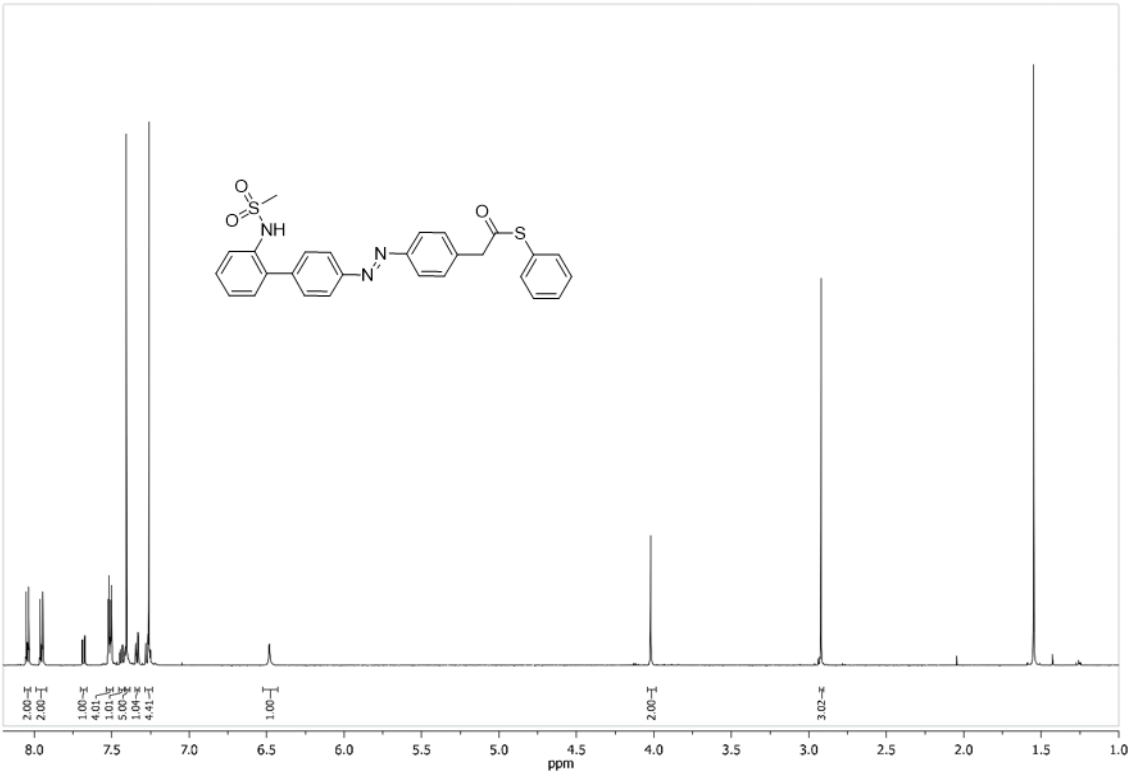

Figure 296: ^{1}H NMR spectrum of compound **13** (500 MHz, $CDCl_3$, 300 K).

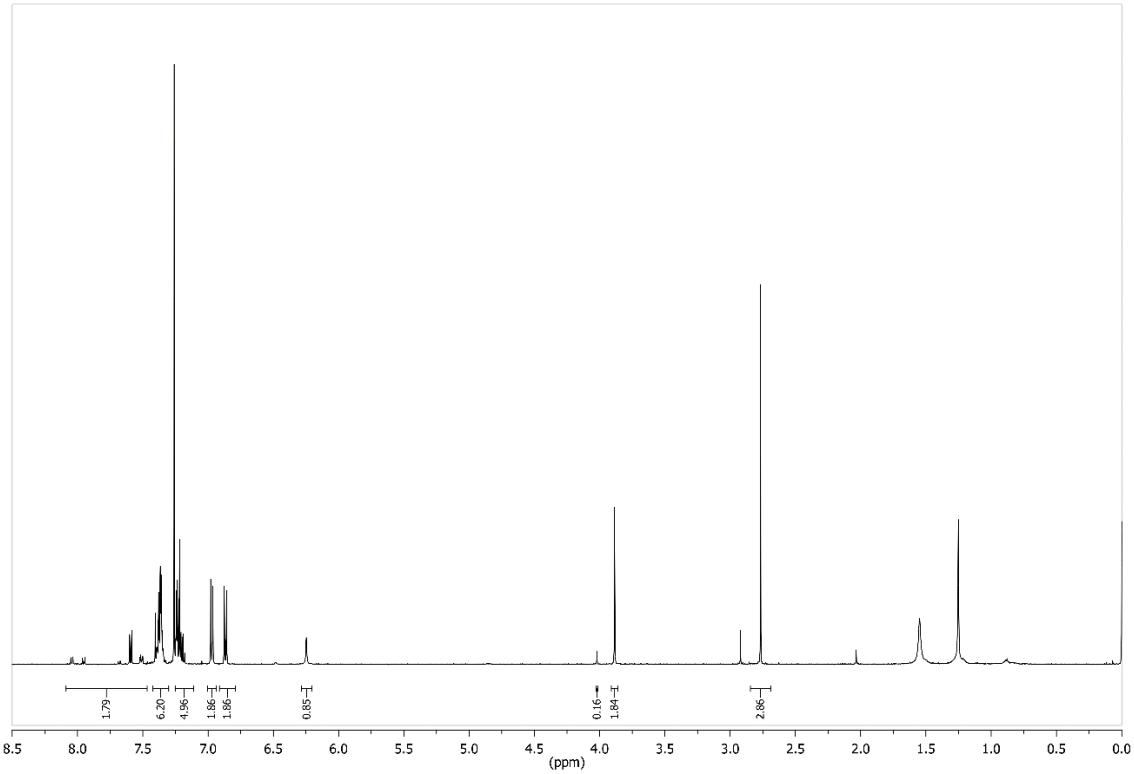

Figure 297: ^{1}H NMR spectrum of compound **13** (*Z*-isomer) (500 MHz, $CDCl_3$, 300 K).

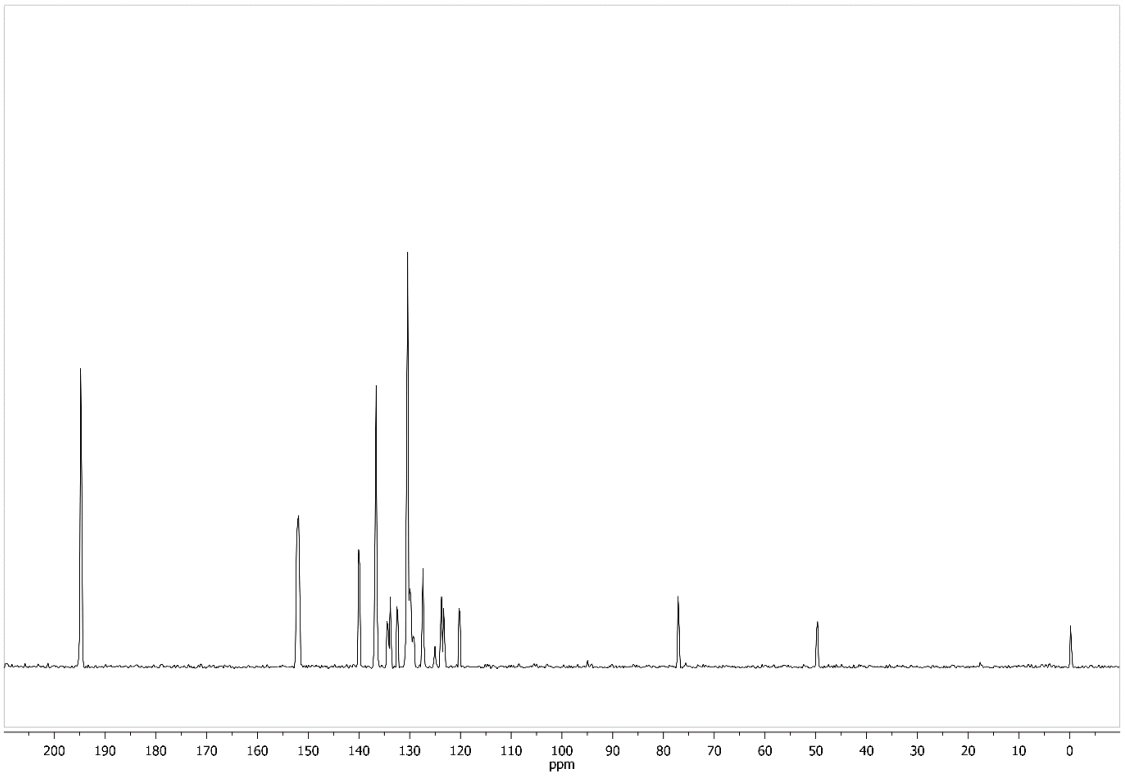

Figure 298: ^{13}C NMR spectrum of compound **13** (126 MHz, $CDCl_3$, 300 K).

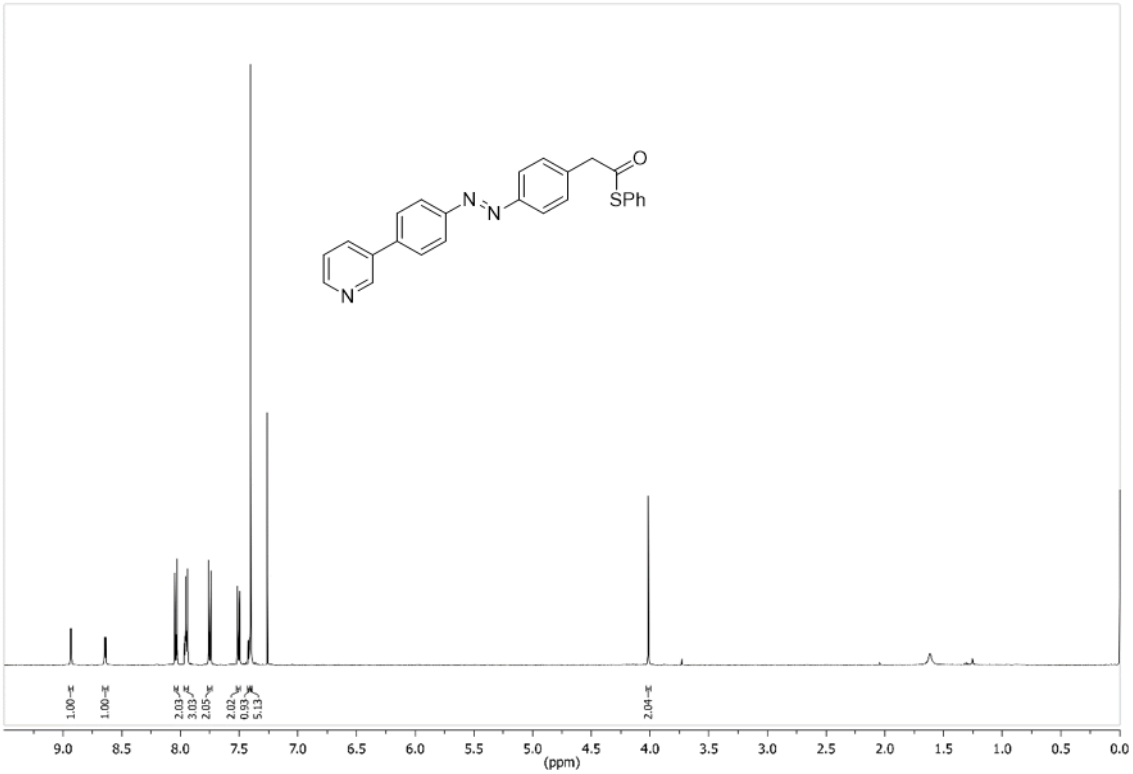

Figure 299: ^{1}H NMR spectrum of compound **14** (500 MHz, $CDCl_3$, 300 K).

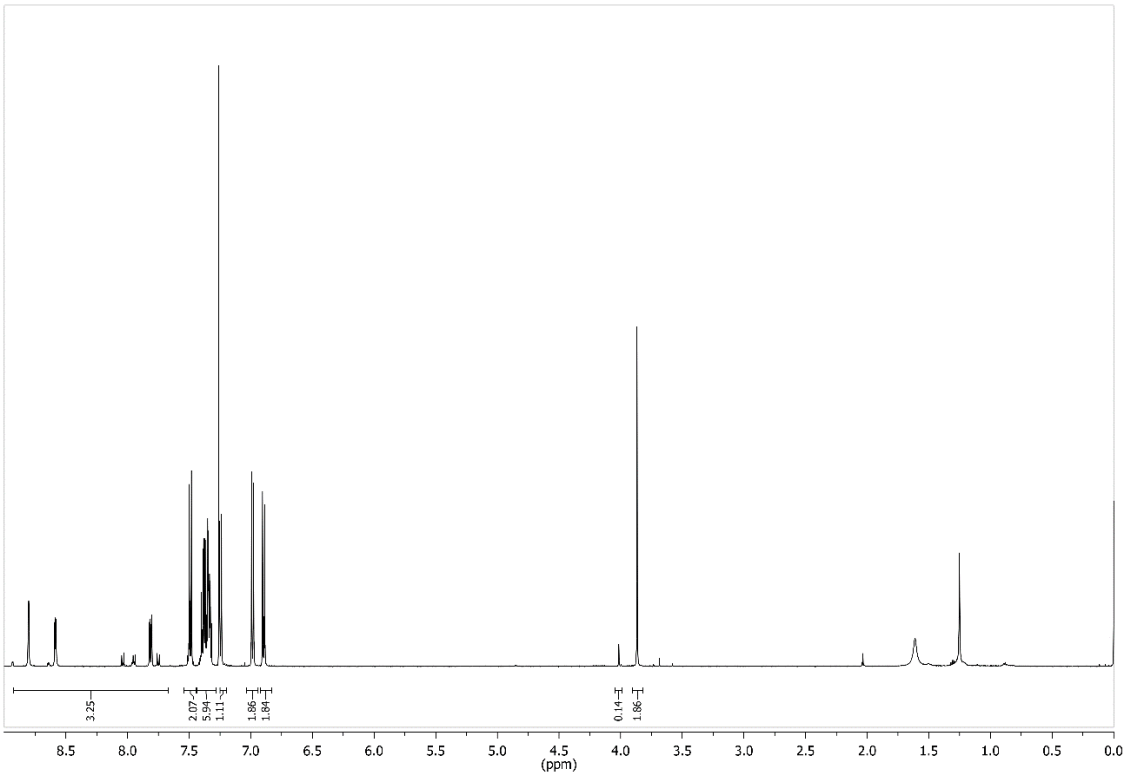

Figure 300: ^{1}H NMR spectrum of compound **14** (*Z*-isomer) (500 MHz, $CDCl_3$, 300 K).

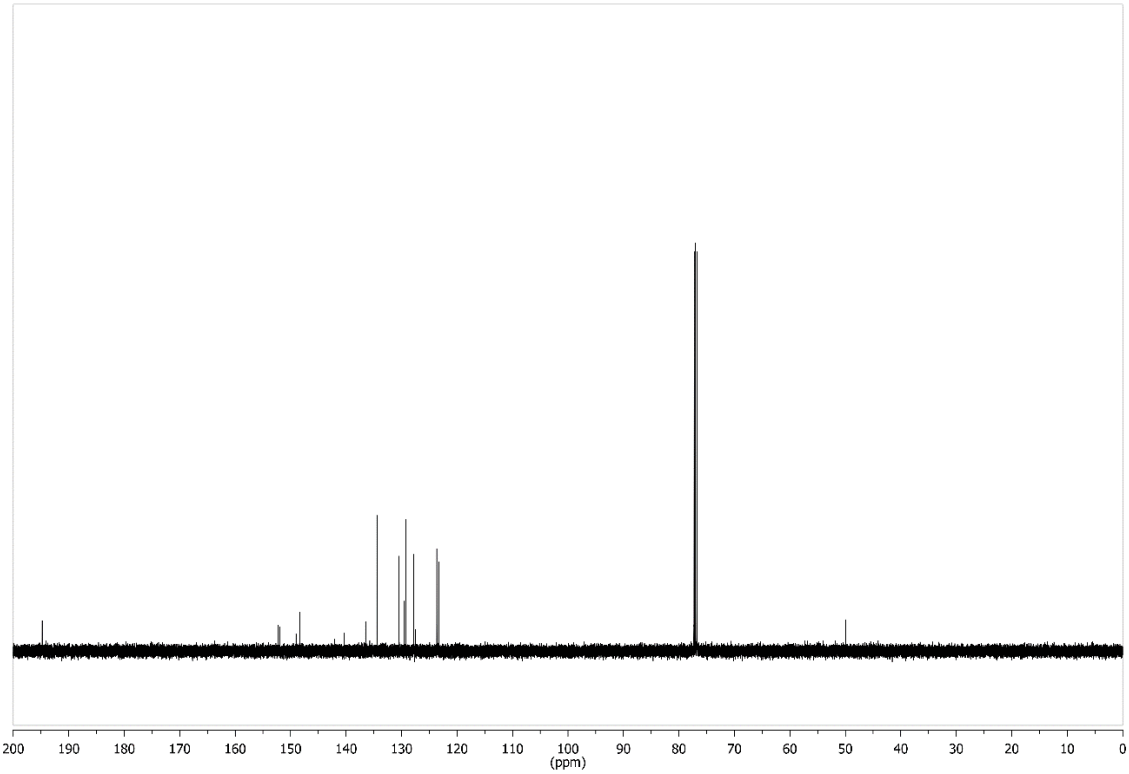

Figure 301: ^{13}C NMR spectrum of compound **14** (126 MHz, $CDCl_3$, 300 K).

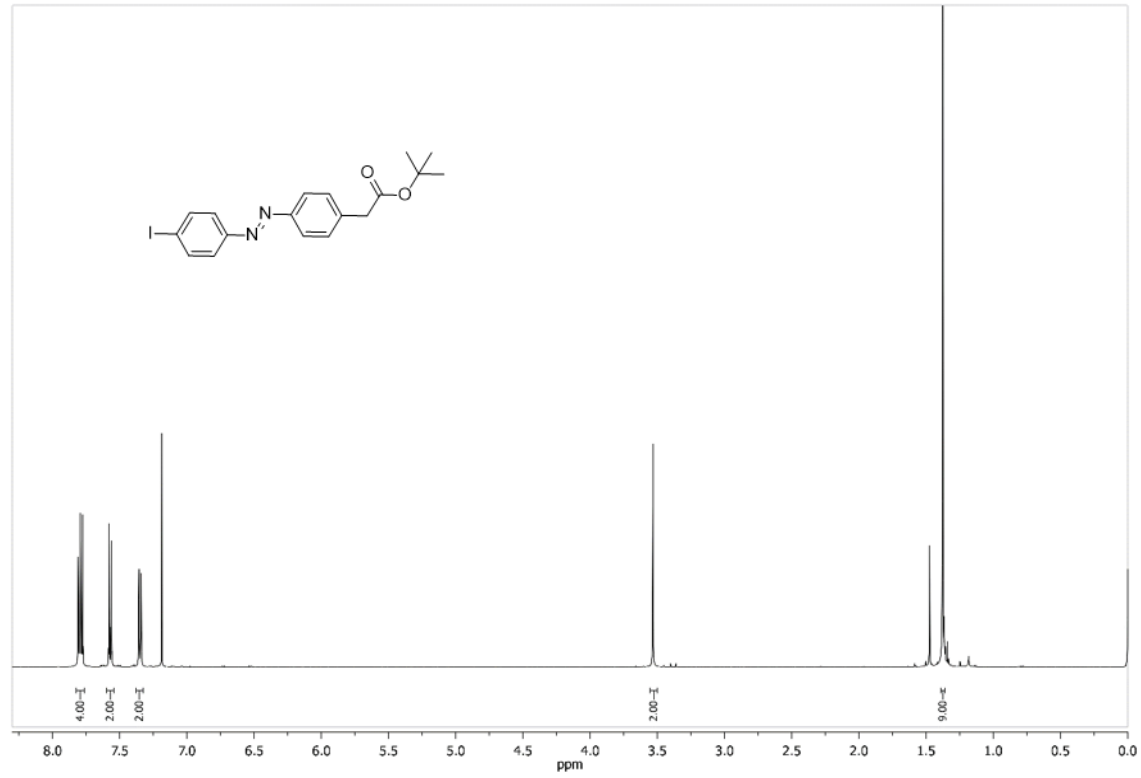

Figure 302: ^{1}H NMR spectrum of compound **23** (500 MHz, $CDCl_3$, 300 K).

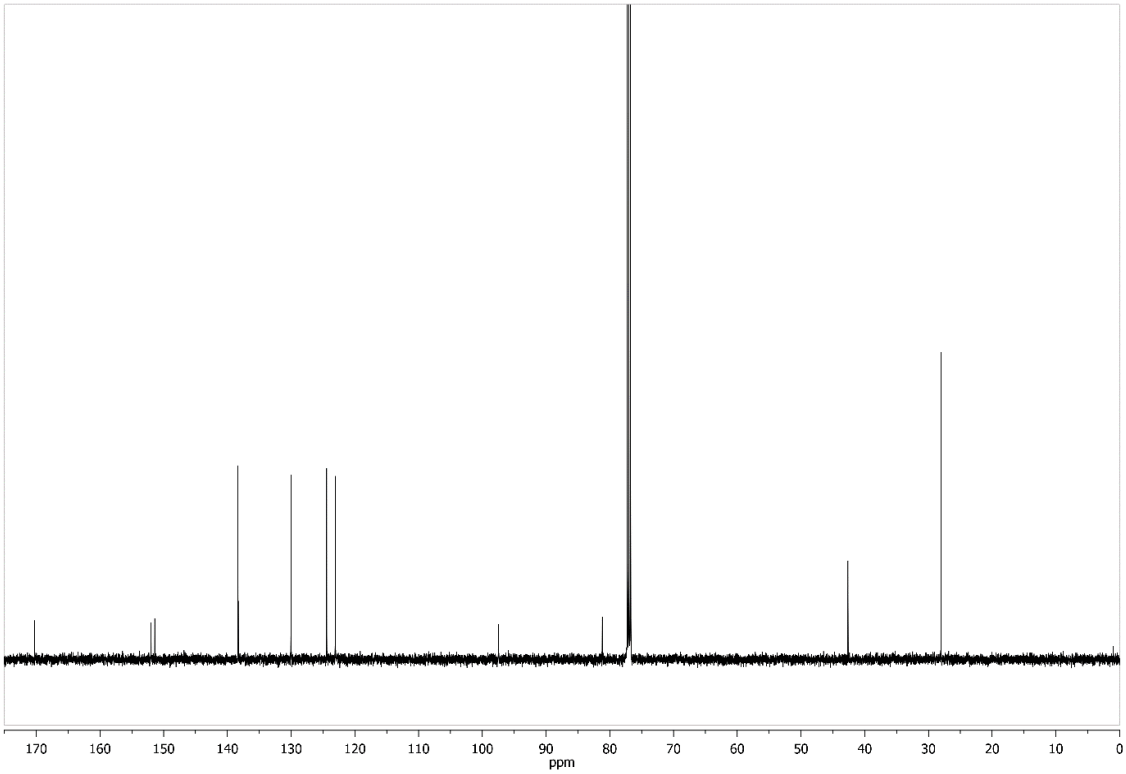

Figure 303: ^{13}C NMR spectrum of compound **23** (126 MHz, $CDCl_3$, 300 K).

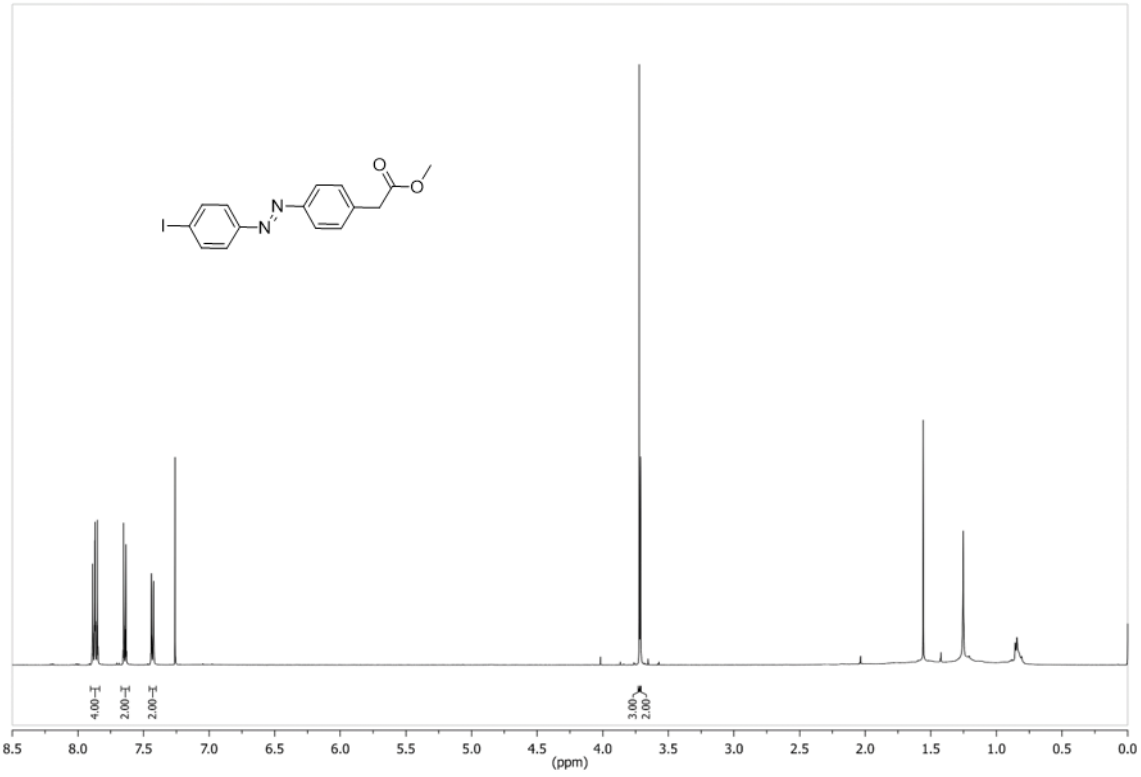

Figure 304: ^{1}H NMR spectrum of compound **24** (500 MHz, $CDCl_3$, 300 K).

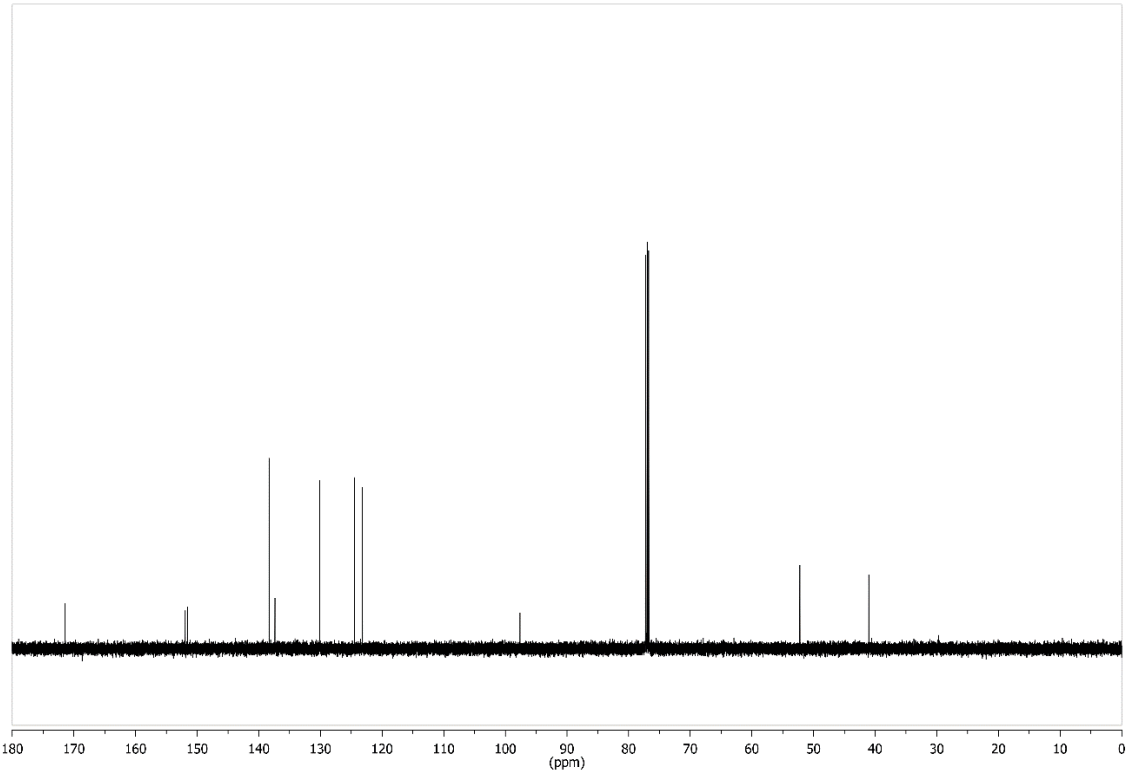

Figure 305: ^{13}C NMR spectrum of compound **24** (126 MHz, $CDCl_3$, 300 K).

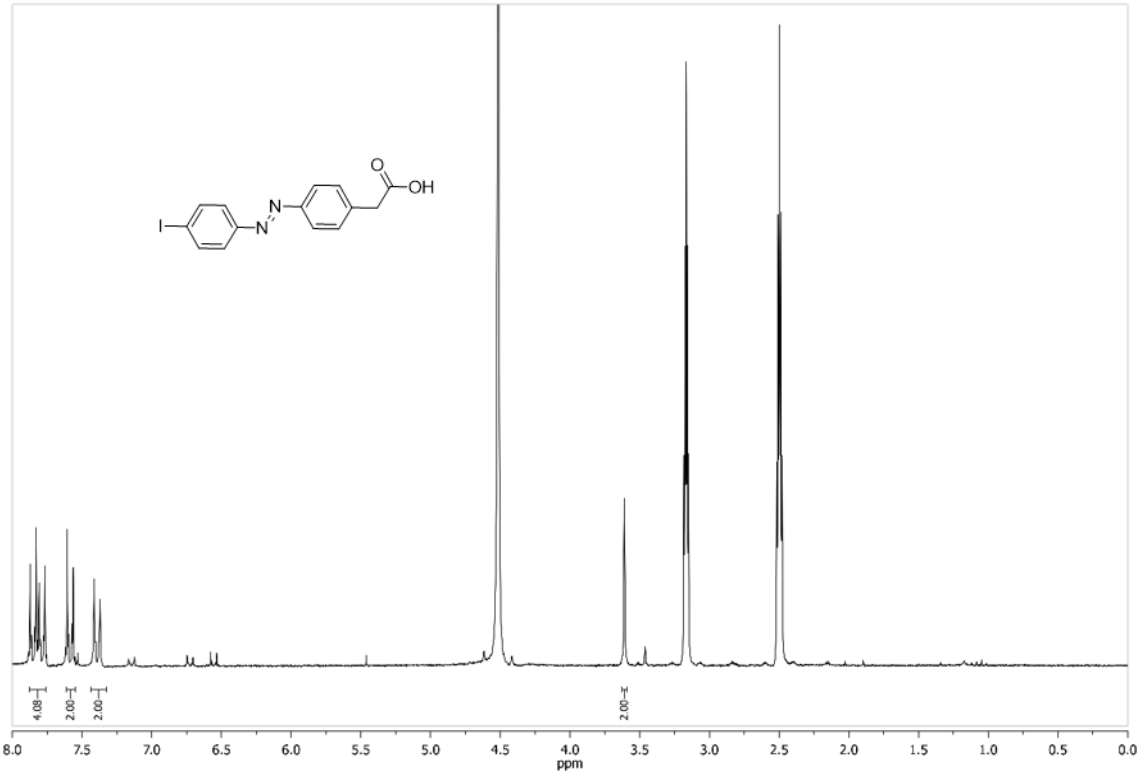

Figure 306: ^{1}H NMR spectrum of compound **25** (600 MHz, MeOD, 300 K).

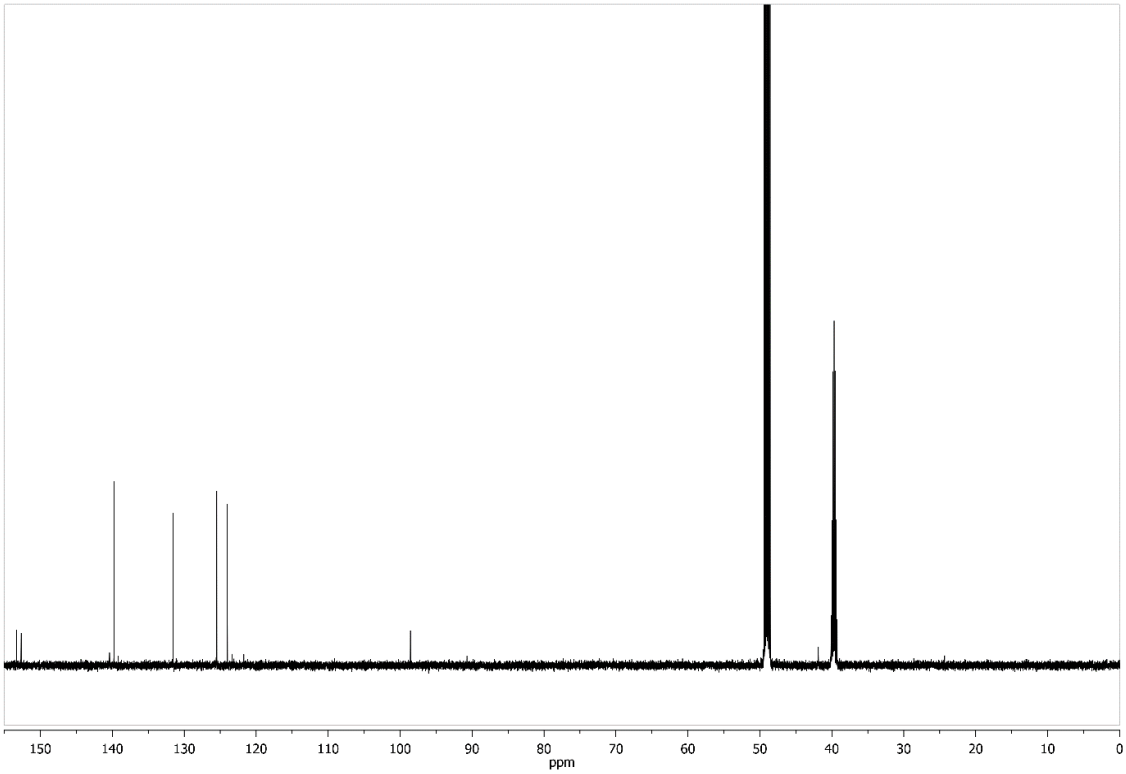

Figure 307: ^{13}C NMR spectrum of compound **25** (151 MHz, MeOD, 300 K).

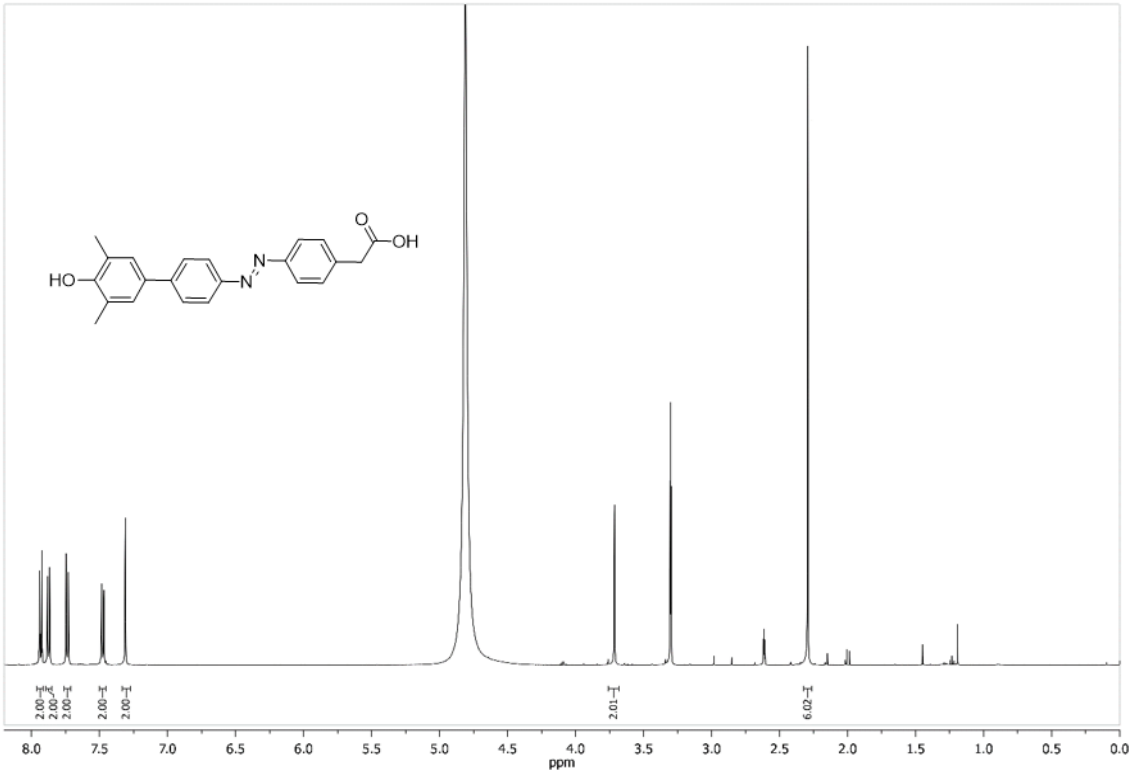

Figure 308: ^{1}H NMR spectrum of compound **30** (500 MHz, MeOD, 300 K).

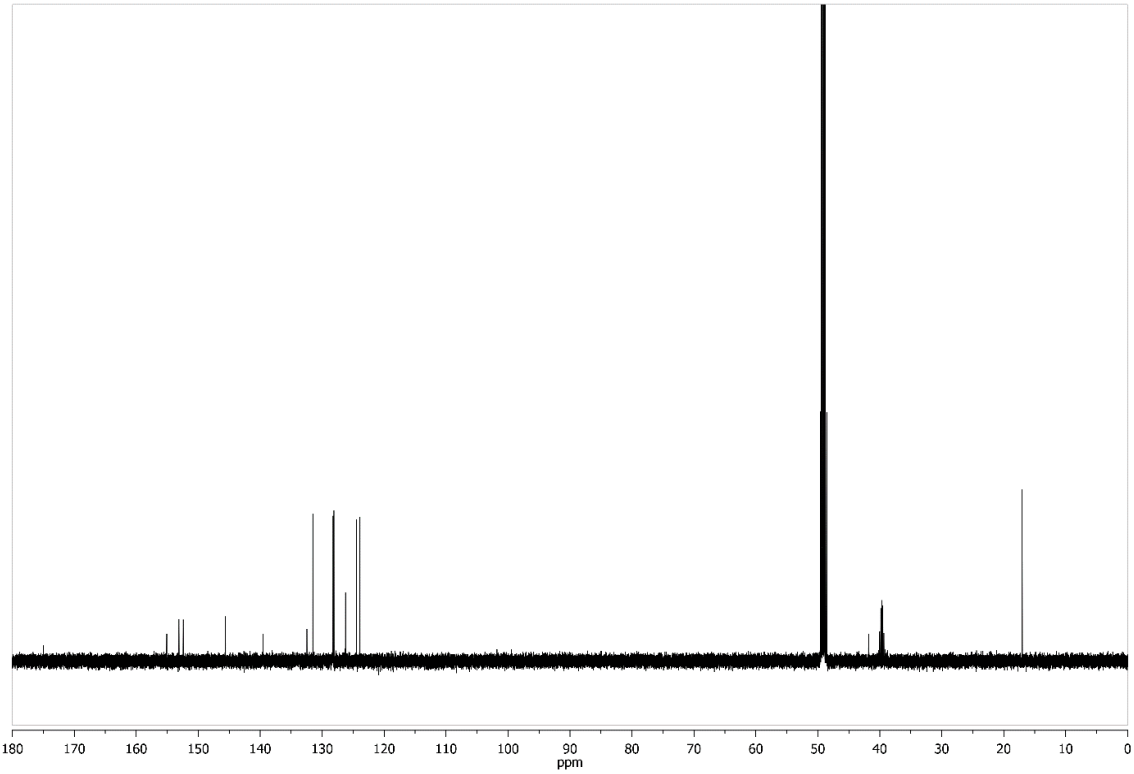

Figure 309: ^{13}C NMR spectrum of compound **30** (126 MHz, MeOD, 300 K).

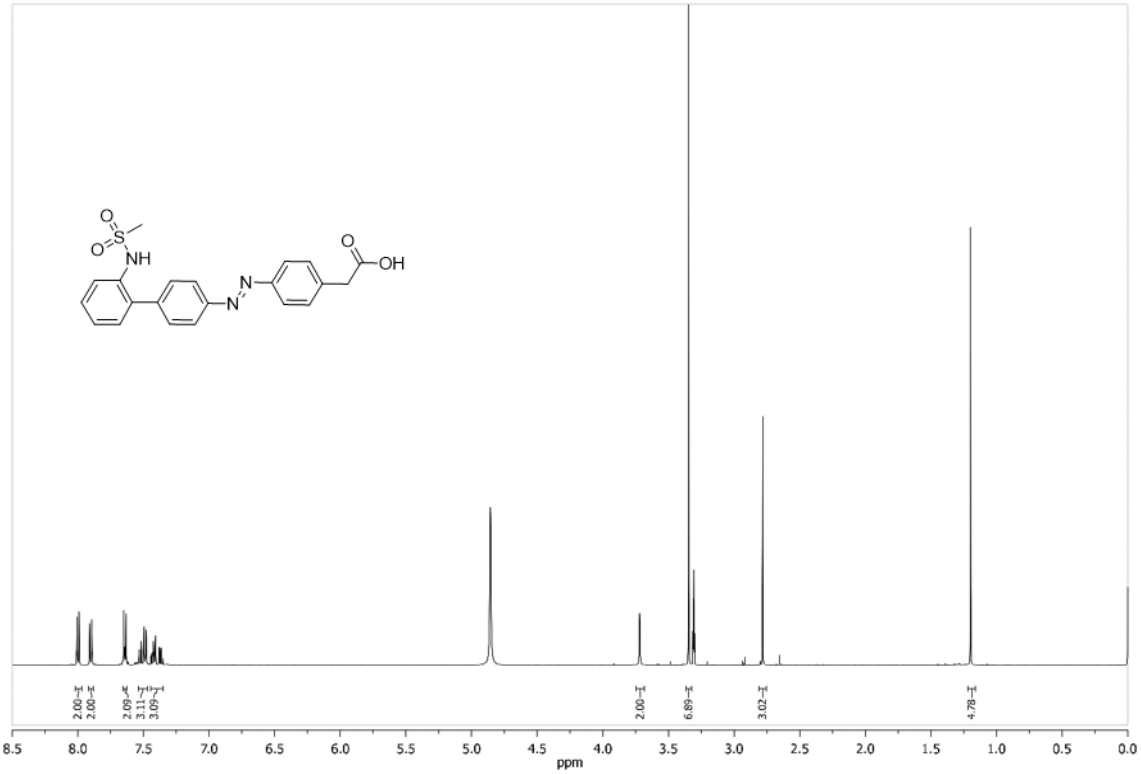

Figure 310: ^{1}H NMR spectrum of compound **31** (500 MHz, MeOD, 300 K).

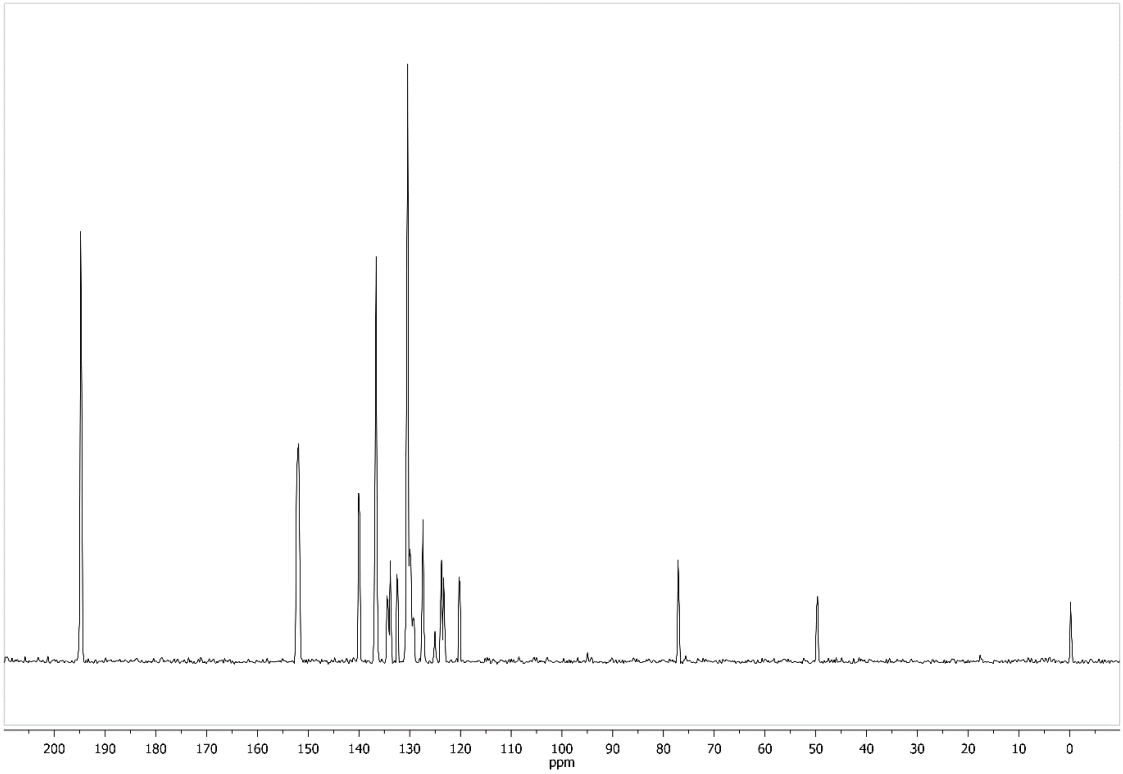

Figure 311: ^{13}C NMR spectrum of compound **31** (126 MHz, MeOD, 300 K).

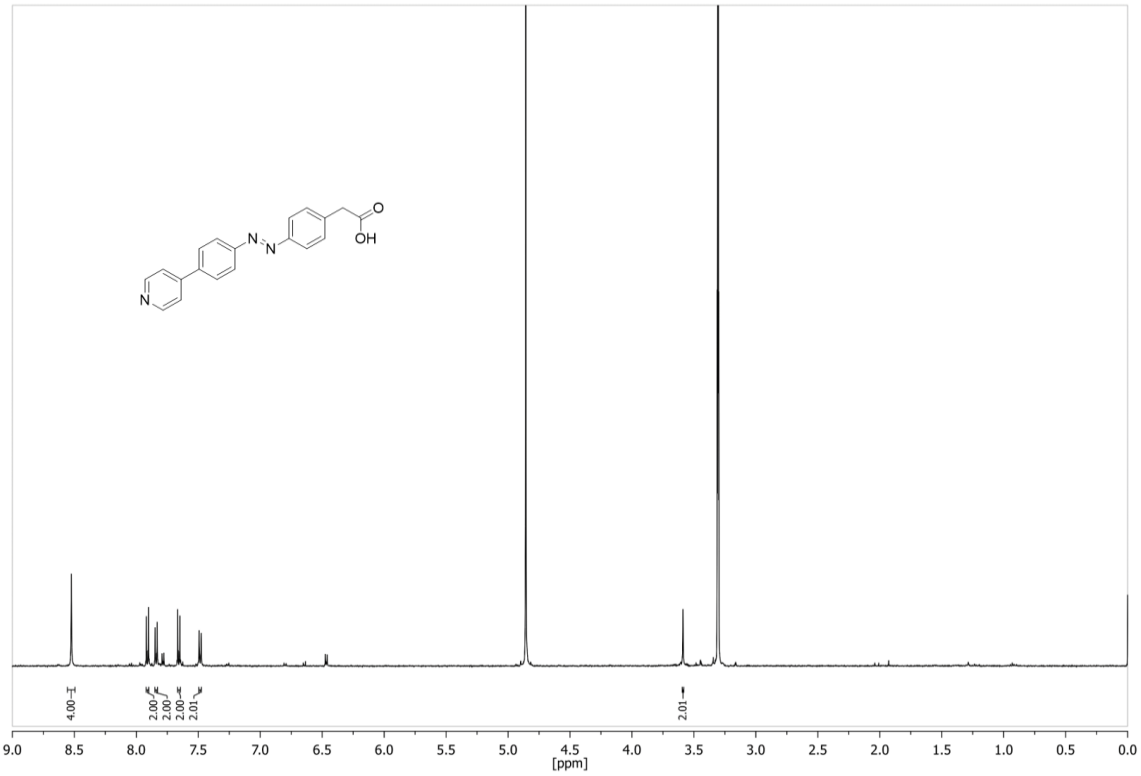

Figure 312: ^{1}H NMR spectrum of compound **32** (500 MHz, MeOD, 300 K).

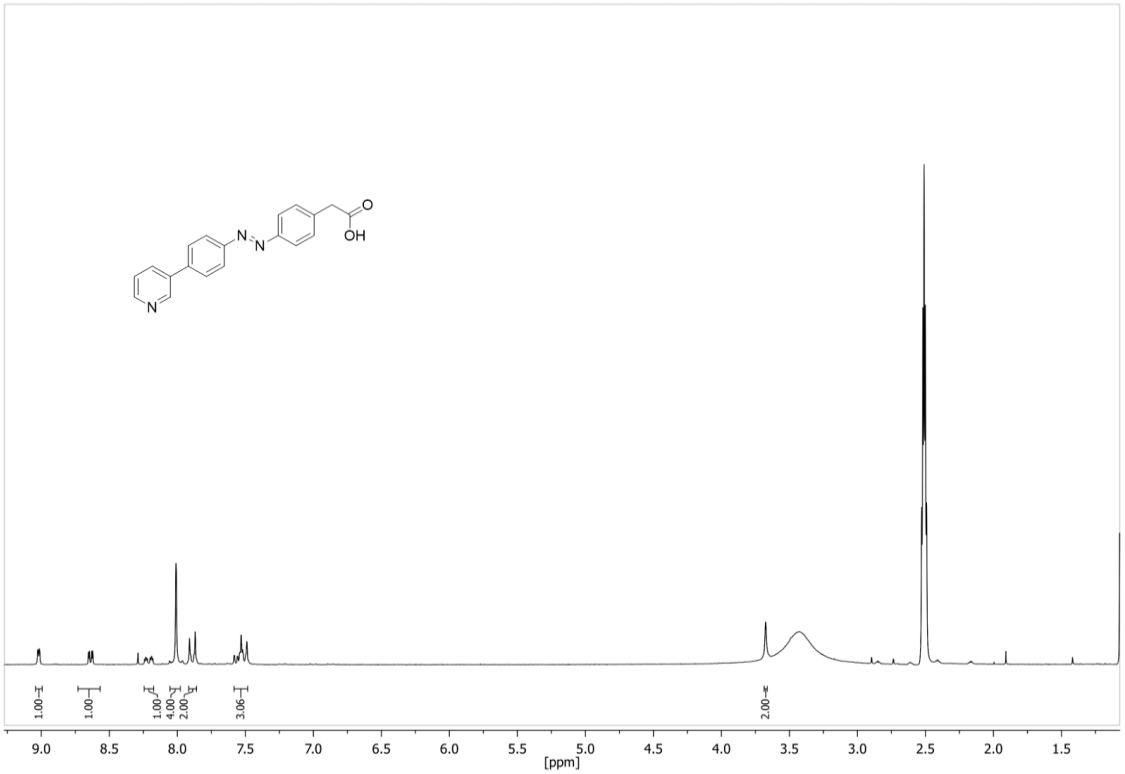

Figure 313: ^{1}H NMR spectrum of compound **33** (500 MHz, DMSO-*d6*, 300 K).

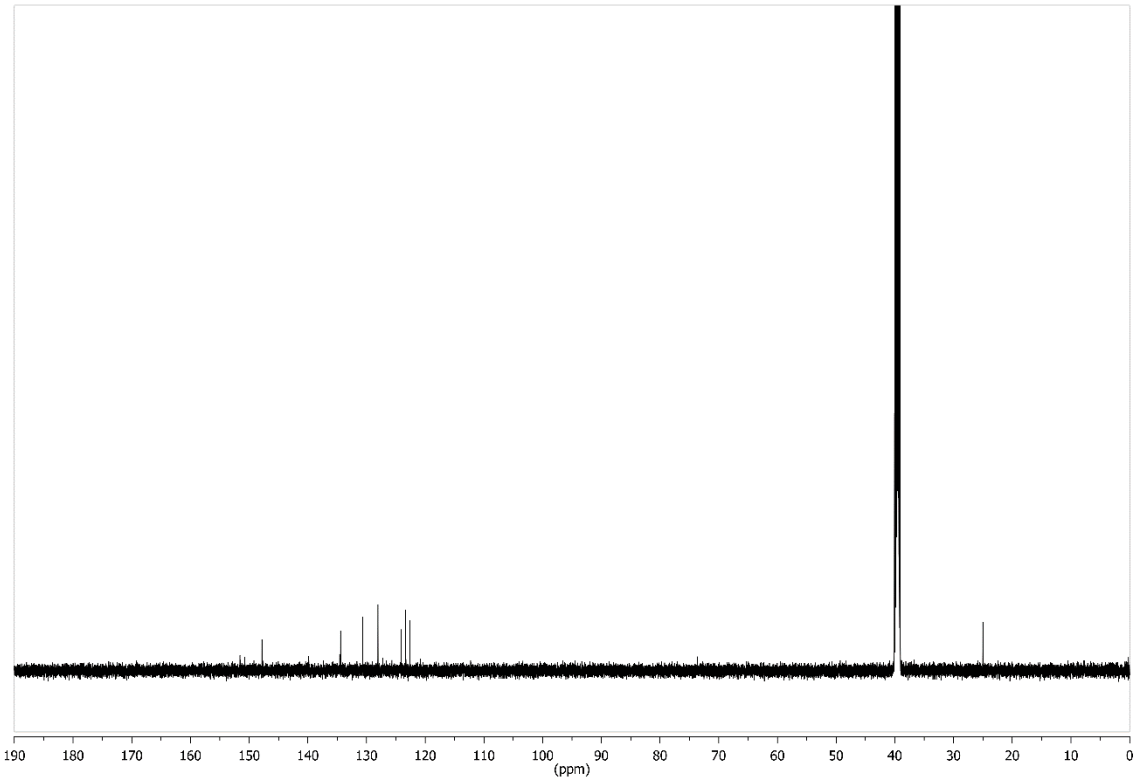

Figure 314: ^{13}C NMR spectrum of compound **33** (151 MHz, DMSO-*d6*, 300 K).

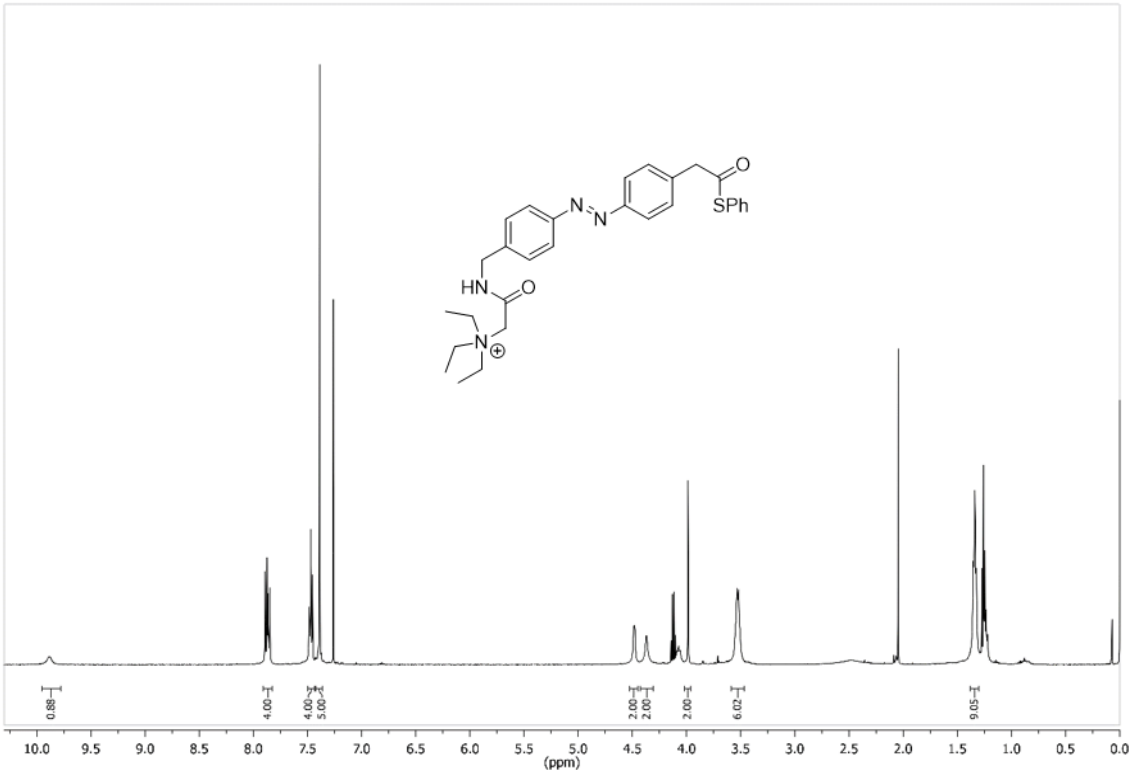

Figure 315: ^{1}H NMR spectrum of compound **35** (500 MHz, $CDCl_3$, 300 K).

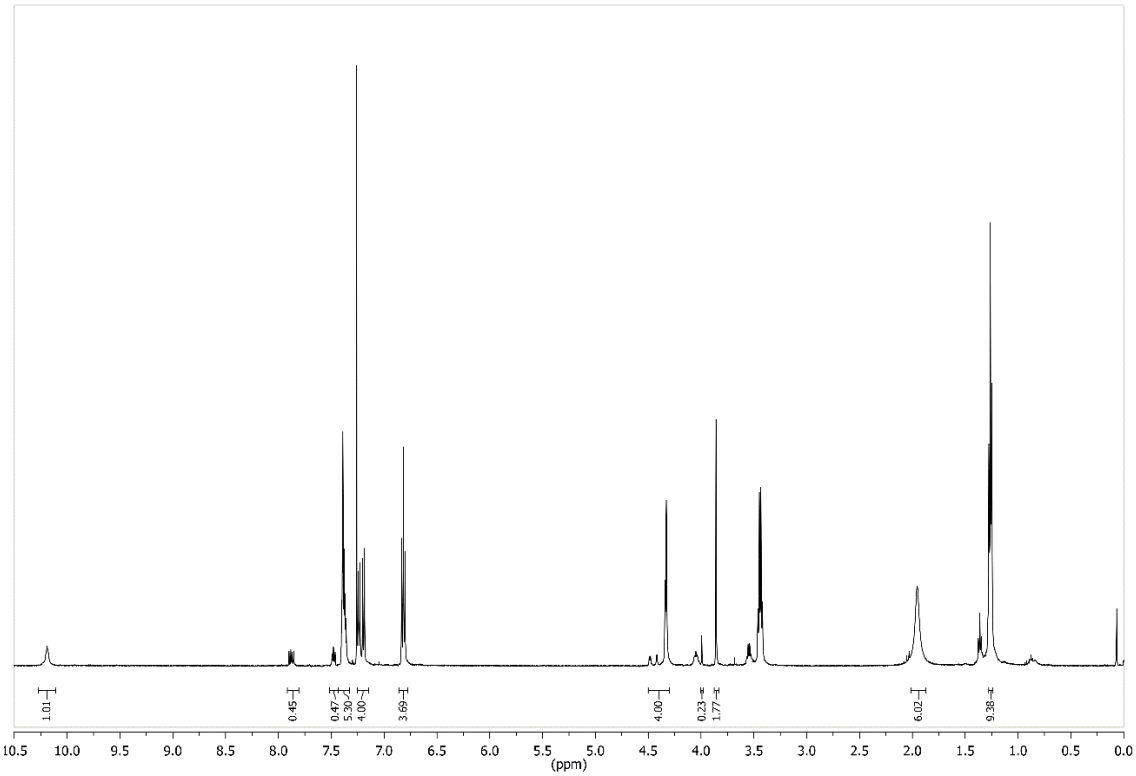

Figure 316: ^{1}H NMR spectrum of compound **35** (*Z*-isomer) (500 MHz, $CDCl_3$, 300 K).

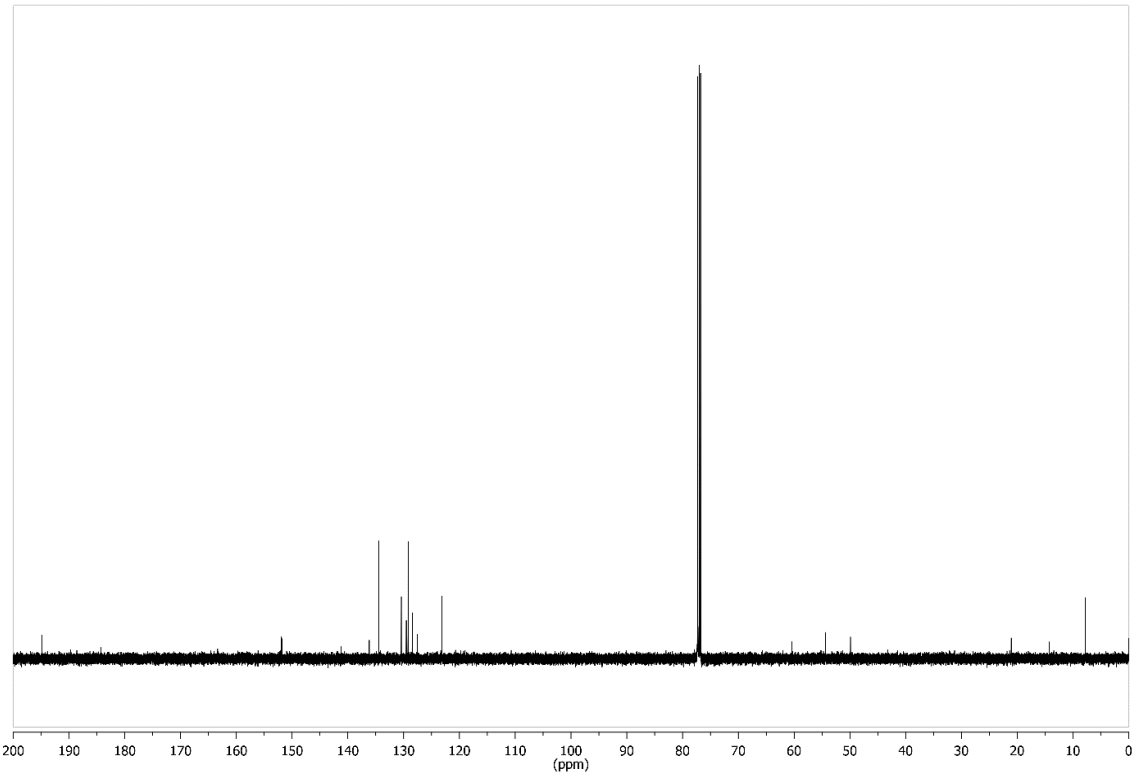

Figure 317: ^{13}C NMR spectrum of compound **35** (126 MHz, $CDCl_3$, 300 K).

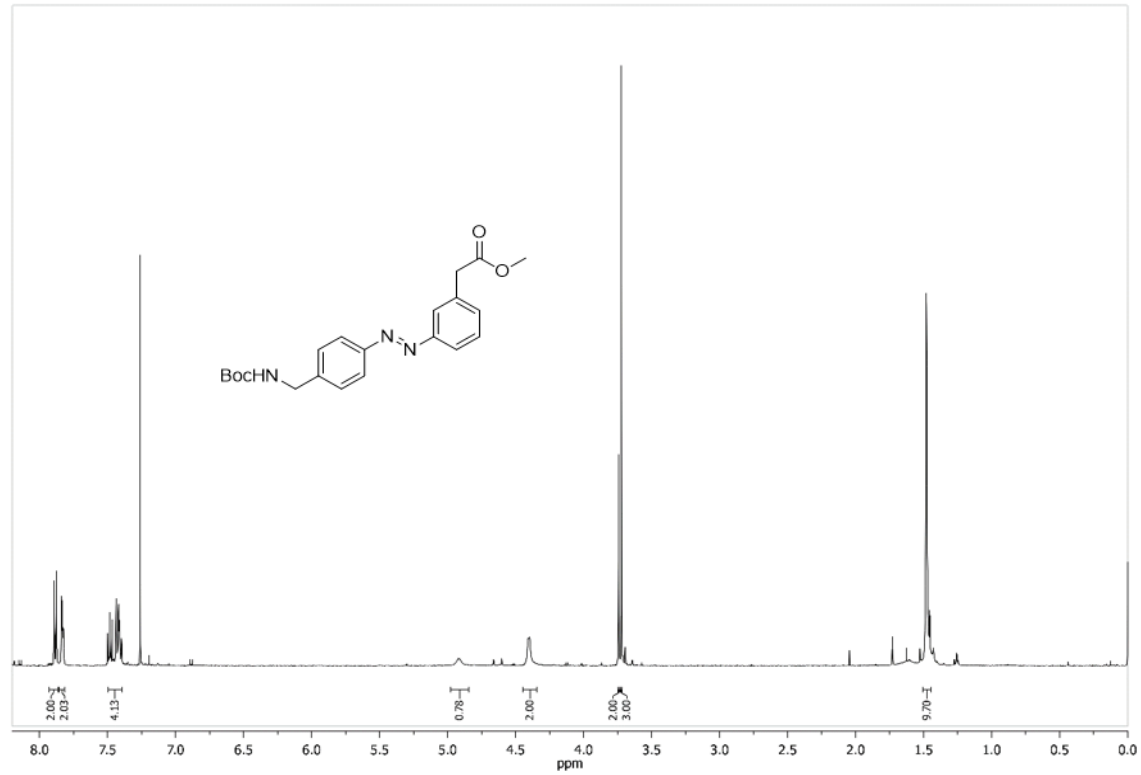

Figure 318: ^{1}H NMR spectrum of compound **52** (500 MHz, $CDCl_3$, 300 K).

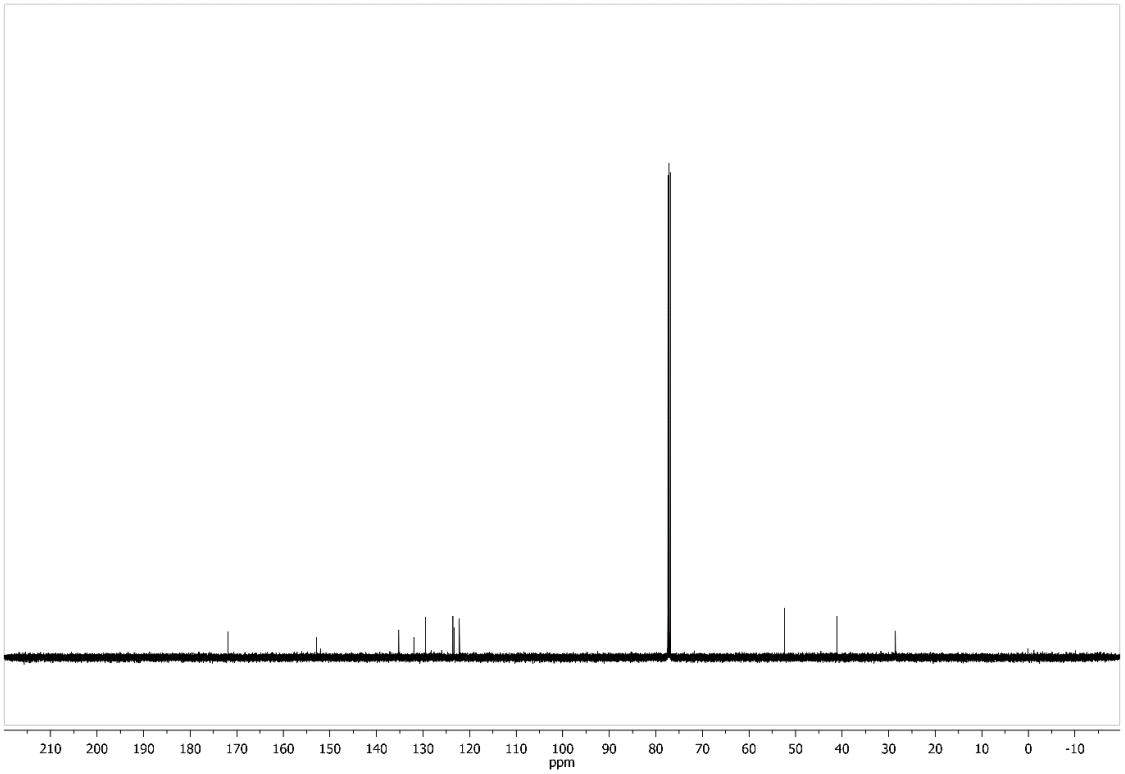

Figure 319: ^{13}C NMR spectrum of compound **52** (126 MHz, $CDCl_3$, 300 K).

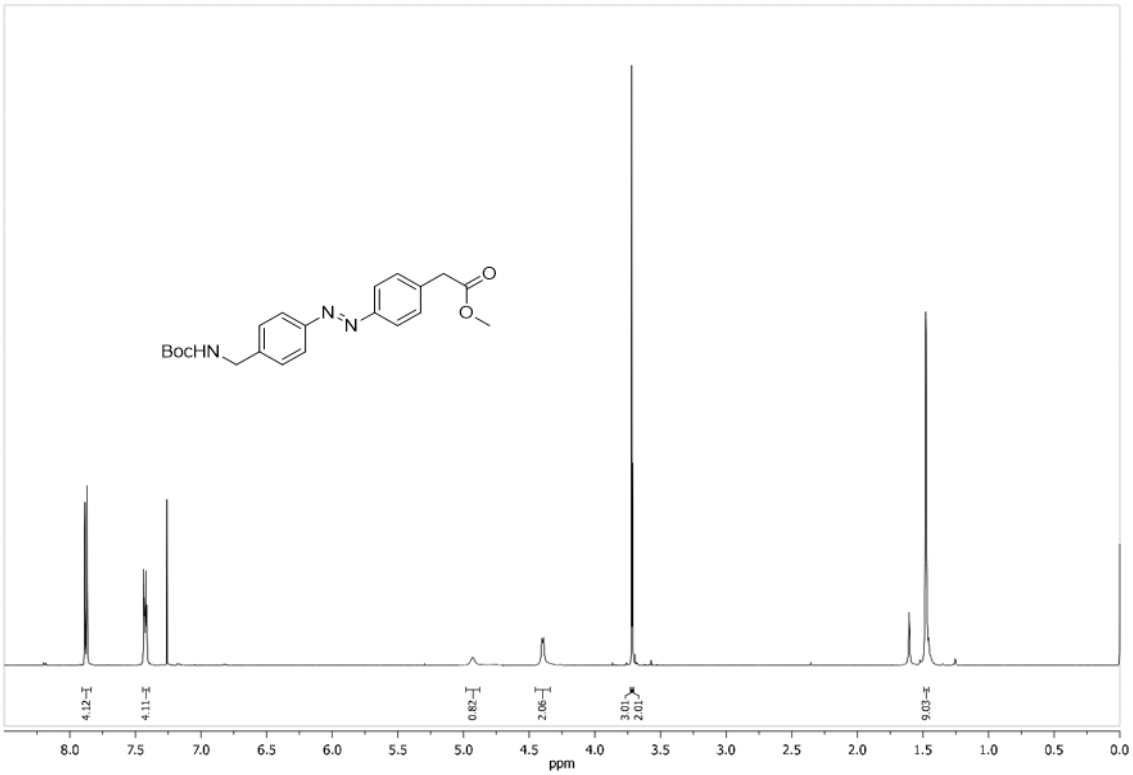

Figure 320: ^{1}H NMR spectrum of compound **53** (500 MHz, $CDCl_3$, 300 K).

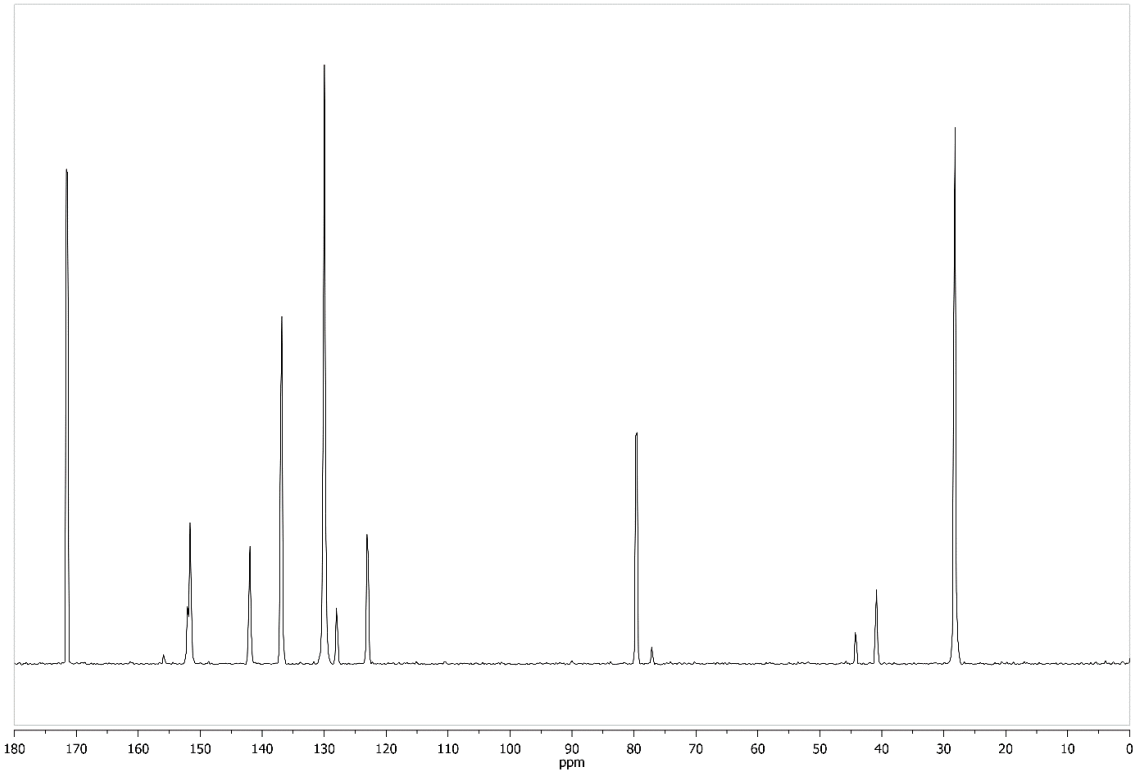

Figure 321: ^{13}C NMR spectrum of compound **53** (126 MHz, $CDCl_3$, 300 K).

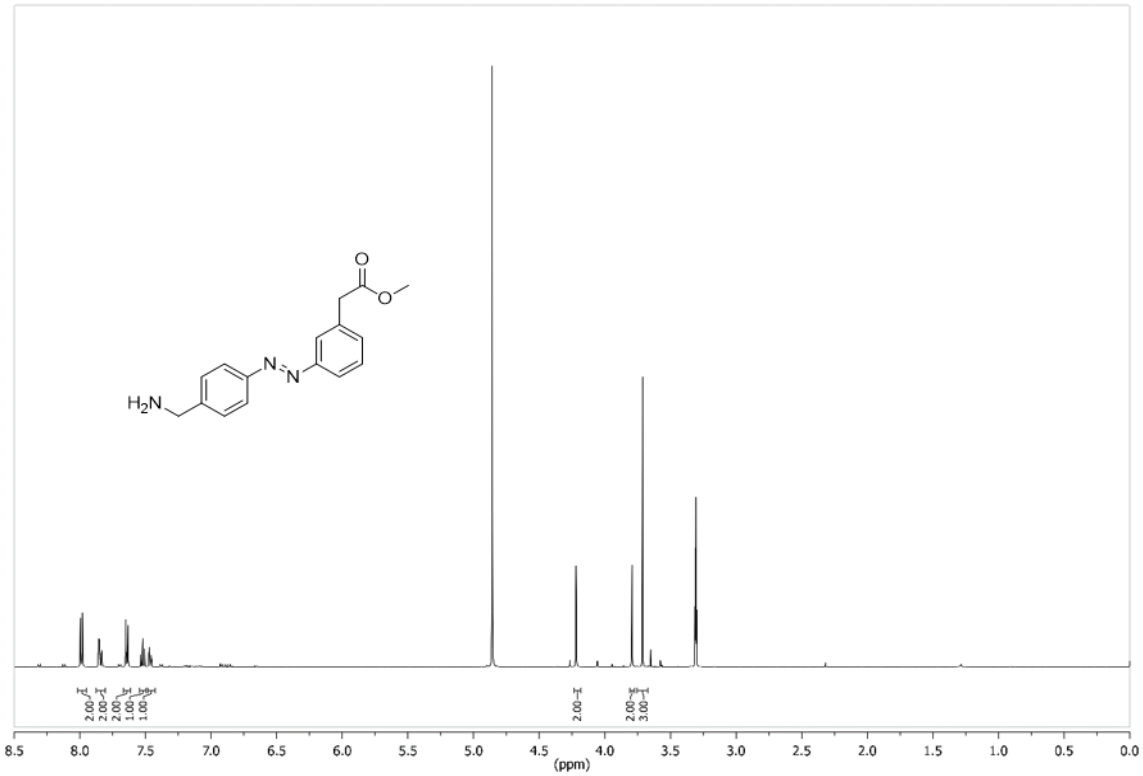

Figure 322: ^{1}H NMR spectrum of compound **54** (500 MHz, MeOD, 300 K).

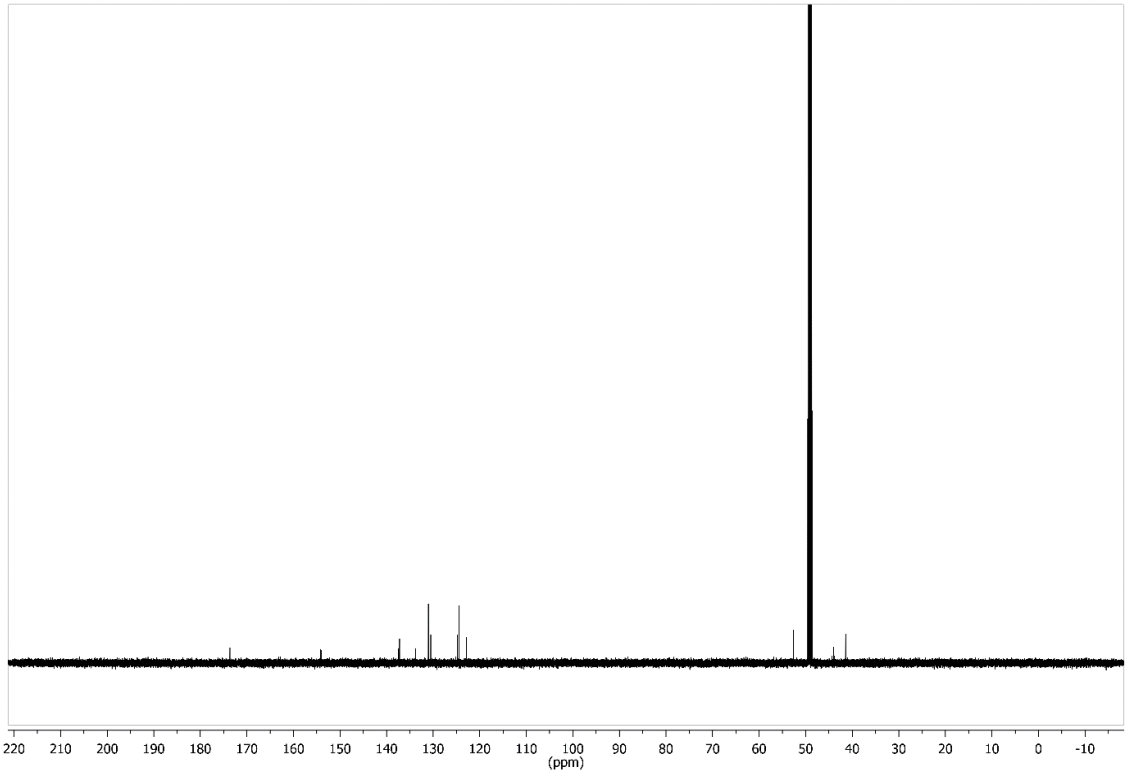

Figure 323: ^{13}C NMR spectrum of compound **54** (126 MHz, MeOD, 300 K).

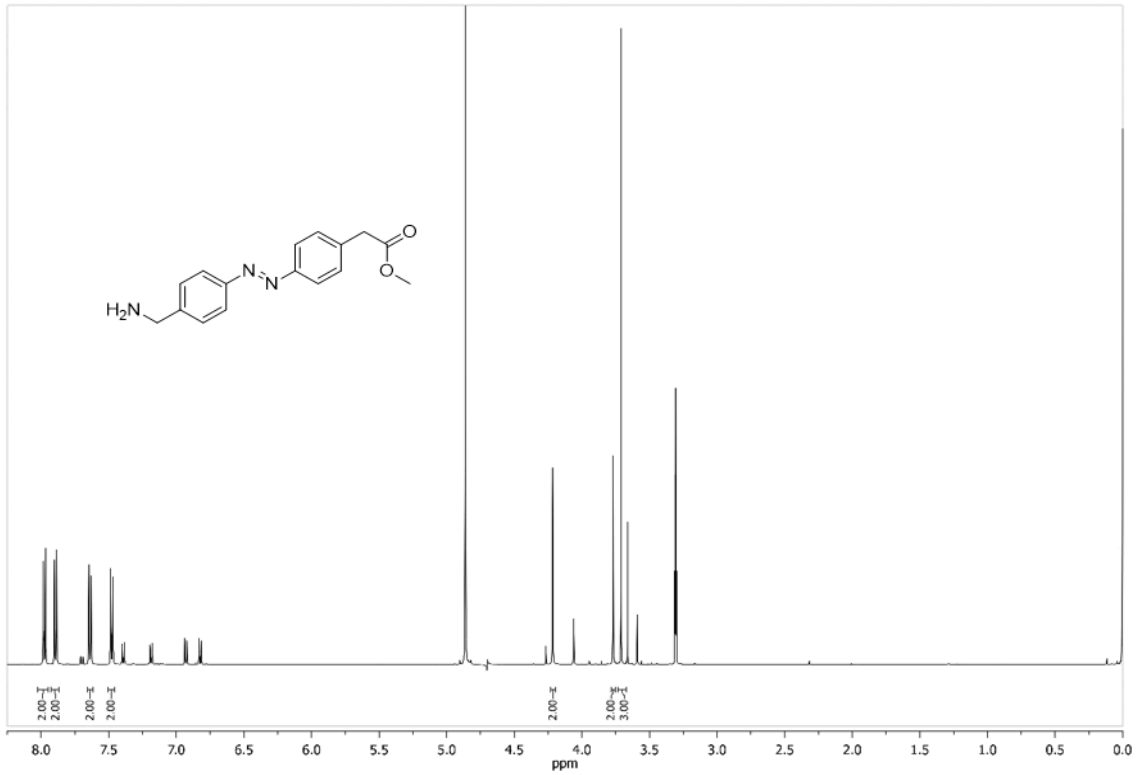

Figure 324: ^{1}H NMR spectrum of compound **55** (500 MHz, MeOD, 300 K).

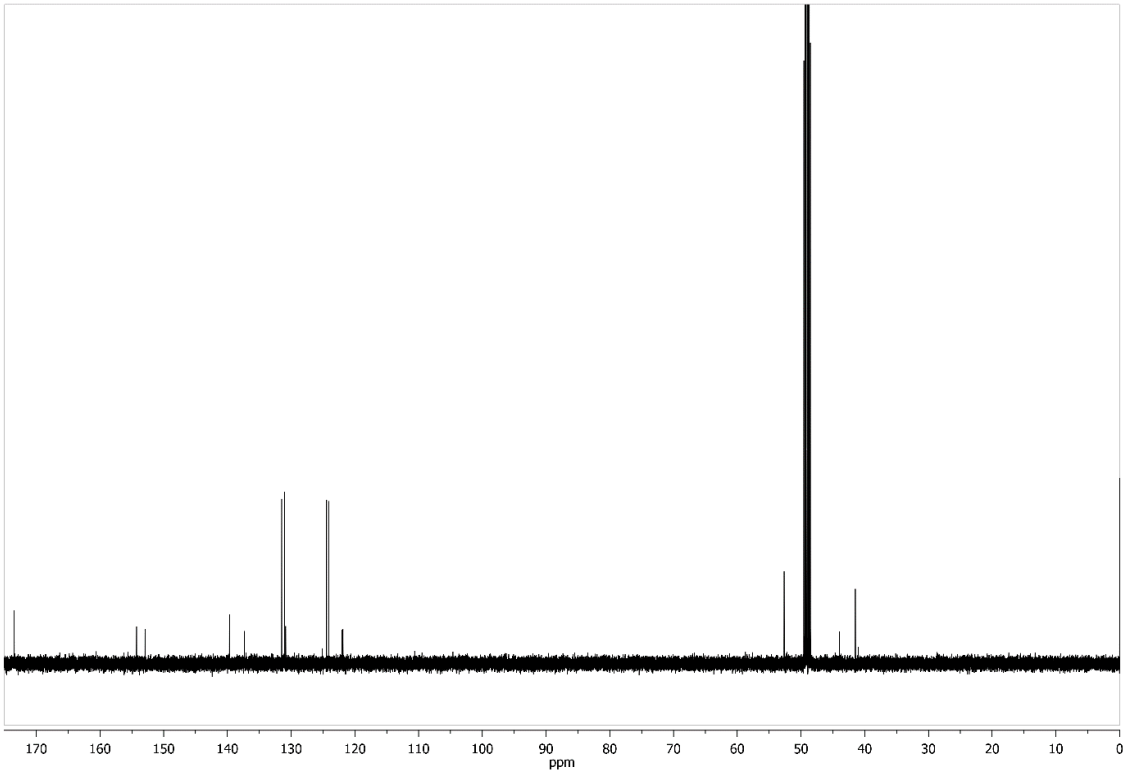

Figure 325: ^{13}C NMR spectrum of compound **55** (126 MHz, MeOD, 300 K).

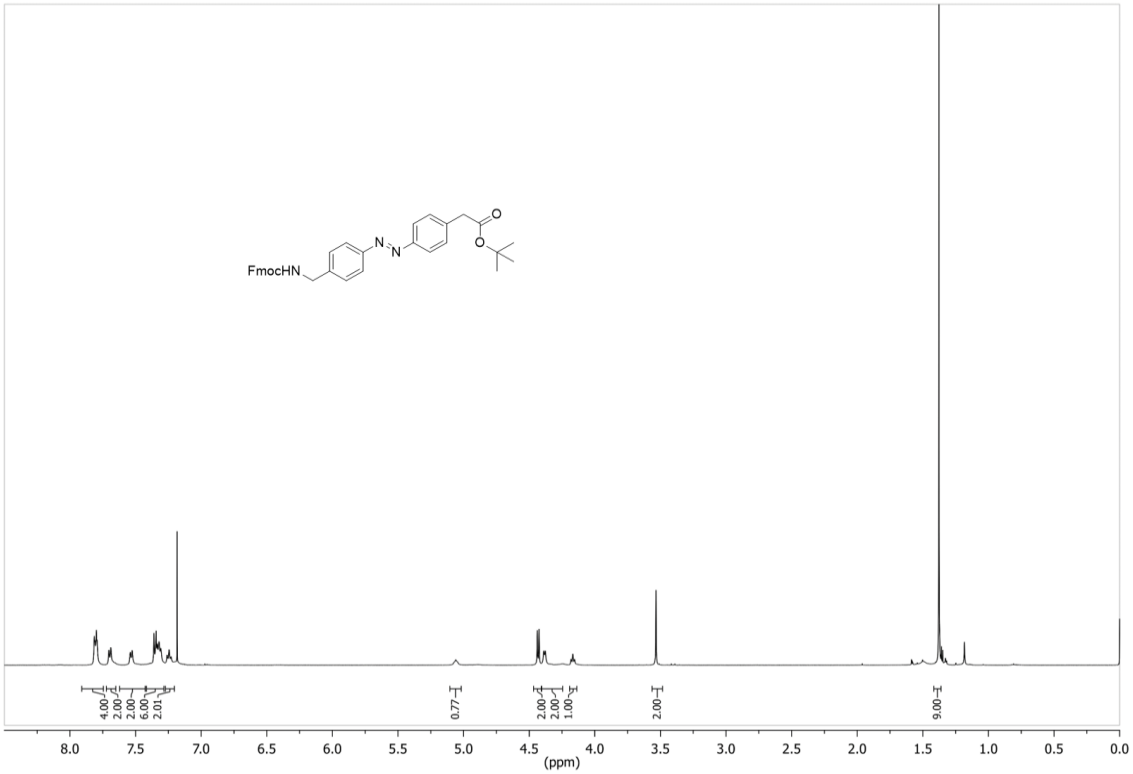

Figure 326: ^{1}H NMR spectrum of compound **56** (500 MHz, $CDCl_3$, 300 K).

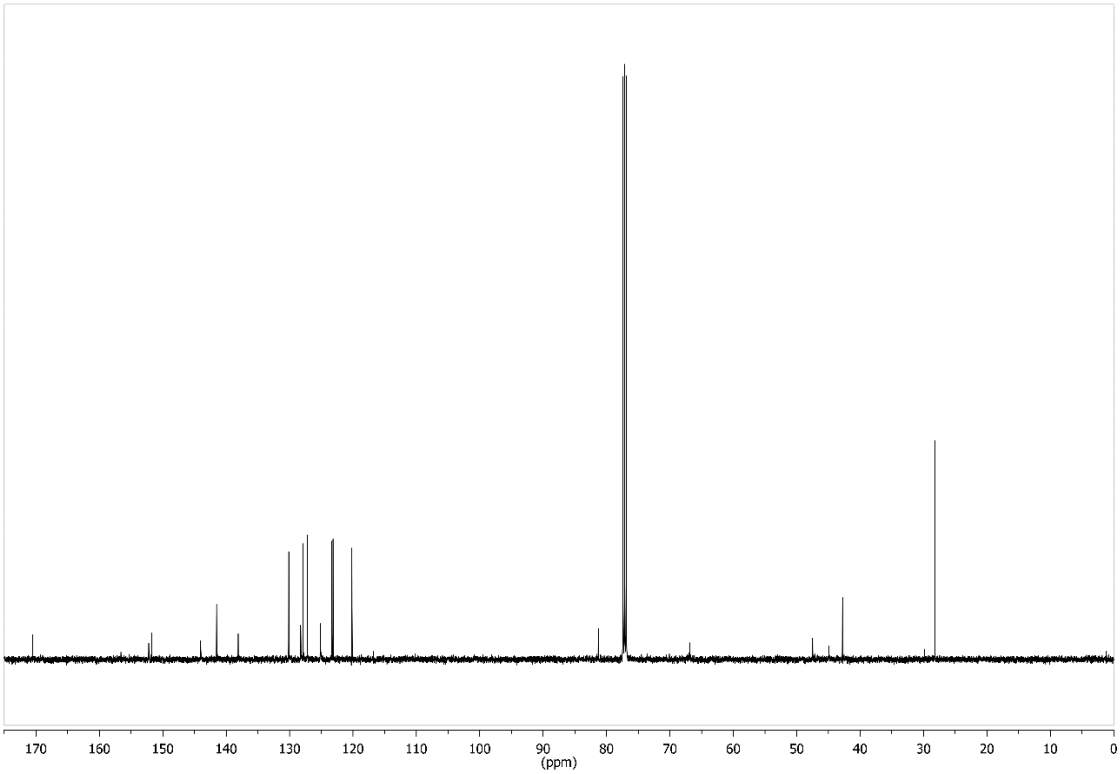

Figure 327: ^{13}C NMR spectrum of compound **56** (126 MHz, $CDCl_3$, 300 K).

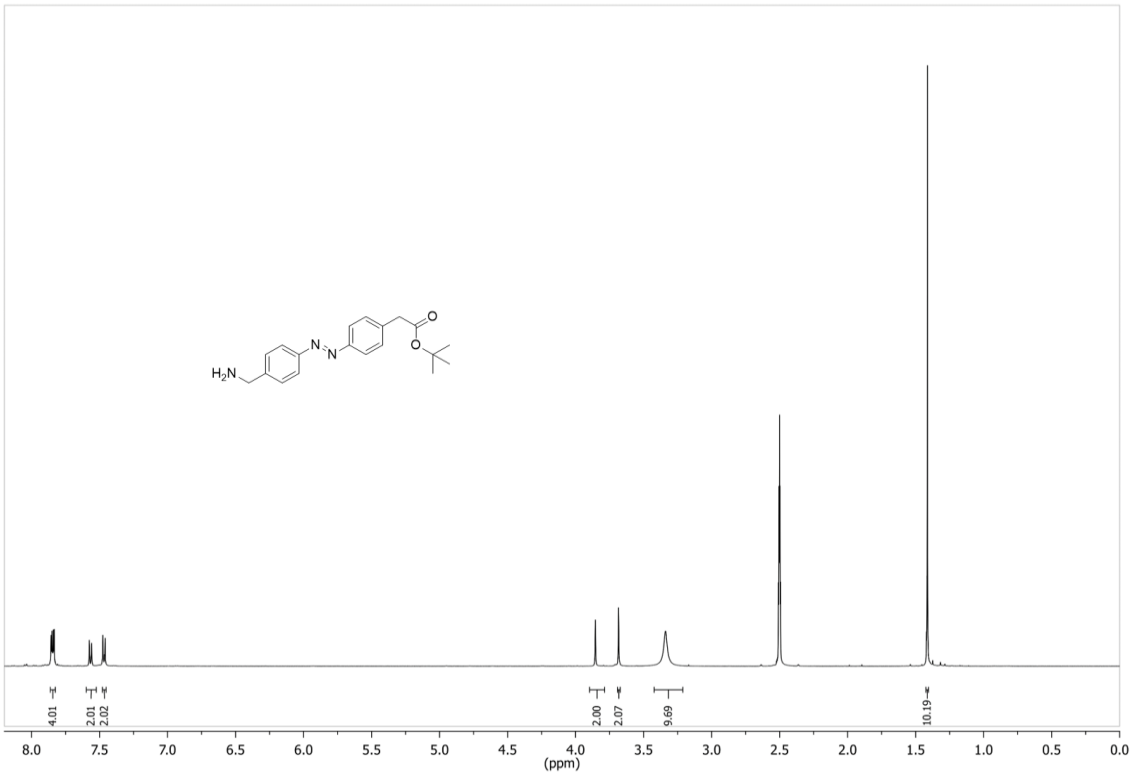

Figure 328: ^{1}H NMR spectrum of compound **57** (500 MHz, DMSO-*d6*, 300 K).

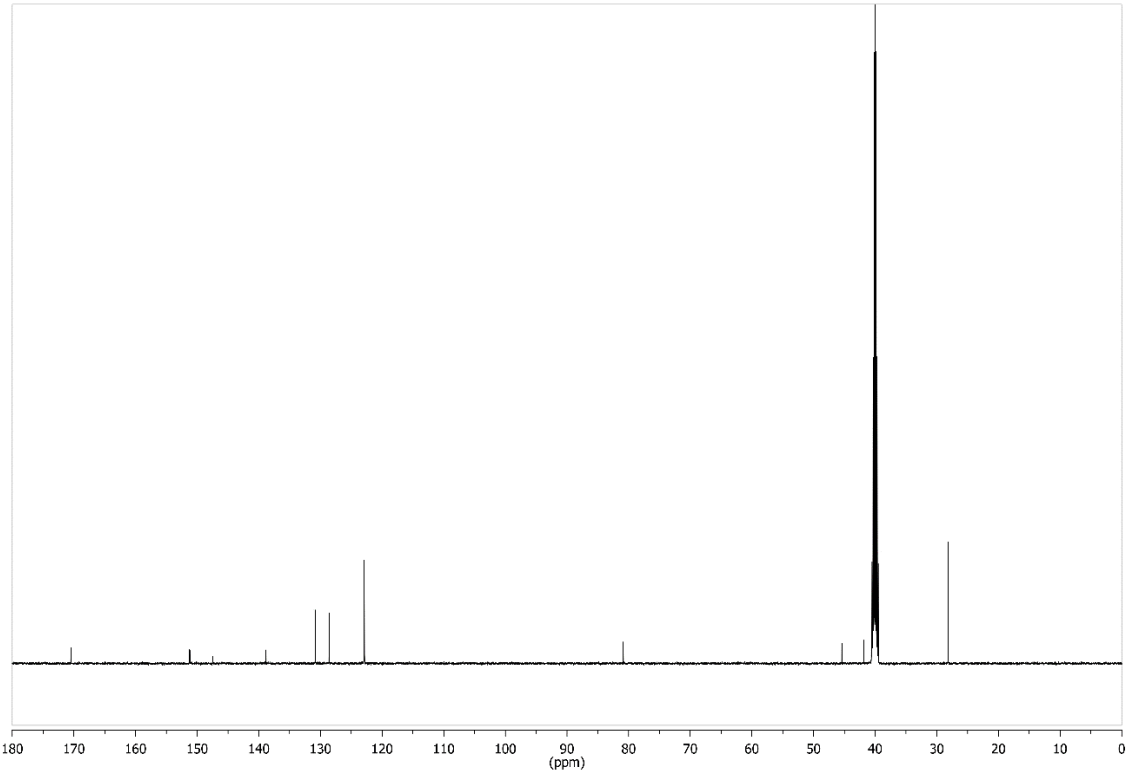

Figure 329: ^{13}C NMR spectrum of compound **57** (126 MHz, DMSO-*d6*, 300 K).

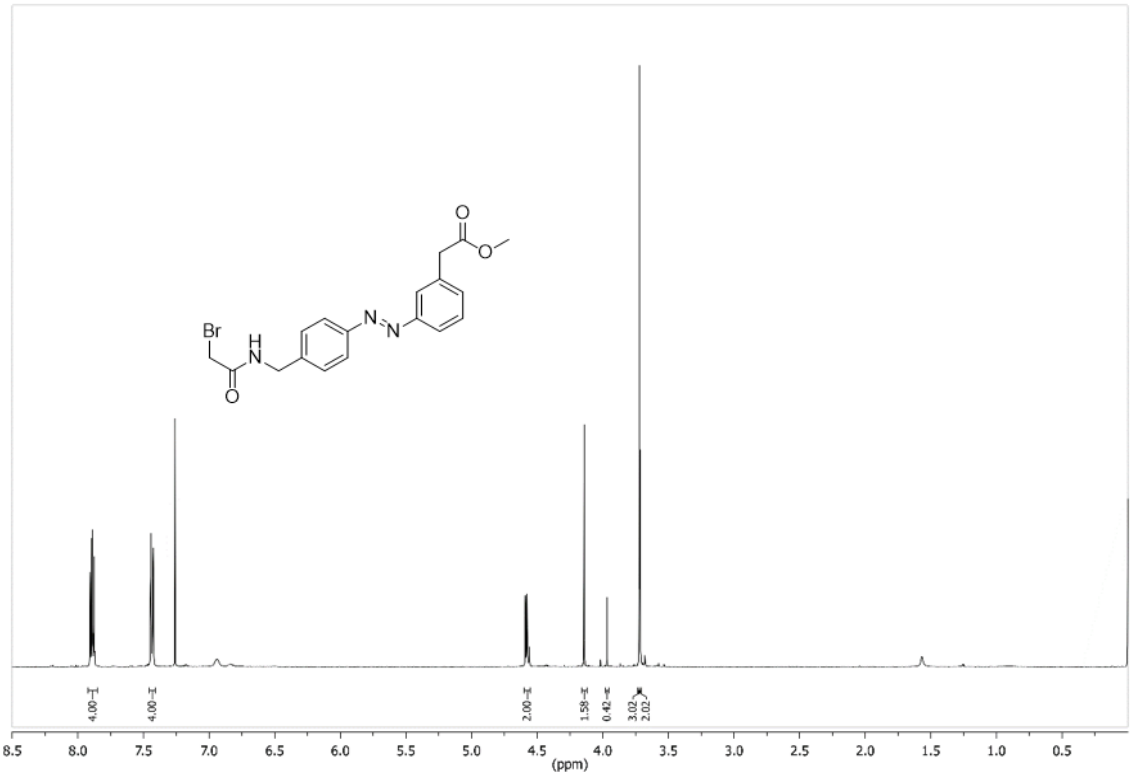

Figure 330: ^{1}H NMR spectrum of compound **59** (500 MHz, $CDCl_3$, 300 K).

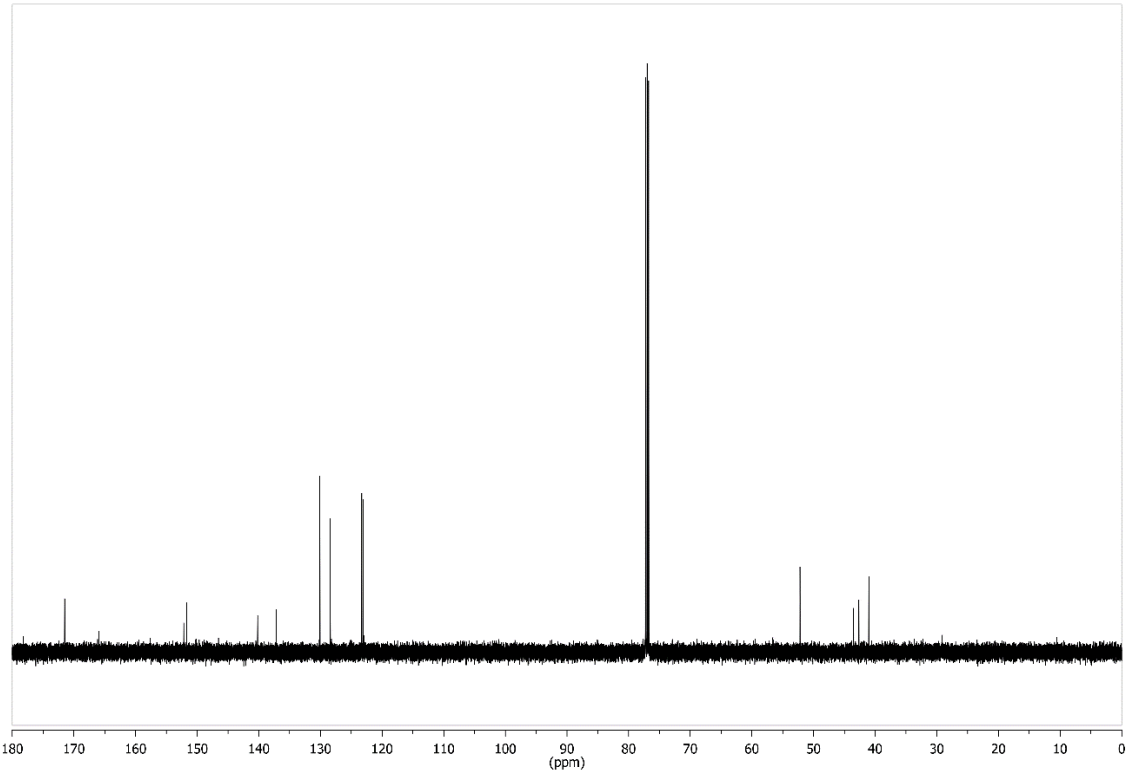

Figure 331: ^{13}C NMR spectrum of compound **59** (126 MHz, $CDCl_3$, 300 K).

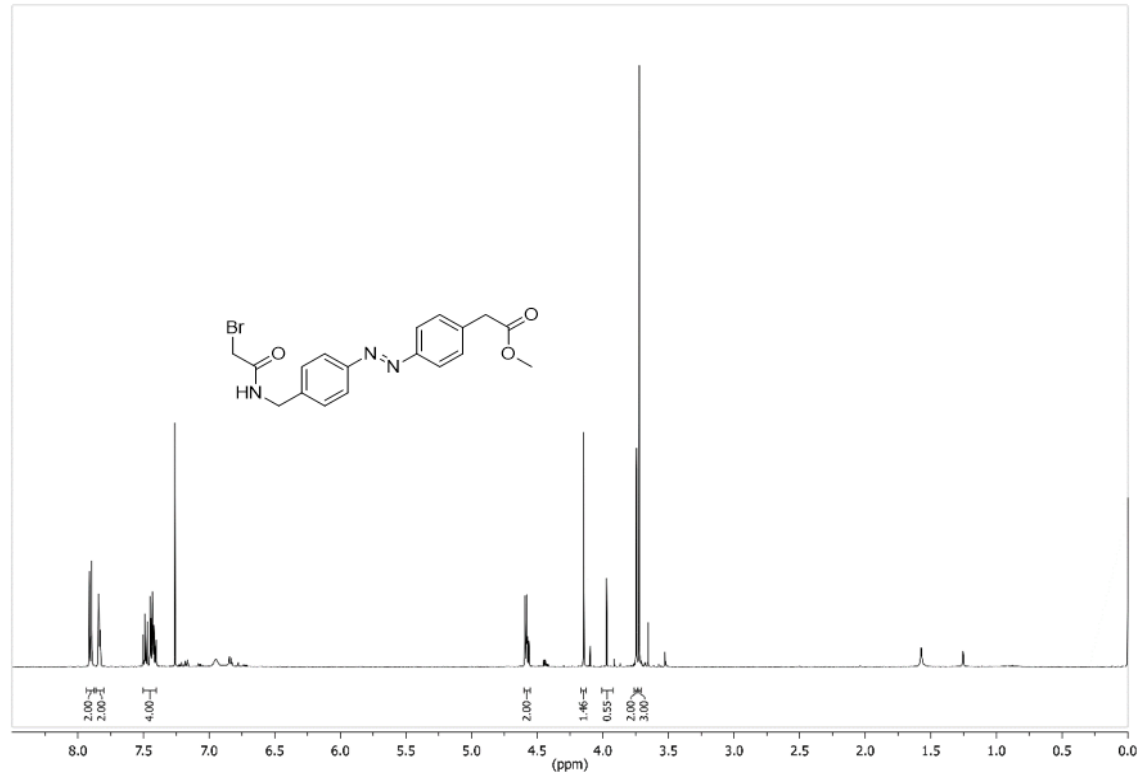

Figure 332: ^{1}H NMR spectrum of compound **60** (500 MHz, $CDCl_3$, 300 K).

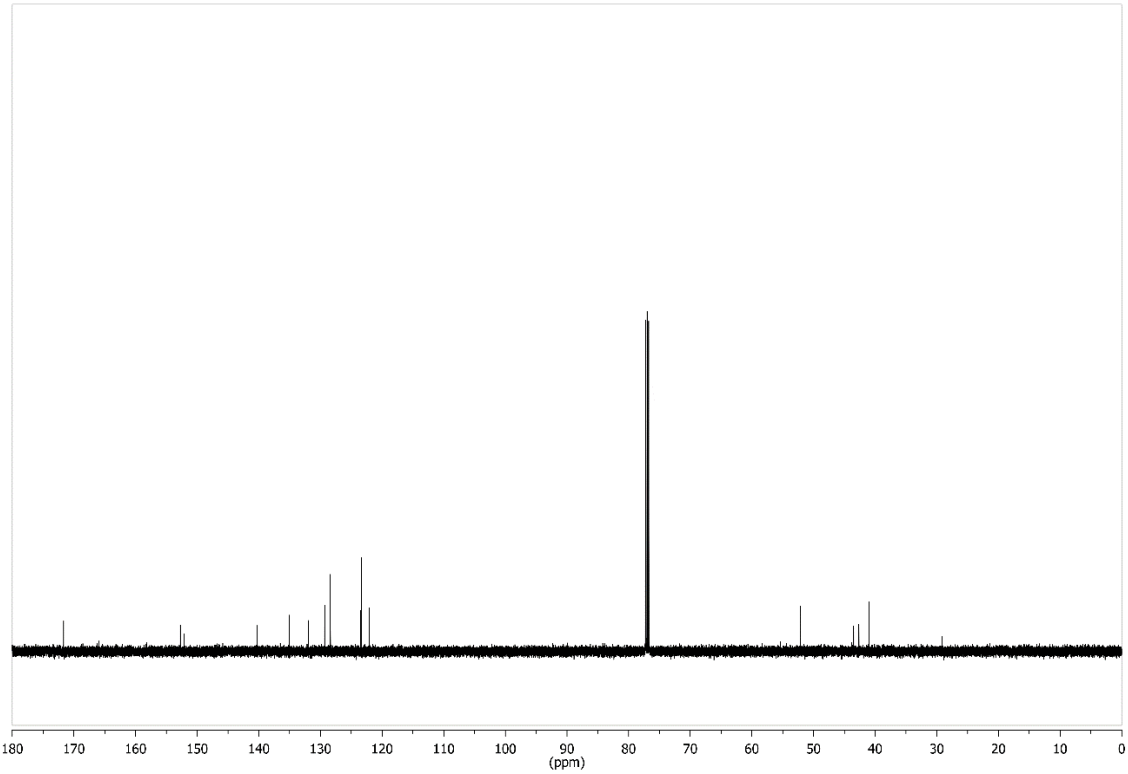

Figure 333: ^{13}C NMR spectrum of compound **60** (126 MHz, $CDCl_3$, 300 K).

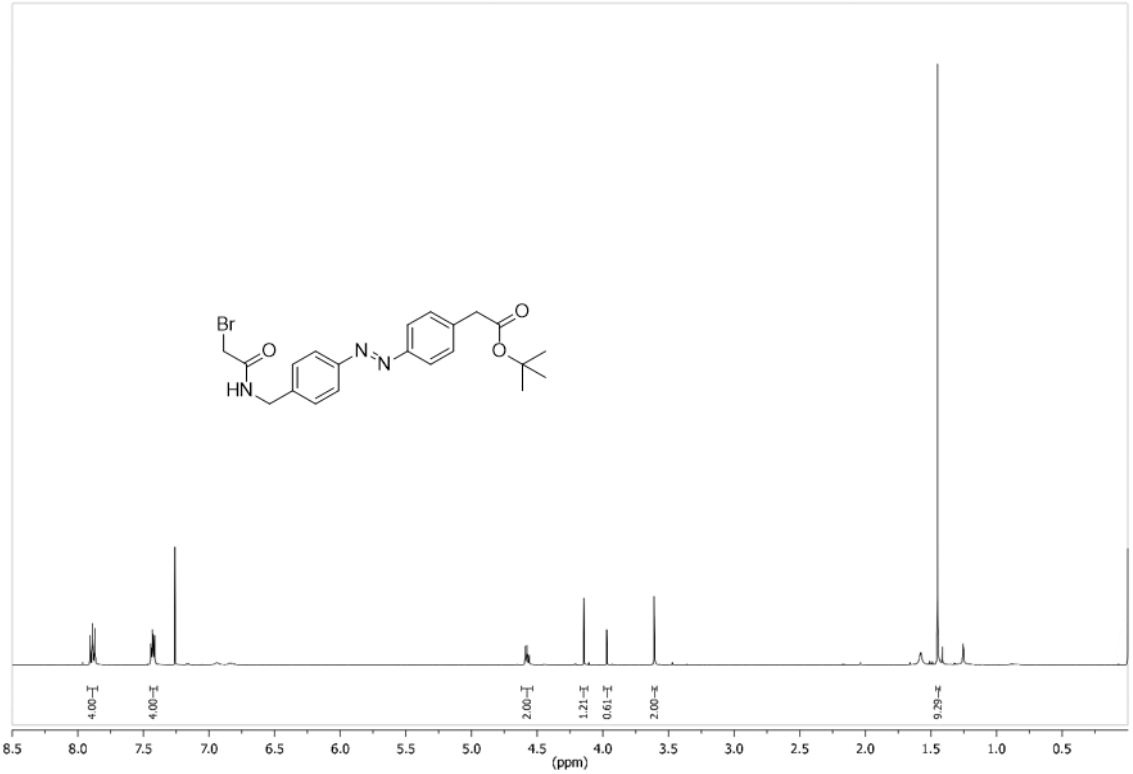

Figure 334: ^{1}H NMR spectrum of compound **61** (500 MHz, $CDCl_3$, 300 K).

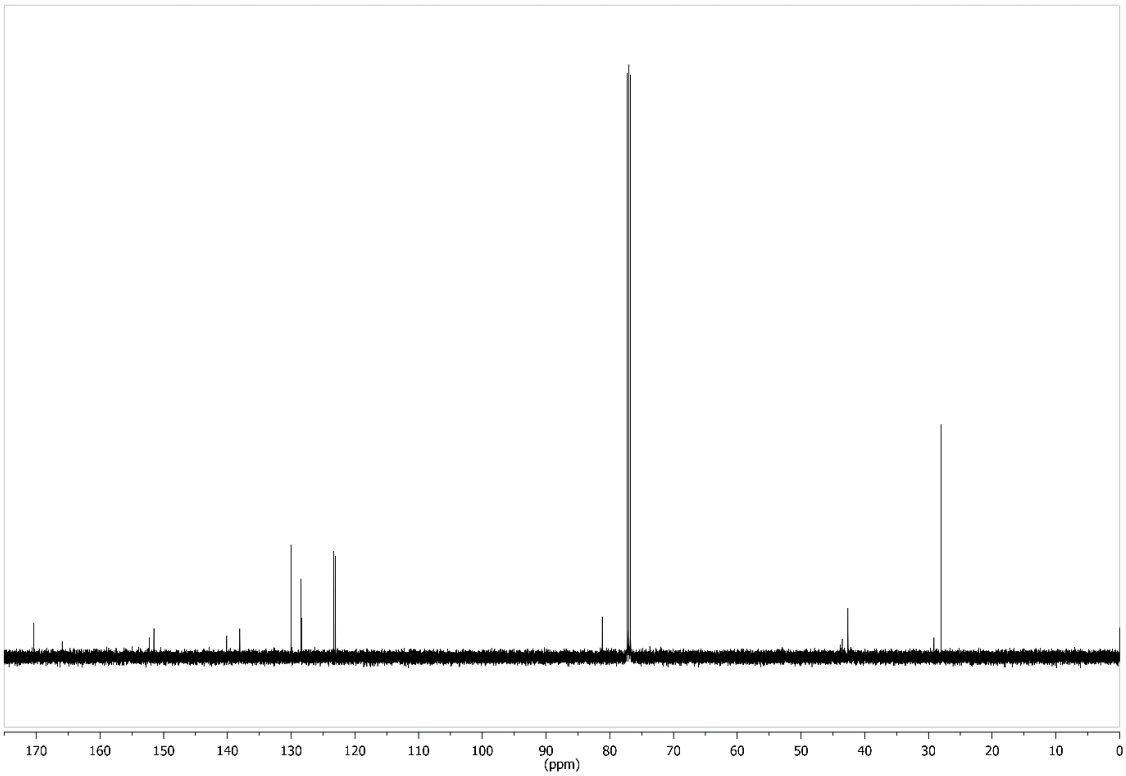

Figure 335: ^{13}C NMR spectrum of compound **61** (126 MHz, $CDCl_3$, 300 K).

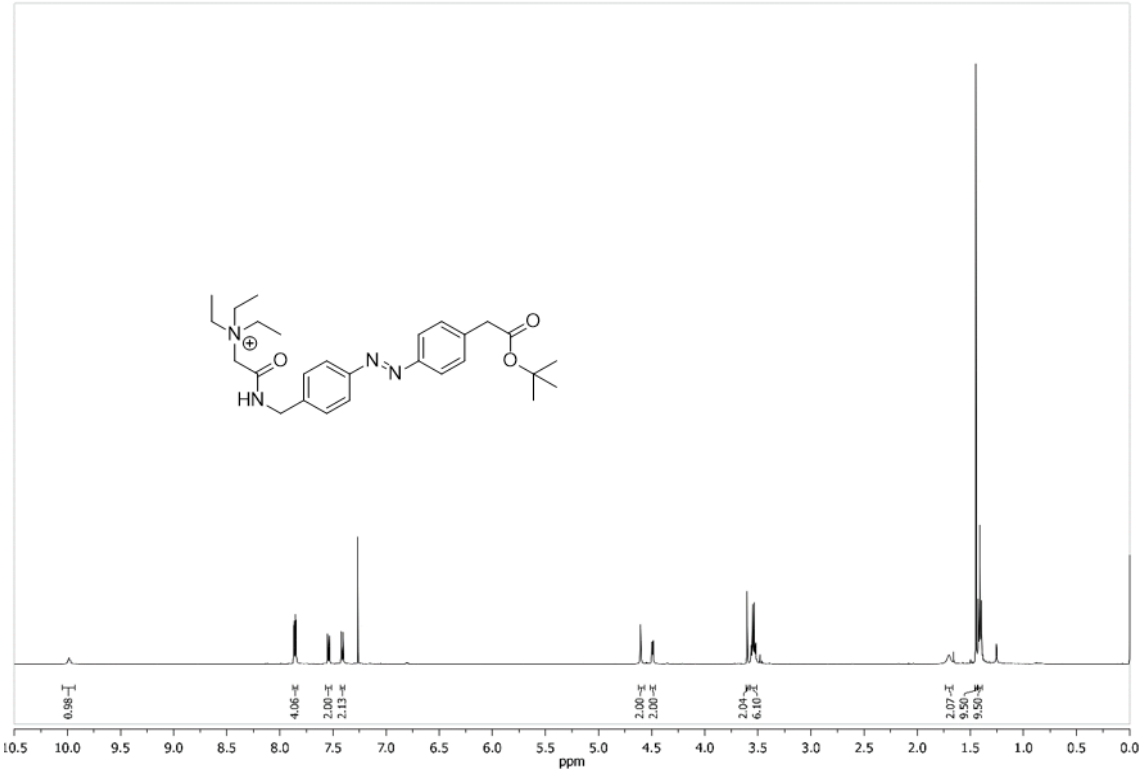

Figure 336: ^{1}H NMR spectrum of compound **62** (500 MHz, $CDCl_3$, 300 K).

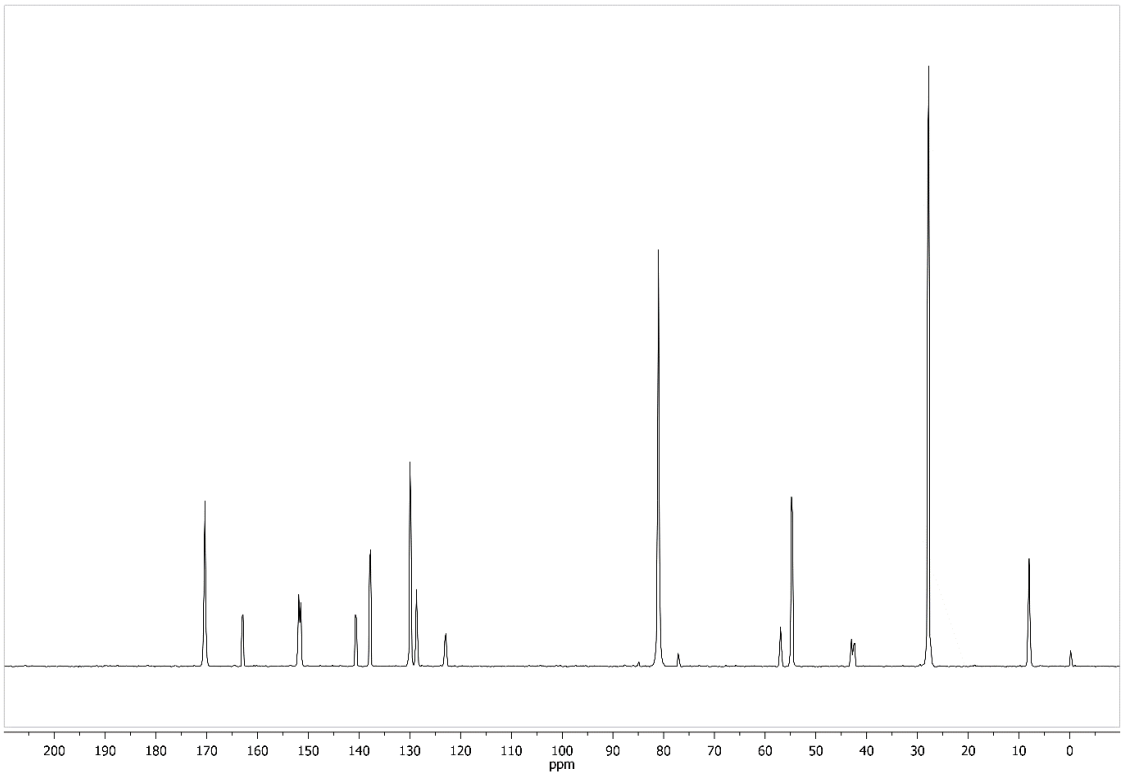

Figure 337: ^{13}C NMR spectrum of compound **62** (126 MHz, $CDCl_3$, 300 K).

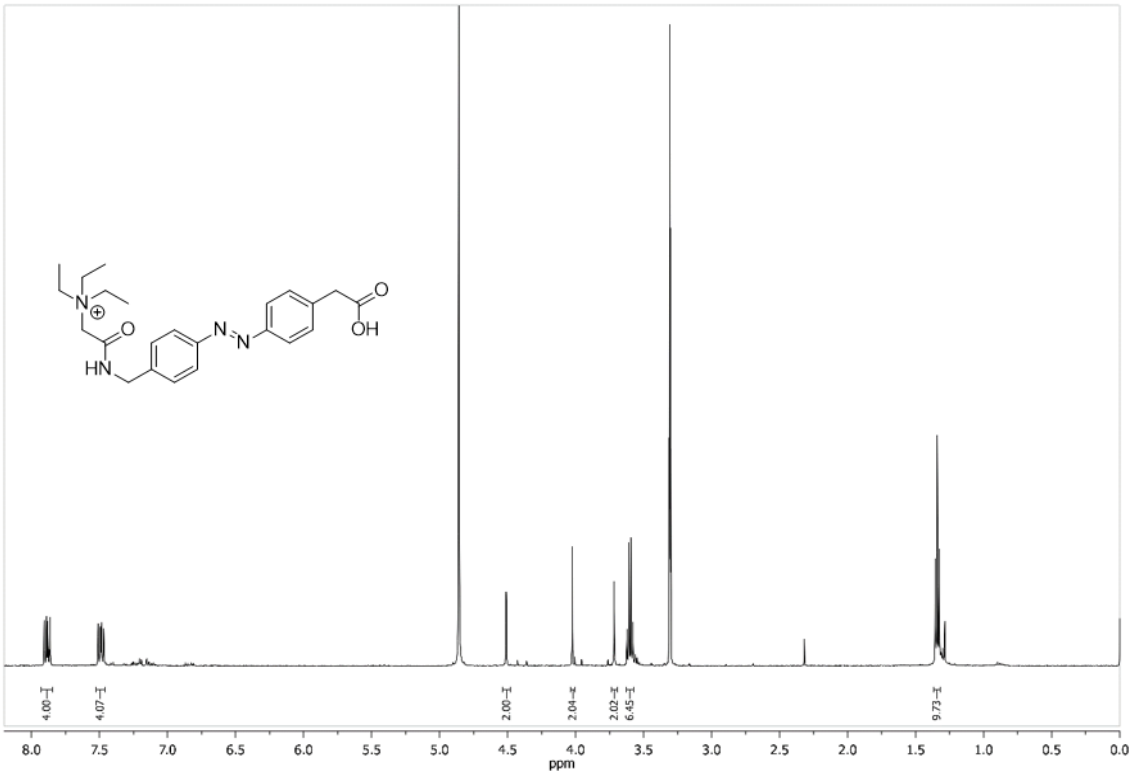

Figure 338: ^{1}H NMR spectrum of compound **63** (500 MHz, MeOD, 300 K).

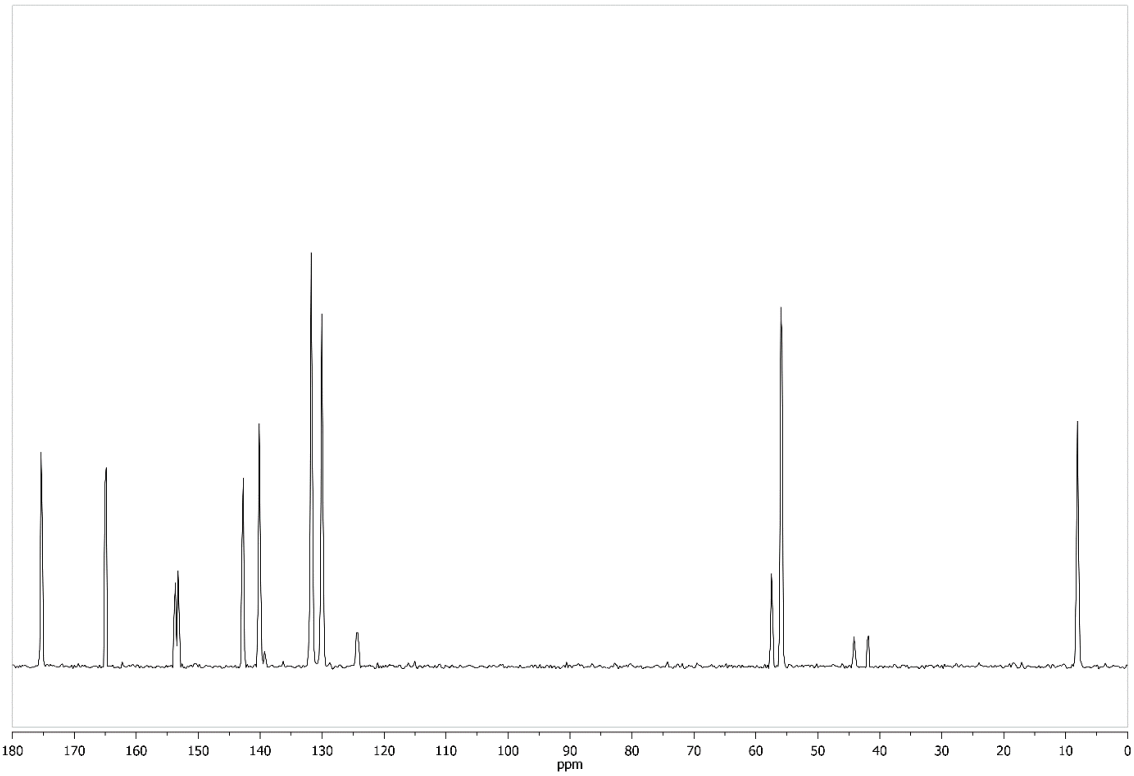

Figure 339: ^{13}C NMR spectrum of compound **63** (126 MHz, MeOD, 300 K).

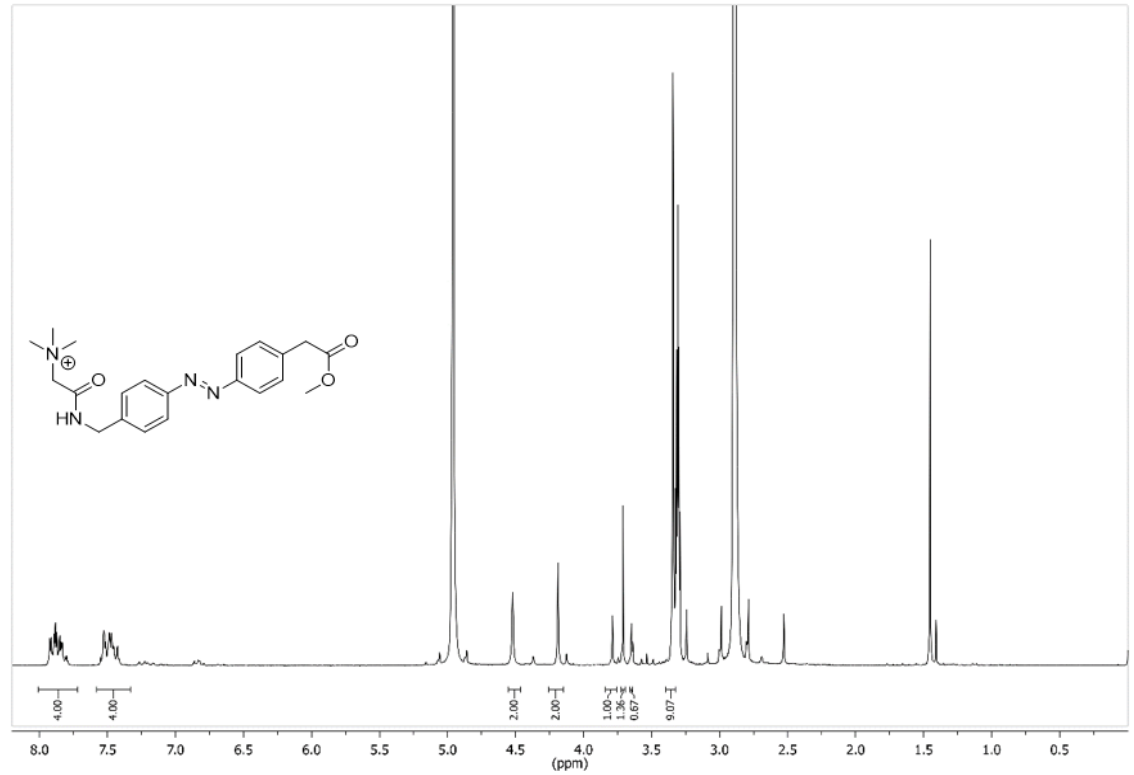

Figure 340: ^{1}H NMR spectrum of compound **65-I** (200 MHz, MeOD, 300 K).

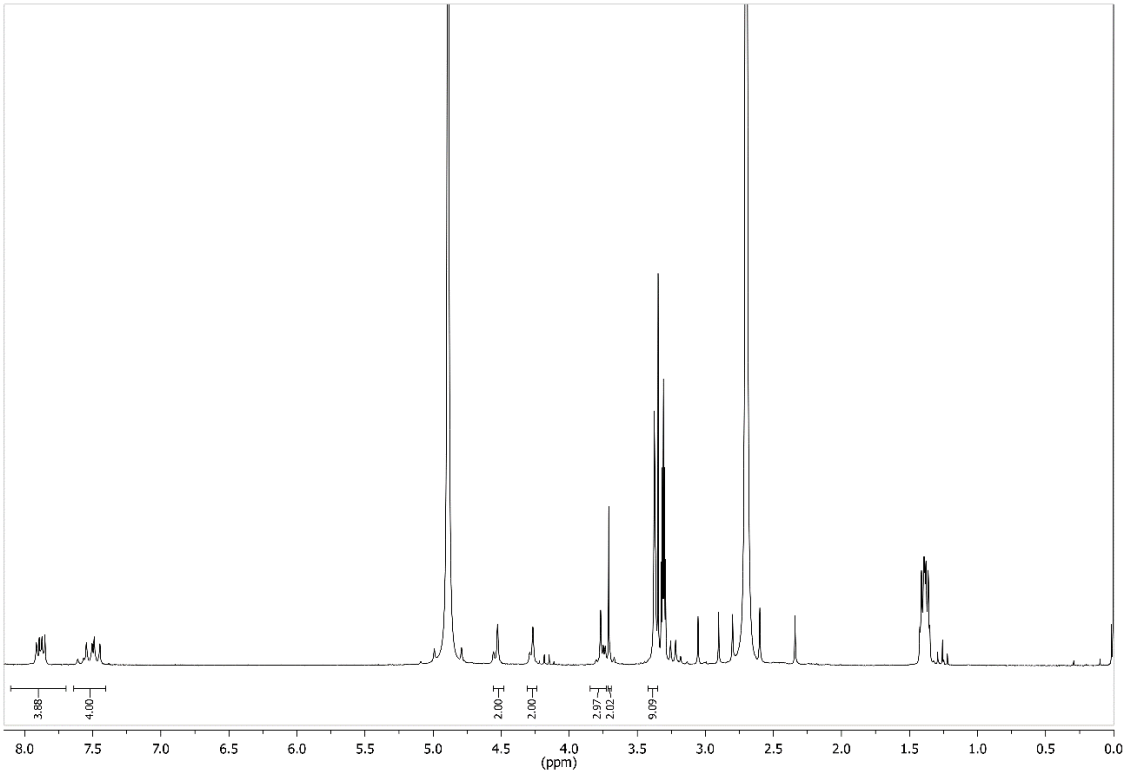

Figure 341: ^{1}H NMR spectrum of compound **65-II** (200 MHz, MeOD, 300 K).

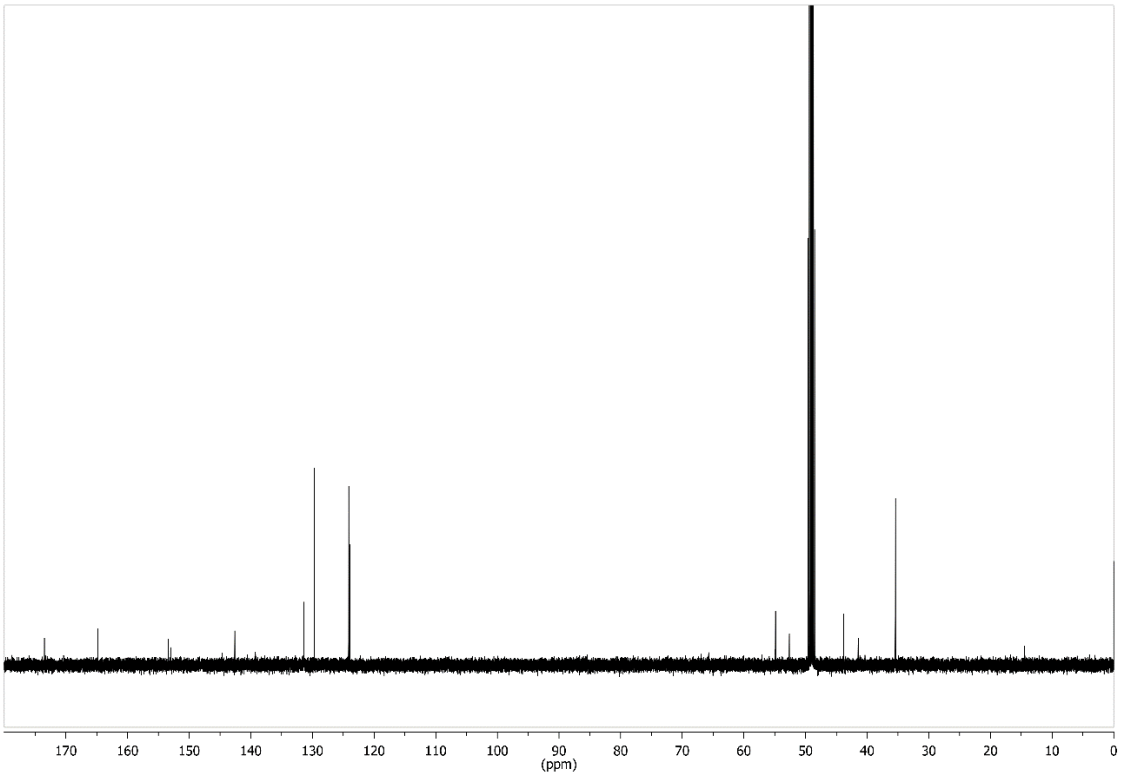

Figure 342: ^{13}C NMR spectrum of compound **65-II** (126 MHz, MeOD, 300 K).

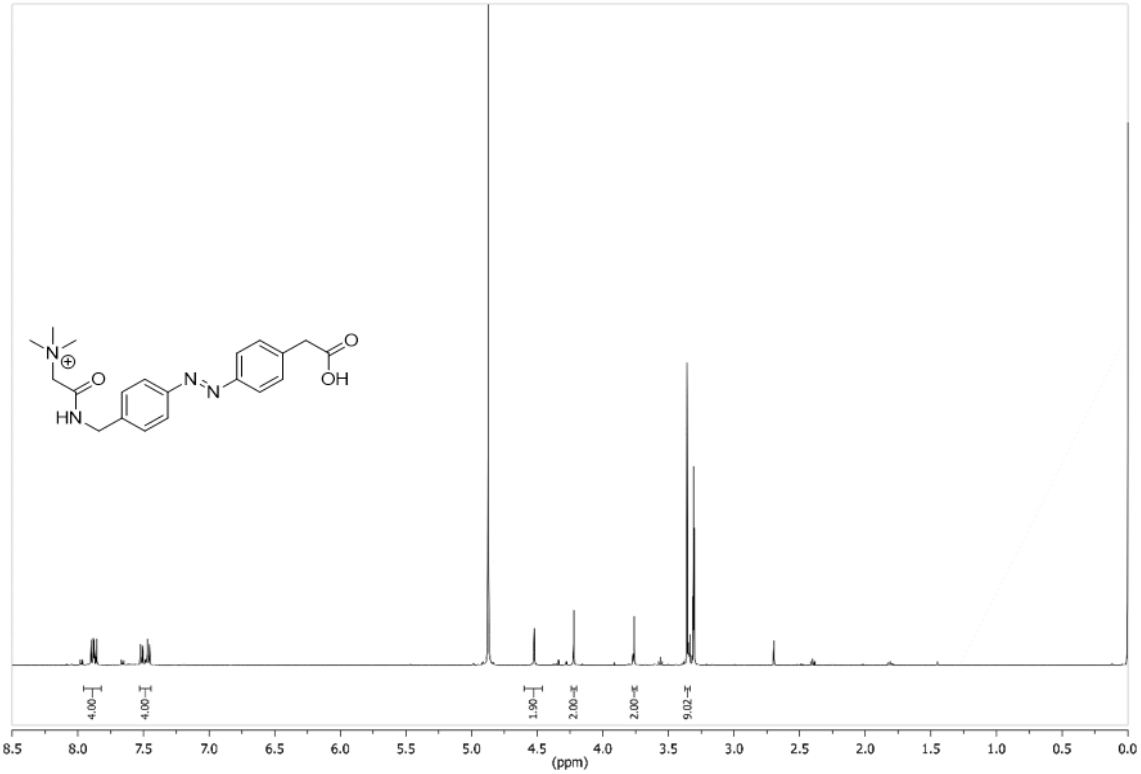

Figure 343: ^{1}H NMR spectrum of compound **66** (500 MHz, MeOD, 300 K).

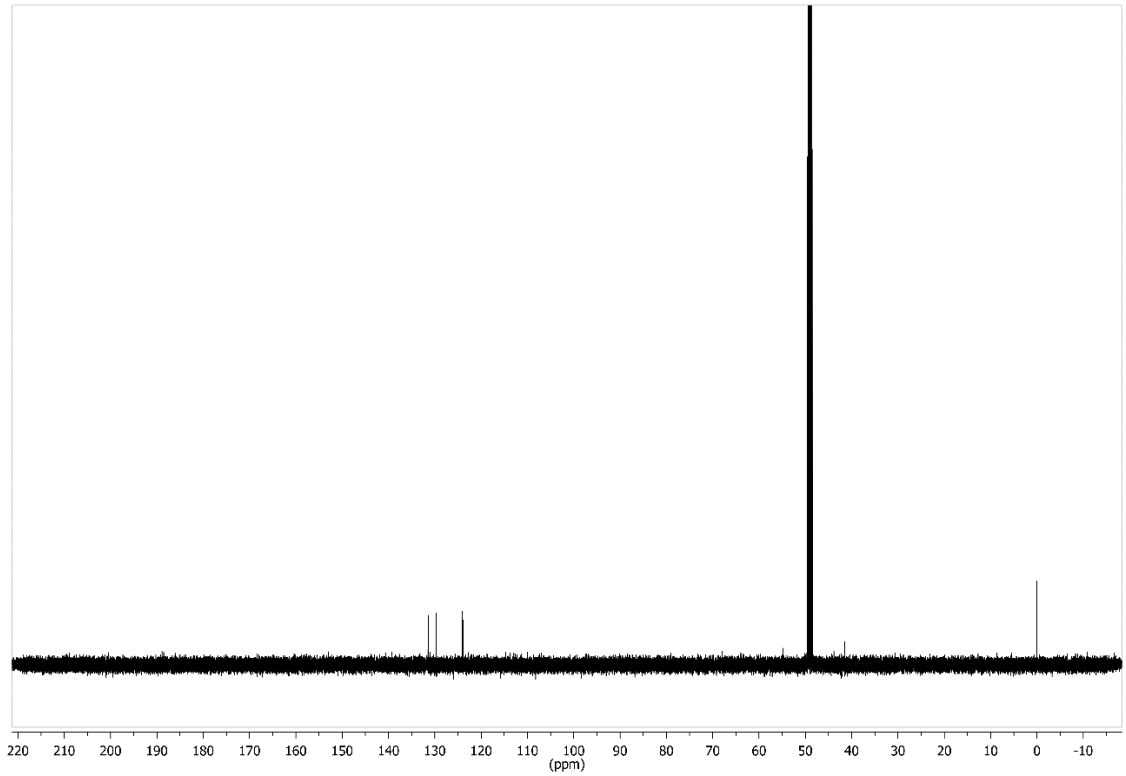

Figure 344: ^{13}C NMR spectrum of compound **66** (126 MHz, MeOD, 300 K).

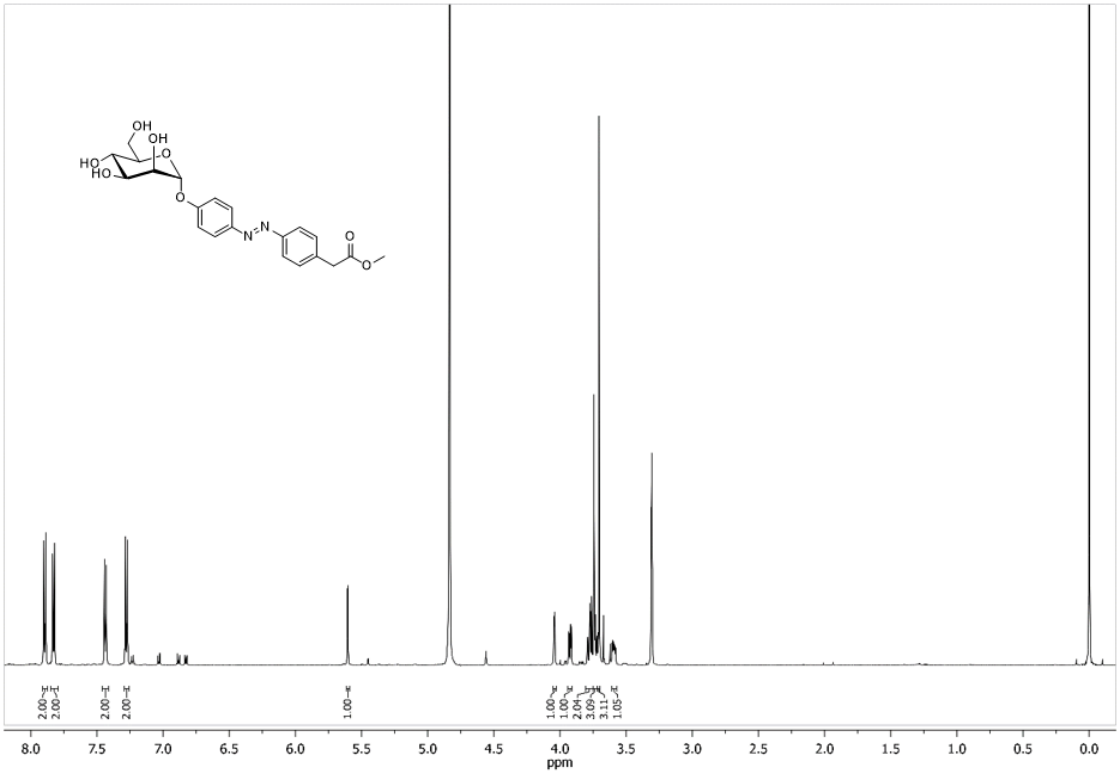

Figure 345: [1]H NMR spectrum of compound **70** (500 MHz, MeOD, 300 K).

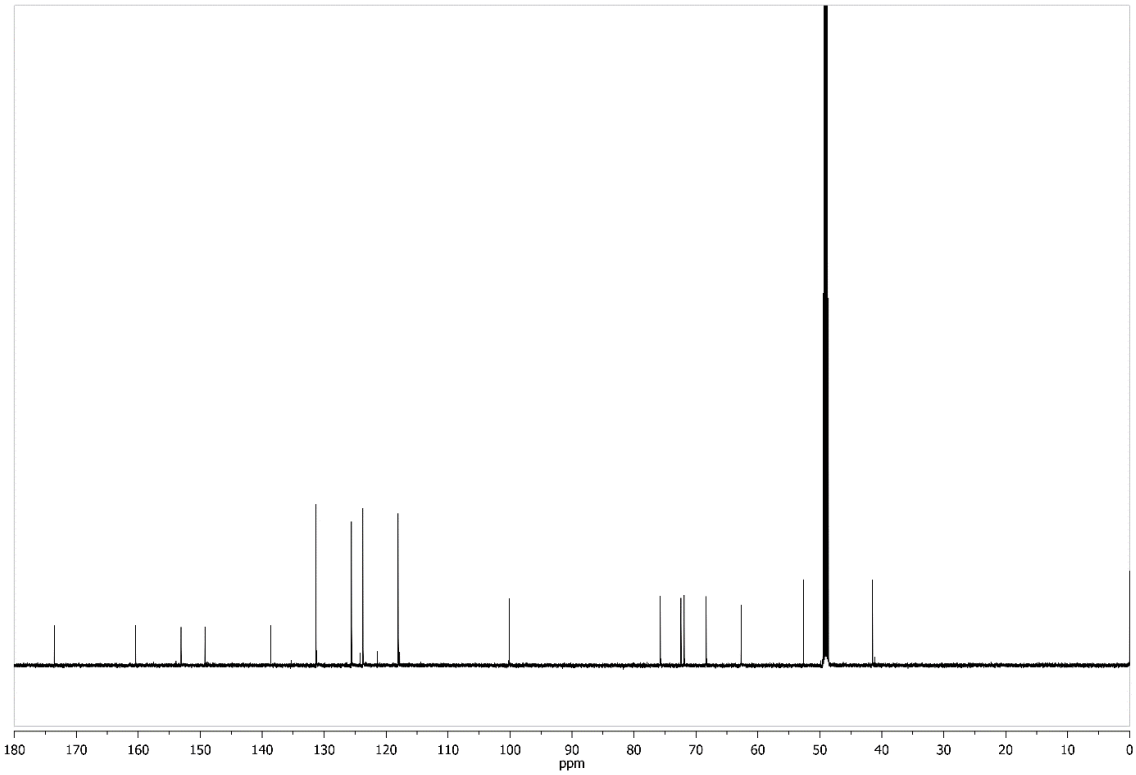

Figure 346: [13]C NMR spectrum of compound **70** (126 MHz, MeOD, 300 K).

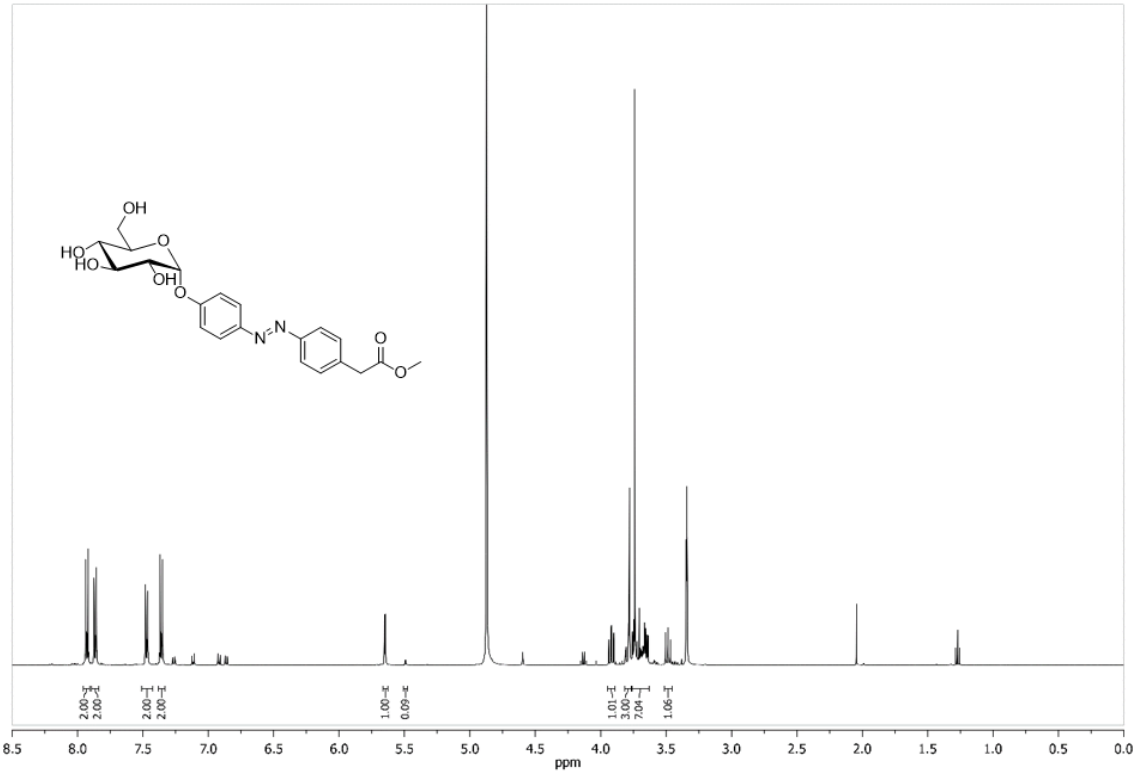

Figure 347: ^{1}H NMR spectrum of compound **71** (500 MHz, MeOD, 300 K).

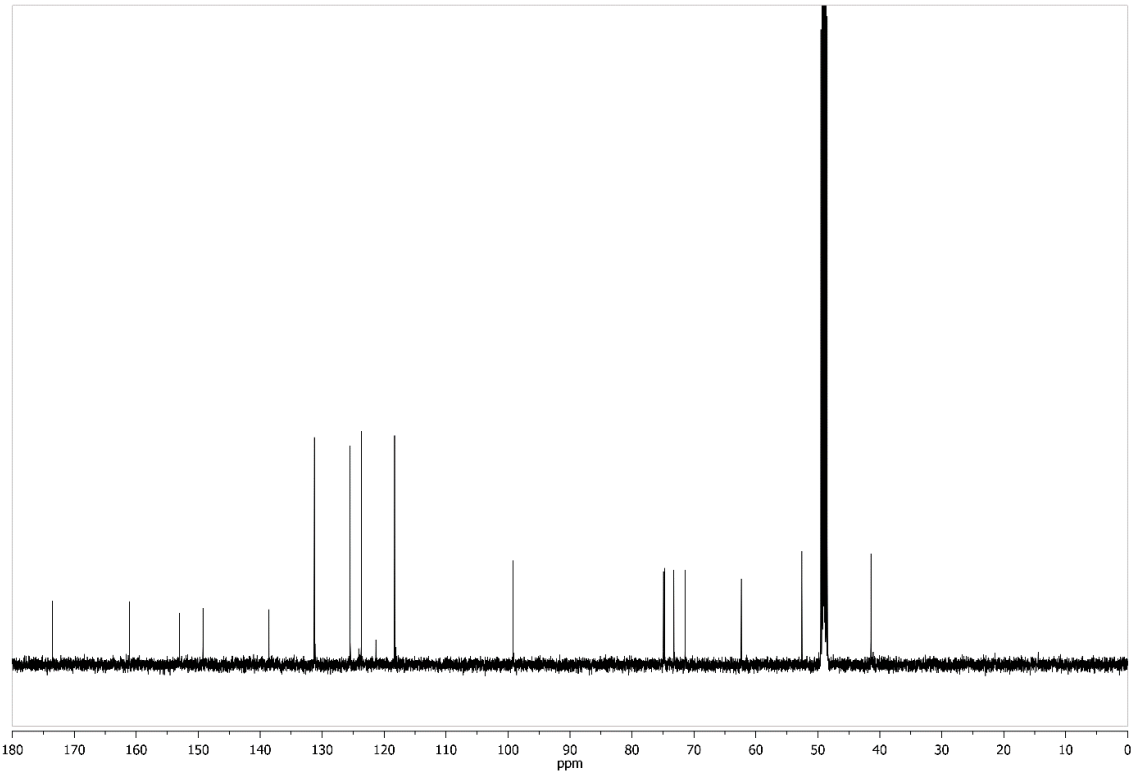

Figure 348: ^{13}C NMR spectrum of compound **71** (126 MHz, MeOD, 300 K).

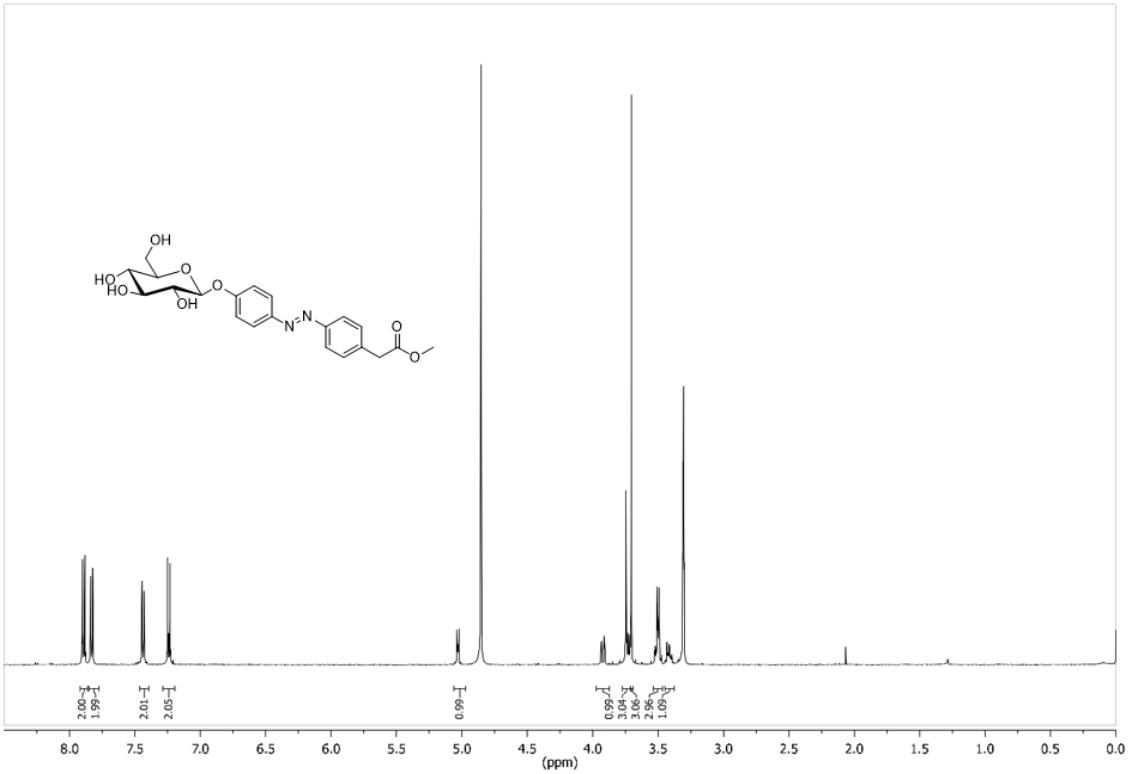

Figure 349: [1]H NMR spectrum of compound **72** (500 MHz, MeOD, 300 K).

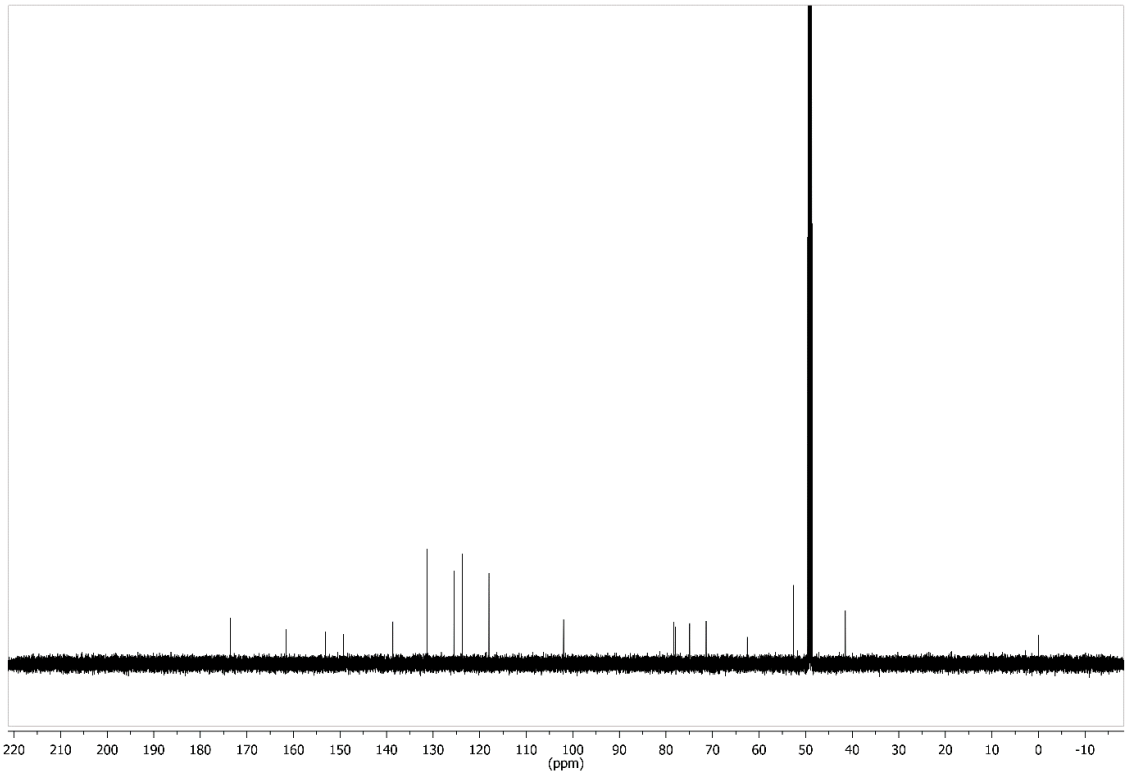

Figure 350: [13]C NMR spectrum of compound **72** (126 MHz, MeOD, 300 K).

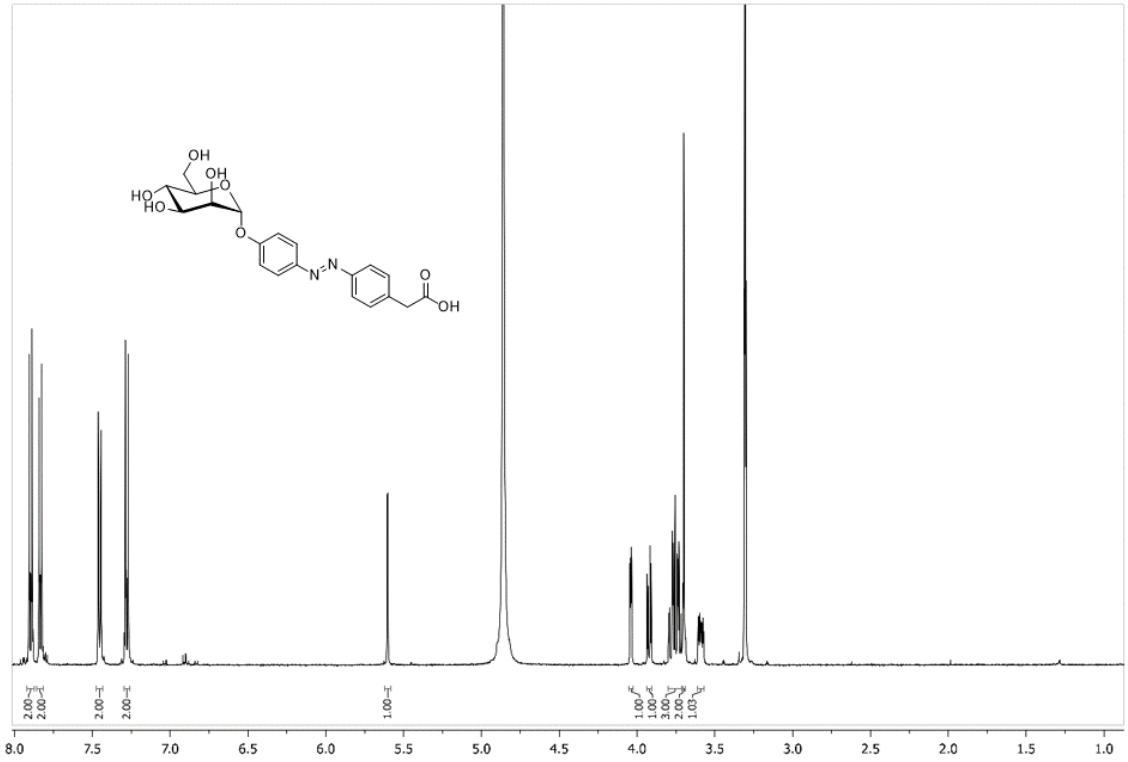

Figure 351: ^{1}H NMR spectrum of compound **73** (500 MHz, MeOD, 300 K).

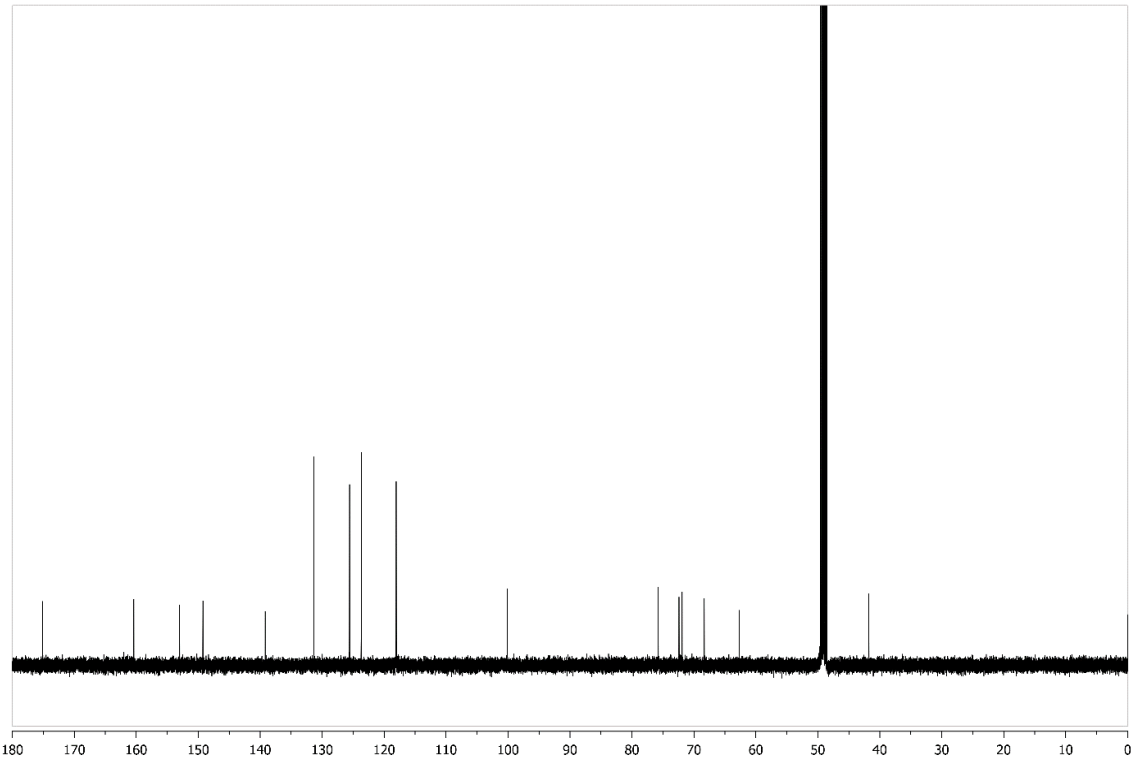

Figure 352: ^{13}C NMR spectrum of compound **73** (126 MHz, MeOD, 300 K).

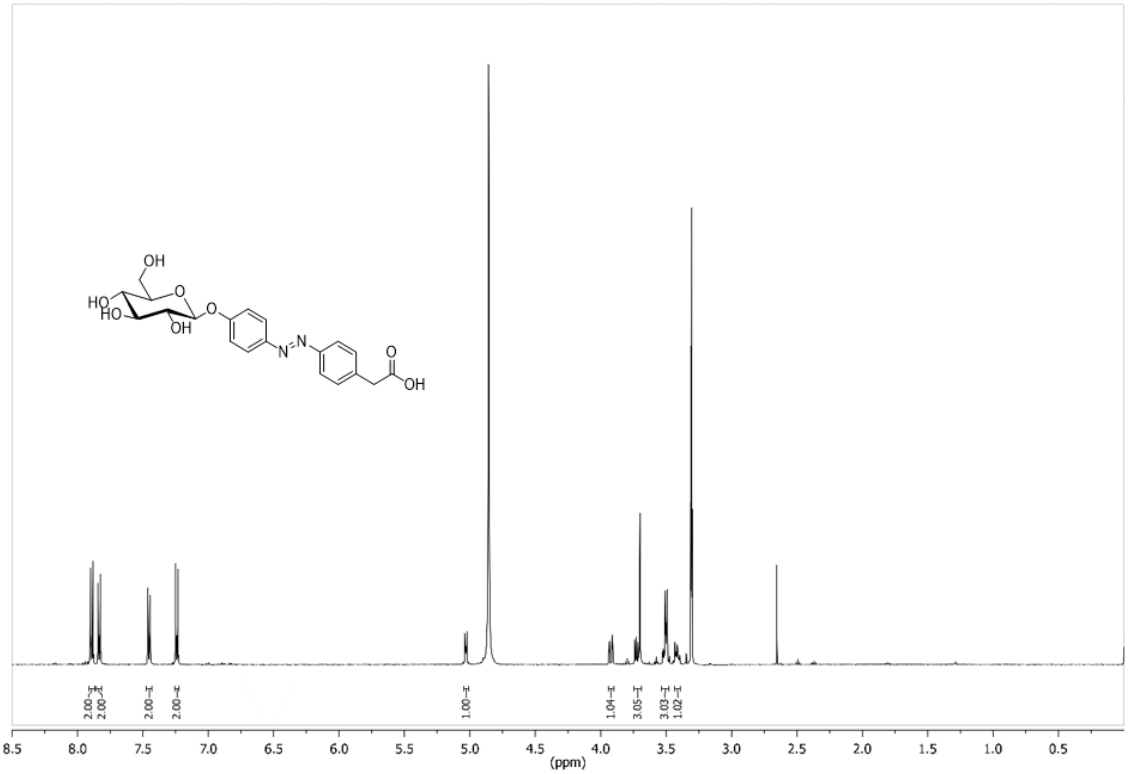

Figure 353: ^{1}H NMR spectrum of compound **75** (500 MHz, MeOD, 300 K).

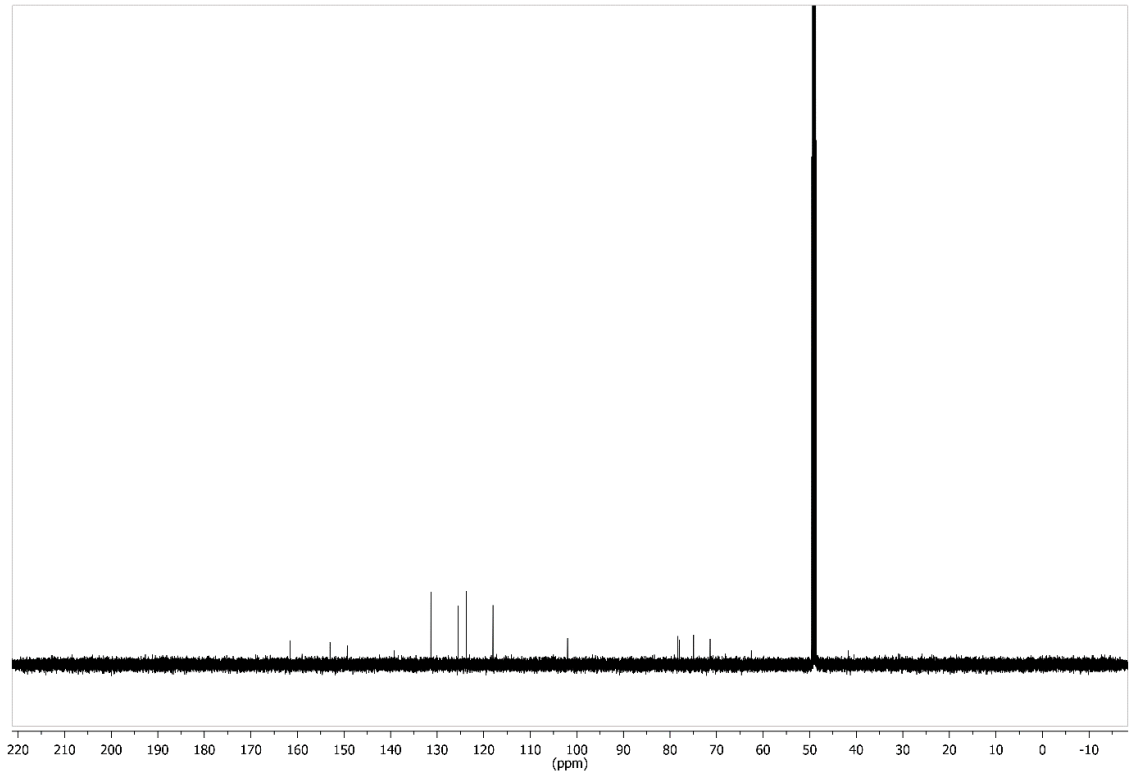

Figure 354: ^{13}C NMR spectrum of compound **75** (126 MHz, MeOD, 300 K).

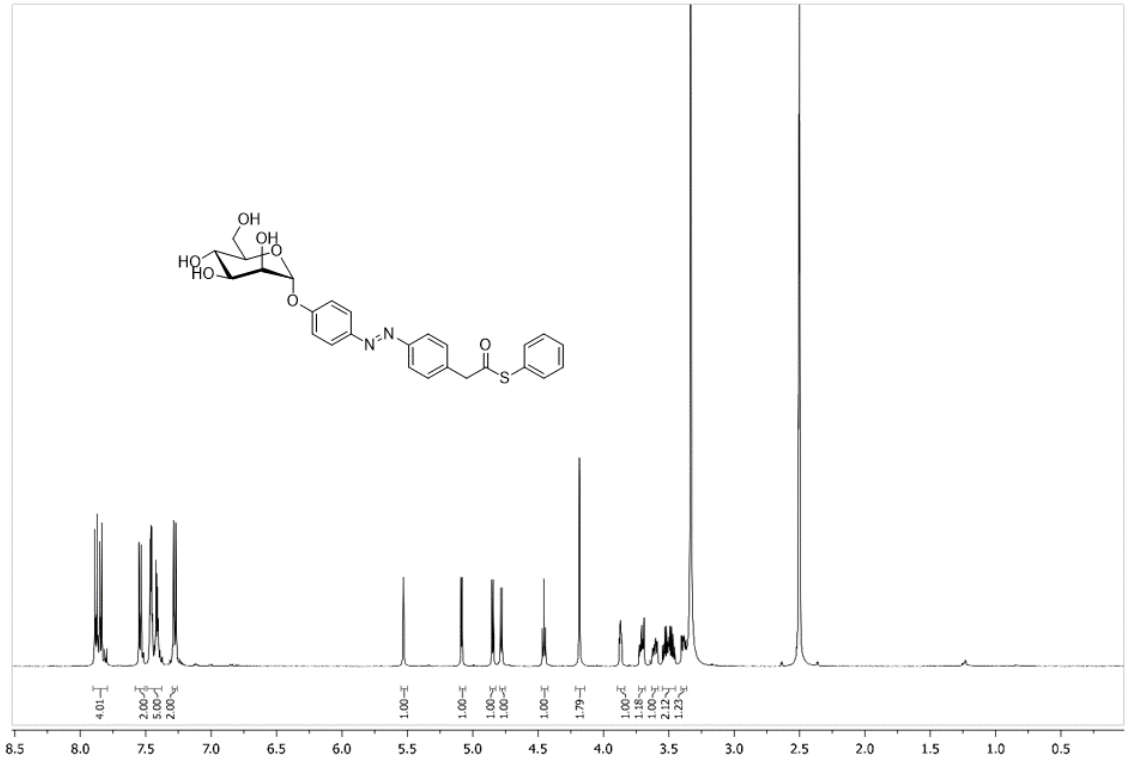

Figure 355: ^{1}H NMR spectrum of compound **78** (500 MHz, MeOD, 300 K).

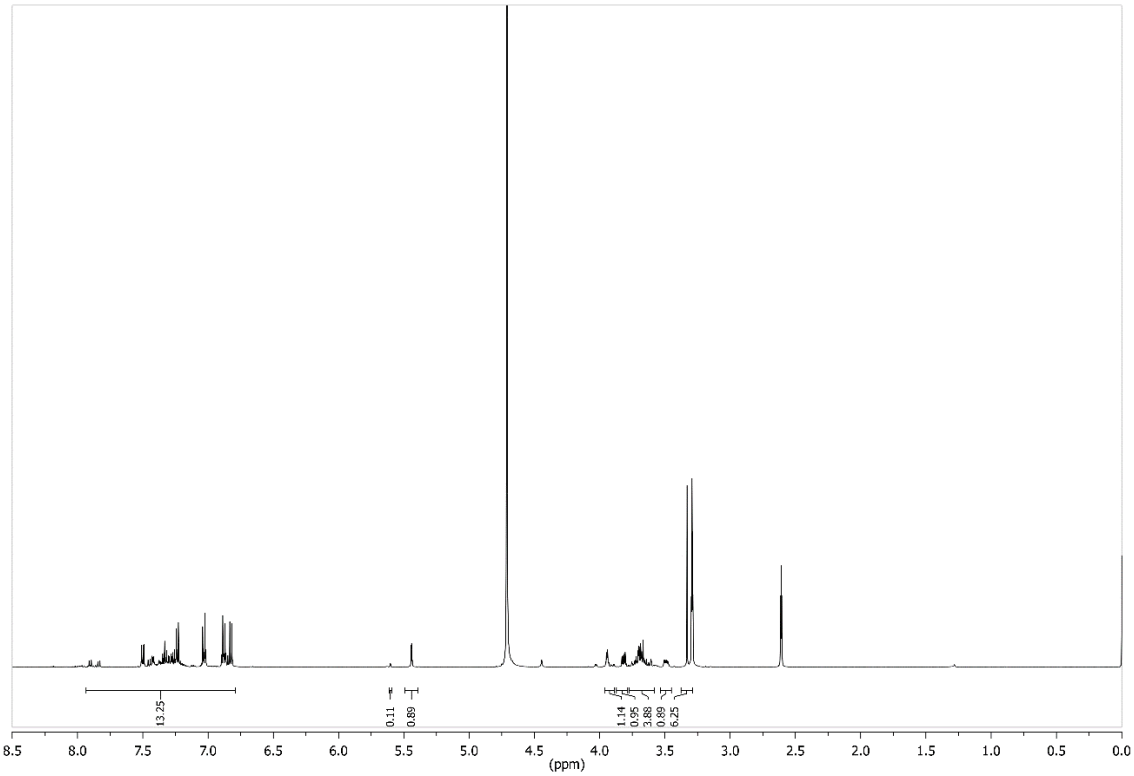

Figure 356: ^{1}H NMR spectrum of compound **78** (*Z*-isomer) (500 MHz, MeOD, 300 K).

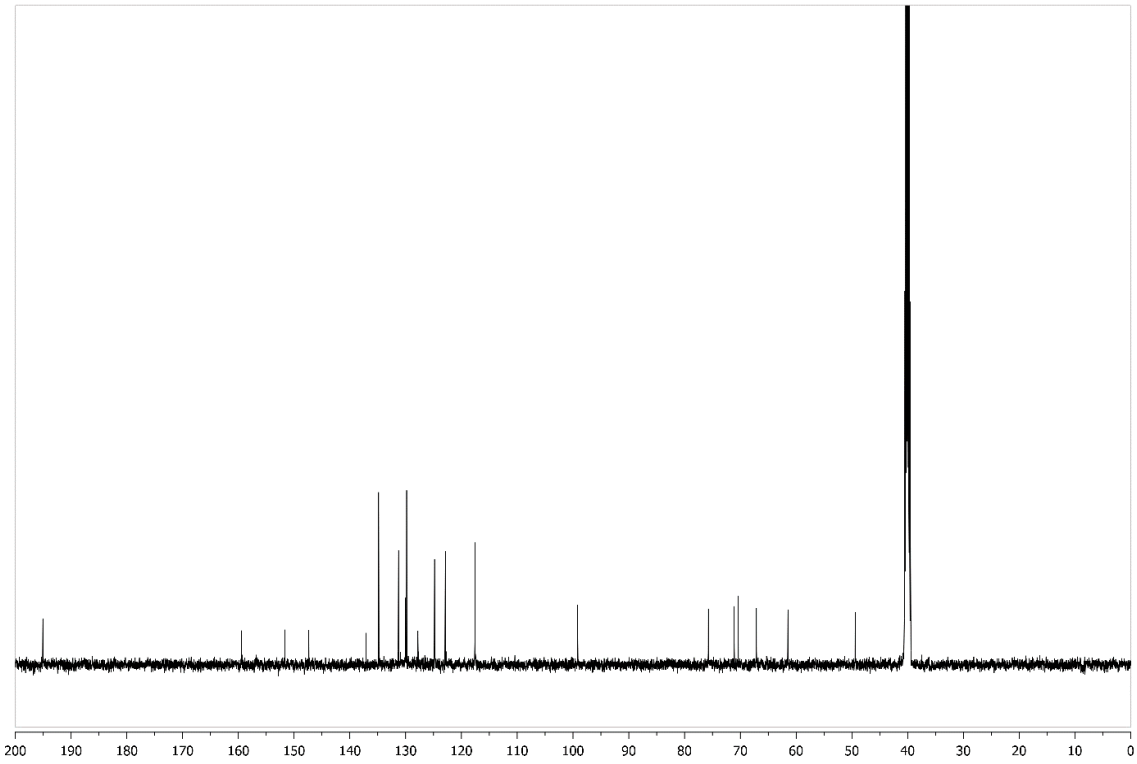

Figure 357: ^{13}C NMR spectrum of compound **78** (126 MHz, MeOD, 300 K).

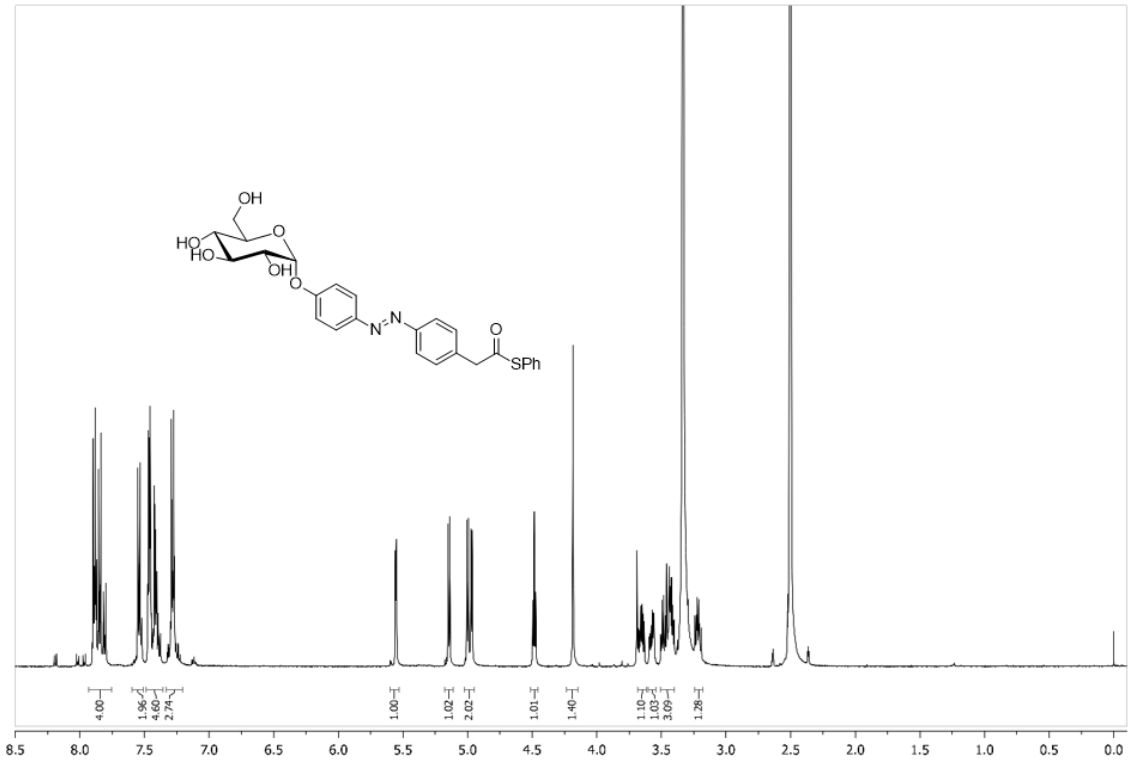

Figure 358: ^{1}H NMR spectrum of compound **79** (500 MHz, MeOD, 300 K).

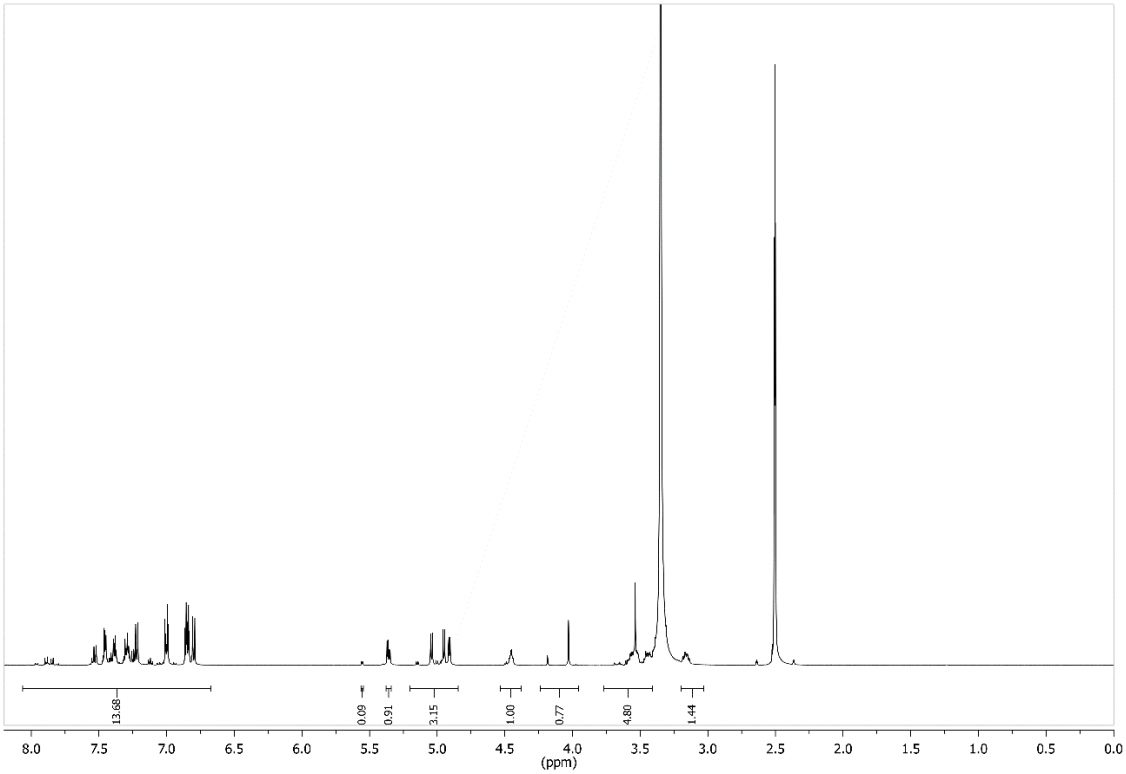

Figure 359: : ^{1}H NMR spectrum of compound **79** (*Z*-isomer) (500 MHz, MeOD, 300 K).

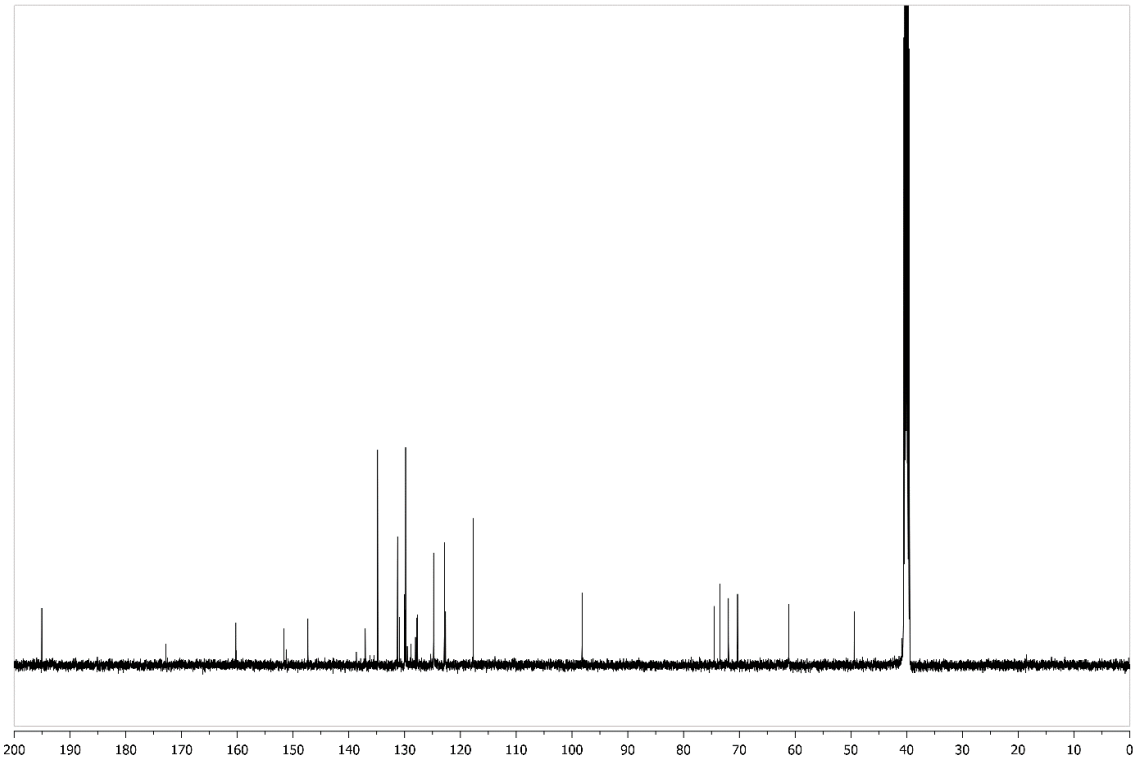

Figure 360: ^{13}C NMR spectrum of compound **79** (126 MHz, MeOD, 300 K).

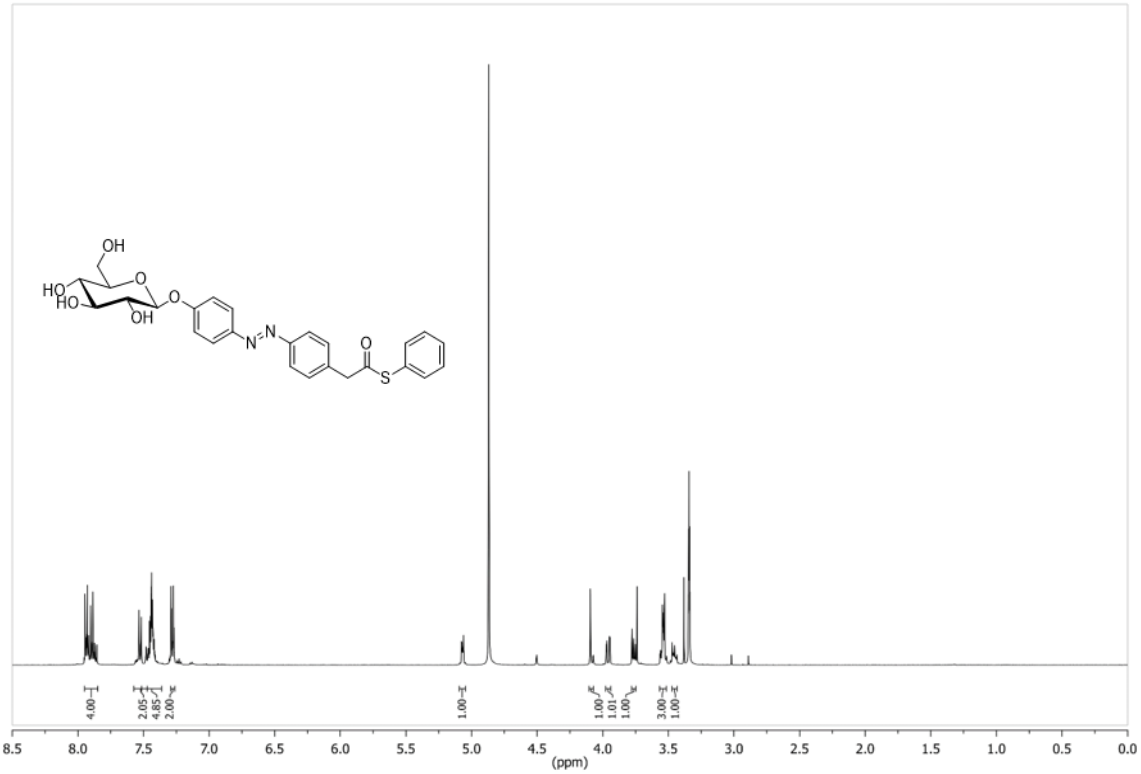

Figure 361: ^{1}H NMR spectrum of compound **80** (500 MHz, MeOD, 300 K).

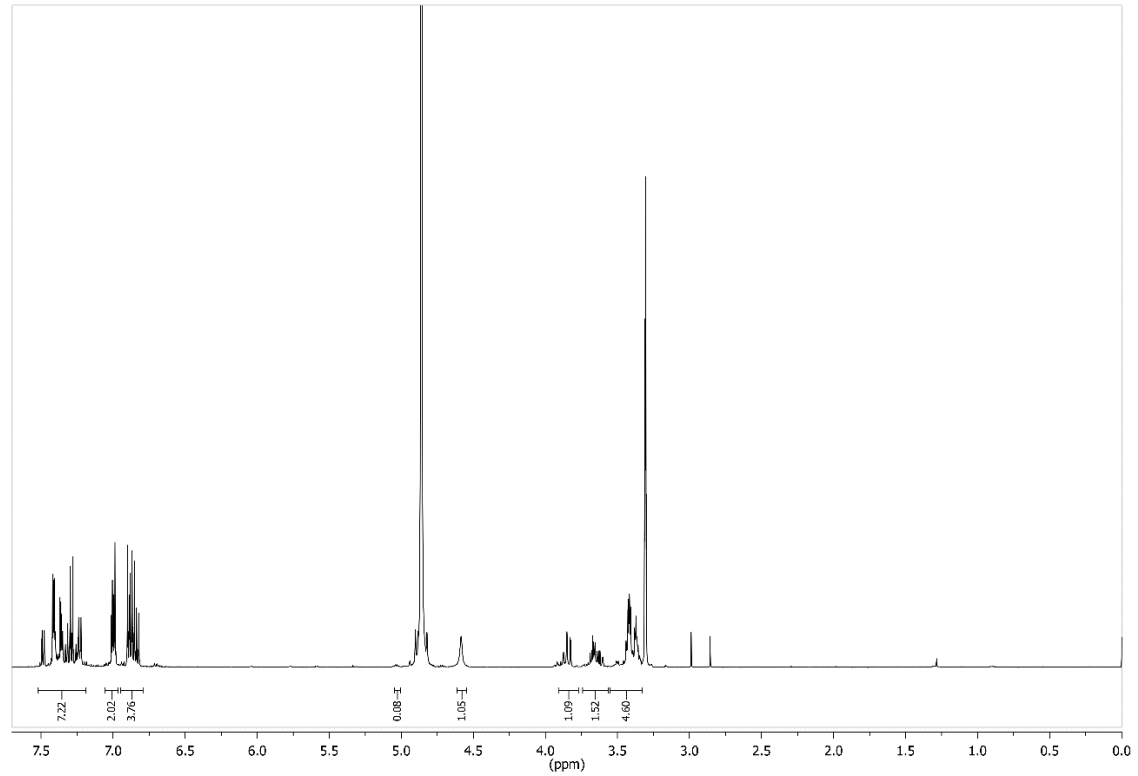

Figure 362: ^{1}H NMR spectrum of compound **80** (*Z*-isomer) (500 MHz, MeOD, 300 K).

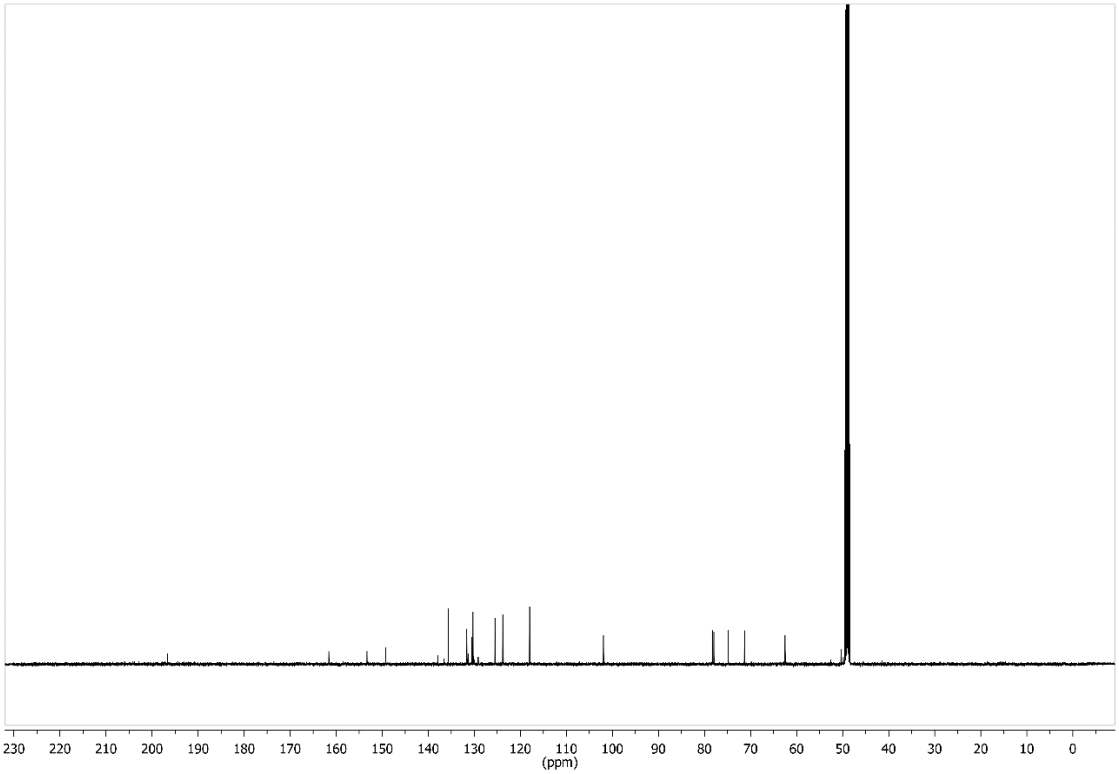

Figure 363: ^{13}C NMR spectrum of compound **80** (126 MHz, MeOD, 300 K).

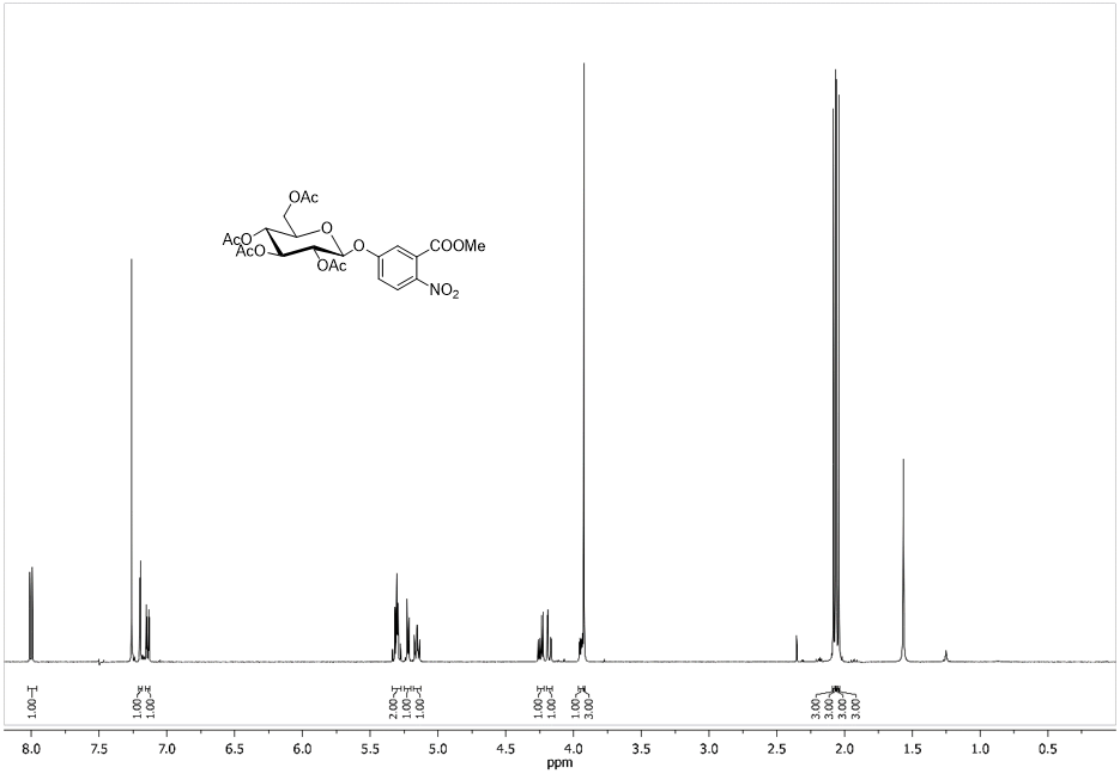

Figure 364: ^{1}H NMR spectrum of compound **92** (500 MHz, $CDCl_3$, 300 K).

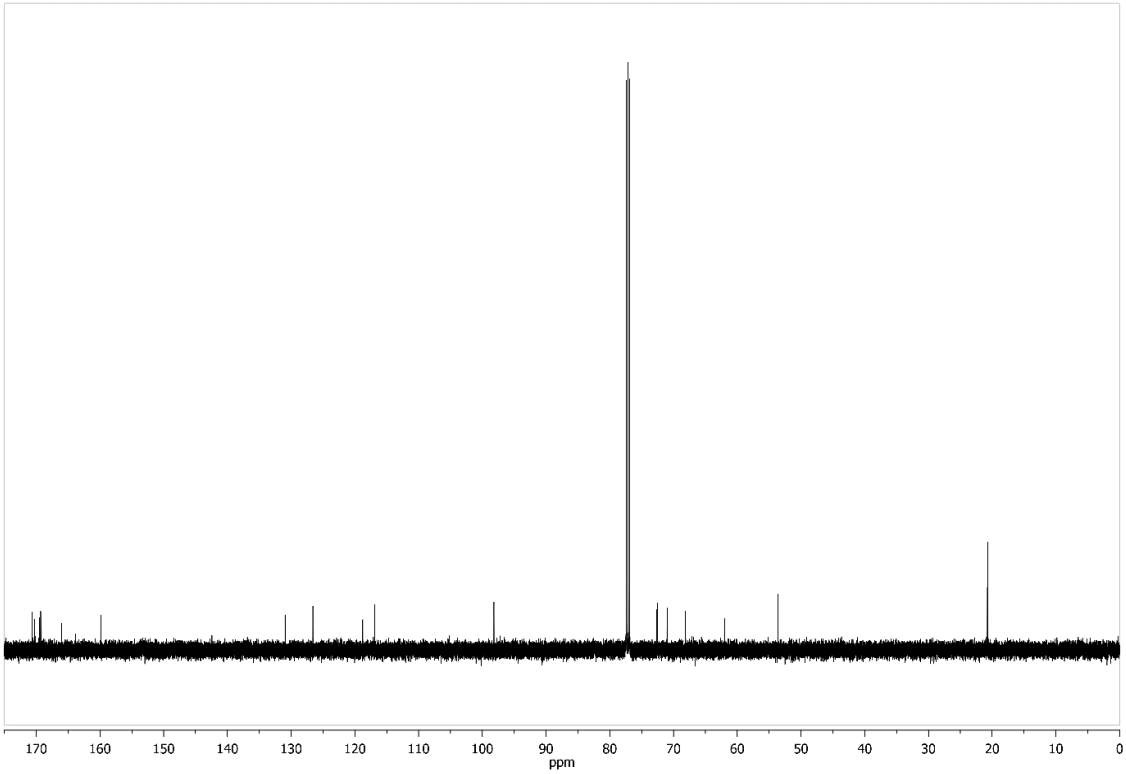

Figure 365: ^{13}C NMR spectrum of compound **92** (126 MHz, $CDCl_3$, 300 K).

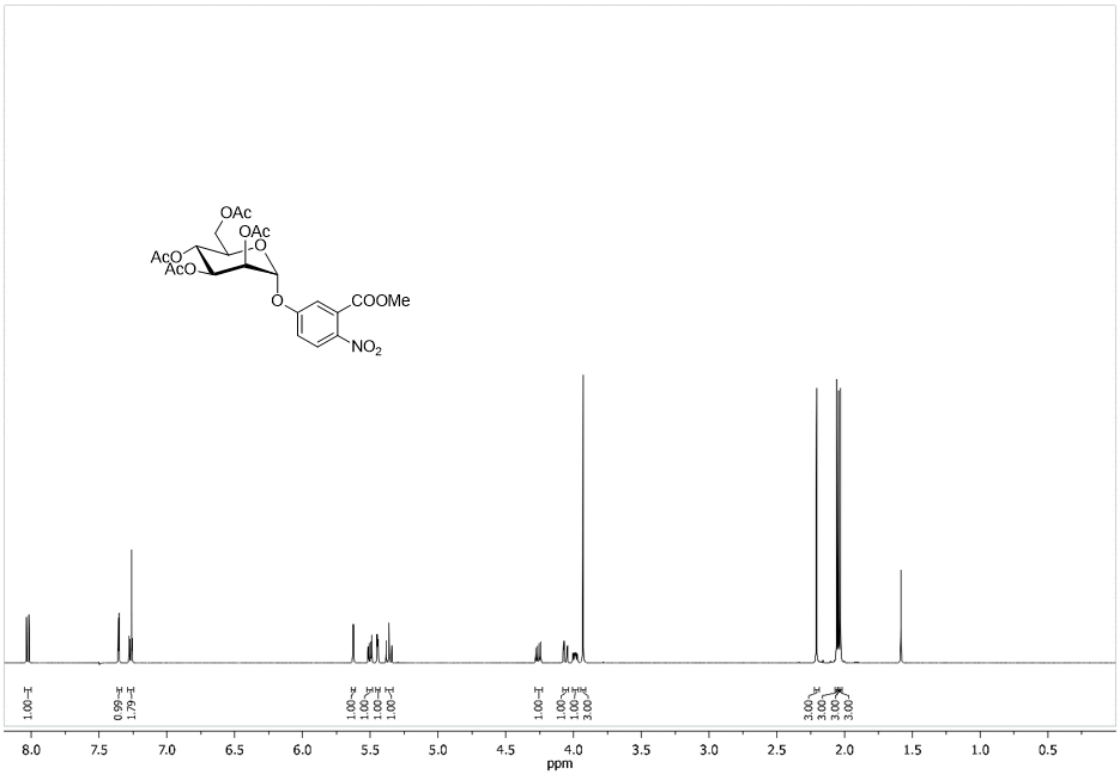

Figure 366: ^{1}H NMR spectrum of compound **93** (500 MHz, $CDCl_3$, 300 K).

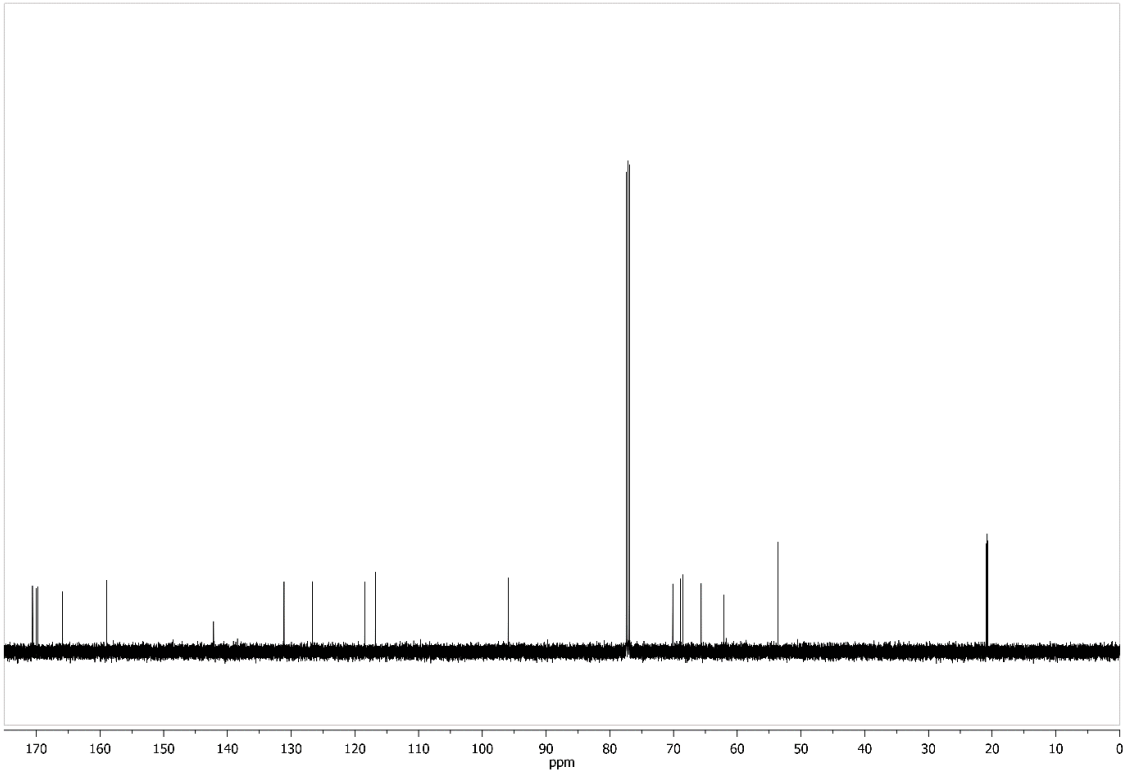

Figure 367: ^{13}C NMR spectrum of compound **93** (126 MHz, $CDCl_3$, 300 K).

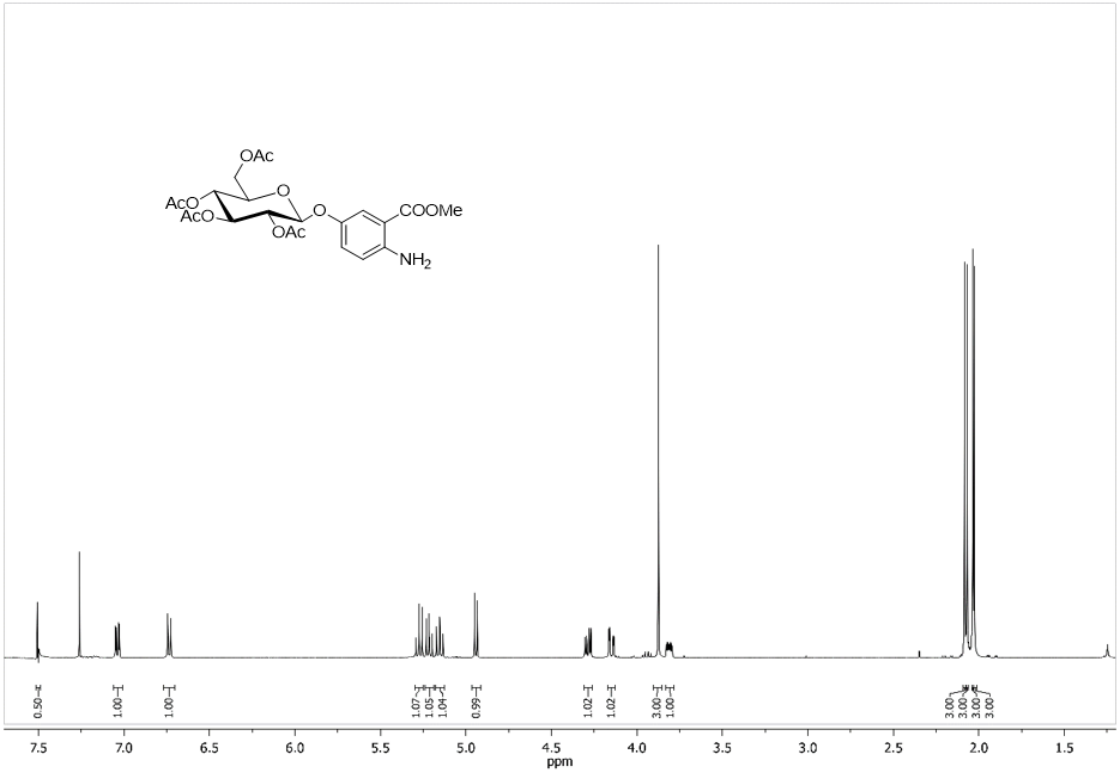

Figure 368: ^{1}H NMR spectrum of compound **94** (500 MHz, $CDCl_3$, 300 K).

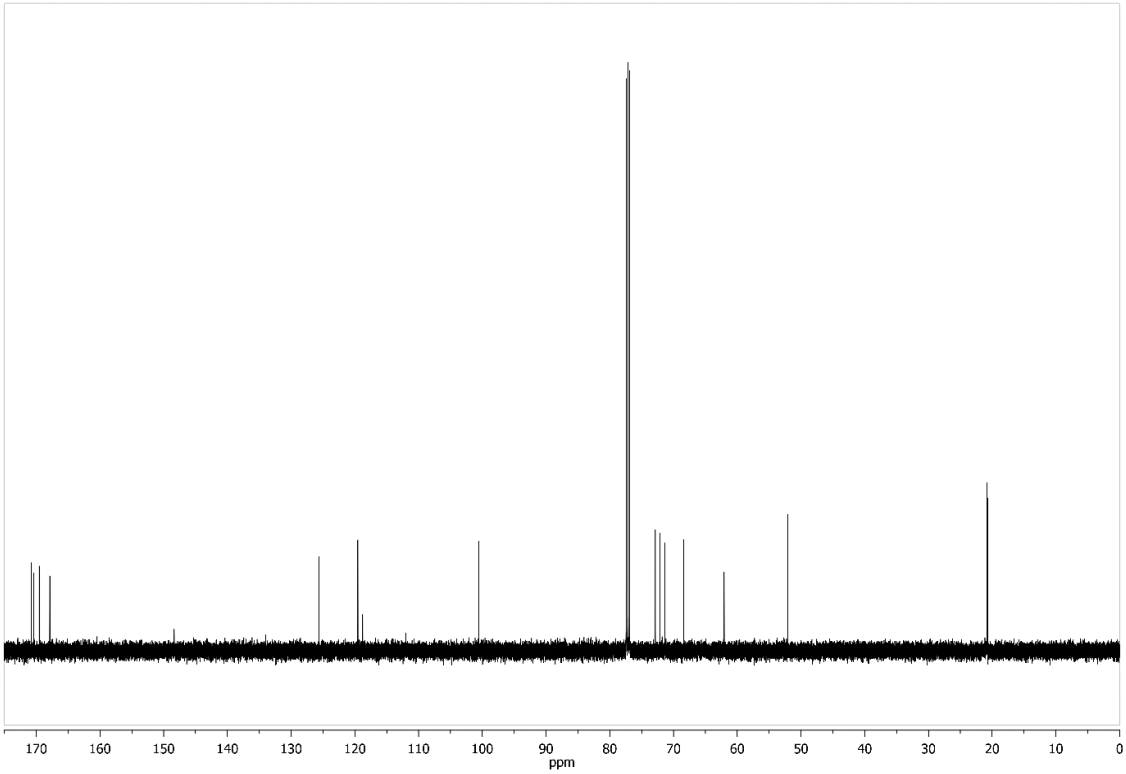

Figure 369: ^{13}C NMR spectrum of compound **94** (126 MHz, $CDCl_3$, 300 K).

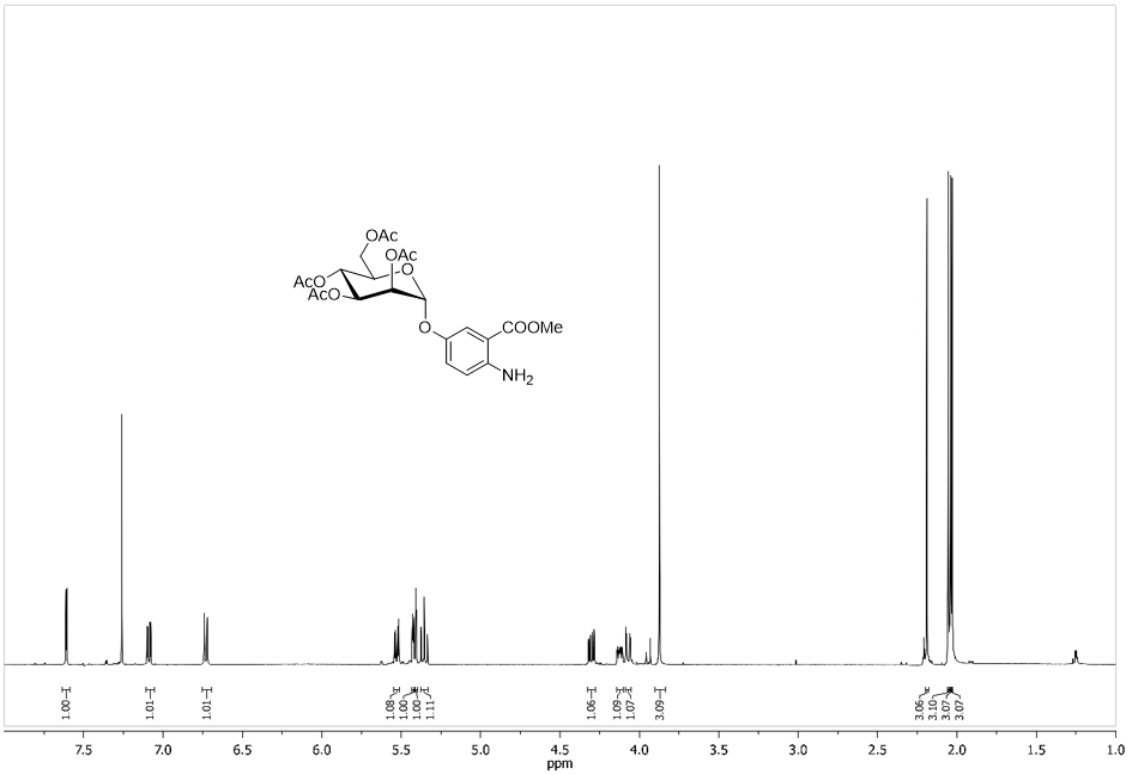

Figure 370: ^{1}H NMR spectrum of compound **95** (500 MHz, $CDCl_3$, 300 K).

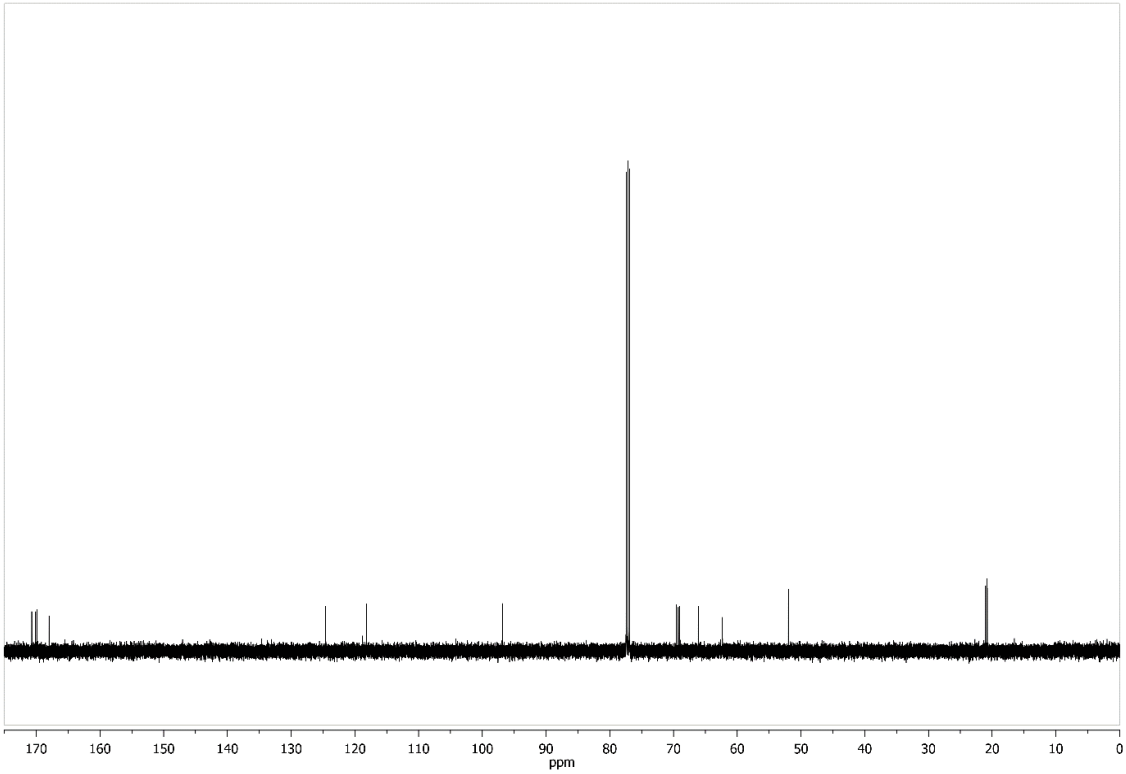

Figure 371: ^{13}C NMR spectrum of compound **95** (126 MHz, $CDCl_3$, 300 K).

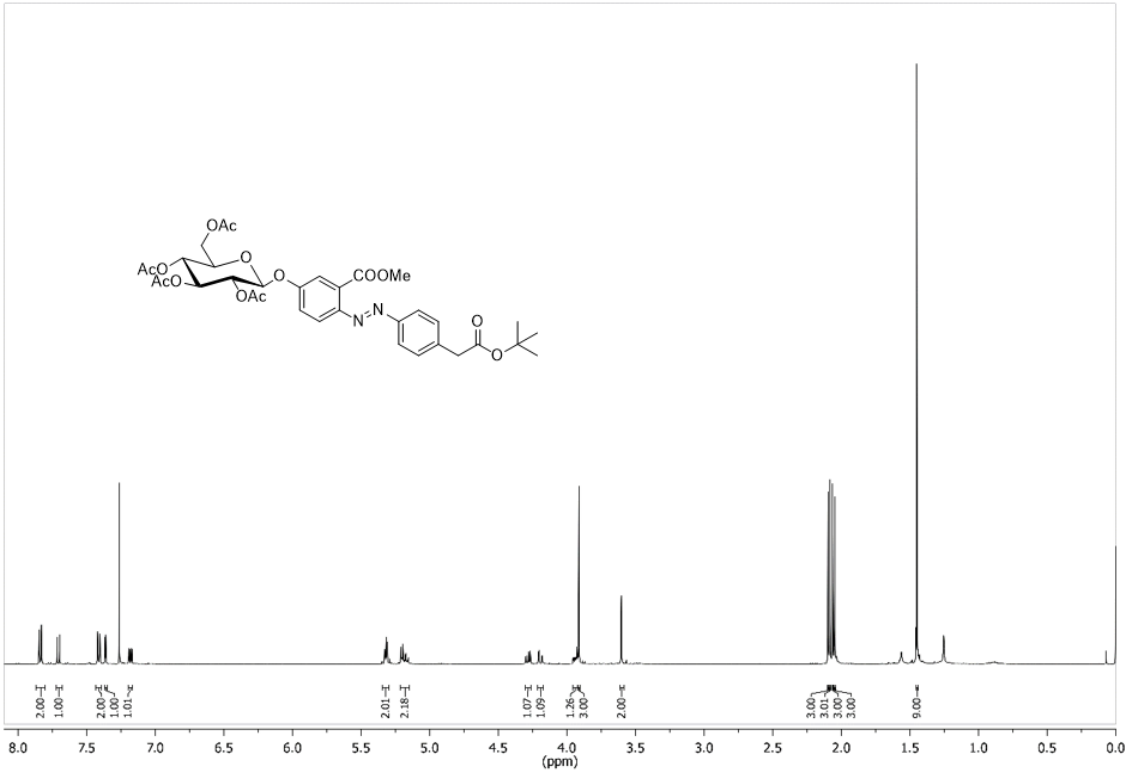

Figure 372: ^{1}H NMR spectrum of compound **96** (500 MHz, $CDCl_3$, 300 K).

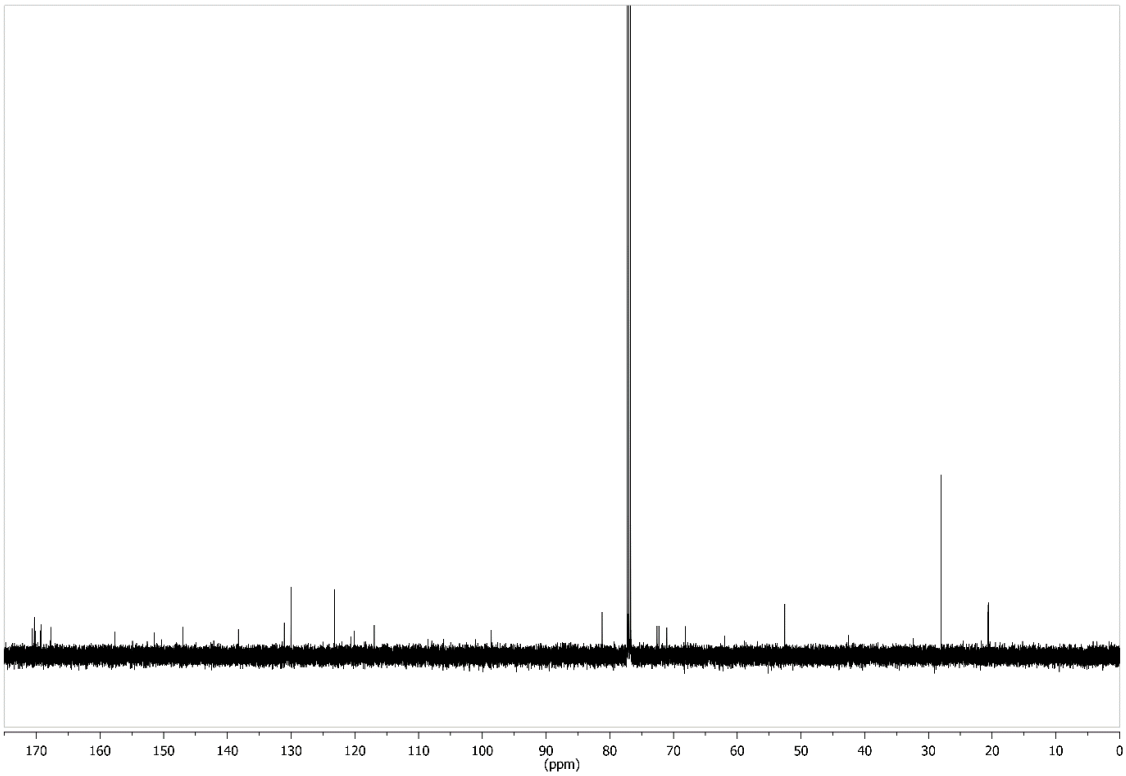

Figure 373: ^{13}C NMR spectrum of compound **96** (126 MHz, $CDCl_3$, 300 K).

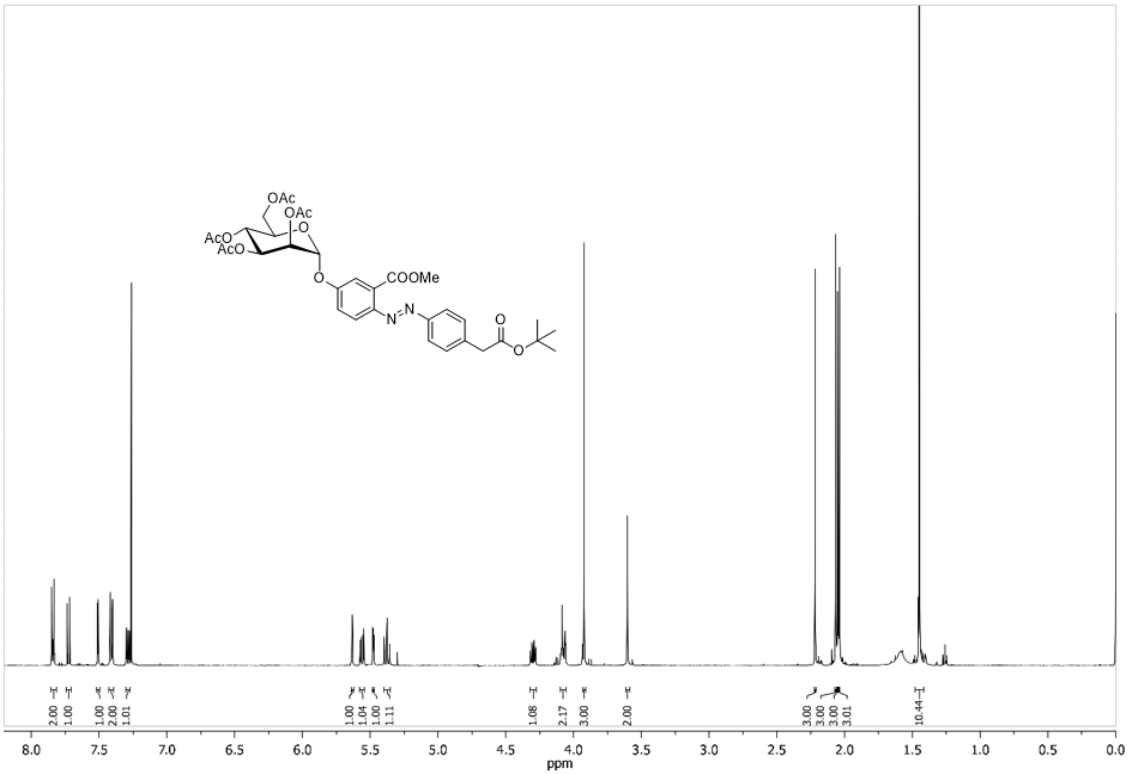

Figure 374: ^{1}H NMR spectrum of compound **97** (500 MHz, $CDCl_3$, 300 K).

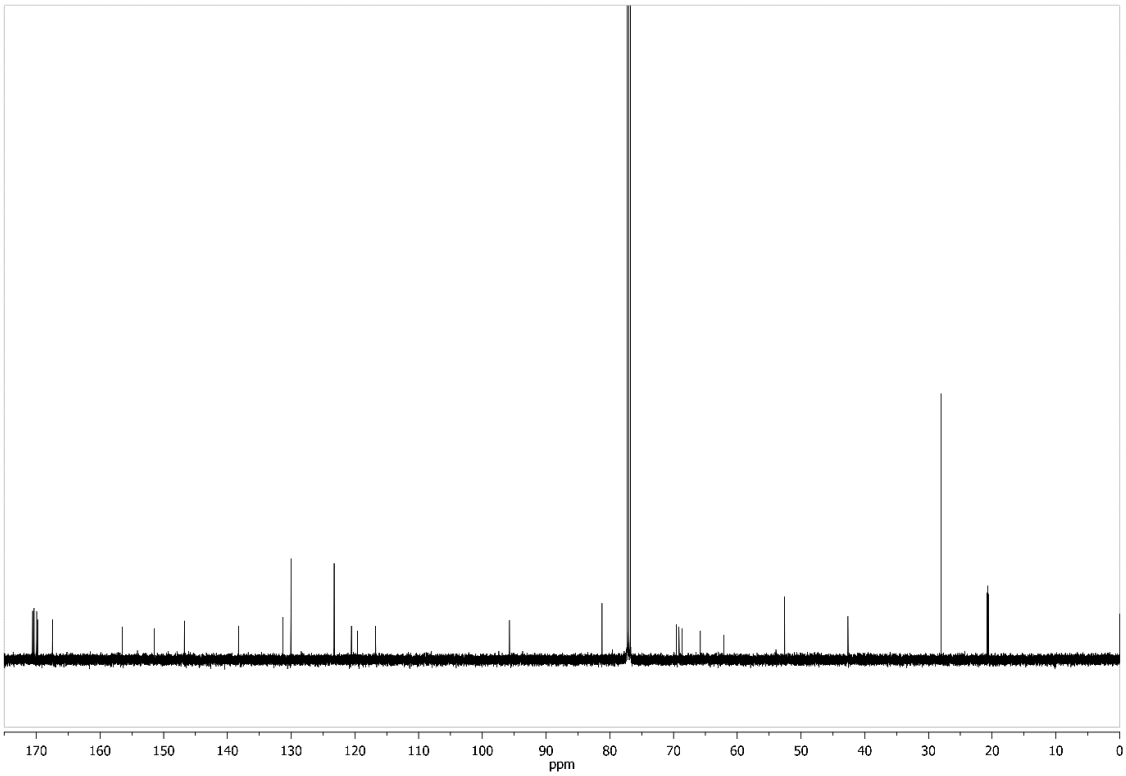

Figure 375: ^{13}C NMR spectrum of compound **97** (126 MHz, $CDCl_3$, 300 K).

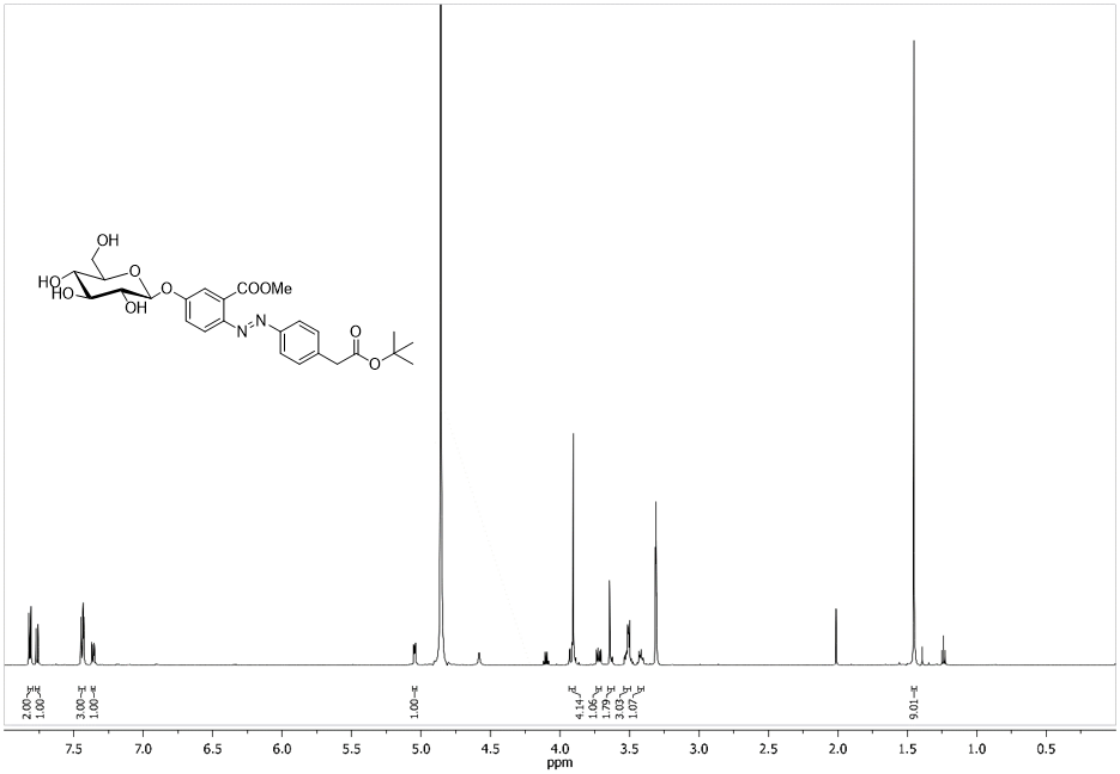

Figure 376: ^{1}H NMR spectrum of compound **98** (500 MHz, MeOD, 300 K).

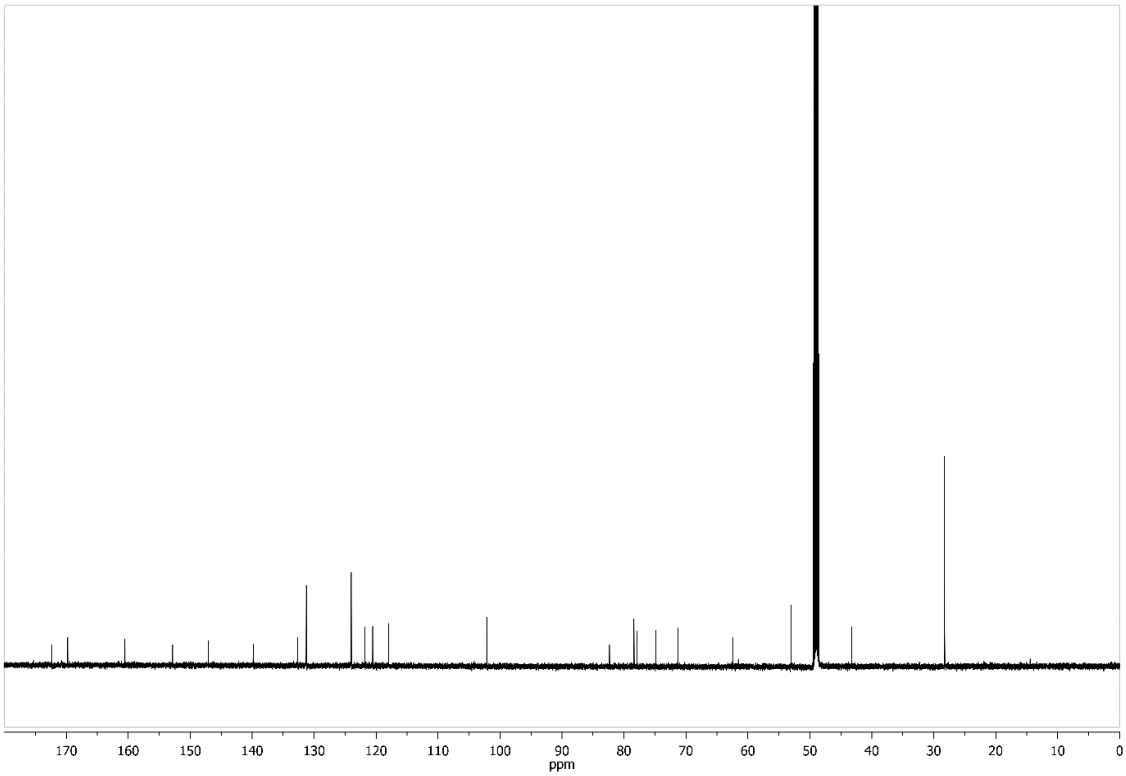

Figure 377: ^{13}C NMR spectrum of compound **98** (126 MHz, MeOD, 300 K).

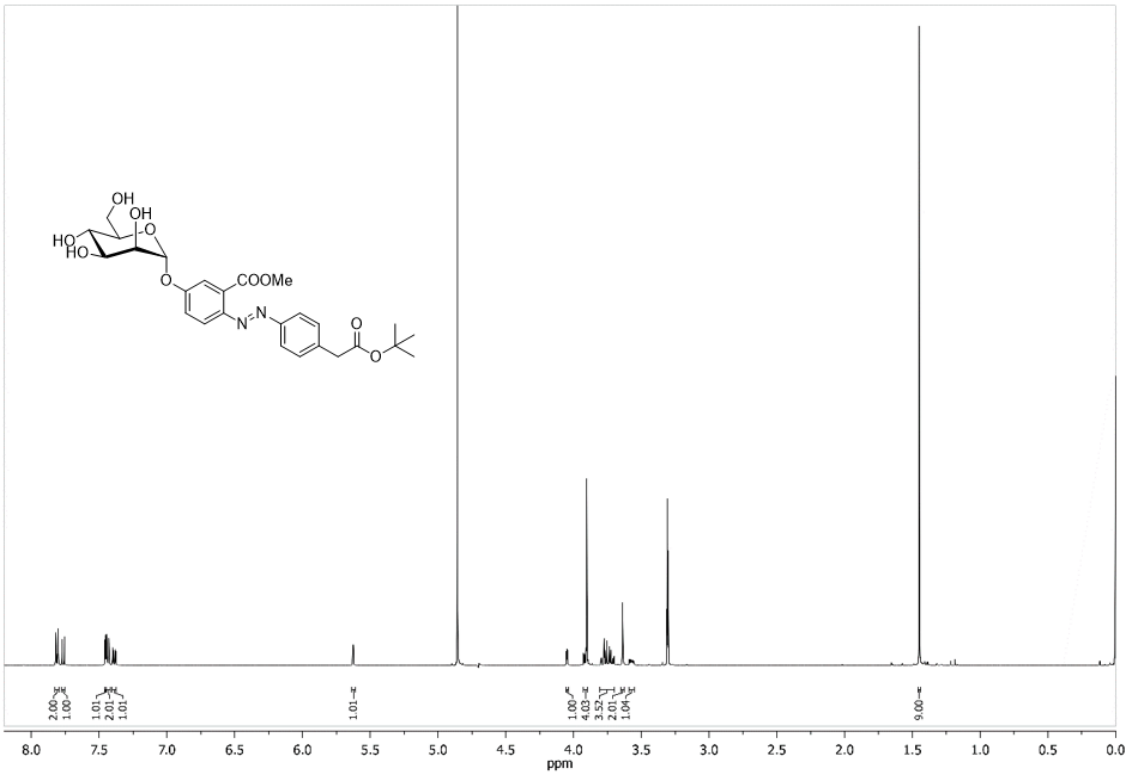

Figure 378: ^{1}H NMR spectrum of compound **99** (500 MHz, MeOD, 300 K).

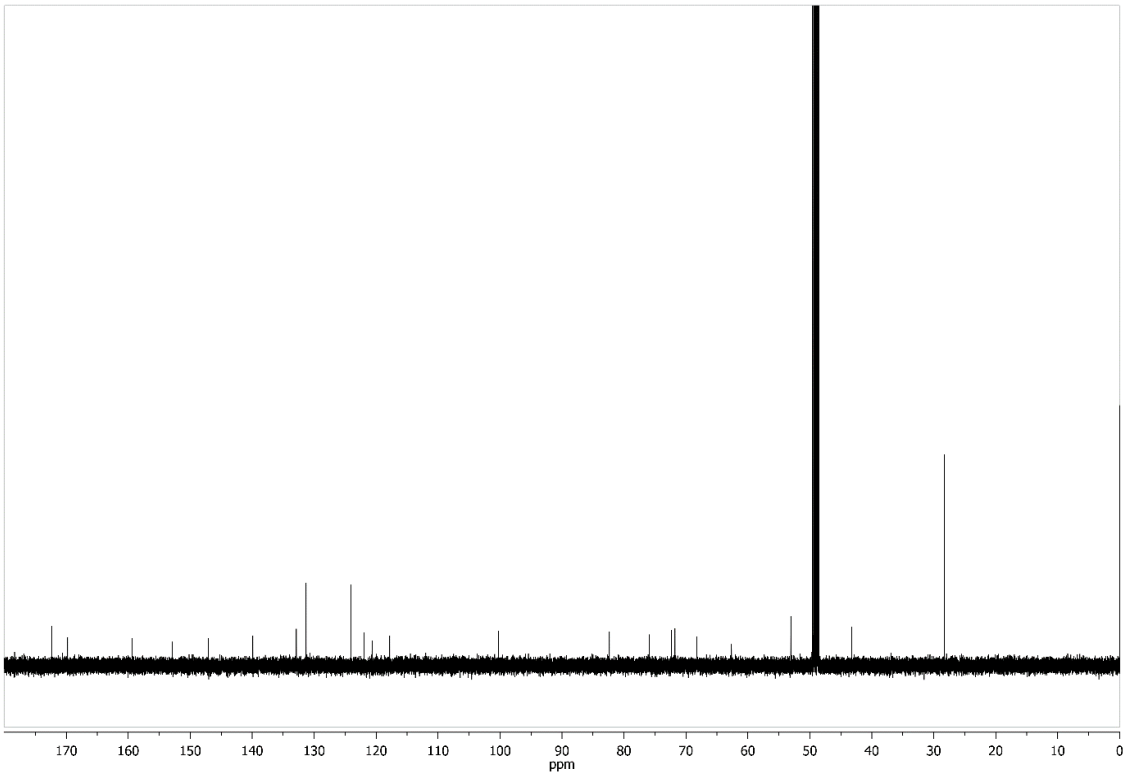

Figure 379: ^{13}C NMR spectrum of compound **99** (126 MHz, MeOD, 300 K).

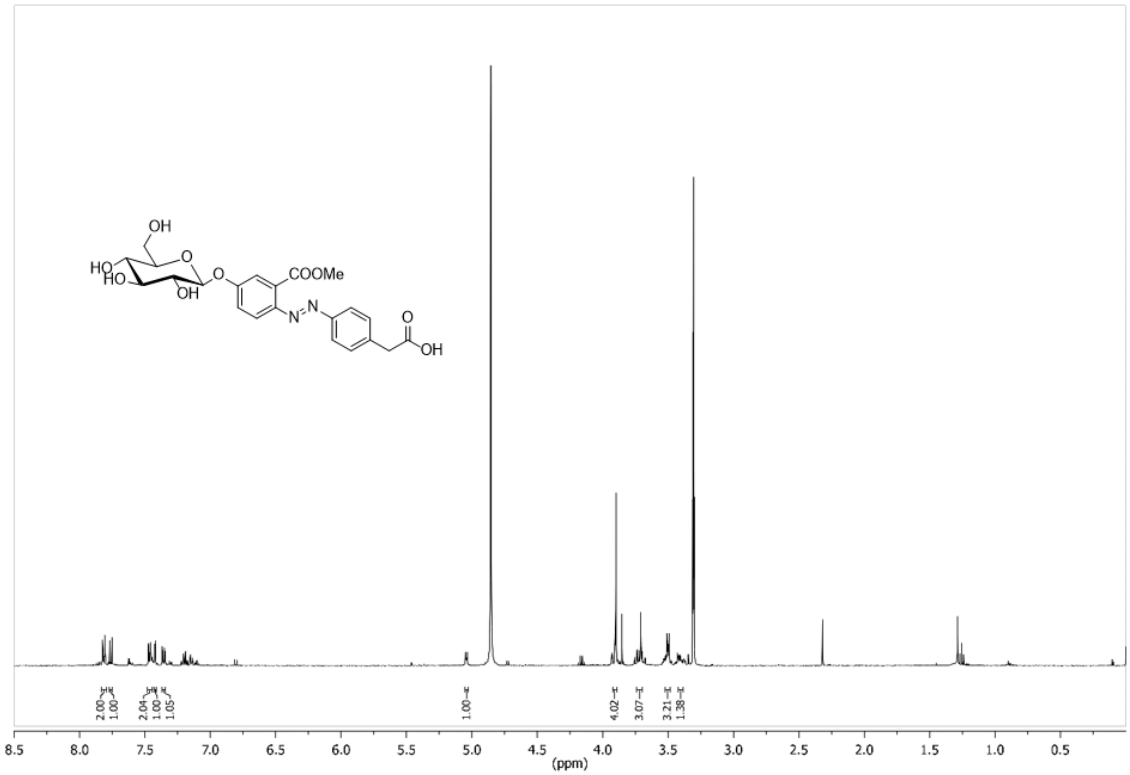

Figure 380: ^{1}H NMR spectrum of compound **100** (500 MHz, MeOD, 300 K).

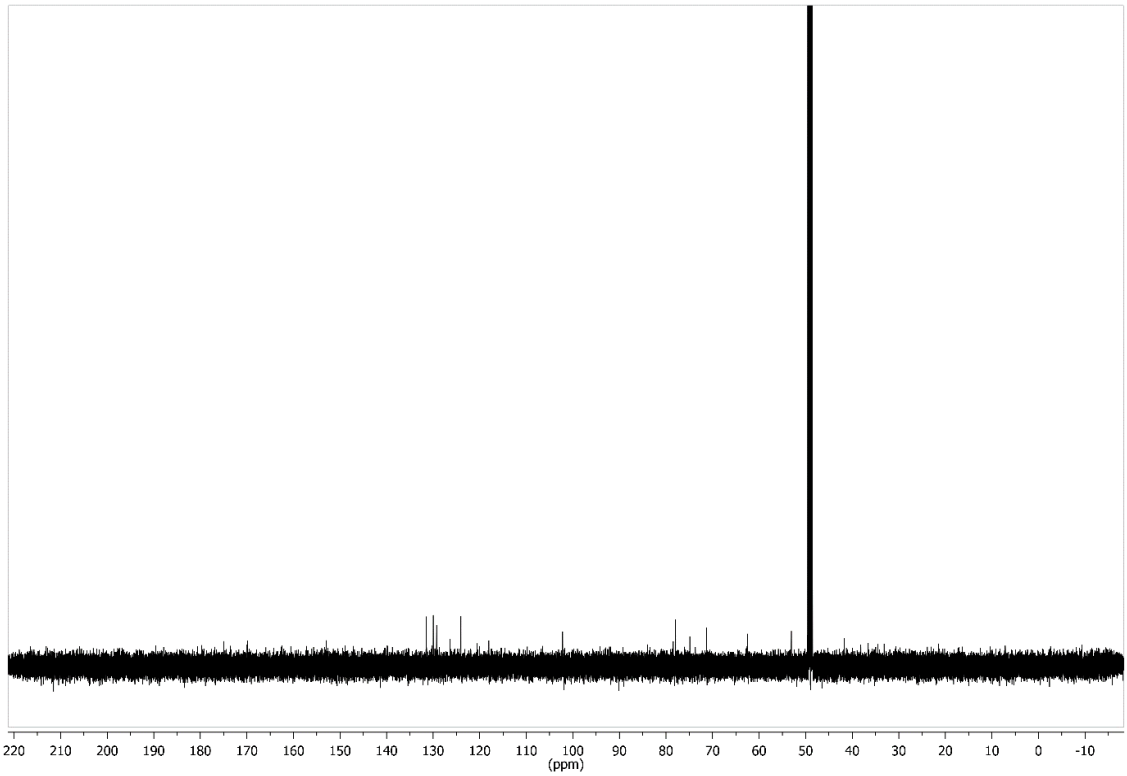

Figure 381: ^{13}C NMR spectrum of compound **100** (126 MHz, MeOD, 300 K).

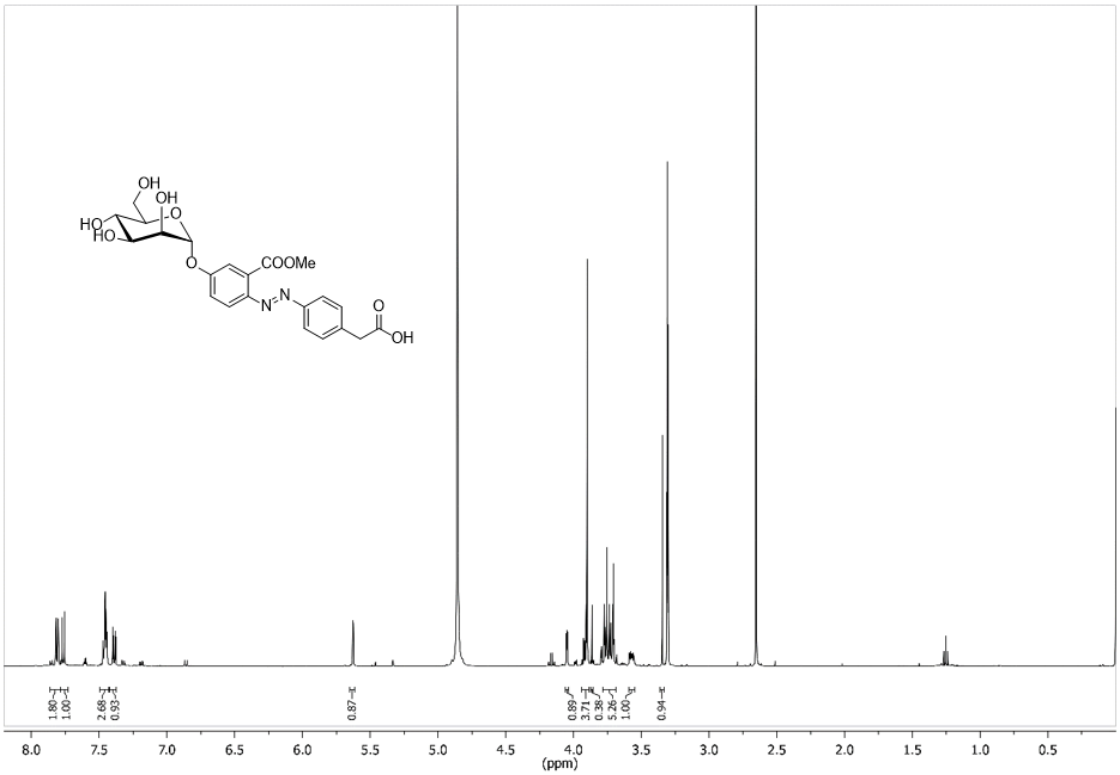

Figure 382: ^{1}H NMR spectrum of compound **101** (500 MHz, MeOD, 300 K).

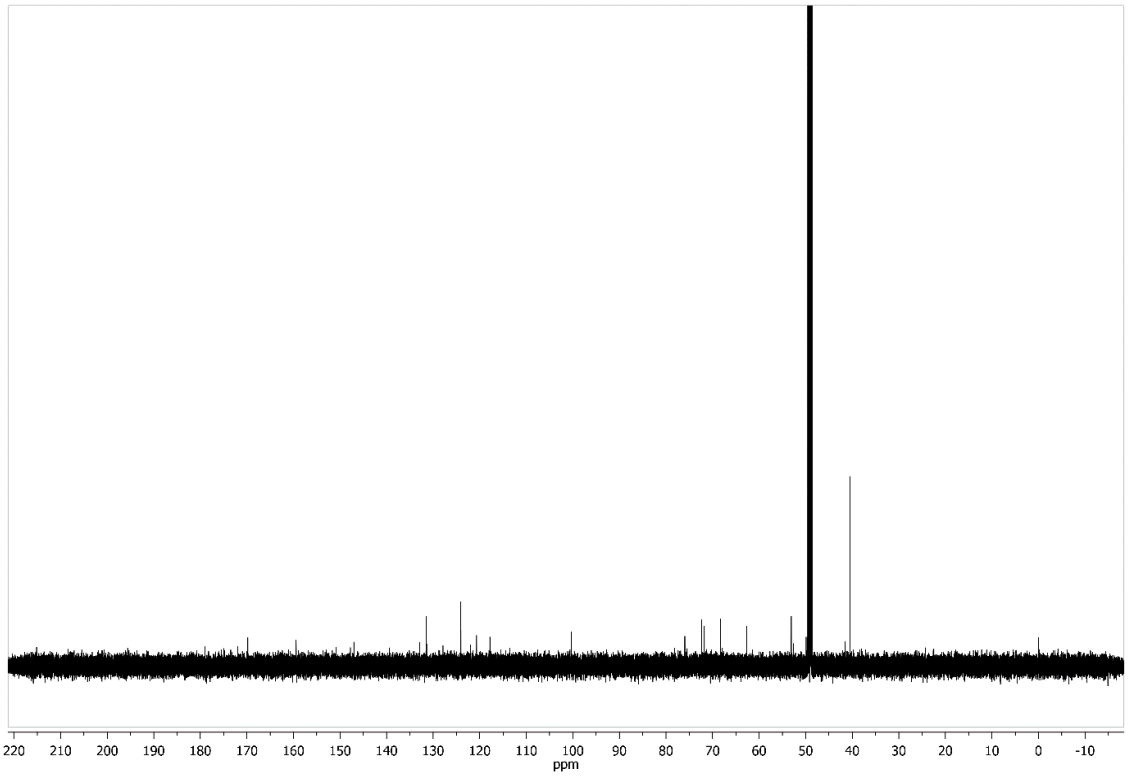

Figure 383: ^{13}C NMR spectrum of compound **101** (126 MHz, MeOD, 300 K).

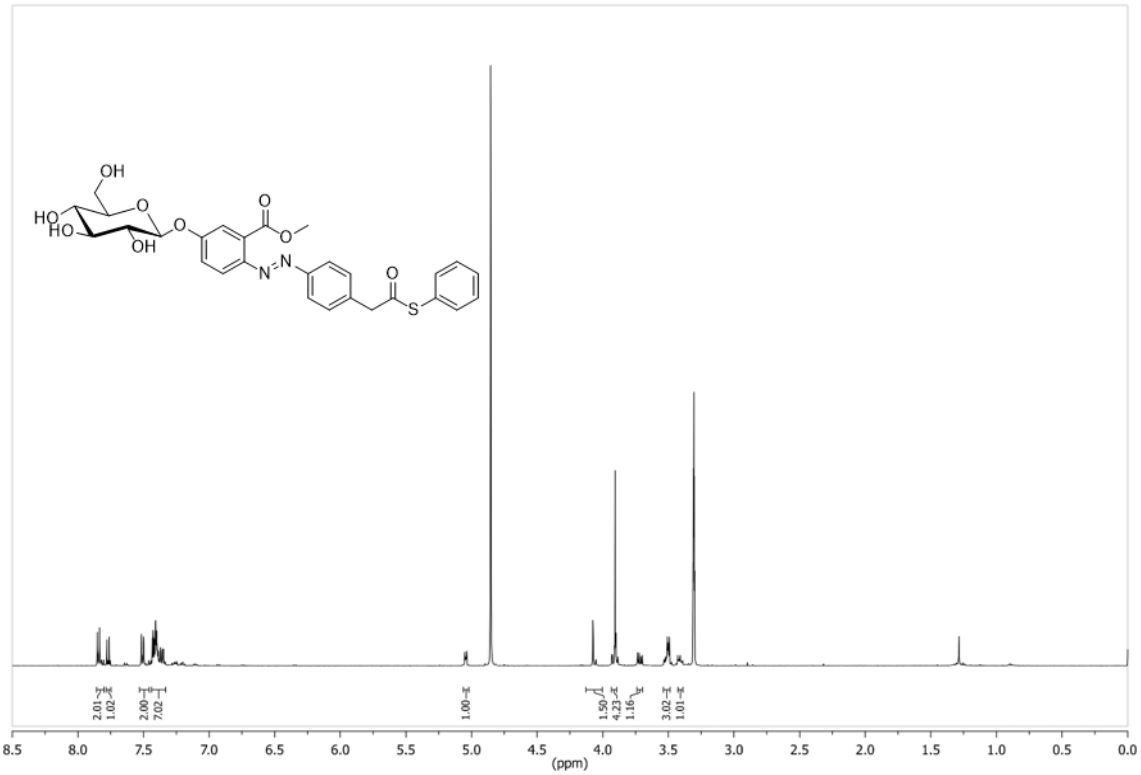

Figure 384: ^{1}H NMR spectrum of compound **102** (500 MHz, MeOD, 300 K).

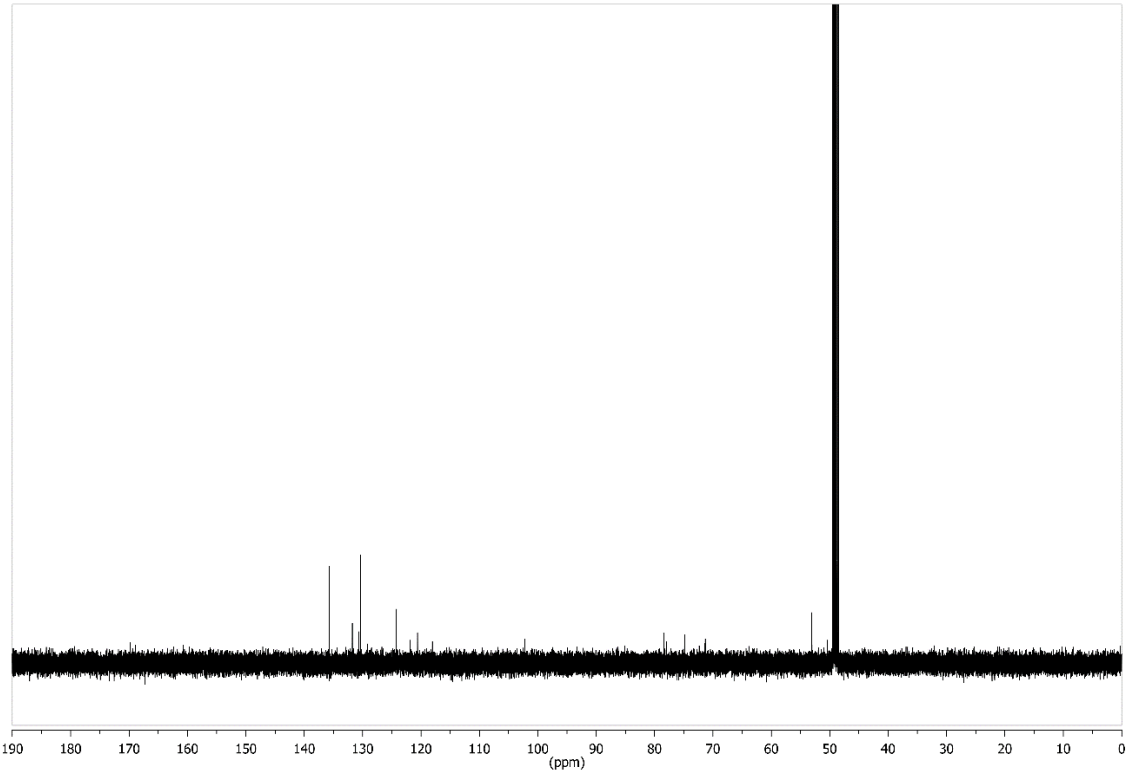

Figure 385: ^{13}C NMR spectrum of compound **102** (126 MHz, MeOD, 300 K).

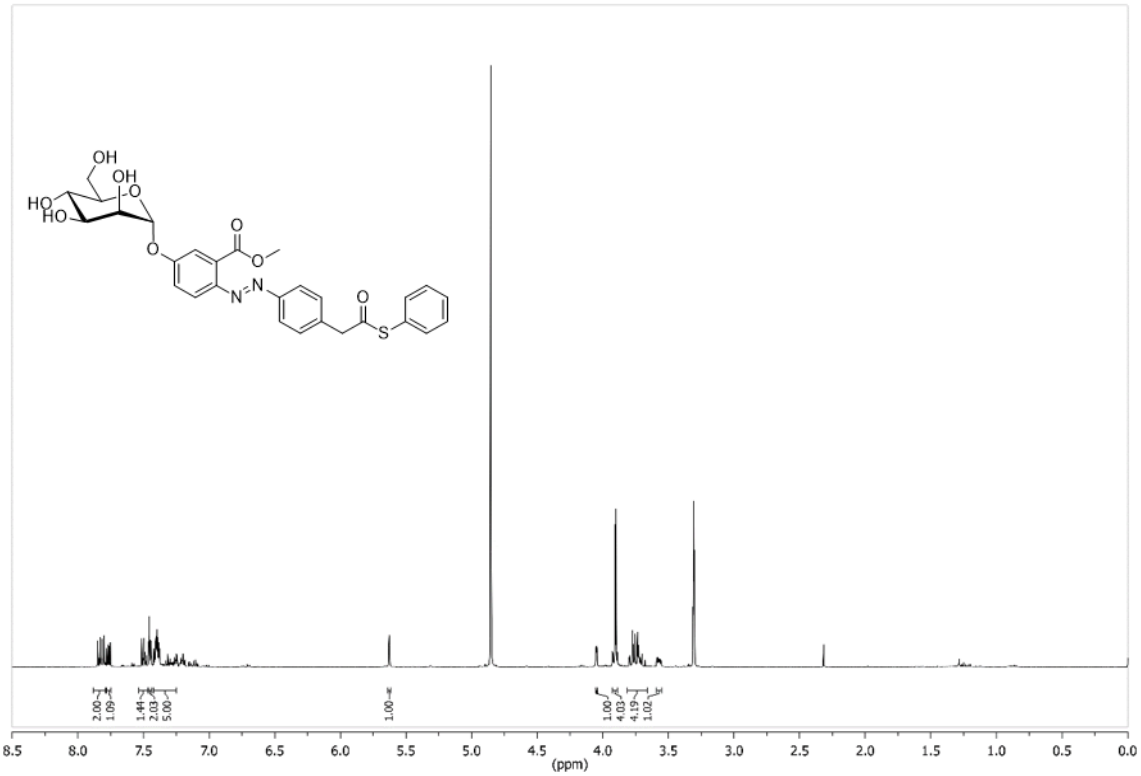

Figure 386: ^{1}H NMR spectrum of compound **103** (500 MHz, MeOD, 300 K).

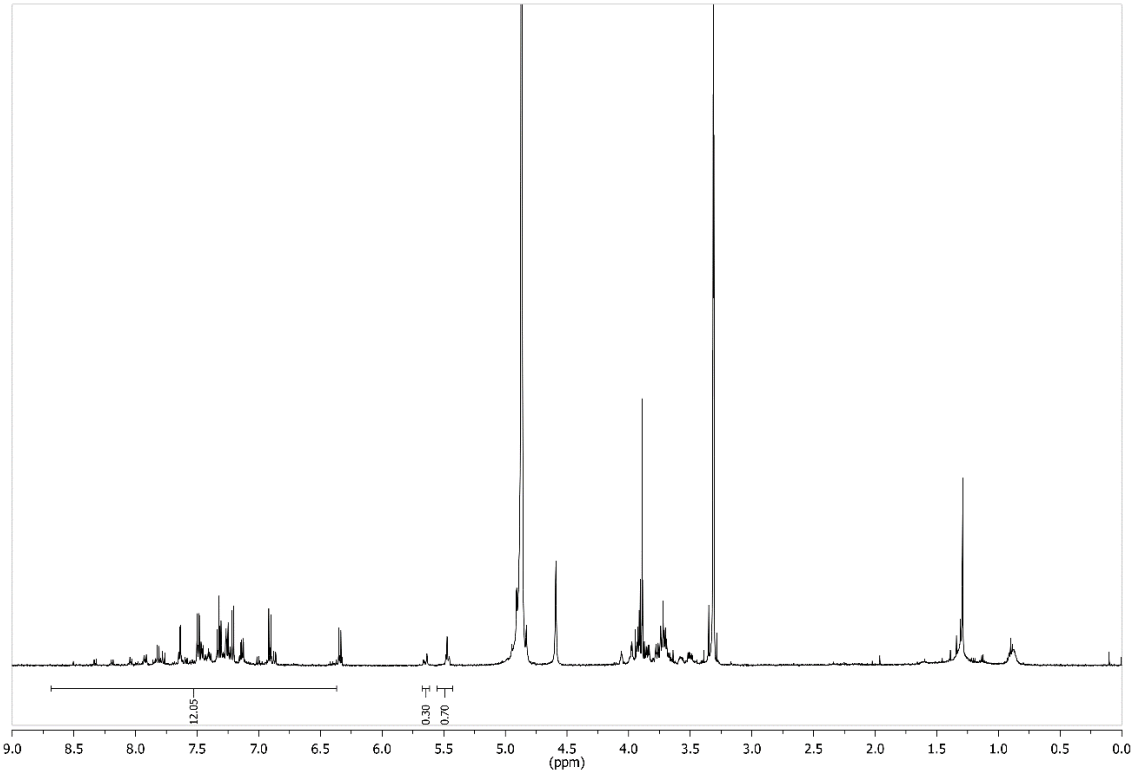

Figure 387: ^{1}H NMR spectrum of compound **103** (*Z*-isomer) (500 MHz, MeOD, 300 K).

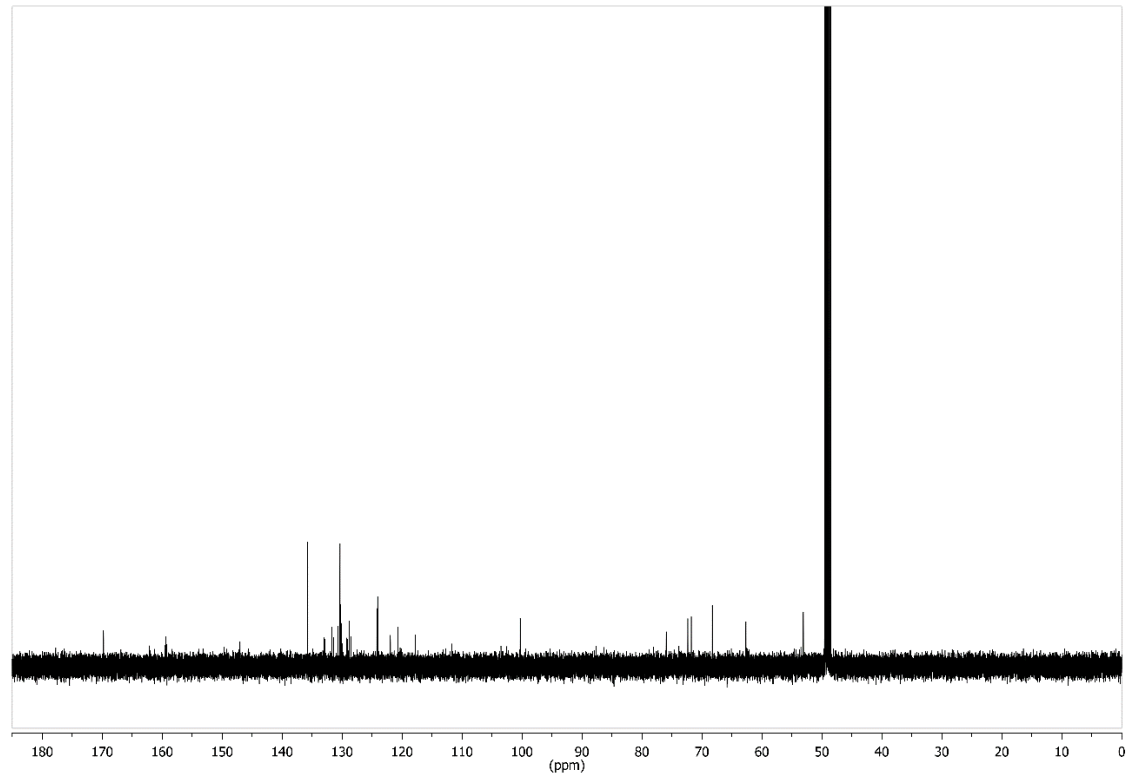

Figure 388: ^{13}C NMR spectrum of compound **103** (126 MHz, MeOD, 300 K).

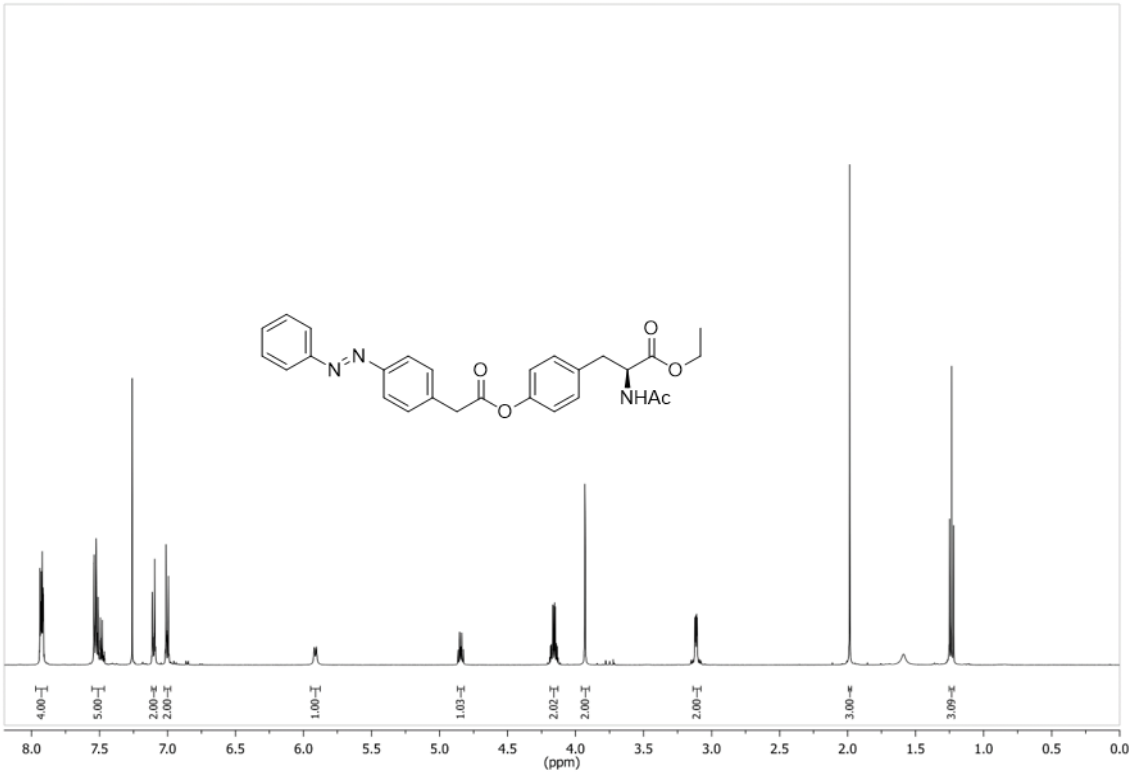

Figure 389: ^{1}H NMR spectrum of compound **108** (500 MHz, $CDCl_3$, 300 K).

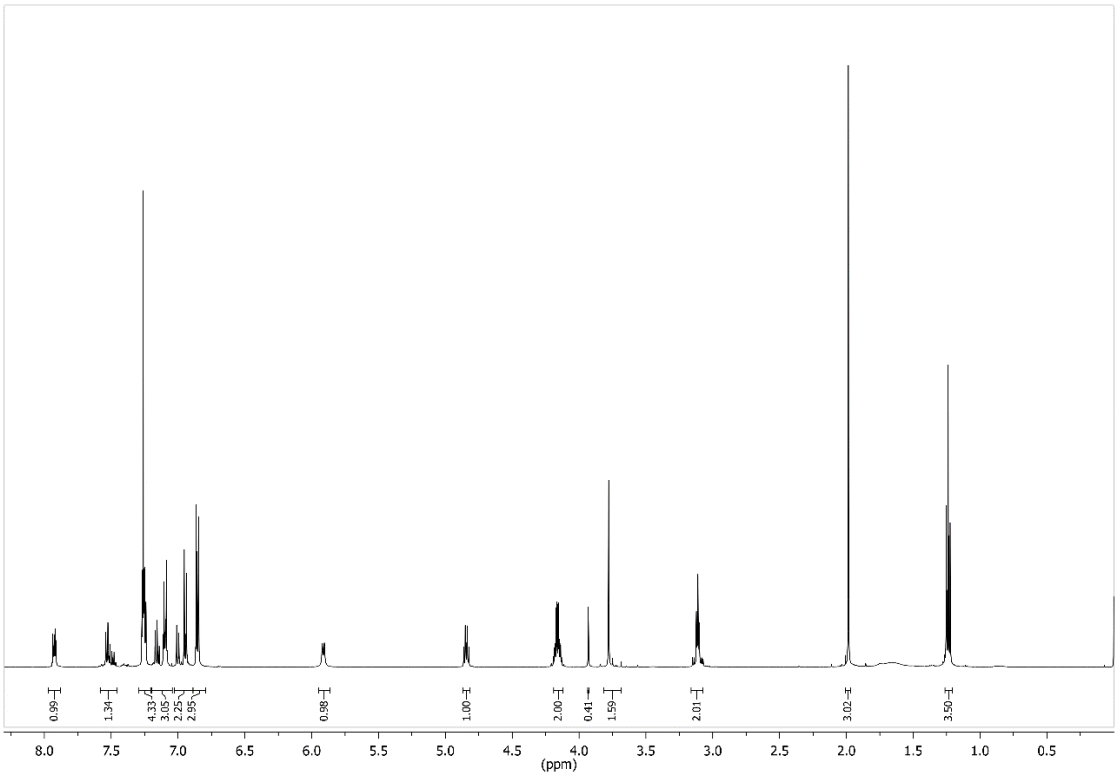

Figure 390: ^{1}H NMR spectrum of compound **108** (*Z*-isomer) (500 MHz, $CDCl_3$, 300 K).

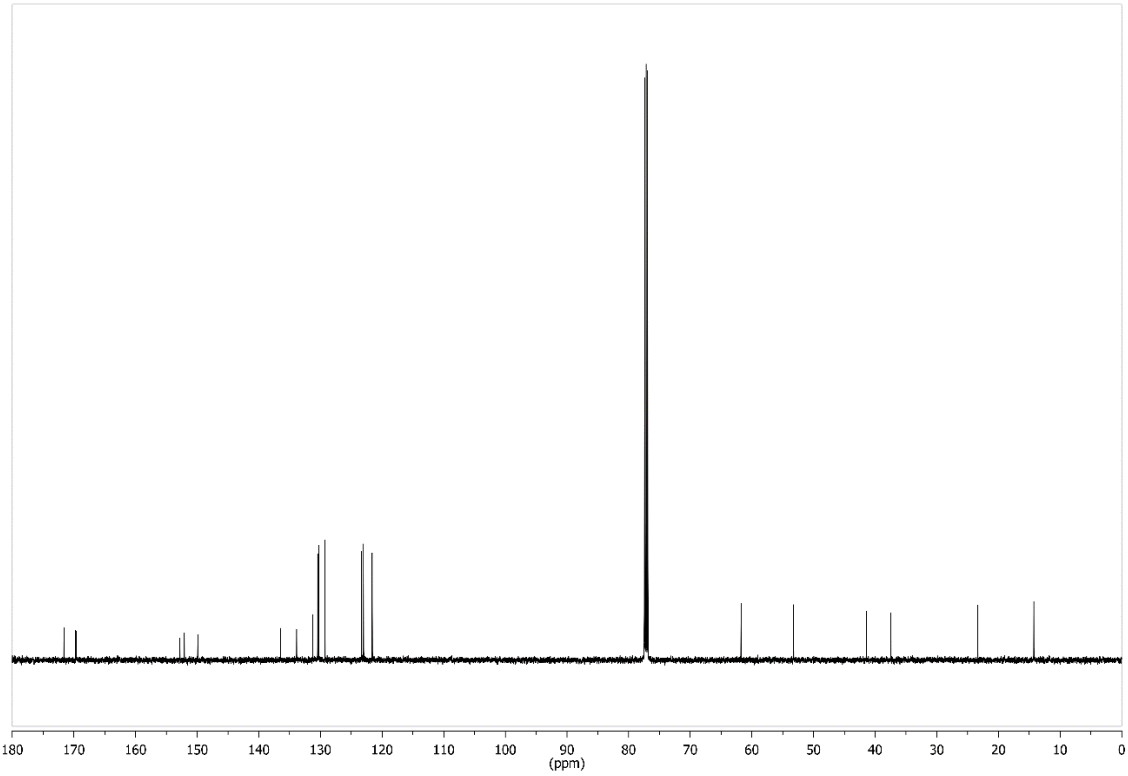

Figure 391: ^{13}C NMR spectrum of compound **108** (126 MHz, $CDCl_3$, 300 K).

8.5.4 UV/Vis spectra of synthesised compounds

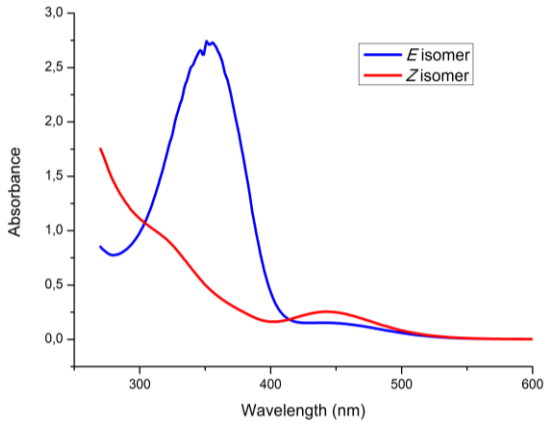

Figure 392: UV spectra of compound **8**. The spectrum of the *E*-isomer (in blue) was recorded after 16 h storage at 40 °C and the spectrum of the *Z*-isomer (in red) was recorded after irradiation with 365 nm for 15 min. Irradiation with 440 nm restored the *E*-isomer. Spectra were recorded in DCM at 293 K.

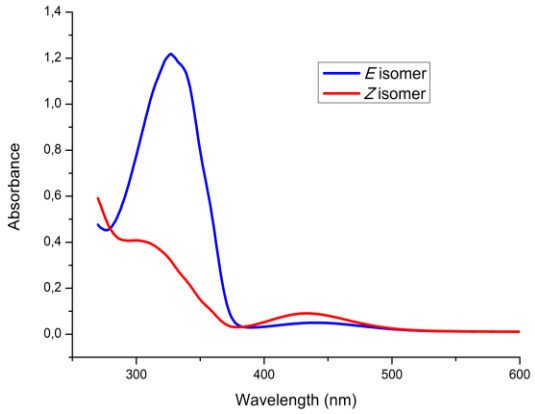

Figure 393: UV spectra of compound **9**. The spectrum of the *E*-isomer (in blue) was recorded after 16 h storage at 40 °C and the spectrum of the *Z*-isomer (in red) was recorded after irradiation with 365 nm for 15 min. Irradiation with 440 nm restored the *E*-isomer. Spectra were recorded in DCM at 293 K.

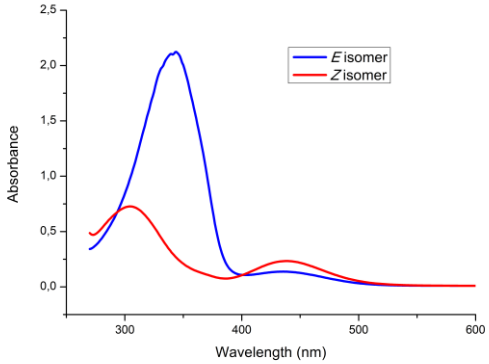

Figure 394: UV spectra of compound **10**. The spectrum of the *E*-isomer (in blue) was recorded after 16 h storage at 40 °C and the spectrum of the *Z*-isomer (in red) was recorded after irradiation with 365 nm for 15 min. Irradiation with 440 nm restored the *E*-isomer. Spectra were recorded in DCM at 293 K.

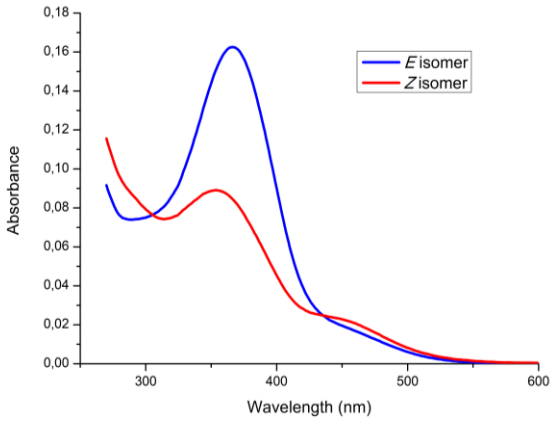

Figure 395: UV spectra of compound **11**. The spectrum of the *E*-isomer (in blue) was recorded after 16 h storage at 40 °C and the spectrum of the *Z*-isomer (in red) was recorded after irradiation with 365 nm for 5 min. Irradiation with 440 nm restored the *E*-isomer. Spectra were recorded in DCM at 293 K.

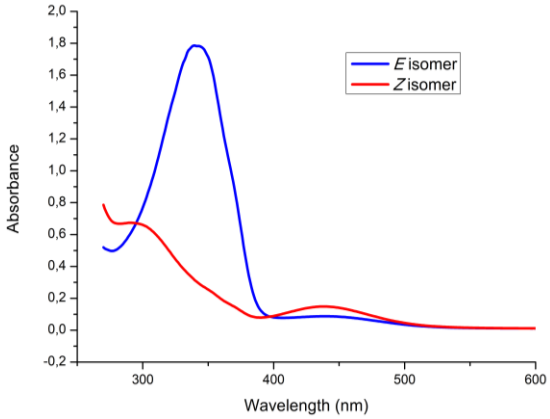

Figure 396: UV spectra of compound **12**. The spectrum of the *E*-isomer (in blue) was recorded after 16 h storage at 40 °C and the spectrum of the *Z*-isomer (in red) was recorded after irradiation with 365 nm for 5 min. Irradiation with 440 nm restored the *E*-isomer. Spectra were recorded in DCM at 293 K.

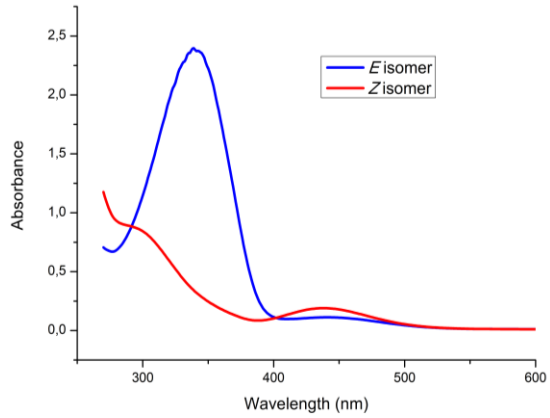

Figure 397: UV spectra of compound **13**. The spectrum of the *E*-isomer (in blue) was recorded after 16 h storage at 40 °C and the spectrum of the *Z*-isomer (in red) was recorded after irradiation with 365 nm for 5 min. Irradiation with 440 nm restored the *E*-isomer. Spectra were recorded in DCM at 293 K.

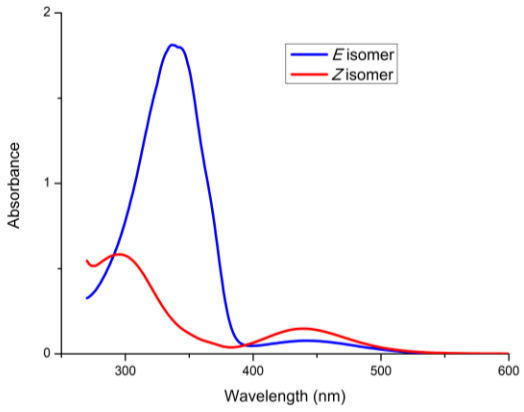

Figure 398: UV spectra of compound **14.** The spectrum of the *E*-isomer (in blue) was recorded after 16 h storage at 40 °C and the spectrum of the *Z*-isomer (in red) was recorded after irradiation with 365 nm for 5 min. Irradiation with 440 nm restored the *E*-isomer. Spectra were recorded in DCM at 293 K.

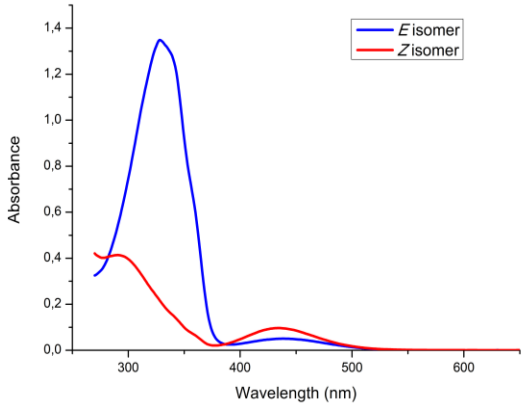

Figure 399: UV spectra of compound **35**. The spectrum of the *E*-isomer (in blue) was recorded after 16 h storage at 40 °C and the spectrum of the *Z*-isomer (in red) was recorded after irradiation with 365 nm for 5 min. Irradiation with 440 nm restored the *E*-isomer. Spectra were recorded in DCM at 293 K.

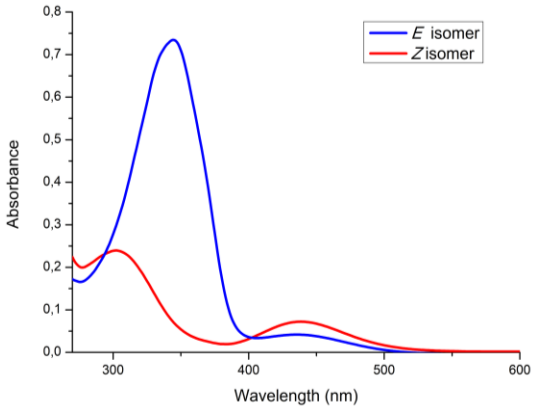

Figure 400: UV spectra of compound **78**. The spectrum of the *E*-isomer (in blue) was recorded after 16 h storage at 40 °C and the spectrum of the *Z*-isomer (in red) was recorded after irradiation with 365 nm for 5 min. Irradiation with 440 nm restored the *E*-isomer. Spectra were recorded in MeOH at 293 K.

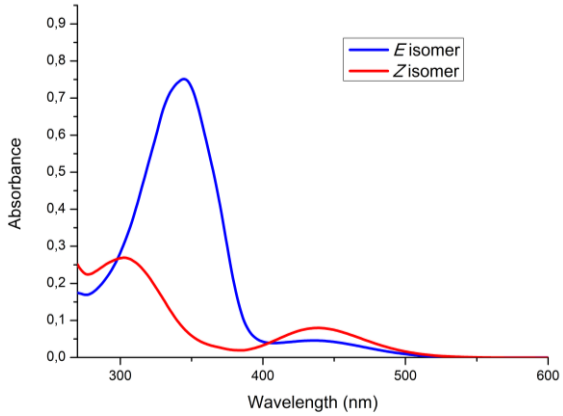

Figure 401: UV spectra of compound **79**. The spectrum of the *E*-isomer (in blue) was recorded after 16 h storage at 40 °C and the spectrum of the *Z*-isomer (in red) was recorded after irradiation with 365 nm for 5 min. Irradiation with 440 nm restored the *E*-isomer. Spectra were recorded in MeOH at 293 K.

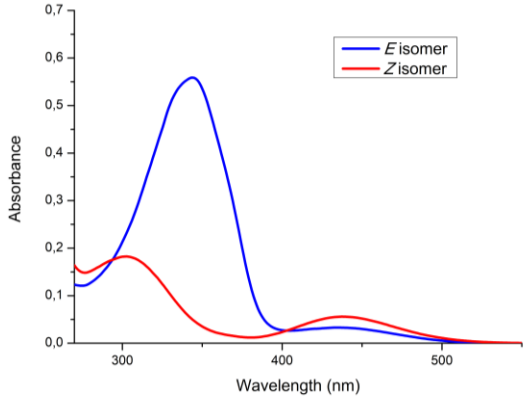

Figure 402: UV spectra of compound **80**. The spectrum of the *E*-isomer (in blue) was recorded after 16 h storage at 40 °C and the spectrum of the *Z*-isomer (in red) was recorded after irradiation with 365 nm for 5 min. Irradiation with 440 nm restored the *E*-isomer. Spectra were recorded in MeOH at 293 K.

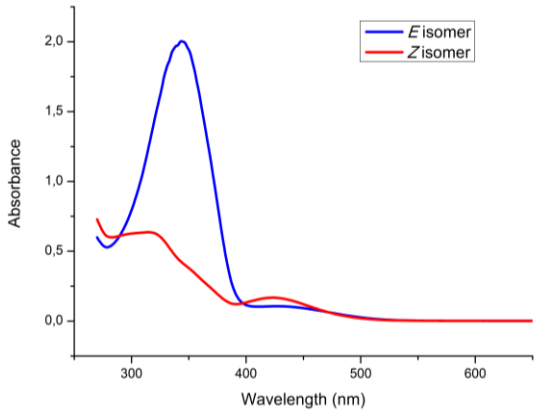

Figure 403: UV spectra of compound **102**. The spectrum of the *E*-isomer (in blue) was recorded after 16 h storage at 40 °C and the spectrum of the *Z*-isomer (in red) was recorded after irradiation with 365 nm for 5 min. Irradiation with 440 nm restored the *E*-isomer. Spectra were recorded in MeOH at 293 K.

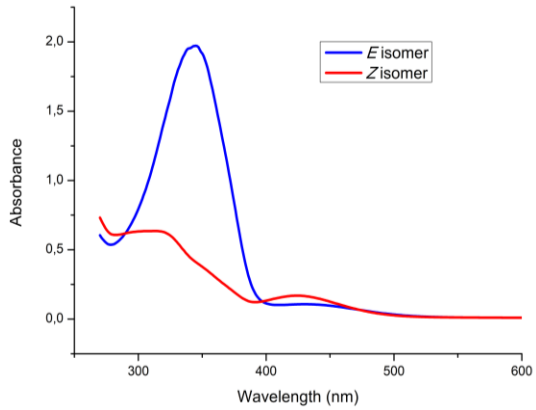

Figure 404: UV spectra of compound **103**. The spectrum of the *E*-isomer (in blue) was recorded after 16 h storage at 40 °C and the spectrum of the *Z*-isomer (in red) was recorded after irradiation with 365 nm for 5 min. Irradiation with 440 nm restored the *E*-isomer. Spectra were recorded in MeOH at 293 K.

8.6 Supporting information for chapter 6: Red-shifted azobenzene glycoconjugates for *in vivo photoswitching* expriments

8.6.1 Synthesis of compounds

3,5-Dichloro-4-nitrophenol 5[414]

Sulfuric acid (1.79 mL in 10.0 mL of water) was added to an ice-cold solution of 3,5-dichlorophenol **2** (4.00 g, 24.7 mmol) and sodium nitrite (2.32 g, 33.6 mmol) in water (70 mL). The reaction mixture was then stirred for 6 hours under reflux while additional sodium nitrite (10.1 g, 146 mmol) was added in portions. Afterwards the mixture was stirred for additional 16 h at room temperature. After extraction with ethyl acetate (3 x 150 mL) the combined organic layers were washed with water (250 mL) and sat. NaCl solution (250 mL). The organic layer was dried over $MgSO_4$, filtered and the solvent removed under reduced pressure. The raw product was purified by column chromatography (cyclohexane/ ethyl acetate 7:1 → 2:1). Finally, the product **5** was crystallised in cyclohexane in the cold as a brownish solid.

Yield: 1.90 g (9.14 mmol; 37 %; lit.: 12 %[414]);

TLC: R_f = 0.35 (cyclohexane/ ethyl acetate 2:1);

^{1}H-NMR: ($CDCl_3$, 200 MHz, 300 K): δ = 6.90 (s, 2H, Ar-H_{ortho}), 5.64 (s, 1H, OH) ppm.

3,5-Dichloro-4-aminophenol 6

3,5-Dichloro-4-nitrophenol **5** (500 mg, 2.40 mmol) was dissolved in methanol (30 mL) and a catalytic amount of palladium catalyst on charcoal was added. The mixture was stirred under hydrogen atmosphere for 16 h at room temperature. The mixture was then filtered with a syringe filter device (Ø = 0.45 µm) before the solvent was removed under reduced pressure. The product was obtained quantitatively as a slightly brown solid.

Yield: 425 mg (2.39 mmol; 99 %);

TLC: R_f = 0.0 (cyclohexane/ ethyl acetate 2:1).

3,5-Dichloro-4-nitrophenyl 2,3,4,6-tetra-*O*-acetyl-α-D-mannopyranoside 10

Borontrifluoride diethyletherate (543 µl, 4.33 mmol) was added to a solution of mannose trichloroacetimidate **9** (426 mg, 865 µmol) and 3,5-Dichloro-4-nitrophenol **5** (180 mg, 865 µmol) in dry DCM (12 mL) at 0 °C. The reaction mixture was stirred at room temperature for 48 h. The solvent was removed under reduced pressure and the crude product was purified by column chromatography (cyclohexane/ ethyl acetate, 3:1→ 2:1) to obtain mannoside **10** as a colourless solid.

Yield: 329 mg (616 µmol; 71 %);

TLC: R_f = 0.21 (cyclohexane/ ethyl acetate 2:1);

^{1}H-NMR: (200 MHz, $CDCl_3$, 300 K, TMS): δ = 7.22 (s, 2H, Ar-H), 5.55-5.52 (d, $^3J_{1,2}$ = 1.7 Hz, 1H, H-1), 5.64-5.51 (m, 2H, H-2, H-3), 5.39-5.27 (dd~t, $^3J_{3,4}$ = 9.7 Hz, 1H, H-4), 4.35-4.21 (dd, $^3J_{5,6}$ = 6.4 Hz, $^2J_{6,6'}$ = 12.3 Hz, 1H, H-6), 4.14-3.93 (m, 2H, H-5, H-6'), 2.20, 2.07, 2.06, 2.04 (each s, each 3H, CH_3) ppm.

3,5-Dichloro-4-aminophenyl 2,3,4,6-tetra-*O*-acetyl-α-D-mannopyranoside 11

Mannoside **10** (329 mg, 616 µmol) was dissolved in methanol (30 mL) and a catalytic amount of palladium catalyst on charcoal was added. The mixture was stirred under hydrogen atmosphere for 4 h at room temperature. The mixture was then filtered with a syringe filter device (Ø = 0.45 µm) before the solvent was removed under reduced pressure. The product **11** was obtained quantitatively as a colourless solid.

Yield: 306 mg (602 µmol; 98 %);

TLC: R_f = 0.2 (cyclohexane/ ethyl acetate 1:1).

4,4'-Azobis(3,5-Dichlorophenol) 16

Azobenzene derivative **13** (300 mg, 1.40 mmol), NCS (936 mg, 7.01 mmol) and $Pd(OAc)_2$ (31.4 mg, 0.14 mmol) were dissolved in acetic acid (16 mL) and stirred at 130 °C for 16 h in an autoclave vessel. The residue was dissolved in DCM (100 mL) and washed with sat. NaCl solution (40 mL). The organic layer was dried over $MgSO_4$, filtered and the solvent removed under reduced pressure. The crude product was filtered over silica (cyclohexane → cyclohexane/ ethyl acetate 2:1) to obtain a crude product of

compound **16** as a red solid which was transposed directly to the synthesis of compound **18**.

4-{[2,4-Bis(2,3,4,6-tetra-*O*-acetyl-α-D-mannopyranosidoxy)-5-chloro-4-hydroxy-phenyl]hydrazino}-2,5-dichlorophenyl 2,3,4,6-tetra-*O*-acetyl-α-D-manno-pyranoside 18

Borontrifluoride diethyletherate (106 µl, 284 µmol) was added to a solution of mannose trichloroacetimidate **9** (140 mg, 284 µmol) and azobenzene derivative **16** (100 mg, 284 µmol) in dry DCM (15 mL) at 0 °C. The reaction mixture was stirred at room temperature for 16 h. The solvent was removed under reduced pressure and the crude product was purified by column chromatography (cyclohexane/ ethyl acetate, 4:1→ 2:1) to obtain mannoside **18** as a colourless solid.

Yield: 329 mg (616 µmol; 71 %);

TLC: R_f = 0.19 (cyclohexane/ ethyl acetate 4:1);

^{1}H-NMR: (500 MHz, $CDCl_3$, 300 K, TMS): δ = 7.34 (s, 4H, Ar-H), 5.78-5.77 (dd, $^3J_{1,2}$ = 1.8 Hz, $^3J_{2,3}$ = 3.2 Hz 3H, H-2), 5.60-5.57 (dd, $^3J_{2,3}$ = 3.2 Hz, $^3J_{3,4}$ = 10.0 Hz, 3H, H-3), 5.42-5.38 (dd~t, $^3J_{3,4}$ = 10.0 Hz 3H, H-4), 5.36-5.35 (d, $^3J_{1,2}$ = 1.8 Hz, 3H, H-1), 4.78-4.62 (ddd, $^3J_{5,6}$ = 2.3 Hz, $^3J_{5,6'}$ = 4.8 Hz, $^3J_{4,5}$ = 10.1 Hz, 1H, H-5), 4.31-4.28 (dd, $^3J_{5,6}$ = 5.10 Hz, $^2J_{6,6'}$ = 5.10 Hz, 3H, H-6), 4.20-4.16 (dd, $^3J_{5,6'}$ = 2.4 Hz, $^2J_{6,6'}$ = 5.10 Hz, 3H, H-6'), 2.07, 1.97, 1.96, 1.92 (each s, each 9H, CH_3) ppm;

^{13}C-NMR: (126 MHz, MeOD, 300 K): δ = 170.6, 169.9, 169.7 (C=O), 148.5 (Ar-CO), 130.7 (Ar-C), 129.6, 129.1 (Ar-C), 101.2 (C-1), 70.9 (C-5), 69.2 (C-2), 68.6 (C-3), 65.7 (C-4), 62.3 (C-6), 20.8, 20.7 ((C=O)CH_3) ppm;

EI-MS: *m/z* = 1347.4 $[M+Na]^+$; (calc. 1324.253 for $C_{54}H_{63}Cl_3N_2O_{30}$).

***p*-[(*E*)-(*p*'-Acetic acid methyl ester) phenylazo]phenyl 2,3,4,6-tetra-*O*-acetyl-β-D-glucopyranoside 20**

Acetic acid anhydride (505 µL, 5.34 mmol) was added to a solution of glucoside **19** (288 mg, 667 µmol) in pyridine (15 mL) and stirred at room temperature for 2 d. The

solvent was removed under reduced pressure and the crude product was codestilled twice with toluene (2 x 30 mL) to obtain compound **20** quantitatively as an orange solid.

Yield: 400 mg (666 µmol, quant.);

TLC: R_f = 0.42 (cyclohexane / ethyl acetate 1:1);

Rotational value: $[\alpha]_D^{24}$ = +10.4 (c = 2.45 mM, CH_2Cl_2);

^{1}H-NMR ($CDCl_3$, 500 MHz, 300 K): δ = 7.91-7.88 (m, 2H, Ar-H_{ortho}), 7.87-7.84 (m, 2H, Ar-$H_{ortho'}$), 7.44-7.41 (m, 2H, Ar-$H_{meta'}$), 7.12-7.09 (m, 2H, Ar-H_{meta}), 5.35-5.30 (m, 2H, H-2, H-3), 5.21-5.17 (m, 2H, H-1, H-4), 4.33-4.28 (dd, $^2J_{6,6'}$ = 12.3 Hz, $^3J_{5,6}$ = 5.5 Hz, 1H, H-6), 4.21-4.18 (dd, $^2J_{6,6'}$ = 12.3 Hz, $^3J_{H5H6'}$ = 2.4 Hz, 1H, H-6'), 3.94-3.90 (ddd, $^3J_{5,6}$ = 5.5 Hz, $^3J_{5,6'}$ = 2.4 Hz, $^3J_{4,5}$ = 10.0 Hz, 1H, H-5), 3.72 (s, 3H, CH_3), 3.71 (s, 2H, CH_2) 2.09, 2.07, 2.06, 2.05 (s, each 3H, C=OCH_3) ppm;

^{13}C-NMR ($CDCl_3$, 126 MHz, 300 K): δ = 171.5 (CH_2(C=O), 170.6, 170.2, 169.4, 169.3 (C=O), 158.8 (Ar-C_{para}), 151.7 (Ar-$C_{ipso'}$), 148.6 (Ar-C_{ipso}), 136.8 (Ar-$C_{para'}$), 130.0 (Ar-$C_{meta'}$), 124.5 (Ar-C_{ortho}), 122.9 (Ar-$C_{ortho'}$), 117.0 (Ar-C_{meta}),98.7 (C-1), 72.7 (C-3), 72.2 (C-5), 71.1 (C-2), 68.2 (C-4), 61.9 (C-6), 52.2 (CH_3), 41.0 (CH_2), 20.7, 20.6 (C=OCH_3) ppm;

IR (ATR): $\tilde{\nu}$ = 1732, 1597, 1497, 1367, 1215, 1072, 1037, 1030, 844 cm^{-1};

ESI-MS: *m/z* = 601.20280, $[M+H]^+$; (calc. 601.20335 for $C_{29}H_{32}N_2O_{12}$+H).

4-[(*E*)-*4*'-(Acetic acid methyl ester)-3,5-dichlorophenylazo]-3,5-dichlorophenyl 2,3,4,6-tetra-*O*-acetyl-β-D-glucopyranoside 21

Glucoside **20** (50.0 mg, 83.5 µmol), NCS (55.5 mg, 417 µmol) and $Pd(OAc)_2$ catalyst (1.88 mg, 8.37 µmol) were suspended in dry acetic acid (1.0 mL) and stirred under microwave heating at 140 °C for 1 h. The acetic acid was removed subsequently under reduced pressure and the residue dissolved in DCM (40 mL) and washed with phosphate buffer (30 mL) and sat. NaCl solution (30 mL). The organic phase was dried over $MgSO_4$, filtered and the solvent removed under reduced pressure. Compound **21** was obtained after column chromatography (cyclohexane/ ethyl acetate 4:1→ 1:1) as a red solid.

Yield: 20.3 mg (27.5 µmol, 33 %);

TLC: R_f = 0.37 (cyclohexane / ethyl acetate 1:1);

^{1}H-NMR ($CDCl_3$, 500 MHz, 300 K): δ = 7.39 (s, 2H, Ar-$H_{meta'}$), 7.12 (s, 2H, Ar-$H_{meta'}$), 5.34-5.26 (m, 2H, H-2, H-3), 5.16-5.10 (m, 2H, H-1, H-4), 4.24-4.21 (m, 2H, H-6, H-6'), 3.97-3.91 (ddd, $^{3}J_{5,6}$ = 5.2 Hz, $^{3}J_{5,6'}$ = 3.7 Hz, $^{3}J_{4,5}$ = 10.0 Hz, 1H, H-5), 3.74 (s, 3H, CH_3), 3.64 (s, 2H, CH_2) 2.13, 2.09, 2.07, 2.05 (s, each 3H, C=OCH_3) ppm;

^{13}C-NMR ($CDCl_3$, 126 MHz, 300 K): δ = 170.6 (CH_2(C=O), 170.5, 170.1, 169.4, 169.2 (C=O), 156.5 (Ar-C_{para}), 146.7 (Ar-$C_{ipso'}$), 142.9 (Ar-C_{ipso}), 136.0 (Ar-$C_{para'}$), 130.2 (Ar-$C_{meta'}$), 129.3 (Ar-C_{ortho}), 127.3 (Ar-$C_{ortho'}$), 118.0 (Ar-C_{meta}),98.5 (C-1), 72.5 (C-5), 72.5 (C-3), 70.9 (C-2), 68.2 (C-4), 62.1 (C-6), 52.5 (CH_3), 40.1 (CH_2), 20.7, 20.6 (C=OCH_3) ppm.

8.6.2 ^{1}H and ^{13}C NMR spectra of synthesised compounds

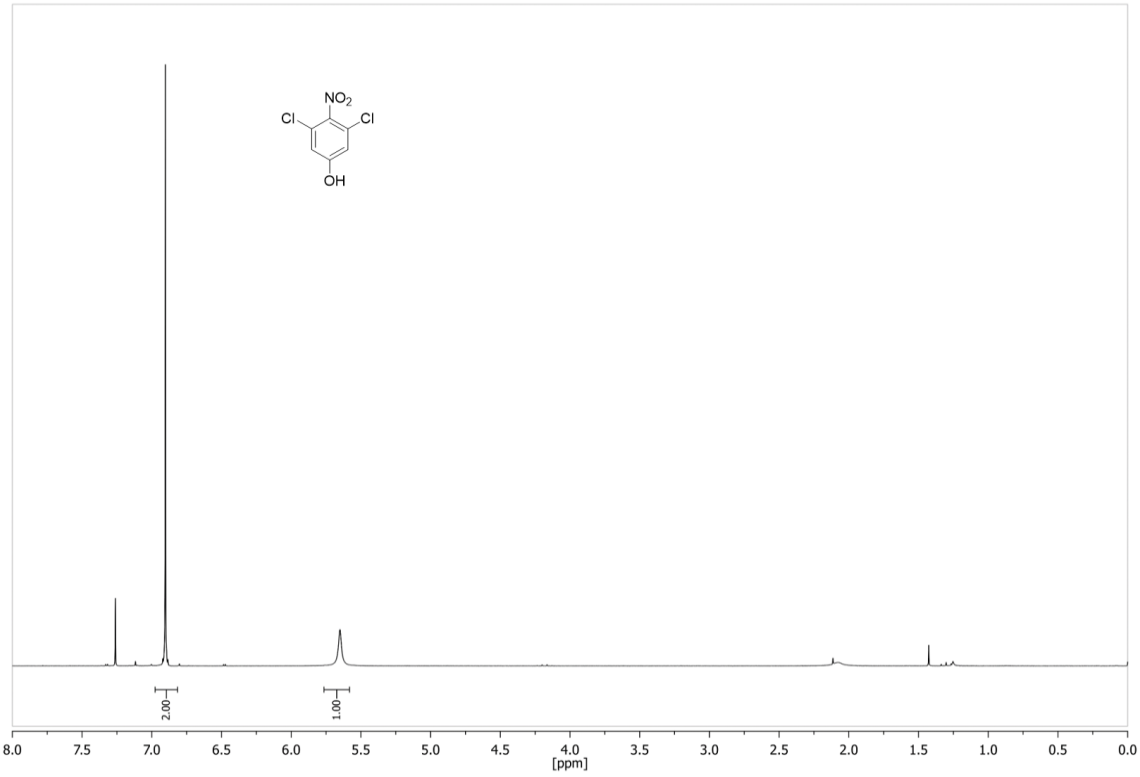

Figure 405: ^{1}H NMR spectrum of compound **5** (200 MHz, $CDCl_3$, 300 K).

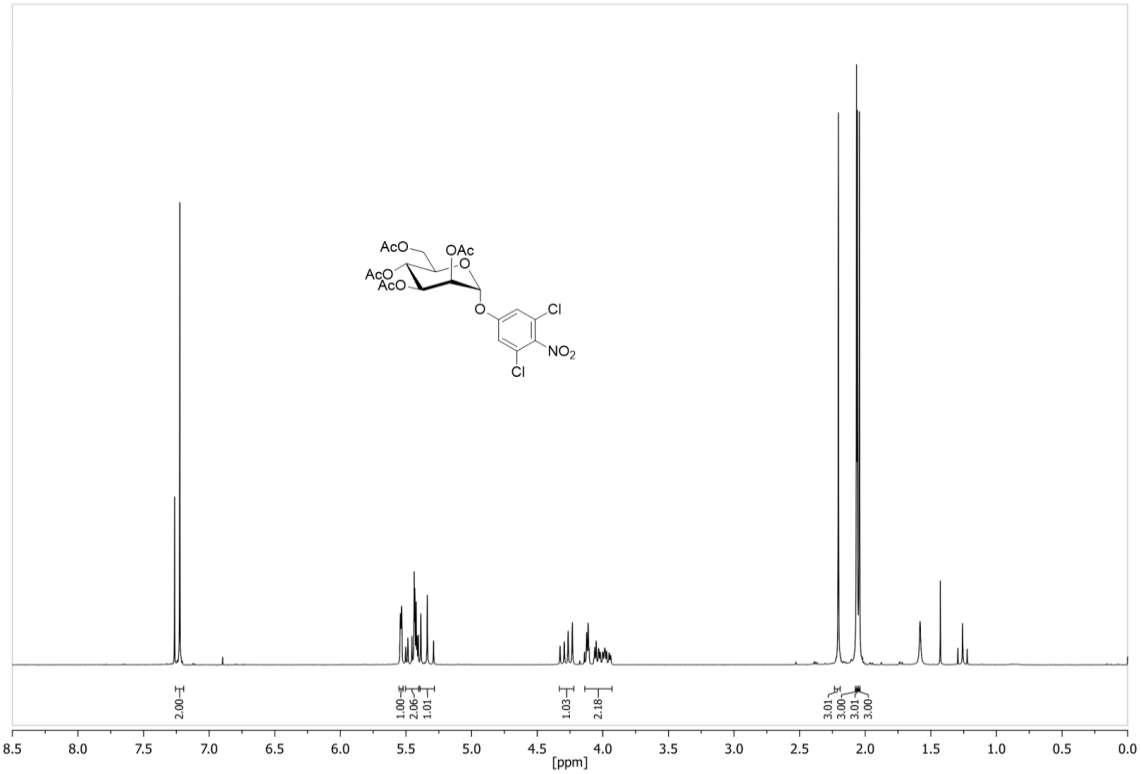

Figure 406: ^{1}H NMR spectrum of compound **10** (200 MHz, $CDCl_3$, 300 K).

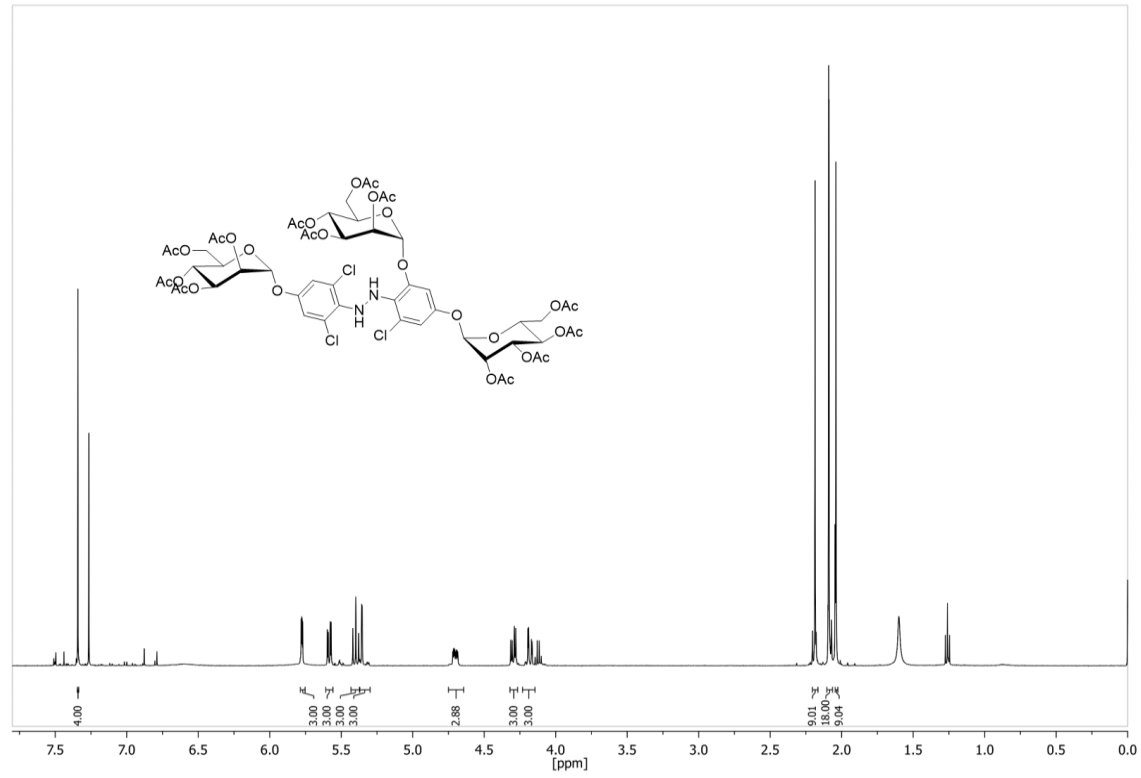

Figure 407: ^{1}H NMR spectrum of compound **18** (500 MHz, $CDCl_3$, 300 K).

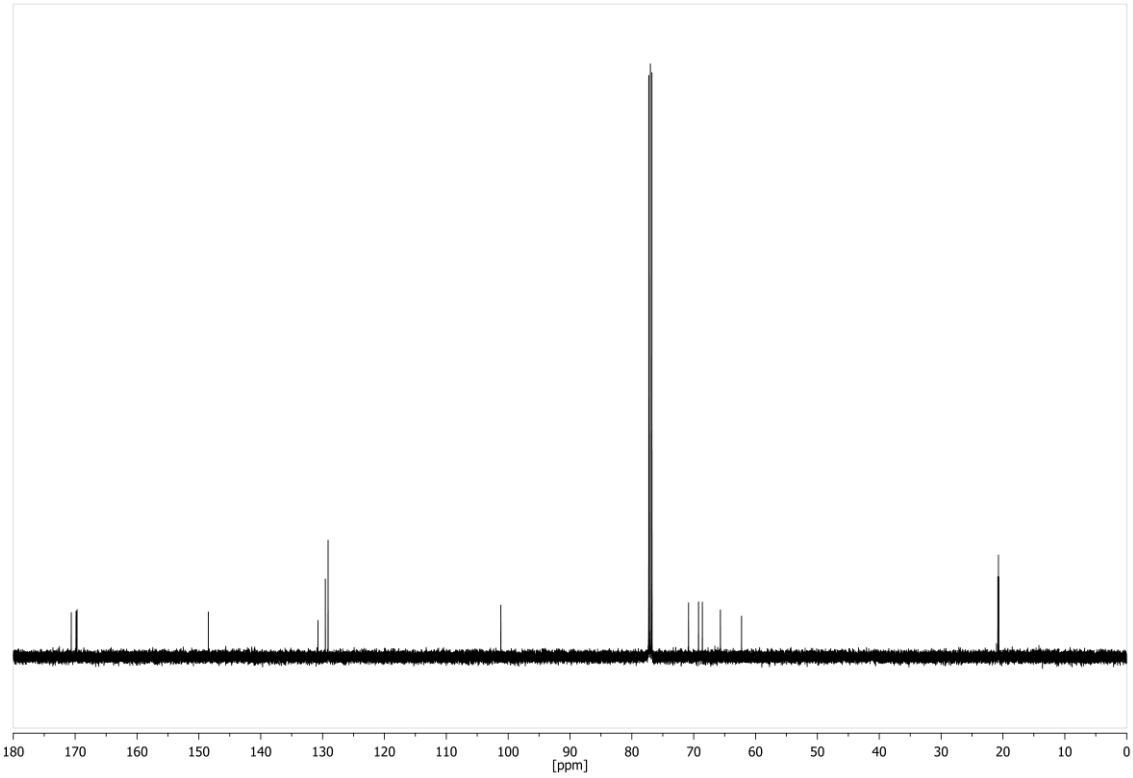

Figure 408: ^{13}C NMR spectrum of compound **18** (126 MHz, $CDCl_3$, 300 K).

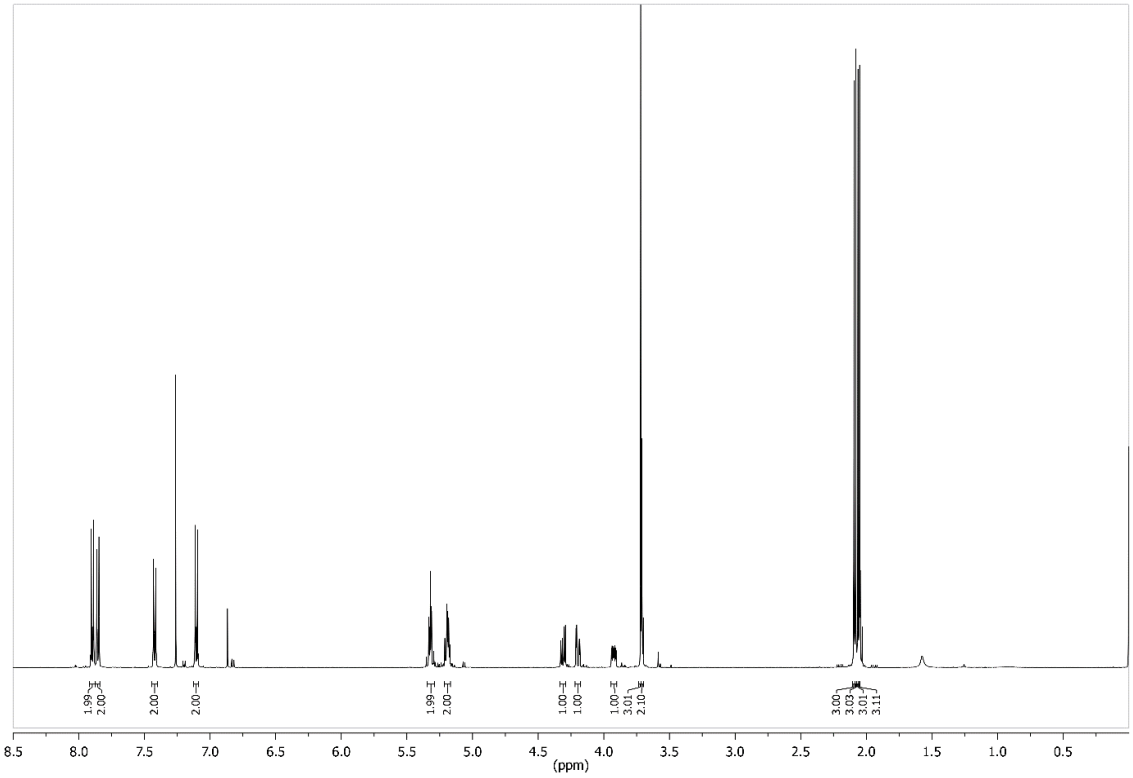

Figure 409: ^{1}H NMR spectrum of compound **20** (500 MHz, $CDCl_3$, 300 K).

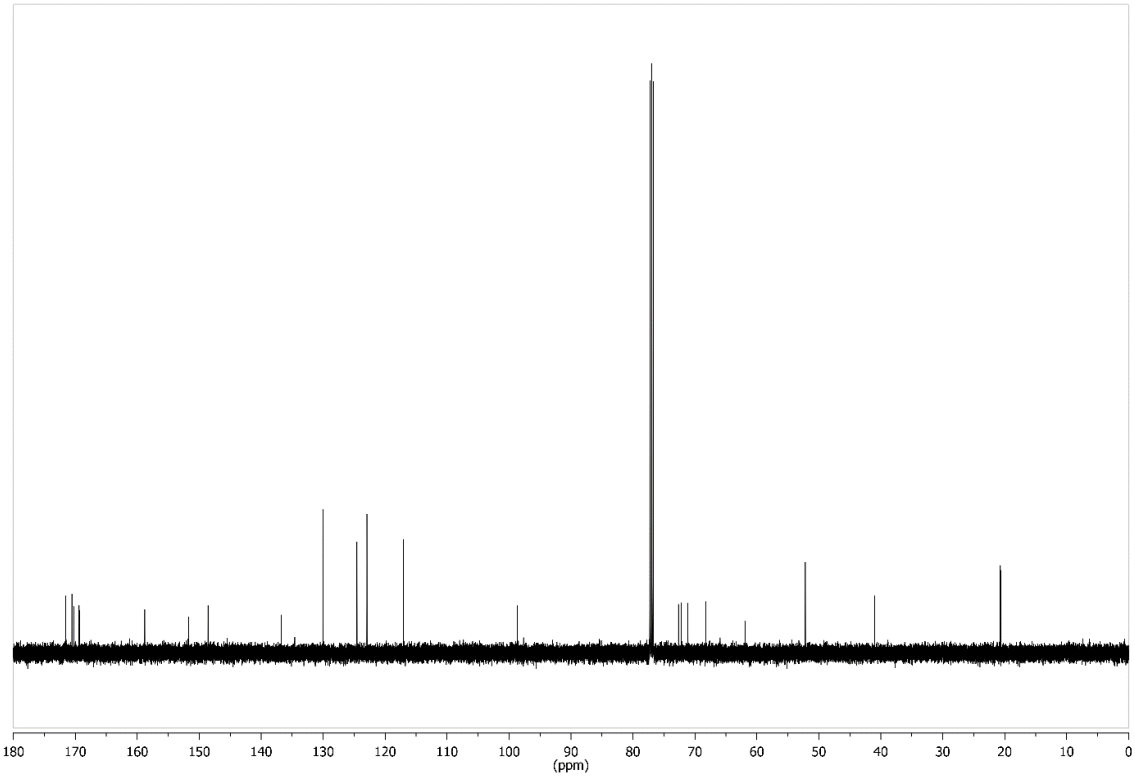

Figure 410: ^{13}C NMR spectrum of compound **20** (126 MHz, $CDCl_3$, 300 K).

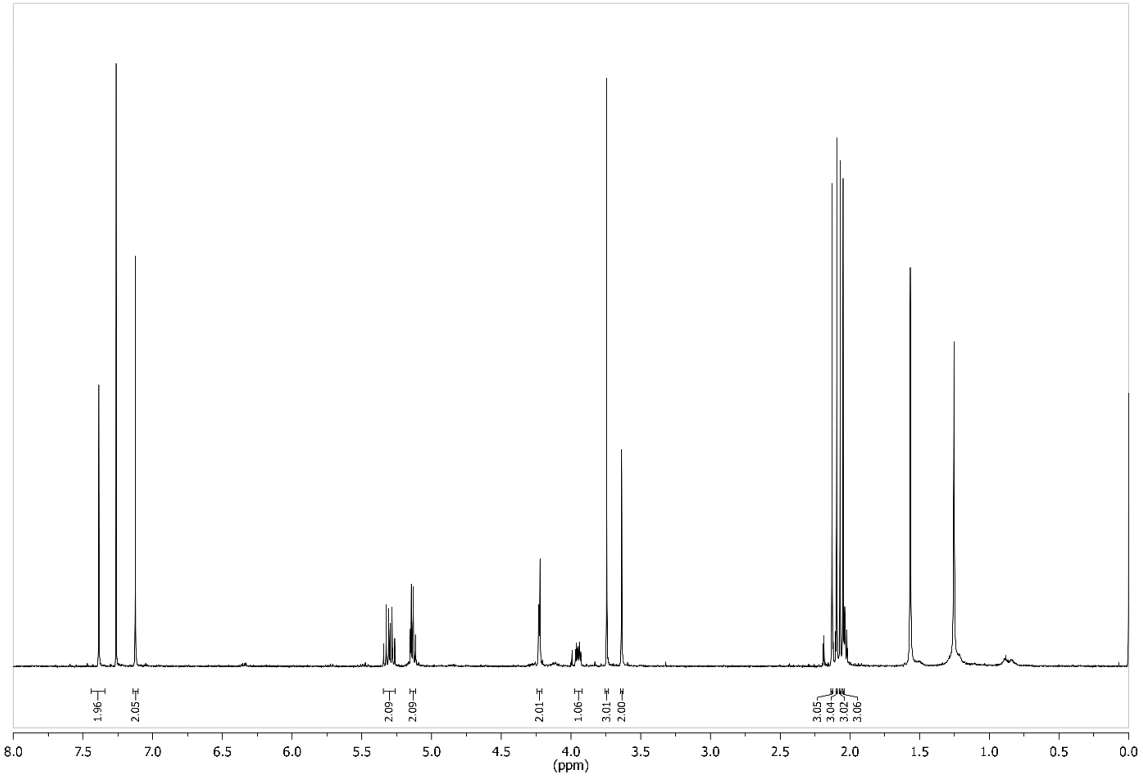

Figure 411: ^{1}H NMR spectrum of compound **21** (500 MHz, $CDCl_3$, 300 K).

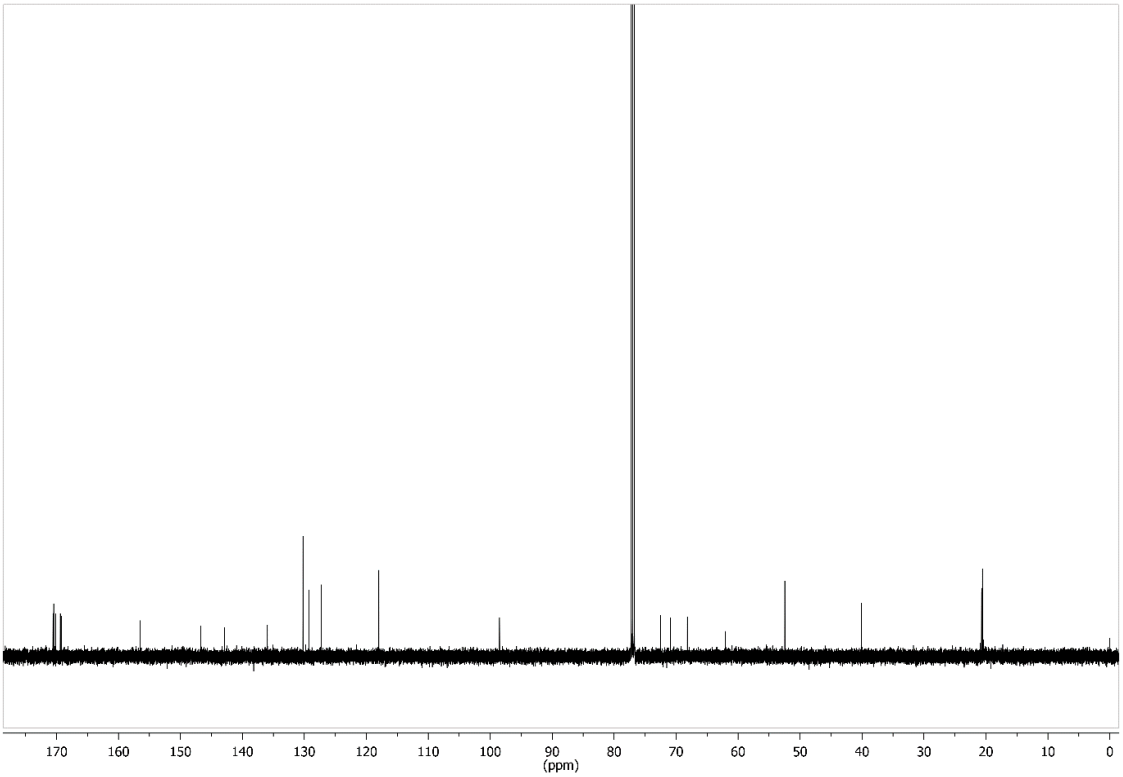

Figure 412: ^{13}C NMR spectrum of compound **21** (126 MHz, $CDCl_3$, 300 K).

9 References

[1] J. D. Watson, F. H. C. Crick, Molecular Structure of Nucleic Acids: A Structure for Deoxyribose Nucleic Acid, *Nature* **1953**, *171*, 737.

[2] M. W. Nirenberg, J. H. Matthaei, The dependence of cell-free protein synthesis in *E. coli* upon naturally occurring or synthetic Polyribonucleotides, *Proc. Natl. Acad. Sci. USA* **1961**, *47*, 1588-1602.

[3] R. W. Holley, J. Apgar, G. A. Everett, J. T. Madison, M. Marquisee, S. H. Merrill, J. R. Penswick, A. Zamir, Structure of a Ribonucleic Acid, *Science* **1965**, *147*, 1462-1465.

[4] D. B. Werz, R. Ranzinger, S. Herget, A. Adibekian, C.-W. von der Lieth, P. H. Seeberger, Exploring the Structural Diversity of Mammalian Carbohydrates ("Glycospace") by Statistical Databank Analysis, *ACS Chem. Biol.* **2007**, *2*, 685-691.

[5] A. Varki, Biological roles of glycans, *Glycobiology* **2017**, *27*, 3-49.

[6] A. Varki, S. Kornfeld, Historical Background and Overview, chapter 1, in *Essentials of Glycobiology*, 3. ed. (Eds.: A. Varki, R. D. Cummings, J. D. Esko et al.), Cold Spring Harbor Laboratory Press, Cold Spring Harbor (NY), **2017**.

[7] W. Völksen, Die Entdeckung der Stärkeverzuckerung (Säurehydrolyse) durch G. S. C. Kirchhoff im Jahre 1811, *Starch - Stärke* **1949**, *1*, 30-36.

[8] E. Fischer, Verbindungen des Phenylhydrazins mit den Zuckerarten, *Ber. Dt. Chem. Ges.* **1884**, *17*, 579-584.

[9] E. Fischer, Verbindungen des Phenylhydrazins mit den Zuckerarten II, *Ber. Dt. Chem. Ges.* **1887**, *20*, 821-834.

[10] E. Fischer, Ueber die Verbindungen des Phynylhydrazins mit den Zuckerarten. III, *Ber. Dt. Chem. Ges.* **1888**, *21*, 988-991.

[11] E. Fischer, J. Hirschberger, Ueber Mannose, *Ber. Dt. Chem. Ges.* **1888**, *21*, 1805-1809.

[12] E. Fischer, Über die Struktur der beiden Methyl-glucoside und über ein drittes Methyl-glucosid, *Ber. Dt. Chem. Ges.* **1914**, *47*, 1980-1989.

[13] Govindjee, D. Krogmann, *Discoveries in Oxygenic Photosynthesis (1727–2003): A Perspective Vol. 80*, **2004**.

[14] F. G. Young, Claude Bernard and the Discovery of Glycogen, *BMJ* **1957**, *1*, 1431-1437.

[15] H. Kornberg, Krebs and his trinity of cycles, *Nat. Rev. Mol. Cell Biol.* **2000**, *1*, 225.

[16] H. L. Kornberg, H. A. Krebs, Synthesis of Cell Constituents from C2-Units by a Modified Tricarboxylic Acid Cycle, *Nature* **1957**, *179*, 988.

[17] H. A. Krebs, K. Henseleit, Untersuchungen uber die Harnstoffbildung im Tierkörper, *Hoppe-Seylers Z. Physiol. Chem.* **1932**, *210*, 33.

[18] L. Cooling, Carbohydrate blood groups, in *Rossi's Principles of Transfusion Medicine*, 5. ed. (Eds.: T. L. Simon, J. McCullough, E. L. Snyder, B. G. Solheim, R. G. Trauss), Wiley, **2016**.

[19] H. P. Schwarz, F. Dorner, Karl landsteiner and his major contributions to haematology, *Br. J. Haematol.* **2003**, *121*, 556-565.

[20] E. Tecle, P. Gagneux, Sugar-coated sperm: Unraveling the functions of the mammalian sperm glycocalyx, *Mol. Reprod. Dev* **2015**, *82*, 635-650.

[21] N. Sharon, H. Lis, Lectins as cell recognition molecules, *Science* **1989**, *246*, 227-234.

[22] M. Ambrosi, N. R. Cameron, B. G. Davis, Lectins: tools for the molecular understanding of the glycocode, *Org. Biomol. Chem.* **2005**, *3*, 1593-1608.

[23] B. K. Brandley, R. L. Schnaar, Cell-Surface Carbohydrates in Cell Recognition and Response, *J. Leukoc. Biol.* **1986**, *40*, 97-111.

[24] T. J. Wiles, R. R. Kulesus, M. A. Mulvey, Origins and virulence mechanisms of uropathogenic Escherichia coli, *Exp. Mol. Pathol.* **2008**, *85*, 11-19.

[25] A. Varki, Biological roles of oligosaccharides: all of the theories are correct, *Glycobiology* **1993**, *3*, 97-130.

[26] T. W. Rademacher, R. B. Parekh, R. A. Dwek, Glycobiology, *Annu. Rev. Biochem* **1988**, *57*, 785-838.

[27] H.-J. Gabius, H.-C. Siebert, S. André, J. Jiménez-Barbero, H. Rüdiger, Chemical Biology of the Sugar Code, *ChemBioChem* **2004**, *5*, 740-764.

[28] C. R. Bertozzi, Kiessling, L. L., Chemical Glycobiology, *Science* **2001**, *291*, 2357-2364.

[29] M. Kukkonen, T. Raunio, R. Virkola, K. Lähteenmäki, P. H. Mäkelä, P. Klemm, S. Clegg, T. K. Korhonen, Basement membrane carbohydrate as a target for bacterial adhesion: binding of type I fimbriae of Salmonella enterica and Escherichia coli to laminin, *Mol. Microbiol.* **1993**, *7*, 229-237.

[30] S. Weinbaum, J. M. Tarbell, E. R. Damiano, The Structure and Function of the Endothelial Glycocalyx Layer, *Annu. Rev. Biomed. Eng.* **2007**, *9*, 121-167.

[31] S. Reitsma, D. W. Slaaf, H. Vink, M. A. M. J. van Zandvoort, M. G. A. oude Egbrink, The endothelial glycocalyx: composition, functions, and visualization, *Pflügers Arch.* **2007**, *454*, 345-359.

[32] G. van Meer, D. R. Voelker, G. W. Feigenson, Membrane lipids: where they are and how they behave, *Nat. Rev. Mol. Cell Biol.* **2008**, *9*, 112-124.

[33] P. Stanley, N. Taniguchi, M. Aebi, N-Glycans, chapter 9, in *Essentials of Glycobiology*, 3 ed. (Eds.: A. Varki, R. Cummings, J. Esko et al.), Cold Spring Harbor Laboratory Press, Cold Spring Harbor (NY), **2017**.

[34] I. Brockhausen, P. Stanley, O-GalNAc Glycans, chapter 10, in *Essentials of Glycobiology* (Eds.: A. Varki, R. Cummings, J. Esko et al.), Cold Spring Harbor Laboratory Press, Cold Spring Harbor (NY), **2017**.

[35] B. F. Becker, M. Jacob, S. Leipert, A. H. J. Salmon, D. Chappell, Degradation of the endothelial glycocalyx in clinical settings: searching for the sheddases, *Br. J. Clin. Pharmacol.* **2015**, *80*, 389-402.

[36] http://www.functionalglycomics.org/static/consortium/Nomenclature.shtml

[37] C. Szymanski, R. Schnaar, M. Aebi, Bacterial and Viral Infections, chapter 42, in *Essentials of Glycobiology*, 3. ed. (Eds.: A. Varki, R. Cummings, J. Esko et al.), Cold Spring Harbor Laboratory Press, Cold Spring Harbor (NY), **2017**.

[38] J. B. Kaper, J. P. Nataro, H. L. T. Mobley, Pathogenic Escherichia coli, *Nat. Rev. Microbiol.* **2004**, *2*, 123.

[39] G. G. Anderson, K. W. Dodson, T. M. Hooton, S. J. Hultgren, Intracellular bacterial communities of uropathogenic *Escherichia coli* in urinary tract pathogenesis, *Trends Microbiol.* **2004**, *12*, 424-430.

[40] P. Heath, Y. Nik, C. Baker, Neonatal meningitis, *Arch. Dis. Child Fetal Neonatal Ed.* **2003**, *88*, F173-F178.

[41] Y. Nguyen, V. Sperandio, Enterohemorrhagic E. coli (EHEC) pathogenesis, *Frontiers in Cellular and Infection Microbiology* **2012**, *2*, 90.

[42] H. Ghazarian, B. Idoni, S. B. Oppenheimer, A glycobiology review: carbohydrates, lectins, and implications in cancer therapeutics, *Acta Histochem.* **2011**, *113*, 236-247.

[43] M. D. Crespo, C. Puorger, M. A. Schärer, O. Eidam, M. G. Grütter, G. Capitani, R. Glockshuber, Quality control of disulfide bond formation in pilus subunits by the chaperone FimC, *Nat. Chem. Biol.* **2012**, *8*, 707.

[44] B. Madison, I. Ofek, S. Clegg, S. N. Abraham, Type 1 fimbrial shafts of Escherichia coli and Klebsiella pneumoniae influence sugar-binding specificities of their FimH adhesins, *Infect. Immun.* **1994**, *62*, 843-848.

[45] D. Choudhury, A. Thompson, V. Stojanoff, S. Langermann, J. Pinkner, S. J. Hultgren, S. D. Knight, X-ray Structure of the FimC-FimH Chaperone-Adhesin Complex from Uropathogenic *Escherichia coli*, *Science* **1999**, *285*, 1061-1066.

[46] B. Fiege, S. Rabbani, R. C. Preston, R. P. Jakob, P. Zihlmann, O. Schwardt, X. Jiang, T. Maier, B. Ernst, The Tyrosine Gate of the Bacterial Lectin FimH: A Conformational Analysis by NMR Spectroscopy and X-ray Crystallography, *ChemBioChem* **2015**, *16*, 1235-1246.

[47] N. Firon, S. Ashkenazi, D. Mirelman, I. Ofek, N. Sharon, Aromatic alpha-glycosides of mannose are powerful inhibitors of the adherence of type 1 fimbriated Escherichia coli to yeast and intestinal epithelial cells, *Infect. Immun.* **1987**, *55*, 472-476.

[48] N. Sharon, I. Ofek, Safe as mother's milk: carbohydrates as future anti-adhesion drugs for bacterial diseases, *Glycoconj J* **2000**, *17*, 659-664.

[49] N. Sharon, Carbohydrates as future anti-adhesion drugs for infectious diseases, *Biochim. Biophys. Acta* **2006**, *1760*, 527-537.

[50] M. Vetsch, D. Erilov, N. Molière, M. Nishiyama, O. Ignatov, R. Glockshuber, Mechanism of fibre assembly through the chaperone–usher pathway, *EMBO Reports* **2006**, *7*, 734-738.

[51] L. Gross, Bacterial Fimbriae Designed to Stay with the Flow, *PLOS Biology* **2006**, *4*, e314.

[52] H. Remaut, C. Tang, N. S. Henderson, J. S. Pinkner, T. Wang, S. J. Hultgren, D. G. Thanassi, G. Waksman, H. Li, Fiber Formation across the Bacterial Outer Membrane by the Chaperone/Usher Pathway, *Cell* **2008**, *133*, 640-652.

[53] T. Feizi, B. Mulloy, Carbohydrates and glycoconjugates: Glycomics: the new era of carbohydrate biology, *Curr. Opin. Struc.t Biol.* **2003**, *13*, 602-604.

[54] D. B. Konrad, J. A. Frank, D. Trauner, Synthesis of Redshifted Azobenzene Photoswitches by Late-Stage Functionalization, *Chem. Eur. J.* **2016**, *22*, 4364-4368.

[55] V. Poonthiyil, F. Reise, G. Despras, T. K. Lindhorst, Microwave-assisted facile synthesis of red-shifted azobenzene glycoconjugates, *Eur. J. Org. Chem.*, doi:10.1002/ejoc.201801078.

[56] R. Phillips, T. Ursell, P. Wiggins, P. Sens, Emerging roles for lipids in shaping membrane-protein function, *Nature* **2009**, *459*, 379-385.

[57] E. H. G. Backus, J. M. Kuiper, J. B. F. N. Engberts, B. Poolman, M. Bonn, Reversible Optical Control of Monolayers on Water through Photoswitchable Lipids, *J. Phys. Chem. B* **2011**, *115*, 2294-2302.

[58] S. R. Dennison, Z. Akbar, D. A. Phoenix, T. J. Snape, Interactions between suitably functionalised conformationally distinct benzanilides and phospholipid monolayers, *Soft Matter* **2012**, *8*, 3258-3264.

[59] S. Fahs, F. B. Rowther, S. R. Dennison, Y. Patil-Sen, T. Warr, T. J. Snape, Development of a novel, multifunctional, membrane-interactive pyridinium salt with potent anticancer activity, *Bioorg. Med. Chem. Lett.* **2014**, *24*, 3430-3433.

[60] T. Sato, Y. Ozaki, K. Iriyama, Molecular Aggregation and Photoisomerization of Langmuir-Blodgett Films of Azobenzene-Containing Long-Chain Fatty Acids and Their Salts Studied by Ultraviolet-Visible and Infrared Spectroscopies, *Langmuir* **1994**, *10*, 2363-2369.

[61] T. J. Hester, S. R. Dennison, M. J. Baker, T. J. Snape, Functionalising the azobenzene motif delivers a light-responsive membrane-interactive compound with the potential for photodynamic therapy applications, *Org. Biomol. Chem.* **2015**, *13*, 8067-8070.

[62] M. Tanaka, T. Sato, Y. Yonezawa, Permeability enhancement in phospholipid bilayer containing azobenzene derivative around the phase transition temperature, *Langmuir* **1995**, *11*, 2834-2836.

[63] Q. Zhao, Y. Wang, Y. Yan, J. Huang, Smart Nanocarrier: Self-Assembly of Bacteria-like Vesicles with Photoswitchable Cilia, *ACS Nano* **2014**, *8*, 11341-11349.

[64] D.-Y. Liu, W.-L. Wang, S.-H. Xu, H.-L. Liu, Photo-Responsivity of Azobenzene-Containing Glycolipid within Liquid-Gas Interface, *Acta Phys. -Chim. Sin.* **2017**, 836-844.

[65] D. Liu, S. Wang, S. Xu, H. Liu, Photocontrollable Intermittent Release of Doxorubicin Hydrochloride from Liposomes Embedded by Azobenzene-Contained Glycolipid, *Langmuir* **2017**, *33*, 1004-1012.

[66] E. Fahy, S. Subramaniam, H. A. Brown, C. K. Glass, A. H. Merrill, R. C. Murphy, C. R. H. Raetz, D. W. Russell, Y. Seyama, W. Shaw, T. Shimizu, F. Spener, G. van Meer, M. S. VanNieuwenhze, S. H. White, J. L. Witztum, E. A. Dennis, A comprehensive classification system for lipids, *Eur. J. Lipid Sci. Technol.* **2005**, *107*, 337-364.

[67] S. Subramaniam, E. Fahy, S. Gupta, M. Sud, R. W. Byrnes, D. Cotter, A. R. Dinasarapu, M. R. Maurya, Bioinformatics and Systems Biology of the Lipidome, *Chem. Rev.* **2011**, *111*, 6452-6490.

[68] H. Watson, Biological membranes, *Essays Biochem.* **2015**, *59*, 43-69.

[69] B. Alberts, A. Johnson, J. Lewis, M. Raff, K. Roberts, P. Walter, *Molecular Biology of the Cell*, 4. ed., Garland Science, New York, **2002**.

[70] S. Roke, J. Schins, M. Müller, M. Bonn, Vibrational spectroscopic investigation of the phase diagram of a biomimetic lipid monolayer, *Phys. Rev. Lett.* **2003**, *90*, 128101.

[71] V. M. Kaganer, H. Möhwald, P. Dutta, Structure and phase transitions in Langmuir monolayers, *Rev. Mod. Phys.* **1999**, *71*, 779-819.

[72] R. Maget-Dana, The monolayer technique: a potent tool for studying the interfacial properties of antimicrobial and membrane-lytic peptides and their interactions with lipid membranes, *Biochim. Biophys. Acta, Rev. Biomembr.* **1999**, *1462*, 109-140.

[73] S. Garcia-Manyes, G. Oncins, F. Sanz, Effect of temperature on the nanomechanics of lipid bilayers studied by force spectroscopy, *Biophys. J.* **2005**, *89*, 4261-4274.

[74] M. Kranenburg, B. Smit, Phase behavior of model lipid bilayers, *J. Phys. Chem. B* **2005**, *109*, 6553-6563.

[75] K. Simons, R. Ehehalt, Cholesterol, lipid rafts, and disease, *J. Clin. Invest.* **2002**, *110*, 597-603.

[76] K. Simons, E. Ikonen, Functional rafts in cell membranes, *Nature* **1997**, *387*, 569 EP -.

[77] K. Yasuhara, Y. Sasaki, J.-i. Kikuchi, A photo-responsive cholesterol capable of inducing a morphological transformation of the liquid-ordered microdomain in lipid bilayers, *Colloid. Polym. Sci.* **2008**, *286*, 1675-1680.

[78] J. A. Frank, H. G. Franquelim, P. Schwille, D. Trauner, Optical Control of Lipid Rafts with Photoswitchable Ceramides, *J. Am. Chem. Soc.* **2016**, *138*, 12981-12986.

[79] R. Turanský, M. Konôpka, N. L. Doltsinis, I. Stich, D. Marx, Switching of functionalized azobenzene suspended between gold tips by mechanochemical, photochemical, and opto-mechanical means, *Phys. Chem. Chem. Phys.* **2010**, *12*, 13922-13932.

[80] J. L. Zhang, J. Q. Zhong, J. D. Lin, W. P. Hu, K. Wu, G. Q. Xu, A. T. S. Wee, W. Chen, Towards single molecule switches, *Chem. Soc. Rev.* **2015**, *44*, 2998-3022.

[81] S. K. Patel, J. Cao, A. R. Lippert, A volumetric three-dimensional digital light photoactivatable dye display, *Nat. Commun.* **2017**, *8*, 15239.

[82] P. L. Anelli, N. Spencer, J. F. Stoddart, A molecular shuttle, *J. Am. Chem. Soc.* **1991**, *113*, 5131-5133.

[83] Y. Norikane, N. Tamaoki, Light-driven molecular hinge: a new molecular machine showing a light-intensity-dependent photoresponse that utilizes the trans-cis isomerization of azobenzene, *Org. Lett.* **2004**, *6*, 2595-2598.

[84] N. Koumura, R. W. Zijlstra, R. A. van Delden, N. Harada, B. L. Feringa, Light-driven monodirectional molecular rotor, *Nature* **1999**, *401*, 152-155.

[85] T. Kudernac, N. Ruangsupapichat, M. Parschau, B. Maciá, N. Katsonis, S. R. Harutyunyan, K.-H. Ernst, B. L. Feringa, Electrically driven directional motion of a four-wheeled molecule on a metal surface, *Nature* **2011**, *479*, 208-211.

[86] C. K. Lee, D. A. Davis, S. R. White, J. S. Moore, N. R. Sottos, P. V. Braun, Force-induced redistribution of a chemical equilibrium, *J. Am. Chem. Soc.* **2010**, *132*, 16107-16111.

[87] P. Weis, D. Wang, S. Wu, Visible-Light-Responsive Azopolymers with Inhibited π–π Stacking Enable Fully Reversible Photopatterning, *Macromolecules* **2016**, *49*, 6368-6373.

[88] J. Chen, P. Zhang, G. Fang, P. Yi, X. Yu, X. Li, F. Zeng, S. Wu, Synthesis and characterization of novel reversible photoswitchable fluorescent polymeric nanoparticles via one-step miniemulsion polymerization, *J. Phys. Chem. B* **2011**, *115*, 3354-3362.

[89] K. E. B. Doncom, C. F. Hansell, P. Theato, R. K. O'Reilly, pH-switchable polymer nanostructures for controlled release, *Polym. Chem.* **2012**, *3*, 3007.

[90] R. H. Bisby, C. Mead, C. G. Morgan, Active uptake of drugs into photosensitive liposomes and rapid release on UV photolysis, *Photochem. Photobiol.* **2000**, *72*, 57-61.

[91] M. Borowiak, W. Nahaboo, M. Reynders, K. Nekolla, P. Jalinot, J. Hasserodt, M. Rehberg, M. Delattre, S. Zahler, A. Vollmar, D. Trauner, O. Thorn-Seshold, Photoswitchable Inhibitors of Microtubule Dynamics Optically Control Mitosis and Cell Death, *Cell* **2015**, *162*, 403-411.

[92] M. A. Kienzler, E. Y. Isacoff, Precise modulation of neuronal activity with synthetic photoswitchable ligands, *Curr. Opin. Neurobiol.* **2017**, *45*, 202-209.

[93] A. M. Packer, B. Roska, M. Häusser, Targeting neurons and photons for optogenetics, *Nat. Neurosci.* **2013**, *16*, 805-815.

[94] L. Laprell, I. Tochitsky, K. Kaur, M. B. Manookin, M. Stein, D. M. Barber, C. Schön, S. Michalakis, M. Biel, R. H. Kramer, M. P. Sumser, D. Trauner, R. N. van Gelder, Photopharmacological control of bipolar cells restores visual function in blind mice, *J. Clin. Invest.* **2017**, *127*, 2598-2611.

[95] T. Fehrentz, M. Schönberger, D. Trauner, Optochemical genetics, *Angew. Chem. Int. Ed. Engl.* **2011**, *50*, 12156-12182.

[96] G. S. Hartley, The Cis-form of Azobenzene, *Nature* **1937**, *140*, 281.

[97] H. Rau, Spektroskopische Eigenschaften organischer Azoverbindungen, *Angew. Chem.* **1973**, *85*, 248-258.

[98] H. Rau, Spectroscopic Properties of Organic Azo Compounds, *Angew. Chem. Int. Ed. Engl.* **1973**, *12*, 224-235.

[99] G. S. Hartley, 113. The cis-form of azobenzene and the velocity of the thermal cis→trans-conversion of azobenzene and some derivatives, *J. Chem. Soc.* **1938**, *0*, 633-642.

[100] Z. F. Liu, K. Hashimoto, A. Fujishima, Photoelectrochemical information storage using an azobenzene derivative, *Nature* **1990**, *347*, 658-660.

[101] E. Merino, M. Ribagorda, Control over molecular motion using the cis-trans photoisomerization of the azo group, *Beilstein J. Org. Chem.* **2012**, *8*, 1071-1090.

[102] J. J. Lange, J. M. Robertson, I. Woodward, X-Ray Crystal Analysis of Trans-Azobenzene, *Proc Math Phys Eng Sci.* **1939**, *171*, 398-410.

[103] A. Mostad, C. Rømming, A refinement of the crystal structure of cis-azobenzene, *Acta Chem. Scand* **1971**, *25*, 3561.

[104] G. C. Hampson, J. M. Robertson, 78. Bond lengths and resonance in the cis-azobenzene molecule, *J. Chem. Soc.* **1941**, 409.

[105] O. Sadovski, A. A. Beharry, F. Zhang, G. A. Woolley, Spectral Tuning of Azobenzene Photoswitches for Biological Applications, *Angew. Chem.* **2009**, *121*, 1512-1514.

[106] K. A. Bello, J. Griffiths, Azo dyes with absorption bands in the near infrared, *J. Chem. Soc., Chem. Commun.* **1986**, 1639.

[107] M. A. Salvador, P. Almeida, L. V. Reis, P. F. Santos, Near-infrared absorbing delocalized cationic azo dyes, *Dyes Pigment.* **2009**, *82*, 118-123.

[108] Y. Li, B. O. Patrick, D. Dolphin, Near-Infrared absorbing azo dyes: synthesis and x-ray crystallographic and spectral characterization of monoazopyrroles, bisazopyrroles, and a boron-azopyrrole complex, *J. Org. Chem.* **2009**, *74*, 5237-5243.

[109] J. L. Magee, W. Shand, H. Eyring, Non-adiabatic Reactions. Rotation about the Double Bond *, *J. Am. Chem. Soc.* **1941**, *63*, 677–688.

[110] D. Y. Curtin, E. J. Grubbs, C. G. McCarty, Uncatalyzed syn-anti Isomerization of Imines, Oxime Ethers, and Haloimines 1, *J. Am. Chem. Soc.* **1966**, *88*, 2775–2786.

[111] C. R. Crecca, A. E. Roitberg, Theoretical study of the isomerization mechanism of azobenzene and disubstituted azobenzene derivatives, *J. Phys. Chem. A* **2006**, *110*, 8188–8203.

[112] H. Rau, E. Lueddecke, On the rotation-inversion controversy on photoisomerization of azobenzenes. Experimental proof of inversion, *J. Am. Chem. Soc.* **1982**, *104*, 1616–1620.

[113] H. M. D. Bandara, S. C. Burdette, Photoisomerization in different classes of azobenzene, *Chem. Soc. Rev.* **2012**, *41*, 1809–1825.

[114] J. Garcia-Amoros, M. Diaz-Lobo, S. Nonell, D. Velasco, Fastest thermal isomerization of an azobenzene for nanosecond photoswitching applications under physiological conditions, *Angew. Chem. Int. Ed. Engl.* **2012**, *51*, 12820-12823.

[115] T. J. White, N. V. Tabiryan, S. V. Serak, U. A. Hrozhyk, V. P. Tondiglia, H. Koerner, R. A. Vaia, T. J. Bunning, A high frequency photodriven polymer oscillator, *Soft Matter* **2008**, *4*, 1796.

[116] J. García-Amorós, D. Velasco, Recent advances towards azobenzene-based light-driven real-time information-transmitting materials, *Beilstein J. Org. Chem.* **2012**, *8*, 1003-1017.

[117] E. Deniz, S. Ray, M. Tomasulo, S. Impellizzeri, S. Sortino, F. M. Raymo, Photoswitchable fluorescent dyads incorporating BODIPY and 1,3oxazine components, *J. Phys. Chem. A* **2010**, *114*, 11567–11575.

[118] J. Buback, M. Kullmann, F. Langhojer, P. Nuernberger, R. Schmidt, F. Würthner, T. Brixner, Ultrafast bidirectional photoswitching of a spiropyran, *J. Am. Chem. Soc.* **2010**, *132*, 16510–16519.

[119] H. Görner, Photochromism of nitrospiropyrans: effects of structure, solvent and temperature, *Phys. Chem. Chem. Phys.* **2001**, *3*, 416–423.

[120] S. Kobatake, S. Takami, H. Muto, T. Ishikawa, M. Irie, Rapid and reversible shape changes of molecular crystals on photoirradiation, *Nature* **2007**, *446*, 778–781.

[121] L. F. Kadem, K. G. Suana, M. Holz, W. Wang, H. Westerhaus, R. Herges, C. Selhuber-Unkel, High-Frequency Mechanostimulation of Cell Adhesion, *Angew. Chem. Int. Ed. Engl.* **2017**, *56*, 225–229.

[122] L. F. Kadem, K. G. Suana, M. Holz, W. Wang, H. Westerhaus, R. Herges, C. Selhuber-Unkel, High-Frequency Mechanostimulation of Cell Adhesion, *Angew. Chem.* **2017**, *129*, 231–235.

[123] C. L. van Oosten, C. W. M. Bastiaansen, D. J. Broer, Printed artificial cilia from liquid-crystal network actuators modularly driven by light, *Nat. Mater.* **2009**, *8*, 677–682.

[124] A. H. Gelebart, M. Mc Bride, A. P. H. J. Schenning, C. N. Bowman, D. J. Broer, Photoresponsive Fiber Array: Toward Mimicking the Collective Motion of Cilia for Transport Applications, *Adv. Funct. Mater.* **2016**, *26*, 5322-5327.

[125] J. Garcia-Amorós, M. Martínez, H. Finkelmann, D. Velasco, Photoactuation and thermal isomerisation mechanism of cyanoazobenzene-based liquid crystal elastomers, *Phys. Chem. Chem. Phys.* **2014**, *16*, 8448–8454.

[126] Y. Yu, T. Ikeda, Photodeformable Polymers: A New Kind of Promising Smart Material for Micro- and Nano-Applications, *Macromol. Chem. Phys.* **2005**, *206*, 1705–1708.

[127] T. Mirfakhrai, J. D. W. Madden, R. H. Baughman, Polymer artificial muscles, *Mater. Today* **2007**, *10*, 30–38.

[128] N. Li, J. Lu, H. Li, E.-T. Kang, Nonlinear optical properties and memory effects of the azo polymers carrying different substituents, *Dyes Pigment.* **2011**, *88*, 18-24.

[129] Z. Li, M. Wang, H. Li, J. He, N. Li, Q. Xu, J. Lu, Rewritable ternary data storage devices based on polymethacrylate containing pendent azobenzene–naphthalene with the combined effects of conformation change and charge traps, *J. Mater. Chem. C* **2017**, *5*, 8593-8598.

[130] R. Hagen, T. Bieringer, Photoaddressable Polymers for Optical Data Storage, *Adv. Mater.* **2001**, *13*, 1805-1810.

[131] Y. Li, T. Su, S. Li, Y. Lai, B. He, Z. Gu, Polymeric micelles with π–π conjugated moiety on glycerol dendrimer as lipophilic segments for anticancer drug delivery, *Biomater. Sci.* **2014**, *2*, 775-783.

[132] D. He, H. Zhuang, H. Liu, H. Liu, H. Li, J. Lu, Adjustment of conformation change and charge trapping in ion-doped polymers to achieve ternary memory performance, *J. Mater. Chem. C* **2013**, *1*, 7883.

[133] A. Mourot, T. Fehrentz, Y. Le Feuvre, C. M. Smith, C. Herold, D. Dalkara, F. Nagy, D. Trauner, R. H. Kramer, Rapid optical control of nociception with an ion-channel photoswitch, *Nat. Methods* **2012**, *9*, 396-402.

[134] J. A. Frank, M. Moroni, R. Moshourab, M. Sumser, G. R. Lewin, D. Trauner, Photoswitchable fatty acids enable optical control of TRPV1, *Nat. Commun.* **2015**, *6*, 7118.

[135] P. Gorostiza, M. Volgraf, R. Numano, S. Szobota, D. Trauner, E. Y. Isacoff, Mechanisms of photoswitch conjugation and light activation of an ionotropic glutamate receptor, *Proc. Natl. Acad. Sci. USA* **2007**, *104*, 10865-10870.

[136] A. A. Beharry, G. A. Woolley, Azobenzene photoswitches for biomolecules, *Chem. Soc. Rev.* **2011**, *40*, 4422–4437.

[137] D. G. Whitten, P. D. Wildes, J. G. Pacifici, G. Irick, Solvent and substituent on the thermal isomerization of substituted azobenzenes. Flash spectroscopic study, *J. Am. Chem. Soc.* **1971**, *93*, 2004-2008.

[138] T. Asano, T. Yano, T. Okada, Mechanistic study of thermal Z-E isomerization of azobenzenes by high-pressure kinetics, *J. Am. Chem. Soc.* **1982**, *104*, 4900–4904.

[139] T. Asano, T. Okada, Thermal Z-E isomerization of azobenzenes. The pressure, solvent, and substituent effects, *J. Org. Chem.* **1984**, *49*, 4387–4391.

[140] T. Asano, T. Okada, Further kinetic evidence for the competitive rotational and inversional Z-E isomerization of substituted azobenzenes, *J. Org. Chem.* **1986**, *51*, 4454–4458.

[141] C.-W. Chang, Y.-C. Lu, T.-T. Wang, E. W.-G. Diau, Photoisomerization dynamics of azobenzene in solution with S1 excitation: a femtosecond fluorescence anisotropy study, *J. Am. Chem. Soc.* **2004**, *126*, 10109–10118.

[142] B. Marcandalli, L. P.-D. Liddo, C. Di Fede, I. R. Bellobono, Solvent and substituent effects on thermal cis–trans-isomerization of some 4-diethylaminoazobenzenes, *J. Chem. Soc., Perkin Trans. 2* **1984**, 589–593.

[143] C.-H. Ho, K.-N. Yang, S.-N. Lee, Mechanistic study of trans?cis isomerization of the substituted azobenzene moiety bound on a liquid-crystalline polymer, *J. Polym. Sci., Part A: Polym. Chem.* **2001**, *39*, 2296–2307.

[144] D. M. Shin, D. G. Whitten, Solvent-induced mechanism change in charge-transfer molecules. Inversion versus rotation paths for the Z .fwdarw. E isomerization of donor-acceptor substituted azobenzenes, *J. Am. Chem. Soc.* **1988**, *110*, 5206–5208.

[145] S. Smith, F. B. Abdallah, The Kinetics of the Cis-to-Trans Thermal Isomerization of 4-Anilino-4'- Nitroazobenzene are Highly Influenced by Solvent Polarity, *J. Therm. Catal.* **2017**, *08*.

[146] J. Garcia-Amorós, W. A. Massad, S. Nonell, D. Velasco, Fast isomerizing methyl iodide azopyridinium salts for molecular switches, *Org. Lett.* **2010**, *12*, 3514-3517.

[147] J. Garcia-Amorós, M. C. R. Castro, P. Coelho, M. M. M. Raposo, D. Velasco, Fastest non-ionic azo dyes and transfer of their thermal isomerisation kinetics into liquid-crystalline materials, *Chem. Commun.* **2016**, *52*, 5132–5135.

[148] J. Garcia-Amorós, M. Reig, A. Cuadrado, M. Ortega, S. Nonell, D. Velasco, A photoswitchable bis-azo derivative with a high temporal resolution, *Chem. Commun.* **2014**, *50*, 11462–11464.

[149] A. A. Beharry, O. Sadovski, G. A. Woolley, Azobenzene photoswitching without ultraviolet light, *J. Am. Chem. Soc.* **2011**, *133*, 19684-19687.

[150] D. Bléger, J. Schwarz, A. M. Brouwer, S. Hecht, o-Fluoroazobenzenes as readily synthesized photoswitches offering nearly quantitative two-way isomerization with visible light, *J. Am. Chem. Soc.* **2012**, *134*, 20597-20600.

[151] S. Samanta, A. Babalhavaeji, M.-x. Dong, G. A. Woolley, Photoswitching of ortho-substituted azonium ions by red light in whole blood, *Angew. Chem. Int. Ed. Engl.* **2013**, *52*, 14127-14130.

[152] M. Dong, A. Babalhavaeji, S. Samanta, A. A. Beharry, G. A. Woolley, Red-Shifting Azobenzene Photoswitches for in Vivo Use, *Acc. Chem. Res.* **2015**, *48*, 2662-2670.

[153] R. H. Bisby, C. Mead, C. G. Morgan, Wavelength-programmed solute release from photosensitive liposomes, *Biochem. Biophys. Res. Commun.* **2000**, *276*, 169-173.

[154] R. H. Bisby, C. Mead, A. C. Mitchell, C. G. Morgan, Fast laser-induced solute release from liposomes sensitized with photochromic lipid: effects of temperature, lipid host, and sensitizer concentration, *Biochem. Biophys. Res. Commun.* **1999**, *262*, 406-410.

[155] R. H. Bisby, C. Mead, C. G. Morgan, Photosensitive liposomes as 'cages' for laser-triggered solute delivery: the effect of bilayer cholesterol on kinetics of solute release, *FEBS Lett.* **1999**, *463*, 165-168.

[156] Y. Lei, J. K. Hurst, Photoregulated Potassium Ion Permeation through Dihexadecyl Phosphate Bilayers Containing Azobenzene and Stilbene Surfactants, *Langmuir* **1999**, *15*, 3424-3429.

[157] X.-M. Liu, B. Yang, Y.-L. Wang, J.-Y. Wang, New Nanoscale Pulsatile Drug Delivery System, *Chem. Mater.* **2005**, *17*, 2792-2795.

[158] C. G. Morgan, E. W. Thomas, S. S. Sandhu, Y. P. Yianni, A. C. Mitchell, Light-induced fusion of liposomes with release of trapped marker dye is sensitised by photochromic phospholipid, *Biochim. Biophys. Acta, Rev. Biomembr.* **1987**, *903*, 504-509.

[159] C. G. Morgan, R. H. Bisby, S. A. Johnson, A. C. Mitchell, Fast solute release from photosensitive liposomes: an alternative to 'caged' reagents for use in biological systems, *FEBS Lett.* **1995**, *375*, 113-116.

[160] C. G. Morgan, E. W. Thomas, Y. P. Yianni, S. S. Sandhu, Incorporation of a novel photochromic phospholipid molecule into vesicles of dipalmitoylphosphatidylcholine, *Biochim. Biophys. Acta, Rev. Biomembr.* **1985**, *820*, 107-114.

[161] T. Sato, M. Kijima, Y. Shiga, Y. Yonezawa, Photochemically controlled ion permeability of liposomal membranes containing amphiphilic azobenzene, *Langmuir* **1991**, *7*, 2330-2335.

[162] R. H. Bisby, C. Mead, C. G. Morgan, Active Uptake of Drugs into Photosensitive Liposomes and Rapid Release on UV Photolysis¶, *Photochem. Photobiol.* **2000**, *72*, 57.

[163] C. Pernpeintner, J. A. Frank, P. Urban, C. R. Roeske, S. D. Pritzl, D. Trauner, T. Lohmüller, Light-Controlled Membrane Mechanics and Shape Transitions of Photoswitchable Lipid Vesicles, *Langmuir* **2017**, *33*, 4083-4089.

[164] S. Geng, Y. Wang, L. Wang, T. Kouyama, T. Gotoh, S. Wada, J.-Y. Wang, A Light-Responsive Self-Assembly Formed by a Cationic Azobenzene Derivative and SDS as a Drug Delivery System, *Sci. Rep.* **2017**, *7*, 39202.

[165] A. Engel, D. J. Müller, Observing single biomolecules at work with the atomic force microscope, *Nat. Struct. Mol. Biol.* **2000**, *7*, 715-718.

[166] A. Berquand, M. P. Mingeot-Leclercq, Y. F. Dufrêne, Real-time imaging of drug-membrane interactions by atomic force microscopy, *Biochim. Biophys. Acta* **2004**, *1664*, 198-205.

[167] C. Demetzos, Differential Scanning Calorimetry (DSC): A Tool to Study the Thermal Behavior of Lipid Bilayers and Liposomal Stability, *Journal of Liposome Research* **2008**, *18*, 159-173.

[168] V. Holy, J. Kuběna, I. Ohlidal, K. Lischka, W. Plotz, X-ray reflection from rough layered systems, *Phys. Rev. B* **1993**, *47*, 15896-15903.

[169] E. Chason, T. M. Mayer, Thin film and surface characterization by specular X-ray reflectivity, *Crit. Rev. Solid State Mater. Sci.* **1997**, *22*, 1-67.

[170] J. Daillant, K. Quinn, C. Gourier, F. Rieutord, Grazing incidence surface scattering of X-rays, *J. Chem. Soc., Faraday Trans.* **1996**, *92*, 505-513.

[171] L. Névot, P. Croce, Caractérisation des surfaces par réflexion rasante de rayons X. Application à l'étude du polissage de quelques verres silicates, *Rev. Phys. Appl. (Paris)* **1980**, *15*, 761-779.

[172] Y. Fujii, Recent Developments in the X-ray Reflectivity Analysis, *AJPA* **2016**, *4*, 27-49.

[173] O. H. Seeck, B. M. Murphy, *X-Ray Diffraction: Modern Experimental Techniques*, Taylor & Francis Group, **2014**.

[174] F. Reise, J. E. Warias, K. Chatterjee, N. R. Krekiehn, O. Magnussen, B. M. Murphy, T. K. Lindhorst, Photoswitchable Glycolipid Mimetics: Synthesis and Photochromic Properties of Glycoazobenzene Amphiphiles, *Chem. Eur. J.* **2018**, doi:10.1002/chem.201803112.

[175] P.-H. Amvam-Zollo, P. Sinaÿ, Streptococcus pneumoniae type XIV polysaccharide: synthesis of a repeating branched tetrasaccharide with dioxa-type spacer-arms, *Carbohydr. Res.* **1986**, *150*, 199-212.

[176] S. Zhang, R.-O. Moussodia, H.-J. Sun, P. Leowanawat, A. Muncan, C. D. Nusbaum, K. M. Chelling, P. A. Heiney, M. L. Klein, S. André, R. Roy, H.-J. Gabius, V. Percec, Mimicking biological membranes with programmable glycan ligands self-assembled from amphiphilic Janus glycodendrimers, *Angew. Chem. Int. Ed. Engl.* **2014**, *53*, 10899-10903.

[177] S. Cecioni, V. Oerthel, J. Iehl, M. Holler, D. Goyard, J.-P. Praly, A. Imberty, J.-F. Nierengarten, S. Vidal, Synthesis of dodecavalent fullerene-based glycoclusters and evaluation of their binding properties towards a bacterial lectin, *Chemistry* **2011**, *17*, 3252-3261.

[178] L. Ballell, K. J. Alink, M. Slijper, C. Versluis, R. M. J. Liskamp, R. J. Pieters, A new chemical probe for proteomics of carbohydrate-binding proteins, *Chembiochem : a European journal of chemical biology* **2005**, *6*, 291-295.

[179] G. Zemplén, E. Pacsu, Über die Verseifung acetylierter Zucker und verwandter Substanzen, *Ber. Dtsch. Chem. Ges. (A and B)* **1929**, *62*, 1613-1614.

[180] V. Chandrasekaran, T. K. Lindhorst, Sweet switches: azobenzene glycoconjugates synthesized by click chemistry, *Chem. Commun.* **2012**, *48*, 7519-7521.

[181] H. R. Pfaendler, F. K. Maier, S. Klar, W. Göggelmann, Racemic and enantiomericall-trans-fecapentaene-12 and -14, *Liebigs Ann. Chem.* **1988**, *1988*, 449-454.

[182] B. Neises, W. Steglich, Einfaches Verfahren zur Veresterung von Carbonsäuren, *Angew. Chem.* **1978**, *90*, 556-557.

[183] M. J. Clemente, J. Fitremann, M. Mauzac, J. L. Serrano, L. Oriol, Synthesis and characterization of maltose-based amphiphiles as supramolecular hydrogelators, *Langmuir* **2011**, *27*, 15236-15247.

[184] L. Latxague, S. Ziane, O. Chassande, A. Patwa, M.-J. Dalila, P. Barthélémy, Glycosylated nucleoside lipid promotes the liposome internalization in stem cells, *Chem. Commun.* **2011**, *47*, 12598-12600.

[185] MacroModel, Version 10.4, from Maestro release 2015-4, Schrödinger, LLC, New York, NY, 2015.

[186] Maestro, Version 10.4, Schrödinger, LLC, New York, NY, 2015

[187] N. R. Krekiehn, M. Müller, U. Jung, S. Ulrich, R. Herges, O. M. Magnussen, UV/Vis Spectroscopy Studies of the Photoisomerization Kinetics in Self-Assembled Azobenzene-Containing Adlayers, *Langmuir* **2015**, *31*, 8362-8370.

[188] X. Song, J. Li, S. Zhang, Supramolecular liquid crystals induced by intermolecular hydrogen bonding between benzoic acid and 4-(alkoxyphenylazo) pyridines, *Liq. Cryst.* **2003**, *30*, 331-335.

[189] A. El-Hawiet, E. N. Kitova, J. S. Klassen, Quantifying Carbohydrate–Protein Interactions by Electrospray Ionization Mass Spectrometry Analysis, *Biochemistry* **2012**, *51*, 4244-4253.

[190] S. J. North, P. G. Hitchen, S. M. Haslam, A. Dell, Mass spectrometry in the analysis of N-linked and O-linked glycans, *Curr. Opin. Struc.t Biol.* **2009**, *19*, 498-506.

[191] Y. Yao, K. Shams-Ud-Doha, R. Daneshfar, E. N. Kitova, J. S. Klassen, Quantifying Protein-Carbohydrate Interactions Using Liquid Sample Desorption Electrospray Ionization Mass Spectrometry, *J. Am. Soc. Mass. Spectrom.* **2015**, *26*, 98-106.

[192] F.-A. Maria del Carmen, D. Dolores, B. Manuel Alvaro, M. Filipa, C. Javier, J.-B. Jesus, Protein-Carbohydrate Interactions Studied by NMR: From Molecular Recognition to Drug Design, *Curr. Protein Pept. Sci.* **2012**, *13*, 816-830.

[193] L. P. Calle, B. Echeverria, A. Franconetti, S. Serna, M. C. Fernández-Alonso, T. Diercks, F. J. Cañada, A. Ardá, N.-C. Reichardt, J. Jiménez-Barbero, Monitoring Glycan–Protein Interactions by NMR Spectroscopic Analysis: A Simple Chemical Tag That Mimics Natural CH–π Interactions, *Chem. Eur. J.* **2015**, *21*, 11408-11416.

[194] T. K. Dam, C. F. Brewer, Thermodynamic Studies of Lectin−Carbohydrate Interactions by Isothermal Titration Calorimetry, *Chem. Rev.* **2002**, *102*, 387-430.

[195] S. Leavitt, E. Freire, Direct measurement of protein binding energetics by isothermal titration calorimetry, *Curr. Opin. Struc.t Biol.* **2001**, *11*, 560-566.

[196] G. Safina, Application of surface plasmon resonance for the detection of carbohydrates, glycoconjugates, and measurement of the carbohydrate-specific interactions: A comparison with conventional analytical techniques. A critical review, *Anal. Chim. Acta* **2012**, *712*, 9-29.

[197] G. Safina, I. B. Duran, M. Alasel, B. Danielsson, Surface plasmon resonance for real-time study of lectin-carbohydrate interactions for the differentiation and identification of glycoproteins, *Talanta* **2011**, *84*, 1284-1290.

[198] C. Wang, V. K. Yadavalli, Investigating biomolecular recognition at the cell surface using atomic force microscopy, *Micron* **2014**, *60*, 5-17.

[199] C. Tse-Wen, Binding of cells to matrixes of distinct antibodies coated on solid surface, *J. Immunol. Methods* **1983**, *65*, 217-223.

[200] J. C. Love, L. A. Estroff, J. K. Kriebel, R. G. Nuzzo, G. M. Whitesides, Self-Assembled Monolayers of Thiolates on Metals as a Form of Nanotechnology, *Chem. Rev.* **2005**, *105*, 1103-1170.

[201] J. Su, M. Mrksich, Using MALDI-TOF Mass Spectrometry to Characterize Interfacial Reactions on Self-Assembled Monolayers, *Langmuir* **2003**, *19*, 4867-4870.

[202] S. Fukui, T. Feizi, C. Galustian, A. M. Lawson, W. G. Chai, Oligosaccharide microarrays for high-throughput detection and specificity assignments of carbohydrate-protein interactions, *Nat. Biotechnol.* **2002**, *20*, 1011-1017.

[203] T. Feizi, F. Fazio, W. C. Chai, C. H. Wong, Carbohydrate microarrays - a new set of technologies at the frontiers of glycomics, *Curr. Opin. Struc.t Biol.* **2003**, *13*, 637-645.

[204] Y. Liu, S. Palma Angelina, T. Feizi, Carbohydrate microarrays: key developments in glycobiology, *Biol. Chem.* **2009**, *390*, 647.

[205] T. Puvirajesinghe, J. Turnbull, Glycoarray Technologies: Deciphering Interactions from Proteins to Live Cell Responses, *Microarrays* **2016**, *5*, 3.

[206] N. Laurent, J. Voglmeier, S. L. Flitsch, ChemInform Abstract: Glycoarrays — Tools for Determining Protein—Carbohydrate Interactions and Glycoenzyme Specificity, *ChemInform* **2009**, *40*.

[207] K. R. Love, P. H. Seeberger, Carbohydrate Arrays as Tools for Glycomics, *Angew. Chem. Int. Ed.* **2002**, *41*, 3583-3586.

[208] S. Park, J. C. Gildersleeve, O. Blixt, I. Shin, Carbohydrate microarrays, *Chem. Soc. Rev.* **2013**, *42*, 4310-4326.

[209] M. B. Biskup, J. U. Müller, R. Weingart, R. R. Schmidt, New Methods for the Generation of Carbohydrate Arrays on Glass Slides and Their Evaluation, *ChemBioChem* **2005**, *6*, 1007-1015.

[210] O. Blixt, S. Head, T. Mondala, C. Scanlan, M. E. Huflejt, R. Alvarez, M. C. Bryan, F. Fazio, D. Calarese, J. Stevens, N. Razi, D. J. Stevens, J. J. Skehel, I. van Die, D. R. Burton, I. A. Wilson, R. Cummings, N. Bovin, C.-H. Wong, J. C. Paulson, Printed covalent glycan array for ligand profiling of diverse glycan binding proteins, *Proc. Natl. Acad. Sci. USA* **2004**, *101*, 17033-17038.

[211] P.-H. Liang, S.-K. Wang, C.-H. Wong, Quantitative Analysis of Carbohydrate−Protein Interactions Using Glycan Microarrays: Determination of Surface and Solution Dissociation Constants, *J. Am. Chem. Soc.* **2007**, *129*, 11177-11184.

[212] J. L. de Paz, C. Noti, P. H. Seeberger, Microarrays of Synthetic Heparin Oligosaccharides, *J. Am. Chem. Soc.* **2006**, *128*, 2766-2767.

[213] C.-Y. Huang, D. A. Thayer, A. Y. Chang, M. D. Best, J. Hoffmann, S. Head, C.-H. Wong, Carbohydrate microarray for profiling the antibodies interacting with Globo H tumor antigen, *Proc. Natl. Acad. Sci. USA* **2006**, *103*, 15-20.

[214] M. D. Disney, P. H. Seeberger, The Use of Carbohydrate Microarrays to Study Carbohydrate-Cell Interactions and to Detect Pathogens, *Chem. Biol.*, *11*, 1701-1707.

[215] D. M. Ratner, E. W. Adams, J. Su, B. R. O'Keefe, M. Mrksich, P. H. Seeberger, Probing Protein–Carbohydrate Interactions with Microarrays of Synthetic Oligosaccharides, *ChemBioChem* **2004**, *5*, 379-383.

[216] M. A. Brun, M. D. Disney, P. H. Seeberger, Miniaturization of Microwave-Assisted Carbohydrate Functionalization to Create Oligosaccharide Microarrays, *ChemBioChem* **2006**, *7*, 421-424.

[217] B. T. Houseman, E. S. Gawalt, M. Mrksich, Maleimide-Functionalized Self-Assembled Monolayers for the Preparation of Peptide and Carbohydrate Biochips, *Langmuir* **2003**, *19*, 1522-1531.

[218] Y. Zhang, S. Luo, Y. Tang, L. Yu, K.-Y. Hou, J.-P. Cheng, X. Zeng, P. G. Wang, Carbohydrate−Protein Interactions by "Clicked" Carbohydrate Self-Assembled Monolayers, *Anal. Chem.* **2006**, *78*, 2001-2008.

[219] X.-L. Sun, C. L. Stabler, C. S. Cazalis, E. L. Chaikof, Carbohydrate and Protein Immobilization onto Solid Surfaces by Sequential Diels−Alder and Azide−Alkyne Cycloadditions, *Bioconjugate Chem.* **2006**, *17*, 52-57.

[220] M. C. Bryan, F. Fazio, H.-K. Lee, C.-Y. Huang, A. Chang, M. D. Best, D. A. Calarese, O. Blixt, J. C. Paulson, D. Burton, I. A. Wilson, C.-H. Wong, Covalent Display of Oligosaccharide Arrays in Microtiter Plates, *J. Am. Chem. Soc.* **2004**, *126*, 8640-8641.

[221] S. R. Hanson, W. A. Greenberg, C. H. Wong, Probing Glycans With the Copper(I)-Catalyzed [3+2] Azide–Alkyne Cycloaddition, *Mol. Inform.* **2007**, *26*, 1243-1252.

[222] B. T. Houseman, M. Mrksich, Carbohydrate Arrays for the Evaluation of Protein Binding and Enzymatic Modification, *Chem. Biol.* **2002**, *9*, 443-454.

[223] L.-H. Liu, M. Yan, Perfluorophenyl Azides: New Applications in Surface Functionalization and Nanomaterial Synthesis, *Acc. Chem. Res.* **2010**, *43*, 1434-1443.

[224] Y. Miura, T. Yamauchi, H. Sato, T. Fukuda, The self-assembled monolayer of saccharide via click chemistry: Formation and protein recognition, *Thin Solid Films* **2008**, *516*, 2443-2449.

[225] M. Kleinert, T. Winkler, A. Terfort, T. K. Lindhorst, A modular approach for the construction and modification of glyco-SAMs utilizing 1,3-dipolar cycloaddition, *Org. Biomol. Chem.* **2008**, *6*, 2118-2132.

[226] L. Ban, M. Mrksich, On-Chip Synthesis and Label-Free Assays of Oligosaccharide Arrays, *Angew. Chem.* **2008**, *120*, 3444-3447.

[227] M. Mrksich, Using self-assembled monolayers to model the extracellular matrix, *Acta Biomater.* **2009**, *5*, 832-841.

[228] P. M. Dietrich, T. Horlacher, P.-L. Girard-Lauriault, T. Gross, A. Lippitz, H. Min, T. Wirth, R. Castelli, P. Seeberger, W. E. S. Unger, Multimethod Chemical Characterization of Carbohydrate-Functionalized Surfaces, *J. Carbohydr. Chem.* **2011**, *30*, 361-372.

[229] P. M. Dietrich, T. Horlacher, P.-L. Girard-Lauriault, T. Gross, A. Lippitz, H. Min, T. Wirth, R. Castelli, P. H. Seeberger, W. E. S. Unger, Adlayers of Dimannoside Thiols on Gold: Surface Chemical Analysis, *Langmuir* **2011**, *27*, 4808-4815.

[230] T. Fyrner, H.-H. Lee, A. Mangone, T. Ekblad, M. E. Pettitt, M. E. Callow, J. A. Callow, S. L. Conlan, R. Mutton, A. S. Clare, P. Konradsson, B. Liedberg, T.

Ederth, Saccharide-Functionalized Alkanethiols for Fouling-Resistant Self-Assembled Monolayers: Synthesis, Monolayer Properties, and Antifouling Behavior, *Langmuir* **2011**, *27*, 15034-15047.

[231] C. Grabosch, M. Kind, Y. Gies, F. Schweighofer, A. Terfort, T. K. Lindhorst, A 'dual click' strategy for the fabrication of bioselective, glycosylated self-assembled monolayers as glycocalyx models, *Org. Biomol. Chem.* **2013**, *11*, 4006-4015.

[232] M. Hartmann, P. Betz, Y. Sun, S. N. Gorb, T. K. Lindhorst, A. Krueger, Saccharide-Modified Nanodiamond Conjugates for the Efficient Detection and Removal of Pathogenic Bacteria, *Chem. Eur. J.* **2012**, *18*, 6485-6492.

[233] C. Fessele, S. Wachtler, V. Chandrasekaran, C. Stiller, T. K. Lindhorst, A. Krueger, Thiourea-Bridged Nanodiamond Glycoconjugates as Inhibitors of Bacterial Adhesion, *Eur. J. Org. Chem.* **2015**, *2015*.

[234] X. L. Sun, W. Cui, C. Haller, E. L. Chaikof, Site-Specific Multivalent Carbohydrate Labeling of Quantum Dots and Magnetic Beads, *ChemBioChem* **2004**, *5*, 1593-1596.

[235] P. Babu, S. Sinha, A. Surolia, Sugar−Quantum Dot Conjugates for a Selective and Sensitive Detection of Lectins, *Bioconjugate Chem.* **2007**, *18*, 146-151.

[236] J. M. d. l. Fuente, A. G. Barrientos, T. C. Rojas, J. Rojo, J. Cañada, A. Fernández, S. Penadés, Gold Glyconanoparticles as Water-Soluble Polyvalent Models To Study Carbohydrate Interactions, *Angew. Chem. Int. Ed.* **2001**, *40*, 2257-2261.

[237] M. D. Disney, J. Zheng, T. M. Swager, P. H. Seeberger, Detection of Bacteria with Carbohydrate-Functionalized Fluorescent Polymers, *J. Am. Chem. Soc.* **2004**, *126*, 13343-13346.

[238] P. D. Rye, Sweet and Sticky: Carbohydrate-Coated Magnetic Beads, *Biotechnol. J.* **1996**, *14*, 155.

[239] M. Hartmann, A. K. Horst, P. Klemm, T. K. Lindhorst, A kit for the investigation of live Escherichia coli cell adhesion to glycosylated surfaces, *Chem. Commun.* **2010**, *46*, 330-332.

[240] C. Fessele, T. Lindhorst, Effect of Aminophenyl and Aminothiahexyl α-D-Glycosides of the Manno-, Gluco-, and Galacto-Series on Type 1 Fimbriae-Mediated Adhesion of Escherichia coli, *Biology* **2013**, *2*, 1135.

[241] C. Grabosch, M. Hartmann, J. Schmidt-Lassen, T. K. Lindhorst, Squaric Acid Monoamide Mannosides as Ligands for the Bacterial Lectin FimH: Covalent Inhibition or Not?, *ChemBioChem* **2011**, *12*, 1066-1074.

[242] M. E. Terlizzi, G. Gribaudo, M. E. Maffei, UroPathogenic Escherichia coli (UPEC) Infections: Virulence Factors, Bladder Responses, Antibiotic, and Non-antibiotic Antimicrobial Strategies, *Front. Cell Infect. Mi.* **2017**, *8*, 1566.

[243] M. A. Bartlett, M. Yan, Fabrication of Polymer Thin Films and Arrays with Spatial and Topographical Controls, *Adv. Mater.* **2001**, *13*, 1449-1451.

[244] M. Yan, J. Ren, Covalent Immobilization of Ultrathin Polymer Films by Thermal Activation of Perfluorophenyl Azide, *Chem. Mater.* **2004**, *16*, 1627-1632.

[245] L. Liu, M. H. Engelhard, M. Yan, Surface and Interface Control on Photochemically Initiated Immobilization, *J. Am. Chem. Soc.* **2006**, *128*, 14067-14072.

[246] M. Yan, Photochemically Initiated Single Polymer Immobilization, *Chemistry* **2007**, *13*, 4138-4144.

[247] J. P. Gann, M. Yan, A Versatile Method for Grafting Polymers on Nanoparticles, *Langmuir* **2008**, *24*, 5319-5323.

[248] S. A. Al-Bataineh, R. Luginbuehl, M. Textor, M. Yan, Covalent Immobilization of Antibacterial Furanones via Photochemical Activation of Perfluorophenylazide, *Langmuir* **2009**, *25*, 7432-7437.

[249] L.-H. Liu, M. Yan, Simple Method for the Covalent Immobilization of Graphene, *Nano Lett.* **2009**, *9*, 3375-3378.

[250] H. Wang, L. Li, Q. Tong, M. Yan, Evaluation of Photochemically Immobilized Poly(2-ethyl-2-oxazoline) Thin Films as Protein-Resistant Surfaces, *ACS Appl. Mater. Interfaces* **2011**, *3*, 3463-3471.

[251] T. Kubo, X. Wang, Q. Tong, M. Yan, Polymer-Based Photocoupling Agent for the Efficient Immobilization of Nanomaterials and Small Molecules, *Langmuir* **2011**, *27*, 9372-9378.

[252] G. Zorn, D. G. Castner, A. Tyagi, X. Wang, H. Wang, M. Yan, Analysis of the surface density and reactivity of perfluorophenylazide and the impact on ligand immobilization, *J. Vac. Sci. Technol.* **2015**, *33*, 021407.

[253] M. Sundhoro, J. Park, K. W. Jayawardana, X. Chen, H. S. N. Jayawardena, M. Yan, Poly(HEMA-co-HEMA-PFPA): Synthesis and preparation of stable

micelles encapsulating imaging nanoparticles, *J. Colloid Interface Sci.* **2017**, *500*, 1-8.

[254] G. T. Carroll, D. Wang, N. J. Turro, J. T. Koberstein, Photochemical Micropatterning of Carbohydrates on a Surface, *Langmuir* **2006**, *22*, 2899-2905.

[255] G. T. Carroll, D. Wang, N. J. Turro, J. T. Koberstein, Photons to illuminate the universe of sugar diversity through bioarrays, *Glycoconjugate J.* **2007**, *25*, 5.

[256] Z. Pei, H. Yu, M. Theurer, A. Waldén, P. Nilsson, M. Yan, O. Ramström, Photogenerated Carbohydrate Microarrays, *ChemBioChem* **2007**, *8*, 166-168.

[257] O. Norberg, L. Deng, M. Yan, O. Ramström, Photo-Click Immobilization of Carbohydrates on Polymeric Surfaces - A Quick Method to Functionalize Surfaces for Biomolecular Recognition Studies, *Bioconjugate Chem.* **2009**, *20*, 2364-2370.

[258] A. Tyagi, X. Wang, L. Deng, O. Ramström, M. Yan, Photogenerated Carbohydrate Microarrays to Study Carbohydrate-Protein Interactions using Surface Plasmon Resonance Imaging, *Biosens. Bioelectron,* **2010**, *26*, 344-350.

[259] O. Norberg, L. Deng, T. Aastrup, M. Yan, O. Ramström, Photo-Click Immobilization on Quartz Crystal Microbalance Sensors for Selective Carbohydrate-Protein Interaction Analyses, *Anal. Chem.* **2011**, *83*, 1000-1007.

[260] L. Deng, O. Norberg, S. Uppalapati, M. Yan, O. Ramström, Stereoselective synthesis of light-activatable perfluorophenylazide-conjugated carbohydrates for glycoarray fabrication and evaluation of structural effects on protein binding by SPR imaging, *Org. Biomol. Chem.* **2011**, *9*, 3188-3198.

[261] M. Sundhoro, H. Wang, S. T. Boiko, X. Chen, H. S. N. Jayawardena, J. Park, M. Yan, Fabrication of carbohydrate microarrays on a poly(2-hydroxyethyl methacrylate)-based photoactive substrate, *Org. Biomol. Chem.* **2016**, *14*, 1124-1130.

[262] N. Maalouli, A. Barras, A. Siriwardena, M. Bouazaoui, R. Boukherroub, S. Szunerits, Comparison of photo- and Cu(i)-catalyzed "click" chemistries for the formation of carbohydrate SPR interfaces, *Analyst* **2013**, *138*, 805-812.

[263] Y. Lu, S. Song, C. Hou, S. Pang, X. Li, X. Wu, C. Shao, Y. Pei, Z. Pei, Facile fabrication of branched-chain carbohydrate chips for studying carbohydrate-protein interactions by QCM biosensor, *Chin. Chem. Lett.* **2018**, *29*, 65-68.

[264] L.-H. Liu, H. Dietsch, P. Schurtenberger, M. Yan, Photoinitiated Coupling of Unmodified Monosaccharides to Iron Oxide Nanoparticles for Sensing Proteins and Bacteria, *Bioconjugate Chem.* **2009**, *20*, 1349-1355.

[265] X. Wang, O. Ramstrom, M. Yan, A photochemically initiated chemistry for coupling underivatized carbohydrates to gold nanoparticles, *J. Mater. Chem.* **2009**, *19*, 8944-8949.

[266] P. M. Sivakumar, N. Moritsugu, S. Obuse, T. Isoshima, H. Tashiro, Y. Ito, Novel Microarrays for Simultaneous Serodiagnosis of Multiple Antiviral Antibodies, *PLoS ONE* **2013**, *8*, e81726.

[267] M. Mammen, S. K. Choi, G. M. Whitesides, Polyvalent Interactions in Biological Systems: Implications for Design and Use of Multivalent Ligands and Inhibitors, *Angew. Chem. Int. Ed.* **1998**, *37*, 2754-2794.

[268] L. L. Kiessling, J. E. Gestwicki, L. E. Strong, Synthetic Multivalent Ligands as Probes of Signal Transduction, *Angew. Chem. Int. Ed. Engl.* **2006**, *45*, 2348-2368.

[269] C. Fasting, C. A. Schalley, M. Weber, O. Seitz, S. Hecht, B. Koksch, J. Dernedde, C. Graf, E. W. Knapp, R. Haag, Multivalency as a Chemical Organization and Action Principle, *Angew. Chem. Int. Ed.* **2012**, *51*, 10472-10498.

[270] J. W. Wehner, M. Hartmann, T. K. Lindhorst, Are multivalent cluster glycosides a means of controlling ligand density of glycoarrays?, *Carbohydr. Res.* **2013**, *371*, 22-31.

[271] J. F. W. Keana, S. X. Cai, ChemInform Abstract: New Reagents for Photoaffinity Labeling: Synthesis and Photolysis of Functionalized Perfluorophenyl Azides, *ChemInform* **1990**, *21*, 3640–3647.

[272] A. Welle, F. Billard, J. Marchand-Brynaert, Tri- and Tetravalent Photoactivable Cross-Linking Agents, *Synthesis* **2012**, *44*, 2249-2254.

[273] L. Möller, C. Hess, J. Paleček, Y. Su, A. Haverich, A. Kirschning, G. Dräger, Towards a biocompatible artificial lung: Covalent functionalization of poly(4-methylpent-1-ene) (TPX) with cRGD pentapeptide, *Beilstein J. Org. Chem.* **2013**, *9*, 270-277.

[274] A. P. Krapcho, C. S. Kuell, Mono-Protected Diamines. N-tert-Butoxycarbonyl-α,ω-Alkanediamines from α,ω-Alkanediamines, *Synth. Commun.* **1990**, *20*, 2559-2564.

[275] K. Prime, G. Whitesides, Self-assembled organic monolayers: model systems for studying adsorption of proteins at surfaces, *Science* **1991**, *252*, 1164-1167.

[276] J. Schmidt-Lassen, T. K. Lindhorst, Exploring the meaning of sugar configuration in a supramolecular environment: comparison of six octyl glycoside micelles by ITC and NMR spectroscopy, *MedChemComm* **2014**, *5*, 1218-1226.

[277] D. S. K. Tsui, P. A. J. Gorin, Methods for the preparation of alkyl 1,2-orthoacetates of d-glucopyranose and d-galactopyranose in high yield, *Carbohydr. Res.* **1985**, *144*, 137-147.

[278] S. Matsumura, K. Imai, S. Yoshikawa, K. Kawada, T. Uchibor, Surface activities, biodegradability and antimicrobial properties of n-alkyl glucosides, mannosides and galactosides, *J. Am. Oil Chem. Soc.* **1990**, *67*, 996-1001.

[279] Y. M. Chabre, C. Contino-Pépin, V. Placide, T. C. Shiao, R. Roy, Expeditive Synthesis of Glycodendrimer Scaffolds Based on Versatile TRIS and Mannoside Derivatives, *J. Org. Chem.* **2008**, *73*, 5602-5605.

[280] Y. M. Chabre, P. P. Brisebois, L. Abbassi, S. C. Kerr, J. V. Fahy, I. Marcotte, R. Roy, Hexaphenylbenzene as a Rigid Template for the Straightforward Syntheses of "Star-Shaped" Glycodendrimers, *J. Org. Chem.* **2011**, *76*, 724-727.

[281] E. Benoist, A. Loussouarn, P. Remaud, J.-F. Chatal, J.-F. Gestin, Convenient and Simplified Approaches to N-Monoprotected Triaminopropane Derivatives: Key Intermediates for Bifunctional Chelating Agent Synthesis, *Synthesis* **1998**, *1998*, 1113-1118.

[282] R. Adamo, Q.-Y. Hu, A. Torosantucci, S. Crotti, G. Brogioni, M. Allan, P. Chiani, C. Bromuro, D. Quinn, M. Tontini, F. Berti, Deciphering the structure-immunogenicity relationship of anti-Candida glycoconjugate vaccines, *Chem. Sci.* **2014**, *5*, 4302-4311.

[283] T. K. Lindhorst, S. Kotter, U. Krallmann-Wenzel, S. Ehlers, Trivalent [small alpha]-D-mannoside clusters as inhibitors of type-1 fimbriae-mediated adhesion of Escherichia coli: structural variation and biotinylation, *J. Chem. Soc., Perkin Trans. 1* **2001**, 823-831.

[284] R. Das, B. Mukhopadhyay, Use of 'click chemistry' for the synthesis of carbohydrate-porphyrin dendrimers and their multivalent approach toward lectin sensing, *Tetrahedron Lett.* **2016**, *57*, 1775-1781.

[285] S. N. Georgiades, J. Clardy, Synthetic libraries of tyrosine-derived bacterial metabolites, *Bioorg. Med. Chem. Lett.* **2008**, *18*, 3117-3121.

[286] A. Paquet, Further studies on the use of the thallium salt of N-hydroxysuccinimide for the preparation of succinimidyl esters, *Can. J. Chem.* **1979**, *57*, 2775-2778.

[287] M. Farrugia, N. Trotter, S. Vijayasarathy, A. A. Salim, Z. G. Khalil, E. Lacey, R. J. Capon, Isolation and synthesis of N-acyladenine and adenosine alkaloids from a southern Australian marine sponge, Phoriospongia sp, *Tetrahedron Lett.* **2014**, *55*, 5902-5904.

[288] T. D. Davis, C. J. Gerry, D. S. Tan, General Platform for Systematic Quantitative Evaluation of Small-Molecule Permeability in Bacteria, *ACS Chem. Biol.* **2014**, *9*, 2535-2544.

[289] J. Danklmaier, H. Hünig, Synthesis of acyclic analogs of N-acetylmuramyl-L-alanyl-D-isoglutamine (MDP), *Liebigs Ann. Chem.* **1990**, *1990*, 145-150.

[290] J. Salta, J. Dernedde, H.-U. Reissig, Synthesis of multivalent carbohydrate mimetics with aminopolyol end groups and their evaluation as L-selectin inhibitors, *Beilstein J. Org. Chem.* **2015**, *11*, 638-646.

[291] T. K. Lindhorst, C. Kieburg, Saccharid-Ummantelung oligovalenter Amine: Synthese Thioharnstoff-verbrückter Cluster-Glycoside aus Glycosylisothiocyanaten, *Angew. Chem.* **1996**, *108*, 2083-2086.

[292] Z. Zhou, X. Wu, A. Kresak, M. Griswold, Z.-R. Lu, Peptide targeted tripod macrocyclic Gd(III) chelates for cancer molecular MRI, *Biomaterials* **2013**, *34*, 7683-7693.

[293] S. Venkataraman, N. Veronica, Z. X. Voo, J. L. Hedrick, Y. Y. Yang, 2-Amino-1,3-propane diols: a versatile platform for the synthesis of aliphatic cyclic carbonate monomers, *Polym. Chem.* **2013**, *4*, 2945-2948.

[294] E. M. Sletten, C. R. Bertozzi, From Mechanism to Mouse: A Tale of Two Bioorthogonal Reactions, *Acc. Chem. Res.* **2011**, *44*, 666-676.

[295] E. Saxon, C. R. Bertozzi, Cell Surface Engineering by a Modified Staudinger Reaction, *Science* **2000**, *287*, 2007-2010.

[296] E. M. Sletten, C. R. Bertozzi, Bioorthogonale Chemie – oder: in einem Meer aus Funktionalität nach Selektivität fischen, *Angew. Chem.* **2009**, *121*, 7108-7133.

[297] E. M. Sletten, C. R. Bertozzi, Bioorthogonal Chemistry: Fishing for Selectivity in a Sea of Functionality, *Angew. Chem. Int. Ed.* **2009**, *48*, 6974-6998.

[298] H. Staudinger, J. Meyer, Über neue organische Phosphorverbindungen III. Phosphinmethylenderivate und Phosphinimine, *Helv. Chim. Acta* **1919**, *2*, 635-646.

[299] V. V. Rostovtsev, L. G. Green, V. V. Fokin, K. B. Sharpless, A Stepwise Huisgen Cycloaddition Process: Copper(I)-Catalyzed Regioselective "Ligation" of Azides and Terminal Alkynes, *Angew. Chem. Int. Ed.* **2002**, *41*, 2596-2599.

[300] C. W. Tornøe, C. Christensen, M. Meldal, Peptidotriazoles on Solid Phase: [1,2,3]-Triazoles by Regiospecific Copper(I)-Catalyzed 1,3-Dipolar Cycloadditions of Terminal Alkynes to Azides, *J. Org. Chem.* **2002**, *67*, 3057-3064.

[301] R. Huisgen, 1.3-Dipolare Cycloadditionen Rückschau und Ausblick, *Angew. Chem.* **1963**, *75*, 604-637.

[302] R. Huisgen, 1,3-Dipolar Cycloadditions. Past and Future, *Angew. Chem. Int. Ed. Engl.* **1963**, *2*, 565-598.

[303] K. Totani, H. Miyazawa, S. Kurata, Y. Ito, Magnetic beads-assisted mild enrichment procedure for weak-binding lectins, *Anal. Biochem.* **2011**, *411*, 50-57.

[304] M. Caragata, A. K. Shah, B. L. Schulz, M. M. Hill, C. Punyadeera, Enrichment and identification of glycoproteins in human saliva using lectin magnetic bead arrays, *Anal. Biochem.* **2016**, *497*, 76-82.

[305] A. K. Shah, K.-A. Lê Cao, E. Choi, D. Chen, B. Gautier, D. Nancarrow, D. C. Whiteman, P. R. Baker, K. R. Clauser, R. J. Chalkley, N. A. Saunders, A. P. Barbour, V. Joshi, M. M. Hill, Glyco-centric lectin magnetic bead array (LeMBA) − proteomics dataset of human serum samples from healthy, Barrett′s esophagus and esophageal adenocarcinoma individuals, *Data Brief.* **2016**, *7*, 1058-1062.

[306] N. Hao, K. Neranon, O. Ramström, M. Yan, Glyconanomaterials for biosensing applications, *Biosens. Bioelectron.* **2016**, *76*, 113-130.

[307] M. Marradi, F. Chiodo, I. Garcia, S. Penades, Glyconanoparticles as multifunctional and multimodal carbohydrate systems, *Chem. Soc. Rev.* **2013**, *42*, 4728-4745.

[308] S. Igde, S. Röblitz, A. Müller, K. Kolbe, S. Boden, C. Fessele, T. K. Lindhorst, M. Weber, L. Hartmann, Linear Precision Glycomacromolecules with Varying Interligand Spacing and Linker Functionalities Binding to Concanavalin A and the Bacterial Lectin FimH, *Macromol. Biosci.* **2017**, *17*, 1700198.

[309] V. Ladmiral, E. Melia, D. M. Haddleton, Synthetic glycopolymers: an overview, *Eur. Polym. J.* **2004**, *40*, 431-449.

[310] C. von der Ehe, C. Weber, M. Gottschaldt, U. S. Schubert, Immobilized glycopolymers: Synthesis, methods and applications, *Prog. Polym. Sci.* **2016**, *57*, 64-102.

[311] T. Hatakeyama, T. Fukuda, N. Yamasaki, An Assay for Lectin Activity Using Dextran Derivatives, *Biosci. Biotechnol. Biochem.* **1992**, *56*, 2072-2073.

[312] K. Negishi, Y. Mashiko, E. Yamashita, A. Otsuka, T. Hasegawa, Cellulose Chemistry Meets Click Chemistry: Syntheses and Properties of Cellulose-Based Glycoclusters with High Structural Homogeneity, *Polymers* **2011**, *3*, 489.

[313] C. Xu, O. Spadiut, A. C. Araújo, A. Nakhai, H. Brumer, Chemo-enzymatic Assembly of Clickable Cellulose Surfaces via Multivalent Polysaccharides, *ChemSusChem* **2012**, *5*, 661-665.

[314] T. Hasegawa, M. Umeda, M. Numata, C. Li, A.-H. Bae, T. Fujisawa, S. Haraguchi, K. Sakurai, S. Shinkai, 'Click chemistry' on polysaccharides: a convenient, general, and monitorable approach to develop (1→3)-β-d-glucans with various functional appendages, *Carbohydr. Res.* **2006**, *341*, 35-40.

[315] N. Kawagoe, Y. Kasori, T. Hasegawa, Highly C6-selective and quantitative modification of cellulose: nucleoside-appended celluloses to solubilize single walled carbon nanotubes, *Cellulose* **2011**, *18*, 83-93.

[316] L. Cui, J. A. Cohen, K. E. Broaders, T. T. Beaudette, J. M. J. Fréchet, Mannosylated Dextran Nanoparticles: A pH-Sensitive System Engineered for Immunomodulation through Mannose Targeting, *Bioconjugate Chem.* **2011**, *22*, 949-957.

[317] K. Izawa, T. Hasegawa, Tosylated and azidated inulins as key substrates for further chemical modifications to access inulin-based advanced materials: An inulin-based glycocluster, *Bioorg. Med. Chem. Lett.* **2012**, *22*, 1189-1193.

[318] J. H. Prestegard, J. Liu, G. O. Widmalm, Oligosaccharides and Polysaccharides, chapter 3, in *Essentials of Glycobiology*, 3. ed. (Eds.: A. Varki, R. Cummings, J. Esko et al.), Cold Spring Harbor Laboratory Press, Cold Spring Harbor (NY), **2017**

[319] S. P. Massia, J. Stark, D. S. Letbetter, Surface-immobilized dextran limits cell adhesion and spreading, *Biomaterials* **2000**, *21*, 2253-2261.

[320] B. Liberelle, A. Merzouki, G. D. Crescenzo, Immobilized carboxymethylated dextran coatings for enhanced ELISA, *J. Immunol. Methods* **2013**, *389*, 38-44.

[321] R. L. Whistler, Solubility of Polysaccharides and Their Behavior in Solution, in *Carbohydrates in Solution, Vol. 117* (Ed.: S. I. Horace), American Chemical Society, **1973**, pp. 242-255.

[322] D. Klemm, *Polysaccharides II*, Springer Berlin Heidelberg, **2006**.

[323] J.-P. Ebran, N. Dendane, O. Melnyk, Carbohydrate microarrays in 96-well polystyrene microtiter plates, *Methods Mol Biol* **2012**, *808*, 377-391.

[324] M. Böcher, T. Böldicke, M. Kieß, U. Bilitewski, Synthesis of mono- and bifunctional peptide–dextran conjugates for the immobilization of peptide antigens on ELISA plates: properties and application, *J. Immunol. Methods* **1997**, *208*, 191-202.

[325] C. Kieburg, K. Sadalapure, Thisbe K. Lindhorst, Glucose-Based AB2-Building Blocks for the Construction of Branched Glycopeptidomimetics, *Eur. J. Org. Chem.* **2000**, *2000*, 2035-2040.

[326] Franziska Reise, master thesis, Christiana Albertina University Kiel (Kiel), **2014**.

[327] T. Heinze, N. Michealis, S. Hornig, Reactive polymeric nanoparticles based on unconventional dextran derivatives, *Eur. Polym. J.* **2007**, *43*, 697-703.

[328] P. Lemechko, E. Renard, J. Guezennec, C. Simon-Colin, V. Langlois, Synthesis of dextran-graft-PHBHV amphiphilic copolymer using click chemistry approach, *React. Funct. Polym.* **2012**, *72*, 487-494.

[329] M. Poláková, M. Beláňová, K. Mikušová, E. Lattová, H. Perreault, Synthesis of 1,2,3-Triazolo-Linked Octyl (1→6)-α-d-Oligomannosides and Their Evaluation in Mycobacterial Mannosyltransferase Assay, *Bioconjugate Chem.* **2011**, *22*, 289-298.

[330] S. D. Knight, J. Bouckaert, *Structure, Function, and Assembly of Type 1 Fimbriae, Vol. 288*, Springer, Berlin, Heidelberg, **2009**.

[331] O. Michel, B. J. Ravoo, Carbohydrate Microarrays by Microcontact "Click" Chemistry, *Langmuir* **2008**, *24*, 12116-12118.

[332] F. H. Crick, Thinking about the brain, *SciAm.* **1979**, *241*, 219-232.

[333] L. Fenno, O. Yizhar, K. Deisseroth, The Development and Application of Optogenetics, *Annu Rev Neurosci.* **2011**, *34*, 389-412.

[334] F. Crick, The impact of molecular biology on neuroscience, *Philos. Trans. Royal Soc. B* **1999**, *354*, 2021-2025.

[335] N. A. Repina, A. Rosenbloom, A. Mukherjee, D. V. Schaffer, R. S. Kane, At Light Speed: Advances in Optogenetic Systems for Regulating Cell Signaling and Behavior, *Annu. Rev. Chem. Biomol. Eng.* **2017**, *8*, 13-39.

[336] E. S. Boyden, F. Zhang, E. Bamberg, G. Nagel, K. Deisseroth, Millisecond-timescale, genetically targeted optical control of neural activity, *Nat. Neurosci.* **2005**, *8*, 1263.

[337] https://www.nobelprize.org/prizes/chemistry/2016/prize-announcement/, 9 Nov 2018, Nobel Media AB, Prize announcement.

[338] B. L. Feringa, The Art of Building Small: From Molecular Switches to Motors (Nobel Lecture), *Angew. Chem. Int. Ed.* **2017**, *56*, 11060-11078.

[339] S. Keiper, J. S. Vyle, Reversible Photocontrol of Deoxyribozyme-Catalyzed RNA Cleavage under Multiple-Turnover Conditions, *Angew. Chem.* **2006**, *118*, 3384-3387.

[340] H. Asanuma, X. Liang, H. Nishioka, D. Matsunaga, M. Liu, M. Komiyama, Synthesis of azobenzene-tethered DNA for reversible photo-regulation of DNA functions: hybridization and transcription, *Nat. Protoc.* **2007**, *2*, 203.

[341] Y. Liu, D. Sen, Light-regulated Catalysis by an RNA-cleaving Deoxyribozyme, *J. Mol. Biol.* **2004**, *341*, 887-892.

[342] J. H. Harvey, D. Trauner, Regulating Enzymatic Activity with a Photoswitchable Affinity Label, *ChemBioChem* **2008**, *9*, 191-193.

[343] D. Matsunaga, H. Asanuma, M. Komiyama, Photoregulation of RNA Digestion by RNase H with Azobenzene-Tethered DNA, *J. Am. Chem. Soc.* **2004**, *126*, 11452-11453.

[344] R. J. Mart, R. K. Allemann, Azobenzene photocontrol of peptides and proteins, *Chem. Commun.* **2016**, *52*, 12262-12277.

[345] U. Kusebauch, S. A. Cadamuro, H. J. Musiol, M. O. Lenz, J. Wachtveitl, L. Moroder, C. Renner, Photocontrolled Folding and Unfolding of a Collagen Triple Helix, *Angew. Chem. Int. Ed.* **2006**, *45*, 7015-7018.

[346] L. Nevola, A. Martín-Quirós, K. Eckelt, N. Camarero, S. Tosi, A. Llobet, E. Giralt, P. Gorostiza, Light-Regulated Stapled Peptides to Inhibit Protein–Protein Interactions Involved in Clathrin-Mediated Endocytosis, *Angew. Chem. Int. Ed.* **2013**, *52*, 7704-7708.

[347] J. Levitz, A. T. Popescu, A. Reiner, E. Y. Isacoff, A Toolkit for Orthogonal and in vivo Optical Manipulation of Ionotropic Glutamate Receptors, *Front. Mol. Neurosci.* **2016**, *9*, 2.

[348] P. Gorostiza, E. Y. Isacoff, Optical Switches for Remote and Noninvasive Control of Cell Signaling, *Science* **2008**, *322*, 395-399.

[349] D. M. Barber, M. Schönberger, J. Burgstaller, J. Levitz, C. D. Weaver, E. Y. Isacoff, H. Baier, D. Trauner, Optical control of neuronal activity using a light-operated GIRK channel opener (LOGO), *Chem. Sci.* **2016**, *7*, 2347-2352.

[350] A. Rullo, A. Reiner, A. Reiter, D. Trauner, E. Y. Isacoff, G. A. Woolley, Long wavelength optical control of glutamate receptor ion channels using a tetra-ortho-substituted azobenzene derivative, *Chem. Commun.* **2014**, *50*, 14613-14615.

[351] T. Fehrentz, M. Schönberger, D. Trauner, Optochemische Genetik, *Angew. Chem.* **2011**, *123*, 12362-12390.

[352] M. Banghart, K. Borges, E. Isacoff, D. Trauner, R. H. Kramer, Light-activated ion channels for remote control of neuronal firing, *Nat. Neurosci.* **2004**, *7*, 1381.

[353] J. Levitz, J. Broichhagen, P. Leippe, D. Konrad, D. Trauner, E. Y. Isacoff, Dual optical control and mechanistic insights into photoswitchable group II and III metabotropic glutamate receptors, *Proc. Natl. Acad. Sci. USA* **2017**, *114*, E3546-E3554.

[354] M. Volgraf, P. Gorostiza, R. Numano, R. H. Kramer, E. Y. Isacoff, D. Trauner, Allosteric control of an ionotropic glutamate receptor with an optical switch, *Nat. Chem. Biol.* **2005**, *2*, 47.

[355] A. J. Link, M. L. Mock, D. A. Tirrell, Non-canonical amino acids in protein engineering, *Curr. Opin. Biotechnol.* **2003**, *14*, 603-609.

[356] W. Lei, S. P. G., Expanding the Genetic Code, *Angew. Chem. Int. Ed.* **2005**, *44*, 34-66.

[357] W. Lei, S. P. G., Die Erweiterung des genetischen Codes, *Angew. Chem.* **2005**, *117*, 34-68.

[358] T. Willemse, K. Van Imp, R. J. M. Goss, H. W. T. Van Vlijmen, W. Schepens, B. U. W. Maes, S. Ballet, Suzuki–Miyaura Diversification of Amino Acids and Dipeptides in Aqueous Media, *ChemCatChem* **2015**, *7*, 2055-2070.

[359] C. D. Spicer, B. G. Davis, Selective chemical protein modification, *Nat. Commun.* **2014**, *5*, 4740.

[360] O. Boutureira, G. J. L. Bernardes, Advances in Chemical Protein Modification, *Chem. Rev.* **2015**, *115*, 2174-2195.

[361] E. Baslé, N. Joubert, M. Pucheault, Protein Chemical Modification on Endogenous Amino Acids, *Chem. Biol.* **2010**, *17*, 213-227.

[362] J. M. Chalker, G. J. L. Bernardes, Y. A. Lin, B. G. Davis, Chemical Modification of Proteins at Cysteine: Opportunities in Chemistry and Biology, *Chem. Asian J.* **2009**, *4*, 630-640.

[363] N. Lundell, T. Schreitmüller, Sample Preparation for Peptide Mapping— A Pharmaceutical Quality-Control Perspective, *Anal. Biochem.* **1999**, *266*, 31-47.

[364] M. E. B. Smith, F. F. Schumacher, C. P. Ryan, L. M. Tedaldi, D. Papaioannou, G. Waksman, S. Caddick, J. R. Baker, Protein Modification, Bioconjugation, and Disulfide Bridging Using Bromomaleimides, *J. Am. Chem. Soc.* **2010**, *132*, 1960-1965.

[365] D. P. Gamblin, S. van Kasteren, G. J. L. Bernardes, J. M. Chalker, N. J. Oldham, A. J. Fairbanks, B. G. Davis, Chemical site-selective prenylation of proteins, *Mol. BioSyst.* **2008**, *4*, 558-561.

[366] S. I. van Kasteren, H. B. Kramer, H. H. Jensen, S. J. Campbell, J. Kirkpatrick, N. J. Oldham, D. C. Anthony, B. G. Davis, Expanding the diversity of chemical protein modification allows post-translational mimicry, *Nature* **2007**, *446*, 1105.

[367] L. Wofsy, H. Metzger, S. J. Singer, Affinity Labeling—a General Method for Labeling the Active Sites of Antibody and Enzyme Molecules*, *Biochemistry* **1962**, *1*, 1031-1039.

[368] B. R. Baker, Factors in the design of active-site-directed irreversible inhibitors, *J. Pharm. Sci.* **1964**, *53*, 347-364.

[369] W. B. Lawson, H. J. Schramm, Modification of a Methionine Residue Near the Active Site of Chymotrypsin, *J. Am. Chem. Soc.* **1962**, *84*, 2017-2018.

[370] T. Hayashi, I. Hamachi, Traceless Affinity Labeling of Endogenous Proteins for Functional Analysis in Living Cells, *Acc. Chem. Res.* **2012**, *45*, 1460-1469.

[371] I. Hamachi, T. Nagase, S. Shinkai, A General Semisynthetic Method for Fluorescent Saccharide-Biosensors Based on a Lectin, *J. Am. Chem. Soc.* **2000**, *122*, 12065-12066.

[372] W. Haruto, M. Masayoshi, K. Yoichiro, T. Yousuke, T. Shinya, H. Itaru, Affinity-Labeling-Based Introduction of a Reactive Handle for Natural Protein Modification, *Chem. Asian J.* **2008**, *3*, 1134-1139.

[373] G. Chen, A. Heim, D. Riether, D. Yee, Y. Milgrom, M. A. Gawinowicz, D. Sames, Reactivity of Functional Groups on the Protein Surface: Development of Epoxide Probes for Protein Labeling, *J. Am. Chem. Soc.* **2003**, *125*, 8130-8133.

[374] Y. Takaoka, H. Tsutsumi, N. Kasagi, E. Nakata, I. Hamachi, One-Pot and Sequential Organic Chemistry on an Enzyme Surface to Tether a Fluorescent Probe at the Proximity of the Active Site with Restoring Enzyme Activity, *J. Am. Chem. Soc.* **2006**, *128*, 3273-3280.

[375] T. Yousuke, O. Akio, H. Itaru, Protein Organic Chemistry and Applications for Labeling and Engineering in Live-Cell Systems, *Angew. Chem. Int. Ed.* **2013**, *52*, 4088-4106.

[376] S. Tsukiji, M. Miyagawa, Y. Takaoka, T. Tamura, I. Hamachi, Ligand-directed tosyl chemistry for protein labeling in vivo, *Nat. Chem. Biol.* **2009**, *5*, 341.

[377] S. Tsukiji, H. Wang, M. Miyagawa, T. Tamura, Y. Takaoka, I. Hamachi, Quenched Ligand-Directed Tosylate Reagents for One-Step Construction of Turn-On Fluorescent Biosensors, *J. Am. Chem. Soc.* **2009**, *131*, 9046-9054.

[378] Y. Koshi, E. Nakata, M. Miyagawa, S. Tsukiji, T. Ogawa, I. Hamachi, Target-Specific Chemical Acylation of Lectins by Ligand-Tethered DMAP Catalysts, *J. Am. Chem. Soc.* **2008**, *130*, 245-251.

[379] F.-I. Beiroth, dissertation thesis, Christian-Albrechts Universität zu Kiel (Kiel), **2015**.

[380] Z. Song, Y. Takaoka, Y. Kioi, K. Komatsu, T. Tamura, T. Miki, I. Hamachi, Extended Affinity-guided DMAP Chemistry with a Finely Tuned Acyl Donor for Intracellular FKBP12 Labeling, *Chem. Lett.* **2015**, *44*, 333-335.

[381] I. Stamer, master thesis, Christiana Albertina University Kiel (Kiel), **2014**.

[382] Glide, Schrödinger, version 10.1, from Maestro release 2017-4, LLC, New York, NY, 2017.

[383] Maestro, Version 10.1, Schrödinger, LLC, New York, NY, 2013.

[384] J. H. Harvey, B. K. Butler, D. Trauner, Functionalized azobenzenes through cross-coupling with organotrifluoroborates, *Tetrahedron Lett.* **2007**, *48*, 1661-1664.

[385] N. Miyaura, A. Suzuki, Palladium-Catalyzed Cross-Coupling Reactions of Organoboron Compounds, *Chem. Rev.* **1995**, *95*, 2457-2483.

[386] S. R. Chemler, D. Trauner, S. J. Danishefsky, The B-Alkyl Suzuki–Miyaura Cross-Coupling Reaction: Development, Mechanistic Study, and Applications in Natural Product Synthesis, *Angew. Chem. Int. Ed.* **2001**, *40*, 4544-4568.

[387] R. I. Dowell, C. J. Springer, D. H. Davies, E. M. Hadley, P. J. Burke, F. T. Boyle, R. G. Melton, T. A. Connors, D. C. Blakey, A. B. Mauger, New Mustard Prodrugs for Antibody-Directed Enzyme Prodrug Therapy: Alternatives to the Amide Link, *J. Med. Chem.* **1996**, *39*, 1100-1105.

[388] M. Hu, L. Li, H. Wu, Y. Su, P.-Y. Yang, M. Uttamchandani, Q.-H. Xu, S. Q. Yao, Multicolor, One- and Two-Photon Imaging of Enzymatic Activities in Live Cells with Fluorescently Quenched Activity-Based Probes (qABPs), *J. Am. Chem. Soc.* **2011**, *133*, 12009-12020.

[389] L. Hu, B. Liu, D. R. Hacking, 5′-[2-(2-Nitrophenyl)-2-methylpropionyl]-2′-deoxy-5-fluorouridine as a potential bioreductively activated prodrug of FUDR: synthesis, stability and reductive activation, *Bioorg. Med. Chem. Lett.* **2000**, *10*, 797-800.

[390] S. Katayama, N. Ae, T. Kodo, S. Masumoto, S. Hourai, C. Tamamura, H. Tanaka, R. Nagata, Tricyclic Indole-2-carboxylic Acids: Highly in Vivo Active and Selective Antagonists for the Glycine Binding Site of the NMDA Receptor, *J. Med. Chem.* **2003**, *46*, 691-701.

[391] J. Xie, F. Yang, M. Zhang, C. Lam, Y. Qiao, J. Xiao, D. Zhang, Y. Ge, L. Fu, D. Xie, Antiproliferative activity and SARs of caffeic acid esters with mono-substituted phenylethanols moiety, *Bioorg. Med. Chem. Lett.* **2017**, *27*, 131-134.

[392] E. Moreau, S. Fortin, J. Lacroix, A. Patenaude, J. L. C. Rousseau, R. C-Gaudreault, N-Phenyl-N′-(2-chloroethyl)ureas (CEUs) as potential antineoplastic agents. Part 3: Role of carbonyl groups in the covalent binding to the colchicine-binding site, *Biorg. Med. Chem.* **2008**, *16*, 1206-1217.

[393] L. Ulysse, J. Chmielewski, The synthesis of a light-switchable amino acid for inclusion into conformationally mobile peptides, *Bioorg. Med. Chem. Lett.* **1994**, *4*, 2145-2146.

[394] L. Lee, Y. R. Leroux, P. Hapiot, A. J. Downard, Amine-Terminated Monolayers on Carbon: Preparation, Characterization, and Coupling Reactions, *Langmuir* **2015**, *31*, 5071-5077.

[395] A. Aemissegger, D. Hilvert, Synthesis and application of an azobenzene amino acid as a light-switchable turn element in polypeptides, *Nat. Protoc.* **2007**, *2*, 161.

[396] W. Adam, C.-G. Zhao, K. Jakka, Dioxirane Oxidations of Compounds other than Alkenes, in *Organic Reactions*, Wiley, **2008**.

[397] G. P. Moloney, G. R. Martin, N. Mathews, A. Milne, H. Hobbs, S. Dodsworth, P. Y. Sang, C. Knight, M. Williams, M. Maxwell, R. C. Glen, Synthesis and Serotonergic Activity of Substituted 2,N-Benzylcarboxamido-5-(2-ethyl-1-dioxoimidazolidinyl)-N,N-dimethyltrypt- amine Derivatives: Novel Antagonists for the Vascular 5-HT1B-like Receptor, *J. Med. Chem.* **1999**, *42*, 2504-2526.

[398] J. Juodaityte, N. Sewald, Synthesis of photoswitchable amino acids based on azobenzene chromophores: building blocks with potential for photoresponsive biomaterials, *J. Biotechnol.* **2004**, *112*, 127-138.

[399] R. Roy, F. D. Tropper, T. Morrison, J. Boratynski, Syntheses and transformations of glycohydrolase substrates into protein conjugates based on Michael additions, *J. Chem. Soc., Chem. Commun.* **1991**, 536-538.

[400] V. Chandrasekaran, J. Eugen, H. Kobarg, F. D. Sönnichsen, T. K. Lindhorst, Synthesis and Photochromic Properties of Configurationally Varied Azobenzene Glycosides, *ChemistryOpen* **2014**, *3*, 99-108.

[401] H. Madani, A. S. Thompson, M. D. Threadgill, An expedient synthesis of 7-O-functionalised pyrrolo[2,1-c][1,4]benzodiazepine-5,11-diones, *Tetrahedron* **2002**, *58*, 8107-8111.

[402] C. S. Hung, J. Bouckaert, D. Hung, J. Pinkner, C. Widberg, A. DeFusco, C. G. Auguste, R. Strouse, S. Langermann, G. Waksman, S. J. Hultgren, Structural basis of tropism of Escherichia coli to the bladder during urinary tract infection, *Mol. Microbiol.* **2002**, *44*, 903-915.

[403] J. Bouckaert, J. Berglund, M. Schembri, E. De Genst, L. Cools, M. Wuhrer, C. S. Hung, J. Pinkner, R. Slättegård, A. Zavialov, D. Choudhury, S. Langermann, S. J. Hultgren, L. Wyns, P. Klemm, S. Oscarson, S. D. Knight, H. De Greve, Receptor binding studies disclose a novel class of high-affinity inhibitors of the Escherichia coli FimH adhesin, *Mol. Microbiol.* **2005**, *55*, 441-455.

[404] Maestro, Release 2017-4, Schrödinger, LLC, New York, NY, 2017

[405] LigPrep, version 10.4, from Maestro release 2015-4, Schrödinger, LLC, New York, NY, 2015.

[406] G. Madhavi Sastry, M. Adzhigirey, T. Day, R. Annabhimoju, W. Sherman, Protein and ligand preparation: parameters, protocols, and influence on virtual screening enrichments, *J. Comput. Aided Mol. Des.* **2013**, *27*, 221-234.

[407] Schrödinger Suite 2017-4: Protein Preparation Wizard; Epik, Schrödinger, LLC, New York, NY, 2016; Impact, Schrödinger, LLC, New York, NY, 2016; Prime, Schrödinger, LLC, New York, NY, 2017.

[408] MacroModel, from Maestro release 2017-4, Schrödinger, LLC, New York, NY, 2017.

[409] R. T. Gephart, D. L. Huang, M. J. B. Aguila, G. Schmidt, A. Shahu, T. H. Warren, Catalytic C-H Amination with Aromatic Amines, *Angew. Chem.* **2012**, *124*, 6594-6598.

[410] R. T. Gephart, D. L. Huang, M. J. B. Aguila, G. Schmidt, A. Shahu, T. H. Warren, Catalytic C-H Amination with Aromatic Amines, *Angew. Chem. Int. Ed.* **2012**, *51*, 6488-6492.

[411] S. Samanta, A. A. Beharry, O. Sadovski, T. M. McCormick, A. Babalhavaeji, V. Tropepe, G. A. Woolley, Photoswitching Azo Compounds in Vivo with Red Light, *J. Am. Chem. Soc.* **2013**, *135*, 9777-9784.

[412] M. J. Hansen, M. M. Lerch, W. Szymanski, B. L. Feringa, Direct and Versatile Synthesis of Red-Shifted Azobenzenes, *Angew. Chem. Int. Ed.* **2016**, *55*, 13514-13518.

[413] M. J. Hansen, M. M. Lerch, W. Szymanski, B. L. Feringa, Direct and Versatile Synthesis of Red-Shifted Azobenzenes, *Angew. Chem.* **2016**, *128*, 13712-13716.

[414] S. N. Joshi, S. M. Vyas, M. W. Duffel, S. Parkin, H. J. Lehmler, Synthesis of Sterically Hindered Polychlorinated Biphenyl Derivatives, *Synthesis* **2011**, *7*, 1045-1054.

[415] J. F. W. Keana, S. X. Cai, Functionalized Perfluorophenyl Azides: New Reagents for Photoaffinity Labeling, *J. Fluorine Chem.* **1989**, *43*, 151-154.

[416] J. F. W. Keana, S. X. Cai, New reagents for photoaffinity labeling: synthesis and photolysis of functionalized perfluorophenyl azides, *J. Org. Chem.* **1990**, *55*, 3640-3647.

[417] L. C. Kreider, E. Friesen, Rotational Relationships of Alkyl Glucosides, *J. Am. Chem. Soc.* **1942**, *64*, 1482-1483.

[418] H. Akita, E. Kawahara, K. Kato, Chemoenzymatic synthesis of rhodiooctanoside isolated from Chinese medicines, rhodiolae radix, *Tetrahedron: Asymmetry* **2004**, *15*, 1623-1629.

[419] K. Shinoda, T. Yamanaka, K. Kinoshita, Surface Chemical Properties in Aqueous Solutions of Non-ionic Surfactants Octyl Glycol Ether, α-Octyl Glyceryl Ether and Octyl Glucoside, *J. Phys. Chem.* **1959**, *63*, 648-650.

[420] C. A. Sanhueza, M. M. Baksh, B. Thuma, M. D. Roy, S. Dutta, C. Préville, B. A. Chrunyk, K. Beaumont, R. Dullea, M. Ammirati, S. Liu, D. Gebhard, J. E. Finley, C. T. Salatto, A. King-Ahmad, I. Stock, K. Atkinson, B. Reidich, W. Lin, R. Kumar, M. Tu, E. Menhaji-Klotz, D. A. Price, S. Liras, M. G. Finn, V. Mascitti, Efficient Liver Targeting by Polyvalent Display of a Compact Ligand for the Asialoglycoprotein Receptor, *J. Am. Chem. Soc.* **2017**, *139*, 3528-3536.

[421] A. Reisner, J. A. J. Haagensen, M. A. Schembri, E. L. Zechner, S. Molin, Development and maturation of Escherichia coli K-12 biofilms, *Mol. Microbiol.* **2003**, *48*, 933-946.

[422] I. V. Shishkov, F. Rominger, P. Hofmann, Remarkably Stable Copper(I) α-Carbonyl Carbenes: Synthesis, Structure, and Mechanistic Studies of Alkene Cyclopropanation Reactions, *Organometallics* **2009**, *28*, 1049-1059.

[423] H. P. Ward, E. F. Jenkins, Use of paranitrophenylacetyl chloride for the identification of alcohols, ethers, phenols and amines, *J. Org. Chem.* **1945**, *10*, 371-373.

[424] J. Lee, J. Lee, M. Kang, M. Shin, J.-M. Kim, S.-U. Kang, J.-O. Lim, H.-K. Choi, Y.-G. Suh, H.-G. Park, U. Oh, H.-D. Kim, Y.-H. Park, H.-J. Ha, Y.-H. Kim, A. Toth, Y. Wang, R. Tran, L. V. Pearce, D. J. Lundberg, P. M. Blumberg, N-(3-Acyloxy-2-benzylpropyl)-N‘-[4-(methylsulfonylamino)benzyl]thiourea Analogues: Novel Potent and High Affinity Antagonists and Partial Antagonists of the Vanilloid Receptor, *J. Med. Chem.* **2003**, *46*, 3116-3126.